Tectonic and Magmatic Evolution of the Snake River Plain Volcanic Province

Editors
Bill Bonnichsen
Craig M. White
Michael McCurry

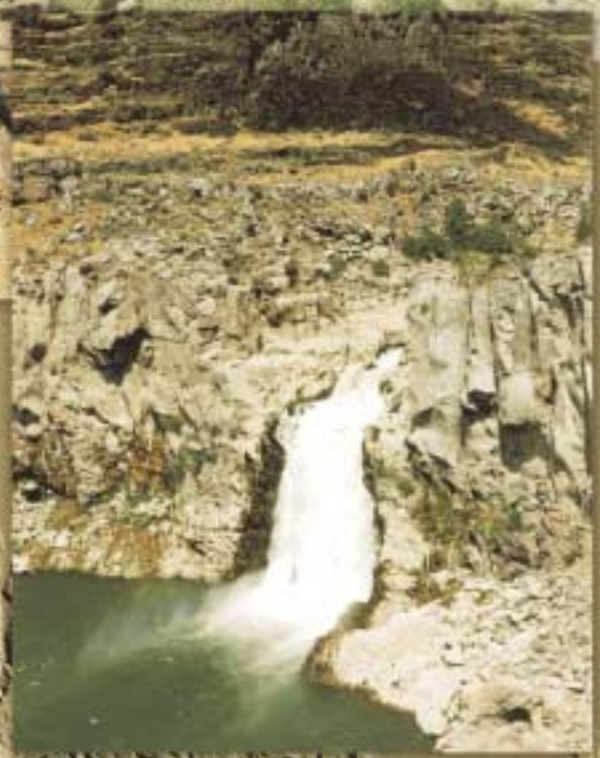

Cover photographs

Front:

(Top) Spectacular erosional pinnacles developed in unit XI of the Cougar Point Tuff, West Fork of Jarbidge Canyon, Nevada.

(Middle left) The welded ignimbrite layers that constitute the Cougar Point Tuff, Black Rock escarpment, Bruneau Canyon.

(Bottom left) Near-vertical rhyolite sheets in the vent area of the Pole Creek Top segment of the Jump Creek Rhyolite, Pole Creek canyon, Oregon.

(Bottom right) The north cataract of the 55-meter-high Twin Falls waterfall on the Snake River, north of Kimberly. The south cataract was appropriated for electrical power production in the mid 1930s.

Back:

(Top) Lizard Butte near Marsing, an erosional remnant of an inner crater-wall basaltic spatter layer deposited during a phreatomagmatic eruption. It lies on Lake Idaho sediments.

(Middle right) Big Southern Butte in the eastern Snake River Plain as viewed from the east. This 5-kilometer-wide butte is a composite rhyolite dome that rises to more than 700 meters above the surrounding plain.

(Middle left) Widely spaced vertical joints in the densely welded part of a tuff layer at the top of the Browns Bench escarpment have created this imposing line-up of giant, 15-meter-high anthropomorphic figures.

(Bottom right) View of the southwest side of Snake River Canyon near Swan Falls Dam, where basalt flows that erupted from Sinker Butte lie on basaltic tuff layers which had erupted earlier from that tuff cone.

(Bottom left) A erosional pinnacle of basalt spatter lying on lake sediments and phreatomagmatic tuff, west flank of Guffey Butte east of Walters Ferry.

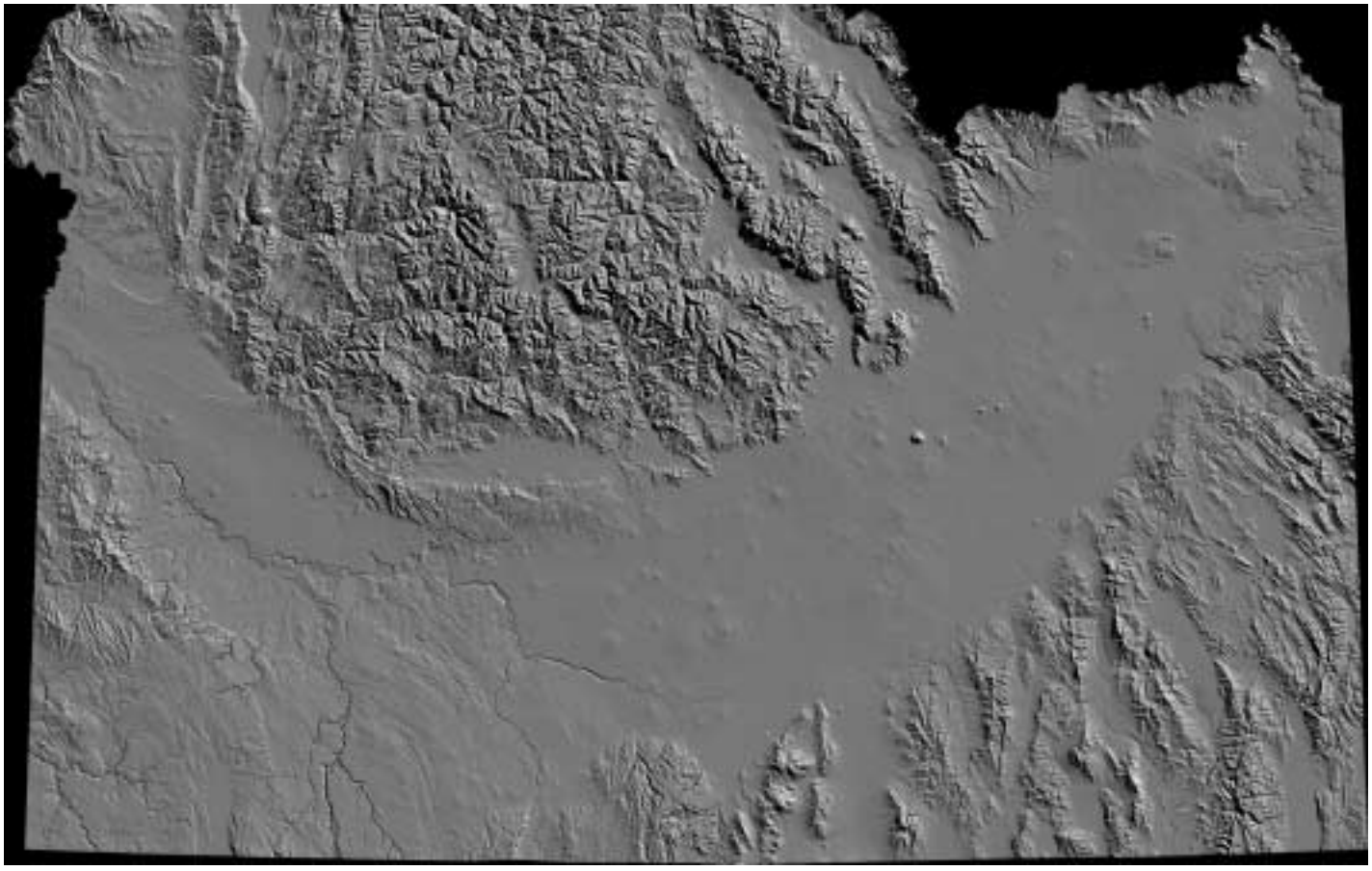

Computer-generated, shaded-relief image of the Snake River Plain region created from the U.S. Geological Survey's digital elevation data.

Tectonic and Magmatic Evolution of the Snake River Plain Volcanic Province

The Arch of Arch Canyon, where Cougar Creek was diverted from one side of an entrenched meander loop to the other and through a large gas cavity in the Dorsey Creek rhyolite.

Tectonic and Magmatic Evolution of the Snake River Plain Volcanic Province

Edited By
Bill Bonnichsen
Craig M. White
Michael McCurry

Idaho Geological Survey
University of Idaho
Moscow, Idaho
Bulletin 30
2002

Idaho Geological Survey Press

ISBN 1-55765-029-2

Contents

Contributing Authors viii

Preface ix

Chapter One: Evolution and Tectonics 1

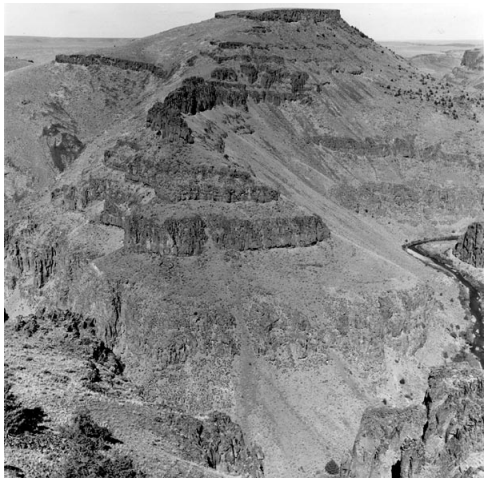

Yellowstone Plume Head: Postulated Tectonic Relations to the Vancouver Slab, Continental Boundaries, and Climate
By Kenneth L. Pierce, Lisa A. Morgan, and Richard W. Saltus 5

Tracking the Western Margin of the North American Craton Beneath Southeastern Oregon: A Multidisciplinary Approach
By James G. Evans, Andrew Griscom, Phyllis F. Halvorson, and Michael L. Cummings 35

A Model for the Origin of the Western Snake River Plain As an Extensional Strike-slip Duplex, Idaho and Oregon
By Peter Hooper, Jenda Johnson, and Chris Hawkesworth 59

Geologic and Tectonic History of the Western Snake River Plain, Idaho and Oregon
By Spencer H. Wood and Drew M. Clemens 69

Detrital Zircon Evidence for Pleistocene Drainage Reversal at Hagerman Fossil Beds National Monument, Central Snake River Plain, Idaho
By Paul Karl Link, H. Gregory McDonald, C. Mark Fanning, and Andrew E. Godfrey 105

Extension and Subsidence of the Eastern Snake River Plain, Idaho
By David W. Rodgers, H. Thomas Ore, Robert T. Bobo, Nadine McQuarrie, and Nick Zentner 121

Chapter Two: Products of Rhyolite Volcanism 157

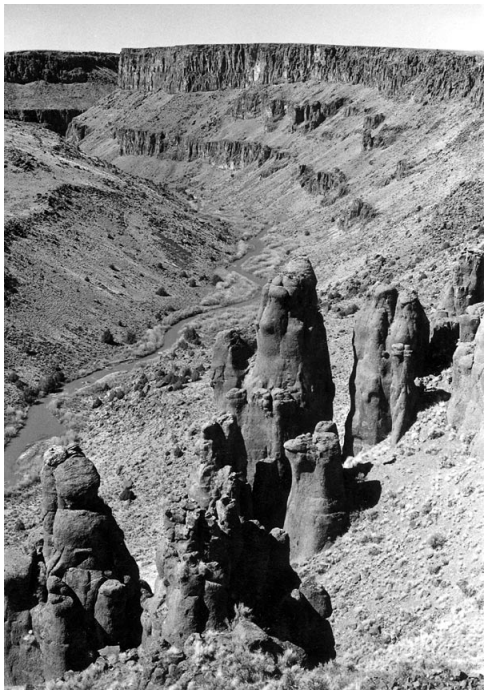

Bulk Major and Trace Element Evidence for a Time-Space Evolution of Snake River Plain Rhyolites, Idaho
By Scott S. Hughes and Michael McCurry 161

Petrology and Geochemistry of the Miocene Tuff of McMullen Creek, Central Snake River Plain, Idaho
By Karen E. Wright, Michael McCurry, and Scott S. Hughes 177

Transition From Ash-Flow to Voluminous Lava-Flow Activity, Bruneau-Jarbidge Eruptive Center, Southwestern Idaho
By William H. Hirt 195

The Juniper Mountain Volcanic Center, Owyhee County, Southwestern Idaho: Age Relations and Physical Volcanology
By Curtis R. Manley and William C. McIntosh 205

Chapter Three: Products of Basaltic Volcanism 229

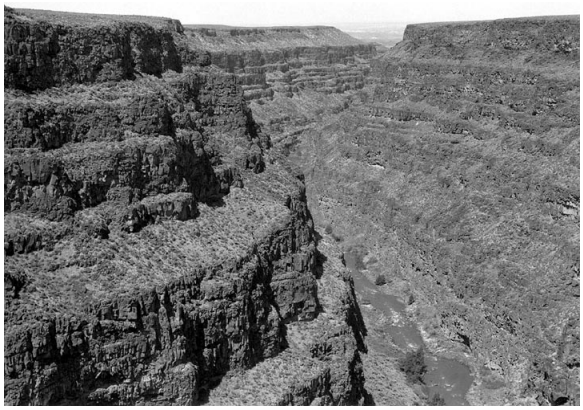

Late Miocene, Pliocene, and Pleistocene Geology ov Southwestern Idaho With Emphasys on Basalts in the Bruneau-Jarbidge, Twin Falls, and Western Snake River Plain Regions
By Bill Bonnichsen and Martha M. Godchaux 233

Temporal Controls on Basalt Genesis and Evolution on the Owyhee Plateau, Idaho and Oregon
By Kurt A. Shoemaker and William K. Hart 313

Geochemical and Sr-Isotopic Variations in Western Snake River Plain Basalts, Idaho
By Craig M. White, William K. Hart, Bill Bonnichsen, and Debra Matthews 329

Origin and Evolution of the Western Snake River Plain: Implications From Stratigraphy, Faulting, and the Geochemistry of Basalts Near Mountain Home, Idaho
By John W. Shervais, Gaurav Shroff, Scott K. Vetter, Scott Matthews, Barry B. Hanan, James J. McGee 343

Evolution of Quaternary Tholeiitic Basalt Eruptive Centers on the Eastern Snake River Plain, Idaho
By Scott S. Hughes, Paul H. Wetmore, and Jason L. Casper 363

Syneruptive Magma-Water and Posteruptive Lava-Water Interactions in the Western Snake River Plain, Idaho, During the Past 12 Million Years
By Martha M. Godchaux and Bill Bonnichsen 387

Overview and Synthesis of Lithologic Controls on Aquifer Heterogeneity in the Eastern Snake River Plain, Idaho
By John A. Welhan, Chad M. Johannesen, Linda L. Davis, Kelly S. Reeves, and John A. Glover 435

Volcanic Hazards of the Idaho National Engineering and Environmental Laboratory, Southeast Idaho
By William R. Hackett, Richard P. Smith, and Soli Khericha 461

Contributing Authors

Bobo, Robert T., p. 121-155
Bonnichsen, Bill, p. 233-312, 329-342, 387-434

Casper, Jason L., p. 363-385
Clemens, Drew M., p. 69-103
Cummings, Michael L., p. 35-57

Davis, Linda L., p. 435-460

Evans, James G., p. 35-57

Fanning, C. Mark, p. 105-119

Glover, John A., p. 435-460
Godchaux, Martha M., p. 233-312, 387-434
Godfrey, Andrew E., p. 105-119
Griscom, Andrew, p. 35-57

Hackett, William R., p. 461-482
Halvorson, Phyllis F., p. 35-57
Hanan, Barry B., p. 343-361
Hart, William K., p. 313-328, 329-342
Hawkesworth, Chris, p. 59-67
Hirt, William H., p. 195-204
Hooper, Peter, p. 59-67
Hughes, Scott S., p. 161-176, 177-194, 363-385

Johannesen, Chad M., p. 435-460
Johnson, Jenda, p. 59-67

Khericha, Soli, p. 461-482

Link, Paul Karl, p. 105-119

Manley, Curtis R., p. 205-227
Matthews, Debra, p. 329-342
Matthews, Scott, p. 343-361
McCurry, Michael, p. 161-176, 177-194
McDonald, H. Gregory, p. 105-119
McGee, James J., p. 343-361
McIntosh, William C., p. 205-227
McQuarrie, Nadine, p. 121-155
Morgan, Lisa A., p. 5-33

Ore, H. Thomas, p. 121-155

Pierce, Kenneth L., p. 5-33

Reeves, Kelly S., p. 435-460
Rodgers, David W., p. 121-155

Saltus, Richard W., p. 5-33
Shervais, John W., p. 343-361
Shoemaker, Kurt A., p. 313-328
Shroff, Gaurav, p. 343-361
Smith, Richard P., p. 461-482

Vetter, Scott K., p. 343-361

Welhan, John A., p. 435-460
Wetmore, Paul H., p. 363-385
White, Craig M., p. 329-342
Wood, Spencer H., p. 69-103
Wright, Karen, p. 177-194

Zentner, Nick, p. 121-155

Preface

The Snake River Plain (SRP) has been recognized for more than a century as a distinctive physiographic feature of the western United States that extends 600 km in an east-west arc across southern Idaho into eastern Oregon. It is distinguished from the surrounding terrain by its lower elevations and lower relief and by a surface geology that consists entirely of Neogene volcanic and sedimentary rocks. In response to ideas proposing the existence of a "hot-spot track" across southern Idaho, the definition of the SRP has expanded during the last two decades to encompass the northeast-trending line of bimodal eruptive centers from southeastern Oregon through the Yellowstone Plateau. Because it has been twenty years since publication of "Cenozoic Geology of Idaho," the last volume of papers with significant emphasis on the SRP, we felt it was indeed time to bring together a new collection of invited papers from different perspectives on the magmatic, structural, and tectonic evolution of this complex geologic system.

We have organized the book into three chapters based on shared topics among papers. Chapter 1 presents the overall magmatic and tectonic evolution of the SRP. Pierce and others begin with the geologic consequences of the emerging Yellowstone mantle plume around 17 Ma. Evans and others discuss the implications along the western edge of the SRP system where it crosses the proposed boundary between the North American craton to the east and accreted terranes to the west. Hooper and others address the origin of the northwest-trending structural basin of the western SRP. Wood and Clemens review the western SRP's geologic and tectonic history, focusing mainly on the sequence of lacustrine sedimentary rocks that accumulated in Pliocene-Pleistocene Lake Idaho. Link and others describe the Pleistocene fluvial system associated with the eastern margin of Lake Idaho in the Hagerman area. Finally, Rodgers and others move the discussion to the eastern SRP to examine the structural deformation of that region.

Chapter 2 offers aspects on the silicic end member of the bimodal SRP volcanic system. Hughes and McCurry present a model for the evolution of SRP rhyolites in time and space as the locus of magmatism migrated eastward. Wright and others report on the petrology of the Miocene tuff of McMullen Creek in the central SRP, presenting a case for the presence of large mantle-derived mass components in some SRP rhyolites. For the southwestern SRP, Hirt discusses two large intracaldera lava flows associated with the Bruneau-Jarbidge eruptive center, and Manley and

McIntosh direct attention to the age relations and physical volcanology of rhyolites at the Juniper Mountain eruptive center.

Chapter 3 is devoted to the SRP's basaltic system. Bonnichsen and Godchaux open with an extensive survey of basaltic volcanism in the western and central SRP. Four papers cover basalt petrogenesis and its tectonic implications: Shoemaker and Hart on the Owyhee Plateau, White and others on the western SRP, Shervais and others on the Mountain Home area, and Hughes and others on the eastern SRP. Godchaux and Bonnichsen discuss the many ways basaltic magmas interacted with external water in the western SRP. Welhan and others present an overview of the basalt flow dominated eastern SRP aquifer. Hackett and others conclude the chapter with an assessment of the hazards posed by basaltic volcanism at the Idaho National Engineering and Environmental Laboratory.

In acknowledgment of the efforts that have made this volume possible, we are foremost grateful for the encouraging support of our affiliated organizations: the Idaho Geological Survey at the University of Idaho, the Department of Geosciences at Boise State University, and the Department of Geosciences at Idaho State University. We are sincerely thankful to the authors not only for their substantial scientific contributions but also for their calm forbearance and understanding as time progressed on this project. We further wish to commend the many reviewers who worked selflessly to improve the clarity and quality of presentations in these papers. We are also pleased to extend deserved recognition to the important contributions of two individuals vital in the book's production: To B. Benjamin E. Studer at the Idaho Geological Survey for preparing and revising the numerous illustrations and tables to meet digital publishing requirements and for tackling this challenging work from the original artwork and software files submitted in nearly as many formats, versions, and styles as there are papers. To Barbara A. Ham of the University of Idaho's Printing and Design Services for meticulously putting together the final layout and design of the book. Finally, we wish to express our gratitude and appreciation to Roger C. Stewart, the manager of publications and communications at the Idaho Geological Survey, for his dedication to detail in all aspects of preparing this book for publication.

Bill Bonnichsen
Idaho Geological Survey

Craig M. White
Boise State University

Michael McCurry
Idaho State University

CHAPTER ONE

Evolution and Tectonics

Triplet Butte and Bruneau Canyon, where the Bruneau River has eroded through the welded ignimbrite layers that constitute the Cougar Point Tuff.

Cougar Point Tuff overlying the tilted Bieroth volcanics, Bruneau Canyon near Rowland, Nevada.

Triguero Homestead rhyolite at Triguero Homestead, Bruneau Canyon.

(Clockwise from top left)*: Dorsey Creek rhyolite, Jarbidge Canyon. Bonneville Flood boulders. Sheep Creek rhyolite, Bruneau Canyon. Shoshone Falls of the Snake River. Lake beds formed in Pliocene Lake Idaho.*

Cowan Homestead near Cougar Creek.

Primitive cabin at Roberson Place along Sheep Creek.

Indian Batt Cabin, Bruneau Canyon.

Yellowstone Plume Head: Postulated Tectonic Relations to the Vancouver Slab, Continental Boundaries, and Climate

Kenneth L. Pierce,[1] Lisa A. Morgan,[2] and Richard W. Saltus[2]

ABSTRACT

We trace the Yellowstone hotspot track back to an apparent inception centered near the Oregon-Nevada border. We and others have concluded this is the locus of a starting plume or plume head. Consideration of this plume-head model leads us to discuss the following three implications.

(1) The apparent center of the relic plume head is about 250 km west of the location where both the trends of the younger hotspot track and the inferred plate motions would place the hotspot at 16 Ma. A possible explanation for this discrepancy is the westward deflection of the plume up the bottom of the inclined Vancouver slab. Plate tectonic reconstructions and an intermediate dip for the Vancouver slab indicate a plume head would have intersected the Vancouver slab.

(2) The postulated arrival of the plume head at the base of the lithosphere is temporally associated with the eruption of the Columbia River and Oregon Plateau flood basalts at 14-17 Ma; however, these basalts were erupted several hundred kilometers north of the apparent plume center. The postulated plume center is symmetrically located near the midpoint of the 1,100-km-long Nevada-Oregon rift zone. Strontium isotopic variations reflect crustal and mantle lithosphere variations along the trend of this rift zone, with the basalt area of Oregon and Washington lying west of the 0.704 line in oceanic crust, the apparent center in northern Nevada between the 0.704 and 0.706 line in intermediate crust, and the area of central and southern Nevada east of the 0.706 line in Precambrian continental crust. Geophysical modeling is consistent with a dense crust north of the Nevada-Oregon border and an asthenospheric low-density body that extends several hundred kilometers south and north of the Nevada-Oregon boundary. A reconstruction of the initial contact of the plume head with the lithosphere suggests relatively thin lithosphere at 17 Ma beneath Oregon and Washington, which would favor the spreading of the plume northward in this direction, more decompression melting in this "thinspot" area, and the eruption of basalt through dense, oceanic lithosphere. Thus, preferential extrusion of flood basalts north of the plume center may be the result of differences in the pre-plume lithosphere, and not the location of the center of the plume head.

(3) A plume head rising into the base of the lithosphere is expected to produce uplift, which we estimate to be about 1 km with a north-south dimension of 1,000 km. This plume-head uplift, followed by subsidence, is consistent with Cenozoic paleobotanical altitude estimates. Other climatic indicators show major aridity about 15 Ma in areas in the inferred precipitation shadow east of the inferred uplift. Indicators of climate about 7 Ma are compatible with an eastward migration of uplift to a site between the plume-head area and the present Yellowstone crescent of high terrain. The warm Neogene "climate optimum" correlates with 14- to 17-Ma flood basalt and rhyolite volcanism. The continued effects of Yellowstone plume-head uplift and ensuing plume-tail uplift, if real, could provide regional uplift that is geophysically plausible. Climatic modeling has shown that uplift of the age and latitude of the postulated Yellowstone plume-head uplift, if allied with Himalayan and perhaps other uplifts, could result in the late Cenozoic cooling

Editors' note: The manuscript was submitted in July 1998 and has been revised at the authors' discretion.

[1]U.S. Geological Survey, Northern Rocky Mountain Science Center, Box 3492, Montana State University, Bozeman, MT 59717-3492.

[2]U.S. Geological Survey, Box 25046, Federal Center, Denver, CO 80225 (MS 966 and 964).

Pierce, K.L., L.A. Morgan, and R.W. Saltus, 2002, Yellowstone plume head: Postulated tectonic relations to the Vancouver slab, continental boundaries, and climate, *in* Bill Bonnichsen, C.M. White, and Michael McCurry, eds., Tectonic and Magmatic Evolution of the Snake River Plain Volcanic Province: Idaho Geological Survey Bulletin 30, p. 5-33.

that lead to the Pliocene-Pleistocene ice ages (Kutzbach and others, 1989; Ruddiman and others, 1989, 1997).

Thus, the postulated Yellowstone plume head could have played an important role in the late Cenozoic geologic history of the northern, interior part of the U.S. Cordillera. Future studies of the kind briefly discussed here should provide a better evaluation of the Yellowstone plume head concept.

Key words: hotspot, Yellowstone, plume head, starting plume, Columbia River basalt, mantle, Basin and Range

INTRODUCTION

A common explanation of hotspot tracks, such as the one responsible for the Hawaiian Islands, is that they are generated by the interaction of a relatively fixed deep thermal plume with a moving lithospheric plate. Richards and others (1989) suggested that mantle plumes initiate as larger plume heads that produce associated flood basalts and then evolve into narrower plume tails associated with later, smaller volume volcanism. Thermal mantle plumes are controversial in part because they cannot be directly investigated; the narrow plume tails are too small in cross section to be imaged seismically. Mantle plumes are thought by many, however, to explain an important and still poorly resolved piece of the generally accepted plate-tectonic model.

A starting plume head rises slowly from deep in the mantle and is fed from below by a much thinner tail or chimney in which heated material is rising through the "tail pipe" an order of magnitude faster than the plume head rises. Thus, as the plume head rises, it inflates to diameters of hundreds or perhaps more than a thousand kilometers before it slowly impacts the base of the lithosphere. Upon rising the last 150 km or so, decompression melting in the plume head results in the eruption of flood basalts. In his presidential address to the Geological Society of America, George Thompson (1998) argued for the importance of deep mantle plumes in general and the Yellowstone plume head and tail in particular, concluding that "The paradigm of deep mantle plumes, like plate tectonics or asteroid impacts, supplies a wonderful unifying concept for geoscientists and for communicating our science to the world at large."

Plume heads produce a large area of uplift that starts before their actual arrival at the base of the lithosphere (Hill and others, 1992). Hotspot swells with heights of 1-2 km and diameters of 800-1,200 km (Crough, 1978) are associated with current hotspot positions commonly inferred to be plume tails. The partial melting of upwelling hot mantle produces two materials that are both lighter than the original mantle (density about 3.3 g/cc): basalt melt (density about 3.0 g/cc) that rises upward and restite residuum (density perhaps about 3.0 g/cc) that stays in the mantle (Morgan and others, 1995).

Despite the apparent unifying appeal, many dispute the mantle plume idea. For example, in the Pacific plate near the Hawaiian, Society, and Marquesas hotspots, Katzman and others (1998) determined that upper mantle velocities were high and not low as predicted by traditional hotspot thermal models. They suggest Richter-type convective rolls above the 660-km discontinuity that are oriented parallel to plate velocity rather than a deep thermal plume. Don Anderson (1998 and references therein) argues against the mantle-plume explanation of hotspots, particularly the deep-seated mantle plume idea, and presents alternative explanations to plume arguments.

In contrast, the recent book "The Earth's Mantle" contains many chapters by different authors who support the concepts of deep mantle plumes and starting plumes or plume heads. Griffiths and Turner (1998) argue for a starting plume head fed by a plume tail. Davies (1998) describes mantle convection with descending slabs and rising plumes. On the basis of chemical considerations, Campbell (1998) argues for a deep plume source for ocean island basalts. From seismological and experimental studies, Jackson and Rigden (1998) argue that the mantle is grossly uniform in chemical composition throughout and that phase transformations provide an adequate explanation for the seismically observed radial structure. In another book, Garnero and others (1998) recognize an ultralow velocity zone that may represent partial melting at the core-mantle boundary. A correlation of this zone with surface hotspot distribution and an anti-correlation with descended slabs suggest whole mantle convection may intersect just above the core-mantle boundary.

In testing the Yellowstone plume hypothesis, we were led into the problem of addressing the initial stages of the Yellowstone plume head by tracking the Yellowstone hotspot back to the west from its present location at the Yellowstone Plateau (Pierce and Morgan, 1990, 1992; Figure 1, hotspot track; Anders and others, 1989; Rodgers and others, 1990; Malde, 1991; Smith and Braile, 1993; Mueller and others, 1999). The hotspot track is associated with a northeastward progression of rhyolitic volcanic fields, faulting, and uplift. The segment containing the 10-Ma and younger rhyolitic volcanic progression is linear in both rate and trend and is reflected in the topographic depression of the eastern Snake River Plain (SRP). In contrast, the segment containing the 10-Ma and older rhyolitic progression includes two calderas active about 10 Ma but spaced 100-200 km apart (Morgan and others, 1997). The progression associated with rhyolitic

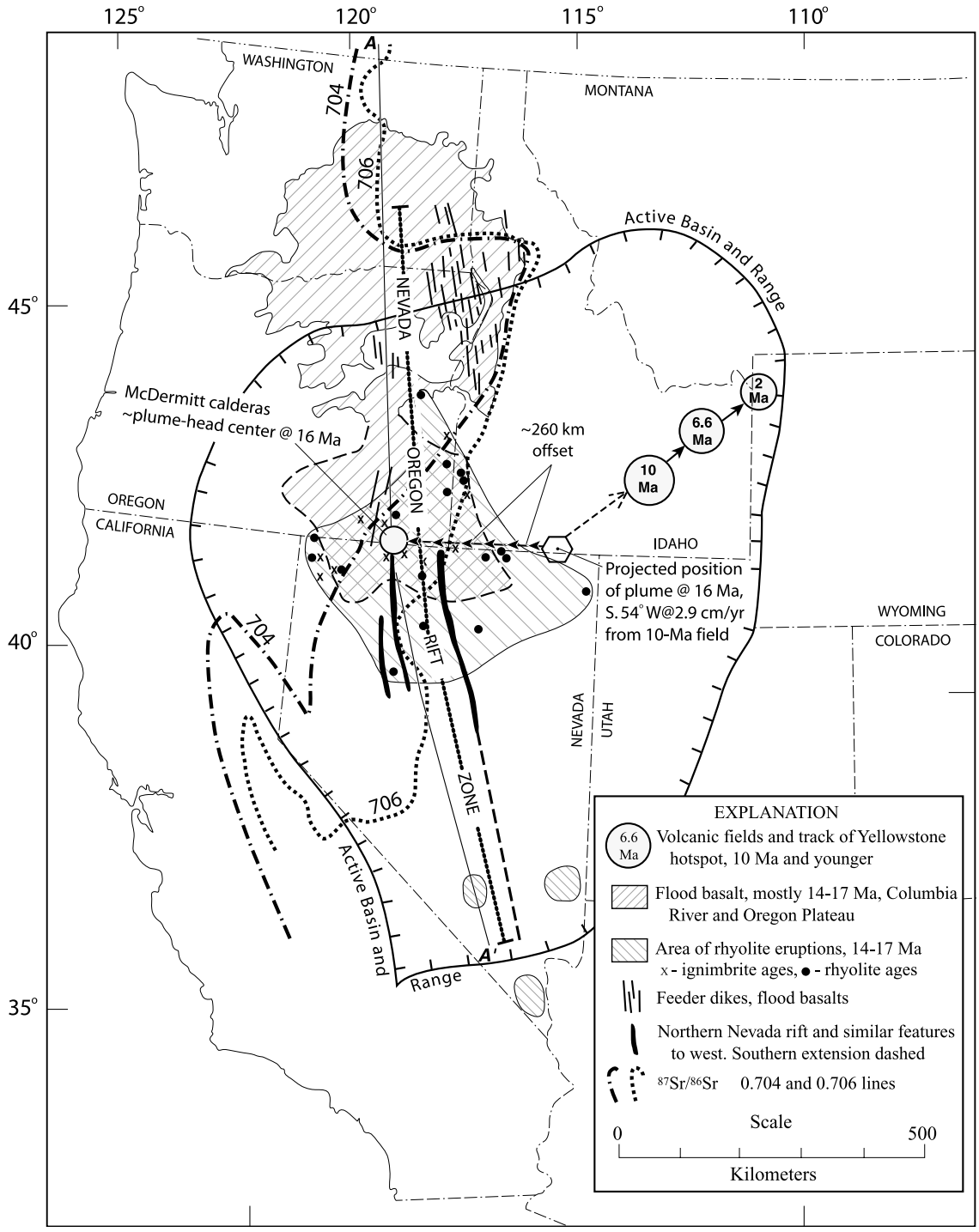

Figure 1. Map of western United States showing the track of the Yellowstone hotspot (after Pierce and Morgan, 1992, Figure 23). The 10- to-2-Ma track is compatible with plate motion, whereas the 10- to 16-Ma track has apparent rates three times faster than predicted. Projecting back from 10 Ma, we infer the plume was located at the site of the hexagon. As shown by the arrowed line, the geologic location of the inferred plume head was about 260 km further west at about the McDermitt caldera. Assuming the Vancouver slab was in the subsurface (Figures 2 and 3), buoyant rise up the slab may have deflected the plume head westward the 260 km shown by the arrowed line. Strontium lines after Reed (1993) with modifications in Washington from Robert Fleck (written commun., 1998) and southeastern Idaho from Leeman and others (1992). Transect A-A′ is portrayed in Figure 5. See Wagner and others (2000) for addition of 16-Ma Lovejoy Basalt in northern California to the Columbia River and Oregon Plateau group of basalts. The area of active basin and range in northwest Montana is not shown.

volcanism becomes increasingly diffuse to the southwest.

The earliest stages of this Yellowstone style volcanism can be projected back in space and time along this trend to the McDermitt caldera complex along the Nevada-Oregon boundary about 16 Ma (Malde, 1991; Thompson and Gibson, 1991; Pierce and Morgan, 1992) and to the northern part of the northern Nevada rift (Zoback and Thompson, 1978). As pointed out by Pierce and Morgan (1992), the 10-Ma and younger trend has an orientation of N. 54º E. and an apparent rate of 2.9 cm/year whereas the 10-Ma and older trend has an orientation of N. 75º E. and an apparent rate of 7.0 cm/year. These differences in apparent orientation and rate compound the problem of clearly identifying the initial hotspot starting location.

Based largely, however, on the track of the Yellowstone hotspot and its Columbia River-Oregon Plateau flood basalt association, the initial stages of the Yellowstone starting plume (plume head) have been inferred to begin at about 17 Ma beneath the northern Basin and Range Province (Zoback and Thompson, 1978; Hooper, 1990; Duncan and Richards, 1991; Thompson and Gibson, 1991; Draper, 1991; Zoback and others, 1994; Camp, 1995; Parsons, 1995). The large sublithospheric density deficit required to support high topography at this location is interpreted by Parsons and others (1994) and Saltus and Thompson (1995) to be the remnants of the Yellowstone plume head.

Our location of the center of the plume head near McDermitt is coincident with the northern part of the northern Nevada rift. On the basis of the age of the rift and extensive dating of associated volcanic sequences and mineralization, John and others (2000) and John and Wallace (2000) further develop the conclusion of Zoback and Thompson (1978) that the origin of the northern Nevada rift is related to the location of the Yellowstone hotspot at the rift about 15-16.5 Ma.

If we assume the nascent Yellowstone starting plume intercepted the lithosphere centered near the Nevada-Oregon border about 17 Ma, then the following possible relationships need to be examined and have implications for understanding the region: (1) The rising plume head may have interacted with and been diverted westward by the inclined Vancouver slab of oceanic lithosphere. This interaction may explain the anomalously high apparent volcanic migration rate from 16 to 10 Ma, which does not correspond with a known change in rate of the North American plate. (2) Differences in the character of the pre-plume lithosphere along a NNW-SSE 1,000-km-long trend centered near McDermitt may account for the different geologic features observed, particularly the 14.5- to 17.5-Ma major pulse of Columbia River-Oregon Plateau flood basalt eruptions north of the center of the plume head (assumed to be near the McDermitt caldera complex) and the dike injection along the 500-km-long northern Nevada rift and associated 14- to 17-Ma basaltic and silicic volcanism near and south of this center. (3) Significant topographic domal uplift above the plume head may have had great impact on past global and northwest U.S. climates and may explain regional changes in topography since the middle Miocene. If geologic observations support these three relations, this may provide support to the plume-head hypothesis. In addition to the three relations described above, the current high regional heat flow (Blackwell, 1989; Lachenbruch and Sass, 1978) and ongoing extension of the Basin and Range region of the North American plate may also relate to the stagnant Yellowstone plume head.

PROBLEMS INVOLVING PAST LOCATIONS OF THE YELLOWSTONE HOTSPOT

Zoback and Thompson (1978) first suggested that the Yellowstone hotspot surfaced in northern Nevada about 16 Ma. Malde (1991) noted that the oldest set of calderas along the Yellowstone hotspot track erupted the 16.1-Ma rhyolites of the McDermitt field (Rytuba and McKee, 1984, Figure 1). Several others have also postulated the McDermitt area near the Nevada-Oregon border (Figure 1) to be the approximate location of a large starting plume (Yellowstone plume head, Thompson and Gibson, 1991; Draper, 1991; Pierce and Morgan, 1992; Parsons and others, 1994; Zoback and others, 1994; Camp, 1995).

Placing the starting position in the McDermitt area raises some problems, as noted but not explained by Pierce and Morgan (1992). The apparent rate of hotspot migration from 16 to 10 Ma is 7 cm/year, more than twice the 10-Ma to present 2.9 cm/year apparent rate (Pierce and Morgan, 1992). On the basis of intervals of very high fault offset, Anders and others (1994) determined a plate migration rate, accounting for extension, of 22 km/m.y. (km/m.y. = mm/year), quite compatible with a global hotspot (but excluding Yellowstone) plate tectonic rate of 22 ± 8 km/m.y. (Alice Gripps, written commun., 1991, in Pierce and Morgan, 1992).

Projecting the trend of the 2- to 10-Ma hotspot track back to 16 Ma yields a location near the Idaho-Utah border about 250 km east of the apparent starting plume centered near McDermitt. West of the 10-Ma Picabo volcanic field, successively older fields have a very crude trend that ends up at McDermitt, but this direction of hotspot migration from 16 to 10 Ma is N. 75º E., about 20º differ-

ent from the direction of N. 54º E. from 10 to 2 Ma.

We have not accounted for the amount of extension (Rodgers and others, 1990) after 16 Ma over the present distance of 430 km between the McDermitt area and the 10-Ma Picabo volcanic field, other than to assume the observed post-10-Ma rate of 29 km/m.y. is the vector sum of the plate rate and the extension rate. If extension has been constant after 16 Ma, this is only about 25 percent of the total calculated rate of "migration" based on Anders' (1994) estimation of 22 km/m.y. for plate motion combined with 7 km/m.y. of tectonic extension to result in a combined rate of 29 km/m.y. One observation that suggests extension has been minor is the smooth, relatively unfaulted topography between McDermitt and the central SRP as shown on the shaded relief map of the U.S. (Thelin and Pike, 1991). This broad plateau is formed largely of 10- to 16-Ma volcanic strata (Luedke and Smith, 1981, 1982, 1983) suggesting little faulting since that time.

Other evidence based on fission track studies in the eastern Basin and Range Province, however, suggests major extension occurred between 20 and 15 Ma (Elizabeth Miller, written commun., 1999). Local extension east of McDermitt is indicated by opening of the western SRP (a few tens of kilometers), and by opening of the Raft Valley by the eastward sliding of the Black Pine and Sublette Ranges off the Albion Range (Covington, 1983; also shown in Pierce and Morgan, 1992, Figure 11). If extension east of McDermitt is as large as 260 km, this could then explain the 260 km westward offset of the 16-Ma plume location (Figure 1) in the last 16 Ma, and the following hypothesis of westward deflection by the Vancouver slab would not be needed.

RECONCILIATION BASED ON WESTWARD DEFLECTION BY THE VANCOUVER SLAB

We suggest here that the apparent discrepancy between both rate and azimuth of hotspot migration can be explained by the westward displacement of the plume head when it rose into the east-dipping Vancouver (or Juan de Fuca) slab (Figures 2 and 3). Geist and Richards (1993) suggested that the Yellowstone plume intercepted the Vancouver slab before 17 Ma, but they argued that the downward and strong northeast motion of the Vancouver plate trapped the plume for some time and carried it northward to near the common borders of Washington, Oregon, and Idaho where it eventually broke through the slab and produced the Columbia River flood basalts (Figure 1). We modify their idea of interaction with the Vancouver slab by suggesting that buoyant gravitational forces would be more effective than tractive forces and that the plume would buoyantly rise along the lower surface of the inclined slab, rather than being dragged northward and held down by the northeastward-moving and descending Vancouver slab. For a plume beneath a horizontal plate, tractive forces, where not opposed to gravity, do appear significant. We also propose a starting plume (or plume head) interacting with the Vancouver slab rather than an already existing plume tail (or chimney) that previously had been located beneath the Pacific Ocean as proposed by others (Geist and Richards, 1993; Duncan, 1982). The possible interaction of the Vancouver slab with the Yellowstone plume has been proposed by several others (Leeman, 1982; Duncan, 1982; Draper, 1991; Hill and others, 1992; and Hooper and Hawksworth, 1993).

To reconstruct the interaction of the Vancouver slab with the Yellowstone hotspot, we have used the plate tectonic reconstruction of Severinghaus and Atwater (1990; Figure 2). We have projected the track of the Yellowstone hotspot back in time on the basis of its 2- to 10-Ma rate of 2.9 cm/year at S. 54º W. (includes both plate rate and extension rate, Pierce and Morgan, 1992), using reconstructions for 30, 20, 10, 0 Ma (Severinghaus and Atwater, 1990). Projecting the direction and rate from 2-10 Ma back to 16 Ma is warranted for the paleomap models of global plate motion (Malcolm Ross, written commun., 1998, based on paleomap programs). Such models show the North American plate having no more than a 4-degree change in direction and 3 percent variation in rate over the last 20 Ma. However, a 12-degree change in direction and a 17 percent increase in rate are indicated about 20-21 Ma, which is before the volcanism we associate with the Yellowstone hotspot.

Figure 3 is a time sequence of cross sections incorporating the above rate with plume rise models and plate tectonic reconstructions. For the plume head, we have used a rise rate of 0.1 m/year (100 km/m.y.) suggested by Richards and others (1989) going back in time (and downward) from its interception with the North American plate (lithosphere) about 17 Ma ago. We estimate the volume of the plume head in the upper mantle to be roughly 400 cubic km based on the following: (1) the volumes erupted from the Columbia River-Oregon Plateau flood basalts (Hooper, 1997; Carlson and Hart, 1988), assuming 5-30 percent of partial melting (202-368 cubic km; Coffin and Eldholm, 1994), plus (2) the linear extent of erupted and injected material along the 500-km Nevada rift zone (Zoback and others, 1994); and (3) the residual mass deficit shown by Parsons and others (1994) for the northern Nevada area that is comparable to the expected deficit produced by a small plume head with a diameter of about

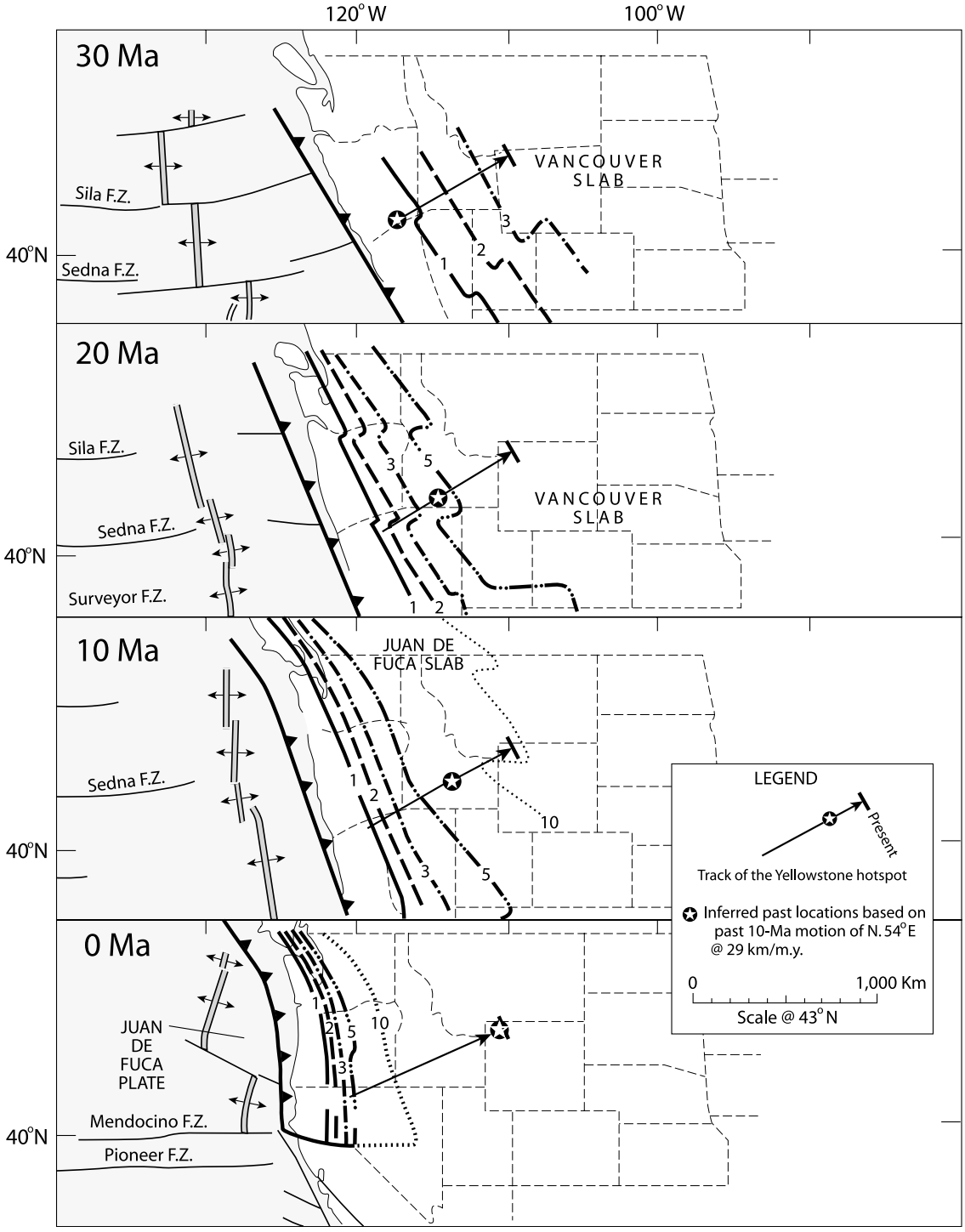

Figure 2. Location of the Yellowstone plume relative to the North American plate and the Vancouver slab (or Juan de Fuca slab; from Severinghaus and Atwater, 1990). The plume is assumed to be fixed in the mantle and now 50 km northeast of the 2.1-Ma caldera that started the Yellowstone Plateau volcanic field. Hotspot migration of 29 km/m.y. from 2 to 10 Ma is plotted as a circled star on the line of section. This rate of 29 km/m.y. is close to the plate motion rate of 22 ± 8 km/m.y. and includes tectonic extension that probably accounts for the apparent difference of 7 km/m.y. Cross sections are drawn to go through the McDermitt caldera and are nearly parallel to plate motion and to the inclination of the Vancouver slab. The reconstruction of Severinghaus and Atwater (1990) accounts for deformation, and the numbers on the Vancouver slab indicate the thermal state of the slab with 1 meaning solid enough to have earthquakes and 10 meaning nearly the same as the surrounding mantle.

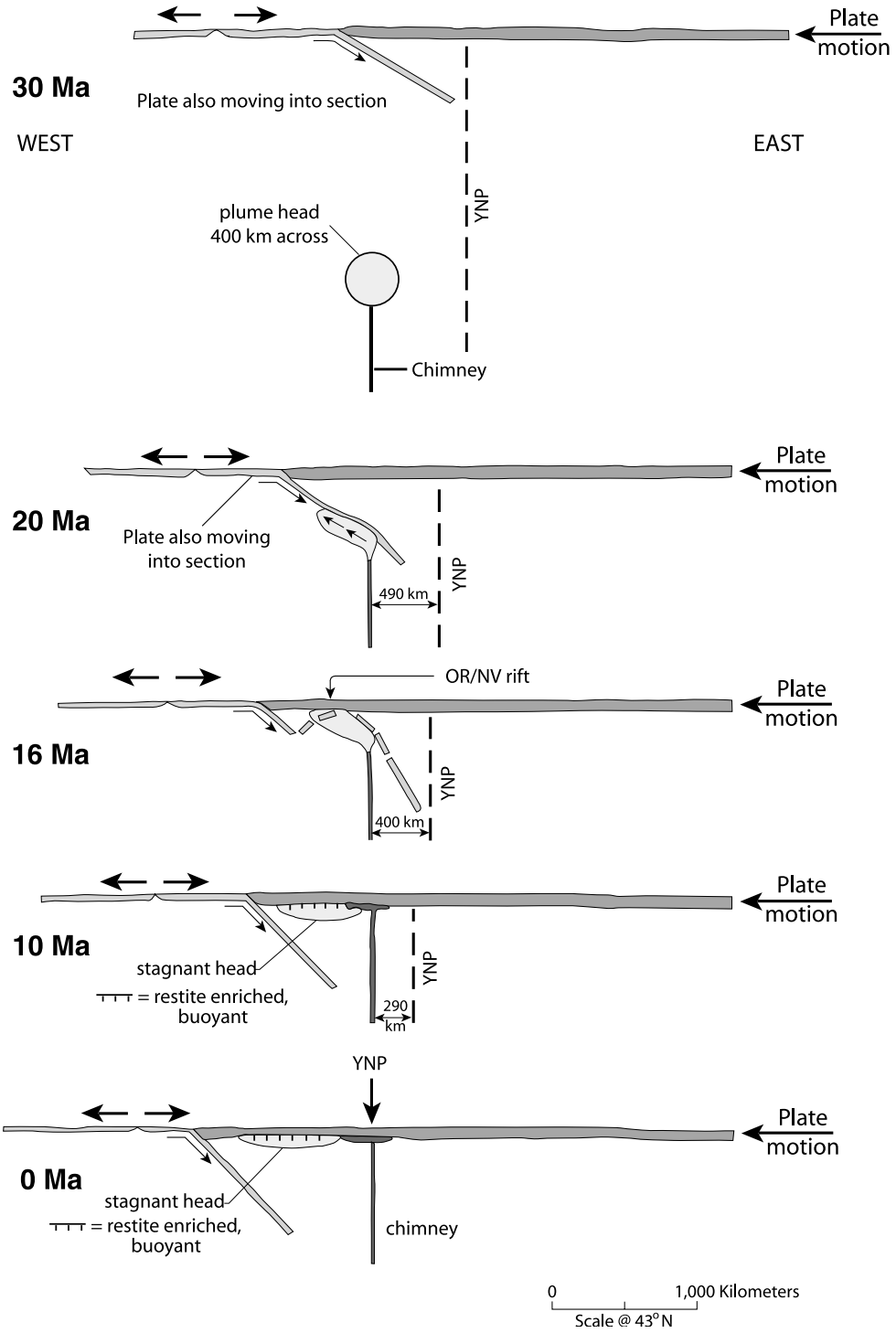

Figure 3. Postulated westward deflection of the Yellowstone plume head by buoyant rise up the inclined Vancouver slab. Time sequence from 30 Ma (top) to present (bottom) with position of plume held fixed in the mantle. At 20 Ma, the plume head has intersected the inclined Vancouver slab and is being displaced westward, and by 16 Ma the plume center is beneath McDermitt (along the Nevada-Oregon rift), about 260 km west of its feeding plume tail. As the plume flattens, the area of the plume in this cross section diminishes to about half because of spreading in the third dimension. The inclination of the Vancouver slab is shown to increase from 30 Ma to the present (see text under heading “Reconciliation Based . . .”). This cartoon does not account for interaction with the 660- and 410-km discontinuities, or curvature of the earth.

400 km and 100ºC-300ºC hotter than the surrounding asthenosphere (Hill and others, 1992). We assume the chimney (tail) of the Yellowstone plume has been held fixed over time (Figure 3) and that the North American plate has migrated at 22 km/m.y. and the hotspot has migrated at 29 km/m.y. (plate motion plus extension). As already noted, we assume the heated material in the tail is rising at about 1.0 m/year, which is an order of magnitude faster than the rate of the ascending plume head (0.1 m/year; or 100 km/m.y.). Thus, ascending material in the plume tail would contribute to inflation of the more slowly rising plume head.

The inclination of the Vancouver slab is difficult to constrain. About 50 Ma, it is thought to have been flat (see discussion in Atwater, 1989, p. 46-49). At present, the dip as far inland as the Cascades-Columbia Plateau boundary is 12 degrees (Parsons and others, 1998). Further inland and with more difficult techniques, Rasmussen and Humphreys (1988) estimate a dip of about 65 degrees near the Washington-Oregon boundary, and VanDecar (1991) estimates the dip to be about 60 degrees beneath Washington. Seismic imaging by van der Lee and Nolet (1997) shows remnants of the Vancouver slab at 500 km beneath the area near Salt Lake City, suggesting a time-averaged dip of about 30 degrees; they suggest a flat slab extending 1,000 km inland at 50 Ma, and at about 30 degrees dip extending more than 50 km inland at 30 Ma. Geist and Richards (1993) draw about a 35 degrees slab dip at 20 Ma. We have drawn a dip of about 40 degrees at 30 Ma that steepens to 45 degrees at 16 Ma and 50 degrees at present.

By about 20 Ma, the starting plume intercepted the Vancouver slab (Figure 3). If gravitational buoyancy dominates over tractive forces, the buoyant plume head would be deflected to the west by the west-rising lower surface of the Vancouver slab. We suggest the tractive force that the Vancouver slab could exert on the relatively low viscosity plume head, particularly by dragging the plume head down, would be minor compared to the buoyant rise of an expanding starting plume. Put more simply, how would the hot, low viscosity plume head stick to the steeply inclined slab? Also, consideration must be given to the slope angle of the descending slab. If the slope is as steep as 60 degrees, as inferred by Rasmussen and Humphreys (1988), traction would have even less of an effect on the ascending plume and thus would not block it.

Buoyant rise directly up the slab would displace the plume head to S. 70º W. That the deflection appears to be essentially to the west may reflect a small component of northward drag due to the northeasterly movement of the Vancouver slab relative to the North American plate.

With this westward offset by the Vancouver slab, the apparent rate of migration of volcanism between 16 and 10 Ma is an additive combination of the projected plate motion plus extension of 29 km/m.y. for 6 m.y. equaling 175 km plus the 250 km net offset by the Vancouver plate (Figure 1). This results in an apparent migration of approximately 420 km in 6 m.y., solved so as to yield the apparent migration rate of 70 km/m.y.

OTHER PROPOSED LOCATIONS OF THE YELLOWSTONE HOTSPOT

A number of proposals for the location of the Yellowstone hotspot at different times have been advanced (Figure 4). We conclude that the Yellowstone hotspot was centered near McDermitt on the Nevada-Oregon border, a location also advocated by Zoback and Thompson (1978), Malde (1991), Thompson and Gibson (1991), Draper (1991), Pierce and Morgan (1990, 1992), Parson and other (1994), Zoback and others (1994), Camp, (1995), John and others (2000), and John and Wallace (2000).

Geist and Richards (1993) suggest the Yellowstone plume was trapped for some time and carried northward by the Vancouver slab to a position beneath the main extrusion area of the Columbia River basalts. Our idea builds on the Vancouver slab interaction suggested by Geist and Richards (1993). We propose that buoyant forces dominated tractive ones and that the plume head was centered near the Nevada-Oregon border.

In the next section and earlier (Pierce and Morgan, 1992), we argue that the nascent Yellowstone plume intercepted the lithosphere near the McDermitt caldera area and that the apparent asymmetry related to the rhyolitic track of the Yellowstone hotspot with respect to the location of the Columbia River-Oregon Plateau flood basalts is due to changes in pre-plume lithosphere thickness and crustal composition. We argue herein and in our prior paper (Pierce and Morgan, 1992) that the asymmetry is merely apparent. In fact, the 1,100-km-long Nevada-Oregon rift can be considered an equal, but overlooked, component to the early stages of the plume head interception of the base of the lithosphere, as are the voluminous flood basalt eruptions to the north. Both components are symmetrical to the McDermitt area. Specifically, the Columbia River-Oregon Plateau basalts, located primarily north of the McDermitt center and north and off the trend of the hotspot track, are the product of a thinner, more mafic, younger accreted crust (Hooper, 1997) where the flood basalts surfaced while the northern Nevada rift developed in thicker, Proterozoic to Paleozoic, mafic to transitional accreted crust. From 14 to

16 Ma in northern Nevada and adjacent parts of Oregon and Idaho, there was widespread silicic volcanism, although the locations of the calderas have not been well established (Figure 1; Luedke and Smith, 1981, 1982, 1983).

Oppliger and others (1997) suggest that the 34- to 43-Ma Carlin-type gold mineralization at Carlin, Nevada, is associated with an "incubation period" of an early Yellowstone plume. They cite the rich abundance of gold and related siderophile elements in the Carlin deposits as being plume related and note that these enriched elements are thought to be derived from the core-mantle boundary where many think thermal plumes originate. We suggest, however, that having the Yellowstone plume beneath northern Nevada at 34-43 Ma is difficult to reconcile considering the rate and direction of motion of the North American plate (Figure 4) and the current location of the Yellowstone hotspot. Assuming a rate of 29 km/m.y. in a direction of S. 55º W. from Yellowstone places a 40-Ma plume somewhere near Sacramento, California, quite distant from Carlin, Nevada. The lack of volcanic deposits or related rifts that may have recorded the passage of a thermal plume in a time-transgressive pattern to the south-

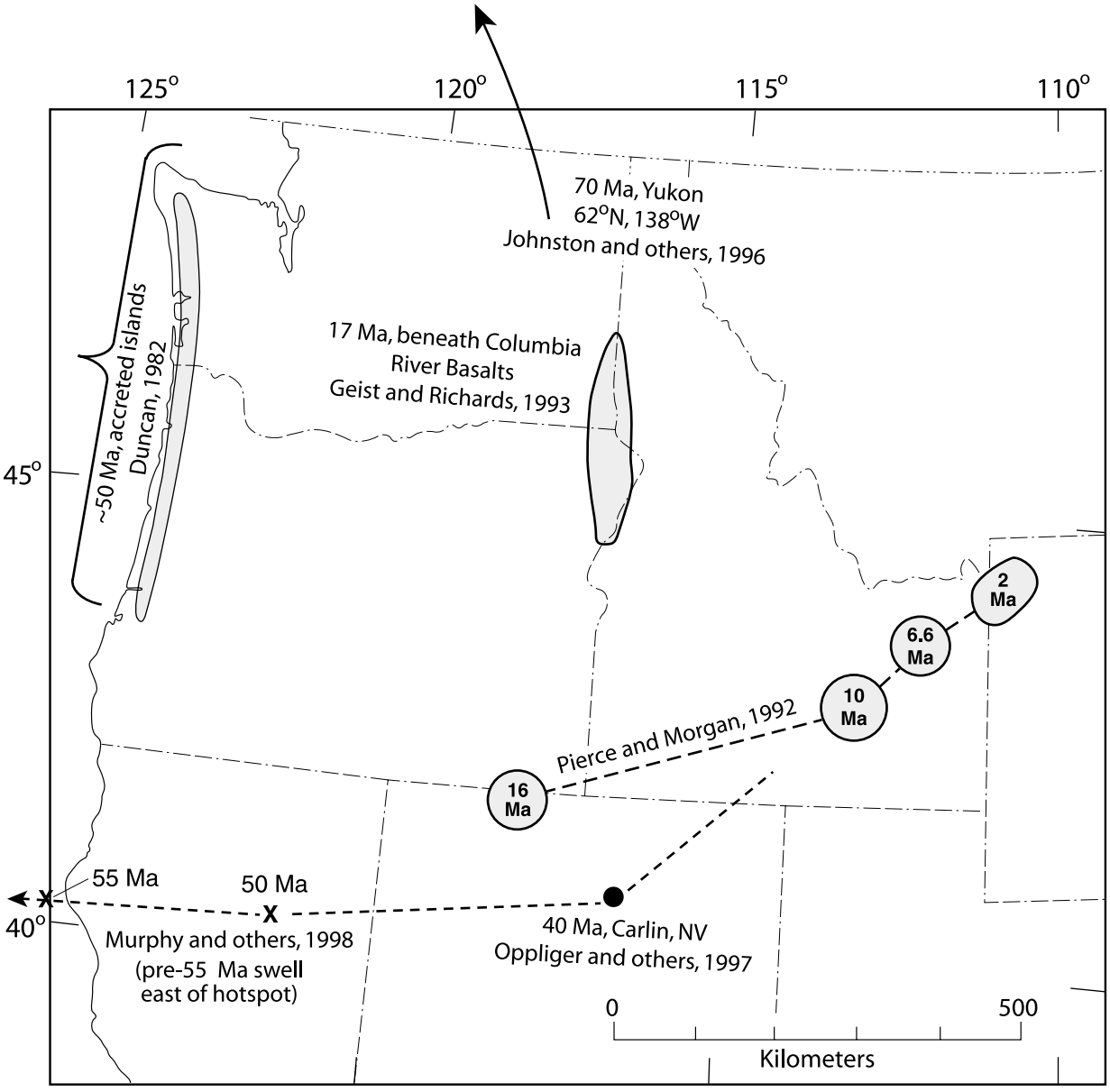

Figure 4. Some positions for the Yellowstone hotspot at different times as postulated by others and by us. The location between 50 and 17 Ma presents a problem that is avoided if the Yellowstone plume starts at 17 Ma.

west from McDermitt is striking. Furthermore, given our conclusion that the Yellowstone plume head intercepted the lithosphere at about 17 Ma near McDermitt, we cannot reconcile the proposal by Oppliger and others (1997) that the hotspot was southeast of McDermitt and only 380 km from the 10 Ma position of the hotspot. Such a location would yield an anomalously slow plate tectonic migration rate of 11 km/m.y.; this rate would also include any basin and range extension (Figure 4).

In a related paper by the same authors, Murphy and others (1998) suggest that before 40 Ma, the Yellowstone hotspot was further west (Figure 4) and the hotspot track had been subducted in advance of the time when the actual plume went under the North American plate about 55 Ma. Thus, the hotspot track and associated swell more than 1,500 km long were subducted prior to 55 Ma. Their paper stresses the idea that subduction of a hotspot track swell could add buoyancy to the subducted slab and affect the Cretaceous-early Tertiary orogeny. Their hotspot track differs in rate and orientation from that determined by the hotspot track volcanism (Pierce and Morgan, 1992), by hotspot faulting (Anders, 1994), and by plate motion (Alice Gripps in Pierce and Morgan, 1992, p. 6).

Bob Duncan (1982) proposed "a captured island chain in the Coast Range of Oregon and Washington" and attributes this to the Yellowstone hotspot (Figure 4). He suggested that the plume was shielded from surfacing between about 17 Ma and perhaps 30 Ma and inferred that the plume was trapped during this interval beneath the Vancouver slab. More recently, part of this "captured island" terrain, termed Siletzia and dated at 51-55 Ma, has also been ascribed to a Yellowstone hotspot origin by Pyle and others (1997). If the hotspot existed before 17 Ma and was active offshore between 50 and 60 Ma (Duncan, 1982; Pyle and others, 1997), yet was shielded from surfacing between 17 and perhaps 25 Ma by the sinking Vancouver slab, we would expect to see some surface manifestation of this plume west of McDermitt between 25 and 50 Ma. Furthermore, if the plume existed before 17 Ma, why does the Nevada-Oregon rift (Pierce and Morgan, 1992; Zoback and others, 1994; Parsons and others, 1994) appear to represent a 17-Ma event extending about 500 km both north and south of the Oregon-Nevada border centered in the McDermitt area and overlain by rhyolitic hotspot track volcanic rocks at McDermitt? How do these models (Duncan, 1982; Pyle and others, 1997) account for such a change in magnitude of processes going from relatively small volcanic events in the late Eocene in areas well away from the current trend of the hotspot track to an approximately 40-Ma period of quiescence and a sudden large event at 17 Ma?

We also suggest that given our understanding of plate motions and rates during this period, it is difficult to reconcile a Yellowstone hotspot off the coast of the Oregon-Washington border considering its present location under the Yellowstone Plateau and its track over the past 16 m.y., which points towards Sacramento and the Great Valley of California.

Johnston and others (1996) proposed a late Cretaceous location of the Yellowstone hotspot in the Yukon (Figure 4). This idea depends on the 50-Ma location now on the Washington-Oregon coast and has the same problems as discussed above.

In conclusion, we concur with Draper (1991) that no connection exists between the 0- to 17-Ma Yellowstone hotspot and the various models for an inferred Yellowstone hotspot 50-60 Ma off the coast of Oregon and Washington (Duncan, 1982; Pyle and others, 1997). Furthermore, the westward displacement of the Yellowstone plume head by the inclined Vancouver slab, as predicted from plate tectonic and plume histories, seems physically plausible and explains the problem of an apparent increase in plate motion (plus extension) by more than 250 percent (from 7 cm/year between 10 and 16 Ma to 2.9 cm/year after 10 Ma).

One possible test of the interrelation of the Yellowstone plume head with the Vancouver slab might be to look for the effects of the slab and associated subducted sediments in the chemistry of the Washington and Oregon basalts. Takahahshi and others (1998) suggest that the Grande Ronde units of the Columbia River flood basalt result from the melting of a plume head that contained fragments of recycled, old, oceanic crust. The arclike geochemical signature of these basalts (high Ba/La ratios; Hooper and Hawkesworth, 1993) leads Hooper (1997) and Shervais and others (1997) to suggest the entrainment of a subduction component into the plume head that is consistent with our proposed interaction with the Vancouver slab.

THE YELLOWSTONE STARTING PLUME: TRANSECT ALONG THE NEVADA-OREGON RIFT ZONE

The apparent asymmetry associated with the Yellowstone starting plume at 14-17 Ma can be explained by changes in the thickness and composition of the lithosphere along a north-south axis parallel to the Nevada-Oregon rift zone (Figures 1 and 5). We place the initial plume head center at the McDermitt caldera complex along the Nevada-Oregon border (Figure 1). The Columbia River-Oregon Plateau flood basalts extend for hundreds of kilometers to the north of, and give a lop-sided

appearance to, the track of the Yellowstone hotspot, although we emphasize that this plume-head center is at about the midpoint of the Nevada-Oregon rift zone. Nonetheless, the location of these flood basalts with respect to the inferred initial location of the starting plume requires explanation. Geist and Richards (1993) explained this northward location of the Columbia River flood basalts by a northward diversion of the plume head by the northward-moving Vancouver slab.

We suggest that a south-to-north change from an older cratonic crust with a thicker lithospheric mantle to a younger, more oceanic crust with a thinner lithospheric mantle (Figure 5) controlled the surface eruption of flood basalts from the plume (Zoback and Thompson, 1978; Pierce and Morgan, 1992; Zoback and others, 1994; Parsons and others, 1994; Takahahshi and others, 1998). As noted by Hooper (1997), nearly all of the Columbia River basalts erupted through fissures in thinner lithosphere made up of accreted oceanic crustal material. The earliest eruptions occurred along a north-south suture on the west side of the Precambrian crust and perpendicular to the minimum principal stress of the regional mid-Miocene state of stress (Zoback and others, 1994) and parallel to a Miocene back-arc spreading system (Zoback and others, 1981; Parsons, 1995). This denser, more mafic crust would facilitate basaltic melts rising to the surface and being erupted because (1) the denser crust increases the lithostatic pressure per crustal unit depth on the magma chamber and (2) the mafic material is more refractory and thus less likely to melt. That the plume head uplift resulted in north-south rifting rather than the classic tensional rifts at 120 degree angles appears to relate to this east-west orientation of the minimum principal stress.

The extent of flood basalt now appears to include northern California and the Lovejoy Formation dated about 16 Ma (Wagner and Saucedo, 1990; Page and others, 1995; Wagner and others, 2000). Wagner (oral commun., 1999) estimates the volume of this basalt to be near 75,000 cubic km, including much basalt beneath the northern Sacramento Valley.

The northern Nevada rift zone was intruded by 14- to 17-Ma mafic magmas (Zoback and Thompson, 1978; Zoback and others, 1994). This extension zone continues northward to the feeder dikes of the Oregon Plateau and Columbia River flood basalts and southward along the extension of the northern Nevada rift into southern Nevada (Blakely and Jachens, 1991) and may include the 14- to 17-Ma rhyolites of southern Nevada. All together, these extensional features form the 1,100-km-long, 17-Ma Nevada-Oregon rift zone and center on the inferred initial sublithospheric position of the Yellowstone plume head (Pierce and Morgan, 1992). Although feeder dikes for the Columbia River flood basalts are as much as 500 km north of this inferred center, White and McKenzie (1989) note that if mantle plumes coincide with active rifts, large-volume basalt eruptions can extend along rifts for 2,000 km (half distance = 1,000 km). Although some plume heads are associated with radial dikes extending thousands of kilometers (Thompson, 1998), the linear N. 20º-25º W. Nevada-Oregon rift zone indicates that at 17 Ma from eastern Washington to southern Nevada, the least principal stress was horizontal and oriented N. 65º-70º E. (Zoback and Thompson, 1978; Christiansen and McKee, 1978; Zoback and others, 1994).

Figure 5 shows modern geologic and geophysical characteristics along a north-south cross section parallel to the 14- to 17-Ma Nevada-Oregon rift zone (A-A', Figure 1). West of the $^{87}Sr/^{86}Sr$ 0.704 line is young, mafic oceanic terrane in Oregon and Washington in the area of flood basalt extrusion. East of the $^{87}Sr/^{86}Sr$ 0.706 line is Precambrian, continental crust in southern Nevada. General differences along the north-south section are as follows, using McDermitt as the midpoint: Transect A shows basalts occurring in the farthest north segment; rhyolites, basalts, and tuffaceous sediments are exposed in the middle with trachybasalts exposed farther south; mafic intrusives with rhyolites occur in the southernmost segment. Transect B shows the terrane to the north as mostly Mesozoic and younger mafic oceanic and oceanic accreted terranes and the terrane to the south as increasing in age from a Paleozoic magmatic arc (Elison and others, 1990) to an interval along the Sr 0.706 line between a Paleozoic arc (to the west) and late Proterozoic sedimentary rocks (to the east; Link and others, 1993). Transect C shows that heat flow has a broad culmination over the inferred position of the plume head near the Nevada-Oregon border. Transect D shows terrain altitude changes from north to south: higher terrain in Canada descending to about 300 m on the Oregon-Washington border, then a bench above 1,500 m in southern Oregon and northern Nevada, to a culmination in central Nevada at about 2,400 m, and finally a decrease to about 300 m in southern Nevada. Transect E is the average of complete Bouguer gravity anomaly values based on stacking (averaging) of five parallel profiles centered on A-A' (Figure 1). The averaged profile shows prominent steps near the Washington-Oregon border and in southern Nevada separated by a major low (Saltus and Thompson, 1995).

Transect F is a two-dimensional model of the gravity profile. The southern boundary of anomalous asthenosphere on it is based on seismic, heat-flow, and isotopic constraints (Saltus and Thompson, 1995); the northern boundary of anomalous asthenosphere is based, by analogy, on the position of the complementary step in gravity

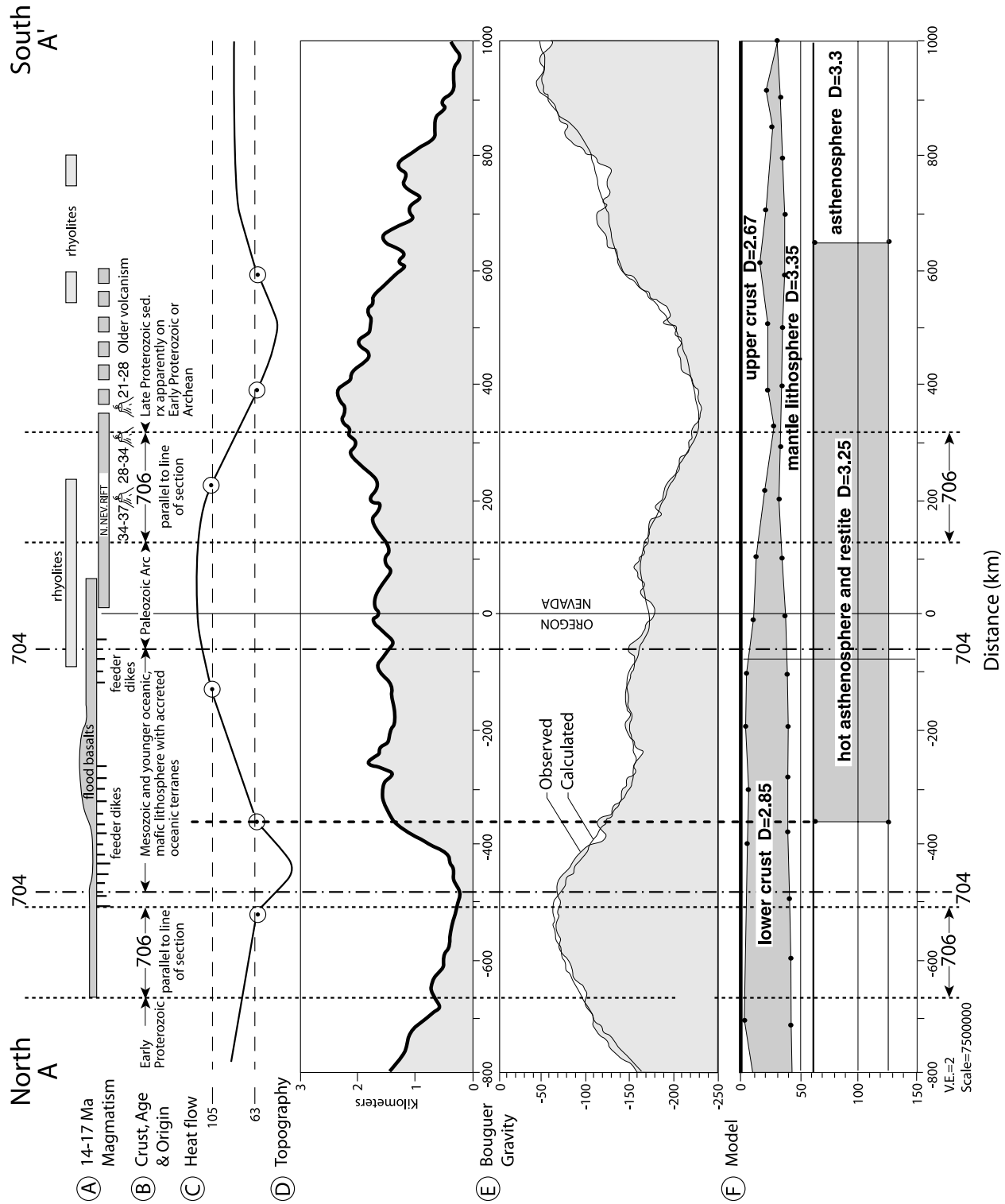
North
A
South
A'
704
706
rhyolites
flood basalts
feeder dikes
N.NEV.RIFT
Paleozoic Arc
Mesozoic and younger oceanic, mafic lithosphere with accreted oceanic terranes
Early Proterozoic
parallel to line of section
34-37
28-34
21-28
Older volcanism
Late Proterozoic sed. rx apparently on Early Proterozoic or Archean
A 14-17 Ma Magmatism
B Crust, Age & Origin
C Heat flow
105
63
D Topography
Kilometers
E Bouguer Gravity
OREGON
NEVADA
Observed
Calculated
F Model
upper crust D=2.67
mantle lithosphere D=3.35
asthenosphere D=3.3
lower crust D=2.85
hot asthenosphere and restite D=3.25
V.E.=2
Scale=7500000
Distance (km)

and topography near the Washington-Oregon border. For the Lake Lahontan basin, Adams and others (1999) conclude that upper mantle viscosity is 2-3 orders of magnitude less than in stable shield areas. The crust-mantle boundary in the model is an average of three different western U.S. Moho maps presented in Geological Society of America Memoir 172 (Mooney and Weaver, 1989; Pakiser, 1989; Braile and others, 1989). We have allowed the midcrustal interface between felsic upper crust and mafic lower crust to vary in order to fit the remaining anomalies. To aid understanding, we have used absolute densities, albeit these are somewhat arbitrary; the gravity model is only sensitive to lateral variations in relative density, not to the absolute values. The model indicates that the gravity data are consistent with the seismically determined average Moho, with our hypothesized anomalous hot or light asthenosphere (hot plume head and restite, both assumed to be 0.05 g/cubic cm lighter than regular asthenosphere, Figure 5), and with a crust which ranges from generally mafic (shown as lower crust) in the north to generally felsic (shown as upper crust) in the south.

Figure 6 illustrates schematically along a north-south axis how a spreading plume head 500-1,000 km across (Hill, 1972) might interact along the section A-A' with crustal changes reflected by the $^{87}Sr/^{86}Sr$ 0.704 and 0.706 lines (Figure 1). To the north of center is relatively thin, dense, accreted oceanic crustal lithosphere, whereas to the south of center is progressively older, more silicic, more continental crustal material (Kistler, 1983; Elison and others, 1990; Mooney and Braile, 1989; Camp, 1995; Link and others, 1993). The rising and spreading plume head (density of 3.25 g/cc) would undergo decompression melting above a depth of about 150 km, producing a basaltic melt (density 3.0 g/cc) and also leaving a restite (also density 3.0 g/cc). North of the McDermitt area, voluminous flood basalts erupted through the Chief Joseph dike swarm that is associated with the foliated and sheared suture zone between the Precambrian continental crust on the east and the oceanic lithosphere and intraoceanic island arc terranes on the west (Hooper, 1997; Camp, 1995; Snee and others; 1995; Vallier, 1995) also delineated by the $^{87}Sr/^{86}Sr$ 0.704 and 0.706 lines (Figure 1). As observed by Hooper (1997), a significant lithospheric signature is present in all but the earliest of the Columbia River basalts and, in fact, varies spatially through time. The Columbia River basalts can be divided into three basic subgroups of enriched subcontinental lithospheric mantle that were entrained into the plume head.

For the Mesozoic and younger oceanic accreted terrane north of the midpoint, plume-head material would flow towards higher areas or "thinspots" at the base of the lithosphere, thereby allowing for an increase in decompression melting and forming basaltic magmas (Thompson and Gibson, 1991; Sleep, 1990). According to Hooper (1997), the Columbia River basalts were mantle-generated magmas that had relatively long residence times in reservoirs at the base of the crust and that erupted periodically and rapidly through NNW-SSE-oriented fissures to form the voluminous flood basalts. Because crust in this area was relatively dense, thin, and weak and was adjacent to a major tectonic boundary of thicker, more competent continental lithosphere (Hooper, 1997), the basaltic magma would be readily able to rise to the surface where it formed flood basalts of the Columbia River and Oregon Plateau. As described by Camp (1995), basalt flows become younger to the north and reflect the northward spread of the plume head as it intersected the lithosphere and pancaked outward. In addition to the northward migration of

Figure 5. Geological and geophysical characteristics along section A-A' (see Figure 1). From McDermitt, this section goes south, parallel to the Nevada-Oregon rift zone and north parallel to the feeder dikes of the Columbia River and Oregon Plateau basalts. The strontium isotopic boundaries($^{87}Sr/^{86}Sr$) define crustal changes with Precambrian silicic continental crust inside (continentward) the 706 line and Mesozoic and younger mafic oceanic crust outside (oceanward) the 704 line ($^{87}Sr/^{86}Sr$ 0.704 and 0.706 shown here as 704 and 706).

A. 14- to 17-Ma magmatism near and along the Nevada-Oregon rift zone, which is about 1,100-km long (from Figure 1). The rhyolite overlaps both the southern part of the flood basalts and the mafic, rift-filling dikes of the northern Nevada rift. The 14- to 17-Ma rhyolites fade out roughly in the area where 21- to 37-Ma magmatism had already occurred, perhaps related to crustal depletion.

B. Crustal ages and origin. Strontium boundaries from Reed (1993, Plate 1, except where updated in Washington by Robert Fleck, written commun., 1998, and in southwest Idaho by Leeman and others, 1992). Precambrian areas from Link and others (1993, Figure 34 and p. 552-557). Northern Nevada from divisions by Elison and others (1990). Oregon after Draper (1991, p. 315), suggesting 2-4 km volcanic and volcaniclastic rock over 15-20 km of oceanic crustal material. Carlson and Hart (1987, Figure 8) show this area as new crust over depleted upper mantle.

C. Heat flow (in mWm^{-2}) from Morgan and Gosnold (1989).

D. Regional topography from averaging of five parallel profiles spaced 15 km apart and centered on section A-A'.

E. Regional complete Bouguer gravity anomaly from averaging of five parallel profiles spaced 15 km apart and centered on section A-A'. The data are from the Decade of North American Geology (DNAG) compilation for the conterminous United States (available on CD-ROM from National Geophysical Data Center, Boulder, Colorado; Hittelman and others, 1994). Thin line shows fit to model shown in F (below).

F. Gravity model of lithosphere and upper asthenosphere. Crust-mantle boundary taken from an average of several Moho maps (Mooney and Weaver, 1989; Pakiser, 1989; Braile and others, 1989). Southern boundary of "hot asthenosphere" taken from Saltus and Thompson (1995). Northern boundary of "hot asthenosphere" interpreted here to coincide with the gravity-topographic step centered at about 380 km on A-A'. The boundary between the upper (felsic) and lower (mafic) crust was allowed to vary between sea level and the Moho to match the Bouguer anomalies. This simple model shows that the gravity data are consistent with a crust that is largely mafic to the north and felsic to the south.

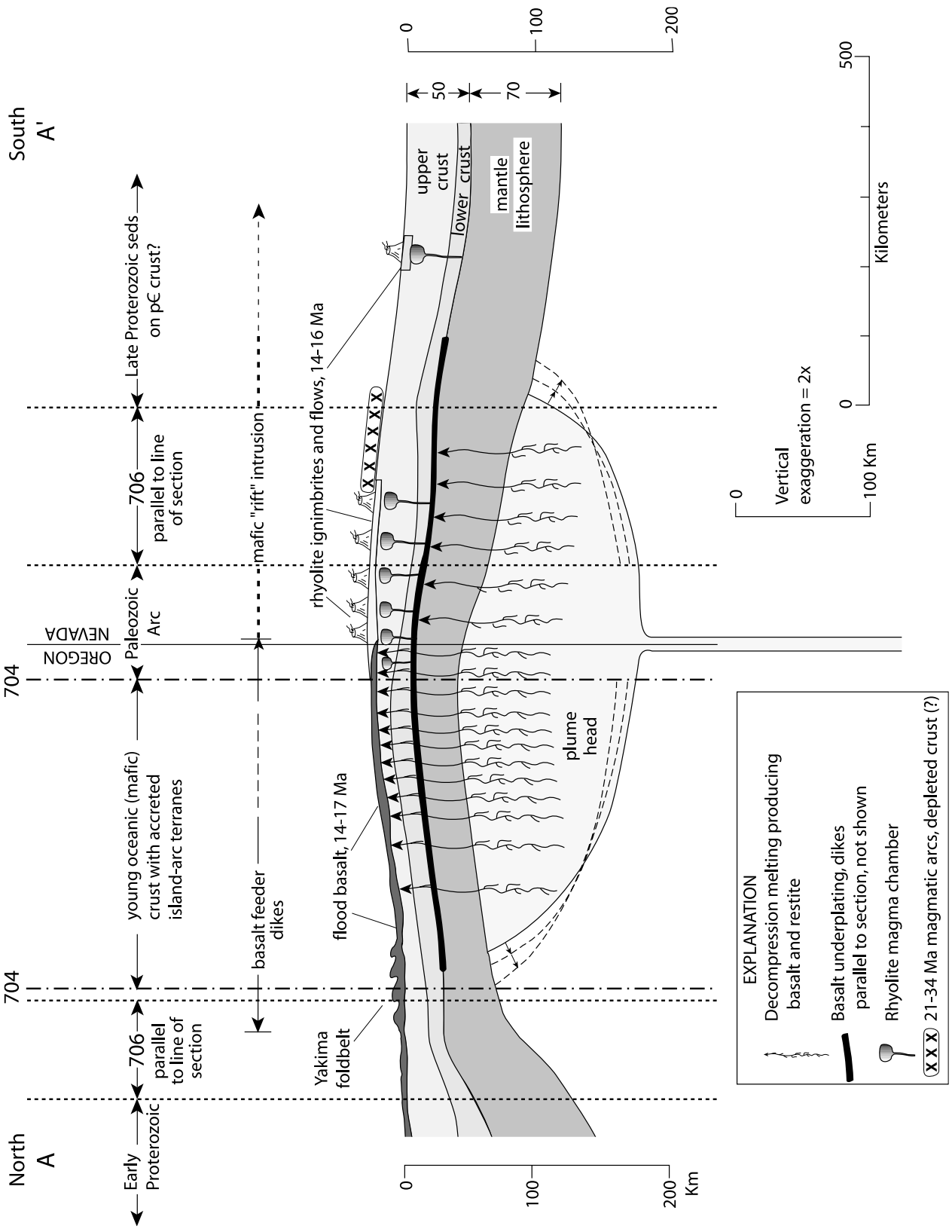
North
A
South
A'
Early Proterozoic
706
parallel to line of section
704
young oceanic (mafic) crust with accreted island-arc terranes
basalt feeder dikes
Yakima foldbelt
flood basalt, 14-17 Ma
OREGON
NEVADA
Paleozoic Arc
704
706
parallel to line of section
mafic "rift" intrusion
rhyolite ignimbrites and flows, 14-16 Ma
X X X X X
Late Proterozoic seds on pЄ crust?
upper crust
lower crust
mantle lithosphere
plume head
0
100
200
Km
50
70
0
100
200
500
Kilometers
0
Vertical exaggeration = 2x
0
100 Km
EXPLANATION
Decompression melting producing basalt and restite
Basalt underplating, dikes parallel to section, not shown
Rhyolite magma chamber
X X X 21-34 Ma magmatic arcs, depleted crust (?)

basalt flows, Camp (1995) also documents a northward progression of uplift during Columbia River basalt time. Between 14 and 17 Ma, northward-directed compression formed the east-west Yakima folds and associated thrusts (Hooper, 1990; Reidel and others, 1989), also consistent with plume-head uplift from the south.

Magmatism from near and to the south of the Nevada-Oregon border was different from the flood basalts farther north (Figure 1): (1) rhyolites and basalts erupted in the region of the northern Nevada rift, (2) trachybasalts erupted in the central area, (3) unexposed basaltic dikes, inferred by observed magnetic anomalies, and isolated rhyolitic volcanic fields are in the south (Zoback and others, 1994). We think the following processes occurred beneath this area: decompression melting generated hot basalt that rose into the silicic crust where, due to the higher melting temperature of basalt, heat from the basaltic melt produced silicic magmas that then rose higher in the crust to form high-level magma chambers from which erupted rhyolitic ignimbrites and lava flows.

Undoubtedly, the cross section along A-A' would have been somewhat different at 17 Ma. In particular, in northern and central Nevada, the lithosphere was probably thicker and has been subsequently thinned by basin and range extension. A significant amount of basaltic underplating, which we associate with the starting plume, has thickened the crust near the Moho in Nevada (Thompson and others, 1989). Crustal thickness may also have been thinner to the north before basaltic underplating associated with the 15-Ma and younger volcanism, and the mantle lithosphere was likely thin beneath this young oceanic terrane. The hot, spreading plume head may have thinned the mantle lithosphere by thermal and mechanical erosion. Because topographic changes also have transpired over the last 17 m.y., the area above the plume head would have been topographically higher when the plume head first intersected the North American plate at 17 Ma than it is today. As suggested by Parsons and others (1994), the 1-km-high present topography centered on McDermitt results from the residual effect of low-density Yellowstone plume material.

The plume head and associated Nevada-Oregon rift are spatially near the center of the active Basin and Range Province (Figure 4). We suggest a causal relationship exists between the inferred plume head and changes in the Basin and Range. Upon impact with the lithosphere, the plume head would decrease its ascension rate; this impact is associated in time and space with a change in Basin and Range extension and volcanism. While not advocates of a plume origin for this region, Christiansen and Yeats (1992) note, "The bimodal rhyolite-basalt magmatism of the Great Basin region is mostly younger than 17 Ma, following a widespread magmatic lull. By about 17 Ma, significant uplift had begun to be the dominant factor in the 1,600-km region that encompassed the Great Basin region, the Columbia Intermontane region, and surrounding areas." For the 14- to 10-Ma interval, they write (p. 388 and Plate 7): "Regional extension in the continental interior changed to widely distributed normal faulting between about 14 and 10 Ma with accelerated uplift of the region from the Sierra Nevada to the High Plains."

Furthermore, northward migration of the source of flood basalts is represented in the spreading of the plume head (Camp, 1995). The remarkable N. 20º-25º W. orientation of the 1,100-km Oregon-Nevada rift zone indicates the minimum principal stress over this great length at 17 Ma was about N. 65º-70º E. and subparallel to the west coast (Zoback and Thompson, 1978; Zoback and others, 1994).

Figure 6. Geologic cartoon along line of section A-A' showing emplacement of postulated Yellowstone plume head. The plume head spreads out (pancakes, mushrooms) upon rising into the lithosphere, but it can rise further beneath the thinner lithosphere (young thin mafic crust and lithospheric mantle) beneath Oregon. Decompression melting (squiggly vertical lines) produces basalt magma that rises upward and interacts differently with the crust: (A) in Oregon, magma rises through the dense, more oceanic crust and surfaces as the Columbia River and Oregon Plateau flood basalts, and (B) in Nevada and southern Oregon, basalt magma melts silicic lower crustal material that then rises into upper crust forming magma chambers (oval pods) and rhyolitic ignimbrite eruptions, shown as volcanoes, and (C) in northernmost Nevada and southern Oregon, both processes have operated. The restite from decompression melting remains in the mantle but is buoyant and contributes to long-lasting uplift (Morgan and others, 1995). At the time of emplacement, doming above the plume head may be 1-2 km (exaggerated in drawing). The northward gravitational push from this doming may have produced the Yakima fold belt near the northern end of the section.

SOUTHERN OREGON RHYOLITE BELT AND THE PLUME HEAD

Many have suggested that the southern Oregon rhyolite belt appears to contradict the plate-tectonic Yellowstone hotspot hypothesis in that it is a similar-aged volcanic progression that advances WNW across southern Oregon (MacLeod and others, 1976; Christiansen and Yeats, 1992, p. 381-382). The vector of this progression makes a 120-degree angle with the vector of the SRP-YP volcanic progression (Figure 1). Both emanate from the tri-state boundary area and have similar ages. Pierce and Morgan (1992, p. 32-33) note significant differences in the rhyolitic volcanism between the eastern SRP-YP trend and the southern Oregon trend that suggest different processes for the two progressions. Differences in the two

volcanic provinces include the time of inception (the southern Oregon belt began about 10 Ma and McDermitt erupted at 16.1 Ma), the style of volcanism (small rhyolitic domes and small-volume ignimbrites are typical in southern Oregon whereas large-volume ignimbrite eruptions are typical in the SRP-YP province), and the volcanic migration rates. The Brothers strike-slip fault zone forms the northern part of the southern Oregon rhyolite trend. It also separates basin and range and associated extension on the south from the High Lava Plains with much less extension on the north. The map pattern of the Brothers fault zone (Walker and others, 1981; Pezzopane and Weldon, 1993) is represented by short, small-offset, normal faults that are arranged in en echelon patterns oriented 10-20 degrees clockwise from the overall Brothers fault-zone trend. These extensional openings are associated with right lateral shear that may have provided conduits for volcanic eruptions. Draper (1991) suggests that both the spreading Yellowstone plume head and the activity on the Brothers fault zone started in northern Nevada-southern Oregon and migrated to the WNW. Volcanism followed this WNW migration of fault activity and plume spreading.

Possible mechanisms that might explain the northwesterly volcanic progression in southern Oregon include (1) counterflow associated with the WNW flow at the base of the lithosphere; (2) plume spreading (Sleep, 1997); and (3) the up-and-out-welling at the edge of a hot, thick body that might produce a WNW drag (Figure 7). A mechanism that might drag the western margin of the Yellowstone plume head further westward and produce the volcanic trend observed in southern Oregon is the counterflow or backflow occurring in the acute angle between the descending Vancouver slab and southwest-advancing North American plate (Draper, 1991). In addition to this counterflow, Eugene Humphreys (oral commun., 1997) and others suggest a thermal convective upwelling along the gradient of the edge of any hot mass in the mantle.

Draper (1991) notes that no younger basalts overlie the Columbia River basalts. He attributes this to a combination of (1) magma reservoir depletion exhausted by the eruption of the Columbia River and Steens Mountain basalts and (2) extension beginning at about 10 Ma that forced the plume head to spread out laterally at the base of the crust. This process resulted in abbreviated magma residence times and generated primitive high-alumina olivine tholeiitic magmas to the west of the Columbia River basalts. Draper (1991) suggests that as extension increased with time, smaller volumes of primitive magmas erupted. According to Draper (1991), the processes of extension combined with a laterally expanding plume head under a crust depleted in low melting-point components. The result produced decreasing volumes of rhyolitic material over time. The WNW progression of silicic activity in the southern Oregon belt (Figures 7 and 8) was concentrated along the edge of the westward-expanding plume head influenced by the sinking Vancouver slab.

In contrast to this minor rhyolitic activity in southern Oregon, large volumes of rhyolitic ignimbrites, tephra, and lavas erupted along the SRP during this comparable interval of time (Bonnichsen, 1982; Perkins and others, 1998; Morgan and others, 1997; Morgan and others, 1984; Morgan and McIntosh, written commun. 2000; Christiansen, 1984). The northeast progression of rhyolitic volcanism in the SRP-YP has been attributed to the North American plate directly overriding the chimney or tail phase of the thermal plume (Pierce and Morgan, 1992) that melted a continuous supply of undepleted crustal material (Draper, 1991). In conclusion, we concur with Draper (1991) that the southern Oregon rhyolite belt may reflect NW migration of either faulting or spreading of the Yellowstone plume head and that this progression does not necessarily negate the SRP-YP as a hotspot track of a thermal mantle plume.

PLUME-HEAD UPLIFT AND ASSOCIATED CLIMATE PATTERNS

Plume heads are expected to cause uplift of 1 km or more and have diameters as much as 1,500 to 2,500 km (Hill and others, 1992). We estimate the Yellowstone plume head was originally a 400-km-diameter sphere. A considerable size is suggested by the 15-17-Ma volcanic activity along the 1,100-km length of the Nevada-Oregon rift zone. Parsons and others (1994; and Tom Parsons, written commun., 1998) consider a minimum 800-km diameter for the flattened plume head based on the current mass deficit in the upper mantle that extended over much of Nevada and parts of Utah and Oregon. Given the elongate pattern of tectonic and volcanic activity aligned subparallel to the Precambrian margin of the North American plate (Camp, 1995) as well as parallel to the back-arc margin inland from the Pacific Ocean (Zoback and others, 1981; Parsons, 1995), we favor (Figure 9) an elongate north-south spreading plume head similar to that proposed by Camp (1995).

Within the Columbia River basalts (Figure 9 and Table 1), northward offlap of basalt units with time is shown by Camp (1995, Figure 4) to reflect south-to-north migration of uplift, with local uplift rates of about 2/3 mm/year. This parallels the northward migration of Columbia River basalt source areas (Camp, 1995).

Estimates of past altitudes are difficult to reconstruct, but a modern leaf-morphology technique based on paleoenthalpy differences between sea level and inland localities has promising results (Figure 9 and Table 1). From detailed analysis of leaf physiognomy, Wolfe and others (1997) suggest that at about 15-16 Ma the surface of west central-Nevada was more than 1 km higher than now. We have reservations about this technique, in part because its results conflict with numerous studies that we find of merit for late Cenozoic uplift in the Colorado Rocky Mountains. But we do find this result for Nevada surprisingly compatible with our altitude estimate, general location, and age for plume-head uplift. Further east, an Eocene fossil-leaf flora is compatible with eastward migration of Yellowstone hotspot uplift: just south of the present location of the Yellowstone hotspot is a 50-Ma locality that is estimated to have been elevated 0.9 km to its present altitude sometime in the last 50 Ma and therefore after the Laramide orogeny (Figure 9; Wolfe and

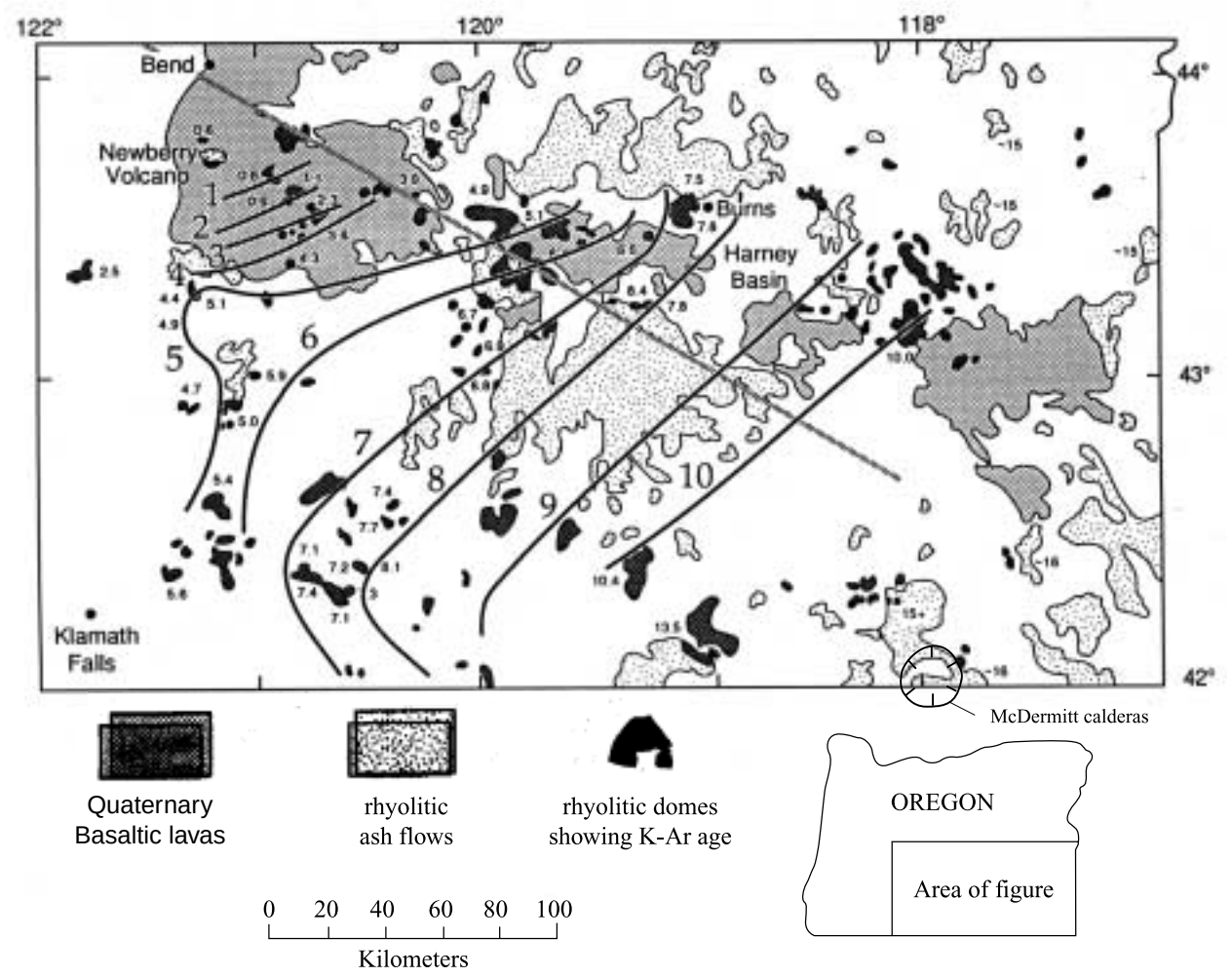

Figure 7. Age progression of silicic lava domes of the southern Oregon rhyolite belt. This figure shows upper Miocene and younger volcanic rocks and is copied from Christiansen and Yeats (1992, Figure 55). The rhyolite domes and their ages were shown by MacLeod and others (1976) to have such a systematic northwest decrease in age that ages could be contoured in 1-million-year increments. This northwest age progression is a key argument against a plume origin for the Yellowstone hotspot (Lipman, 1992; Christiansen and Yeats, 1992). See Figure 9 for our suggestions about how the southern Oregon rhyolite belt might be reconciled with a thermal plume origin of the Yellowstone hotspot. Both the southern Oregon rhyolite belt and the Yellowstone hotspot track start in the region near McDermitt, but they become younger in nearly opposite directions at the same time. The silicic domes (dark) form two belts that trend N. 75º W. The northern belt ends at Newberry caldera and parallels the Brothers fault zone (gray line) which is actually a complex en echelon pattern of normal faults whose trend of about 10 degrees clockwise to the overall pattern (Walker and Nolf, 1981) suggests a right lateral component (Pezzopane and Weldon, 1993). Between 10 and 17 Ma, ignimbrites and other silicic volcanism are widespread in the southern Oregon, northern Nevada and southwestern Oregon area (Figure 1; Pierce and Morgan, 1992;) but have no systematic progression with age in southeast Oregon (MacLeod and others, 1976, p. 470).

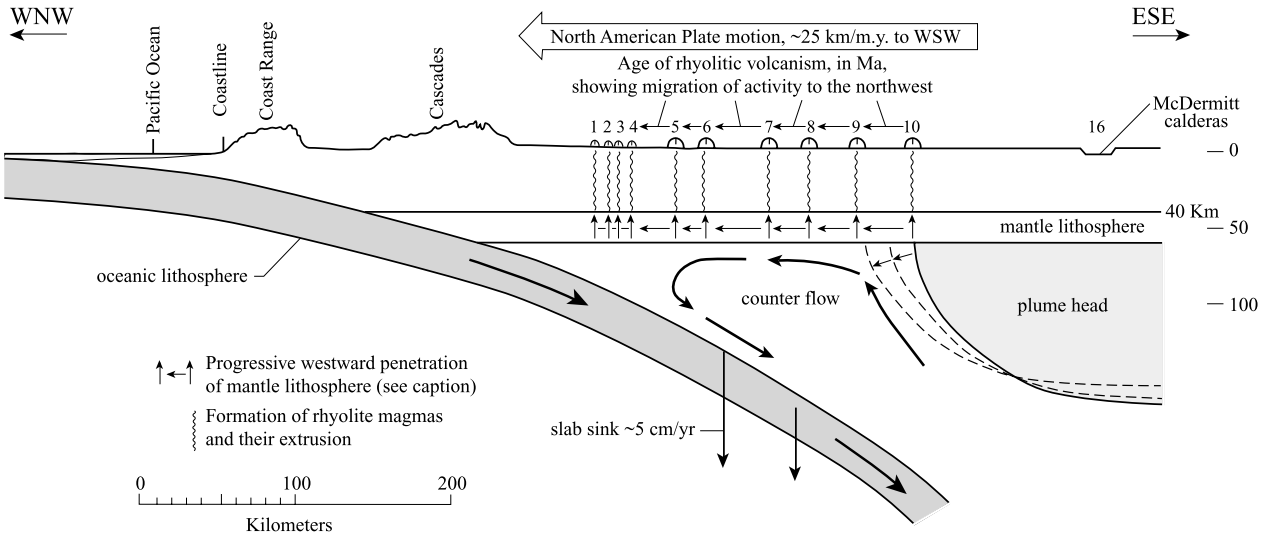

Figure 8. Geologic sketch (after Draper, 1991) along the southern Oregon rhyolite belt parallel to the trend of the Brothers fault zone. The mounds numbered 10 to 1 represent contours on the age of rhyolitic volcanism in Ma (MacLeod and others, 1976). Following Draper (1991), we suggest several factors may have acted separately or in combination to produce the penetration of mantle lithosphere by basaltic melts to form rhyolite magma from crust: (1) the cracking of mantle lithosphere by westward-migrating activity on the Brothers fault zone, (2) the westward-spreading plume head, and (3) the thermal erosion of mantle lithosphere associated with counterflow. The fracturing of the lithosphere along the Brothers fault zone (MacLeod and others, 1976; Carlson and Hart, 1987; Pezzopane and Weldon, 1993) appears to have provided the conduits for volcanism as well as its overall northwest trend. The most reasonable mechanism for the northwest progression of rhyolitic volcanism may be a northwest progression of faulting to form the Brothers fault zone. Such a northwest progression of faulting might have been accompanied by a northwestward migration of plume-head material aided by both the general outward migration of the plume head and the counter flow between the Vancouver slab and North American plate (Draper, 1991). If the two proceeded together, the faulting may have caused fracturing of the mantle lithosphere, permitting the erosion and stoping from below of the mantle lithosphere (a mechanism suggested by George Thompson, oral commun., 1998) and thus forming an inverted channel enhancing both outward (northwestward) plume-head flow and decompression melting by thinning of the lithosphere. Although Draper (1991) drew a similar diagram, we include this version because many have argued that this northwestward volcanic progression negates the Yellowstone hotspot as a mantle plume, and we think these factors offer a mantle-plume compatible explanation. The geometry of the subducting slab is based on a fairly well-controlled section by Parsons and others (1998) near the Oregon-Washington border.

others, 1998). This is compatible with uplift associated with the hotspot as it migrated 650 km from the plume-head area at 16 Ma to its current position at Yellowstone at 2 Ma.

Our hypothesized uplift of 1 km over a north-south distance of 1,000 km (Figure 9) should have a significant effect on local weather patterns. The expected effect would be increased precipitation on the west side from the orographic moisture extraction of rising airmasses coming inland (eastward) from the Pacific Ocean and then orographic drying and aridity east of the crest as these airmasses descend the lee side of the uplift. A precipitation shadow would extend further inland (east) as long as the main moisture source was from the Pacific. This pattern is analogous to the present Sierra Nevada with a wet west side, a dry east side, and a precipitation shadow extending far eastward across the Great Basin.

The geologic history of the Tertiary Bozeman Group in the Montana-Idaho area suggests the climate became more arid about 15 Ma at the time the plume-head uplift would have culminated (Table 1 and Figure 9, locations 9 and 10; Thompson and others, 1982; Fields and others, 1985). In the Yellowstone Valley north of Yellowstone Park, 15-Ma saline lake deposits with gypsum and anhydrite formed because of aridity. Furthermore, associated rodent fossils at nearby localities suggest aridity was more severe than at 20 Ma (Table 1, location 11; Barnosky and Labar, 1989).

Figure 9. Uplift and climatic patterns that may relate to Yellowstone plume (both head and tail). The dashed line shows the pancaked plume with an original spherical diameter as suggested by Parsons and others (1994) of about 400 km but elongated north-south as suggested by Camp (1995) parallel to the Nevada-Oregon rift zone. Table 1 describes the various localities, areas, and transects shown here. One of the main climatic parameters listed is orographic dryness (light shading) in the lee of the inferred Yellowstone plume-head uplift. In general, observations of uplift and climate are compatible with uplift above the plume head followed by uplift migrating to the east associated with the plume tail (chimney) to the "Yellowstone crescent of high terrain" associated with the present plume tail (Pierce and Morgan, 1992) or a similar 650-m-high altitude anomaly that Smith and Braille (1993) associated with the current Yellowstone hotspot.

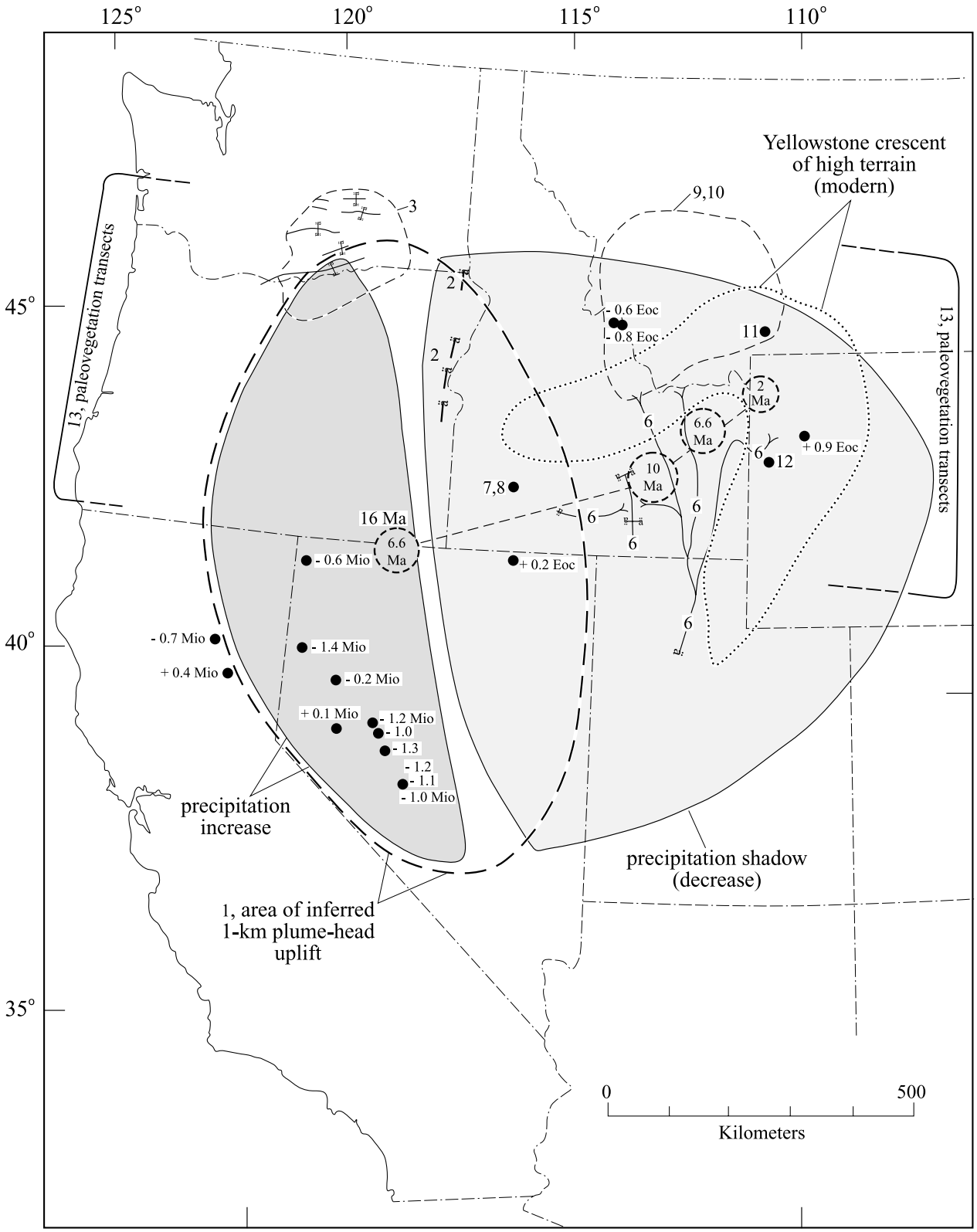
125°
120°
115°
110°
45°
40°
35°
Yellowstone crescent of high terrain (modern)
13, paleovegetation transects
13, paleovegetation transects
9,10
3
2
2
- 0.6 Eoc
- 0.8 Eoc
11
2 Ma
6
6.6 Ma
+ 0.9 Eoc
6
12
10 Ma
7,8
6
6
6
6
16 Ma
6.6 Ma
- 0.6 Mio
+ 0.2 Eoc
- 0.7 Mio
+ 0.4 Mio
- 1.4 Mio
- 0.2 Mio
+ 0.1 Mio
- 1.2 Mio
- 1.0
- 1.3
- 1.2
- 1.1
- 1.0 Mio
precipitation increase
precipitation shadow (decrease)
1, area of inferred 1-km plume-head uplift
0
500
Kilometers

Table 1. A sampling of possible indicators of uplift, altitude, and precipitation shadow that may be related to Yellowstone hotspot plume uplift.

Location	Age	Unit	Comments	References
1	~15? Ma	Low density anomaly in the mantle	Large, low-density anomaly in the mantle interpreted to be Yellowstone plume head. Diameter about 800 km and associated with active basin and range.	Parsons and others, 1994
2	17.5-14 Ma	Columbia River basalt	Offlap and thickness of subsequent CRB units indicate south to north uplift, locally at a rate of 0.67 mm/year	Camp, 1995
3	17-14 Ma and continuing	Yakima fold belt	The Yakima fold belt on the northern margin of the CRB was formed by south to north compression. CRB flows were being deformed shortly after their emplacement. We here suggest that the age and pattern of deformation are consistent with Yellowstone plume head uplift and north-directed gravitational forces on the north flank of the uplift (perhaps others have already suggested this).	See Reidel and others (1989) for age and geometry of structure.
4 = "Mio"	~14-16 Ma	Middle Miocene leaves	Paleobotanical analysis using leaf physiognomy of middle Miocene assemblages indicates subsequent subsidence (-) or uplift of stated amount in km. "When the standard error is applied to two coeval sites, the combination of the two errors produces a standard error in the estimated difference in altitude of ~760 m."	Wolfe and others, 1997
5 = "Eoc"	~40-50 Ma	Eocene leaves	Paleobotanical analysis using leaf physiognomy of Eocene assemblages indicates subsequent subsidence (-) or uplift of stated amount in km.	Wolf and others, 1998
6	9?-5? Ma	Late Miocene	Drainage divide on present Snake River Plain 75 km east of Twin Falls with drainage west of this divide down present Snake River Plain and out towards California, and east of this divide drainage from Jackson Hole and north of SRP southward into present Bonneville Basin. This suggests an ancestral high (hotspot?) east of Twin Falls in the late Miocene.	Taylor and Bright, 1987
7	5-9.5 Ma	Chalk Hills Fm.	Fish ecology and oxygen-isotope analysis on fish otolith suggest warm, moist climate with milder winters (16° C warmer than present) and cool summers (1° C cooler than present). Oxygen isotope (SMOW) calculated for water -15.5 per mil and annual cycle in fish from -16.6 to -13.5 per mil.	Smith and Patterson, 1994
8	5-9.5 Ma	Chalk Hills Fm.	Water in glass spheres has δ D value of -147 per mil, whereas present-day meteoric water at site has value of -125 per mil. This value is as high as that for drainages in the highest country at the upper end of the hotspot track in the mountains surrounding Yellowstone (Irving Friedman, written commun., 1998), suggesting the possibility that this area was much higher at the time of deposition.	Friedman and others, 1993
9	16 Ma	Bozeman Group	Change from a wetter to a more arid climate at about 16 Ma may reflect inception of precipitation shadow from plume head.	Fields and others, 1985

Table 1. Continued.

Location	Age	Unit	Comments			References
10	~15 Ma	Six Mile-Renova unconformity	Climate change from wet to dry ~15 Ma (and dry to wet ~ 20 Ma).			Thompson and others, 1982
11	15 Ma	Hepburn Mesa Fm. Barstovian	Saline lake deposit with gypsum and halite indicates aridity and drier than present. Rodent type suggests even more arid than semiarid Arikareean. May be in precipitation shadow of plume uplift to west.			Barnosky and Labar, 1989
12	~8-6? Ma	Camp Davis Fm.	Lake sediments rich in carbonate suggest dryness. Oxygen isotopes (-5.4 to 8.7 per mil, SMOW) "are the lightest yet reported for a nonmarine carbonate." Lake water estimated to be -20.7 to -34.8 per mil. SMOW and modern precipitation to be -16.5 per mil, SMOW (-30 per mil oxygen SMOW converts to -160 per mil Deuterium). Either much higher than present or in major precipitation shadow (of plume uplift?) or a combination of the above. The similarity in age to the Chalk Hills Formation but the much lighter isotopes suggests this site may have been in a precipitation shadow related to uplift associated with the plume tail.			Drummond and others, 1993
13	Transect from Pacific Coast inland to Rocky Mountains					
			East. Washington & Oregon	Idaho	Rocky Mountains	
13a	12-17 Ma	Barstovian/Late Hemingfordian	Deciduous hardwood forest and Taxodium swamp.	Deciduous hardwood forest and Taxodium swamp.	Montane conifer forest with steppe openings. Precipitation shadow?	Leopold and Denton 1987, Table 7
13b similar to 4	8-12 Ma	Clarendonian	Clarendonian Montane conifer and deciduous forest, Taxodium swamp.	Montane conifer and deciduous forest.	Montane conifer forest with steppe openings. Precipitation shadow?	Leopold and Denton 1987, Table 7

Paleobotanical transects from eastern Washington and Oregon to the Rocky Mountains (Figure 9 and Table 1, locality 13; Leopold and Denton, 1987,) show clear drying inland but no compelling evidence for plume-head uplift. Between 12-17 Ma, vegetation reconstructions show deciduous hardwood forest and *Taxodium* swamps in eastern Oregon and Washington and northern Idaho, and montane conifer forest with steppe openings in central Wyoming and Colorado. Between 8-12 Ma, reconstructions show conifer forest and deciduous forests in eastern Oregon and Washington, montane in southern Idaho, and montane conifer forests with steppe openings in northwest Wyoming. The Rocky Mountain localities are permissible of a precipitation shadow in the lee of plume-head uplift to the west.

The following history of vegetation in the SRP area is compatible with the decrease in altitude (Leopold and Wright, 1985) that may have followed plume-head and tail-related uplift: (1) Miocene—deciduous and conifer forest; (2) Pliocene—conifer forest with some open grassland and increasing numbers of grazing horses; and (3) Pleistocene—steppe vegetation and alkaline lakes.

In Jackson Hole, 7.5- to 10.3-Ma lacustrine beds (Love and others, 1997) have carbonate that Drummond and others (1993) concluded had the lightest $^{18}O/^{16}O$ ratio yet recorded for nonmarine carbonate sequences (Figure 9 and Table 1, locality 12). In the similar-aged 7-Ma Chalk Hills Formation in the western SRP (Figure 9 and Table 1, locality 8), deuterium in glass spheres is 22 per mil lighter than modern water (Friedman and others, 1993), which may suggest that the western SRP was higher at 7 Ma. Also from the Chalk Hills Formation, oxygen iso-

tope studies of fish otoliths range from -16.6 to -13.5 per mil in water calculated to have been -15.5 per mil. These data also suggest the water source for the 7-Ma Chalk Hills Formation was at a higher than present elevation. Uplift associated with the inferred 7-Ma plume position near Pocatello (Pierce and Morgan, 1992) may have resulted both in higher terrain in the Chalk Hills area of the western SRP and orographically drier climates east of this highland resulting in very light oxygen isotopes in the Jackson Hole area. Amundson and others (1996) summarize for the western United States some available information on oxygen isotope distribution.

Using the regional distribution and paleobiogeography of mollusks, Taylor and Bright (1987, Figure 5) locate a late Miocene (5?–9? Ma) drainage divide near American Falls (about 75 km east of Twin Falls) with drainage east of this divide going south into the present Bonneville Basin (Figure 9 and Table 1, locality 6). Wood and Clemens (this volume) also invoke a northeast shifting drainage divide to explain an increase in drainage basin size associated with a rise of Lake Idaho from a low about 6-7 Ma to a high near 5.5 Ma (their Figure 7).

GENERAL CLIMATE HISTORY

The marine record of climate change shows overall cooling throughout the Cenozoic, which in finer detail includes some steps, plateaus, and peaks (Figure 10). Coffin and Eldholm (1994, and references therein) show the correlation between the Columbia Plateau "large igneous province" and the 14-17 Ma Miocene warm interval, which was followed by cooling. The 14- to 17-Ma climatic optimum is recognized in deep-sea sites (Figure 10 shows the compilation by Barron and Keller, 1982, Figure 1, and site 747 on Kerguelen Plateau by Wright and Miller, 1992). A major global warming at 18-15 Ma also is recognized on land by "dramatic northward movement of temperate deciduous forests north of the Arctic Circle in Alaska and northern Canada" (Thomas Ager, written commun., 1996). Hodell and Woodruff (1994) attribute this middle Miocene climatic optimum to the warming effect of carbon dioxide and other material associated with extrusion of the Columbia River flood basalts. Significant carbon dioxide emissions probably accompany flood basalt and other volcanic activity (Arthur and others, 1985; McClean, 1985; Leavitt, 1982; Rampino, 1991).

Self and others (1997) estimate that the volatile release from the Rosa unit of the Columbia River basalt introduced significant amounts of S, Cl, and Fl into the upper troposphere and possibly the lower stratosphere, thus significantly affecting the global atmosphere. Eruptions of this type, composition, and magnitude sustained over periods of decades, would have "strong, detrimental effects on global climate" (Self and others, 1997). After 14 Ma, most of the total volume of the Columbia River basalt had been erupted (Baksi, 1989) and emissions of carbon dioxide associated with plume-head volcanism decreased, compatible with the cooling of climate by 14 Ma.

Although uplifts affect climate patterns, Raymo and others (1988) and Raymo and Ruddiman (1992) postulate the largest effect on climate associated with the uplift of the Himalayan-Tibet areas was through the reduction in carbon dioxide during enhanced silicate weathering of fresh material kept exposed by accelerated erosion on tectonically steepened terrain. Carbon-dioxide changes related to plume-head volcanism and uplift are consistent with the climate history in the 17- to 10-Ma time interval shown in Figure 10 as follows: (1) carbon dioxide buildup in atmosphere associated with 15- to 17-Ma Oregon Plateau and Columbia River flood basalts and (2) carbon-dioxide reduction associated with silicate weathering due to erosion and dissection of plume-head uplift starting about 15 Ma.

DISCUSSION OF PLUME-HEAD UPLIFT AND CLIMATE

Studies by Ruddiman, Kutzbach, and colleagues suggest that late Cenozoic plateau uplift could have forced changes that led to the "late Cenozoic climatic deterioration" that culminated in the Pliocene-Pleistocene ice ages (Ruddiman and Kutzbach, 1989; Kutzbach and others, 1989; Ruddiman and others, 1989). They suggest plateau uplift in southern Asia and the American West, including the Sierra Nevada, Colorado Plateau, Basin and Range, Rocky Mountains, and High Plains (Ruddiman and others, 1989). However, Molnar and England (1990a, 1990b) strongly question the late Cenozoic uplift of the American West. Much new paleobotanical analysis using the methods of Wolfe (1993) or similar methods has also cast doubt on general uplift in the western U.S. and particularly that of the Rocky Mountains (Gregory and Chase, 1992) and the Colorado Plateau. Also, House and others (1998) conclude the Sierra Nevada has been high since the Cretaceous on the basis of thermal history and apatite (U-Th)/He ages. In addition, Molnar and England (1990a) examine the geophysical basis of uplift and question evidence suggesting true uplift as distinct from isostatic uplift associated with erosion.

The mechanism of uplift associated with a plume head or tail does provide a driving process below the lithosphere to explain epeirogenic-type uplift. We suggest that

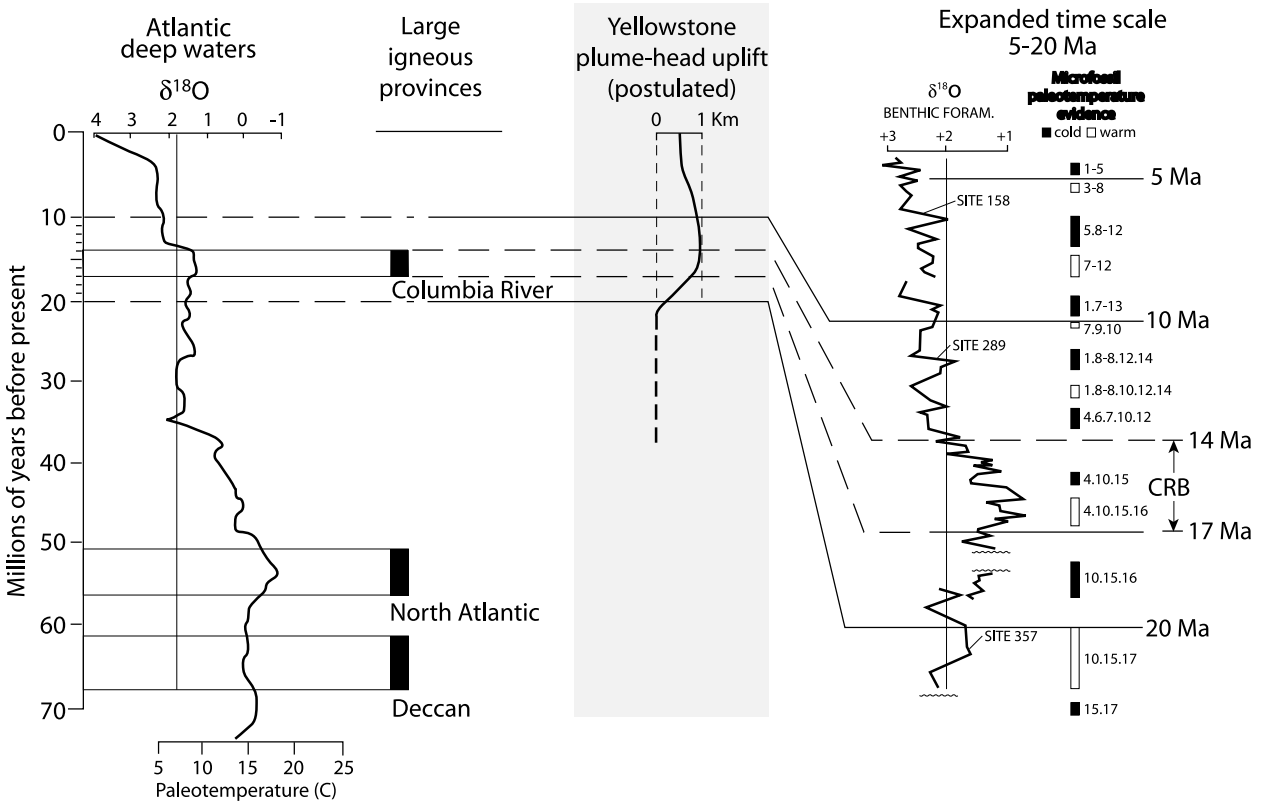

Figure 10. Temporal relations among Cenozoic climate proxies, "large igneous provinces" (flood basalts), and postulated Yellowstone plume-head uplift. Atlantic deep waters (after Miller and others, 1987, as shown in Barron and Baldauf, 1989). The 14- to 17-Ma middle Miocene "climatic optimum" (expanded plot, right side from Barron and Keller, 1982) has been associated with the Columbia River-Oregon Plateau flood basalts (CRB, for example, Hodell and Woodruff, 1994). After the Miocene "climatic optimum," cooling continued eventually to the Pliocene-Pleistocene ice ages. Uplift associated with the Yellowstone plume head is a candidate for a "plateau uplift" whose plume-head mechanism could produce significant late Cenozoic uplift (Figure 9). Global climatic modeling by Kutzbach and others (1989) and Ruddiman and others (1997) shows that "plateau uplifts" could produce late Cenozoic climatic cooling in the Northern Hemisphere that might lead to the Pliocene-Pleistocene ice ages. Late Cenozoic Yellowstone plume uplift (head and tail) could also diminish atmospheric CO_2 leading to cooling, by the mechanism of Raymo and Ruddiman (1992) and Ruddiman and others (1997). Plume-head uplift does not have the geophysical problem of a plausible mechanism of how the isostatic balance of the lithosphere could rapidly change that Molnar and England (1990a, 1990b) used to challenge the validity of late Cenozoic "plateau uplifts."

broad plume-head uplift (see Figure 9) was substantial by about 17 Ma and was followed by gradual subsidence in the head area. For the Lahontan basin in the west-central Basin and Range, viscosity estimates for upper mantle are 2-3 orders of magnitude less than in stable cratonic areas (Adams and others, 1999), an observation consistent with the hypothesis of a residual but still hot plume head. The uplift migrated northeastward to the present Yellowstone crescent of high terrain (Figure 9) that is associated with the current plume tail (Pierce and Morgan, 1992). The geoid anomaly that now centers on the Yellowstone Plateau (Pierce and Morgan, 1992; Pierce and others, 1992; Smith and Braille, 1993, Figure 7) and, more importantly, the larger plume-head uplift might provide a late Cenozoic broad uplift that could affect climate patterns in the ways modeled by Kutzbach and others (1989). Evidence (Table 1) for uplift, migrating drainage divides, and an orographic precipitation shadow suggests uplift associated with the plume head and ensuing tail may have occurred. A much more complete analysis of existing and new evidence is needed to evaluate plume-head uplift and possible relations to climatic patterns, but we hope this brief outline suggests avenues for future research.

CONCLUSIONS

We were led to the hypothesis of a 17-Ma Yellowstone plume head by tracing the Yellowstone hotspot track back to the area of the McDermitt volcanic field on the Nevada-Oregon border. We think the Yellowstone hotspot

track is best explained by a mantle plume particularly because of the following evidence (Pierce and Morgan, 1992): (1) the volcanism that progressed from 10 Ma to 2 Ma is coincident with both the rate and orientation predicted by plate motion; (2) the belts of faulting and uplift are oriented about this volcanic progression like the bow wave of a boat with uplift occurring in advance (northeast) of volcanism; (3) a large geoid anomaly centers on Yellowstone; (4) $^{3}He/^{4}He$ ratios near 16 suggest a deep mantle source, and most important (5) the scale of associated faulting and uplift is more than 400 km across suggesting a deep, sublithospheric process.

Upon backtracking the hotspot to its start near McDermitt, we find that a plume head (a sphere about 400 km in diameter) explains the following observations (Figure 1): (1) the much wider dispersal of 14- to 16-Ma rhyolitic volcanism than that after 10 Ma, (2) the association of the inferred plume head with the 14- to 17-Ma Columbia River and Oregon Plateau basalts, (3) the plume-head location near the midpoint of the 1,100-km-long, 16- to 17-Ma, Nevada-Oregon rift zone, and (4) no continuous manifestation of a hotspot before 17 ma.

If one accepts the Yellowstone plume-head hypothesis, the following three topics merit attention.

1. The westward displacement of the plume head upward along the inclined Vancouver slab (Figures 2 and 3). Plate tectonic reconstructions suggest the rising plume head rose upward into the Vancouver slab. We suggest its buoyant rise was deflected westward by the up-to-the-west inclination of the Vancouver slab. This could explain an unresolved problem with the hotspot track between the 10-Ma Picabo volcanic field and the 16-Ma McDermitt area that calls for a rate too high (70 km/m.y.) and a trend more easterly (about 20 degrees clockwise) than indicated by both the post-10-Ma progression of volcanism and faulting (about 29 ± 5 km/m.y. to the N. $54^{\circ} \pm 5^{\circ}$ E.) and the known rate and direction of North American plate motion (about 22 ± 8 km/m.y. to the S. $56^{\circ} \pm 17^{\circ}$ W.; Pierce and Morgan, 1992, p. 6).

2. The oblique transection of the craton margin by the plume head going from Mesozoic accreted oceanic lithosphere in the north to Precambrian craton in the south (Figures 5 and 6). Our best estimate is that the plume head contacted the lithosphere about 17 Ma near the Oregon-Nevada border beneath the McDermitt volcanic field. Reconstructions of crust and mantle lithosphere properties suggest a thinner, denser, oceanic lithosphere was present to the north in Oregon and Washington than was present in Nevada. This permitted the mantle plume head to migrate preferentially towards this "thinspot" and thus favor more decompression melting. The greater crustal density favored the eruption of the Columbia River and Oregon Plateau flood basalts. The 16- to 17-Ma Nevada-Oregon rift zone is defined by the N. 20° W. orientation of the following 16-17 Ma features: (1) the northern Nevada rift, (2) the extension of this rift into southern Nevada, and (3) the feeder dikes to the Columbia River and Oregon Plateau flood basalts. Although flood basalts are north of the inferred plume center, the plume is at the midpoint of this 16-Ma rift zone. The composition of erupted or intruded magmatic material can be explained by differences in crustal composition: (1) flood basalts are restricted to the oceanic, mafic crust and (2) rhyolites are restricted to more continental crust where the partial melt of mantle basalt melted silicic crustal material, which rose upward to form magma chambers that erupted to produce rhyolite flows and ignimbrites, leaving the heat-supplying basalt at depth.

3. Plume-head uplift and associated climatic patterns (Figures 8 and 9). A plume head is expected to produce significant uplift. On the basis of several observations, we prefer roughly 1 km of uplift over an oblong north-south ellipse of 1,100 km. Paleobotanical analysis of leaves suggest that at 15 Ma, central and northern Nevada was about 1 km higher than the present. A precipitation shadow is expected to occur east of this postulated uplift; evidence of marked aridity about 15 Ma is found near the common boundaries of Montana, Wyoming, and Idaho. About 7 Ma, uplift associated with eastward hotspot migration is predicted to migrate to the area of the central SRP; paleo-mollusk studies suggest a drainage divide in this area near American Falls, and other studies suggest aridity to the east of this uplift. The Yellowstone plume head may provide a mechanism for regional uplift that is geophysically plausible. Notably, the plume-head mechanism can cause geologically rapid uplift without requiring crustal thickening. Modeling studies suggest this kind of uplift could have contributed to late Cenozoic cooling that led to the ice ages (Kutzbach and others, 1989; Ruddiman and others, 1997).

A more thorough evaluation of the plume-head hypothesis and its implications regarding (1) westward offset up the inclined Vancouver slab, (2) lithospheric changes along the Nevada-Oregon rift zone, and (3) uplift and associated climatic changes all require much additional study.

ACKNOWLEDGMENTS

We have discussed these ideas with many colleagues during the last few years. We have particularly benefited from discussions with George Thompson, Tom Parsons, Mike Coffin, Norm Sleep, Robert Duncan, Eugene Humphreys, Vic Camp, Alan Wallace, Anita Grunder, Scott Lundstrom, Margaret Hiza, Silvio Pezzopane, and

Bob Thompson. We wish to thank Spence Wood, Tom Parsons, and Mike McCurry for technical review of an earlier version of this paper, and Roger Stewart for thorough and quite helpful editorial reviews.

REFERENCES

Adams, K.D., S.G. Wesnousky, and B.G. Bills, 1999, Isostatic rebound, active faulting, and potential geomorphic effects in the Lake Lahontan basin, Nevada and California: Geological Society of America Bulletin, v. 111, p. 1739-1756.

Amundson, Ronald, Oliver Chadwick, Carol Kendall, Yang Wang, and Michael DeNiro, 1996, Isotopic evidence for shifts in atmospheric circulation patterns during the late Quaternary in mid-North America: Geology, v. 24, p. 23-36.

Anders, M.H., 1994, Constraints on North American plate velocity from Yellowstone hotspot deformation field: Nature, v. 369, p. 53-55.

Anders, M.H., J.W. Geissman, L.A. Piety, and J.T. Sullivan, 1989, Parabolic distribution of circum-eastern Snake River Plain seismicity and latest Quaternary faulting: Migratory pattern and association with the Yellowstone hotspot: Journal of Geophysical Research, v. 94. no. B2, p. 1589-1621.

Anderson, D.L., 1998, The edges of the mantle, *in* Michael Gurnis, M.E. Wysession, Elise Kittle, and B.A. Buffett, eds., The Core-Mantle Boundary Region: American Geophysical Union, Geodynamics Series, v. 28, p. 255-271.

Arthur, M.A., W.E. Dean, and S.O. Schlanger, 1985, Variations in the global carbon cycle during the Cretaceous related to climate, volcanism, and changes in atmospheric CO_2, *in* E.T. Sundquist and W.H. Broecker, eds., The Carbon Cycle and Atmospheric CO_2: Natural Variations Archean to Present: American Geophysical Union Geophysical Monograph 32, p. 504-529.

Atwater, Tanya, 1989, Plate tectonic history of the northeast Pacific and western North America, *in* E.L. Winterer, D.M. Hussong, and R.W. Decker, eds., The Eastern Pacific Ocean and Hawaii: The Geology of North America, Geological Society of America, Denver, Colorado, p. 21-72.

Baksi, A.K., 1989, Reevaluation of the timing and duration of extrusion of the Imnaha, Picture Gorge, and Grande Ronde Basalts, Columbia River Group, *in* S.P. Reidel and P.R. Hooper, Volcanism and Tectonism in the Columbia River Flood Basalt Province: Geological Society of America Special Paper 239, p. 105-111.

Barnosky, A.D., and W.J. Labar, 1989, Mid-Miocene (Barstovian) environmental and tectonic setting near Yellowstone National Park, Wyoming and Montana: Geological Society of America Bulletin, v. 101, p. 1448-1456.

Barron, J.A., and J.G. Baldauf, 1989, Tertiary cooling steps and paleoproductivity as reflected by diatoms and biosiliceous sediments, *in* W.H. Berger, V.S. Smetacck, and G. Wefer, eds., Productivity of the Ocean: Present and Past: John Wiley and Sons, p. 341-354.

Barron, J.A., and Gerta Keller, 1982, Widespread Miocene deep-sea hiatuses: Coincidence with periods of global cooling: Geology, v. 10, p. 577-581.

Blackwell, D.D., 1989, Regional implications of heat flow of the Snake River Plain, northwestern United States: Tectonophysics, v. 164, p. 323-343.

Blakely, R.J., and R.C. Jachens, 1991, Regional study of mineral resources in Nevada: Insights from three-dimensional analysis of gravity and magnetic anomalies: Geological Society of America Bulletin, v. 103, p. 795-803.

Bonnichsen, Bill, 1982, The Bruneau-Jarbidge eruptive center, southwestern Idaho, *in* Bill Bonnichsen and R.M. Breckenridge, eds., Cenozoic Geology of Idaho: Idaho Bureau of Mines and Geology Bulletin 26, p. 237-254.

Braile, L.W., W.J. Hinze, R.R.B. von Frese, and G.R. Keller, 1989, Seismic properties of the crust and uppermost mantle of the conterminous United States and adjacent Canada, *in* L.C. Pakiser and W.D. Mooney, eds., Geophysical Framework of the Continental United States: Geological Society of America Memoir 172, p. 655-680.

Camp, V.E., 1995, Mid-Miocene propagation of the Yellowstone mantle plume head beneath the Columbia River basalt source region: Geology, v. 23, no. 5, p. 435-438.

Campbell, I.H., 1998, The mantle's chemical structure: Insights from melting products of mantle plumes, *in* Ian Jackson, ed., The Earth's Mantle: Cambridge University Press, p. 259-310.

Carlson, R.W., and W.K. Hart, 1987, Crustal genesis of the Oregon Plateau: Journal of Geophysical Research, v. 92, p. 6191-6206.

_____, 1988, Flood basalt volcanism in the northwestern United States, *in* J.D. Macdougall, ed., Continental Flood Basalts: Kluwer Academic Publishers, Dordrecht, The Netherlands, p. 35-61.

Christiansen, R.L., 1984, Yellowstone magmatic evolution: Its bearing on understanding large-volume explosive volcanism, *in* Explosive Volcanism: Inception, Evolution, and Hazards, Studies in Geophysics: National Academy Press, p. 84-95.

Christiansen, R.L., and E.H. McKee, 1978, Late Cenozoic volcanic and tectonic evolution of the Great Basin and Columbia intermontane regions, *in* R.B. Smith and G.P. Eaton, eds., Cenozoic Tectonics and Regional Geophysics of the Western Cordillera: Geological Society of America Memoir 152, p. 283-311.

Christiansen, R.L, and R.S. Yeats, 1992, Post-Laramide geology of the U.S. Cordilleran region, *in* B.C. Burchfiel, P.W. Lipman, and M.L. Zoback, eds., The Cordilleran Orogen: Conterminous U.S.: The Geology of North America: Geological Society of America, v. G-3, p. 261-406.

Coffin, M.F., and Olav Eldholm, 1994, Large igneous provinces: Crustal structure, dimensions, and external consequences: Reviews of Geophysics, v. 32, p. 1-36.

Covington, H.R., 1983, Structural evolution of the Raft River basin, Idaho, *in* D.M. Miller, V.R. Todd, and K.A. Howard, eds., Tectonic and Stratigraphic Studies in the Eastern Great Basin: Geological Society of America Memoir 157, p. 229-237.

Crough, S.T., 1978, Thermal origin of mid-plate hot-spot swells: Geophysical Journal of the Royal Astronomical Society, v. 55, p. 451-469.

Davies, G.F., 1998, Plates, plumes, mantle convection, and mantle evolution, *in* Ian Jackson, ed., The Earth's Mantle: Cambridge University Press, p. 228-258.

Draper, D.S., 1991, Late Cenozoic bimodal magmatism in the northern Basin and Range Province of southeastern Oregon: Journal of Volcanology and Geothermal Research, v. 47, p. 299-328.

Drummond, C.N., B.H. Wilkinson, K.C. Lohmann, and G.R. Smith, 1993, Effect of regional topography and hydrology on the lacustrine isotopic record of Miocene paleoclimate in the Rocky Mountains: Palaeogeography, Palaeoclimatology, Palaeoecology, v. 101, p. 67-79.

Duncan, R.A., 1982, A captured island chain in the Coast Range of Oregon and Washington: Journal of Geophysical Research, v. 87, p. 10,827-10,837.

Duncan, R.A., and M.A. Richards, 1991, Hotspots, mantle plumes, flood basalts, and true polar wander: Reviews in Geophysics, v. 29, p. 31-50.

Elison, M.W., R.C. Speed, and R.W. Kistler, 1990, Geologic and isotopic constraints on the crustal structure of the northern Great Basin: Geological Society of America Bulletin, v. 102, p. 1077-1092.

Fields, R.W., D.L. Rasmussen, A.R. Tabrum, and R. Nichol, 1985, Cenozoic rocks of the intermontane basins of western Montana and eastern Idaho, *in* R.M. Flores and S.S. Kaplan, eds., Cenozoic Paleogeography of the West-Central United States: Society of Economic Paleontologists and Mineralogists, Rocky Mountain Section, p. 9-36.

Friedman, Irving, Jim Glean, R.A. Shepherd, and A.J. Guide, III, 1993, Deuterium fractionation as water diffuses into silicic volcanic ash: Geophysical Monograph 78, p. 321-323.

Garnero, E.J., Justin Revenaugh, Quentin Williams, Thorne Lay, and L.H. Kellogg, 1998, Ultralow velocity zone at the core-mantle boundary, *in* Michael Gurnis, M.E. Wysession, Elise Kittle, and B.A. Buffett, eds., The Core-Mantle Boundary Region: American Geophysical Union, Geodynamics Series, v. 28, p. 319-334.

Geist, Dennis, and Mark Richards, 1993, Origin of the Columbia Plateau and Snake River Plain: Deflection of the Yellowstone plume: Geology, v. 21, p. 789-792.

Gregory, K.M., and C.G. Chase, 1992, Tectonic significance of paleobotanically estimated climate and altitude of the late Eocene erosion surface, Colorado: Geology, v. 20, p. 581-585.

Griffiths, R.W., and J.S. Turner, 1998, Understanding mantle dynamics through mathematical models and laboratory experiments, *in* Ian Jackson, ed., The Earth's Mantle: Cambridge University Press, p. 191-227.

Hill, D.P., 1972, Crustal and upper-mantle structure of the Columbia Plateau from long-range seismic-refraction measurements: Geological Society of America Bulletin, v. 83, p. 1639-1648.

Hill, R.I., I.H. Campbell, G.F. Davies, and R.W. Griffiths, 1992, Mantle plumes and continental tectonics: Science, v. 256, p. 186-193.

Hittleman, A.M., D.T. Dater, R.W. Buhmann, and S.D. Racey, 1994, Gravity—1994 edition (CD-ROM): National Geophysical Data Center, Boulder, Colorado (request flier SE-0703).

Hodell, D.A., and Fay Woodruff, 1994, Variations in the strontium isotopic ratio of seawater during the Miocene: Stratigrapic and geochemical implications: Paleoceanography, v. 9, p. 405-426.

Hooper, P.R., 1990, The timing of crustal extension and the eruption of continental flood basalts: Nature, v. 345, p. 246-249.

_____, 1997, The Columbia River flood basalt province: Current status, *in* J.J. Mahoney and M.F. Coffin, eds., Large Igneous Provinces: Continental, Oceanic, and Planetary Flood Volcanism: American Geophysical Monograph 100, p. 1-27.

Hooper, P.R., and C.J. Hawkesworth, 1993, Isotopic and geochemical constraints on the origin and evolution of the Columbia River basalt: Is there a Ba/La ratio argument for the Vancouver slab?: Journal of Petrology, v. 34, p. 1203-1246.

House, M.A., B.P. Warnicke, and K.A., Farley, 1998, Dating topography of the Sierra Nevada, California, using apatite (U/Th)/He ages: Nature, v. 396, p. 66-69.

Jackson, Ian, and S.M. Rigden, 1998, Composition and temperature of the earth's mantle: Seismological models interpreted through experimental studies of earth materials, *in* Ian Jackson, ed., The Earth's Mantle: Cambridge University Press, p. 405-460.

John, D.A., A.R. Ponce, R.B. Fleck, and J.E. Conrad, 2000, New perspectives on the geology and origin of the northern Nevada rift, *in* J.K. Cluer, J.G. Price, E.M. Struhsacker, R.F. Hardyman, and C.L. Morris, eds., Geology and Ore Deposits 2000: The Great Basin and Beyond: Geological Society of Nevada Symposium Proceedings, May 15-18, 2000, p. 127-154.

John, D.A., and A.R. Wallace, 2000, Epithermal gold-silver deposits related to the northern Nevada rift, *in* J.K. Cluer, J.G. Price, E.M. Struhsacker, R.F. Hardyman, and C.L. Morris, eds., Geology and Ore Deposits 2000: The Great Basin and Beyond: Geological Society of Nevada Symposium Proceedings, May 15-18, 2000, p. 155-175.

Johnston, S.T., P.J. Wynne, Don Francis, C.J.R. Hart, R.J. Enkin, and D.C. Engebretson, 1996, Yellowstone in Yukon: The late Cretaceous Carmaks Group: Geology, v. 24, p. 997-1000.

Katzman, Rafael, Li Zhao, and T.H. Jordan, 1998, High-resolution, two dimensional vertical tomography of the central Pacific mantle using ScS reverberations and frequency-dependent travel times: Journal of Geophysical Research, v. 103, p. 17,933-17,971.

Kistler, R.W., 1983, Isotope geochemistry of plutons in the northern Great Basin: Geothermal Resources Council, Davis, California, Special Report 13, p. 3-8.

Kutzbach, J.E., P.J. Guetter, W.F. Ruddiman, and W.L. Prell, 1989, Sensitivity of climate to late Cenozoic uplift in southern Asia and the American West: Numerical experiments: Journal of Geophysical Research, v. 94, p. 18,393-18,407.

Lachenbruch, A.H., and J.H. Sass, 1978, Models of an extending lithosphere and heat flow in the Basin and Range Province: Geological Society of America Memoir 152, p. 209-250.

Leavitt, S.W., 1982, Annual volcanic carbon dioxide emission: An estimate from eruption chronologies: Environmental Geology, v. 4, p. 15-21.

Leeman, W.P., 1982, Development of the Snake River Plain-Yellowstone Plateau province, Idaho and Wyoming: An overview and petrologic model, *in* Bill Bonnichsen and R.M. Breckenridge, eds., Cenozoic Geology of Idaho: Idaho Bureau of Mines and Geology Bulletin 26, p. 155-178.

Leeman, W.P., J.S. Oldow, and W.K. Hart, 1992, Lithosphere-scale thrusting in the western U.S. Cordillera as constrained by Sr and Nd isotopic transitions in Neogene volcanic rocks: Geology, v. 20, p. 63-66.

Leopold, E.B., and M.F. Denton, 1987, Comparative age of grassland and steppe east and west of the northern Rocky Mountains: Annals of the Missouri Botanical Garden, v. 74, p. 841-867.

Leopold, E.B., and V.C. Wright, 1985, Pollen profiles of the Plio-Pleistocene transition in the Snake River Plain, Idaho, *in* Late Cenozoic History of the Pacific Northwest: American Association for the Advancement of Science, Pacific Division, San Francisco, p. 323-348.

Link, P.K., N. Christie-Blick, J.H. Stewart, J.M.G. Miller, W.J. Devlin, and M. Levy, 1993, Late Proterozoic strata of the United States Cordillera, *in* P.K. Link and others, Middle and Late Proterozoic stratified rocks of the western U.S. Cordillera, Colorado Plateau, and Basin and Range Province, *in* J.C. Reed, M.E. Bickford, R.S. Houston, P.K. Link, D.W. Rankin, P.K. Sims, and W.R. Van Schmus, eds., PreCambrian: Conterminous U.S.: Geological Society of America, The Geology of North America, Boulder, v. C-2, p. 536-558.

Lipman, P.W., 1992, Magmatism in the Cordilleran United States: Progress and problems, *in* B.C. Burchfiel, P.W. Lipman, and M.L. Zoback, eds., The Cordilleran Orogen: Conterminous U.S.: The Geology of North America: Geological Society of America, v. G-3, p. 481-514.

Love, J.D., L.A. Morgan, and W.C. McIntosh, 1997, The Teewinot Formation: Evidence for late Miocene basin formation in response to volcanism, faulting, and uplift associated with the Yellowstone hotspot?: Geological Society of America Abstracts with Programs, v. 29, no. 6, p. A-365.

Luedke, R.G., and R.L. Smith, 1981, Map showing distribution and age of late Cenozoic volcanic centers in California and Nevada: U.S. Geological Survey Miscellaneous Geologic Investigations Map, I-1091-C, scale 1:1,000,000.

_____, 1982, Map showing distribution and age of late Cenozoic volcanic centers in Oregon and Washington: U.S. Geological Survey Miscellaneous Geologic Investigations Map, I-1091-D, scale 1:1,000,000.

_____, 1983, Map showing distribution and age of late Cenozoic volcanic centers in Idaho, western Montana, west-central South Dakota, and northwestern Wyoming: U.S. Geological Survey Miscellaneous Geologic Investigations Map, I-1091-E, scale 1:1,000,000.

MacLeod, N.S., G.W. Walker, and E.H. McKee, 1976, Geothermal significance of eastward increase in age of upper Cenozoic rhyolitic domes in southeastern Oregon: Proceedings of the Second United Nations Symposium on the Development and Use of Geothermal Resources, v. 1, Washington, D.C., U.S. Government Printing Office, p. 456-474.

Malde, H.E., 1991, Quaternary geology and structural history of the Snake River Plain, Idaho and Oregon, *in* R.B. Morrison, ed., Quaternary Nonglacial History of the Conterminous U.S.: Geological Society of America, The Geology of North America, v. K-2, ch. 4, p. 251-282.

McClean, D.M., 1985, Mantle degassing induced dead ocean in the Cretaceous-Tertiary transition, *in* E.T. Sundquist and W.H. Broecker, eds., The Carbon Cycle and Atmospheric CO_2: Natural Variations Archean to Present: American Geophysical Union Geophysical Monograph 32, p. 493-503.

Miller, K., R.G. Fairbanks, and G.S. Mountain, 1987, Tertiary isotope synthesis, sea level history, and continental margin erosion: Paleooceanography, v. 2, p. 1-19.

Molnar, Peter, and Philip England, 1990a, Surface uplift, uplift of rocks, and exhumation of rocks: Geology, v. 18, p. 1173-1177.

_____, 1990b, Late Cenozoic uplift of mountain ranges and global climate change: Chicken or egg?: Nature, v. 346, p. 29-34.

Mooney, W.D., and L.W. Braile, 1989, The seismic structure of the continental crust and upper mantle of North America, *in* A.W. Bally and A.R. Palmer, eds., The Geology of North America—An Overview: Geological Society of America, The Geology of North America, v. A, p. 39-52.

Mooney, W.D, and C.S. Weaver, 1989, Regional crustal structure and tectonics of the Pacific coastal states: California, Oregon, and Washington, *in* L.C. Pakiser and W.D. Mooney, eds., Geophysical Framework of the Continental United States: Geological Society of America Memoir 172, p. 129-161.

Morgan, J.P., W.J. Morgan, and Evelyn Price, 1995, Hotspot melting generates both hotspot volcanism and a hotspot swell?: Journal of Geophysical Research, v. 100, p. 8045-8062.

Morgan, L.A., D.J. Doherty, and W.P. Leeman, 1984, Ignimbrites of the eastern Snake River Plain: Evidence for major caldera forming eruptions: Journal of Geophysical Research, v. 89, no. B10, p. 8665-8678.

Morgan, L.A., and W.C. McIntosh, 2002, $^{40}Ar/^{39}Ar$ ages of silicic volcanic rocks in the Heise volcanic field, eastern Snake River Plain, Idaho: Timing of volcanism and tectonism, *in* Bill Bonnichsen, C.M. White, and Michael McCurry, eds., Tectonic and Magmatic Evolution of the Snake River Plain Volcanic Province: Idaho Geological Survey Bulletin 30.

Morgan, L.A., W.C. McIntosh, and K.L. Pierce, 1997, Inferences for changes in plume dynamics from stratigraphic framework studies of ignimbrites, central Snake River Plain, Idaho: Geological Society of America Abstracts with Programs, v. 29, no. 6, p. A-299.

Morgan, Paul, and W.D. Gosnold, 1989, Heat flow and thermal regimes of the continental United States, *in* L.C. Pakiser and W.D. Mooney, eds., Geophysical Framework of the Continental United States: Geological Society of America Memoir 172, p. 493-522.

Mueller, K.J., P.K. Cerveny, M.E. Perkins, and L.W. Snee, 1999, Chronology of polyphase extension in the Windermere Hills, northeast Nevada: Geological Society of America Bulletin, v. 111, p. 11-27.

Murphy, J.B., G.L. Oppliger, and G.H. Brimhall, Jr., 1998, Plume-modified orogeny: An example from the western United States: Geology, v. 26, p. 731-734.

Oppliger, G.L., J.B Murphy, and G.H. Brimhall, Jr., 1997, Is the ancestral Yellowstone hotspot responsible for the Tertiary Carlin mineralization in the Great Basin of Nevada?: Geology, v. 25, no. 7, p. 627-630.

Page, W.D., T.L. Sawyer, and P.R. Renne, 1995, Tectonic deformation of the Lovejoy Basalt, a late Cenozoic strain gage across the northern Sierra Nevada and Diamond Mountains, California, in W.D. Page, trip leader, Quaternary Geology Along the Boundary Between the Modoc Plateau, Southern Cascade Mountains, and Northern Sierra Nevada: Friends of the Pleistocene, 1995 Pacific Cell Field Trip: PG&E, San Francisco, Appendix 3-3, 11 p.

Pakiser, L.C., 1989, Geophysics of the Intermontane system, *in* L.C. Pakiser and W.D. Mooney, eds., Geophysical Framework of the Continental United States: Geological Society of America Memoir 172, p. 235-247.

Parsons, Tom, 1995, The Basin and Range Province, *in* K.H. Olsen, ed., Continental Rifts: Evolution, Structure, Tectonics, Developments: Geotectonics 25, Elsevier, Amsterdam, p. 277-324.

Parsons, Tom, G.A. Thompson, and N.H. Sleep, 1994, Mantle plume influence on the Neogene uplift and extension of the U.S. western Cordillera?: Geology, v. 22, p. 83-86.

Parsons, Tom, A.M. Trehu, J.H. Luetgert, Kate Miller, Fiona Kilbride, R.E. Wells, M.A. Fisher, Ernst Flueh, U.S. Ten Brink, and N.I. Christensen, 1998, A new view into the Cascade subduction zone and volcanic arc: Implications for earthquake hazards along the Washington margin: Geology, v. 26, p. 199-202.

Perkins, M.E., F.H. Brown, W.P. Nash, W. McIntosh, and S.K. Williams, 1998, Sequence, age, and source of silicic fallout tuffs in middle to late Miocene basins of the Basin and Range Province: Geological Society of America Bulletin, v. 110, p. 344-360.

Pezzopane, S.K., and R.J. Weldon, II, 1993, Tectonic role of active faulting in central Oregon: Tectonics, v. 12, p. 1140-1169.

Pierce, K.L., D.G. Milbert, and R.W. Saltus, 1992, Geoid dome culminates on Yellowstone: Yellowstone hotspot fed by a thermal mantle plume?: Eos, Transactions of the American Geophysical Union, v. 73, p. 284.

Pierce, K.L., and L.A. Morgan, 1990, The track of the Yellowstone hotspot: Volcanism, faulting, and uplift: U.S. Geological Survey Open-File Report 90-415, 49 p.

_____ 1992, The track of the Yellowstone hotspot: Volcanism, faulting, and uplift, *in* P.K. Link, M.A. Kuntz, and L.B. Platt, eds., Regional Geology of Eastern Idaho and Western Wyoming: Geological Society of America Memoir 179, p. 1-53.

Pyle, D.G., B.B. Hanan, D.W. Graham, and R.A. Duncan, 1997, Siletzia-geochemistry and geochronology of Yellowstone hotspot volcanism in a suboceanic setting: Geological Society of America Abstracts with Programs, v. 29, no. 6, p. A-298.

Rampino, M.R., 1991, Volcanism, climate change, and the geologic record: Society of Economic Paleontologists and Mineralogists, Special Publication 45, p. 9-18.

Rasmussen, J., and E. Humphreys, 1988, Tomographic image of the Juan de Fuca plate beneath Washington and western Oregon using teleseismic P-wave travel times: Geophysical Research Letters, v. 15, p. 1417-1420.

Raymo, M.W., and W.F. Ruddiman, 1992, Tectonic forcing of late Cenozoic climate: Nature, v. 359, p. 117-122.

Raymo, M.W., W.F. Ruddiman, and P.N. Froelich, 1988, The influence of late Cenozoic mountain building on oceanic geochemical cycles: Geology, v. 16, p. 649-653.

Reed., J.C., Jr., 1993, Map of the Precambrian rocks of the conterminous United States, *in* J.C. Reed, M.E. Bickford, R.S. Houston, P.K. Link, D.W. Rankin, P.K. Sims, and W.R. Van Schmus, eds., Precambrian: Conterminous U.S.: Geological Society of America, The Geology of North America, Boulder, v. C-2, plate 1.

Reidel, S.P, N.P. Campbell, K.R. Fecht, and K.A. Lindwey, 1989, Late Cenozoic structure and stratigraphy of south central Washington, *in* Regional Geology of Washington State: Washington Department of Natural Resources Bulletin 80, p. 159-180.

Richards, M.A., R.A. Duncan, and V.E. Courtillot, 1989, Flood basalts and hotspot tracks: Plume heads and tails: Science, v. 246, p. 103-107.

Rodgers, D.W., W.R. Hackett, and H.T. Ore, 1990, Extension of the Yellowstone Plateau, eastern Snake River Plain, and Owyhee Plateau: Geology, v. 18, p. 1138-1141.

Ruddiman, W.F., and J.E. Kutzbach, 1989, Forcing of late Cenozoic Northern Hemisphere climate by plateau uplift in southern Asia and the American West: Journal of Geophysical Research, v. 94, p. 18,409-18,427.

Ruddiman, W.F., J.E. Kutzbach, and I.C. Prentice, 1997, Testing the climatic effects of orography and CO_2 with general circulation and Biome models, *in* W.F. Ruddiman, ed., Tectonic Uplift and Climate Change: Plenum Press, New York, p. 204-235.

Ruddiman, W.F., W.L. Prell, and M.E. Raymo, 1989, Late Cenozoic uplift in southern Asia and the American West: Rationale for general circulation modeling experiments: Journal of Geophysical Research, v. 94, p. 18,379-18,391.

Ruddiman, W.F., M.E. Raymo, W.L. Prell, and J.E. Kutzbach, 1997, The uplift-climate connection: A synthesis, *in* W.F. Ruddiman, ed., Tectonic Uplift and Climate Change: Plenum Press, New York, p. 471-515.

Rytuba, J.J., and E.H. McKee, 1984, Peralkaline ash flow tuffs and calderas of the McDermitt volcanic field, southeast Oregon and north central Nevada: Journal of Geophysical Research, v. 89, no. B10, p. 8616-8628.

Saltus, R.W., and G.A. Thompson, 1995, Why is it downhill from Tonopah to Las Vegas?: A case for a mantle plume support of the high northern Basin and Range: Tectonics, v. 14, p. 1235-1244.

Self, Stephen, Thorvaldur Thordarson, and Laszlo Keszthelyi, 1997, Emplacement of continental flood basalt lava flows, *in* J.J. Mahoney and M.F. Coffin, eds., Large Igneous Provinces: Continental, Oceanic, and Planetary Flood Volcanism: American Geophysical Monograph 100, p. 381-410.

Severinghaus, Jeff, and Tanya Atwater, 1990, Cenozoic geometry and thermal state of the subducting slabs beneath western North America, *in* B.P. Wernicke, ed., Basin and Range Extensional Tectonics Near the Latitude of Las Vegas, Nevada: Geological Society of America Memoir 176, p. 1-22.

Shervais, John, Scott Vetter, and Barry Hanan, 1997, Shaking the plume's tail: Basaltic volcanism in the central Snake River Plain, Idaho: Geological Society of America Abstracts with Programs, v. 29, no. 6, p. A-300.

Sleep, N.H., 1990, Hotspots and mantle plumes: Some phenomenology: Journal of Geophysical Research, v. 95, no. B5, p. 6715-6736.

_____, 1997, Lateral flow and ponding of starting plume material: Journal of Geophysical Research, v. 102, no. B5, p. 10,001-10,012.

Smith, G.R., and W.P. Patterson, 1994, Mio-Pliocene seasonality on the Snake River Plain: Comparison of faunal and oxygen isotopic evidence: Palaeogeography, Palaeoclimatology, Palaeoecology, v. 107, p. 291-302.

Smith, R.B., and L.W. Braille, 1993, Topographic signature, space-time evolution, and physical properties of the Yellowstone-Snake River Plain volcanic system: The Yellowstone hotspot, *in* A.W. Snoke, J.R. Steidtmann, and S.M. Roberts, eds., Geology of Wyoming: Geological Survey of Wyoming Memoir No. 5, p. 694-754.

Snee, L.W., Karen Lund, J.F. Sutter, D.E. Balcer, and K.V. Evans, 1995, An $^{40}Ar/^{39}Ar$ chronicle of the tectonic development of the Salmon River suture zone, western Idaho, *in* T.L. Vallier and H.C. Brooks, eds., Geology of the Blue Mountains Region of Oregon, Idaho, and Washington: Petrology and Tectonic Evolution of Pre-Tertiary Rocks of the Blue Mountain Region: U.S. Geological Survey Professional Paper 1438, p. 359-414.

Takahahshi, Eiichi, Katsuji Nakajima, and T.L. Wright, 1998, Origin of the Columbia River basalts; melting model of a heterogeneous plume head: Earth and Planetary Science Letters, v. 162 (1-4), p. 63-80.

Taylor, D.W., and R.C. Bright, 1987, Drainage history of the Bonneville Basin, *in* Cenozoic Geology of Western Utah: Utah Geological Association Publication 16, p. 239-256.

Thelin, Gail, and R.J. Pike, 1991, Landforms of the conterminous United States—A digital shaded relief portrayal: U.S. Geological Survey Miscellaneous Geologic Investigations Map I-2206, scale 1:3,500,000.

Thompson, G.A., 1998, Deep mantle plumes and geoscience vision, Geological Society of America, and presidential address: GSA Today, April 1996, p. 17-25.

Thompson, G.A., R. Catchings, E. Goodwin, S. Holbrook, C. Jarchow, C. Mann, J. McCarthy, and D. Okaya, 1989, Geophysics of the western Basin and Range Province, *in* L.C. Pakiser and W.D. Mooney, eds., Geophysical Framework of the Continental United States: Geological Society of America Memoir 172, p. 177-203.

Thompson, G.R., R.W. Fields, and David Alt, 1982, Land-based evidence for Tertiary climatic variations: Northern Rockies: Geology, v. 10, p. 413-417.

Thompson, R.N., and S.A. Gibson, 1991, Subcontinental mantle plumes, hotspots, and pre-existing thinspots: Journal of the Geological Society, London, v. 148, p. 973-977.

Vallier, T.L., 1995, Petrology of pre-Tertiary igneous rocks in the Blue Mountains province of Oregon, Idaho, and Washington: Implications for the geologic evolution of a complex island arc: U.S. Geological Survey Professional Paper 1438, p. 125-209.

Van der Lee, Susan, and Guust Nolet, 1997, Seismic image of the subducted trailing fragments of the Vancouver plate: Nature, v. 386, p. 266-269.

VanDecar, J.C., 1991, Upper-mantle structure of the Cascadia Subduction Zone from non-linear teleseismic travel-time inversion: University of Washington Ph.D. dissertation, 177 p.

Wagner, D.L., and G.J. Saucedo, 1990, Age and stratigraphic relationships of Miocene volcanic rocks along the eastern margin of the Sacramento Valley, California, *in* R.V. Ingersoll and T.H. Nilsen, eds., Sacramento Valley Symposium and Guidebook, Pacific Section S.E.P.M., v. 65, p. 143-151.

Wagner, D.L., G.J. Saucedo, and T.L.T. Grose, 2000, Tertiary volcanic rocks of the Blairsden area, northern Sierra Nevada, California, *in* E.R. Brooks and L.T. Dida, eds., Field Guide to the Geology and Tectonics of the Northern Sierra Nevada—NAGT Far Western Section Fall Conference: California Division of Mines and Geology Special Publication 122, p. 155-172.

Walker, G.W., and Bruce Nolf, 1981, High lava plains, Brothers fault zone to Harvey Basin, Oregon, *in* D.A. Johnston and Julie Donnelly-Nolan, eds., Guides to Some Volcanic Terranes in Washington, Idaho, Oregon, and Northern California: U.S. Geological Survey Circular 838, p. 105-111.

White, R.S., and D.P. McKenzie, 1989, Magmatism at rift zones: The generation of volcanic continental margins and flood basalts: Journal of Geophysical Research, v. 94, no. B6, p. 7685-7729.

Wolfe, J.A., 1993, A method for obtaining climate parameters from leaf assemblages: U.S. Geological Survey Bulletin 2040, 71 p.

Wolfe, J.A., C.E. Forest, and Peter Molnar, 1998, Paleobotanical evidence on Eocene and Oligocene paleoaltitudes in mid-latitude western North America: Geological Society of America Bulletin, v. 110, p. 664-678.

Wolfe, J.A., H.E. Schorn, C.E. Forest, and Peter Molnar, 1997, Paleobotanical evidence for high altitudes in Nevada during the Miocene: Science, v. 276, p. 1672-1675.

Wood, S.H., and Clemens, D.M., 2002, Geologic and tectonic history of the western Snake River Plain, Idaho and Oregon, *in* Bill Bonnichsen, C.M. White, and Michael McCurry, eds., Tectonic and Magmatic Evolution of the Snake River Plain Volcanic Province: Idaho Geological Survey Bulletin 30.

Wright, J.D., and K.G. Miller, 1992, Miocene stable isotope stratigraphy, site 747, Kerguelen Plateau: Proceedings Ocean Drilling Program, Scientific Results, v. 120, p. 855-866.

Zoback, M.L., R.E. Anderson, and G.A. Thompson, 1981, Cainozoic evolution of the state of stress and style of tectonism of the Basin and Range Province of the western United States: Philosophical Transactions of the Royal Society of London, v. A300, p. 407-434.

Zoback, M.L., E.H. McKee, R.J. Blakely, and G.A. Thompson, 1994, The northern Nevada rift: Regional tectono-magmatic relations and middle Miocene stress direction: Geological Society of America Bulletin, v. 106, p. 371-382.

Zoback, M.L., and G.A. Thompson, 1978, Basin and Range rifting in northern Nevada: Clues from a mid-Miocene rift and its subsequent offsets: Geology, v. 6, p. 111-116.

Tracking the Western Margin of the North American Craton Beneath Southeastern Oregon: A Multidisciplinary Approach

James G. Evans,[1] Andrew Griscom,[2] Phyllis F. Halvorson,[3] and Michael L. Cummings[4]

ABSTRACT

On the basis of balanced cross sections and strontium and neodymium isotopic compositions of volcanic and plutonic rocks in western Idaho and eastern Oregon, Leeman and others (1992) suggested that the Cretaceous boundary between the western margin of North America and the Mesozoic accreted terranes, including the boundary between oceanic and continental crust as demarcated by the western Idaho suture zone, was thrust as much as 150 km eastward during the Sevier orogeny. According to their model, the Sevier-age decollement cuts down into the upper mantle as deep as the zone of segregation of basalt magma, and an autochthonous oceanic-cratonic suture in the lithospheric mantle underlies eastern Oregon. Results of a recent mineral resource assessment of southeastern Oregon that includes analyses of geophysical, geologic, and geochemical data suggest an approximate location for the decollement-truncated suture at depth. The prime candidate for its surface projection is a set of near-coincident, northeast-trending geophysical gradient belts that transect the southeastern Oregon Tertiary volcanic province. These physical discontinuities delineate regional gravity, aeromagnetic, and aeroradioactivity anomaly domains. The potential-field gradient belts flank long-wavelength anomalies produced by sources that could lie at mid or lower crustal depths, but probably not in the upper mantle. The aeroradioactivity gradients, although produced by sources in the surface skin only, broadly reflect a regional contrast in radioelement geochemistry, with lithologies to the southeast more typical of a continental lithosphere.

The set of discontinuities generally trends northeastward from about lat 42º30'N., long 119º30'W., to about lat 44º10'N., long 117º50'W., where it intersects the accreted terranes. Its further northeastward continuation is problematical; the potential-field elements, at least, are truncated by major northeast-trending structures, and the radiometric trends become indistinct. Additional hints as to the location of the suture under Oregon are suggested by xenoliths in volcanic and plutonic rocks and by possible suture-related localization of Cenozoic volcanism and hydrothermal activity. If the geophysical gradients directly overlie the Mesozoic continental-oceanic mantle suture at depth, east-west separation of the continent-ocean lithospheric mantle boundary as measured from the western Idaho suture zone to the K/eTh boundary at lat 44ºN. is approximately 125 km. This separation, however, may include up to tens of kilometers of late Tertiary extension, so that 125 km is the maximum possible Sevier translation of the western Idaho suture zone relative to eastern Oregon at this latitude. If the suture generally dips east at depth, the Sevier translation would be increased accordingly.

Key words: western margin of North American craton, western Idaho suture zone, Sevier orogeny, Mesozoic continental-oceanic mantle suture

INTRODUCTION

The western margin of the North American craton between lat 42ºN. and 46º15'N. has been depicted as trend-

Editors' note: The manuscript was submitted in June 1998 and has been revised at the authors' discretion.

[1]U.S. Geological Survey, 904 W. Riverside, Room 202, Spokane, WA, 99210-1087

[2]U.S. Geological Survey (retired), 345 Middlefield Road, Menlo Park, CA, 94025

[3]610 Thayer Rd., Bonny Doon, CA, 95060

[4]Geology Department, Portland State University, Portland, OR 97207

Evans, J.G., Andrew Griscom, P.F. Halvorson, and M.L. Cummings, 2002, Tracking the western margin of the North American Craton beneath southeastern Oregon: A multidisciplinary approach, *in* Bill Bonnichsen, C.M. White, and Michael McCurry, eds., Tectonic and Magmatic Evolution of the Snake River Plain Volcanic Province: Idaho Geological Survey Bulletin 30, p. 35-57.

ing north-northeast, partly along the steeply dipping western Idaho suture zone, which separates accreted oceanic terranes to the west from the Cretaceous Idaho batholith on the east (Figure 1; Lund and Snee, 1988; Fleck and Criss, 1988; Farmer, 1988; Strayer and others, 1989). Mesozoic granites that postdate the western Idaho suture zone have $^{87}Sr/^{86}Sr$ ratios greater than 0.706 east of the zone and less than 0.704 to the west of it in westernmost Idaho and eastern Oregon (Armstrong and others, 1977; Fleck and Criss, 1985). These differences in strontium isotopic ratios are interpreted to reflect the presence of underlying continental (east) and oceanic (west) lithospheric mantle. $^{87}Sr/^{86}Sr$ ratios in Neogene volcanic rocks between about long 116°30'W. (the approximate longitude of the western Idaho suture zone) and long 119°W., however, are 0.7035-0.706 for basalt and 0.705-0.708 for rhyolite, and $^{143}Nd/^{144}Nd$ ratios are 0.5125-5128 for basalt and 0.5124-0.517 for rhyolites (Leeman and others, 1992). Leeman and others interpreted these ratios to indicate magma derivation from both continental and oceanic lithospheric mantle. According to their model, based on balanced cross sections through the western Idaho suture zone to the Montana fold and thrust belt, and the Sr and Nd isotopic data, the basal decollement of the late Mesozoic and early Tertiary Sevier orogeny dips gently westward into the upper mantle below depths of segregation of basaltic magma. Oceanic lithospheric mantle has been thrust an estimated 150 km generally eastward over a shelf of older continental lithospheric mantle, truncating the earlier formed suture zone in the mantle. According to this model, the autochthonous part of the continental-oceanic suture beneath the decollement would be present beneath eastern Oregon. The purpose of this paper is to present geologic, geophysical, and geochemi-

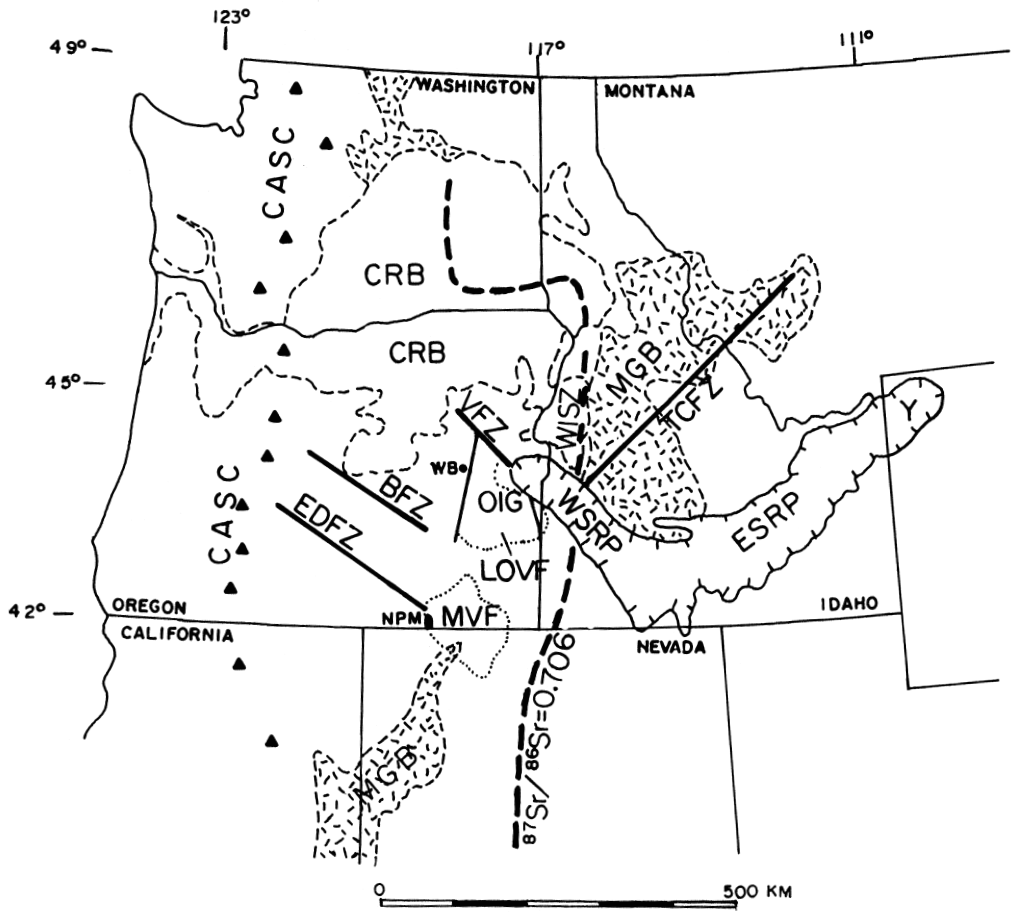

Figure 1. Tectonic framework of eastern Oregon. BFZ, Brothers fault zone; CASC, Cascade Range; CRB, Columbia River Basalt Group; EDFZ, Eugene-Denio fault zone; LOVF, Lake Owyhee volcanic field; MGB, Mesozoic granitic batholiths; MVF, McDermitt volcanic field; NPM, northern Pueblo Mountains; OIG, Oregon-Idaho graben, showing generalized fault margins (thin north-northeast- and north-northwest-trending lines); ESRP, eastern Snake River Plain; TCFZ, Trans-Challis fault zone; VFZ, Vale fault zone; WB, Westfall Butte; $^{87}Sr/^{86}Sr = 0.706$ line (in part coincides with western Idaho suture zone, WISZ); WSRP, western Snake River Plain.

cal evidence indicating the location of the truncated autochthonous suture at lower crustal or upper mantle depths under southeastern Oregon.

GEOLOGIC EVIDENCE

The geologic evidence for the types of basement under eastern Oregon derives from xenoliths ranging in size from a few millimeters to a few hundred meters in Mesozoic and Tertiary volcanic and hypabyssal to plutonic rocks. While xenoliths do not conclusively support a particular model, they indicate that certain types of basement rock were in contact with magma emplaced under parts of Oregon in the middle to late Tertiary and imply regional differences in crustal composition.

XENOLITHS IN MIOCENE VOLCANIC ROCKS OF THE OREGON-IDAHO GRABEN

Xenoliths of granitic gneiss were found in volcanic rock units in the 50 by 100 km, north-trending, middle Miocene Oregon-Idaho graben (Ferns and others, 1993a, b; Cummings and others, 2000; Figure 1). The graben coincides with the Lake Owyhee volcanic field of Rytuba and others (1991), a region of abundant and rhyolitic to basaltic volcanism mostly associated with the graben's early subsidence. The graben developed during the middle Miocene beginning at about 15 Ma with caldera-forming eruptions chiefly along its axis and relatively large-volume rhyolite flows along both margins (Ferns and others, 1993a, b; Cummings and others, 2000). Pre-graben stratigraphy exposed on both margins includes a 1-km-thick section of Columbia River-type basalt (Evans, 1990a, b; Evans, 1996, Evans and Keith, 1996; Evans and Binger, 1997; Binger, 1997; Ekren and others, 1981, 1982) that is believed to floor the younger graben. Griscom and Halvorson (1994) show that gravity and magnetic patterns over the central graben can be modeled by a basalt slab 1.8 km thick at a depth of 2 km under relatively low-density graben fill. As much as 1 km of the underlying basalt is accounted for by the known thickness of the flood-basalt sequence in the region. Therefore, as much as 0.8 km of the model slab under the graben may be basalt and gabbro sills, dikes, and plutons that underplated it during its middle Miocene evolution. Cummings and others (1996) model a 1.4 km-thick slab beneath the central graben at a depth greater than 2 km. Orthopyroxene-bearing gabbro xenoliths in shallow intrusions suggest gabbro sills and plutons are an important component of this slab. An exposed example of such an intrusion-thickened basalt slab is found in the northern Pueblo Mountains (Figure 1), where basalt and gabbro sills increase the apparent thickness of the exposed section of Steens Basalt by as much as 0.25 km (Evans, unpub. mapping, 1995, Ladycomb Peak 7.5-minute quadrangle). Relatively small-volume silicic to basaltic flows erupted within the graben until about 8 Ma, when east-west extension ceased and northeast-southwest extension began in the western Snake River Plain (SRP).

Highly recrystallized partially melted granitic gneiss xenoliths, about fist-size, in intragraben basalt flows (Cummings, 1991) are present at least 50 km west of where the $^{87}Sr/^{86}Sr = 0.706$ line is commonly drawn in southwest Idaho near the Idaho-Oregon state line (Figure 1). The locations of the xenoliths suggest that much of the Oregon-Idaho graben could be underlain by metamorphosed crust, presumably contiguous with metamorphosed crust, likely to be continental, exposed in southwestern Idaho (Ekren and others, 1981; Evans, unpub. mapping, 1996, DeLamar and Flint 7.5-minute quadrangles).

XENOLITHS IN VOLCANIC ROCKS AT WESTFALL BUTTE

Millimeter- to centimeter-sized xenoliths of recrystallized radiolarian chert and argillite were found in three volcanic rock units in the Westfall Butte area, about 10 km west of the Oregon-Idaho graben (Figure 1). Chert and argillite are common lithologies in the Mesozoic Baker terrane of northeastern Oregon (Brooks, 1979), and their presence suggests that Baker terrane is present under Westfall Butte. The butte itself is a small, middle Miocene, silicic to basaltic volcanic edifice built on Columbia River-type basalt and relatively thin middle Miocene volcanic and sedimentary rocks on the rim of a caldera (Evans and Binger, 1997).

The oldest volcanic rock unit containing the xenoliths is the 15-Ma Dinner Creek Welded Tuff (Kittleman and others, 1965; Fiebelkorn and others, 1983), which overlies the basalt of Malheur Gorge and is at least 120 m thick just north of Westfall Butte. Here, the Dinner Creek probably constitutes the upper part of the intracaldera pyroclastic facies.

Hunter Creek Basalt (Kittleman and others, 1965), an extensive icelandite or basaltic andesite that overlies the Dinner Creek, also contains xenoliths of chert and argillite. The basalt may have erupted from dikes about 10 km to the east (Brooks and O'Brien, 1992) along the western margin of the Oregon-Idaho graben soon after the Dinner Creek was emplaced. The youngest rock unit with xenoliths of chert and argillite is the basal pyroclas-

tic breccia of the Westfall Butte Volcanics (Evans and Binger, 1997), which overlie the Hunter Creek basalt. The xenoliths of radiolarian chert and argillite in these rock units are similar to rock types in the Baker terrane (Brooks, 1979). The nearest outcrops of Baker terrane rocks are about 60 km north of Westfall Butte (Silberling and others, 1987; Walker and MacLeod, 1991). Thus, an accreted terrane source of the chert and argillite apparently underlies an area at least 10 km by 5 km to judge from the areal distribution of vent sources and may connect with the Baker terrane. The xenoliths do not clearly indicate whether their source is oceanic lithosphere, as is assumed to the north, or another unknown configuration of cratonal crustal blocks and slabs that contain oceanic lithologies.

XENOLITHS IN PRE-TERTIARY ROCKS OF THE NORTHERN PUEBLO MOUNTAINS

Xenoliths of quartzite as much as 0.4 km long are present in intrusions of the Jurassic volcano-plutonic complex of the northern Pueblo Mountains in southern Harney County, Oregon (Figure 1; Harrold, 1972; Rowe, 1970; Tower, 1972; Evans, unpub. mapping, 1995, Ladycomb Peak 7.5-minute quadrangle). The complex includes granite, granite pegmatite, monzonite, granodiorite, diorite, basaltic trachyandesite, trachyandesite, dacite, and rhyolite (Brown, 1996; Evans, unpub. mapping and analytical data, 1995). This rock suite has been interpreted as the metavolcanic part of a magmatic arc (Roback and others, 1987; Brown, 1996), but apparently below clearly extrusive phases and probably largely hypabyssal, as no flow structure or vents were identified (Evans, unpub. mapping, 1995). The rocks have been variably metamorphosed to greenschist facies or albite-epidote hornfels facies.

Silberling and others (1987) and Silberling (1991) assigned pre-Tertiary rocks of the northern Pueblo Mountains to their Black Rock terrane and suggested that the protoliths of at least some metamorphic rocks there are Lower Permian in age. This interpretation apparently is based in part on interpretations of some of the metaigneous rocks as extrusive metavolcanic rocks and of the schist unit on the east flank of the Pueblo Mountains as derived from metavolcanic or deep-sea protoliths (Roback and others, 1987). However, a gradational zone as much as 10 m wide between the schist and the metaigneous rocks (Evans, unpub. mapping, 1995; Brown, 1996) suggests that the schist was derived from the volcano-plutonic complex. Differences in mineralogy and composition between the schist and igneous complex are attributed by Brown (1996) to the introduction of water in a 3- to 5-km-wide, 20-km-long, north-northeast-trending sheer zone. Brown (1996) theorizes that the Pueblo Mountains zone may be part of a regional ductile shear zone that may encompass the western Idaho suture zone and a similar shear zone in the Pine Forest Range, Nevada.

The quartzite xenoliths (Harrold, 1972; Rowe, 1970; Tower, 1972; Evans, unpub. mapping, 1996) may represent a mature sediment that is common in cratonic shelf-facies protolith. By itself, however, this association in the Pueblo Mountains is not clearly diagnostic of plate-tectonic setting because quartzose sandstones in the Hurwall Formation are found in the Wallowa terrane in association with Martin Bridge Limestone (Follo, 1994). A shelf-facies protolith would necessarily pre-date metamorphism and would therefore be most likely Precambrian or Paleozoic in age, implying that the pre-Tertiary rocks of the Pueblo Mountains, which are 135 km west of the $^{87}Sr/^{86}Sr = 0.706$ line, are underlain by continental crust, part of the Mesozoic craton of North America.

In summary, the xenolith data suggest that a Mesozoic cratonic margin may pass between Westfall Butte and the northern Pueblo Mountains somewhere near the western margin of the Oregon-Idaho graben. As outlined below, regional geophysical data are consistent with this hypothesis and provide further constraints on the character of the substrate.

GEOPHYSICAL EVIDENCE

The sources of gravity, aeromagnetic, and airborne radiometric data for eastern Oregon and the methods of processing the data to derive interpretations of structure and lithology are described in a preliminary mineral resource assessment of southeastern Oregon (Griscom and Halvorson, 1994). These sources will be fully documented in a forthcoming final assessment report (Evans, in prep.); brief descriptions are provided in the following sections. Geophysical data are used to focus on a particular candidate for the deep crustal or upper mantle suture. Each map was modified for this report by eliminating the Griscom-Halvorson color scale of the original plates and half of the original contours before reduction to a scale of approximately 1:2,000,000.

INTERPRETATION OF GRAVITY DATA

Figure 2 is an isostatic residual gravity map of eastern Oregon. A standard Airy-Heiskanen model was used

in data reduction, with density of topography 2,670 kg per cubic m, standard crustal thickness at sea level 25 km, and crust-mantle density contrast 400 kg per cubic m. The map is based on about 4,730 gravity stations obtained from Oregon State University (Lillie, 1977), the U.S. Geological Survey (Plouff, 1976, 1977, 1984, 1987), Griscom and Conradi (1975), and the National Geophysical Data Center. Structural interpretations from the gravity data are shown in Figure 3. Detrital and volcanic rocks range in density from 1,500 to 2,500 kg per cubic m, whereas massive basalt flows may have densities as high as 3,200 kg per cubic m. Long-wavelength anomaly sources are mostly concealed beneath the Miocene and younger cover, and there is little subsurface geologic information to assist in the interpretation.

Many prominent high-amplitude negative anomalies are clearly due to low-density sedimentary and volcaniclastic deposits, most located in fault-bounded alluviated basins or calderas (Griscom and Halvorson, 1994). Other, less prominent lows are believed to be due to relatively low-density granitic plutons concealed in the subsurface. Anomaly lows associated with the Steens and Logan Valley calderas are large enough to appear on small-scale regional maps (e.g., Riddihough and others, 1986).

Some anomaly highs in the northern part of the area are possibly caused by relatively high-density mafic plutons. The arcuate gravity high (greater than 24 mGal) near the northeast corner of the map coincides in part with exposures of the mafic Sparta complex (Walker and MacLeod, 1991). The high (greater than 24 mGal) area to the south may reflect an ultramafic complex under the Huntington Formation, a Triassic volcanic arc (Walker and MacLeod, 1991), or, alternatively, a concealed Mesozoic or Tertiary gabbro pluton.

Most of the linear boundaries are probably faults (Figure 3). Curvilinear belts of steep gradient in the southeast corner of the area embrace anomaly lows inferred to represent concealed plutons, possibly of Mesozoic age with peripheral contact-metamorphic rocks that may cause the curvilinear highs. The large, deep equidimensional low over Steens Mountain, in the southwestern part of the map, is alternatively interpreted as a caldera, granitic pluton, or sedimentary basin (Gettings and Blank, 1974), although the caldera interpretation is currently favored (Blank, oral commun., 1999). Interbedded tuff and arkose exposed along the eastern flank of Steens Mountain (Evans, unpub. mapping, 1995, Fields and V Lake 7.5-minute quadrangles) suggest a combined caldera and granitic pluton model. The broad low extending northerly along long 118ºW. from the Long Ridge caldera at the Oregon-Nevada state line (Rytuba and McKee, 1984) may be the expression of a concealed Miocene pluton.

Five first-order regional density boundaries—four with northeasterly trends—are expressed by gradients on the flanks of the longer wavelength anomalies (Figure 3). According to Griscom and Halvorson (1994), the four northeast-trending major boundaries are extensions of prelate Cenozoic upper crustal zones that transect the Cascade Range to the southwest (Blakely and Jachens, 1990). The northernmost two boundaries appear to relate in part to Tertiary uplift of the Blue Mountains, possibly beginning in Eocene or earliest Oligocene (Walker, 1990), which exposed Mesozoic basement rocks and truncated structures associated with the western SRP and the Oregon-Idaho graben. The major boundary extending north-south just east of long 118ºW. may be related to middle Miocene structures and parallels, in part, the western margin of the middle Miocene Oregon-Idaho graben (Figure 1). North-trending gravity boundaries and linear gravity highs within the graben are associated with mapped fault zones. Average isostatic anomaly values over the graben are about 5 to 10 mGals higher than gravity levels to the west. This difference may result from the presence of flood basalts and mafic intrusive rocks beneath and within the graben fill (Griscom and Halvorson, 1994; Cummings and others, 1996).

INTERPRETATION OF MAGNETIC DATA

Aeromagnetic surveys used in this study are documented in Boler (1978), U.S. Geological Survey (1972, 1984), High Life Helicopters and QEB, Inc. (1981), and Bond and Zietz (1987). Figure 4 is a map of residual total-intensity aeromagnetic anomalies over southeastern Oregon after the removal of the International Geomagnetic Reference Field and reduction to the pole. The latter process assumes normal or antinormal induced magnetization and computes the field that would be observed at the geomagnetic north pole (vertical induction). Interpretation of the magnetic map is here restricted to main features; interpretation of the numerous high-frequency (short spatial wavelength) anomalies that characterize most volcanic terrain, including southeastern Oregon, is beyond the scope of this report. In general, mafic volcanic rocks such as basalt and andesite are strongly magnetic and produce intense magnetic anomalies; however, in places along the western margin of the Oregon-Idaho graben, magnetite-rich rhyolites also have very strong magnetic signatures. Volcanic rocks chilled rapidly from a melt may possess a large remanant magnetization in addition to induced magnetization. In Tertiary rocks, this remanence is generally near-normal or near-antinormal

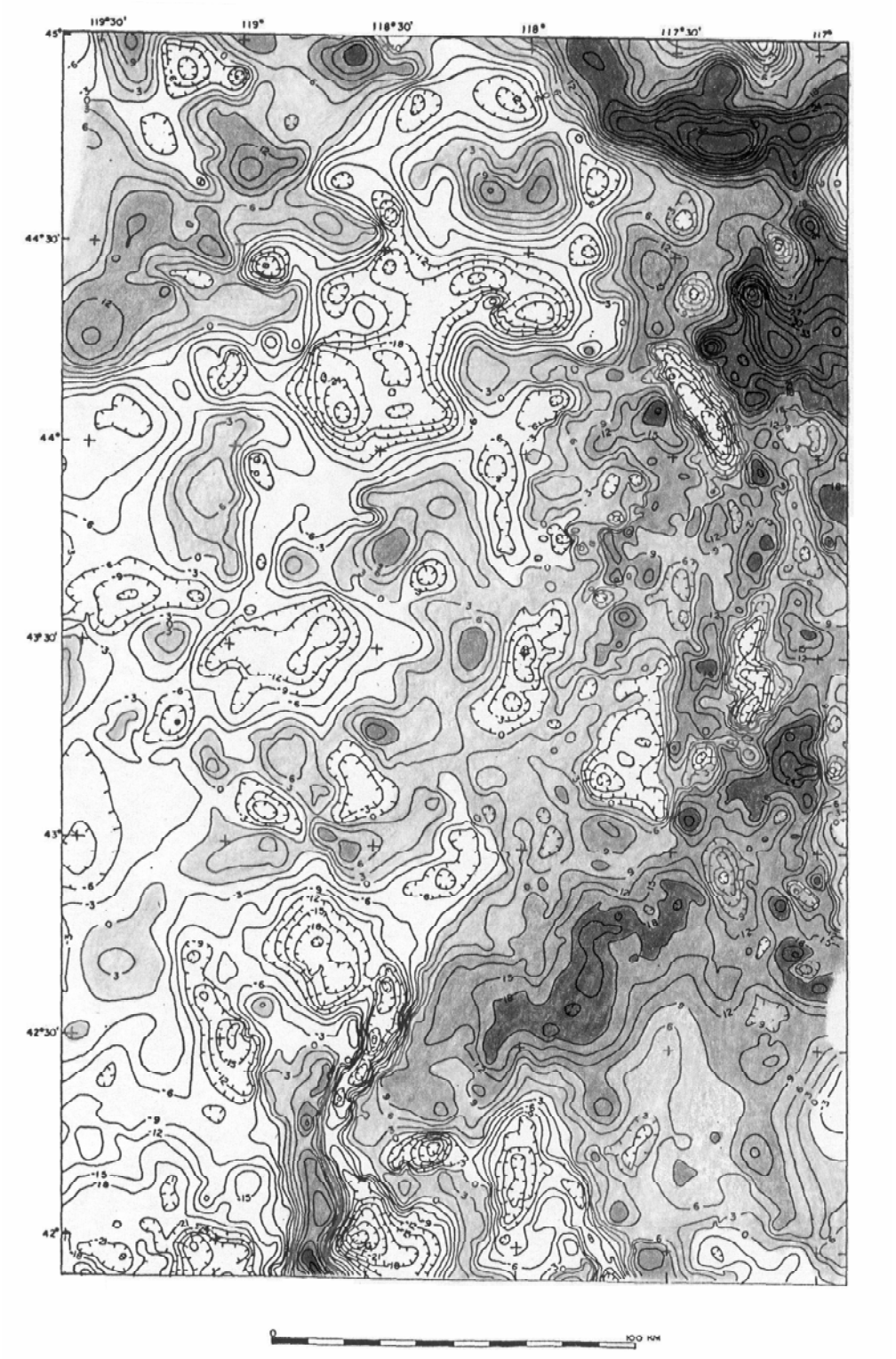

Figure 2. Isostatic residual gravity anomaly map of southeastern Oregon and parts of southwestern Idaho and north-central Nevada. Contour interval 5 milligals (mGal). Black represents values >18 mGal; dark gray, 9 to 18 mGal; light gray, 0 to 9 mGal; white, <0 mGal. Scale approximately 1:2,000,000.

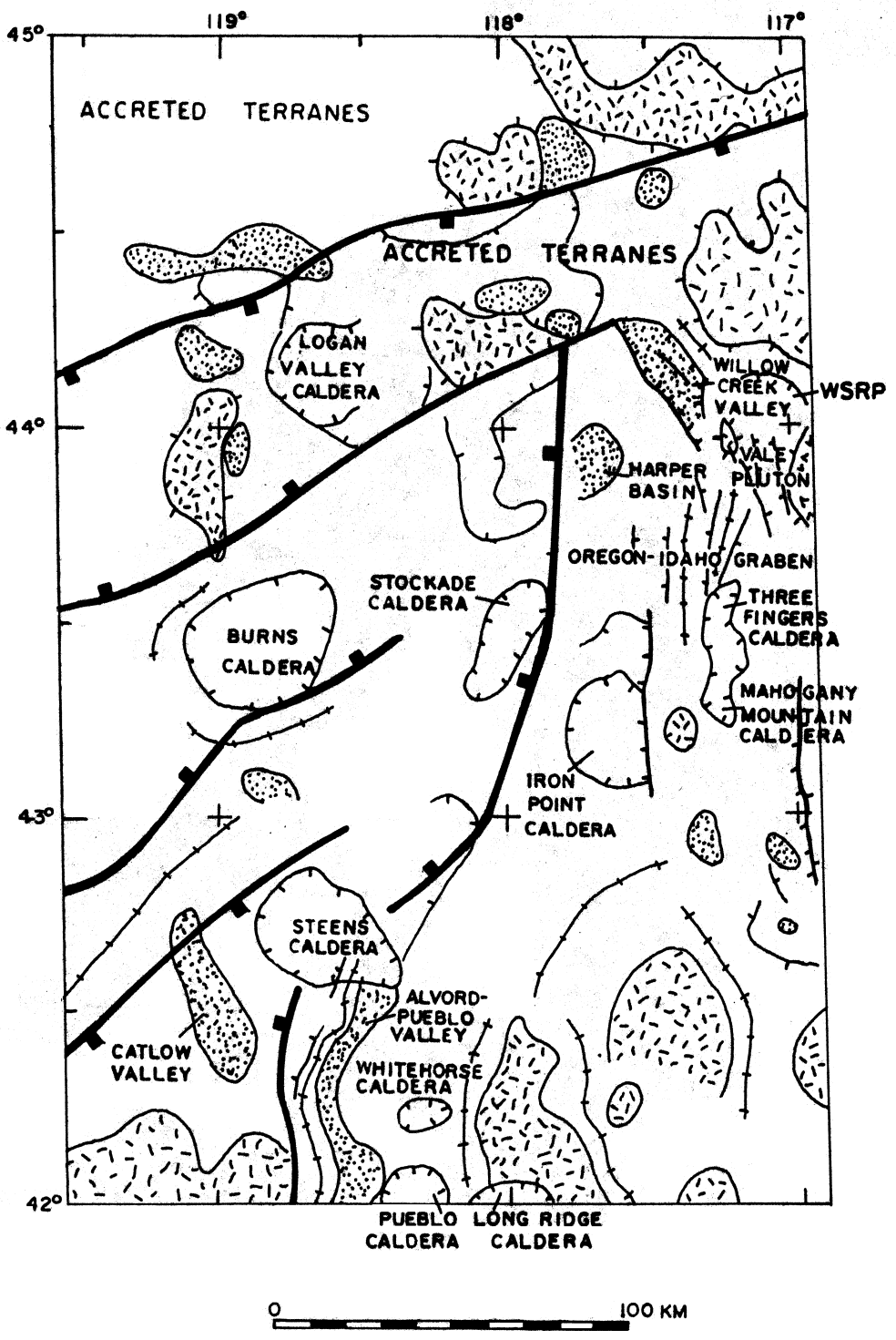

Figure 3. Structural elements interpreted from isostatic residual gravity map (Figure 2). Heavy lines indicate inferred major deep crustal density boundaries, with square teeth on lower-density side (Griscom and Halvorson, 1994). Areas of thick pyroclastic fill associated with calderas are enclosed by hachured lines; areas of thick basin fill bounded by basin-range faults are stippled; unexposed plutons are shown by dashed pattern, with widely spaced hachures pointing outward for those of high density. Selected faults are shown by thin lines with hachures on downthrown side; axes of density highs, by two-sided hachured lines; areas of relatively thick, relatively dense volcanic rocks, by pattern of V's. WSRP, western Snake River Plain. Scale approximately 1:2,000,000.

with respect to the present field, unless rotated subsequent to emplacement. Some sharply negative anomalies on Figure 4 probably are attributable to sources whose magnetization is predominantly antinormal remanence. Weakly magnetic rocks, such as sedimentary strata, are essentially "transparent," and are commonly associated with anomaly depressions or with areas of relatively smooth magnetic field with long-wavelength anomalies.

Another way to display the magnetic data is in the form of a magnetic potential map (Figure 5). Magnetic potential maps are prepared from data that are first reduced to the pole, then integrated to obtain the scalar potential; in some cases, the potential is multiplied by a constant to obtain an equivalent gravity anomaly, resulting in a "pseudogravity" map. For a discussion of the method see Blakely (1995). The transformation from magnetic map to magnetic potential map acts as a filter in that short wavelength anomalies are relatively suppressed and long wavelength anomalies enhanced, as in an upward continuation filter. Thus this transformation emphasizes the contribution of deep-seated magnetic rock masses.

The magnetic potential map (Figure 5) shows a broad belt of highs trending northeast across the entire map. High values in the northeast are associated spatially with the Oregon-Idaho graben and reflect the thick flood-basalt section inferred to underlie the graben and numerous mafic intrusions mapped in or inferred to underlie the graben.

Figure 6 shows the interpretations of the aeromagnetic (Figure 4) and magnetic potential data (Figure 5). Griscom and Halvorson (1994) attributed most prominent magnetic highs to concealed plutons associated with calderas at the south margin of the magnetic map near the Long Ridge caldera and near lat 43ºN. along the east border of the map in the southern part of the Oregon-Idaho graben. A few areas of exposed highly magnetic mafic volcanic rock produce magnetic highs with a "bird's-eye maple" anomaly pattern. Circular "bull's-eye" magnetic lows, especially those that appear to interrupt linear magnetic features, are interpreted to be the magnetic expression of calderas, presumably filled with weakly magnetic silicic volcanic and sedimentary rocks. Most linear boundaries are interpreted as faults or fault zones, which are shown as thinner lines on Figure 6 (see caption). The largest pluton in the southeastern corner of the area may be of Mesozoic age. The row of four small interpreted plutons within the graben near lat 43ºN. may be of Miocene age and associated with graben volcanism. Magnetic lineations trending N. 20º W. in the center of Figure 6 are approximately colinear with the northern Nevada rift (Stewart and others, 1975; Zoback and Thompson, 1978; Zoback and others, 1994). Magnetic lineaments extending southeast die out a little to the north of the Oregon-Nevada state line but appear heading towards an intersection with the state line at about long 117º35'W., close to where the northern Nevada rift intersects the state line.

Five first-order, long spatial wavelength magnetic-domain boundaries inferred from the magnetic-potential map trend northeasterly across the study region. These boundaries closely parallel and are nearly orthogonal to the predominant trends of the Oregon-Idaho graben and western SRP and locally coincide with three major density discontinuities inferred from the gravity data (Figures 2 and 3), suggesting common origin as major crustal block margins. The longest element of the magnetic set trends northeast from about lat 43º30'N. and truncates mapped structures at the northwestern end of the western SRP and the northern end of the Oregon-Idaho graben; otherwise, no displacement of mid to late Cenozoic structures is evident. Thus, the magnetic domain boundaries appear to be older than middle Miocene, although likely reactivated in the northeast in the late Tertiary to accommodate extension related to development of the Oregon-Idaho graben and the western SRP. However, they could be younger than an early Tertiary stage of east-west extension (Gromme and others, 1986), and the blocks may be extended Mesozoic crust. The two remaining major structures inferred from the magnetic data, both north-trending (Figure 6), are in part associated with the margins of the Oregon-Idaho graben.

INTERPRETATION OF AERORADIOACTIVITY DATA

The aeroradiometric surveys used to construct the aeroradioactivity maps (Figures 7-9) were flown in conjunction with the National Uranium Resource Evaluation (NURE) program (Bernardi and Robbins, 1982; Geodata International, Inc., 1980a; 1980b; High Life Helicopters, Inc. and QEB, Inc., 1981). Figures 7 to 9 present maps of percent potassium (K), parts per million (ppm) equivalent U (eU), and ppm equivalent Th (eTh) detected by the NURE surveys over eastern Oregon. Comparisons of these radioactivity maps with a geologic map of Oregon (Walker and MacLeod, 1991) show that broad radiation anomalies or anomaly domains have characteristic lithologic associations. Large areas of basalt and andesite in the northwestern part of the study area are, for example, low in U, Th, and K. Higher K concentrations occur in the south and east and correlate with ash flows and associated rhyolitic volcanic rocks of middle Miocene age (Figure 7). South of lat 43º30'N., the lower concentrations of K are associated either with late Miocene or

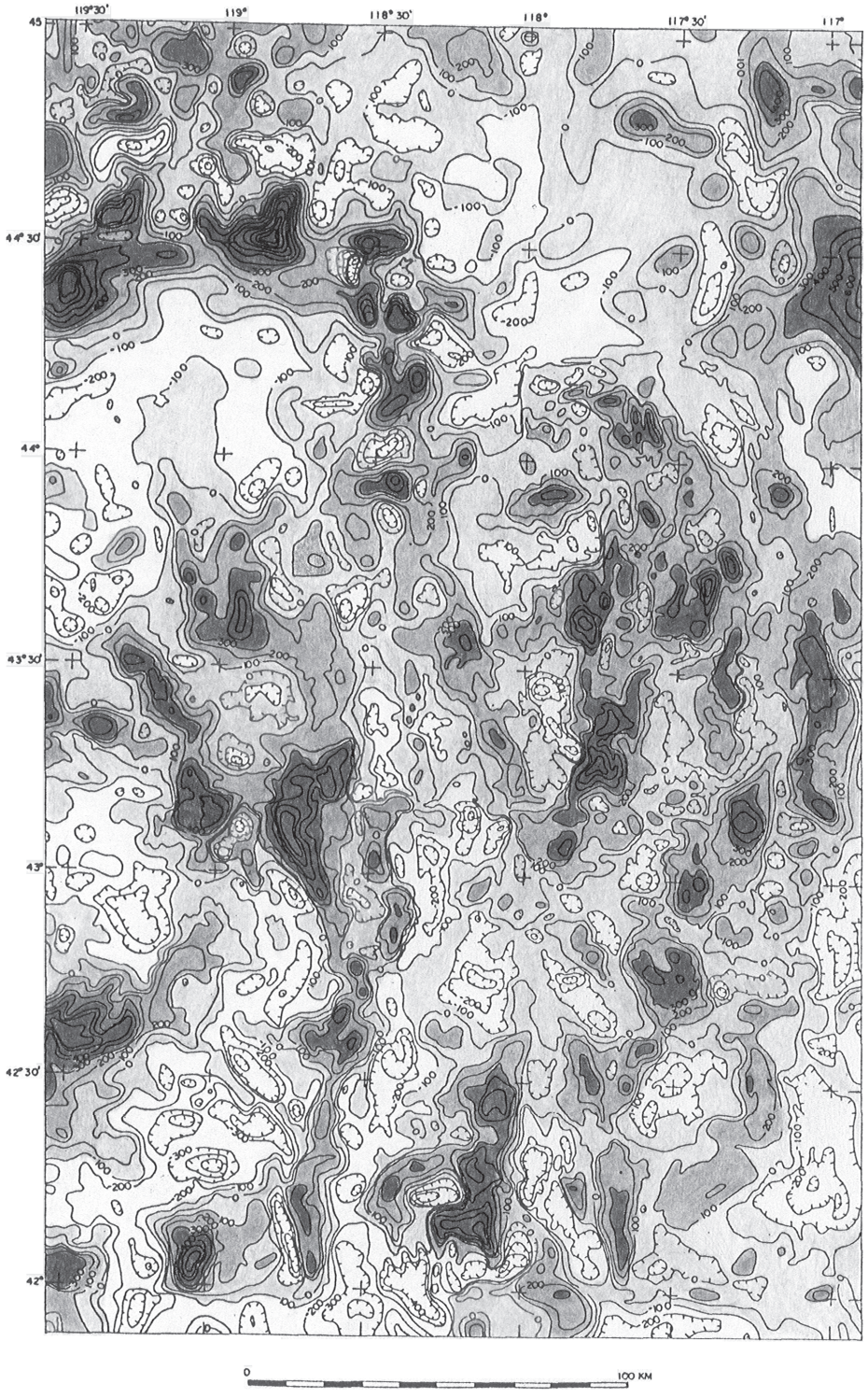

Figure 4. Map of residual total-intensity aeromagnetic anomalies reduced to the pole and draped at 2,000 feet (610 m) above ground for southeastern Oregon and parts of southwestern Idaho and north-central Nevada. Black represents magnetic intensities >300 nanoteslas (nT); dark gray, 100 to 300 nT; light gray, -100 to 100 nT; white <-100 nT. Scale approximately 1:2,000,000.

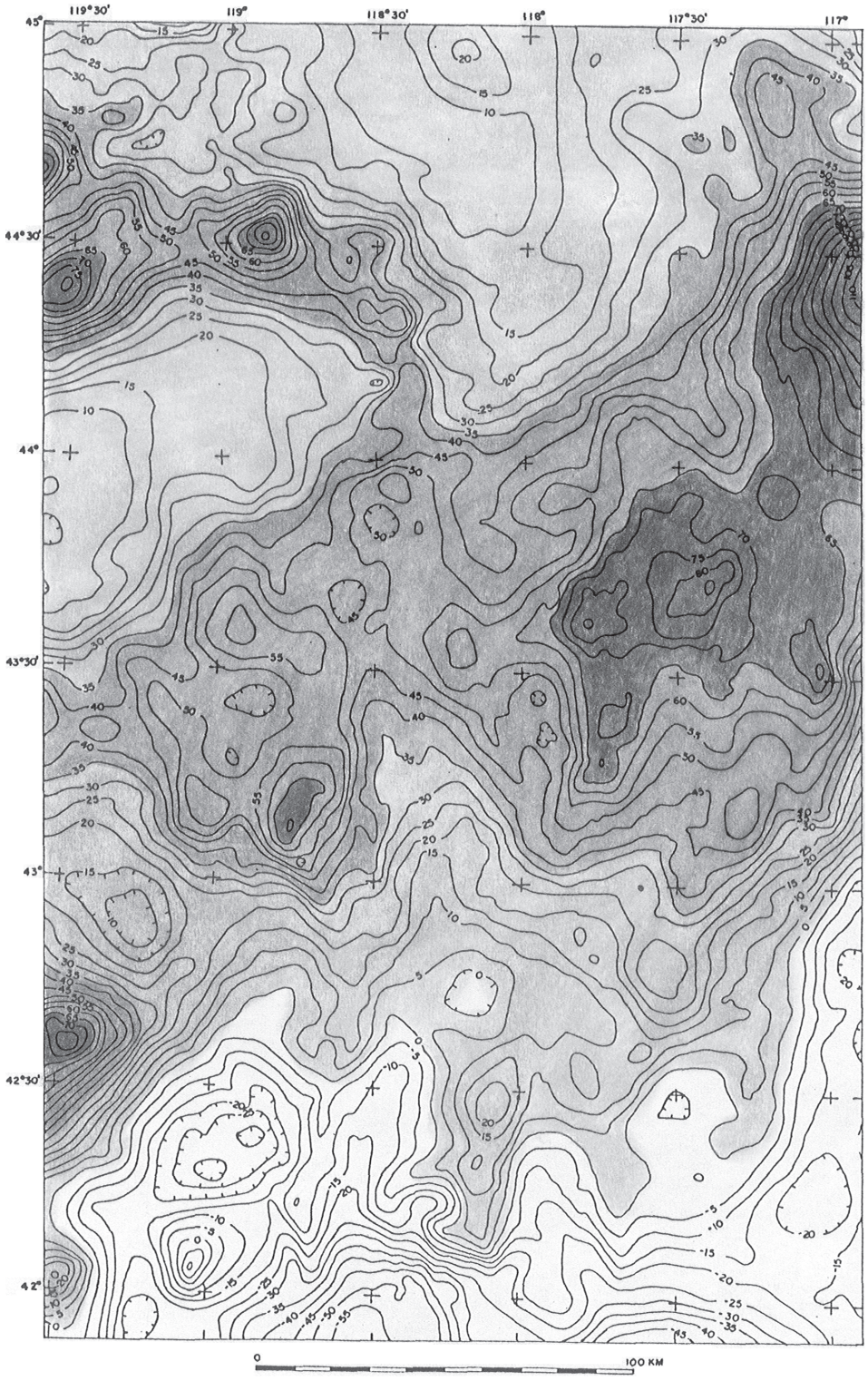

Figure 5. Magnetic potential map of southeastern Oregon and parts of southwestern Idaho and north-central Nevada. Contour interval 5 nanoteslas x square meters (nTm^2). Black represents values >65 nTm^2; dark gray, 35 to 65 nTm^2; light gray, 0 to 35 nTm^2; white, <0 nTm^2. Scale approximately 1:2,000,000.

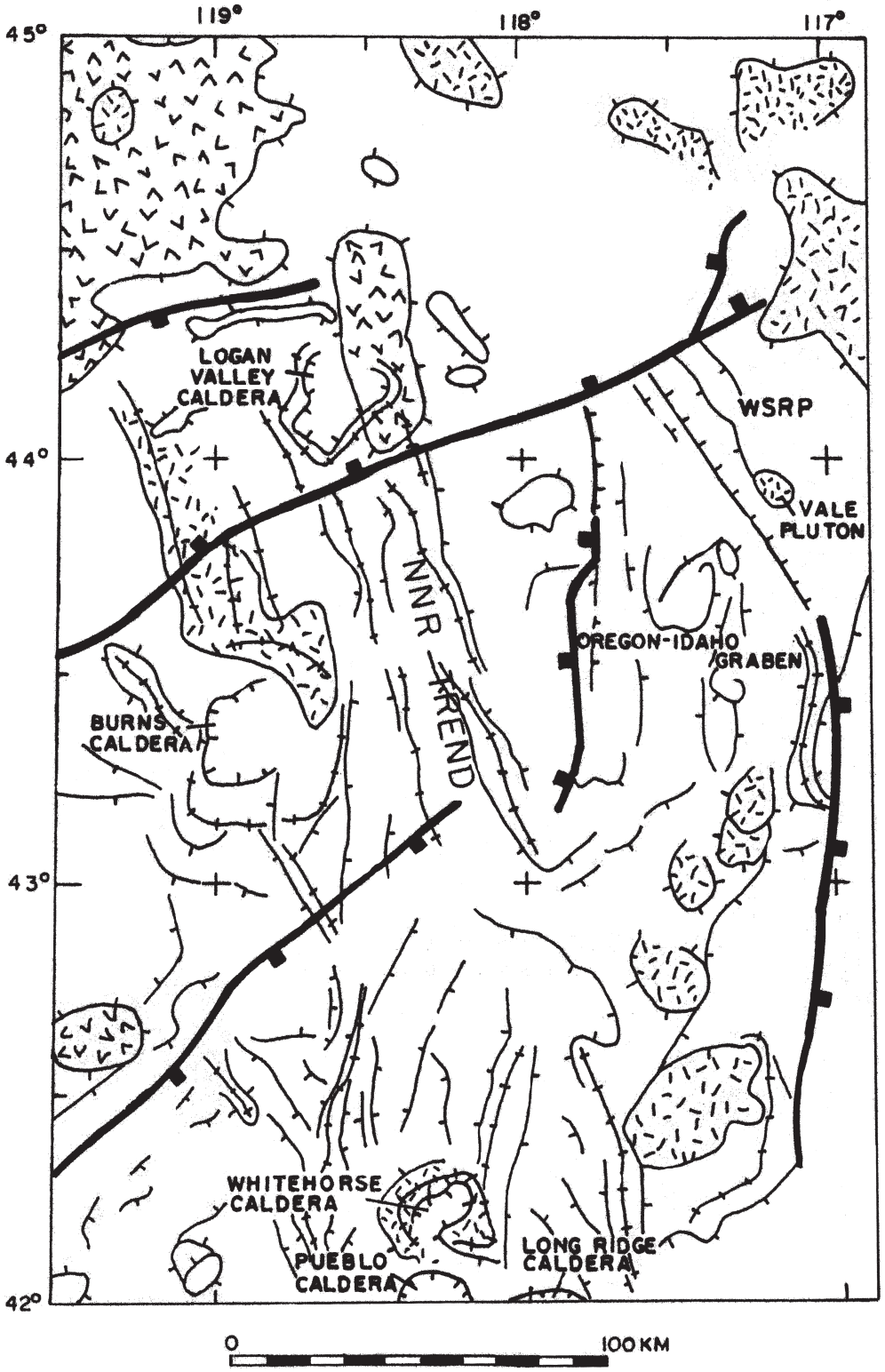

Figure 6. Structural elements interpreted from magnetic residual total-intensity and magnetic potential maps (Figures 4 and 5). NNR TREND, trend of northern Nevada rift. Other symbols same as shown in Figure 3. Scale approximately 1:2,000,000.

younger basalt flows, or with early to middle Miocene Steens Basalt. In places, Steens Basalt tends to be associated with high potassium values, evidently because of widespread younger ash flow cappings.

The eU and eTh (Figures 8 and 9) maps, like the K map (Figure 7), show a general increase of radioactivity to the southeast. The highest concentrations are just east of long 117ºW. where K is as much as 2.45 percent, eU is as much as 3.4 ppm, and eTh is as much as 16 ppm. Instrumental neutron activation analyses for Th concentration in basalt and rhyolite from the Oregon-Idaho graben and from areas west of Westfall Butte near Beulah Reservoir (Cummings, unpub. data, 1996) are consistent with above concentration estimates.

The eU and eTh data also show a linear belt of high concentrations trending N. 70º W. across the centers of the maps (Figures 8 and 9). This belt can also be seen, but less clearly, in the K map (Figure 7). The belt appears to correlate with a row of middle Miocene and younger vents that have erupted siliceous volcanic rocks with enhanced concentrations of U, Th, and K (Figures 7-9). This trend was noted informally by Mark L. Ferns (Oregon Department of Geology and Mineral Industries, Baker City), his Stockade Mountain trend, and corresponds to a zone of intense rock alteration and gold mineralization.

Because U, Th, and K tend to be associated with each other and to vary similarly in geologic materials, element ratios of their concentrations are often more informative than the absolute concentrations of the individual elements because the ratios tend to be independent of variations in lithology. Figure 10 is a map of the ratio K/eTh for the study area. Southeastern Oregon consists of two ratio domains: a relatively high-K/eTh domain to the northwest and a largely low-K/eTh domain to the southeast. This result appears to be independent of rock units in the region. Both K and eTh increase to the south and east, but eTh more rapidly, a distribution emphasized by the ratio map. Thus the two domains on the K/eTh map are predominantly an enhanced expression of eTh concentration. The boundary, drawn along the southeastern flank of the northeast-trending K/eTh ridge across the middle of the study area at approximately the K/eTh = 0.30 contour (Griscom and Halvorson, 1994), separates two volcanic terranes that have a distinctive mean compositional difference in the trace element Th. This is a very significant result because it implies a major crustal or mantle source difference across the boundary. The relatively high eTh in the southeastern part of Oregon (Figure 9) is continuous with a region of very high eTh concentration in the portion of southwest Idaho near the Oregon-Idaho state line not far from exposures of granitic rocks (Figure 9). These relations and the expected low K/eTh ratio for granitic rocks (Darnley and Ford, 1987) suggest that the domain of low K/eTh occurs in rocks with sources in a continental crust. Therefore, the domain boundary at the K/eTh = 0.30 contour may be regarded as the "surface trace" of the northwestern margin of continental crust under eastern Oregon.

In view of the extensive dispersal of lithologies that inevitably results in volcanic terrains subjected to lava and pyroclastic eruptions as well as erosional processes, the concept that representative samples of the uppermost few centimeters (perhaps 0.5 m for surficial materials) can delineate a deeply buried continental margin may seem counterintuitive at best. But the K/eTh domain boundary is distinct, if somewhat diffuse, and its trend clearly transects the study area northeasterly. Moreover, correlations with other geophysical and geochemical features, discussed below, suggest that this boundary indeed reflects significant differences in crustal and subcrustal lithologies.

Figure 11 is a composite of principal structural elements interpreted from gravity and magnetic data (Figures 3 and 6), with the addition of radiometric features from the K/eTh ratio map (Figure 10). Also shown are geochemical features, as discussed in the following section.

GEOCHEMICAL EVIDENCE

Superimposed on the geophysical features in Figure 11 are the boundaries of tracts favorable for the presence of hot-spring Au-Ag deposits and associated epithermal deposits and for volcanogenic U deposits (Peters and others, 1996). The western limits of these two tracts are near the density, magnetic, and K/eTh boundaries in the center of the figure. Nowhere are the tracts present more than a few kilometeres west of the K/eTh boundary except in the vicinity of Westfall Butte, where this boundary apparently is interrupted by northeast-trending structures.

The tract boundaries are based on multidisciplinary criteria. For the hot-spring Au-Ag deposits, seven sets of data were used: (1) geochemistry, (2) surface mineralogy, (3) rock alteration, (4) regional structure as derived from (5) surficial geology, (6) remote sensing (thematic mapper), and (7) geophysical anomalies on the gravity, magnetic, and radiometric maps discussed above. Thus this tract boundary was not determined completely independently of the first-order structural boundary. However, the first six data sets were considered to be of paramount importance.

For volcanogenic U deposits, three criteria were used: (1) locations of alkaline to peralkaline silicic igneous rocks from the surface to 1 km depth, (2) known U, Mo,

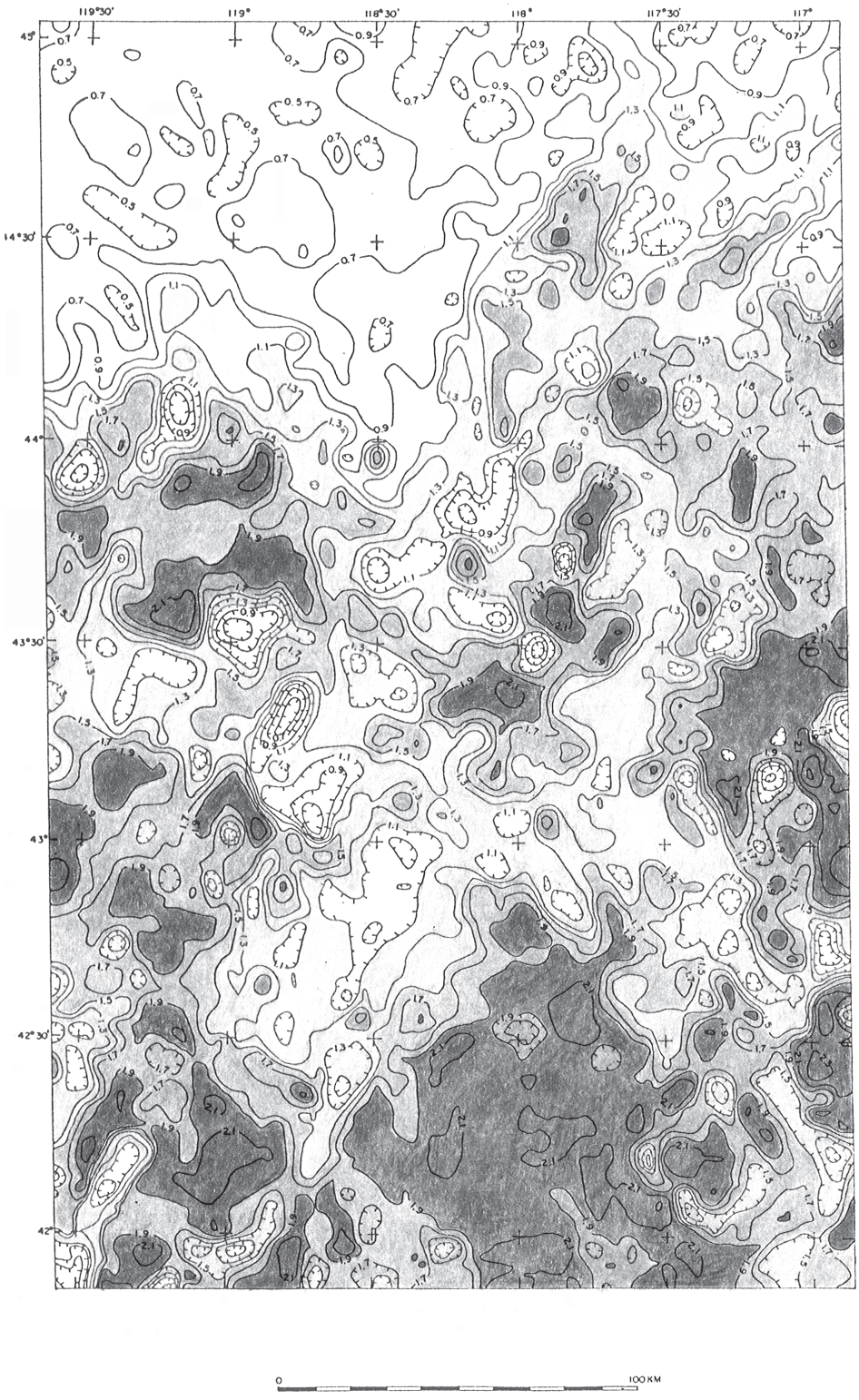

Figure 7. Aeroradioactivity map of percent potassium (K), southeastern Oregon and parts of southwestern Idaho and north-central Nevada. Contour interval 0.2 percent K. Black represents values >1.9 percent; dark gray, 1.5 to 1.9 percent; light gray 1.1 to 1.5 percent; white, <1.1 percent. Scale approximately 1:2,000,000.

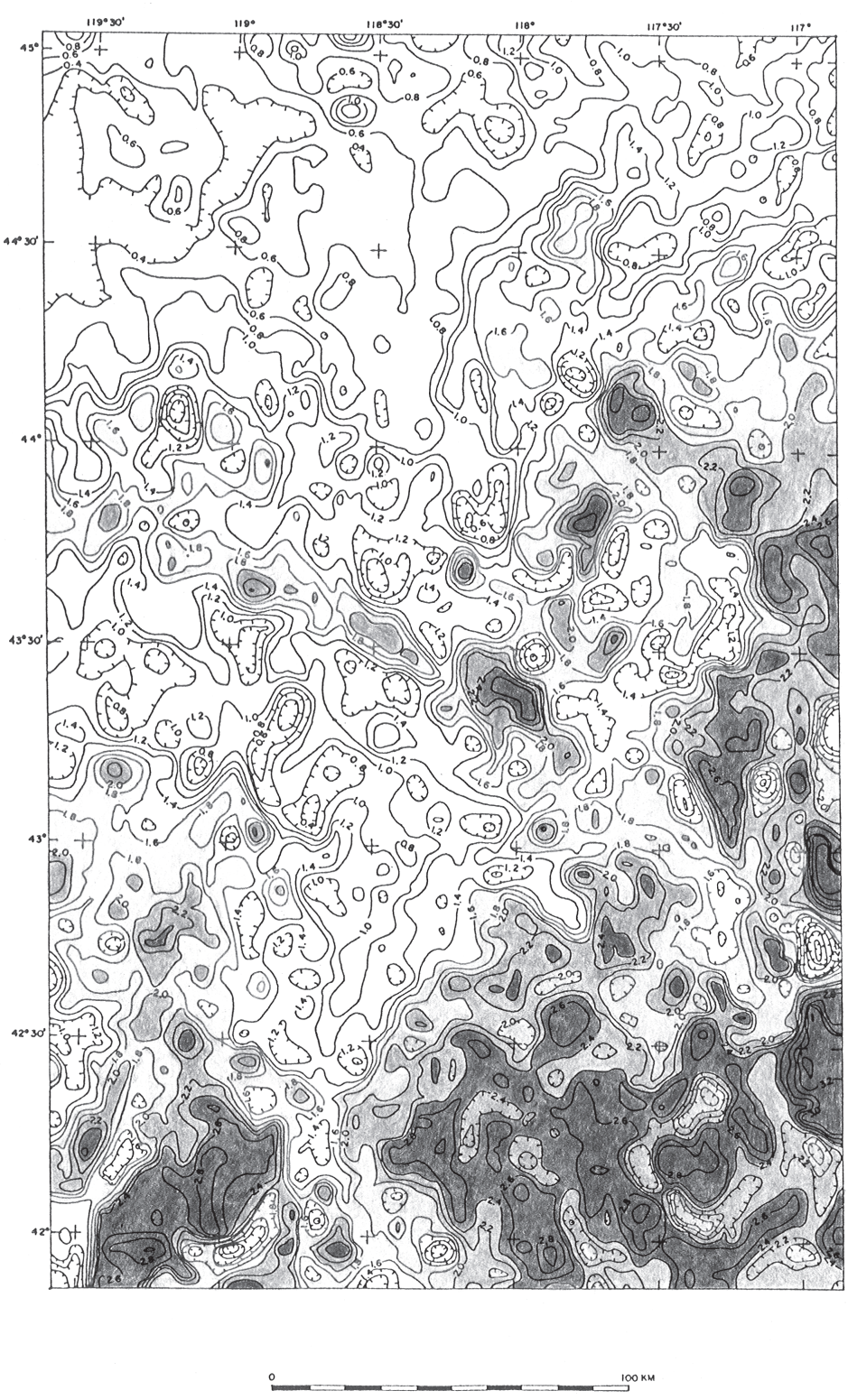

Figure 8. Aeroradioactivity map of parts per million (ppm) equivalent uranium (eU), southeastern Oregon and parts of southwestern Idaho and north-central Nevada. Contour interval is 0.2 ppm U. Black represents values >2.4 ppm; dark gray, 2.0 to 2.4 ppm; light gray, 1.6 to 2.0 ppm; white, <1.6 ppm. Scale approximately 1:2,000,000.

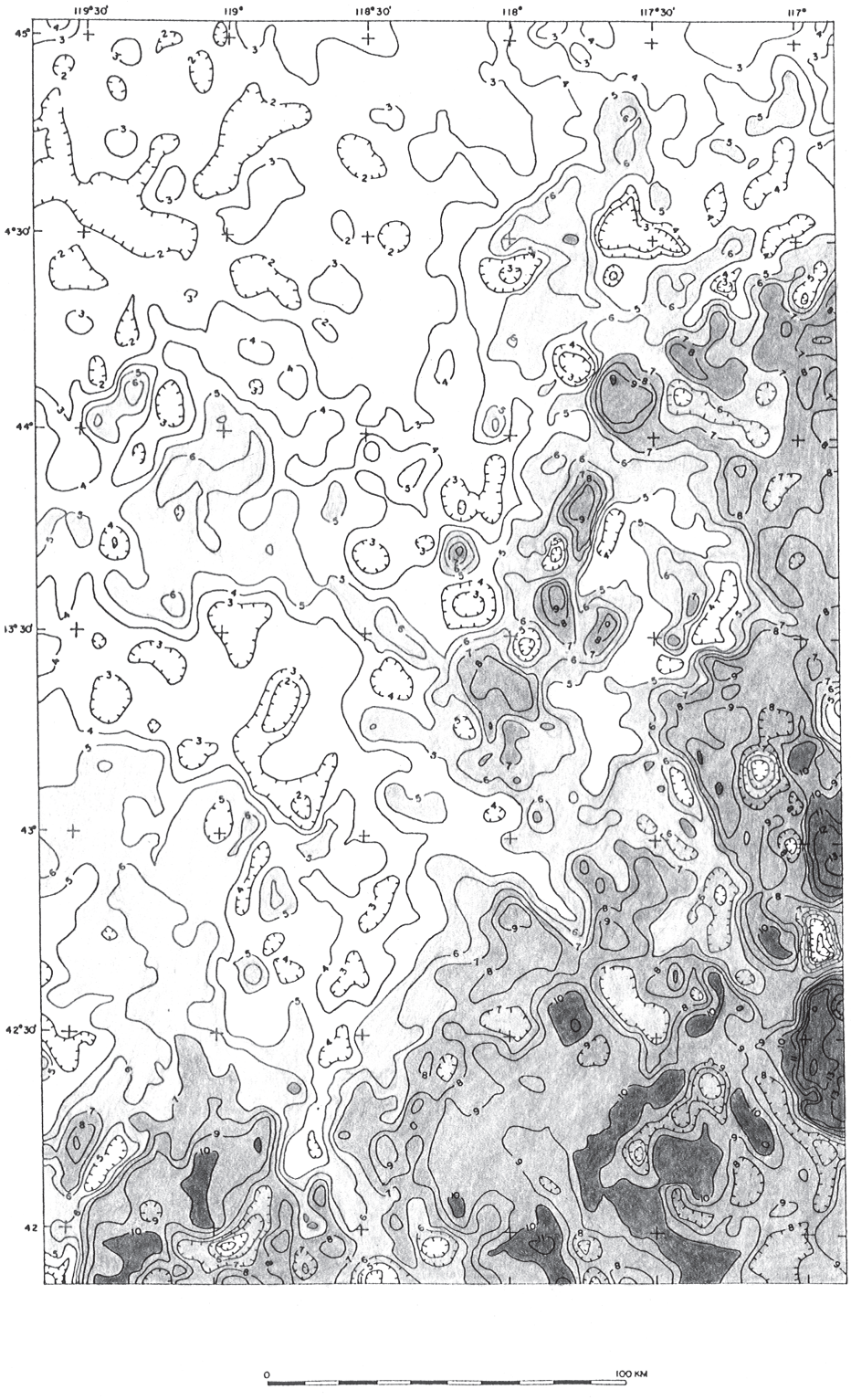

Figure 9. Aeroradioactivity map of ppm equivalent thorium (eTh), southeastern Oregon and parts of southwestern Idaho and north-central Nevada. Contour interval is 1 ppm Th. Black represents values >10 ppm; dark gray, 7 to 10 ppm; light gray, 5 to 7 ppm; white, <5 ppm. Scale approximately 1:2,000,000.

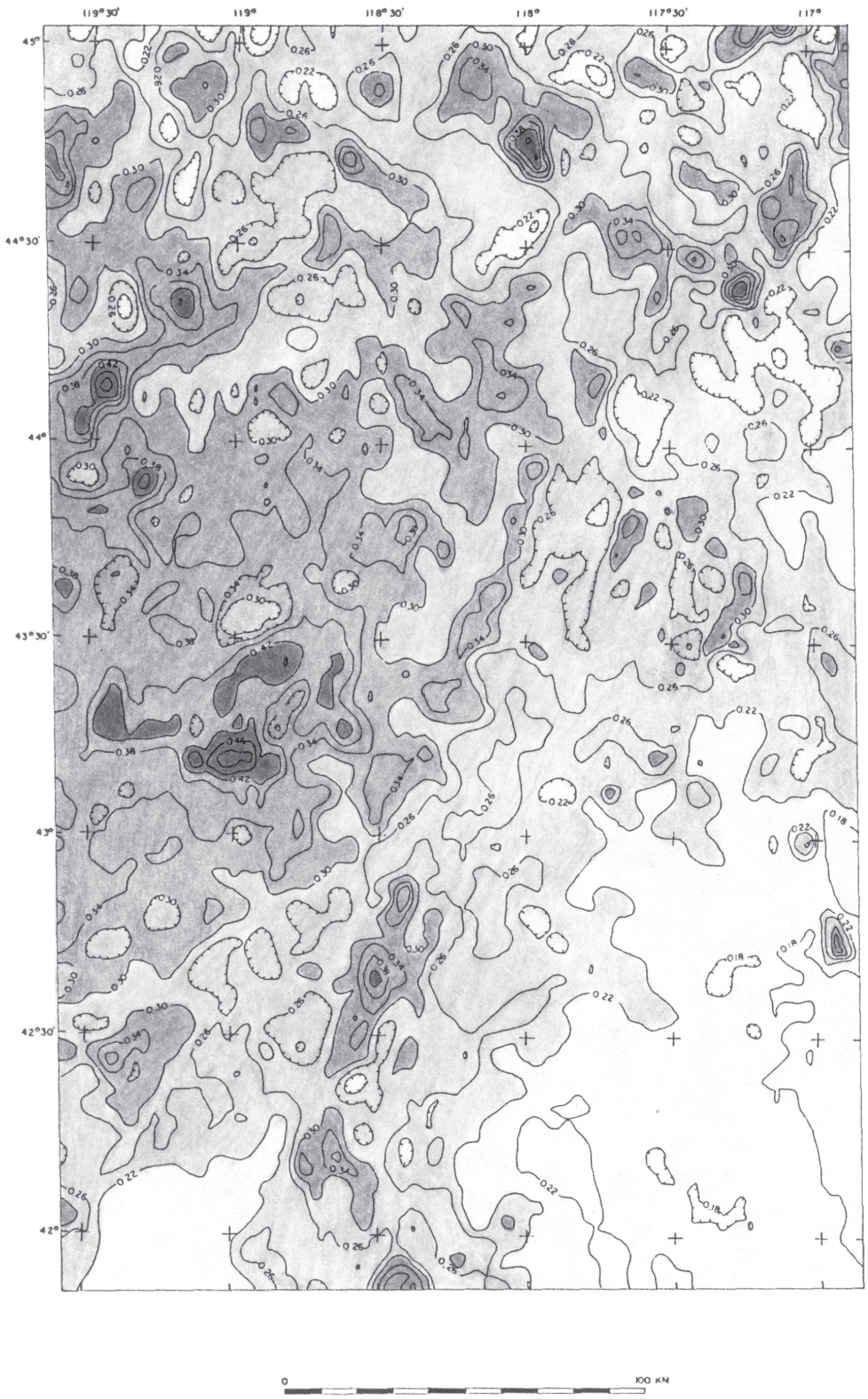

Figure 10. Map showing the ratio percent K divided by ppm eTh, southeastern Oregon and parts of southwestern Idaho and north-central Nevada. Contour interval 0.04. Black represents values >0.42; dark gray, 0.30 to 0.42; light gray, 0.22-0.30; white, <0.22. Scale approximately 1:2,000,000.

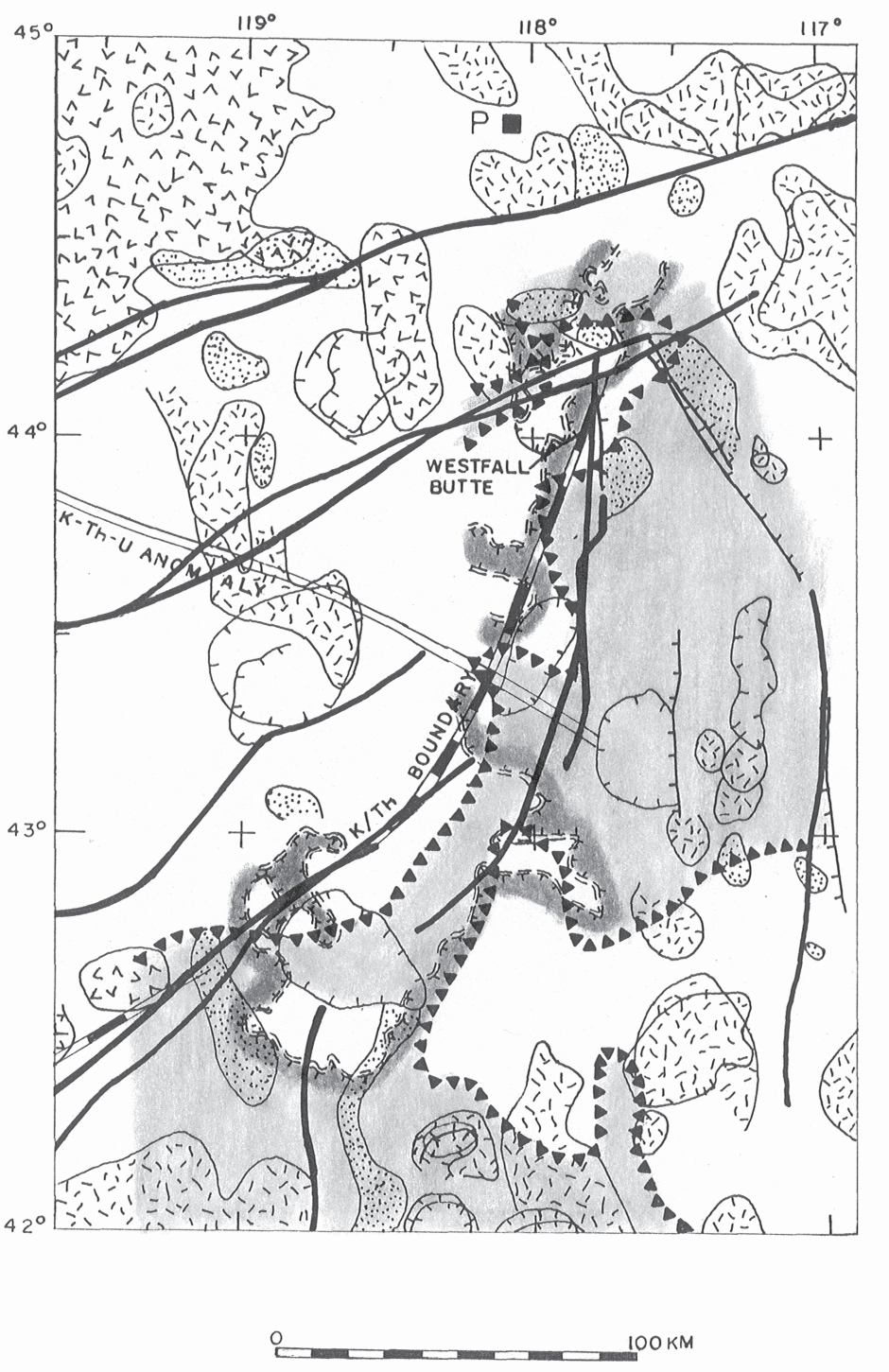

Figure 11. Summary of geologic, geophysical, and geochemical features of southeastern Oregon and parts of southwestern Idaho and north-central Nevada. Geologic, density, and magnetic features compiled from Figures 3 and 6. Aeroradiometric features include: (1) K/eTh = 0.30 boundary from Figure 10 and (2) axis of percent K, eTh, and eU anomaly from Figures 7-9. Geochemical features include: (1) external boundary of tract favorable for occurrence of hot-springs Au and Ag deposits shown by solid triangles with apexes of triangles pointing into favorable tract, colored light gray and (2) western boundary of tract favorable for occurrence of volcanogenic uranium deposits, shown by double dashed line with hachures on side facing tract, dark gray on tract side of boundary. P, solid square, is estimated projection of continental-oceanic suture on extended cross section of Leeman and others (1992).

and Hg mineralization or areas with more than 1.4 ppm in eU, and (3) known U prospects and occurrences and associated Hg deposits. Inasmuch as a radiometric map (Figure 8) was used for one of the three criteria, this tract was likewise not delimited completely independently of geophysical data. It should be noted that aeroradiometric data alone would not have served to determine the tract boundary, chiefly because of the wide traverse spacing and the variable terrain clearance of the surveys.

The close spatial relation of tract limits to the K/eTh boundary and associated density and magnetic features strongly suggests that a northeast-trending geophysically defined first-order structure in some way influences localization of regional hydrothermal activity and mineralization and that the crust to the southeast of these structures has characteristics more favorable for hot-spring Au-Ag and volcanogenic U deposits, than crust to the northwest. The gneissic xenoliths in volcanic rocks in the Oregon-Idaho graben, quartzite xenoliths in the metavolcano-plutonic complex of the northern Pueblo Mountains, and the relatively high eU and eTh concentrations in southeastern Oregon, all suggest that the basement difference is compositional, that is, the difference between continental (southeast) and oceanic (northwest) crust, with the implication that the two types of crust are underlain by continental and oceanic upper mantle, respectively.

DISCUSSION

The southwestern segment of the suture between cratonic North America and the Mesozoic accreted terranes, as inferred from the gravity, aeromagnetic, and aeroradioactivity data (Figures 3, 6, and 11), trends N. 55º E. from about lat 42º30'N., long 119º30'W., to about lat 43ºN., long 118º30'W. From there, the boundary trends N. 20º E. to about lat 44º15'N., long 117º50'W. Based on a density boundary (Figure 2), the suture may extend in the subsurface for as much as 50 km north of the northern terminus of the K/eTh boundary. It is unclear whether the approximate trace, largely drawn on the K/eTh = 0.30 contour, consists of intersecting structures or is one continuous arcuate zone of structures. If the K/eTh boundary corresponds closely to the contact of the craton and accreted terranes, the Oregon-Idaho graben could lie entirely on the continental side of the K/eTh boundary. The small volcanic center at Westfall Butte is just west of the K/eTh boundary, and therefore would probably overlie accreted terrane, consistent with the occurrence of radiolarian chert and argillite xenoliths in the volcanic rocks there. The surface trace of the suture as drawn in Figure 11 would be close to or west of most of the Neogene volcanic samples that have transitional Sr and Nd isotopes (Leeman and others, 1992).

Figure 12 shows the K/eTh line of the present study in relation to key regional structures and the western Idaho suture zone. The line of cross section of Leeman and others (1992) is also shown. Extending their line of cross section farther into eastern Oregon, and assuming 150 km of eastward translation of the western Idaho suture zone during the Sevier orogeny, and vertical dip of the suture zone, the autochthonous part would intersect the extended cross section at a point P as indicated on Figure 11. This point is located in Baker Valley at lat 44º49'N., long 118º5'W., or about 80 km north and 25 km west of the northern end of the K/eTh boundary. If the average dip of the autochthonous suture is easterly, as indicated on the cross section of Leeman and others (1992), the projection of its autochthonous segment could be considerably farther northeast.

The minimum east-west separation between the western Idaho suture zone and the K/eTh boundary/suture, as measured along lat 44ºN. near the northern end of the boundary, is about 125 km (Figure 12), suggesting that if the K/eTh boundary indeed reflects the autochthonous suture, an easterly dip of the upper segment is required to match the 150 km of east-west translation suggested by Leeman and others (1992). If the suture dips eastward, as shown on cross sections of Leeman and others (1992), then the east-west separation is greater than 125 km. It is unclear what portion of this distance can be accounted for within the Oregon-Idaho graben and the western SRP. Extension related to formation of these two grabens may include structures beyond the graben margins, such as the north-northwest-trending late Miocene to Pliocene and Quaternary faults with related basaltic volcanism in the Swede Flat quadrangle, 10 km southwest of the western SRP (Evans, unpub. mapping, 1994).

The maximum depth of gravity and magnetic sources adjacent to the K/eTh boundary and coincident or nearby gravity and magnetic boundaries may be estimated using the approximation of Smith (1959). If g_{max} = magnitude of the gravity anomaly and g_h = its horizontal gradient,

$$\text{depth to top of gravity source} \leq 0.86\, g_{max}/g_h.$$

Maximum depth calculations from seven points along density and magnetic potential boundaries (Figures 3 and 6) coincident with or near the K/eTh boundary range from about 7.54 to 20.8 km (Figure 13). If calculations are made using a constant of 0.65 for 2-dimensional sources, the depths would decrease by about 25 percent. The pattern of source depths along the several kinds of geophysical boundaries suggests that the subsurface suture may consist of a zone as much as 20 km wide.

The estimates of depths to anomaly sources support the alternative model rejected by Leeman and others

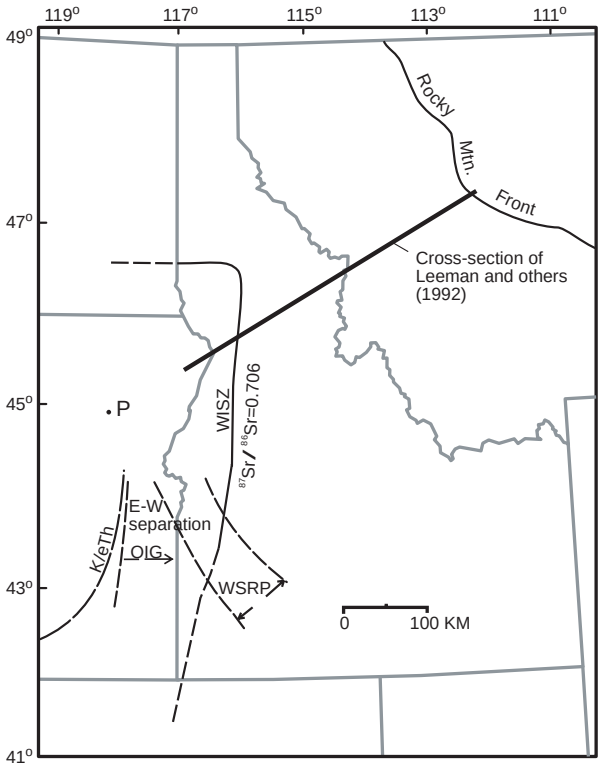

Figure 12. Map of eastern Oregon and adjacent parts of Washington and Nevada, and Idaho and adjacent parts of Montana, Wyoming, and Utah. Map shows geographic relations among the projection "P" of the autochthonous segment of the western Idaho suture zone inferred from an extended cross section based on the cross section of Leeman and others (1992); the $^{87}Sr/^{86}Sr = 0.706$ line, which coincides with the western Idaho suture zone (WISZ) north of the western Snake River Plain (WSRP); the K/eTh boundary; the minimum east-west separation at lat 44ºN. proposed for the oceanic-continental suture in this report; the Oregon-Idaho graben (OIG); and the Rocky Mountain Front.

(1992) that the the Sevier-age decollement cuts the crust rather than the mantle lithosphere (Figure 14). Overlap of continental and oceanic lithospheric mantle may occur if the autochthonous segment of the western Idaho suture zone decreases in dip to the east. This geometry would be consistent with accretion of the Wallowa-Seven Devils volcanic arc, the easternmost accreted terrane, to the continent in central Oregon (Lund, 1984; Ave Lallemant and others, 1980) and subsequent northward translation along a transpressive fault (Lund, 1984; Lund and Snee, 1988). Structural transition between the steeper and more gently dipping parts of the continental-oceanic boundary may not be as smooth as shown on Figure 14. A very gentle westward dip of the Sevier decollement and a shallow eastward dip of the suture zone at depth would allow for the coincidence of the Mesozoic 0.706 line and the Cenozoic 0.706 lines suggested by $^{87}Sr/^{86}Sr$ of Neogene basalts and rhyolites (Leeman and others, 1992).

SUMMARY

Leeman and others (1992) have proposed, on the basis of mass conservation from preliminary balanced cross sections and magma source regions inferred from $^{87}Sr/^{86}Sr$ and $^{143}Nd/^{144}Nd$ ratios, that shortening during the Sevier orogeny involved eastward translation of the vertical to steeply eastward dipping western Idaho suture zone about 150 km along a gently west-dipping decollement that penetrated the upper mantle. This model implies that a shelf of continental lithospheric mantle lies at depth somewhere under eastern Oregon as much as 150 km west of the $^{87}Sr/^{86}Sr = 0.706$ line and the suture zone. Xenoliths in volcanic and plutonic rocks in southeast Oregon suggest that much of the region between lat 42ºN. and 44ºN. and long 117ºW. to 119º30'W. may be underlain by basement rock with cratonic affinities. Geophysical data, especially the eU and eTh concentrations and K/eTh ratios, for the region are consistent with the hypothesis that continental-type crust and presumably continental upper mantle underlie much of southeastern Oregon, and suggest that the approximate location of the surface trace of the concealed suture between the craton and accreted terranes is a zone extending between lat 42º30'N., long 119º30'W., and lat 44º10'N., long 117º45'W. Segments of this continental-oceanic crustal boundary were no doubt deformed during mid- to late-Cenozoic extension; in places, they may have influenced the location of Miocene volcanism. Since collision of the accreted terranes with the North American craton in the Cretaceous, the boundary may have undergone east-west translation of no more than 125 km at lat 44ºN., possibly along a Sevier-age decollement, as proposed by Leeman and others (1992), and the top of the autochthonous segment may be at mid to low crustal depths.

ACKNOWLEDGMENTS

The information upon which this paper is based was derived from two cooperative projects: (1) geologic mapping of the Vale and Mahogany Mountain 30 x 60 minute quadrangles (Ferns and others, 1993a, b), which involved the collaboration of the Oregon Department of Geology and Mineral Industries, Portland State University, and the U.S. Geological Survey, and (2) quantitative mineral resource assessment of the Bureau of Land Management's Malheur, Jordan, and Andrews Resource Areas (Smith, 1994; Peters and others, 1996; Evans, unpub. report), which involved the collaboration of the U.S. Bureau of Land Management, U.S. Bureau of Mines (until 1994), and the U.S. Geological Survey. Comments of William P. Leeman, Department of Geology and Geophysics, Rice

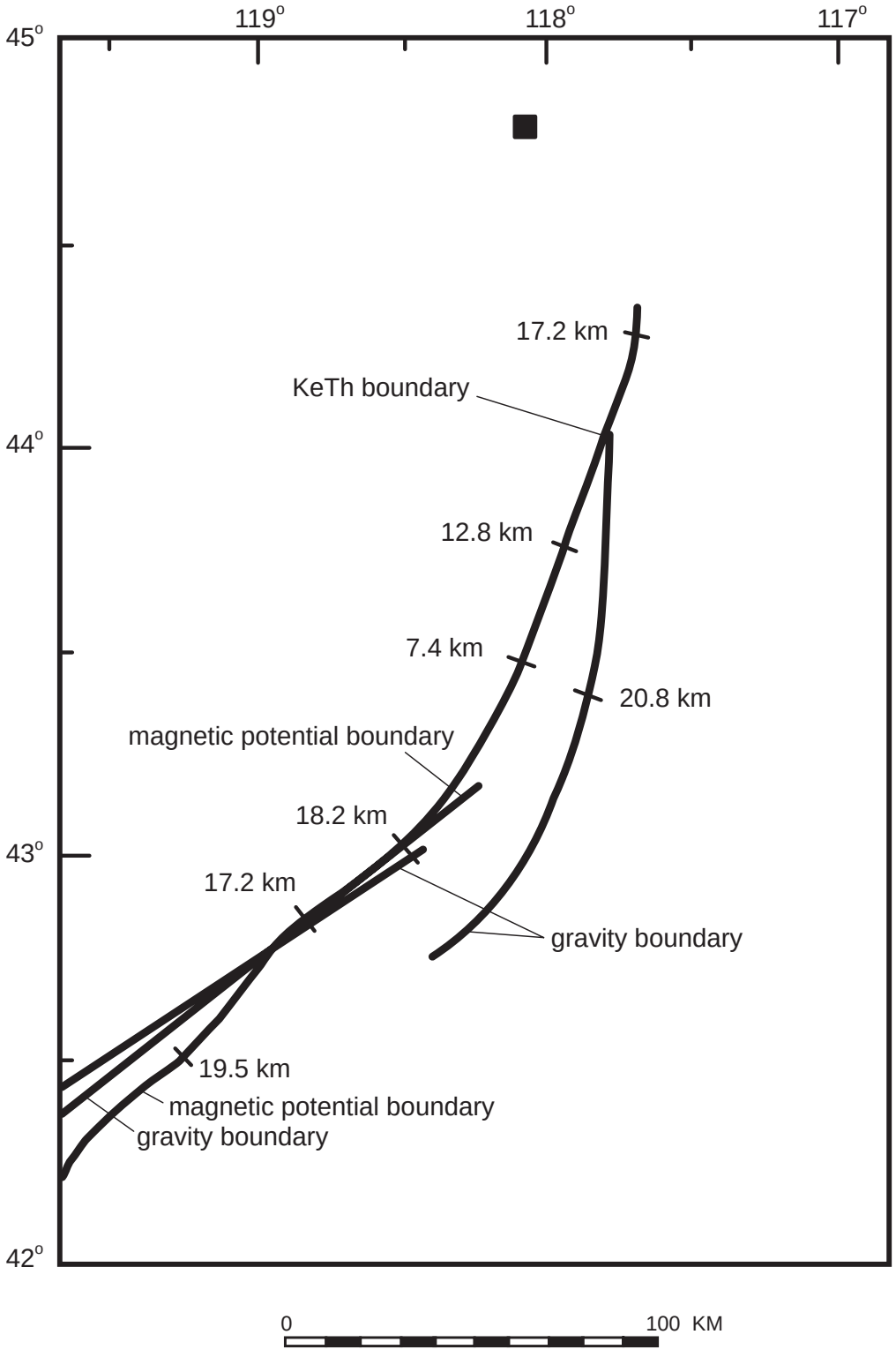

Figure 13. Gravity and magnetic boundaries that coincide with or are close to the K/eTh boundary along which maximum depths to sources were calculated. The dashed northern extension of the K/eTh boundary under the accreted terranes of the southern Blue Mountains is suggested by gravity data in Figure 2. The solid square is the projected trace of the autochthonous segment of the western Idaho suture zone from cross sections of Leeman and others (1992).

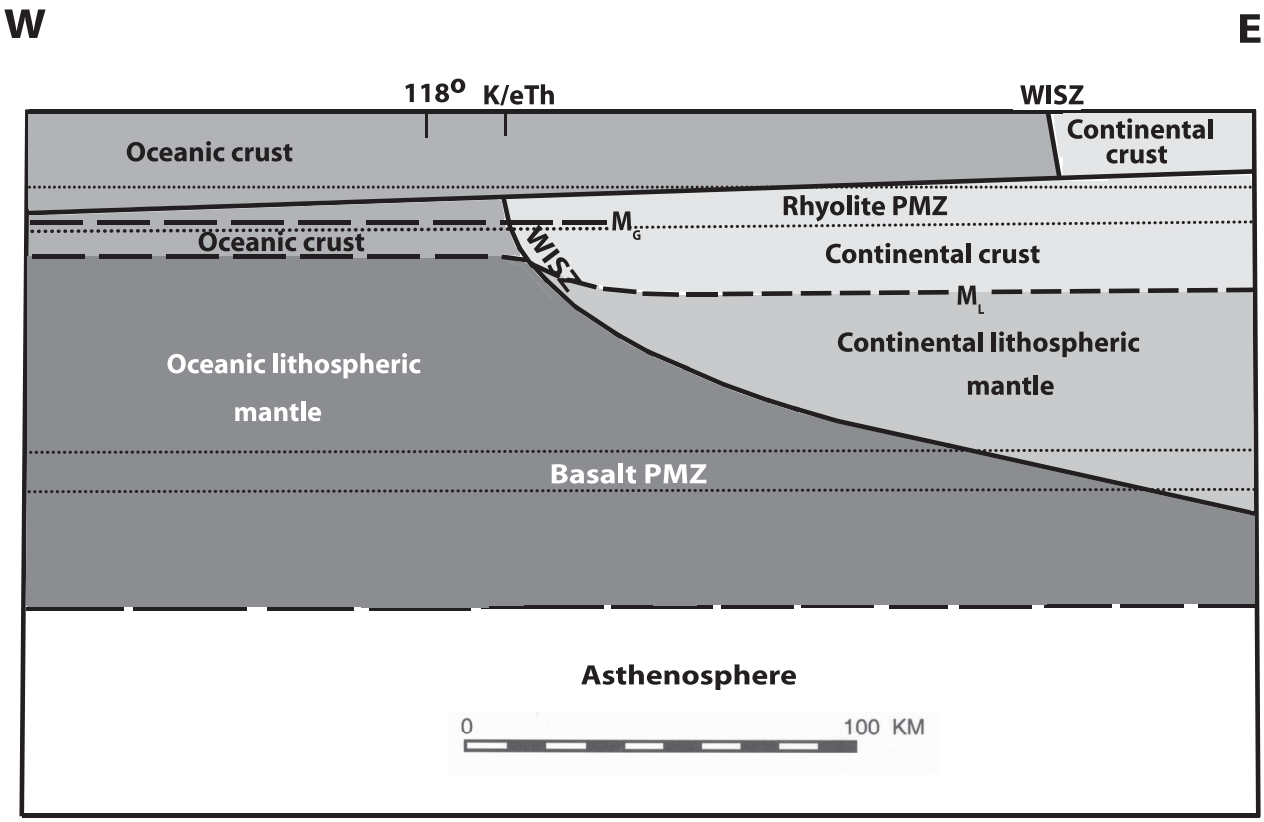

Figure 14. East-west cross section along lat 44ºN. showing 125 km separation of segments of western Idaho suture zone along a regional decollement. The western Idaho suture zone is drawn about 20 km deep under eastern Oregon. M_G, model depth of Moho used by Griscom and Halvorson (1994) and drawn only under the study area in eastern Oregon and westernmost Idaho; M_L, depth of Moho used by Leeman and others (1992); K/eTh = 0.30 boundary; PMZ, top of partial melt zone as shown by Leeman and others (1992); LM, lithospheric mantle; WISZ, western Idaho suture zone. Crust colored light gray; lithospheric mantle, dark gray. No vertical exaggeration.

University; H. Richard Blank, U.S. Geological Survey, Spokane Field Office; and Mark L. Ferns, Oregon Department of Geology and Mineral Industries, Baker City Office, greatly improved the manuscript.

REFERENCES

Armstrong, R.L., W.H. Taubeneck, and P.O. Hales, 1977, Rb-Sr and K-Ar geochronology of Mesozoic granitic rocks and their Sr isotopic composition, Oregon, Washington, and Idaho: Geological Society of America Bulletin, v. 88, p. 397-411.

Ave Lallemant, H.G., D.W. Phelps, and J.F. Sutter, 1980, ^{40}Ar-^{39}Ar ages of some pre-Tertiary plutonic and metamorphic rocks of eastern Oregon and their geologic relationships: Geology, v. 8, p. 371-374.

Bernardi, M.L., and J.W. Robbins, 1982, National uranium resources evaluation, Baker quadrangle, Oregon and Idaho: Bendix Field Engineering Corporation Report PGY-1112(82), Grand Junction, Colorado; prepared for U.S. Department of Energy under contract no. DE-AC07-76GJ01664, 34 p.

Binger, G.B., 1997, The volcanic stratigraphy of the Juntura region, eastern Oregon: Washington State University M.S. thesis, 206 p.

Blakely, R.J., 1995, Potential Theory in Gravity and Magnetic Applications: New York, Cambridge University Press, 441 p.

Blakely, R.J., and R.C. Jachens, 1990, Volcanism, isostatic residual gravity, and regional tectonic setting of the Cascade volcanic province: Journal of Geophysical Research, v. 95, no. B12, p. 19,439-19,451.

Boler, F.M., 1978, Aeromagnetic measurements, magnetic source depths, and the Curie point isotherm in the Vale-Owyhee, Oregon, geothermal area: Corvallis, Oregon State University M.S. thesis, 104 p.

Bond, K.R., and Isidore Zietz, 1987, Composite magnetic anomaly map of the conterminous United States west of 96º longitude: U.S. Geological Survey Geophysical Investigations Map GP-997, scale 1:2,500,000.

Brooks, H.C., 1979, Plate tectonics and the geologic history of the Blue Mountains: Oregon Geology, v. 41, no. 5, p. 71-80.

Brooks, H.C., and J.P. O'Brien, 1992, Geology and mineral resources map of the Westfall quadrangle, Malheur County, Oregon: Oregon Department of Geology and Mineral Industries Geologic Map Series GMS-71, scale 1:24,000.

Brown, M.A., 1996, The pre-Tertiary geology, structural evolution, and geochronology of the Pueblo Mountains, Nevada-Oregon: Rice University M.S. thesis, 75 p.

Cummings, M.L., 1991, Geology of the Deer Butte Formation, Malheur County, Oregon: Faulting, sedimentation, and volcanism in a post-caldera setting: Sedimentary Geology, v. 74, p. 345-362.

Cummings, M.L., J.G. Evans, M.L. Ferns, and K.R. Lees, 2000, Stratigraphic and structural evolution of the middle Miocene synvolcanic Oregon-Idaho graben: Geological Society of America Bulletin, V. 112, no. 5, p. 668-682.

Cummings, M.L., A.G. Johnson, and K.M. Cruikshank, 1996, Intragraben fault zones and hot-spring deposits in the Oregon-Idaho graben: A geophysical study, *in* A.R. Coyner and P.L. Fahey, eds., Geology and Ore Deposits of the American Cordillera: Geological Society of Nevada Symposium, Reno/Sparks, April, 1995, p. 1047-1062.

Darnley, A.G., and K.L. Ford, 1989, Regional airborne gamma-ray surveys: A review, *in* G.D. Garland, ed., Proceedings of Exploration '87: Ontario Geological Survey Special Volume 3, p. 229-240.

Ekren, E.B., D.H. McIntyre, E.H. Bennett, and H.E. Malde, 1981, Geologic map of Owyhee County west of longitude 116ºW.: U.S. Geological Survey Miscellaneous Geologic Investigations Map I-1256, scale 1:125,000.

Ekren, E.B., D.H. McIntyre, E.H. Bennett, and R.F. Marvin, 1982, Cenozoic stratigraphy of western Owyhee County, Idaho, *in* Bill Bonnichsen and R.M. Breckenridge, eds., Cenozoic Geology of Idaho: Idaho Bureau of Mines and Geology Bulletin 26, p. 215-235.

Evans, J.G., 1990a, Geology and mineral resources map of the Jonesboro quadrangle, Malheur County, Oregon: Oregon Department of Geology and Mineral Industries Geological Map Series GMS-66, scale 1:24,000.

———, 1990b, Geology and mineral resources map of the South Mountain quadrangle, Malheur County, Oregon: Oregon Department of Geology and Mineral Industries Geological Map Series GMS-67, scale 1:24,000.

———, 1996, Geology of the Monument Peak quadrangle, Malheur County, Oregon: U.S. Geological Survey Miscellaneous Field Studies Map MF-2317, scale 1:24,000.

Evans, J.G., and G.B. Binger, 1997, Geologic map of the Westfall Butte quadrangle, Malheur County, Oregon: U.S. Geological Survey Open-File Report OF-97-481, scale 1:24,000.

Evans, J.G., and W.J. Keith, 1996, Geologic map of the Tims Peak quadrangle, Malheur County, Oregon: U.S. Geological Survey Miscellaneous Field Studies Map MF-2316, scale 1:24,000.

Farmer, G.L., 1988, Isotope geochemistry of Mesozoic and Tertiary igneous rocks in the western United States and implications for the structure and composition of deep continental lithosphere, *in* W.G. Ernst, ed., Metamorphism and Crustal Evolution of the Western United States (Rubey Volume VII): Englewood Cliffs, New Jersey, Prentice-Hall, p. 87-109.

Ferns, M.L., H.C. Brooks, J.G. Evans, and M.L. Cummings, 1993a, Geologic map of the Vale 30 x 60 minute quadrangle, Malheur County, Oregon, and Owyhee County, Idaho: Oregon Department of Geology and Mineral Industries Geological Map Series GMS-77, scale 1:100,000.

Ferns, M.L., J.G. Evans, and M.L. Cummings, 1993b, Geologic map of the Mahogany Mountain 30 x 60 minute quadrangle, Malheur County, Oregon, and Owyhee County, Idaho: Oregon Department of Geology and Mineral Industries Geological Map Series GMS-78, scale 1:100,000.

Fiebelkorn, R.B., G.W. Walker, N.S. MacLeod, E.H. McKee, and J.G. Smith, 1983, Index to K-Ar determinations for the State of Oregon: Isochron/West, no. 37, p. 3-60.

Fleck, R.J., and R.E. Criss, 1985, Strontium and oxygen isotopic variations in Mesozoic and Tertiary plutons of central Idaho: Contributions to Mineralogy and Petrology, v. 90, p. 291-308.

———, 1988, Location, age, and tectonic significance of the western Idaho suture zone (WISZ) and its relation to the Idaho batholith: Geological Society of America Abstracts with Programs, v. 20, p. 414.

Follo, M.F., 1994, Sedimentology and stratigraphy of the Martin Bridge Limestone and Hurwal Formation (Upper Triassic to Lower Jurassic) from the Wallowa terrane, Oregon, *in* T.L. Vallier and H.C. Brooks, eds., Geology of the Blue Mountains Region of Oregon, Idaho, and Washington: Stratigraphy, Physiography and Mineral Resources of the Blue Mountans Region: U.S. Geological Survey Professional Paper 1439, p. 1-27.

Geodata International, Inc., 1980a, Aerial radiometric and magnetic survey, Jordan Valley [1º by 2º] National Topographic Map, Idaho and Oregon: Grand Junction, Colorado, U.S. Department of Energy, National Uranium Resource Evaluation Program Report GJBX-095(80), v. 2, 205 p.

———, 1980b, Aerial radiometric and magnetic survey, Adel National Topographic Map, Oregon, 1º x 2º sheet: U.S. Department of Energy Open-File Report GJBX-104(80), v. 2, 145 p.

Gettings, M.E., and H.R. Blank, Jr., 1974, Structural interpretation of aeromagnetic and gravity data from Steens Mountain, Oregon (abs.): Eos, Transactions of the American Geophysical Union, v. 55, no. 5, p. 557.

Griscom, Andrew, and Arthur Conradi, Jr., 1975, Principal facts and preliminary interpretation for gravity and continuous truck-mounted magnetometer profiles in the Alvord Valley, Oregon: U.S. Geological Survey Open-File Report 75-293, 20 p., 18 plates, 9 tables.

Griscom, Andrew, and P.F. Halvorson, 1994, Geophysical interpretation of the Malheur-Jordan resource area, Malheur County, Orgeon, *in* C.L. Smith, ed., Mineral and Energy Resources of the BLM's Malheur, Jordan, and Andrews resource areas, southeastern Oregon: U.S. Geological Survey Administrative Report to the Bureau of Land Management, Ch. D, 20 p.

Gromme, C.S., M.E. Beck, Jr., R.E. Wells, and D.C. Engbretson, 1986, Paleomagnetism in the Tertiary Clarno Formation of central Oregon and its significance for the tectonic history of the Pacific Northwest: Journal of Geophysical Research, v. 91, no. B14, p. 14,089-14,103.

Harrold, J.L., 1972, Geology of the north-central Pueblo Mountains, Harney County, Oregon: Oregon State University M.S. thesis, 135 p.

High Life Helicopters, Inc., and QEB, Inc., 1981, Airborne gamma-ray spectrometer and magnetometer survey, Burns quadrangle, Oregon, 1º by 2º sheet: Grand Junction, Colorado, U.S. Department of Energy, National Uranium Resource Evaluation Program, GJBX-104(80).

Kittleman, L.R., A.R. Green, A.M. Kohnson, J.M. McMurray, R.G. Russell, and D.A. Weeden, 1965, Cenozoic geology of the Owyhee region, southeastern Oregon: University of Oregon Museum of Natural History Bulletin 1, 45 p.

Leeman, W.P., J.S. Oldow, and W.K. Hart, 1992, Lithosphere-scale thrusting in the western U.S. Cordillera as constrained by Sr and Nd isotopic transitions in Neogene volcanic rocks: Geology, v. 20, no. 1, p. 63-66.

Lillie, R.J., 1977, Subsurface geologic structure of the Vale, Oregon, Known Geothermal Resource Area from the interpretation of seismic reflection and potential field data: Oregon State University M.S. thesis, 52 p.

Lund, Karen, 1984, Tectonic history of a continent-island arc boundary: West-central Idaho: Pennsylvania State University Ph.D. dissertation, 207 p.

Lund, Karen, and L.W. Snee, 1988, Metamorphism, structural development, and age of the continent-island arc juncture in west-central Idaho, *in* W.G. Ernst, ed., Metamorphism and Crustal Evolution of the Western United States (Rubey Volume VII): Englewood Cliffs, New Jersey, Prentice-Hall, p. 296-331.

Peters, S.G., G.T. Spanski, H.C. Brooks, J.G. Evans, R.R. Carlson, G.K. Lee, K.A. Connors, J.J. Rytuba, Andrew Griscom, G.V. Albino, P.F. Halvorson, and R.P. Ashley, 1996, Deposit models, tracts, and estimation of endowment for undiscovered metallic resources in the BLM's Malheur, Jordan, and Andrews Resource Areas, southeast-

ern Oregon: U.S. Geological Survey Administrative Report to the Bureau of Land Management, 69 p.

Plouff, Donald, 1976, Principal facts for gravity observations near McDermitt, Nevada: U.S. Geological Survey Open-File Report 76-599, 21 p.

———, 1977, List of principal facts and gravity anomalies for an area between Orovada, Nevada, and Adel, Oregon: U.S. Geological Survey Open-File Report 77-683, 40 p.

———, 1984, Interpretation of aeromagnetic and gravity data, Charles Sheldon Wilderness Study Area, Nevada and Oregon, *in* U.S. Geological Survey and U.S. Bureau of Mines, Mineral Resources of the Charles Sheldon Wilderness Study Area, Humboldt County, Nevada, and Harney County, Oregon: U.S. Geological Survey Bulletin 1538-B, p. 35-50, plate 2, scale 1:125,000.

———, 1987, Gravity observations by the U.S. Geological Survey in northwest Nevada, southeast Oregon, and northeast California, 1984-1986: U.S. Geological Survey Open-File Report 87-639, 33 p.

Riddihough, Robin, Carol Finn, and Richard Couch, 1986, Klamath-Blue Mountain lineament: Geology, v. 14, no. 6, p. 528-531.

Roback, R.C., D.B. Vander Meulen, H.D. King, Donald Plouff, S.R. Munts, and S.L. Willett, 1987, Mineral resources of the Pueblo Mountains Wilderness Study Area, Harney County, Oregon, and Humboldt County, Nevada: U.S. Geological Survey Bulletin 1740-B, 30 p., scale 1:48,000.

Rowe, W.A., 1970, Geology of the south-central Pueblo Mountains, Oregon-Nevada: Oregon State University M.S. thesis, 81 p.

Rytuba, J.J., and E.H. McKee, 1984, Peralkaline ash-flow tuff and calderas of the McDermitt volcanic field, southeast Oregon and north-central Nevada: Journal of Geophysical Research, v. 89, no. B10, p. 8616-8628.

Rytuba, J.J., D.B. Vander Meulen, V.E. Barlock, and M.L. Ferns, 1991, Hot spring gold deposits in the Lake Owyhee volcanic field, eastern Oregon, *in* R.H. Buffa and A.R. Coyner, eds., Geology and Ore Deposits of the Great Basin: Geological Society of Nevada Field Trip Guide no. 10, p. 633-712.

Silberling, N.J., 1991, Allochthanous terranes of western Nevada—current status, *in* G.L. Raines, R.E. Lisle, R.W. Schafer, and W.H. Wilkinson, eds., Geology and Ore Deposits of the Great Basin: Geological Society of Nevada and U.S. Geological Survey, v. I, p. 101-102.

Silberling, N.J., D.L. Jones, M.C. Blake, Jr., and D.G. Howell, 1987, Lithotectonic terrane map of the western conterminous United States: U.S. Geological Survey Miscellaneous Field Studies Map MF-1874-C, scale 1:2,500,000.

Smith, C.L., ed., 1994, Mineral and energy resources of the BLM's Malheur, Jordan, and Andrews resource areas, southeastern Oregon: U.S. Geological Survey Administrative Report to the Bureau of Land Management, 294 p.

Smith, R.A., 1959, Some depth formulas for local gravity interpretations: Geophysical Prospecting, v. 7, p. 55-63.

Stewart, J.H., G.W. Walker, and F.J. Kleinhampl, 1975, Oregon-Nevada lineament: Geology, v. 3, p. 265-268.

Strayer, L.M., R.D. Hyndman, J.W. Sears, and P.E. Myers, 1989, Direction and shear sense during suturing of the Seven Devils-Wallowa terrane against North America in western Idaho: Geology, v. 17, p. 1025-1028.

Tower, D.B., 1972, Geology of the central Pueblo Mountains, Harney County, Oregon: Oregon State University M.S. thesis, 96 p.

U.S. Geological Survey, 1972, Aeromagnetic map of the Adel and parts of the Burns, Boise, and Jordan Valley 1° x 2° quadrangles, Oregon: U.S. Geological Survey Open-File Report 72-390, scale 1:250,000.

———, 1984, Aeromagnetic map of east-central Oregon: U.S. Geological Survey Open-File Report 84-512, 2 sheets, scale 1:250,000.

Walker, G.W., 1990, Paleocene(?), Eocene, and Oligocene(?) rocks of the Blue Mountains region, *in* G.W. Walker, ed., Geology of the Blue Mountains Region of Oregon, Idaho, and Washington: Cenozoic Geology of the Blue Mountains Region: U.S. Geological Survey Professional Paper 1437, p. 13-27.

Walker, G.W., and N.S. MacLeod, 1991, Geology of Oregon: U.S. Geological Survey, scale 1:500,000.

Zoback, M.L., E.H. McKee, R.J. Blakely, and G.A. Thompson, 1994, The northern Nevada rift: Regional tectono-magmatic relations and middle Miocene stress direction: Geological Society of America Bulletin, v. 106, no. 3, p. 371-382.

Zoback, M.L., and G.A. Thompson, 1978, Basin and range rifting in northern Nevada: Clues from a mid-Miocene rift and its subsequent offsets: Geology, v. 6, p. 111-116.

A Model for the Origin of the Western Snake River Plain as an Extensional Strike-Slip Duplex, Idaho and Oregon

Peter Hooper,[1] Jenda Johnson,[2] and Chris Hawkesworth[3]

ABSTRACT

Field, chemical, and age data indicate that the graben forming the western Snake River Plain (SRP) has a right lateral strike-slip component contemporaneous with the formation of the Oregon-Idaho graben, which was initiated at 15.3 Ma ± 0.5 Ma. In age, in orientation, and in its pattern of associated faults, the western SRP is similar to extensional strike-slip duplexes or pull-apart structures previously described across a large part of northeast Oregon between the western SRP and the Olympic-Wallowa lineament. These structures have been attributed to Miocene east-west extension. We conclude that the western SRP originated primarily because of Basin and Range-related extension and, unlike the eastern SRP, that it is associated only indirectly with the Yellowstone hot spot.

Key words: graben, Basin and Range, extensional strike-slip duplex, pull-apart structure, Miocene, Yellowstone hot spot

INTRODUCTION

The western Snake River Plain (SRP), unlike the eastern SRP, does not lie in the track of the Yellowstone hot spot. It is a graben filled with sediment and dense basalt, creating an arcuate gravity high (Figure 1; Mabey, 1984; Malde, 1991; Wood and Clemens, this volume). The western SRP in Oregon also includes the Vale fault zone, regarded by Lawrence (1976) and subsequent authors as the northern limit of the Basin and Range extensional province. The graben trends WNW-ESE and appears to separate an area of active east-west extension to the south from an area of more limited extension to the north. If this interpretation is correct, then the western SRP must include a component of "right-lateral shear couple" (Pierce and Morgan, 1992, p. 8).

Recent mapping in east-central Oregon covered part of the western end of the western SRP (Figure 1; Ferns and others, 1993). The mapping identified the 50-km-wide Oregon-Idaho graben (OIG) which terminates to the north along the Adrian fault zone, the southern boundary of the western SRP (Figure 1; Ferns and others, 1993; Cummings and others, 2000). The use of major- and trace-element analyses to correlate the many volcanic units disrupted by faulting across the OIG and western SRP (Lees, 1994; Binger, 1997; Johnson and others, 1998), together with many new $^{40}Ar/^{39}Ar$ age determinations (Lees, 1994; Hooper and others, 2002), has clarified both the stratigraphic sequence (Figure 2) and the volcanic and tectonic evolution of this complex area.

This paper provides new evidence in support of significant right-lateral displacement across the western SRP. With the OIG, the western SRP displays a geometry of associated structures similar to those described across the broad zone between the western SRP and the Olympic-Wallowa lineament (OWL) to the north (Figure 1; Gehrels and others, 1980; Hooper and Conrey, 1989; Mann, 1989; Mann and Meyer, 1993). These structures have been attributed to extensional strike-slip duplexes (pull-apart structures). We suggest that the proposed tectonic model of extensional strike-slip duplexes is applicable to a wide area of northeast Oregon, including the western SRP. We also suggest that the model is consistent with the expla-

Editors' note: The manuscript was submitted in June 1998 and has been revised at the authors' discretion.

[1]Department of Geology, Washington State University, Pullman, WA 99164
[2]U.S. Geological Survey, HVO, P.O. Box 51, HI 96718
[3]Department of Earth Sciences, University of Bristol, Bristol, BS8 1RJ, U.K.

Hooper, Peter, Jenda Johnson, and Chris Hawkesworth, 2002, A model for the origin of the western Snake River Plain as an extensional strike-slip duplex, Idaho and Oregon, *in* Bill Bonnichsen, C.M. White, and Michael McCurry, eds., Tectonic and Magmatic Evolution of the Snake River Plain Volcanic Province: Idaho Geological Survey Bulletin 30, p. 59-67.

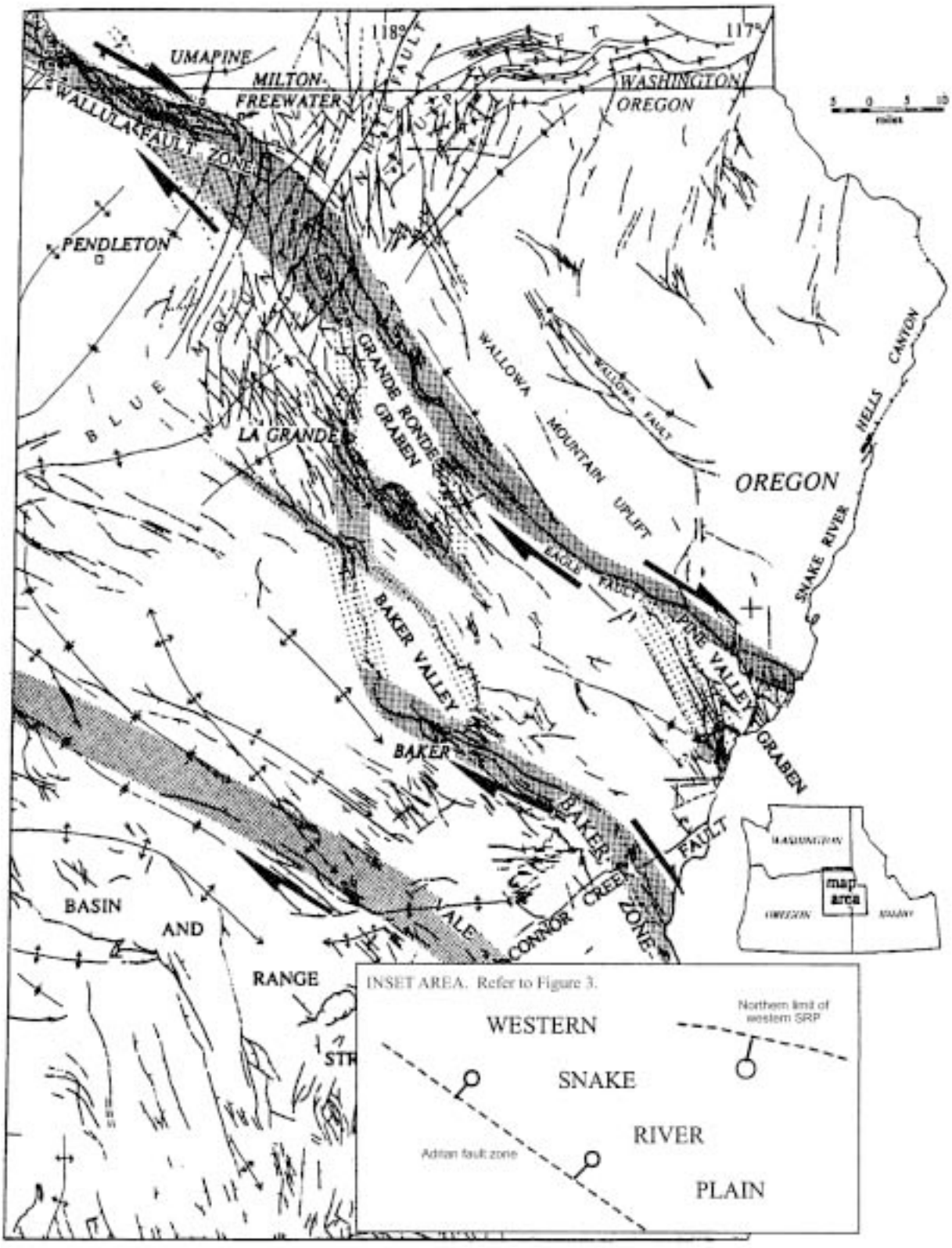

Figure 1. The structural elements of northeast Oregon. Modified from Mann and Meyer (1993) and derived originally from Brooks and others (1976), Walker (1977), Mann (1989), and Hooper and Conrey (1989), among others.

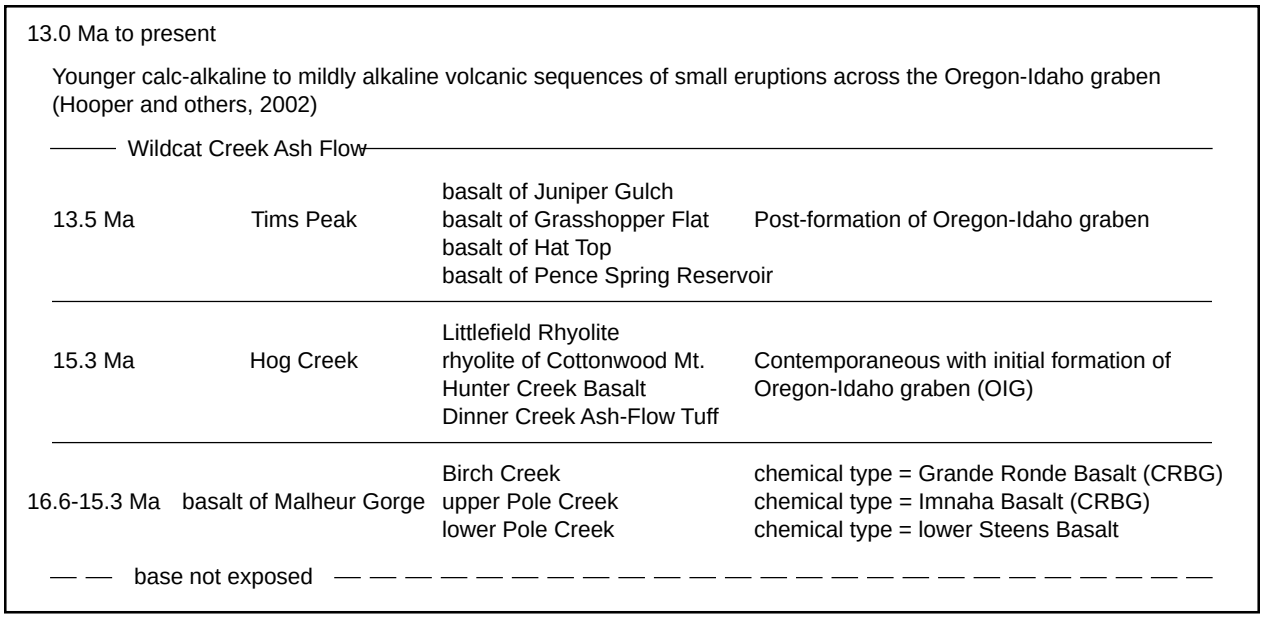

Figure 2. Stratigraphic sequence and $^{40}Ar/^{39}Ar$ ages for the lower volcanic units exposed in the horst of the Malheur Gorge area, south of the Adrian fault zone, in east-central Oregon. The basalt of Malheur Gorge is exposed again along the north and western margins of the western SRP where it can be traced into flows assigned to the Imnaha and Grande Ronde Basalt Formations of the Columbia River Basalt Group (CRBG, Figure 3).

nation for increasing Basin and Range extension from north to south by right-lateral displacement along major WNW-ESE lineaments as suggested by Lawrence (1976).

THE WESTERN SNAKE RIVER PLAIN IN OREGON

Along the Oregon-Idaho border the western SRP is clearly a graben. A major fault immediately south of Farewell Bend on the Snake River (Figure 3) drops flows of the basalt of Malheur Gorge (equivalent to the Columbia River Basalt Group), which lie at the surface north of Farewell Bend, to approximately 300 m below the surface in the Kirby bore hole south of Farewell Bend (Figure 3; Bennett and others, 1996). The southern margin of the western SRP is formed by the WNW-ESE-trending Adrian fault zone that drops the Hunter Creek Basalt (15.3 Ma; Figure 2) 200-300 m from south to north. Younger flows of olivine basalt (7-8 Ma) thicken northwards across the fault zone (Ferns and others, 1993).

The basalt of Malheur Gorge is exposed in a broad arc west and southwest of Farewell Bend (Figure 3; Lees, 1994; Hooper and others, 2002). The flows lie unconformably on the pre-Tertiary units of the Blue Mountains Province to the north and west, which implies that the graben dies out westwards. The outcrop pattern, not yet mapped in detail, means that the exposed western margin of the basalt of Malheur Gorge lies progressively farther east going from south to north across the width of the western SRP (Figure 3). A break in the basalt exposures across Bully Creek (Figure 3), which follows the Adrian fault zone, implies that some graben formation extends west to longitude 118ºW along the southern margin of the western SRP (Figure 3).

Near the Oregon-Idaho border the Adrian fault zone is displaced to the south, apparently by right-lateral motion along predominantly normal north-south faults (Figure 3; Ferns and others, 1993). Mabey (1984) also records that farther east into Idaho both sides of the western SRP are displaced southwards on the east side of a north-south right-lateral strike-slip fault. Right-lateral displacement along north-south faults provide a potential explanation for the discrepancy between the WNW-ESE orientation of the southern margin of the western SRP in Oregon and the apparent overall NW-SE trend of the whole western SRP as now exposed in Idaho. Finally, the western SRP in Oregon incorporates the Vale fault zone (Figure 3; Ferns and others, 1993, Figure 1). This is a stack of conspicuous NW-SE-trending faults that is entirely confined to the western SRP.

In summary, the western SRP in Oregon is a 50-km-wide, WNW-ESE-trending graben lying between Farewell Bend and the Adrian fault zone. The graben is 200-300 m deep along the Idaho border, significantly less than its depth farther east near Boise (Wood and Clemens, this volume), and it dies out rapidly to the west. The graben encloses the NW-SE stack of the Vale faults and is dis-

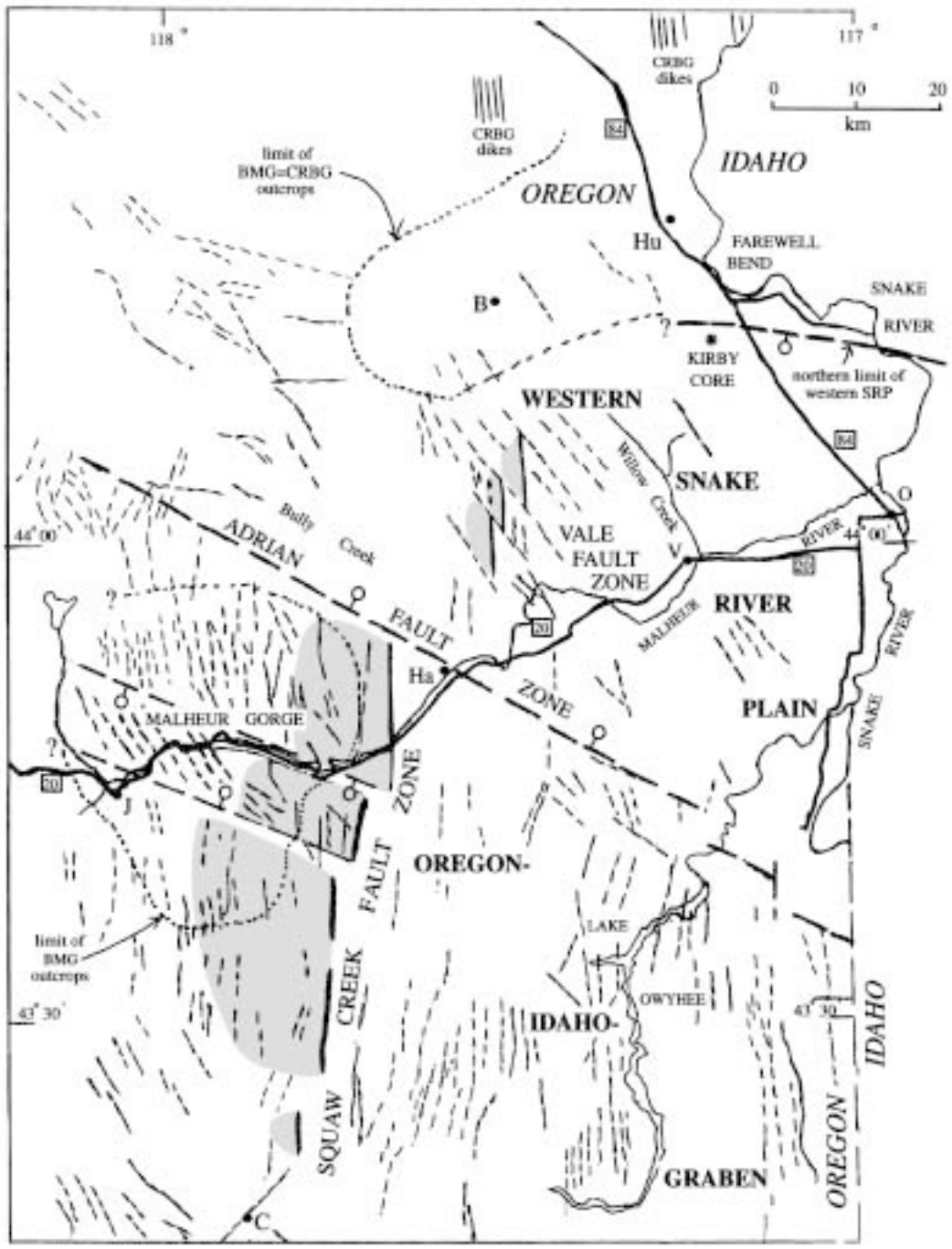

Figure 3. Geologic sketch map of the Oregon part of the western Snake River Plain (SRP) and the northern part of the Oregon-Idaho graben (OIG). Fault patterns from Walker (1977) and modified from Ferns and others (1993), Evans (1990a, 1990b), Johnson and others (1998), Jim Evans (written commun., 1996), and Howard Brooks (written, commun., 1996). Gray stipple represents the extent of the rhyolite of Cottonwood Mountain (north) and the Littlefield Rhyolite (south); both erupted around 15.3 Ma along the Squaw Creek fault zone which forms the western margin of the OIG (Ferns and others, 1993; Lees, 1994; Binger, 1997). The Adrian fault zone represents the southern margin of the western SRP, displaced to the south on its eastern end by dominantly normal faults that form the eastern margin of the OIG along the Oregon-Idaho border (Ferns and others, 1993). Note that the rhyolites and the faulted western margin of the OIG are displaced right laterally by the WNW-ESE-trending Malheur Gorge half graben, the WNW-ESE-trending Adrian fault zone, and again by the stack of NW-SE-trending faults that form the Vale fault zone. Outcrops of the basalt of Malheur Gorge are also consistent with a similar degree of right-lateral translation across the WNW-ESE structures. Towns: Hu-Huntington; B-Brogan; V-Vale; O-Ontario; Ha-Harper; J-Juntura, and C-Cowley.

placed locally by north-south right-lateral strike-slip faults associated with the Oregon-Idaho graben. As discussed below, this fault pattern is typical of right-lateral extensional strike-slip duplexes (Woodcock and Fischer, 1986). The eastward displacement of the western margin of the basalt of Malheur Gorge from south to north, together with the obvious east-west extension to the south and the lack of such obvious extension to the north, together suggest right-lateral displacement across the graben.

THE OREGON-IDAHO GRABEN

The Oregon-Idaho graben (OIG) is a large fault-bounded basin lying immediately south of the western SRP in Oregon. Over 100 km long from north to south and approximately 50 km wide, the OIG extends west from the Oregon-Idaho border to the Malheur Gorge (Figure 3; Ferns and others, 1993; Cummings and others, 2000). On its eastern margin, the OIG is bounded by down-to-the-west normal faults with a north-south trend approximately parallel to, and immediately east of, the Oregon-Idaho boundary (Ferns and others, 1993; Cummings and others, 2000). On the west, the OIG is bounded by the Squaw Creek fault zone, composed of down-to-the-east normal faults (Figure 3; Ferns and others, 1993). The entire OIG basin with its sedimentary-volcanic fill is cut by north-south-trending normal faults to form a sequence of internal horst-graben structures (Cummings and others, 2000). The graben was initiated at 15.3 Ma (Cummings and others, 2000; Hooper and others, 2002). We assume that the OIG, like the many other north-south grabens of the Basin and Range Province, was the result of east-west extension (e.g., Walker, 1977; Kendal and others, 1981).

The OIG is terminated to the north by the Adrian fault zone, the southern margin of the western SRP, and these two major structures overlap. The Adrian fault zone, which apparently terminates the OIG (Ferns and others, 1993), is locally displaced by faults associated with the OIG, as noted above. In addition, the western boundary of the OIG extends into, and is displaced across, the western SRP. The western boundary of the OIG, the Squaw Creek fault zone, was intruded by the rhyolite of Cottonwood Mountain and the Littlefield Rhyolite (Figure 2). The rhyolite of Cottonwood Mountain and its north-south-faulted contact can be traced north into the western SRP. It is offset right laterally both as it crosses the WNW-ESE-trending Adrian fault zone and again as it crosses the successive NW-SE trending faults of the Vale fault zone (Figure 3) within the western SRP. We conclude, therefore, that these two structures, the western SRP and the OIG, are largely contemporaneous and complementary. The east-west extension that formed the OIG was terminated to the north by right-lateral motion across the western SRP between 15.3 Ma and 7 Ma.

The Squaw Creek fault zone that forms the west side the OIG has an average trend just east of north (Ferns and others, 1993). In detail, it is composed of many short north-south segments with en echelon displacement to the east as it progresses northwards (Figure 3; Evans, 1990a, 1990b; Ferns and others, 1993). To the south the Squaw Creek fault zone appears to join onto the northern end of the Steens Mountain fault (Walker, 1977), which is a true NNE-trending structure. The essentially north-south alignment of most of these fault segments, together with the persistent north-south trend of the many normal faults and smaller horst-graben structures within the OIG, leads us to conclude that the direction of extension responsible for the OIG was east-west.

THE HALF GRABEN OF MALHEUR GORGE

Evans (1990a, 1990b) mapped a narrow half graben trending WNW-ESE west from the western edge of the OIG through the eastern end of the Malheur Gorge (Figure 3). The northeastern side of the structure is a fault that drops units of 15.3 Ma and older (basalt of Malheur Gorge, and units of the Hogs Creek sequence—the Dinner Creek Ash-Flow Tuff, rhyolite of Cottonwood Mountain, Hunters Creek Basalt and the Littlefield Rhyolite, Figure 2) down to the south. The southwestern margin of the half graben is formed by a series of stepped faults and a northeasterly dip of the same older volcanic units (Figure 3; Evans, 1990a, 1990b; Ferns and others, 1993). In the Stemler Ridge quadrangle, the westward continuation of this structural zone fails to deform the younger (13.5 Ma) Tims Peak Basalt, which lies unconformably on the older units (Johnson and others, 1998). The Malheur Gorge structure is, therefore, a narrow WNW-ESE-trending half graben active primarily between 15.3 Ma and 13.5 Ma.

The half graben displaces the rhyolite of Cottonwood Mountain and the Littlefield Rhyolite of the Hogs Creek sequence, which were emplaced along the initial boundary faults of the OIG at 15.3 Ma (Ferns and others, 1993; Cummings and others, 2000). No striae have been reported along the Malheur Gorge fault, but the half graben appears to displace the margins of the Littlefield Rhyolite both laterally and vertically, implying oblique normal/right-lateral strike-slip motion (Figure 3). The western margin of the rhyolite is displaced a minimum of 5 km to the west, as the northeastern side of the struc-

ture is crossed north to south, and as much as 15 km if one compares the southern side of the half graben with the northern. Similarly, the eastern margin of the rhyolite, which lies along the western margin of the OIG, is displaced a minimum of 6 km across the line of the half graben (see Ferns and others, 1993). We conclude that the WNW-ESE-trending Malheur Gorge structure is an extensional right-lateral strike-slip duplex or pull-apart structure.

FAULT PATTERNS

The fault pattern across the Malheur Gorge half graben as recorded by Evans (1990a, 1990b), Ferns and others (1993) and Johnson and others (1998) is emphasized in Figure 3. To the north, between the Malheur Gorge half graben and the western SRP, north-south normal faults predominate. These are well exposed along the northern margin of the Stemler Ridge quadrangle. Here, a parallel stack of north-south normal faults dips steeply to the east, dissecting flows of the 13.5 Ma Tims Peak Basalt, which dip gently to the west, repeating the same part of the flow stratigraphy many times (Johnson and others, 1998). This typical example of listric faulting (Trudgill and Cartwright, 1994) implies east-west extension. A similar pattern of north-south normal faults dominates the area to the south of the Malheur Gorge half graben (Figure 3; Ferns and others, 1993). However, within the half graben the dominant trend of the faults is NW-SE. No striae have been observed on the NW-SE fault planes, and the degree of lateral displacement, if any, is not known. The vertical component can be recorded from the displacement of the gently dipping basalt flows. Right-lateral displacement on the NW-SE fault planes can only be inferred on the present evidence by comparison with similarly oriented faults within the western SRP, as described below.

Within the WNW-ESE-trending western SRP a similar fault pattern is apparent. Faults to the north and south of the plain, including the grabens of the Weiser valley, Idaho (Fitzgerald, 1984), the feeder dikes to the Columbia River basalts on Pedro and Lookout Mountains to the north (Figure 3) and the fault pattern of the OIG to the south, are N-S to NNW-SSE. In contrast, the fault pattern within the Oregon part of the western SRP is dominated by the stack of parallel NW-SE faults of the Vale fault zone. As noted above, these NW-SE faults systematically move the faulted eastern margin of the rhyolite of Cottonwood Mountain to the southeast (Figure 3), implying systematic right-lateral displacement along these NW-SE faults.

Extensional strike-slip duplexes have been described from a large area of northeastern Oregon between the western SRP and the Olympic-Wallowa lineament. This whole area may be interpreted as a continuing sequence of such structures (compare Figure 1 with Figure 4a). Particularly good examples of extensional duplex structures are the Wallula fault zone (Figure 1 and Figure 4a; Hooper and Conrey, 1989; Mann and Meyer, 1993) and the Grande Ronde and Baker grabens (Barrash and others, 1980, 1983; Gehrels and others, 1980; Gehrels, 1981; Kendal and others, 1981; White, 1981; Mann, 1989; Bailey, 1990; Hooper and Swanson, 1990; Mann and Meyer, 1993). These structures are elongated along boundary faults with a WNW-ESE trend. They may include deep basins or grabens with NNW-SSE to N-S marginal normal faults (Grande Ronde and Baker grabens). They are crossed by stacks of parallel NW-SE faults (Figure 4). This is the dominant pattern in type extensional strike-slip duplexes (Figure 4a; Woodcock and Fischer, 1986). This pattern of faults was described as long ago as 1906 by W.S. Gilbert in his classic account of strike-slip displacement along the San Andreas Fault during the great California earthquake of that year (Johnson and others, 1997).

EXTENT OF RIGHT-LATERAL DISPLACEMENT

Evidence for right-lateral displacement along the western SRP may be summarized as follows: (1) the development of the OIG on the south side of the western SRP, which we assume represents some significant degree of east-west extension, and the lack of evidence for equivalent extension on the north side; (2) the en echelon east-stepping of the faulted margin of the rhyolite of Cottonwood Mountain from south to north across the western SRP (Figure 3); and (3) the apparent stepping to the east of the basalt of Malheur Gorge crossing the western SRP from south to north (Figure 3). Farther north, NNW-SSE-trending CRBG feeder dikes are widespread on both Pedro Mountain and Lookout Mountain due north of the Vale fault zone (Figure 3). From this we deduce a maximum right-lateral displacement of 20 to 30 km across the whole western SRP in Oregon.

The right-lateral displacement across the western SRP was not confined to a single strike-slip fault plane. Rather, it was dispersed across numerous small faults with small increments of displacement over a 50-km-wide zone using NW-SE as well as WNW-ESE fault planes.

The structural style and orientation of the western SRP is similar to that of the extensional strike-slip duplexes described from other parts of northeast Oregon in age

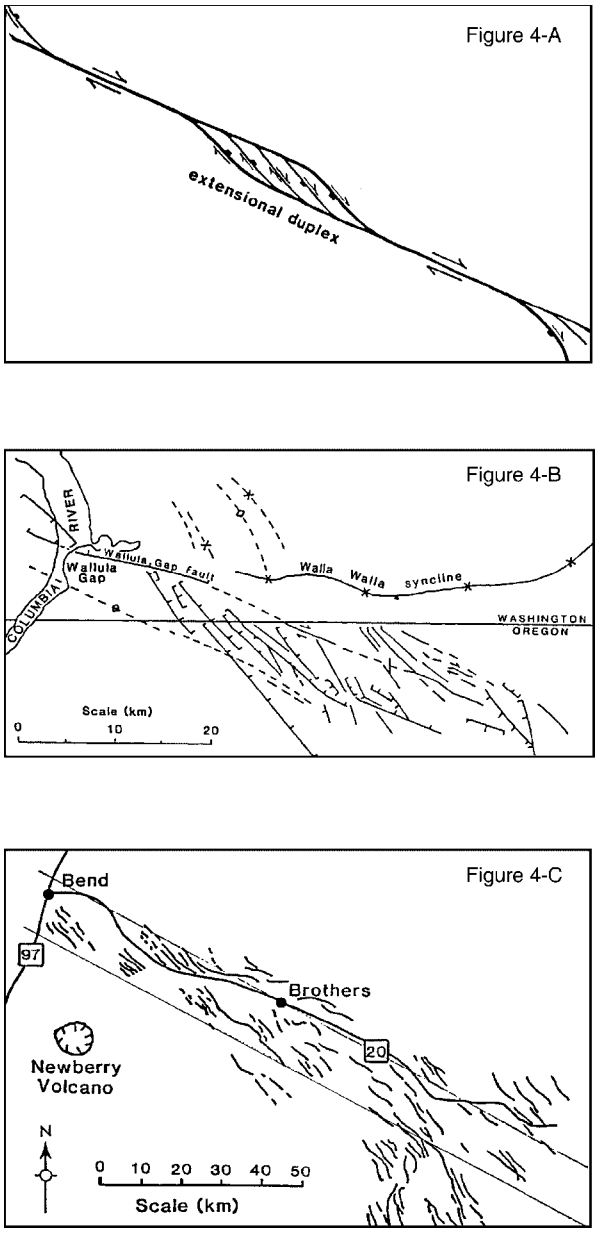

Figure 4. Fault patterns associated with WNW-ESE right-lateral extensional strike-slip duplexes or pull-apart structures. (A) Theoretical model from Woodcock and Fischer (1986). (B) The Wallula fault zone on the Olympic-Wallowa lineament (Hooper and Conrey, 1989; Mann and Meyer, 1993). (C) The western end of the Brothers fault zone (Walker and Nolf, 1981). These fault patterns can be compared to those across the Malheur Gorge half graben and the western SRP apparent in Figure 3.

(15.5-13.5 Ma), WNW-ESE trend, and structural style (Figure 1). We conclude that the western SRP, like the Malheur Gorge structure, is best interpreted as an extensional strike-slip duplex formed by greater east-west extension on its southern than on its northern side. Greater east-west extension along the southern side of the WNW-ESE-oriented western SRP created the graben and a significant component of right-lateral displacement.

DISCUSSION

Lawrence (1976) regarded the Vale fault zone as the northern limit of the Basin and Range Province. He suggested that the increased extension to the south was accomplished by right-lateral displacement along major WNW-ESE lineaments from the Brothers fault zone south into California and Nevada. More recently Hooper and Conrey (1989), Mann (1989) and Mann and Meyer (1993) have extended the zone of east-west extension north to the Olympic-Wallowa lineament. Despite general agreement that the degree of extension did increase southwards, many geologists have remained skeptical of the Lawrence hypothesis. This is partly due to failure to identify in the field any individual WNW-ESE fault planes with horizontal striae accompanied by clear evidence of right-lateral displacement of geologic units. Similar objections have been raised to the suggestion that the Olympic-Wallowa lineament was a more northerly example of a regional WNW-ESE lineament formed by extension-related right-lateral shear (Hooper and Conrey, 1989; Mann and Meyer, 1993; see Reidel and Tolan, 1994). Across east-central Oregon, including the western SRP, fault striae remain elusive. On the other hand, the pattern of right-lateral displacement of geologic boundaries across both WNW-ESE fault zones (Malheur Gorge; Adrian fault zone) and NW-SE faults (the Vale fault zone) in east-central Oregon is evident. We suggest that the modified form of Lawrence's model proposed here, in which the change in degree of east-west extension is achieved primarily by right-lateral motion along broad WNW-ESE zones rather than along a few individual fault planes, implies the potential opening of the WNW-ESE zones in an east-west direction to form narrow grabens and a lack of the compressional forces across those planes which would likely create striae.

Additional evidence for interpreting the western SRP in Oregon as an extensional strike-slip duplex or pull-apart structure is found in the associated fault patterns. The combination of N-S grabens, separated by WNW-ESE fault zones which enclose NW-SE right-lateral strike-slip faults is consistent across northeast Oregon (Figure 1; Hooper and Conrey, 1989; Mann and Meyers, 1993) and is clearly displayed by the Oregon-Idaho graben and across the western SRP (Figure 3). Similarities in the fault patterns across northeast Oregon with those patterns developed in type extensional strike-slip duplexes (Woodcock and Fischer, 1986) are illustrated in Figure 4.

It is clear from Figure 1 that the whole area from the

Olympic-Wallowa lineament to the western SRP has undergone right-lateral torque transgressed by WNW-ESE zones or corridors within which the strike-slip motion has been concentrated. Recognition that increased extension to the south is accomplished by the many extensional strike-slip duplexes widely dispersed over northeast Oregon goes a long way towards explaining the lack of obvious strike-slip fault planes with clearly developed horizontal striae. This torque and right-lateral translation has not, however, been accommodated by internal clockwise rotation, as might have been expected (Wells and Heller, 1988; Hooper and Conrey, 1989; Bailey, 1990), but rather by stacks of parallel NW-SE faults, each with small increments of right-lateral displacement, which again spread the translation across a wide zone rather than confining it to a single fault plane.

The extent to which the model of strike-slip duplexes can be applied to all of eastern Oregon is not yet clear. Pezzopane and Weldon (1993) conclude that east-westerly extension is associated with dextral shear across much of Oregon. However, in the model advocated here, the formation of well-developed extensional strike-slip duplexes depends not only on east-west extension but also on a relatively rapid change in the degree of that extension from south to north. The maximum change in the degree of extension will occur at the terminus of the extensional province, that is between the western SRP and the Olympic-Wallowa lineament. One would expect, therefore, that the extensional strike-slip duplex model is better developed in this northernmost zone of the Basin and Range Province. Further south, in central and southern Oregon, the amount of extension is likely to have changed less rapidly with latitude and a simpler regime of north-south-trending extensional grabens separated by more widely spaced zones of WNW-ESE extensional strike-slip duplexes would be anticipated. Typical north-south graben topography is well developed on either side of the Brothers fault zone in south and central Oregon. The Brothers fault zone has a WNW-ESE trend and is crossed by numerous NW-SE faults in a pattern that appears similar to that of the Wallula fault zone along the Olympic-Wallowa lineament (Walker and Nolf, 1981; Hooper and Conrey, 1989; Pezzopane and Weldon, 1993).

We conclude that the western SRP is an extensional strike-slip duplex or pull-apart structure resulting both from east-west Basin and Range extension and from the rapid decrease in the degree of that extension from south to north. Most of the observed extension occurred relatively suddenly between 15.3 Ma and 13.5 Ma, immediately following the eruption of the main volume of hot-spot related flood basalt (Hooper and others, 2002), although further displacement within the western SRP continued until at least 7 Ma (Ferns and others, 1993; Wood and Clemens, this volume). Thus, while the western SRP is not directly related to the Yellowstone hot spot, unlike the eastern SRP (Pierce and Morgan, 1992), there may be a less direct association. It is possible that the lithosphere was weakened in the proximity of the hot spot so encouraging greater extension in that southeastern area of Oregon immediately following the hot-spot eruption between 16.6 Ma and 15.3 Ma (Hooper and others, 2002).

If the proposed tectonic model has any validity, then the western SRP is unlikely to have formed as part of the north-south zone of weakness or thin spot in the lithosphere which may have channeled the flood basalt eruption (Thompson and Gibson, 1991; Zoback and others, 1994). We believe that such a zone of weakness did run north-south parallel to, and just west of, the boundary separating the older cratonic North American plate from the thinner accreted oceanic terranes. We suggest, however, that this zone of weakness did not include either the northern Nevada rift or the western SRP, both of which are better associated with the extension that immediately followed the flood basalt eruption (Hooper and others, 2002). If the OIG was formed largely by east-west extension, then the original eruptions of flood basalt from Steens Mountain may have erupted close to the present Oregon-Idaho border. The zone of weakness would have extended northwards from there to the Washington border where the greatest volume of flood basalt was vented.

ACKNOWLEDGMENTS

We thank Jim Evans, Mark Ferns, Howard Brooks, and Mike Cummings for the generous way they have shared their knowledge of the geology of east-central Oregon with us, making available not only their views but also their many unpublished maps. They provided samples of many volcanic units to complement our own collections for chemical analysis. We are grateful to Kate Lees and Ben Binger for their hard work in the field and laboratory. They provided most of the new dates and chemical analyses on which our structural analysis is based. Thanks to John Watkinson for his advice on the correct structural terminology and to Paul Link and Bill Bonnichsen for their constructive reviews.

REFERENCES

Bailey, D.G., 1990, Geochemistry and petrogenesis of Miocene volcanic rocks in the Powder River volcanic field, northeastern Oregon: Washington State University Ph.D. dissertation, 341 p.

Barrash, Warren, J.G. Bond, J.G. Kauffman, and R. Venkatakrishnan,

1980, Geology of the La Grande area, Oregon: Geoscience Research Consultants, Special Paper 6, 47 p.

Barrash, Warren, J.G. Bond, and R. Venkatakrishnan, 1983, Structural evolution of the Columbia Plateau in Washington and Oregon: American Journal Science, v. 283, p. 897-935.

Bennett, J.C., R.M. Conrey, and P.R. Hooper, 1996, Imnaha Basalt: The stratigraphy of a borehole in Malheur County, Oregon: Geological Society of America, Abstracts with Programs, v. 28, no. 5, p. 48.

Binger, G.B., 1997, The volcanic stratigraphy of the Juntura region, eastern Oregon: Washington State University M.S. thesis, 206 p.

Brooks, H.C., J.R. McIntyre, and G.W. Walker, 1976, Geologic map of the Oregon part of the Baker 1º by 2º quadrangle: Oregon Department of Geology and Mineral Industries GMS-7, scale 1:250,000.

Cummings, M.L., J.G. Evans, M.L. Ferns, and K.R. Lees, 2000, Stratigraphic and structural evolution of the middle Miocene syn-volcanic Oregon-Idaho graben: Geological Society of America Bulletin, v. 112, p. 668-682.

Evans, J.G., 1990a, Geology and mineral resources map of the Jonesboro quadrangle, Malheur County, Oregon: Oregon Department of Geology and Mineral Industries GMS-67, scale 1:24,000.

———, 1990b, Geology and mineral resources map of the South Mountain quadrangle, Malheur County, Oregon: Oregon Department of Geology and Mineral Industries GMS-66, scale 1:24,000.

Ferns, M.L., H.C. Brooks, J.G. Evans, and M.L. Cummings, 1993, Geologic map of the Vale 30 x 60 minute quadrangle, Malheur County, Oregon, and Owyhee County, Idaho: Oregon Department of Geology and Mineral Industries/GMS-78, scale 1:100,000.

Fitzgerald, J.F., 1984, Geology and basalt stratigraphy of the Weiser embayment, west-central Idaho, *in* Bill Bonnichsen and R.M. Breckenridge, eds., Cenozoic Geology of Idaho: Idaho Bureau of Mines and Geology Bulletin 26, p. 103-128.

Gehrels, G.E., 1981, The geology of the western half of the La Grande basin, northeastern Oregon: University of Southern California M.S. thesis, 97 p.

Gehrels, G.E., R.R. White, and G.A. Davis, 1980, The La Grande pull-apart basin, northeastern Oregon: Geological Society of America, Abstracts with Program, v. 12, p. 107.

Hooper, P.R., G.B. Binger, and K.R. Lees, 2002, Ages of the Steens and Columbia River flood basalts and their relationship to extension-related calc-alkalic volcanism in eastern Oregon: Geological Society of America Bulletin, v. 114, p. 43-50.

Hooper, P.R., and R.M. Conrey, 1989, A model for the tectonic setting of the Columbia River basalt eruption, *in* S.P. Reidel and P.R. Hooper, eds., Volcanism and Tectonism in the Columbia River Flood-Basalt Province: Geological Society America Special Paper 239, p. 293-306.

Hooper, P.R., and D.A. Swanson, 1990, The Columbia River Basalt Group and associated volcanic rocks of the Blue Mountains Province, *in* George Walker, ed., Geology of the Blue Mountains Region: U.S. Geological Survey Professional Paper 1437, p. 63-100.

Johnson, A.M., R.A.W. Flaming, K.M. Cruikshank, S. Martosudarmo, N.A. Johnson, K.M. Johnson, and Wei, 1997, Analecta of structures formed during the 28th June 1992 Landers-Big Bear, California earthquake sequence: U.S. Geological Survey Open-File Report 97-94, 59 p.

Johnson, J.A., P.R. Hooper, C.J. Hawkesworth, and G.B. Binger, 1998, Geologic map of the Stemler Ridge quadrangle, Malheur County, southeastern Oregon: U.S. Geological Survey Open-File Report OF 98-105, scale 1:24,000.

Kendal, J.J., R.C. Dale, and G.A. Davis, 1981, The structural relationship of the Olympic-Wallowa lineament, Hite fault system and La Grande fault system, the Blue Mountains of Umatilla County, Oregon: Geological Society of America, Abstracts with program, v. 13, p. 64.

Lawrence, R.D., 1976, Strike-slip faulting terminates the Basin and Range Province in Oregon: Geological Society of America Bulletin, v. 87, p. 846-850.

Lees, K.R., 1994, Magmatic and tectonic changes through time in the Neogene volcanic rocks of the Vale area, Oregon: Milton Keynes, Open University, U.K., Ph.D. dissertation, 283 p.

Mabey, D.R., 1984, Geophysics and tectonics of the Snake River Plain, Idaho, *in* Bill Bonnichsen and R.M. Breckenridge, eds., Cenozoic Geology of Idaho: Idaho Bureau of Mines and Geology Bulletin 26, p. 139-153.

Malde, H.E., 1991, Quaternary geology and structural history of the Snake River Plain, Idaho and Oregon, *in* R.B. Morrison, ed., Quaternary Non-Glacial Geology: Conterminous U.S.: Geological Society of America, The Geology of North America, v. K-2, p. 251-281.

Mann, G.M., 1989, Seismicity and late Cenozoic faulting in the Brownlee Dam area—Oregon-Idaho: A preliminary report. U.S. Geological Survey Open-File Report 89-429, 46 p.

Mann, G.M., and C.E. Meyer, 1993, Late Cenozoic structure and correlations to seismicity along the Olympic-Wallowa lineament, northwest United States: Geological Society of America Bulletin, v. 105, p. 853-871.

Pezzopane, S.K., and R.J. Weldon, 1993, Tectonic role of active faulting in central Oregon: Tectonics, v. 12, p. 1140-1169.

Pierce, K.L., and L.A. Morgan, 1992, The track of the Yellowstone hot spot: Volcanism, faulting and uplift: Geological Society of America Memoir 179, p. 1-53.

Reidel, S.P., and T.L. Tolan, 1994, Late Cenozoic structure and correlation to seismicity along the Olympic-Wallowa lineament, northwestern United States: Discussion and reply, Geological Society of America Bulletin, v. 106, p. 1634-1638.

Thompson, R.N., and S.A. Gibson, 1991, Subcontinental mantle plumes, hot spots and pre-existing thin spots: Journal of Geophysical Research, v. 148, p. 973-977.

Trudgill, B., and J. Cartwright, 1994, Relay-ramp forms and normal-fault linkages, Canyons National Park, Utah: Geological Society of America Bulletin, v. 106, p. 1143-1157.

Walker, George, 1977, Geologic map of Oregon east of the 121st meridian: U.S. Geological Survey Miscellaneous Investigation Series, Map I-902, scale 1:500,000.

Walker, George, and B. Nolf, 1981, High lava plains, Brothers fault zone to Harney Basin, Oregon, *in* D.A. Johnston and J. Donnelly-Nolan, eds., Guides to Some Volcanic Terranes in Washington, Idaho, Oregon, and Northern California: U.S. Geological Survey Circular 838, p. 105-113.

Wells, Ray, and Paul Heller, 1988, The relative contribution of accretion, shear and extension to Cenozoic tectonic rotation in the Pacific Northwest: Geological Society of America Bulletin, v. 100, p. 325-338.

White, R.R., 1981, Structural geology of the eastern half of the La Grande Basin, northeastern Oregon: University of Southern California M.S. thesis, 132 p.

Wood, Spencer, and Drew Clemens, 2002, Geologic and tectonic history of the western Snake River Plain, Idaho and Oregon, *in* Bill Bonnichsen, Mike McCurry, and Craig White, eds., Tectonic and Magmatic Evolution of the Snake River Plain Volcanic Province: Idaho Geological Survey Bulletin 30.

Woodcock, Nigel, and Mike Fischer, 1986, Strike-slip duplexes: Journal of Structural Geology, v. 8, no. 7, p. 725-735.

Zoback, Mary Lou, Edwin McKee, Richard Blakely, and George Thompson, 1994, The northern Nevada rift: Regional tecto-magmatic relations and middle Miocene stress direction: Geological Society of America Bulletin, v. 106, p. 371-382.

Geologic and Tectonic History of the Western Snake River Plain, Idaho and Oregon

Spencer H. Wood[1] and Drew M. Clemens[2]

ABSTRACT

The western Snake River Plain is a Neogene-aged intracontinental rift basin, about 70 km wide and 300 km long, trending northwest across the southern Idaho batholith. Its southeastern end merges with the northeast-trending eastern plain, a structural downwarp associated with extension along the track of the Yellowstone hot spot. Orientation of the western plain rift is parallel to several regional northwest-trending crustal discontinuities, such as the Olympic-Wallowa lineament and the Brothers fault zone, suggesting that the rift failed along zones of lithospheric weakness, as the lithosphere was softened by the passing hot spot. Crustal refraction data and gravity show that the rift is not simply underlain by granitic rock, despite its appearance of having broken and extended the southern end of the Idaho batholith. Instead, the crust beneath 1 to 2 km of basin fill is mostly of mafic composition down to the top of the mantle, about 42 km deep beneath the plain. North and south of the plain, the upper crust has velocities more typical of granitic rock. South of the plain, beneath the 9-11 Ma Bruneau-Jarbidge eruptive center of silicic volcanics, is a zone of slightly high seismic velocity at a depth of 23 km that could be restite or an underplate of basalt related to formation of the silicic magma.

In this paper we show that some (12-10 Ma) rhyolite flows and domes erupted near the margins of the plain, but that thick rhyolite does not occur in deep wells in the subsurface of the plain northwest of Boise. For this reason, we suspect that much of the area of the plain was an upland and not a large depositional basin during the period of silicic volcanism.

Geochronology of volcanic rocks on both sides indicate major faulting began about 11 Ma and was largely finished by 9 Ma. Since about 9 Ma, slip rates have been low (less than 0.01 mm/year) with the exception of a short (about 10-km) segment of late Quaternary faulting in the Halfway Gulch-Little Jacks Creek area on the south side.

Earliest sediment of the plain is associated with basalt volcanism and high rates of faulting. Interbedded arkose, mudstone, and volcanic ash constitute this earliest sediment mapped as the Chalk Hills Formation. Local basalt lava fields (dated 10-7 Ma) occur at several levels in the Chalk Hills Formation. An active rift environment is envisioned with lakes interconnected at times by a river system.

The faulted and tilted Chalk Hills Formation is dissected by an erosion surface at the basin margins, indicating a regression of lakes to the deeper basins. Depositional records of the regression are generally absent from the margins, but we suggest that the east Boise fan aquifer sediments and deep basin fill might be such a record. Nothing is known of the cause of the regression of the Chalk Hills lake.

A transgressive lacustrine sequence encroached over slightly deformed and eroded Chalk Hills Formation on the plain margins, locally leaving basal coarse sand, or a thin beach pebble layer now iron-oxide cemented. The upper part of this transgression deposited shoreline oolitic sand deposits, indicating increased alkalinity of a closed lake. In the Boise foothills, much of the exposed sediment appears to be this transgressive lacustrine sequence

Editors' note: The manuscript was submitted in July 1998 and has been revised at the authors' discretion.

[1]Department of Geosciences, Boise State University, Boise, ID 83725
[2]U.S. Army Corps of Engineers, CENAE-EP-HC, 696 Virginia Road, Concord, MA 01742

Wood, S.H., and D.M. Clemens, 2002, Geologic and tectonic history of the western Snake River Plain, Idaho and Oregon, *in* Bill Bonnichsen, C.M. White, and Michael McCurry, eds., Tectonic and Magmatic Evolution of the Snake River Plain Volcanic Province: Idaho Geological Survey Bulletin 30, p. 69-103.

where it is mapped as the Terteling Springs Formation, with shoreline sands and small deltas interfingering basinward with lake muds. The lake rose to its highest elevation of about 3,600 feet (1,100 m) in a period of less than a few million years. At that highest level, it overtopped the spill point into ancestral Hell's Canyon and the Columbia-Salmon river drainage. Reliable geochronology constrains the time of overflow between 6.4 and 1.7 Ma and is in need of better resolution. The rise in lake level may have been indirectly caused by regional tectonic movement of the migrating uplift of the Yellowstone hot spot, as an associated Continental Divide migrated about 200 km eastward from the Arco area to its position in Yellowstone National Park over the period 6 Ma to present. In doing so, the catchment area of the Snake River may have increased as much as 50,000 square km. Captured runoff associated with the shifting topographic divide is hypothesized to have caused the level of Lake Idaho to rise to its spill point about 4 million years ago.

Downcutting of the outlet was apparently slow (about 120 m/Ma) during which time sandy sediment eroded from the basin margins and filled the remaining lake basin with interbedded mud and sand of lacustrine delta systems. This sedimentary sequence of a slowly lowering base level constitutes most of the Glenns Ferry Formation and the main sand-bearing aquifer section of the western plain. It is represented in the Boise foothills by a 60-m-thick unit of coarse sand with Gilbert-type foreset bedding called the Pierce Park sand. Subsequently, fluvial systems with gradients necessary to produce braidplain sandy gravel deposits flowed to the outlet region near Weiser. These gravel deposits should decrease in age and altitude to the northwest, and at Weiser these oldest gravels occur at elevation 2,500 feet.

During the late stages of the draining of Lake Idaho, basalt volcanism resumed in the western plain, focusing along a line of vents that trends obliquely across the plain at about N. 70º W., named here the Kuna-Mountain Home volcanic rift. Both sublacustrine and subaerial volcanoes erupted and built a basalt upland with elevations of highest shields to 3,600 feet over the last 2.2 million years. Aligned vents and fissures of these volcanoes indicate the present orientation of the principal tectonic stress is N. 70º W., contrasting with the N. 45º W. boundary of the plain and the N. 30º W. alignment of vents in the eastern plain. This N. 70º W. alignment is similar to the same vent features of Quaternary basalt fields in eastern Oregon, suggesting that a province of similar tectonic stress orientation includes the western plain and much of eastern Oregon.

Key words: rift, Cenozoic faulting, lacustrine sediments, Quaternary volcanoes

INTRODUCTION

The western part of the Snake River Plain is an intracontinental rift basin about 70 km wide and 300 km long. It is a normal-fault bounded basin with relief due to both tilting toward the center of the basin and evolving normal fault systems. Maximum depth of Neogene sedimentary fill in the basin is 2-3 km. The offset of older volcanic rocks exceeds 4 km in places. We show here that the rift-basin structure evolved mostly within the last 9.5 million years contrary to estimates by others (Mabey, 1982; Malde, 1991) who have loosely stated the basin began forming 16 to 17 million years ago.

The contiguous lowland of the eastern and western Snake River Plain confused geologists for many years who tried to ascribe a common structural origin to the entire arcuate lowland of southern Idaho (called the "smile face" of Idaho as it appears on physiographic maps). Lindgren (1898) and Kirkham (1939) described the plain as an arcuate structural downwarp. They did not recognize the fault boundaries of the western plain. Malde (1959) was first to report the normal fault boundaries of the western plain.

The eastern part of the plain is not a tectonic rift because it is not fault bounded. Instead, it is a downwarp forming a spectacular low topographic corridor across the actively extending northern Basin and Range Province (Parsons and others, 1998). By all measures, the eastern plain is an unusual lowland formed perhaps by a curious interplay of magmatism and extension (Parsons and others, 1998; McQuarrie and Rodgers, 1998).

The western plain can be more simply explained as a basin and range structure whose formation was triggered by the magmatism of the migrating Yellowstone hot spot (Clemens, 1993). Its orientation is the same as the many northwest-trending half grabens that flank the eastern plain and developed in the "wake" of the northeast-migrating hot spot. In contrast to those half-graben systems, however, the western plain is a much larger feature, 70 km wide compared to less than 30 km wide for the Grand Valley or Lemhi Valley grabens. The western plain lies north of the track of the hot spot. In the hot-spot tectonic model proposed by Anders and others (1989) and Pierce and Morgan (1992), one might expect symmetrically disposed half-graben systems formed beyond the parabolic-shaped "wake" as the hot spot passed by. No corresponding major graben system of similar proportions and age occurs south of the track in the northwestern Utah area.

As shown in Figure 1, the western plain cuts obliquely across an older north-trending Oregon-Idaho graben dated 15.5 to 10.5 Ma (Cummings and others, 2000). It also truncates the south end of the west-central Idaho fault belt identified by Hamilton (1963), a relatively young

system of north-trending normal faults. Early in its history the western plain underwent rapid subsidence and became the locus for the major lacustrine system of Lake Idaho, which persisted from about 9.5 to 1.7 Ma. The lake system underwent a substantial lowering about 6 Ma and then refilled. The 7.8-Ma duration of the lake system is long but typical of other rift lakes, such as east African Lake Malawi discussed by Johnson and Ng'ang'a (1990).

The western plain rift basin is similar in dimensions and structure to intracontinental rifts elsewhere in the world, such as those in east Africa, the Baikal Rift in eastern Russia, and the Rio Grande Rift in southwestern United States. The structure is a complex of half grabens and full grabens similar to that reported by Bosworth (1985) in other continental rift settings. The volcanism of the western plain differs from those rifts by its association with a migrating continental hot spot indicated by a pattern of time-transgressive silicic volcanism.

Practical geological interest in the western plain is largely inspired by the great ground-water resources in the sedimentary fill, and to a lesser extent by the geothermal ground water in the deep volcanic rocks. These resources are essential to the economy of semiarid southwestern Idaho. Recent pumpage has been about 0.3 million acre-feet/year (0.37 cubic km/year; Newton, 1991). Ground-water development has been mostly within the upper 800 feet (250 m) of section and has been spectacularly successful with some wells in sand aquifers producing 3,000 gallons/minute (1,600 cubic m/day; Squires and others, 1992). Many wells, however, are drilled into thick mudstone sections with poor production. The distribution of sand aquifers in the fluvial-lacustrine section is complex, but in just the last few years we are gaining a clearer understanding of the depositional history and gross features of the sedimentary architecture (Squires and others, 1992; Wood, 1994). Toward this end, we have turned the unsuccessful oil and natural gas exploration in the basin to our advantage. We have examined the scattered data on deep holes drilled by petroleum companies mostly in the years between 1950 and 1985 (Wood, 1994). This information and recent studies have improved the ground-water models now being developed for managing the resource and averting conflicts over ground-water use.

In this study, we review geophysical data on the western plain and interpret seismic-reflection data and deep drill-hole data to understand both the tectonic framework of the basin and the sedimentary facies of the basin fill. We incorporate available K-Ar and $^{39}Ar/^{40}Ar$ ages of volcanic rocks and paleomagnetic data for a chronology of events that produced the plain. We elucidate features of the sedimentary fill pertinent to the location of sand aquifers in the predominantly mud sediments of the lake system. From these data and geomorphological considerations, we propose a model for the history of the great lake system that filled the basin and its eventual overflow into ancestral Hell's Canyon. We also discuss Qua-

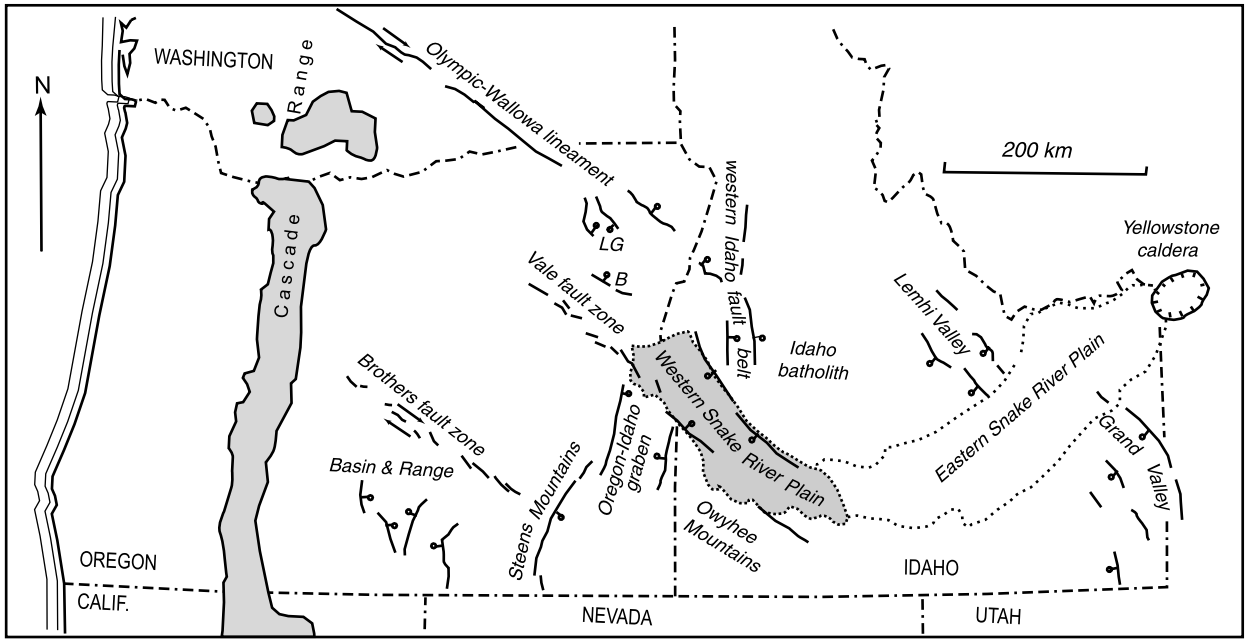

Figure 1. Regional setting of the western Snake River Plain showing related geologic features and emphasizing northwest-trending, late Cenozoic fault structures in Oregon and Idaho. LG—La Grande graben, B—Baker Valley.

ternary geomorphic features of the fluvial system that followed the draining of the lake and tectonic aspects of the Quaternary basalt fields that cover part of the western Snake River Plain.

CRUSTAL STRUCTURE AND TECTONICS

Basic to understanding the origin of the western plain is the following question. What is it about the earth's crust that causes a wide northwest-trending sag and graben just here in southern Idaho? The upper crust extended several kilometers to form this 50- to 70-km-wide rift. The northwest trend of the western plain cuts across north- to south-trending older Miocene extensional structures. The northwest trend, however, is the same as that of several smaller late Cenozoic graben basins northwest of the plain (La Grande Valley, Baker Valley). These basins show late Quaternary faulting on their margins (Pezzopane and Weldon, 1993). Several major lineaments of the northwest United States also have the same northwest-southeast trend (the Olympic-Wallowa lineament, Vale fault zone, and the Brothers fault zone). The lineaments are spaced 70 to 200 km apart through eastern Oregon (Figure 1). Parts of some lineaments are expressed by normal faults. Many of the lineaments show small amounts of late Cenozoic right-lateral movement expressed as *en echelon* normal faults or pull-apart basins. Displacements are but a few kilometers, thought to accommodate differences in extension across the lineament structures (Lawrence, 1976). The pervasive northwest structural trends suggest an orientation for zones of lithosphere weakness that have responded to late Cenozoic stress systems. While inherited zones of weakness might explain the orientation of the western plain, it does not explain the geographic position or width.

The western plain cuts across the southern part of the Mesozoic Idaho batholith, with the Owyhee Mountains segment (Taubeneck, 1971) split off to the south of the main outcrop (Figure 2). The elevation of most of the batholith mountains to the north, as well as the crest of the Owyhee Mountains, is about 8,000 feet (2,440 m). Southwest of the Owyhee Mountains is the Owyhee Plateau, a region of low relief (elevation about 5,500 feet, 1,680 m) extending into northern Nevada and southeastern Oregon. Flows of hot-spot rhyolite and basalt that form the plateau are relatively little deformed by faulting or tilting, and little is known of the underlying crust.

If the western plain is an ordinary graben, it should be underlain by downfaulted granitic rocks of the Idaho batholith. According to Hill and Pakiser's (1967) interpretation of deep crustal refraction data, a significant layer of rock having the velocity of granite (V_P of 5.5-6.4 km/s) does not underlie the plain. Prodehl (1979) reinterpreted the refraction data and concluded similarly that granitic-rock velocities are restricted beneath the western plain. Instead, the plain is underlain below 8-km depth by high-velocity material, V_p = 6.6-6.8 km/s (Figure 3). This contrasts with crust south of the plain (Mountain City to Elko), where 6.1 km/s material extends down to an 18-km depth. We have no refraction data north of the plain; however, the very existence of the extensive Idaho batholith north of the plain indicates granitic crust. The depth to the base of the batholith has not been gravity modeled to our knowledge, although Cowan and others (1986) illustrate it in their cross section to extend to 8 to 10 km. The thickness of most great granite batholiths is probably not more than 15 km, and the erosion of roof rock has probably reduced the depth to the base of the granite of exposed batholiths to less 10 km (Bott and Smithson, 1967; Leake, 1990). By analogy with the Sierra Nevada batholith, granitic rock there extends to a depth of 10 to 15 km and appears to be underlain by a root of low velocity (6.5 km/s) material to a depth of 40 km (Fliedner and others, 1996). In addition, a relatively low-velocity upper mantle material is detected to a 60-km depth. It is reasonable to assume that at one time granite beneath the plain was 8 to 10 km thick, but has been intruded by significant quantities of basaltic rock.

A large positive gravity anomaly is associated with the western plain (about +100 milligals) relative to the bordering batholith regions (Mabey, 1982). The anomaly has two peculiar features (Figure 4). It is composed of a broad positive anomaly paralleling the margins of the plain (N. 40º W.). Superposed on this is a narrow (30-km-wide) feature of about +25 milligals that trends obliquely (N. 70º W.) across the plain, south of Mountain Home, for a distance of 140 km (shown in Figure 4 by the southeastern region enclosed by the -105 milligal contour). The narrow anomaly can be accounted for by the Quaternary basalt field, but the broad anomaly must arise from a deep high-density body. Mabey (1982) modeled a single gravity profile perpendicular to the plain, near Mountain Home, and reproduced the gravity data with a deep body of density 2.9 g/cm^3 from 9 to 18 km and a shallow body of the same density from 3 to 6 km depth. A density of 2.9 g/cm^3 is appropriate for solid basalt or gabbro in contrast to a density of 2.65 g/cm^3 for granitic rocks, and less than 2.3 g/cm^3 for sedimentary rocks. Both the seismic refraction data and gravity data indicate that the sediment and volcanic fill are underlain by material in the intermediate crust having appropriate velocity and density of diabase or gabbro intrusive rocks, and not material typical of granite.

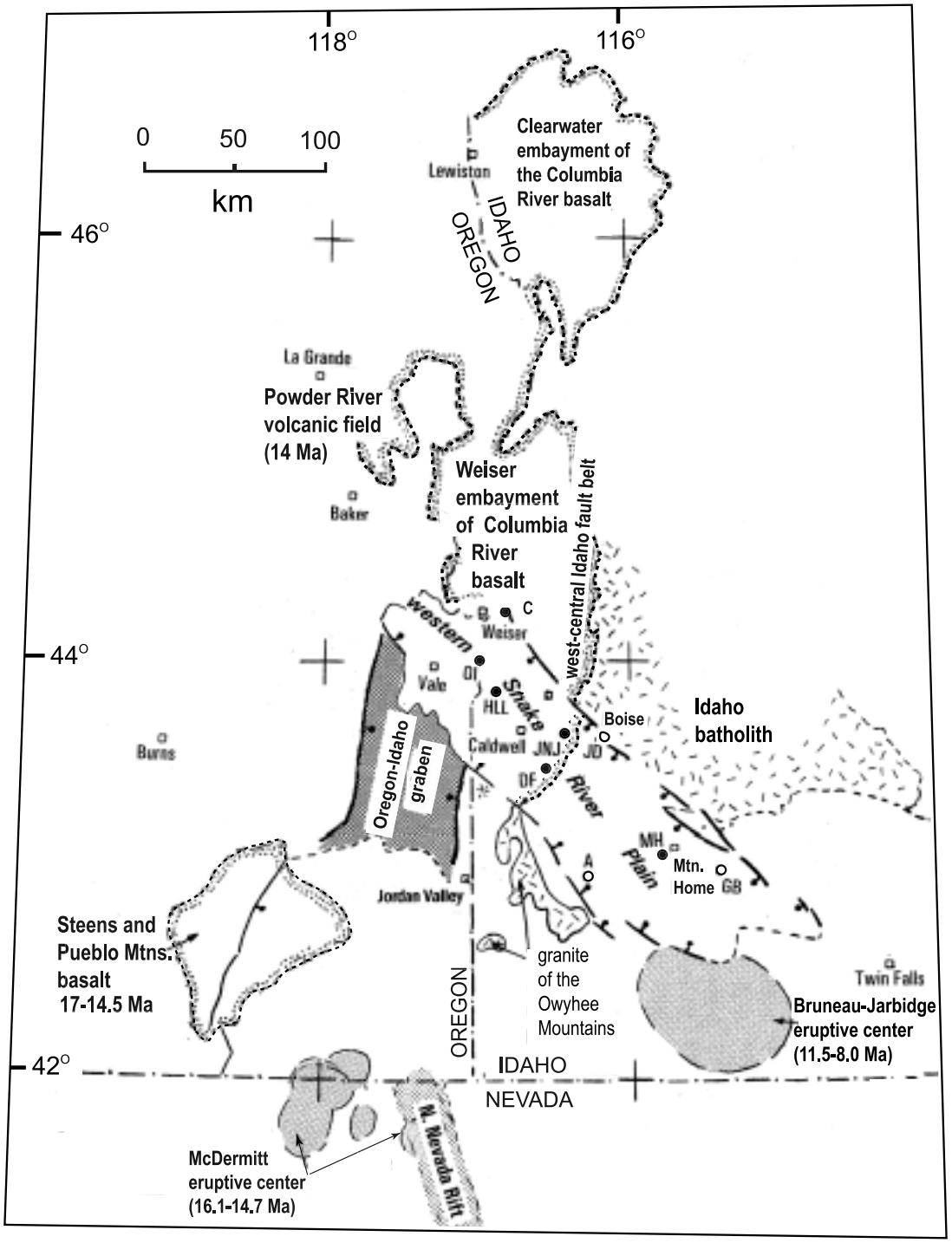

Figure 2. Map showing tectonic features surrounding the western Snake River Plain and locations of deep wells into volcanic basement. Wells only in deep basalt are shown with a solid circle: C—Chrestesen No. A-1; OI—Ore-Ida Foods No. 1; HLL—Highland Land and Livestock No. 1; JNJ—J.N. James No. 1; DF—Deer Flat No. 1; and MH—Mountain Home Air Force Base Geothermal Test. Wells in deep rhyolite are shown with an open circle: JD—Boise Julia Davis Park; A—Anschutz Federal No. 1; and GB—Griffith-Bostic No. 1. Tectonic feature locations and reference sources: northern Nevada rift (Zoback and others, 1994); Oregon-Idaho graben (Cummings and others, 2000); rhyolite-field eruptive centers (Bonnichsen, 1982; Pierce and Morgan, 1992; McCurry and others, 1997); and the Columbia River and Steens Mountain basalt areas (Hooper and Swanson, 1990; Lees, 1994; Hooper and others, 2002a, 2002b.).

A substantial accumulation of Miocene basalt lava lies beneath the sediments of the western plain. We show a hypothesized contact of lavas with underlying intrusive basalt (Figure 3). The deepest drill hole in the plain at Meridian (J.N. James well, 4.3 km deep) penetrates a thick basalt section and bottoms in basalt flows having a geochemical affinity with the Columbia River Basalt Group (Clemens, 1993; Figure 5). No inclusions of deep crustal rocks are known from western plain basalt, so we can only speculate on the geophysical results that either the underlying crust contains insignificant remnant granite greatly intruded by Cenozoic diabase and gabbro, or it is entirely filled with mafic intrusives.

Extension could have thinned the granite, but as we

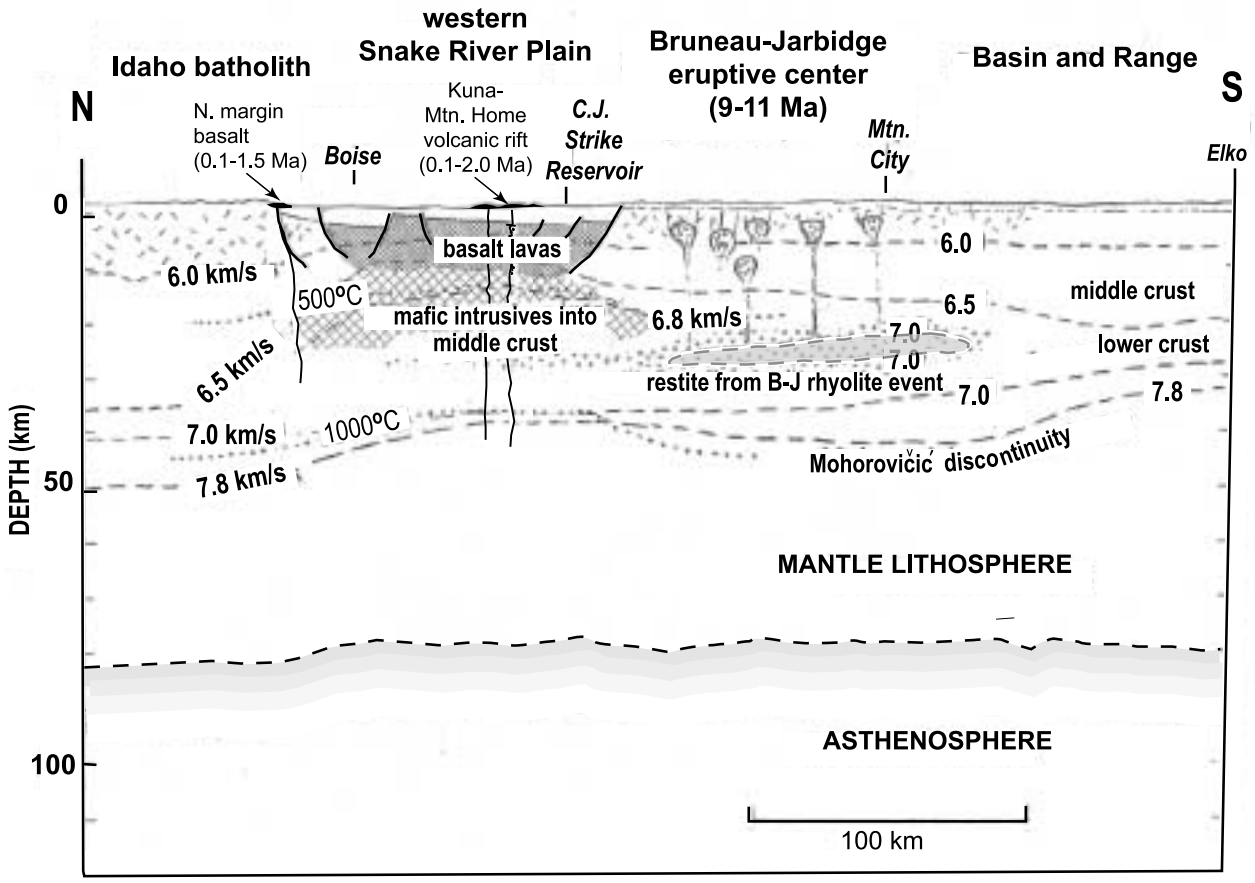

Figure 3 (A)

Figure 3. **(A)** Lithosphere structure interpreted principally from crustal structure beneath the western Snake River Plain and adjacent areas. Interpretation is based on the seismic refraction line of Hill and Pakiser (1967) and the reinterpretation by Prodehl (1979). Location of seismic line shown on map. Noteworthy is the upward bulge of material, with $V_P > 6.6$ km/s beneath the western plain believed to be mafic rock, and the overlying thin (~5 km) layer with velocity between 6.0 and 6.5, believed to be basalt flows or granite intruded by basalt. Prodehl's interpretation shows a high velocity layer ($V_P > 7.0$ km/s) that lies in the deep crust beneath what is now recognized as the Bruneau-Jarbidge rhyolite eruptive center along the track of the hot spot. We suggest the high-velocity layer might be restite remaining from the partial melt and extraction of rhyolite melt. It is important to realize that the crustal refraction velocities shown beneath the plain are obtained from arrivals into a string of detectors, south of Boise, and are an average of the crust between Boise and C.J. Strike. No experiments have explored structure beneath the Idaho batholith. The batholith structure shown is inferred from a section by Hyndman (1978) and Cowan and others (1986) and by analogy to the Sierra Nevada batholith shown by Fliedner and others (1996). Mafic intrusives in the intermediate crust were first suggested by Mabey (1976) from gravity data. Diagrammatic diapirs of silicic melts beneath the B-J area were suggested by Leeman (1989). Dotted-line isotherms are from heat-flow models of Brott and others (1978). One can only guess the depth of the asthenosphere at about 90 km (see Smith and Braile, 1993, Figure 35, for the eastern plain, and by analogy to the Rio Grande Rift, Baldridge and others, 1984, Figure 2).

(B) Prodehl's (1979) reinterpretation of refraction data and crustal structure from Boise to Elko.

(C) Map showing the location of the seismic refraction line. Labeled triangles are shot points, and circles are detector positions.

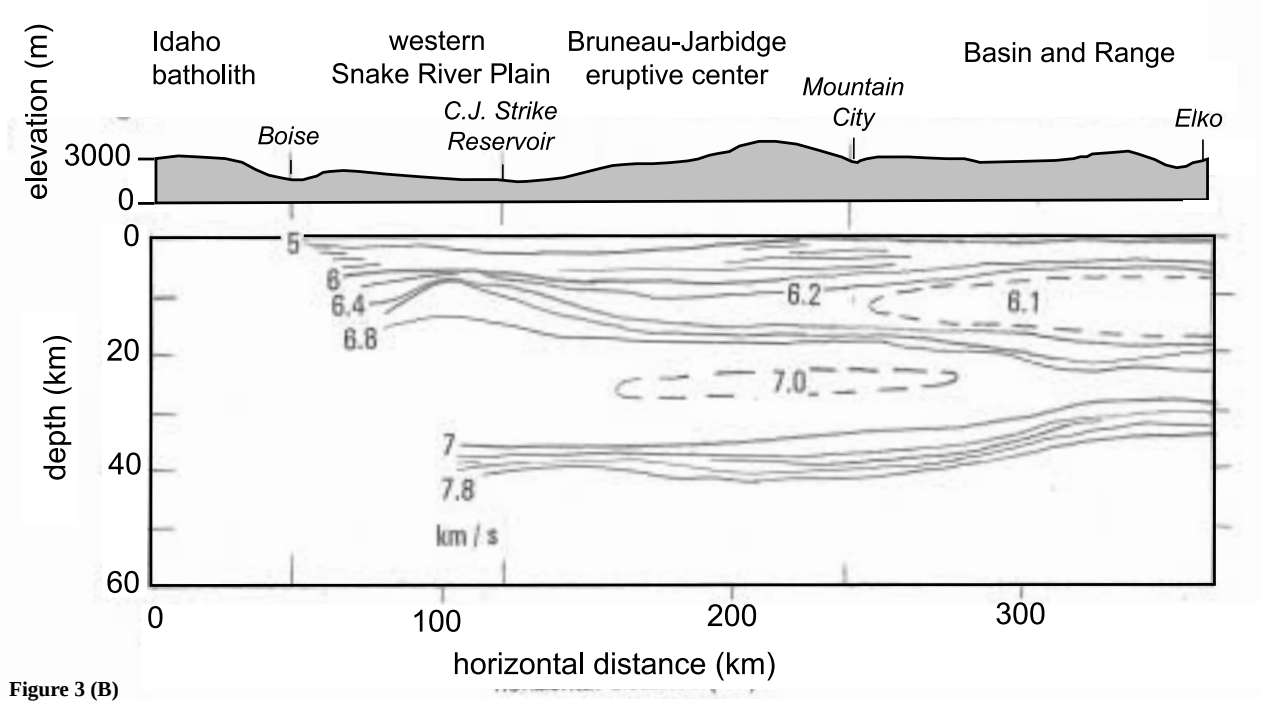

Figure 3 (B)

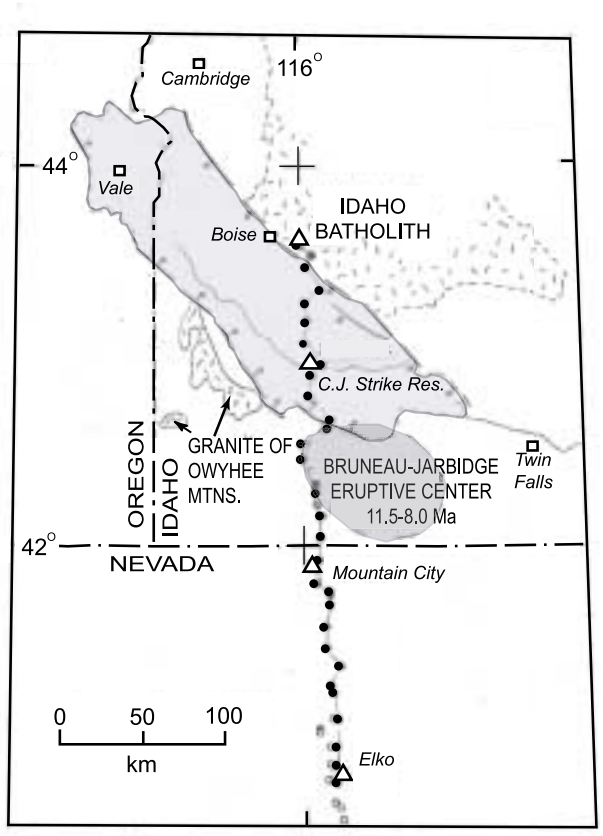

Figure 3 (C)

will show, it is unlikely that this process has greatly altered the thickness of the granite. To evaluate extension, we have added up the vertical dip-slip fault offset of the basement volcanic rock, shown on Figure 5, and assuming 45-degree dipping normal fault planes, we obtain only about 2 km of vertical offset and therefore a corresponding 2 km of horizontal extension of the 60 km width, or about 3 percent extension. Such an evaluation using only fault offset does not take into account the component of basin extension expressed by subsidence due to downwarping. If, instead of faulting, we consider the volume of the basin to have been created by extension of the upper 10 km of crust, we obtain an extension of about 10 percent. This value of extension is comparable to the 7 to 14 percent extension determined for the east African rift basins by Rosendahl and others (1992) and around 10 percent for the Rhine and Baikal rifts (Park, 1988, p. 84). It seems unlikely that extension of 10 percent could thin the granite so that it is undetectable from seismic refraction velocity measurement.

Although the western plain would not be regarded as strongly extended, with about 10 percent extension, the modification of the composition of the middle and lower crust below 8-km depth is considerable. Our preferred explanation is that the middle and lower crust under the western plain has been so invaded by mafic intrusives that it has a seismic velocity (6.6 km/s) similar to that indicated for diabase by Christiansen and Mooney (1995). Dense, high-velocity rock could also form in the middle

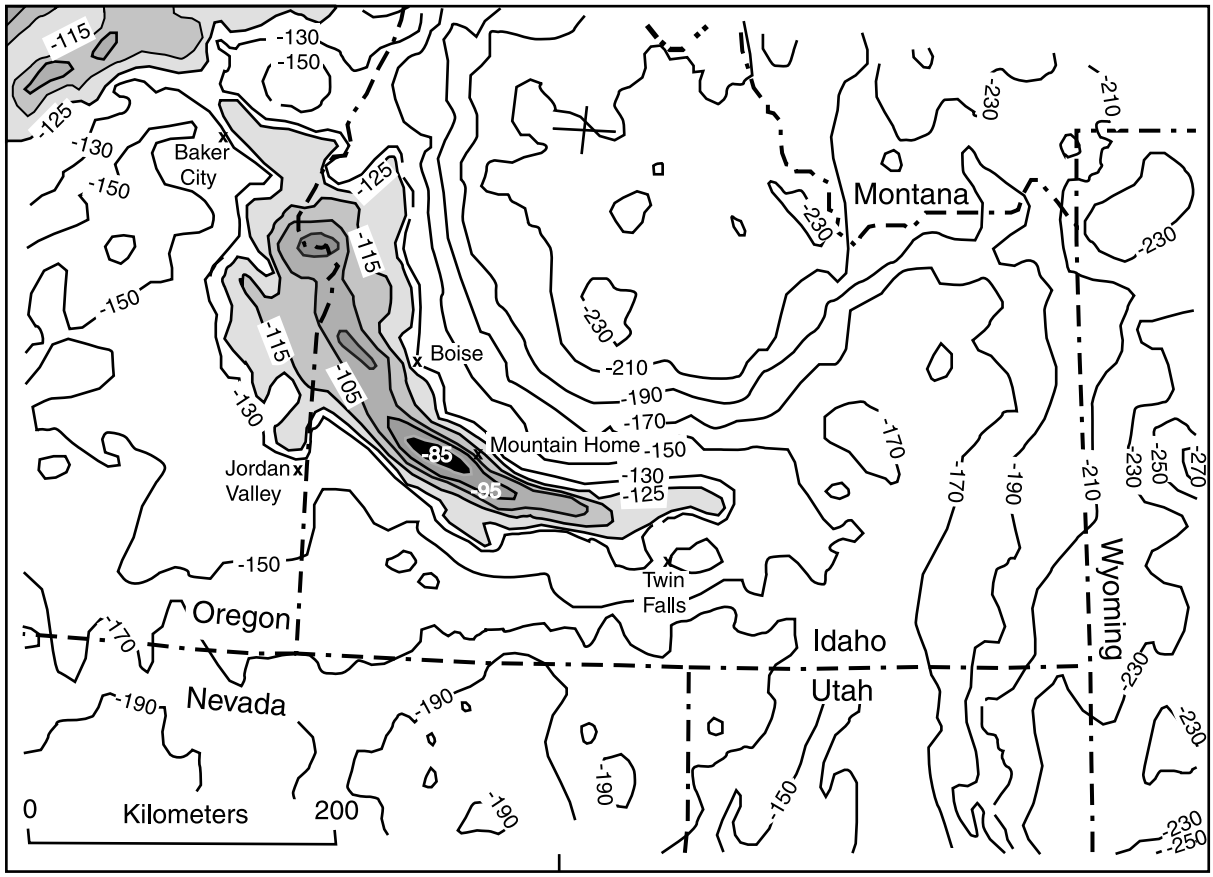

Figure 4. Map of Bouguer gravity anomalies of the western Snake River Plain region. Noteworthy is the high gravity anomaly of the western plain indicating rock of high density beneath the plain. Contour interval is 20 milligals, except for values more positive than -130 milligals. The areas of more than -125 milligals are shaded and contoured every 10 milligals. Map is from the Gravity Anomaly Map Committee (1987). Values are terrain corrected in areas of high relief. Bouguer anomalies are calculated by subtracting the theoretical attraction of rock mass above sea level using a standard crustal density of 2.670 g/cm^3. This attempts to remove the effects of varying topographic relief. Thus Bouguer anomalies result from masses above sea level with densities different from 2.67 g/cm^3, or from any lateral variation of density below sea level. In continental regions, the regional values are negative because topography is usually isostatically compensated by low density crust extending below sea level. Theoretically, corrected gravity will be zero only at sea-level measuring points.

crust by magmatic differentiation or by partial melting and eruption of the silicic component, leaving a residual mafic material; however, the volume of silicic volcanics erupted from the plain area appears to be too small (less than 500 cubic km) to account for a residual volume of high velocity rock in the intermediate crust. Most of the silicic magma of the region erupted from vents south of the western plain.

Crustal velocities in the western plain are different from those in the eastern plain, where such large lateral variations in velocity of the upper and middle crust are not detected. This led Braile and others (1982) and Wendlandt and others (1991) to infer that rising basalt may not have yet significantly modified the middle crustal composition of the eastern plain.

From the reinterpretation of the western-plain seismic refraction profile by Prodehl (1979), one might infer from his velocity model that granitic material lies south of the plain, between depths of 6 to 15 km, and that an anomalous 10-km-thick high-velocity layer of 7.0 km/s lies deep in the crust from 20 to 30 km (Figure 3). The location of that layer coincides with the roots of the large Bruneau-Jarbidge rhyolite eruptive center identified by Bonnichsen (1982) and located along the track of the Yellowstone hot spot (Figure 2). A deep-crustal high-velocity layer in this position supports the idea of a remnant of deep crustal underplate of plume basalt suggested by Leeman (1989). Alternatively, the layer could be the mafic residual of deep crust from which 2,000 cubic km of rhyolite is estimated by Pierce and Morgan (1992) to have erupted from the Bruneau-Jarbidge area.

Thus, rifting by downwarping and normal faulting

along northwest-trending boundary faults initiated extension of the western-plain crust, cutting through the south end of the batholith. It is possible that a pre-existing lithosphere structure along this trend was particularly vulnerable to weakening by heating and extension caused by the passing hot spot 10 to 11 million years ago. The rifting process involved the injection of large amounts of basaltic magma into the middle crust beneath the western plain, and that process may have greatly extended the early rift, more so than is estimated by our examination of the basin volume or faulting of the Miocene basalt basement. Basaltic magma may have been injected into the downfaulted block of granite. Humphreys and others (1999) suggest that much of the subsidence of the eastern plain is caused by the weight of added basalt to the crust, and that explanation invoked by Baldridge and others (1995, p. 455) for other continental rifts, may also apply to the western plain. Again, we point out that the actual track of the hot spot adjacent to the south side of the western plain appears to correlate with a high-velocity (7.0 km/s) body in the deep crust that may contain injected basalt or mafic residue from hot-spot volcanism. In contrast, beneath the western plain the high velocities and inferred injected basalt extend upward to a much shallower depth (8 km). These interpretations of older seismic refraction data indicate that deep-crustal seismic experiments and a reevaluation of gravity data using modern methods would contribute to our knowledge of the Bruneau-Jarbidge eruptive center, the western plain, the batholith, and the effect of the migrating hot spot on the crust.

Because the plain is the product of extension and has clear evidence of high-angle, normal faulting at the surface, it is appropriate to question whether these high-angle faults shoal in dip at depth and merge with low-angle detachment faults. Recently proposed models of extended terrane show such detachments at the brittle ductile transition at depths of 15 to 30 km beneath the Basin and

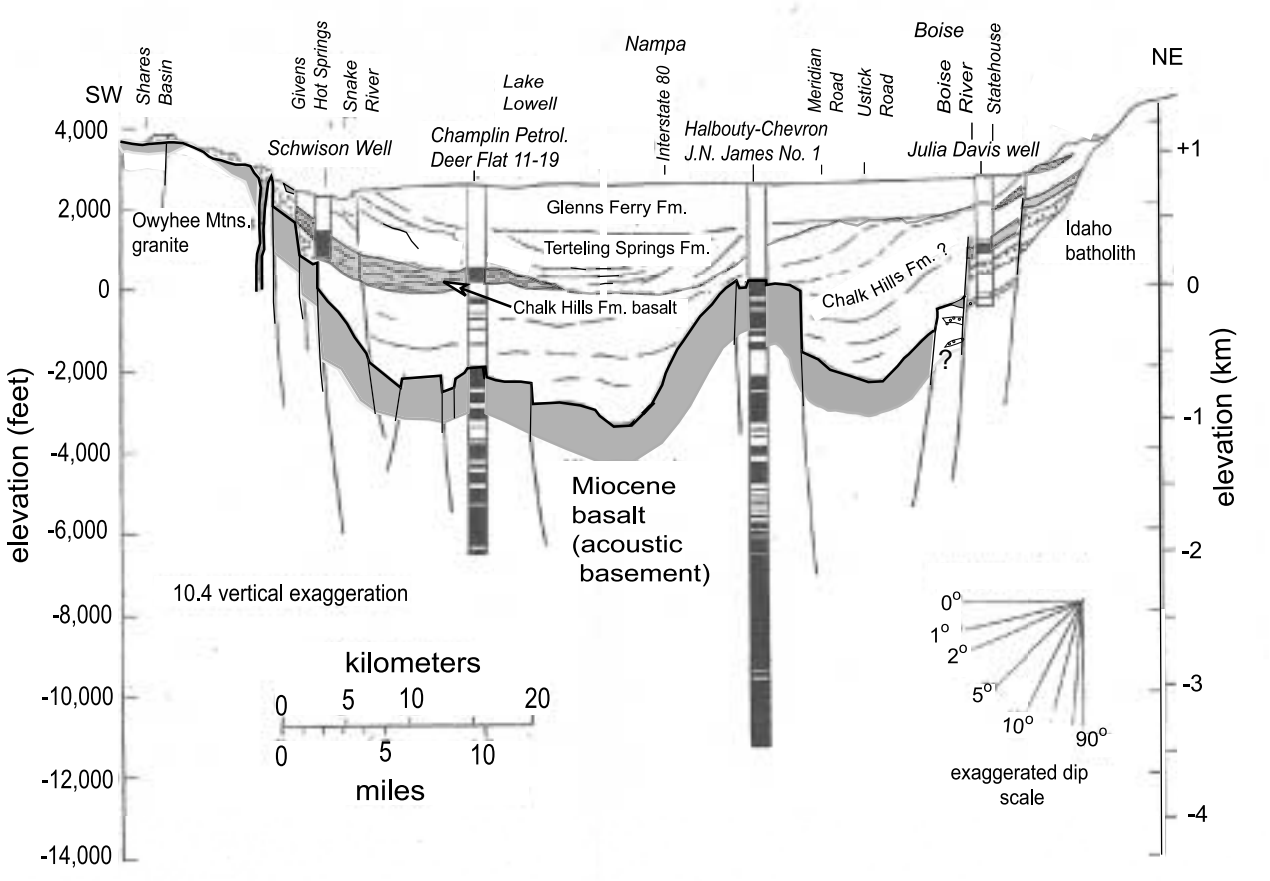

Figure 5. Section across the western plain showing the basalt occurrence (dark pattern) in the deep wells and the configuration of sedimentary fill and associated basalt from seismic reflection data. Shaded outline is the top of Miocene basalt. Stippled pattern is rhyolite that occurs in wells only at the margins of the plain.

Range Province (Wernicke, 1992). Fault block rotation, indicating the curvature of some faults at depth, occurs only along the northeast margin faults at the west end of the Mount Bennett Hills. Wood (1989) shows that the blocks have rotated to northeast dips of 12 to 25 degrees. We have no geophysical observations on the nature of faults deeper than 6 km, but certainly we allow that they could greatly decrease in dip and merge with detachments at depth as they approach the ductile middle crust. The crust is considered ductile below about 13 km because that is the limiting depth of earthquakes in this region.

THE BEGINNING OF THE WESTERN SNAKE RIVER PLAIN BASIN

We address here the time at which the western Snake River Plain first became a depositional basin. Previous workers have loosely assumed it began about 17 to 16 Ma (Mabey, 1982; Malde, 1991), associating the western plain graben with the beginning of large-scale extension in the Basin and Range Province to the south. We believe that the graben basin did not begin forming until 11 Ma. Our presumption is that evidence for the formation of the incipient plain must be (1) northwest-oriented normal faulting and downwarping of the western plain area and (2) accumulation of sediments in a basin.

STRUCTURES BEFORE THE WESTERN PLAIN GRABEN

Before formation of the western plain, extensional-fault and dike structure had a more north-south trend (Figure 1). Extensional faults and dikes were a north-south orientation during the eruption of Columbia River basalt north of the plain in the interval 17 to 14 Ma (Hooper and Swanson, 1990), in the Steens Mountains (Minor and others, 1987), and in the northern Nevada rift from 18 to 14 M (Zoback and others, 1994). The north- to south-trending Weiser embayment of the Columbia River Basalt Group was a basin that accumulated at least 2.1 km of basalt prior to formation of the western plain (well logs from 1978 Phillips Petroleum Chrestesen No. A-1). Columbia River basalts onlap the batholith at the eastern margin of the embayment. It is not known whether this margin is a result of basin downwarping or if it is partly a fault boundary. The Weiser embayment is oriented north to south similar also to the Clearwater embayment (Figure 2). From surface mapping, other workers have reported that the Weiser embayment contains up to 0.7 km of Imnaha Basalt (17.2-16.5 Ma), as much as 0.2 km of Grande Ronde Basalt (16.5-15.6 Ma), and 0.3 km of the younger (< 15 Ma) but undated Weiser Basalt (Hooper and Swanson, 1990; Fitzgerald, 1982; Hooper and Hawkesworth, 1993).

South of the western plain, Cummings and others (2000) have discovered a north- to south-trending basin they have named the Oregon-Idaho graben (Figures 1 and 2). The bounding faults on this graben formed 15.5 to 10.5 Ma. The basin filled with bimodal (rhyolite and basalt) volcanic assemblages and sediments over 2 km thick. Dike orientations in the basin generally trend north to northeast (Ferns and others, 1993). The basin was later truncated by the northwest faulting that formed the western plain. The east side of the Oregon-Idaho graben and the east side of the Weiser embayment coincide with a north-trending zone of steep gravity gradient, where the Bouguer value increases about 25 milligals from the area on the east underlain by granitic batholith to the basalt-filled basin on the west (illustrated in Figure 4 and in more detail by Figure 2-1 of Wood and Anderson, 1981). Though rhyolite eruptives are more conspicuous at the surface of the Oregon-Idaho graben, the gravity data suggest a thick graben fill of dense basalt that contrasts with lower density granitic rock to the east (illustrated just north of Jordan Valley, in Figure 4).

The spatial arrangement of the Weiser embayment basin across the western plain from the Oregon-Idaho graben tempts one to correlate these two north-northeast trending structures (Figure 2). The ages of basalt fill of the Weiser embayment span the time of the pre-Ore-Ida graben accumulation of at least 0.6 km of tholeiitic basalt and latite and also the accumulation of 2 km of lava flows and volcaniclastic sedimentary fill in the graben. Pre-graben tholeiitic basalt also occurs in a 1-km-thick section to the adjacent east in the Owyhee Mountain upon which Pansze (1974) obtained a whole-rock K-Ar age of 17 Ma (Ekren and others, 1982; Cummings and others, 2000). Basalt dikes within this Owyhee Mountains section trend north-south (Ekren and others, 1981). Therefore, it seems likely that north- and north-northeast-trending basins were the dominant structural-basin pattern before the western Snake River Plain graben formed.

Several deep wells (greater than 2.7 km deep) in the northwestern part of the western plain penetrate thick sections of basalt and tuffaceous sediment beneath the lacustrine sediment (Clemens, 1993). Figure 2 shows a western group of deep wells, drilled only in basalt at depth, that did not intersect rhyolite. The J.N. James No. 1 well was drilled by the Halbouty-Chevron group to a depth of 4.3 km in the center of the western plain at a site 25 km west of Boise. Beneath 0.7 km of lacustrine sediment, the well contains a 1.59-km-thick section of basalt lying upon a 1.37-km-thick sequence of mostly basaltic tuff,

and a bottom section of 0.2-km-thick basalt (Figure 5). The chemistry of five samples of bottom basalt cuttings from 4.08 to 4.11 km in depth were analyzed for major, trace, and REE elements (Clemens, 1993) and fall within the range of Columbia River basalts, being most like the olivine tholeiites of the Powder River volcanic field (Figure. 2) that erupted 14 Ma in the La Grande and Baker grabens (Hooper and Conrey, 1989), but also having some characteristics of the Imnaha Basalt (Peter Hooper, written commun., 1993; Clemens, 1993). We have not yet analyzed the other basalts in the well. The most one can conclude is that no significant rhyolite occurs in this well and that the lower basalt is similar to the basalt in the Weiser embayment.

The Highland Land and Livestock No. 1 well (3.64 km deep) and Ore-Ida No. 1 well (3.06 km deep) drilled through similar sections of interbedded basalt and sediment to a total depth beneath the upper 1.1 km and 1.4 km of lacustrine sediment, respectively. Samples from the Ore-Ida well were submitted for K-Ar dating by participating companies. The resulting dates are known, but laboratory details are not available. Basalt cuttings from a depth of 2.18 km in the Ore-Ida well yielded a whole-rock age of 16.2 ± 1.8 Ma, and core from a depth of 2.50 km a whole-rock age of 9.0 ± 1.8 Ma. The stratigraphic contradiction in the ages suggests that either the apparently older sample has gained radiogenic argon or the older age is correct. The apparently younger and deeper sample could have lost argon by the hydrothermal alteration of the basalt, and therefore the sample could be older. Nevertheless, the 9.0 Ma age can be regarded as a minimum age for this basalt.

THE INCEPTION OF SILICIC VOLCANISM AND UPLIFT

It is widely advocated that the Yellowstone hot spot was first manifested in eruptions of the Imnaha Basalt about 17.5 Ma along north and north-northwest-trending fissures in the Hell's Canyon area (Hooper and Swanson, 1990), as eruptions of the Steens Basalt (16.1 Ma), as eruptions and caldera collapse of several rhyolite centers near McDermott, Nevada, and as basalt dike emplacement along the N-NW-trending northern Nevada rift about 17 Ma (Pierce and Morgan, 1992; Zoback and others, 1994). During the inception of silicic volcanism (17-14 Ma), the rhyolite erupted from vents scattered over a broad region encompassing most of southwest Idaho south of the western plain and adjacent parts of Nevada and Oregon. By 11 Ma, silicic volcanic vents were centered mostly in the Bruneau-Jarbidge region (Bonnichsen and others, 1989) but were also distributed to the northwest along the future site of the western plain graben (Figure 6). The actual vent areas for many of the larger volume tuffs and flows have not been located, but many emanated from the Bruneau-Jarbidge region. Rhyolite vents are evident along the margins of the western plain. Jenks and others (1993) mapped a thick rhyolite breccia with unbrecciated dikes and sills, near Little and Big Jacks Creek, which they called the rhyolite of Horse Basin. They suggest it erupted from a buried NW-trending fissure near the edge of the plain. A faulted 1-km-diameter dome occurs south of Givens Hot Springs at the southwest edge of the plain and edge of the Owyhee Mountains (S.H. Wood, unpub. mapping). Clemens and Wood (1993) and Clemens (1993) have obtained K-Ar ages on near-source rhyolite lava flows of 11.8 to 11.0 Ma near and west of Boise on the north margin. It appears that eruptions of domes and small flows may have accompanied the beginning of the active phase of northwest-trending faulting, but that rhyolite volcanism had largely ceased by the time the basin began to form.

Most of the 12-10 Ma rhyolite accumulations on the margins of the western plain are without significant sedimentary interbeds (Wood and Gardner, 1984). The only known exception is from recent drilling in the subsurface beneath north Boise (City of Boise, Julia Davis Park well; Figure 5) where two rhyolite flows are separated by 130 m of coarse arkosic sand and batholith-derived gravel. The lowest flow is underlain by 60 m of similar coarse sediment at the bottom of the 0.98-km-deep well (P.N. Naylor, written commun. 1998). This sediment occurrence might be explained by local downfaulting associated with the eruptions adjacent to the batholith mountains. Perhaps this was the site of early basin initiation accompanying the rhyolite eruptions, but lack of a fine-grained lacustrine facies in the deep section precludes association with a deep basin. Likewise, the 2.3-km section of rhyolite in the Anschutz-Federal well on the south margin of the plain is without significant sedimentary interbeds (McIntyre, 1979). Elsewhere around the western plain, the lack of sediment in the nearly continuous pile of rhyolite eruptives suggests that during time of silicic volcanism the area was an upland. One would expect to find caldera basins; however, Ekren and others (1984) were impressed by the lack of conspicuous caldera features associated with silicic volcanism south of the plain in the region east of the Oregon border.

We believe it is significant that the deep wells in the center of the western plain, discussed above, have not drilled sections of rhyolite, despite abundant and thick rhyolite on the northeast and southwest margins. The lack of rhyolite beneath the plain is indeed surprising, and we can only conclude that the center of the present plain was formerly an upland of older basalt.

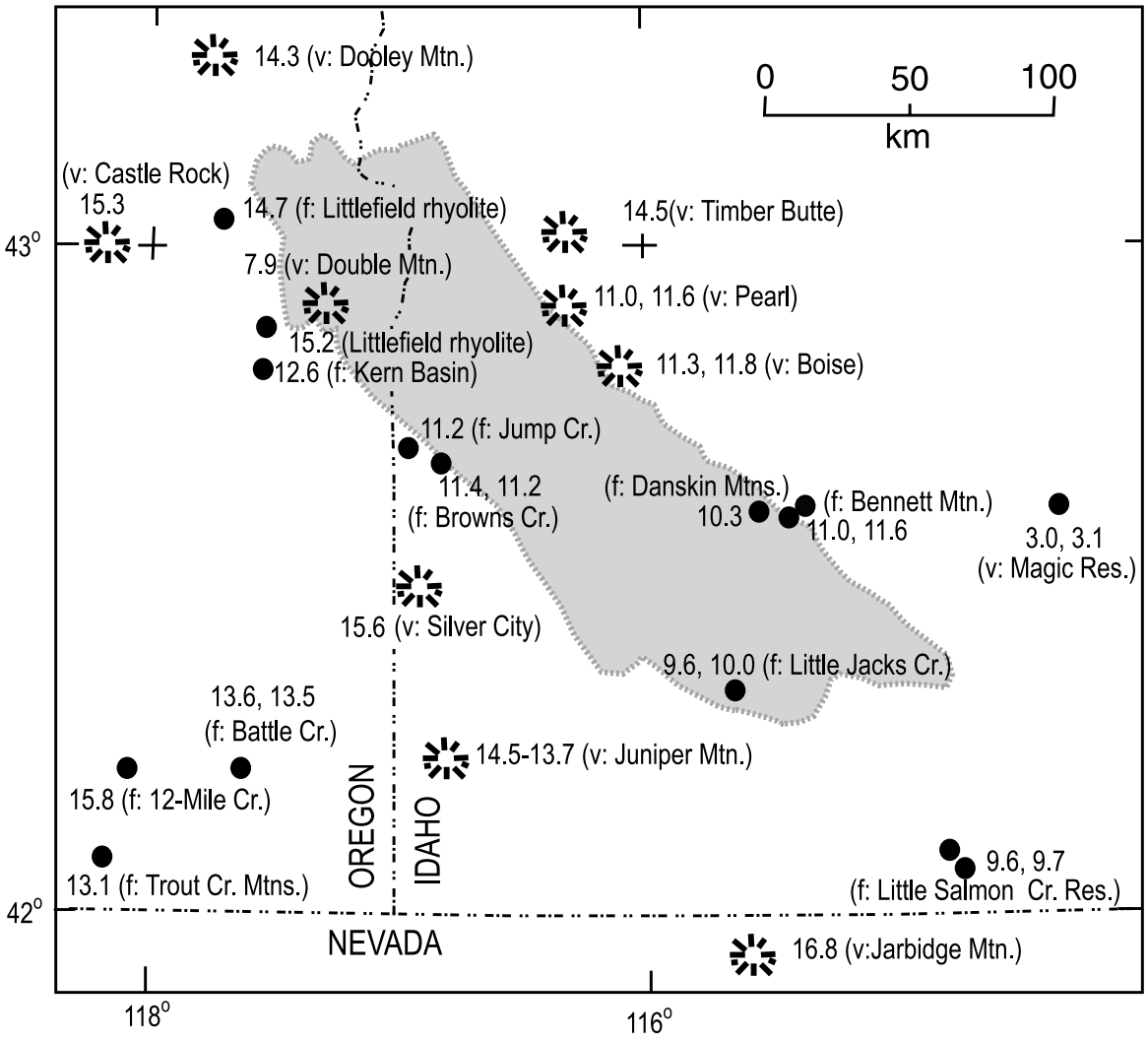

Figure 6. K-Ar ages (Ma) of rhyolite vents (v) and tuffs or lava flows (f) adjacent to the western Snake River Plain from Neill (1975) and Armstrong and others (1980) quoted in Ekren and others (1981, 1984), Clemens (1993), and Clemens and Wood (1991, 1993a, 1993b), Walker and others (1974), Dalrymple and others (1967), MacLeod and others (1975), Ferns and Cummings (1992), Rytuba and Vander Meulen (1991), and Ar-Ar ages from Lees (1992), and Manley and McIntosh (1999). All K-Ar ages calculated using 1976 constants except Trout Creek, 12 Mile Creek, Battle Creek, Salmon Creek, Jarbidge, and Silver City, which may be 0.1 to 0.4 Ma older than shown if recalculated.

East of Boise are two wells that drilled deep rhyolite near the margins of the plain (Anschutz-Federal and Griffith-Bostic). Rhyolite beneath sediment and basalt in the Griffith-Bostic well east of Mountain Home shows that the faulting has displaced rhyolite erupted 10.3 Ma to a depth of 2.0 km (Clemens and Wood, 1993). There the well bottomed in rhyolite at least 0.9 km thick, and the total rhyolite thickness is judged to be about 2.3 km (Wood, 1989). The Anschutz-Federal well (45 km southwest of Mountain Home) drilled through 2.2 km of rhyolite and bottomed in granite (McIntyre, 1979; Ekren and others, 1981). The center of the western plain southeast of Boise has not been explored by deep drilling, so we cannot be certain that rhyolite is absent from the subsurface there. The deepest well is 1.3 km deep at Mountain Home Air Force Base (elevation 3,022 feet, 921 m). This well drilled through 0.75 km of basalt beneath 0.55 km of lacustrine sediment (Lewis and Stone, 1988), a section similar to those in the center of the western plain shown in Figure 5.

Pierce and Morgan (1991) emphasized the broad uplift of 0.5-2.0 km that occurs as the hot spot migrates, and it is shown most graphically by their Plate 1 of topography. Others have suggested that simple vertical expansion due to heating the crustal lithosphere can account for uplift of that order, followed by cooling subsidence

after passage of the hot spot (Brott and Blackwell, 1978). Blackwell (1989) estimates the thermal effect to be 200-250 km wide. This estimate can be projected back in time to the western plain region to suggest that the area was on the north edge of a volcanic highland at 14-11 Ma and not a basin. Before eruption of rhyolite in the western plain area, the geologic evidence discussed earlier shows only north-trending basins laying generally west of the batholith that accumulated basalt. Mapping the rhyolite flow directions in the future should help to reconstruct the topographic picture and confirm or refute the presence and nature of the uplift as the hot spot passed by the position of the western plain.

HISTORY OF GRABEN FAULTING IN THE WESTERN PLAIN

The geochronology of the major graben that forms the western plain has been determined at two localities by correlating dated surface volcanic units to their subsurface equivalents (Figure 7). The offset of volcanic units at the south side of the Bennett Mountains show that most of the 2.8 km offset occurred between 11 and 9.5 Ma. Offset units on the north side of the Owyhee Mountains indicate the 2.2 km of offset was largely completed by 9 Ma, but the date for the onset of vertical movement is not well constrained.

A history of faulting in eastern Idaho along northwest-trending basin and range structures associated with hot-spot migration can be compared with that for the western plain. Anders and others (1989) determined that the rapid rate of faulting south of the eastern plain was constrained in time between 2 and 3 Ma, with vertical slip rates of about 1 mm/year (Figure 7). For the western plain, we derive somewhat smaller slip rates of 0.5 mm/year for the two boundary faults on either side of the plain. Basin relief formed by hot-spot-triggered normal faulting seems to evolve over just a few million years, and then vertical slip rates become very slow (less than 0.01 mm/year). From these fault histories, we argue that most of the western-SRP basin relief was formed in a rather short geologic time between 11.0 and 9.5 Ma. This is not to imply that these normal fault systems become totally inactive after the main period of displacement, but only to note that the average long-term slip rates become very low following the main episode of activity.

The only segment of western-SRP faults shown to have late Quaternary activity is the Owyhee Mountain front 55 km southwest of Mountain Home in the Halfway Gulch-Little Jacks Creek area (Beukelman, 1997). The Halfway Gulch fault trends N. 60º W. to N. 75º W.

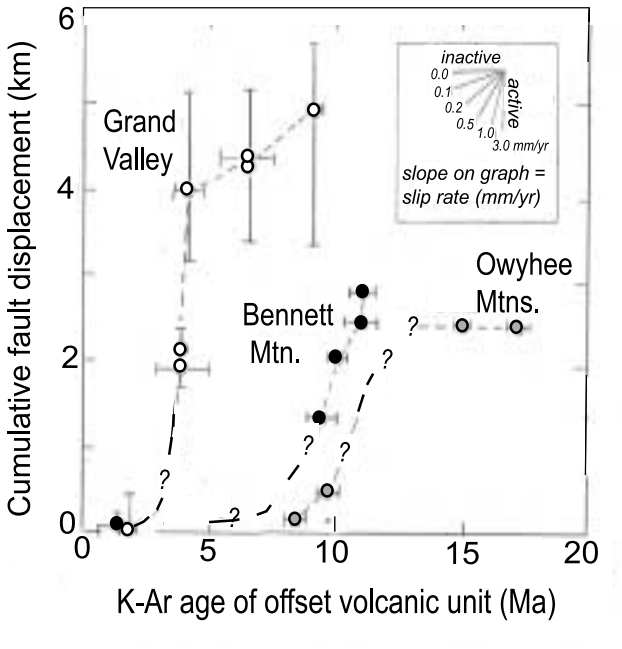

Figure 7. Displacement histories of normal faults bounding the western plain graben (Bennett Mountain is north of and includes the Griffith-Bostic well shown as GB in Figure 2; Owyhee Mountains-Anschutz well is shown as A in Figure 2; modified after Clemens, 1993) and of the Grand Valley fault oriented perpendicular to the eastern plain. Location of Grand Valley fault shown in Figure 1 (after Anders and others, 1989). Illustration shows that basin relief from normal faulting evolves rapidly over a very few million years and that vertical slip rates sharply wane afterwards.

A mappable, late Quaternary scarp occurs along the mountain front for a very short length of only 5.3 km, with a maximum scarp height of 7.7 m. The total length of the system of mappable young faults is less than 12 km, which is unusually short for such large vertical displacement. Scarp-degradation age estimates are about 20,000 years. An associated fault (Water-Tank fault), 7.6 km northeast of the mountain front, strikes N. 35-50º W. and has a 3.6-m Quaternary scarp. A trench-stratigraphic study on the Water-Tank fault shows five episodes of surface rupture within an estimated 26,000 years and estimated average vertical slip rates within these time periods of 0.08 to 0.2 mm/year (Beukelman, 1997). These Quaternary vertical slip rates greatly exceed the long-term slip rates shown in Figure 7 for the Owyhee Mountain front just 20 km to the northwest. This difference in slip rates suggests that episodic reactivation may occur on suitably oriented faults (Beukelman, 1997).

THE EARLIEST SEDIMENT IN THE WESTERN PLAIN: BANBURY BASALT AND THE CHALK HILLS FORMATION

Throughout the western plain margins, a section of basalt flows and pyroclastic layers interbedded with tuffaceous mudstone commonly rests unconformably upon the granite of the Idaho batholith, the late Miocene rhyolite, or the basalt of the Miocene Columbia River Group. At the south margin of the Weiser embayment near Emmett, coarse sand and tuffaceous sediment rest unconformably on Weiser basalt of the Columbia River Basalt Group. Near the plain margins, the lower basaltic material may be interbedded with gravels and sands derived from the batholith. Some of these basaltic rocks have been called the Banbury Basalt. The formation name has been incorrectly applied to any basalt within the sedimentary sequence of the plain. It is unlikely that the Banbury Basalt is a continuous unit or that basalts of identical age occur along the margins and beneath the plain. Basalt eruptive centers probably occurred sporadically in many places and spanned a considerable time after rhyolite volcanism ceased. Bonnichsen and others (1997, p. 401) make a crucial observation that the period of western-plain basalt volcanism following the rhyolite is confined to about 2 million years from 9 to 7 Ma, although we believe that the inception of basalt volcanism extends back to about 10 Ma for reasons indicated in the following discussion.

In some places, sediments may dominate in the basal section, and geologists might call the section the Chalk Hills Formation or the Banbury Basalt with interbedded sediment. We recommend that the term Banbury Basalt be restricted to the basalt field in the vicinity of Banbury Hot Springs, and not be extended to other basalt fields intercalated with sediment of the Chalk Hills Formation. We further recommend that each contiguous basalt field be given a separate name, and each be considered as a member of the Chalk Hills Formation.

In its type area, the Banbury Basalt is about 330 m thick (Malde and Powers, 1961). Armstrong and others (1980) reviewed the age of this basalt section, where it overlies Idavada rhyolite dated 10.1 and 11.0 Ma and encloses a silicic ash K-Ar dated at 10.2 Ma (sample KA 830, whole-rock on coarse ash; Evernden, 1964). Armstrong and others (1980) report two whole-rock K-Ar age determinations of 13.8 ± 1.5 and 8.1 ± 0.7 Ma. These disparate ages were then averaged and reported as 9.4 ± 0.6 Ma, although the validity of averaging such ages is questionable. Ekren and others (1981) report that all the flows they measured had normal magnetic polarity, which suggests the Banbury Basalt erupted during the normal interval between 10.1 and 8.8 Ma.

In the Boise area, a basalt tuff-dominated unit resting on rhyolite or granite is about 200 m thick in drill holes beneath the city, and thinner discontinuous patches occur in the foothills upon the batholith on both the north and south sides of the plain. Clemens (1996) has reported on an undated 4-m-thick rhyolite ash in the lower part of this unit in the Boise foothills.

In the Boise area, the beginning of fluvial-lacustrine sedimentation is dated at before 9.5 Ma by the basalt of Aldape Park intercalated with sediment that crops out in the foothills, and is correlated to the subsurface in geothermal wells. This basalt yields a modified whole-rock K-Ar age of 9.5 ± 0.6 Ma and has a normal magnetic polarity (Clemens and Wood, 1993). A whole-rock K-Ar age of a basalt might be open to question, but the age is within the normal polarity episode from 8.8 to 10.1 Ma, and the other normal episodes are either younger than 8.2 Ma or older than 11.3 Ma, leading us to believe it is a valid age. This basalt layer overlies 150 m of fluvial-lacustrine sediment beneath which is about 200 m of basalt, tuff, and sediment resting upon rhyolite or granitic rocks. Therefore, 150 m of basin sediment was deposited in the Boise area before 9.5 Ma but after emplacement of an earlier basal basalt. We do not have reliable radiometric dates or magnetic polarity on the basalt tuff unit, but it lies on rhyolite dated 11.3 and 11.8 Ma (Clemens and Wood, 1993). We conclude that the 150 m section of sediment beneath the dated basalt marks the beginning of the basin in the western plain between 11.3 and 9.5 Ma.

Sediment that rests on the older basalts, rhyolite, or the Idaho batholith is usually mapped as the Chalk Hills Formation or in some localities as the arkosic sands of the Poison Creek Formation. These formation distinctions are poorly defined and not useful because the arkosic sands are just a fluvial facies that may have a lacustrine equivalent. These sediments are the first clear evidence of the basin in the western plain. Systematic mapping and study of these rocks are yet to be done, but we will review here our present knowledge of the Chalk Hills Formation. The bottommost sediments are usually coarse sand and pebble gravel derived mostly from the Idaho batholith and older volcanics. These sands are interbedded with mudstones which become more prevalent upwards in the section. Within the first 100 m, the section grades upward into tuffaceous muds and clays and many volcanic ash beds, predominantly gray silicic ash and lapilli, but with some basaltic ash beds. Some ash and lapilli beds exceed 20 m in thickness. Pillow basalts occur within these sediments south of Walters Ferry and over an area called the Teapot volcanic complex by Bonnichsen and others (1997) and mapped by Ekren and others(1981) as

basalt of the Murphy area.

We have mapped and measured a 100-m section just south of Walters Ferry in the vicinity of Chalky (sec. 35, T. 2 S., R. 3 W.) and show the complexity of the basal sediments and volcanics of the Chalk Hills Formation in Figure 8. The rhyolite of Browns Creek (11.1 Ma) is overlain by reddish pahoehoe basalt erupted subaerially. The basalt is then overlain by noncalcareous silts with channel arkosic sands in a 50-m sequence that fines upward. Upon this sequence is 30 m of cliff-forming gray silicic ash, mostly silt size, that fines upward. Over the ash are basalt lapilli layers and palagonite tuff. The top of the section here is a 15-m-thick complex of pillow basalt and dikes, called the "Teapot volcanic complex" with a $^{40}Ar/^{39}Ar$ age of 7.95 ± 0.2 Ma (Craig White, written commun., 1997; Bonnichsen and others, 1997). The section beneath the pillow basalt is faulted down to the northeast about 20 m by a northwest-trending normal fault that does not appear to cut the pillow basalt unit.

Swirydczuk and others (1982), Kimmel (1982), and Middleton and others (1985) describe sections of the Chalk Hills Formation on the south margin of the plain. None are measured with respect to the base of the formation. Most are within 50 m of the top of the formation as defined by an oolitic sand and a slight angular unconformity. Kimmel (1982) had some success in tracing ash layers in the formation and obtained nine fission-track ages on glass from the ash layers. Ages ranged from 6.1 to 9.1 Ma with standard deviations of 0.5 to 1.2 Ma. Some question exists regarding the reliability of glass fission track ages, but they are within the range of two whole-rock K-Ar ages on basalt in the lower part of the unit reported by Armstrong (1975) at 8.2 ± 0.7 and 8.6 ± 0.5 Ma.

Perkins and others (1998) examined Kimmel's (1979) stratigraphic section no. 14 (SE $^1/_4$, sec. 19, T. 7 S., R. 4 E.). From trace and major element chemistry, they were able to correlate the ash layers within this Chalk Hills Formation section to regional volcanic ash falls. Ages of these ashes range from 7.49 to 6.4 Ma. The 6.4-Ma ash correlates to the Walcott Tuff on which several whole-rock K-Ar ages, ranging between 6.3 ± 0.3 and 6.5 ± 0.1 Ma, are reported by Morgan (1992). The age of this ash is important because it establishes the youngest known age for Chalk Hills Formation deposition before the formation was partly eroded during a regression of the lake system.

Kimmel's (1979) section no. 14 was examined in this study. The sediments rest upon the subaerial flow basalt of Al Sadie Ranch that rests upon the rhyolite of Horse Basin mapped by Jenks and others (1993). The lower 25 m of sediment is a nonlacustrine sequence of fluvial deposits and paleosols overlain by basalt tuff. The top of the basalt tuff is reworked in part and shows hummocky cross-stratification of shoreline storm waves. The cross-stratified tuff is overlain by 50 m of lacustrine deposits containing the volcanic ashes and fish fossils. From this reexamination and from Perkins and other's (1998) ash chronology, we conclude that the Chalk Hills Formation lake transgressed over this area at some time before 7.49 Ma and that basalt eruptives preceded the lake transgres-

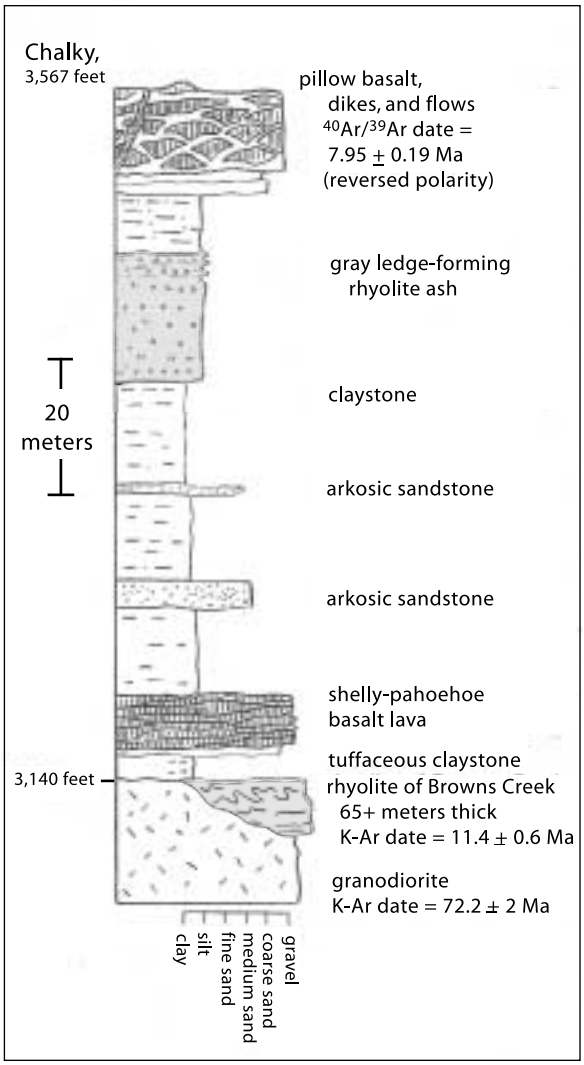

Figure 8. Columnar section of the Chalk Hills Formation at "Chalky" on the south side of the western plain near Walters Ferry (sec. 35, T. 2 S., R. 3 W.). This section was called a reference section (PC-2) for the Poison Creek Formation by Ekren and others (1981), but we regard the Poison Creek as a facies of the Chalk Hills Formation (see text). Section contains two sequences of basalt separated by claystone and a thick rhyolite ash bed. $^{40}Ar/^{39}Ar$ age of 7.95 Ma on the upper basalt is from Craig White (written commun., 1997), and the K-Ar dates on rhyolite and granite are referenced in Ekren and others (1981, 1984). Recalculated age on the Reynolds Creek flow of the Browns Creek rhyolite from Bill Bonnichsen (written commun., 2000).

sion at this locality. The lake then regressed from this site at some time after 6.5 Ma.

The Chalk Hills Formation is relatively thin, about 100 m, along the margins of the plain. It is much thicker beneath the plain (Figure 5). In the type area at the head of Little Valley, Malde and Powers (1962) report the Chalk Hills Formation to be about 90 m thick where it overlies the Banbury Basalt. Ekren and others (1981) report a thickness over 100 m. Sheppard (1991) describes a 100-m-thick section near Oreana that rests on the rhyolite of Little Jacks Creek. The rhyolite of Little Jacks Creek is K-Ar dated at 9.6 ± 1.5 and 10.0 ± 2.0 Ma by Neill (1975; ages recalculated by Bill Bonnichsen (written commun., 2000). The Oreana section contains a 13-m-thick marker gray rhyolite ash, about 35 m above the base, and at least twenty other ash layers interbedded with fine sediment. Sheppard (1991) noted several thin (less than 25 cm) basalt ash layers in the upper part of the formation. The occurrence of one thick (more than 10 m) gray ash within the Chalk Hills Formation and of basaltic ash near the top appears to correlate with our 100-m section (Figure 8) at Chalky near Walters Ferry, about 38 km to the northwest. Thick ash could have erupted from sources to the east; however, at a locality 10 km south of Marsing ($SE^1/_4$ sec. 32, T. 2 N., R. 4 W.) is a 100-m section that contains a 1.5-m layer of rhyolite pumice blocks up to a meter in diameter, 80 m above the base. The layer can only be from a local eruption of a rhyolite dome beneath the lake water (Wood and Wood, 1999), and it shows that at least one rhyolite system continued to erupt near the southeast margin of the western plain during deposition of the formation.

Sheppard (1991) discusses the chemistry of the "Chalk Hills lake," drawing information from an examination of ostracodes by R.M. Forester. The ostracode fauna indicate that at one time the lake-water salinity was greater than 300 mg/l and less than 3,000 mg /l and had a pH about 8 to 9. The water chemistry, though somewhat alkaline, is consistent with lake water supporting the freshwater fish fauna described by Smith and others (1982), not unlike many of the fish-populated Great Basin lakes of today.

Smith and Patterson (1994) show that the water of the "Chalk Hills lake" produced carbonates that are extremely depleted in the heavy oxygen isotope (^{18}O). This suggested to them that the lake was maintained by tributaries of high elevation watersheds and that the waters were little affected by evaporation. They also report that the lake had an unusual mix of fish fauna. Cold-water fish (Salmon and trout species) occur with warm-water species of catfish and sunfish. The lake contained no sculpins or whitefish (cold-water species). It has not yet been resolved if any of the fish were anadromous (Gerald Smith, oral commun., 1995).

Much of the Chalk Hills Formation sediment is noncalcareous mudstone. We are unaware of any significant carbonate facies in the formation. Kimmel (1979) does not describe any calcareous sediment in the many stratigraphic sections he measured. Gypsum partings and veins occur locally near the base of Chalk Hills Formation mudstones. Within thick siltstone layers is a 0.3-m gypsum layer in sec. 23, T. 21 S., R. 46 E., Malheur County, Oregon (Kimmel, 1979, p. 262) and gypsum is associated with volcanic ash layers in Owyhee County, Idaho (sec. 19, T. 7 S., R. 4 E.; Kimmel, 1982). We have noted selenite and satin spar as veins and partings in laminated bentonitic mudstone at the base of the formation north of Marsing (sec. 4 and 5, T. 1 N., R. 4 W.). Kimmel (1979) interpreted these as "displacement gypsum" probably formed by shallow ground-water precipitation in the lake muds. Veins and partings of gypsum in mudrocks suggest that shallow ground water was enriched in sulfate and calcium, and this probably occurred beneath local areas of restricted lake waters that underwent seasonal evaporation. However, we wish to emphasize that the gypsum occurs early in the history of deposition and not in the bulk of the later Chalk Hills Formation.

Kimmel (1982) puzzled (as we have also) over the fall in lake level at the end of Chalk Hills Formation deposition and the subsequent rise in lake level and deposition of the transgressive unit and the Glenns Ferry Formation. He gave several alternate hypotheses for the major lake fluctuation, which we believe reached its lowest elevation at some time after 6.4 Ma. One of these hypotheses involves both tectonic movement and downcutting of the outlet to produce a low lake level, and then basalt volcanism blocking the outlet. Tectonic movement was significant based upon the faulted and slightly tilted nature of most of Chalk Hills Formation and our analysis of rates of faulting (Figure 7). Therefore, it is possible that the basin and its outlet were tectonically lowered. There is no evidence in the sediments of major evaporation in the upper part of the formation to suggest climate change or reduced inflow; however, the stratigraphy of the formation is in need of review to understand the lowering of the lake level. We know nothing of the location of the outlet, but basalt volcanism blocking an outlet in the western plain region is an unlikely cause of the subsequent rise in lake level because Bonnichsen and others (1997) do not find significant basalt volcanism in the western region for the interval between 7 and 2.2 Ma. Rhyolite volcanism, however, was active in what is now the eastern plain region, and that volcanism combined with uplift of the hot-spot region could account for blocking an eastern outlet, if it existed there.

We visualize an environment of a large basin with sporadic basalt volcanism and high rates of basin-relief formation by faulting. At many localities around the plain, basalt volcanic rocks underlie the basal fluvial or lacustrine sediments and are also intercalated with the sediments. From Kimmel's (1982) work, the interconnected Chalk Hills lakes apparently extended from the Bruneau area to the Oregon border, a distance of at least 110 km. From Smith and others' (1982) and Sheppard's (1991) work, the lakes were at times slightly alkaline, but they supported a fresh-water fish fauna. This suggests a system of river interconnections through the evolving topography in the basin, but perhaps not as great a flow-through as the present Snake River discharge. From the above discussion of stratigraphy in the Boise area, the "Chalk Hills lake system" is younger than 10.1 Ma and includes basalt dated 9.4 Ma in the Boise foothills and a pillow basalt complex on the south side of the plain dated at 7.95 ± 0.19 Ma. For the youngest date on the Chalk Hills, we go to the south side of the plain and use Kimmel's (1982) glass fission-track ages between 6.1 and 9.1 Ma, but accepting the uncertainty of these ages. Identification of the Walcott tuff (6.4 Ma) by Perkins and others (1998) in the upper part of the formation establishes a maximum age for the drop in lake level at the end of "Chalk Hills Time." The top of the formation has been removed by erosion marked by a slight unconformity at most localities. Future research should focus on finding a complete upper section in order to better understand events leading to the drop in lake level and the resulting unconformity.

DROP IN LAKE LEVEL AT THE END OF "CHALK HILLS TIME"

A key problem is defining the top of the Chalk Hills Formation. Swirydczuk and others (1979, 1980) show convincingly that a lacustrine shoreline sequence transgresses over beveled, gently tilted strata of the Chalk Hills Formation in the Oreana area. Kimmel (1982) concluded that the Chalk Hills lake lowered or completely drained at the end of the Miocene, and then filled again. Smith and others (1982) suggest that about 1 million years of geologic record is missing in the hiatus between the beveled lake deposits of the Chalk Hills Formation and the transgressive shoreline deposits, and that the missing time is somewhere in the 6 to 4 Ma interval. In some places, the contact is an unconformity with underlying Chalk Hills Formation dipping 4 to 12 degrees basinward, overlain by lake beds dipping less than 4 degrees. At these localities, the upper part of the Chalk Hills Formation has been eroded away. If lakes persisted in the deeper parts of the basin, sediment preserved in the subsurface may contain a more complete sedimentary record. Figure 5 shows the seismically imaged deep sediment that is thought to be the upper part of the Chalk Hills sedimentary record. Because part of the Chalk Hills Formation has been eroded from the margins and we have not, as yet, identified this unconformity in the subsurface, the decline in lake level at the time of the upper Chalk Hills is poorly understood. Apparently, the duration of a lake system could be from 10.1 to about 6 Ma as illustrated in Figure 9.

The transgressive sequence marked by the lowest occurrence of oolitic shoreline sand has been used as the definition of the base of the Glenns Ferry Formation (Malde and Powers, 1962). In the Boise foothills area (Figure 10), lenses of oolitic sand occur over a 120-m-vertical section within the upper part of a shoreline facies that W.L. Burnham and S.H. Wood (written commun., 1992) have named the Terteling Springs Formation. We regard most of the Terteling Springs Formation as a transgressive unit. We have not been able to find a clear indicator in the Boise area of the top of the Chalk Hills Formation. We have found a record of lake-level rise but have not found a record of lake-level drop similar to the unconformity on the south side of the plain.

Possibly, the subsurface alluvial fan deposits of southwest Boise, delineated by Squires and others (1992) and shown in Figure 11, are a record of lake-level fall in Chalk Hills Formation time because the base of the fan rests upon clayey sediments at a subsurface elevation of 2,000 to 2,400 feet (610 to 730 m). The subsurface fan is overlain by lake deposits at about elevation 2,700 feet (820 m). Ed Squires (written commun., 1990) has mapped an outcrop of oolitic sands in the Mayfield area to the east at elevation 3,600 feet overlying the fan deposits. From these relationships, he concludes a lake transgressed over the alluvial fan deposits. If so, then the subsurface alluvial fan deposits are much older than we have previously thought and are contemporaneous with the upper Chalk Hills Formation.

THE TRANSGRESSIVE LACUSTRINE SEQUENCE

A history of the major water-level fluctuations of Lake Idaho is hypothesized in Figure 9. Some event caused the lake level to rise and transgress over the Chalk Hills Formation. The upper part of this transgressive sequence contains oolite lenses marking shoreline regions. Repenning and others (1994, p. 72) thoroughly reviewed

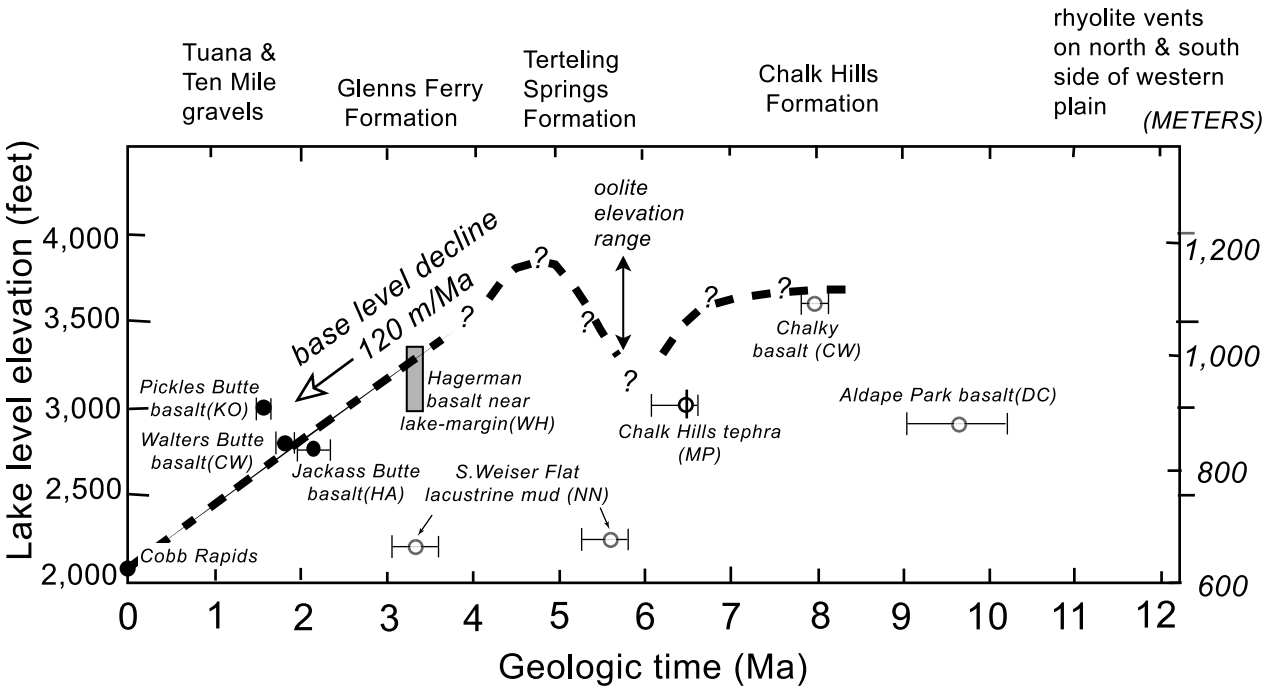

Figure 9. Plot of elevation of lake deposits versus time. This plot does not take into account tectonic deformation that may have altered the elevation of lake deposits. Most localities are on the margin of the plain, which has not been so much affected by tectonic movement or compaction subsidence (Wood, 1994). Points on the graph are dates on lacustrine sediment, or basalt associated with or overlying the lacustrine section: K-Ar dates on basalt are from DC (Clemens and Wood, 1993) and HA (Amini and others, 1984); zircon fission track ages on silicic ash are from NN (Nancy Naeser, published in Thompson, 1991); $^{40}Ar/^{39}Ar$ ages on basalt are from CW (Craig White, written commun., 1997), KO (Othberg and others, 1995), and WH (Hart and others, 1999); and tephrochronology is from MP (Perkins and others, 1998).

previous work on the Glenns Ferry Formation. They proposed that the locally oolitic, rusty-stained sandstone, taken by Malde and Powers (1962) as the base of the Glenns Ferry Formation, be given separate formational recognition. Our mapping on the north side of the plain supports that proposal, for we see at least 120 m of an oolite lens-bearing section up to elevation 3,800 feet (1,160 m). The stratigraphic diagram (Figure 12) shows this relationship in the Boise foothills with oolite lenses up to 3,200 feet (975 m). The lower elevation (3,200 feet) shown in the section is because of the southwest dip of the strata. In principle, this transgressive sequence should have an equivalent open lake facies that may be quite thick. We believe the mudstone facies of the Terteling Springs Formation to be that open lake facies. Consequently, the basinward equivalents of oolite facies on the south side of the plain need to be reexamined because there should be a substantial correlative section of mudstone. Only the 30 m beneath the oolite is described in the literature on this section (Swirydczuk and others, 1980a, 1980b, 1982).

An important implication of a transgressive or rising lake-level sequence is that sand and coarse clastics will be deposited near the shoreline and that deltas will not prograde significantly into the lake basin. Therefore, much of the incoming sand is stored as nearshore sediment, and not deposited in the open lake where only muds are deposited. The rising lake level also suggests that the lake does not have a spillway. A closed basin might have been forming. A steadily filling closed basin perhaps explains the oolites in the upper part of the section. The lake was becoming increasingly alkaline from evaporation as it rose to higher levels, thus favoring precipitation of calcium carbonate. Swirydczuk and others (1980b) compare the lake chemistry at the time of oolite deposition with that of Pyramid Lake, Nevada (pH of 9, and 4,700 mg/l total dissolved solids, but supporting a healthy trout population). Finally, the lake overtopped a spill point and began to slowly drain. As soon as drainage was established, the lake would have become less alkaline.

THE LAKE-LEVEL FLUCTUATION AT 6-4 MA AND A PLAUSIBLE EXPLANATION

The history of lake levels shown in Figure 9 ignores the effects of differential tectonic movement, which with

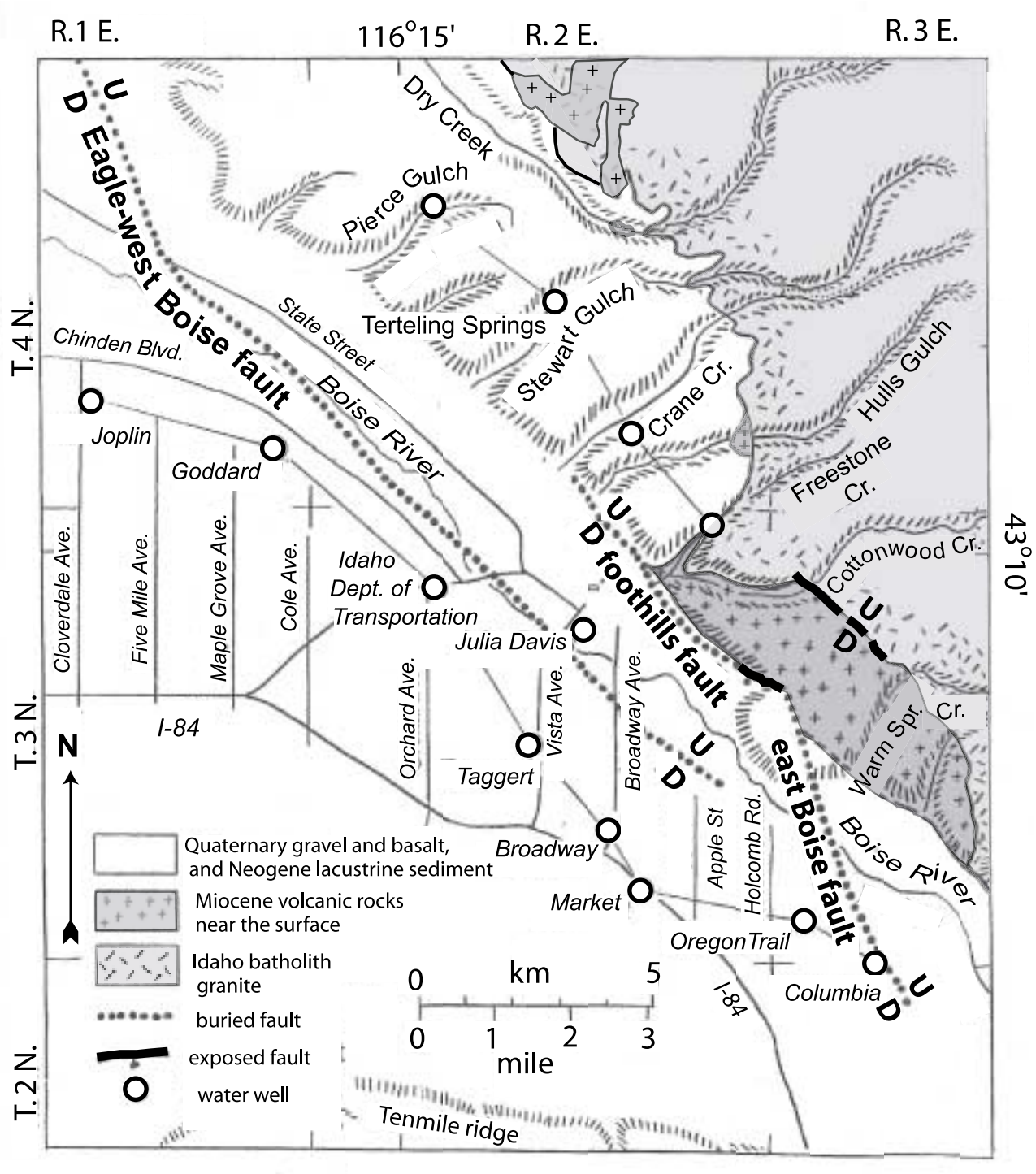

Figure 10. Geologic map of the Boise area showing locations of stratigraphic cross sections of Figure 11 and Figure 12.

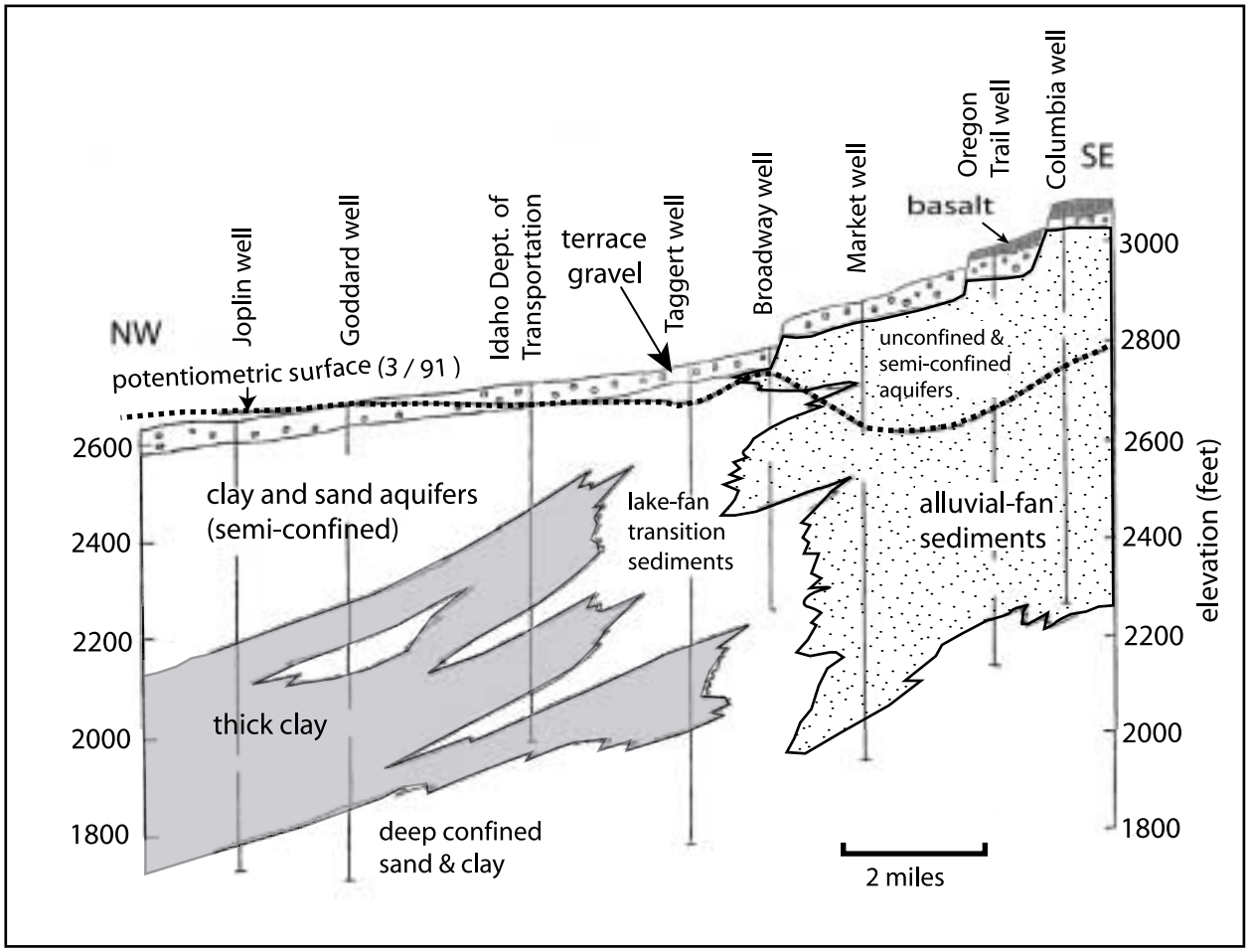

Figure 11. Cross section showing stratigraphy of alluvial fan and lake sediment aquifers beneath Boise (from Squires and others, 1992).

the present knowledge is difficult to unravel from other causes of lake-level fluctuation. We list the possible causes of secular lake-level fluctuations (Table 1) but will pursue only our favored mechanism to keep the discussion short. At the outset, we must state that our study of the Chalk Hills Formation is very limited. The accumulation of the formation is likely a result of continued tectonic foundering of the basin area. The subsequent fall in lake level, about 6 to 7 Ma, is poorly documented and without a satisfactory explanation. The rapid tectonic foundering of the basin, the change to a more arid climate, or the establishment of a lower outlet are all favored possible explanations.

The lake-level rise, marked by the transgressive sequence (oolite section and the upper Terteling Springs Formation), is well documented (Swirydczuk and others, 1980a, 1980b). We propose that the major lake-level fluctuation at about 6 Ma was caused by new stream inflows associated with the migrating Yellowstone hot-spot

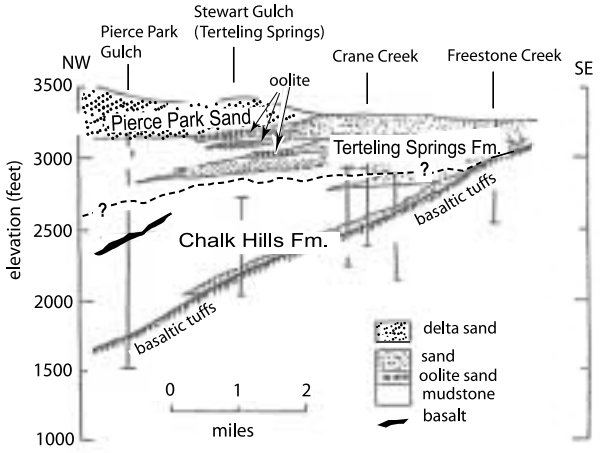

Figure 12. Stratigraphic cross section showing lake margin facies in the Boise foothills and the distribution of oolitic sands. Location of section shown in Figure 10.

Table 1. Causes of lake-level fluctuations.

RISE IN LAKE LEVEL
Increased inflow
Increased runoff
Increased precipitation
Decreased evapotranspiration in catchment
Diversion of major stream into basin by capture or damming
Decreased evaporation from lake surface
Decrease in surface area
A climate change, colder or more humid
Filling of lake basin by sediment
Rise in elevation of the outlet
Landslide, glacier-ice, or lava-flow damming
Relative tectonic warping or faulting of outlet area
DECLINE IN LAKE LEVEL
Decreased inflow
Decreased runoff
Precipitation decrease
Increase in evapotranspiration in catchment region
Diversion of a major tributary stream from basin by capture or damming
Increase in evaporation from lake surface
Warmer or dryer climate
Increase in lake surfacearea
Sediment compaction
Fall in the level of the outlet
Progressive downcutting of outlet
Breaching of a landslide, glacier-ice, or lava-flow dam
Spillover and establishment of a new and lower outlet
Tectonic lowering of outlet by warping or faulting

uplift. An uplifted region about 400 km across with a maximum uplift of 0.5 to 1 km is currently centered on the locus of rhyolite volcanism at Yellowstone (Pierce and Morgan, 1992). The hot-spot model implies a broad northeast-migrating continental uplift region. A migrating uplift also implies an eastward-migrating drainage divide (Figure 13).

Anderson (1947) proposed that the Continental Divide had shifted eastward about 160 km in late Tertiary time. He was intrigued by the peculiar shift in directions of the Salmon River and drainages north of the eastern plain. We realize now that the hot-spot uplift provides a mechanism for his observations. Taylor and Bright (1987) also suspected that the migrating uplift was responsible for drainage changes in the region. Cox (1989) suggested this has been a characteristic of continental hot spots. The Continental Divide may have shifted about 200 km from a position near Arco, where it was associated with the Heise Volcanic field about 6 Ma, to its present position in Yellowstone National Park.

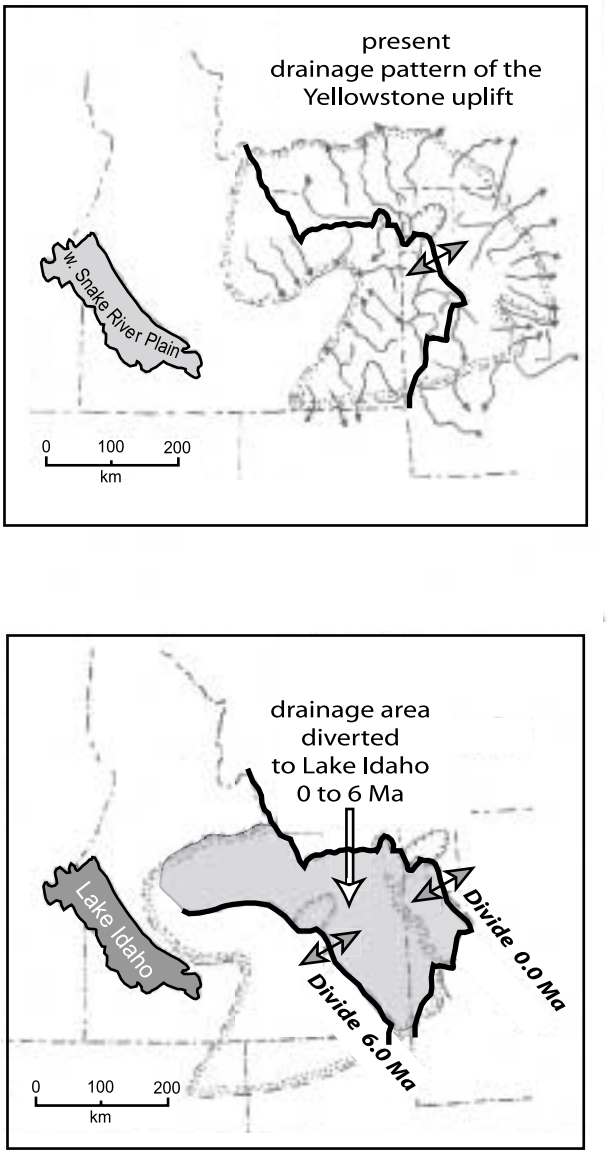

Figure 13. Map showing the area that may have diverted drainage to Lake Idaho, 6 to 0 Ma, on account of eastward-migrating uplift associated with the Yellowstone hot spot.

The idea of a shifting drainage divide could explain a part of the history of lakes in the western plain. About 6 Ma, the lake that was depositing the Chalk Hills Formation declined to a low level. The shifting drainage divide does not offer a simple explanation for the decline to a low level; however, some earlier spillover into another lower elevation basin, a climate change decreasing inflow and increasing evaporation, or an increase in the rate of subsidence could account for the lake-level lowering. Then, about 4.5 Ma the lake began to rise, transgressing over the older Chalk Hills lacustrine deposits. We propose here that the eastward-migrating uplift with

a west slope captured major rivers or allowed major drainage diversions into the western plain basin (Figure 13). We suggest that drainages that had formerly flowed east to the Missouri or Colorado drainages, or into Basin and Range dead ends, now flowed down the west slope of the uplift into Lake Idaho. Such major diversions could have increased the inflow into Lake Idaho causing it to rise to its spill point about 4.0 Ma.

THE SPILLOVER OF LAKE IDAHO INTO HELL'S CANYON AND THE DEPOSITION OF THE GLENNS FERRY FORMATION

Wheeler and Cook (1954) published a key concept in deciphering the history of Lake Idaho. They propose that headward erosion to the south by a tributary to the Salmon-Columbia river system captured the waters of Lake Idaho in the late Cenozoic. Although we differ in the details, the spillover into ancestral Hell's Canyon seems certain. They believed spillover and capture occurred at the Oxbow because of the peculiar bends of the Snake River. The Oxbow and its trend are more satisfactorily explained by diversion of the downcutting river by the resistant northeast-trending mylonite zone in the pre-Tertiary rocks. Wood (1994) believed the capture occurred near the present Cobb Rapids by Weiser. We now believe the spillover point was a divide about 5 km above the present confluence of the Burnt River with the Snake River through a low gap between the present Slaughterhouse Range and Dead Indian Ridge (Figure 14). Our observations are mostly from topographic maps: the area has not been systematically mapped and searched for remnant patches of lake sediment and gravel to test these ideas. We hypothesize a former low divide at about 3,600 feet (1,100 m) in elevation at the headwaters of a steep-gradient, north-draining tributary. The lake, which lay to the south, rose and overtopped this divide. A similar divide exists today at Henley Basin (Figure 14), 8 km to the northeast, a gap similar to that which must have existed at the spillover. This gap is the 3,200-foot (980-m) elevation divide between the north-flowing Rock Creek and the south-flowing Hog Creek. It is a gap through which rising lake water also could have flowed over into ancestral Hell's Canyon, had it not already done so in the gap to the southwest, presumed to have been slightly lower at the time of spillover. That this gap is presently 3,200 feet (989 m) is not really a problem, since in the past several million years, it could have been lowered by erosion 400 feet (120 m; this assumes a reasonable denudation rate of the divide area of 200 feet/Ma or 6 cm/Ka). Note also on Figure 15, that the river gradient steepens in the 20-mile (32-km) reach from the mouth of Rock Creek to Cobb Rapids, suggesting that the smoothed remnant of the former knickpoint created by the spillover has migrated about 10 miles (16 km) above the spillover point.

We hypothesize that most streams on the south side of the Blue Mountains formerly flowed to the south-southeast into the lake. The Burnt River and many nearby creeks have this direction; however, the Burnt River turns sharply northeast in its lowest 4-km reach below Huntington, where we believe it was captured and diverted from its southerly course by the downcutting Snake River.

Repenning and others (1994, p. 71-72) and Van Tassell and others (2001) suggest that the spillover occurred in the early Pliocene, rather than with the onset of the ice ages of the late Pliocene as previously suggested by Othberg (1988) and Wood (1994). Repenning and others (1994) propose that much of the Glenns Ferry Formation deposition occurred after the lake had found the Hell's Canyon outlet, which they believe happened between 3 and 4 million years ago. Othberg (1994) also suggests that the basin may have filled earlier than late Pliocene. He further suggests that the lake drained slowly while flood-plain aggradation continued in the basin. He does associate the beginning of widespread gravel deposition over the plain with a change in stream regimen caused by late Pliocene climates. From his study of gravel terraces and deposits of the Boise Valley, he indicates that basin aggradation gave way to valley cutting in the early Pleistocene.

The time when spillover occurred is not well constrained. Lacking is accurate geochronology tied to traceable marker beds and detailed stratigraphic work in the upper Glenns Ferry Formation. The timing of spillover assumed by other workers rests upon magnetic polarity changes in sedimentary section determined by Neville and others (1979) and Conrad (1980) in scattered stratigraphic sections that were not tied to radiometrically dated ashes or flows or by geologic mapping. We believe the reliable geochronology is as follows: (1) the 6.4-Ma date near the top of the Chalk Hills Formation determined by Perkins and others (1998); (2) the Ar-Ar ages obtained by Hart and others (1999) on basalt at Hagerman and paleomagnetism of sediment determined by Neville and others (1979) and the volcanic ash correlations of Izett (1981) that indicate ages between 3 and 4 Ma for the Hagerman section; and (3) the Ar-Ar age of 1.67 Ma for the subaerially erupted basalt at Pickles Butte obtained by Othberg (1994). These dates reliably set the maximum age for the beginning of the transgressive sequence, the age when the lake shore was near Hagerman, and the age when the lake basin filled with sediment and river gravel

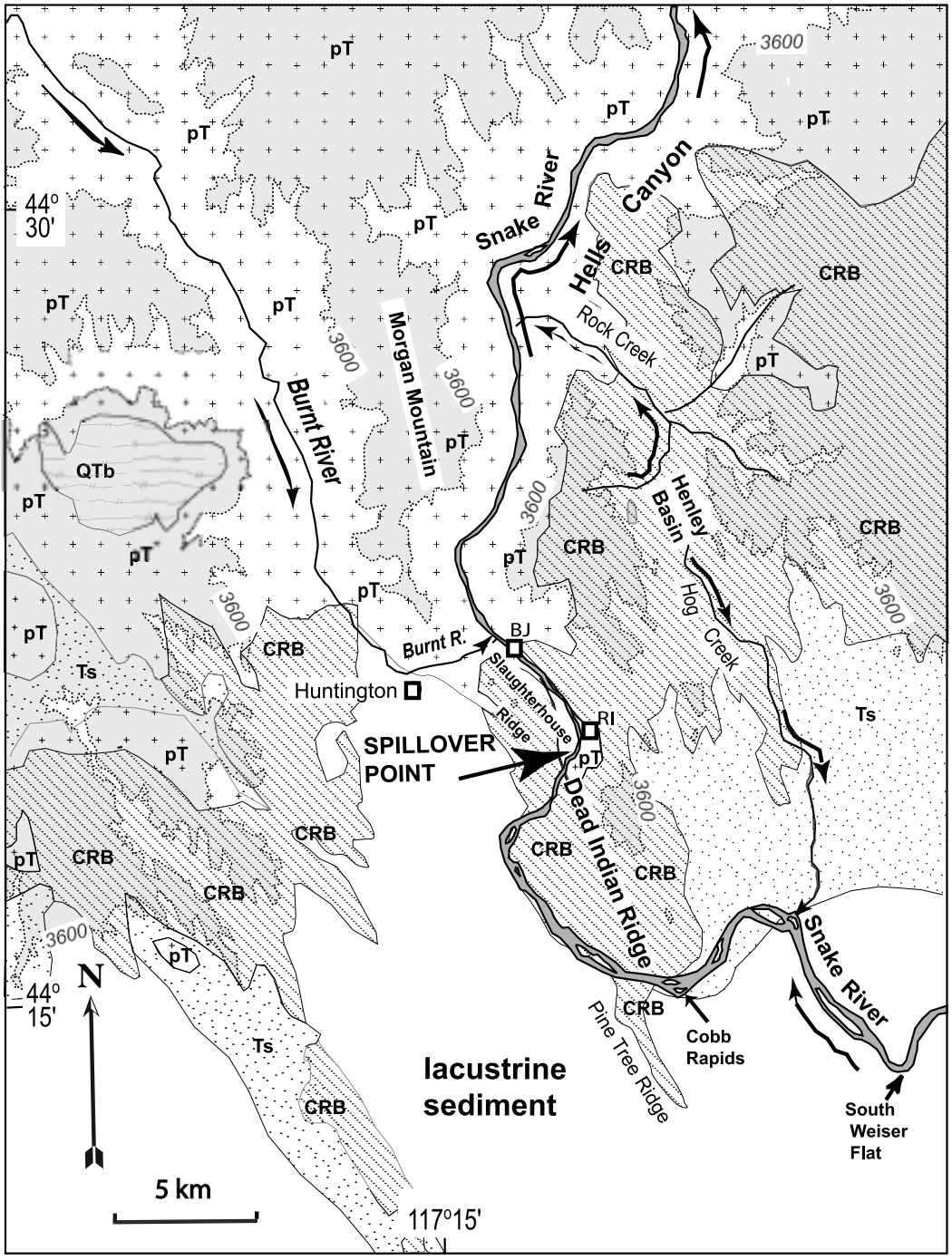

Figure 14. Present topography above 3,600 feet (shaded area) and geology at the upper end of Hell's Canyon showing the proposed spill point of Pliocene Lake Idaho. We hypothesize that the headwaters of a north-flowing tributary of ancestral Hell's Canyon were between Blakes Junction (BJ) and Rock Island Station (RI). The Pliocene divide between the Columbia-Salmon River system and Lake Idaho was between the present Slaughterhouse Ridge and Dead Indian Ridge. That divide was overtopped when the lake rose to about 3,600 feet. Henley Basin is a similar divide that still exists between north-flowing Rock Creek and south-flowing Hot Creek. The knickpoint formed by the capture has subsequently migrated 9 km up to Cobb Rapids (see Figures 15 and 17). As the river canyon lowered, a tributary creek on the west captured the lower part of the south-flowing Burnt River. Geologic units are pT—pre-Tertiary rocks of the Olds Ferry terrane (Vallier, 1998); CRB—Columbia River Basalt Group; Ts—older deformed lacustrine and fluvial sediment, probably equivalent to Sucker Creek and Chalk Hills Formations; QTb—cinder cone and basalt flows of probable Pliocene age; lacustrine sediment—younger sediment of Lake Idaho.

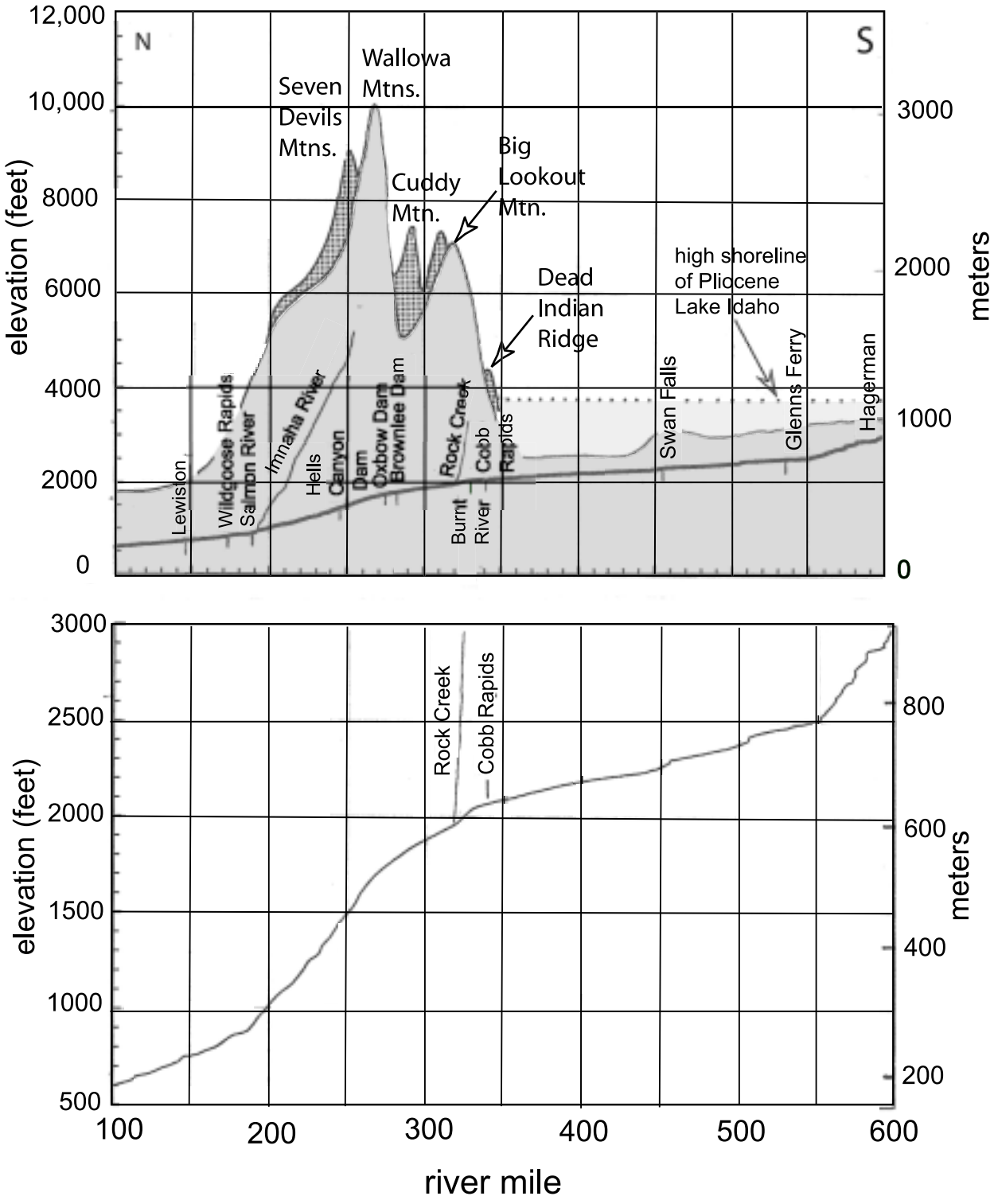

Figure 15. Longitudinal profile of the Snake River showing the change in gradient from Hell's Canyon to the Snake River Plain. Included is the profile of the Imnaha River, which has a source in the high Wallowa Mountains, and Rock Creek, which has headwaters at a divide similar to the proposed spillover location shown in Figure 14. It is thought the ancestral upper Snake River had a similar high-gradient profile at the time it breached the divide into the western plain and began draining Lake Idaho.

deposited over lake sediment near Marsing, respectively. Therefore the rise, spillover, fall, and sediment infilling of the lake occurred at sometime between 6.4 Ma and 1.67 Ma. Van Tassell and others (2001) and Smith and others (2000) provide new geochronological and paleontological evidence suggesting that Lake Idaho connected to the Columbia River drainage at some time between 3.8 and 2 Ma.

It will be important to establish whether the Hagerman section represents a transgressive sequence of lacustrine deposits over beach deposits, deposits of a highstand of the lake, or fluvial deposits over lacustrine deposits. We believe the facies at Hagerman could be the transgressive stage, the highstand, or a facies of the early stages of draining an alkaline lake. Our contention is that the medium and fine sand interbedded with calcareous silt and clay throughout the 250- to 400-foot (75-120 m) sections described by Malde (1972) at Fossil Gulch and Peters Gulch indicate lake conditions of a closed alkaline lake, or one just beginning to drain. Wood (1994) described 1,000 feet (300 m) of very calcareous claystone overlain by 800 feet (240 m) of interbedded fluvial and deltaic sand interbedded with moderately calcareous silt in a geothermal well beneath Caldwell. South of Marsing, the lacustrine sediments above the Chalk Hills Formation and beach gravels are composed of 300 feet (90 m) of noncalcareous mudstone (with gypsum cemented ashes and gypsum veins) conformably overlain by 1,000 feet (300 m) of very calcareous mudstone interbedded with fine and medium sand in the upper part (S.H. Wood, unpub. mapping). We believe the thick calcareous sediments are a record of an alkaline lake of a closed basin.

We constructed the diagram of Figure 9 without knowing that Hearst (1999) had published a similar hypothetical diagram of lake-level elevations over time. She shows the spillover as having occurred about 2.7 to 2.5 Ma, based upon a re-evaluation of the geochronology of Kimmel (1982), Neville and others (1979), and Repenning and others (1994). She accepts the glass fission-track ages of Kimmel (1982) and finds that they concur reasonably with paleontological age estimates of fauna in the Glenns Ferry Formation. Her work has caused us to rethink the ages in our Figure 9. Kimmel's (1982) dates are on volcanic ash within 17 m of the base of the Glenns Ferry Formation. The ages range from 2.2 to 3.3 Ma, and since they are based upon fission tracks in glass and not in zircon, and because they are near the base of the formation, we suspect they may be too young for that part of the section. The ages of 5.5 ± 0.4 Ma and 3.3 ± 1.0 Ma at south Weiser Flat, shown in Figure 7, are fission-track ages on zircons from volcanic ash within lacustrine sediments, but we are uncertain of their correlation to the Glenns Ferry Formation. These ages on ash date a time of deposition of noncalcareous lacustrine mudstone at that site at the northwest end of the western plain basin. Future work should focus on better dates on volcanic ashes in the section explored by Hearst (1999) and the section in the Boise foothills where major sand units prograde over lacustrine muds in the upper part of the section and are an indication of falling lake level after the lake spilled over the outlet into Hell's Canyon.

We realize now that the slow downcutting of the bedrock outlet and deepening of Hell's Canyon are good explanations for features of the final phase of Lake Idaho. Helpful to our understanding were the typical rates of downcutting of bedrock canyons by major rivers (Schumm and others, 1991). Rates are typically about 150 m/Ma. We have added comparative data from other studies that support these relatively slow rates (Table 2). A reconstructed history of lake levels (Figure 9) suggests that the lake level lowered at a rate of about 120 m/Ma. Although climate change may have affected the stream regimen, the rates of downcutting of Hell's Canyon, and the lake levels, we do not think that climate change is necessary to explain the sequence of major events in the late history of Lake Idaho.

A slow lowering of base level would have caused the erosion of sands from the lake margins and delivered sand into the basin by delta progradation, a feature noted in the center of the basin by Wood (1994) but its significance not clearly understood at the time. The abrupt change from deep lake mudstone to prodelta and delta deposits occurs over much of the western plain where it is detected by geophysical logs (Figure 16). We believe this change is a result of the slowly lowering lake level and of sandy sediment prograding into and filling the basin. Wood (1994) calculated from the relief of prodelta slopes that the lake water into which the deltas prograded was at least 255 m deep. Not until the entire western part of the lake was filled did streams flow across the plain to the outlet. At Weiser, the highest gravel deposits are about elevation 2,500 feet (762 m), and we believe these record the time at which the lake basin completely filled with sediment and stream gradients had aggraded across the plain so that braided streams transported gravel across the plain to the outlet area, leaving deposits known as the Tuana Gravel and the Tenmile Gravel (Sadler and Link, 1996; Othberg, 1994). The ages of the gravels must decrease across the plain to the west, but it is believed that the streams were continuous to the outlet near Weiser by about 1.7 Ma (Othberg, 1994). These highest gravels have subsequently been incised by the Snake River and tributaries about 120 m. Cobb Rapids of the Snake River at elevation 2,080 feet (635 m; Figure 17) is the present knickpoint in Miocene basalt as the river changes grade

Table 2. Rates of river incision into bedrock canyons (after Schumm and Ethridge, 1994).

Rate (cm/1,000yr)	Rock Type	Location	Reference
4.0	granite	SE Australia	*Brittlebank, 1900
9.6	basalt	SE Australia	*Brittlebank, 1900
9.5	conglomerate	Arizona	*Rice, 1980
24.8	sandstone	Arizona	*Rice, 1980
30.0	sedimentary rock	Colorado	*Larsen et al., 1975
7.0	metamorphic rock	Colorado	*Scott, 1975
37.0	limestone and basalt	Utah	*Hamblin et al.,1981
2.6	limestone and basalt	Utah	*Hamblin et al., 1981
8.7	granite	Sierra Nevada, west slope, California	*Huber, 1981
50.0	unknown	Dearborn River, Montana	Foley, 1980
5 to 10	granite	Boise River, Idaho	Howard, et al., 1982
30 to 70	Quaternary intracanyon basalt	South Fork Boise River, Idaho	Howard, et al., 1982
15 to 16	Eocene lacustrine sediment	Wind River, Wyoming	Chadwick et al., 1997
11 to 16	granite and metamorphic rock	Middle Fork Salmon River, Idaho	Meyer and Leidecker, 1999

*Schumm and Ethridge's (1994) table contains references to data prior to 1981, which are not referenced in this paper.

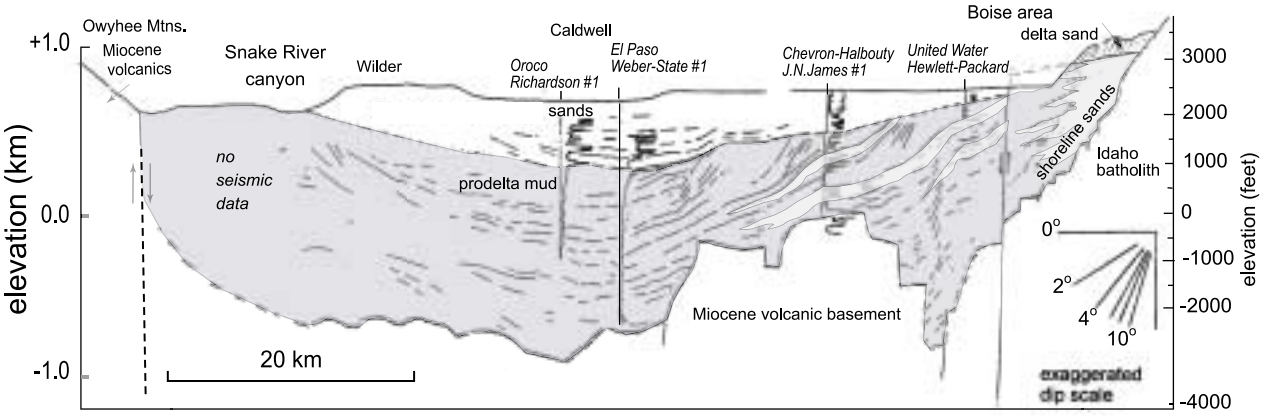

Figure 16. Tracing from seismic reflection section across the western Snake River Plain showing the upper sequence of fluvial-deltaic sediments and character of resistivity logs in wells. Resistivity-log excursions to the right are fresh-water aquifer sands, and the monotonous, near zero, resistivity values are indicative of mudstones. Notice the abrupt change upward from pro-delta muds to the sandy section of the delta systems, delta plain, and fluvial sands in the Caldwell area. Deposition may have been continuous in the center of the plain, but beds appear truncated by erosion to the east, and this surface to the east may be the unconformity at the top of the Chalk Hills Formation. The deltaic deposits in the Richardson well are discussed by Wood (1994). Line of section extends from Terteling Springs in Stewart Gulch shown in Figure 10 westward through the J.N. James well to the Caldwell area shown on Figure 2.

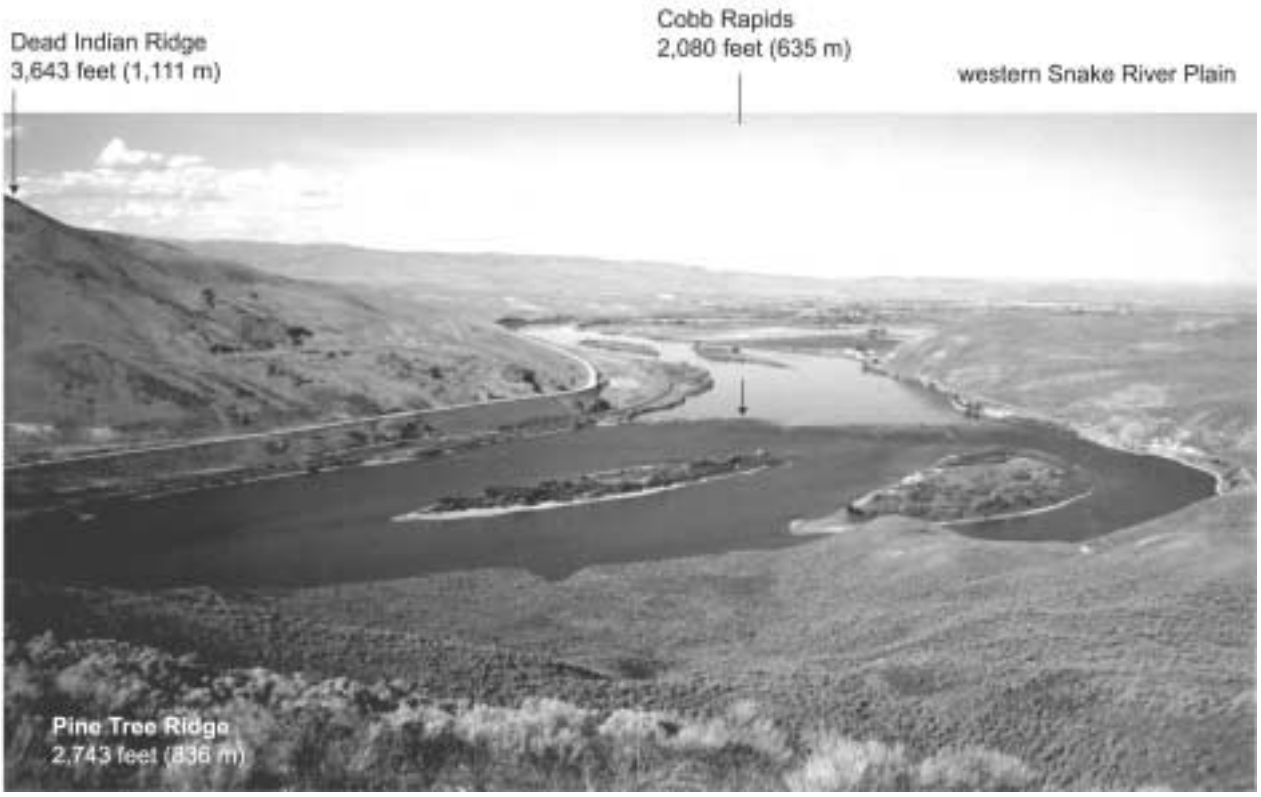

Figure 17. Photograph looking east and upriver of Cobb Rapids of the Snake River near Weiser. Cobb Rapids is the knickpoint of the river profile between the low gradient plain and the high gradient Hell's Canyon reach.

from the plain (1.6 feet/mile, 0.0003) and descends at steeper gradient (4.9 feet/mile, 0.0009) and a convex profile into Hell's Canyon (Figure 15).

LATE PLIOCENE AND QUATERNARY VOLCANISM IN THE WESTERN PLAIN

The resumption of basalt volcanism in the western plain region began around 2.2 Ma. At the western side of the plain, Lees (1994) obtained $^{40}Ar/^{39}Ar$ dates and subdivided the late Cenozoic basalts into two groups. On the older group of olivine basalts, shown by Walker and MacLeod (1991) as Pliocene and Miocene, Hooper and others (2001b) obtained dates ranging from 8 to 13 Ma, which they called the Sourdough and Keeney sequences. The younger group with dates of 1.9 to 0.8 Ma, they named the Kivett sequence. This basalt chronology of Hooper and others (2001b) is roughly consistent with that of Bonnichsen and others (1997) who show a 9-7 Ma basalt episode in the western plain, followed by a 5-Ma-long hiatus in basalt volcanism and then a second episode from about 2.2 Ma to as recently as 100,000 years ago.

Hooper and others (2001b) also dated Malheur Butte, a volcanic neck that is higher (elevation 2,661 feet, 811 m) than Lake Idaho sediment in the surrounding hills (elevation 2,300-2,550 feet, 670-780 m). Fine-grained, blue-gray andesite (about 2 percent plagioclase) yielded a whole-rock $^{40}Ar/^{39}Ar$ date of 0.8 ± 0.7 Ma. We have determined that the andesite is intrusive into an older bentonitic claystone, but we cannot determine from field relationships if it intrudes into or is overlain by the Glenns Ferry Formation. Lees (1994) suspected that flows of Malheur Butte lay buried beneath the lake sediment, but we find it is clearly intrusive into uplifted older sediment.

Basalt volcanism in the western plain beginning about 2.2 Ma erupted a volume of about 300 cubic km (see basalt-isopach map by Whitehead, 1992) from a group of vents with an alignment that is oblique to the orientation of the plain and its boundary faults (Figure 18). We call this basalt field of the western plain the Kuna-Mountain Home volcanic-rift zone. Although small in volume compared to the total late Neogene and Quaternary basalt of the eastern plain (estimated to be 40,000 cubic km

by Kuntz, 1992, p. 231), the western plain basalt field shares characteristic forms of basalt fields of the eastern plain. The vents are marked by numerous shield volcanoes distributed from near Mountain Home to the Kuna-Melba area. Other vents of this age also occur along the north margin of the plain near Boise (Othberg, 1994; Othberg and others, 1995) and within the Idaho batholith north of the plain (Howard and Shervais, 1982; Vetter and Shervais, 1992). Some intracanyon flows from these vents traveled down stream valley, up to 75 km distance, and spilled onto the plain, but their total volume is substantially less than the vents within the plain, probably less than 10 cubic km. A number of basalt vents erupted into the declining stages of Lake Idaho along the south side of the plain (Godchaux and others, 1992), and we used ages on Walters Butte and Pickles Butte to help date the level of the lake in Figure 9. Bonnichsen (written commun., 2000) has pointed out to us that some vents lie off the main line of shields, but we believe the bulk of the volume erupted from the zone shown in Figures 19.

Basalt eruptions from the volcanic rift zone constructed an upland of coalescing large shield volcanoes, generally higher than 3,100 feet (945 m) in elevation, that has confined the Snake River to a southerly course through the plain. Big Foot Butte shield is fully 8 km in diameter, and elevation at the top is 3,535 feet (1,078 m). The Initial Point shield is 10 km in diameter and has built up to an elevation of 3,240 feet (988 m). Most of the lava field erupted upon a surface that is 2,400 to 2,500 feet (730-760 m) in elevation (Wood, 1997). In the area of Little Joe Butte, Whitehead (1992) shows Quaternary basalt down to 1,300 feet (400 m) in elevation, where the basalt is determined to be 1,500 feet (460 m) thick on the basis of resistivity soundings. Two water wells drilled the basalt column down to elevation 1,880 feet (573 m), where they are still in the basalt section (Cinder Butte Farms Well, sec. 27, T. 2 S., R. 4 E.; and Big "D," Inc. Well, sec. 28, T. 2 S., R. 4. E.). The deep basalt in this area appears confined to a zone about 10 km wide over the main vent area and may be partly composed of dikes and sills; however, the driller of the Cinder Cone Butte well described red cinders at elevation 2,048 feet (624 m), and the driller of the Sabin well (sec. 25) described subsurface red lava at the 2,108-foot (647-m) elevation. The red color suggests these are subaerially erupted basalt cinders. In most other wells, basalt rests upon gravel and sand sediment at and above elevation 2,050 feet (625 m). The deep basalts here are poorly understood, particularly the low elevation of the sediment surface upon which most of basalt rests in this local area (i.e., about 2,050 feet, 625 m). We do not believe that the lake deposits of the western plain were incised to that depth before the eruption of basalt lavas. The present Snake River elevation just southeast of this area is 2,340 feet (713 m). Probably, this area of low-elevation basalt-sediment contact has experienced relative downfaulting associated with the basalt volcanism.

An ancestral canyon of the Snake River (filled by basalt) trends northwestward in the subsurface from Swan Falls to near Melba and Bowmont, a feature originally identified by Malde (1987) and called the "Canyon 3 Stage." Malde (1991) estimates the floor of the canyon at elevation 2,150 feet (655 m) on the basis of well data

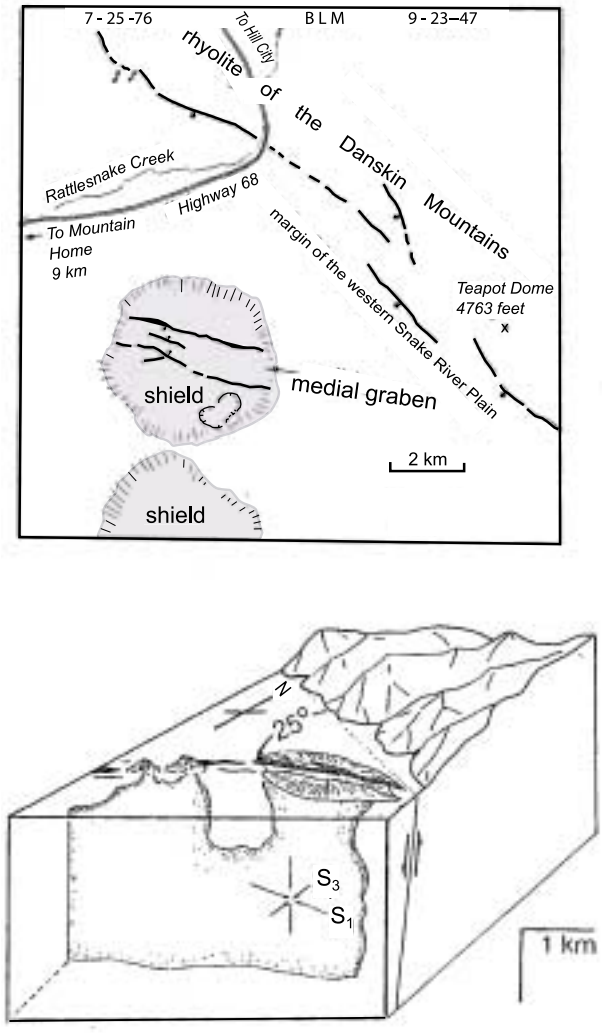

Figure 18. The air-photo tracing shows the northeast margin of the western plain 9 km northeast of Mountain Home. Tracing shows the N. 70° W. trend of fissures in the Pleistocene shield volcano and the N. 45° W. trend of the faults on the margins of the plain. Block diagram shows the inferred direction of principal stress-controlling feeder dike systems for the Kuna-Mountain Home volcanic rift zone. S_1 is the maximum principal stress, and S_3 is the minimum principal stress.

in the Melba area. He believed the canyon went through to the Boise River drainage to the north. We are unable to find the well data cited by Malde. Wood (1981, unpub. mapping) found water wells that drilled basalt down to 2,330 feet (710 m) in elevation near Nampa and U.S. Highway 30, but not down to 2,150 feet (655 m). There is evidence for the incision of the older lake deposits and infilling intracanyon basalt down to 2,330 feet (710 m) in elevation, but not to 2,150 feet (655 m) as suggested by Malde (1991). Determining elevations of the base of gravels overlain by subsurface intracanyon basalt is important to understanding the evolution of the Quaternary deposits and the history of incision of lake deposits (Othberg, 1994). The river at Swan Falls is now at 2,285 feet (697 m) in elevation. It is unlikely the river previously had a lower base level. Base level is established by the bedrock knickpoint at Cobb Rapids (elevation 2,080 feet, 634 m) 100 miles (160 km) downstream (Figures 14 and 15). Incision below 2,300 feet at Swan Falls would require the eroding stream to have had a lesser gradient than now (1.7 feet/mile, 0.0003), or that the Cobb Rapids area has been significantly uplifted in the Quaternary, neither of which seems likely. An elevation range of 2,300 to 2,400 feet (700-730 m) appears to be the deepest level of Quaternary incision in the Swan Falls-Nampa area of the plain.

The western plain basalt field has characteristics identical to the individual volcanic rift zones of the eastern plain, as defined by Kuntz (1992) to be linear arrays of basalt volcanic landforms and structures. The landforms include fissures, spatter ramparts, tephra cones, lava cones, shield volcanoes, and dikes at depth. The structures include noneruptive fissures, faults, and small grabens. The term "rift" needs clarification because we regard the western plain as a tectonic or continental rift, but we define here a volcanic rift zone that cuts obliquely across the western plain. A tectonic rift is a large graben structure not necessarily associated with volcanism. Kuntz (1992) shows that volcanic rift zone alignments are collinear with the strike orientation of active basin-range normal faults on both sides of the eastern plain. The length of the Kuna-Mountain Home volcanic rift zone is about 100 km, similar to typical 80-km lengths of zones in the eastern plain.

Fissures and faults within shield volcanoes of the western plain have the same alignment as the volcanic vents, about N. 70º W., indicating structural control of magma vents related to the regional tectonic stress system. This alignment is about 25 degrees counterclockwise from the bounding fault systems of the western plain (Figure 18). Nakamura and Uyeda (1980), Zoback and Zoback (1991), and Conner and Conway (2000) show such features are reliable indicators of tectonic stress direction whereby the volcano alignment is perpendicular to the least principal stress direction.

Remarkably, the alignments within volcanic rift zones change from the eastern plain to the western plain. Eastern plain zones are mostly aligned N. 30º W., whereas the one zone in the western plain is N. 70º W., and this change in orientation occurs over a distance of 80 km from the Richfield-Burley Butte zone (Shoshone lava field) to the easternmost group of vents near Mountain Home. That general trend N. 70º W. is also characteristic of eastern Oregon Quaternary basalt fields (aligned vents and fissures) and to the distribution of Quaternary basalt fields across the state westward to the Cascade Range (Figure 19). These Quaternary volcanic trends may indicate a province of relatively uniform stress orientation east of the Cascades and including the western plain, that is a different province from the eastern plain region.

CONCLUSIONS

The western Snake River Plain is a normal-fault bounded basin, 70-km wide and 300-km long. The amount of extension that formed the western-plain sedimentary basin is about 10 percent, similar to intracontinental rift basins elsewhere in the world such as Lake Baikal and those in east Africa. Exposed strata on the margins and seismic reflection data show as much as 2 km of basin relief formed by both faulting and by downwarping toward the basin axis. Fault structures are both half and full grabens. The western plain structure contrasts greatly with the northeast-trending eastern plain where extension is not expressed by faulting at the margins but solely by downwarping associated with basalt intrusion in fissure systems oriented perpendicular to the axis of the eastern plain.

Previously published seismic refraction data show that the intermediate and deep crust beneath the western plain is mafic rock, whereas the margins of the plain are granitic rock. The basin sediments are underlain first by basalt lavas which are underlain by middle crustal rock so invaded by mafic intrusives that the original granite is no longer recognizable by seismic refraction-derived velocities. This indicates the plain is not a simple graben of downfaulted granitic crust. The data also show a high velocity layer at a depth of 23 km restricted to the area beneath the Bruneau-Jarbidge eruptive center southeast of the plain. This layer could be restite or an underplate of basalt related to the formation of silicic magma.

The northwest orientation of the western plain basin appears to follow a pre-existing lithosphere weaknesses or megafabrics of the northwestern United States. This

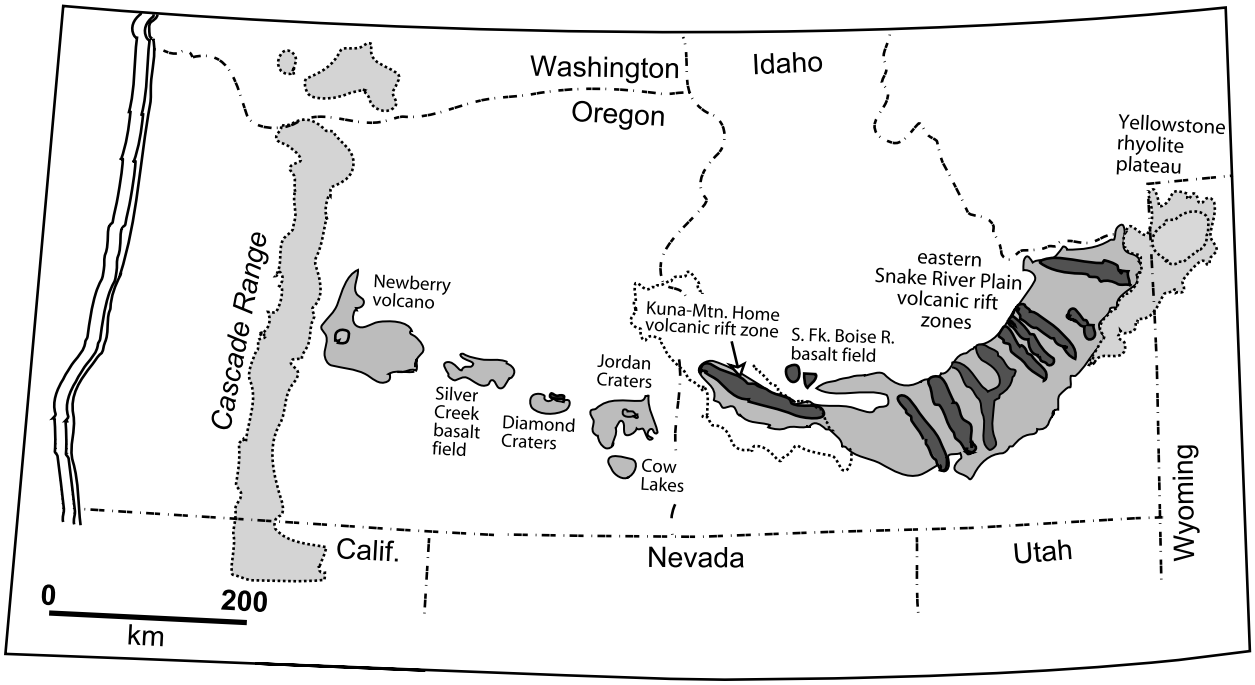

Figure 19. Map showing Quaternary basalt fields of eastern Oregon and southwest Idaho. Darkest shading is the basalt vent area. Note the contrast in the orientation of the volcanic rift zones between the eastern and the western plain. Orientation of the Kuna-Mountain Home volcanic rift zone of the western plain parallels those of eastern Oregon basalt fields, suggesting a similar orientation of tectonic stress direction in the Quaternary but a direction that differs markedly from the eastern Snake River Plain.

orientation is expressed in other structures such as the Olympic-Wallowa lineament, the Brothers fault zone, and the Baker-La Grande grabens.

The geologic and tectonic history of the western Snake River Plain is intimately involved with magmatism as shown by the following sequence of events and features:

(1) Before the basin formed, widespread and voluminous rhyolite volcanism occurred south of the plain, and the early Columbia River and Steens basalt erupted over Mesozoic rocks north and south of the plain, 17-13 Ma. Local eruptions of rhyolite occurred along the fault margins of the plain as the basin began to form about 12-11 Ma.

(2) Timing of the beginning of the basin coincides with the lodging of the hot spot at the Bruneau-Jarbidge rhyolite eruptive center, 11.5-8 Ma, southeast of the western plain. We suggest that heating of the lithosphere initiated the structure and also caused basalt magma intrusion as the basin extended.

(3) Deep wells in the center of the western plain drilled through sediments to basalt flows and basalt tuff exceeding 2.5 km in thickness, and have not drilled through rhyolite. Rhyolite sequences without significant sedimentary interbeds, as much as 2-km thick, occur on the margins of the plain. Lack of rhyolite in deep drill holes suggests that much of the plain area was an upland during the early eruptions of rhyolite from the Bruneau-Jarbidge center.

(4) Normal faulting that formed the western plain basin began about 11 Ma and amounted to over 2 km of offset by 9 Ma. Since that time, long-term average rates of vertical slip have been low (<0.01 mm/year), except for an active fault segment 55 km southwest of Mountain Home. Broad downwarping toward the center of the basin and compaction subsidence of the thick sedimentary fill have since lowered the center of the basin about 0.3 km with respect to the margins.

(5) Earliest sedimentation in the western plain is accompanied by eruptions of local basalt fields dated 10 to 7 Ma. The sediments are mapped as the Chalk Hills Formation. We find that the Poison Creek Formation of arkosic sand and the Banbury Basalt are local features and should be considered as facies and local basalt fields within the Chalk Hills Formation.

(6) The lake systems that deposited the Chalk Hills Formation declined in lake level at some time between 6 and 4 Ma, resulting in erosion of the Chalk Hills Formation from the margins of the lake. Reasons for the decline in lake level are not known.

(7) On the basis of fault history, we assume that elevations of lake-level features preserved as shoreline fea-

tures on the margins of the lake have changed little in the past 6 million years. This assumption allows reconstruction of the history of Lake Idaho as the basin refilled, overflowed, and the outlet was downcut.

(8) Between 6 and 4 Ma, lake levels rose and deposited a transgressive sequence over an unconformity surface on the Chalk Hills Formation. The shoreline transgressive sequence is identified by pebbly sands and oolitic-sand deposits in its upper part. We interpret the oolite occurrence as a product of increasing alkalinity in the lake water, as lake levels rose in a closed basin. We speculate that the lake-level rise was caused by captured drainages associated with the eastward-migrating hot-spot uplift.

(9) The lake overtopped a spill point into ancestral Hell's Canyon at a point between Huntington and Weiser. The spill point appears to be near Dead Indian Ridge at about elevation 3,600 feet (1,100 m). The time when the lake began to drain is poorly constrained, but we speculate it was about 4 Ma.

(10) Overtopping of the spill point connected the Snake River to the Columbia-Salmon River system and to the sea. Recent work by Van Tassel and others (2001) suggests the connection was established between 3.8 and 2 Ma. An implication is that once the lake began to drain, the alkalinity of lake water should have decreased, and this perhaps explains the lack of calcareous muds in the uppermost part of the Lake Idaho stratigraphic section.

(11) In the subsurface of the northwestern part of the western plain, an abrubt transition occurs upward in the section from thick mudstone to overlying deltaic sands. We interpret these sands to be the result of lowering lake level, erosion of lake-margin sands, and delivery of sand to the unfilled basin. The resulting upper section of deltaic sands and fluvial deposits is as much as 400 m thick, and these interbedded sands and muds constitute the main freshwater aquifer section of the western plain.

(12) Ages and elevations of basalt deposited over flood-plain sediment and gravel near the margins of the western plain indicate erosion of the outlet resulting in lake-level decline at an average rate of 120 m/Ma over the past 4 Ma.

(13) The process of filling of the remaining lake basin from southeast to the northwest outlet implies that flood-plain and stream-channel deposits should become younger to the northwest. The lake basin filled with sediment by about 1.6 Ma, and braided stream systems depositing cobble gravel flowed to the outlet.

(14) The resumption of basalt volcanism in the western plain began about 2.2 Ma. Much of the volcanism is expressed as a field of shield volcanoes that trends obliquely across the plain from Mountain Home to Kuna with an orientation of N. 70º W. Fissures and faults within the shields have similar orientations, suggesting the vents are controlled by a regional stress system such that the maximum principal stress is similarly oriented and that the least principal stress is aligned perpendicularly at N. 20º E.

(19) Late Quaternary fault activity occurred on a segment of the southeastern boundary fault system, 55 km southwest of Mountain Home, that trends N. 30º W. to N. 70ºW. The N. 70º W. orientation of some active faults is parallel to the Quaternary Kuna-Mountain Home volcanic rift zone, which suggests that episodic reactivation may occur on faults oriented suitably with respect to the present system of tectonic stress.

Examining the history of the western Snake River Plain brings up a number of questions for future research. Is the basalt crust beneath the western plain a product of early injection of basalt magma, similar to processes thought to be presently occurring in the eastern plain? Is the deep-crustal high-velocity zone beneath the Bruneau-Jarbidge center related to the rhyolite volcanism? These two questions might be answered by deep-crustal seismic exploration and a reevaluation of gravity data. Additionally, such a project might give new data on the way in which hot-spot magmatism has altered the lithosphere.

Other aspects of the western plain that should be a focus of research are as follows: The paleotopography and implied uplift of the region during eruption of rhyolite might be reconstructed if flow directions of rhyolite were mapped. Chronology of the "Chalk Hills" lake is poorly constrained, particularly the time of the lake level decline. Better stratigraphic study and chronology are needed of this formation to understand the processes that affected the lake. Further, the chronology of the lake level rise and overtopping of the spill point is poorly known. Detailed stratigraphy and geochronology combined with an interpretation of lacustrine-sediment geochemistry may significantly contribute to knowledge of the history of Lake Idaho.

We have suggested that the principal tectonic stress orientation indicated by Quaternary basalt vents and active faulting is about N. 70º W., and that a similar orientation is expressed by basalt fields in eastern Oregon. More detailed study of the vents throughout the region is needed to verify this. Also borehole breakouts as indicators of tectonic-stress orientation in future deep wells should be studied with compass-oriented borehole imaging or 4-arm caliper logs.

ACKNOWLEDGMENTS

Our studies of the western plain have been supported at various times by the Idaho Department of Water Re-

sources, United Water Idaho, Idaho State Board of Education, Los Alamos National Laboratory, J.R. Simplot Company, and Boise State University faculty research grants. This study contains new information developed for the Treasure Valley Hydrologic Study of the Idaho Department of Water Resources. Our ideas have been shaped through discussion and data shared by many colleagues. We would like to thank Ed Squires, Dan Brown, Terry Scanlon, Patrick Naylor, David Hawk, Lee Liberty, Dora Gallegos, Gregg Beukelman, Kurt Othberg, Craig White, Ken Pierce, Grant Meyer, and the late Will Burnham. A special thanks to Bill Bonnichsen for an insightful review and information on areas he has explored far more than any other person. Many thanks also to Gary Fuis for reviewing and clarifying parts of the manuscript.

REFERENCES

Amini, H., H.H. Hehnert, and J.D. Obradovich, 1984, K-Ar ages of late Cenozoic basalts from the western Snake River Plain, Idaho: Isochron/West, v. 41, p. 7-11.

Anders, M.H., J.W. Geissman, L.A. Piety, and J.T. Sullivan, 1989, Parabolic distribution of circumeastern Snake River Plain seismicity and latest Quaternary faulting: Migratory pattern and association with the Yellowstone hotspot: Journal of Geophysical Research, v. 94, p. 1589-1621.

Anderson, A.L., 1947, Drainage diversion in the northern Rocky Mountains of east-central Idaho: Journal of Geology, v. 55, p. 61-75.

Armstrong, R.L., J.E. Harakal, and W.M. Neill, 1980, K-Ar dating of Snake River Plain (Idaho) volcanic rocks—New results: Isochron/West, v. 27, p. 5-10.

Armstrong, R.L., W.P. Leeman, and H.E. Malde, 1975, K-Ar dating, Quaternary and Neogene volcanic rocks of the Snake River Plain, Idaho: American Journal of Science, v. 275, p. 225-251.

Baldridge, W.S., G.R. Keller, and L.W. Braile, 1995, Continental rifting: A final perspective, *in* K.H. Olsen, ed., Continental Rifts: Evolution, Structure, Tectonics: Elsevier Science, Amsterdam, p. 453-459.

Baldridge, W.S., K.H. Olsen, and J.F. Callender, 1984, Rio Grande Rift: Problems and perspectives, *in* W.S. Baldridge, P.W. Dickerson, R.E. Riecker, and J. Zidek, eds., Rio Grande Rift: New Mexico Geological Society Guidebook, 35th Field Conference, p. 1-12.

Beukelman, G.S., 1997, Evidence of active faulting in the Halfway Gulch-Little Jacks Creek area of the western Snake River Plain, Idaho: Boise State University M.S. Thesis, 170 p.

Blackwell, D.D., 1989, Regional implications of heat flow of the Snake River Plain, northwestern United States: Tectonophysics, v. 164, p. 323-343.

Bonnichsen, Bill, 1982, Rhyolite lava flows in the Bruneau-Jarbidge eruptive center, southwestern Idaho and vicinity, *in* Bill Bonnichsen and R.M. Breckenridge, eds., Cenozoic Geology of Idaho: Idaho Geological Survey Bulletin 26, p. 103-128.

Bonnichsen, Bill, R.L. Christiansen, L.A. Morgan, F.J. Moye, W.R. Hackett, W.P. Leeman, N. Honjo, M.D. Jenks, and M.M. Godchaux, 1989, Excursion 4A: Silicic volcanic rocks in the Snake River Plain-Yellowstone Plateau Province, *in* C.E. Chapin and J. Zidek, eds., Field Excursions to Volcanic Terranes of the Western United States, v. II, Cascades and Intermountain West: New Mexico Bureau of Mines and Mineral Resources Memoir 47, p. 135-182.

Bonnichsen, Bill, C. White, and M.M. Godchaux, 1997, Basaltic volcanism, western Snake River Plain [section within Mike McCurry, Bill Bonnichsen, Craig White, M.M. Godchaux, and S.S. Hughes, 1997, Bimodal basalt-rhyolite magmatism in the central and western Snake River Plain, Idaho and Oregon, *in* P.K. Link and B.J. Kowallis, Proterozoic to Recent Stratigraphy, Tectonics, and Volcanology, Utah, Nevada, Southern Idaho and Central Mexico: Brigham Young University Geology Studies, v. 42, pt. 1, p. 381-422], p. 399-422.

Bosworth, W., 1985, Geometry of propagating continental rifts: Nature, v. 316, p. 625-627.

Bott, M.H.P., and S.B. Smithson, 1967, Gravity investigations of subsurface shape and mass distributions of granite batholiths: Geological Society of America Bulletin, v. 78, p. 859-878.

Braile, L.W., R.B. Smith, J. Ansorge, M.R. Baker, M.A. Sparlin, C. Prodehl, M.M. Schilly, J.H. Healy, S. Mueller, and K.H. Olsen, 1982, The Yellowstone-Snake River Plain seismic profiling experiment: Crustal structure of the eastern Snake River Plain: Journal of Geophysical Research, v. 87, p. 2597-2609.

Brott, C.A., D.D. Blackwell, and J.C. Mitchell, 1978, Tectonic implications of the heat flow of the Snake River Plain, Idaho: Geological Society of America Bulletin, v. 89, p. 1697-1707.

Chadwick, O.A., R.D. Hall, and F.M. Phillips, 1997, Chronology of Pleistocene glacial advances in the central Rocky Mountains: Geological Society of America Bulletin, v. 109, p. 1443-1452.

Christensen, N.I., and W.D. Mooney, 1995, Seismic velocity structure and composition of the continental crust: A global view: Journal of Geophysical Research, v. 100, p. 9761-9788.

Clemens, D.M., 1993, Tectonics and silicic volcanic stratigraphy of the western Snake River Plain, Idaho: Arizona State University M.S. thesis, 209 p.

———, 1996, The Barber ash, a tephrachronology case study in southwestern Idaho, U.S.A.: Compass, v. 71, no. 2, p. 58-68.

Clemens, D.M., and S.H. Wood, 1991, K-Ar age of silicic volcanic rocks within the lower Columbia River Basalt Group at Timber Butte, Boise and Gem counties, west-central Idaho: Isochron/West, v. 57, p. 3-7.

———, 1993a, Radiometric dating, volcanic stratigraphy, and sedimentation in the Boise foothills, northeastern margin of the western Snake River Plain, Ada County, Idaho: Isochron/West, v. 59, p. 3-10.

———, 1993b, Late Cenozoic volcanic stratigraphy and geochronology of the Mount Bennett Hills, Snake River Plain, Idaho: Isochron/West, v. 60, p. 3-14.

Conner, C.B., and M.F. Conway, 2000, Basalt volcanic fields, *in* H. Sigurdsson, ed., Encyclopedia of Volcanoes: Academic Press, New York, p. 331-343.

Conrad, G.S., 1980, Biostratigraphy and mammalian paleontology of the Glenns Ferry Formation from Hammett to Oreana, Idaho: Idaho State University Ph.D. dissertation, 334 p.

Cowan, D.S., and C.J. Potter (principal compilers) with contributions from M.T. Brandson, D.M. Fountain, D.W. Hyndman, S. Y. Johnson, B.T.R. Lewis, K.J. McLain, and D.A. Swanson, 1986, Centennial continent/ocean transect #9, B-3 Juan de Fuca spreading ridge to Montana thrust belt: Geological Society of America, Decade of North American Geology, 12 p., 3 sheets.

Cox, K.G., 1989, The role of mantle plumes in the development of continental drainage systems: Nature, v. 342, p. 873-877.

Cummings, M.L., J.G. Evans, M.L. Ferns, and K.R. Lees, 2000, Stratigraphic and structural evolution of the middle Miocene synvolcanic Oregon-Idaho graben: Geological Society of America Bulletin, v. 112, p. 668-682.

Dalrymple, G.B., A. Cox, R.R. Doell, and C.S. Gromme, 1967, Pliocene geomagnetic polarity epochs: Earth and Planetary Science Letters, v. 2, p. 163-173.

Ekren, E.B., D.H. McIntyre, and E.H. Bennett, 1984, High-temperature, large-volume, lava-like ash-flow tuffs without calderas: U.S. Geological Survey Professional Paper 1272, 76 p.

Ekren, E.B., D.H. McIntyre, E.H. Bennett, and H.E. Malde, 1981, Geologic map of Owyhee County, Idaho, west of longitude 116º W.: U.S. Geological Survey Map I-1256, scale 1:125,000.

Ekren, E.B., D.H. McIntyre, E.H. Bennett, and R.F. Marvin, 1982, Cenozoic stratigraphy of western Owyhee County, Idaho, *in* Bill Bonnichsen and R.M. Breckenridge, eds., Cenozoic Geology of Idaho: Idaho Geological Survey Bulletin 26, p. 215-235.

Evernden, J.F., D.E. Savage, G.H. Curtis, and G.T. James, 1964, Potassium-argon dates and the Cenozoic mammalian chronology of North America: American Journal of Science, v. 262, p. 145-198.

Ferns, M.L., and M.L. Cummings, 1992, Geology and mineral resources map of The Elbow quadrangle, Malheur County, Oregon: Oregon Department of Geology and Mineral Industries Geological Map Series GMS-62, scale 1:24,000.

Ferns, M.L., H.C. Brooks, J.G. Evans, and M.L. Cummings, 1993, Geologic map of the Vale 30 x 60 minute quadrangle, Malheur County, Oregon, and Owyhee County, Idaho: Oregon Department of Geology and Mineral Industries Map GMS-77, scale 1:100,000.

Fitzgerald, J.F., 1982, Geology and basalt stratigraphy of the Weiser embayment, west-cental Idaho, *in* Bill Bonnichsen and R.M. Breckenridge, eds., Cenozoic Geology of Idaho: Idaho Geological Survey Bulletin 26, p. 103-128.

Fliedner, M.M., S. Ruppert, and Southern Sierra Nevada Continental Dynamics Working Group, 1996, Three-dimensional crustal structure of the southern Sierra Nevada from seismic fan profiles and gravity modeling: Geology, v. 24, p. 367-370.

Foley, M.G., 1980, Quaternary diversion and incision, Dearborn River, Montana: Summary: Geological Society of America Bulletin, v. 91, pt. 1, p. 567-577.

Godchaux, M.M., Bill Bonnichsen, and M.D. Jenks, 1992, Types of phreatomagmatic volcanoes in the western Snake River Plain, Idaho, USA: Journal of Volcanology and Geothermal Research, v. 52, p. 1-25.

Gravity Anomaly Map Committee, 1987, Gravity anomaly map of North America, 1:5,000,000: Decade of North American Geology, Continent-Scale Map-002, Geological Society of America.

Izett, G.A., 1981, Volcanic ash beds: Recorders of upper Cenozoic silicic pyroclastic volcanism in the western United States: Journal of Geophysical Research, v. 86, p. 10,200-10,222.

Hamilton, W., 1962, Late Cenozoic structure of west-central Idaho: Geological Society of America Bulletin, v. 73, p. 511-516.

Hart, W.K., M.E. Brueseke, P.R. Renne, and H.G. McDonald, 1999, Chronostratigraphy of the Pliocene Glenns Ferry Formation, Hagerman Fossil Beds National Monument, Idaho (abs.): Geological Society of America Abstracts with Programs, v. 31, no. 4, p. A-15.

Hearst, J., 1999, Depositional environments of the Birch Creek local fauna (Pliocene:Blancan), Owyhee County, Idaho, *in* W.A. Akersten, H.G. McDonald, D.J. Meldrum, and M.E.T. Flint, eds., And Whereas . . . Papers on the Vertebrate Paleontology of Idaho Honoring John A. White, Volume 1: Idaho Museum of Natural History Occasional Paper 36, p. 56-93.

Hill, D.P., and L.C. Pakiser, 1967, Seismic-refraction study of crustal structure between the Nevada Test Site and Boise, Idaho: Geological Society of America Bulletin, v. 78, p. 685-704.

Hooper, P.R., G.B. Binger, and K.R. Lees, 2002a, Ages of the Steens and Columbia River flood basalts and their relationship to extension-related calc-alkalic volcanism in eastern Oregon: Geological Society of America Bulletin, v. 114, p. 43-50.

———, 2002b, Correction: Geological Society of America Bulletin, v. 114, p. 923-924.

Hooper, P.R., and R.M. Conrey, 1989, A model for the tectonic setting of the Columbia River basalt eruptions, *in* S.P. Reidel and P.R. Hooper, eds., Volcanism and Tectonism in the Columbia River Flood-Basalt Province: Geological Society of America Special Paper 239, p. 293-306.

Hooper, P.R., and C.J. Hawkesworth, 1993, Isotopic and geochemical constraints on the origin and evolution of the Columbia River basalt: Journal of Petrology, v. 34, p. 1203-1246.

Hooper, P.R., and D.A. Swanson, 1990, The Columbia River Basalt Group and associated volcanic rocks of the Blue Mountains Province: U.S. Geological Survey Professional Paper 1437, p. 63-99.

Howard, K.A., J.W. Shervais, and E.H. McKee, 1982, Canyon-filling lavas and lava dams on the Boise River, Idaho, and their significance for evaluating downcutting during the last two million years, *in* Bill Bonnichsen and R.M. Breckenridge, eds., Cenozoic Geology of Idaho: Idaho Geological Survey Bulletin 26, p. 629-642.

Humphreys, E.D., K. Dueker, D. Schutt, and R. Saltzer, 1999, Lithosphere and asthenosphere structure and activity in Yellowstone's wake: Geological Society of America Abstracts with Programs, v. 31, no. 4, p. A-17.

Hyndman, D.W., 1978, Major tectonic elements and tectonic problems along the line of section from northeastern Oregon to west-central Montana: Geological Society of America Map and Chart Series, MC-28C.

Jenks, M.D., and Bill Bonnichsen, 1989, Subaqueous basalt eruptions into Pliocene Lake Idaho, *in* V.E. Chamberlain, R.M. Breckenridge, and Bill Bonnichsen, eds., Guidebook to the Geology of Northern and Western Idaho and Surrounding Areas: Idaho Geological Survey Bulletin 28, p. 17-34.

Jenks, M.D., Bill Bonnichsen, and M.M. Godchaux, 1993, Geologic maps of the Grand View-Bruneau area, Owyhee County, Idaho: Idaho Geological Survey Technical Report 93-2, 21 p., scale 1:24,000.

Johnson, T.C., and P. Ng'ang'a, 1990, Reflection on a rift lake, *in* B.J. Katz, ed., Lacustrine Basin Exploration: American Association of Petroleum Geologists Memoir 50, p. 113-136.

Kimmel, P.G., 1979, Stratigraphy and paleoenvironments of the Miocene Chalk Hills Formation and Pliocene Glenns Ferry Formation in the western Snake River Plain, Idaho: University of Michigan Ph.D. dissertation, 331 p.

———, 1982, Stratigraphy, age, and tectonic setting of the western Snake River Plain, Oregon and Idaho, *in* Bill Bonnichsen and R.M. Breckenridge, eds., Cenozoic Geology of Idaho: Idaho Geological Survey Bulletin 26, p. 103-128.

Kirkham, V.R.D., 1931, The Snake River downwarp: Journal of Geology, v. 39, p. 456-482.

Kuntz, M.A., H.R. Covington, and L.J. Schorr, 1992, An overview of basaltic volcanism of the eastern Snake River Plain, Idaho, *in* P.K. Link, M.A. Kuntz, and L.B. Platt, eds., Regional Geology of Eastern Idaho and Western Wyoming: Geological Society of America Memoir 179, p. 227-267.

Lawrence, R.D., 1976, Strike-slip faulting terminates the Basin and Range Province in Oregon: Geological Society of America Bulletin, v. 87, p. 846-850.

Leake, B.E., 1990, Granite magmas: Their sources, initiation, and consequences of emplacement: Journal of the Geological Society of London, v. 147, p. 579-589.

Leeman, W.P., 1989, Origin and development of the Snake River Plain—An overview, *in* R.P. Smith and W.F. Downs, eds., Snake River Plain-Yellowstone Volcanic Province: 28th International Geological Congress Guidebook T305, American Geophysical Union, Washington, D.C., p. 4-12.

Lees, K., 1994, Magmatic and tectonic changes through time in the Neogene volcanic rocks of the Vale area, Oregon, northwestern USA:

Milton Keynes, Great Britain, The Open University Ph.D. dissertation, 284 p.

Lewis, R.E., and M.A.J. Stone, 1988, Geohydrologic data from a 4,403-foot geothermal test hole, Mountain Home Air Force Base, Elmore County, Idaho: U.S. Geological Survey Open-file Report 88-166, 30 p.

Lindgren, W., 1898, Description of the Boise quadrangle, Idaho: U.S. Geological Survey Geologic Atlas, Folio 103, 7 p.

Mabey, D.R., 1976, Interpretation of a gravity profile across the western Snake River Plain, Idaho: Geology, v. 4, p. 53-55.

———, 1982, Geophysics and tectonics of the Snake River Plain, Idaho, *in* Bill Bonnichsen and R.M. Breckenridge, eds., Cenozoic Geology of Idaho: Idaho Geological Survey Bulletin 26, p. 139-154.

MacLeod, N.S., G.S. Walker, and E.H. McKee, 1975, Geothermal significance of eastward increase in age of upper Cenozoic rhyolitic domes in southeastern Oregon, *in* Proceedings, Second United Nations Symposium on the Development and Use of Geothermal Resources, v. 1, p. 465-474.

Malde, H.E., 1959, Fault zone along northern boundary of western Snake River Plain, Idaho: Science, v. 130, p. 272.

———, 1972, Stratigraphy of the Glenns Ferry Formation from Hammett to Hagerman, Idaho: U.S. Geological Survey Bulletin 1331-D, 19 p.

———, 1991, Quaternary geology and structural history of the Snake River Plain, Idaho and Oregon, *in* R.B. Morrison, ed., Quaternary Nonglacial Geology, Conterminous U.S.: Geology of North America, Geological Society of America, v. K-2, p. 251-280.

Malde, H.E., and H.A. Powers, 1962, Upper Cenozoic stratigraphy of the western Snake River Plain, Idaho: Geological Society of America Bulletin, v. 73, p. 1197-1220.

Manley, C.R., and W.C. McIntosh, 1999, The Juniper Mountain volcanic center, Owyhee County, SW Idaho: Age relations, physical volcanology, and magmatic evolution: Geological Society of America Abstracts with Programs, v. 31, no. 4, p. A-24.

McCurry, Mike, Bill Bonnichsen, Craig White, M.M. Godchaux, and S.S. Hughes, 1997, Bimodal basalt-rhyolite magmatism in the central and western Snake River Plain, Idaho and Oregon, *in* P.K. Link and B.J. Kowallis, eds., Proterozoic to Recent Stratigraphy, Tectonics, and Volcanology, Utah, Nevada, Southern Idaho and Central Mexico: Brigham Young University Geology Studies, v. 42, pt. 1, p. 381-422.

McIntyre, D.H., 1979, Preliminary description of Anschutz Federal No. 1 drill hole, Owyhee County, Idaho: U.S. Geological Survey Open-File Report 79-651, 15 p.

McQuarrie, N., and D.W. Rodgers, 1998, Subsidence of a volcanic basin by flexure and lower crustal flow: Tectonics, v. 17, p. 203-220.

Meyer, G.M., and M.E. Leidecker, 1999, Fluvial terraces along the Middle Fork Salmon River, Idaho, and their relation to glaciation, landslide dams, and incision rates: A preliminary analysis and river-mile guide, *in* S.S. Hughes and G.D. Thackray, eds., Guidebook to the Geology of Eastern Idaho: Idaho Museum of Natural History, p. 219-235.

Middleton, L.T., M.L. Porter, and P.G. Kimmel, 1985, Depositional settings of the Chalk Hills and Glenns Ferry Formations west of Bruneau, Idaho, *in* R.M. Flores and S.S. Kaplan, eds., Cenozoic Paleogeography of the West-Central United States: Society of Economic Paleontologists and Mineralogists, Rocky Mountain Section, p. 37-53.

Minor, S.A., J.J. Rytuba, M.J. Grubensky, D.B. Vander Meulen, C.A. Goeldner, and K.J. Tegtmeyer, 1987, Geologic map of the High Steens and Little Blitzen Gorge Wilderness Study Areas, Harney County, Oregon: U.S. Geological Survey Map MF-1876, scale 1:24,000.

Morgan, L.A., 1992, Stratigraphic relations and paleomagnetic and geochemical correlations of ignimbrites of the Heise volcanic field, eastern Snake River Plain, eastern Idaho and western Wyoming, *in* P.K. Link, M.A. Kuntz, and L.B. Platt, eds., Regional Geology of Eastern Idaho and Western Wyoming: Geological Society of America Memoir 179, p. 215-226.

Nakamura, K. and S. Uyeda, 1980, Stress gradient in back-arc regions and plate subduction: Journal of Geophysical Research, v. 85, p. 6419-6428.

Neill, W.M., 1975, Geology of the southeastern Owyhee Mountains and environs, Owyhee County, Idaho: Stanford University M.S. thesis, 59 p.

Neville, C., N.D. Opdyke, E.H. Lindsay, and N.M. Johnson, 1979, Magnetic stratigraphy of Pliocene deposits on the Glenns Ferry Formation, Idaho, and its implications for North American mammalian biostratigraphy: American Journal of Science, v. 279, p. 503-526.

Newton, G.D., 1991, Geohydrology of the regional aquifer system, western Snake River Plain, southwestern Idaho: U.S. Geological Survey Professional Paper 1408-G, 52 p.

Othberg, K.L., 1988, Changeover from basin-filling to incision in the western Snake River Plain: Geological Society of America Abstracts with Programs, v. 20, no. 6, p. 461.

———, 1994, Geology and geomorphology of the Boise Valley and adjoining areas, western Snake River Plain, Idaho: Idaho Geological Survey Bulletin 29, 54 p.

Othberg, K.L., Bill Bonnichsen, C.C. Swisher III, and M.M. Godchaux, 1995, Geochronology and geochemistry of Pleistocene basalts of the western Snake River Plain and Smith Prairie, Idaho: Isochron/West, v. 62, p. 16-29.

Pansze, A.J., Jr., 1975, Geology and ore deposits of the Silver City-Delamar-Flint region, Owyhee County, Idaho: Idaho Bureau of Mines and Geology Pamphlet 161, 79 p.

Park, R.G., 1988, Geological Structures and Moving Plates: Blackie and Sons, Glasgow, 337 p.

Parsons, T., G.A. Thompson, and R.P. Smith, 1998, More than one way to stretch: A tectonic model for extension along the plume track of the Yellowstone hotspot and adjacent Basin and Range Province: Tectonics, v. 17, p. 221-234.

Perkins, M.E., F.H. Brown, W.P. Nash, W. McIntosh, and S.K. Williams, 1998, Sequence, age, and source of silicic fallout tuffs in middle to late Miocene basins of the Basin and Range Province: Geological Society of America Bulletin, v. 110, p. 344-360.

Pezzopane, S.K., and R.J. Weldon, 1993, Tectonic role of active faulting in central Oregon: Tectonics, v. 12, p. 1140-1169.

Pierce, K.L., and L.A. Morgan, 1992, The track of the Yellowstone hot spot: Volcanism, faulting, and uplift, *in* P.K. Link, M.A. Kuntz, and L.B. Platt, eds., Regional Geology of Eastern Idaho and Western Wyoming: Geological Society of America Memoir 179, p. 1-53.

Prodehl, C., 1979, Crustal structure of the western United States: U.S. Geological Survey Professional Paper 1034, 74 p.

Repenning, C.A., T.R. Weasma, and G.R. Scott, 1994, The early Pleistocene (latest Blancan-earliest Irvingtonian) Froman Ferry fauna and history of the Glenns Ferry Formation, southwestern Idaho: U.S. Geological Survey Bulletin 2105, 86 p.

Rosendahl, B.R., E. Kilembe, and K. Kaczmarick, 1992, Comparison of the Tanganyika, Malawi, Rukwa, and Turkana Rift zones from analysis of seismic reflection data: Tectonophysics, v. 213, p. 235-256.

Rytuba, J.J., and D.B. Vander Meulen, 1991, Hot-spring precious-metal systems in the Lake Owyhee volcanic field, Oregon-Idaho, *in* G.L. Raines, R.E. Lisle, R.W. Schafer, and W.H. Wilkinson, eds., Geology and Ore Deposits of the Great Basin: Symposium Proceedings, Geological Society of Nevada, Reno, p. 1085-1096.

Sadler, J.L. and P.K. Link, 1996, The Tuana Gravel: Early Pleistocene response to longitudinal drainage of a late-stage rift basin, western Snake River Plain, Idaho: Northwest Geology, v. 26, p. 46-62.

Schumm, S.A., and F.G. Ethridge, 1994, Origin, evolution, and morphology of fluvial valleys, *in* Incised Valley Systems; Origin and Sedimentary Sequences, Society of Economic Paleontologists and Mineralogists Special Publication 51, Society for Sedimentary Geology, Tulsa, p. 11-27.

Sheppard, R.A., 1991, Zeolite diagenesis of tuffs in the Miocene Chalk Hills Formation, western Snake River Plain, Idaho: U.S. Geological Survey Bulletin 1963, 27 p.

Smith, G.R., N. Morgan, and E. Gustafson, 2000, Fishes of the Pliocene Ringold Formation of Washington and history of the Columbia River drainage: University of Michigan Museum of Paleontology Papers on Paleontology, v. 32, 42 p.

Smith, G.R., K. Swirydczuk, P.G. Kimmel, and B.H. Wilkinson, 1982, Fish biostratigraphy of late Miocene to Pleistocene sediments of the western Snake River Plain, Idaho, *in* Bill Bonnichsen and R.M. Breckenridge, eds., Cenozoic Geology of Idaho: Idaho Geological Survey Bulletin 26, p. 519-541.

Smith, G.R., and W.P. Patterson, 1994, Mio-Pliocene seasonality on the Snake River Plain: Comparison of faunal and oxygen isotopic evidence: Paleogeography, Paleoclimatology, Paleoecology, v. 107, p. 291-302.

Smith, R.B., and L.W. Braile, 1993, Topographic signature, space-time evolution, and physical properties of the Yellowstone-Snake River Plain volcanic system: The Yellowstone hotspot, *in* A.W. Snoke, J.R. Steidtmann, and S.M. Roberts, eds., Geology of Wyoming: Geological Survey of Wyoming Memoir No. 5, p. 694-754.

Squires, E., S.H. Wood, and J.L. Osiensky, 1992, Hydrogeologic framework of the Boise aquifer system, Ada County, Idaho: Idaho Water Resources Research Institute, Research Technical Completion Report 14-08-0001-0G1559-06, University of Idaho, 114 p.

Swirydczuk, K., G.P. Larson, and Gerald R. Smith, 1982, Volcanic ash beds as stratigraphic markers in the Glenns Ferry and Chalk Hills Formations from Adrian, Oregon, to Bruneau, Idaho, *in* Bill Bonnichsen and R.M. Breckenridge, eds., Cenozoic Geology of Idaho: Idaho Bureau of Mines and Geology Bulletin 26, p. 543-558.

Swirydczuk, K., B.H. Wilkinson, and G.R. Smith, 1979, The Pliocene Glenns Ferry oolite: Lake-margin carbonate deposition in the southwestern Snake River Plain: Journal of Sedimentary Petrology, v. 49, p. 995-1004.

———, 1980a, The Pliocene Glenns Ferry oolite-I: Lake-margin carbonate deposition in the southwestern Snake River Plain—Reply: Journal of Sedimentary Petrology, v. 50, p. 999-1001.

———, 1980b, The Pliocene Glenns Ferry oolite-II: Sedimentology of oolitic lacustrine terrace deposits: Journal of Sedimentary Petrology, v. 50, p. 1237-1248.

Taylor, D.W., and R.C. Bright, 1987, Drainage history of the Bonneville Basin, *in* Cenozoic Geology of Western Utah—Sites for Precious Metal and Petroleum Accumulations: Utah Geological Society Publication 16, p. 239-256.

Taubeneck, W.H., 1971, Idaho batholith and its southern extension: Geological Society of America Bulletin, v. 82, p. 1899-1928.

Thompson, R.S., 1991, Pliocene environments and climates of the western United States: Quaternary Science Reviews, v. 10, p. 115-132.

Vallier, Tracey, 1998, Islands and Rapids: A Geological Story of Hell's Canyon: Confluence Press, Lewiston, Idaho, 151 p.

Van Tassell, J., M. Ferns, V. McConnell, and G.R. Smith, 2001, The mid-Pliocene Imbler fish fossils, Grande Ronde Valley, Union County, Oregon, and the connection between Lake Idaho and the Columbia River: Oregon Geology, v. 63, p. 77-96.

Vetter, S.K., and J.W. Shervais, 1992, Continental basalts of the Boise River group near Smith Prairie, Idaho: Journal of Geophysical Research, v. 97, p. 9043-9061.

Walker, G.W., G.B. Dalrymple, and M.A. Lanphere, 1974, Index to potassium-argon ages of volcanic rocks of Oregon: U.S. Geological Survey Miscellaneous Field Studies, Map MF-569, 2 sheets.

Walker, G.W., and N.S. MacLeod, 1991, Geologic map of Oregon: U.S. Geological Survey, scale 1:500,000.

Wendlandt, R.F., W.S. Baldridge, and E.R. Neumann, 1991, Modification of the lower crust by continental rift magmatism: Geophysical Research Letters, v. 18, p. 1759-1762.

Wernicke, B., 1992, Extensional tectonics in the western United States: Geology of North America, v. G-3, The Cordilleran Orogen, Conterminous U.S.: Geological Society of America, Boulder, Colorado., p. 553-582.

Wheeler, H.E., and E.F. Cook, 1954, Structural and stratigraphic significance of the Snake River capture, Idaho-Oregon: Journal of Geology, v. 62, p. 525-536.

Whitehead, R.L., 1992, Geohydrologic framework of the Snake River Plain, Idaho and eastern Oregon: U.S. Geological Survey Professional Paper 1408-B, 32 p.

Wood, S.H., 1989, Silicic volcanic rocks and structure of the western Mount Bennett Hills and adjacent Snake River Plain, Idaho, *in* R.P. Smith and K.L. Ruebelmann, eds., Snake River Plain-Yellowstone Volcanic Province: 28th International Geological Congress, Guidebook T305, American Geophysical Union, Washington, D.C., p. 69-77.

———, 1994, Seismic expression and geological significance of a lacustrine delta in Neogene deposits of the western Snake River Plain, Idaho: American Association of Petroleum Geologists Bulletin, v. 78, p. 102-121.

———, 1997, Structure contour map of the base of Quaternary basalt in the western Snake River Plain: Idaho Department of Water Resources, Treasure Valley Hydrologic Project, Boise, scale 1:100,000.

Wood, S.H., and J.E. Anderson, 1981, Geology, *in* J.C. Mitchell, ed., Geothermal Investigations in Idaho, Part 11, Geological, Hydrological, Geochemical, and Geophysical Investigations of the Nampa-Caldwell and Adjacent Areas, Southwestern Idaho: Idaho Department of Water Resources Water Information Bulletin 30, p. 9-31.

Wood, S.H., and J.N. Gardner, 1984, Silicic volcanic rocks of the Miocene Idavada Group, Bennett Mountain, Elmore County, southwestern Idaho: Final contract report to the Los Alamos National Laboratory from Boise State University, 39 p., 1 map, scale 1:100,000.

Wood, Steven, and S.H. Wood, 1999, Large pumice-block layer marks sublacustrine rhyolite-dome eruption in the Miocene Chalk Hills Formation, near Marsing, Idaho, western Snake River Plain: Geological Society of America Abstracts with Programs, v. 31, no. 4, p. A-62.

Zoback, M.L., E.H. McKee, R.J. Blakely, and G.A. Thompson, 1994, The northern Nevada rift: Regional tectono-magmatic relations and middle Miocene stress direction: Geological Society of America Bulletin, v. 106, p. 371-382.

Zoback, M.D., and M.L. Zoback, 1991, Tectonic stress field of North America and relative plate motions, *in* D.B. Slemmons, E.R. Engdahl, M.D. Zoback, and D.D. Blackwell, eds., Neotectonics of North America: Geological Society of America Map Volume 1, p. 339-365.

Detrital Zircon Evidence for Pleistocene Drainage Reversal at Hagerman Fossil Beds National Monument, Central Snake River Plain, Idaho

Paul Karl Link,[1] H. Gregory McDonald,[2]
C. Mark Fanning,[3] and Andrew E. Godfrey[4]

ABSTRACT

The Pliocene Glenns Ferry Formation at Hagerman Fossil Beds National Monument represents flood-plain and fluvial aggradation between 4 and 3.2 Ma. Detrital zircon populations from the main body of the Glenns Ferry Formation match those of the present Big and Little Wood rivers, which flow southward, draining the Soldier and Pioneer mountains.

Unconformably above the Glenns Ferry Formation, the Pliocene(?) and lower Pleistocene Tuana Gravel contains fluvial sands and gravels deposited by cycles of west- and north-prograding drainage. Regional base-level started to lower around 3.2 Ma, controlled by cutting of the outlet to the western Snake River Plain through Hells Canyon. The uppermost Glenns Ferry Formation and Tuana Gravel contain distinctive zircon assemblages, including 160 to 140 Ma (Middle Jurassic) grains derived from the Contact pluton south of Jarbidge, Nevada, and late Eocene (42-37 Ma) grains derived from voluminous volcanics of northern Nevada.

The detrital zircon populations indicate a drainage reversal in the Hagerman area between 3.2 and 1.5 Ma from south-flowing streams with provenance in the Wood River drainage of central Idaho, which fed the Glenns Ferry Formation, to north-flowing streams with provenance in the Salmon Falls Creek drainage of northern Nevada, which fed the Tuana Gravel. This is consistent with suggestions by Repenning and others (1995) of a Pliocene drainage connection between the Hagerman area and the Sacramento and Humboldt River systems to the south and west, based on distributions of pygmy muskrat *Pliopotamys minor,* giant beaver *Protocastoroides idahoensis*, the turtle *Clemmys*, fossil fish and mollusks. Both detrital zircon signatures of the Glenns Ferry Formation and Tuana Gravel are different than those of the Recent Snake River west of Twin Falls, leaving unresolved questions about when the Snake River established its present northwestward course.

Key words: detrital-zircon, Idaho, Snake River Plain, Pleistocene, Hagerman

INTRODUCTION

Late Miocene to Recent eastward migration of the continental divide across Idaho followed the crest of the tumescent topographic bulge associated with the Snake River Plain-Yellowstone hot spot (Figure 1; Pierce and Morgan, 1992; Smith and Siegel, 2000). Neogene drainage reversals have been documented south and east of Pocatello in the Portneuf, Bear, and Rock Creek drainages, where the Snake River has captured parts of streams that formerly drained south and east (Ore and others, 1996; Ore; 1999). One of the most famous drainage captures was at Red Rock Pass, the dam to late Pleistocene

Editors' note: The manuscript was submitted in June 1998 and has been revised at the authors' discretion.

[1]Department of Geosciences, Idaho State University, Pocatello, ID 83209
[2]National Park Service, P.O. Box 25287, Denver, CO 80225
[3]Research School of Earth Sciences, Australian National University, Canberra ACT, 2601, Australia
[4]U.S. Department of Agriculture, Forest Service, 324 25th St., Ogden, UT 84401

Link, P.K., H.G. McDonald, C.M. Fanning, and A.E. Godfrey, 2002, Detrital zircon evidence for Pleistocene drainage reversal at Hagerman Fossil Beds National Monument, central Snake River Plain, Idaho, *in* Bill Bonnichsen, C.M. White, and Michael McCurry, eds., Tectonic and Magmatic Evolution of the Snake River Plain Volcanic Province: Idaho Geological Survey Bulletin 30, p. 105-119.

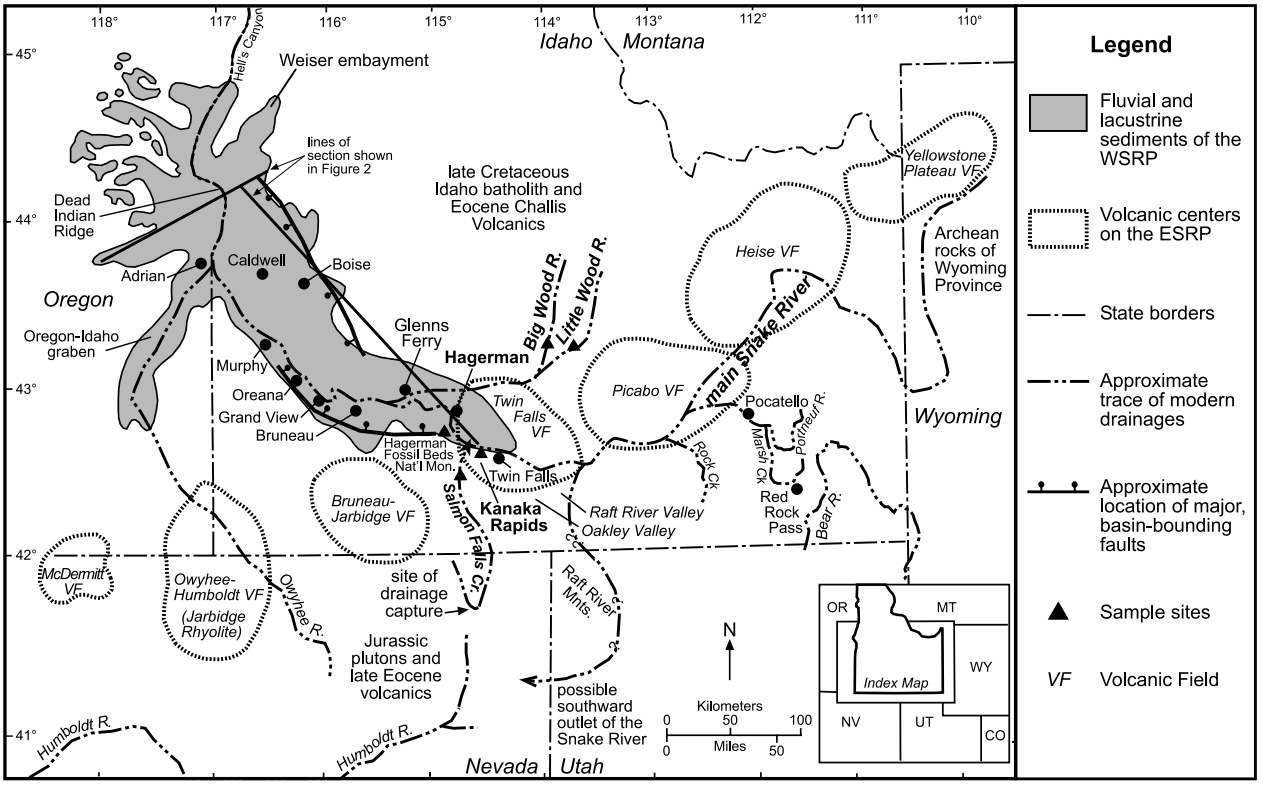

Figure 1. Location map for Snake River Plain (SRP) region showing localities mentioned in the text (modified from Middleton and others, 1985; Pierce and Morgan, 1992; Sadler and Link, 1996). Neogene volcanic fields are shown, as well as approximate fault boundaries of western SRP and extents of Lake Idaho. Stratigraphic cross section lines of Figure 2 are shown.

Lake Bonneville (Bright and Ore, 1987; Link and others, 1999b).

The western Snake River Plain (SRP) formed after about 11.5 Ma coincident with the initial development of the Bruneau-Jarbidge eruptive center (Wood, 1994, this volume; Bonnichsen, this volume) as a rapidly subsiding continental rift on the northwest shoulder of the SRP-Yellowstone hot spot, which is hypothesized to have formed a tumescent topographic bulge about 100 km in radius and elevated by 0.5 to 1 km (Pierce and Morgan, 1992). From 8.5 to 2 Ma the western SRP contained a large freshwater lake system (Lake Idaho) and related fluvial systems in which the Idaho Group (Poison Creek, Chalk Hills, Glenns Ferry, Tuana, and Bruneau formations, Figures 2 and 3) was deposited. The fossiliferous Glenns Ferry Formation at Hagerman Fossil Beds National Monument (Figure 3) represents flood-plain and marsh facies that accumulated on the eastern side of Lake Idaho about 4 to 3.2 Ma (Malde, 1972; McDonald and others, 1996).

Subsidence of the eastern SRP began about 10 Ma and progressed northeastward, caused by crustal loading of a lower-crustal mafic sill (McQuarrie and Rodgers, 1998), as well as thermal subsidence from detumescence of the topographic bulge, and superimposed on early Basin and Range uplifts and basins (Pierce and Morgan, 1992; Ore and others, 1996; Sadler and Link, 1996; Rodgers and others, this volume).

We use the new tool of detrital zircon geochronology to constrain models of paleodrainage in Recent and Neogene sands in the central SRP area. As we describe below, our data are consistent with the drainage model of Repenning and others (1995), where Lake Idaho and the late Miocene and Pliocene Snake River had connections to the south, in Nevada, and thence to the Sacramento system, with drainage reversal to the west occurring in latest Pliocene or early Pleistocene time (Link and others, 1999a). However, the location and timing of the southward drainage connection are not constrained and require further study.

METHODOLOGY

We collected sand samples from the Glenns Ferry Formation and Tuana Gravel at Hagerman Fossil Beds National Monument and from several modern rivers that drain mountainous regions north and south of the SRP.

Because these first- and second-order stream systems drain country with known geology, the detrital zircon signatures of their sands are predictable and explainable (Link and others, 2000). In the northeastern SRP, comparing the detrital zircon signatures of modern rivers with subsurface Quaternary strata has allowed a highly precise evaluation of paleodrainage patterns (Geslin and others, 1999, 2002).

Ages of detrital zircon grains were obtained on the sensitive high-resolution ion microprobe (SHRIMP) at Australian National University. The uranium-lead ages of about fifty random, medium- to fine-sand sized detrital zircon grains from each sample are presented in Figure 4 and compiled in Table 1. Representative parts of the data are shown in stratigraphic context for the Glenns Ferry Formation at Hagerman in Figure 3.

The plots of Figures 3 and 4 show relative-probability spectra created from individual detrital zircon ages and errors, which are assigned Gaussian distributions and then summed together in 1 Ma bins. This method has proven useful in determining provenance signatures of source terranes and depositional basins, and is refined over a histogram in that it incorporates the precision of each age determination into the plot (Ireland, 1992; Ireland and others, 1998; Geslin and others, 1999, 2002).

GLENNS FERRY FORMATION

The Pliocene Glenns Ferry Formation (of the Idaho Group, Figure 2) contains lacustrine and fluvial sediments and ashes interbedded with basaltic lava flows (Malde

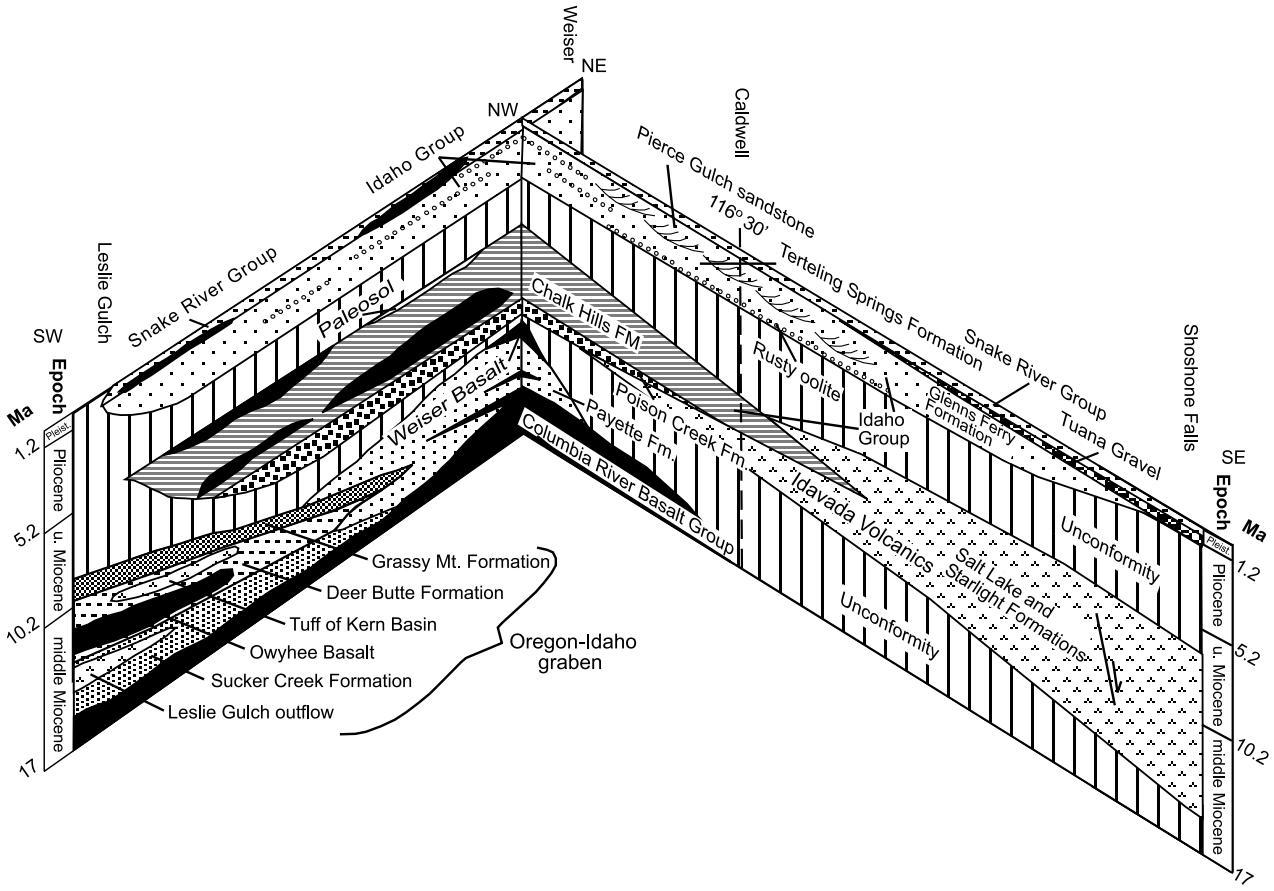

Figure 2. Correlation diagram of Neogene and Pleistocene stratigraphic units of the western SRP and Oregon-Idaho graben. Locations of cross section lines are shown on Figure 1. Chronological listing of the main sources: (Malde and others, 1963; Kittleman and others, 1965; Kittleman, 1973; Malde and Powers, 1972; Armstrong and others, 1975, 1980; McIntyre, 1979; Nakai, 1979; Ekren and others, 1981; Fitzgerald, 1982; Bonnichsen, 1982; Wood and Gardner, 1984; Bonnichsen and Kauffman, 1987; Lewis and Stone, 1988; Lawrence, 1988a, 1988b; Reidel and Hooper, 1989; Worl and others, 1991, 1995; Sheppard, 1991; Pierce and Morgan, 1992; Clemens, 1993; Clemens and Wood, 1993a, 1993b; Ferns and others, 1993; Honjo and others, 1992; Wood, 1994; Kellogg and others, 1994; Williams, 1994; Cummings and others, 1994; Gibbons, 1995; Sadler and Link, 1996; Hughes and others, 1996; McCurry and others, 1996, 1997; Ferns, 1997; Morgan and others, 1998; Perkins and others, 1998; Cummings and others, 2000).

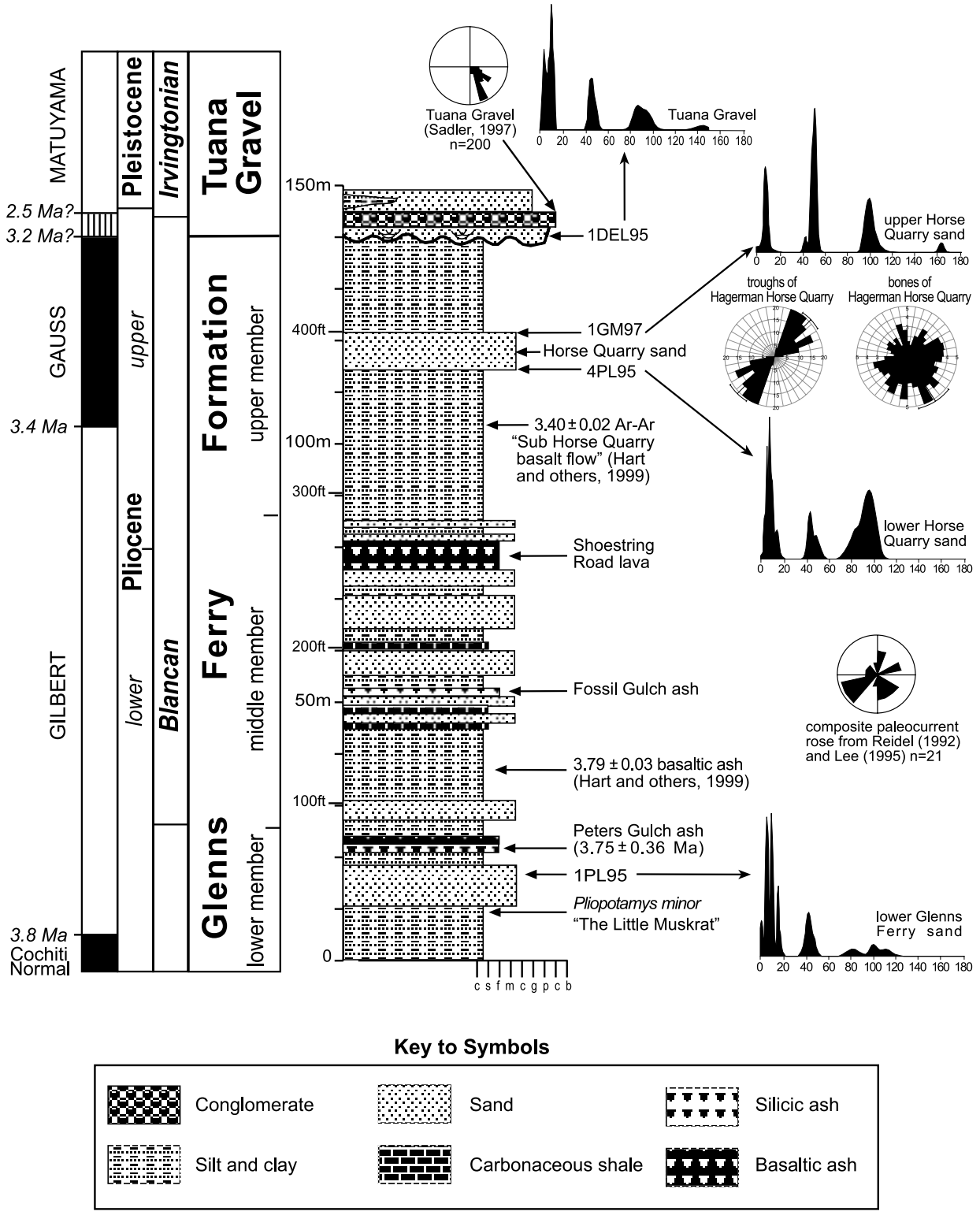

Figure 3. Stratigraphic column showing strata exposed at Hagerman Fossil Beds National Monument. Locations of detrital zircon samples and radiometric ages are shown. Detrital zircon plots (less than 160 Ma zircons only) are shown for four stratigraphic samples. Paleocurrent roses are shown for the middle Glenns Ferry Formation (Riedel, 1992; Lee and others, 1995), the Horse Quarry sands (data from G.M. McDonald, 1998) and the Tuana Gravel (Sadler, 1997). Column after Lee and others (1995) and Sadler and Link (1996).

and Powers, 1962). At Hagerman Fossil Beds National Monument, the oldest exposed beds of the Glenns Ferry Formation crop out. These sediments of calcareous silt, clay, and fine- to medium-grained sand (Figure 3) were deposited on a poorly drained, marshy flood plain and are locally abundantly fossiliferous. The Hagerman flood-plain exposures lie east of, and are older than, lacustrine facies present from Glenns Ferry westward to Grand View (Malde and Powers, 1962; Malde and others, 1963; Malde, 1972; Kimmel, 1982; Middleton and others, 1985; Kraus and Middleton, 1987). Coarser grained and likely younger Glenns Ferry lithofacies, consisting of north- and south-derived fluvial sands, are present in outcrops on the northern and southern margins of the western SRP (Malde, 1972).

Regionally, ages and chemostratigraphic correlations obtained from Glenns Ferry Formation ashes and basalt lava flows span about 4.5 to 1.6 Ma (Figure 2; Perkins and others, 1995). The most recent dating at Hagerman Fossil Beds National Monument indicates that a basaltic ash 50 feet above the Peter's Gulch ash (Figure 3) is 3.79 ± 0.03 Ma and the sub-Horse Quarry basalt flow is 3.40 ± 0.02 Ma (Hart and others, 1999; this volume).

Vertebrate fossils found within the Glenns Ferry Formation have been used to define the Blancan and earliest Irvingtonian land mammal ages (Figure 3; Lundelius and others, 1987). Repenning (1987) used the presence of the pygmy muskrat, *Pliopotamys minor*, in the lower part of the Glenns Ferry Formation at Hagerman as characteristic of Blancan 3 faunas.

About 183 m (600 feet) of flood-plain facies of the lower part of the Glenns Ferry Formation are exposed in steep cliffs on the west side of the Snake River at Hagerman Fossil Beds National Monument (Figure 3). The exposures are divided into lower, middle, and upper members, following Zakrzewski (1969), Bjork (1970), and Lee and others (1995). The upper member contains the upper and lower "Horse Quarry" sand beds (Figure 3) from which abundant fossil horse-skeletons have been collected, including *Equus simplicidens*, the Idaho State Fossil (McDonald and others, 1996). The middle member contains rhyolitic ashes and basalt lavas (Hart and others, 1999).

The Glenns Ferry Formation at Hagerman contains linear fluvial sands encased in ephemeral lake and flood-plain muds. The sediments were deposited in a meandering stream and flood-plain system dotted with ephemeral ponds and marshes. They are home to the extraordinarily diverse Hagerman local fauna, the oldest known fauna in the Glenns Ferry Formation (McDonald and others, 1996). Stream-channel sands of the lower part of the Glenns Ferry Formation at Hagerman are generally vertically stacked (Lee and others, 1995). The aggrading flood-plain muds may have caused streams to become more or less permanently established in meander belts. Paleocurrent measurements from cross-bedded sands (Figure 3) suggest a high-sinuosity stream system and no clear transport direction.

Malde (1972) noted that sequences several hundred feet thick of the lower and middle parts of the Glenns Ferry Formation were deposited in aggrading sedimentary environments with little lateral migration of facies. This amount of deposition suggests subsidence at about the same rate as sedimentation, or 22.8 cm per Ka (using 183 m in 800 Ka) at Hagerman.

The upper part of the Glenns Ferry Formation is younger west of Hagerman (Figure 2), as indicated by latest Pliocene and Pleistocene vertebrate faunas (Repenning and others, 1995; Sankey, 1996). Thus, the eastern margin of Lake Idaho migrated northwestward from west of Hagerman near 4 Ma to 1.5 Ma at Froman Ferry on the north side of the Snake River southwest of Caldwell (Repenning and others, 1995). Its maximum extent was near 3.5 Ma during deposition of the Glenns Ferry Formation at Hagerman Fossil Beds National Monument.

TUANA GRAVEL

The Tuana Gravel (Malde and Powers, 1962, 1972; Malde and others, 1963; Sadler and Link, 1996; Sadler and others, 1997; Sadler, 1997) is a sand- and gravel-bearing unit with an erosional base near the top of the Neogene and Pleistocene Idaho Group (Figures 2 and 3). Regionally it is present on the south side of the western SRP from east of Boise to Hagerman. Pleistocene gravel-bearing formations of the western SRP include the Tuana, Tenmile, Black Mesa, and other similar units. They form prominent high-level braid-plain deposits above the Snake, Boise, and other rivers of the western SRP, and likely are older to the southeast (Othberg and Stanford, 1992; Othberg, 1994).

At Hagerman, the Tuana Gravel lies unconformably on the Glenns Ferry Formation on a scoured contact (Figure 2, 3) and contains 10 to 60 m of gravel, sand, and subordinate silt and mud. Its age is poorly constrained at late Pliocene and early Pleistocene, about 3.2 to 1 Ma. The Tuana contains alluvial-fan and braided-stream deposits of two ancestral drainages, Salmon Falls Creek on the east and the Bruneau River on the west (Malde and Powers, 1972).

In Hagerman Fossil Beds National Monument, the Tuana Gravel is about 20 m thick (Figure 3) and contains greenish, trough cross-bedded sand and granule conglom-

erate in three, 10-m-thick upward-fining cycles (Sadler and Link, 1996; Sadler and others, 1997). Paleocurrent measurements from trough cross-beds and imbricated gravel clasts suggest flow to the north-northwest on a broad northwest-sloping braid-plain. The Tuana does not represent a single catastrophic event.

Unconformity-bounded upward-fining sedimentary cycles in the Tuana at Hagerman are likely related to base-level lowering caused by progressive cutting of the outlet to the western SRP at Dead Indian Ridge south of Hells Canyon (Wood, 1994; Repenning and others, 1995; Sadler and Link, 1996). Pleistocene glacial climatic variation likely also contributed to cycles of stream aggradation and incision (Pierce and Scott, 1982; Malde, 1991; Othberg, 1994; Repenning and others, 1995).

DETRITAL ZIRCON DATA

SAMPLE LOCATIONS

In addition to samples from the stratigraphic section exposed at Hagerman Fossil Beds National Monument, medium-grained sand samples were taken from accessible localities of the Big and Little Wood rivers north of Shoshone, the main Snake River at Kanaka Rapids, and Salmon Falls Creek near its mouth (Figure 1). The statistical limitations of this sampling strategy are obvious. Testing these signatures with a more complete sampling strategy is a logical next step.

ZIRCON POPULATIONS

In the discussion below, we first summarize the various zircon populations, then discuss provenance signatures from modern streams and the Glenns Ferry and Tuana formations. Zircon age plots are shown in Figure 4 and compiled in Table 1.

Archean Zircons

A few Archean (2,500-2,600 Ma) zircons are present in most samples, notably except Salmon Falls Creek. Most Archean zircons are likely recycled through Proterozoic or Phanerozoic sandstones exposed in the Montana-Idaho-Wyoming thrust belt. Some in the modern Snake River could have been derived directly from Wyoming Province basement.

Proterozoic Zircons

Paleoproterozoic and Mesoproterozoic (2,000-950 Ma) zircons are present in all samples except Salmon Falls Creek and were likely recycled through the Mesoproterozoic (about 1,470-1,370 Ma) Belt Supergroup (Link, 1999; Winston and others, 1999) or through Neoproterozoic to Permian sands of the Cordilleran miogeocline (Smith and Gehrels, 1994).

Paleozoic Zircons

Paleozoic zircons are scarce and potentially valuable as provenance tracers, because they must have come from specific plutons within the miogeocline or in the Roberts Mountains Allochthon to the south. A smattering of Silurian and Devonian zircons with an age range of 430 to 393 Ma is present in the Tuana Gravel, main Snake, middle Glenns Ferry and Big Wood samples. The Beaverhead Mountains pluton in eastern Idaho is a unique Ordovician coarse-grained granite with an age of 483 Ma (Rb-Sr, Evans and Zartman, 1988). Grains from the Beaverhead pluton provide a fingerprint for drainages from the northern border of the eastern SRP (Geslin and others, 1999, 2002). No detrital grains in the Hagerman area overlap with ages of the Beaverhead pluton.

Jurassic Zircons

Middle Jurassic (144-169 Ma) detrital zircons are abundant in Salmon Falls Creek (14 percent) and Tuana Gravel (11 percent) and are present as one grain in the upper Horse Quarry sand. Middle Jurassic (160-140 Ma) plutons are common in northern Nevada, part of voluminous magmatism that occurred during intra-Cordilleran arc shortening (Camilleri and others, 1997; Wyld and Wright, 1997). There are several plutons with ages from 140 to 150 Ma in Elko County, Nevada (Coats, 1987), including the Contact pluton of the Granite Range, which crops out along Salmon Falls Creek about 25 km south of the Idaho border.

Cretaceous and Paleocene Zircons

Numerous grains in most samples except Salmon Falls Creek span the age range of 105 to 80 Ma and were derived from the Late Cretaceous Idaho batholith, exposed both in the central Idaho mountains north of Hagerman and to the southwest in the Owyhee Mountains. In the Challis and Hailey 1° x 2° quadrangles, intrusive rocks of

Figure 4. Detrital zircon plots from Glenns Ferry and Tuana formations and modern streams of the central SRP. On left are plots of all zircon grains. On right are plots only of grains less than 200 Ma. Plots show Gaussian frequency for 1 Ma intervals. Each sample represents about fifty detrital grains. See Table 1 for data.

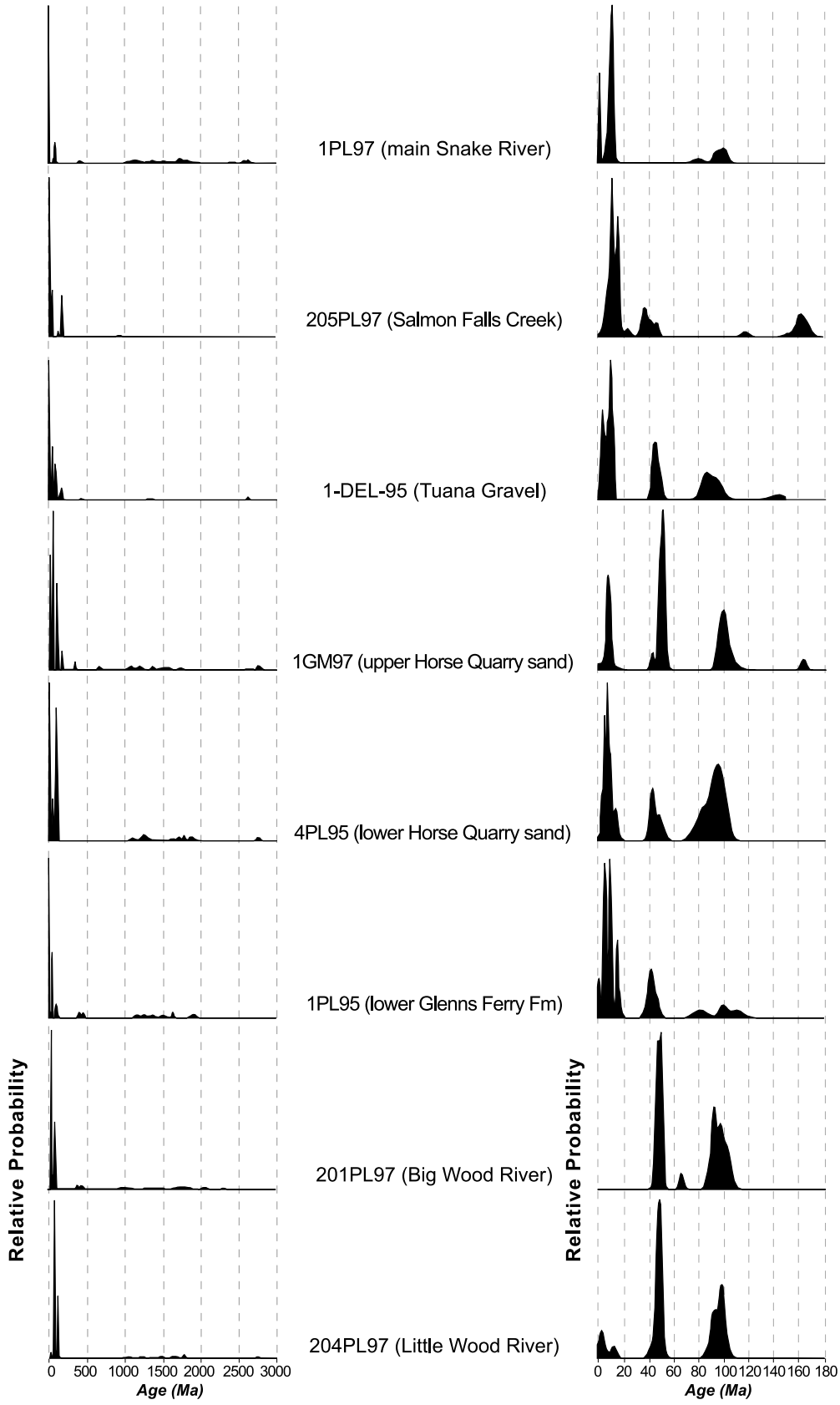
1PL97 (main Snake River)
205PL97 (Salmon Falls Creek)
1-DEL-95 (Tuana Gravel)
1GM97 (upper Horse Quarry sand)
4PL95 (lower Horse Quarry sand)
1PL95 (lower Glenns Ferry Fm)
201PL97 (Big Wood River)
204PL97 (Little Wood River)
Relative Probability
Relative Probability
0 500 1000 1500 2000 2500 3000
Age (Ma)
0 20 40 60 80 100 120 140 160 180
Age (Ma)

Table 1. Ages of detrital zircon grains using SHRIMP at Australian National University. Only $^{206}Pb/^{238}U$ ages are shown. Grains are sequenced from young to old. Note large standard deviation of some analyses and resulting age uncertainty for grains less than 10 Ma.

	Little Wood River **204PL97**	**Big Wood River** **201PL97**	**lower Glenns Ferry Formation 1PL95**	**lower Horse Quarry sand 4PL95**	**uppermost Horse Quarry sand 1GM97**	**Tuana Gravel Tuana Gravel 1-DEL-95**	**Salmon Falls Creek 205PL97**	**main Snake River 1PL97**
	$^{206}Pb/^{238}U$ *Age(Ma)*	$^{206}Pb/^{238}U$ *Age(Ma)*	$^{206}Pb/^{238}U$ *Age(Ma)*	$^{206}Pb/^{238}U$ *Age(Ma)*	$^{206}Pb/^{238}U$ *Age(Ma)*	$^{206}Pb/^{238}U$ *Age(Ma)*	$^{206}Pb/^{238}U$ *Age(Ma)*	$^{206}Pb/^{238}U$ *Age(Ma)*
1	3.0 ± 2.7	45.5 ± 1.1	1.4 ± 0.9	3.9 ± 0.9	4.2 ± 6.5	2.5 ± 1.3	6.2 ± 2.5	0.7 ± 0.2
2	3.4 ± 1.6	46.1 ± 1.2	4.4 ± 0.3	5.7 ± 0.4	6.9 ± 4.4	3.1 ± 1.7	6.9 ± 1.2	1.0 ± 0.2
3	4.6 ± 3.3	46.5 ± 1.9	5.3 ± 0.5	5.9 ± 1.2	7.1 ± 1.1	3.5 ± 1.1	7.0 ± 2.3	1.5 ± 0.3
4	12.9 ± 1.8	47.1 ± 1.6	6 ± 1	6.5 ± 6.7	7.2 ± 0.5	3.8 ± 0.6	7.3 ± 2.2	5.9 ± 1.2
5	42.5 ± 2.2	47.2 ± 1.0	6.6 ± 0.9	7.6 ± 0.6	7.5 ± 1.0	4.1 ± 0.7	9.5 ± 1.5	7.9 ± 1.2
6	45.8 ± 2.2	47.7 ± 0.7	6.9 ± 0.5	7.9 ± 0.5	8.3 ± 0.6	5.9 ± 0.5	9.7 ± 1.9	8.8 ± 0.6
7	45.9 ± 1.0	48.6 ± 1.3	8.7 ± 2.7	8.6 ± 0.7	9.2 ± 0.5	5.9 ± 0.8	9.7 ± 3.3	9.1 ± 1.1
8	46.5 ± 0.9	48.8 ± 1.3	9.5 ± 0.4	10.0 ± 0.9	10.5 ± 0.9	7.7 ± 0.5	9.8 ± 1.1	9.9 ± 2.1
9	47.2 ± 1.2	49.0 ± 1.0	9.9 ± 0.9	10.3 ± 1.1	42.9 ± 1.2	8.1 ± 0.6	9.8 ± 5.5	10.4 ± 0.7
10	47.4 ± 1.0	49.8 ± 1.0	10.6 ± 0.8	11.9 ± 2.7	47.9 ± 0.8	8.8 ± 0.9	10.0 ± 2.3	10.5 ± 0.9
11	47.8 ± 1.3	49.9 ± 1.6	11.4 ± 1.0	14.9 ± 1.4	48.8 ± 0.9	9.2 ± 0.7	10.1 ± 0.8	10.6 ± 1.0
12	48.3 ± 1.3	50.3 ± 1.0	15.6 ± 0.5	43.1 ± 2.0	48.9 ± 1.2	10.0 ± 0.6	10.3 ± 0.3	10.7 ± 1.2
13	48.7 ± 1.0	50.4 ± 1.3	17.1 ± 1.3	44.1 ± 2.3	49.0 ± 2.2	10.2 ± 0.7	10.9 ± 0.3	10.9 ± 1.1
14	48.7 ± 1.2	50.8 ± 0.8	40.8 ± 2.6	44.5 ± 1.4	49.5 ± 1.5	10.5 ± 0.5	11.1 ± 0.7	10.9 ± 1.4
15	48.8 ± 1.4	51.4 ± 1.0	42.4 ± 1.7	49.0 ± 1.9	50.0 ± 1.6	10.7 ± 0.7	11.1 ± 2.3	11.1 ± 0.4
16	48.9 ± 2.8	66.1 ± 1.6	43.5 ± 2.2	52.0 ± 2.6	50.3 ± 1.4	10.7 ± 0.9	11.2 ± 0.9	11.2 ± 1.9
17	49.3 ± 0.9	87.4 ± 1.9	47.2 ± 2.2	62.4 ± 17	50.7 ± 1.0	12.0 ± 0.6	11.7 ± 1.8	11.4 ± 1.3
18	49.9 ± 1.4	91.1 ± 1.7	82.3 ± 5.0	78.4 ± 3.8	51.0 ± 1.2	12.3 ± 0.5	12.2 ± 0.8	11.7 ± 1.2
19	50.1 ± 0.9	91.6 ± 1.1	100 ± 3	82.3 ± 3.8	51.0 ± 1.3	44.1 ± 1.7	12.2 ± 3.0	79.2 ± 4.4
20	50.4 ± 1.6	91.7 ± 1.5	111 ± 5	84.9 ± 2.7	51.2 ± 1.0	44.2 ± 1.4	12.7 ± 1.9	93.2 ± 2.3
21	51.4 ± 1.2	91.8 ± 3.0	404 ± 11	87.0 ± 3.6	51.9 ± 1.6	44.3 ± 1.5	14.2 ± 0.6	96.5 ± 2.9
22	87.4 ± 2.5	93.9 ± 3.2	455.6 ± 13	90.7 ± 3.3	52.0 ± 1.1	46.2 ± 1.5	14.2 ± 1.6	98.4 ± 2.6
23	90.0 ± 1.5	94.7 ± 2.7	1196 ± 25	91.5 ± 3.1	52.1 ± 1.2	46.5 ± 1.5	14.5 ± 2.0	101 ± 2
24	90.8 ± 1.7	96.6 ± 1.8	1243 ± 52	95.1 ± 3.8	52.2 ± 1.7	46.7 ± 1.4	14.5 ± 2.5	423 ± 16
25	91.5 ± 1.5	96.6 ± 5.2	1268 ± 28	95.2 ± 3.3	94.1 ± 1.8	49.6 ± 1.5	15.2 ± 0.8	1036 ± 35
26	93.3 ± 1.2	97.2 ± 2.7	1483 ± 31	95.5 ± 3.3	96.2 ± 2.2	49.7 ± 1.7	15.3 ± 1.3	1041 ± 39
27	95.0 ± 2.5	97.8 ± 3.1	1642 ± 35	95.6 ± 4.1	96.5 ± 2.1	84.0 ± 3.5	15.6 ± 0.3	1049 ± 34
28	95.8 ± 1.9	98.0 ± 2.9	1698 ± 33	97.1 ± 4.6	98.0 ± 2.7	85.2 ± 2.4	15.7 ± 1.0	1082 ± 26
29	97.1 ± 1.8	98.4 ± 5.2	1758 ± 49	98.5 ± 3.3	98.6 ± 2.1	86.2 ± 3.3	16.3 ± 2.1	1110 ± 45
30	97.4 ± 1.6	102 ± 2	1905 ± 45	101 ± 4	98.9 ± 2.0	88.1 ± 2.4	17.0 ± 1.0	1117 ± 28
31	97.6 ± 2.3	103 ± 3		101 ± 4	100 ± 2	91.2 ± 4.0	23.5 ± 1.9	1163 ± 20
32	98.3 ± 1.8	104 ± 3		101 ± 5	101 ± 3	92.5 ± 2.6	35.9 ± 2.2	1334 ± 46
33	98.9 ± 2.3	393 ± 7		102 ± 4	102 ± 3	95.2 ± 3.8	37.2 ± 1.6	1349 ± 32
34	99.1 ± 3.3	439 ± 9		102 ± 4	104 ± 5	95.7 ± 4.3	37.2 ± 1.8	1410 ± 34
35	101.4 ± 2.6	464 ± 12		901 ± 25	105 ± 4	98.3 ± 3.3	37.4 ± 2.9	1435 ± 21
36	964 ± 23	971 ± 33		1024 ± 30	162 ± 2	144.5 ± 4.7	39.5 ± 2.5	1490 ± 23
37	1009 ± 28	985 ± 22		1168 ± 35	336 ± 5	159.7 ± 4.6	41.9 ± 1.4	1533 ± 46
38	1057 ± 24	991 ± 13		1229 ± 32	658 ± 13	162.4 ± 4.8	45.3 ± 1.9	1593 ± 32
39	1185 ± 24	1011 ± 36		1367 ± 31	1082 ± 20	167.4 ± 5.3	47.2 ± 1.5	1618 ± 53
40	1224 ± 25	1255 ± 17		1563 ± 39	1102 ± 15	430.0 ± 13	118 ± 3	1736 ± 62
41	1270 ± 23	1329 ± 14		1613 ± 47	1183 ± 22	1246 ± 33	153 ± 4	1736 ± 39
42	1499 ± 20	1426 ± 42		1669 ± 44	1198 ± 31	2220 ± 64	160 ± 3	1805 ± 44
43	1510 ± 22	1454 ± 27		1730 ± 51	1232 ± 15		162 ± 2	1810 ± 33
44	1601 ± 25	1480 ± 26		1760 ± 52	1316 ± 16		162 ± 3	1834 ± 79
45	1675 ± 40	1655 ± 27		2643 ± 67	1331 ± 26		162 ± 3	1840 ± 37
46	1696 ± 32	1715 ± 40		1477 ± 32			165 ± 4	1860 ± 45
47	1700 ± 30	1806 ± 23		1537 ± 20			167 ± 2	1877 ± 27
48	1800 ± 21	1859 ± 29		2637 ± 51			169 ± 4	1920 ± 29
49	1827 ± 42	1860 ± 35		2673 ± 38			918 ± 17	1990 ± 43
50	2598 ± 42	1908 ± 35		2863 ± 81				2385 ± 38
51		1911 ± 29						2589 ± 33
52								2590 ± 145

the Idaho batholith terrane are 95 to 75 Ma (Kiilsgaard and Bennett, 1995; Vallier and Brooks, 1987). When considering the entire Idaho batholith, Fisher (1995, p. 5) gives an age range of 112 to 70 Ma. Only in the complex border zone on the west side of the batholith are any ages greater than 100 Ma (to 120 Ma). The only Jurassic intrusive rocks in the Challis 1º x 2º sheet are small bodies (less than 1 km in diameter) along the Salmon River south of Challis (Fisher and others, 1992; Hobbs and others, 1991). Notably, there are no Idaho batholith ages in the 160- to 140-Ma range.

The Big Wood River sample contains one Paleocene (66 Ma) grain. This could have been derived from Paleogene diorite intrusions west of Hailey (Deer Creek, Bellevue, and Croesus stocks; Worl and others, 1991, 1995).

Early and Middle Eocene Zircons

Early and middle Eocene (50-42 Ma) zircons are present in all drainages except the Snake River. These were derived from volcanic rocks erupted during the Challis magmatic episode that produced mainly 50- to 45-Ma intermediate and felsic flows, pyroclastic rocks, and several intrusive phases in a large area of south-central and southwestern Idaho (Ekren and others, 1981; McIntyre and others, 1982; Janecke and Snee, 1993; Fisher and others, 1992; Snider, 1995; M'Gonigle and Dalrymple, 1996; Link and Janecke, 1999).

Late Eocene Zircons

Late Eocene (42-37 Ma) zircons are moderately abundant in Salmon Falls Creek and distinct in age from Challis zircons. These are likely derived from voluminous 43- to 34-Ma andesitic to rhyolitic volcanic rocks in northern and central Nevada (Stewart, 1980).

Neogene and Pleistocene Zircons

Late Miocene zircons, younger than 17 Ma, are present in most samples. Due to the lower resolution of U-Pb SHRIMP scans for detrital studies, the precision of our U-Pb dates is low for some Neogene zircons. Thus, individual ages may not be directly matched with a coeval volcanic field of a specific source area. In general, these grains are derived from the volcanic rocks of the SRP-Yellowstone volcanic system.

Only Salmon Falls Creek contains 17- to 14-Ma grains derived from the Owyhee-Humboldt, McDermitt, or Oregon-Idaho graben volcanic fields in southwestern-most Idaho and southeastern Oregon (Figure 1). The main Snake River contains three Pleistocene (1.8-0.5 Ma) grains consistent with Pliocene or Pleistocene capture by the Snake River of drainage from the Yellowstone volcanic field, which formerly flowed to the east to the Green or Bighorn river systems (Fritz and Sears, 1993).

MODERN STREAM SIGNATURES

The provenance signatures of the modern streams are predictable, that is, with sample size of one (Figure 4). Specific ages of each grain are listed in Table 1.

Central Idaho Provenance Area

The Little Wood River has one Archean (2,598 Ma) grain, a few Proterozoic (1,800-964 Ma) grains, and many Cretaceous (98-87 Ma), Eocene (51-46 Ma), and Neogene (13-3 Ma) grains consistent with derivation from Paleozoic sedimentary rocks, Idaho batholith, and Challis Volcanic Group of south-central Idaho. The Big Wood River signature is similar and has scattered Proterozoic (1,911-971 Ma) grains, one Ordovician (439 Ma) grain, one Devonian (393 Ma) grain, numerous Cretaceous (104-91 Ma) grains, one Paleocene (66 Ma) grain, and numerous Eocene grains. Miocene grains are surprisingly absent.

Northern Nevada Provenance Area

Salmon Falls Creek contains abundant Jurassic (169-153 Ma) grains, no Cretaceous grains less than 100 Ma, only two Challis-age Eocene (47-45 Ma) grains, scattered late Eocene (42 to 37 Ma) and early Miocene (23.5 Ma) grains, distinctive 17- to 14-Ma grains from the Jarbidge rhyolite of the Owyhee-Humboldt volcanic field, and abundant middle and late Miocene (13-7 Ma) grains. The lack of voluminous Idaho batholith and Challis grains, the presence of late Eocene grains derived from volcanic rocks in northern Nevada, and the grains from the Owyhee-Humboldt volcanic field plus the common Jurassic grains make this southern provenance distinctive.

Main Snake River

The main Snake River does not have a unique signature, but only one sample has been dated. It contains a variety of Archean (2,590-2,385 Ma) and Proterozoic (1,990-1,041 Ma) grains, one Silurian (423 Ma) grain, a few Cretaceous grains, no Eocene grains, and several Neogene (1.8-0.5 Ma) grains from the Yellowstone volcanic plateau. Further sampling of the Snake River upstream of major tributaries will help define the timing of progressive westward drainage capture.

INTERPRETATION

Glenns Ferry and Tuana samples can be confidently matched to the central Idaho and northern Nevada provenance areas, respectively, demonstrating a drainage reversal during deposition of the Horse Quarry sand of the uppermost Glenns Ferry Formation. Glenns Ferry sands, rich in Challis volcanic, Idaho batholith, and reworked Proterozoic grains, were derived from the Little and Big Wood river drainage area in central Idaho.

Detrital zircons in the Tuana Gravel are similar to the northern Nevada signature of Salmon Falls Creek. The lack of late Eocene grains in the Tuana may reflect post-Tuana southward enlargement of the Salmon Falls drainage area. We interpret the first appearance of south-derived zircons in the uppermost Horse Quarry sand of the Glenns Ferry Formation and Tuana Gravel to record initial drainage reversal near 3.2 Ma caused by cutting of the outlet to the western SRP (Wood, 1994, this volume). The base level of the newly north-draining western SRP progressively dropped, and Lake Idaho shrank northwestward. In the Hagerman area, three cycles of stream rejuvenation are recorded in the Tuana Gravel, likely related to early phases of this lowering of base level. The main stem of the Snake River need not have been present during any deposition at Hagerman.

DRAINAGE DEVELOPMENT: THE LITTLE MUSKRAT, THE GIANT BEAVER, AND THE TUMESCENT BULGE

The late Miocene location of the drainage outlet of Lake Idaho (if there was one) is controversial. Conventional wisdom, based on the similarity of living and fossil freshwater fish and mollusks, holds that Lake Idaho drained westward, up the modern Owyhee River in southeast Oregon, then southward or westward to the Sacramento River in California and ultimately to San Francisco Bay (Wheeler and Cook, 1954; Miller, 1965; Taylor, 1966, 1985; Smith, 1975; Smith and others, 1982; Middleton and others, 1985; Malde, 1991). This paleodrainage model is based on "a combination of well-founded interpretations and a gossamer of speculation" (Taylor and Bright, 1987, p. 249).

A fatal flaw in the proposal of drainage of Lake Idaho to the southwest through southeast Oregon is that the sediments or channel for this alleged westward drainage are not present. Instead, southeast Oregon was a topographically high rhyolite plateau from 17 Ma to at least 10 Ma, with eruption and deposition of rhyolitic epiclastic rocks of the Oregon-Idaho graben (Sucker Creek, Deer Butte, and Grassy Mountain formations, Ferns and others, 1993; Cummings and others, 2000; Figure 2). Further, the Chalk Hills Formation is locally evaporitic and may not have had an outlet.

The Chalk Hills and Glenns Ferry faunas suggest a connection to the Sacramento and Humboldt drainages to the south and west and do not have close affinities with Columbia River basin faunas until the late Pliocene (Repenning and others, 1995, p. 66-67). The "little muskrat" *Pliopotamys minor* is present in 4.1-Ma beds in the Sacramento River basin, in less than 3.6-Ma Glenns Ferry Formation beds at Hagerman, and in the Columbia River basin at about 2.9 Ma (Taunton fauna of the Ringold Formation). This progression is taken to indicate a migratory route northward and westward from the Sacramento to the Lake Lahontan basin in Nevada to Hagerman and down the Snake River through Hells Canyon. Muskrats are dependent on marshy and stream environments and are unable to travel cross-country; thus, their distribution indicates a connected drainage system (Figure 5).

One way to account for muskrats migrating from the Humboldt drainage into Salmon Falls Creek would be by stream capture of a segment of a former south-flowing drainage by the south-expanding drainage basin of Salmon Falls Creek. Such a scenario may have occurred at Henry, Nevada, along Highway 93 about 20 miles south of Jackpot (see Figure 5), where the present headwaters of Salmon Falls Creek flow southeasterly (their former course into the Great Basin) and then abruptly turn to the northeast (Bonnichsen, written commun., 2000).

The distribution path of the "giant beaver," *Protocastoroides idahoensis*, present in the Birch Creek fauna of the Glenns Ferry Formation (about 2.6 Ma, Hearst, 1998) and in the 2.9 Ma Taunton fauna, may also have waited for the cutting of Hells Canyon (Repenning and others, 1995). A smaller (older) relative of the giant beaver (*P. intermedius*) is present lower in the section at Hagerman. Two microtine rodents (voles), *Mimomys (Cosomys)* and *Mimomys (Ophiomys)*, have similar distributions from Hagerman to the Columbia system.

Pliocene turtles at Hagerman also have connections with the Lahontan basin. Turtles are currently absent from the Snake River drainage, but during the Pliocene they were common in southern Idaho with two extinct species present at Hagerman, *Trachemys idahoensis* and *Clemmys owyheensis*. In the west the genus *Clemmys* is represented by a single species, *C. marmorata*. The range of the modern western pond turtle is currently restricted to west of the crest of the Cascade and Sierra mountain ranges with a small outlying isolated population in the Truckee and Carson rivers in Nevada. The remnant Nevada population in the Lahontan basin suggests the former existence

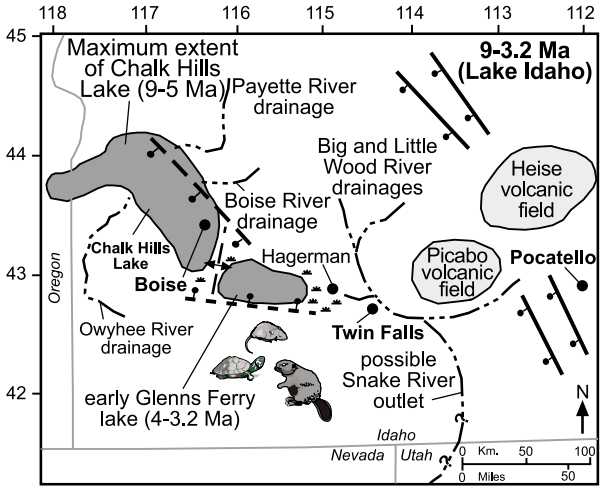

Figure 5. Paleogeographic synthesis for Lake Idaho, about 9 to 3 million years ago. Near Hagerman, at the southeast corner of Lake Idaho, streams and marshes were home to a diverse set of Pliocene animals, including immigrants from Nevada (shown), the Giant Beaver (*Protocastoroides idahoensis*), the Pygmy Muskrat (*Pliopotamys minor*), and fossil turtles (genus *Clemmys*). We show the eastern segment of the modern Snake River, and perhaps the eastern part of Lake Idaho, as draining to the south through northern Nevada to the Sacramento River. We also show a discontinuous Lake Idaho basin, with a medial high formed as an accommodation zone, following half-graben models of Lambiase (1990), Leeder (1995), and Faulds and Varga (1998).

of an aquatic connection between the SRP and the Sacramento River system in California via this part of Nevada.

The proposed paleodrainage of Repenning and others (1995) coursed southward from the SRP by a route (yet-to-be-discovered) to the Humboldt River of the Lahontan basin in northern Nevada, westward to Winnemucca and the Black Rock Desert, and thence to the Alturas lake basin and the Pit River, a tributary to the Sacramento River in northeastern California (Figure 5).

Geologic evidence for this drainage is permissive. There are sediments of about the right age in the several Basin and Range valleys, e.g., Honey Lake, California (Taylor and Smith, 1981), but the location of the south-flowing major stream draining from the SRP is not known. The Salmon Falls Creek canyon, proposed in the diagrams of Link and others (1999a), is not a candidate because it contains late Miocene and Pliocene basalt that flowed northward (Bonnichsen, written commun., 2000). The drainage connection may have been through the Oakley-Grouse Creek valley or the Raft River Valley east of Twin Falls (Figure 1 and 5). The Oakley Valley near Artesian City contains over 400 m of late Miocene rhyolite and four interbeds of sediment included in the Idavada volcanics (Struhsacker and others, 1983). The Raft River Valley contains up to 1,700 m of Miocene to Recent ignimbrite and sediment, mainly of the Salt Lake Formation (Williams and others, 1982). Some of these sediments may be lacustrine.

Several issues remain to be resolved about where, when, and if the eastern or any part of the Snake River entered the Great Basin in late Miocene time. We acknowledge the preliminary nature of our conclusions and the sparse data on which they are founded. Further detrital zircon work will more closely define both the signatures of Neogene sands of Idaho and Nevada as well as those of the modern river systems.

ACKNOWLEDGMENTS

This synthesis grows from M.S. research at Hagerman Fossil Beds National Monument by Dana E. Lee and Jeremy L. Sadler, directed by McDonald and Link (Lee and others, 1995; McDonald and others, 1996; Sadler and Link, 1996; Sadler and others, 1997; Sadler, 1997). Detrital zircon geochronology was performed at Australian National University by Fanning. Spencer H. Wood of Boise State University was extremely helpful and candid about his interpretations of the western SRP on a fine field trip in 1998 and provided a rigorous review of the manuscript. Preparation of the digital elevation models for southern Idaho through the Neogene (Link and others, 1999a; Reading and others, 1999) was coordinated by Godfrey, with technical assistance from Russell W. Reading and David E. Prevedel of the U.S.D.A. Forest Service GIS Center of Excellence in Ogden, Utah. Drafting assistance at Idaho State University was by James W. Riesterer and Diana Boyack.

The Hagerman work was funded under Subagreement 4 to Cooperative Agreement No. CA-9000-0-0013 between Idaho State University and the National Park Service, Pacific West Field Area. The eastern SRP and detrital zircon work was funded by the U.S. Department of Energy through the Idaho Water Resources Research Institute, Contract DE-FG07-96ID13420.

REFERENCES

Armstrong, R.L, J.E. Harakal, and W.M. Neill, 1980, K-Ar dating of Snake River Plain (Idaho) volcanic rocks—New results: Isochron/West, no. 27, p. 5-10.

Armstrong, R.L., W.P. Leeman, and H.E. Malde, 1975, K-Ar dating of Quaternary and Neogene volcanic rocks of the Snake River Plain, Idaho: American Journal of Science, v. 275, p. 225-251.

Bjork, P.R., 1970, The carnivora of the Hagerman local fauna (late Pliocene) of southwestern Idaho: Transactions of the American Philosophical Society, v. 60, 54 p.

Bonnichsen, Bill, 1982, The Bruneau-Jarbidge eruptive center, southwestern Idaho, *in* Bill Bonnichsen and R.M. Breckenridge, eds., Cenozoic Geology of Idaho: Idaho Bureau of Mines and Geology

Bulletin 26, p. 237-254.

Bonnichsen, Bill, and D.J. Kauffman, 1987, Physical features of rhyolite lava flows in the Snake River Plain volcanic province, southwestern Idaho, *in* J.H. Fink, ed., The Emplacement of Silicic Domes and Lava Flows: Geological Society of America Special Paper 212, p. 119-145.

Bright, R.C., and H.T. Ore, 1987, Evidence for the spillover of Lake Bonneville, southeastern Idaho, *in* S. Beus, ed., Geological Society of America Centennial Field Guide 2—Rocky Mountain Section, p. 143-146.

Camilleri, Phyllis, Adolph Yonkee, Jim Coogan, Peter Decelles, Allen McGrew, and Michael Wells, 1997, Hinterland to foreland transect through the Sevier orogen, northeast Nevada to north-central Utah: Structural style, metamorphism, and kinematic history of a large contractional orogenic wedge: Brigham Young University Geology Studies, v. 42, part I, p. 297-309.

Christiansen, R.L., and E.H. McKee, 1978, Late Cenozoic volcanic and tectonic evolution of the Great Basin and Columbia Intermontane regions, *in* R.B. Smith and G.P. Eaton, eds., Cenozoic Tectonics and Regional Geophysics in the Western Cordillera: Geological Society of America Memoir 152, p. 283-312.

Clemens, D.M., 1993, Tectonics and silicic volcanic stratigraphy of the western Snake River Plain, southwestern Idaho: Arizona State University M.S. thesis, 209 p.

Clemens, D.W., and S.H. Wood, 1993a, Radiometric dating, volcanic stratigraphy, and sedimentation in the Boise foothills, northeastern margin of the western Snake River Plain, Ada County, Idaho: Isochron/West, no. 59, p. 3-10.

Clemens, D.W., and S.H. Wood, 1993b, Late Cenozoic volcanic stratigraphy and geochronology of the Mount Bennett Hills, central Snake River Plain, Idaho: Isochron/West, no. 60, p. 3-14.

Coats, R.R., 1987, Geology of Elko County, Nevada: Nevada Bureau of Mines and Geology Bulletin 101, 112 p.

Cummings, M.L., J.G. Evans, and M.L. Ferns, 1994, Stratigraphic and structural evolution of the middle Miocene Oregon-Idaho graben, Malheur County, Oregon, *in* D.A. Swanson and R.S. Haugerud, eds., Geologic Field Trips in the Pacific Northwest: Department of Geological Sciences, University of Washington, v. 1, p. 1G1-1G17.

Cummings, M.L., J.G. Evans, M.L. Ferns, and K.R. Lees, 2000, Stratigraphic and structural evolution of the middle Miocene synvolcanic Oregon-Idaho graben: Geological Society of America Bulletin, v. 112, p. 668-682.

Ekren, E.B., D.H. McIntyre, E.H. Bennett, and H.E. Malde, 1981, Geologic map of Owyhee County, Idaho, west of longitude 116ºW.: U.S. Geological Survey Miscellaneous Geologic Investigations Map I-1256, scale 1:125,000.

Evans, K.V., and R.E. Zartman, 1988, Early Paleozoic alkalic plutonism in east-central Idaho: Geological Society of America Bulletin, v. 100, p. 1981-1987.

Faulds, J.E., and R.J. Varga, 1998, The role of accommodation zones and transfer zones in the regional segmentation of extended terranes, *in* J.E. Faulds and J.H. Stewart, eds., Accommodation Zones and Transfer Zones: The Regional Segmentation of the Basin and Range Province: Geological Society of America Special Paper 323, p. 1-46.

Ferns, M.L., 1997, Field trip guide to the eastern margin of the Oregon-Idaho graben and the middle Miocene calderas of the Lake Owyhee volcanic field: Oregon Geology, v. 59, no. 1, p. 9-20.

Ferns, M.L., H.C. Brooks, J.G. Evans, and M.L. Cummings, 1993, Geologic map of the Vale 30 x 60 minute quadrangle, Malheur County, Oregon and Owyhee County, Idaho: Oregon Department of Geology and Mineral Industries, Map GMS-77, scale 1:100,000.

Fisher, F.S., 1995, Geologic setting and history of mineralization, *in* F.S. Fisher and K.M. Johnson, eds., Geology and Mineral Resource Assessment of the Challis 1º x 2º Quadrangle, Idaho: U.S. Geological Survey Professional Paper 1525, p. 4-6.

Fisher, F.S., D.H. McIntyre, and K.M. Johnson, 1992, Geologic map of the Challis 1º x 2º quadrangle, Idaho: U.S. Geological Survey Miscellaneous Investigations Series Map I-1819, scale 1:250,000.

Fitzgerald, J.F., 1982, Geology and basalt stratigraphy of the Weiser embayment, west-central Idaho, *in* Bill Bonnichsen and R.M. Breckenridge, eds., Cenozoic Geology of Idaho: Idaho Bureau of Mines and Geology Bulletin 26, p. 103-128.

Fritz, W.J., and J.W. Sears, 1993, Tectonics of the Yellowstone hotspot wake in southwestern Montana: Geology, v. 21, p. 427-430.

Geslin, J.K., P.K. Link, and C.M. Fanning, 1999, High-precision provenance determination using detrital-zircon ages and petrography of Quaternary sands on the eastern Snake River Plain, Idaho: Geology, v. 27, no. 4, p. 295-298.

Geslin, J.K., P.K. Link, J.W. Riesterer, M.A. Kuntz, and C.M. Fanning, 2002, Pliocene and Quaternary stratigraphic architecture and drainage systems of the Big Lost Trough, northeastern Snake River Plain, Idaho, *in* P.K. Link and L.L. Mink, eds., Geology, Hydrogeology and Environmental Remediation, Idaho National Engineering and Environmental Laboratory, Eastern Snake River Plain, Idaho: Geological Society of America Special Paper 353, p. 11-26.

Gibbons, A.B., 1995, Tertiary sedimentary rocks of the Payette Formation (Miocene) and the lower part (Miocene and Pliocene) of the Idaho Group, Hailey 1º x 2º quadrangle and vicinity, west-central Idaho, *in* R.G. Worl, P.K. Link, G.R. Winkler, and K.M. Johnson, eds., Geology and Mineral Resources of the Hailey 1º x 2º quadrangle and the Western Part of the Idaho Falls 1º x 2º quadrangle, Idaho: U.S. Geological Survey Bulletin 2064, p. K1-K9.

Hart, W.K., M.E. Brueske, P.R. Remme, and H.G. McDonald, 1999, Chronostratigraphy of the Pliocene Glenns Ferry Formation, Hagerman Fossil Beds National Monument, Idaho: Geological Society of America Abstracts with Programs, v. 31, no. 4, p. A-15.

Hearst, J.M., 1998, Depositional environments of the Birch Creek local fauna (Pliocene: Blancan), Owyhee County, Idaho, *in* W.A. Akersten, H.G. McDonald, J. Meldrum, and M.T. Flints eds., And Whereas…Papers on the Vertebrate Paleontology of Idaho Honoring John A. White, Vol. 1: Idaho Museum of Natural History Occasional Paper 36, p. 56-93.

Hobbs, S.W., W.H. Hays, and D.H. McIntyre, 1991, Geological map of the Bayhorse area, central Custer County, Idaho: U.S. Geological Survey Miscellaneous Investigations Series Map I-1882, scale 1:62,500.

Honjo, Norio, Bill Bonnichsen, W.P. Leeman, and J.C. Stormer, 1992, Mineralogy and geothermometry of high-temperature rhyolites from the central and western Snake River Plain: Bulletin of Volcanology, v. 54, p. 220-237.

Hughes, S.S., J.L., Parker, A.M. Watkins, and Mike McCurry, 1996, Geochemical evidence for a magmatic transition along the Yellowstone hot-spot track: Northwest Geology, v. 26, p. 63-80.

Ireland, T.R., 1992, Crustal evolution of New Zealand: Evidence from age distributions of detrital zircons in western province paragneiss and Torlesse greywacke: Geochimica et Cosmochimica Acta, v. 56, p. 911-920.

Ireland, T.R., T. Flottman, C.M. Fanning, G.M. Gibson, and W.V. Preiss, 1998, Development of the early Paleozoic Pacific margin of Gondwana from detrital-zircon ages across the Delamerian orogen: Geology, v. 26, p. 243-246.

Janecke, S.U., and L.W. Snee, 1993, Timing and episodicity of middle Eocene volcanism and onset of conglomerate deposition, Idaho: Journal of Geology, v. 101, p. 603-621.

Kellogg, K.S., S.S. Harlan, H.H. Mehnert, L.W. Snee, W.R. Hackett, and D.W. Rodgers, 1994, Major 10.2-Ma rhyolitic volcanism in the east-

ern Snake River Plain, Idaho—Isotopic age and stratigraphic setting of the Arbon Valley Tuff Member of the Starlight Formation: U.S. Geological Survey Bulletin 2091, 18 p.

Kiilsgaard, T.H., and E.H. Bennett, 1995, Idaho batholith terrane, *in* F.S. Fisher and K.M. Johnson, eds., Geology and Mineral Resource Assessment of the Challis 1º x 2º quadrangle, Idaho: U.S. Geological Survey Professional Paper 1525, p. 36-40.

Kimmel, P.G., 1982, Stratigraphy, age, and tectonic setting of the Miocene-Pliocene lacustrine sediments of the western Snake River Plain, Oregon and Idaho, *in* Bill Bonnichsen and R.M. Breckenridge, eds., Cenozoic Geology of Idaho: Idaho Bureau of Mines and Geology Bulletin 26, p. 559-578.

Kittleman, L.R., 1973, Guide to the geology of the Owyhee region of Oregon: University of Oregon, Museum of Natural History Bulletin 21, 61 p.

Kittleman, L.R., A.R. Green, A.R. Hagood, A.M. Johnson, J.M. McMurray, R.G. Russell, and D.A. Weeden, 1965, Cenozoic stratigraphy of the Owyhee region, southeastern Oregon: University of Oregon, Museum of Natural History Bulletin 1, 45 p.

Kraus, M.J., and L.T. Middleton, 1987, Contrasting architecture of two alluvial suites in different structural settings, *in* F.G. Ethridge, R.M. Flores, and M.D. Harvey, eds., Recent Developments in Fluvial Sedimentology: Society of Economic Paleontologists and Mineralogists Special Publication 39, p. 253-262.

Lambiase, J.J., 1990, A model for tectonic control of lacustrine stratigraphic sequences in continental rift basins, *in* B.J. Katz, ed., Lacustrine Basin Exploration: American Association of Petroleum Geologists Memoir 50, p. 265-276.

Lawrence, D.C., 1988a, Geology and revised stratigraphic interpretation of the Miocene Sucker Creek Formation, Malheur County, Oregon: Boise State University M.S. thesis, 54 p.

———, 1988b, Geologic field trip guide to the northern Succor Creek area, Malheur County, Oregon: Oregon Geology, v. 50, no. 2, p. 15-21.

Lee, D.E., P.K. Link, and H.T. Ore, 1995, Characterization of the Glenns Ferry Formation in the Fossil Gulch area, Hagerman Fossil Beds National Monument: Idaho Museum of Natural History, Geology Report 1, Completion Report for National Park Service Subagreement 3 to Contract CA-9000-0-0013, 59 p.

Leeder, M.R., 1995, Continental rifts and proto-oceanic rift troughs, *in* C.J. Busby and R.V. Ingersoll, eds., Tectonics of Sedimentary Basins: Blackwell Science, Cambridge Massachusetts, p. 119-148.

Lewis, R.E., and M.A.J. Stone, 1988, Geohydrologic data from a 4,403-foot geothermal test hole, Mountain Home Air Force Base, Elmore County, Idaho: U.S. Geological Survey Open-File Report 88-166, 30 p.

Link, P.K., 1999, Regional Geologic perspectives on the Belt Supergroup gained since Belt Symposium II, 1983, *in* R.B. Berg, ed., Belt Symposium III: Montana Bureau of Mines and Geology Special Publication 112, p. 2-10.

Link, P.K., J.K. Geslin, and C.M. Fanning, 2000, Detrital zircon "barcodes" from Modern and Neogene sands of the Snake River Plain, Idaho: Defining a provenance area requires several grains and single grains mean little: Geological Society of America Abstracts with Programs, v. 32, no. 6, p. A-25.

Link, P.K., and S.U. Janecke, 1999, Geology of east-central Idaho: Geologic roadlogs for the Big and Little Lost River, Lemhi, and Salmon River valleys, *in* S.S. Hughes and G.D. Thackray, eds., Guidebook to the Geology of Eastern Idaho: Idaho Museum of Natural History, p. 295-334.

Link, P.K., D.S. Kaufman, and G.D. Thackray, 1999b, Field guide to Pleistocene Lakes Thatcher and Bonneville and the Bonneville Flood, southeastern Idaho, *in* S.S. Hughes and G.D. Thackray, eds., Guidebook to the Geology of Eastern Idaho: Idaho Museum of Natural History, p. 251-266.

Link, P.K., R.W. Reading, A.E. Godfrey, and D. Prevedel, 1999a, Topographic development of the Snake River Plain, Idaho, *in* S.S. Hughes and G.D. Thackray, eds., Guidebook to the Geology of eastern Idaho: Idaho Museum of Natural History, back cover.

Lundelius, E.L., Jr., and eight others, 1987, The North American Quaternary sequence, *in* M.O. Woodburne, ed., Cenozoic Mammals of North America: University of California Press, p. 236-268.

Mabey, D.R., 1982, Geophysics and tectonics of the Snake River Plain, Idaho, *in* Bill Bonnichsen and R.M. Breckenridge, eds., Cenozoic Geology of Idaho: Idaho Geological Survey Bulletin 26, p. 139-154.

Malde, H.E., 1972, Stratigraphy of the Glenns Ferry Formation from Hammett to Hagerman, Idaho: U.S. Geological Survey Bulletin 1331-D, 19 p.

———, 1991, Quaternary geology and structural history of the Snake River Plain, Idaho and Oregon, *in* R.B. Morrison, ed., Quaternary Nonglacial Geology, Conterminous U.S.: Geological Society of America, The Geology of North America, v. K-2, p. 251-280.

Malde, H.E., and H.A. Powers, 1962, Upper Cenozoic stratigraphy of western Snake River Plain, Idaho: Geological Society of America Bulletin, v. 73, p. 1197-1220.

———, 1972, Geologic map of the Glenns Ferry-Hagerman area, west-central Snake River Plain, Idaho: U.S. Geological Survey, Miscellaneous Geologic Investigations Map I-696, scale 1:48,000, 2 sheets.

Malde, H.E., H.A. Powers, and C.H. Marshall, 1963, Reconnaissance geologic map of west-central Snake River Plain, Idaho: U.S. Geological Survey Miscellaneous Investigations Map I-373, scale 1:125,000, 1 sheet.

McCurry, Mike, Bill Bonnichsen, Craig White, M.M. Godchaux, and S.S. Hughes, 1997, Bimodal basalt-rhyolite magmatism in the central and western Snake River Plain, Idaho and Oregon: Brigham Young University Geology Studies, v. 42, part 1, p. 381-422.

McCurry, Mike, A.M. Watkins, J.L. Parker, K.E. Wright, and S.S. Hughes, 1996, Preliminary volcanological constraints for sources of high-grade, rheomorphic ignimbrites of the Cassia Mountains, Idaho: Implications for the evolution of the Twin Falls volcanic center: Northwest Geology, v. 26, p. 81-91.

McDonald, G.H., P.K. Link, and D.E. Lee, 1996, An overview of the geology and paleontology of the Pliocene Glenns Ferry Formation, Hagerman Fossil Beds National Monument: Northwest Geology, v. 26, p. 16-45.

McIntyre, D.H., 1979, Preliminary description of Anschutz Federal No. 1 drill hole, Owyhee County, Idaho: U.S. Geological Survey Open-File Report 79-651, 14 p.

McIntyre, D.H., E.B. Ekren, and R.F. Hardyman, 1982, Stratigraphic and structural framework of the Challis volcanics in the eastern half of the Challis 1º x 2º quadrangle, Idaho, *in* Bill Bonnichsen and R.M. Breckenridge, eds., Cenozoic Geology of Idaho: Idaho Bureau of Mines and Geology Bulletin 26, p. 3-22.

M'Gonigle, J.W., and G.B. Dalrymple, 1996, $^{40}Ar/^{39}Ar$ ages of Challis volcanic rocks and the initiation of Tertiary sedimentary basins in southwestern Montana: U.S. Geological Survey Bulletin 2132, 17 p.

McQuarrie, Nadine, and D.W. Rodgers, 1998, Subsidence of a volcanic basin by flexure and lower crustal flow: The eastern Snake River Plain, Idaho: Tectonics, v. 17, p. 203-220.

Middleton, L.T., M.L. Porter, and P.G. Kimmel, 1985, Depositional settings of the Chalk Hills and Glenns Ferry Formations west of Bruneau, Idaho, *in* R.M. Flores and S.S. Kaplan, eds., Cenozoic Paleogeography of the West-Central United States: Rocky Mountain Section of the Society of Economic Paleontologists and Mineralogists, p. 37-53.

Miller, R.R., 1965, Quaternary freshwater fishes of North America, *in* H.E. Wright and D.G. Frey, eds., The Quaternary of the United States: Princeton University Press, p. 569-581.

Morgan, L.A., K.L. Pierce, W.C. McIntosh, 1998, The volcanic track of the Yellowstone hot spot: An Update: Yellowstone Science, v. 20, p. 44.

Nakai, T.S., 1979, Stratigraphy of the Payette Formation, Washington County, Idaho: University of Idaho M.S. thesis, 187 p.

Ore, H.T., 1999, Topographic and geomorphic development of southeastern Idaho, segments from an essay, *in* S.S. Hughes and G.D. Thackray, eds., Guidebook to the Geology of Eastern Idaho: Idaho Museum of Natural History, p. 254-255.

Ore, H.T., T.V. Reid, and P.K. Link, 1996, Pre-Bonneville-level, catastrophic overflow of Plio-Pleistocene Lake Bonneville, south of Rockland, Idaho: Northwest Geology, v. 26, p. 1-15.

Othberg, K.L., 1994, Geology and geomorphology of the Boise Valley and adjoining areas, western Snake River Plain, Idaho: Idaho Geological Survey Bulletin 29, 54 p.

Othberg, K.L., and L.R. Stanford, 1992, Geologic map of the Boise Valley and adjoining area, western Snake River Plain, Idaho: Idaho Geological Survey Geologic Map 18, scale 1:100,000.

Perkins, M.E., F.H. Brown, W.P. Nash, William McIntosh, and S.K., Williams, 1998, Sequence, age, and source of silicic fallout tuffs in middle to late Miocene basins of the northern Basin and Range Province: Geological Society of America Bulletin, v. 110, no. 3, p. 344-360.

Perkins, M.E., W.P. Nash, F.H. Brown, and R.J. Fleck, 1995, Fallout tuffs of Trapper Creek Idaho—A record of Miocene explosive volcanism in the Snake River Plain volcanic province: Geological Society of America Bulletin, v. 107, p. 1484-1506.

Pierce, K.L., and L.A. Morgan, 1992, The track of the Yellowstone hot spot: Volcanism, faulting, and uplift, *in* P.K. Link, M.A. Kuntz, and L.B. Platt, eds., Regional Geology of Eastern Idaho and Western Wyoming: Geological Society of America Memoir 179, p. 1-53.

Pierce, K.L., and W.E. Scott, 1982, Pleistocene episodes of alluvial-gravel deposition, southeastern Idaho, *in* Bill Bonnichsen and R.M. Breckenridge, eds., Cenozoic Geology of Idaho: Idaho Bureau of Mines and Geology Bulletin 26, p. 685-702.

Reading, R.W., A.E. Godfrey, D. Prevedel, and P.K. Link, 1999, Digital elevation models of topographic development of the Snake River Plain: Geological Society of America Abstracts with Programs, v. 31, no. 4, p. A-53.

Reidel, J.L., 1992, Existing conditions of large landslides at Hagerman Fossil Beds National Monument: National Park Service Report, 34 p.

Reidel, S.P., and P.R. Hooper, eds., 1989, Volcanism and tectonism in the Columbia River flood-basalt province: Geological Society of America Special Paper 239, 386 p.

Repenning, C.A., 1987, Biochronology of the microtine rodents of the United States, *in* M.O. Woodburne, ed., Cenozoic Mammals of North America: University of California Press, p. 236-268.

Repenning, C.A., T.R. Weasma, and G.R. Scott, 1995, The early Pleistocene (latest Blancan-earliest Irvingtonian) Froman Ferry fauna and history of the Glenns Ferry Formation, southwestern Idaho: U.S. Geological Survey Bulletin 2105, 86 p.

Sadler, J.L., 1997, Sedimentology and stratigraphy of the Pleistocene Tuana Gravel at Hagerman Fossil Beds National Monument, Idaho: Idaho State University M.S. thesis, 40 p.

Sadler, J.L., and P.K. Link, 1996, The Tuana Gravel: Early Pleistocene response to longitudinal drainage of a late-stage rift basin, western Snake River Plain, Idaho: Northwest Geology, v. 26, p. 46-62.

Sadler, J.L., P.K. Link, and H.T. Ore, 1997, Sedimentologic and stratigraphic evaluation of the Pleistocene Tuana Gravel at Hagerman Fossil Beds National Monument, Idaho: Idaho Museum of Natural History, Geology Report 2, Completion report for National Park Service, Hagerman, Idaho, Subagreement of Contract CA-9000-0-0013, 40 p.

Sankey, J.T., 1996, Vertebrate paleontology and magnetostratigraphy of the upper Glenns Ferry (latest Pliocene) and lower Bruneau (Pliocene-Pleistocene) Formations, near Murphy, southwestern Idaho: Journal of the Idaho Academy of Sciences, v. 32, p. 71-88.

Sheppard, R.A., 1991, Zeolitic diagenesis of tuffs in the Miocene Chalk Hills Formation, western Snake River Plain, Idaho: U.S. Geological Survey Bulletin 1963, 19 p.

Smith, Moira, and George Gehrels, 1994, Detrital zircon geochronology and the provenance of the Harmony and Valmy Formations, Roberts Mountains Allochthon, Nevada: Geological Society of America Bulletin, v. 106, p. 968-979.

Smith, G.R., 1975, Fishes of the Pliocene Glenns Ferry Formation, southwest Idaho: University of Michigan Museum of Paleontology, Papers on Paleontology, v. 14, p. 1-68.

Smith, G.R., Krystyna Swirydczuk, P.G. Kimmel, and B.H. Wilkinson, 1982, Fish biostratigraphy of the late Miocene to Pleistocene sediments of the western Snake River Plain, Idaho, *in* Bill Bonnichsen and R.M. Breckenridge, eds., Cenozoic Geology of Idaho: Idaho Bureau of Mines and Geology Bulletin 26, p. 519-541.

Smith, R.B., and L.J. Siegel, 2000, Windows into the earth: The geologic story of Yellowstone and Grant Teton National Parks: Oxford University Press, 242 p.

Snider, L.G., 1995, Stratigraphic framework, geochemistry, geochronology, and eruptive styles of Eocene volcanic rocks in the White Knob Mountains area, southeastern Challis volcanic field, central Idaho: Idaho State University M.S. thesis, 212 p.

Stewart, J.H., 1980, Geology of Nevada: Nevada Bureau of Mines and Geology Special Publication 4, 136 p.

Struhsacker, E.M., C. Smith, and R.M. Capuano, 1983, An evaluation of exploration methods for low-temperature geothermal systems in the Artesian City area, Idaho: Geological Society of America Bulletin, v. 94, p. 58-79.

Taylor, D.W., 1966, Summary of North American Blancan nonmarine mollusks: Malacologia, v. 4, p. 1-172.

———, 1995, Evolution of fresh-water drainages and mollusks in western North America, *in* C.J. Smiley, ed., Late Cenozoic History of the Pacific Northwest: American Association for the Advancement of Science, Pacific Division, p. 265-321.

Taylor, D.W., and R.C. Bright, 1987, Drainage history of the Bonneville Basin, *in* R.S. Kopp and R.E. Cohenour, eds., Cenozoic Geology of Western Utah—Sites for Precious Metal and Hydrocarbon Accumulations: Utah Geological Association Publication 16, p. 239-256.

Taylor, D.W., and G.R. Smith, 1981, Pliocene molluscs and fishes from northeastern California and northwestern Nevada: University of Michigan, Museum of Paleontology Contributions, v. 25, p. 339-413.

Vallier, T.L., and H.C. Brooks, 1987, The Idaho batholith and its border zone: A regional perspective, *in* T.L. Vallier and H.C. Brooks, eds., Geology of the Blue Mountains Region of Oregon, Idaho, and Washington: The Idaho Batholith and Its Border Zone: U.S. Geological Survey Professional Paper 1436, p. 1-8.

Wheeler, H.E., and E.F. Cook, 1954, Structural and stratigraphic significance of the Snake River capture, Idaho-Oregon: Journal of Geology, v. 62, p. 525-536.

Williams, P.L., H.R. Covington, and K.L., Pierce, 1982; Cenozoic stratigraphy and tectonic evolution of the Raft River basin, Idaho: *in* Bill Bonnichsen and R.M. Breckenridge, eds., Cenozoic Geology of Idaho: Idaho Bureau of Mines and Geology Bulletin 26, p. 491-504.

Williams, S.K., 1994, Late Cenozoic tephrostratigraphy of deep sediment cores from the Bonneville basin, northwest Utah: Geological Society of America Bulletin, v. 106, p. 1517-1530.

Winston, Don, P.K. Link, and Nate Hathaway, 1999, The Yellowjacket is not the Prichard and other heresies: Belt Supergroup Correlations, Structure and Paleogeography, east-central Idaho, *in* S.S. Hughes and G.T. Thackray, eds., Guidebook to the Geology of Eastern Idaho: Idaho Museum of Natural History, p. 3-20.

Wood, S.H., 1994, Seismic expression and geological significance of a lacustrine delta in Neogene deposits of the western Snake River Plain, Idaho: American Association of Petroleum Geologists Bulletin, v. 78, p. 102-121.

Wood, S.H., and J.N. Gardner, 1984, Silicic volcanic rocks of the Miocene Idavada Group, Bennett Mountain, southwestern Idaho: Final Contract Report to the Los Alamos National Laboratory from Boise State University, unpaginated.

Worl, R.G., T.H. Kiilsgaard, E.H. Bennett, P.K. Link, R.S. Lewis, V.E. Mitchell, K.M. Johnson, and L.D. Snyder, 1991, Geologic map of the Hailey 1º x 2º quadrangle, Idaho: U.S. Geological Survey Open-File Report 91-340, scale 1:250,000.

Worl, R.G., P.K. Link, G.R. Winkler, and K.M. Johnson, eds., 1995, Geology and mineral resources of the Hailey 1º x 2º quadrangle and the western part of the Idaho Falls 1º x 2º quadrangle, Idaho: U.S. Geological Survey Bulletin 2064, Chapters A-R, variously paginated.

Wyld, S.J., and J.E. Wright, 1997, Triassic-Jurassic tectonism and magmatism in the Mesozoic continental arc of Nevada: Classic relations and new developments: Brigham Young University Geology Studies, v. 42, part I, p. 197-224.

Zakrzewski, R.J., 1969, The rodents from the Hagerman local fauna, upper Pliocene of Idaho: University of Michigan Museum of Paleontology Contributions, v. 23, no. 1, p. 1-36.

Extension and Subsidence of the Eastern Snake River Plain, Idaho

David W. Rodgers,[1] H. Thomas Ore,[1] Robert T. Bobo,[2]
Nadine McQuarrie,[3] and Nick Zentner[4]

ABSTRACT

The deformational history of the eastern Snake River Plain (SRP) is interpreted from rocks, structures, and landforms within and adjacent to it. Crustal extension is manifested by west-dipping normal faults that define a half-graben fault style along the north and south margins of the plain. Cumulative extension averages 15-20 percent and diminishes only slightly from the south margin to the north, evidence of no lateral shear beneath the plain. Miocene-Quaternary volcanic and sedimentary rocks fill the half grabens and provide evidence of two pulses of extension that migrated northeast through time. One pulse of minor extension began 16-11 Ma and ended 11-9 Ma, and a second pulse of major extension began 11-9 Ma and lasted a few million years in any one location as it migrated eastward to the eastern edge of the Basin and Range, where it continues today. Because many Miocene faults project into the eastern SRP with no evidence of diminishing offset, normal faults are interpreted to have characterized the eastern SRP in middle and late Miocene time. Since then, upper crustal extension has been accommodated primarily by mafic dike injection.

Subsidence of eastern SRP rocks relative to Basin and Range rocks is manifested by the accumulation of a thick volcanic succession, crustal flexure of its margins, and marginal normal faults. Northeast-striking marginal normal faults only accommodated 2-5 percent extension associated with crustal flexure, not downfaulting of eastern SRP crust. Crustal flexure along the northern margin of the eastern SRP is evidenced by Cretaceous fold hinges whose southward plunges increase regularly toward the plain. Isoplunge contours define a zone of flexure about 20 km wide that accommodated 4.5-8.5 km of subsidence of eastern SRP rocks. Age-depth relations of eastern SRP volcanic rocks indicate 1.7 km of rock subsidence since 8.0 Ma, 3.1 km since 8.5 Ma, and the initiation of subsidence before 10 Ma.

Subsidence of the eastern SRP surface relative to the Basin and Range surface is manifested by axial drainage that extends 50 km beyond the SRP margins. Streams that are tributary to the Snake River have deeply incised Basin and Range valleys along the southern margin of the eastern SRP, a process attributed to SRP surface subsidence and consequent base level lowering of the Snake River. The age and amount of surface subsidence are recorded by a strath terrace near Pocatello that cuts across tilted 7.3-Ma basin fill and is perched 900 m above the modern plain. Drainage reversals at tributary stream headwaters provide evidence of ongoing Pleistocene subsidence.

Space-time patterns of extension and subsidence are used to support a three-stage model of deformation. Stage 1 involved minor half-graben normal faulting and possibly regional subsidence of the proto-eastern SRP. Stage 2 involved regional rock subsidence and major extension via normal faulting. Extension was focused slightly east of coeval silicic magmatism, and both migrated northeast after 11 Ma. Deformation and coeval magmatism were widely dispersed across the plain at about 10 Ma. Stage 3 has involved ongoing rock subsidence, surface

Editors' note: The manuscript was submitted in June 1998 and has been revised at the authors' discretion.

[1]Department of Geosciences, Idaho State University, Pocatello, ID 83209-8072
[2]595 Ford Road, McKenzie, TN 38201
[3]Division of Geological and Planetary Sciences, California Institute of Technology, Pasadena, CA 91125
[4]Department of Geology, Central Washington University, Ellensburg, WA, 98926

Rodgers, D.W., H.T. Ore, R.T. Bobo, Nadine McQuarrie, and Nick Zentner, 2002, Extension and subsidence of the eastern Snake River Plain, Idaho, *in* Bill Bonnichsen, C.M. White, and Michael McCurry, eds., Tectonic and Magmatic Evolution of the Snake River Plain Volcanic Province: Idaho Geological Survey Bulletin 30, p. 121-155.

subsidence after about 7 Ma, and extension via dike injection after about 4 Ma. Stage 3 deformation has been located west of coeval silicic magmatism.

Key words: Yellowstone, Snake River Plain, Basin and Range, extensional tectonics, lower crustal flow, crustal subsidence

INTRODUCTION

The eastern Snake River Plain (SRP) is a bimodal magmatic province with little surficial evidence of crustal deformation. A few basaltic rift zones, rare normal faults, and a relatively low regional elevation are the only indication of crustal movement. In contrast, the adjacent Basin and Range Province is characterized by a relatively high regional elevation and widespread normal faults that accommodate both crustal extension and vertical offset. Structural and geomorphic features clearly indicate that different deformational processes are currently operating in the two provinces, but what causes the differences and what defines the transition remain difficult to discern. The two provinces also experienced temporal changes in deformation style and kinematics. The eastern SRP evolved during the past 16 Ma through a complicated process of magmatism and deformation, but little is known about the Neogene deformational history during the eruption of voluminous rhyolites and the early stages of basaltic magmatism. Neogene rocks and structures of the eastern SRP that probably record this earlier history are concealed beneath Quaternary basalts.

Fortunately, footwall uplifts of the adjacent Basin and Range contain rocks and structures that record several pulses of late Cenozoic deformation. Some pulses were restricted to the Basin and Range, whereas others were more extensive and affected what is now the eastern SRP. The late Cenozoic rocks have been studied by some workers, notably Kirkham (1927, 1931), Trimble (1980), Trimble and Carr (1976), Allmendinger (1982), Kellogg (1992), Pierce and Morgan (1992), and especially Anders and his coworkers (Anders and others, 1989; Rodgers and Anders, 1990; Anders and others, 1993; Anders, 1994) who used the tectonic tilts of Neogene rocks to interpret that the locus of Basin and Range faulting migrated eastward and away from the eastern SRP through time.

Similarly, we have worked in late Cenozoic rocks of the Basin and Range, but we have focused along the eastern SRP margins where structures, basin fill, and geomorphology record deformation that may have affected the eastern SRP. Results indicate that crustal extension and subsidence occurred in the eastern SRP throughout the Neogene and that deformation was intricately tied to the rise of magma, its accumulation within the crust, and the space-time pattern of eruptions. Our objective in this paper is to document the Neogene and Quaternary deformational history, the space-time pattern of deformation and magmatism, and the landscape evolution to develop an evolutionary model of eastern SRP deformation. Most of the data and interpretations in this paper were first presented in Master's theses by Zentner (1989), Bobo (1991), and McQuarrie (1997) who worked under the supervision of D.W. Rodgers and H.T. Ore. Except for some abstracts and one paper (McQuarrie and Rodgers, 1998), the information was not widely disseminated or integrated, a situation this paper attempts to rectify.

STRUCTURAL SETTING

A complicated pattern of crustal extension has affected the eastern SRP region (Figure 1). The eastern SRP itself appears relatively unextended with just a few late Quaternary volcanic rift zones presumed to overlie mafic dikes. Neogene to early Quaternary structures are completely obscured by younger basalt flows. Beyond the eastern SRP are normal faults of the Basin and Range Province, some of which are active as indicated by arcuate zones of high topography, high seismicity, and high to moderate Quaternary slip rates that are almost symmetrically distributed about the eastern SRP. Most workers attribute the modern extensional pattern to the Yellowstone magmatic system and its interaction with the southwest-drifting North American plate, though the actual mechanics of this process are unclear. To better understand the interaction between extension and magmatism, a few workers have studied the older Neogene history of normal faults near the eastern SRP. Anders and others (1989, 1993) measured the ages and rates of faulting both north and south of the eastern SRP, and interpreted them in terms of a migrating "seismic parabola" shaped like the modern one. Rodgers and others (1990) compiled the space-time relations of SRP magmatism and faulting south of the SRP and proposed a model of concomitant tectonic activity, wherein the SRP experienced crustal extension (via normal faulting, ductile attenuation, and magma injection) before, during, and after magmatism at any one locality. Recent studies, in particular new dating and correlation techniques, have revised data and interpretations concerning the space-time pattern of extension. One goal of this paper is to present information that will explain the interaction of extension and magmatism on the eastern SRP.

Perhaps as unusual as the pattern of crustal extension is the pattern of subsidence in the eastern SRP. First recognized by King (1878) as "a depressed area which subsided very gently with minimal faulting" (Kirkham,

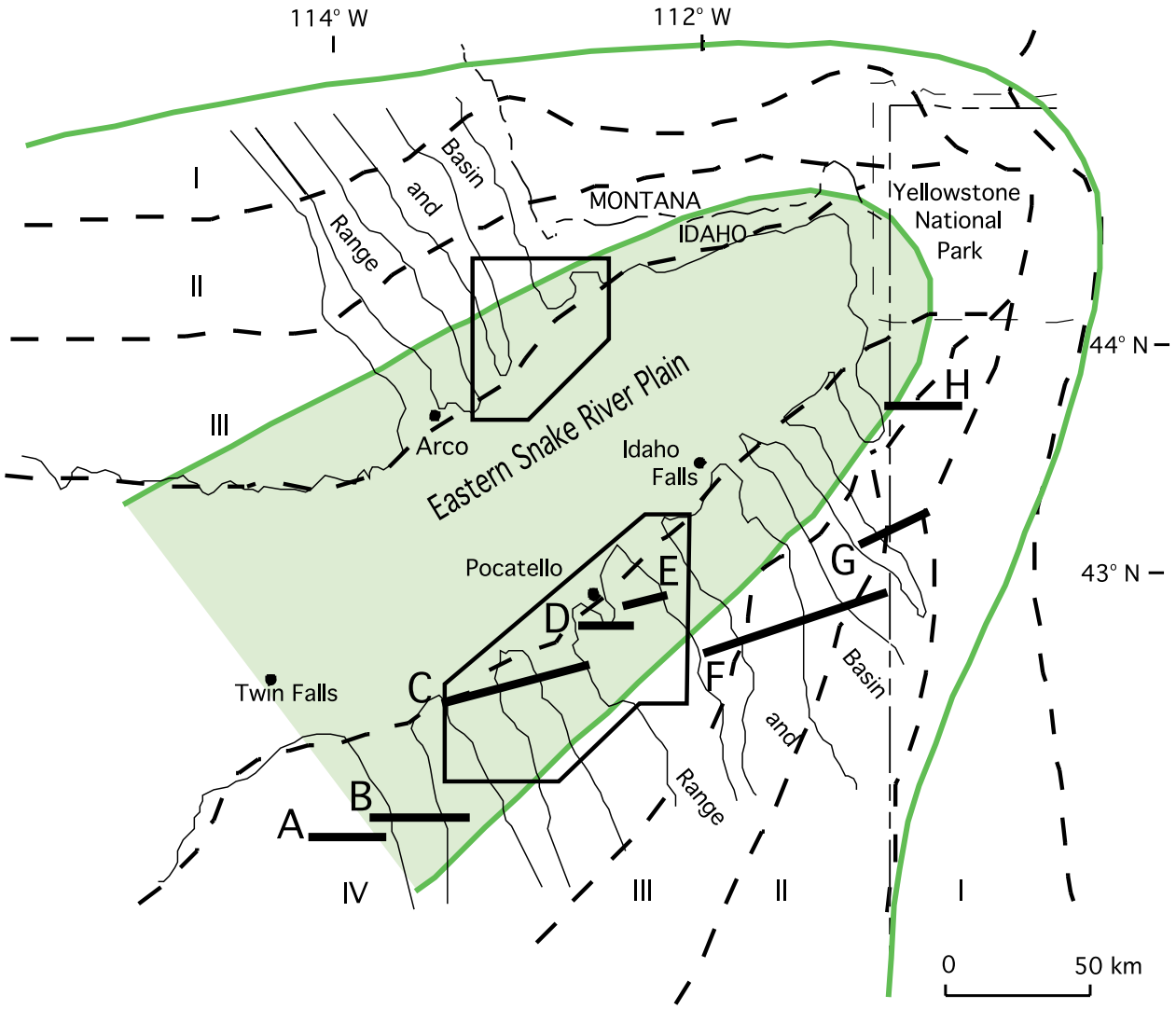

Figure 1. Geography and tectonic domains of eastern SRP and adjacent Basin and Range Province. Dashed lines divide Quaternary fault zones (I, II, III, IV) of Pierce and Morgan (1992). Gray lines define seismic parabola of Anders and others (1989). Polygons indicate locations of study areas shown in Figure 2. Lines labeled A-H indicate locations of composite cross section shown in Figures 3 and 4.

1931), the eastern SRP shows over 2 km of topographic relief and as much as 8 km of structural relief (McQuarrie, 1997) compared to adjacent regions. Surface subsidence is also apparent within the eastern SRP, as manifested by a southwestward decline in elevation along its axis. Brott and others (1981) proposed that thermal contraction in the wake of a hot spot was an important subsidence mechanism, and Leeman (1982) proposed that crustal densification by mafic magma was significant. Quantitative subsidence analyses were performed by a few workers, notably Brott and others (1981) and Anders and Sleep (1992), who studied along-axis subsidence, and McQuarrie and Rodgers (1998) who studied cross-axis subsidence. A useful approach adopted in the latter study was to consider the eastern SRP a basin, similar to sedimentary basins, such that its margins record flexure and faulting associated with basin formation and that its volcanic fill records the subsidence history. Although our basin analysis of the eastern SRP is still underway, initial results (Zentner, 1989; McQuarrie and Rodgers, 1998) suggest a close relation between subsidence and crustal densification by mafic magma. In this paper, we discuss the subsidence record and available age constraints to aid in understanding the space-time pattern of eastern SRP intrusive activity.

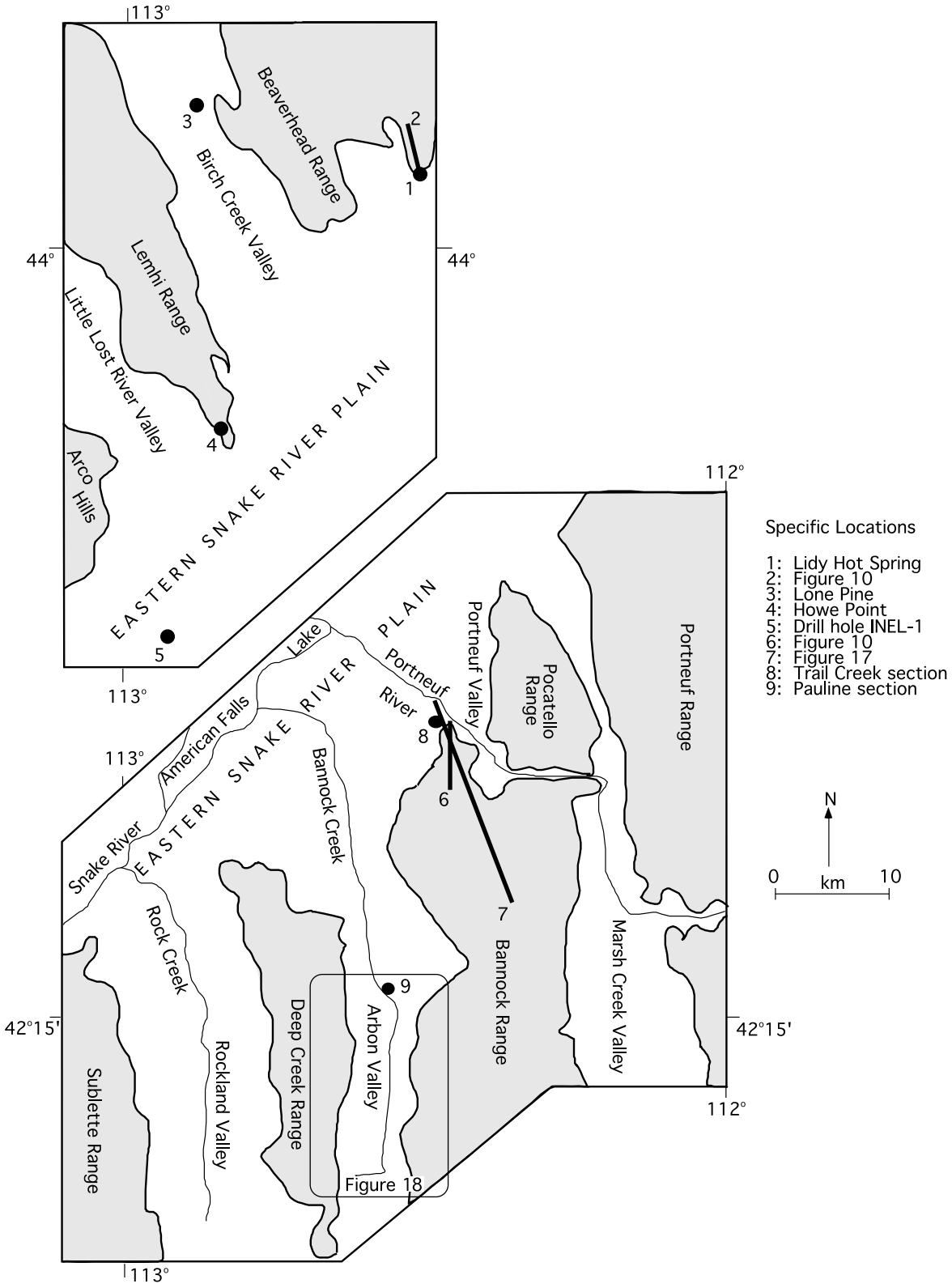

Figure 2. Geographic maps along the north and south margins of the eastern Snake River Plain showing geographic features and specific locations mentioned in text. Location of maps shown in Figure 1.

CRUSTAL EXTENSION

The eastern SRP is surrounded by extended crust of the Basin and Range Province. Nowhere along the plain margins have any workers identified eastern SRP-parallel strike-slip faults, orographic bending, or minor pull-apart basins that would indicate abrupt termination or lateral offset of the Basin and Range faults. Until such structures are found, it must be inferred that the eastern SRP crust experienced a kinematic history similar to that of the adjacent Basin and Range Province.

Normal faulting and dike injection are two processes that accommodated much of the eastern SRP extension. Dikes were the main means by which Pliocene-Quaternary mafic magma rose from mantle through the crust (Kuntz, 1992). Basaltic dikes are not observed in the eastern SRP today but are inferred from Quaternary volcanic rift zones that cut across the eastern SRP (Kuntz and others, 1992). Their absence at the surface today merely reflects ongoing subsidence and accumulation of younger volcanic rocks.

Large normal faults are similarly not observed on the surface of the eastern SRP. We interpret, however, that they exist at depth beneath the plain, because faults in the surrounding Basin and Range project directly into the plain and timing relations (discussed below) suggest many faults were active before basalt magmatism commenced on the plain. To understand this early phase of extension, we have studied the Miocene history of Basin and Range faulting and then projected it into the eastern SRP.

PLIOCENE-QUATERNARY EXTENSION OF THE EASTERN SNAKE RIVER PLAIN

Late Quaternary volcanic rift zones are present on the eastern SRP and are interpreted to overlie basalt dikes that accommodated crustal extension (Kuntz and others, 1992; Kuntz, 1992; Hackett and others, 1996). The rift zones are parallel to the Basin and Range faults and in places are nearly colinear with them. Rodgers and others (1990) first proposed that dike emplacement was the main extensional mechanism in the Pliocene-Quaternary eastern SRP, and Parsons and Thompson (1991) and Parsons and others (1998) provided analytical evidence that dikes could accommodate a similar amount of extension as that along adjacent Basin and Range faults.

Quaternary volcanic rift zones are concentrated in the northern half of the eastern SRP but are uncommon in the southern half (Kuntz and others, 1992). We suggest that this pattern reflects along-strike changes in Quaternary strain magnitude similar to those in the adjacent Basin and Range Province (Anders and others, 1989; Pierce and Morgan, 1992). The actively extending northern half of the eastern SRP is compatible with Pierce and Morgan's (1992) fault zone III along the northern margin of the eastern SRP, and the relatively inactive southern half of the eastern SRP is compatible with fault zone IV along the southern margin of the eastern SRP where normal faults are inactive (Pierce and Morgan, 1992). This view of Quaternary deformation makes the Snake River the axis of the regionally extensive zones of seismicity and Quaternary extensional activity, such that these patterns are symmetrically distributed about the modern Snake River. In this interpretation, the margins of the eastern SRP are thought to mark a fundamental change in extensional style but not a significant change in extensional kinematics.

MIOCENE EXTENSION OF THE EASTERN SNAKE RIVER PLAIN

The eastern SRP extensional history before basaltic magmatism is speculative because the older structures are concealed beneath younger basalt. However, normal faults along the north and south margins of the eastern SRP are exposed. They provide a record of Miocene deformation that can be extrapolated beneath the eastern SRP, a procedure justified by the absence of plain-parallel strike-slip faults and the geometry of crustal flexure (McQuarrie and Rodgers, 1998; and described below).

Basin and Range Faults South of the Eastern Snake River Plain

The style and kinematics of Basin and Range extension south of the eastern SRP were studied by compiling geologic maps and cross sections into one regional cross-section (Rodgers and others, 1994; Figures 3 and 4). Because the goal was to extrapolate extension into the eastern SRP, the section was located close to the eastern SRP wherever extensive, high quality mapping was available. The construction of each cross section is described in Figure 3, and the regional style and kinematics of faulting is summarized below. The age of faulting is addressed in a subseqent section on basin fill.

Extension occurred along normal faults that generally define a half-graben style. Nearly all normal faults dip 25º-60º W. Most faults with small offset dip more steeply, and faults (or fault sets) with more offset dip more gently, evidence of domino-style tilting during fault slip. Some faults, like the Grand Valley fault and Aspen Range fault, are influenced by older west-dipping thrust ramps (Royse and others, 1975). Other west-dipping faults may have been controlled by other west-dipping thrusts (e.g.,

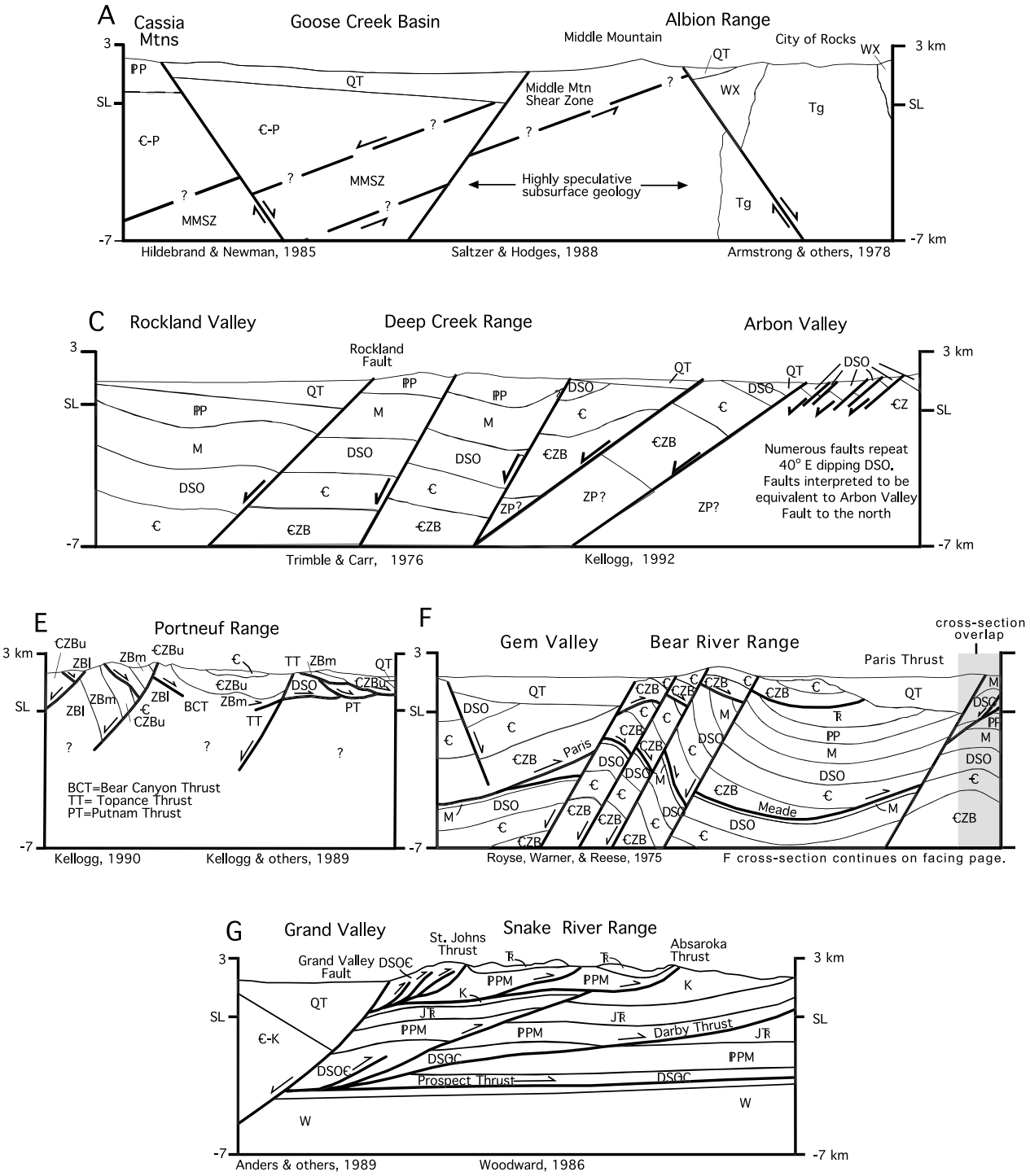

Figure 3. Cross sections of Basin and Range south of the eastern Snake River Plain, showing geometry and style of faulting. Location of cross sections shown in Figure 1. From Rodgers and others (1994) and compiled from sources listed below cross sections.

Figures 3A and 3B. The western end of the cross section is in the Cassia Mountains which bound the Owyhee Plateau, a relatively unextended middle Miocene rhyolite plateau. The Albion Range is a metamorphic core complex flanked by two different detachment faults, the Eocene-Oligocene Middle Mountain shear zone (with rocks metamorphosed at 20+ km; Saltzer and Hodges, 1988) and the early to middle Miocene Raft River fault (with 25 km slip; Covington, 1983). West of the Albion Range is the relatively unextended middle Miocene Goose Creek Basin and to the east is the middle Miocene Raft River Valley. Space problems associated with the contrasting detachments have not been addressed in this cross section.

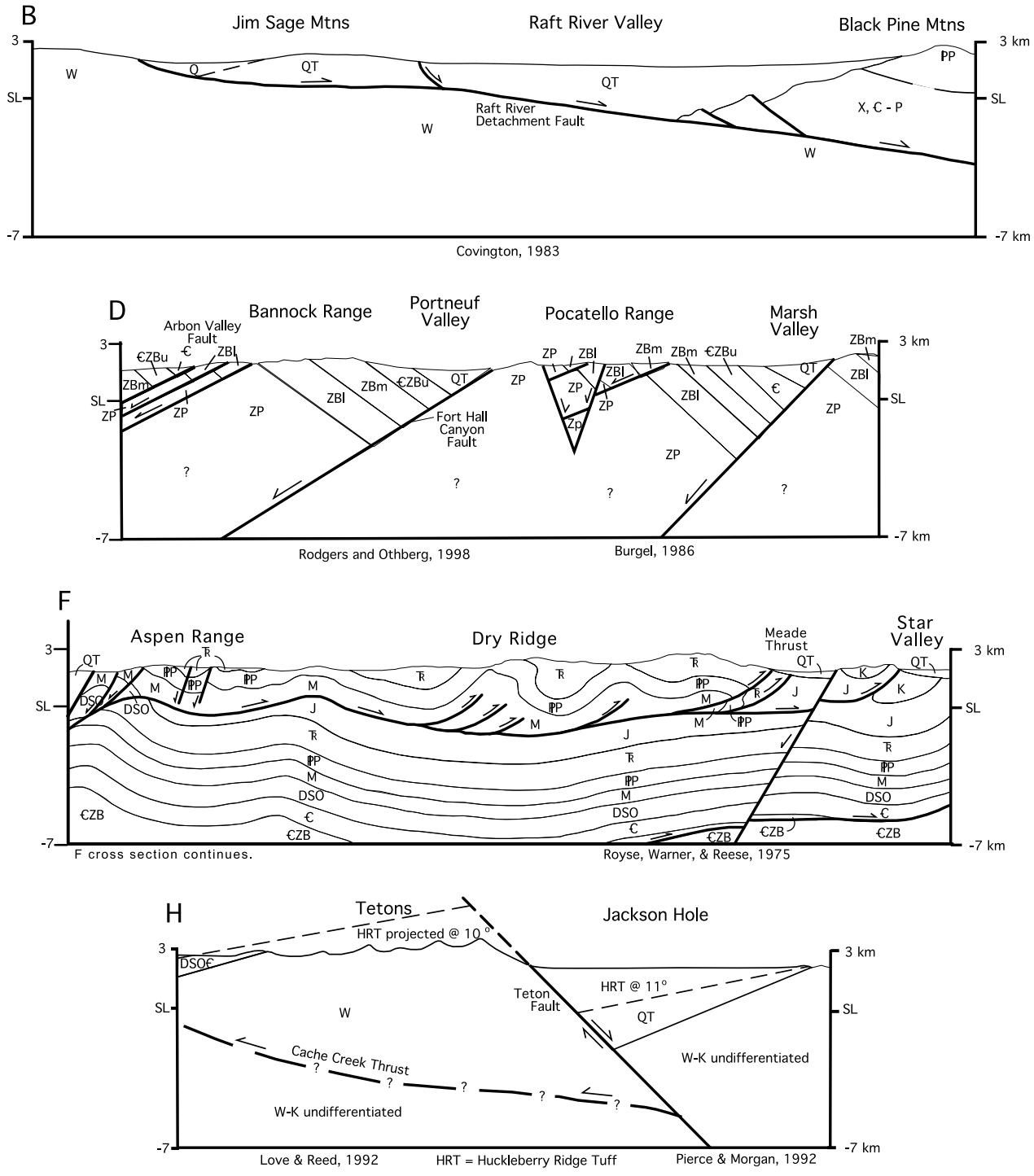

Figure 3C. One major fault lies within the Deep Creek Range, and one borders it on the west. Early(?) to middle Miocene rocks in Rockland Valley dip gently east, whereas bedrock and early(?) to middle Miocene rocks in Arbon Valley dip more steeply east. The fault geometry in Arbon Valley is not well-characterized: Trimble and Carr (1976) show repeated sections of Paleozoic bedrock plus Miocene basin fill that we have reinterpreted to be bounded by several west-dipping normal faults. The overall westward decrease in age of exposed bedrock in Arbon Valley was interpreted by Rodgers and Janecke (1992) to reflect a concealed Mesozoic thrust ramp. Two problems remain in this section: whether the Raft River detachment exists at depth, and whether the geometry of the fault in western Arbon Valley is correct (because the fault shows major slip without forming a deep basin). *(Caption continues on the next page.)*

Figures 3D and 3E. Late Proterozoic to Middle Cambrian rocks are exposed in the Bannock Range and Pocatello Range. These once deep-seated rocks were probably uplifted twice, first along a ramp of the Mesozoic Putnam thrust (whose deep structure is unknown and not shown) and later along Miocene normal faults (Rodgers and Janecke, 1992). The normal faults are more gently dipping (25-45 degrees) than faults elsewhere in the regional cross section. The comparatively shallow basins may reflect prolonged uplift above regional base level or the close spacing of normal faults. The Portneuf Range is cut by normal faults, but the dominant structure is a duplex system associated with the Putnam thrust (Kellogg and others, 1989; Kellogg, 1990).

Figure 3F. This cross section is only slightly modified from Royse and others (1975), who recognized a few normal faults superimposed on Mesozoic thrust faults. Normal faults in the Bear River Range are shown as uniformly west-dipping, though Royse and others (1975) show a few east-dipping faults. The location of the normal fault that bounds the Aspen Range may have been determined by a footwall ramp in the Meade thrust.

Figures 3G and 3H. Anders and others (1989) proposed 4 km of middle to late Miocene slip on the Grand Valley fault. Royse and others (1975) showed this fault merging with the Absaroka thrust, but we believe that 4-km slip requires a more deeply rooted geometry. No major normal faults cut through the Snake River Range (Woodward, 1986) or the next range north, the Tetons (Love and others, 1992). Along the Teton fault, the hanging wall was vertically downfaulted 2.5 km since emplacement of the 2.0 Ma Huckleberry Ridge Tuff (HRT) and 5 km since a 5.5-Ma tuff was emplaced (Pierce and Morgan, 1992). We estimate 10 km of total offset, measured along the Teton fault from the projected hanging wall trace of the 5.5-Ma tuff to the projected footwall trace of the HRT. Jackson Hole is the east edge of the Basin and Range Province.

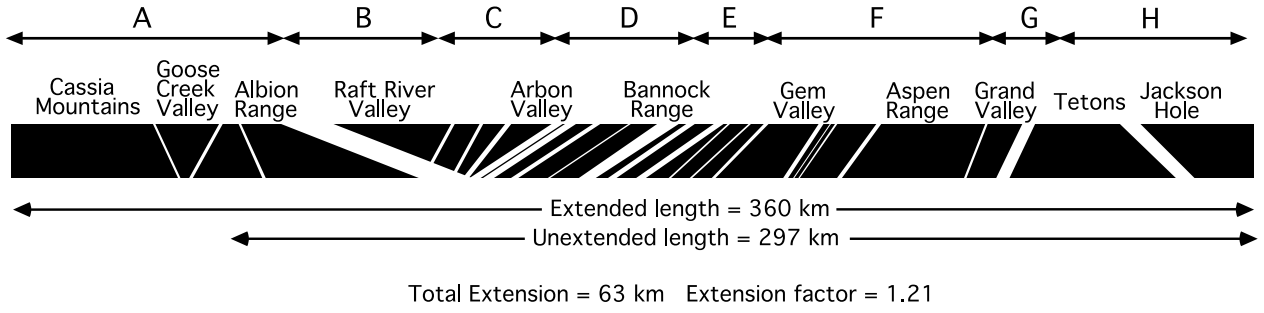

Figure 4. A schematic representation of the composite cross section shown in Figure 3 (and located in Figure 1), which summarizes fault geometry and kinematics. The slant and width of gaps reflect the dip and offset along Neogene-Quaternary normal faults.

Arbon Valley faults by Arbon Valley ramp), by inferred late Proterozoic rift-related faults, or by the west-thickening Paleozoic sedimentary sequence. Two major faults dip east. The Teton fault may have been controlled by the geometry of the underlying, east-dipping Cache Creek thrust fault (Lageson, 1992). What controlled the east dip of the Raft River detachment is unclear.

The spacing of normal faults is irregular. Faults are closely spaced in the central region, from Arbon Valley to the Aspen Range, and widely spaced from Jackson Hole to the Aspen Range and from Rockland Valley to the Cassia Mountains. Fault spacing appears to be inversely proportional to depth to crystalline basement, suggesting that deep-seated sedimentary rocks with subhorizontal weaknesses may have facilitated half-graben faulting. Alternatively, fault spacing may reflect proximity to the volcanic province to the north: Pierce and Morgan (1992) and Parsons and others (1998) noted that Basin and Range faults are more closely spaced near the SRP and suggested that they formed when the brittle-ductile transition was shallow because of an elevated geothermal gradient associated with magmatic activity.

The cumulative extension by middle Miocene to recent normal faults is about 63 km across a modern distance of 360 km, yielding 21 percent extension (Figure 4). Three faults account for half of the extension—the Raft River detachment (17 km from 17-7 Ma; Covington, 1983), the Fort Hall Canyon fault (7 km), and the Teton fault (7 km). Significant slip along each fault is also shown by the metamorphosed Archean or Late Proterozoic rocks in their footwalls (although in each place, uplift occurred in two phases). The most highly extended region is from Arbon Valley to Gem Valley, where numerous faults accommodated nearly 80 percent extension. As expected in a half-graben fault system, faults in this region dip more gently (25°-40° W.), and basin fill dips more steeply (25°-40° E.) than elsewhere. The region may be highly extended either because of its thick sedimentary sequence or because of reactivation of older thrust ramps or Proterozoic faults. Alternatively, the region may have experienced two magmatic events, each of which weakened the crust and allowed it to extend.

Basin and Range Faults North of the Eastern Snake River Plain

A continuous cross section through the entire Basin and Range just north of the eastern SRP has not been completed, but previous studies have estimated Basin and Range extension in the region. In east-central Idaho, three large normal faults, the Lost River, Lemhi, and Beaverhead faults, bound adjacent ranges (Figure 2). The faults generally strike northwest, dip southwest, and are bound on the southwest by sediment-filled basins as much as 3.5 km deep and on the northeast by ranges that rise as much as 2 km above the basins. The pattern of earthquakes as well as geodetic studies associated with the 1983 M_s = 7.3 Borah Peak earthquake on the Lost River fault clearly show it is a planar fault that dips about 50 degrees and extends to 16 km depth (Richins and others, 1987; Barrientos and others, 1987). All three faults are approximately 120 km in length. Janecke (1993) constructed balanced cross sections to measure 10-15 percent extension across east-central Idaho. Anders and others (1993) used tectonic tilts of fault blocks to measure 11 percent extension across southwestern Montana and east-central Idaho.

The typical Basin and Range landscape is absent to the west in central Idaho, replaced by highlands with few sedimentary basins. Across the White Knob and Pioneer Mountains, north- to northwest-striking, west-dipping normal faults are spaced 5-20 km apart and cut through fault blocks tilted 10º-25º E. (Rodgers and others, 1995). In the Smoky and Boulder Mountains (located 50 km north of the eastern SRP), Basin and Range faults have similarly broken the crust into gently northeast-tilted blocks (Rodgers and others, 1995) bounded by faults with relatively long continuous map traces. Major faults include the Sun Valley fault zone along the east side of the Wood River Valley, the Boulder fault along the front of the Boulder Mountains, and the Big Smoky fault along Big Smoky Creek. Offset along these faults was accompanied by 10-15 degrees of tilting to the northeast, as shown by regional outcrop patterns of subplanar volcanic and hypabyssal contacts (e.g., Mahoney, 1987) and sparse measurements of the attitudes of Eocene Challis Group volcaniclastic rocks. Overall, the typical east-northeastern tectonic tilt of 15 degrees indicates about 15 percent extension has been accommodated by Basin and Range faults.

In summary, two styles of Basin and Range faulting are evident north of the eastern SRP: widely spaced, segmented half-graben faults with significant offset and associated sedimentary basins and more closely spaced, relatively short half-graben faults with small offset and no associated basins. The contrast in style appears to correlate with a change in upper crustal rock type: Major faults to the east cut through a thick section of sedimentary rock, whereas minor faults to the west cut through the Eocene Challis volcanic field characterized by plutonic rock at shallow depths. Despite these differences, the cumulative extension throughout the region is consistently estimated at about 15 percent in a NE to ENE direction.

EXTENSION OF THE EASTERN SNAKE RIVER PLAIN

The absence of eastern SRP-parallel strike-slip faults, orographic bending, or minor pull-apart basins along the margins of the eastern SRP provide strong evidence that the eastern SRP experienced a kinematic history similar to that of the adjacent Basin and Range Province. Where individual faults can be traced from the Basin-Range into the eastern SRP, they progressively die out and overlap with volcanic rift zones (Quaternary faults) or are buried by younger rocks without showing evidence of diminished slip (Miocene-Pliocene faults). Because the Basin and Range experienced about 20 percent (south) to 15 percent (north) upper crustal extension, we interpret the crust of the eastern SRP to be similarly extended 15-20 percent in an ENE direction. Dikes and normal faults accommodated the extension in the upper crust, whereas the lower crust probably extended through dike injection and ductile attenuation. We predict that beneath the veneer of Quaternary basalt on the eastern SRP, the upper crust has structural relief and irregular topography reminiscent of the Basin and Range Province.

BASIN FILL: A RECORD OF EXTENSION AND MAGMATISM FROM 16 TO 0 MA

The stratigraphy of rock units in basins that flank the eastern SRP provides an excellent record of tectonism through time. Most basins formed as subsiding half grabens during active volcanism on the eastern SRP and thus contain a fairly complete stratigraphic record of both distal and proximal volcanic activity. The intercalated volcanic and sedimentary rocks, informally termed basin fill, are exposed today because of postdepositional tilting or deep incision by late Cenozoic streams, particularly along the southern margin of the eastern SRP where fault activity has ceased. We describe the evolution of two basins adjacent to the eastern SRP, one to the north and one to the south, to understand the initiation and duration of extension in the region.

Arbon Valley

Arbon Valley (Figure 2) is separated from the Bannock Range by the west-dipping Arbon Valley fault and from the Deep Creek Range by minor normal faults. Trimble and Carr (1976) defined the Neogene Starlight Formation in northern Arbon Valley where it consists of a lower member, a middle volcanic member (the tuff of Arbon Valley), and an upper member. Hladky and Kellogg (1987) remapped some of Arbon Valley prior to Bobo's (1991) detailed study of the Starlight Formation. Based on the latter work, we describe the stratigraphy and age of the Starlight Formation at two locations (Figure 5) and interpret depositional environments in the basin and their relation to eastern SRP tectonics.

The Trail Creek section, located in the northeastern corner of Arbon Valley, contains about 1,000 m of gently east-tilted Starlight Formation. The lower half includes a multitude of intercalated limestone and reworked tuffs. The limestones are interpreted to be lacustrine by lithology, primary sedimentary structures, and the type of fossils they contain. The intercalated tuffs indicate periods of silicic volcanism that inundated the lakes with voluminous pyroclastic material, temporarily exterminating the flora and fauna. New dating and correlation of ashes based upon their chemistry indicate an age range for these rocks from 15.65 Ma to older than 12.67 Ma (D.W. Rodgers, unpub. data). Basalt and 12.67-Ma rhyolite tuff are the next units upsection. Planar bedding and very fine ash laminae suggest emplacement of primary air-fall deposits into standing water. Paleocurrents indicate the flow or flows came from the southwest. The tuff is overlain by clast-supported conglomerate that is interpreted to be the channel deposits of a major meandering stream. Paleocurrent data indicate southeasterly flow, away from what is now the eastern SRP. Above the conglomerate is about 250 m of mostly loess-covered terrain containing rare outcrops of the 10.2 Ma tuff of Arbon Valley. The tuff of Arbon Valley heralds the beginning of massive, silicic volcanism that flooded much of Arbon Valley with deposits of pyroclastic flows and epiclastic tuffs. The number of exposures and the thicknesses of outcrops decrease to the south, ceasing altogether just south of Pauline, providing evidence of a source vent to the north. With the exception of an overlying 7.9-Ma porphyry lava, which occurs only in the extreme northern part of the valley, almost no basin fill is preserved above the tuff of Arbon Valley, indicating an end to deposition essentially after 10.2 Ma in this location.

The Pauline section of the Starlight Formation, located in central Arbon Valley, is dominantly siliciclastic. Drilling data indicate that bedrock is overlain by about 50 m of sandstone, which is overlain by about 10 m of exposed tuffaceous conglomerate intercalated with lenses of clay, sand, and tuff. This is overlain by two, nearly 100-m-thick sections of pebble-, cobble-, and boulder-conglomerate that locally fine upward. Pebble imbrications indicate a dominant northeast paleocurrent direction. The conglomerates are interpreted to be proximal and upper middle fan-facies fanglomerates with the coars-

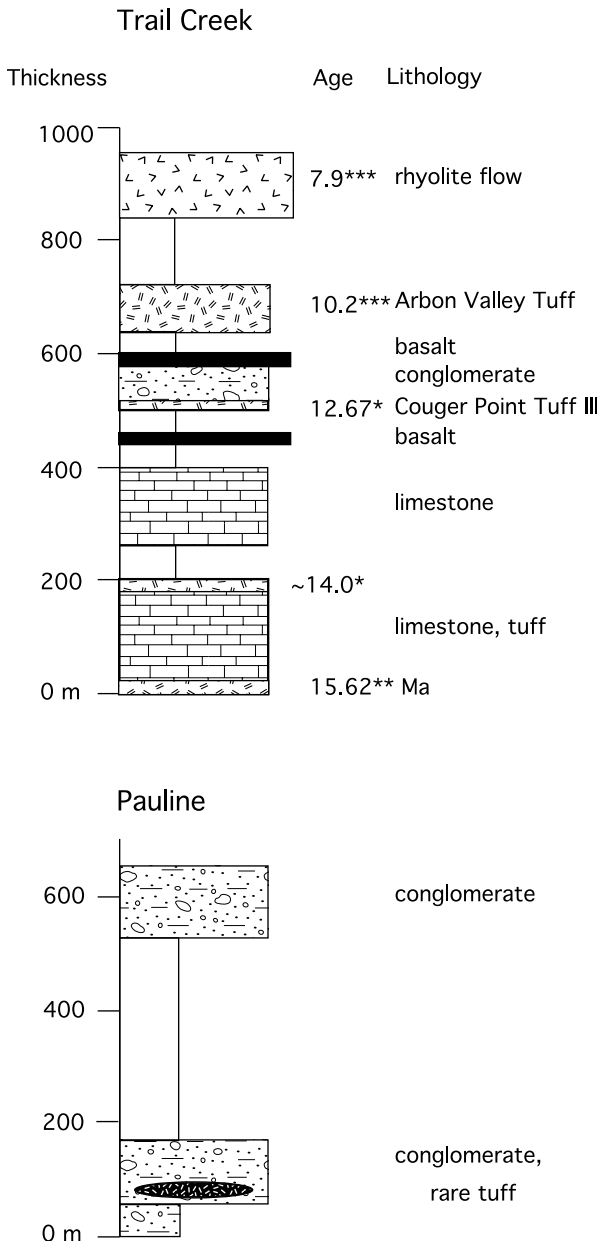

Figure 5. Stratigraphic columns of basin fill from Arbon Valley (modified from Bobo, 1991). Location of sections shown in Figure 2. Trail Creek section includes correlation ages (*) and $^{40}Ar/^{39}Ar$ ages (**) from David Rodgers (unpub. data), and $^{40}Ar/^{39}Ar$ ages (***) from Kellogg and others (1994).

est deposits representing channel lag deposits and the beds of pebbles, sand, and mud being sheetflood deposits. The tuff deposits and tuffaceous matrix testify to distant volcanic activity.

Thus, Arbon Valley evolved as a typical half graben: Erosion of horst blocks furnished siliciclastic sediments, and periodic eruptions from distant volcanoes provided significant quantities of silicic ash. Sediments were transported to the graben and produced rocks ranging from boulder conglomerates to fine mudstone in alluvial fan, fluvial flood-plain, and lacustrine environments. Trunk streams discharged into lakes that indicate a long-lived, poorly integrated, endorheic drainage system. In the northern part of the basin, proximal volcanism initiated with the emplacement of the 10.2-Ma tuff of Arbon Valley and 7.9-Ma lava flows. A second (or ongoing) pulse of faulting resulted in gentle to moderate half-graben tilting of the basin fill.

These results support the interpretation that Basin and Range faulting occurred before and during voluminous SRP magmatism in the region. From 16 to 10 Ma, when northern Arbon Valley subsided and filled, magmatism was focused to the west at the Owyhee Plateau and Twin Falls volcanic center. Syn- to post-10-Ma tilting of basin fill reflects extension that was approximately coeval with the eruption of the Arbon Valley tuff, the final 8.6-Ma volcanism in the Twin Falls volcanic center (Williams and others, 1990), or initial 6.5-Ma volcanism in the Heise volcanic field perhaps 50 km north of Arbon Valley (Morgan and others, 1984).

Southern Birch Creek Valley

Southern Birch Creek Valley (Figure 2) is bounded on the east by the Blue Dome segment of the west-dipping Beaverhead normal fault. Rodgers and Anders (1990) interpreted the stratigraphy and evolution of basin fill in the Lone Pine vicinity and in places throughout southern Birch Creek Valley. McBroome (1981), Kuntz and others (1984; 1994a), Rodgers and Zentner (1988), and Hodges and Rodgers (1999) described the stratigraphy of Howe Point at the southern end of Birch Creek Valley. Rodgers and Anders (1990) suggested a northward migration of both fault initiation and cessation for southern Birch Creek Valley. In this paper, we focus on fault initiation and its timing relative to proximal eruption of rhyolite volcanic rocks.

Angular unconformities and disconformities separate all units exposed at Howe Point (Figure 6). The Medicine Lodge beds, which include 90 m of fanglomerate with minor lacustrine limestone and volcanic ash, accumulated about 16.1 Ma as determined by the age of intercalated volcanic ash near the top of the sequence. Though no syn-depositional fault was observed, these rocks are typical of half-graben basin fill and thus interpreted to reflect the earliest Basin and Range tectonism in the region. Attitudes of these and overlying rocks provide evidence of 23 degrees of south-southeastward tilting between 16-10 Ma, followed by 52 degrees of east-northeastward tilting between 10-0 Ma (Figure 7). These two tilt directions are most simply interpreted as an early pulse of flexure associated with eastern SRP subsidence (described below) and as progressive tilting associated with ongoing Basin and Range tectonics. Furthermore, all rocks older than 6.0 Ma are very gently folded about an ENE-trending axis, which McQuarrie and Rodgers (1998) interpreted in terms of a late, minor (12 degrees) pulse of subsidence-related flexure.

In contrast, Neogene rock units near Lone Pine are more commonly separated by disconformities (Figure 8), suggesting no significant tilting of the Neogene section until after Pliocene-Pliestocene conglomerate deposition (Rodgers and Anders, 1990). Despite fewer angular unconformities, the existence of a fault-bounded basin during Medicine Lodge accumulation is supported by the presence of conglomerate east and west of correlative limestone and by the eastward shift in depocenters from the Medicine Lodge beds basin to the Lone Pine basalt basin. Faulting just before the accumulation of Lone Pine basalt is strongly supported by the map pattern and basalt thickness, indicating the basalt filled an asymmetric valley with stream channels projecting into the Lemhi Range. Significant tilting, and by inference faulting along the Beaverhead fault, did not begin at Lone Pine until after deposition of Pliocene-Pliestocene conglomerate.

These data clearly show a northward decrease in the initial age and amount of extensional displacement, a pattern interpreted by Rodgers and Anders (1990) to reflect the outward migration of a Neogene seismic parabola.

TIMING OF REGIONAL EXTENSION

Stipulating that many Basin and Range faults project onto the eastern SRP and that the eastern SRP and adjacent Basin and Range Province share a common kinematic history, the age or ages of extension in the two provinces should be similar. Thus, the timing of Basin and Range normal faulting can be used to indicate the timing of eastern SRP extension.

In addition to detailed analysis of associated basin fill, such as described above for Arbon Valley and Birch Creek Valley, the age of normal faulting can be determined by cross-cutting relations between faults and datable rocks, by thermochronologic studies of uplifted fault blocks, and (for active terrains) by the study of fault scarps

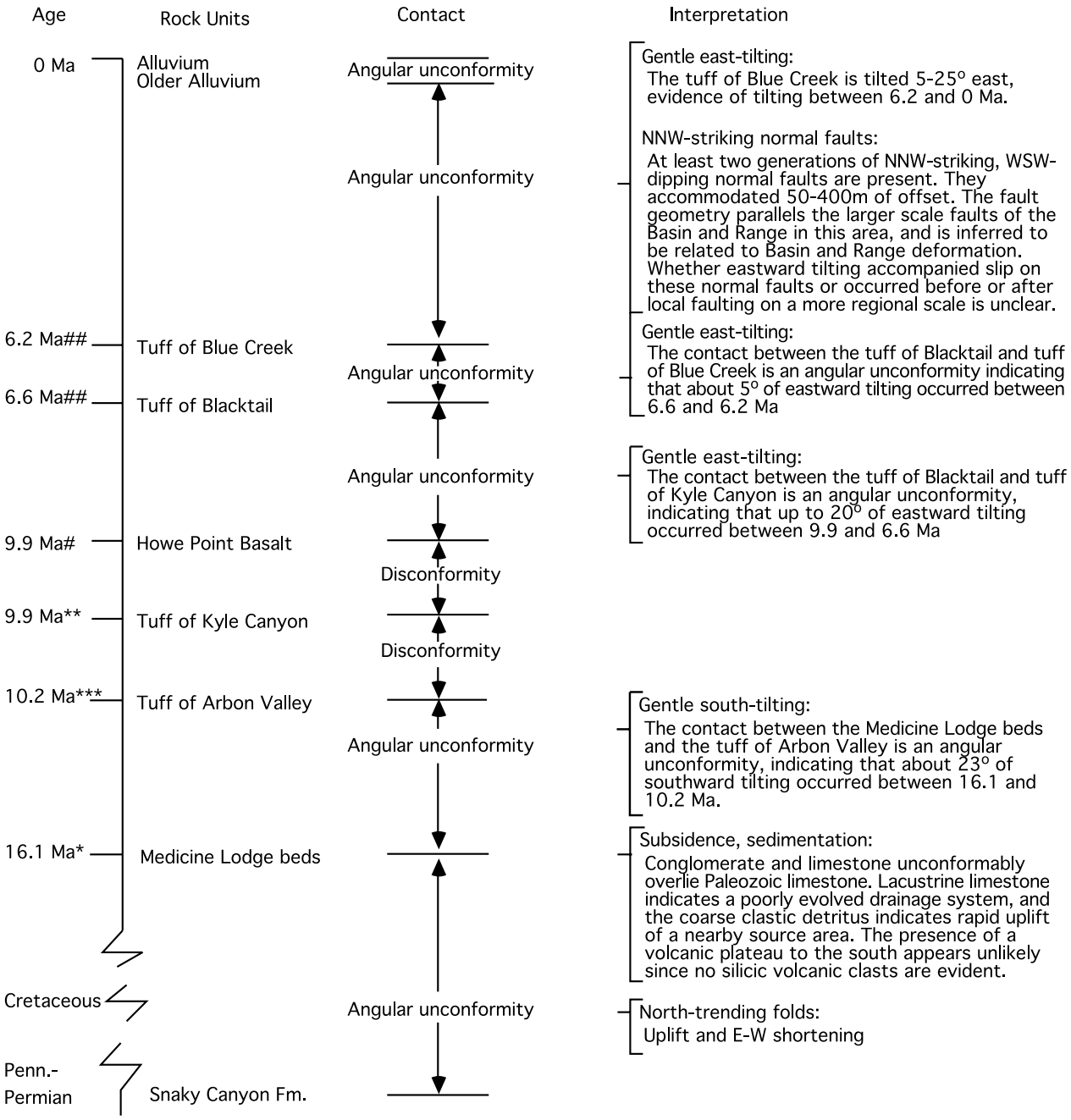

Figure 6. Summary of deformation and basin filling at Howe Point in southernmost Birch Creek Valley. See Figure 2 for location of Howe Point. Sources of radiometric ages: (*) from Anders (unpublished), (**) from Morgan and others (1984), (***) Kellogg and others (1994), and (##) from Rodgers and Anders (1990). Figure modified from Rodgers and Zentner (1988).

and geomorphic features. Unfortunately, cross-cutting relations are rarely exposed, and no late Cenozoic fission-track or $^{40}Ar/^{39}Ar$ ages have been reported from uplifted footwalls for the region, apparently because of insufficient uplift or difficulty in obtaining adequate samples. To interpret the ages of normal faulting across the region, we summarize the ages and texture of basin fill along the southern margin of the eastern SRP. In concert with existing neotectonic data, such as the relative degrees of Quaternary fault activity (Turko and Knuepfer, 1991; Pierce and Morgan, 1992) and the ages of recent individual fault events based on trenching, these data indicate the space-time pattern of extension that we interpret to have affected the eastern SRP.

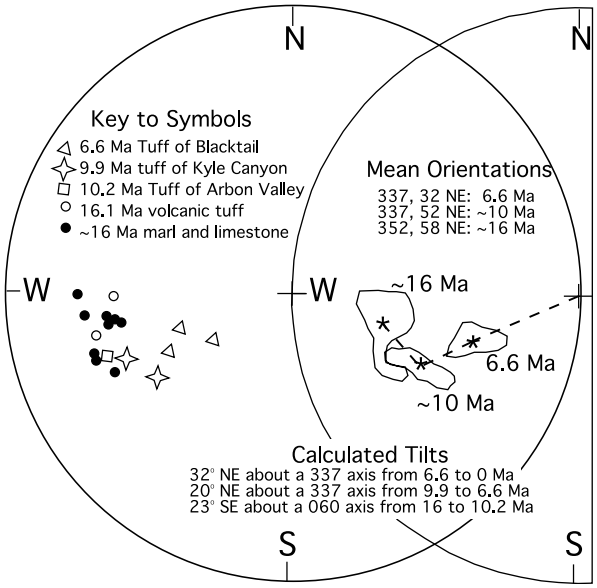

Figure 7. Lower hemisphere, equal area projection of poles to bedding and compaction foliation in Miocene rocks at Howe Point, southernmost Birch Creek Valley. Left figure shows measured orientations of rocks. Right figure shows mean orientations of rocks in three age groups. The calculated tilts would generate the angular unconformities between groups. These data provide evidence of eastern SRP flexure from 16-10 Ma and Basin and Range tilting from 10-0 Ma.

Figure 9 summarizes the interpreted age span of extension in several localities across southern Idaho and adjacent regions. The figure assumes that basin filling was associated with extensional faulting. The figure also presents an incomplete record of extension because the lower basin fill in several localities is undated. The figure does not indicate north-to-south variations in extensional age or extensional pulses unaccompanied by basin filling. Although more field-based study of extensional tectonics is needed throughout the region to clarify the detailed pattern of extension, Figure 9 shows a regional pattern first recognized by Allmendinger (1982) that we interpret as two periods of Neogene extension.

First, the entire region extended in the middle Miocene. Basins in southern Idaho generally contain less than 1,000 m of volcanic and fine-grained sedimentary rocks, evidence of only minor extension at this time in contrast to northern Nevada where signficant extension is indicated by basins with more than 3,000 m of basin fill. Basin filling began as early as 15.7 Ma in Arbon Valley and before 10.2 Ma in Buckskin Basin, Swan Valley, and Jackson Hole. Basin filling ceased by about 12 Ma in Arbon Valley and 9 Ma in Jackson Hole, but slow subsidence continued in other regions (Figure 9).

A second period of extension affected southern Idaho and western Wyoming during the last 9 million years, as manifested by the accumulation of thick, coarse-grained basin fill or the rapid tilting of basin fill (Figure 9). We infer that most of the extension across southern Idaho and western Wyoming occurred during this second pulse of extension. Both the beginning and end of this extensional pulse becomes younger from west to east, evidence that an east-migrating pulse of major extension passed across southern Idaho. The modern coincidence of this pulse with the Quaternary fault zones of Pierce and Morgan (1992) and the seismic parabola of Anders and others (1989) is strong evidence that the same pattern and migration of normal faults existed during the late Neogene.

CRUSTAL SUBSIDENCE

Although high in regional elevation, the eastern SRP is a topographic and structural depression (Figure 1). Along its axis, the surface slopes gently southwest from an elevation of about 3 km on the Yellowstone Plateau to 1.5 km near Twin Falls. Across its axis, the surface is relatively flat, with a subtle axial highland. At its margins, the terrain rises from elevations of 1.5-2 km on the lava plains to 2-4 km in the valleys and mountains of the Basin and Range. Two wavelengths of cross-axis topography are evident: a short wavelength depression about 40 km wider than the eastern SRP, and a long wavelength depression about 150 km wider than the eastern SRP. Short wavelength, cross-axis structural relief is manifested by marginal Paleozoic and Miocene rocks that dip gently toward the eastern SRP.

Kirkham (1927, 1931) first recognized and described the “Snake River downwarp” by noting a number of geomorphic features and some tilted rocks that consistently dipped toward the eastern SRP. Suppe and others (1975) insightfully described regional topography and emphasized the downwarp’s relation to hot-spot magmatism. Surface subsidence along the axis of the eastern SRP that increased as a function of distance from the Yellowstone Plateau was documented by Reilinger and others (1977) and modeled as thermal contraction (Brott and others, 1981; Blackwell and others, 1992) or as a relative increase in loading by dense magmatic intrusions (Anders and Sleep, 1992). Indeed, it is the gradual northeast to southwest decrease in eastern SRP elevation that supports the theory that the eastern SRP marks the passage of western North America over a mantle plume.

Because vertical motions of the crust are intricately tied to other tectonic processes, the subsidence history of the eastern SRP is an important record of events otherwise obscured by younger events and rocks. Subsidence

data can be obtained from several eastern SRP sources, including drill holes, topography, seismic, and gravity studies, or from analysis of the eastern SRP margins where faults, tilted rocks, and angular unconformities are present. Many other workers have described and interpreted the eastern SRP data (Reilinger and others, 1977; Doherty and others, 1979; Pankratz and Ackermann, 1982; Greensfelder, 1981; Sparlin and others, 1982; Blackwell and others, 1992; Anders and Sleep, 1992; Saltzer and Humphreys, 1997; Peng and Humphreys, 1998), but few have focused on subsidence recorded along the eastern SRP margins. In the following sections, we describe the

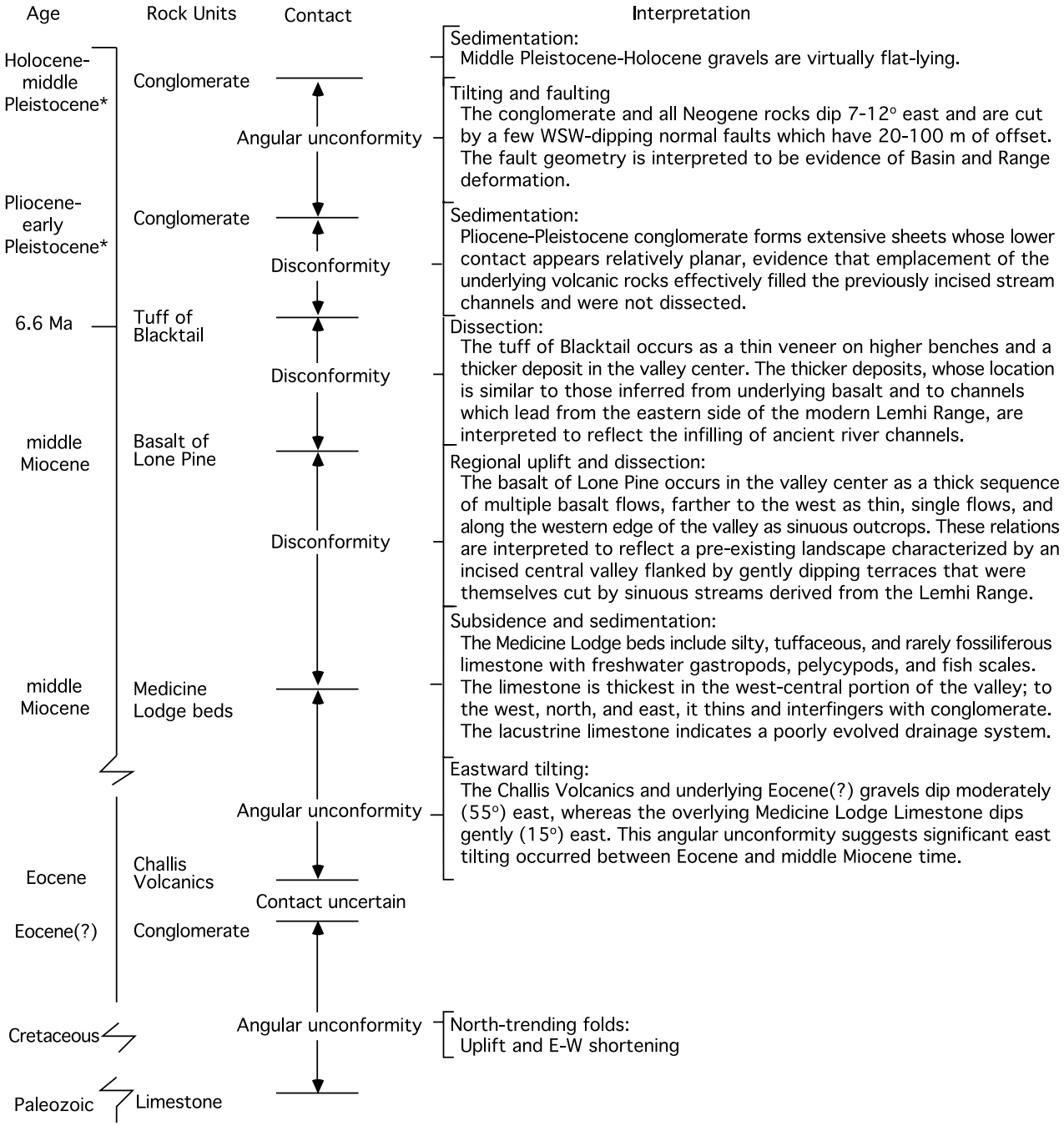

Figure 8. Summary of deformation and basin filling at Lone Pine in southern Birch Creek Valley. See Figure 2 for location of Lone Pine. Ages (*) from Scott (1982).

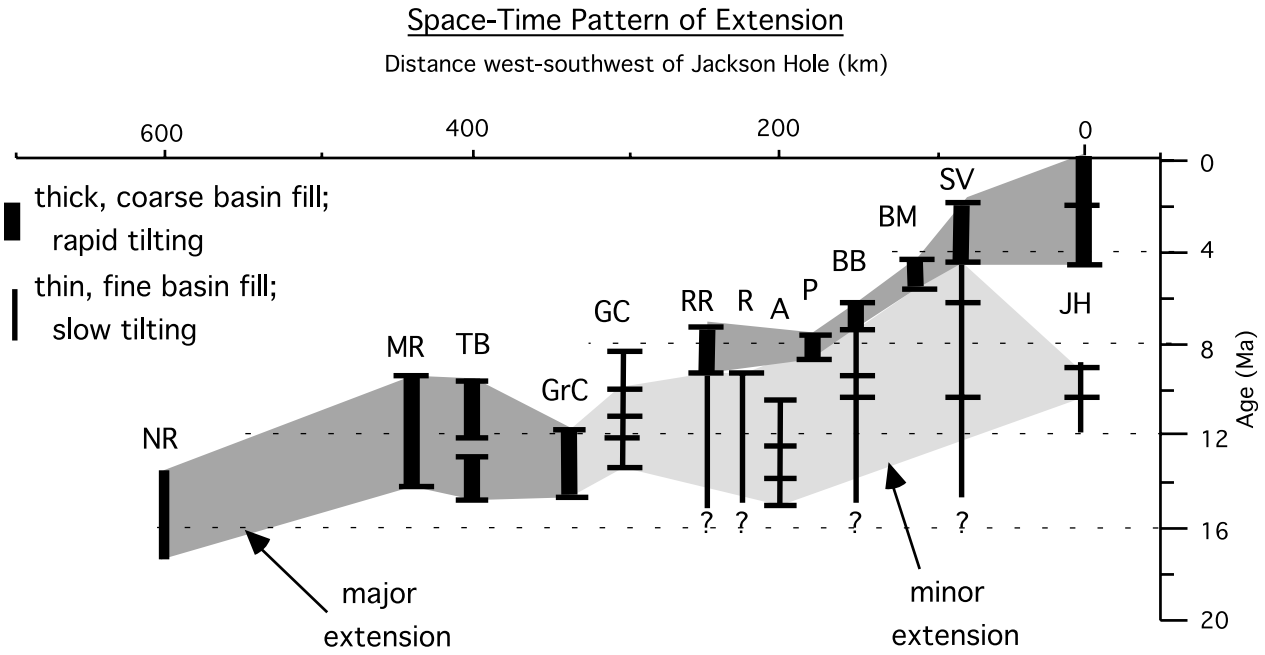

Figure 9. Interpreted age span of extension in specific localities across southern Idaho and adjacent Nevada and Wyoming. Horizontal bars indicate dated volcanic rocks. Extension manifested by dike injection (NR), relative rates of basin-fill tilting (SV), normal faults cut by volcanic rocks (BM), and the age span of basin fill (all other localities). Dark shading indicates a pulse of major extension and light shading a pulse of minor extension. Localities and sources of data include northern Nevada rift (NR; Zoback and Thompson, 1978), Mary's River (MR; Mueller and Snoke, 1993), Toano basin (TB; Mueller and Snoke, 1993), Grouse Creek Valley (GrC; Compton, 1983), Goose Creek Valley (GC; Perkins and others, 1995), Raft River Valley (RR; Williams and others, 1982), Rockland Valley (R; Trimble and Carr, 1976; this paper), Arbon Valley (A; Bobo, 1991; this paper), Portneuf Valley (P; this paper), Buckskin Basin (BB; Kellogg and Marvin, 1988), Blackfoot Mountains (BM; Allmendinger, 1982), Swan Valley (SV; Anders and others, 1989; Anders, 1990), and Jackson Hole (JH; Love, 1977; Love and others, 1992; Pierce and Morgan, 1992; Perkins and Nash, 1994). Figure modified from Rodgers and others (1990, 1994).

results of several studies undertaken to document the style, geometry, and timing of eastern SRP subsidence. These data, in conjunction with previous studies of the eastern SRP itself, provide a new view of crustal processes associated with magmatism and deformation.

Two types of eastern SRP subsidence will be discussed. Both are measured relative to rocks and elevations of the adjacent Basin and Range Province, not to an external reference plane such as sea level (England and Molnar, 1990). One type is rock subsidence, characterized by a decrease in vertical position. Where rock subsidence is accommodated via structural tilting we use the term crustal flexure. The other type is surface subsidence, characterized by a reduced elevation of the earth's surface. Where surface subsidence is manifested by regional topographic gradients, we use the term downwarping.

NORMAL FAULTING

Based on seismic velocity data from the 1978 Yellowstone-eastern SRP seismic experiment, Sparlin and others (1982), Braile and others (1982), and Smith and others (1982) suggested that the eastern SRP experienced subsidence by downdropping, half-graben style, along a normal fault at its northern margin. If the fault exists, it is concealed beneath the Quaternary basalts of the eastern SRP and thus unavailable for structural analysis. However, other northeast-striking normal faults are present just beyond the eastern SRP in the Basin and Range. To document fault style and geometry, Zentner (1989) mapped normal faults in the southern Beaverhead Range (Figure 2) where they offset Neogene ash-flow tuff whose distinct lithologies, instantaneous emplacement, and widespread lateral extent make them ideal for study. Zentner (1989) also used published maps adjacent to the entire eastern SRP to determine the lateral extent of similar faults. More recently, Kellogg (1990) and Rodgers and Othberg (1999) have mapped similar faults in the northern Portneuf and Bannock Ranges (Figure 2). The results of these studies are reported below.

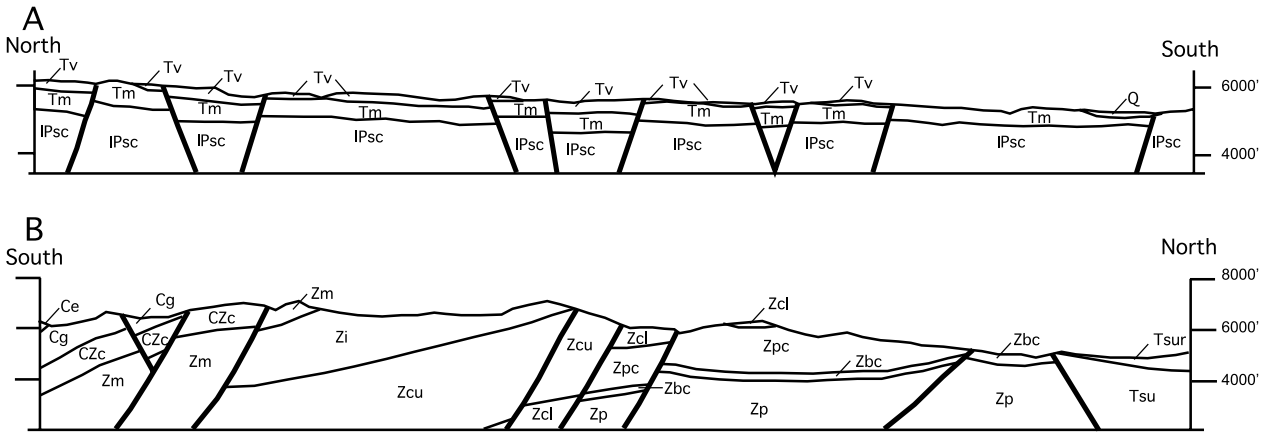

Figure 10. Cross sections showing fault patterns adjacent to the eastern SRP. A is north to south cross section near Lidy Hot Spring (located in Figure 2). B is south to north cross section in the northern Bannock Range (located in Figure 2). After Zentner (1989) and Rodgers and Othberg (1999).

Lidy Hot Springs, Southern Beaverhead Range

The Lidy Hot Springs area at the southern tip of the Beaverhead Mountains (Figure 2) contains a sequence of sedimentary rocks and ash-flow tuffs (Embree and others, 1982). Two distinct normal fault sets are apparent in the study area, a northwest-striking set and a northeast-striking set. The faults cut all rock units of the area, except the Quaternary gravel, and truncate each other at various locations throughout the field area.

The NNW-striking normal fault set comprises a series of faults spaced 0.1 to 0.7 km apart. No fault surfaces are exposed, but fault traces are located where formations are juxtaposed contrary to their depositional order. Strikes of faults in this set average N. 25º W.; their dips range from 55-65 degrees both northeast and southwest. Individual faults offset the ash-flow sheets as much as 250 m. Calculations of the area's width before and after extension show that the area was extended about 7 percent northeast-southwest by these faults. The age of the fault set is between the age of the youngest unit offset by faults (4.3-Ma tuff of Kilgore) and the age of the oldest unit (Quaternary alluvium) not offset. Because the normal faults are parallel to major Basin and Range normal faults in the region, they are interpreted to reflect Basin and Range extension.

The ENE-striking normal fault set (Figure 10) comprises faults that are spaced 0.3 to 0.7 km apart and generally extend several kilometers in length. They show no evidence of strike-slip movement, which discredits ideas that the eastern SRP represents a major strike-slip zone between regions of differential extension (Pratt, 1982). Strikes of the faults in this set average around N. 60º E., and their dips are 70-80 degrees both northwest and southeast. Individual faults offset the ash-flow tuffs up to 100 m. Calculations of the area's width before and after extension show that the area was extended only 2 percent northwest-southeast. Cross-cutting relations with rocks and the NNW-striking fault set indicate that both fault sets were active at the same time.

Northern Bannock Range

Northeast-striking normal faults were mapped in detail in the northern Bannock Range (Figure 2) by Rodgers and Othberg (1999) and in the northern Portneuf Range (Figure 2) by Kellogg (1990). Here, normal faults cut Proterozoic to Middle Cambrian strata that previously experienced both Cretaceous shortening and Basin and Range extension. The eastern SRP-parallel faults strike east-northeast to northeast, are spaced 1-5 km apart, dip moderately to steeply southeast, and typically show 100-1,000 m of normal slip (Figure 10). The cumulative result of fault offset is to uplift rocks in the north more than rocks in the south. The Bannock Range faults postdate regional tilting associated with 9-7.3 Ma basin formation, show a mutually cross-cutting relation with the range-bounding fault, and do not cut across 0.6 Ma basalt.

Normal Faults Along the Margins of the Eastern Snake River Plain

To document the regional extent and pattern of northeast-striking normal faults along the margins of the eastern SRP, Zentner (1989) compiled published geologic maps of areas within 50 km of it. As shown in Figure 11,

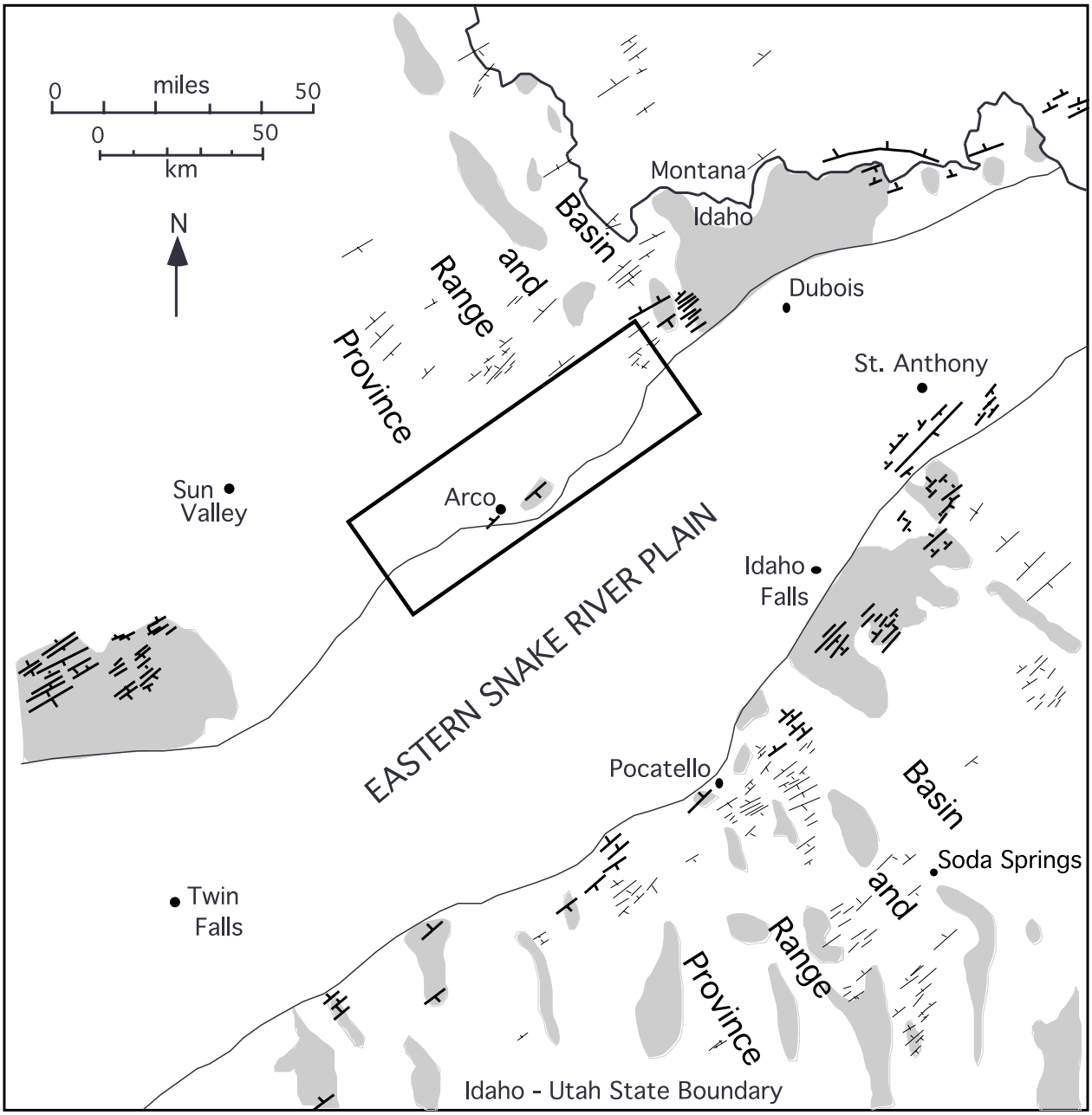

Figure 11. Compilation of northeast-striking normal faults adjacent to the eastern SRP from Zentner (1989). Faults that cut rocks older than 10 Ma are represented by thin lines, whereas faults that cut 10 Ma and younger rocks are indicated by thick lines. Distribution of Tertiary rocks younger than 10 Ma is shaded. Northeast-striking faults younger than 10 Ma are restricted to a 30-km zone adjacent to the eastern SRP. Rectangle is location of Figure 12. Sources of data include Albee and Cullins (1965), Armstrong and others (1978), Burgel (1986), Carlson (1968), Cluer and Cluer (1986), Corbett (1978), Cress (1981), Garmezy (1981), Hladky (1986), Kellogg (1990), Kellogg and others (1989), LeFebre (1984), Oriel (1980), Oriel and Moore (1985), Pierce and others (1983), Schmidt (1962), Skipp (1988), Skipp and others (1990, 1992), Trimble (1980), Trimble and Carr (1976), Waldrop (1975), Witkind (1972, 1976).

northeast-striking faults are present throughout southern Idaho, western Wyoming, and southwestern Montana and are both adjacent to and distant from the eastern SRP.

Because southern Idaho has experienced a protracted deformational history, northeast-striking faults in the region may have formed during Mesozoic thrusting, Neogene Basin and Range faulting, or Neogene development of the eastern SRP. To discriminate faults of different ages, northeast-striking faults that cut rocks younger than about 10 Ma are distinguished from faults that cut rocks older than 10 Ma (Figure 11). The ages of faults in pre-10 Ma rocks are uncertain: they may also be younger than 10 Ma, or they may be older than 10 Ma and therefore unrelated to the eastern SRP.

Figure 11 shows that northeast-striking faults younger than 10 Ma are restricted to two zones, each about 30 km wide, along the northern and southern margins of the eastern SRP. Tertiary rocks not cut by northeast-striking faults are more than 30 km from the eastern SRP margins, indicating that the zones of faults are situated near the margins of the eastern SRP. Because of their orientation, their proximity to the eastern SRP, and their similar age to the eastern SRP, these faults are inferred to be related to the development of the eastern SRP. Although the kinematics of these faults are in most places unknown, where they have been studied (Allmendinger, 1982; Smith, 1966; Hladky, 1986; Pogue, 1984) the faults show normal dip-slip displacements of less than 1 km. Thus, their style and geometry appear to be identical to the northeast-striking faults of the Lidy Hot Springs, Portneuf, and Bannock regions.

The age of the northeast-striking normal faults across the region is poorly constrained. Zentner (1989) and Allmendinger (1982) determined the age of faulting to be between 4.7 Ma and about 2.0 Ma, and Rodgers and Othberg (1999) bracketed the age of faults between 7.3 and about 0.6 Ma.

Interpretation of Northeast-Striking Normal Faults

Before this study, it was assumed that since the plain is a structural basin, the northeast-striking normal faults must have accommodated the downdropping of the plain (Sparlin and others, 1982). Certainly the structural parallelism of the northeast-striking normal faults and the axis of the eastern SRP, as well as the coeval development of the faults and eastern SRP, support the interpretation that the faults and eastern SRP are genetically related. Zentner's (1989) mapping, however, shows that the net vertical displacement along these normal faults is minimal, and many of the faults dip away from the eastern SRP's axis. Thus, the exposed northeast-striking normal faults clearly do not contribute to a structural downdropping towards the plain. Alternate interpretations of plain-parallel normal faults include (1) regional northwest-southeast extension, (2) faulting along caldera margins, (3) horizontal thermal contraction, and (4) extension related to crustal flexure. We believe the first three options are not supported by the distribution, geometry, and kinematics of faulting. However, the zone of normal faults is coincident with a zone of downwarping first described by Kirkham (1927, 1931). Recognizing the coincidence of faults and downwarped crust, Zentner (1989) proposed that the minor northeast-striking normal faults along both margins of the eastern SRP formed as the rigid uppermost crust flexed downward beneath the eastern SRP. As observed in foreland basins and subducting oceanic slabs (Turcotte and Schubert, 1982), such flexure would be accompanied by extensional structures of uniform orientation, restricted extent, and variable dips identical to the faults observed in this study. This interpretation is most consistent with the available data and is strongly supported by the more recent work of McQuarrie (1997; and summarized below), who measured the extent and amount of crustal flexure and confirmed that it was coincident with the zone of northeast-striking normal faults. Thus, the normal faults along the margins of the eastern SRP are interpreted to reflect extension due to crustal flexure.

ROCK SUBSIDENCE AND CRUSTAL FLEXURE

Subsidence of the eastern SRP and the associated downwarping and flexure of the adjacent Basin and Range are manifested by surface tilts and 1- to 20-degree structural dips of late Cenozoic rocks toward the eastern SRP (Kirkham, 1927, 1931; Trimble and Carr, 1976; Rodgers and Anders, 1990; Houser, 1992). To systematically measure the amount and distribution of crustal flexure and to interpret the mechanisms of eastern SRP crustal subsidence, McQuarrie (1997; and McQuarrie and Rodgers, 1998) completed a quantitative analysis of crustal flexure along the northwestern margin of the eastern SRP.

Crustal Flexure

Crustal flexure adjacent to the eastern SRP should cause Cretaceous fold hinges in Paleozoic rocks to tilt toward the plain. If these fold hinges were originally horizontal, the amount of flexure can be determined. McQuarrie (1997) measured the plunges of 313 Cretaceous fold hinges, and locally the dip of Neogene vol-

canic rocks, to quantify the amount of flexure. Fold data indicate a regular pattern of orientations: fold hinges trend southeast approximately perpendicular to the trend of the eastern SRP, plunge 0º-25º SE., and show a progressively increasing plunge to the southeast. After accounting for tilting due to Basin and Range extension, the fold data were contoured to smooth out irregularities, emphasize overall trends, and provide numerical values for areas with no measured folds. The map of contoured fold hinges shows a consistent pattern throughout the study area (Figure 12). The contour lines parallel the axis of the eastern SRP and define a narrow downwarped zone that extends approximately 10-20 km north of the eastern SRP. They also show a southeastward increase in plunge, to a maximum of 25º SE. A second-order trend is the prominent pattern of reentrants and salients that give a scalloped appearance to the contours. The reentrants make sharp curves inward on both the ranges (Pioneer Mountains and the Appendicitis Hills) and the intervening valleys (Little Lost River Valley and Birch Creek Valley) and have both closely and widely spaced contours (Figure 12).

Cross sections show that measured structural relief due to flexure is much greater than the 1.5 km indicated by topographic relief and that the structural surface de-

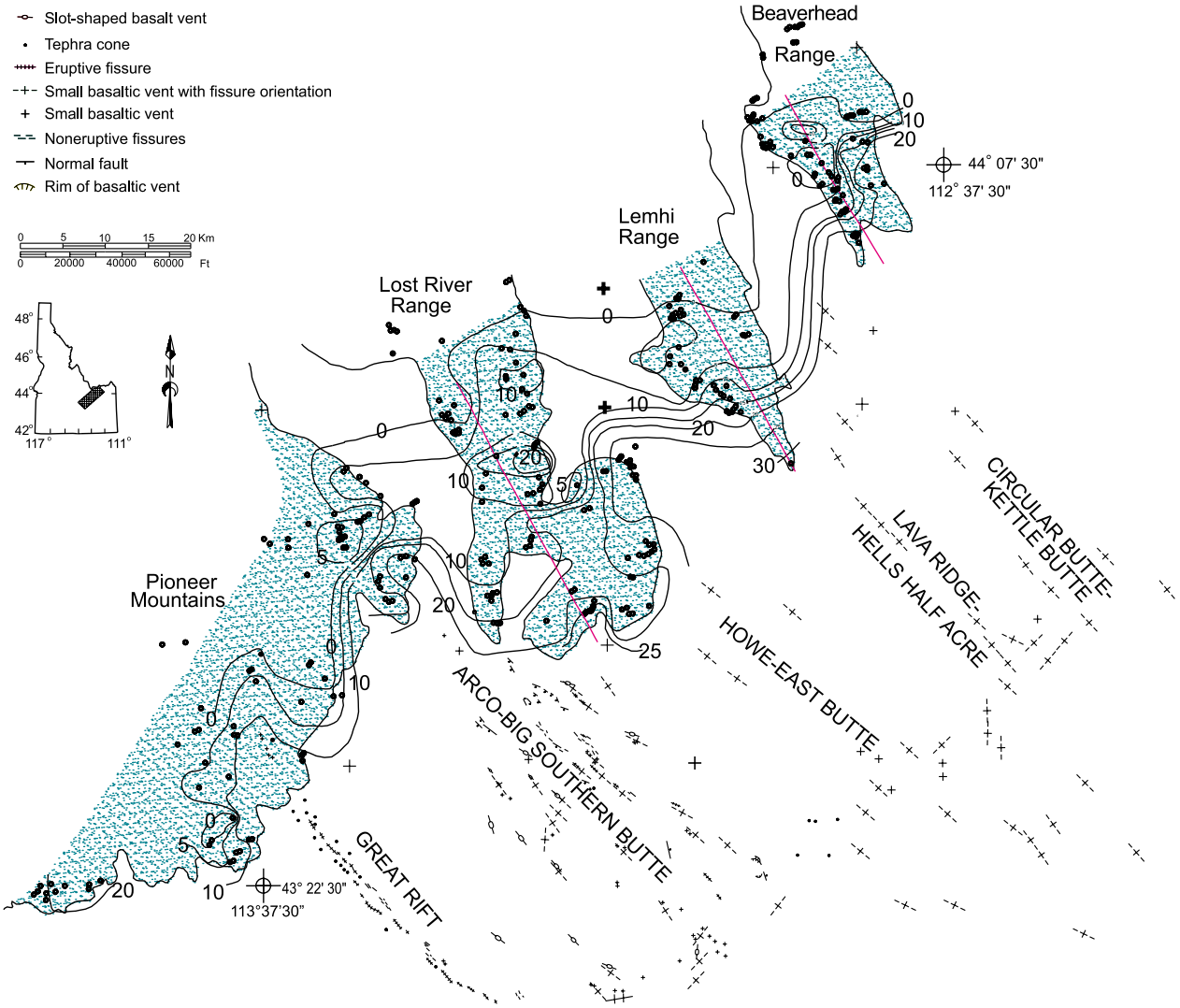

Figure 12. Summary of crustal flexure along the northern margin of the eastern SRP. Black dots in the ranges are locations where Cretaceous fold plunges were measured. Contours represent lines of equal southward fold plunge through the study area. The contour interval is 5º. Fold plunges increase from 0º to greater than 20º to the south. Also shown are Quaternary volcanic rift zones on the eastern SRP (after Kuntz and others, 1992), which emphasize their spatial correlation to reentrant contours. Location of figure is shown in Figure 11. Modified from McQuarrie (1997).

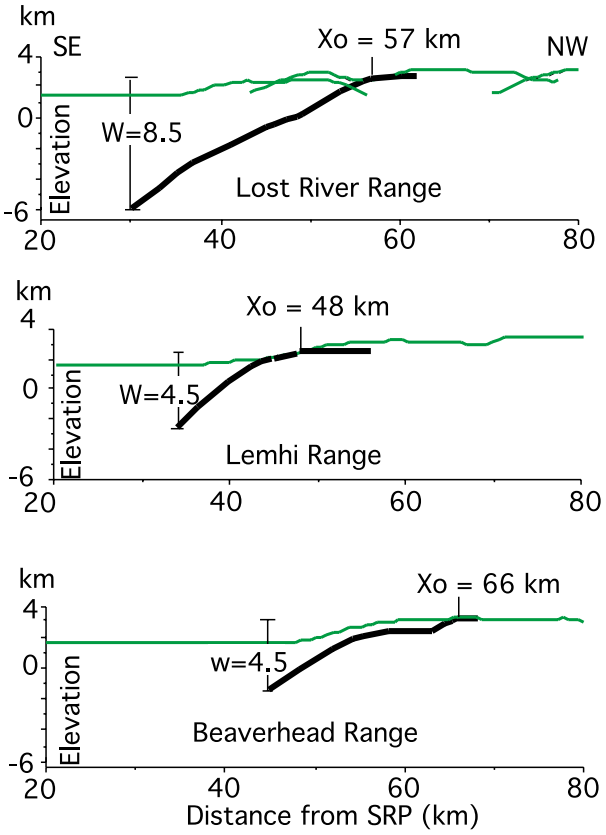

Figure 13. Cross sections of crustal flexure and topography along the northern margin of the eastern SRP. Topographic downwarping is shown by thin lines that are average elevations of ranges measured along each ridge crest. Crustal flexure is shown by bold lines that represent the projected plunge of folds measured along the surface. W = minimum amount of measured crustal flexure. X_0 is half-width of eastern SRP, measured from 0º plunge to eastern SRP axis. Sections are located in Figure 12. Figure from McQuarrie (1997).

lineated by plunge values does not parallel topography (Figure 13). Structural relief ranges from 4.5 to 8.5 km, amounts which represent the minimum rock subsidence of the eastern SRP with respect to the Basin and Range.

Crustal flexure has not been systematically examined beyond the study area of McQuarrie (1997), although such work is currently underway. The ubiquitous development of topographic downwarping along the eastern SRP margins is a good indication that crustal flexure everywhere flanks the eastern SRP and is supported by measurements of tilted structural markers elsewhere (Trimble and Carr, 1976; Houser, 1992; Rodgers, unpubl. data, 1995).

Eastern Snake River Plain Loading Mechanisms

The pattern of subsidence and downwarping reveals that a laterally extensive, crustal to lithospheric process has affected the greater eastern SRP region. McQuarrie (1997) and McQuarrie and Rodgers (1998) attributed regional subsidence of both rocks and the surface to the isostatic compensation of a load emplaced on or beneath the eastern SRP; the load is imposed by crustal layers that are thicker or denser than correlative layers in the adjacent Basin and Range. Loading by thermal contraction of the eastern SRP was rejected because heat flow is greater on the eastern SRP (107 mWm^{-2}) than on the adjacent Basin and Range (80 mWm^{-2}; Blackwell and others, 1992). Loading by the 5- to 8-km-thick sequence of basalts and underlying sediments and rhyolites, which constitute the "basin fill" of the eastern SRP, was also rejected because these rocks have relatively low densities (2.5 g cm^{-3} according to Sparlin and others, 1982). Loading generated by dense mafic rock that was emplaced into the eastern SRP crust is the preferred mechanism, and previous work suggests that such rocks are present at depth (Leeman, 1982; Sparlin and others, 1982; Greensfelder, 1981; Anders and Sleep, 1992).

Flexural Modeling

Flexural modeling was used to test the hypothesis that a dense crustal layer or layers beneath the eastern SRP could generate the appropriate load to produce the observed downwarping and flexure along the eastern SRP flanks and to provide a range of load dimensions that could produce the measured flexure as well as estimates of crustal strength and depth of compensation. A flexure model developed for the study of an aulocogen (Nunn and Aires, 1988) was applied to eastern SRP subsidence, with the exception that no extension was included. As reported in McQuarrie and Rodgers (1998) and shown in Figure 14, the main results of modeling include the following:

(1) Subsidence was isostatically compensated in the lower crust, not asthenosphere, because only crustal compensation allows for the development of a relatively narrow, deep basin like the eastern SRP. Compensation in the lower crust is supported by a flat Moho (Sparlin and others, 1982; Peng and Humphreys, 1998), by a close relationship between topography and Bouguer gravity suggesting compensation by plastic flow within the upper 20 km of the crust (Eaton and others, 1978), and by a high heat flow sufficient for partial melting or subsolidus grain-boundary relaxation of the lower crust (Greensfelder, 1981; Blackwell and others, 1992).

(2) The calculated strength of the Basin and Range crust is very low, as expected with such a high heat flow. Flexural parameters of 5-10 km are slightly lower than

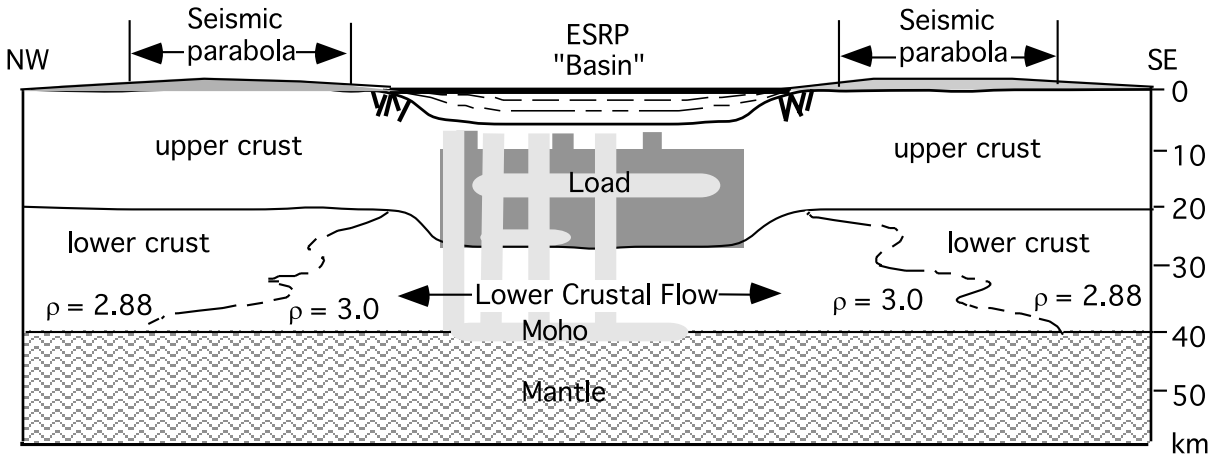

Figure 14. Summary figure depicting crustal flexure and subsidence associated with the eastern SRP. Figure shows (1) an extensive midcrustal load emplaced by 10 Ma (black area), (2) a post-Neogene load related to the volcanic rift zones (gray area), (3) 5-8 km of downwarped Basin and Range crust, (4) a northeast-striking fault set associated with flexure of the crust (Zentner, 1989), (5) an angular unconformity between the downwarped fold hinges and volcanic rocks of the SRP (dashed lines), (6) a flat Moho, and (7) lower crustal flow from beneath the eastern SRP to the extending Basin and Range (seismic parabola). Figure from McQuarrie and Rodgers (1998).

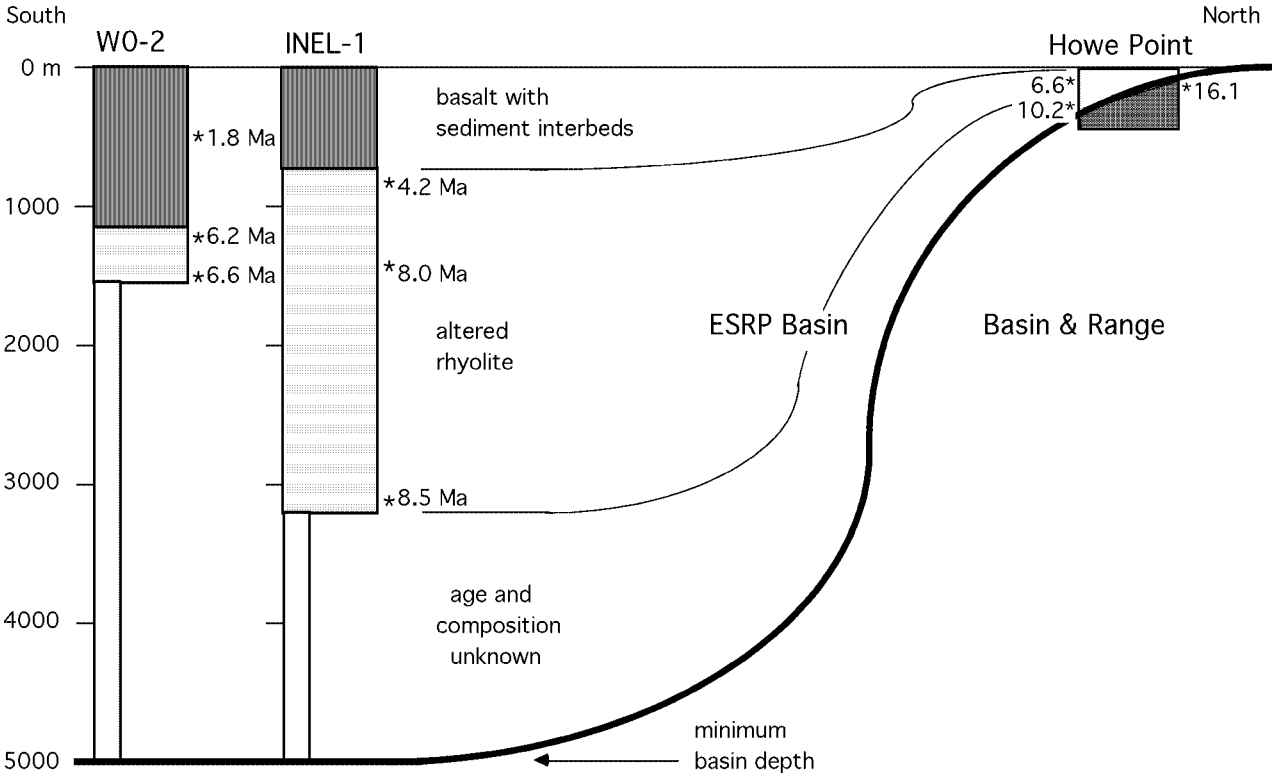

Figure 15. Schematic cross section along the northern margin of the eastern SRP showing age-depth relations of various horizons and rock units. See text for discussion. Data from Morgan and others (1984), Anderson and others (1997), McQuarrie and Rodgers (1998), and M. McCurry (oral commun., 1999).

previous estimates of about 12 km (Anders and others, 1993; Lowry and Smith, 1995), and much lower than that typical of cratonal regions.

(3) The eastern SRP crustal layering proposed by Sparlin and others (1982) would induce somewhat less subsidence and a wider depression than is actually observed. To produce a close match between model and actual flexure curves, a middle crustal sill must have a half width of 40-50 km, roughly coincident with the borders of the eastern SRP, and a thickness ranging from 17 to 25 km if its average density is 2.88 g cm^{-3}.

Age and Rate of Rock Subsidence

The age of initial rock subsidence is unknown because the oldest rocks in the eastern SRP basin have not been penetrated by drilling. Instead, two deep drill holes located south of the Lemhi Range on the eastern SRP provide partial evidence of the subsidence history of the eastern SRP. As shown in Figure 15, holes WO-2 and INEL-1 penetrated the basalt sequence and terminated in altered rhyolite. New ages of 8.0 and 8.5 Ma (SHRIMP U-Pb, zr) were obtained from rhyolite at depths of 1,482 m and 3,060 m in hole INEL-1 (M. McCurry, oral commun., 1999). These ages differ from preliminary fission track ages of identical rocks (Morgan and others, 1984) but are believed to be more accurate based on the improved methodology.

A rock subsidence curve can be compiled using the age-depth relations of volcanic rocks in INEL-1 and WO-2 (Figure 16). According to these data, 3.1 km of subsidence occurred since 8.5 Ma, and the remaining subsidence (between 1.4 and 4.4 km) occurred before 8.5 Ma. The smooth curve shown in Figure 16 indicates rapid (1.5 km/m.y.) subsidence before 8 Ma and slow (0.2 km/m.y.) subsidence since 8 Ma. If subsidence at INEL-1 was due to regional processes, the curve implies that regional eastern SRP subsidence started about 10 Ma. Alternatively, the rapid accumulation rate, rock texture (Morgan and others, 1984), and absence of correlative rocks in nearby ranges may be evidence that INEL-1 rhyolitic rocks accumulated in a fault-bounded basin, perhaps a caldera. In this scenario, the INEL-1 ages record significant local subsidence between 8.5 and 8 Ma and about 1.7 km of regional subsidence since 8 Ma. In this interpretation, most of the calculated regional subsidence (between 2.8 and 5.8 km) occurred before 8 Ma but is not manifested in the drill hole data.

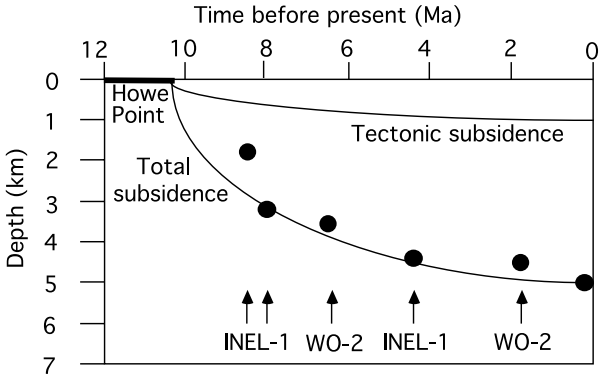

Figure 16. Eastern SRP subsidence graph constrained by INEL-1 and WO-2 well log data. Figure assumes 5 km of subsidence measured relative to correlative rocks in the adjacent Basin and Range (see Figure 13). The total subsidence is a combination of tectonic subsidence (due to midcrustal densification) and subsidence due to the weight of basin-filling volcanic and sedimentary rocks. Age-depth relations in WO-2 are from Hackett and others (1994) and Anderson and others (1997). Other data are from McBroome (1981), Morgan and others (1984), and M. McCurry (oral commun., 1999). Initial subsidence at Howe Point (16-10 Ma) from Figure 7.

SURFACE SUBSIDENCE AND TECTONIC GEOMORPHOLOGY

The eastern SRP and surrounding regions are characterized by axial drainage, wherein tributary streams flow toward the eastern SRP and its trunk river, the Snake River, which itself flows southwest along the axis of the eastern SRP. This geomorphic system reflects tectonic processes, including first-order surface subsidence and second-order fault and volcanic rift patterns, and climatic processes. Because the drainage system is strongly influenced by regional surface subsidence, we can use it to study subsidence through time. In particular, the extent and initiation of surface subsidence should be recorded by the extent and age of axial drainage development. To this end, a region immediately south of the eastern SRP was studied to describe landscape evolution during eastern SRP development. The study area encompasses Arbon Valley to the Portneuf Range including two streams, the Portneuf River and Bannock Creek (Figure 2).

Maximum Basin Filling

A low gradient surface is perched at higher elevations in the northern Bannock Range (Figure 17), as much as 900 m above the eastern SRP. Near Kinport Peak, the surface cuts across tilted Proterozoic rocks, whereas to the south it cuts across tilted Miocene basin fill. The surface is generally undissected by modern streams and is overlain by rare but distinctive white quartzite cobbles derived from the Ordovician Swan Peak Quartzite. The surface is fringed by dissected, lower-elevation terrain

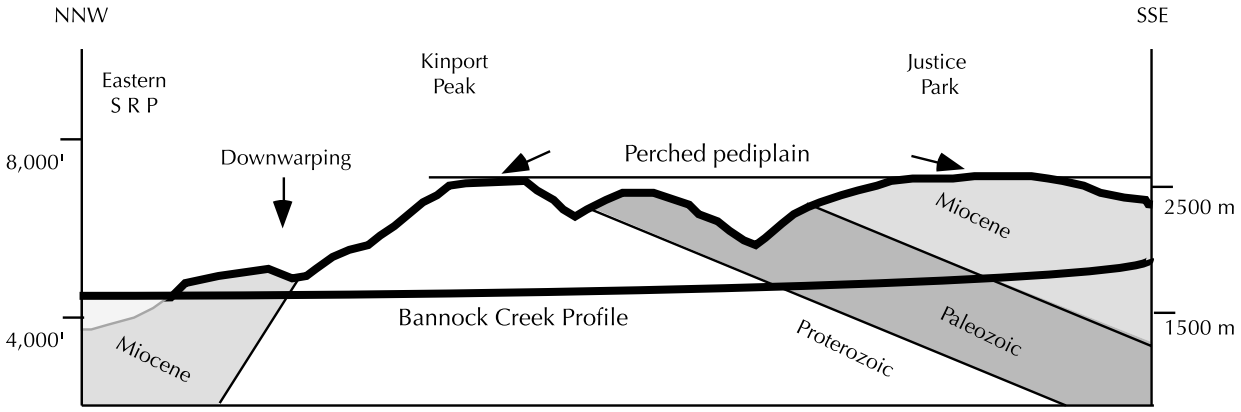

Figure 17. Schematic cross-section of high-level pediplain surface in northern Bannock Range. Surface is at an elevation of about 7,200 feet and cuts across east-tilted Proterozoic, Paleozoic, and Miocene rocks. South of Kinport Peak, the vertical distance between the mountain profile and the superimposed Bannock Creek profile represents the maximum incision interpreted for valleys like Arbon Valley and Portneuf Valley. North of Kinport Peak, crustal flexure and downwarping has occurred. Location of cross section shown in Figure 2. Vertical exaggeration is about 5.

that ultimately grades to the Portneuf River and Bannock Creek.

The perched surface and overlying cobbles are interpreted to be a regional pediplain with lag concentrate resulting from fluvial processes. The surface, although discontinuous and irregular today, must have been laterally continuous across the northern Bannock Range and must have formed after Basin and Range tilting was completed (post-7.3 Ma; Figure 9). The profound implication is that after Basin and Range faulting ceased the top of the northern Bannock Range and the Portneuf and Arbon valleys were at the same elevation as one another and as the eastern SRP. Miocene basin fill must have filled the valleys to the tops of the intervening ranges, 800 to 900 m above the modern valley floors. An alternative explanation, that the terrace was uplifted relative to the modern valleys during renewed Basin and Range faulting, is untenable because (1) basin fill is present immediately below the terrace, (2) the terrace is at similar elevations on either side of a major Basin and Range fault, and (3) the horizontal terrace shows no indication of eastward tilting that would accompany faulting. Our preferred interpretation is that basin fill accumulated to the level of the pediplain and that this low-relief surface may have been graded to the eastern SRP before its surface subsided, or to a regional base level to the east. Paleocurrent information relating to processes on this surface has not been found.

Basin Emptying

The Bannock and Portneuf rivers are consequent streams that flow north to the Snake River. The rivers flow parallel to the structural grain imparted by rocks

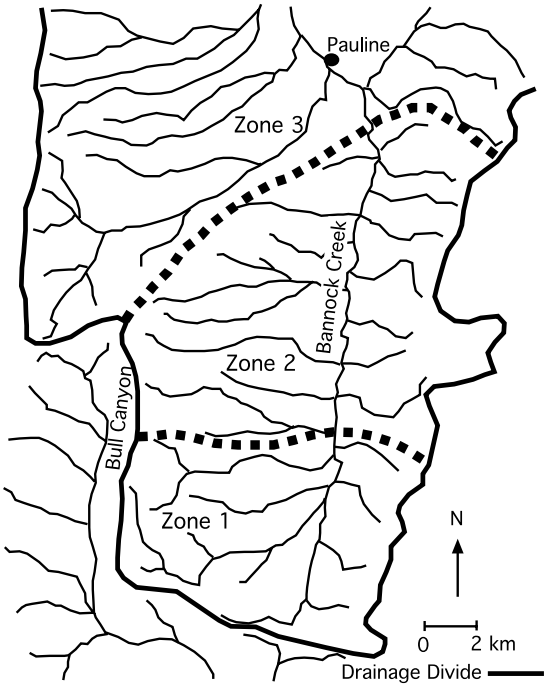

Figure 18. Bannock Creek drainage patterns in southern Arbon Valley. Location shown in Figure 2. Tributary streams in zone 1 have "barbed" confluence angles with Bannock Creek, and other streams undergo an abrupt change in direction from south to north. Tributaries show perpendicular confluence angles in zone 2 and acute confluence angles in zone 3. A related geomorphic feature is the offset drainage divide in the Deep Creek Range: Knox Canyon discharges into Arbon Valley, and Bull Canyon discharges south into the Bonneville Basin, but the divide that separates the two is 10-12 km north of the Arbon Valley divide. The drainage patterns are interpreted to reflect headward (southward) erosion of Bannock Creek. Headward migration and progressive stream capture are recorded where streams incise nonresistant gravels, but where streams incise resistant bedrock the divide is relatively fixed. The Arbon Valley divide has migrated 10 km south since incision into bedrock and about 23 km south since the early to middle Pleistocene terraces of Arbon Valley were formed. From Bobo (1991).

and faults, preferentially incising nonresistant late Cenozoic basin fill and impeded by bedrock horsts. By incising the land, they have created subsequent valleys such as the Marsh Creek, Portneuf, and Arbon valleys (Figure 2). In these young valleys, Miocene basin fill from 0 to 600 m below the pediplain is generally absent, and basin fill from 600 to 900 m below the surface is partially incised or concealed beneath younger deposits.

We attribute valley incision to surface subsidence of the eastern Snake River Plain and the ancestral Snake River that flowed over it; the reduction in base level of the Bannock and Portneuf rivers induced significant downcutting by these tributary streams. In this scenario, widespread erosion occurred first but was later replaced by several smaller cut-and-fill cycles, which we interpret to reflect the second-order effects of Pleistocene climate change and basaltic volcanism on the eastern SRP.

The age of incision and inferred surface subsidence has not been systematically studied. Incision by the Portneuf River system began after 7.3 Ma, the youngest age of basin fill beneath the pediplain. About 700 m of incision was completed before a prominent bajada surface developed along the Portneuf River, which is interpreted to be early to middle Pleistocene (Scott, 1982). About 900 m of incision was completed when the ancestral Portneuf River channel was filled by the Portneuf Valley basalt, which yielded a whole rock K-Ar date of 580 Ka (Pierce and Scott, 1982). The base of the basalt is at the same level as the modern Portenuf River, evidence of minimal incision since that time. The age of incision by Bannock Creek is partially recorded near its headwaters, where the drainage pattern is interpreted to record 23 km of headward migration induced by base level change (Figure 18; Bobo, 1991). Because the incised substrate is alluvial gravel of early to middle Pleistocene age (Scott, 1982), migration is interpreted to be the result of middle to late Pleistocene surface subsidence of the eastern SRP. Other mechanisms of base level change, such as localized incision of eastern SRP basalts by the Snake River or pluvial lake formation in the Bonneville Basin, may have been contributing factors as well.

DISCUSSION

CRUSTAL DEFORMATION MODEL

In an earlier paper (Rodgers and others, 1990, p. 1,140), we proposed a model of eastern SRP deformation that emphasized extension and the role of a mantle plume:

> *East of the locus of volcanism, the crust extended by normal faulting at shallow levels and ductile attenuation at depth. Sedimentary basins formed and were filled by horst-derived clastic detritus. Basins east-northeast of the locus of volcanism were progressively obliterated as the continent drifted over the plume, but basins north or south of the path of volcanism were preserved. Over the plume, the crust extended by normal faulting at very shallow levels and magma injection at depth. North and south of the plume, the crust continued to extend by faulting and ductile attenuation, resulting in basins filled with plume-derived volcanic detritus. West of the plume, minor extension in the volcanic province was accommodated by the injection of basalt dikes and by rare normal faults.*

Some revision of this model is needed to account for the space-time patterns of extension and subsidence summarized in this paper and by Pierce and Morgan (1992) and McQuarrie and Rodgers (1998). As before, deformation is described in relation to transgressing silicic volcanism (Figure 19). Data and interpretations used to build the new model are summarized in Figure 20, and the new model is illustrated in Figure 21 and described below. The model is predicated on the interpretation that rocks and structures similar to those beside the eastern SRP were formerly present on the eastern SRP, but have since subsided and been covered by younger volcanic and sedimentary rocks.

Stage 1 (16-11 Ma)

In the initial stage of deformation, the "proto-eastern SRP" was characterized by half-graben development. Basin fill included thin sequences of carbonate rocks, fine-grained clastic rocks, air-fall tuff and rare basalt that compose the Beaverdam Formation in Goose Creek, the lower Starlight Formation in Arbon Valley, the Medicine Lodge beds throughout the northeast margin of the eastern SRP, and the Teewinot Formation in Jackson Hole. The rocks accumulated in lacustrine and fluviolacustrine environments and were flanked by mountains or highlands, as shown by the uncommon intercalation of pebble conglomerate and by regional facies patterns in at least two basins (Goose Creek and Birch Creek) indicative of Basin and Range morphology. Sedimentation rates of 50-80 m/m.y. are interpreted to reflect slow basin subsidence due to slow rates of extension. Available age constraints (Figure 9) indicate the basins existed from 16 to 9 Ma overall, with basin initiation from 16 to about 11 Ma and an east-migrating basin cessation from 11 to 9 Ma.

Rocks in the lower Starlight Formation and Medicine Lodge beds are not areally restricted to individual half grabens, but they are restricted to the margins of the east-

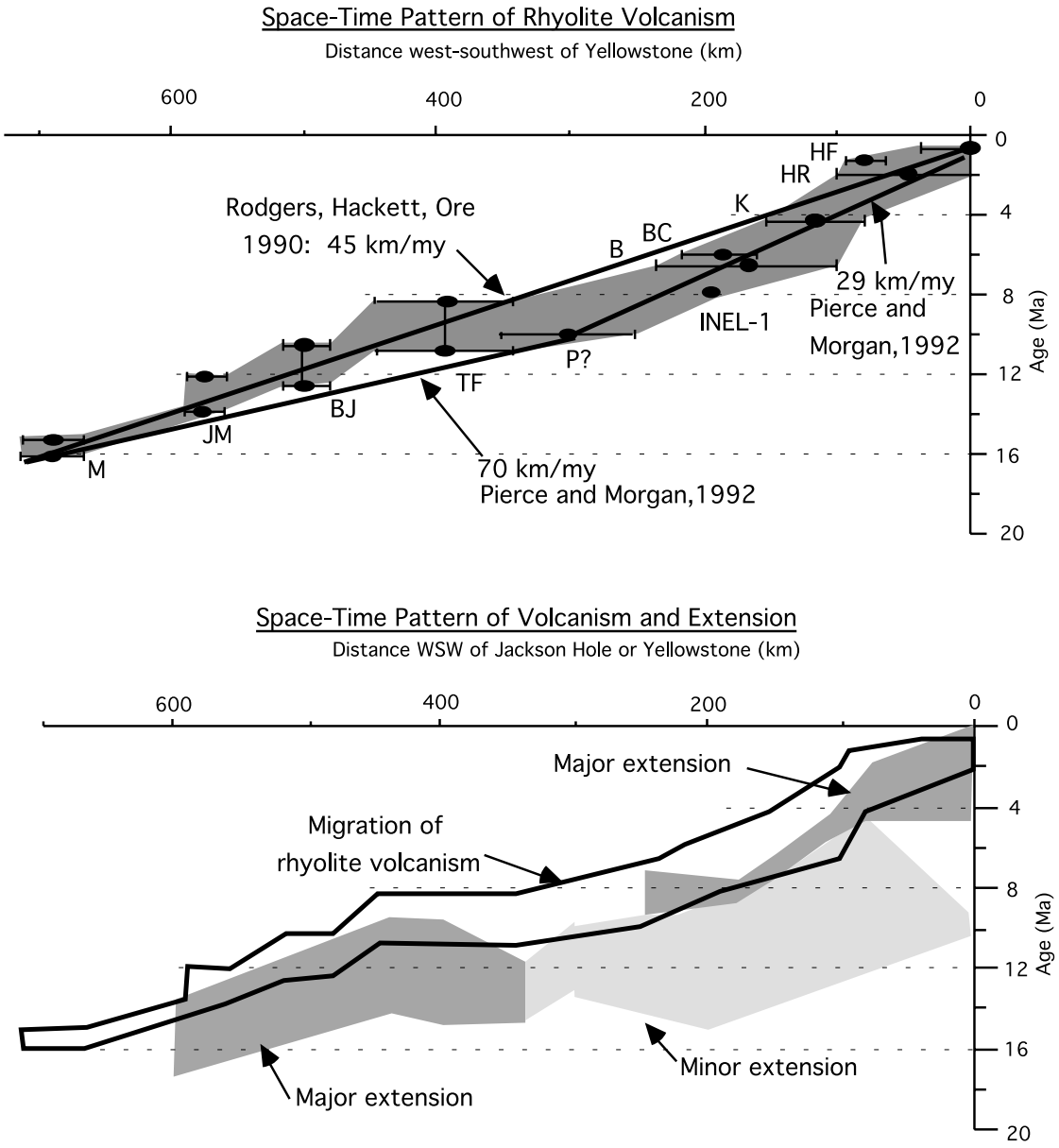

Figure 19. Space-time pattern of rhyolite magmatism and its relation to extension (see Figure 9). The duration of rhyolite magmatism from the Owyhee Plateau to Yellowstone Plateau is shown, including the following volcanic fields and calderas: McDermitt (M), Juniper Mountain (JM), Bruneau-Jarbidge (BJ), Twin Falls (TF), Picabo (P), INEL-1 drill hole, Blacktail (B), Blue Creek (BC), Kilgore (K), Huckleberry Ridge (HR), Henry's Fork (HF), and Yellowstone. The eastward migration of silicic magmatism is a first-order pattern of the eastern SRP, supported by most data with the following caveats: (1) well WO-2 on the INEEL was drilled within the inferred caldera of the 6.6 Ma tuff of Blacktail but met a Blacktail outflow sheet instead of intracaldera fill (Hackett and others, 1994); (2) wells INEL-1 and WO-2 intersected thick rhyolite units that were previously undocumented along the eastern SRP margins (Hackett and others, 1994, M. McCurry, oral commun., 1999) indicating the marginal record is incomplete here and possibly elsewhere; (3) the 10.2 Ma tuff of Arbon Valley (from the Picabo caldera) is petrologically distinct (Trimble and Carr, 1976; Kellogg and others, 1994) and perhaps petrogenetically distinct from other eastern SRP rhyolites; and (4) silicic magmatism was widespread across the central and eastern SRP from 8.5-11.5 Ma. Neogene rhyolite magmatism migrated northeast at a constant rate (Armstrong and others, 1975; Rodgers and others, 1990) or two constant rates before and after 10 Ma (Pierce and Morgan, 1992). Note that the difference between Pierce and Morgan's volcanic migration rate (29 ± 5 km/m.y.) and the Basin and Range extension rate (4-6 km/m.y; see Figure 4) is equivalent to the independently calculated North America plate migration rate of 22 ± 8 km/m.y. (Gripp and Gordan, 1990), evidence in support of a hot-spot origin for the eastern SRP. Sources of data include Bonnichsen (1982), Christiansen (1984), Ekren and others (1982, 1984), Kellogg and others (1994), Morgan and others (1984), Perkins and others (1995), Pierce and Morgan (1992), Rytuba and McKee (1984), and sources listed in Figure 9.

ern SRP. In addition, the age and lithologies of these two units are identical at two points (Trail Creek and Howe Point; Figure 2) on opposite margins. A speculative hypothesis is that the smaller half-graben basins were integrated across the proto-eastern SRP, and that integration was due to regional subsidence. Documenting regional subsidence during stage 1 would be significant because it could relate stages 1 and 2: Subsidence was induced by regional dike injection and densification of the crust, which heated and weakened the lower crust allowing the upper crust to fail in extension and form minor half grabens. After a few million years of dike injection, regional

Feature	Description	Evidence	Reference
Late Quaternary Rift Zones			
Width and distribution	Narrow, discrete	Exposed vents and fisures	1
	Broad, diffuse	Exposed and subsurface vents	2
Extension direction	W to WSW	Trend of rift zones	
Extension amount	Unknown		
Neogene-Late Quaternary Normal Faults			
Cumulative extension			
Direction	W to WSW	Strike of normal faults	
Amount	20% (south), 10-15% (north)	Restored cross sections	Figs. 3 & 4; 4
Older extension			
Amount	Inferred minor	Thin, fine-grained clastic and carbonate basin fill Sedimentation rates of 50-80 m/m.y.	3
Age	Migrated ENE through time began 16 to 10 Ma ended 11 to 9 Ma	Age of basin fill, south margin	Fig. 9
Relation to volcanism	Prior to initial silicic eruptions	Space-time pattern	Fig. 19
Younger extension			
Amount	Inferred major	Thick, coarse-grained clastic basin fill Sedimentation rates of 100-300 m/m.y.	3
Age	Migrated ENE through time began 10 Ma, ongoing today	Age of basin fill, south margin	Fig. 9 5, 6
	Migrated outward from SRP	Age pattern of rapid tilting of basin fill	7
Relation to volcanism	Preceding and beside initial silicic eruptions	Space-time pattern	Fig. 19
Neogene-Quaternary Rock Subsidence			
Amount	4.5 to 8.5 km Decreases north to south(?) Increases near Pleistocene rifts	Crustal flexure, north margin	8
Age	Began 16-10 Ma, ongoing today	Howe Point unconformity	Fig. 7
Rate	Decreases through time	Subsidence curve	Fig. 16
Relation to magmatism	Coeval and after silicic eruptions	Age-depth relations in INEL-1 drill hole	Fig. 15
	Coeval with midcrustal intrusion	Subsidence model	8
	Coeval with basaltic eruptions		
Neogene-Quaternary Surface Subsidence			
Amount	900 m Unknown along north margin	Pocatello perched pediplain, incised valleys	Fig. 17
Age	Younger than 7.3 Ma	Age of basin fill below Pocatello terrace	3
Relation to volcanism	After silicic eruptions Coeval with basaltic eruptions	Age of rhyolite near Pocatello	

References:
(1) Kuntz, 1992; (2) Wetmore and others, 2000; (3) this paper; (4) Janecke, 1993; (5) Rodgers and others, 1990; (6) Pierce and Morgan, 1992; (7) Anders and others, 1989; (8) McQuarrie and Rodgers, 1998

Figure 20. Summary of Miocene to Quaternary deformation, eastern SRP.

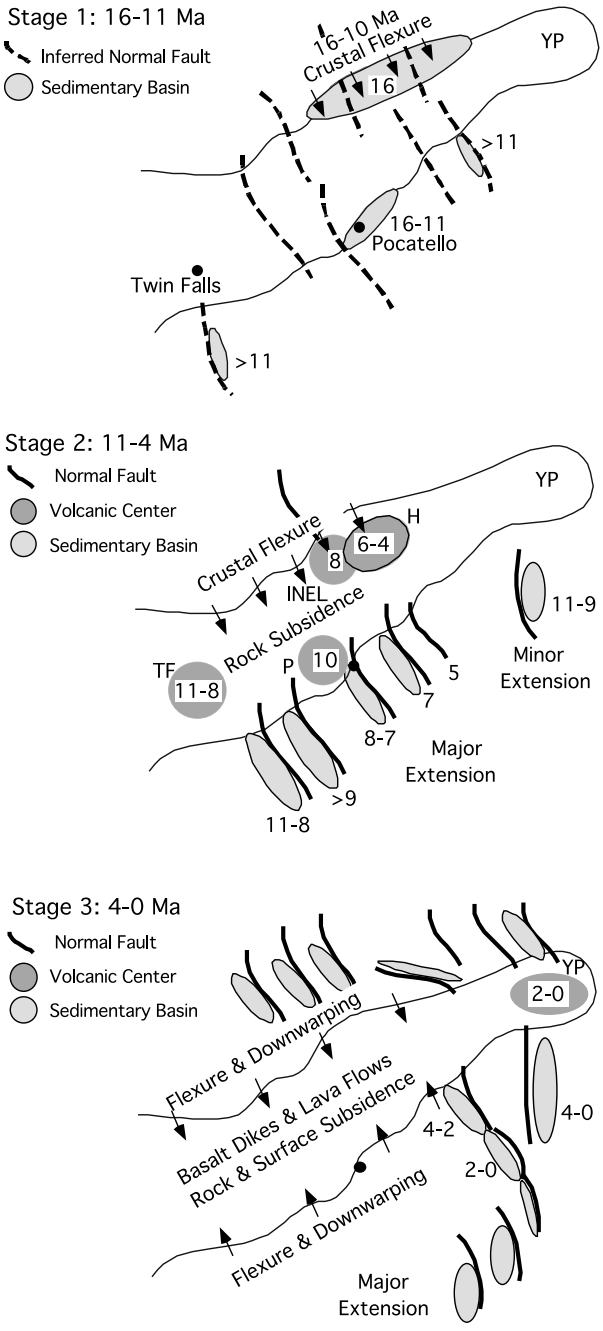

Figure 21. Schematic maps of the eastern SRP showing the space-time pattern of extension, subsidence, sedimentation, and volcanism during deformational stages 1, 2, and 3. The ages (shown in millions of years) associated with each deformational event are useful approximations, but because of the transgressive nature of tectonism they may not be accurate for all locations. Major silicic volcanic centers include Twin Falls (TF), Picabo (P), INEL-1 drill hole (INEL), Heise (H), and Yellowstone Plateau (YP). Data and references presented in Figures 9 and 19.

subsidence, and upper crustal extension, partial melting of the lower crust created silicic melts that erupted periodically across the region during stage 2.

Stage 2 (11-4 Ma)

In the second stage of deformation, a major pulse of extension swept eastward from longitude 115° to its current position on the Yellowstone Plateau. The upper crust extended by normal faulting, and the lower crust presumably extended and thinned by lower crustal flow and dike injection. Extension is manifested along the eastern SRP margins by half grabens with distinctively thick sequences of clastic rocks including the upper Starlight Formation in Raft River Valley, Rockland Valley, Arbon Valley, Portneuf Valley, and Buckskin Basin. Sedimentation rates of 100-300 m/m.y. are interpreted to reflect rapid subsidence and rapid rates of extension. Extension is also manifested by normal faults in the Blackfoot Mountains, by rapidly tilted basin fill in Swan Valley, Grand Valley, and Jackson Hole, and by current patterns of seismicity, elevation, and Quaternary faults in the circum-eastern SRP. Cumulative extension along the eastern SRP margins, which decreases slightly from south (20 percent) to north (10-15 percent), mostly occurred during this event. The extension rate was 4-6 km/m.y. from 11 to 0 Ma (depending upon how much extension occurred from 16-11 Ma versus 11-0 Ma). As measured along the southern margin of the eastern SRP, this extensional event migrated eastward from 11 to 0 Ma, preceding and beside initial silicic magmatism at any one place on the eastern SRP (Rodgers and others, 1990; Pierce and Morgan, 1992). Based only on data from southern Birch Creek Valley (Figure 7; Rodgers and Anders, 1990), extension was coeval along the north margin.

The eastern SRP experienced significant rock subsidence with respect to the adjacent Basin and Range. At least 4.5 km total subsidence occurred near the north margin and was accommodated by a narrow zone of crustal flexure and northeast-striking normal faults. Rock subsidence along the southern margin has not been studied, although northeast-striking normal faults and downwarping are widespread there. Regional subsidence was driven by the emplacement of dense mafic dikes and sills in the middle crust and accentuated by the accumulation of volcanic and sedimentary rocks on the surface (Figure 16). Most of the subsidence along the north margin occurred during or before local silicic magmatism from 8.5 to 6.0 Ma (Figure 21), evidence that the midcrustal sill formed during or before the pulse of silicic magmatism.

Silicic volcanism and thermal expansion may have

created a (migrating?) topographic highland, similar to the modern Yellowstone Plateau, across some of the eastern SRP (Fritz and Sears, 1993), but more paleocurrent data from marginal half-graben basin fill are needed to document this. East of and beside silicic volcanism on the plain, half grabens that formed during the extensional pulse probably created a rugged Basin and Range topography characterized by north-trending valleys and mountains. However, the rugged landscape experienced truncation and filling near the end of Stage 2 as shown by the presence of a regional pediplain across mature half grabens in the northern Bannock Range.

Stage 3 (4-0 Ma)

In the third stage of deformation, the eastern SRP has experienced dike injection, rock subsidence, and surface subsidence. Extension via upper crustal dike injection has occurred beneath volcanic rift zones (Rodgers and others, 1990; Hackett and others, 1996). Exposed rift zones are rather sharply defined (Kuntz and others, 1992), but the distribution of late Pleistocene subsurface vents is more diffuse (Hughes and others, this volume). The direction of extension changes within the southeastern half of the eastern SRP: ranges south of here trend north, whereas volcanic rift zones north of here trend northwest, and the Great Rift itself bends in this region (Pierce and Morgan, 1992, and references therein). The amount of extension shows a similar pattern of change. The southeastern edge of the eastern SRP appears to be the locus of lowest strain, with extension increasing gradually and symmetrically away to the arcuate zones of seismicity, high topography, and active Quaternary faults documented by Anders and others (1989) and Pierce and Morgan (1992). Indeed, calculations suggest that the amount of strain via dike injection on the plain is the same order of magnitude as that accommodated by normal faults north of the plain (Parsons and others, 1998).

Rock subsidence has continued during stage 3, but the amount and rate of subsidence (about 1,000 m in 4 m.y.) have been significantly less than that during stage 2. Quaternary subsidence is indicated along the northern margin of the plain where flexure contours define a pattern of reentrants that coincide with late Quaternary volcanic rift zones (Figure 12), and along the south margin where the Pleistocene Raft Formation is gently tilted northward (Houser, 1992). Cumulative rock subsidence has been at least 4.5 km, evidence of a midcrustal dike and sill complex at least 17 km thick. As in stage 2, subsidence during stage 3 has been accommodated at deeper levels by the ductile flow of lower crust to the Basin and Range from the eastern SRP.

Surface subsidence and the emplacement of basalt lava flows have created the modern eastern SRP during stage 3. Surface subsidence is manifested by downwarping of rocks along both margins of the plain, by axial drainage throughout the region, by as much as 900 m of incision of a perched pediplain near Pocatello, by drainage reversals of streams tributary to the Snake River, and by theodolite surveys of the modern surface (Reilinger and others, 1977). The age of surface subsidence is only known to be younger than 7.3 Ma, although further study may significantly improve the constraints. Basalt thins and the plain increases in elevation to the east (Brott and others, 1981), evidence of an eastward migration of basalt volcanism and subsidence during stage 3.

CRITIQUE OF TECTONIC MODELS

The revised deformation model can be used to test various tectonic models for the origin of the province. Tectonic models for the origin and development of the SRP-Yellowstone system include a propagating rift (Hamilton, 1987; 1989), a crustal flaw (Eaton and others, 1978), a transform fault (Christiansen and McKee, 1978), an origin by meteorite impact (Alt and others, 1988), a hot-spot track (Morgan, 1972; Suppe and others, 1975; Pierce and Morgan, 1992, and references therein), and a self-propagating convective melt (Saltzer and Humphreys, 1997). All but the last model were critiqued in detail by Pierce and Morgan (1992), who concluded that a two-phase hot-spot model was uniquely supported by most of the magmatic, deformational, geophysical, and sedimentary data. Without repeating the discussion of Pierce and Morgan (1992), what follows is a brief critique of the tectonic models (except the crustal flaw and meteorite impact models, for which we have no relevant data) based upon the space-time relations described in this paper.

Eastward-Propagating Rift

We have found no faults that accommodated downfaulting of the eastern SRP, nor have we observed northeast-striking dikes while mapping along its margins. Flexure along its margins is similar to monoclines that border a few rifts (Sengor, 1995), but flexure is interpreted to reflect vertical subsidence of the eastern SRP without horizontal (NW-SE) extension. In a few localities, we have documented mutual cross-cutting relations between Basin and Range faults and flexure-related normal faults, indicating NE-SW extension and crustal flexure occurred synchronously. Eastern SRP-parallel normal faults in the adjacent Basin and Range Province show only minor offset and are interpreted to be a consequence

of crustal flexure (Zentner, 1988), not regional NW-SE extension. Overall, the structural data of the region provide little support for interpreting the eastern SRP as an eastward-propagating extensional rift (Hamilton, 1987, 1989).

Transform Fault at the Northern End of the Basin and Range

Nowhere along the margins of the eastern SRP have we or others identified eastern SRP-parallel strike-slip faults, orographic bending, or minor pull-apart basins that would indicate lateral offset of the crust (see discussion in Pierce and Morgan, 1992). The amount of Basin and Range extension diminishes slightly to the north, and the direction changes by 30 degrees, but these are small differences that do not require a transform system. Crustal flexure has affected both margins of the eastern SRP: documented flexure on the north side appears greater than the estimated flexure on the south side, but again the small difference in kinematics does not require a transform system. Further work is needed to document the inception of Basin and Range faulting on the north side of the eastern SRP and to seek a significant age difference between initial extension on the north and south, but the available data are in favor of a broadly symmetrical pattern of extension and subsidence through time.

Mantle Plume or Self-Propagating Convective Instability

Much of the history outlined in this paper is compatible with previously proposed models that the eastern SRP marks the passage of North America over a mantle plume (Pierce and Morgan, 1992, and references therein) or self-propagating convective instability (Saltzer and Humphreys, 1997), now located beneath the Yellowstone Plateau. In particular, these models are well-supported by the space-time patterns of extension, subsidence, and tectonic geomorphology manifested during stages 2 and 3 of the deformation model presented above. The models differ from one another in mantle dynamics and kinematics: the plume model incorporates a deep mantle source, whereas the instability model involves lengthwise convection cells in the asthenospheric mantle that are instigated by lithospheric shear (Saltzer and Humphreys, 1997). However, the models as currently conceived are indistinguishable in crustal dynamics and kinematics: the crust of the eastern SRP, Yellowstone Plateau, and adjacent Basin and Range would host the same deformational processes and experience the same deformational history in either case.

We conclude by emphasizing that whatever tectonic model is ultimately chosen for the eastern SRP, that model must incorporate crustal deformation before silicic volcanism. Half-graben normal faulting occurred in front of and prior to silicic volcanism in any one location. Regional rock and surface subsidence may have preceded silicic volcanism as well, although more evidence is needed to document this process. The leading edge of the migrating Yellowstone system was manifested on the surface by crustal extension and basin formation, and possibly by mafic plutonism at depth.

SUGGESTIONS FOR FUTURE WORK

The deformational model outlined in this paper is supported by evidence of the style, kinematics, and timing of extension and subsidence observed in isolated places along the margins of the eastern SRP. The model should be tested and revised by completing similar studies in many more places along the margins. Some suggestions include:

(1) Determine the ages of initial and rapid extension along the north margin of the eastern SRP by describing and dating half-graben basin fill in several locations and by measuring the angular unconformities between different units.

(2) Estimate the amount of crustal flexure along the south margin by measuring fold plunges or tilted Miocene rocks and calculating a best-fit flexural curve.

(3) Estimate the rate of crustal flexure along the north and south margins by measuring the angularity across unconformities in differentially flexed Neogene rocks.

(4) Document the age and amount of surface subsidence along the south and north margins wherever appropriate erosional surfaces are preserved.

(5) Study the stratigraphy and sedimentology of the Medicine Lodge beds and lower Starlight Formation to characterize the tectonic setting of the eastern SRP before silicic volcanism initiated.

(6) Complete high resolution gravity studies of the eastern SRP to identify concealed half grabens beneath the volcanic rocks.

(7) Obtain precise ages on basalt and rhyolite in drill holes on the eastern SRP to better define age-depth relations and to document the initial age of voluminous basalt eruptions.

COMMENTS ON RESEARCH SINCE MANUSCRIPT ORIGINALLY SUBMITTED

Additional data and interpretations about deforma-

tion near the eastern SRP have been presented since our paper was written and submitted over five years ago. Janecke and others (2000) discuss eastern SRP-parallel normal faults of the northeastern Basin and Range Province. Whereas Zentner (1988) documented late Cenozoic activity on faults within 30 km of the eastern SRP, Janecke and others (2000) identified late Cenozoic movement on faults farther from the plain. They proposed that crustal subsidence within the arc of high topography and seismicity has induced a secondary strain field, characterized by approximately plain-perpendicular extension, that is superimposed on the Basin and Range strain field. This model is compatible with the one proposed by Zentner (1988) and discussed in our paper, if two strain fields exist in association with two wavelengths of crustal flexure. Both strain fields involve plain-perpendicular extension, but the amount of extension is much smaller than the amount of plain-parallel "Basin and Range" extension.

Hough (2001) addresses the age and rate of crustal flexure in the Lidy Hot Springs region (Figure 2) along the northeastern margin of the eastern SRP. He measured the plunges of six map-scale fold hinges in Paleozoic rocks and used these to locate a flexural hinge that roughly parallels the eastern SRP margin. The flexural hinge separates horizontal folds (to the north) from folds with 25-degree southward plunges (to the south), similar to the one identified by McQuarrie and Rodgers (1998). Hough (2001) found that the Medicine Lodge beds, which overlie the folded Paleozoic rocks, have the same orientation north and south of the flexural hinge, evidence that the Medicine Lodge beds postdate the flexure recorded by Paleozoic folds. The Medicine Lodge beds in this region are undated, but inferred to be middle Miocene (Skipp and others, 1979), and contain tuff that is chemically similar to eastern SRP tuffs (Hough, 2001). Hough also recognized disconformable contacts between Medicine Lodge beds and overlying 6.6-6.2 Ma volcanic rocks, and a minor amount of post-6.2 Ma eastward tilting. Hough proposed a Neogene history that includes the deposition of the Medicine Lodge beds at Howe Point (about 16 Ma), an initial pulse of southward flexure everywhere along the eastern SRP margin (between 16 and 10 Ma according to Figure 7), the deposition of the Medicine Lodge beds at Lidy Hot Springs, the emplacement of 6.6 to 6.2 Ma volcanic rocks everywhere along the eastern SRP margin, and the eastward tilting of Lidy Hot Springs rocks due to Basin and Range faulting. This history matches that of deformation proposed in our paper and awaits confirmation by dates on the Medicine Lodge beds at Lidy Hot Springs.

Kuntz and others (2002) analyze exposed structures of the eastern SRP, including tension cracks, eruptive fissures, concealed dikes, and faults. Their mapping shows that dike systems of the eastern SRP average 20 km long but may be as much as 40 km long. They interpreted some structures, like the Arco rift zone, to represent continuations of normal faults adjacent to the eastern SRP.

The Big Lost trough has recently been defined by Geslin and others (2002) and Bestland and others (2002) as a subbasin of the eastern SRP. With upper Pliocene-Quaternary rocks as much as 200 m deeper than correlative rocks beyond the subbasin, the Big Lost trough provides evidence of non-uniform subsidence across the eastern SRP. The trough is located immediately south of the Lost River Range, coincident with the greatest amount of crustal flexure along the eastern SRP margin (Figure 13).

Humphreys and others (2000) propose that Yellowstone tectonism is intricately related to the progression of magmatism across the High Lava Plains of Oregon, because the bilateral symmetry of this broader tectonic system argues against a simple hotspot origin for the Yellowstone system. Expanding upon the model of Saltzer and Humphreys (1997), they proposed that partial melting beneath these two magmatic tracks has left a residuum of uppermost mantle. This residuum would block the rise of underlying hot, fertile mantle rock, causing it to be bilaterally deflected to the leading tips of the two tracks. The larger volume of magma along the Yellowstone track is attributed in part to greater crustal extension there than in eastern Oregon. With regard to the Yellowstone-eastern SRP, this model differs from the hotspot model in mantle dynamics but not in crustal dynamics, and it is compatible with the deformational processes described in this paper.

ACKNOWLEDGMENTS

This research was supported by grants from the Idaho State Board of Education and NASA Idaho Space Grant Consortium. The authors thank Geology faculty and students at Idaho State University for provocative discussions and the 1993 Advanced Structure class for compiling regional cross sections through southeastern Idaho. Thanks also to Bill Hackett, Roger Stewart, and Bill Bonnichson for detailed reviews that added clarity and focus to the paper.

REFERENCES

Albee, H.F., and H.L. Cullins, 1965, Preliminary map of the Poker Peak and Palisades Reservoir quadrangles, Bonneville County, Idaho, and Lincoln County, Wyoming: U.S. Geological Survey Geologic Map GQ-1260.

Allmendinger, R.W., 1982, Sequence of late Cenozoic deformation in the Blackfoot Mountains, southeastern Idaho, *in* Bill Bonnichsen and R.M. Breckenridge, eds., Cenozoic Geology of Idaho: Idaho Bureau of Mines and Geology Bulletin 26, p. 505-516.

Alt, David, J.M. Sears, and D.W. Hyndman, 1988, Terrestrial maria: The origins of large basalt plateaus, hotspot tracks and spreading ridges: Journal of Geophysical Research, v. 96, p. 647-662.

Anders, M.H., 1990, Late Cenozoic evolution of Grand and Swan Valleys, Idaho, *in* Sheila Roberts, ed., Geologic Field Tours of Western Wyoming and Parts of Adjacent Idaho, Montana, and Utah: Geological Survey of Wyoming Public Information Circular 29, p. 15-25.

———, 1994, Constraints on North American plate velocity from the Yellowstone hotspot deformational field: Nature, v. 369, p. 53-55.

Anders, M.H., J.W. Geissman, L.A. Piety, and J.T. Sullivan, 1989, Parabolic distribution of circum-eastern Snake River Plain seismicity and latest Quaternary faulting: Migratory pattern and association with the Yellowstone hotspot: Journal of Geophysical Research, v. 94, p. 1589-1621.

Anders, M.H., and N.H. Sleep, 1992, Magmatism and extension: The thermal and mechanical effects of the Yellowstone hotspot: Journal of Geophysical Research, v. 97, p. 15,379-15,394.

Anders, M.H., Mark Spiegelman, D.W. Rodgers, and J.T. Hagstrum, 1993, The growth of fault-bounded tilt blocks: Tectonics, v. 12, p. 1451-1459.

Anderson, S.R., and M.J. Liszewski, 1997, Stratigraphy of the unsaturated zone and the Snake River Plain aquifer at and near the Idaho National Engineering Laboratory, Idaho: U.S. Geological Survey Water-Resources Investigations Report 97-4183, 65 p.

Armstrong, F.C., 1969, Geologic map of the Soda Springs quadrangle, southeastern Idaho: U.S. Geological Survey Miscellaneous Investigations Map I-557, scale 1:48,000.

Armstrong, R.L., W.P. Leeman, and H.E. Malde, 1975, K-Ar dating, Quaternary and Neogene volcanic rocks of the Snake River Plain, Idaho: American Journal of Science, v. 275, p. 225-251.

Armstrong, R.L., J.F. Smith, H.R. Covington, and P.L. Williams, 1978, Preliminary geologic map of the west half of the Pocatello 1º x 2º quadrangle, Idaho: U.S. Geological Survey Open-File Report 78-1018, scale 1:250,000.

Barrientos, S.E., R.S. Stein, and S.N. Ward, 1987, Comparison of the 1959 Hebgen Lake, Montana, and the 1983 Borah Peak, Idaho, earthquakes from geodetic observations: Bulletin of the Seismological Society of America, v. 77, p. 784-808.

Bestland, E.A., P.K. Link, M.A. Lanphere, and D.E. Champion, 2002, Paleoenvironments of sedimentary interbeds in the Pliocene and Quaternary Big Lost trough, eastern Snake River Plain, Idaho, *in* P.K. Link and L.L. Mink, eds., Geology, Hydrogeology, and Environmental Remediation: Idaho National Engineering and Environmental Laboratory, Eastern Snake River Plain, Idaho: Geological Society of America Special Paper 353, p. 27-44.

Blackwell, D.D., Shari Kelley, and J.L. Steele, 1992, Heat flow modeling of the Snake River Plain, Idaho: U.S. Department of Energy Report for contract DE-AC07-761DO1570, 109 p.

Bobo, R.T., 1991, Basin evolution of Arbon Valley and its relation to Snake River Plain volcanism and Basin and Range tectonics: Idaho State University M.S. thesis, 82 p.

Bonnichsen, Bill, 1982, The Bruneau-Jarbidge eruptive center, southwestern Idaho, *in* Bill Bonnichsen and R.M. Breckenridge, eds., Cenozoic Geology of Idaho: Idaho Bureau of Mines and Geology Bulletin 26, p. 237-254.

Braile, L.W., R.B. Smith, J. Ansorge, M.R. Baker, M.A. Sparlin, C. Prodehl, M.M. Schilly, J.H. Healy, S. Mueller, and K.H. Olsen, 1982, The Yellowstone-Snake River Plain seismic profiling experiment: Crustal structure of the eastern Snake River Plain: Journal of Geophysical Research, v. 87, no. B4, p. 2597-2609.

Brott, C.A., D.D. Blackwell, and J.P. Ziagos, 1981, Thermal and tectonic implications of heat flow in the eastern SRP, Idaho: Journal of Geophysical Research, v. 86, no. B12, p. 11,709-11,734.

Bruhn, R.L., D. Wu, and J-J. Lee, 1992, Final report on structure of the southern Lemhi and Arco fault zone, Idaho: Informal report contract no. EGG-NPR-10680, 25 p.

Burgel, W.D., 1986, Structural geology of the Rapid Creek area, Pocatello Range, north of Inkom, southeast Idaho: Idaho State University M.S. thesis, 72 p.

Burgel, W.D., D.W. Rodgers, and P.K. Link, 1987, Mesozoic and Cenozoic structures of the Pocatello region, southeastern Idaho, *in* W.R. Miller, ed., The Thrust Belt Revisited: Wyoming Geological Association, 37th Annual Field Conference Guidebook, p. 91-100.

Carlson, R.A., 1968, Geology and petrography of the volcanic rocks south of Hawkins Basin, S.E. Idaho: Idaho State University M.S. thesis, 66 p.

Christiansen, R.L., 1984, Yellowstone magmatic evolution: Its bearing on understanding large volume explosive volcanism, *in* Explosive Volcanism: Inception, Evolution, Hazards: National Academy Press, Washington, D.C., p. 84-95.

Christiansen, R.L., and E.H. McKee, 1978, Late Cenozoic volcanic and tectonic evolution of the Great Basin and Columbia intermountain regions, *in* R.B. Smith and G.P. Eaton, eds., Cenozoic Tectonics and Regional Geophysics of the Western Cordillera: Geological Society of America Memoir 152, p. 283-311.

Cluer, J.K., and B.L. Cluer, 1986, The late Cenozoic Camas Prairie rift, south-central Idaho: Contributions to Geology, University of Wyoming, v. 24, no. 1, p. 91-101.

Compton, R.R., 1983, Displaced Miocene rocks on the west flank of the Raft River-Grouse Creek core complex, Utah, *in* D.M. Miller, V.R. Todd, and K.A. Howard, eds., Tectonic and Stratigraphic Sudies in the Eastern Great Basin: Geological Society of America Memoir 157, p. 271-280.

Corbett, M.K., 1978, Geologic map of the northern Portneuf Range: U.S. Geological Survey Open-File Report 78-1018, scale 1:48,000.

Covington, H.R., 1983, Structural evolution of the Raft River basin, Idaho, *in* D.M. Miller, V.R. Todd, and K.A. Howard, eds., Tectonic and Stratigraphic Sudies in the Eastern Great Basin: Geological Society of America Memoir 157, p. 229-238.

Cress, L.D., 1981, Stratigraphy and structure of the south half of the Deep Creek Mountains, Oneida and Power counties, Idaho: Colorado School of Mines Ph.D. dissertation, 251 p.

Dixon, J.S., 1980, Regional structural synthesis, Wyoming salient of western Overthrust Belt: American Association of Petroleum Geologists Bulletin, v. 66, p. 1560-1580.

Doherty, D.J., L.A. McBroome, and M.A. Kuntz, 1979, Preliminary geologic interpretation and lithological log of the exploratory test well (INEL-1), Idaho National Engineering Laboratory, eastern Snake River Plain, Idaho: U.S. Geological Survey Open-File Report 79-1248, 10 p.

Eaton, G.P., R.R. Wahl, H.L. Prostka, D.R. Mabey, and M.D. Kleinkopf, 1978, Regional gravity and tectonic patterns: Their relation to late Cenozoic epeirogeny and lateral spreading in the western Cordillera, *in* R.B. Smith and G.P. Eaton, eds., Cenozoic Tectonics and Regional Geophysics of the Western Cordillera: Geological Society of America Memoir 152, p. 51-92.

Ekren, E.B., D.H. McIntyre, and E.H. Bennett, 1984, High-temperature, large volume, lavalike ash-flow tuffs without calderas in southwestern Idaho: U.S. Geological Survey Professional Paper 1272, 73 p.

Ekren, E.B., D.H. McIntyre, E.H. Bennett, and R.F. Marvin, 1982, Cenozoic stratigraphy of western Owyhee countty, Idaho, *in* Bill Bonnichsen and R.M. Breckenridge, eds., Cenozoic Geology of

Idaho: Idaho Bureau of Mines and Geology Bulletin 26, p. 215-236.

Embree, G.F., L.A. McBroome, and D.J. Doherty, 1982, Preliminary stratigraphic framework of the Pliocene and Miocene rhyolites, eastern Snake River Plain, Idaho, *in* Bill Bonnichsen and R.M. Breckenridge, eds., Cenozoic Geology of Idaho: Idaho Bureau of Mines and Geology Bulletin 26, p. 333-334.

England, P., and P. Molnar, 1990, Surface uplift, uplift of rocks, and exhumation of rocks: Geology, v. 18, p. 1173-1177.

Fritz, W.J., and J.W. Sears, 1993, Tectonics of the Yellowstone hotspot wake in southwestern Montana: Geology, v. 21, p. 427-430.

Garmezy, Larry, 1981, Geology and tectonic evolution of the southern Beaverhead Range, east-central Idaho: Pennsylvania State University M.S. thesis, 155 p.

Geslin, J.K., P.K. Link, J.W. Riesterer, M.A. Kuntz, and C.M. Fanning, 2002, Pliocene and Quaternary stratigraphic architecture and drainage systems of the Big Lost trough, northeastern Snake River Plain, Idaho, *in* P.K. Link and L.L. Mink, eds., Geology, Hydrogeology, and Environmental Remediation: Idaho National Engineering and Environmental Laboratory, Eastern Snake River Plain, Idaho: Geological Society of America Special Paper 353, p. 11-26.

Greensfelder, R.W., 1981, Lithospheric structure of the eastern Snake River Plain, Idaho: Stanford University Ph.D. dissertation, 188 p.

Gripp, A.E., and R.G. Gordan, 1990, Current plate velocities relative to hot-spots incorporating the NUVEL-1 global plate motion model: Geophysical Research Letters, v. 17, p. 1109-1112.

Hackett, W.R., M.H. Anders, and R.C. Walter, 1994, Preliminary stratigraphic framework of rhyolites from corehole WO-2, Idaho National Engineering Laboratory: Caldera-related, late-Tertiary silicic volcanism of the eastern Snake River Plain (abs.): Proceedings of the VII International Symposium on the observation of the continental crust through drilling: International Continental Drilling Program, Santa Fe, New Mexico, unpaginated.

Hackett, W.R., S.M. Jackson, and R.P. Smith, 1996, Paleoseismology of volcanic environments, *in* J.P. McCalpin, ed., Paleoseismology: Academic Press, New York, p. 147-182.

Hamilton, Warren, 1989, Crustal geologic processes of the United States, *in* L.C. Pakiser and W.D. Mooney, eds., Geophysical Framework of the Continental United States: Geological Society of America Memoir 172, p. 743-781.

———, 1987, Plate-tectonic evolution of the western U.S.A.: Episodes, v. 10, p. 271-276.

Henderson, E.P., 1991, Neogene basin filling of Goose Creek basin, south-central Idaho, northwestern Utah, and northeastern Nevada: Geological Society of America Abstracts with Programs, v. 23, no.4, p. 32.

Hildebrand, R.T., and K.R. Newman, 1985, Miocene sedimentation in the Goose Creek basin, south-central Idaho, northeastern Nevada, and northwestern Utah, *in* R.M. Flores and S.S. Kaplan, eds., Cenozoic Paleogeography of West-Central United States: Society of Economic Paleontologists and Mineralogists, Rocky Mountain Section, Symposium 3, p. 55-70.

Hladky, F.R., 1986, Geology of an area north of the narrows of Ross Fork Canyon, northernmost Portneuf Range, Fort Hall Indian Reservation, Bannock and Bingham counties, Idaho: Idaho State University M.S. thesis, 110 p.

Hladky, F.R., and K.S. Kellogg, 1987, Geologic map of the western part of the Fort Hall Indian Reservation, Idaho: U.S. Geological Survey, Branch of Central Mineral Resources, 38 p.

Hodges, M.K.V., and D.W. Rodgers, 1999, Middle Miocene initiation of Basin-Range faulting and eastern Snake River Plain subsidence—evidence from east-central Idaho: Geological Society of America Abstracts with Programs, v. 31, no. 4, p. A-17.

Hough, B.G., 2001, Temporal constraints on crustal flexure adjacent to the eastern Snake River Plain, Idaho: Idaho State University M.S. thesis, 82 p.

Houser, B.B., 1992, Quaternary stratigraphy of an area northeast of American Falls Reservoir, eastern Snake River Plain, Idaho, *in* P.K. Link, M.A. Kuntz, and L.B. Platt, eds., Regional Geology of Eastern Idaho and Western Wyoming: Geological Society of America Memoir 179, p. 269-288.

Humphreys, E.D., K.G. Duecker, D.L. Schutt, and R.B. Smith, 1990, Beneath Yellowstone: Evaluating plume and nonplume models using teleseismic images of the upper mantle: GSA Today, v. 10, no. 12, p. 1-7.

Janecke, S.U., 1993, Estimates of late Cenozoic extension, east-central Idaho: Geological Society of America Abstracts with Programs, v. 25, no. 5, p. 56.

Janecke, S.U., M.E. Perkins, and R.B. Smith, 2000, Normal fault patterns around the Yellowstone hot spot: A new model: Geological Society of America Abstracts with Programs, v. 32, no. 7, p. A-45.

Kellogg, K.S., 1990, Geologic map of the south Putnam Mountain quadrangle, Bannock and Caribou counties, Idaho: U.S. Geological Survey Geologic Quadrangle Map GQ-1665, scale 1:24,000.

———, 1992, Cretaceous thrusting and neogene block rotation in the northern Portneuf Range region, southeastern Idaho, *in* P.K. Link, M.A. Kuntz, and L.B. Platt, eds., Regional Geology of Eastern Idaho and Western Wyoming: Geological Society of America Memoir 179, p. 95-113.

Kellogg, K.S., S.S. Harlan, H.H. Mehnert, L.W. Snee, K.L. Pierce, W.R. Hackett, and D.W. Rodgers, 1994, Major 10.2-Ma rhyolitic volcanism in the eastern Snake River Plain, Idaho—Isotopic age and stratigraphic setting of the Arbon Valley Tuff Member of the Starlight Formation: U.S. Geological Survey Bulletin 2091, 18 p.

Kellogg, K.S., and R.F. Marvin, 1988, New potassium-argon ages, geochemistry, and tectonic setting of upper Cenozoic volcanic rocks near Blackfoot, Idaho: U.S. Geological Survey Bulletin 1806, 19 p.

Kellogg, K.S., S.S. Oriel, R.E. Amerman, P.K. Link, and F.R. Hladky, 1989, Geologic map of the Jeff Cabin Creek quadrangle, Bannock and Caribou counties, Idaho: U.S. Geological Survey Geologic Quadrangle Map GQ-1669, scale 1:24,000.

King, Clarence, 1878, U.S. Geologic Exploration, Fortieth Parallel Report, v. 1, p. 412-440.

Kirkham, V.R.D., 1927, A geologic reconnaissance of Clark and Jefferson and parts of Butte, Custer, Fremont, Lemhi, and Madison counties, Idaho: Idaho Bureau of Mines and Geology Pamphlet 19, 47 p.

———, 1931, Snake River downwarp: Journal of Geology, v. 39, p. 456-487.

Kuntz, M.A., 1992, A model based perspective of basaltic volcanism, eastern Snake River Plain, Idaho, *in* P.K. Link, M.A. Kuntz, and L.B. Platt, eds., Regional Geology of Eastern Idaho and Western Wyoming: Geological Society of America Memoir 179, p. 289-304.

Kuntz, M.A., S.R. Anderson, D.E. Champion, M.A. Lanphere, and D.J. Grunwald, 2002, Tension cracks, eruptive fissures, dikes, and faults related to late Pliocene-Holocene basaltic volcanism and implication for the distribution of hydraulic conductivity in the eastern Snake River Plain, Idaho, *in* P.K. Link and L.L. Mink, eds., Geology, Hydrogeology, and Environmental Remediation: Idaho National Engineering and Environmental Laboratory, Eastern Snake River Plain, Idaho: Geological Society of America Special Paper 353, p. 111-134.

Kuntz, M.A., D.E. Champion, E.C. Spiker, R.H. Lefebvre, and L.A. McBroome, 1982, The Great Rift and evolution of the Craters of the Moon lava field, Idaho, *in* Bill Bonnichsen and R.M. Breckenridge, eds., Cenozoic Geology of Idaho: Idaho Bureau of Mines and Geology Bulletin 26, p. 423-437.

Kuntz, M.A., H.R. Covington, and L.J. Schoor, 1992, An overview of basaltic volcanism of the Eastern Snake River Plain, Idaho, *in* P.K. Link, M.A. Kuntz, and L.B. Platt, eds., Regional Geology of Eastern Idaho and Western Wyoming: Geological Society of America Memoir 179, p. 227-269.

Kuntz, M.A., Betty Skipp, M.A. Lanphere, W.E. Scott, K.L. Pierce, G.B. Dalrymple, D.E. Champion, G.F. Embree, W.R. Page, L.A. Morgan, R.P. Smith, W.R. Hackett, and D.W. Rodgers, 1994a, Geologic map of the Idaho National Engineering Laboratory and adjoining areas, eastern Idaho: U.S. Geological Survey Miscellaneous Investigations Map I-2330, scale 1:100,000.

Kuntz, M.A., Betty Skipp, W.E. Scott, and W.R. Page, 1984, Preliminary geologic map of the Idaho National Engineering Laboratory and adjoining areas: U.S. Geological Survey Open-File Report 84-281, 25 p.

Lageson, D.R., 1992, Possible Laramide influences on the Teton normal fault, western Wyoming, *in* P.K. Link, M.A. Kuntz, and L.B. Platt, eds., Regional Geology of Eastern Idaho and Western Wyoming: Geological Society of America Memoir 179, p. 183-196.

Leeman, W.P., 1982, Development of the Snake River Plain-Yellowstone Plateau province, Idaho and Wyoming: An overview and petrographic model, *in* Bill Bonnichsen and R.M. Breckenridge, eds., Cenozoic Geology of Idaho: Idaho Bureau of Mines and Geology Bulletin 26, p. 155-177.

LeFebre, G.B., 1984, Geology of the Chinks Peak area, Pocatello Range, Bannock County, Idaho: Idaho State University M.S. thesis, 61 p.

Love, J.D., 1977, Summary of Upper Cretaceous and Cenozoic stratigraphy and of tectonic and glacial events in Jackson Hole, northwestern Wyoming: Wyoming Geological Association 29th Annual Field Conference Guidebook, p. 585-594.

Love, J.D., J.C. Reed, and A.C. Christiansen, 1992, Geologic map of Grand Teton National Park, Teton County, Wyoming: U.S. Geological Survey Map I-2031, scale 1: 62,500.

Lowry, A.R., and R.B. Smith, 1995, Strength and rheology of the western U.S. Cordillera: Journal of Geophysical Research, v. 100, p. 17,947-17,963.

Mahoney, J.B., 1987, The geology of the northern Smoky Mountains and stratigraphy of a portion of the lower Permian Grand Prize Formation, Blaine and Camas counties, Idaho: Idaho State University M.S. thesis, 143 p.

Mansfield, G.R, 1927, Geography, geology and mineral resources of part of southeastern Idaho, with descriptions of Carboniferous and Triassic fossils by G.H. Girty: U.S. Geological Survey Professional Paper 152, 453 p.

McBroome, L.A., 1981, Stratigtraphy and origin of Neogene ash-flow tuffs on the northcentral margin of the eastern Snake River Plain, Idaho: University of Colorado M.S. thesis, 74 p.

McQuarrie, Nadine, 1997, Crustal flexure adjacent to the eastern Snake River Plain, Idaho: Idaho State University, M.S. thesis, 87 p.

McQuarrie, Nadine, and D.W. Rodgers, 1998, Subsidence of a volcanic basin by flexure and lower crustal flow: The eastern Snake River Plain, Idaho: Tectonics, v. 17, p. 203-220.

Miller, D.M., 1980, Structural geology of the northern Albion Mountains, south central Idaho, *in* M.D. Crittenden, P.J. Coney, and G.H. Davis, eds., Cordilleran Metamorphic Core Complexes: Geological Society of America Memoir 153, p. 399-423.

Morgan, L.A., D.J. Doherty, and W.P. Leeman, 1984, Ignimbrites of the eastern Snake River Plain: Evidence for major caldera-forming eruptions: Journal of Geophysical Research, v. 89, no. B10, p. 8665-8678.

Morgan, W.J., 1972, Plate motions and deep mantle convection: Geological Society of America Memoir 132, p. 7-22.

Mueller, K.J., and A.W. Snoke, 1993, Cenozoic basin development and normal fault systems associated with the exhumation of metamorphic complexes in northeastern Nevada, *in* M.M. Lahren, J.H. Trexler, Jr., and Claude Spinosa, eds., Crustal Evolution of the Great Basin and the Sierra Nevada: Cordilleran/Rocky Mountains Section, Geological Society of America Guidebook, Department of Geological Sciences, University of Nevada, Reno, p. 1-34.

Myers, W.B., and Warren Hamilton, 1964, Deformation accompanying the Hebgen Lake earthquake of August 17, 1959: U.S. Geological Survey Professional Paper 435, p. 55-98.

Mytton, J.W., P.L. Williams, and W.A. Morgan, 1990, Geologic map of the Stricker 4 quadrangle, Cassia, Twin Falls, and Jerome counties, Idaho: U.S. Geological Survey Miscellaneous Investigations Series Map I-2052, scale 1:48,000.

Nunn, J.A., and J.R. Aires, 1988, Gravity anomalies and flexure of the lithosphere at the Middle Amazon Basin, Brazil: Journal of Geophysical Research, v. 93, p. 415-428.

Oriel, S.S., and D.W. Moore, 1985, Geologic map of the west and east Palisades Roadless areas, Idaho and Wyoming: U.S. Geological Survey Miscellaneous Field Studies Map MF-1619-B, scale 1:50,000.

Oriel, S.S., and L.B. Platt, 1980, Geologic map of the Preston 1º x 2º quadrangle, southeastern Idaho and western Wyoming: U.S. Geological Survey Miscellaneous Investigation Series Map I-1127, scale 1:250,000.

Pankratz, L.W., and H.D. Ackermann, 1982, Structure along the northwest edge of the Snake River Plain interpreted from seismic refraction: Journal of Geophysical Research, v. 87, no. B4, p. 2676-2682.

Parsons, Tom, and G.A. Thompson, 1991, The role of magma overpressuring in suppressing earthquakes and topography: Worldwide examples: Science, v. 253, p. 1399-1402.

Parsons, Tom, G.A. Thompson, and R.P. Smith, 1998, More than one way to stretch: A tectonic model for extension along the plume track of the Yellowstone hot spot and adjacent Basin and Range Province: Tectonics, v. 17, p. 221-234.

Peng, Xiaohua, and E.D. Humphreys, 1998, Crustal velocity structure across the eastern Snake River Plain and the Yellowstone swell: Journal of Geophysical Research, v. 103, p. 7171-7186.

Perkins, M.E., and W.P. Nash, 1994, Tephrochronology of the Teewinot Formation, Jackson Hole, Wyoming: Geological Society of America Abstracts with Programs, v. 26, no. 6, p. 58-59.

Perkins, M.E., W.P. Nash, F.H. Brown, and R.J. Fleck, 1995, Fallout tuffs of Trapper Creek, Idaho—A record of Miocene explosive volcanism in the Snake River Plain volcanic province: U.S. Geological Survey Bulletin, v. 107, p. 1484-1506.

Pierce, K.L., H.R. Covington, P.L. Williams, and D.H. McIntyre, 1983, Geologic map of the Cotterel Mountains and the northern Raft River Valley, Cassia County, Idaho: U.S. Geological Survey Miscellaneous Investigation Series Map I-1450, scale 1:48,000.

Pierce, K.L., and L.A. Morgan, 1992, The track of the Yellowstone hotspot; volcanism, faulting and uplift, *in* P.K. Link, M.A. Kuntz, and L.B. Platt, eds., Regional Geology of Eastern Idaho and Western Wyoming: Geological Society of America Memoir 179, p. 1-53.

Pierce, K.L., and W.E. Scott, 1982, Pleistocene episodes of alluvial-gravel deposition, southeastern Idaho, *in* Bill Bonnichsen and R.M. Breckenridge, eds., Cenozoic Geology of Idaho: Idaho Bureau of Mines and Geology Bulletin 26, p. 685-702.

Pogue, K.R., 1984, Geology of the Mt. Putnam area, northern Portneuf Range, Bannock and Caribou counties, Idaho: Idaho State University M.S. thesis, 106 p.

Pratt, R.M., 1982, The case for lateral offset of the overthrust belt along the Snake River Plain, *in* R.B. Powers, ed., Geologic Studies of the Cordilleran Thrust Belt: Rocky Mountain Association of Geologists, v. 1, p. 235-246.

Reilinger, R.E., G.P. Citron, and L.D. Brown, 1977, Recent vertical crustal movements from precise leveling data in southwestern Montana, western Yellowstone National Park and the Snake River Plain: Journal of Geophysical Research, v. 82, p. 5349-5359.

Richins, R.D., J.C. Pechmann, R.B. Smith, C.J. Langer, S.K. Goter, J.E. Zwollweg, and J.J. King, 1987, The 1983 Borah Peak, Idaho, earthquake and its aftershocks: Bulletin of the Seismological Society of America, v. 77, no. 3, p. 694-723.

Rodgers, D.W., and M.H. Anders, 1990, Neogene evolution of Birch Creek Valley near Lone Pine, Idaho *in* Sheila Roberts, ed., Geologic Field Tours of Western Wyoming and Parts of Adjacent Idaho, Montana, and Utah: Geological Survey of Wyoming Public Information Circular 29, p. 27-40.

Rodgers, D.W., Mason Estes, Chris Meehan, Terrence Osier, John Preacher, and Ian Warren, 1994, Style, kinematics, and timing of Neogene-Quaternary extension in the northeastern Basin and Range: Geological Society of America Abstracts with Programs, v. 75, p. 61.

Rodgers, D.W., W.R. Hackett, and H.T. Ore, 1990, Extension of the Yellowstone Plateau, eastern Snake River Plain, and Owyhee Plateau: Geology, v. 18, p. 1138-1141.

Rodgers, D.W., and S.U. Janecke, 1992, Tertiary paleogeographic maps of the western Idaho-Wyoming-Montana thrust belt, *in* P.K. Link, M.A. Kuntz, and L.B. Platt, eds., Regional Geology of Eastern Idaho and Western Wyoming: Geological Society of America Memoir 179, p. 83-94.

Rodgers, D.W., P.K. Link, and A.D. Huerta, 1995, Structural framework of mineral deposits hosted by Paleozoic rocks in the northeastern part of the Hailey 1° x 2° quadrangle, south-central Idaho: U.S. Geological Survey Bulletin 2064-B, 18 p.

Rodgers, D.W., and K.L. Othberg, 1999, Geologic map of the Pocatello South quadrangle, Idaho: Idaho Geological Survey Geologic Map 26, scale 1:24,000.

Rodgers, D.W., and N.C. Zentner, 1988, Fault geometries along the northern margin of the eastern Snake River Plain, Idaho: Geological Society of America Abstracts with Programs, v. 20, p. 465.

Royse, Frank, Jr., M.A. Warner, and D.L. Reese, 1975, Thrust belt structural geometry and related stratigraphic problems, Wyoming-Idaho-northern Utah, *in* D.W. Bolyard, ed., Deep Drilling Frontiers of the Central Rocky Mountains: Rocky Mountains Association of Geologists Symposium, Denver, Colorado, p. 41-54.

Ruppel, E.T., 1967, Late Cenozoic drainage reversal, east-central Idaho, and its relation to possible undiscovered placer deposits: Economic Geology, v. 61, p. 648-663.

Rytuba, J.J., and E.H. McKee, 1984, Peralkaline ash flow tuffs and calderas of the McDermitt volcanic field, southeast Oregon and northcentral Nevada: Journal of Geophysical Research, v. 89, p. 8616-8628.

Saltzer, S.D., and K.V. Hodges, 1988, The Middle Mountain shear zone, southern Idaho—Kinematic analysis of an early Tertiary high-temperature detachment: Geological Society of America Bulletin, v. 100, p. 96-103.

Saltzer, R.L., and E.D. Humphreys, 1997, Upper mantle P-wave velocity structure of the eastern Snake River Plain and its relationship to geodynamic models of the region: Journal of Geophysical Research, v. 102, p. 11,829-11,841.

Schmidt, D.L., 1962, Quaternary geology of the Bellevue area in Blaine and Camas counties, Idaho: U.S. Geological Survey Open-File Report 625, 133 p.

Scott, W.E., 1982, Surficial geologic map of the eastern Snake River Plain and adjacent area, 111° to 115°W, Idaho and Wyoming: U.S. Geological Survey Miscellaneous Investigations Map I-1372, scale 1:125,000.

Scott, W.E., K.L. Pierce, and M.H. Hait, Jr., 1985, Quaternary tectonic setting of the 1983 Borah Peak earthquake, central Idaho, *in* R.S. Stein and R.C. Bucknam, eds., Proceedings, Workshop XXVIII on the Borah Peak, Idaho, Earthquake: U.S. Geological Survey Open-File Report 85-290, p. 1-16.

Sengor, A.M.C., 1995, Sedimentation and tectonics of fossil rifts, *in* C.J. Busby and R.V. Ingersoll, eds., Tectonics of Sedimentary Basins: Blackwell Science, Cambridge, Massachusettes, p. 53-118.

Skipp, Betty, 1988, Geologic map of Mackay 4 (Grouse) NE quadrangle, Butte and Custer counties, Idaho: U.S. Geological Survey Open-File report 88-423, scale 1:24,000.

Skipp, Betty, and D.D. Bollmann, 1992, Geologic map of Blizzard Mountain North quadrangle, Butte and Custer counties, Idaho: U.S. Geological Survey Open-File Report 92-280, scale 1:24,000.

Skipp, Betty, M.A. Kuntz, and L.A. Morgan, 1990, Geologic map of Mackay 4 (Grouse) SE quadrangle, Butte and Custer counties, Idaho: U.S. Geological Survey Open-File Report 89-431, scale 1:24,000.

Skipp, Betty, H.J. Prostka, and D.L. Schleicher, 1979, Preliminary geologic map of the Edie Ranch quadrangle, Clark County, Idaho, and Beaverhead County, Montana: U.S. Geological Survey Open-File Report 79-845, scale 1:62,500.

Smith, C.L., 1966, Geology of the eastern Mount Bennett Hills, Camas, Gooding, and Lincoln counties, Idaho: University of Idaho Ph.D. dissertation, 129 p.

Smith, R.B., W.D. Richins, and D.I. Doser, 1985, The 1983 Borah Peak, Idaho, earthquake: Regional seismicity, kinematics of faulting and tectonic mechanism, *in* R.S. Stein and R.C. Bucknam, eds., Proceedings, Workshop XXVIII on the Borah Peak, Idaho, Earthquake: U.S. Geological Survey Open-File Report 85-290, p. 236-263.

Smith, R.B., and N.L. Sbar, 1974, Contemporary tectonics and seismicity of the western United States with emphasis on the Intermountain Seismic Belt: Geological Society of America Bulletin, v. 85, p. 1205-1218.

Smith, R.B., M.M. Schilly, L.W. Braile, J. Ansorge, J.L. Lehman, M.R. Baker, C. Prodehl, J.H. Healy, S. Mueller, and R.W. Greensfelder, 1982, The 1978 Yellowstone-eastern Snake River Plain seismic profiling experiment: Crustal structure of the Yellowstone region and experiment design: Journal of Geophysical Research, v. 87, no. B4, p. 2583-2596.

Sparlin, M.A., L.W. Braile, and R.B. Smith, 1982, Crustal structure of the eastern Snake River Plain determined from ray trace modeling of seismic refraction data: Journal of Geophysical Research, v. 87, no. B4, p. 2619-2633.

Suppe, John, Christine Powell, and Robert Berry, 1975, Regional topography, seismicity, Quaternary volcanism, and the present-day tectonics of the western United States: American Journal of Science, v. 275A, p. 397-436.

Trimble, D.E., 1980, Geology of the Michaud and Pocatello quadrangles, Bannock and Power counties, Idaho: U.S. Geological Survey Bulletin 1400, 88 p.

Trimble, D.E., and W.J. Carr, 1976, Geology of the Rockland and Arbon quadrangles, Power County, Idaho: U.S. Geological Survey Bulletin 1399, 115 p.

Turcotte, D.L., and Gerald Schubert, 1982, Geodynamics: Applications of Continuum Physics to Geological Problems: John Wiley and Sons, New York, 450 p.

Turko, J.M., and P.L.K. Knuepfer, 1991, Late Quaternary fault segmentation from analysis of scarp morphology: Geology, v. 19, p. 718-721.

Waldrop, H.A., 1975, Surficial geologic map of the Henry's Lake quadrangle, Idaho and Montana: U.S. Geological Survey Miscellaneous Investigations Map I-684.

Williams, P.L., H.R. Covington, and K.L. Pierce, 1982, Cenozoic stratigraphy and tectonic evolution of the Raft River Basin, Idaho, *in* Bill

Bonnichsen and R.M. Breckenridge, eds., Cenozoic Geology of Idaho: Idaho Bureau of Mines and Geology Bulletin 26, p. 491-504.

Williams, P.L., J.W. Mytton, and H.R. Covington, 1990, Geologic map of the Stricker 1 quadrangle, Cassia, Twin Falls, and Jerome counties, Idaho: U.S. Geological Survey Miscellaneous Investigations Map I-2078, scale 1:48,000.

Witkind, I.J., 1972, Geologic map of the Henry's Lake quadrangle, Idaho and Montana: U.S. Geological Survey Map I-781-A, scale 1:48,000.

———, 1976, Geologic map of the southern part of the Upper Red Rock Lake quadrangle, southwest Montana and adjacent Idaho: U.S. Geological Survey Miscellaneous Investigations Map I-943, scale 1:48,000.

Woodward, N.B., 1986, Thrust fault geometry of the Snake River Range, Idaho and Wyoming: Geological Society of America Bulletin, v. 97, p. 178-193.

Zentner, N.C., 1989, Neogene normal faults related to the structural origin of the eastern Snake River Plain, Idaho: Idaho State University M.S. thesis, 47 p.

Zoback, M.L., and G.A. Thompson, 1978, Basin and Range rifting in northern Nevada: Clues from a mid-Miocene rift and its subsequent offsets: Geology, v. 6, p. 111-116.

Zoback, M.L., and Mark Zoback, 1980, State of stress in the conterminous United States: Journal of Geophysical Research, v. 85, no. B11, p. 6113-6156.

CHAPTER TWO

Products of Rhyolitic Volcanism

Hoodoos formed by erosion of the Cougar Point Tuff, Black Rock escarpment, Bruneau Canyon.

(Clockwise from top left)*: Lithophysal zone in the Cougar Point Tuff. Flow lobe near margin of Dorsey Creek rhyolite. Red and black breccia in Cedar Tree rhyolite. Sheeting joints in rhyolite of Juniper-Clover area.*

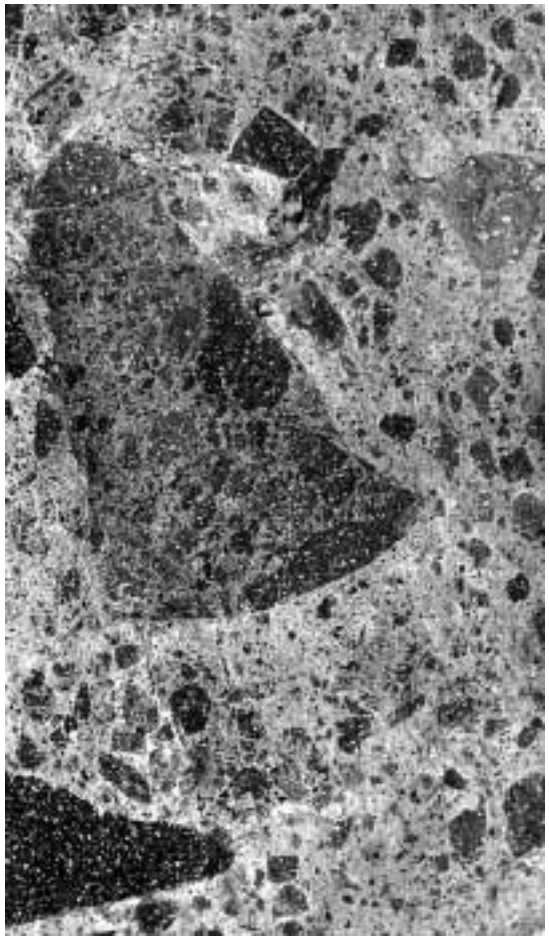

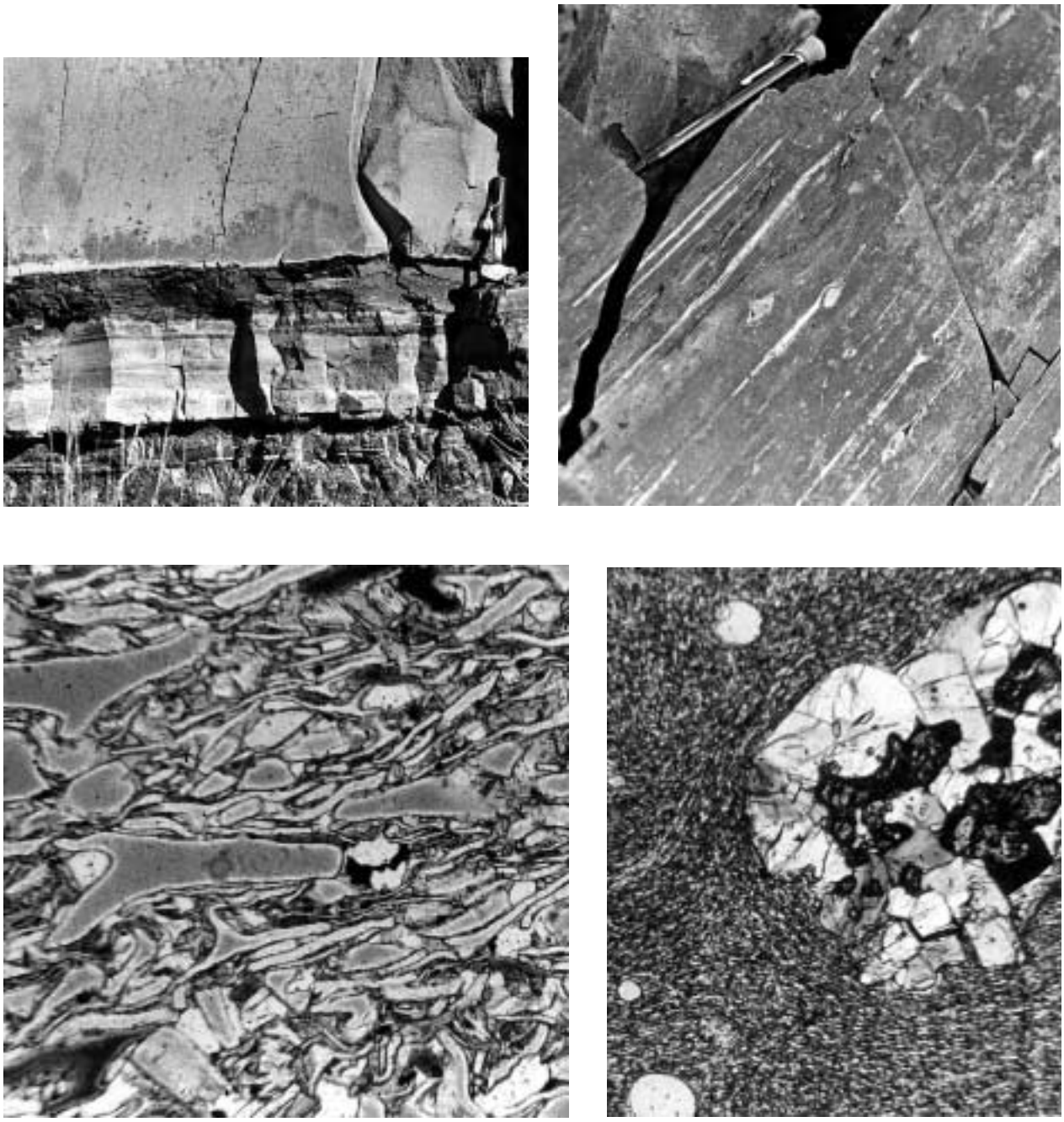

(Clockwise from top left)*: Base of a Cougar Point Tuff unit. Flattened pumice clasts and lithic fragments in the Cougar Point Tuff. Microscopic view of a rhyolite lava flow. Microscopic view of a welded tuff.*

Cabin at Three Forks of Sheep Creek.

Abandoned house near Broken Wagon Draw.

Cowan Place along Sheep Creek.

Bulk Major and Trace Element Evidence for a Time-Space Evolution of Snake River Plain Rhyolites, Idaho

Scott S. Hughes[1] and Michael McCurry[1]

ABSTRACT

Petrologic and geochemical analyses of Miocene rheomorphic tuffs in the Cassia Mountains, compared to existing data for the Yellowstone Plateau-Snake River Plain (SRP) Province, indicate that rhyolitic magmas of the Owyhee-Humboldt, Bruneau-Jarbidge, and Twin Falls volcanic centers experienced shorter crustal residence times than those of the Heise, Yellowstone, and perhaps Picabo volcanic centers. Relatively uniform trace element patterns for high-temperature southwestern rhyolites reflect magma generation in younger, thinner, and more mafic deep crust in comparison to upper crustal realms in the northeastern segment from which magmas derived more varied trace element signatures. We present a model of magma genesis and evolution along the trend of the SRP system that suggests a change in the compositions of silicic magmas and their modes of eruption near long 114ºW. within a region of westward-thinning craton. The model is consistent with current hypotheses that imply lower-crustal magmas in the southwestern segment of the SRP system were erupted from deep sources and that magmas in the northeastern segment coalesced in the upper crust and produced large calderas. Chemical and mineralogical transitions in magmatism occur between the Twin Falls and Picabo volcanic centers. This is 200-300 km east of a sharp, eastward transition from less to more evolved Sr- and Nd-isotopic values within SRP rhyolites near the Oregon-Idaho border. Along the northern margin of the SRP, compositional distinctions among volcanic centers suggest that rhyolites in the Mount Bennett Hills region should be included with the Twin Falls center rather than the Picabo center. The Picabo center is represented by the Arbon Valley Tuff Member of the Starlight Formation and associated rhyolite lavas.

Key words: ignimbrite, ash-flow tuffs, rhyolite, Yellowstone hot spot

Editors' note: The manuscript was submitted in August 1998 and has been revised at the aurthors' discretion.

[1]Department of Geosciences, Idaho State University, Pocatello, ID 83209-8072

INTRODUCTION

Volcanism during the past 16 Ma in the region—from the plateaus of northern Nevada, southeastern Oregon, and southwestern Idaho through the eastern Snake River Plain topographic depression in Idaho to the Yellowstone Plateau in northwestern Wyoming—is the manifestation of a 950-km-long dominantly bimodal (rhyolitic/basaltic) continental tectonic-magmatic system. This time-transgressive system (e.g., Armstrong and others, 1975), currently active beneath Yellowstone National Park, is broadly referred to as the Snake River Plain (SRP) volcanic province. It is represented by thick, Miocene to Quaternary rhyolitic ignimbrites, tuffs, and lava flows exposed mainly along the northern and southern boundaries of the SRP depression, on the Yellowstone Plateau, and on the Owyhee Plateau of southwestern Idaho (Figure 1). The inception of volcanism is recorded by middle Miocene silicic ash-flow tuffs and lavas in the Owyhee-Humboldt region that are contemporaneous with the main series of Columbia River continental flood basalts erupted from dike swarms in northeastern Oregon and southeastern Washington. Ignimbrites in the Owyhee-Humboldt part of the province have been attributed to deep-crustal fissure eruptions owing to the apparent lack of calderas (Ekren and others, 1984); those in the northeastern part of the province (e.g., Christiansen, 1984; Morgan and

Hughes, S.S., and Michael McCurry, 2002, Bulk major and trace element evidence for a time-space evolution of Snake River Plain rhyolites, Idaho, *in* Bill Bonnichsen, C.M. White, and Michael McCurry, eds., Tectonic and Magmatic Evolution of the Snake River Plain Volcanic Province: Idaho Geological Survey Bulletin 30, p. 161-176.

others, 1984) show more surface evidence of caldera formation.

The time-transgressive nature of SRP rhyolitic eruptions implies they are a hot-spot track broadly consistent with a mantle plume being overridden by the North American plate (e.g., Armstrong and others, 1975; Rodgers and others, 1990; Pierce and Morgan, 1992; Smith and Braile, 1993). However, the age progression of rhyolitic volcanism is not uniform throughout the province (Kellogg and others, 1994; Perkins and others, 1995). A volcanic transition occurred about 10 Ma that is associated with a change in direction of the hot-spot track and an abrupt physiographic change from the southwestern Idaho plateaus to the topographic depression of the eastern SRP. Pierce and Morgan (1992) attribute this to a transition in the mantle plume from an expanding-head phase to a narrow-chimney phase. They suggest that this represents the eastward transition from Paleozoic mafic crust to Precambrian sialic crust at about long 114ºW. near the intersection of the western and eastern segments of the SRP. Their model (see Figure 24 in Pierce and Morgan, 1992) is consistent with the general lithospheric transition occurring across a broad cratonic boundary that juxtaposes Mesozoic accreted oceanic terranes west of the Owyhee Plateau and Archean cratonic terranes east of the Idaho and Wyoming fold and thrust belt. Variations in lithologic properties across the province are expected to be manifested in the petrologic and geochemical signatures of rhyolites that define the hot-spot track. Thus, petrologic signatures are related to crustal evolution and the compositions of magmatic sources, as well as to the mechanisms of magma genesis and subsequent processes, especially the amounts of crustal assimilation and crystallization during magmatic evolution.

This paper, a preliminary study that extends the work of Hughes and others (1996), summarizes petrologic and bulk rock chemical variations among rhyolites in the SRP system. Although the bulk rock data do not strictly repre-

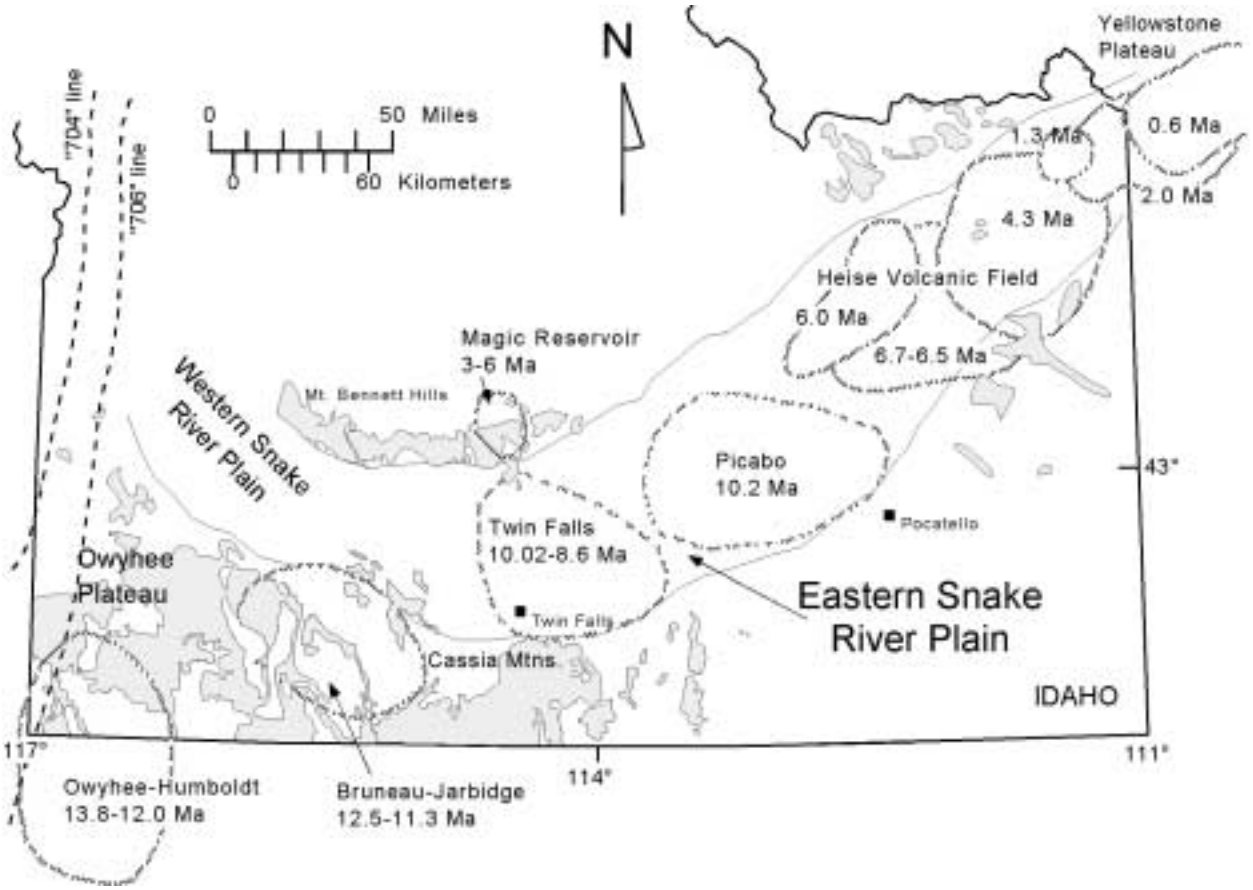

Figure 1. Volcanic centers associated with the eastern Snake River Plain hot-spot track modified from Pierce and Morgan (1992). Dates from Bonnichsen (1982), Christiansen (1984), Ekren and others (1984), Morgan and others (1984), Ryutuba and McKee (1984), Kellogg and Marvin (1988), Kellogg and others (1994), and Perkins and others (1995). $^{87}Sr/^{86}Sr$ isopleth lines (0.704 and 0.706) are derived from Fleck and Criss (1985) and Armstrong and others (1977). Precambrian continental crust lies east of the 0.706 line and accreted Mesozoic oceanic terranes lie west of the 0.704 line; the intermediate zone is Paleozoic mafic crust.

sent melt compositions due to the presence of phenocrysts, most SRP rhyolites contain less than about 20 percent phenocrysts, so their compositions reflect gross time-space changes in petrologic processes. Chemical variations are used in this study to construct a regional petrologic model that outlines the effects of tectonic regimes and lithospheric properties on magma genesis and evolution. Approximately 350 chemical analyses of rhyolitic deposits from the SRP Province are compared among known and inferred eruptive centers. Most of these data were obtained during our recent research in the Cassia Mountains south of Twin Falls for M.S. theses by J. Parker (1996), A. Watkins (1998), and K. Wright (1998).

TIME AND SPACE PROGRESSION OF VOLCANISM

Major inferred SRP silicic volcanic systems in sequence from oldest to youngest are the eruptive centers of Owyhee-Humboldt, Bruneau-Jarbidge, Twin Falls, Picabo, Heise, and Yellowstone Plateau (Figure 1). Each system produced one or more major caldera or fissure-erupted volcanic centers associated with large ash flows. Less is known about the caldera margins or eruption conduits associated with the Picabo and Twin Falls centers than with other SRP silicic volcanic centers. Late Miocene-Pliocene rhyolites on the eastern SRP from Twin Falls to Ashton are covered by as much as 2 km of late Tertiary and Quaternary basaltic lavas and associated volcanic and sedimentary deposits that fill much of the topographic depression (Hackett and others, this volume; Hughes and others, this volume). The SRP rhyolitic eruptive centers apparently represent distinct time-space cycles of volcanism (Armstrong and others, 1975; Morgan and others, 1984; Pierce and Morgan, 1992) with evidence of temporal overlap observed only for Owyhee-Humboldt with Bruneau-Jarbidge and for Twin Falls with Picabo.

Hypotheses of the hot-spot age progression were reviewed in detail by Pierce and Morgan (1992) and include the following: (1) the trace of a stationary deep-seated mantle plume, currently beneath the northeast part of Yellowstone National Park, which contributed much heat to the overriding continental lithospheric plate (Morgan, 1972; Smith and Sbar, 1974); (2) an eastward-propagating rift in the lithosphere, resulting in decompression melting of the asthenosphere (Myers and Hamilton, 1964; Hamilton, 1989); (3) volcanism along a preexisting crustal flaw (Eaton and others, 1975); (4) the propagation of a crack following a transform fault boundary between two regimes of Basin and Range extension (Christiansen and McKee, 1978); and (5) a meteorite impact that initiated the eruption of large volumes of flood basalts (Alt and others, 1988). The most widely accepted of these models explains the SRP system as a hot-spot track created by the North American plate passing over a stationary mantle plume (Armstrong and others, 1975; Leeman, 1982a; Pierce and Morgan, 1992; Smith and Braile, 1993).

Several aspects of the SRP indicate a complex tectonic-magmatic system involving mantle processes other than those attributed to current models of a deep-seated mantle plume. Examples include widespread Quaternary eastern SRP volcanism, which does not follow the rhyolitic time transgression (Armstrong and others, 1980; Kuntz and others, 1992); the 3-6 Ma rhyolites erupted at Magic Reservoir that are adjacent to 10-8 Ma SRP rhyolites (Struhsacker and others, 1982; Honjo and others, 1986); and lithospheric structural and geophysical properties (e.g., Saltzer and Humphries, 1997; McQuarrie and Rodgers, 1998) that are inconsistent with a spatially restricted deep-seated heat source. Recent seismic measurements (Saltzer and Humphries, 1997) indicate a corridor of low-velocity, partially melted, mantle extending beneath the plain to depths as great as 200 km. Crustal velocity structure determined by Sparlin and others (1982) and Peng and Humphreys (1998) indicate a midcrustal, flat-topped gabbroic layer extending across the entire width of the eastern SRP. In a study of crustal flexure and eastern SRP subsidence, McQuarrie and Rodgers (1998) proposed that a regional midcrustal load is related to the elongate mafic sill being emplaced at about 10 Ma, which may have provided the heat source for widespread SRP volcanism at that time. Regional volcanism at about 10 Ma is documented by similar age units of the Twin Falls center exposed in and around the Cassia Mountains (Perkins and others, 1995), by the 10.2 Ma Arbon Valley Tuff of the Picabo center erupted from the inferred Taber caldera near Blackfoot (Kellogg and others, 1994), by the 9.9 Ma tuff of Kyle Canyon exposed at Howe Point about 40 km northeast of Arco (Morgan and others, 1984), and by 11.2 and 8.8 Ma rhyolites intersected in a deep corehole (INEL-1) on the Idaho National Engineering and Environmental Laboratory (Morgan and others, 1984). Moreover, the inferred Picabo center is anomalous in its overall age progression; it is contemporaneous with widespread volcanism from other eruptions of the central SRP Province.

TECTONIC ASSOCIATIONS

The SRP volcanic province is one of several late Tertiary complex magmatic terranes that also include the Cascades magmatic arc, the Columbia River basalts, and the

Oregon Plateau basalts, all of which are adjacent to the Basin and Range Province extensional system. Complexities in the hot-spot track were probably produced by concomitant Basin and Range extensional tectonics, which have been active since 17 Ma, and by subduction along the Cascades arc, at least during the hot-spot track's middle Miocene inception. Geist and Richards (1993) propose that the ascending Yellowstone mantle plume was initially deflected northward by the subducting Farallon plate at about 20 Ma. Their model suggests that the downgoing plate was subsequently penetrated at 17.5 Ma, allowing the plume to ascend and spread out and thus producing the Columbia River basalts and the Yellowstone hot-spot track. Alternatively, an upwelling and thickening plume head became compressed and distorted by the southwest-moving Precambrian cratonic plate (Camp, 1995) before Columbia River and SRP volcanism. Either scenario requires a complex interaction of the plume with dissimilar accreted terranes that is likely to be reflected in compositional differences between the two major provinces.

Calculated rates of movement of the North American continent southwestward range from 2.9 to 7 cm/year, with an average rate of 4 ± 1 cm/year (Smith and Braile, 1993). Pierce and Morgan (1992) indicate a shift in the age progression, along with the 10 Ma volcanic transition, in the hot-spot track near the proposed Picabo volcanic center that relates to a decrease in the rate of hot-spot migration (7 cm/year to 2.9 cm/year) and a change in direction (N. 70º-75º E. to N. 54º E.). Taking into account Basin and Range extension along the hot-spot track and Miocene-Pliocene plate rotation, Rodgers and others (1990) determined a rate of 4.5 cm/year and a direction of N. 56º E. of the volcanic track over the last 16 Ma.

PETROLOGIC COMPARISON OF SRP RHYOLITES

The locations, ages, and lithologies of SRP rhyolites obtained from various sources are summarized in Table 1 for inferring petrogenesis and eruptive styles. Ignimbrites in the Cassia Mountains include the following units (oldest to youngest): the tuffs of Magpie Basin and Big Bluff, which erupted from the Bruneau-Jarbidge center, and the tuffs of Steer Basin, Wooden Shoe Butte, and

Table 1. Summary of locations, ages, ash-flow tuff units, and eruptive mechanisms of six SRP volcanic centers (after Bonnichsen, 1982; Bonnichsen and Citron, 1982; Embree and others, 1982; Christiansen, 1982, 1984; Ekren and others, 1984; Hildreth and others, 1984; Morgan and others, 1984; Neace, 1986; Bonnichsen and Kauffman, 1987; Bonnichsen and others, 1987; Kellogg and Marvin, 1988; Henry and Wolff, 1992; Honjo and others, 1992; Pierce and Morgan, 1992; Kellogg and others, 1994).

Volcanic Center	Owyhee-Humboldt	Bruneau-Jarbidge	Twin Falls	Picabo	Heise	Yellowstone
Location	42ºN 116º-117ºW	42º30'N 115º-116ºW	43ºN 114ºW	43ºN 113ºW	44° N 112ºW	44º30'N 111ºW
Age (Ma)	13.8-12.0	12.5-11.3	10.0-8.6	10.2	6.7-4.3	2.0-0.6
Ash-flow tuff units	tuff of Mill Cr., Swisher Mt. Tuff, Juniper Mt. tuff of the Badlands	Cougar Point Tuff, tuffs of Big Bluff and Magpie Basin	tuffs of McMullen Creek, Wooden Shoe Butte, and Steer Basin	Arbon Valley Tuff Member of the Starlight Formation	tuffs of Blacktail, Blue Creek, and Kilgore	Huckleberry Ridge Tuff, Mesa Falls Tuff, and Lava Creek Tuff
Minerals, common (& rare or accessory)*	Pl, Qtz, Sa, Pgt, Mag, (Opx, Zrn, Ap)	Pl, Qtz, Sa, Cpx, Pgt, Mag, (Fa, Opx, Ilm, Ap, Mnz, Zrn)	Pl, Pgt, Cpx, Qtz, Mag, (Opx, Sa, Ap, Zrn)	Pl, Qtz, Sa, Bt, Cpx (Ap, Zrn)	Pl, Qtz, Sa, Cpx, Opx, Mag, Bt, (Zrn, Ap)	Qtz, Sa, Pl, Cpx, Cam, Fa, Mag, Ilm (Zrn, Aln, Ap)
Anhydrous assemblage?	yes	yes	yes	no	no	no
Rheomorphism?	yes	yes	yes	no	no	no
Magmatic Temperature	>1090ºC	850ºC-1000ºC	1040ºC-1100ºC	not determined	est. ~860ºC	820ºC-900ºC

*Mineral abbreviations (Kretz, 1983): Qtz = quartz, Pl = plagioclase, Sa = sanidine, Pgt = pigeonite, Cpx = Ca clinopyroxene, Opx = orthopyroxene, Mag = magnetite, Cam = Ca clinoamphibole, Fa = fayalite, Ilm = ilmenite, Ap = apatite, Zrn = zircon, Mnz = monazite, Aln = allanite.

McMullen Creek, which erupted from the inferred Twin Falls center. All are characterized by intense welding, basal vitrophyres, massive to platy devitrification zones, and lavalike rheomorphic folding (Williams and others 1990, 1991; Mytton and others, 1990; Parker and others, 1996; Watkins and others, 1996). Anhydrous phenocryst assemblages and rheomorphic folding are common in the high-temperature rhyolites of southwestern SRP centers: Owyhee-Humboldt, Bruneau-Jarbidge, and Twin Falls. Pyroclastic textures are present, but some of the ignimbrites were so hot upon emplacement that they coalesced and flowed under traction or gravitational forces, creating rheomorphic features similar to those of lava flows (Bonnichsen and Citron, 1982; Ekren and others, 1982, 1984; Bonnichsen and Kauffman, 1987; Bonnichsen and others, 1989; Henry and Wolff, 1992; Branney and Kokelaar, 1992; Parker and others, 1996; Watkins and others, 1996; McCurry and others, 1996, 1997). By contrast, many rhyolites in the northeastern Picabo, Heise, and Yellowstone centers contain hydrous phases (biotite or amphibole) and well-developed vapor-phase zones and are poorly to densely welded without much rheomorphism (Morgan and others, 1984; Christiansen, 1984; Hackett and Morgan, 1988; Kellogg and Marvin, 1988).

ESTIMATES OF TEMPERATURES AND VOLATILE CONTENTS

Anhydrous mineral assemblages in southwestern rhyolites were used to infer high magma temperatures, perhaps with low water content (Ekren and others, 1984; Honjo and others, 1992). Eruption temperatures in the Owyhee-Humboldt volcanic center, initially estimated to be as high as 1100ºC (Ekren and others, 1984), were recalculated at 930ºC-960ºC (Honjo and others, 1992), whereas estimates for the Bruneau-Jarbidge rhyolites by Bonnichsen and others (1987) range from 800ºC to 1050ºC.

The presence of biotite as a common phenocryst in the Arbon Valley Tuff Member of the Starlight Formation (Picabo center) and in the ash-flow tuffs of the Heise center is consistent with lower eruption temperatures of these units relative to those of the southwestern volcanic centers. The eruption temperature of the amphibole-bearing Lava Creek Tuff in the Yellowstone center was calculated to be 820ºC-900ºC (Hildreth and others, 1984), and temperatures of three major Yellowstone units were generalized only as greater than 850ºC (Christiansen and Hildreth, 1989). On the basis of similarities in the eruptive style and zirconium concentrations of the Heise and Yellowstone ash-flow tuffs, Perkins and others (1995) suggest similar eruptive temperatures (about 860ºC) for the Heise units. Thus, a transition apparently occurred in which eruption temperatures decreased, and perhaps volatile concentrations increased, from southwest to northeast across the SRP Province.

GEOCHEMICAL VARIATION AMONG SRP RHYOLITIC VOLCANIC CENTERS

The chemistries of rhyolites from the postulated Twin Falls volcanic center are known from 106 analyses, many of which are from the tuffs of Wooden Shoe Butte (Parker, 1996) and Steer Basin (Watkins, 1998). Other analyses used in this compilation are from Bonnichsen and others (1994a, 1994b) for the Bruneau-Jarbidge region and from Ekren and others (1982), Leeman (1982b), Morgan and others (1984), Hildreth and others (1984, 1991), Kellogg and Marvin (1988), Honjo (1990), and Manley (1995). Representative compositions (Table 2) illustrate the dominantly rhyolitic nature of SRP ash-flow units and the regional variation of major and trace elements across the volcanic province. Parker and others (1996) address the problem of chemical variation within an ignimbrite and show that much of the variation in Twin Falls compositions can be attributed to crystal-glass segregation during emplacement.

Figure 2 illustrates the differences in chemical compositions between the southwestern and northeastern SRP volcanic centers. The Yellowstone, Heise, and Picabo centers have higher SiO_2, Na_2O, and total alkalis and lower TiO_2, FeO, and CaO/Al_2O_3 than most samples from the Bruneau-Jarbidge and Twin Falls centers. Notice that units in the Mount Bennett Hills, which were originally included in the Picabo center by Honjo (1990), plot among the data for Twin Falls and Bruneau-Jarbidge centers. The compositional division between the southwestern and northeastern volcanic centers is shown by the broken lines in Figure 2. Aside from a few outlying compositions, the clustering of Bruneau-Jarbidge with Twin Falls compositions and of Yellowstone with Heise compositions is generally apparent, suggesting that some combination of different magma sources and subsequent evolution were operative.

Discrimination of the volcanic centers is also possible using covariations of Ba versus Sr, Zr versus TiO_2, Sm/Eu versus La, and Hf versus Ta (Figure 3) with ranges defining separate clusters for representative units from the northeastern and southwestern volcanic centers. Most samples from the Yellowstone and Heise volcanic centers are characterized by relative depletions of Sr (<60 ppm), Ba (<1100 ppm), Zr (<480 ppm), and TiO_2 (<0.4 weight percent) compared to higher values of these elements from the rhyolites of the Twin Falls centers (Sr =

Table 2. Representative bulk rock analyses of rhyolitic ash-flow tuffs from the Yellowstone-Snake River Plain Province.

Vol. Ctr:	Bruneau-Jarbidge			Twin Falls					Picabo	Heise			Yellowstone Plateau				
Source✦	1	1	1	2	2	2	2	2	3	4	4	4	5	5	5	1	1
Sample	I-569	I-841	I-459	830-10	JPSCH-4	830-07A	830-05	830-01	MC-22	BkTail-2	BluCr-2	tuff of	81yh-96	78yh-40	8yc-413	yg70-13	6yc-135
Unit	CPT-II	CPT-VI	CPT-XV	Tmc	Twsb	Tsb	Tbb	Tmb	AVT	Blacktail	Blue Cr.	Kilgor	HRT	MFT	LCT	intra C	extra C
Major oxides in wt. % normalized to 100% anhydrous																	
SiO_2	76.70	73.30	73.80	75.70	71.90	72.00	74.30	75.00	75.50	76.20	76.50	75.00	75.80	75.70	77.70	77.10	76.10
TiO_2	0.15	0.49	0.42	0.33	0.64	0.62	0.38	0.34	0.15	0.23	0.11	0.21	0.14	0.20	0.08	0.12	0.17
Al_2O_3	12.60	13.00	12.90	12.00	13.10	12.60	12.00	12.20	13.20	12.60	12.60	12.10	12.80	12.50	12.10	11.90	12.40
FeO*	1.30	2.99	2.77	2.26	4.42	4.22	3.17	2.61	1.30	1.43	1.42	1.34	1.72	1.67	1.18	1.57	1.82
MnO	0.02	0.05	0.05	0.03	0.07	0.06	0.05	0.04	0.02	0.03	0.02	0.03	0.03	0.05	0.02	0.04	0.02
MgO	0.36	0.42	0.50	0.11	0.45	0.34	0.10	0.08	0.27	0.23	0.16	0.31	nd	0.37	nd	0.01	0.20
CaO	0.64	1.35	1.40	0.57	2.08	1.64	1.31	0.71	0.96	0.61	0.43	2.51	0.68	0.81	0.44	0.48	0.72
Na_2O	2.56	2.52	2.90	3.15	2.78	3.08	3.40	2.92	3.49	3.04	3.55	3.07	3.36	3.32	3.47	3.83	4.03
K_2O	5.62	5.78	5.18	5.76	4.41	5.38	5.15	6.06	5.11	5.59	5.11	5.39	5.45	5.28	5.08	4.93	4.55
P_2O5	0.02	0.09	0.06	0.03	0.16	0.10	0.05	0.04	0.02	0.05	0.05	0.05	nd	0.04	0.01	nd	0.02
Orig. Sum	99.88	99.72	99.67	98.09	98.93	99.35	99.34	100.37	97.70	100.00	99.99	100.01	99.42	99.71	99.42	99.77	99.39
Trace elements in ppm																	
Sc	1.70	5.70	4.40	3.80	7.20	5.20	4.70	3.70	4.00	nd	nd	nd	nd	nd	nd	1.30	2.00
Cr	nd	nd	nd	1.60	4.80	3.30	2.00	1.40	2.00	nd	nd	nd	nd	nd	nd	nd	nd
Co	0.60	2.70	2.20	1.30	3.90	3.30	1.70	1.30	0.80	nd	nd	nd	nd	nd	nd	0.10	0.30
Rb	313	220	188	229	167	221	222	227	169	240	220	222	250	178	300	214	174
Sr	16	87	81	36	122	94	63	40	51	58	32	22	18	39	nd	0.40	40
Cs	7.20	4.92	4.01	3.58	3.32	4.31	4.14	3.94	2.95	nd	nd	nd	5.00	3.20	6.80	4.00	2.00
Ba	95	989	1155	1083	1225	1190	1330	1170	388	930	1110	943	105	715	28	19	459
La	82.00	78.40	84.60	85.80	82.10	82.90	88.80	84.40	68.40	72.00	85.00	84.00	nd	nd	nd	87.00	59.00
Ce	156	153	158	172	151	162	173	161	133	148	175	165	148	148	116	171	142
Nd	65	62.40	65.50	64	64	65	72	61	57	57	73	74	nd	nd	nd	69	59
Sm	12.80	11.70	11.90	12.90	12.50	12.60	14.30	12.20	10.80	10.00	14.00	13.00	nd	nd	nd	15.80	11.80
Eu	0.22	1.49	1.48	1.28	2.17	1.42	1.86	1.33	0.78	1.30	2.10	1.40	0.22	1.15	0.13	0.37	0.88
Tb	1.15	0.87	0.91	1.82	1.97	1.78	2.01	1.65	1.75	1.00	2.00	1.00	nd	nd	nd	2.49	1.70
Yb	7.80	5.65	6.06	6.00	5.92	6.06	6.90	5.74	6.40	5.00	7.00	6.00	7.10	5.80	10.10	8.57	5.60
Lu	1.17	0.88	0.95	0.89	0.82	0.87	1.05	0.86	0.89	0.80	1.00	0.90	nd	nd	nd	1.25	0.77
Zr	218	483	465	412	690	590	589	483	162	220	222	230	150	285	300	286	228
Hf	8.10	12.90	12.40	12.50	17.50	14.90	16.10	13.80	5.60	9.00	8.00	11.00	5.80	8.00	7.50	11.60	7.30
Ta	5.10	3.13	3.07	3.46	2.69	2.90	3.16	2.90	2.78	nd	nd	nd	4.70	3.45	6.80	5.80	3.20
Th	44.50	32.20	32.30	33.50	18.40	33.00	31.50	33.80	26.9	nd	nd	nd	34.90	26.80	37.50	28.60	22.00
U	12.30	8.50	8.10	7.60	6.70	7.50	7.00	7.10	6.0	nd	nd	nd	7.90	5.90	12.00	7.80	4.00

✦Sources of data: (1) Honjo, 1992; (2) Hughes and others, 1996; (3) unpublished, Idaho State University laboratory; (4) Morgan and others, 1984; (5) Hildreth and others, 1984

*Total Fe reported as FeO

nd = value not determined or out of analytical range

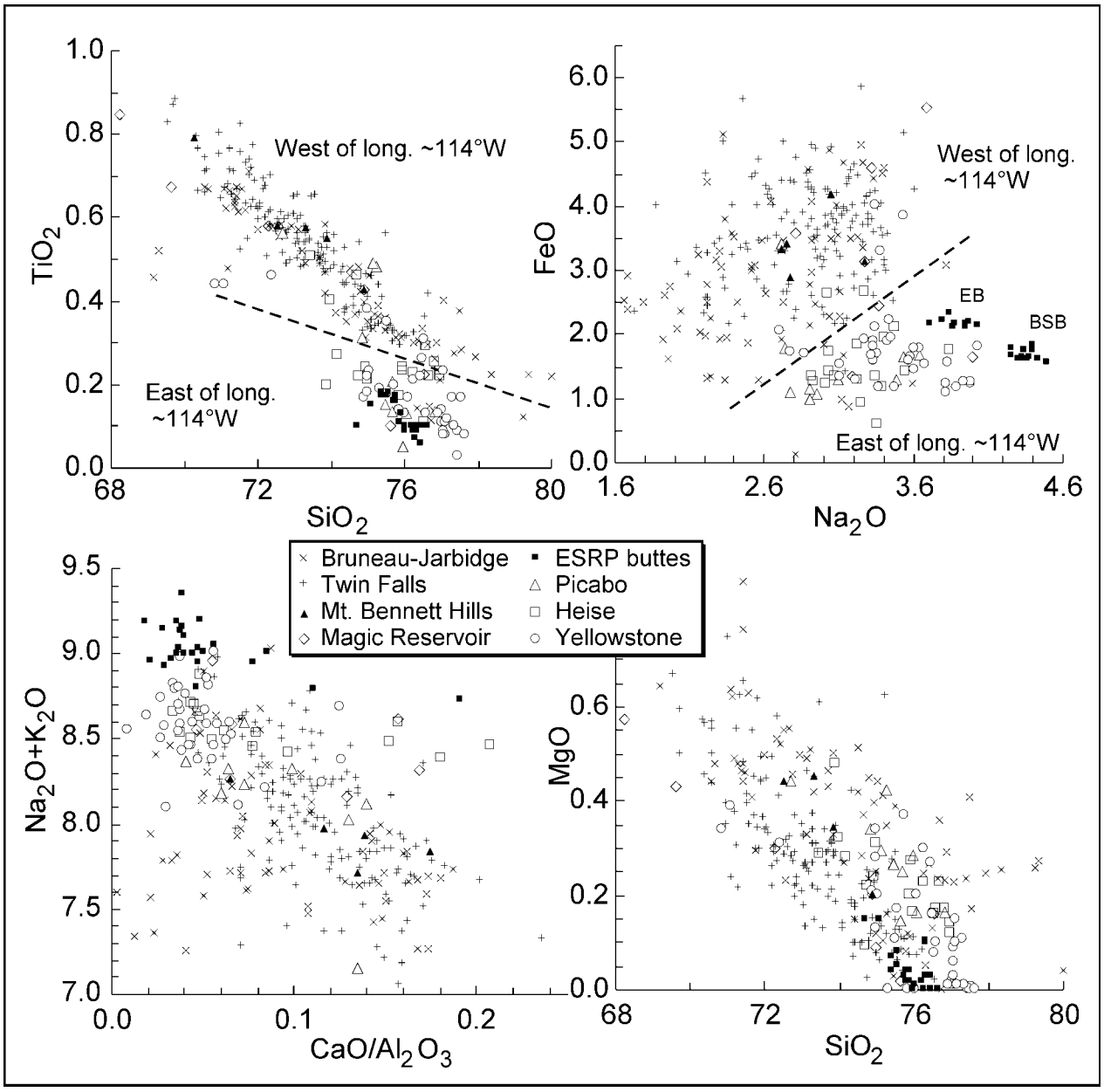

Figure 2. Covariation plots of TiO_2 versus SiO_2, FeO versus Na_2O, Na_2O+K_2O versus CaO/Al_2O_3, and MgO versus SiO_2 for rhyolitic units associated with the SRP Province. Data are from Bonnichsen and others (1994a, 1994b), Ekren and others (1982), Leeman (1982b), Morgan and others (1984), Hildreth and others (1984, 1991), Kellogg and Marvin (1988), Honjo (1990), Manley (1995), and unpublished data from this study by the Idaho State University Laboratory for Environmental Geochemistry. Picabo samples are those represented by the Arbon Valley Tuff Member of the Starlight Formation and associated rhyolites, whereas Mount Bennett Hills samples consistently plot with the Twin Falls and Bruneau-Jarbidge centers. Rhyolites from the 5 Ma Magic Reservoir center and the late Pleistocene eastern SRP rhyolite domes (ESRP buttes) are shown for comparison, although they are not considered to be part of the time-transgressive SRP-Yellowstone hot-spot track.

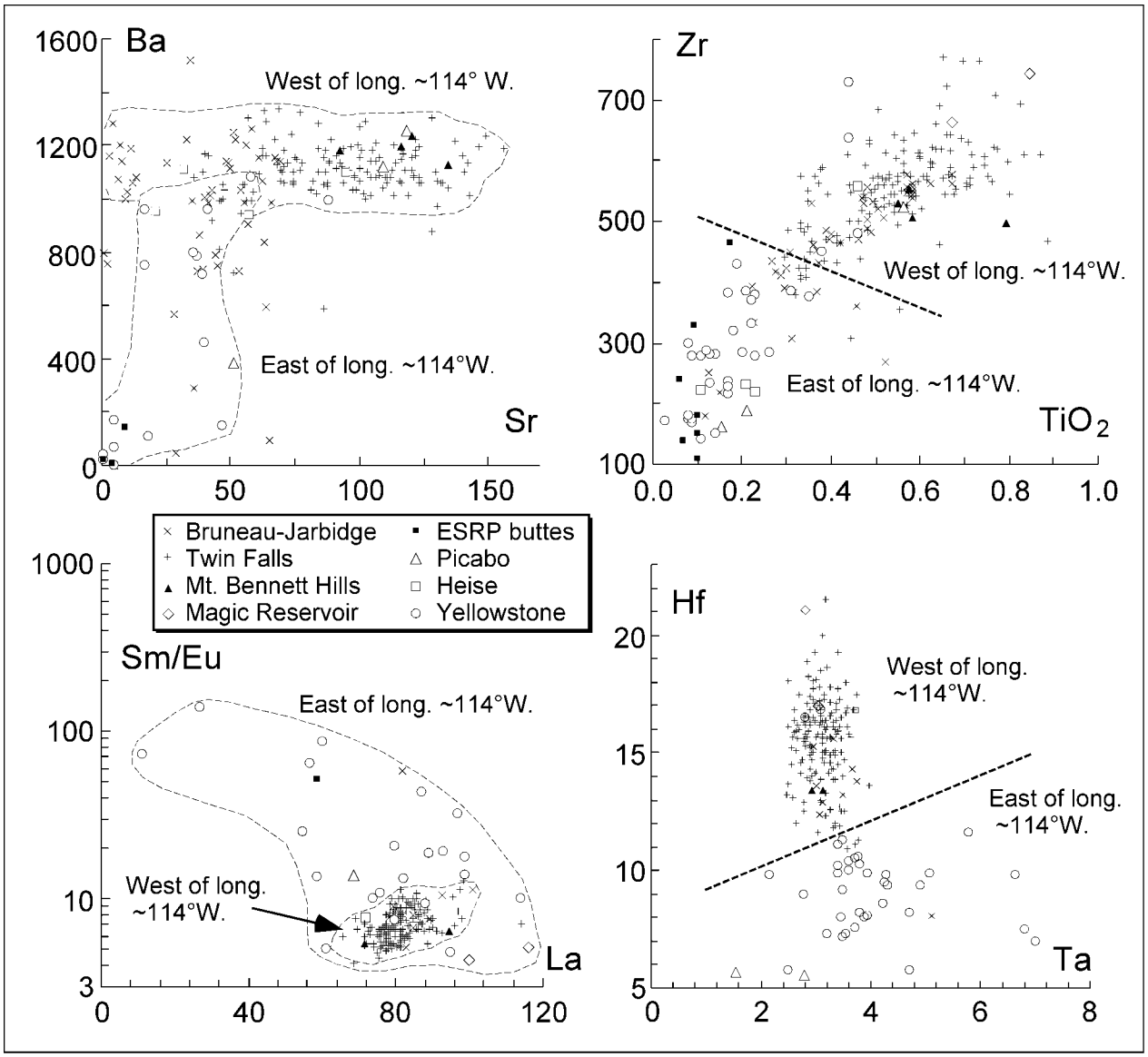

Figure 3. Covariation plots of Ba versus Sr, Zr versus TiO_2, Sm/Eu versus La, and Hf versus Ta for SRP rhyolitic units (all parameters are the same as in Figure 2). See text for explanation.

30-180 ppm, Ba = 600-1400 ppm, Zr = 400-800 ppm, TiO_2 = 0.3-0.9 weight percent). Bruneau-Jarbidge compositions coincide roughly with Twin Falls clusters, except for the lower Sr reported for several samples. Sm/Eu ratios and La (ppm) are significantly more scattered in northeastern centers (Sm/Eu = 5-200; La = 10-120) relative to the tight clustering of data for the southwestern centers. Strong discrimination of the bulk rock compositional differences between the rhyolites is shown by Hf and Ta; southwestern centers have fairly uniform Ta values (2.5-4 ppm) and relatively high Hf (10-22 ppm) compared to northeastern centers with lower Hf (5-11 ppm) and a much wider range in Ta (1.5-7 ppm). These chemical differences are compelling and attest to an overall change in magma generation and evolution. Moreover, Na_2O is significantly higher and K/Na ratios lower in northeastern SRP rhyolites relative to those from southwestern centers (Table 2). Despite these distinctions, no overall differences in the abundances of the alkalis K_2O, Rb, and Cs are apparent throughout the SRP Province.

The chemical signatures of rhyolites originally associated with the Picabo volcanic center include data for samples from two separate regions: (1) the Arbon Valley Tuff Member of the Starlight Formation (Kellogg and others, 1994) and associated rhyolites of Buckskin Basin, Two-and-a-Half Mile Creek, and Stevens Peak near

Pocatello (Kellogg and Marvin, 1988), and (2) the Picabo Tuff, the tuff of Thorn Creek, and other units in and near the Mount Bennett Hills north of Twin Falls (Leeman, 1982b; Honjo, 1990). These data are less well-clustered than the other SRP compositions and yield different chemical signatures. The Mount Bennett Hills samples plot in clusters defined by the Twin Falls and Bruneau-Jarbidge volcanic centers (Figures 2 and 3), and the Arbon Valley Tuff and associated units plot more with Yellowstone-Heise volcanics (Figure 2). Kellogg and others (1994) have demonstrated the bulk chemical affinity of the Arbon Valley Tuff and related volcanics with rocks from the Heise center; however, the meager amount of trace element data (Figure 3) does not confirm an association with Heise units.

If the Picabo center is a distinct SRP volcanic system, it is best represented by the Arbon Valley Tuff and associated rhyolites (Pierce and Morgan, 1992). Conversely, the ash-flow tuffs exposed in the Mount Bennett Hills have strong lithologic and chemical affinities, as well as geographic proximity, to the units of the Cassia Mountains south of Twin Falls (Paul Williams, oral commun., 1995). On the basis of these correlations, the Mount Bennett Hills units (included with either Picabo or Twin Falls centers by Pierce and Morgan, 1992) are probably associated with the Twin Falls volcanic center.

TRACE ELEMENT CONSTRAINTS ON RHYOLITE PETROGENESIS

Trace element data, normalized to average continental lower crust (Taylor and McLennan, 1985; Rudnick and Fountain, 1995), may be used to infer possible mineralogic controls during partial melting and subsequent evolution of these magmas. Trace element patterns for the Cassia Mountains ignimbrites of the Twin Falls volcanic center (Figure 4) and the Bruneau-Jarbidge volcanic center (Figure 5) are less enriched in Ba, Sr, Eu, Ti, and Sc, elements that are more compatible in restite phases, than they are in less compatible elements such as Cs, Rb, Th, U, K, Zr, Hf, and REE. The mineral-liquid equilibria during primary crustal anatexis, the assimilation of partially melted crust, or the fractional crystallization of parental magma could account for the relative abundances of these elements. The patterns suggest that the source restite (after partial melting) for these magmas consisted of plagioclase, pyroxene, and Fe-Ti oxides but did not include significant amounts of alkali feldspar, garnet, zircon, or other trace minerals such as apatite which, if originally present, became incorporated into the silicic magma. The predicted restite assemblage is consistent with the minerals found in granulite-facies

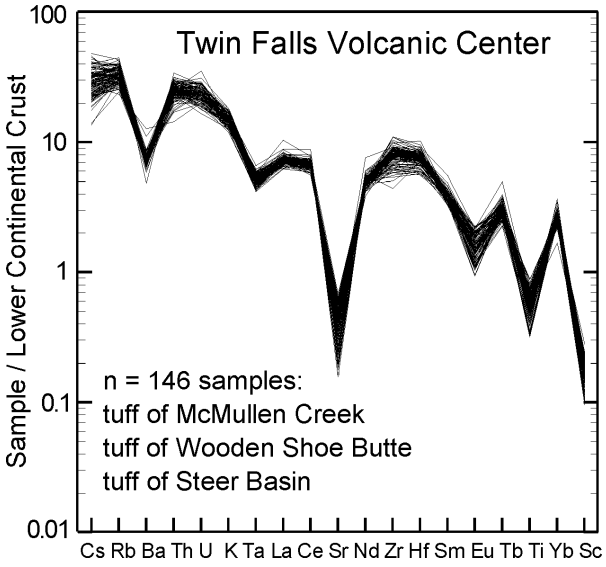

Figure 4. Multielement patterns of Cassia Mountains high temperature rhyolitic ash-flow tuff samples (Twin Falls volcanic center) normalized to average lower continental crust values (Taylor and McLennan, 1985; Rudnick and Fountain, 1995). Elements are shown in order of overall decreasing incompatibility in lower crust and upper mantle regimes. Data from this study.

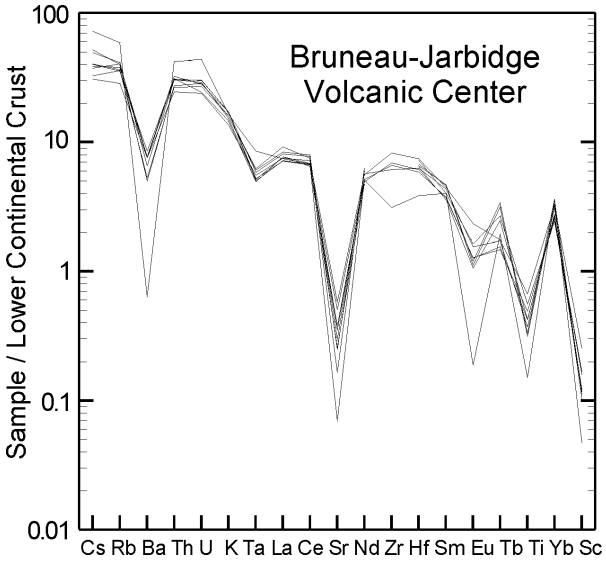

Figure 5. Multielement patterns of high temperature rhyolitic ash-flow tuff samples from the Bruneau-Jarbidge volcanic center normalized to average lower continental crust values (Taylor and McLennan, 1985; Rudnick and Fountain, 1995). Elements are shown in order of overall decreasing incompatibility in lower crust and upper mantle regimes. Data from Bonnichsen and others (1994a, 1994b).

rocks and models mentioned above. Subsequent mineral fractionation also may be responsible, in part, for the observed enrichment patterns, but the process will be manifested more in strongly depleted compatible elements. For low-degrees of melting, this may not be easily distinguished from a partial melt-restite relation.

Most significant is the uniformity among patterns for samples from a given unit, reflecting relatively minor magmatic evolution subsequent to magma generation. Chemical signatures of most Cassia Mountains ash-flow tuffs have no systematic zoning of major or trace elements either vertically within sections or with distance from the thickest section. Any zonation inherent in the magma chamber was either insignificant or mixed, on the scale of hand samples, during eruption. As with major-element variations, the different trace-element abundances in most of the Cassia Mountains units can be related, in part or entirely, to crystal-glass segregation during emplacement (e.g., Parker and others, 1996; Watkins, 1998).

The youngest group of ignimbrites in the Cassia Mountains is distinguished by chemical zonations that cannot be entirely accounted for by depositional processes (Wright, 1998; Wright and others, this volume). Wright suggests that at least some of the compositional variation resulted from fractional crystallization of the observed phenocryst phases. We also recognize multimodal glass shard compositions documented by Perkins and others (1995) for fallout units that appear to be comagmatic with some Cassia Mountains ignimbrites. Taken together, these observations suggest that subtle, small-scale chemical variations occurred within at least some of the source magma chambers.

Yellowstone trace-element patterns (Figure 6) illustrate extreme depletions of compatible elements producing negative anomalies of Ba, Sr, Eu, Ti, and Sc. These signatures may be due primarily to plagioclase, pyroxene, and Fe-Ti oxide fractionation, indicating extensive magma evolution and, hence, long crustal history. Also apparent are slight variations in other elements affected by minor phases, such as Ta in Fe-Ti oxide and Zr in zircon, plus increases in the incompatible elements Th and U related to either fractionation or assimilation. It may be significant that K remains fairly constant, implying a lack of K-feldspar fractionation, even though sanidine occurs as a phenocryst in these rocks. These relations suggest that in the Yellowstone system the initial magmas began crystallizing as soon as they began to ascend from the zone of partial melting. Fractionation likely involved thermodiffusive boundary-layer effects as magmas coalesced into a large shallow chamber and erupted from associated calderas (Hildreth, 1981).

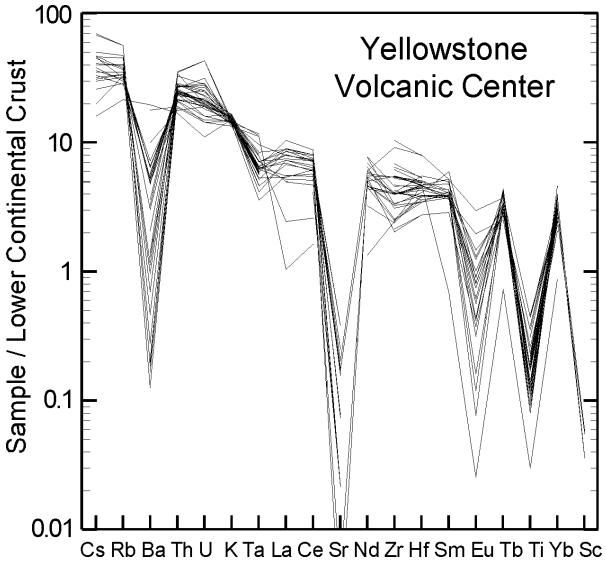

Figure 6. Multielement patterns of Yellowstone rhyolitic ash-flow tuff samples normalized to average lower crustal values (Taylor and McLennan, 1985; Rudnick and Fountain, 1995). Yellowstone rhyolites have significant relative depletion (or lack of enrichment) compared to rhyolitic samples from the Twin Falls volcanic center. Data are from Hildreth and others (1984, 1991) and Honjo (1990).

Similar trace element patterns among Cassia Mountains ignimbrites argue in favor of low residence times for magmas erupted from middle to deep crustal regions, which would produce compositions close to primary partial melts of the lower crust. Eruption of more primitive magma from a deep chamber likely would not produce clearly defined calderas, although some subsidence of the overlying crust might be possible (Lipman, 1997). By contrast, silicic magmas erupted from shallow chambers would yield compositions reflecting significant middle and upper crustal evolution during or after ascent of the magma bodies. The fractionated trace-element patterns of the Yellowstone rhyolites require longer periods of magma evolution before eruption, indicating a long crustal residence time, in accord with field evidence that Yellowstone and Heise rhyolites are derived from shallow caldera systems. The trace-element patterns of Picabo and Heise rhyolites (Figure 7) have depleted Sr, Eu, Ti, and Sc and an overall close affinity to the Yellowstone system, which suggests a similar episode of long crustal residence time in a shallow magma chamber.

LITHOSPHERIC CONTROLS ON SRP RHYOLITE MAGMATISM

Differences in the lithologies, eruptive styles, compositions, and emplacement mechanisms of SRP rhyo-

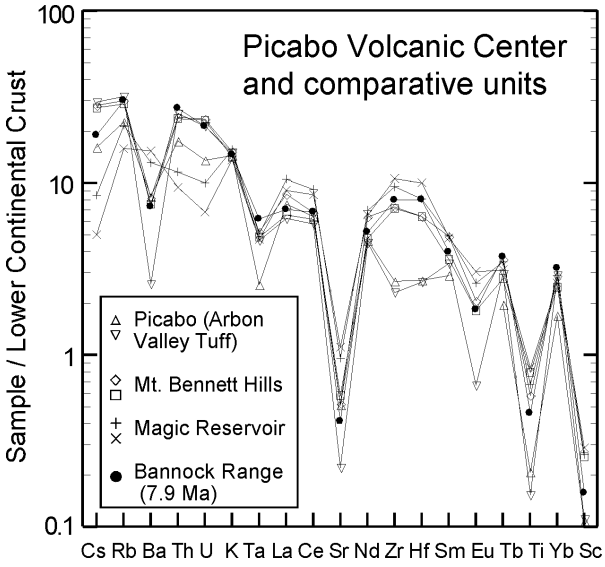

Figure 7. Multi-element patterns of Picabo (Arbon Valley Tuff) and comparative central SRP rhyolite samples normalized to average lower crustal values (Taylor and McLennan, 1985; Rudnick and Fountain, 1995). The two Picabo samples and a 7.9 Ma rhyolite lava from the Bannock Range near Pocatello represent unpublished analyses of samples collected by the authors. Although unconfirmed, the Bannock Range unit may have erupted from the Picabo center. Data for Mount Bennett Hills samples (probably Twin Falls center) and Magic Reservoir samples (not associated with the Yellowstone hot-spot track) are from Honjo (1990).

lites are not coincident with isotopically determined terrane boundaries. Petrochemical differences among SRP rhyolites and basalts may reflect the influence of different lithospheric terranes (Armstrong and others, 1977; Fleck and Criss, 1985; Lund and Snee, 1988), exemplified by a west-to-east transition of age-corrected $^{87}Sr/^{86}Sr$ ratios from less than 0.704 to greater than 0.706, roughly coincident with a N-S line at about long 116º30′W. The map positions of lines marking the $^{87}Sr/^{86}Sr = 0.704$ and 0.706 limits are well-defined in the region between Columbia River basalts and the Mesozoic batholiths in Idaho, but the southern extensions have been subject to different interpretations because of incomplete analytical coverage. Armstrong and others (1977) show a narrow 0.704-0.706 transition extending southward about lat 46ºN. into the Owyhee Plateau; it then splits near lat 43ºN. with the 0.704 limit and continues southwest to yield a widening 0.704-0.706 transition in northern Nevada. Pierce and Morgan (1992) summarize geologic evidence that implies a separation of the 0.704-0.706 line about lat 43ºN. but with the 0.704 limit extending southwestward and the 0.706 limit extending southeastward. This would place SRP rhyolitic centers older than the Twin Falls center within the 0.704-0.706 transition.

Leeman and others (1992) propose that regional isotopic signatures define a narrow accretionary N-S suture zone about long 116º15′W. to long 119ºW. that occurred along a westward-dipping mantle-level decollement during late Mesozoic-early Tertiary Rocky Mountain thrusting. Their model presents a scenario in which magmatism occurring within the suture zone, including the Columbia River basalts (Chief Joseph dike swarm) and westernmost SRP, has transitional isotopic compositions caused by two overlapping sources: accreted oceanic lithosphere and cratonic subcontinental mantle. Volcanic systems lying west of this zone were derived from accreted lithosphere having oceanic affinities, such as the Picture Gorge member of the Columbia River basalts (Monument dike swarm) and some Oregon high lava plains volcanics. Isotopic signatures east of the zone (i.e., much of the SRP system) are representative of cratonic lower crust and subcontinental lithosphere.

Leeman and others' (1992) location of the boundary between the accreted terranes and the craton near the Oregon-Idaho border is also consistent with regional patterns in the Sr- and Nd-iostopic signatures of Mesozoic plutons studied by Farmer and DePaolo (1983). Along the SRP volcanic track, there is thus an apparent decoupling of the transitions in mineralogy and chemical compositions of the rhyolites on one hand (at long 114ºW.) and their isotopic compositions on the other (at long 116º-117ºW.). This decoupling, as well as uncertainties in locating the edge of the craton, may reflect a structural complexity, perhaps due to an irregular thinning of the cratonal lithosphere, near its western rifted margin.

MAGMA GENESIS AND EVOLUTION

Silicic magmas of the Yellowstone and Owyhee-Humboldt centers have been modeled by the partial melting of granulite-facies rocks of the deep crust (Doe and others, 1982; Ekren and others, 1984) extensively modified by mixing with mantle-derived basalt (e.g., Hildreth and others, 1991). According to this model, basaltic magma that is formed by a partial melting of the upper mantle provides material and heat to the lower crust. Rising basaltic magmas spread laterally, owing to density contrasts, and cause the partial melting of the hybridized crust to yield rhyolitic magmas by conductive heating (Huppert and Sparks, 1988; Bergantz and Dawes, 1994). Melting experiments by Whitney (1988) show that, at 8 kbar pressure and low H_2O content (less than about 1.5 weight percent), temperatures in excess of 1100ºC are required to produce a rhyolitic magma from sources in which plagioclase is the only felsic residual phase. More water is necessary to produce separable amounts of rhyolitic magma at lower temperatures.

Support for the involvement of crustal rocks in SRP rhyolite genesis comes from isotopic studies that suggest different source materials for the rhyolites and the basalts. Lead and strontium isotopic ratios in SRP basalts ($^{206}Pb/^{204}Pb$ = 16.1-17.3; $^{87}Sr/^{86}Sr$ = 0.7039-0.7089) indicate upper mantle reservoirs, whereas isotopic ratios of Yellowstone rhyolites ($^{206}Pb/^{204}Pb$ = 16.6-18.1; $^{87}Sr/^{86}Sr$ = 0.7084-0.7268) suggest a lower crustal granulite-facies source (Doe and others, 1982). Hildreth and others (1991) propose that the Yellowstone rhyolites represent either partial melts of lower crustal rocks or a combination of melts from upper crustal plutonic rocks, deep-crustal granulites, and fractionated basalts. Recent Sr and Nd isotopic studies of SRP rhyolites in the central plain indicate less than 20 percent Precambrian crustal component in their magmas (Wright and others, this volume).

MODEL FOR TECTONIC-MAGMATIC TRANSITION

Models of silicic magma genesis and evolution in the SRP system are supported by experiments on the melting of granulites and other lower crustal rocks in high pressure regimes (Watt and Harley, 1993; Beard and others, 1994; Patiño-Douce and Beard, 1995). Thermal requirements are high and argue in favor of a large heat source related to a mantle-derived plume, which caused extensive partial melting in the lithospheric mantle and subsequently in the lower crust. Rhyolitic ash-flow tuffs in the southwestern part of the SRP Province erupted directly from deep-seated magmas in the Owyhee Mountains, which did not produce significant shallow ring fractures or calderas (Ekren and others, 1982, 1984). Magma ascent in northeastern SRP systems caused ring-fracture systems and caldera complexes such as those at Yellowstone (Christiansen, 1984). The physiographic difference between the southwestern and northeastern SRP volcanic centers is thought to be related to a crustal transition from accreted to cratonic terranes, and we argue that this transition is also reflected in different rhyolitic magma compositions, temperatures, and modes of generation.

The explanation of differences between the southwestern and northeastern segments of the SRP Province must address complexities related primarily to mafic magmatism and the various types of continental crust. A schematic model of magma genesis and evolution in the two major regions of the SRP Province is presented in Figure 8 on the basis of geochemical and petrologic constraints outlined above. Silicic magmas are generated at temperatures greater than 1000ºC from deep-crustal sources in which plagioclase and pyroxene dominate the residuum (K-feldspar and quartz probably are not restite phases). The generation of silicic magma is directly related to mafic magma underplating, which causes hybridization and partial melting of the lower crust. The concomitant formation of silicic melts ensues, with the segregation of these melts into separate lower-crustal magma bodies. If these deep-seated magmas coalesce into lower to middle crustal chambers that are tapped during lithospheric extension, high-temperature rhyolites will be erupted without significant secondary evolution in the upper crust. However, if lithospheric extension is insufficient to allow magma ascent through fissures, or if the crust is more stable during lithospheric extension, these magmas will remain as relatively small diapiric bodies that ascend and coalesce in the upper crust. This is more likely to occur in the northeastern segment of the SRP Province where crust is thicker, older, and compositionally different from crust in the southwestern segment.

The transition in magmatism reflects physical changes in lithospheric terrane between the Twin Falls and Picabo volcanic centers. The transition defined by geochemical, mineralogical, and eruptive style variations is not consistent with the currently accepted $^{87}Sr/^{86}Sr$ = 0.706 isopleth that separates Paleozoic and younger accreted terranes from older Precambrian crust. Although the terrane boundary is not precisely defined, the petrogenetic shift as determined by geochemical signatures of rhyolites may eventually lead to a better understanding of this major lithospheric transition.

ACKNOWLEDGMENTS

Funding for this research was provided by National Science Foundation EPSCoR Cooperative Agreement OSR-9350539 to Hughes and McCurry. The authors thank Paul Williams and Bill Bonnichsen for help and discussions during field research. Thoughtful and thorough reviews by Bill Hirt and Bill Hackett significantly improved the quality of arguments presented in this paper.

REFERENCES

Alt, David, J.M. Sears, and D.W. Hyndman, 1988, Terrestrial maria: The origins of large basalt plateaus, hot spot tracks and spreading ridges: Journal of Geology, v. 96, p. 647-662.

Armstrong, R.L., J.E. Harakal, and W.M. Neill, 1980, K-Ar dating of Snake River Plain (Idaho) volcanic rocks—new results: Isochron West, no. 27, p. 5-10.

Armstrong, R.L., W.P. Leeman, and H.E. Malde, 1975, K-Ar dating, Quaternary and Neogene volcanic rocks of the Snake River Plain, Idaho: American Journal of Science, v. 275, p. 225-251.

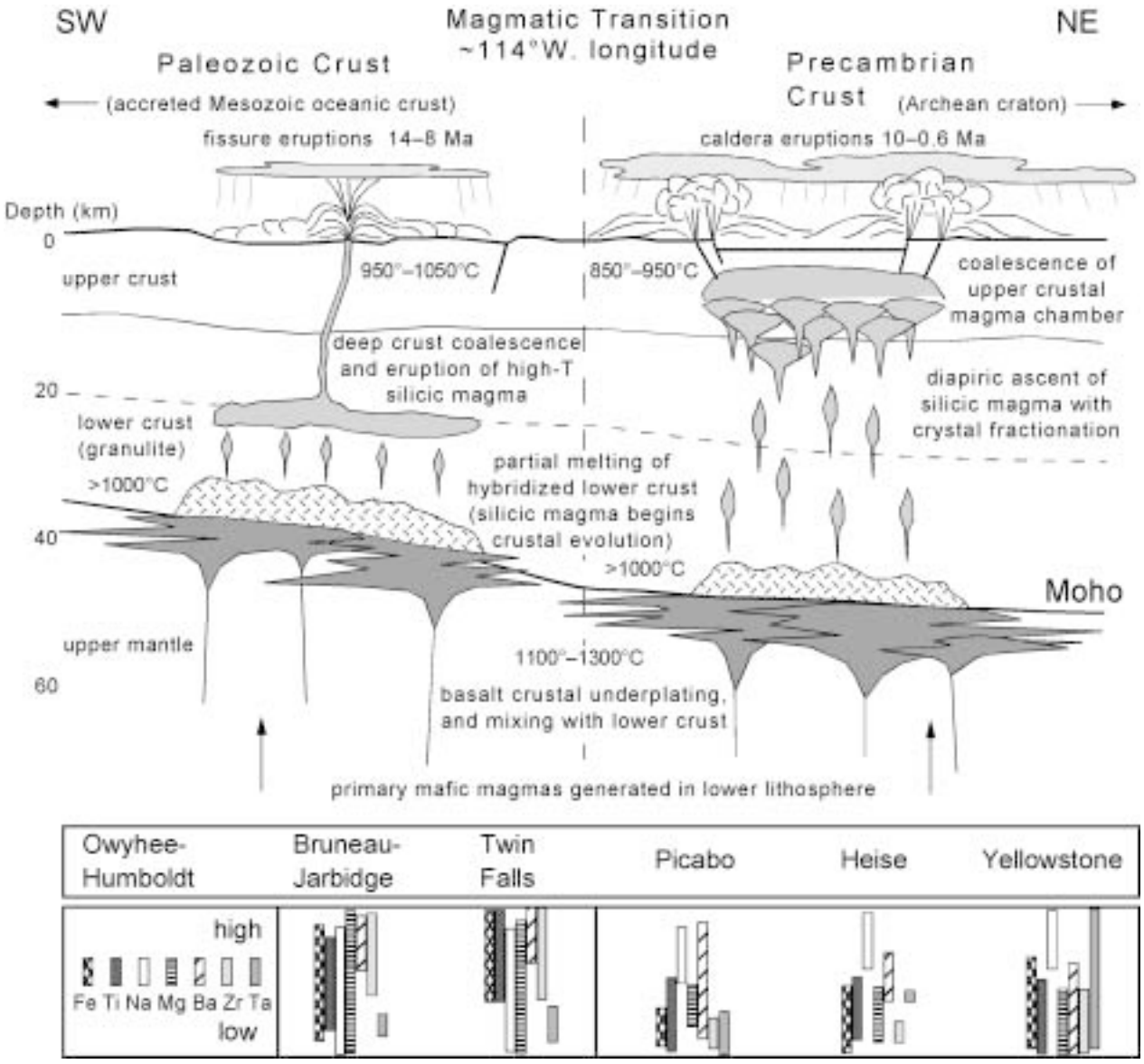

Figure 8. Schematic model of the magmatic transition in the SRP hot-spot tract at long 114ºW. West of the transition, high temperature rhyolites were erupted from regions in the lower or middle crust directly along fissure systems, possibly in response to Basin and Range extension and without significant magmatic differentiation. Calderas were either absent or took the form of crustal downsag in response to eruption from deep-seated sources. East of the transition, parental magmas ascended and coalesced into large upper crustal magma chambers capable of cataclysmic ash eruptions leading to caldera collapse. Relative positions of volcanic centers are from Figure 1. Geochemical signatures are from Table 2 and represent significantly more data from the Bruneau Jarbidge, Twin Falls, and Yellowstone centers than the Heise and proposed Picabo centers.

Armstrong, R.L., W.H. Taubeneck, and P.O. Hales, 1977, Rb-Sr and K-Ar geochronology of Mesozoic granitic rocks and their Sr isotopic composition, Oregon, Washington, and Idaho: Geological Society of America Bulletin, v. 88, p. 397-411.

Beard, J.S., G.E. Lofgren, A.K. Sinha, and R.P. Tollo, 1994, Partial melting of apatite-bearing charnockite, granulite, and diorite: Melt compositions, restite mineralogy, and petrologic implications. Journal of Geophysical Research, v. 99, no. B11, p. 21,591-21,603.

Bergantz, G.W., and R. Dawes, 1994, Aspects of magma generation and ascent in continental lithosphere, *in* M.P. Ryan, ed., Magmatic Systems: Academic Press, New York, p. 291-317.

Bonnichsen, Bill, 1982, The Bruneau-Jarbidge eruptive center, southwestern Idaho, *in* Bill Bonnichsen and R.M. Breckenridge, eds., Cenozoic Geology of Idaho: Idaho Bureau of Mines and Geology Bulletin 26, p. 237-254.

Bonnichsen, Bill, and G.P. Citron, 1982, The Cougar Point Tuff, southwestern Idaho and vicinity, *in* Bill Bonnichsen and R.M. Breckenridge, eds., Cenozoic Geology of Idaho: Idaho Bureau of Mines and Geology Bulletin 26, p. 255-281.

Bonnichsen, Bill, Norio Honjo, and W.P. Leeman, 1987, Relations be-

tween emplacement conditions and physical features in rhyolitic welded tuffs and lava flows, central Snake River Plain, Idaho (abs.): Geological Society of America Abstracts with Programs, v. 19, no. 7, p. 595.

Bonnichsen, Bill, M.D. Jenks, M.M. Godchaux, W.P. Leeman, and M.D. Norman, 1994a, Analyzed rocks from the Glenns Ferry 30 x 60 minute quadrangle, Owyhee, Twin Falls, Gooding, and Elmore counties, southwestern Idaho: Idaho Geological Survey Technical Report 94-4, 1 diskette, 1 plate.

Bonnichsen, Bill, and D.F. Kauffman, 1987, Physical features of rhyolite lava flows in the Snake River Plain volcanic province, southwestern Idaho, *in* J.H. Fink, ed., The Emplacement of Silicic Domes and Lava Flows: Geological Society of America Special Paper 212, p. 119-145.

Bonnichsen, Bill, W.P. Leeman, John Bernt, M.M. Godchaux, and M.D. Jenks, 1994b, Analyzed rocks from the Sheep Creek 30 x 60 minute quadrangle, Owyhee and Twin Falls counties, southwestern Idaho: Idaho Geological Survey Technical Report 94-5, 1 diskette, 1 plate.

Bonnichsen, Bill, W.P. Leeman, M.D. Jenks, and Norio Honjo, 1988, Geologic field trip guide to the central and western Snake River Plain, Idaho, emphasizing the silicic volcanic rocks, *in* P.K. Link and W.R. Hackett, eds., Guidebook to the Geology of Central and Southern Idaho: Idaho Geological Survey Bulletin 27, p. 247-281.

Branney, M.J., and Peter Kokelaar, 1992, A reappraisal of ignimbrite emplacement: Progressive aggradation and changes from particulate to non-particulate flow during emplacement of high-grade ignimbrite: Bulletin of Volcanology, v. 54, p. 504-520.

Camp, V.E., 1995, Mid-Miocene propagation of the Yellowstone mantle plume head beneath the Columbia River basalt source region: Geology, v. 23, p. 435-438.

Christiansen, R.L., 1982, Late Cenozoic volcanism of the Island Park area, eastern Idaho, *in* Bill Bonnichsen and R.M. Breckenridge, eds., Cenozoic Geology of Idaho: Idaho Bureau of Mines and Geology Bulletin 26, p. 345-368.

———, 1984, Yellowstone magmatic evolution: Its bearing on understanding large-volume explosive volcanism, *in* Explosive Volcanism: Inception, Evolution, Hazards: National Academy Press, Washington, D.C., p. 84-95.

Christiansen, R.L., and Wes Hildreth, 1989, Voluminous rhyolitic lavas of broad extent on the Yellowstone Plateau, *in* Continental Magmatism Abstracts: New Mexico Bureau of Mines and Mineral Resources Bulletin v. 131, p. 52.

Christiansen, R.L., and E.H. McKee, 1978, Late Cenozoic volcanic and tectonic evolution of the Great Basin and Columbia intermountain regions, *in* R.B. Smith and G.P. Eaton, eds., Cenozoic Tectonics and Regional Geophysics of the Western Cordillera: Geological Society of America Memoir 152, p. 283-311.

Doe, B.R., W.P. Leeman, R.L. Christiansen, and C.E. Hedge, 1982, Lead and strontium isotopes and related trace elements as genetic tracers in the Upper Cenozoic rhyolite-basalt association of the Yellowstone Plateau volcanic field: Journal of Geophysical Research, v. 87, p. 4785-4806.

Eaton, G.P., R.L. Christiansen, H.M. Iyer, A.M. Pitt, D.R. Mabey, H.R. Blank, Jr., I. Zietz, and M.E. Gettings, 1975, Magma beneath Yellowstone National Park: Science, v. 188, p. 787-796.

Ekren, E.B., D.H. McIntyre, and E.H. Bennett, 1984, High-temperature, large-volume, lavalike ash-flow tuffs without calderas in southwestern Idaho: U.S. Geological Survey Professional Paper 1272, 73 p.

Ekren, E.B., D.H. McIntyre, E.H. Bennett, and R.F. Marvin, 1982, Cenozoic stratigraphy of western Owyhee County, Idaho, *in* Bill Bonnichsen and R.M. Breckenridge, eds., Cenozoic Geology of Idaho: Idaho Bureau of Mines and Geology Bulletin 26, p. 215-236.

Embree, G.F., L.A. McBroome, and D.J. Doherty, 1982, Preliminary stratigraphic framework of the Pliocene and Miocene rhyolite, eastern Snake River Plain, Idaho, *in* Bill Bonnichsen and R.M. Breckenridge, eds., Cenozoic Geology of Idaho: Idaho Bureau of Mines and Geology Bulletin 26, p. 333-343.

Farmer, G.L., and D.J. DePaolo, 1983, Origin of Mesozoic and Tertiary granite in the western United States and implications for pre-Mesozoic crustal structure, 1, Nd and Sr isotopic studies in the geocline of the northern Great Basin: Journal of Geophysical Research, v. 88, p. 3379-3401.

Fleck, R.J., and R.E. Criss, 1985, Strontium and oxygen isotopic variations in Mesozoic and Tertiary plutons of central Idaho: Contributions to Mineralogy and Petrology, v. 90, p. 291-308.

Geist, Dennis, and Mark Richards, 1993, Origin of the Columbia Plateau and Snake River plain: Deflection of the Yellowstone plume: Geology, v. 21, p. 789-792.

Hackett, W.R., and L.A. Morgan, 1988, Explosive basaltic and rhyolitic volcanism of the eastern Snake River Plain, *in* P.K. Link and W.R. Hackett, eds., Guidebook to the Geology of Central and Southern Idaho: Idaho Geological Survey Bulletin 27, p. 283-301.

Hackett, W.R., R.P. Smith, and Soli Khericha, 2002, Volcanic hazards of the Idaho National Engineering and Environmental Laboratory, southeast Idaho, *in* Bill Bonnichsen, C.M. White, and Michael McCurry, eds., Tectonic and Magmatic Evolution of the Snake River Plain Volcanic Province: Idaho Geological Survey Bulletin 30.

Hamilton, W.B., 1989, Crustal geologic processes of the United States, *in* L.C. Pakiser and W.D. Mooney, eds., Geophysical Framework of the Continental United States: Geological Society of America Memoir 172, p. 743-781.

Henry, C.D., and J.A. Wolff, 1992, Distinguishing strongly rheomorphic tuffs from extensive silicic lavas: Bulletin of Volcanology, v. 54, p. 171-186.

Hildreth, Wes, 1981, Gradients in silicic magma chambers: Implications for lithospheric magmatism: Journal of Geophysical Research, v. 86, p. 10,153-10,192.

Hildreth, Wes, A.N. Halliday, and R.L. Christiansen, 1991, Isotopic and chemical evidence concerning the genesis and contamination of basaltic and rhyolitic magma beneath the Yellowstone Plateau volcanic field: Journal of Geology, v. 32, p. 63-138.

Hildreth, Wes, and S. Moorbath, 1988, Crustal contributions to arc magmatism in the Andes of central Chile: Contributions to Mineralogy and Petrology, v. 98, p. 455-489.

Honjo, Norio, 1990, Geology and stratigraphy of the Mount Bennett Hills, and the origin of west-central Snake River Plain rhyolites: Rice University Ph.D. dissertation, 259 p.

Honjo, Norio, Bill Bonnichsen, W.P. Leeman, and J.C. Stormer, Jr., 1992, Mineralogy and geothermometry of high-temperature rhyolites from the central and western Snake River Plain: Bulletin of Volcanology, v. 54, p. 220-237.

Honjo, Norio, K.R. McElwee, R.A. Duncan, and W.P. Leeman, 1986, K-Ar ages of volcanic rocks from the Magic Reservoir eruptive center, Snake River Plain, Idaho: Isochron West, v. 46, p. 15-19.

Hughes, S.S., J.L. Parker, A.M. Watkins, and Mike McCurry, 1996, Geochemical evidence for a magmatic transition along the Yellowstone hotspot track: Northwest Geology, v. 26, p. 63-80.

Hughes, S.S., P.H. Wetmore, and J.L. Casper, 2002, Evolution of Quaternary tholeiitic basalt eruptive centers on the eastern Snake River Plain, Idaho, *in* Bill Bonnichsen, C.M. White, and Michael McCurry, eds., Tectonic and Magmatic Evolution of the Snake River Plain Volcanic Province: Idaho Geological Survey Bulletin 30.

Huppert, H.E., and R.S.J. Sparks, 1988, The generation of granitic magmas by intrusion of basalt into continental crust: Journal of Petrology, v. 29, p. 599-624.

Kellogg, K.S., S.S. Harlan, H.H. Mehnert, L.W. Snee, K.L. Pierce, W.R. Hackett, and D.W. Rodgers, 1994, Major 10.2-Ma rhyolitic volcanism in the eastern snake River Plain, Idaho–Isotopic age and stratigraphic setting of the Arbon Valley Tuff Member of the Starlight Formation: U.S. Geological Survey Bulletin 2091, 18 p.

Kellogg, K.S., and R.F. Marvin, 1988, New potassium-argon ages, geochemistry, and tectonic setting of Upper Cenozoic volcanic rocks near Blackfoot, Idaho: U.S. Geological Survey Bulletin 1806, 19 p.

Kretz, Ralph, 1983, Symbols for rock-forming minerals: American Mineralogist, v. 68, p. 277-279.

Kuntz, M.A., H.R. Covington, and L.J. Schorr, 1992, An overview of basaltic volcanism of the eastern Snake River Plain, Idaho, *in* P.K. Link, M.A. Kuntz, and L.P. Platt, eds., Regional Geology of Eastern Idaho and Western Wyoming: Geological Society of America Memoir 179, p. 227-267.

Leeman, W.P., 1982a, Development of the Snake River Plain-Yellowstone Plateau Province, Idaho and Wyoming: An overview and petrologic model, *in* Bill Bonnichsen and R.M. Breckenridge, eds., Cenozoic Geology of Idaho: Idaho Bureau of Mines and Geology Bulletin 26, p. 155-177.

———, 1982b, Geology of the Magic Reservoir area, Snake River Plain, Idaho, *in* Bill Bonnichsen and R.M. Breckenridge, eds., Cenozoic Geology of Idaho: Idaho Bureau of Mines and Geology Bulletin 26, p. 369-376.

Leeman, W.P., J.S. Oldow, and W.K. Hart, 1992, Lithosphere-scale thrusting in the western U.S. Cordillera as constrained by Sr and Nd isotopic transitions in Neogene volcanic rocks: Geology, v. 20, p. 63-66.

Lipman, P.W., 1997, Subsidence of ash-flow calderas: Relation to caldera size and magma-chamber geometry: Bulletin of Volcanology, v. 59, p. 198-218.

Lund, Karen, and L.W. Snee, 1988, Metamorphism, structural development, and age of the continent-island arc juncture in west-central Idaho, *in* W.G. Ernst, ed., Metamorphism and Crustal Evolution of the Western United States (Rubey Volume): Englewood Cliffs, N.J., Prentice-Hall, p. 296-331.

Manley, C.K., 1995, How voluminous rhyolitic lavas mimic rheomorphic ignimbrites: Eruptive style, emplacement conditions, and formation of tuff-like textures: Geology, v. 23, no. 4, p. 349-352.

McCurry Mike, Bill Bonnichsen, Craig White, M.M. Godchaux, and S.S. Hughes, 1997, Bimodal basalt-rhyolite magmatism in the central and western Snake River Plain, Idaho and Oregon, *in* P.K. Link and B.J. Kowallis, eds., Proterozoic to Recent Stratigraphy, Tectonics, and Volcanology, Utah, Nevada, Southern Idaho and Central Mexico: Geological Society of America Field Trip Guidebook, Brigham Young University Geology Studies, v. 42, part 1, p. 381-422.

McCurry, Mike, A.M. Watkins, J.L. Parker, Karen Wright, and S.S. Hughes, 1996, Preliminary volcanological constraints for sources of high-grade, rheomorphic ignimbrites of the Cassia Mountains: Implications for the evolution of the Twin Falls volcanic center: Northwest Geology, v. 26, p. 81-91.

McQuarrie, Nadine, and D.W. Rodgers, 1998, Subsidence of a volcanic basin by flexure and lower crustal flow: The eastern Snake River Plain, Idaho: Tectonics, v. 17, no. 2, p. 203-220.

Morgan, L.A., D.J. Doherty, and W.P. Leeman, 1984, Ignimbrites of the eastern Snake River Plain: Evidence for major caldera-forming eruptions: Journal of Geophysical Research, v. 89, p. 8665-8678.

Morgan, W.J., 1972, Plate motions and deep mantle convection: Geological Society of America Memoir 132, p. 7-22.

Myers, W.B., and Warren Hamilton, 1964, Deformation accompanying the Hebgen Lake earthquake of August 17, 1959: U.S. Geological Survey Professional Paper 435, p. 55-98.

Mytton, J.W., P.L. Williams, and W.A. Morgan, 1990, Geologic map of the Stricker 4 quadrangle, Cassia County, Idaho: U.S. Geological Survey Miscellaneous Investigations Series Map I-2052, scale 1:48,000.

Neace, T.F., 1986, Eruptive style, emplacement, and lateral variations of the Mesa Falls Tuff, Island Park, Idaho, as shown by detailed volcanic stratigraphy and pyroclastic studies: Idaho State University M.S. thesis, 98 p.

Parker, J.L., 1996, Physical volcanology and geochemistry of the tuff of Wooden Shoe Butte, Cassia Mountains, Idaho: Idaho State University M.S. thesis, 103 p.

Parker, J.L., S.S. Hughes, and Mike McCurry, 1996, Physical and chemical constraints on the emplacement of the tuff of Wooden Shoe Butte, Cassia Mountains, Idaho: Northwest Geology, v. 26, p. 92-106.

Patiño-Douce, A.E., and J.S. Beard, 1995. Dehydration-melting of biotite gneiss and quartz amphibolite from 3 to 15 kbar: Journal of Petrology, v. 36, p. 707-738.

Peng, Xiaohua, and E.D. Humphreys, 1998, Crustal velocity structure across the eastern Snake River Plain and the Yellowstone swell: Journal of Geophysical Research, v. 103, no. B4, p. 7171-7186.

Perkins, M.E., W.P. Nash, F.H. Brown, and R.J. Fleck, 1995, Fallout tuffs of Trapper Creek, Idaho—A record of Miocene explosive volcanism in the Snake River Plain volcanic province: Geological Society of America Bulletin, v. 107, no. 12, p. 1484-1506.

Pierce, K.L., and L.A. Morgan, 1992, The track of the Yellowstone hot spot: Volcanism, faulting, and uplift, *in* P.K. Link, M.A. Kuntz, and L.P. Platt, eds., Regional Geology of Eastern Idaho and Western Wyoming: Geological Society of America Memoir 179, p. 1-53.

Rodgers, D.W., W.R. Hackett, and H.T. Ore, 1990, Extension of the Yellowstone Plateau, eastern Snake River Plain, and Owyhee Plateau: Geology, v. 18, p. 1138-1141.

Rudnick, R.L., and D.M. Fountain, 1995, Nature and composition of the continental crust: A lower crustal perspective: Reviews of Geophysics, v. 33, p. 267-309.

Ryutuba, J.J., and E.H. McKee, 1984, Peralkaline ash flow tuffs and calderas of the McDermitt volcanic field, southeast Oregon and north central Nevada: Journal of Geophysical Research, v. 89, p. 8616-8628.

Saltzer, R.L., and E.D. Humphreys, 1997, Upper mantle P wave velocity structure of the eastern Snake River Plain and its relationship to geodynamic models of the region: Journal of Geophysical Research, v. 102, no. B6, p. 11,829-11,841.

Smith, R.B., and L.W. Braile, 1993, Topographic signature, space-time evolution, and physical properties of the Yellowstone-Snake River Plain volcanic system: The Yellowstone hot spot, *in* A.W. Snoke, J.R. Steidtmann, and S.M. Roberts, eds., Geology of Wyoming: Geological Survey of Wyoming Memoir No. 5, p. 694-754.

Smith, R.B., and N.L. Sbar, 1974, Contemporary tectonics and seismicity of the western United States with emphasis on the Intermountain Seismic Belt: Geological Society of America Bulletin, v. 85, p. 1205-1218.

Sparlin, M.A., L.W. Braile, and R.B. Smith, 1982, Crustal structure of the eastern Snake River Plain determined from ray trace modeling of seismic refraction data: Journal of Geophysical Research, v. 87, p. 2619-2633.

Struhsacker, D.W., P.W. Jewell, J. Zeisloft, and S.H. Evans, Jr., 1982, The geology and geothermal setting of the Magic Reservoir area, Blaine and Camas counties, Idaho, *in* Bill Bonnichsen and R.M. Breckenridge, eds., Cenozoic Geology of Idaho: Idaho Bureau of Mines and Geology Bulletin 26, p. 377-393.

Taylor, S.R., and S.M. McLennan, 1985, The Continental Crust: Its Composition and Evolution: Blackwell, Cambridge, Mass., 312 p.

Watkins, A.M., 1998, Geochemistry, petrography, and stratigraphy of the tuff of Steer Basin, Twin Falls and Cassia counties, Idaho: Idaho State University M.S. thesis, 177 p.

Watkins A.M., M. McCurry, and S.S. Hughes (1996) Preliminary report on the stratigraphy and geochemistry of the tuff of Steer Basin, Cassia Mountains, Idaho, *in* S.S. Hughes and R.C. Thomas, eds., Geology of the Crook in the Snake River Plain, Twin Falls and Vicinity: Northwest Geology, v. 26, p. 107-120.

Watt, G.R., and S.L. Harley, 1993, Accessory phase controls on the geochemistry of crustal melts and restites produced during water-undersaturated partial melting: Contributions to Mineralogy and Petrology, v. 114, p. 550-566.

Whitney, J.A., 1988, The origin of granite: The role and source of water in the evolution of granitic magmas: Geological Society of America Bulletin, v. 100, p. 1886-1897.

Williams, P.L., H.R. Covington, and J.W. Mytton, 1991, Geologic map of the Stricker 2 quadrangle, Twin Falls and Cassia counties, Idaho: U. S. Geological Survey Miscellaneous Investigations Series Map I-2146, 1:48,000.

Williams, P.L., J.W. Mytton, and H.R. Covington, 1990, Geologic map of the Stricker 1 quadrangle, Cassia, Twin Falls, and Jerome counties, Idaho: U.S. Geological Survey Miscellaneous Investigations Series Map I-2078, scale 1:48,000.

Wright, K.E., 1998, Geochemistry and petrology of the tuff of McMullen Creek, Cassia County, Idaho: Idaho State University M.S. thesis, 172 p.

Wright, K.E., Michael McCurry, and S.S. Hughes, 2002, Petrology and Geochemistry of the Miocene tuff of McMullen Creek, central Snake River Plain, Idaho, *in* Bill Bonnichsen, C.M. White, and Michael McCurry, eds., Tectonic and Magmatic Evolution of the Snake River Plain Volcanic Province: Idaho Geological Survey Bulletin 30.

Petrology and Geochemistry of the Miocene Tuff of McMullen Creek, Central Snake River Plain, Idaho

Karen E. Wright,[1] Michael McCurry,[2] and Scott S. Hughes[2]

ABSTRACT

The 8.8 to 8.6 Ma tuff of McMullen Creek is one of three major multiple-ignimbrite sequences that erupted between 10 and 8.6 Ma from within the Twin Falls volcanic field in south-central Idaho. It consists of two simple densely welded cooling units, three moderately to densely welded compound cooling units, and intervening nonwelded fallout tephra.

Phenocrysts and glomeroporphyritic aggregates vary from about 10 to 20 volume percent and consist of plagioclase, pigeonite, ferroaugite, opaques, quartz, Fe-Ti oxides, and accessory zircon and apatite. The presence of orthopyroxene and sanidine phenocrysts distinguish the oldest ignimbrite from the younger four. Bulk SiO_2 concentration for the ignimbrites ranges from 70.3 to 76.2 weight percent, and Sr ranges from 45 to 142 parts per million. Initial Sr-isotopic ratios $(^{87}Sr/^{86}Sr)_i$ range from 0.71024 to 0.71347 for plagioclase separates and from 0.71018 to 0.71300 for whole rocks. Bulk rock ε_{Nd} varies from -6.5 to -7.1.

Neither bulk composition nor phenocryst assemblage shows large-scale stratigraphically systematic variations typical of many ignimbrites in North America. Our analyses indicate that most of the chemical differences in the tuff of McMullen Creek resulted from fractional crystallization prior to eruption, and not from depositional or alteration processes. These features rule out a simple (i.e., top-down) drawdown from a vertically zoned magma chamber. Zonations within the chamber could have been spatially complex, or alternatively, eruptions could have occurred simultaneously from multiple sources—perhaps cupolas at the top of a larger contiguous magma chamber.

Our data support a petrogenetic model wherein magmas parental to the tuff of McMullen Creek were produced by a two-stage process. First, late Archean lower- and middle-continental crust was profoundly modified chemically and thermally by the intrusion of about 90 percent volume percent of Tertiary basaltic dikes and sills. Second, hybrid silicic partial melts from the modified crust ascended into magma chambers within the middle crust and underwent moderate fractional crystallization and assimilation before eruption.

Key words: Snake River Plain, rhyolite petrogenesis, assimilation, isotopes, ignimbrites

INTRODUCTION

The tuff of McMullen Creek (Williams and others, 1990, 1991) is the youngest of a voluminous sequence of rhyolite ignimbrites erupted from the Twin Falls volcanic field (Pierce and Morgan, 1992; McCurry and others, 1996), a little studied but fundamental part of the Snake River Plain (SRP)-Yellowstone hot-spot track system (Pierce and Morgan, 1992; Armstong and others 1975). The Twin Falls volcanic field, located about halfway along the hot-spot track (Figure 1), is distinguished by being near a suture zone between Archean cratonal lithosphere and accreted Mesozoic terranes. The suture zone trends roughly north-south along the Oregon-Idaho border (Leeman and others, 1992). The Twin Falls volcanic field is also in close proximity to a bend in the direction and change in apparent speed of the hot-spot track (Smith

Editors' note: The manuscript was submitted in June 1998 and has been revised at the authors' discretion.

[1]Idaho National Engineering and Environmental Laboratory, PO Box 1625, MS 2025, Idaho Falls, ID 83415

[2]Department of Geosciences, Idaho State University, Pocatello, ID 83209

Wright, K.E., Michael McCurry, and S.S. Hughes, 2002, Petrology and geochemistry of the Miocene tuff of McMullen Creek, central Snake River Plain, Idaho, *in* Bill Bonnichsen, C.M. White, and Michael McCurry, eds., Tectonic and Magmatic Evolution of the Snake River Plain Volcanic Province: Idaho Geological Survey Bulletin 30, p. 177-194.

and Braile, 1993). Preliminary works on the petrology of volcanic rocks in the area (McCurry and others, 1995; Hughes and McCurry, this volume) suggest that the rocks have many chemical and isotopic characteristics that are intermediate or transitional between those in the eastern Snake River Plain and Yellowstone to the northeast (e.g., Hildreth and others, 1991; Morgan and others, 1984; Leeman, 1982) and the oldest parts of the hot-spot track to the southwest (Ekren and others, 1984). In addition, some Nd- and Sr-isotopic characteristics of the rocks appear to be unique (McCurry and others, 1995).

Our study focuses on the petrology and geochemistry of one of the best-exposed, youngest parts of the Twin Falls volcanic field. Our purpose is to better define hot-spot-related magma genesis in a transitional part of the hot-spot track. Our specific objectives are three: (1) to define petrologic and bulk chemical and isotopic characteristics of rhyolite ignimbrites associated with the tuff of McMullen Creek, (2) to determine the origins of patterns of chemical and isotopic variations within the ignimbrites, and (3) to identify the origin of the magmas parental to the rhyolites.

GEOLOGIC SETTING

The SRP-Yellowstone hot-spot track is approximately 90 km wide and 800 km long, stretching northeast from the mutual borders of Idaho, Oregon, and Nevada to its terminus at Yellowstone National Park. It cross cuts Basin-and-Range topography. Rhyolite volcanism along the SRP-Yellowstone hot-spot track is roughly time-transgressive; the inception of large-scale ash-flow eruptions varies from about 14-15 Ma in the southwest to 2.0 Ma

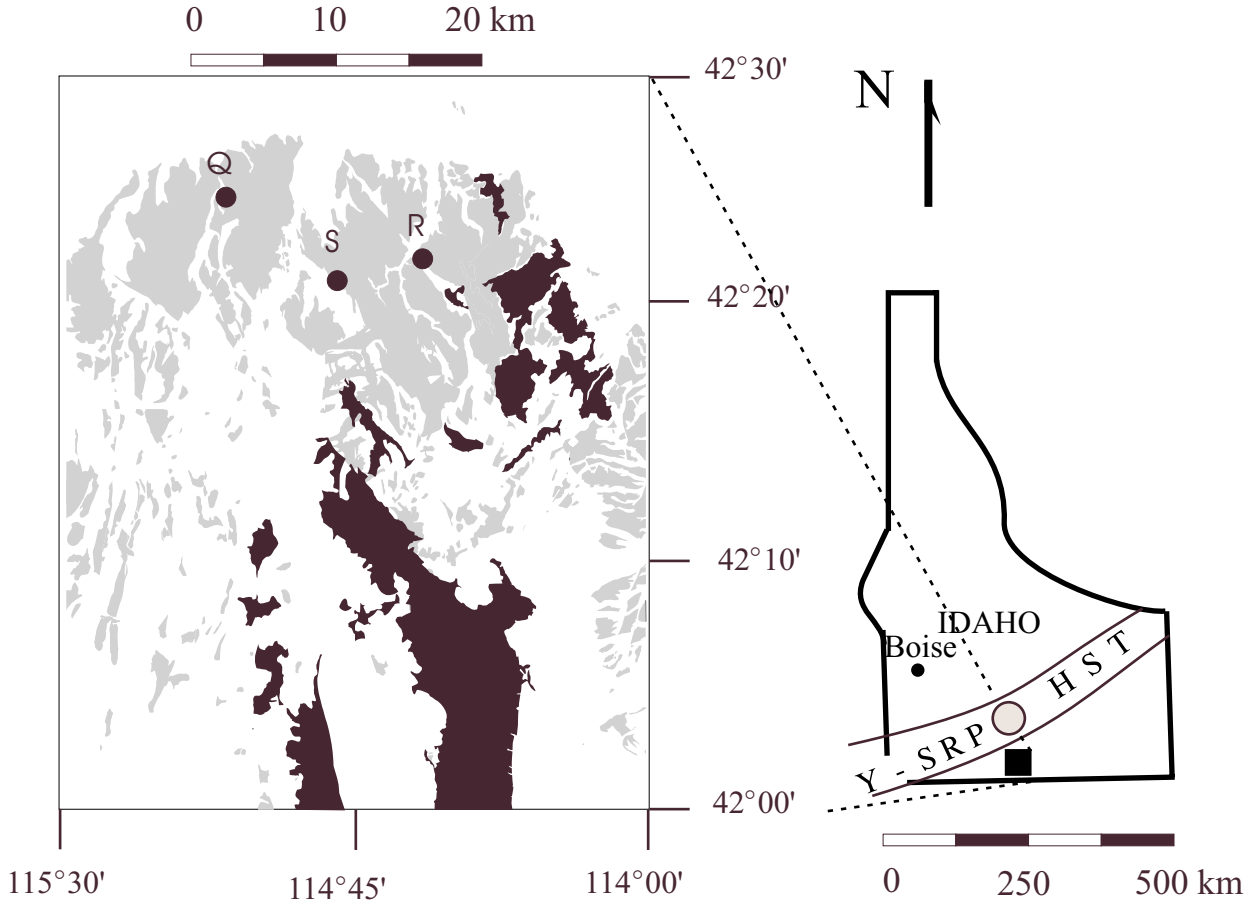

Figure 1. Sketch map of Idaho showing the location of the Cassia Mountains (solid square) as well as the hypothesized Twin Falls volcanic center (stippled). The Snake River Plain-Yellowstone hot-spot track traverses the state (Y-SRP HST). Outcrops of the tuff of McMullen Creek (gray) and pre-Tertiary rocks (black) in the Cassia Mountains. Studied localities in the northern part of the Cassia Mountains are (from west to east) Quarry (Q), Schipper (S), and Rams Horn Ridge (R).

at Yellowstone (Pierce and Morgan, 1992).

Eruptive products of the Twin Falls volcanic field are primarily exposed in the Cassia Mountains located approximately midway between either end of the hot-spot track, near the northern margin of the Basin-and-Range physiographic province (Figure 1). The mountains cover an area about 1,500 square km and have a relief of about 1,100 m.

The oldest exposed rocks in the region are late Paleozoic sedimentary rocks, which are unconformably overlain by Miocene ignimbrites and interbedded volcaniclastic sediments. The Paleozoic rocks were folded and thrust-faulted during the Laramide Orogeny (Younquist and Haegele, 1956). Younger Basin-and-Range normal faults cross-cut many older thrust faults. The entire region is characterized by a broad, domal uplift formed during the late Pliocene or early Pleistocene (Younquist and Haegele, 1956), causing the region to be in a youthful erosional stage. Consequently, the area is strongly dissected by streams, which generally flow from the central part of the dome toward the lower, outer reaches. Canyons are steep walled and narrow; they separate flat-topped areas underlain by ignimbrites.

The region is heavily block faulted. Near-vertical faults are up to 9 km long and have dip-slip displacements as great as 300 m (Mapel and Hail, 1959). Many of the most prominent faults trend northwest to northeast. Some faults cut Miocene ignimbrites; others cut only pre-Tertiary rocks, indicating that normal faulting occurred before and after the emplacement of the Miocene ignimbrite units.

All of the ignimbrites in the area contain linear features indicating direction of transport. McCurry and others (1996) used the orientation of such linear features to propose that the tuff of McMullen Creek originated from the north and flowed southward, spreading radially to form a fanlike pattern. Many of the lineations parallel paleo-topographical features such as north- to northwest-trending horst blocks, suggesting that such features influenced the direction of flow and the depositional patterns of the ignimbrites.

STRATIGRAPHY OF THE TUFF OF MCMULLEN CREEK

Williams and others (1990, 1991) introduced the informal name "tuff of McMullen Creek" for all ignimbrites and intervening fallout tephra located stratigraphically above the tuff of Wooden Shoe Butte. For convenience, we adopt this name and its usage here. We have examined the stratigraphy of the sequence in three localities of the northern Cassia Mountains—the Schipper, Rams Horn Ridge, and Quarry sections (Figure 1)—and have collected approximately fifty-five samples for petrographic and geochemical analyses.

Exposures are strongly biased towards outcrops of densely welded ignimbrites, the focus of this study. Intervening slope-forming areas typically make up 30 percent of the total sequence, but exposures in such areas are very poor or absent. They consist of fine-grained to medium-grained, well-bedded, well-sorted, vitric and vitric-crystal ash. In the measured sections, we observed no evidence of water reworking or soil-profile development.

Williams and others (1990, 1991) document exposures of the tuff of McMullen Creek throughout the Cassia Mountains (Figure 1). The unit varies in thickness from about 95 m in the northern Cassia Mountains to less than 10 m in the south. Individual ignimbrites vary from 2 to 35 m in the north to less than a meter to the south. Exposures of similar looking ignimbrites occur 25 to 15 km to the west and east of the Cassia Mountains (McCurry and others, 1996), as well as along the northern margin of the Snake River Plain (Honjo, 1990; Moye and others, 1988). Rheomorphic lineations present at many localities within and near the Cassia Mountains converge on a point near the city of Twin Falls, suggesting a source is buried beneath the Quaternary basalts in that area (McCurry and others, 1996). The original areal extent (about 5,000 square km) and volume of the unit may therefore have been comparable to major Yellowstone ignimbrites, although individual ignimbrites appear to be thinner and less voluminous.

In the northern Cassia Mountains, the tuff of McMullen Creek contains at least five ignimbrites (Wright, 1998), one more than originally recognized by Williams and others (1990, 1991). We informally refer to ignimbrite-fallout tuff sequences, from stratigraphically lowest to highest, as members 1, 2, 3, 4, and 5 (Figure 2). Members 2 through 5 overlap in their petrographic and geochemical characteristics, whereas member 1 is distinguished by the occurrence of orthopyroxene and sanidine phenocrysts as well as a more evolved bulk chemical composition.

Ages of the various ignimbrites of the tuff of McMullen Creek are not well established, in part because of the absence of sanidine or biotite phenocrysts. Armstrong and others (1975, 1980) report whole-rock K/Ar ages of 8.6 and 8.7 Ma; however, it is not clear which ignimbrites were dated. Perkins and others (1998) report an $^{40}Ar/^{39}Ar$ age of 8.84 Ma on sanidine from a sample of member 1 collected near Trapper Creek, about 30 km southeast of Rock Creek Canyon.

Each of the three studied sections of the tuff of

McMullen Creek (Figure 1) contain four members consisting of densely welded cooling units separated by nonwelded fallout tephra. The uppermost ignimbrite, member 5, forms the tops of mesas at the three localities. Member 1 is exposed only in the Quarry section, which consists of members 1, 3, 4, and 5 (Wright, 1998); other ignimbrites are correlated in Figure 2.

The thickest exposures of the tuff of McMullen Creek occur in cliffs adjacent to Rock Creek (Schipper section) and along Rams Horn Ridge. Brief descriptions of member 4 from the Schipper section and member 1 from the Quarry section are presented below. Members 2 and 5 have lithological and mineralogical features similar to those of member 4. Member 3 is much thinner than the others (2 to 3 m), and poorly exposed. Nomenclature follows that of McCurry and others (1996) and Sparks and others (1973). Lithologic and zonal features are illustrated in Figure 2.

Member 4 is a densely welded, compound cooling unit about 35 m thick that contains many of the layers typically found in the standard ignimbrite of Sparks and others (1973). Layer 1 (the surge layer) is relatively thin (a few centimeters) and laterally discontinuous. Layer 2a (the fine-grained, well-sorted layer) is about 10 cm thick. The base of the 2b layer (the poorly sorted main body of the ignimbrite) is a dense black vitrophyre containing about 15-20 percent phenocrysts of subhedral to euhedral plagioclase, pyroxene and Fe-Ti oxides. Upwards, the layer grades into a lithic- and pumice-rich devitrified and vapor-phase crystallized zone. Lithics compose from 1 to 30 percent of this zone and consist of subangular to angular lithoidal to glassy rhyolites and obsidian clasts up to 10 mm in diameter. Concomitant with an increase in lithic content (between 62 and 72 m on Figure 2), there is a decrease in the degree of welding. Above this lithic-rich zone, the 2b layer grades into a densely welded, vapor-phase crystallized, devitrified section that has horizontal, platy joints (cf., Chapin and Lowell, 1979). Thin, discontinuous layers within this section have a phenocryst content of about 5 percent. These fine-grained layers are probably co-ignimbrite ash-cloud deposits, indicating that the ignimbrite consists of multiple flow units (Wright, 1998). Weakly developed rheomorphic folds occur near the top of the ignimbrite. Capping member 4 is a 0.5 m-thick co-ignimbrite ash deposit that contains 5-7 percent crystals.

Member 1 is exposed at the Quarry locality, but not at the Schipper or Rams Horn Ridge localities. It is approximately 43 m thick and a very densely welded simple cooling unit. Rheomorphic deformation is common and in some places extreme. Welding extends through the base of the ignimbrite for several meters downward into the underlying vitric fallout. Vitrophyric zones occur at the top and bottom of the unit. The absence of the unit at the two other localities is curious, because an apparently correlative unit was identified by Perkins and others (1998) more than 30 km further to the southeast. Member 1 is distinguished from the other ignimbrites in three ways: (1) lower phenocryst abundance (1 to 5 percent), (2) lower lithic content (rare, small rhyolite lithics), and (3) the presence of orthopyroxene and sanidine phenocrysts.

PETROGRAPHY

We considered samples from layer 2b to be most representative of the magma, because it is more poorly sorted than the other layers of the ignimbrite. Moreover, there is a paucity of pumice present in the tuff of McMullen Creek. We examined multiple samples from layer 2b within each ignimbrite of the three stratigraphic sections. With the exception of member 1, they are all similar in phenocryst assemblage, consisting of (in decreasing order of abundance) subhedral to euhedral plagioclase, pigeonite, ferroaugite, Fe-Ti oxides, quartz, and accessory zircon and apatite. Phenocryst contents vary from 6 to 19 volume percent in samples from layer 2b of ignimbrites 2 through 5 (Figure 3); whereas member 1 is distinguished in both its assemblage and lower concentration of phenocrysts (1 to 5 percent). At the Schipper section, member 2 shows a vertically systematic decline in phenocryst content from 19 to 9 percent. However, at Rams Horn Ridge the crystal content appears to vary randomly with stratigraphic height. Although phenocryst content in members 2 through 5 varies widely, the relative proportions of minerals remains about the same. Such apparently random fluctuations, both vertically and horizontally, are typical of the ignimbrites.

Plagioclase occurs in two distinct habits, which we designate type-1 and type-2. Type-1 plagioclase are subhedral to euhedral, normally zoned laths. Most are between 0.5 to 2 mm across and contain inclusions of glass or other phenocrysts, commonly pigeonite, ferroaugite, Fe-Ti oxides, or apatite. Cellular texture is common (Hibbard, 1995). Compositional zonations within the grains parallel the walls of cellular structures, rather than are cut by them, suggesting that the cellular texture results from rapid growth rather than resorption. These grains occur as isolated phenocrysts and within glomeroporphyritic aggregates along with clinopyroxene and Fe-Ti oxides.

Type-2 plagioclase grains are subhedral to euhedral laths commonly broken on at least one side. They range in size from 0.2 to 2 mm across, although most are smaller than 1 mm. They rarely contain inclusions (apatite, Fe-Ti

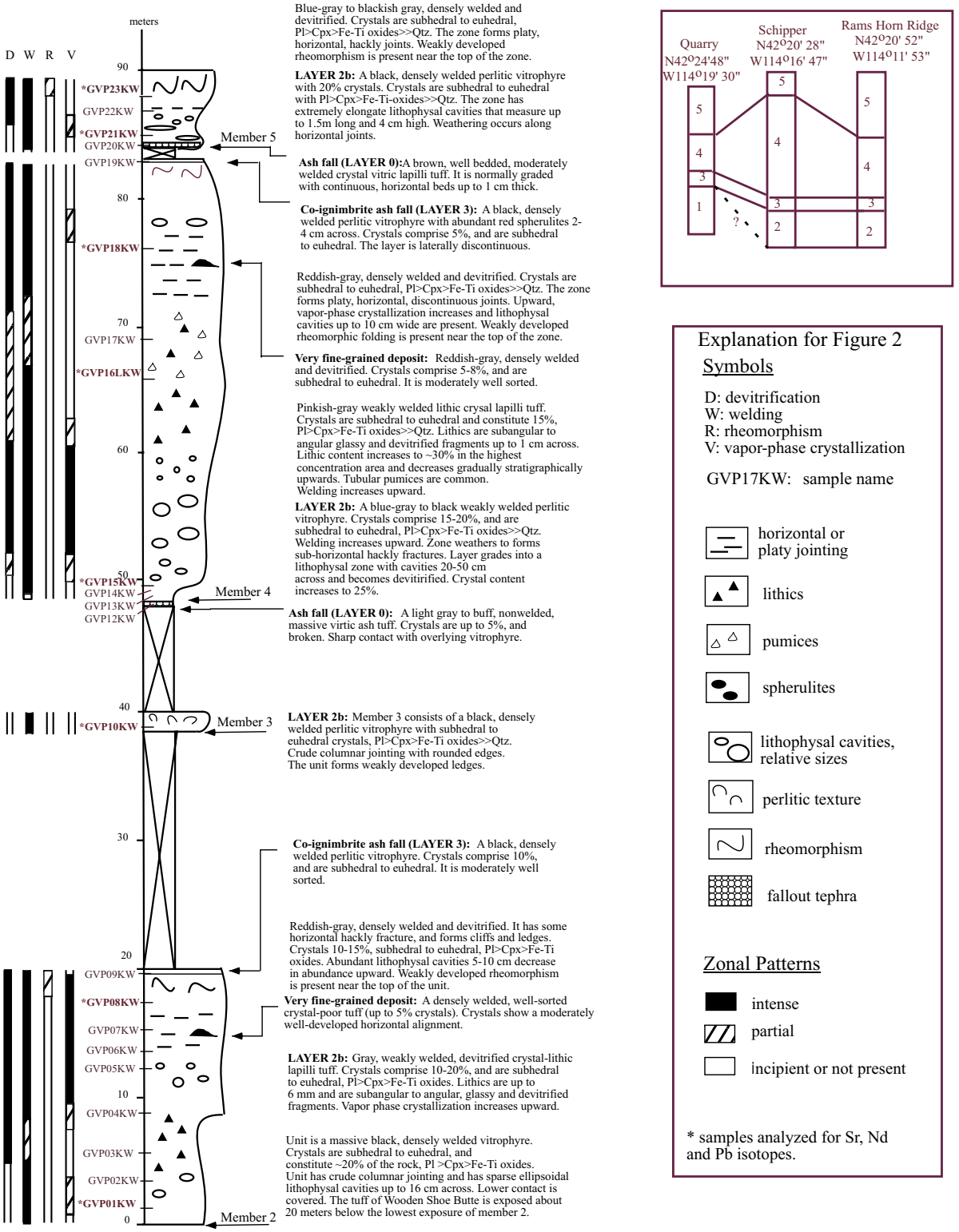

Figure 2. Stratigraphy present at the Schipper locality is shown on left. Symbols described on right. Correlations between localities are illustrated in the fence diagram (upper right).

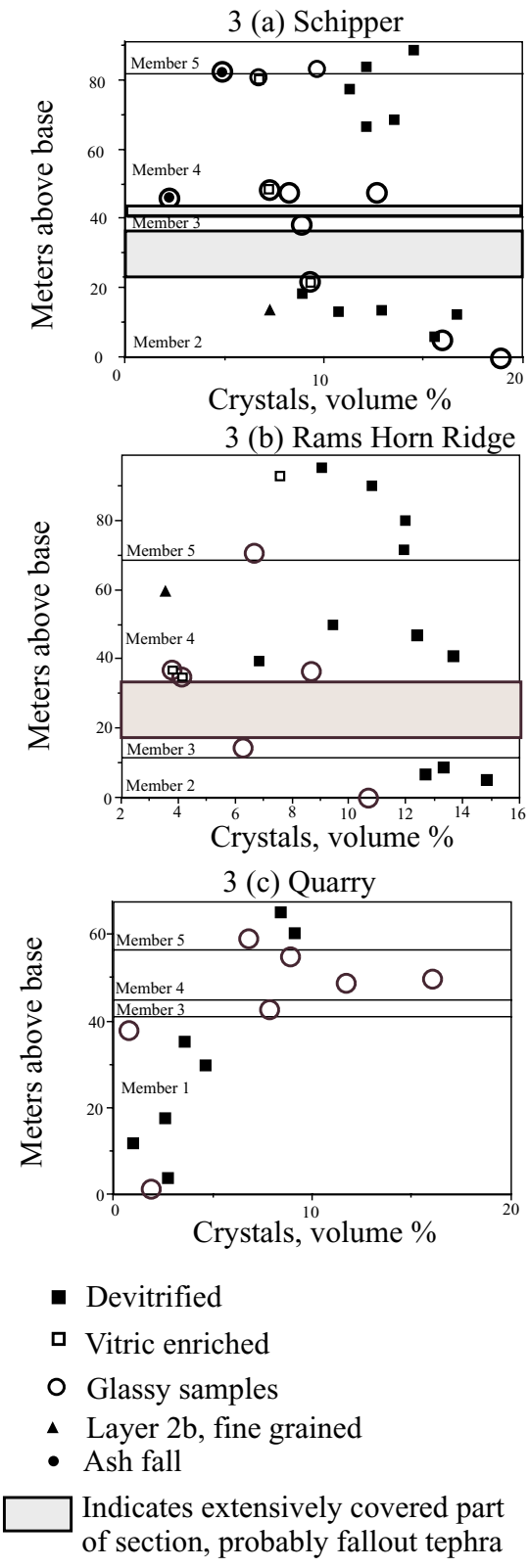

Figure 3. Percentages of phenocrysts with respect to stratigraphy for (a) Schipper, (b) Rams Horn Ridge, and (c) Quarry.

oxides, and clinopyroxene), and in contrast to type-1 plagioclase, they do not occur within glomeroporphyritic aggregates.

Pigeonite and ferroaugite occur as individual subhedral to euhedral prismatic grains from 0.5 to 3 mm across. Many grains appear to be broken. In addition, they occur within glomeroporphyritic aggregates. Inclusions of Fe-Ti oxides and apatite are common.

Approximately half of all phenocrysts observed throughout the tuff are present in the form of glomeroporphyritic aggregates, which typically consist of pigeonite, ferroaugite, plagioclase (type-1), magnetite, and apatite ± zircon. Crystals are anhedral to subhedral, and entire aggregates are typically 2-3 mm across. All phenocrysts in the aggregates are also found as isolated crystals in the matrix.

Glomeroporphyritic aggregates similar to those in the tuff of McMullen Creek have been found in the Bruneau-Jarbidge system. Bonnichsen and Citron (1982) considered these to be protolithic restite material. In their study of Mazama lavas, Nakada and others (1994) demonstrated that similar aggregates are cognate fragments of crystals originally attached to the chilled margin of the magma chamber. We suggest that the latter process is more consistent with our thin section observations, where we see both aggregates and broken single crystals. Many of the broken crystals are type-2 plagioclase grains; there are also rarer broken fragments of clinopyroxene. Since the aggregates are dominantly plagioclase, the disruption of such aggregates should result in a preponderance of broken plagioclase grains.

GEOCHEMISTRY

MAJOR AND TRACE ELEMENTS

We analyzed fifty-five bulk-rock samples (which are aliquots of the samples used for petrographic analysis) for major oxides and twenty-one trace elements. Representative samples from layer 2b of ignimbrites at Schipper and Quarry sections are listed in Table 1. We omitted analyses of samples from Rams Horn Ridge from Table 1 because of their similarity to analyses of Schipper samples. Thus, analyses of samples from all members are represented on Table 1. We carefully collected and prepared the samples to minimize the effects of weathering and xenolithic contamination. Sources of alteration that we could not minimize include devitrification, vapor-phase crystallization, and (for glassy samples) hydration (Noble, 1967). We also recognize that bulk-rock samples of ignimbrites may have undergone substantial crystal-vitric segregation during emplacement of the origi-

Table 1. Major and trace element data for representative samples from the tuff of McMullen Creek. M1, M2, M3, M4, and M5 refer to members 1-5.

	Schipper							Quarry	
	base, M2	top, M2	M3	base, M4	top, M4	base, M5	top, M5	middle, M1	middle, M1
Rock type:	vitrophyre	devitrified	vitrophyre	vitrophyre	devitrified	vitrophyre	devitrified	devitrified	devitrified
Sample:	GVP02KW	GVP08KW	GVP10KW	GVP15KW	GVP18KW	GVP21KW	GVP23KW	SB02AKW	SB03KW
	Major oxides in wt. % normalized to 100% anhydrous								
SiO_2, wt.%	70.5	72.2	72.9	72.6	73.9	74.4	73.7	76.2	74.6
TiO_2	0.75	0.68	0.50	0.60	0.55	0.45	0.50	0.33	0.41
Al_2O_3	13.2	13.1	12.6	12.9	12.5	12.3	12.5	12.0	12.3
FeO	4.58	3.96	3.90	3.90	3.45	3.34	3.71	2.32	2.86
MnO	0.068	0.047	0.064	0.065	0.054	0.059	0.066	0.04	0.04
MgO	0.57	0.26	0.24	0.32	0.19	0.15	0.20	0.09	0.23
CaO	2.27	1.53	1.52	1.76	1.23	1.05	1.27	0.72	1.01
Na_2O	2.91	3.08	2.85	2.75	3.26	2.94	3.29	3.00	3.29
K_2O	4.99	4.96	5.42	5.00	4.78	5.25	4.65	5.23	5.11
P_2O_5	0.17	0.16	0.09	0.12	0.09	0.08	0.10	0.043	0.12
H_2O-	0.44	0.31	0.46	0.35	0.54	0.59	0.55	0.03	0.14
LOI	1.58	0.78	2.56	2.14	0.16	2.25	0.28	0.52	0.39
Original Total	99.20	99.70	100.50	99.50	99.20	98.40	98.60	102.20	99.10
	Trace-Element ICP Analyses								
Rb, ppm	183	168	189						
Ba	1060	1110	1060	1080	1090	1060	1100	1050	1060
Sr	116	96	94	110	98	74	103	55	71
Zr	592	546	555	606	575	547	532	424	478
	NAA Analyses								
Sc, ppm	7.72	6.91	6.75	7.86	6.02	5.31	6.51	4.1	4.82
Cr	8.7	7.2	3.2	2.2	0.4	3.1			
Co	6.01	4.87	3.73	4.73	3.17	2.72	3.02	1.22	1.8
Rb	159	167	157	175	164	188			
Cs	2.42	2.27	2.85	2.81	2.08	2.58	1.76	2.35	2.76
La	75.5	76.4	81	75.4	78.6	81.6	83.7	86.9	81.0
Ce	145	149	167	175	146	155	149	184	147
Nd	55.7	57.8	66.5	60.7	60.8	65.9	71.7	53.1	61.2
Sm	11.5	11.4	11.6	10.4	12.5	11.5	13.2	12.8	12.6
Eu	1.79	1.68	2.21	2.35	1.89	1.90	2.26	1.48	1.68
Tb	1.49	1.46	1.96	1.96	1.63	1.64	1.76	1.86	1.62
Yb	5.24	5.24	6.27	5.69	6.26	6.16	6.10	6.45	5.41
Lu	0.78	0.79	0.91	0.83	0.89	0.94	0.93	0.84	0.85
Hf	16.1	15.6	15.8	18.0	15.5	15.1	16.4	14.0	14.1
Ta	2.51	2.67	3.60	3.55	2.79	3.34	2.99	3.49	3.24
Th	25.8	28.3	30.7	28.5	24.2	26.5	25.5	31.2	29.2
U	5.9	7.2	6.2	6.1	6.5	6.5	6.7	6.5	6.3

nal ignimbrite (Parker, 1996).

The tuff of McMullen Creek is typical of the relatively Fe- and Zr-rich metaluminous rhyolites of the central and western segments of the Snake River Plain hotspot track system (Hughes and McCurry, this volume). Samples from members 2 through 5 (Figure 4) have overlapping, moderate to subtle linear covariations for many major and trace elements (e.g., SiO_2 vs. Al_2O_3, TiO_2, FeO*, MgO, CaO, P_2O_5, Sr, Co, Cr, and Sc); others have apparently random variations (e.g., SiO_2 vs. Cs, Ba, Zr, and Ta), or variations originating from hydration, or vapor-phase alteration (e.g., SiO_2 vs. Na_2O and K_2O). We find no evidence for compositional gaps or for curvilinear compositional trends (see Wright, 1998, for details).

Member 1 is nearly homogeneous and is distinguished from members 2 through 5 by many small but petrologically significant differences in chemical composition (Figure 4). Most elements lie on chemically evolved extensions of linear trends defined by samples from members 2 through 5 (Figure 4). Other differences occur in element ratios. For example, member 1 has a Sm/Eu ratio of ~8.1, significantly higher than the average of 5.9 ± 1.2 for members 2 through 5 and reflective of a more pronounced negative Eu-anomaly for member 1.

Stratigraphic correlations are compared with chemical compositions in Figure 5a-c, using SiO_2 as the repre-

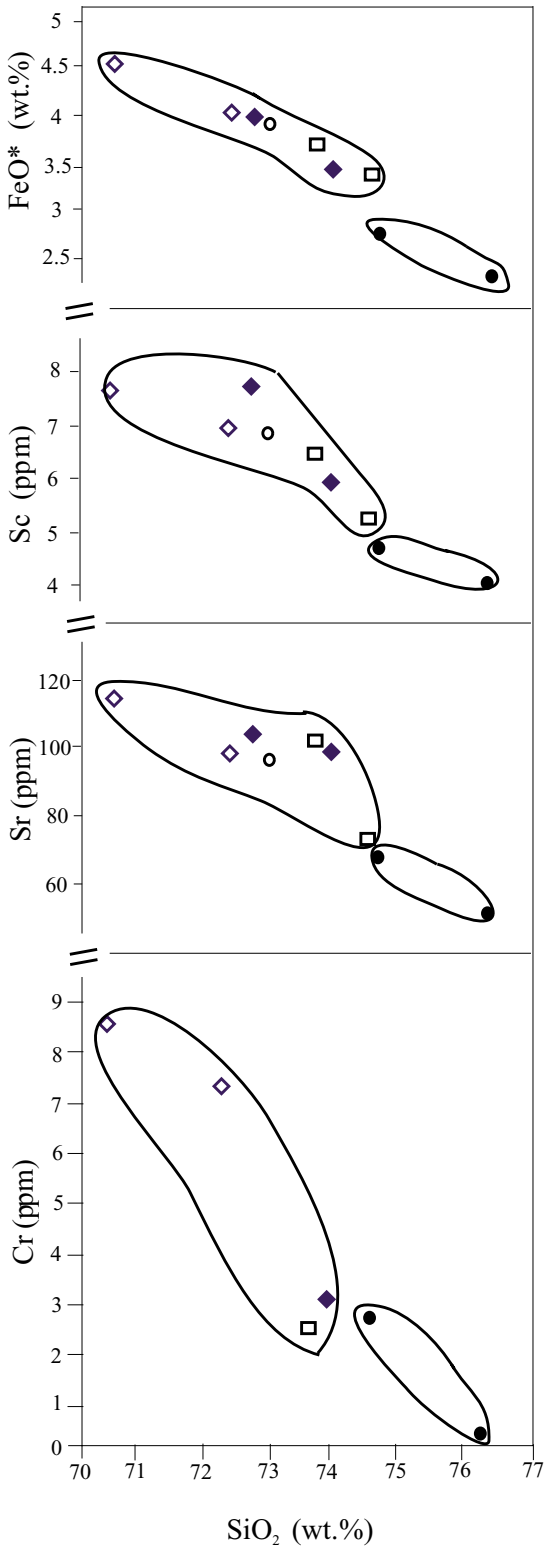

Figure 4. Harker diagrams for representative tuff of McMullen Creek samples. Member 1 (filled circles), member 2 (open diamonds), member 3 (open circles), member 4 (filled diamonds), and member 5 (open squares).

sentative compositional variable (similar variations occur for many other major and trace elements). Considering samples from all layers within each member, systematic vertical variations in chemical composition are either absent or not systematic within the levels of analytical uncertainty. For example, at the Schipper section, member 2 shows a stratigraphically upward decline from 71.0 to 70.2 percent SiO_2, then a steady increase in silica to 72 percent; the same member shows a steady upward decline in SiO_2 content at Rams Horn Ridge of 71.7 to 70.8 percent.

Overall, the tuff of McMullen Creek shows chemical patterns that appear to be repeated in each of the three sample localities. Considering only layer 2b samples from members 2, 4, and 5 at the Schipper section, there is an upward increase in SiO_2 from about 70.5 to 74 percent, and concomitant upward declines in FeO* from 4.3 to 3.5 percent, MgO from 0.4 to 0.18 percent, CaO from 1.9 to 1.2 percent, P_2O_5 from 0.17 to 0.09 percent, and Co from 5 to 3 ppm. Other constituents have little or no systematic vertical variations. Member 3, a thin, apparently low-volume ignimbrite, plots slightly off the trends defined by the other members. Similar patterns are repeated for members 2, 4, and 5 at Rams Horn Ridge and for 4 and 5 at the Quarry locality (Figure 5).

Normalized to a model Archean lower crust (Figure 6), representative samples from all five members of the tuff of McMullen Creek show prominent depletions of Sr, Ti, and Sc and minor depletions of Ba and Ta. Strong enrichments of Rb, Th, and U occur as well as more modest enrichments of Zr and Hf. Enrichment decreases from left to right in Figure 6, suggesting increasing compatibility to source mineralogy.

ISOTOPES

We analyzed eight samples from the Schipper locality for Sr-, Nd-, and Pb-isotopic signatures. Samples were selected from the stratigraphically lowest and highest part of the 2b layers exposed in members 2, 4, and 5; one sample was selected from near the middle of member 3 (Figure 2). Plagioclase separates were obtained from the lower vitrophyre of each member for Sr-isotopic analysis. Other samples represent bulk-rock material, which was carefully prepared to avoid or remove contamination originating from weathering or xenolithic materials. In addition, an aggregate of typical rhyolite lithics from member 4 was separated from a 10 kilogram rock sample and analyzed for its isotopic ratios. Methods for isotopic analyses follow those reported by Wright and Snoke (1993).

Sr- and Nd-isotopic analyses are listed in Table 2, and isotopic variations among members are shown in Figure

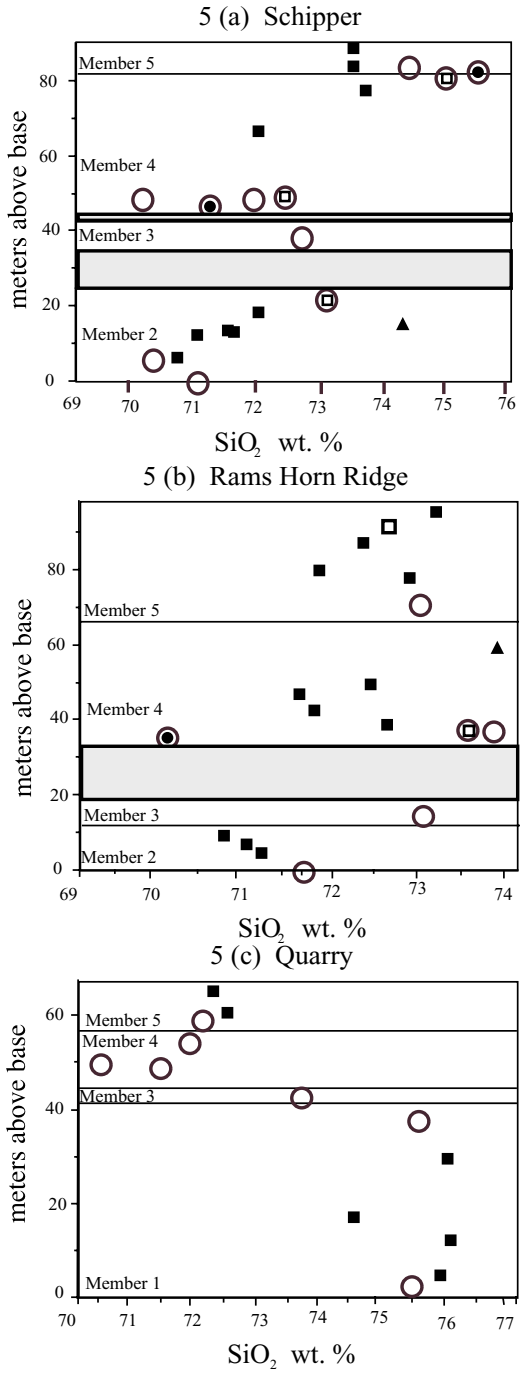

Figure 5. Vertical SiO_2 variations with respect to stratigraphy for (a) Schipper, (b) Rams Horn Ridge, and (c) Quarry. Phenocrysts compose less than 5 percent of vitric enriched samples.

7. Whereas ε_{Nd} variation within each member may not exceed analytical uncertainties, ε_{Nd} variation between members exceeds such uncertainties. There is an apparent shift to less isotopically evolved material between members 2 and 3 and between members 4 and 5 (Figure 7). If we consider data from whole rock analyses only, this behavior is emulated by Sr-isotopic data between members 4 and 5 (Figure 7). Within members 2, 4, and 5, initial $^{87}Sr/^{86}Sr$ ratios trend from more evolved to less evolved; however, within each member, whole rock isotopic data are compared to data generated from plagioclase separates. As is discussed later, this approach may be problematic. Importantly, while the aggregate of accessory lithics contained within member 4 appear to be isotopically similar to member 4, they do not fall on a mixing curve between the isotopic compositions of the top and bottom of member 4. In addition, the tuff of McMullen Creek has isotopic ratios that are distinct from those of hot-spot rhyolites west of the craton margin (Figure 8)

Variations in Pb-isotopic ratios with respect to stratigraphy are plotted in Figure 9. Within a given member, Pb-ratios increase with stratigraphic height (variations in member 4 for $^{208}Pb/^{204}Pb$ and $^{207}Pb/^{204}Pb$ are within 2σ analytical uncertainty for counting statistics); however, like the Sr-isotopic data, Pb-ratios within each member compare whole rock data to data obtained from plagioclase separates. Pb-isotopic ratio changes within and between members closely mimics those of the Sr-isotopic ratios (Figure 9). For example, if we consider data from whole rock analyses only, there is a shift to less isotopically evolved material between members 4 and 5. When comparing data from the plagioclase separates to that of the whole rocks, there is a shift to less isotopically evolved material within members 2, 4, and 5, similar to that shown by the Sr-isotopic data. Finally, Pb-isotopic ratios of tuff of McMullen Creek samples appear to be more similar to those of eastern SRP basalts, than those of rhyolites generated at Yellowstone National Park (Figure 10).

ORIGIN OF GEOCHEMICAL VARIATIONS

MAJOR- AND TRACE-ELEMENT ZONATIONS

One of the questions we have sought to answer is whether or not the ignimbrites of the tuff of McMullen

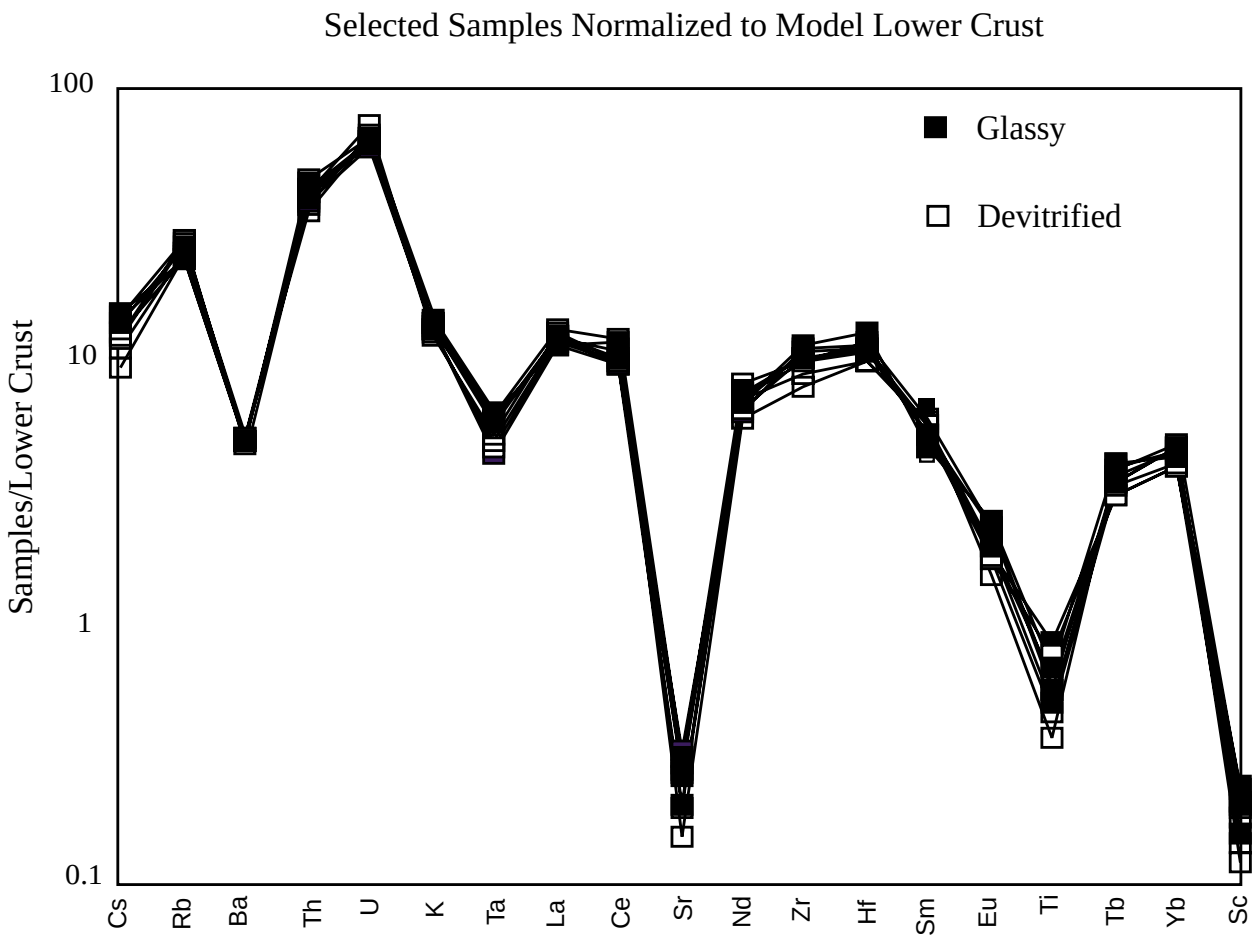

Figure 6. Spider diagram for representative tuff of McMullen Creek samples shown in order of increasing compatibility, normalized to the model lower crust composition of Rudnick and Fountain (1995).

Creek are chemically zoned (cf. Smith, 1979), and if so, what is the origin of the zonations. As demonstrated in Figure 5, overall the tuff of McMullen Creek becomes more chemically evolved stratigraphically upward. That is, SiO_2 concentrations generally increase, whereas FeO* and CaO concentrations decrease. However, upon examining the geochemical patterns in individual members from different spatial locations, we find that the zonations are apparently quite complex and do not have normal zonation patterns common in the Tertiary ignimbrites of the western United States. For example, member 2 at the Schipper locality becomes more silicic upward (Figure 5), whereas the same member becomes less silicic upward (Figure 5) at the Rams Horn Ridge locality. Because of the small number of localities studied, we cannot determine whether systematic geochemical patterns exist with respect to stratigraphy (vertical zonation) or lateral extent (horizontal zonation); however, we can say that the tuff of McMullen Creek is not normally zoned (e.g., Smith, 1979).

Parker (1996) observed similar compositional patterns for the tuff of Wooden Shoe Butte and suggested that they were produced by vitric-crystal partitioning and are therefore an artifact of emplacement processes, rather than of the original magma source. We tested this hypothesis using a simple least-squares-fit mass balance approach for the most heavily sampled members of tuff of McMullen Creek—member 1 at the Quarry locality and members 2 and 4 at Schipper and Rams Horn Ridge. Details of the mass balance approach are found in Wright (1998). Bulk major element analyses for parent and daughter samples were selected from parts of the 2b layers of the ignimbrites, so as to avoid those that appeared altered or contaminated by lithics. Phenocryst abundance and assemblage were established by point counting. Phenocryst compositions were assumed from unpublished

Table 2. Isotopic data for the tuff of McMullen Creek samples. See Figures 1 and 2 for sample locations.

Sample	Sr ppm	Rb ppm	($^{87}Sr/^{87}Sr$)i*	($^{87}Sr/^{87}Sr$)m*	error ±	Sm ppm	Nd ppm	($^{144}Nd/^{143}Nd$)i	($^{144}Nd/^{143}Nd$)m#	error ±
GVP01KW^	535	15	0.710242	0.710252	7	12.5	63.0	0.512265	0.512272	5
GVP08KW	96	183	0.710182	0.710834	8	11.4	57.8	0.512274	0.512281	5
GVP10KW^	634	12	0.710484	0.710498	6	12.5	63.0	0.512296	0.512302	4
GVP15KW^	613	11	0.713465	0.713471	10	12.5	63.0	0.512269	0.512276	4
GVP16LKW	121	221	0.712955	0.71358	7	11.4	53.2	0.512295	0.512302	5
GVP18KW	96	183	0.712995	0.713647	7	12.5	60.8	0.512264	0.512271	4
GVP21KW^	678	6	0.712406	0.712412	7	12.5	63.0	0.512296	0.512303	5
GVP23KW	103	164	0.712253	0.712784	6	13.2	71.7	0.512296	0.512302	6

^ indicates plagioclase separates

Note: values used for CHUR are $^{143}Nd/^{144}Nd = 0.512638$, $^{147}Sm/^{144}Nd = 0.1967$. Decay constants: Sm= 6.54E-12/yr; Rb = 1.42E-11/yr.

Sr and Rb concentrations determined by ICP-AES analysis (except as noted). Sm and Nd concentrations determined by INAA

* corrected for mass fractionation by normalizing to $^{86}Sr/^{88}Sr = 0.1194$

corrected for mass fractionation by normalizing to $^{146}Nd/^{144}Nd = 0.72190$

Repeated analysis of SRM-987 = 0.710247; repeated analysis of BCR-1 yielded $^{144}Nd/^{143}Nd = 0.512633$.

Sample	($^{208}Pb/^{204}Pb$)m*	error ±	($^{207}Pb/^{204}Pb$)m*	error ±	($^{206}Pb/^{204}Pb$)m*	error ±
GVP01KW^	39.502	6	15.694	3	18.635	3
GVP08KW	39.751	4	15.710	3	18.759	1
GVP10KW^	39.524	7	15.692	2	18.623	3
GVP15KW^	39.327	9	15.687	3	18.530	1
GVP16LKW	39.438	7	15.714	3	18.587	4
GVP18KW	39.332	13	15.680	5	18.544	4
GVP21KW^	39.353	4	15.687	2	18.539	2
GVP23KW	39.453		15.707		18.579	

* Isotopic compositions corrected for a mass fractionation of 0.11%.

^ indicates plagioclase separates.

microprobe analyses of samples from the tuff of Steer Basin, a similar ignimbrite deposited in the Cassia Mountains. The phenocryst assemblage throughout the tuff of McMullen Creek is dominated by plagioclase and clinopyroxene (pigeonite), at about a 3:1 ratio; therefore, these phases were used in the modeling process. Results of the mass balance model are shown in Table 3. Models generated require about a 3:1 plagioclase-pigeonite ratio, which is consistent with the observed assemblage in the tuff of McMullen Creek. Although the phenocryst assemblage and proportion used in the model are similar to that observed in the samples, and phenocryst content generally correlates positively with changes in composition, the increase in crystal content is not sufficient to account for the change in bulk composition. Our mixing calculations suggest that about 40 to 90 percent of the variation must be accounted for by processes other than crystal-vitric segregation.

Since crystal-vitric segregation cannot account for all the observed geochemical variation, we infer the remainder to be attributed to variations in original (i.e., pre-eruptive) magma chemistry. Trace-element variations are generally in accord with the direction of changes that would be expected from the mass balance model. Because Sr and Eu have a substantial decrease in concentration among the tuff of McMullen Creek samples, they were used as independent variables to test the fractional crystallization hypothesis. We assumed the only significant Eu- and Sr- bearing mineral phase is plagioclase. We obtained partition coefficients for Sr and Eu by measuring their concentrations in plagioclase phenocrysts and matrix material (Wright, 1998). Calculations using a Raleigh fractionation model, and the same parent-daughter sample pairs in Table 3 adjusted for crystal-vitric segregation, suggest that 2 to 4 percent fractionation is necessary to achieve the observed Eu and Sr concentration differences within each parent-daughter pair.

ISOTOPIC VARIATIONS

An important aspect of petrogenesis and chemical evolution is whether isotopic zonations, similar to major and trace-element zonations found frequently in ignimbrites, can be found in the tuff of McMullen Creek. An initial assumption was that plagioclase separates taken from the lower vitrophyres of each ignimbrite would be isotopically representative of the magma. However, our petrographic observations of glomeroporphyritic aggre-

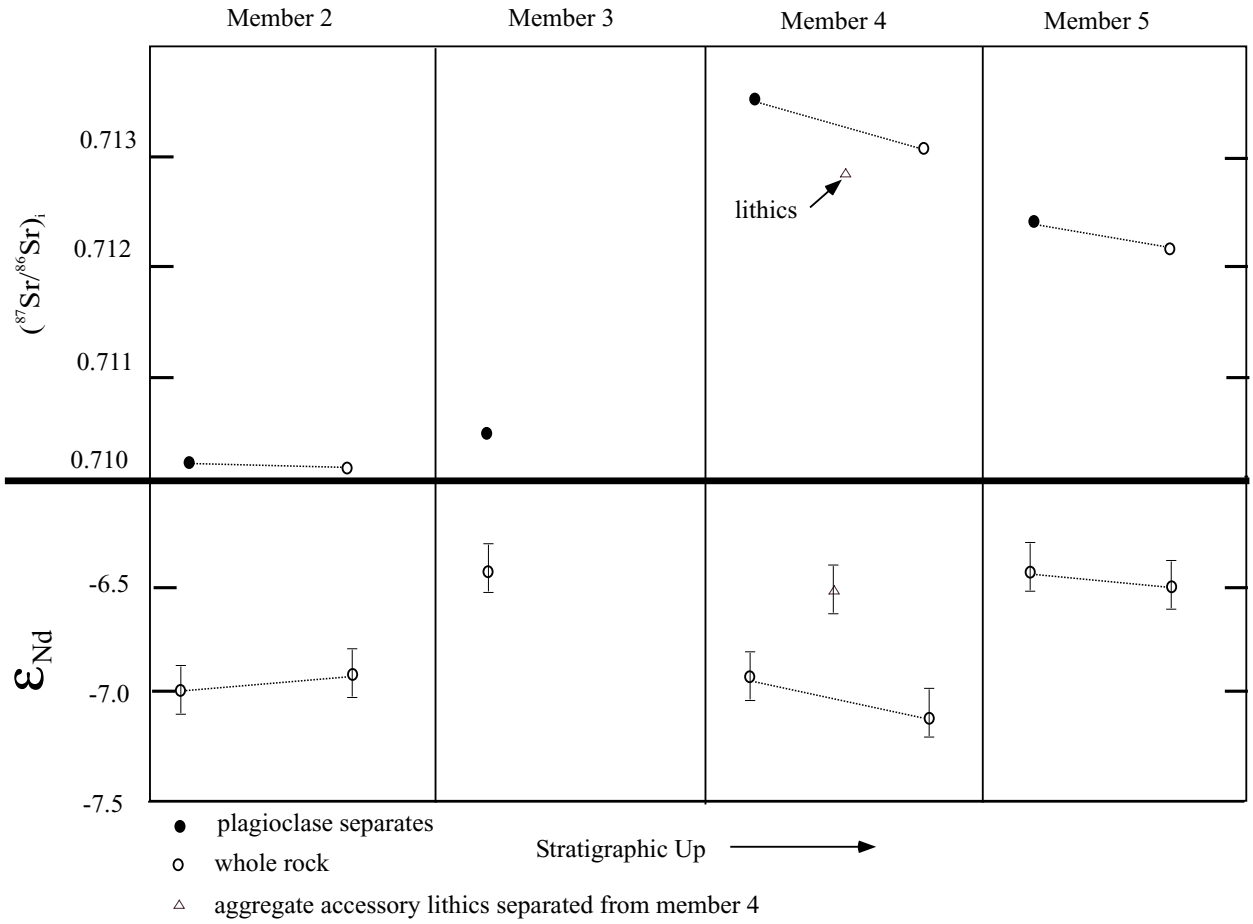

Figure 7. Sr- and Nd-isotopic variations within each member that is exposed at the Schipper locality. Whereas ε_{Nd} variations within each member may be within uncertainties, initial Sr-isotopic ratios are higher at the base of members 2, 4, and 5 (as measured by plagioclase separates) and lower at the top of these members (as measured by bulk rock analyses). Error for Sr-isotopic ratios is smaller than the symbols (open and filled circles).

gates, which we interpret to be cognate fragments originally attached to the walls of the magma chamber, suggest that our initial assumption was invalid. The problem with assuming that mineral separates obtained from the ignimbrites will have isotopic signatures indicative of the magma chamber as a whole is that cognate fragments may have assimilated more country rock than the magma located near the center of the chamber, thereby altering the isotopic ratios of the fragments preferentially. Because of this, it is not possible for us to determine whether or not the chamber was isotopically zoned; however, by comparing the isotopic values of the plagioclase separates with the whole rock data for each ignimbrite, some constraints may be obtained concerning assimilation processes (Wright, 1998).

If we consider whole rock isotopic data only, there appears to be a shift towards less-evolved isotopic ratios between members 2 and 3, and members 4 and 5. A shift to more evolved ratios occurs between members 3 and 4. This may appear to conflict with geochemical data that overall suggest that the tuff of McMullen Creek becomes more evolved (more silicic) stratigraphically upward. However, our mass-balance calculations suggest that fractional crystallization is an important, perhaps dominant, process controlling the geochemical evolution of the magmatic system. If closed-system processes such as fractional crystallization dominate over open-system processes such as assimilation, the isotopic evolution and the geochemical evolution of the magmatic system will tend to be somewhat independent of each other.

PETROGENESIS

Crustal Structure and Isotopic Reservoirs

The SRP-Yellowstone hot-spot track crosses a fundamental lithospheric boundary between early Protero-

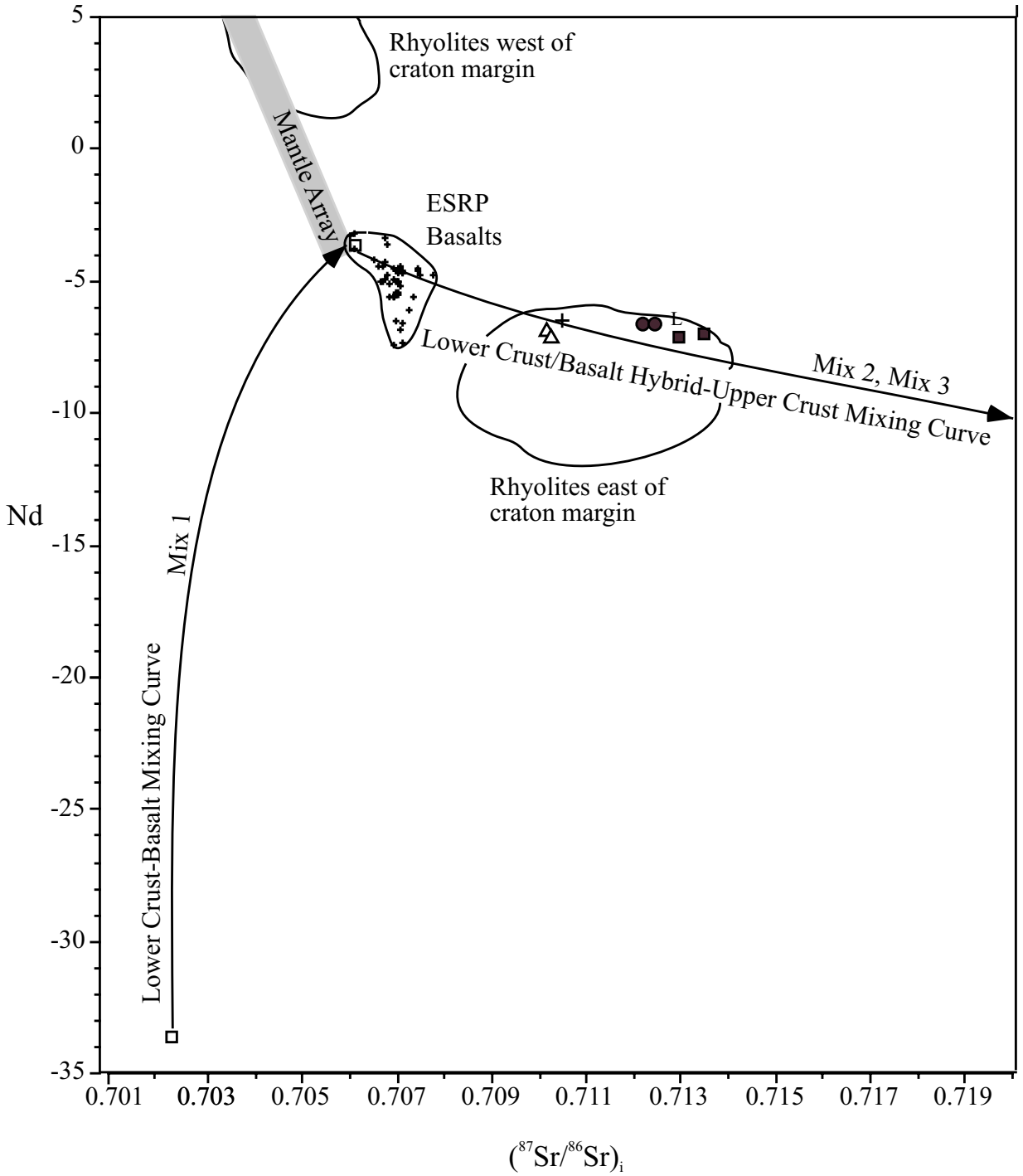

Figure 8. Plot illustrates Sr- and Nd-isotopic fields for rhyolites west of the craton margin, rhyolites east of the craton margin, and ESRP basalts (data comes from Leeman and others, 1992; McCurry, unpublished data, 1999). Isotopic analyses for tuff of McMullen Creek samples are shown with Member 2 (open triangles), Member 3 (plus symbol), Member 4 (filled squares), Member 5 (filled circles), and lithics separated from Member 4 (L). Mixing solutions from Table 4 are plotted.

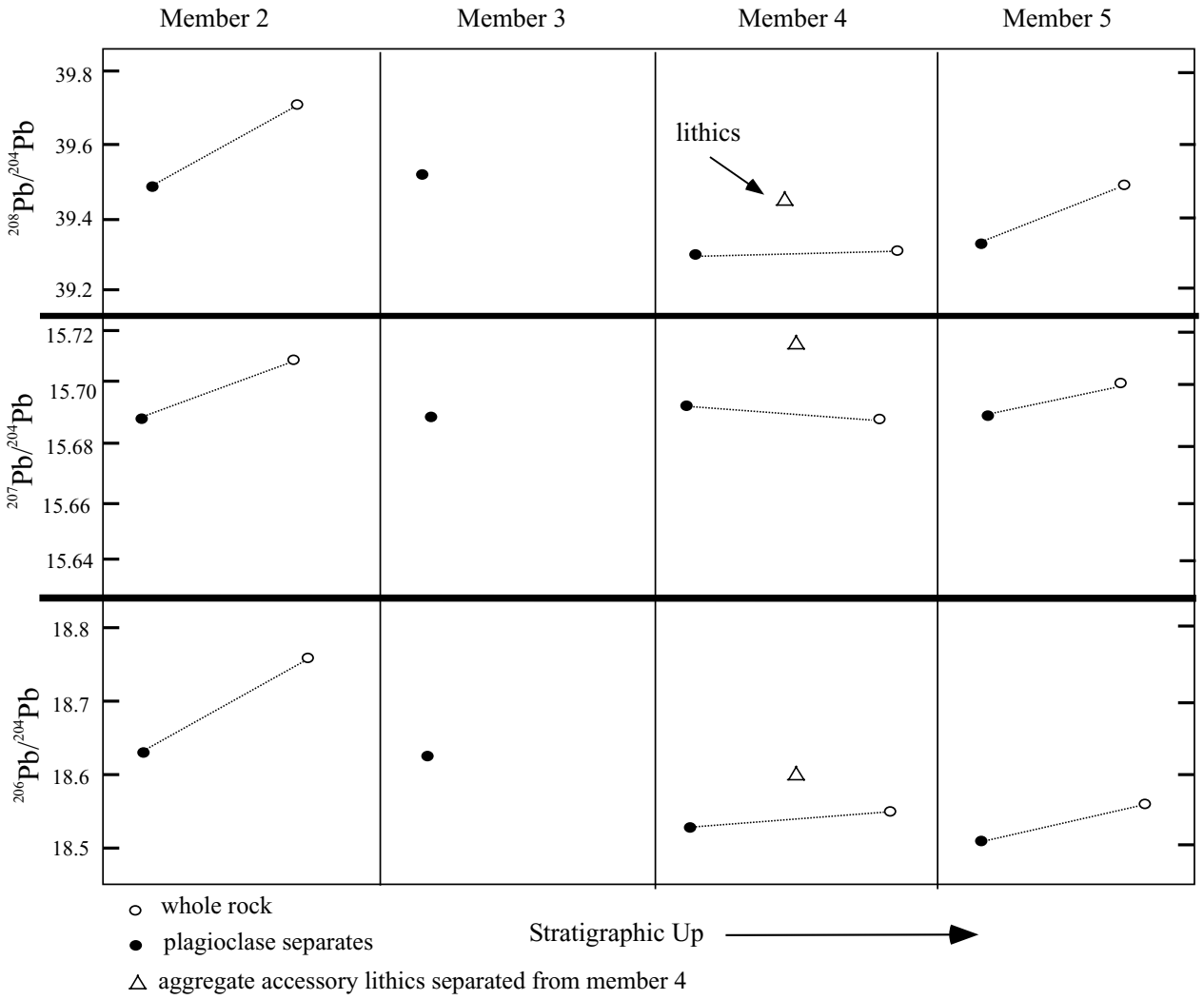

Figure 9. Pb-isotopic variations within each member of the tuff of McMullen Creek. Variations of $^{207}Pb/^{204}Pb$ and $^{208}Pb/^{204}Pb$ for member 4 are within analytical uncertainties (uncertainties are smaller than the symbols). Plagioclase separates yield lower Pb-isotopic ratios than whole rocks from the same member. Middle to upper crust Pb isotopes for all three Pb ratios will be lower than Pb ratios for the tuff of McMullen Creek samples (Leeman and others, 1985).

zoic to late Archean Wyoming terrane to the east and younger, Phanerozoic accreted terrane to the west. However, the precise location and three dimensional geometry of the boundary are poorly understood, primarily due to the lack of suitable exposures in western Idaho and Nevada. There are two, apparently incompatible, interpretations of the location of the contact or boundary, referred to as the 0.706 line between Precambrian ($^{87}Sr/^{86}Sr > 0.706$) and Phanerozoic ($^{87}Sr/^{86}Sr < 0.706$) lithosphere. Leeman and others (1992) place the 0.706 line nearly coincident with the Idaho-Oregon border. This interpretation is consistent with Farmer and DePaolo (1983), who used both Sr and Nd values for their explanation, as well as Strayler and others (1989) who used tectonic reconstructions. In contrast, Elison and others (1990) suggest that the 0.706 line transects northern Nevada and cross-cuts Idaho near the Nevada-Utah border. Elison and others (1990), however, base the location of the 0.706 line on a small number of samples. Moreover, Leeman and others (1985) collected crustal xenoliths significantly west of Elison and others' (1990) 0.706 line that yield metamorphic ages of 2.8 Ga and Nd model ages of 3.1-3.4 Ga. For the purposes of our work, we assume that the boundary between cratonal lithosphere and accreted terrane roughly parallels the Idaho-Oregon border.

Potential isotopic reservoirs that may have contrib-

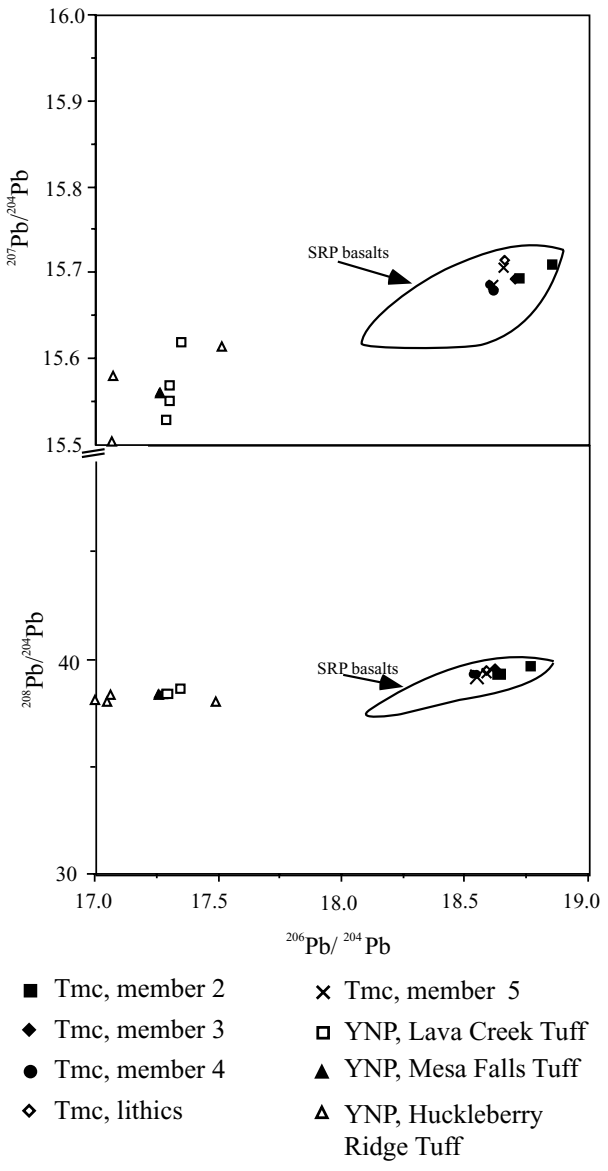

Figure 10. Pb-isotopic ratios of tuff of McMullen Creek rhyolites compared to rhyolites from Yellowstone National Park and eastern SRP basalts. Note that the Pb-isotopic ratios of the tuff of McMullen Creek rhyolites are more similar to those of eastern SRP basalts than those of Yellowstone National Park rhyolites.

uted to the petrogenesis of the tuff of McMullen Creek include upper and lower continental crust, lithospheric mantle, hot-spot plume-type mantle, and Paleozoic and Mesozoic sedimentary rocks. Because isotopic data for sedimentary rocks near the Twin Falls volcanic center have not been published, we obtained isotopic values for sedimentary rocks from Leeman and others (1977); they pertain primarily to the outcrops of the Madison Limestone near Yellowstone National Park. Data concerning subcontinental mantle lithosphere are inferred from Quaternary basalt analyses from the eastern SRP (Hughes and others, 2000). Because the volcanic deposits along the SRP have been altered substantially from those that would have plume-type isotopic signatures, the potential isotopic influence from the plume on the tuff of McMullen Creek rhyolites has been ignored. Data for upper and lower crustal rocks were obtained from Leeman and others (1985). In that work, numerous Sr-, Nd-, and Pb-isotopic analyses of xenoliths found in SRP basalts have been published. Although Leeman and others (1985) suggest the xenoliths are lower crustal in origin, because of their high Sr-isotopic ratios, many of them appear to be more consistent isotopically with upper crustal rocks. Therefore, lower crust compositions were approximated using Spencer-Kilgore sample B2; upper crust compositions were approximated using Albion Range sample YAG-799.

Rhyolite Petrogenesis

Several hypotheses have been proposed to explain the petrogenesis of rhyolites along the Yellowstone hot-spot track. These include fractional fusion of a mantle source, crustal anatexis due to injection of high-temperature mafic magmas, differentiation of basaltic parental magmas (Leeman, 1989), and partial melting of lower crust that has been hybridized by basaltic intrusions (Hildreth and others, 1991).

The first two hypotheses cannot be used to explain the petrogenesis of the tuff of McMullen Creek, as the isotopic signatures of the proposed reservoirs are inconsistent with our isotopic data. Fractional crystallization of a primitive SRP basalt with minor crustal contamination is consistent with our isotopic data. Extreme fractionation of basalt can produce melts that are rhyolitic in composition with regard to major element chemistry and many trace elements. Assimilation of upper crustal rocks will result in the enrichment of incompatible elements such as Ba, Cs, and Th into the melt. This relative enrichment of incompatible elements and relative depletion of compatible elements are apparent in Figure 6. However, there are two difficulties with this hypothesis: (1) Cassia Mountains rhyolites do not show evidence of extreme fractional crystallization. Substantial plagioclase fractionation should be evident in the form of large depletions of Sr in Figure 6, but this has not occurred. (2) If basalt is parental to the rhyolite, intermediate composition rocks might also be expected to be present; intermediate rocks are present at other regions of the SRP (i.e., Craters of the Moon). However, no rocks of intermediate composition have been found in the Cassia Mountains region.

Table 3. Results of mass balance calculations based upon phenocryst segregation between parent and daughter compositions for several members of the tuff of McMullen Creek. Observed phenocryst difference is the percentage of phenocrysts in the parent rock minus the percentage of phenocrysts in the daughter rock. Predicted phenocryst difference is the amount of phenocryst segregation required to satisfy chemical differences. Because the observed difference is substantially less than predicted, this modeling suggests that crystal-vitric segregation cannot account for all the observed geochemical variations.

	Quarry M1	Schipper M2	Schipper M4	Rams Horn Ridge M2	Rams Horn Ridge M4
Parent Sample	SB03KW	GVP02KW	GVP15KW	RH04KW	RH12KW
Daughter Sample	SB02AKW	GVP08KW	GVP18KW	RH01KW	RH07KW
Observed phenocryst difference	2.4%	7.2%	1.4%	2.6%	0.8%
Predicted phenocryst difference	6.2%	11.9%	7.8%	4.7%	6.7%
Maximum percentage of geochemical variations possible by crystal-vitric segregation	39%	61%	18%	55%	12%

However, no rocks of intermediate composition have been found in the Cassia Mountains region.

The hypothesis of Hildreth and others (1991) is also consistent with the observed data. If the lower crust were pervasively hybridized by basalt, it would become isotopically and geochemically very similar to basalt. Partial melts of such a hybrid could rise to midcrustal levels where further differentiation, contamination, and eruption could take place.

To produce a basalt-lower crust hybrid with an ε_{Nd} of around -4, a 90 percent basalt component is required (Figure 8, Table 4). The resulting $^{87}Sr/^{86}Sr$ would be 0.705. Partial melts of this hybrid material would rise to midcrustal levels where the assimilation of 12 to 18 percent upper crust component would be necessary to produce rhyolites with the observed isotopic ratios (Figure 8, Table 4). The resulting basalt component of erupting rhyolites would be 74-80 percent (basalt is 90 percent of mix 1; mix 1 is 82-88 percent of mix 2 and mix 3, the mixes from which the rhyolites are produced).

CONCLUSIONS

We propose that Tertiary basaltic magmas invaded and pervasively hybridized isotopically with Archean lower and middle continental crust during the earliest phase of hot-spot and continental crust interaction in the central SRP region. As much as 90 percent of the mass within the mid- and lower-crust may have been added during this time. The thermal pulse associated with the emplacement of the mantle-derived magmas subsequently resulted in widespread partial melting of the hybridized crustal material. These melts ascended into magma chambers in the mid- or upper-crust where they underwent moderate fractional crystallization and assimilation.

Bulk compositional variations within ignimbrites of the tuff of McMullen Creek are complex and are partly influenced by mixing and segregation processes associated with the eruption and emplacement of the deposits. However, at least 40 percent of the observed variations are magmatic in nature. Thus, we infer some composi-

Table 4. Strontium- and neodymium-isotope mixing models. Components used to create mixing curves illustrated on Figure 8. $(^{87}Sr/^{86}Sr)_t$ and $(^{143}Nd/^{144}Nd)_t$ refer to ratio values at 8.6 Ma. Data for components 2 and 3 come from Leeman and others (1985). Data for component 1 come from Hughes and others (2000).

Components	Mixing Proportions	$(^{87}Sr/^{86}Sr)_t$	$(^{143}Nd/^{144}Nd)_t$	ε_{Nd}	Sr, ppm	Nd, ppm
1	100% SRP basalt	0.705991	0.512470	-3.2	247	26
2	100% Spencer Kilgore B2	0.70235	0.510906	-33.2	634	6.76
Mix 1	90% component 1, 10% component 2	0.705180	0.512426	-4.17	286	24
3	Albion Range YAG-799	0.805646	0.511266	-26.2	115	19
Mix 2	82% Mix 1, 18% component 3	0.713339	0.512255	-7.5	255	23
Mix 3	88% Mix 1, 12% component 3	0.710410	0.512313	-6.4	265	24

tional heterogeneity existed within the source chamber or chambers, albeit not necessarily a systematic vertical zonation. These variations are best explained by fractional crystallization from a common parental magma.

The upward trend towards more evolved compositions as seen in members 2 through 5 suggests that the parental magma may have become increasingly felsic over time, possibly reflecting the presence of a long-lived magma chamber in the middle crust.

ACKNOWLEDGMENTS

Funding for this research was provided by State of Idaho Natioinal Science Foundation EPSCoR Cooperative Agreement OSR-9350539. Irradiation of samples for INAA analyses was provided by the Radiation Center, Oregon State University, Brian Dodd, Director. Isotopic analyses of samples were provided by Jim Wright, Rice University. We would also like to thank Curtis Manley for his thoughtful and thorough editing of this manuscript.

REFERENCES

Armstrong, R.L., J.E. Harakel, and W.M. Neill, 1980, K-Ar dating of Snake River Plain (Idaho) volcanic rocks—new results: Isochron/West, no. 27, p. 5-10.

Armstrong, R.L., W.P. Leeman, and H.E. Malde, 1975, K-Ar dating, Quaternary and Neogene volcanic rocks of the Snake River Plain, Idaho: American Journal of Science, v. 275, p. 225-251.

Bonnichsen, Bill, and G.P. Citron, 1982, The Cougar Point Tuff, southwestern Idaho and vicinity, *in* Bill Bonnichsen and R.M. Breckenridge, eds., Cenozoic Geology of Idaho: Idaho Bureau of Mines and Geology Bulletin 26, p. 255-281.

Chapin, C.E., and G.R. Lowell, 1979, Primary and secondary flow structures in ash-flow tuffs of the Gribbles Run paleovalley, central Colorado, *in* C.E. Chapin and W.E. Elston, eds., Ash-Flow Tuffs: Geological Society of America Special Paper 180, p. 137-153.

Ekren, E.B., D.H. McIntyre, and E.H. Bennett, 1984, High temperature, large-volume, lavalike ash-flow tuffs without calderas in southwestern Idaho: U.S. Geological Survey Professional Paper 1272, 73 p.

Elison, M.W., R.C. Speed, and R.W. Kistler, 1990, Geologic and isotopic constraints on the crustal structure of the northern Great Basin: Geological Society of America Bulletin, v. 102, p. 1077-1092.

Farmer, G.L., and D.J. DePaolo, 1983, Origin of Mesozoic and Tertiary granite in the western United States and implications for pre-Mesozoic crustal structure, 1, Nd and Sr isotopic studies in the geocline of the northern Great Basin: Journal of Geophysical Research v. 88, p. 3379-3401.

Hibbard, M.J., 1995, Petrography to Petrogenesis: Prentice-Hall, Englewood Cliffs, 587 p.

Hildreth, Wes, A.N. Halliday, and R.L. Christiansen, 1991, Genesis and contamination of basaltic and rhyolitic magma beneath the Yellowstone Plateau volcanic field: Journal of Petrology, v. 32, p. 63-138.

Honjo, Norio., 1990, Geology and stratigraphy of the Mount Bennett Hills, and the origin of west-central Snake River Plain rhyolites: Rice University Ph.D. dissertation, 259 p.

Hughes, S.S., Michael McCurry, and D.J. Geist, 2000, Regional geochemical correlations and magmatic evolution of basalt flow groups at INEEL, *in* P.K. Link, L.L. Mink, and Dale Ralston, eds., Geology, Hydrogeology and Environmental Remediation, Idaho National Engineering and Environmental Laboratory, Eastern Snake River Plain: Geological Society of America Special Paper 353, p. 151-173.

Leeman, W.P., 1982, Development of the Snake River Plain-Yellowstone Plateau province, Idaho and Wyoming: An overview and petrologic model, *in* Bill Bonnichsen and R.M. Breckenridge, eds., Cenozoic Geology of Idaho: Idaho Bureau of Mines and Geology Bulletin 26, p. 155-177.

———, 1989, Origin and development of the Snake River Plain (SRP)—An overview, *in* R.P. Smith and W.F. Down, eds., IGC Field Trip T305: Field Guide to the Snake River Plain-Yellowstone Volcanic Province, Volcanism and Plutonism of Western North America: American Geophysical Union, Washington, D.C., v. 2, p. T305:4-T305:12.

Leeman, W.P., B.R. Doe, and Joseph Whelan, 1977, Radiogenic and stable isotope studies of hot-spring deposits in Yellowstone National Park and their genetic implications: Geochemical Journal, v. 11, p. 65-74.

Leeman, W.P., M.A. Menzies, D.J. Matty, and G.F. Embree, 1985, Strontium, neodymium and lead isotopic compositions of deep crustal xenoliths from the Snake River Plain: Evidence for Archean basement: Earth and Planetary Science Letters, v. 75, p. 354-368.

Leeman, W.P., J.S. Oldow, and W.K. Hart, 1992, Lithosphere-scale thrusting in the western U.S. Cordillera as constrained by Sr and Nd isotopic transitions in Neogene volcanic rocks: Geology, v. 20, p. 63-66.

Mapel, W.J., and W.J. Hail, Jr., 1959, Tertiary geology of the Goose Creek district, Cassia County, Idaho, Box Elder County, Utah, and Elko County, Nevada: U.S. Geological Survey Bulletin 1055-H, p. 217-254.

McCurry, Michael, A.M. Watkins, J.L. Parker, Karen Wright, and S.S. Hughes, 1996, Preliminary volcanological constraints for sources of high-grade, rheomorphic ignimbrites of the Cassia Mountains, Idaho: Implications for the evolution of the Twin Falls volcanic center, *in* S.S. Hughes and R.C. Thomas, eds., Northwest Geology, v. 26, p. 81-91.

McCurry, Michael, K.E. Wright, and S.S. Hughes, 1995, Nd- and Sr-isotopic characteristics of ignimbrites along the south-central part of the Snake River Plain—Yellowstone hotspot track: Eos, Transactions, American Geophysical Union, v. 76(46), p. F656.

Morgan, L.A., D.J. Doherty, and W.P. Leeman, 1984, Ignimbrites of the eastern Snake River Plain: Evidence of major caldera-forming eruptions: Journal of Geophysical Research, v. 89, p. 8665-8678.

Moye, F.J., W.P. Leeman, W.R. Hackett, Bill Bonnichsen, Norio Honjo, and C. Clarke, 1988, Cenozoic volcanic stratigraphy of the Lake Hills, Blaine Co., Idaho, and bearing on development of the Snake River Plain Province: Geological Society of America Abstracts with Programs, v. 20, p. 434.

Nakada, Setsuya, C.R. Bacon, and A.E. Gartner, 1994, Origin of phenocrysts and compositional diversity in pre-Mazama rhyodacite lavas, Crater Lake, Oregon: Journal of Petrology, v. 35, p. 127-162.

Noble, D.C., and W.P. Leeman, 1989, Sodium, potassium, and ferrous iron contents of some secondarily hydrated natural silicic glasses: American Mineralogist, v. 52, p. 280-286.

Parker, J.L., 1996, Physical volcanology and geochemistry of the tuff of Wooden Shoe Butte, Cassia Mountains, Idaho: Idaho State University M.S. Thesis, 105 p.

Perkins, M.E., F.H. Brown, W.P. Nash, William McIntosh, and S.K. Williams, 1998, Sequence, age, and source of silicic fallout tuffs in middle to late Miocene basins of the northern Basin and Range Prov-

ince: Geological Society of America Bulletin, v. 110, p. 344-360.
Pierce, K.L., and L.A. Morgan, 1992, The track of the Yellowstone hotspot: Volcanism, faulting and uplift, *in* P.K. Link, M.A. Kuntz, and L.B. Platt, eds., Regional Geology of Eastern Idaho and Western Wyoming: Geological Society of America Memoir 179, p. 1-53.
Rudnick, R.L., and D.M. Fountain, 1995, Nature and composition of the continental crust: A lower crust perspective: Reviews of Geophysics, v. 33., no. 3, p. 267-310.
Smith, R.B., and L.W. Braile, 1993, Topographic signature, space-time evolution, and physical properties of the Yellowstone-Snake River Plain volcanic system: The Yellowstone hotspot, *in* A.W. Snoke, J.R. Steidtmann, and S.M. Roberts, eds., Geology of Wyoming: Geological Survey of Wyoming Memoir 5, p. 694-754.
Smith, R.L., 1979. Ash-flow magmatism: Geological Society of America Special Paper 180, 5-27.
Sparks, R.S.J., Steve Self, and G.P.L. Walker, 1973, Products of ignimbrite eruptions: Geology, v. 1, p. 115-118.
Strayler, L.M. IV, D.W. Hyndman, J.W. Sears, and P.E. Myers, 1989, Direction and shear sense during suturing of the Seven Devils-Wallowa terrane against North America in western Idaho: Geology, v. 17, p. 1025-1028.
Williams, P.L., H.R. Covington, and J.W. Mytton, 1991, Geologic map of the Stricker 2 quadrangle, Twin Falls and Cassia counties, Idaho: U.S. Geological Survey Miscellaneous Investigations Series Map I-2078, 1:48,000.
Williams, P.L., J.W. Mytton, and H.R. Covington, 1990, Geologic map of the Stricker 1 quadrangle, Cassia, Twin Falls, and Jerome counties, Idaho: U.S. Geological Survey Miscellaneous Investigations Series Map I-2078, 1:48,000.
Wright, J.E., and A.W. Snoke, 1993, Tertiary magmatism and mylonitization in the Ruby-East Humbolt metamorphic core complex, northeastern Nevada: U-Pb geochronology and Sr, Nd, and Pb isotope geochemistry: Geological Society of America Bulletin, v. 105, no. 7, p. 935-952.
Wright, K.E., 1998, Geochemistry and Petrology of the tuff of McMullen Creek, Cassia County, Idaho: Idaho State University M.S. Thesis, 172 p.
Youngquist, W., and J.R. Haegele, 1956, Geological reconnaissance of the Cassia Mountain region, Twin Falls and Cassia counties, Idaho: Idaho Bureau of Mines and Geology Pamphlet 110, 18 p.

Transition From Ash-Flow to Voluminous Lava-Flow Activity, Bruneau-Jarbidge Eruptive Center, Southwestern Idaho

William H. Hirt[1]

ABSTRACT

The Triguero Homestead (TH) and Indian Batt (IB) rhyolites are large intracaldera lava flows that were extruded from the southern part of the Bruneau-Jarbidge eruptive center (BJEC) shortly after the eruptions which produced the youngest members of the Cougar Point Tuff (CPT) about 10.5 Ma. Together with the two youngest members of the CPT (units XIII and XV), these flows define the last of three eruptive "cycles" within which rhyolites become hotter and more mafic over time. The third-cycle rhyolites also span the eruptive center's final transition from ash flows to lavas and suggest that a decrease in the volatile contents of the magmas accompanied other compositional changes that took place during the cycle.

Plagioclases from the TH and IB rhyolites are more calcic, and pyroxenes more magnesian, than those from the associated ash-flow tuffs. The compositions of coexisting augites ($Wo_{35}En_{31}Fs_{34}$) and pigeonites ($Wo_{10}En_{36}Fs_{54}$) indicate an eruptive temperature of about 975ºC for the TH rhyolite. Similarly, the compositions of coexisting augites ($Wo_{36}En_{33}Fs_{31}$) and pigeonites ($Wo_{09}En_{40}Fs_{51}$) indicate an eruptive temperature of about 960ºC for the IB rhyolite. The eruptive temperatures of these lavas were about 30ºC-50ºC higher than that of the ash flow, CPT XV, which immediately preceded them.

Repeated eruptions of relatively felsic rhyolites at the beginnings of each of the three cycles suggest that one or more large, thermally and chemically zoned rhyolite reservoirs developed beneath the BJEC during the formation of the CPT and the oldest overlying lavas. The TH and IB rhyolite flows are interpreted as magmas erupted from the deeper part of the third-cycle reservoir after its volatile-rich upper part had vented to form CPT members XIII and XV, but before compositional gradients within the body had been restored by subsequent differentiation.

Key words: Bruneau-Jarbidge eruptive center, rhyolite, geothermometry

INTRODUCTION

The Bruneau-Jarbidge eruptive center (BJEC) is a bimodal volcanic system that developed above the Yellowstone hot spot in southwestern Idaho during middle to late Miocene time (Bonnichsen, 1982a). The earliest recognized eruptions at the BJEC produced a sequence of nine rhyolite ash-flow tuffs, collectively termed the Cougar Point Tuff (Bonnichsen and Citron, 1982), and were accompanied by subsidence of an approximately 50- by 100-km depression that defines the center (Figure 1). Shortly after the eruption of the youngest ash flow, about 10.5 Ma (Perkins and others, 1998), a sequence of eight to twelve large rhyolite lava flows spread across the floor of the depression (Bonnichsen, 1982b). These flows partially filled the eruptive center and marked the end of its rhyolitic activity at about 8 Ma (Vetter and Shervais, 1997). Subsequent filling of the BJEC by locally derived sediments and post-8 Ma basalts has largely obliterated the original basin, so that present-day exposures of the intrabasinal units are restricted to the canyons that the Bruneau and Jarbidge rivers and their tributaries have incised into the Owyhee Plateau.

The CPT ash flows and at least two of the overlying

Editors' note: The manuscript was submitted in July 1998 and has been revised at the author's discretion.

[1]College of the Siskiyous, 800 College Ave., Weed, CA 96094

Hirt, W.H., 2002, Transition from ash-flow to voluminous lava-flow activity, Bruneau-Jarbidge eruptive center, southwestern Idaho, *in* Bill Bonnichsen, C.M. White, and Michael McCurry, eds., Tectonic and Magmatic Evolution of the Snake River Plain Volcanic Province: Idaho Geological Survey Bulletin 30, p. 195-204.

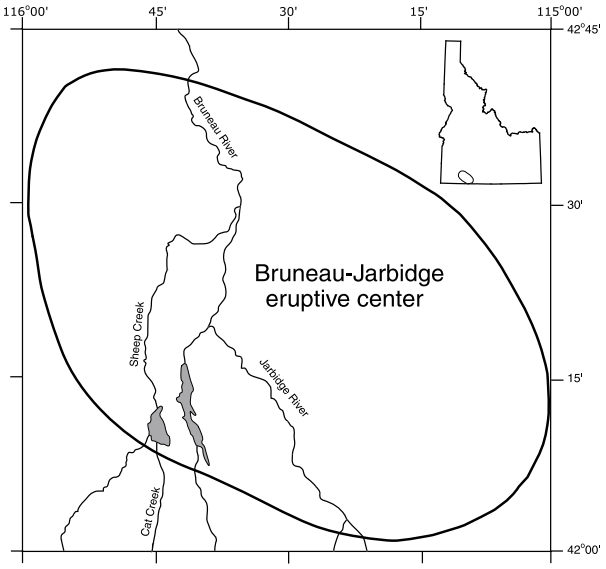

Figure 1. Index map of the BJEC showing the locations of rhyolite lava-flow outcrops in the parts of the Sheep Creek, Cat Creek, and Bruneau River canyons where the TH and IB flows are exposed. The gray outcrop areas include both the TH and IB rhyolites as well as several younger flows, but separate units have not been broken out on this map. Modified from Bonnichsen (1982a).

rhyolite lava flows (TH and IB) can be grouped into three "eruptive cycles" on the basis of trends in their major- and trace-element compositions (Bonnichsen, 1982c). Progressively hotter, more mafic rhyolites were erupted during the course of each cycle (Figure 2), but the second and third cycles began with the eruptions of cooler, more felsic ash-flow tuffs than those that had ended the preceding cycles.

The compositional trends that define these eruptive cycles are superimposed on longer-term changes in the CPT ash flows and their correlative air-fall tephras that include: (1) general increases in eruptive temperatures (Perkins and others, 1995); and (2) shifts towards more "primitive" (mantlelike) Sr and Nd isotopic compositions (Table 1) over time (Cathey and others, 1997). These long-term changes suggest that the eruptive center's lower crustal source rocks may have become increasingly hybridized with mantle-derived magmas during the lifetime of the system (e.g., Riciputi and Johnson, 1990).

The transitions to cooler, more felsic ash flows that mark the beginnings of the second and third eruptive cycles suggest that the reservoir or reservoirs, which once lay beneath the BJEC, had become thermally and compositionally zoned during the periods of repose between cycles. Differentiation that took place during these periods is evidenced by the trends in eruptive temperatures and bulk compositions described earlier (Figure 2), as well as by systematic variations in the types and abundances of phenocrysts found in the CPT units. Within the tuffs erupted during the third cycle, for example, quartz and plagioclase are more abundant upward relative to sanidine in CPT XIII, and fayalite decreases in abundance upward and finally disappears as pigeonite becomes more abundant in CPT XV.

One explanation for the compositional trends among the CPT members is that the rhyolites produced during each eruptive cycle were drawn from a separate differentiated reservoir. A detailed study by Cathey and Nash (1998) has shown, however, that the compositions of pyroxenes and glasses from the CPT cluster into at least seven distinct ranges and that these compositional modes occur repeatedly throughout the ash-flow tuff sequence. These authors suggest, therefore, that the entire CPT was erupted from a single reservoir system rather than three distinct reservoirs. They infer that successive eruptions repeatedly tapped a number of distinct compositional horizons that had developed within this system and persisted during much of its 2.2 million year eruptive history. Although the recurrence of several distinct phenocryst and glass populations supports the interpretation that CPT rhyolites from all three eruptive cycles were drawn from a single reservoir, I will refer to the part of this system that produced CPT XIII, CPT XV, and the TH and IB lava flows as the "third-cycle reservoir" in this paper.

The preceding discussion of the rhyolitic magmatic system that developed beneath the BJEC has been based largely on data from the CPT. Some of the most important elements in the records of rhyolitic volcanism at eruptive centers such as Bruneau-Jarbidge, however, are the intracaldera lava flows. As studies at the Yellowstone Plateau volcanic field have shown, these flows provide glimpses into the development of long-lived magmatic systems at times other than those of major ash-flow eruptions (Hildreth and others, 1984; Hildreth and others, 1991). Unfortunately, the early part of the lava-flow record is unavailable at the BJEC because all but two of the flows that predate the third eruptive cycle have been buried within the center. The two exposed flows crop out between CPT XII and CPT XIII at the Black Rock escarpment (Bonnichsen, 1982a) and may be some of the last rhyolites erupted during the second cycle or some of the first erupted during the third. Unfortunately, no data are yet available from which to infer their relationships to the surrounding tuffs.

The lavas that erupted after CPT XV, on the other hand, are relatively well exposed. The two oldest of these, the TH and IB rhyolites, apparently extend the trend defined by the third-cycle ash-flow tuffs to more mafic whole rock compositions (Table 2). The eruptions of the TH and IB rhyolites also mark the beginning of the final

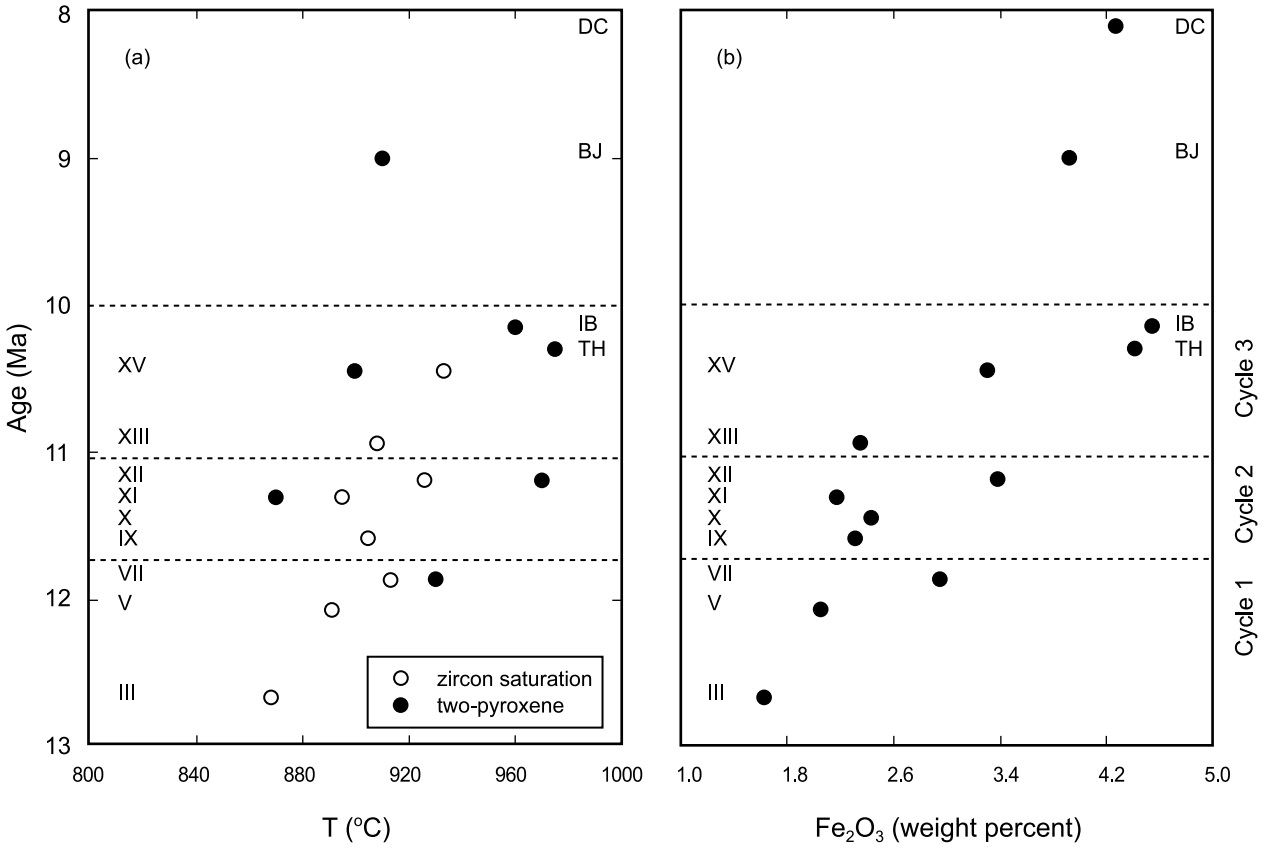

Figure 2. Average (a) eruptive temperatures and (b) Fe_2O_3* (total Fe reported as Fe_2O_3) contents of the CPT ash flows and four overlying rhyolite lava flows plotted versus their ages. Two-pyroxene temperatures are from Honjo and others (1992) and this paper and were calculated using the model of Davidson and Lindsley (1985). Zircon solubility temperatures were calculated using the model of Watson and Harrison (1983) and the compositions of correlative air-fall ashes reported by Perkins and others (1995). Fe_2O_3* percentages are averages of vitrophyre analyses (and, for CPT X, one crystallized rock) reported by Bonnichsen (1982c) and Bonnichsen and others (1994). Each of the averages has been normalized to a major-element total of 100 percent. Ages for all of the CPT members except VII and X are from Perkins and others (1998). The age of the Dorsey Creek rhyolite (DC) is an average of two measurements (8.00 and 8.22 Ma) reported by Bonnichsen (1982a). The ages assigned to the remaining units (CPT VII and X and the TH, IB, and Bruneau Jasper (BJ) rhyolite flows) are arbitrary values consistent with their stratigraphic positions relative to adjacent units for which age measurements or estimates are available.

transition from ignimbrite to lava-flow activity at the BJEC. The goals of this paper are (1) to document the compositions of the plagioclases and pyroxenes from the TH and IB flows and (2) to test whether these mineral compositions and the eruptive temperatures estimated from them extend trends defined by the third-cycle ash-flow tuffs. Such agreement would support the interpretation that the TH and IB flows were drawn from the same thermally and compositionally stratified reservoir that produced CPT units XIII and XV.

SAMPLE DESCRIPTIONS

The Triguero Homestead rhyolite flow directly overlies a part of CPT XV deposited within the BJEC, and is, in turn, overlain by the Indian Batt rhyolite (Figure 3). The contacts between these units are well exposed along the canyons of the Bruneau River and its tributaries in the southwestern part of the eruptive center (Figure 1). Both flows are described by Bonnichsen (1982b), and each consists of a basal vitrophyre that is overlain by a crystalline interval and locally capped by an upper vitrophyre. The samples used in this study, TH-1 and IB-1, were collected from the basal vitrophyres of the flows where they crop out in Cat Creek Canyon, 1.05 km and 0.35 km, respectively, southeast of the confluence of Sheep and Cat creeks.

Both vitrophyres are petrographically similar and consist of approximately 85 volume percent brown glass, 7 percent plagioclase, 4 percent augite, 3 percent pigeonite, 1 percent magnetite and ilmenite, and trace amounts

Table 1. Published Sr and Nd isotopic compositions of the BJEC rhyolites. The calculated initial Sr ratios of CPT members are not successively lower as expected on the basis of the increases in ε_{Nd} values reported for correlative air-fall ashes by Cathey and others (1997). However, the calculated initial ratio for CPT III is probably too low because the relatively high Rb/Sr ratio of this sample magnifies the errors associated with the correction for in situ production of ^{87}Sr. Omitting this datum, a general decrease from first- to third-cycle ignimbrites supports the reported trend towards the eruption of more isotopically "primitive" magmas at the BJEC through time. This trend does not continue into the youngest rhyolite lavas, however, as indicated by the high initial ratio of the Dorsey Creek rhyolite.

Unit	Age (Ma)[1]	Rb (ppm)[2]	Sr (ppm)[2]	$^{87}Sr/^{86}Sr_0$[2]	$^{87}Rb/^{86}Sr_0$	$^{87}Sr/^{86}Sr_i$	ε_{Nd}[3]
DC	8.11	117	108	0.71283	3.136	0.71247	—
CPT XV	10.45	190	79	0.71047	6.960	0.70944	-6.7
CPT XIII	10.94	211	29	0.71234	21.061	0.70907	—
CPT VII	11.83	218	82	0.71165	7.695	0.71035	—
CPT III	12.67	306	14.7	0.71922	60.295	0.70837	-8.0

Notes:

[1]Ages are from Perkins and others (1998) except for DC and CPT VII. The age for DC is an average of the two measurements reported by Bonnichsen (1982a). The age cited for CPT VII is the midpoint of the interval between the ages reported for CPT V and IX by Perkins and others (1998).

[2]The abundances of Rb and Sr and the present-day $^{87}Sr/^{86}Sr$ ratios are from Bonnichsen and Citron (1982).

[3]Values reported by Cathey and others (1997) for air-fall tuffs correlated with these ash flow units.

Table 2. Average chemical compositions of the third-cycle rhyolites from the BJEC. Data are from Bonnichsen (1982c) and Bonnichsen and others (1994).

	CPT XIII (n = 8)	CPT XV (n = 8)	TH lava (n = 10)	IB lava (n = 10)
Oxide wt. %[1]				
SiO_2	75.18	73.41	71.19	70.01
TiO_2	0.28	0.42	0.61	0.66
Al_2O_3	12.36	12.72	13.43	13.92
Fe_2O_3*	2.38	3.30	4.41	4.54
MnO	0.03	0.05	0.06	0.07
MgO	0.36	0.50	0.65	0.79
CaO	0.79	1.14	1.92	2.28
Na_2O	2.71	2.65	2.27	2.69
K_2O	5.87	5.73	5.35	4.90
P_2O_5	0.04	0.08	0.11	0.14
Total	100.00	100.00	100.00	100.00

[1]Each rock composition is an average of the number of analyses listed at the top of the column. These average compositions have been normalized to 100 percent with total Fe reported as Fe_2O_3.

of apatite and zircon (Figure 4). The groundmass glasses in both samples are free of microlites and are cut by perlitic fractures that are probably the result of incipient hydration. Most of the plagioclase crystals are euhedral and are characterized by the presence of weak oscillatory zoning and zones of rounded glass inclusions. Augite and pigeonite crystals are euhedral and not visibly zoned in thin section. They commonly occur in small clots with one another and with the other phenocryst phases. The oxide crystals are euhedral to subhedral and lack obvious exsolution textures. Tiny needles of apatite occur sparingly as inclusions in some plagioclase crystals. Granular aggregates of plagioclase, pyroxenes, and glass that may be xenolithic fragments have been reported in the TH rhyolite (Bill Bonnichsen, written commun., 1991), but none were found in the samples examined for this study.

MINERAL COMPOSITIONS AND THERMOMETRY

The ranges of plagioclase compositions in both lavas are similar (An_{35} to An_{41}) and extend the trend reported by Honjo and others (1992) from CPT units XIII (An_{23} to An_{27}) and XV (An_{29} to An_{33}) to more calcic compositions (Figure 5). The average compositions of crystals from

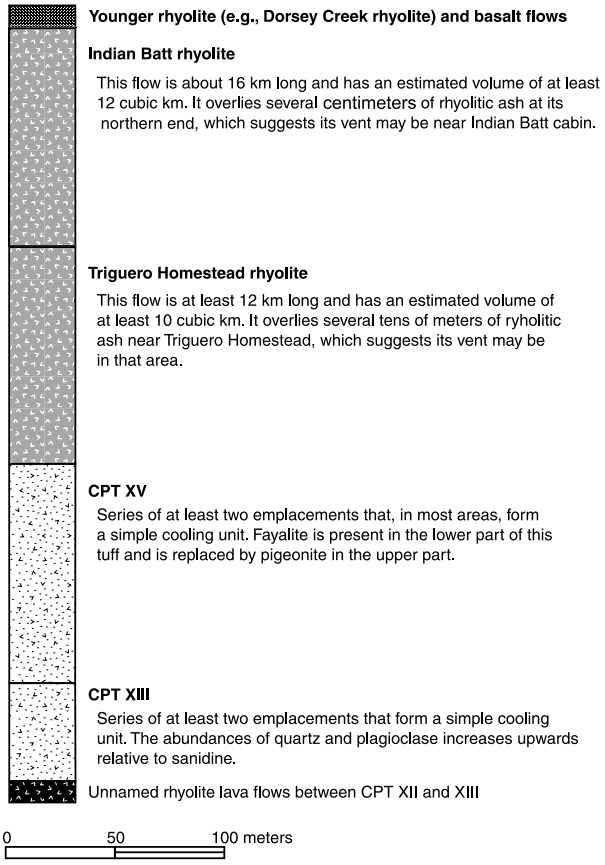

Figure 3. Schematic stratigraphic column for the third-cycle rhyolites from the BJEC. Information on unit thicknesses, phenocryst assemblages, and inferred vent localities is from Bonnichsen (1982b) and Bonnichsen and Citron (1982).

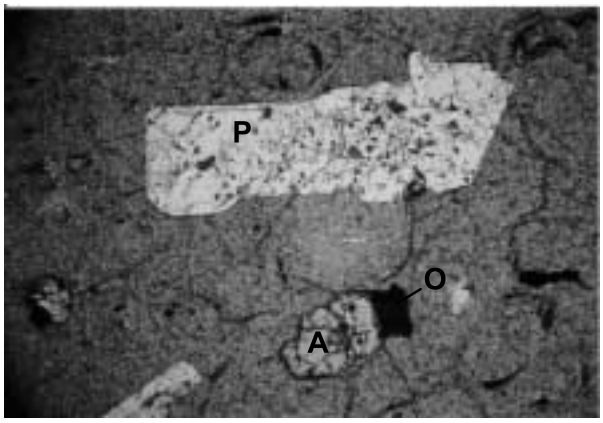

Figure 4. Photomicrograph of Triguero Homestead vitrophyre showing an euhedral plagioclase crystal (P) with glass inclusions, as well as crystals of augite (A), an opaque oxide (O), and perlitic fractures in the groundmass glass. The field of view is approximately 3.5 mm wide.

each lava are given in Table 3. Intriguingly, all three crystals analyzed from TH-1 are reversely zoned (from about An_{37} to An_{40}), whereas three of the four crystals analyzed from IB-1 are normally zoned (from about An_{42} to An_{36}). Because of the small number of crystals analyzed and the limited compositional range of the entire sample suite, it is difficult to know if this difference in zoning is petrologically significant.

In contrast to the plagioclases, the compositions of augites and pigeonites from each of the lavas span narrow ranges and are clearly distinct from one another. Average analyses of TH and IB pyroxenes are given in Table 4, and the compositions of all of the analyzed crystals are plotted in the Di-Hd-En-Fs quadrilateral in Figure 6. To project the compositions of these pyroxenes into the quadrilateral, the abundances of Fe^{2+}, Fe^{3+}, and nonquadrilateral components were calculated using the method outlined by Lindsley (1983). These calculations indicate (1) that Fe^{3+} composes about 7 percent of the total Fe in the TH and IB augites and about 1.5 percent in the pigeonites; and (2) that the total abundances of nonquadrilateral components are similar in the augites from both lavas (about 7 mole percent) and are considerably higher than the abundances of these components in the coexisting pigeonites (about 4 mole percent). The augites ($Wo_{35}En_{31}Fs_{34}$) and pigeonites ($Wo_{10}En_{36}Fs_{54}$) from the TH rhyolite are slightly less magnesian than the augites ($Wo_{36}En_{33}Fs_{31}$) and pigeonites ($Wo_{09}En_{40}Fs_{51}$) from the IB rhyolite.

To calculate the pyroxene equilibration temperatures of the TH and IB rhyolites using the solution model of Davidson and Lindsley (1985), it is necessary to have an independent estimate of the crystallization pressure. Unfortunately, no assemblages suitable for geobarometry have been found in these rhyolites. If the lavas are assumed to sample magmas from the deeper part of the same reservoir that produced the CPT XIII and XV ash flows, however, mineral equilibria from the tuffs can be used to infer at least a minimum pre-eruptive pressure for the lavas. One reaction potentially applicable to the mineral assemblages in the third-cycle tuffs is the solubility of the CaTs ($CaAl_2SiO_6$) component in augite that coexists with quartz and plagioclase. The reaction

$$CaAl_2Si_2O_8 \text{ (plagioclase)} = CaAl_2SiO_6 \text{ (augite)} + SiO_2 \text{ (quartz)}$$

has been calibrated as a geobarometer for high-grade metamorphic rocks by Ellis (1980) and has been used to estimate the crystallization pressure of a felsic igneous rock by Speer (1988).

There are two potential problems with the application of this geobarometer to the third-cycle ash flows,

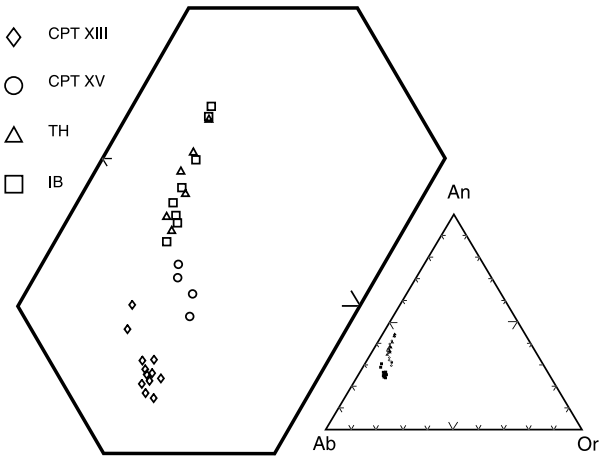

Figure 5. Compositions of plagioclase crystals from the third-cycle rhyolites projected onto the Ab-An-Or ternary diagram. The analyses of plagioclase crystals from CPT XIII and XV are from Honjo and others (1992).

however. First, because the calculated pressures depend somewhat on temperature, only the mineral compositions from member XV, for which an equilibration temperature of 900ºC-910ºC has been estimated by Honjo and others (1992), may be used. Second, as discussed by Creasar (1989), there is considerable uncertainty about how to assign cations to end-member components in calcic pyroxenes. This uncertainty translates into large potential errors in the estimates of the mole fractions of CaTs in even well-analyzed samples. Augites from CPT XV have relatively low Al_2O_3 contents and, even with the most generous assignment of Al to the CaTs component, contain only 1.8 to 1.9 mole percent CaTs. This composition yields an estimated pressure of about 0.6 GPa. The presence of Na, Ti, and Fe^{3+} in amounts sufficient to form components that could include nearly all of the Al in these pyroxenes implies that their actual CaTs contents are probably considerably lower and, thus, so are the estimated pressures. Geophysical evidence indicates that the top of the magma reservoir beneath the Yellowstone volcanic center presently lies at a depth corresponding to a pressure of 0.2 to 0.3 GPa (Hildreth and others, 1984). If the reservoir that produced the third-cycle rhyolites at the BJEC lay at a similar depth, then pressures ranging from 0.2 to 0.6 GPa ought to provide a reasonable bracket for the calculation of equilibration temperatures for the TH and IB pyroxenes.

Calculations using the model of Davidson and Lindsley (1985) for pressures from 0.2 to 0.6 GPa yield temperatures of 972ºC to 976ºC for the TH rhyolite and 959ºC to 963ºC for the IB rhyolite. The differences in the calculated temperatures due to assumed pressure differences are small compared to the uncertainties of ± 20ºC-

Table 3. Average chemical analyses of plagioclase crystals from samples of the basal vitrophyres of the TH and IB rhyolite lava flows.

	TH plagioclase (n = 6)	IB plagioclase (n = 8)
Oxide wt. %[1, 2]		
SiO_2	58.36 (135)	58.01 (272)
Al_2O_3	25.88 (92)	26.11 (130)
Fe_2O_3*	0.58 (07)	0.52 (12)
CaO	7.82 (111)	7.85 (139)
SrO	0.26 (05)	0.24 (09)
BaO	0.12 (09)	0.16 (13)
Na_2O	6.35 (52)	6.32 (60)
K_2O	0.97 (20)	0.97 (25)
Total	100.32	100.18
Cations[3]		
Si	2.616 (52)	2.605 (84)
Al	1.367 (50)	1.382 (87)
Fe^{3+}	0.020 (03)	0.018 (04)
Ca	0.375 (54)	0.378 (70)
Sr	0.007 (01)	0.006 (02)
Ba	0.002 (01)	0.003 (02)
Na	0.552 (43)	0.550 (48)
K	0.055 (12)	0.056 (14)
Total	4.994	4.998
End-members[4]		
Ab	56.2 (4.4)	55.9 (5.3)
An	38.2 (5.4)	38.4 (6.7)
Or	5.6 (1.2)	5.7 (1.5)

Notes:
[1]Wavelength-dispersive analyses conducted using the automated CAMECA microprobe at the University of California, Davis in January 1993. All analyses were carried out at an accelerating voltage of 15 kV, using a beam current of 10 nA, and were reduced using a ZAF routine. The standards used for these analyses were albite (Si, Na), anorthite (Al, Ca), orthoclase (K), fayalite (Fe), synthetic $SrTiO_3$ (Sr), and barite (Ba).
[2] Each analysis is an average of the number of points listed at the top of the column. Standard deviations (2s) are given in parentheses for the last two (or in some cases three) digits.
[3]Average cation numbers calculated on the basis of eight oxygens per formula unit. Standard deviations are given in parentheses.
[4]Average end-member abundances given in mole percent. Standard deviations are given in parentheses.

Table 4. Average chemical analyses of augite and pigeonite crystals from samples of the basal vitrophyres of the TH and IB rhyolite lava flows.

	TH augite (n = 8)	**TH pigeonite (n = 8)**	**IB augite (n = 10)**	**IB pigeonite (n = 10)**
Oxide wt. %[1, 2]				
SiO_2	49.98 (63)	49.67 (85)	50.25 (77)	50.16 (68)
TiO_2	0.37 (11)	0.25 (09)	0.41 (09)	0.21 (10)
Al_2O_3	1.09 (21)	0.53 (09)	1.08 (36)	0.48 (08)
FeO*	21.04 (79)	33.29 (80)	19.43 (56)	31.70 (105)
MnO	0.59 (15)	0.91 (22)	0.56 (09)	0.89 (20)
MgO	10.20 (36)	12.24 (17)	11.03 (58)	13.79 (35)
CaO	16.93 (56)	4.51 (22)	17.61 (49)	4.04 (26)
Na_2O	0.23 (03)	0.06 (05)	0.23 (05)	0.05 (05)
Total	100.43	101.46	100.60	101.32
Cations[3]				
Si	1.939 (13)	1.953 (10)	1.935 (12)	1.956 (15)
Al	0.050 (10)	0.025 (04)	0.049 (17)	0.022 (04)
Ti	0.011 (03)	0.007 (02)	0.012 (03)	0.006 (03)
Fe^{3+}	0.046 (12)	0.015 (06)	0.043 (16)	0.014 (08)
Fe^{2+}	0.637 (29)	1.079 (20)	0.583 (19)	1.020 (32)
Mn	0.019 (05)	0.030 (07)	0.018 (03)	0.029 (06)
Mg	0.590 (15)	0.718 (12)	0.633 (28)	0.802 (17)
Ca	0.704 (20)	0.190 (09)	0.726 (25)	0.169 (11)
Na	0.017 (02)	0.005 (03)	0.017 (04)	0.004 (03)
Total	4.011	4.022	4.016	4.022
End-members[4]				
Wo	34.6 (1.3)	9.9 (0.9)	35.9 (1.8)	8.6 (1.2)
En	31.4 (0.9)	36.0 (0.8)	33.4 (1.4)	40.2 (0.9)
Fs	34.0 (1.4)	54.1 (1.0)	30.7 (1.0)	51.2 (1.7)
nonquad	7.1 (1.2)	4.1 (0.3)	7.0 (1.6)	3.8 (0.8)

Notes:

[1] The analytical procedure was the same as outlined for plagioclase except that the standards used for these analyses were tremolite (Si, Mg), anorthite (Al), synthetic TiO_2 (Ti), fayalite (Fe), rhodonite (Mn), wollastonite (Ca), and omphacite (Na).

[2] Each analysis is an average of the number of points listed at the top of the column. Standard deviations (2s) are given in parentheses for the last two (or in one case three) digits.

[3] Average cation numbers calculated on the basis of six oxygens per formula unit. Fe^{3+} was estimated using the charge-balance method outlined by Lindsley (1983). Standard deviations are given in parentheses.

[4] Average end-member percentages calculated using the program PXPROJ which is based on the procedure of Lindsley and Anderson (1983). Quadrilateral components (Wo, En, and Fs) are normalized to 100 mole percent. Total nonquadrilateral ("nonquad") components are given in mole percent of the original analysis. Standard deviations are given in parentheses.

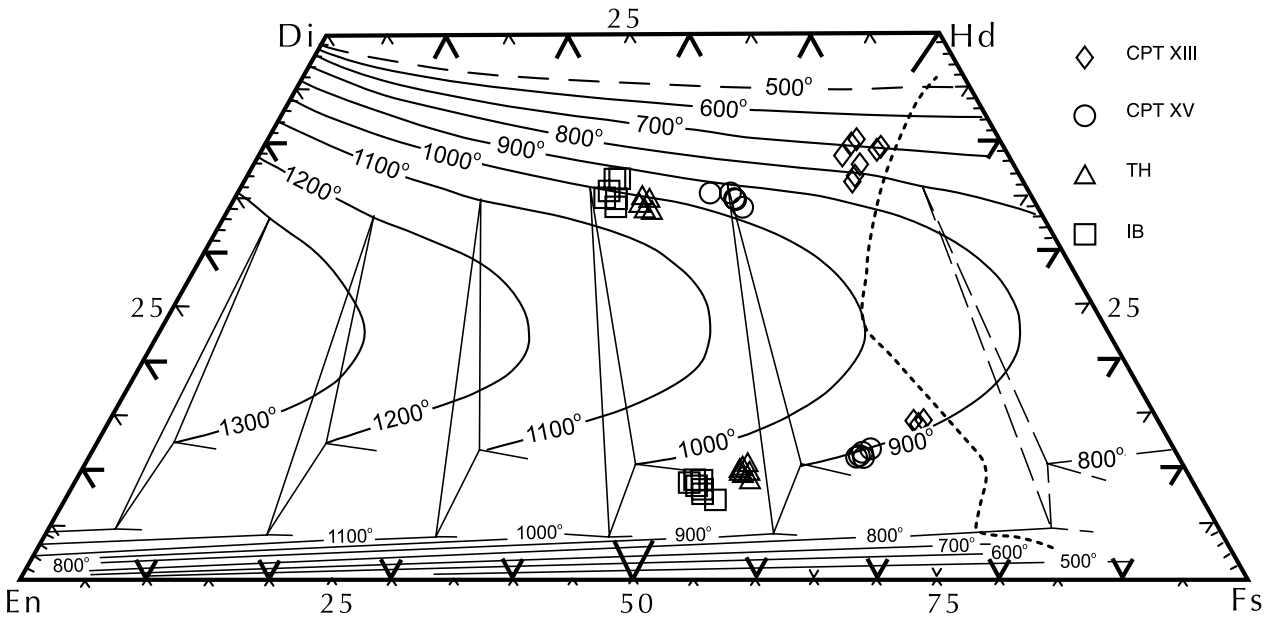

Figure 6. Compositions of pyroxene crystals from the third-cycle rhyolites projected onto the pyroxene quadrilateral. For reference, the data are superimposed upon the isotherms of the graphical geothermometer of Lindsley (1983) at p = 0.5 GPa. Temperatures discussed in the text were not determined graphically but by using the model of Davidson and Lindsley (1985) which yields very similar values (cf. Honjo and others, 1992). The analyses of the pyroxene crystals from CPT XIII and XV are from Honjo and others (1992).

50ºC estimated for this geothermometer (cf. Honjo and others, 1992). The model temperature estimates converge well over the entire pressure and composition range studied, with typical differences between the observed and calculated pigeonite compositions of 2 to 3 mole percent En and 0.2 to 0.4 mole percent Wo. The model fails for the IB pyroxenes at 0.6 GPa because it predicts coexistence of augite and orthopyroxene rather than the observed assemblage of augite and pigeonite. This failure implies that 0.5 to 0.6 GPa is an upper limit for the possible crystallization pressure of pyroxenes the IB rhyolite.

DISCUSSION

The continuity of trends in whole-rock and mineral chemistries suggests that the TH and IB lava flows sampled magmas closely related to those that fed the eruptions of CPT members XIII and XV. The compositions of plagioclases and pyroxenes from the TH and IB rhyolites extend the trends defined by minerals from the third-cycle ash-flow tuffs to more calcic and magnesian compositions, respectively, and record crystallization temperatures about 30ºC-50ºC hotter than those of the preceding ignimbrite (Figure 7).

These data are consistent with the model outlined above in which third-cycle rhyolites were formed in a thermally and compositionally zoned magma reservoir that was cooler and more volatile-rich near its top. The initial eruption of CPT XIII from this body was followed by a period of repose during which the compositional gradient in the upper part of the magma was partially restored. The eruption of CPT XV, which began with fayalite-bearing lavas and progressed to pigeonite-bearing ones, removed the cooler, volatile-enriched upper part of the magma body and led to the last episode of caldera subsidence at the BJEC. The remaining magma in the upper part of the reservoir was hotter but possibly too poor in volatiles to erupt explosively, so it flowed out along the southern ring fracture of the caldera in two pulses to form the TH and, later, IB lava flows. Rhyolite magmas continued to leak from the BJEC magmatic system for another 2 Ma, and formed six to ten additional lava flows. The higher initial Sr ratio of the Dorsey Creek rhyolite (Table 1) relative to those of CPT members XIII and XV suggests, however, that at least some of the members of this group of younger lavas may have come from a different source than that which fed the third eruptive cycle.

Recent studies of rhyolitic volcanism at the Yellowstone Plateau volcanic center reveal that the magma reservoirs associated with the last three major ash-flow eruptions restored their pre-eruptive compositional zonations during periods ranging from 60,000 to 400,000

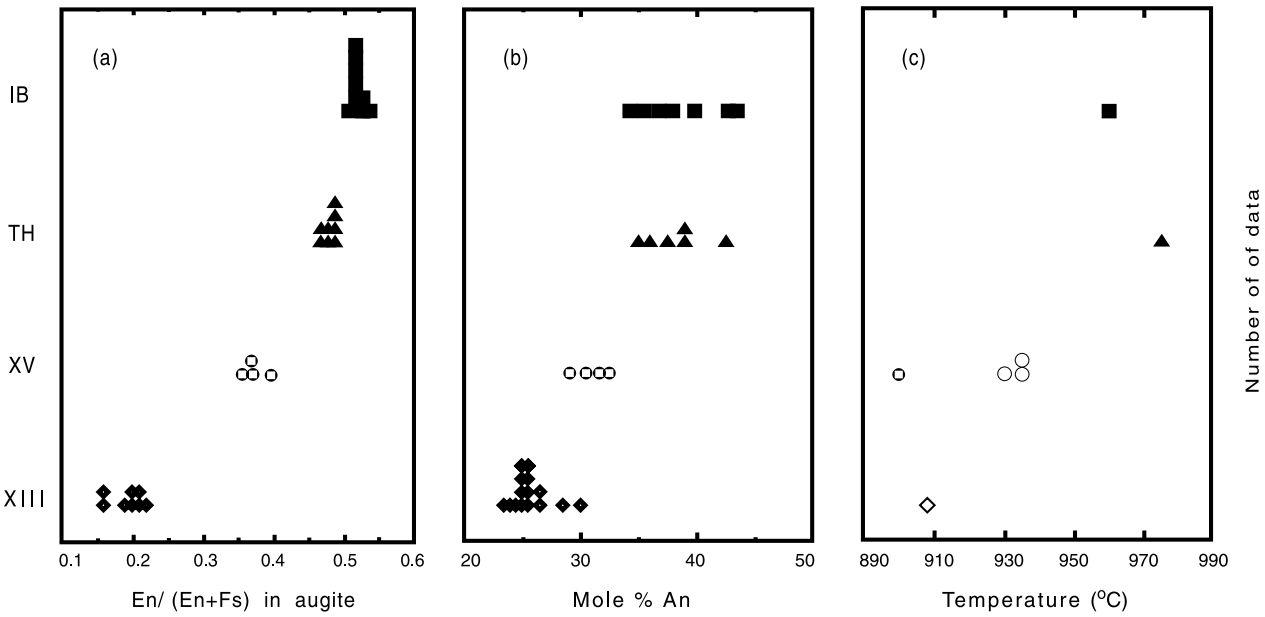

Figure 7. Histograms of (a) the En/(En + Fs) ratios of augites, (b) the anorthite contents of plagioclases, and (c) the calculated eruptive temperatures of the third-cycle rhyolites plotted as functions of their relative stratigraphic heights. In part (c) the solid symbols denote two-pyroxene temperatures and the open symbols denote zircon solubility temperatures. Mineral compositions for CPT XIII and XV are from Honjo and others (1992), and temperature estimates were calculated using the models and data cited in the caption for Figure 2.

years (Hildreth and others, 1984; Ganseki and others, 1996). If the BJEC and Yellowstone Plateau centers developed similarly and the scenario outlined above is correct, then the extrusion of the TH and IB flows probably followed the eruption of CPT member XV by no more than a few tens to perhaps a few hundreds of thousands of years.

ACKNOWLEDGMENTS

I would like to thank Bill Bonnichsen for his enthusiastic support of this work on the petrogenesis of the third-cycle rhyolites, for sharing a wealth of unpublished data, and for escorting me on two sampling trips into the Bruneau-Jarbidge region. This paper has benefitted from detailed and constructive reviews by Curtis Manley and Mike McCurry. I would also like to thank Peter Schiffman and Sarah Roeske for their assistance in carrying out the microprobe analyses and their hospitality while I was working at the University of California, Davis.

REFERENCES

Bonnichsen, Bill, 1982a, The Bruneau-Jarbidge eruptive center, southwestern Idaho, *in* Bill Bonnichsen and R.M. Breckenridge, eds., Cenozoic Geology of Idaho: Idaho Bureau of Mines and Geology Bulletin 26, p. 237-254.

———, 1982b, Rhyolite lava flows in the Bruneau-Jarbidge eruptive center, southwestern Idaho, *in* Bill Bonnichsen and R.M. Breckenridge, eds., Cenozoic Geology of Idaho: Idaho Bureau of Mines and Geology Bulletin 26, p. 283-320.

———, 1982c, Chemical composition of the Cougar Point Tuff and rhyolite lava flows from the Bruneau-Jarbidge eruptive center, Owyhee County, Idaho: Idaho Bureau of Mines and Geology Technical Report 82-1, 22 p.

Bonnichsen, Bill, and G.P. Citron, 1982, The Cougar Point Tuff, southwestern Idaho and vicinity, *in* Bill Bonnichsen and R.M. Breckenridge, eds., Cenozoic Geology of Idaho: Idaho Bureau of Mines and Geology Bulletin 26, p. 255-281.

Bonnichsen, Bill, W.P. Leeman, John Bernt, M.M. Godchaux, and M.D. Jenks, 1994, Analyzed rocks from the Sheep Creek 30 x 60 minute quadrangle, Owyhee and Twin Falls counties, southwestern Idaho: Idaho Geological Survey Technical Report 94-5.

Cathey, H.E., and W.P. Nash, 1998, Compositional gaps in the Cougar Point Tuff: Evidence for tapping of persistent magma volumes by multiple eruptions from a common magma reservoir, 12.7–10.5 Ma: EOS, Transactions American Geophysical Union, v. 79, no. 45, p. F925.

Cathey, H.E., W.P. Nash, and M.E. Perkins, 1997, A hotter hotspot: Chemical variation in the Miocene Cougar Point Tuff, central Snake River Plain: Geological Society of America Abstracts with Programs, v. 29, p. A-299.

Creasar, R.A., 1989, Comment on "Depth and mineralogy of the magma source or pause region for the Carboniferous Liberty Hill pluton, South Carolina": Geology, v. 17, p. 482-483.

Davidson, P.M., and D.H. Lindsley, 1985, Thermodynamic analysis of quadrilateral pyroxenes, part II: Model calibration from experiments and applications to geothermometry: Contributions to Mineralogy and Petrology, v. 91, p. 390-404.

Ellis, D.J., 1980, Osumilite-sapphirine-quartz granulites from Enderby

Land, Antarctica: P-T conditions of metamorphism, implications for garnet-cordierite equilibria and the evolution of the deep crust: Contributions to Mineralogy and Petrology, v. 74, p. 201-210.

Ganseki, C.A., G.A. Mahood, and M.O. McWilliams, 1996, $^{40}Ar/^{39}Ar$ geochronology of rhyolites erupted following collapse of the Yellowstone caldera, Yellowstone Plateau volcanic field: Implications for crustal contamination: Earth and Planetary Science Letters, v. 142, p. 91-107.

Hildreth, Wes, R.L. Christiansen, and J.R. O'Neil, 1984, Catastrophic isotopic modification of rhyolitic magma at times of caldera subsidence, Yellowstone Plateau volcanic field: Journal of Geophysical Research, v. 89, no. B10, p. 8339-8369.

Hildreth, Wes, A.N. Halliday, R.L. Christiansen, 1991, Isotopic and chemical evidence concerning the genesis and contamination of basaltic and rhyolitic magma beneath the Yellowstone Plateau volcanic field: Journal of Petrology, v. 32, p. 63-138.

Honjo, Norio, Bill Bonnichsen, W.P. Leeman, and J.C. Stormer, Jr., 1992, Mineralogy and geothermometry of high-temperature rhyolites from the central and western Snake River Plain: Bulletin of Volcanology and Geothermal Research, v. 54, p. 220-237.

Lindsley, D.H., 1983, Pyroxene thermometry: American Mineralogist, v. 68, nos. 5 and 6, p. 477-493.

Lindsley, D.H., and D.J. Anderson, 1983, A two-pyroxene thermometer: Proceedings of the Thirteenth Lunar and Planetary Science Conference, Part 2, Journal of Geophysical Research, v. 88, supplement, p. A887-A906.

Perkins, M.E., F.H. Brown, W.P. Nash, W. McIntosh, and S.K. Williams, 1998, Sequence, age, and source of silicic fallout tuffs in middle to late Miocene basins of the northern Basin and Range province: Geological Society of America Bulletin, v. 110, p. 344-360.

Perkins, M.E., W.P. Nash, F.H. Brown, and R.J. Fleck, 1995, Fallout tuffs of Trapper Creek, Idaho—A record of Miocene explosive volcanism in the Snake River Plain volcanic province: Geological Society of America Bulletin, v. 107, p. 1484-1506.

Riciputi, L.R., and C.M. Johnson, 1990, Nd- and Pb-isotope variations in the multicyclic central caldera cluster of the San Juan volcanic field, Colorado, and implications for crustal hybridization: Geology, v. 18, no. 10, p. 975-978.

Speer, J.A., 1988, Depth and mineralogy of the magma source or pause region for the Carboniferous Liberty Hill pluton, South Carolina: Geology, v. 16, p. 521-524.

Vetter, S.K., and John Shervais, 1997, Basaltic volcanism of the Bruneau-Jarbidge eruptive center, southwest Idaho: Geological Society of America Abstracts with Programs, v. 29, no. 6, p. A-298.

Watson, E.B., and T.M. Harrison, 1983, Zircon saturation revisited: Temperature and composition effects in a variety of crustal magma types: Earth and Planetary Science Letters, v. 64, p. 295-304.

The Juniper Mountain Volcanic Center, Owyhee County, Southwestern Idaho: Age Relations and Physical Volcanology

Curtis R. Manley[1] and William C. McIntosh[2]

ABSTRACT

Rhyolites erupted near Juniper Mountain in southwestern Idaho record silicic magmatism at the western edge of the North American craton as it passed over the Yellowstone hot spot. New $^{40}Ar/^{39}Ar$ dates reveal that the Juniper Mountain volcanic center was active from 14.5 to 13.7 Ma. Units at the lowest stratigraphic positions are flat-lying and widely distributed, but not equivalent; they vary in age and degree of petrologic evolution. Volcanism appears to have begun with large volumes of ignimbrites, lava flows, or both, with about 68 weight percent SiO_2. Over the next 0.6 m.y., magma compositions evolved to 78 weight percent SiO_2, unit volumes and magmatic temperatures both decreased, and eruptive mode became dominantly lava extrusion. During this period, heat input into the system apparently declined, leading to crystallization and differentiation. However, it seems likely that at about 13.8 Ma a pulse of mafic magma into the base of the magmatic system caused the remelting of material crystallized on the walls of the magma chamber. Magmas low in dissolved water contents (0.75 to 2.6 weight percent) erupted in two or three fountain-fed rhyolite units. These were followed within 0.01 m.y. by eruption of the 15-cubic-km Badlands Lava Flow, which is much less evolved than the preceding units and is rich in fractured phenocrysts (up to 2.5 cm in long dimension) that appear to represent the chamber's crystalline rind. These eruptions essentially marked the end of Juniper Mountain rhyolitic magmatism. The area then subsided and was covered with sediments and basaltic lavas which erupted through the rhyolites between 10 and 7 Ma.

Key words: Badlands Lava Flow, fire fountain, remelting, Ar/Ar, rhyolite

INTRODUCTION

The progressive Snake River Plain (SRP) trend of silicic volcanism from southeastern Oregon (McDermitt caldera, about 17.5 Ma) to Yellowstone National Park (Yellowstone caldera, 2 Ma to present) is generally believed to reflect movement of the North American plate over an essentially fixed mantle hot spot (Rodgers and others, 1990; Pierce and Morgan, 1992; Anders and Sleep, 1992). The western edge of the North American craton is thought to lie just east of the Oregon-Idaho boundary, within or very near the area of the present report (Leeman and others, 1992); the peralkaline volcanic rocks of the McDermitt caldera (off the craton) contrast strongly with the metaluminous rhyolites of the SRP province. Most of the silicic volcanic centers along the eastern part of the SRP have been buried by subsequent sediments and basaltic lava flows (Morgan and others, 1984). In southwestern Idaho, even though basalt lavas erupted over much of the area, the relatively old age and high elevation have led to the erosion of deep river canyons that expose proximal rhyolitic units in the Bruneau-Jarbidge eruptive center, active from about 12 to 9 Ma (Bonnichsen, 1982), and in the Juniper Mountain volcanic center, active from 14.5 to 13.7 Ma.

Editors' note: The manuscript was submitted in July 1998 and has been revised at the authors' discretion.

[1]Department of Geological Sciences, Arizona State University, Tempe, AZ 85287-1404; crmanley@mindspring.com

[2]New Mexico Geochronology Research Laboratory, New Mexico Bureau of Mines, New Mexico Tech, 801 Leroy Place, Socorro, NM 87801-4796

Manley, C.R., and W.C. McIntosh, 2002, The Juniper Mountain volcanic center, Owyhee County, southwestern Idaho: Age relations and physical volcanology, *in* Bill Bonnichsen, C.M. White, and Michael McCurry, eds., Tectonic and Magmatic Evolution of the Snake River Plain Volcanic Province: Idaho Geological Survey Bulletin 30, p. 205-227.

The Juniper Mountain volcanic center (JMVC) is the northern part of a larger, less explored area that Bonnichsen and Kauffman (1987) named the Owyhee-Humboldt eruptive center (OHEC; Figure 1). Juniper Mountain itself is the sole constructional volcano that rises above the rest of the OHEC. Primarily reconnaissance mapping by Ekren and others (1981, 1982, 1984) highlighted the geology of the Juniper Mountain region. Based largely on the widespread nature of their "map units" (one or more "emplacement units," which are individual units emplaced from a single vent) and also on the scattered occurrences of fragmental textures similar in appearance to (and presumed to be) eutaxitic ignimbrite fabrics, Ekren and others (1984) interpreted all the JMVC rhyolites as ignimbrites affected by differing degrees by rheomorphism. The otherwise ubiquitous presence of physical features and textures indicative of emplacement as viscous liquids (lava flows) were cited as evidence that rheomorphism destroyed most ignimbrite textures and that the units had advanced to their final positions by lava-like movement. Since the publication of Ekren and others (1984), several authors have discussed criteria to distinguish voluminous silicic lavas from welded or rheomorphic ignimbrites (e.g., Henry and others, 1988; Henry and Wolff, 1992; Manley, 1995) and have described true effusive lava flows of large volumes and areal extents (Henry and others, 1990; Green and Fitz, 1993; Manley, 1996a).

Due to burial by younger units and only minimal canyon exposures in some areas, the dimensions and details of emplacement of most of the OHEC's rhyolitic units remain unknown. Subsequent to the work of Ekren and others (1981, 1984), isolated local mapping reported in Goeldner and others (1986), Minor and others (1986, 1987), and other publications cited below generally follow the interpretations and conclusions of Ekren and others. Manley (1994a) recognized previously unmapped units and reinterpreted several described earlier by Ekren and others (1981, 1984). This paper presents a current overview of the volcanic history of the OHEC, based on published and unpublished mapping and seventeen new $^{40}Ar/^{39}Ar$ dates on rhyolitic units. The dating methods and results are presented in the appendix and summarized in Tables 1, 2 and 3.

PRE-JUNIPER MOUNTAIN VOLCANIC CENTER GEOLOGIC HISTORY

Granites of the Idaho batholith make up the northern margin of the western SRP graben. Scattered outcrops of granitic and other intrusive rocks south of the western SRP (Figure 1) suggest that the Idaho batholith extends beneath much of southwestern Idaho and underlies the JMVC (Taubeneck, 1971). Largely covering these plutonic rocks are Miocene basalt and trachyandesite (latite) lava flows generally of the same age (about 17-15 Ma) as the earliest (greatest volume) Columbia River basalt units (Bonnichsen, 1983; Tolan and others, 1989) and the phenocryst-poor, high-silica rhyolites of the Silver City Range (about 17-16 Ma). Some of the latter host epithermal silver-gold mineralization (Bonnichsen, 1983; Ekren and others, 1984). Rhyolitic units apparently associated with the JMVC overlie these earlier units; they are found primarily beneath a thin cover of fluviolacustrine sediments and basaltic lava flows blanketing much of the Idaho-Oregon-Nevada region. Major extensional block faulting associated with the formation of the Basin and Range Province and with the passage of the Yellowstone hot spot predated OHEC rhyolitic magmatism. Similar faulting was noted elsewhere along the SRP by Rodgers and others (1990). Units in the Owyhee Mountains and around the southern edge of the OHEC are extensively faulted, but, with only a few exceptions, only faults with minor throws cut the OHEC and JMVC rhyolites or the overlying basalts (Ekren and others, 1981).

Figure 1. Generalized geologic map showing southwestern Idaho, southeastern Oregon, and north-central Nevada. Juniper Mountain and the Juniper Mountain volcanic center are in Idaho in the center of the figure. MVC-McDermitt volcanic center; OHEC-Owyhee Humboldt eruptive center. The Bruneau-Jarbidge eruptive center is just off the figure to the east. Qb-basalts of the Jordan Craters area; TQb-basalts; Trcc-Circle Creek Rhyolite; Trlj-Little Jacks Tuff; Trgc-Garat Crossing Lava Flow; Trb-Badlands Lava Flow; Trbc-Beaver Creek Tuff; Trpr-rhyolite of Petition Reservoir; Trul-Upper Lobes Lava Flows; Trll-Lower Lobes Lava Flow; Trsm-Swisher Mountain Rhyolite; Tr-rhyolite undivided; Trsc-rhyolites of the Silver City Range; black-Tertiary and Cretaceous intrusive rocks and Jurassic metamorphic rocks; white-alluvium, sediments, and miscellaneous volcanic units. Sample locations shown; x suffix indicates sample with compositional data listed in Table 2; a suffix indicates dated sample (Table 1). Only one fault, in unit Trul, is shown (see Figure 2); it is important in the Juniper Mountain area. See Figures 2, 4, and 6 for more detail and sample locations in Juniper Mountain area. More basaltic vents (asterisks) undoubtedly occur in north-central Nevada, but have not been mapped as they have in Idaho and Oregon. Modified from Coats (1968), Stewart and Carlson (1978), Ekren and others (1981, 1982, 1984), Rytuba and McKee (1984), Walker and MacLeod (1991), Willden (1961), and C.R. Manley (unpub. data, 1989-1993).

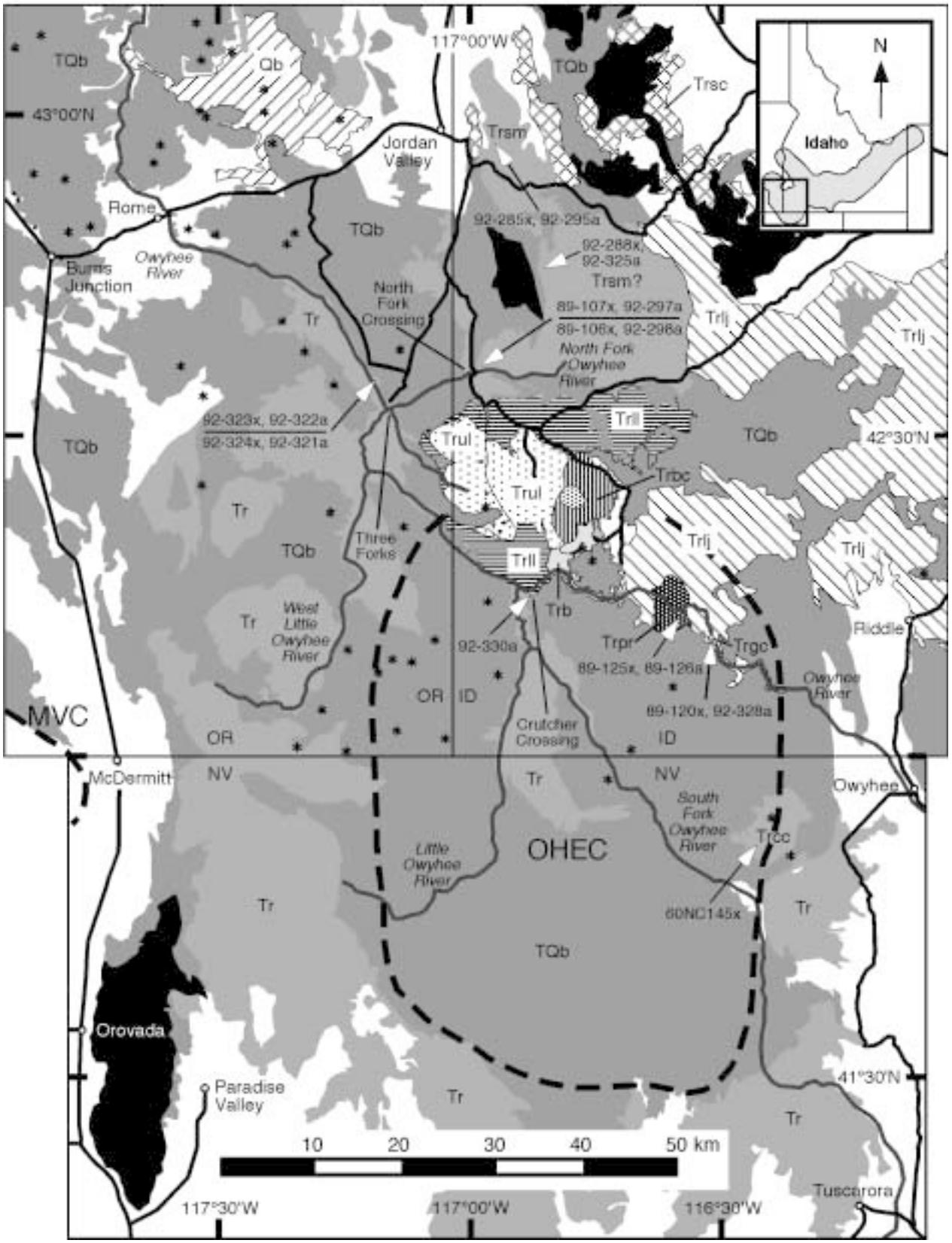
117°00'W
43°00'N
42°30'N
41°30'N
117°30'W
116°30'W
N
Idaho
TQb
Qb
Trsc
Trsm
Jordan Valley
Rome
Burns Junction
Owyhee River
North Fork Crossing
92-285x, 92-295a
92-288x, 92-325a
Trsm?
89-107x, 92-297a
89-106x, 92-298a
North Fork Owyhee River
Trlj
Tr
92-323x, 92-322a
92-324x, 92-321a
Trl
Trul
Trbc
Three Forks
Trll
Trb
West Little Owyhee River
92-330a
Trpr
Trgc
89-125x, 89-126a
89-120x, 92-328a
Riddle
Owyhee River
MVC
OR
ID
NV
Crutcher Crossing
McDermitt
Owyhee
South Fork Owyhee River
Little Owyhee River
OHEC
Trcc
60NC145x
Orovada
Paradise Valley
10 20 30 40 50 km
Tuscarora

UNITS OF THE JUNIPER MOUNTAIN VOLCANIC CENTER AND OWYHEE-HUMBOLDT ERUPTIVE CENTER

THE "SWISHER MOUNTAIN TUFF" AND ITS STRATIGRAPHIC EQUIVALENTS

A huge region of southwestern Idaho, southeastern Oregon, and northern Nevada (Figure 1) is underlain by generally flat-lying rhyolites; bases of these units are not exposed in even the deepest river canyons. Swisher Mountain Tuff, the name chosen by Ekren and others (1981, 1984) for outcrops on Swisher Mountain, east of the town of Jordan Valley, Oregon, was applied by them to all the lowest-exposed rhyolites in the greater OHEC area. The unit's source was inferred to be Juniper Mountain itself. The Swisher Mountain Tuff map unit covers such a huge area and shows such ranges in composition (68 to 77 weight percent SiO_2) and age (14.5 to 14.1 Ma) that it might actually include a dozen or more emplacement units erupted from widely separated vents (Manley, 1994a, and unpub. data, 1989-1993). In addition, some of these units are herein reinterpreted as true lava flows. For these reasons, the continued use of the term "Swisher Mountain Tuff" is not recommended. New names for individual emplacement units must await detailed mapping.

East of Jordan Valley

The Wood Canyon type section of Ekren and others' (1981, 1984) Swisher Mountain Tuff is part of a large body of rock east of the town of Jordan Valley (Figure 1) now dated at 14.21 ± 0.13 Ma (all errors quoted at ± 2σ; Tables 1, 2 and 3). Relations of this body with other rocks originally mapped as Swisher Mountain Tuff to the east and north (Ekren and others, 1981, 1984) are uncertain. Physical features and rock textures of this body indicate that it is a single voluminous extrusive lava flow, now tilted slightly eastward. The Swisher Mountain Rhyolite is suggested as a formal name for this body of rock, with Ekren and others' (1984) original Wood Canyon type section being retained.

North Fork Crossing

Where the Juniper Mountain road crosses the North Fork of the Owyhee River at North Fork Crossing (Figure 1), just east of the Oregon line, at least two thick rhyolitic units are exposed in the near-vertical canyon walls. These units appear to be lava flows. In stratigraphic order, they are dated at 14.22 ± 0.08 Ma and 14.10 ± 0.06 Ma (Tables 1, 2 and 3). The older unit at North Fork Crossing and the unit east of Jordan Valley are identical in age and nearly so in major and trace element composition (Table 2).

Northeast of Juniper Mountain

Part of the Juniper Mountain road northeast of Juniper Mountain itself (Figures 1 and 2) is built on the upper vitrophyre of Ekren and others' (1981, 1984) Swisher Mountain Tuff map unit. Features in the vitrophyre indicate that this body of rock is most likely a lava flow (Manley, 1996b). With a date of 14.31 ± 0.06 Ma (Tables 1, 2 and 3), it is the second oldest of the JMVC units. To the north is a large area of complexly faulted rhyolite apparently continuous with the rhyolite along the road. It was all interpreted to be Swisher Mountain Tuff by Ekren and others (1981, 1984) and has yet to be inspected in more detail. Its aspect suggests a gently resurgent dome in a caldera, but aside from possible lacustrine deposits in the low area between the possible dome and the older Silver City Range (S. Minor, oral commun., 1989), no evidence for caldera collapse is apparent.

Three Forks and Southeastern Oregon

At Three Forks (Figure 1) northwest of Juniper Mountain, river erosion has carved out a wide area, probably once filled primarily by sediments, between the apparent westernmost extent of one of the Swisher Mountain rhyolite units at North Fork Crossing and the easternmost extents of two other large, overlapping rhyolite units. Although the mapping of Ekren and others (1981) did not extend into Oregon, Evans and others (1987) mapped these two units as Swisher Mountain Tuff westward along the Owyhee canyon from Three Forks; together the units reach at least 350 m in thickness. In most places, these units seem to be sheetlike. Contact relations near Three Forks imply that at least one of them is a lava flow. Downstream about 25 km west of Three Forks, the rhyolites disappear beneath the overlying sediments and basaltic lavas (Evans and others, 1987). As exposed along the Wes Hawkins Trail, in stratigraphic order, the units are dated at 14.48 ± 0.04 Ma and 14.09 ± 0.1 Ma (Tables 1, 2 and 3). The older Wes Hawkins unit is the oldest dated unit associated with the JMVC or OHEC. The younger Wes Hawkins unit and the younger unit at North Fork Crossing have identical ages and very similar major and trace element compositions, suggesting they may be related.

Elsewhere in southeastern Oregon, rhyolitic units crop

Table 1. Summary of $^{40}Ar/^{39}Ar$ results for samples from the Juniper Mountain volcanic center and vicinity.

Sample	Unit	Location	Notes	n	K/Ca	±2σ	Age (Ma)	±2σ
92-328	Garat Crossing Lava Flow	Owhyee River Cyn.	type loc.	16	24.2	4.4	13.65	0.04
92-280	Badlands Lava Flow	The Badlands	type loc.	15	24.1	12.2	13.73	0.08
92-325	rhyolite of Mill Creek	Mill Creek	type loc.	15	26.9	6.8	13.77	0.12
91-252	Beaver Creek Tuff	Carter Creek	type loc.	16	25.3	2.2	13.82	0.05
89-126	rhyolite of Petition Reservoir	Owhyee River Cyn.		15	32.2	2.5	13.83	0.04
92-308	Upper Lobes Lava Flows	Juniper Mtn. summit		13	23.6	1.4	13.83	0.06
92-316	Carter Spring Rhyolite	Carter Spring	type loc.	15	28.0	4.6	13.89	0.05
91-211	Lower Lobes Lava Flow	NE of Squaw Ck.		18	17.0	6.9	13.89	0.11
91-204	Upper Lobes Lava Flows	NE of Squaw Ck.	type loc.	15	21.0	2.1	13.90	0.05
92-303	Lower Lobes Lava Flow	Bat Spring	upper unit	15	16.5	2.4	13.95	0.06
92-322	"Swisher Mountain Tuff"	Three Forks (OR)	upper unit	15	15.2	4.0	14.09	0.10
92-297	"Swisher Mountain Tuff"	N. Fork Crossing	upper unit	15	14.3	8.7	14.10	0.06
92-330	"Swisher Mountain Tuff"	Crutcher Crossing		14	16.0	5.1	14.15	0.11
92-295	Swisher Mountain Rhyolite	E. of Jordan Valley	type loc.	15	15.4	9.3	14.21	0.13
92-298	"Swisher Mountain Tuff"	N. Fork Crossing	lower unit	13	14.5	3.8	14.22	0.08
92-302*	"Swisher Mountain Tuff"	mouth of Deep Ck.		7	9.5	4.5	14.31	0.06
92-321	"Swisher Mountain Tuff"	Three Forks (OR)	lower unit	15	14.2	2.1	14.48	0.04

Notes: n = number of individual crystals analyzed by single-crystal laser-fusion; K/Ca = molar ratio calculated from $^{39}Ar_K$ and $^{37}Ar_{Ca}$; * indicates multi-grain analysis; single-crystal analysis used for all other samples.

Sample preparation and irradiation: Sanidine separated by crushing, LST heavy liquid, Frantz and HF, then irradiated in machined Al discs for 7 hours, D-3 position, Nuclear Science Center, College Station, Texas. Neutron flux monitored by Fish Canyon Tuff sanidine FC-1 with an assigned age of 27.84 Ma (Deino and Potts, 1990), relative to Mmhb-1 at 520.4 Ma (Samson and Alexander, 1987).

Instrumentation: Mass Analyzer Products 215-50 mass spectrometer on line with automated, all-metal extraction system at New Mexico Geochronology Research Laboratory, Socorro. Heating: single-crystal laser-fusion, 10W continuous CO_2 laser. Reactive gas cleanup: 1 to 2 minutes, SAES GP-50 getters operated at 20ºC and ~450ºC.

Age calculations: Mean ages calculated using inverse variance weighting of Samson and Alexander (1987); all errors reported at ± 2 σ. Decay constant and isotopic abundances after Steiger and Jaeger (1977). Complete data set in McIntosh (1999).

Analytical parameters: Electron multiplier sensitivity = 7×10^{-17} moles/pA; average system blanks were 210, 3.2, 0.4, 1.5, 1.9×10^{-18} moles at masses 40, 39, 38, 37, 36 respectively. J-factors determined to a precision of ± 0.2% using CO_2 laser-fusion of 4 to 6 single crystals from each of 4 to 6 radial positions around irradiation vessel. Correction factors for interfering nuclear reactions determined using K-glass and CaF_2: $(^{40}Ar/^{39}Ar)_K = 0.00020 \pm 0.0003$; $(^{36}Ar/^{37}Ar)_{Ca} = 0.00026 \pm 0.00002$; and $(^{39}Ar/^{37}Ar)_{Ca} = 0.00070 \pm 0.00005$.

out over large areas possibly never covered by younger basaltic lavas (Figure 1; Walker and Repenning, 1966; Walker and MacLeod, 1991). This area has not been studied sufficiently to delineate individual emplacement units or to characterize eruptive styles.

Northern Nevada

In the southern part of the OHEC, south of the main Owyhee River, fluviolacustrine sediments capped in some areas by roughly 10 to 6 Ma basaltic lavas (Hart and others, 1984) cover nearly all the rhyolitic units. In the canyons of the Little Owyhee River and the Owyhee River's South Fork, Ekren and others (1981, 1984) mapped their Swisher Mountain Tuff south to the Nevada border. Using that same stratigraphic framework, Ach and others (1986) and Foord and others (1987) further mapped the Swisher Mountain Tuff in southern Idaho and northern Nevada, respectively. Foord and others (1987) noted a magmatic vent feeding a rhyolite unit in the river canyon, demonstrating that some of the Swisher Mountain Tuff had a local source and was not erupted from Juniper Mountain. Coats (1968), Peterson and others (1986), and Wallace and others (1988) also mapped local volcanic units in northern Nevada.

LOWER LOBES LAVA FLOW

Ekren and others (1981, 1984) originally mapped the Juniper Mountain edifice as composed of two units, the lower one a broad, tabular bench and the upper one the more shieldlike summit of the mountain. The lower unit was originally interpreted as an ignimbrite and informally named the lower lobes of Juniper Mountain. More recent

Table 2. Compositions of representative samples from the Juniper Mountain volcanic center and vicinity.

Sample	**92-324**	**92-323**	**89-106**	**89-107**	**92-285**	**89-80**	**89-54**	**89-65**	**89-26**
Unit	**"Swisher Mountain Tuff"**		**"Swisher Mountain Tuff"**		**Swisher Mountain Rhyolite**	**Lower Lobes Lava Flow**		**Upper Lobes Lava Flows**	
Unit age (Ma)	14.48	14.09	14.22	14.10	14.21	13.95	13.89	13.90	13.83
±2σ (Ma)	±0.04	±0.10	±0.08	±0.06	±0.13	±0.06	±0.11	±0.05	±0.06
Notes	lower unit	upper unit	lower unit	upper unit	type locality	E of Juniper Mtn	W of Juniper Mtn	W flank of Juniper Mtn	summit
Location	Wes Hawkins Trail near Three Forks		North Fork Crossing		Wood Canyon	Bat Spring	Squaw Creek	Squaw Creek	Little Smith Ck
State	OR		ID		ID	ID	ID	ID	ID
Lithology	cryst.	cryst.	cryst.	cryst.	cryst.	cryst.	cryst.	cryst.	cryst.
Major Oxides (wt.%):									
SiO_2	68.5	74.3	72.1	74.5	71.8	75.2	75.3	77.0	78.1
TiO_2	0.54	0.46	0.51	0.42	0.57	0.35	0.31	0.23	0.13
Al_2O_3	17.4	12.8	13.9	12.9	13.6	12.7	12.7	12.2	12.0
FeO*	3.06	2.56	2.90	2.71	3.19	2.48	2.25	1.87	1.40
MnO	0.04	0.02	0.03	0.01	0.03	0.03	0.02	0.01	0.02
MgO	0.34	0.17	0.07	0.00	0.33	0.01	0.02	0.00	0.00
CaO	1.36	0.95	1.19	0.70	1.52	0.46	0.57	0.34	0.31
Na_2O	3.22	3.27	3.90	3.19	3.62	3.22	3.25	2.95	2.87
K_2O	5.33	5.38	5.31	5.50	5.29	5.53	5.48	5.40	5.22
P_2O_5	0.20	0.09	0.09	0.04	0.11	0.01	0.02	0.01	0.00
Orig. Total	101.6	99.5	99.6	97.3	99.7	97.7	97.3	97.5	96.9
Trace Elements (ppm):									
Ba	1283	1700	2019	1109	1325	841	827	483	48
Rb	174	182	163	195	173	201	201	210	280
Sr	105	92	112	64	109	40	41	23	3
Zr	463	485	634	443	472	421	381	302	212

Notes: Sample 89-106 and those with 90-, 91- and 92- prefixes were analyzed by wavelength dispersive X-ray fluorescence (WDXRF) and inductively coupled plasma-mass spectrometry at Washington State University, November 1992. All other samples with 89- prefixes analyzed by WDXRF at Stanford University, May 1990.

SU data corrected to WSU analyses with internal standards.

Lithology of sample: cryst. = crystalline; vit. = vitrophyric.

Table 2. Continued.

Sample	**89-125**	**91-252**	**91-215**		**90-171**	**92-288**	**91-249**		**90-177R**	**89-120**	**60NC145**
Unit	**rhyolite of Petition Reservoir**	**Beaver Creek Tuff**	**Carter Spring Rhyolite**			**rhyolite of Mill Creek**	**Badlands Lava Flow**			**Garat Crossing Lava Flow**	**Circle Creek Rhyolite**
Unit age (Ma)	13.83	13.82	13.89			13.77	13.73			13.65	11.9**
±2σ (Ma)	±0.04	±0.05	±0.05			±0.12	±0.08			±0.04	±0.5
Notes		densely welded	spatter ring		lava flow	type locality	aphyric		pheno-rich	type locality	type locality
Location	Owyhee Canyon	Carter Creek	Carter Spring type area			Mill Creek	NW margin		over vent	Garat Crossing	Circle Creek
State	ID	ID	ID			ID	ID			ID	NV
Lithology	cryst.	cryst.	cryst.		vit.	cryst.	cryst.		vit.	vit.	vit.
Major Oxides (wt.%):											
SiO_2	77.5	78.3	76.9		76.8	72.9	78.1		74.9	75.9	74.2
TiO_2	0.10	0.12	0.11		0.11	0.56	0.11		0.31	0.30	0.29
Al_2O_3	12.1	11.5	12.2		12.2	14.2	11.8		12.7	12.3	12.8
FeO*	1.37	1.27	1.31		1.36	1.68	1.25		2.16	1.98	2.41
MnO	0.02	0.01	0.01		0.02	0.01	0.02		0.03	0.02	0.04
MgO	0.00	0.00	0.00		0.00	0.00	0.00		0.12	0.08	0.36
CaO	0.21	0.37	0.41		0.63	1.25	0.39		1.03	0.86	0.99
Na_2O	3.43	3.09	3.32		3.13	3.93	3.28		2.90	2.74	2.96
K_2O	5.28	5.28	5.64		5.78	5.34	4.99		5.78	5.78	5.91
P_2O_5	0.01	0.02	0.07		0.01	0.10	0.02		0.05	0.02	0.04
Orig. Total	96.9	100.1	99.7		98.7	100.2	100.0		99.0	95.3	100.0
Trace Elements (ppm):											
Ba	33	98	82		65	1517	146		567	605	820
Rb	327	265	294		287	178	302		242	209	nd
Sr	0	11	15		7	112	12		52	47	40
Zr	180	204	212		207	553	171		308	282	400

Notes: Continued.

*Total Fe is expressed as FeO. All compositions recalculated on an anhydrous basis. Compositional data from Manley (1994a); sample 60NC145 from Coats (1968).

**Dates are $^{40}Ar/^{39}Ar$ single crystal laser determinations (Table 1), except sample 60NC145, dated by K-Ar by Coats (1968); date recalculated according to the constants of Steiger and Yaeger (1977).

Table 3. Stratigraphic relations in the Juniper Mountain volcanic center and surrounding areas

Juniper Mountain volcanic center proper		vents likely located in outlying areas	
		Circle Creek Rhyolite in northern NV	**11.9 ± 0.5 Ma***
13.73 ± 0.08 Ma	Badlands Lava Flow	Garat Crossing Lava Flow southeast of Juniper Mountain	**13.65 ± 0.04 Ma**
similar ages; compositionally and petrographically identical			
		rhyolite of Mill Creek north of Juniper Mountain	**13.77 ± 0.12 Ma**
13.89 ± 0.05 Ma	Carter Spring Rhyolite		
13.82 ± 0.05 Ma	Beaver Creek Tuff		
13.83 ± 0.06 Ma	Upper Lobes Lava Flows on summit of Juniper Mountain	rhyolite of Petition Reservoir southeast of Juniper Mountain	**13.83 ± 0.04 Ma**
identical ages; very similar compositions; widely separated vents			
13.90 ± 0.05 Ma	Upper Lobes Lava Flows near Squaw Creek		
13.89 ± 0.11 Ma	Lower Lobes Lava Flow near Squaw Creek		
13.95 ± 0.06 Ma	Lower Lobes Lava Flow east of Juniper Mountain		
14.10 ± 0.06 Ma	"Swisher Mountain Tuff" (upper unit) at North Fork Crossing	"Swisher Mountain Tuff" (upper unit) near Three Forks, OR	**14.09 ± 0.10 Ma**
identical ages; very similar compositions			
14.15 ± 0.11 Ma	"Swisher Mountain Tuff" at Crutcher Crossing		
14.22 ± 0.08 Ma	"Swisher Mountain Tuff" (lower unit) at North Fork Crossing	Swisher Mountain Rhyolite east of town of Jordan Valley	**14.21 ± 0.13 Ma**
identical ages; very similar compositions			
		"Swisher Mountain Tuff" east of Juniper Mountain	**14.31 ± 0.06 Ma**
		"Swisher Mountain Tuff" (lower unit) near Three Forks, OR	**14.48 ± 0.04 Ma**

Notes: All dates are $^{40}Ar/^{39}Ar$ determinations on sanidine (Table 1; Fig. A1), except * which is K-Ar (Table 2).

mapping indicates that the unit probably is a single huge rhyolite lava flow with an overall ovoid plan shape (Figure 2; Manley, 1994a, and unpub. data, 1989-1993). Its volume is roughly 230 cubic km. Parts of the flow front are lobate, with lobe widths of several kilometers. Large ogives (flow folds) are preserved where the original flow surface is exposed. On the basis of ogive orientation, Ekren and others (1984) suggested that the vent is buried beneath younger basalts at a location just northeast of the Beaver Creek Tuff (see below); this still seems likely. The unit is here formally renamed the Lower Lobes Lava Flow, and the type section (Figure 2) is defined as the eastern wall of Cougar Canyon in the $NE^1/_4$ sec. 11, T. 10 S., R. 3 W., where the vitrophyric basal crumble breccia

overlies vitrophyric material mapped as Swisher Mountain Tuff by Ekren and others (1981, 1984). Compositions (Table 2) and new dates of 13.95 ± 0.06 Ma and 13.89 ± 0.11 Ma (Tables 1 and 3) from samples 30 km apart are consistent with the Lower Lobes Lava Flow being a single emplacement unit.

On the northwestern flank of Juniper Mountain (near sample 89-65 on Figure 2), northward-advancing flow fronts of the Lower Lobes Lava Flow overlie rhyolite mapped by Ekren and others (1981) as Swisher Mountain Tuff. To the south, the Swisher Mountain unit thins quickly and disappears beneath the Lower Lobes Lava Flow. The map of Ekren and others (1981) shows the Swisher Mountain Tuff exposed in the bed of Squaw Creek far upstream and closer to the center of Juniper Mountain itself. This relationship was cited as showing that Juniper Mountain was higher than the surrounding units because it was domed up by a hypabyssal intrusion postdating all rhyolite volcanism (Ekren and others, 1981). Instead, this part of Squaw Creek

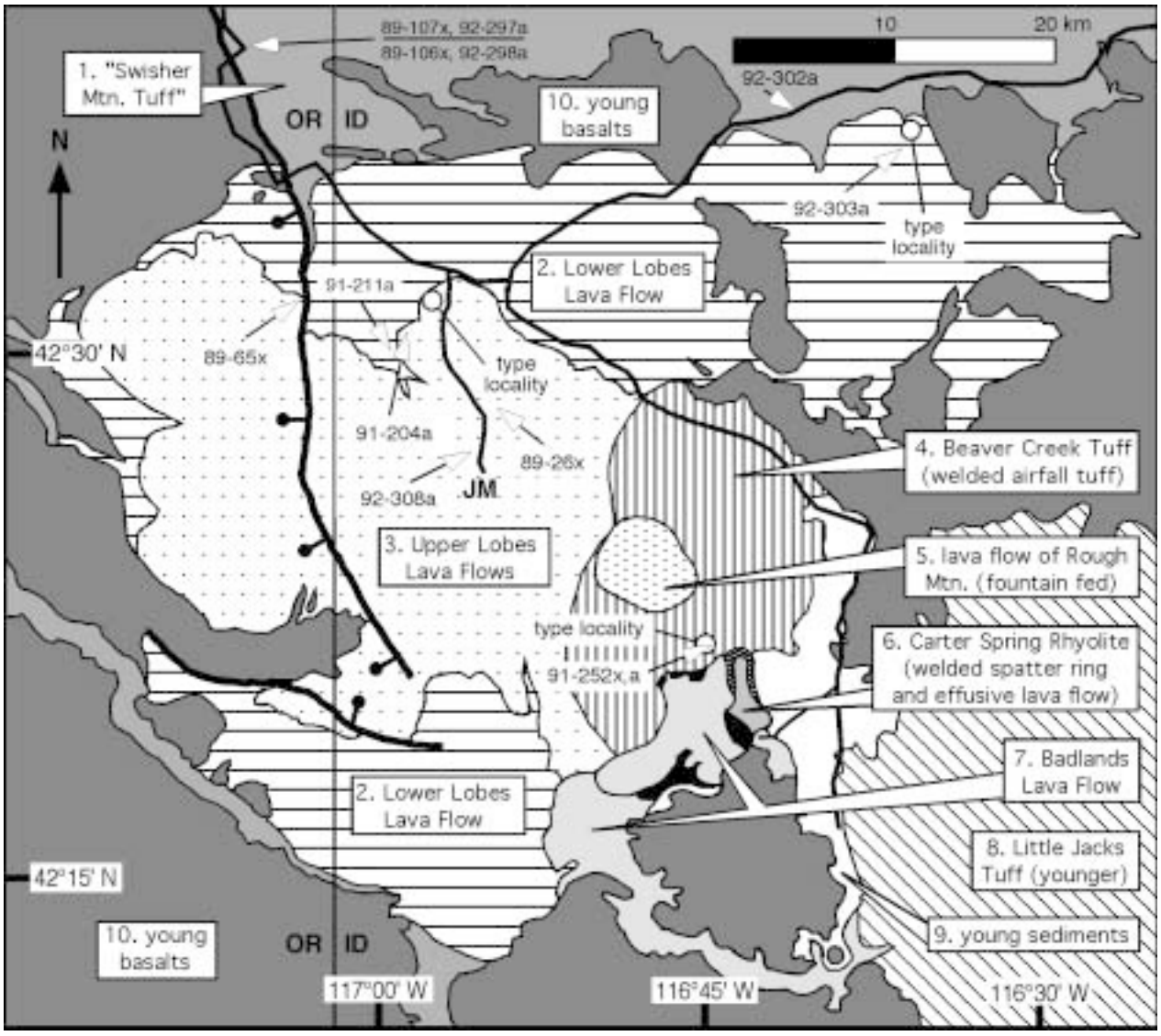

Figure 2. Geologic sketch map of units of the Juniper Mountain volcanic center. Juniper Mountain (JM) proper is a stack of overlapping rhyolite lavas (Upper Lobes Lava Flows) sitting on the Lower Lobes Lava Flow and draped on the southeastern flank by the Beaver Creek Tuff, a welded fall unit fed by a tall (?) fire fountain. The Carter Spring Rhyolite tephra ring was also fed by fountaining or spatter eruptions. Its vent lies within a few kilometers of the fissure that fed the Badlands Lava Flow. Numbering of units is based on stratigraphic relations within the area of the figure. Sample locations shown as in Figure 1. Type sections shown by open dots. Modified from Ekren and others (1981, 1982, 1984) and C.R. Manley (unpub. data, 1989-1993).

is cut solely through the Lower Lobes Lava Flow, the base of which is unexposed. There is thus no evidence of intrusive doming.

UPPER LOBES LAVA FLOWS

Ekren and others (1984) described the summit shield of Juniper Mountain proper as composed of one or more tuffs and informally named the unit the upper lobes of Juniper Mountain. Identifying the unit as composed of tuffs was apparently based solely on exposures on the southeastern flank of Juniper Mountain. These rocks are tuffaceous and are now termed the Beaver Creek Tuff (see below). The upper lobes unit of Juniper Mountain is herein redefined as a sequence of overlapping rhyolite lava flows or flow lobes with well-preserved but poorly exposed basal vitrophyre layers and crumble breccias and with poorly preserved upper vitrophyre layers and carapace breccias. The unit is here formally named the Upper Lobes Lava Flows. The type section (Figure 2) is designated as exposures resting on the upper vitrophyre of the Lower Lobes Lava Flow in the SW¼ sec. 35, T. 10 S., R. 5 W. The lack of obvious soils implies no long hiatuses between extrusions of the Upper Lobes Lava Flows, consistent with dates of 13.90 ± 0.05 Ma and 13.83 ± 0.06 Ma for samples at the base and summit of Juniper Mountain, respectively (Tables 1, 2 and 3).

RHYOLITE OF PETITION RESERVOIR

Exposed along the canyon of the Owyhee River southeast of Juniper Mountain are two units originally correlated with the tuff of The Badlands by Ekren and others (1981, 1984). The larger of these units was later assigned to the upper rhyolite of Juniper Mountain by Sawlan and others (1987). This larger unit is here informally renamed the rhyolite of Petition Reservoir; it has now been dated at 13.83 ± 0.04 Ma (Tables 1 and 3). It is petrographically and compositionally distinct from the Badlands Lava Flow (see below) and is the most evolved in trace element composition (Figure 8; Table 2) of all the JMVC rhyolites. Steep margins and other contact relations with the overlying Little Jacks Tuff imply that the rhyolite of Petition Reservoir is probably a large lava flow fed by a local vent and not a remnant of a more extensive ignimbrite.

BEAVER CREEK TUFF

The Beaver Creek Tuff (Figure 2; Table 2) is a rhyolitic, welded fall unit (roughly 8 cubic km). It was the first clearly noneffusive unit erupted from the JMVC magmatic system. The unit is formally named for exposures along Beaver and Carter creeks on the southeastern flank of Juniper Mountain, especially in the NE¼ sec. 24, T. 12 S., R. 4 W. (near sample 91-252 on Figure 2). The upper vitrophyre of the Beaver Creek Tuff is preserved, although poorly exposed, beneath the northern margin of the younger Carter Spring Rhyolite spatter ring (see below) in the S½ sec. 18, T. 12 S., R. 3 W. Stratigraphically-lower exposures (Figure 3) are pinkish crystalline rhyolite with a foliation subparallel to the slope of the unit's present surface. Lithic fragments are as much as 10 cm in diameter but are not abundant. Near the eastern edge of the unit where it is only poorly welded, small, partially flattened pumice clasts are clearly visible in outcrop and can be removed by hand from the matrix. The Beaver Creek Tuff, stratigraphically beneath the Carter Spring Rhyolite, has been dated at 13.82 ± 0.05 Ma (Tables 1 and 3).

Figure 3. Field photograph of subparallel layering in densely welded fall deposits of the Beaver Creek Tuff as exposed in the drainage of Carter Creek. Hammer for scale.

LAVA FLOW OF ROUGH MOUNTAIN

The lava flow of Rough Mountain (Figure 2) is as yet undated and incompletely mapped. It stratigraphically overlies the Beaver Creek Tuff at that unit's highest point, assumed to be at or near its vent. No vitrophyric material has been found in outcrops of the lava flow of Rough Mountain. All material so far observed is crystalline and pinkish, in contrast to other lavas of the JMVC, which are various shades of gray. The oxidized pink color of the rock, the extremely low pre-eruptive water content (see below), and the unit's association with the Beaver Creek Tuff all suggest that the lava flow of Rough Mountain is a secondary lava flow—the product of a fire-fountain or spatter-type eruption (Manley, 1994b, 1996b). The unit was most likely fed by the same vent from which the Beaver Creek Tuff erupted.

CARTER SPRING RHYOLITE

The Carter Spring Rhyolite, here formally defined, consists of two contrasting eruptive units: an oval-shaped welded spatter ring with the long-dimension trending N-S, and an effusive lava flow largely confined to the interior of the ring (Figure 4; Table 2). The spatter ring is composed of beds of dense, crystalline rhyolite that largely dip inward toward the presumed location of the vent, apparently a N-S-trending dike between 0.5 and 1.5 km long. The designated type section is along a drainage gully in the SE¼ sec. 19, T. 12 S., R. 3 W. (Figure 4). Here, the dips of the beds (toward the vent) increase smoothly from 46 degrees in the topographically and stratigraphically lowest exposures to 84 degrees in the uppermost (and nearest the vent) preserved exposures. The degree of welding in the deposit increases with increasing stratigraphic height and proximity to the vent, so that in the material closest to the vent, individual clasts can no longer be discerned. In this material, "bedding" was likely formed both by primary deposition of hot pyroclasts and by gravity-driven syn- and post-depositional viscous flow. However, at a location on the northeastern lip of the ring, thin (several centimeters thick) interlayers of vitrophyric material with scattered spherulites indicate that hiatuses in deposition (due either to hiatuses in the eruption or to shifting winds) allowed some of the tephra to quench to glass after welding. The Carter Spring Rhyolite has been dated at 13.89 ± 0.05 Ma (Tables 1 and 3).

Evidence that tephra production was highly variable is seen in allochthonous exposures of the southeastern part of the spatter ring. Clast-supported beds of coarse blocks up to 20 cm in diameter, welded together and with a paucity of fines and with voids between some blocks (Figure 5a), are juxtaposed with beds of welded shards

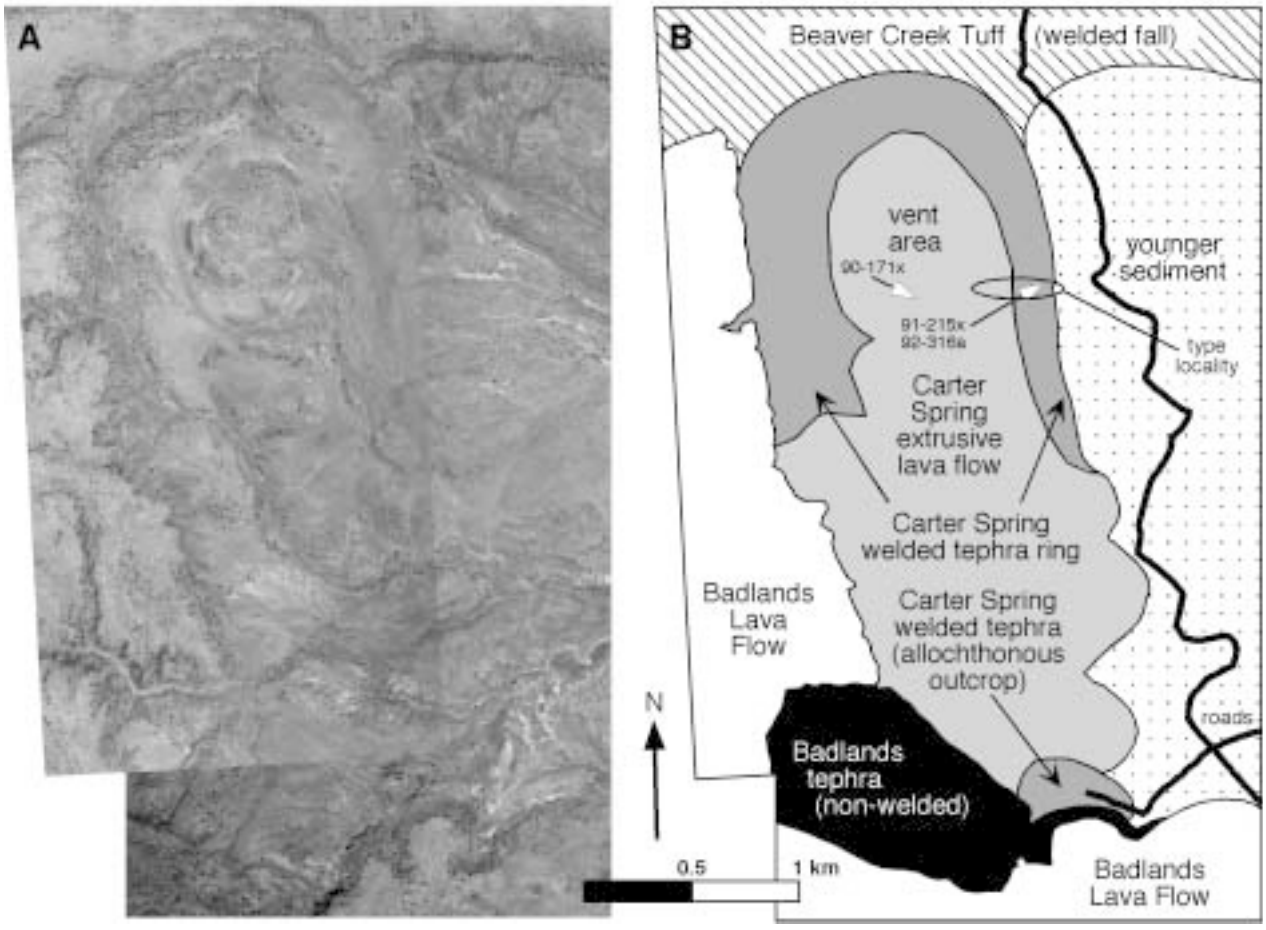

Figure 4a, b. The Carter Spring Rhyolite. (a) Mosaic of aerial photographs. (b) Geologic sketch map showing the fountain-fed spatter (welded tephra) ring and later effusive lava flow; sample locations and type section as in Figures 1 and 2.

with an average grain size of roughly 1 mm (Figure 5b). In the fine-grained beds, shards show thick bubble walls that broke by perpendicular fracture (Figure 5c), indicating a silly-putty-like plastic rheology instead of the highly brittle fracture seen in most high-silica rhyolites. Diversity in tephra size and morphology indicates an eruptive style between Hawaiian and Strombolian, and the possibility that deposition was affected by strong or shifting winds.

The Carter Spring Rhyolite is better preserved and exposed than units of the Taylor Creek Rhyolite in western New Mexico (Duffield, 1990), which also appear to have been fountain-fed. The Carter Spring Rhyolite retains the original morphology of its welded tephra deposit, though most nonwelded to poorly welded material that originally draped the welded tephra has been removed by erosion.

Filling the tephra ring is a small rhyolite lava flow erupted from near the northern end of the dike. Foliations wrapping completely around that part of the flow above the conduit indicate the lava apparently extruded coherently and did not erupt by fountaining. At the southern end of the welded spatter ring, which was the lowest topographically, the weight of the extrusive lava flow apparently disrupted the ring and shoved some of it perhaps several hundred meters further south. The lava then spilled through the breach and spread eastward away from the ring (Figure 4).

BADLANDS LAVA FLOW

The youngest rhyolite units in the immediate area of Juniper Mountain were interpreted by Ekren and others (1981, 1984) to be the erosional remnants of an extensive ignimbrite they informally named the tuff of The Badlands. That part of the unit that includes the geographic area known as The Badlands is a lava flow, not an ignimbrite. It is here formally named the Badlands Lava Flow. The type section is designated by exposures of near-vent tephra, lava, and vitrophyric basal crumble breccia along an erosional gully in sec. 31, T. 12 S., R. 3 W. (Figure 6). The unit has now been dated at 13.73 ± 0.08 Ma (Tables 1 and 3). The Badlands Lava Flow was described in detail by Manley (1995; 1996a, 1996b). Its original volume was at least 15 cubic km, but an unknown amount lies buried beneath younger units. This unit erupted on a greater slope than did the Lower Lobes Lava Flow, and so it is both irregular and asymmetric in shape, with large and small lobes that flowed distances up to 9 km downslope from the vent (Figures 2 and 6). Original flow-lobe thicknesses ranged from about 40 to 200 m, depending on underlying slope and the rheology of the

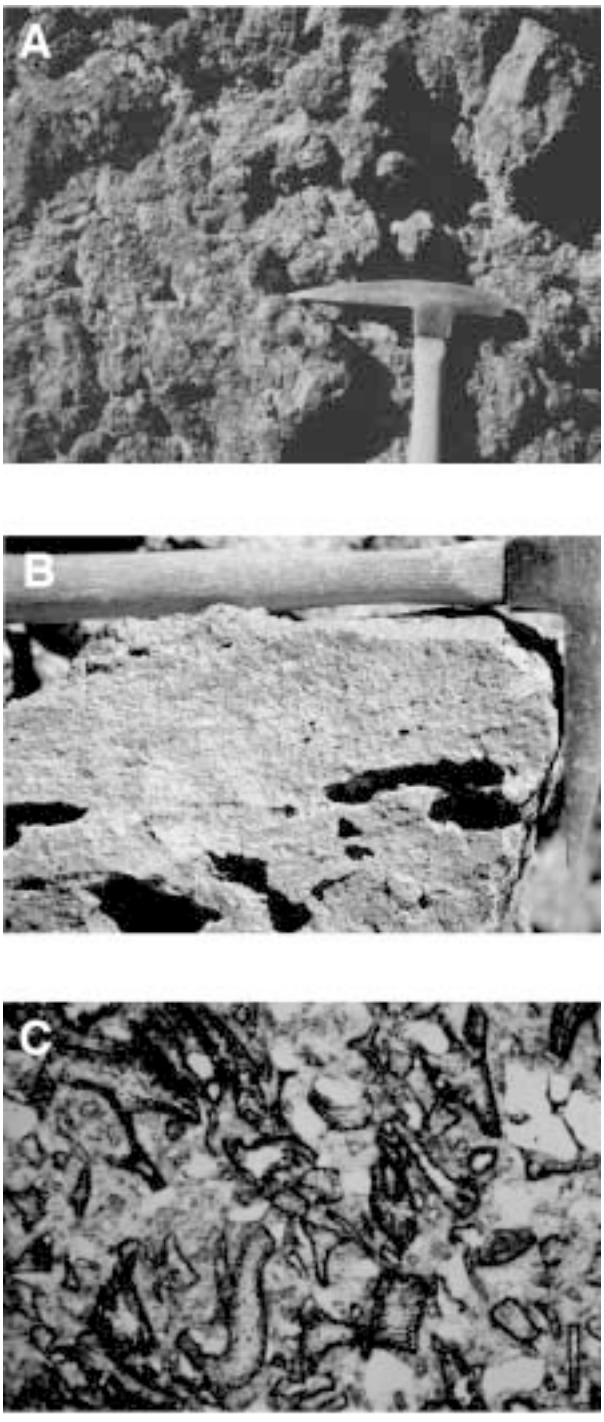

Figure 5a, b, c. Photographs of tephra from the Carter Spring Rhyolite spatter (welded tephra) ring. (a) Bed of clast-supported tephra from the allochthonous outcrop of the spatter ring (at south in Figure 4). Hammer for scale. (b) Fine-grained bed from type section on east side of the spatter ring. Hammer for scale. (c) Photomicrograph of fine-grained spatter ring tephra (from allochthonous outcrop) showing silly-putty-like breakage of thick-walled shards. Horizontal field of view is 6.25 mm.

mixed magma (both aphyric and phenocryst-rich magma erupted simultaneously; Manley, 1995; 1996a). Eruptive temperatures, based on Fe-Ti oxide equilibria, were about 830ºC (Manley, 1995). Eruption occurred from a fissure at least 7 km long. Although the evidence that the unit is a lava flow is unequivocal, many samples of the upper and lower vitrophyres show microscopic fragmental textures created by comminution and welding of pumiceous blocks from the lava's macroscopically brecciated carapace (Manley, 1996b). Identical textures in outcrops of

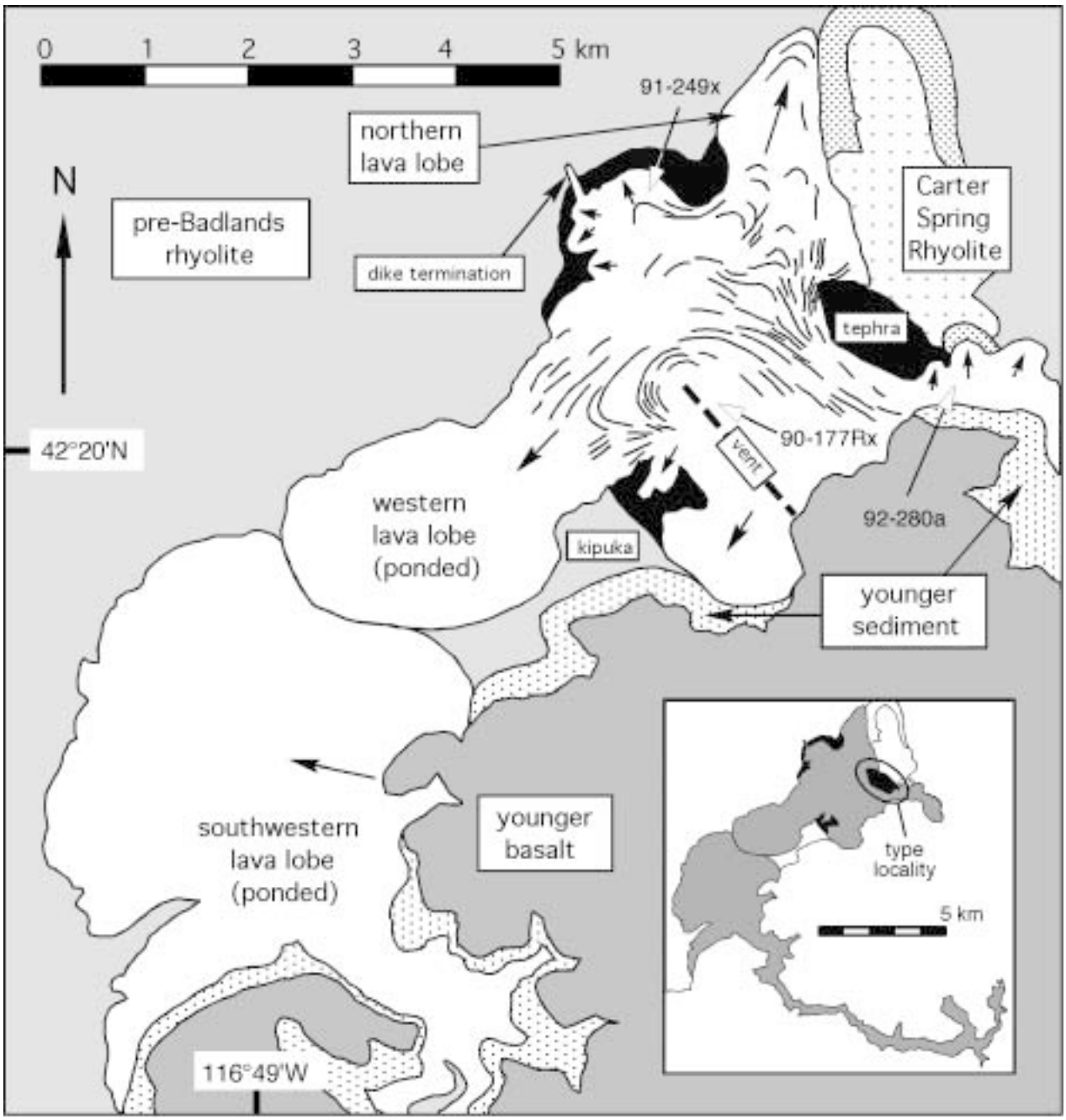

Figure 6. Detailed geologic sketch map of exposed vent area of the Badlands Lava Flow. White is the Badlands Lava Flow. Black is early tephra deposits of the Badlands Lava Flow. Inset at lower right shows known extent of unit (gray) and location of type section. Flow foliations reveal position and orientation of vent fissure. Arrows indicate flow directions of largest lava flow lobes. The Carter Spring Rhyolite is immediately east of the Badlands Lava Flow's northern lava lobe. The aphyric lithology is found primarily in small lobes near the dike termination. Greatest local slope is to the southwest from the vent. Sample locations are shown as in Figure 2. Modified from Manley (1995).

the Swisher Mountain Tuff northeast of Juniper Mountain convinced Ekren and others (1984) that that unit was an ignimbrite.

Small rhyolitic lava flow eruptions usually begin with sub-Plinian explosive behavior that forms a ring of loose tephra around the vent. As explosive activity is replaced by the effusion of lava, the tephra ring can be covered or shoved out of the way. The exposed vent area of the Badlands Lava Flow looks like a larger version (Manley, 1996a) of the vent areas of small lava flows. Initial explosive activity along the WNW-trending dike that fed the Badlands Lava Flow produced ridges of tephra up to 60 m high that parallel the dike. The tephra is composed of oxidized lithic blocks and juvenile pumice and ash, and, unlike the Beaver Creek Tuff and the tephra of the Carter Spring Rhyolite, is not welded. By chance, the tephra deposit on the north side of the dike was shoved farther north against that part of the Carter Spring Rhyolite spatter ring that had itself been moved south by the Carter Spring Rhyolite's extrusive lava.

Near the dike termination where the flow lobes are composed of the aphyric rhyolite, scattered marekanites up to about 4 cm in diameter are the only remaining obsidian from the lava's otherwise perlitic, eroded upper vitrophyre. The presence of these nodules in association with chert and agate debitage (N. Sudman and A. Bronsdon, oral commun., 1992) in areas not downstream from this source implies that the obsidian was transported and utilized by prehistoric Native Americans. Marekanites and other debitage are especially common around the Carter Spring Rhyolite and westward toward the obsidian source.

Ekren and others (1981, 1984) mapped a large area west of the fault on the west side of Juniper Mountain (Figure 2) as the largest remnant of their tuff of The Badlands. The units in this area are actually downfaulted parts of the Lower Lobes Lava Flow and Upper Lobes Lava Flows east of the fault (Manley, unpub. data, 1989-1993).

GARAT CROSSING LAVA FLOW

Like the rhyolite of Petition Reservoir, a rhyolite unit at Garat Crossing, in the bottom of the Owyhee River canyon southeast of Juniper Mountain, was mapped as part of the tuff of The Badlands by Ekren and others (1981, 1984). The morphology of the Garat Crossing unit shows that it is a thick lava flow with its base unexposed and much of its upper vitrophyre removed by erosion. Therefore, it is here formally renamed the Garat Crossing Lava Flow. The type section is at Garat Crossing in the SW$^1/_4$ sec. 19, T. 14 S., R. 1 W. The unit has now been dated at 13.65 ± 0.04 Ma (Tables 1 and 3). It is thus extremely similar in age, composition (Table 2), and petrographic character (Manley, 1994a) to the Badlands Lava Flow, and the two units very likely erupted from the same magma reservoir through widely separated vents.

RHYOLITE OF MILL CREEK

The informally named rhyolite of Mill Creek replaces the previously proposed tuff of Mill Creek. Ekren and others (1981, 1984) informally named the tuff of Mill Creek for exposures in a restricted area north of Juniper Mountain. They concluded it was older than—but clearly related to—the Swisher Mountain Tuff, which locally overlies it as mapped. Although its composition (Table 2) is very similar (except for a low Fe content) to many other units mapped as Swisher Mountain Tuff, the age of 13.77 ± 0.12 Ma (Table 1) is about 0.3 Ma younger than the youngest Swisher Mountain Tuff sample analyzed in this study (Tables 1 and 3). It is thus much more mafic than units of similar age; whether this is due to problems with the dating or is a true exception to the overall petrologic trend is presently unknown. The unit's physical features are also at odds with the previous interpretation that the unit is an ignimbrite. They include an upper pumiceous breccia, a probable basal crumble breccia, and jointing that implies viscous (lava-like) flow at the time that crystallization was beginning (Manley, 1992). These features suggest that the unit is a lava flow, not a tuff, and so the rhyolite of Mill Creek is suggested as a better name.

DISTAL AIR-FALL ASHES FROM THE OWYHEE-HUMBOLDT ERUPTIVE CENTER

A distal record of the volcanism along the SRP trend, including that of the JMVC and OHEC, has been compiled by Perkins and others (1995, 1998) and Nash and others (1996) from fallout deposit ash beds in depositional basins outside the SRP. Relative and absolute dating has provided a stratigraphic framework for understanding the ashes, and ash shard compositions have been matched to proximal ash and tuff deposits in several of the eruptive centers along the SRP. Ashes that these authors dated, by relative methods, at between 13.9 Ma and 12.8 Ma were thought to have erupted from the JMVC-OHEC. They show compositions more evolved and Zr temperatures cooler than younger ashes from further east along the hot-spot track. These ash beds seem to record only the younger JMVC activity—perhaps the Lower Lobes Lava Flow and younger units.

The widespread nature of the ash beds linked to JMVC volcanism contrasts with both the apparently effusive (nonexplosive) character of the identified rhyolitic units

and the paucity of outcropping ash layers between rhyolites in the JMVC area. For example, the Badlands Lava Flow eruption began with sub-Plinian activity, and this deposited near-vent tephra and might have created a significant fallout ash layer, but only the coarse near-vent tephra has been found. In addition, most of the unit erupted effusively as a lava flow with no evidence of accompanying explosive activity. The effusive eruptions of the Lower Lobes Lava Flow and Upper Lobes Lava Flows also imply that any early explosive phase would have been minor. If the welded fall deposit of the Beaver Creek Tuff was emplaced by fire fountaining as envisioned above, the volume of fine ash material lofted high into the atmosphere by convection in the eruptive column should have been minimal (see below), implying only a minor contribution to distal depositional basins. Future work may correlate specific JMVC rhyolite units with individual ash beds, as has been done with certain units of the Cougar Point Tuff of the Bruneau-Jarbidge eruptive center (Perkins and others, 1995, 1998).

POST-JUNIPER MOUNTAIN VOLCANIC CENTER GEOLOGIC HISTORY

CIRCLE CREEK RHYOLITE

The Circle Creek Rhyolite of Coats (1968) is the only rhyolite emplacement unit mapped in detail in the northern Nevada portion of the OHEC. Dated at 11.9 ± 0.5 Ma (Coats, 1968, recalculated using the constants of Steiger and Jaeger, 1977) by K-Ar methods (Figure 1; Table 2), it is much younger than the JMVC-related rhyolites in Idaho and Oregon. Erosion of overlying sediments and basaltic lavas has exposed a roughly 90-square-km area of the surface of this unit, but no margins or cross-sectional views. Coats mapped surficial areas of closed flow-foliation and believed each of these must denote lava erupted from a separate magmatic vent. On this basis, he felt the unit was a "lava flow" fed by a large number of closely spaced magmatic vents active simultaneously—an arrangement not reported elsewhere. The unit is more likely a lava flow fed by a possibly-segmented fissure vent. Diapirism is common in the upper parts of rhyolite lavas (Fink, 1980) and could also account for closures in flow layering in the uppermost vitrophyre of the Circle Creek Rhyolite.

LITTLE JACKS TUFF

Lying stratigraphically above the Badlands Lava Flow and the rhyolite of Petition Reservoir is a widespread, multiple-cooling unit rhyolite termed the Little Jacks Tuff (Figure 1) and K-Ar dated at between 10 and 9.6 Ma (Ekren and others, 1984). Its source area appears to be northeast of the JMVC, where the Owyhee Plateau meets the edge of the western SRP. The Little Jacks Tuff is a series of five or more ignimbrites or lavas, or some of each.

YOUNGER BASALTIC VOLCANISM

After eruption of the Little Jacks Tuff, the Owyhee-Humboldt eruptive center was largely covered by fluviolacustrine sediments and then by basaltic lava flows erupted primarily from low shield volcanoes (Figure 1). Basalt volcanism around the JMVC lasted from about 10 to 6 Ma (Hart and Carlson, 1983, 1985; Hart and others, 1984), indicating that any local rhyolitic magma reservoirs had by then cooled sufficiently that rising basaltic magmas could propagate through them to the surface.

SUBSIDENCE OF THE OWYHEE-HUMBOLDT STRUCTURAL BASIN

Unlike most silicic volcanic centers of the SRP (Bonnichsen, 1982; Morgan and others, 1989) and elsewhere, the JMVC shows no clear evidence of "caldera-type" collapse associated with eruptions of even its most voluminous units (Ekren and others, 1981, 1984). It does, however, sit at the northern edge of a circular basin (the OHEC), approximately 90 km in diameter, that extends south into Nevada and west into Oregon (Figure 1). Outcrops in the canyons of the Owyhee River and its tributaries show that rhyolite underlies the entire circular area. The basal contacts of the lowermost rhyolites are not exposed, so the full thickness of rhyolite is unknown (Ekren and others, 1981).

After JMVC rhyolitic volcanism ended, the OHEC was buried by fine-grained fluviolacustrine sediments (Ekren and others, 1981), indicating that the area was a shallow depositional basin at that time. Whether flexure of the basin began before rhyolitic volcanism ceased is unclear. The Carter Spring Rhyolite and the Badlands Lava Flow preferentially flowed south in the direction of the center of the present basin, but this may simply reflect the southward slope of the primary surface of the underlying Beaver Creek Tuff. The younger basaltic lava flows and shield volcanoes that overlie rhyolites and sediments south and east of Juniper Mountain clearly show the effects of southward tilt. The flexure's northern structural hinge appears to be located approximately along the northern margin of the Lower Lobes Lava Flow (Figure

2). The upper surfaces of basaltic mesas overlying this unit are nearly flat-lying to the north, but they have a southward slope south of the apparent hinge. Subsidence of the basin by at least 200 m is likely, based on topographic evidence.

Flexural subsidence of this great circular region may have resulted from both the cooling of the underlying crust after it passed over the Yellowstone mantle plume and the loading of the lower to middle crust by basaltic intrusions. Presumably the same processes would also have operated beneath the neighboring Bruneau-Jarbidge eruptive center and the other SRP eruptive centers, but similar late subsidence is not observed in those locations.

FIRE-FOUNTAINING ON THE OWYHEE PLATEAU

Fire fountaining is commonly considered an eruptive mode confined to basalts and other magma compositions much more mafic than rhyolite. Nevertheless, several silicic units, including two erupted from the Yellowstone caldera, and all or much of the Taylor Creek Rhyolite in southwestern New Mexico (Duffield, 1990; Webster and Duffield, 1991, 1994) have been interpreted to be fountain-fed. All such units seem to have pre-eruptive water contents lower than average. Many have high F contents: melt inclusions from the Taylor Creek Rhyolite contain up to 3 weight percent F (Webster and Duffield, 1991, 1994). By itself, a low water content could strongly influence the eruptive style of a silicic magma. In Plinian and sub-Plinian eruptions, rhyolitic magma, commonly with pre-eruptive water contents of 4 to 6 weight percent (Lowenstern, 1995), vesiculates to the point of explosive comminution as it rises in the conduit toward the Earth's surface. This produces tephra with a large proportion of fine ash particles. The dense eruptive column above the vent efficiently entrains and heats outside air, convecting most of the tephra high into the atmosphere and far from the vent. Magma with a lower pre-eruptive water content will become less comminuted and will produce a much smaller proportion of ash-sized tephra, leading to a lower density eruptive column. Entrainment of air and resultant convection are thus minimal; the clasts can be emplaced ballistically in what is essentially a fire fountain. Thus, more of the tephra falls nearer the vent and remains hot enough to weld, forming a welded fall deposit. High magmatic F contents may also play an important role by decreasing the viscosity (Dingwell and others, 1985) of such a magma sufficiently that it is still able to rise through the conduit and erupt.

The JMVC units that show physical evidence of fountaining activity during their emplacement also have low pre-eruptive water contents and in some cases high F contents. Melt inclusions in euhedral quartz crystals from the Beaver Creek Tuff average 2.61 weight percent H_2O and 2,760 parts per million F (Manley, 1994a, 1994b). In the overlying lava flow of Rough Mountain, melt inclusions in euhedral quartz crystals contain the lowest H_2O contents (averaging 0.76 weight percent) and the highest F contents (averaging 8,100 parts per million) of analyzed JMVC rocks (Manley, 1994a, 1994b), and they apparently are the lowest pre-eruptive water contents yet determined for any rhyolite (Lowenstern, 1995).

Fountain-fed and effusive lava vented in turn to form the Carter Spring Rhyolite unit. Melt inclusions hosted in euhedral quartz from the fountain-fed tephra average 0.95 weight percent H_2O and have F contents of 2,660 parts per million (Manley, 1994a). Melt inclusions from the lava flow indicate a higher pre-eruptive water content of about 1.97 weight percent and 3,100 parts per million F (Manley, 1994a).

The Beaver Creek Tuff and the lava flow of Rough Mountain are physically very similar (R.L. Christiansen, oral commun., 1993) to the Sulphur Creek Tuff and Canyon Lava Flow of Yellowstone (Christiansen, 2001). These latter two units, both strongly ^{18}O-depleted rhyolites, were erupted immediately following resurgent doming within the Yellowstone caldera after its collapse due to the eruption of the Lava Creek Tuff (Hildreth and others, 1984; Gansecki and others, 1996). The Sulphur Creek Tuff (at least 13 cubic km) is a welded fall unit formed by energetic fire-fountaining behavior. The Canyon Lava Flow (about 5 cubic km) apparently fountained or erupted effusively from the same vent, deforming the underlying and still hot Sulphur Creek Tuff (Christiansen, 2001).

MIXED-MAGMA EVIDENCE FOR DIFFERENTIATION IN THE BADLANDS LAVA FLOW MAGMA CHAMBER

Evidence for the rise of evolved magmatic liquids, presumably along the wall of the magma chamber, and their accumulation at the top of the chamber is present in early tephra from the Badlands Lava Flow eruption and in the pattern of the mixing between the phenocryst-rich (30 percent phenocrysts, with sanidine crystals up to 2.5 cm in long dimension) and the aphyric (less than 1 percent phenocrysts) lava lithologies (Manley, 1996a). Populations of quartz phenocrysts from the lava and the tephra reveal that small, fresh crystals were grow-

ing in the aphyric magma at the top of the chamber (represented by early-erupted tephra and by early lava that vented from near the dike termination), while crystals in the underlying, dominant volume of phenocryst-rich magma were large (up to 0.5 cm), fractured, and corroded (Manley, 1996d). The aphyric lava has essentially the same major element composition as the liquid (excluding the phenocrysts) of the phenocryst-rich lava, but it has increased incompatible element and decreased compatible element contents (Manley, 1994a), indicating that further crystal fractionation occurred to form the aphyric liquid.

MAGMATIC HISTORIES ALONG THE SNAKE RIVER PLAIN

MAGMATISM OF THE JUNIPER MOUNTAIN VOLCANIC CENTER

A generalized history of the greater JMVC magmatic system can be summarized from the stratigraphic, compositional, and geochronologic analyses reported here. Between 14.5 Ma and 14.09 Ma, low-silica (69 to 74 weight percent SiO_2) rhyolite magmas erupted as voluminous lava flows and possibly ignimbrites over a large area of southwestern Idaho, southeastern Oregon, and northern Nevada. Where two units overlap, the younger unit is the more evolved. In the Juniper Mountain area, effusive volcanism continued, with compositions increasing to 78 weight percent SiO_2 (Figures 7 and 8) and unit areas, volumes, and magmatic temperatures decreasing, implying that the magmatic system was cooling, crystallizing and differentiating, and dying out.

Then at about 13.8 Ma, two or three fountain-fed rhyolites erupted on and near Juniper Mountain, followed at 13.7 Ma by the large Badlands Lava Flow (Figure 7). The Badlands Lava Flow shows petrographic evidence that it was at least partly derived by the melting of previously solidified rhyolitic magma, akin to several of the post-caldera rhyolites (including the two fountain-fed units) at Yellowstone (Bindeman and Valley, 2000). The remelting hypothesis is also consistent with the low water contents of the fountain-fed units, if the material that melted had previously lost much of its volatile content during crystallization (Manley, 1996c).

The remelting of the rhyolitic material represented by the Beaver Creek Tuff, lava flow of Rough Mountain, Carter Spring Rhyolite, and Badlands Lava Flow (approximately 25 cubic km) implies a substantial pulse of heat into the magmatic system, presumably by the intrusion of mantle-derived basaltic magmas. The extent of the area affected by the thermal pulse and the remelting is unknown, but the Garat Crossing Lava Flow is very similar to the Badlands Lava Flow, and these units and the rhyolite of Mill Creek are all less evolved than other young units of the JMVC. If these magmas were all remobilized by remelting, the thermal pulse must have affected at least a 1,700-square-km area of the crust. This is a large area but much smaller than that apparently involved in the early phase of volcanism between about 14.5 and 14.09 Ma. A similar process is thought to have occurred during geologically recent time in the central Andes (de Silva and others, 1994).

DIFFERENCES BETWEEN THE JUNIPER MOUNTAIN VOLCANIC CENTER AND BRUNEAU-JARBIDGE ERUPTIVE CENTER

The JMVC and the neighboring Bruneau-Jarbidge eruptive center (BJEC), the next younger eruptive center east along the SRP, though only separated by about 50 km, had very different eruptive and magmatic histories. The JMVC produced large-volume rhyolite lava flows and a few late fountain-fed rhyolites, but no units can yet confidently be identified as ignimbrites, and no caldera seems to be present (Ekren and others, 1981, 1984). The least-evolved (and oldest) units exposed near Juniper Mountain have 72 weight percent SiO_2, while the most-evolved units reach 78 weight percent. No basalts are found intercalated with these rhyolites. The system as a whole shows decreases with time in both unit volume and eruption temperature (Manley, 1994b), and an increase with time in degree of evolution (Figures 7 and 8), indicating a single, progressively cooling and fractionating magma chamber (at least until the melting event that resulted in the eruption of the fountain-fed units).

Figure 7. Plot of SiO_2 vs. FeO (total) concentrations in samples from the Juniper Mountain volcanic center and vicinity. Labeled fields show samples with similar degree of evolution or multiple samples from a single unit. The trend of the majority of the units (white circles) progresses in age (Tables 1 and 2) from least to most evolved (ages in Ma in white boxes), while units associated with the hypothesized melting event (black circles) show a reversed age-evolution trend (see Figure 8).

Figure 8a, b. Incompatible-compatible element plots of Rb vs. Sr concentrations in samples from the Juniper Mountain volcanic center and vicinity, showing behavior indicating that the rhyolites are primarily related by crystal fractionation. (a) Linear plot, showing concave trend of majority of samples (white circles; see Figure 7). Labeled fields show samples with similar degree of evolution or multiple samples from a single unit. Note that all units associated with the hypothesized melting event (black circles) plot above the main concave trend. (b) Log-log plot showing straight-line trend for same set of samples.

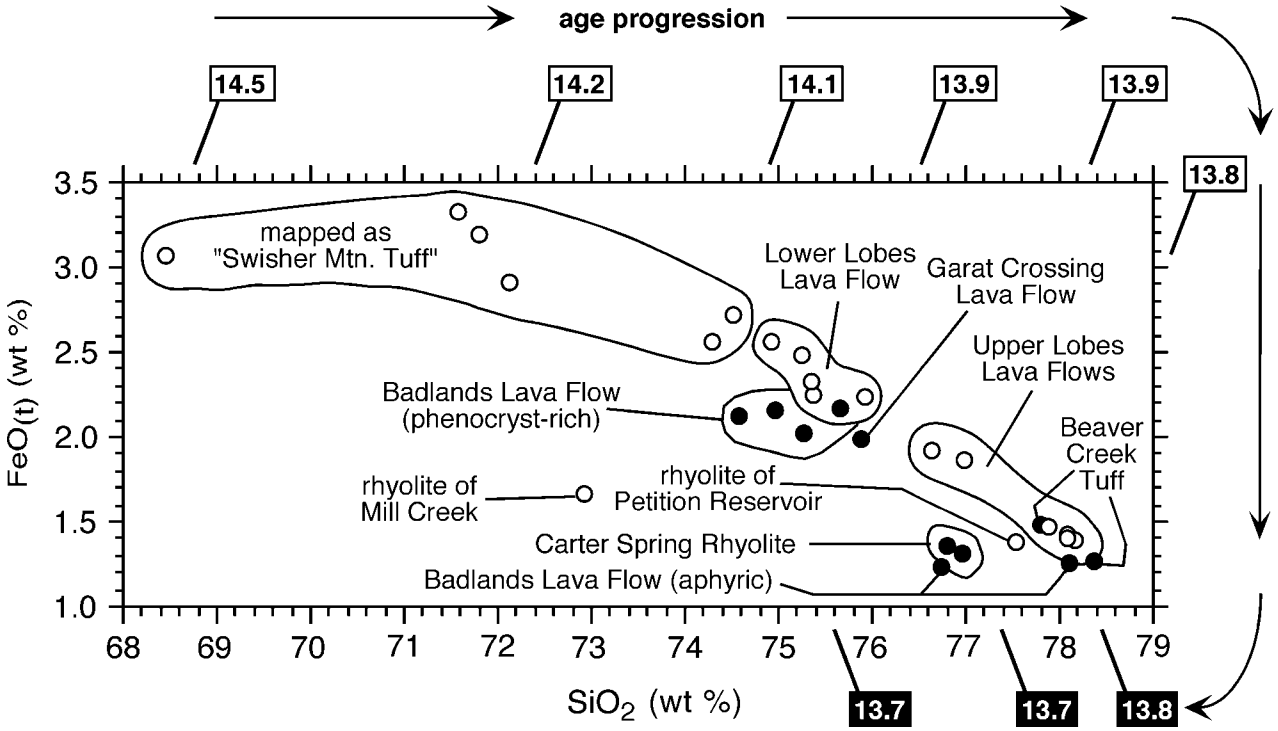

Figure 7.

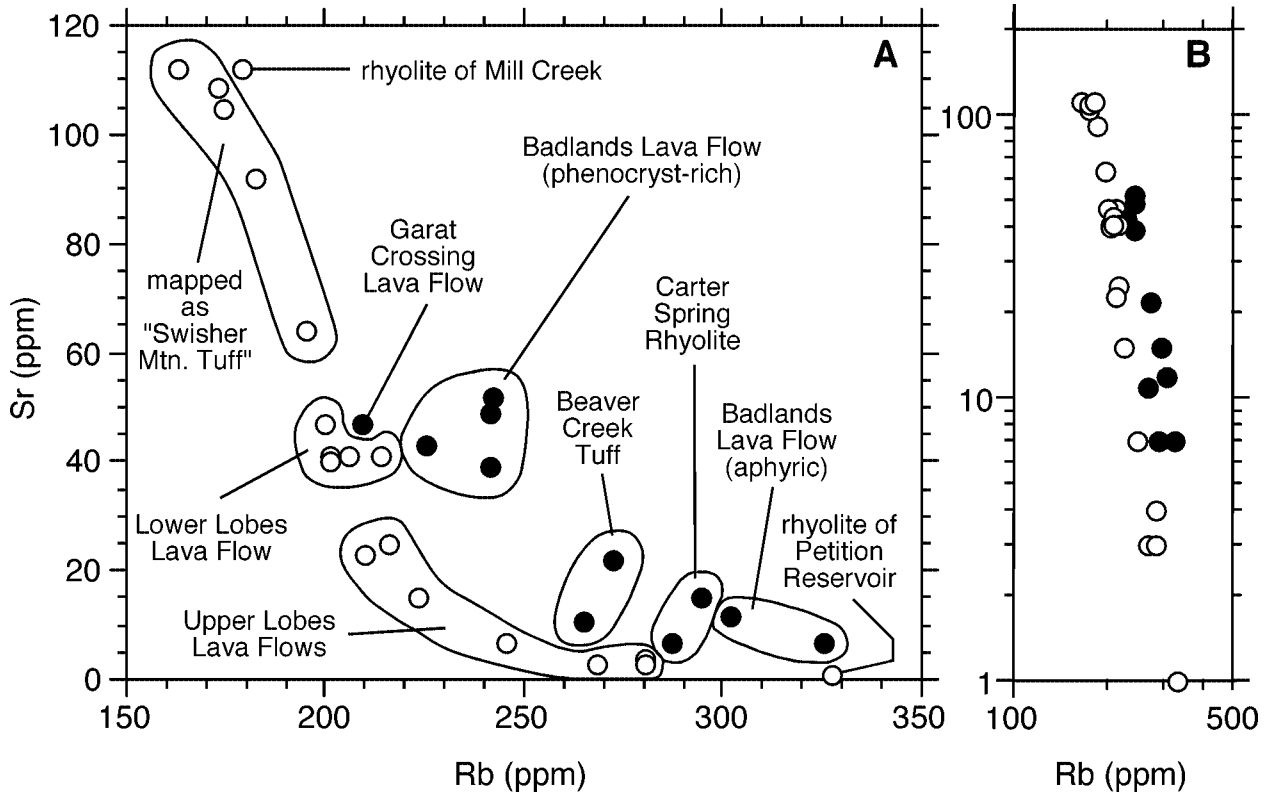

Figure 8.

In contrast, the 12-9 Ma BJEC erupted a sequence of widespread ignimbrites that caused the (possibly gradual) collapse of an ovoid caldera; large-volume lavas (Bonnichsen, 1982; Bonnichsen and Citron, 1982; Bonnichsen and Kauffman, 1987) then filled the caldera. Three eruption cycles of increasingly less-evolved magma compositions indicate tapping and reestablishment of a zoned system recharged at depth. Overall, eruptive temperatures are higher (Honjo and others, 1992; Perkins and others, 1995, 1998) and rhyolite compositions less evolved than those of the JMVC; SiO_2 contents range from 69 to 75 weight percent, with the rhyolite lava flows being the least evolved (Bonnichsen, 1982; Perkins and others, 1995). Basalt lavas, erupted outside the caldera, are intercalated with the rhyolites (Bonnichsen, 1982).

These differences in evolutionary trend and eruptive style may reflect differences in coupling of the hot-spot heat source with the crust. Possible variables include (1) crustal lithology (Idaho batholith rocks possibly underlying the JMVC (Taubeneck, 1971) may not extend as far east as the BJEC), (2) increases in hot-spot heat or mass flux during activity of the BJEC, and (3) timing and rate of extension ahead of the hot spot, which acts to translate the crust over the hot spot at rates greater than the velocity of the North American plate as a whole (Rodgers and others, 1990).

ACKNOWLEDGMENTS

Bill Bonnichsen, Robert Christiansen, Drew Clemens, Michael Cummings, Jon Fink, Virginia Gillerman, Marty Godchaux, Chris Henry, and Spencer Wood all visited the JMVC and offered important insights on various units. Rick Hervig provided valuable guidance and advice as well as instruction and assistance with the ion microprobe. John Holloway allowed the use of laboratory equipment and sample preparation facilities, and Ken Domanik assisted greatly with the internally heated, gas pressure-vessel during the high-pressure revitrification of some melt inclusions. Michael Hochella assisted with XRF analyses at Stanford University. Diane Johnson and Charles Knaack performed analyses at Washington State University. Michael Sawlan provided copies of his field mapping near Juniper Mountain. Jim Clark assisted with electron microprobe standardization. Reviews of the manuscript by Richard P. Smith and Michael McCurry are gratefully acknowledged, as are editorial comments by Roger Stewart. Portions of this work were funded by National Science Foundation grants EAR 90-18216 to R. Hervig and EAR 91-05329 to J. Fink and by a Stanford School of Earth Sciences McGee Fund grant and Geological Society of America Research Grants 4266-89 and 4498-90 to C.R. Manley. Support was provided to W.C. McIntosh by the New Mexico Bureau of Mines and Mineral Resources. The development of the New Mexico Geochronology Research Laboratory was aided by National Science Foundation grant EAR 92-064438. Lisa Peters and Richard Esser assisted with $^{40}Ar/^{39}Ar$ analyses.

APPENDIX: $^{40}Ar/^{39}Ar$ METHODS AND RESULTS

Sanidine crystals separated from seventeen samples of selected rhyolitic units were dated using single-crystal laser-fusion (SCLF) $^{40}Ar/^{39}Ar$ methods similar to those described in McIntosh and Chamberlin (1994). Table 1 summarizes the results and provides details of procedures and analytical parameters. Table A1 provides geographic coordinates and brief site descriptions of the dated samples. The complete set of analytical data, including probability distribution diagrams for individual analyses, is given in McIntosh (1999).

Precise weighted mean ages were obtained from sixteen of the seventeen samples; these data are characterized by tightly grouped, approximately Gaussian distributions of individual age analyses, high radiogenic yields (>94 percent), and consistent K/Ca values. Mean ages of these samples range from 14.48 Ma to 13.65 Ma, with 2σ uncertainties generally from $\pm$ 0.3 percent to $\pm$ 0.9 percent (Table 1). The remaining sample (92-302) yielded a less precise age of 14.67 $\pm$ 0.49 Ma, because of the small size of individual crystals and consequently low signal-to-noise ratios. On the basis of the single-crystal results, the possibility of contaminant grains seemed low, so this sample was reanalyzed as several multi-crystal aliquots to improve precision, yielding a more precise weighted mean age of 14.31 $\pm$ 0.06 Ma. Xenocrysts or altered sanidine crystals were rare or absent in all samples. Only three sanidine crystals were sufficiently discordant to be excluded from calculations of weighted mean ages (one crystal each from samples 92-298, 92-321 and 92-330). The data are sufficiently precise to resolve several separate eruptive episodes within the short (0.8 m.y.) eruptive life span of the Juniper Mountain volcanic center (Figure A1).

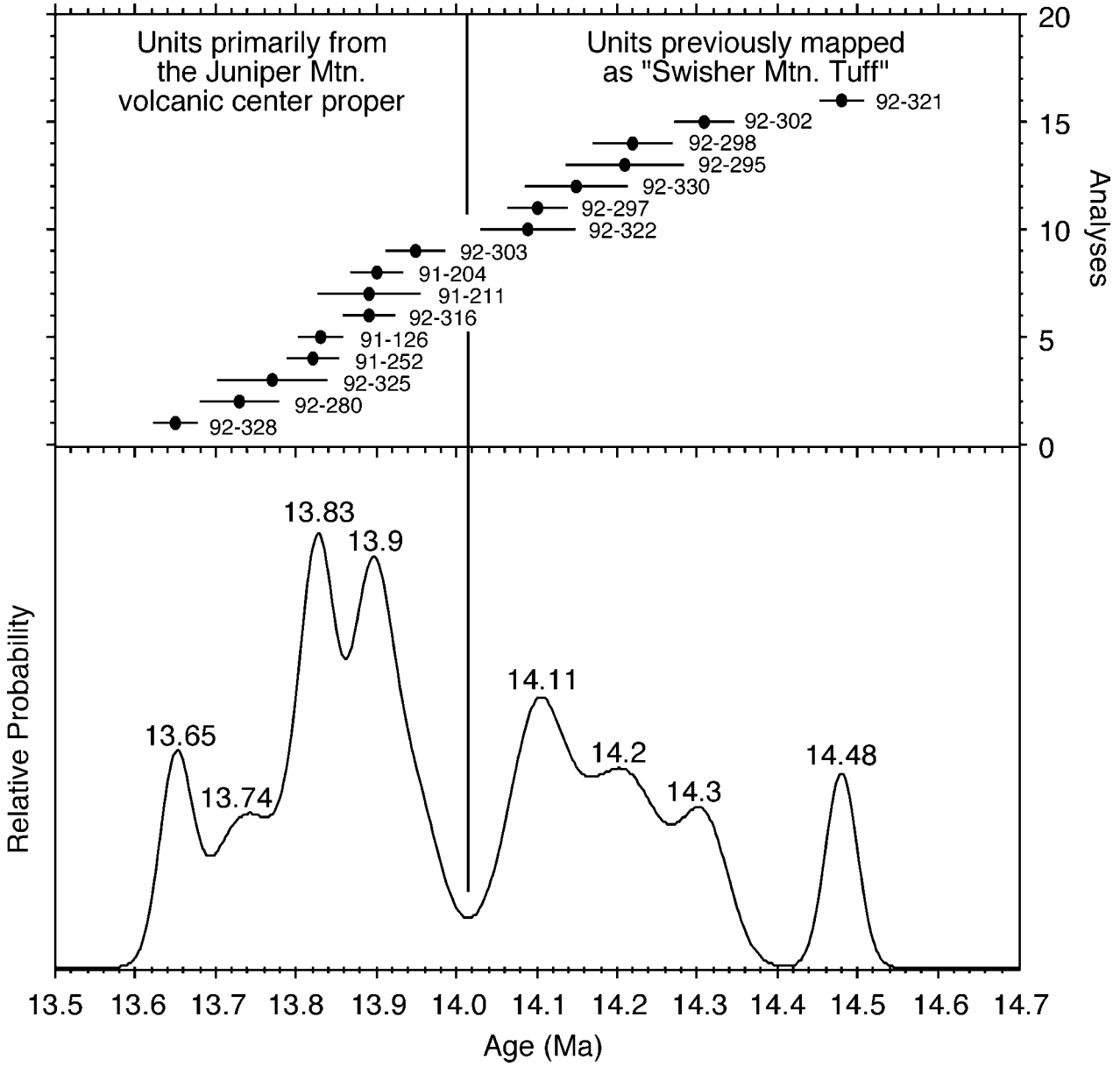

Figure A1. Summary of all $^{40}Ar/^{39}Ar$ ages determined from JMVC rhyolites. Individual analyses with respective 2σ uncertainties are shown at top. At bottom is a composite probability diagram incorporating dates and uncertainties from all samples. Note hiatus between units at the lowest stratigraphic levels (mapped as Swisher Mountain Tuff by Ekren and others, 1981, 1984) and units of the JMVC proper.

Table A1. Locations of $^{40}Ar/^{39}Ar$-dated samples from the Juniper Mountain volcanic center and vicinity.

Sample	Township and Range Location				7.5' Topo. Quad.	W Long.	N Lat.	Site Description
92-328	SW¼ SW¼	sec. 19	T. 14S	R. 1W	Piute Basin East, ID	116.5058	42.1858	Auto-silicified top of crystalline core of Garat Crossing Lava Flow at bottom of E Owyhee River canyon.
92-280	NE¼ SE¼	sec. 31	T. 12S	R. 3W	Brace Flat, ID	116.7312	42.3377	Auto-silicified top of crystalline core of tongue of Badlands Lava Flow covering tephra rampart.
92-325	SE¼ SW¼	sec. 31	T. 7S	R. 4W	Combination Ridge, ID	116.8546	42.7667	Crystalline core of NE-tilted lava flow forming high, steep hills above Mill Creek.
91-252	NE¼ NE¼	sec. 24	T. 12S	R. 4W	Brace Flat, ID	116.7479	42.3687	Crystalline welded air-fall tuff, dipping to S, exposed in Carter Creek (N bank).
89-126	NE¼ SW¼	sec. 10	T. 14S	R. 2W	Piute Basin East, ID	116.5618	42.2188	Crystalline rhyolite from unit exposed N and S of Owyhee River (sample from S canyon rim).
92-308	SW¼ SE¼	sec. 13	T. 11S	R. 5W	Smith Creek, ID	116.8732	42.4616	Auto-silicified top of crystalline core of one of the Upper Lobes Lava Flows at summit of Juniper Mtn.
92-316	NE¼ SE¼	sec. 19	T. 12S	R. 3W	Brace Flat, ID	116.7320	42.3625	Crystalline welded air-fall tuff from NE portion of elongate tephra ring S of Carter Creek.
91-211	NE¼ NW¼	sec. 10	T. 11S	R. 5W	Bedstead Ridge, ID	116.9162	42.4854	Upper vitrophyre of the Lower Lobes Lava Flow as exposed in the canyon of upper Squaw Creek.
91-204	NE¼ NE¼	sec. 3	T. 11S	R. 5W	Fairylawn, ID	116.9045	42.5013	Crystalline core of one of the Upper Lobes Lava Flows directly overlying the Lower Lobes Lava Flow.
92-303	NE¼ SW¼	sec. 11	T. 10S	R. 3W	Slack Mountain, ID	116.6628	42.5650	Crystalline core of the Lower Lobes Lava Flow in W bank of Cougar Canyon at Bat Spring.
92-322	NE¼ SW¼	sec. 22	T. 34S	R. 45E	Three Forks, OR	117.1833	42.5767	Auto-silicified top of crystalline core of younger lava flow on Wes Hawkins Trail in Owyhee River canyon.
92-297	NW¼ NW¼	sec. 6	T. 10S	R. 5W	Fairylawn, ID	116.9763	42.5878	Upper vitrophyre of younger lava flow at North Fork Crossing (SE canyon rim).
92-330	NE¼ NW¼	sec. 36	T. 13S	R. 5W	Red Basin, ID	116.8738	42.2507	Auto-silicified top of crystalline core of lava flow on N side of Owyhee River at Crutcher Crossing.
92-295	SW¼ NE¼	sec. 24	T. 6S	R. 5W	Stonehouse Creek, ID	116.8767	42.8876	Crystalline core of E-tilted Swisher Mtn. Rhyolite near confluence of Jordan Creek and Duck Creek.
92-298	NE¼ SW¼	sec. 36	T. 9S	R. 6W	Fairylawn, ID	117.9925	42.5964	Upper vitrophyre of older lava flow at North Fork Crossing (NW canyon rim).
92-302	SE¼ SW¼	sec. 4	T. 10S	R. 3W	Slack Mountain, ID	116.6992	42.5779	Upper vitrophyre of lava flow exposed along road opposite the mouth of Deep Creek canyon.
92-321	NW¼ SW¼	sec. 22	T. 34S	R. 45E	Three Forks, OR	117.1847	42.5779	Crystalline core of older lava flow on Wes Hawkins Trail in Owyhee River canyon.

Notes: Auto-silicification occurred during primary cooling of the upper portions of many of these flows.

REFERENCES

Ach, J.A., H.D. King, A.R. Buehler, and D.O. Capstick, 1986, Mineral resources of the Little Owyhee River Wilderness Study Area, Owyhee County, Idaho: U.S. Geological Survey Bulletin 1719C, 10 p.

Anders, M.H., and N.H. Sleep, 1992, Magmatism and extension: The thermal and mechanical effects of the Yellowstone hotspot: Journal of Geophysical Research, v. 97, p. 15,379-15,393.

Bindeman, I.N., and J.W. Valley, 2000, Formation of low-$\delta^{18}O$ rhyolites after caldera collapse at Yellowstone, Wyoming, USA: Geology, v. 28, p. 719-722.

Bonnichsen, Bill, 1982, The Bruneau-Jarbidge eruptive center, southwestern Idaho, *in* Bill Bonnichsen and R.M. Breckenridge, eds., Cenozoic Geology of Idaho: Idaho Bureau of Mines and Geology Bulletin 26, p. 237-254.

———, 1983, Epithermal gold and silver deposits, Silver City-De Lamar district, Idaho: Idaho Bureau of Mines and Geology Technical Report 83-4, 29 p.

Bonnichsen, Bill, and G.P. Citron, 1982, The Cougar Point Tuff, southwestern Idaho and vicinity, *in* Bill Bonnichsen and R.M. Breckenridge, eds., Cenozoic Geology of Idaho: Idaho Bureau of Mines and Geology Bulletin 26, p. 255-281.

Bonnichsen, Bill, and D.F. Kauffman, 1987, Physical features of rhyolite lava flows in the Snake River Plain volcanic province, southwestern Idaho, *in* J.H. Fink, ed., The Emplacement of Silicic Domes and Lava Flows: Geological Society of America Special Paper 212, p. 119-145.

Christiansen, R.L., 2001, The Quaternary and Pliocene Yellowstone Plateau volcanic field of Wyoming, Idaho, and Montana: U.S. Geological Survey Professional Paper 729-G, 145 p.

Coats, R.R., 1968, The Circle Creek Rhyolite, a volcanic complex in northern Elko County, Nevada, *in* R.R. Coats, R.L. Hay, and C.A. Anderson, eds., Studies in Volcanology; Williams Volume: Geological Society of America Memoir 116, p. 69-106.

Deino, A.L., and Richard Potts, 1990, Single-crystal $^{40}Ar/^{39}Ar$ dating of the Olorgesailie Formation, southern Kenya Rift: Journal of Geophysical Research, v. 95, p. 8453-8470.

de Silva, S.L., S. Self, P.W. Francis, R.E. Drake, and Carlos Ramirez R., 1994, Effusive silicic volcanism in the Central Andes: The Chao dacite and other young lavas of the Altiplano-Puna Volcanic Complex: Journal of Geophysical Research, v. 99, p. 17,805-17,825.

Dingwell, D.B., C.M. Scarfe, and D.J. Cronin, 1985, The effect of fluorine on viscosities in the system Na_2O-Al_2O_3-SiO_2: Implications for phonolites, trachytes and rhyolites: American Mineralogist, v. 70, p. 80-87.

Duffield, W.A., 1990, Eruptive fountains of silicic magma and their possible effects on the tin content of fountain-fed lavas, *in* H.J. Stein and J.L. Hannah, eds., Ore-Bearing Granite Systems: Petrogenesis and Mineralizing Processes: Geological Society of America Special Paper 246, p. 251-261.

Ekren, E.B., D.H. McIntyre, and E.H. Bennett, 1984, High-temperature, large-volume, lavalike ash-flow tuffs without calderas in southwestern Idaho: U.S. Geological Survey Professional Paper 1272, 76 p.

Ekren, E.B., D.H. McIntyre, E.H. Bennett, and H.E. Malde, 1981, Geologic map of Owyhee County, Idaho, west of longitude 116 degrees W: U.S. Geological Survey Miscellaneous Geologic Investigations Map I-256, scale 1:125,000.

Ekren, E.B., D.H. McIntyre, E.H. Bennett, and R.F. Marvin, 1982, Cenozoic stratigraphy of western Owyhee County, Idaho, *in* Bill Bonnichsen and R.M. Breckenridge, eds., Cenozoic Geology of Idaho: Idaho Bureau of Mines and Geology Bulletin 26, p. 215-235.

Evans, J.G., J.D. Hoffman, D.M. Kulik, and J.M. Linne, 1987, Mineral resources of the Owyhee Canyon Wilderness Study Area, Malheur County, Oregon: U.S. Geological Survey Bulletin 1719E, 18 p.

Fink, J.H., 1980, Gravity instability in the Holocene Big and Little Glass Mountain rhyolitic obsidian flows, northern California: Tectonophysics, v. 66, p. 147-166.

Foord, E.F., M.J. Luessen, D.S. Hovorka, J.L. Plesha, V.J.S. Grauch, Harlan Barton, H.D. King, D.O. Capstick, R.T. Mayerle, A.R. Buehler, and P.N. Gabby, 1987, Mineral resources of the Owyhee Canyon and South Fork Owyhee River Wilderness Study Areas, Elko County, Nevada, and Owyhee County, Idaho: U.S. Geological Survey Bulletin 1719F, 20 p.

Gansecki, C.A., G.A. Mahood, and M.O. McWilliams, 1996, $^{40}Ar/^{39}Ar$ geochronology of rhyolites erupted following collapse of the Yellowstone Caldera, Yellowstone Plateau volcanic field: Implications for crustal contamination: Earth and Planetary Science Letters, v. 142, p. 91-108.

Goeldner, C.A., M.G. Sawlan, H.D. King, R.A. Winters, A.M. Leszcykowski, and D.E. Graham, 1986, Mineral resources of the Battle Creek, Yatahoney Creek, and Juniper Creek Wilderness Study Areas, Owyhee County, Idaho: U.S. Geological Survey Bulletin 1719B, 10 p.

Green, J.C., and T.J. Fitz III, 1993, Extensive felsic lavas and rheoignimbrites in the Keweenawan Midcontinent Rift plateau volcanics, Minnesota: Petrographic and field recognition: Journal of Volcanology and Geothermal Research, v. 54, p. 177-196.

Hart, W.K., J.L. Aronson, and S.A. Mertzman, 1984, Areal distribution and age of low K, high-alumina olivine tholeiite magmatism in the northwestern Great Basin, U.S.A.: Geological Society of America Bulletin, v. 95, p. 186-195.

Hart, W.K., and R.W. Carlson, 1983, K-Ar ages of late Cenozoic basalts from southeastern Oregon, southwestern Idaho, and northern Nevada: Isochron/West, no. 38, p. 23-26.

———, 1985, Distribution and geochronology of Steens Mountain-type basalts from the northwestern Great Basin: Isochron/West, no. 43, p. 5-10.

Henry, C.E., J.G. Price, J.N. Rubin, and S.E. Laubach, 1990, Case study of an extensive silicic lava: The Bracks Rhyolite, Trans-Pecos Texas: Journal of Volcanology and Geothermal Research, v. 43, p. 113-132.

Henry, C.E., J.G. Price, J.N. Rubin, D.F. Parker, J.A. Wolff, Stephen Self, Richard Franklin, and D.A. Barker, 1988, Widespread, lavalike silicic volcanic rocks of Trans-Pecos Texas: Geology, v. 16, p. 509-512.

Henry, C.E., and J.A. Wolff, 1992, Distinguishing strongly rheomorphic tuffs from extensive silicic lavas: Bulletin of Volcanology, v. 54, p. 171-186.

Hildreth, Wes, R.L. Christiansen, and J.R. O'Neil, 1984, Catastrophic isotopic modification of rhyolitic magma at times of caldera subsidence, Yellowstone Plateau volcanic field: Journal of Geophysical Research, v. 89, p. 8339-8369.

Honjo, Norio, Bill Bonnichsen, W.P. Leeman, and J.C. Stormer, Jr., 1992, Mineralogy and geothermometry of high-temperature rhyolites from the central and western Snake River Plain: Bulletin of Volcanology, v. 54, p. 220-237.

Hope, R.A., and R.R. Coats, 1976, Preliminary geologic map of Elko County, Nevada: U.S. Geological Survey Open-File Report 76-779, scale 1:100,000.

Leeman, W.P., J.S. Oldow, and W.K. Hart, 1992, Lithosphere-scale thrusting in the western U.S. Cordillera as constrained by Sr and Nd isotopic transitions in Neogene volcanic rocks: Geology, v. 20, p. 63-66.

Lowenstern, J.B., 1995, Applications of silicate melt inclusions to the study of magmatic volatiles, *in* J.F.H. Thompson, ed., Magmas, Flu-

ids and Ore Deposits: Mineralogical Association of Canada Short Course 23, p. 71-99.

Manley, C.R., 1992, Extended cooling and viscous flow of large, hot rhyolite lavas: Implications of numerical modeling results: Journal of Volcanology and Geothermal Research, v. 53, p. 27-46.

———, 1994a, On voluminous rhyolite lava flows: Arizona State University Ph.D. dissertation, 314 p.

———, 1994b, Rhyolitic fire-fountaining on the Owyhee Plateau, SW Idaho: Very low-H_2O magmas from higher-H_2O magmatic systems (abs.): Eos, Transactions, American Geophysical Union, v. 75, p. 751.

———, 1995, How voluminous rhyolite lavas mimic rheomorphic ignimbrites: Eruptive style, emplacement conditions, and formation of tuff-like textures: Geology, v. 23, p. 349-352.

———, 1996a, Physical volcanology of a voluminous rhyolite lava flow: The Badlands lava, Owyhee Plateau, SW Idaho: Journal of Volcanology and Geothermal Research, v. 71, p. 129-153.

———, 1996b, In situ formation of welded tuff-like textures in the carapace of a voluminous silicic lava flow, Owyhee County, SW Idaho: Bulletin of Volcanology, v. 57, p. 672-686.

———, 1996c, Rhyolitic fire-fountains, low pre-eruptive volatile contents, and petrogenesis by wall-rock melting (abs.): Eos, Transactions, American Geophysical Union, v. 77, p. 818.

———, 1996d, Morphology and maturation of melt inclusions in quartz phenocrysts from the Badlands rhyolite lava flow, southwestern Idaho: American Mineralogist, v. 81, p. 158-168.

McIntosh, W.C., 1999, $^{40}Ar/^{39}Ar$ analytical data from the Juniper Mountain volcanic center, Owyhee County, southwestern Idaho: New Mexico Bureau of Geology and Mineral Resources Open File AR-4, 20 p.

McIntosh, W.C., and R.M. Chamberlin, 1994, $^{40}Ar/^{39}Ar$ geochronology of Middle to Late Cenozoic ignimbrites, mafic lavas, and volcaniclastic rocks in the Quemado Region, New Mexico: New Mexico Geological Society Guidebook, v. 45, p. 165-185.

Minor, S.A., H.D. King, D.M. Kulik, D. Sawatzky, and D.O. Capstick, 1987, Mineral resources of the Upper Deep Creek Wilderness Study Area, Owyhee County, Idaho: U.S. Geological Survey Bulletin 1719G, 14 p.

Minor, S.A., D. Sawatzky, and A.M. Leszcykowski, 1986, Mineral resources of the North Fork Owyhee River Wilderness Study Area, Owyhee County, Idaho: U.S. Geological Survey Bulletin 1719A, 9 p.

Morgan, L.A., D.J. Doherty, and W.P. Leeman, 1984, Ignimbrites of the eastern Snake River Plain—Evidence for major caldera-forming eruptions: Journal of Geophysical Research, v. 89, p. 8665-8678.

Nash, W.P., M.E. Perkins, J.N. Christensen, D.-C. Lee, and A.N. Halliday, 1996, Temporal variation in $^{143}Nd/^{144}Nd$ and $^{176}Hf/^{177}Hf$ in silicic magmas of the Yellowstone hotspot (abs.): Eos, Transactions, American Geophysical Union, v. 77, suppl., p. 823.

Perkins, M.E., F.H. Brown, W.P. Nash, William McIntosh, and S.K. Williams, 1998, Sequence, age, and source of silicic fallout tuffs in Middle to Late Miocene basins of the northern Basin and Range Province: Geological Society of America Bulletin, v. 110, p. 344-360.

Perkins, M.E., W.P. Nash, F.H. Brown, and R.J. Fleck, 1995, Fallout tuffs of Trapper Creek, Idaho—A record of Miocene explosive volcanism in the Snake River Plain volcanic province: Geological Society of America Bulletin, v. 107, p. 1484-1506.

Peterson, J.A., W.D. Heran, and A.M. Leszcykowski, 1986, Mineral resources of the North Fork of the Little Humboldt River Wilderness Study Area, Humboldt County, Nevada: U.S. Geological Survey Bulletin 1732A, 10 p.

Pierce, K.L., and L.A. Morgan, 1992, The track of the Yellowstone hot spot: Volcanism, faulting, and uplift, *in* P.K. Link, M.A. Kuntz, and L.B. Platt, eds., Regional Geology of Eastern Idaho and Western Wyoming: Geological Society of America Memoir 179, p. 1-53.

Rodgers, D.W., W.R. Hackett, and H.T. Ore, 1990, Extension of the Yellowstone Plateau, eastern Snake River plain, and Owyhee Plateau: Geology, v. 18, p. 1138-1141.

Rytuba, J.J., and E.H. McKee, 1984, Peralkaline ash flow tuffs and calderas of the McDermitt volcanic field, southeast Oregon and north central Nevada: Journal of Geophysical Research, v. 89, p. 8616-8628.

Samson, S.D., and C.E. Alexander, 1987, Calibration of the interlaboratory $^{40}Ar/^{39}Ar$ dating standard, Mmhb-1: Isotope Geoscience, v. 66, p. 27-34.

Sawlan, M.G., H.D. King, J.D. Hoffman, D.M. Kulik, P.N. Gabby, D.O. Capstick, and A.R. Buehler, 1987, Mineral Resources of the Owyhee River Canyon and Deep Creek-Owyhee River Wilderness Study Areas, Owyhee County, Idaho: U.S. Geological Survey Bulletin 1719D, 12 p.

Steiger, R.H., and E. Jaeger, 1977, Subcommission on geochronology: Convention on the use of decay constants in geo- and cosmochronology: Earth and Planetary Science Letters, v. 36, p. 359-362.

Stewart, J.H., and J.E. Carlson, 1978, Geologic map of Nevada: U.S. Geological Survey, scale 1:500,000.

Taubeneck, W.H., 1971, Idaho batholith and its southern extension: Geological Society of America Bulletin, v. 82, p. 1899-1928.

Tolan, T.L., S.P. Reidel, M.H. Beeson, J.L. Anderson, K.R. Fecht, and D.A. Swanson, 1989, Revisions to the estimates of the areal extent and volume of the Columbia River Basalt Group, *in* S.P. Reidel and P.R. Hooper, eds., Volcanism and Tectonism in the Columbia River Flood-Basalt Province: Geological Society of America Special Paper 239, p. 1-20.

Walker, G.W., and N.S. MacLeod, 1991, Geologic map of Oregon: U.S. Geological Survey, scale 1:500,000.

Walker, G.W., and C.A. Repenning, 1966, Reconnaissance geologic map of the west half of the Jordan Valley quadrangle, Malheur County, Oregon: U.S. Geological Survey Miscellaneous Geologic Investigations Map I-457, scale 1:250,000.

Wallace, A.R., R.L. Turner, V.J.S. Grauch, J.L. Plesha, M.D. Krohn, J.S. Duval, and P.N. Gabby, 1988, Mineral resources of the Little Humboldt River Wilderness Study Area, Elko County, Nevada: U.S. Geological Survey Bulletin 1732B, 20 p.

Webster, J.D., and W.A. Duffield, 1991, Volatiles and lithophile elements in Taylor Creek Rhyolite: Constraints from glass inclusion analysis: American Mineralogist, v. 76, p. 1628-1645.

———, 1994, Extreme halogen abundances in tin-rich magma of the Taylor Creek Rhyolite, New Mexico: Economic Geology, v. 89, p. 840-850.

Willden, Ronald, 1961, Preliminary geologic map of Humboldt County, Nevada: U.S. Geological Survey Mineral Investigations Field Studies Map MF-236, scale 1:200,000.

CHAPTER THREE

Products of Basaltic Volcanism

Basalt flows in the walls of Bruneau Canyon at Scenic View.

Salmon Butte, a cinder and spatter cone near Rogerson.

Castle Butte, a tuff cone near Grand View.

The tuff and cinder vent of the Seventy One Gulch volcanic field, near Bruneau.

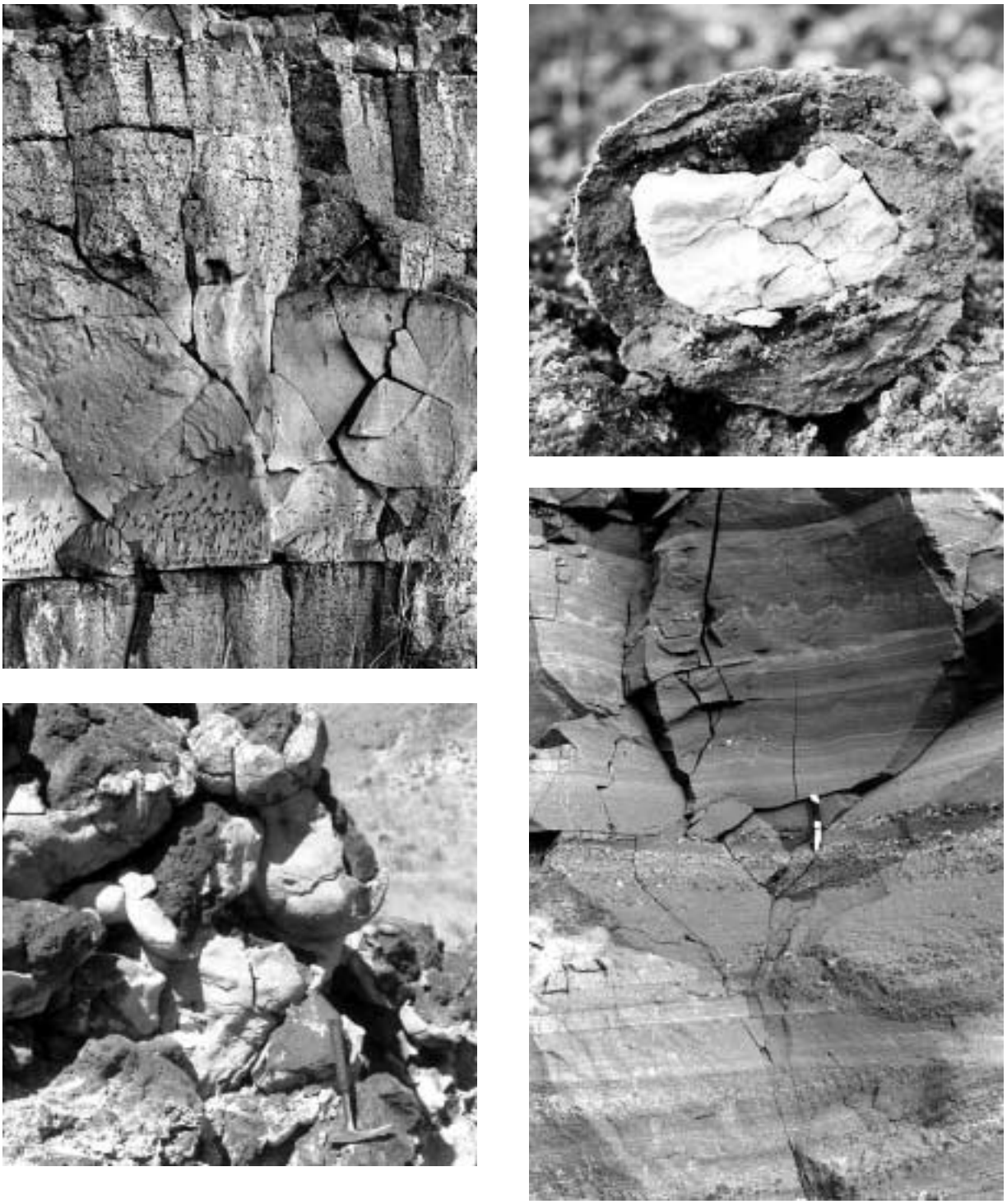

(Clockwise from top left)*: A thin basalt flow. Basaltic bomb cored by sediments. Phreatomagmatic tuffs erupted from Sinker Butte. Basalt pillows with limestone overgrowths.*

Tindall homestead, Marys Creek.

Stone building at Black Rock Crossing, Bruneau Canyon.

Wickahoney ranch house, near Wickahoney Creek.

Late Miocene, Pliocene, and Pleistocene Geology of Southwestern Idaho With Emphasis on Basalts in the Bruneau-Jarbidge, Twin Falls, and Western Snake River Plain Regions

Bill Bonnichsen[1] and Martha M. Godchaux[2]

ABSTRACT

In southwestern Idaho, the development of the Snake River Plain (SRP) and its basaltic volcanism followed a succession of Eocene, Oligocene, and middle Miocene volcanic events. Then in the late Miocene, about 1 to 3 million years before the outpourings of basalt began, an astonishing amount of rhyolitic volcanism dominated the early evolution of the SRP. These rhyolite eruptions formed a major part of the Yellowstone hotspot track. The SRP basaltic volcanism that followed the rhyolite eruptions shows a complex development pattern. The early (about 10-5 Ma), widely distributed part formed mainly from subaerial eruptions of high-Al (most primitive), Al-enhanced, and SROT basalt that resulted in small shields and elongate subaerial flows. Such basalts cap much of the plateaus and plains of the Bruneau-Jarbidge and Twin Falls regions. The later (about 5 Ma or less) part of the basaltic volcanism, however, mainly accompanied the western SRP rifting. The area affected by these later eruptions cuts across the hotspot track in the northern parts of the Bruneau-Jarbidge and Twin Falls regions. These later eruptions were dominated by Fe-enhanced basalt, ferrobasalt (most evolved), and alkali-rich basalt.

In the western SRP rift where a large lake, Lake Idaho, existed for several million years, basalt erupted between about 9-7 Ma and 2.2-0.4 Ma and was deposited in highly varied fashions determined by the availability of water. The eruptions ranged from effusive to very explosive, and the results include subaerial flows, water-affected basalt, pillow deltas, fragmental subaqueous basalt accumulations, and a variety of basaltic tuffs. Much of the 9-7 Ma basalt was erupted subaqueously and some apparently in rather deep water. The extrusion of this basalt likely accompanied the most pronounced period of NE-SW extension during which the rift-basin mainly formed. Between 7 and about 2.2 Ma, only minor amounts of basalt were erupted in the western SRP, although much was being erupted in the adjacent Twin Falls and Bruneau-Jarbidge regions.

Starting at about 2.2 Ma, basalt again was erupted abundantly in the western SRP and continued until about 0.4 Ma. Simultaneously, Lake Idaho gradually drained and was replaced by river systems that eventually cut deep canyons. During this time, the style of volcanism changed from subaqueous and emergent eruptions that formed tuff cones, subaqueous pillow-basalt deposits and debris-flows of basaltic tuff to subaerial eruptions that formed maars, tuff rings, and pillow deltas where subaerially erupted basalt flowed into lakes and streams. As the area dried out, the volcanic style changed to the formation of cinder and spatter cones and small shields that emitted subaerial flows. During the Pleistocene, the basalt became more and more iron-rich. Between about 1.2 and 0.8 Ma, nearly all the materials being erupted were ferrobasalt. At about 0.8 Ma, the composition changed again, to basalt low in iron but enriched in alkalis. Deformation of basalt flows and associated lake sediments, both by faulting and tilting of originally subhorizontal layers, lasted until as recent as a million years ago.

Key words: basalt, Bruneau-Jarbidge eruptive cen-

Editors' note: The manuscript was submitted in December 2003.

[1]Idaho Geological Survey, Morrill Hall, Third Floor, University of Idaho, Moscow, ID 83844-3014

[2]Department of Geography and Geology, Mount Holyoke College, South Hadley, MA 01075

Bonnichsen, Bill, and M.M. Godchaux, 2002, Late Miocene, Pliocene, and Pleistocene geology of southwestern Idaho with emphasis on basalts in the Bruneau-Jarbidge, Twin Falls, and western Snake River Plain regions, *in* Bill Bonnichsen, C.M. White, and Michael McCurry, eds., Tectonic and Magmatic Evolution of the Snake River Plain Volcanic Province: Idaho Geological Survey Bulletin 30, p. 233-312.

ter, ferrobasalt, maars, phreatomagmatic volcanism, shields, Snake River Plain, Twin Falls eruptive center, tuff rings, western Snake River Plain rift

INTRODUCTION

The Snake River Plain (SRP) volcanic province has several tectonic subdivisions (Figure 1), including physiographic areas that are the result of crustal extension, massive amounts of rhyolitic volcanism, and features that may have resulted from deep-seated magma injection or removal. The province is a topographically depressed and elongated feature that developed progressively from southwest to northeast likely in response to the southwestward passage of the North American plate over a deeper zone in the Earth from which copious amounts of magma were being generated, e.g., the Yellowstone hotspot. The younger eastern part of the province is a more marked topographic depression than is the older southwestern part, commonly referred to as the Owyhee Plateau. Together, the two are thought to show the trace of where North America rode over the Yellowstone hotspot.

The wide valley of the SRP curves like a broad smile across southern Idaho. Its eastern part is the eastern SRP near the younger Yellowstone area. The western part, however, diverges from the hotspot track to follow a wide, southeast-to-northwest-trending valley known as the western Snake River Plain. The western SRP valley coincides with a fault-bounded, topographically depressed complex graben, or rift. The rift evolved over a fairly long period, has much internal variation in vertical displacement, and was a zone along which significant quantities of volcanic rock were erupted. The western SRP rift, as it evolved, was the site of pull-apart stretching of the crust, so that the final crustal zone is considerably wider than when it started. These, then, are the three main elements of the SRP volcanic province in southwestern Idaho: the Owyhee Plateau, the southwestern part of the eastern SRP, and the western SRP graben or rift, which extends almost perpendicularly from the main SRP hotspot trend. The part of the SRP volcanic province where these three elements converge commonly is called the central SRP (Figure 1, inset).

Voluminous rhyolitic volcanism occurred in southwestern Idaho and vicinity as the southwestern part of the SRP developed. This happened principally in three main stages as the three large zones referred to as the Owyhee-Humboldt, Bruneau-Jarbidge, and Twin Falls eruptive centers were successively formed from about 14 to 8 million years ago. Each eruptive center appears to have the form of a broad structural basin filled with volcanic and younger sedimentary deposits. Where the margins of the eruptive centers are exposed, faults are revealed that indicate downward displacement of the interiors of the basins relative to their surroundings. Through most of their extents, however, these basins have not been eroded deeply enough to clearly show their margins. These eruptive centers are mainly filled with large volumes of rhyolitic and basaltic ejecta, and much of the subsidence associated with their interiors probably occurred during and immediately after the volcanism. In their structural and volcanic attributes, the eruptive centers are seen to be very much like calderas, except that they are larger than most calderas. Each eruptive center likely was developed from several caldera-forming eruptions that collectively gave rise to the broad basins that now constitute the axis of the elongate SRP volcanic province, and that extend northeastward as a series of younger buried calderas to the Yellowstone area.

The SRP hotspot track progressively developed from southwest to northeast (Pierce and Morgan, 1992; Pierce and others, this volume). This happened primarily between about 14 Ma ago and the present. The process followed a major regional magmatic episode that included the development of most of the Columbia River Basalt Group and the eruption of other large basaltic and rhyolitic volcanic groups in Idaho and adjacent regions of Washington, Oregon, and Nevada about 17 to 14 Ma ago. Within the immediate vicinity of the SRP province, volcanism during this period formed the lower basalts and latites and the Silver City rhyolite group in the Owyhee Range (Ekren and others, 1981, 1984) and a thick sequence of rhyolitic lavas and intercalated ignimbrites in the Jarbidge Range of north-central Nevada (Coats, 1964). These volcanic rocks are the time equivalents to the Columbia River Basalt Group. Many geologists believe that this massive volcanic episode between 17 and 14 Ma was related to the initial interaction of the Yellowstone hotspot and the base of the lithosphere, and that the later development of the hotspot track toward the northeast along the trace of the Owyhee Plateau, the eastern SRP, and the Yellowstone area was a continuation of that process.

The objective of this paper is to broadly describe the geologic features of southwestern Idaho and the basaltic volcanism associated with the evolution of the SRP in much of the region. We have prepared a comprehensive conceptual framework for understanding the SRP-associated basalts of southwestern Idaho on the basis of stratigraphy and age, chemical variations, physical volcanology, and the geologic environment into which they were erupted.

GEOLOGIC SETTING

Exposed in the highlands surrounding the central and

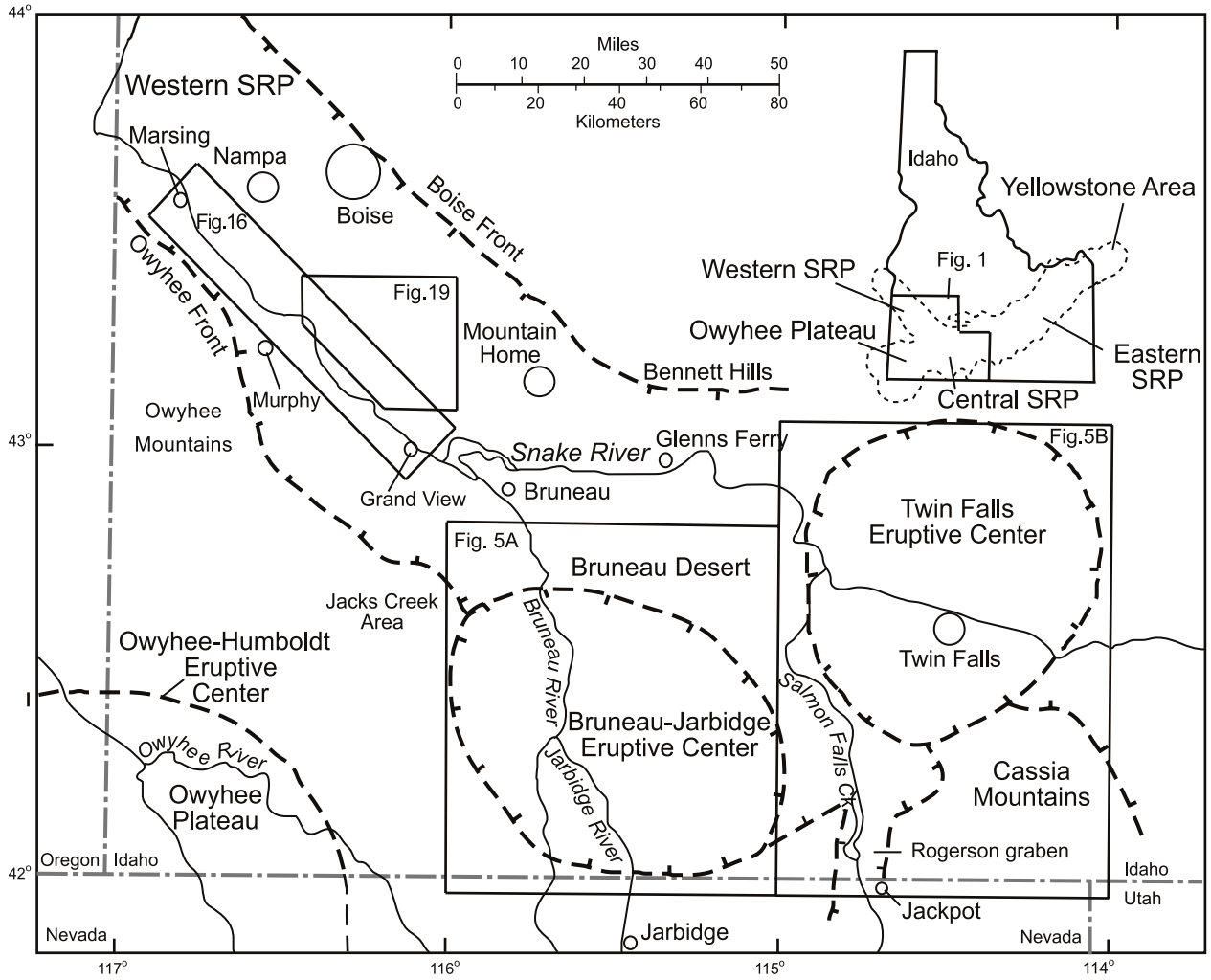

Figure 1. Index map of southwestern Idaho.

western SRP and the Owyhee Plateau are several rock groups that are older than the SRP. These include Paleozoic and Mesozoic marine sedimentary rocks, Cretaceous and Eocene dioritic to granitic plutons, and Eocene, Oligocene, and Miocene volcanic rocks. Except for the Paleozoic and Mesozoic sedimentary rocks, the main groups of pre-SRP rocks are summarized in the stratigraphic columns in Figure 2. The oldest rocks shown are granitic; those in the Owyhee Mountains region adjacent to the western SRP, the Silver City granite, are generally considered to be part of the Idaho batholith, whereas those in northern Nevada adjacent to the Bruneau-Jarbidge region are not. Granitic rocks of the Idaho batholith occur north of the central SRP and part of the western SRP, so granitic rocks likely occur at depth beneath much of southwestern Idaho.

Eocene volcanic rocks of intermediate and silicic composition occur at a few localities around the margins of the SRP province. These rocks are similar in age and composition to the Challis Volcanics of central Idaho and probably represent a southward continuation of that volcanic province. The Eocene volcanic rocks include the thick mass of dacitic welded pyroclastic material in the Rough Mountain area on the south side of the western SRP (Ekren and others, 1981), the Bieroth Volcanics in northernmost Nevada just south of the Idaho border in the Bruneau Canyon area (Bushnell, 1967; Bernt and Bonnichsen, 1982), and several occurrences in the Bennett Mountain area north of the central SRP (Malde and others, 1963; Worl and others, 1991). A relatively small area of Oligocene volcanic rocks, the Salmon Creek Volcanics (Figure 2), are in the northwestern part of the Owyhee Mountains. They generally are andesitic in composition (Ekren and others, 1981).

During the middle Miocene, volcanism in the Owyhee Mountains and in the Jarbidge Mountains in northern

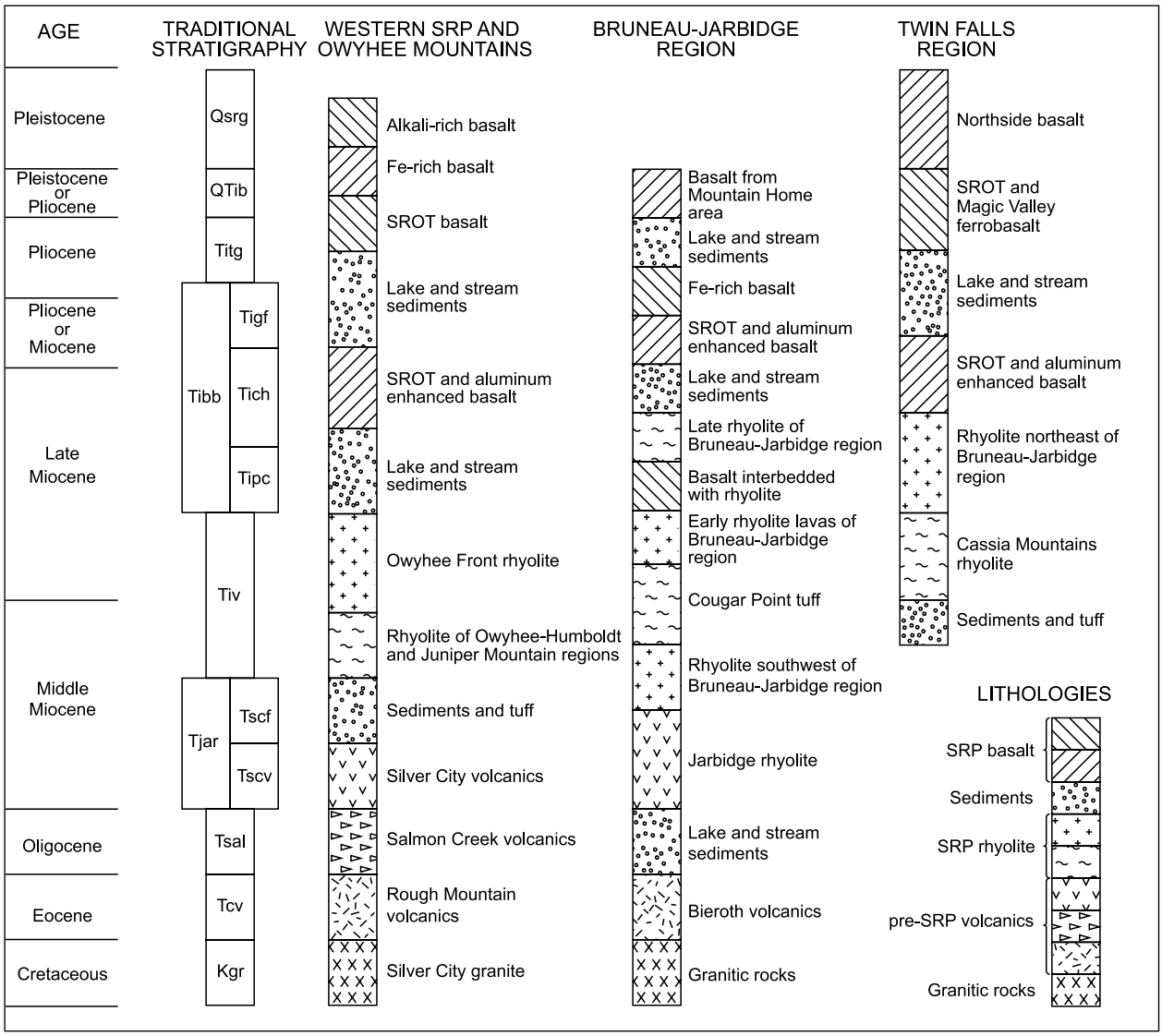

Figure 2. Stratigraphic columns for the western SRP and Owyhee Mountains, the Bruneau-Jarbidge region, and the Twin Falls region compared to the traditional stratigraphy of southwestern Idaho. The traditional stratigraphic units are identified as follows: Qsrg—Snake River Group, QTib—Bruneau Formation of the Idaho Group, Titg—Tuanna Gravel and Tenmile Gravel of the Idaho Group, Tigf—Glenns Ferry Formation of the Idaho Group, Tich—Chalk Hills Formation of the Idaho Group, Tipc—Poison Creek Formation of the Idaho Group, Tibb—Banbury Basalt of the Idaho Group, Tiv—Idavada Volcanics, Tscf—Sucker Creek Formation, Tscv—Silver City volcanics, Tjar—Jarbidge rhyolite, Tsal—Salmon Creek volcanics, Tcv—Challis Volcanics, Kgr—granitic rocks. Sources include Stearns and others (1938), Malde (1991), Malde and Powers (1962, 1972), Malde and others (1963), Armstrong and others (1975), Kimmel (1982), Swirydczuk and others (1982), Bonnichsen (1982a, 1982b), Bonnichsen and Citron (1982), Ekren and others (1981), Williams and others (1990, 1991), Covington and Weaver (1989, 1990a, 1990b, 1990c, 1991), and Lindholm, 1996). SROT is Snake River olivine tholeiite.

Nevada produced an abundance of rhyolite and basalt. In the Owyhee Mountains, this period of volcanism consisted of earlier basaltic eruptions, mainly between 17 Ma and 16 Ma, followed by rhyolite eruptions, mostly as domes, mainly between 16 Ma and 15 Ma. In adjacent parts of Malheur County, Oregon, voluminous rhyolitic volcanism occurred during this time and also formed several calderas (Ferns and others, 1993a, 1993b; Cummings and others, 2000). The 17-16 Ma basalts also are quite voluminous and apparently erupted mainly from north-south dikes. The basalts were accompanied by modest amounts of ferrolatite, latite, and andesite. Along the western side of the northern part of the Owyhee Mountains, the middle Miocene basalts have been cut by several north-south normal faults and a series of westward-tilted blocks formed presumably as a result of east-west

directed extension. North of the western SRP, similarly faulted and tilted basalts occur in the Horseshoe Bend region and continue much farther north, almost to Lewiston. In both areas, the faulted and westward-tilted zones of the Columbia River Basalt Group lie immediately west of the exposed western margin of the Idaho batholith (Figure 3, lower panel).

At the end of the middle Miocene and throughout most of the late Miocene, an enormous amount of rhyolitic volcanism associated with the development of the SRP occurred in southwest Idaho and vicinity. Most of this happened between about 14.5 and 6.0 million years ago. Well over half of the known volume of rhyolite in the SRP-Yellowstone Province was erupted during this time in the form of large-volume, high-temperature ignimbrites that constitute most of the volume and numerous accompanying rhyolite lava flows that make up the rest. Moreover, most of this volume actually was erupted in a narrower time range, between about 12.0 and 10.0 million years ago, that has been referred to as the "ignimbrite flare-up" (Perkins and others, 1995). Detailed consideration of the nature and causes of the rhyolitic volcanism is beyond the scope of this paper; however, brief summaries of the main aspects of the SRP-associated rhyolitic volcanism in various parts of the SRP are included in the discussions of the different parts of the region.

Starting at about 11.7 Ma, the rhyolitic volcanism associated with the western SRP rift got underway with the eruption of rhyolitic lavas along the southwestern margin of what is now the western SRP rift. When this volcanism started, there already was some sort of widespread lake in the region (Godchaux and Bonnichsen, this volume). This pulse of rhyolitic volcanism was contemporaneous with, and contiguous to, the developing Bruneau-Jarbidge eruptive center to the southeast. Also about this time, there was a general rotation in the apparent extensional stress directions in southwestern Idaho. This can be seen in the orientation of normal faults of different ages on regional geologic maps, such as the one by Ekren and others (1981). Before this time, the extension direction generally was oriented east-west, but afterward the extension direction was oriented about northeast-southwest, subparallel to the direction that the Yellowstone hotspot track eventually would follow.

Sometime after the extension-direction orientation had changed to northeast-southwest, the stretching of the crust in southwest Idaho commenced as the Bruneau-Jarbidge eruptive center was being formed over the hotspot. Eventually this northeast-southwest stretching led to rifting of the western SRP region, with widening in the range of several to perhaps more than 10 km. At present, it is unclear exactly when this northeast-southwest widening

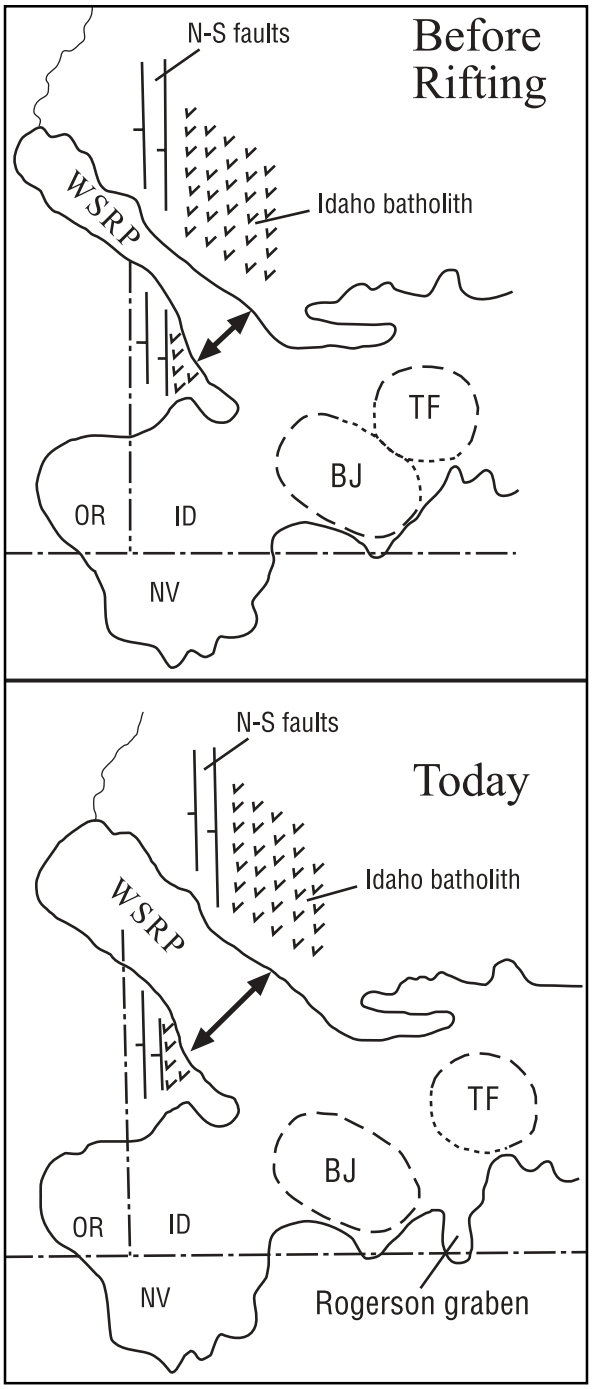

Figure 3. Diagram showing the effect of rifting on the western Snake River Plain. The upper panel is the region before the major late Miocene rifting, and the lower panel is the region today. The extension direction is southeast-northwest, parallel to the arrows. This extension offset the zone of north-south faults and the western edge of the Idaho batholith on opposite sides of the western Snake River Plain (WSRP). The Bruneau-Jarbidge (BJ) and Twin Falls (TF) eruptive centers would essentially have been one large structural basin before the late Miocene rifting. The development of the Rogerson graben probably represents part of the extension on the south side of the SRP that occurred during the southwest-northeast widening of the western SRP.

started, how many episodes there might have been, and what was the total amount of extension. However, by using north-south elongate structural markers and assuming that they initially were straight-line features, the amount of extension can be estimated (Figure 3). The amount of extension might roughly range between 20 and 40 percent of the present width of the western SRP. The structural markers are the western margin of the Idaho batholith and the zone of tilted, middle Miocene fault blocks immediately west of the batholith. Much of the widening probably occurred during the 9 to 7 Ma period when a large amount of basaltic volcanism occurred in the western SRP. There may have been some widening before this, and some has likely occurred as recently as about a million years ago, based on the apparent ages of faults and folds that deform basalt flows and sediments within the western SRP. The amount of widening seems to vary along the length of the western SRP, with more in the southeastern part where the rift merges into the main SRP.

In addition, the zone of rifting likely does not stop at the margin of the main SRP. Rather, we suggest that such a zone of widening continues into and across the main SRP hotspot track to merge with extensional features associated with the Basin and Range Province immediately to the south. The Rogerson graben likely was produced during this general extension event. The interior of the central SRP likely underwent as much or more stretching as has occurred in the western SRP, but it is largely unrecognized because the extended part of the central SRP is buried under later, largely undeformed sediments and young basalt flows. If the above is essentially correct, then the present positions of the Bruneau-Jarbidge and Twin Falls eruptive centers, as shown in Figure 1, have been modified from where these large features initially were formed relative to one another. The crude reconstruction of their relative positions in the upper, before rifting, panel of Figure 3 suggests that the Twin Falls center may simply have been the continuation to the northeast of the zone of collapse that started in the Bruneau-Jarbidge region, and that there is not as much significance to the integrity of these individual eruptive centers as we and other geologists have assumed in the past. Regardless, the rest of our paper will follow the concept that these eruptive centers have enough of their original validity so as to form a reasonable geologic framework into which the SRP basalts can be fitted for descriptive purposes. Thus, our discussion of the distribution of SRP basalt in southwest Idaho is organized into basaltic volcanism associated with (1) the Bruneau-Jarbidge region, (2) the Twin Falls region, and (3) the western SRP region.

THE PHYSICAL NATURE OF BASALTIC VOLCANISM IN SOUTHWESTERN IDAHO

In southwestern Idaho, SRP basaltic volcanism has been occurring sporadically for the past 11.5 to 12.0 Ma. It has appeared in different areas at different times, and the basalt composition has varied as the SRP volcanic system has evolved. Much of the volcanism is associated with the last part of the igneous development in the Owyhee-Humboldt, the Bruneau-Jarbidge, and the Twin Falls regions along the southwest-northeast axis of the SRP hot-spot track. The rest of the volcanism is associated with the development of the western SRP rift. The basalt that erupted in the Owyhee-Humboldt and Bruneau-Jarbidge regions formed subaerial flows and shield volcanoes scattered about on the Owyhee Plateau. The eruptions in the western SRP and Twin Falls regions formed a wider variety of volcano and flow types because lakes were present during some of the volcanism. Much of this volcanism is younger than, and differs somewhat chemically from, the basalts of the Owyhee Plateau region, although considerable overlap in time and composition occurs.

MINERALOGY AND TEXTURES

The SRP basalts of southwestern Idaho are similar in their mineralogy but vary in their textural and structural attributes. The phenocryst minerals are olivine and plagioclase. Olivine phenocrysts typically range from Fo_{85} to Fo_{60}, and plagioclase phenocrysts from An_{80} to An_{60}. Groundmass olivines are as iron-rich as Fo_{40}, and groundmass plagioclases are as sodic as An_5 (Leeman, 1982). Either or both of these minerals may be present as phenocrysts in a given flow, and they vary widely in abundance and size from flow to flow, and even within individual flows. In some basalts, olivine and plagioclase appear as single crystals, whereas in other basalts either or both occur in cumulophyric aggregates. In some rocks they are clearly xenocrysts. Pyroxenes and other minerals that commonly occur as phenocrysts in basalt have not been seen as phenocrysts in the hundreds of flows that we have investigated in the SRP region.

Groundmass material in the SRP basalts includes abundant pyroxenes (principally clinopyroxenes with generally subcalcic augite compositions), opaque oxide minerals (principally intermediate members of the ilmenite-hematite and magnetite-ulvospinel-chromite-spinel solid solution series), plagioclase (commonly as microphenocrysts), olivine, and interstitial glass of varying color and composition. Other minerals might occur

in small amounts in southwest Idaho basalts, but we have not found them in our admittedly meager petrographic investigations. Although many basalt flows contain plagioclase xenocrysts, and some contain olivine xenocrysts, xenoliths are rare and nearly always are fragments of rocks that occur very near the Earth's surface. Basalt fragments are the most common xenolith type, and most appear to be earlier-formed cognate fragments of the enclosing basalt. At phreatomagmatic vents, lithic fragments of near-surface sediments commonly have been entrained in basaltic cinder and spatter deposits. We have seen no ultramafic inclusions and very rarely gabbros as inclusions.

VOLCANOES

In the western SRP, Owyhee Plateau, and central SRP, nearly all basalt volcanoes are monogenetic. These have many forms, including simple and complex shields; dike vents; cinder-, spatter-, and tuff-cones and rings; maars; and subaqueous vent complexes. As we have used the terms, simple shields have erupted from a single point or from points distributed along a linear zone, whereas complex shields have erupted from several points that generally are distributed in a nonlinear fashion. The shields and dike vents were formed mainly by Icelandic and Hawaiian style eruptions in relatively dry subaerial environments and produced lava flows. In some instances, the subaerial lavas flowed over wet ground or into bodies of water to form pillow basalts of various types and hydrated basalt referred to as water-affected basalt (WAB) where sufficient time allowed the hot lava and surface water to interact. The cinder and spatter cones were formed mainly during Strombolian style eruptions in subaerial environments that might have been a little wetter than where shields were formed. Lava flows were erupted from some of the cinder and spatter cones. Maars and tuff rings were formed mainly by Surtseyan and Taalian styles of phreatomagmatic eruptions sometimes combined with Strombolian style magmatic eruptions in subaerial environments where a substantial amount of meteoric water, mainly ground water, was available. Tuff cones constructed from mixtures of basaltic tuff, cinders, spatter, and perhaps accompanying small lava flows generally formed in emergent environments in which mainly Surtseyan style eruptions started in shallow water and during which the accumulated volcanic products built up to levels above the lake or river surface (Godchaux and others, 1992; Godchaux and Bonnichsen, this volume). Subaerial and perhaps subaqueous lava flows were erupted from the tuff cones. Subaqueous vents produced hyaloclastite and massive tuff-breccia deposits, accumulations of pillows and pillow fragments, and invasive blobs and flows. Subaqueous eruptions in shallow water probably were mainly Surtseyan, but those in deeper water likely consisted of the relatively effusive eruption of lava with little or no accompanying explosive activity.

Many of the geologic units that resulted from the basaltic volcanism consist primarily of lava flows. In most instances where the source volcano has been identified, these units carry the name of the source volcano: e.g., the basalt of Austin Butte. In other instances where the source is unknown or more than one source is involved, other names have been used, e.g., the basalt of Little Blue Table. In many instances, however, the products of one volcano or a few related volcanoes are diverse, including flows, spatter, cinders, and tuffs; we generally have used the term "volcanic complex" to collectively include all of these materials in the name of the resulting unit, e.g., Seventy One Gulch volcanic complex. In addition, groups of smaller but mappable units such as flows may be from related sources. For these groups, we commonly have used the descriptive terms "volcanic field" or "basalt field" to indicate this close relationship and to designate them as single entities for purposes of discussion, e.g., the Saylor Creek ferrobasalt field.

LAVA FLOWS

Hundreds of basalt flows associated with the evolution of the SRP volcanic province occur in southwestern Idaho. Perhaps two hundred of these have been traced back to the volcanoes from which they erupted, but many others, typically exposed in canyon walls at lower stratigraphic levels, have not. Most of the basalt flows were erupted under subaerial conditions from small shield volcanoes, typically 100 m or less high and 4 km or less in diameter. A smaller number of basalt flows were erupted from cinder and spatter cones and even tuff cones; these mainly occur in the western SRP. Several hundred kilometers of excellent canyon-wall exposures occur in southwestern Idaho, thus the interiors of many of the basalt flows are clearly exposed. Only a few of the volcanoes, however, have been eroded or faulted to the extent that their interiors are well exposed. In many places, basalt lavas ran into lakes and rivers, or were erupted in shallow to deep lake environments. A brief discussion of some of the results of these processes is given later in our section on the interaction of basaltic lava and water, and many more details are presented in the accompanying paper by Godchaux and Bonnichsen (this volume).

The southwestern Idaho basalt flows vary widely in length and volume. Some flows are only a few tens of meters long and have volumes of only a few thousand cubic meters. By contrast, other flows have been traced more than 50 km from their vents, and the largest single-source flows appear to have volumes as great as 20 cubic

km or more. The largest southwestern Idaho basalt units that erupted from single sources are mainly in the central SRP region, whereas many of the smallest units are concentrated in the western SRP. Individual basalt flows tend to be thin, typically between 2 m and 10 m thick, although a few considerably thicker ones have been noted. These thicker flows tend to be where lava may have been ponded near vents or in topographic depressions.

Both pahoehoe and aa flows have been noted, with most, by far, being pahoehoe. Throughout much of southwestern Idaho, the subaerial basaltic lavas erupted onto relatively flat ground and spread across gentle slopes away from their source vents. This has imparted a sheetlike character to many of the individual flows. A single flow of this type typically is only a few meters thick. Lava tubes similar to those in many eastern SRP flows do not occur in these thin sheet flows. For many basalt units erupted from a single vent, only a single sheet spread any distance from the vent. Closer to the volcanoes, however, two to several individual flows may be stacked on one another, even though all are from the same monogenetic volcano. In some situations, the stacking of flows represents a series of sheets that were emplaced into a topographic depression such as a canyon. In other situations, however, the stacking of flows from a single source implies pauses during the eruption sequence, so that later material flowed over previously solidified earlier flows from the same source. In many of these situations, the flows become progressively less voluminous upwards in the sequence from that particular source, so that in effect many of the shields appear to have formed as the last phase of a particular eruption, which likely started out as lava effusion from short fissures now buried beneath their shields.

Except in certain areas around the central axial zone of the western SRP and in the area north of the Snake River in the central SRP, few open lava tubes exist in the southwestern Idaho basalt flows, even though the flows in many regions clearly have spread many kilometers from their source vents. Only in the axial part of the western SRP are there lengthy, large-diameter, open lava tubes. These tubes likely resulted from slightly greater slopes at the time of eruption than in regions where the terrain is flatter. Throughout southwestern Idaho, surface features on the basalt lava flows are poorly exposed or have been eroded entirely. Furthermore, most flow tops at the Earth's surface typically are covered by loess or other sedimentary deposits, or soil and vegetation. In the canyon walls, however, many of the original basalt-flow surface features are preserved, along with many internal structural features of the flows. Although detailed studies of the internal features have not been made, our observations are consistent with sheet-flow emplacement. Evidently most molten lava transport took place in flow interiors, with solidification occurring both at the base and top of the sheet as the lava spread farther and farther from its source, rather than lava traveling mainly in tubes and levee-bounded channels. In this respect, the southwestern Idaho basalt flows differ somewhat from basalt flows described in many other places including the eastern SRP (Greeley, 1982; Kuntz and others, 1992) where the molten lava was distributed primarily in channels and tubes. As a consequence, many of the southwestern Idaho flows tend to be broader and thinner for a given length than those where the terrain was steeper at the time of eruption. Some basalt flows contain evidence of inflation and multiple-injection emplacement modes.

PYROCLASTIC DEPOSITS

Many of the basalt eruptions in southwest Idaho, and especially in the western SRP region, produced pyroclastic deposits, both in the vent areas and at distal locations. Some of these deposits were formed by subaerial eruptions, whereas others were formed by subaqueous or emergent eruptions in lacustrine environments to produce significant amounts of phreatomagmatic tuff. This diversity of environments and eruptive styles led to a corresponding variety of volcano forms, ranging from cinder and spatter constructs to maar and tuff ring complexes to tuff cones, as the eruptive environment ranged from relatively dry to relatively wet and the proportion and duration of phreatomagmatic activity waxed and waned. Cinder and spatter deposits, mainly at and near vents, probably record conditions of the modest availability of surface and ground water to facilitate the Strombolian style of low-intensity explosivity associated with such eruptions. In others instances, much more water was available, so that phreatomagmatic, strongly explosive, Surtseyan, Taalian, and perhaps even Vulcanian or Subplinian styles of eruptions occurred; such more energetic explosions were capable of spreading volcanic ash to distances much farther from the vents. More discussion of some of the phreatomagmatic eruptions in the western SRP region are presented in the accompanying paper by Godchaux and Bonnichsen (this volume). As a note of clarification, in this paper we have liberally used the term "spatter." As well as true spatter consisting of accumulations of pyroclastically emplaced lava clots, we include as spatter some deposits that might be referred to by others as thoroughly welded or sintered cinder, lapilli, or volcanic ash deposits.

A variety of basaltic pyroclastic deposits are associated with the explosive basaltic eruptions, especially in the western SRP region. Most of the preserved pyroclas-

tic eruptive products are proximal deposits, which accumulated at and near their vents, but some are distal deposits, which accumulated as much as tens of kilometers away. The proximal deposits consist of various tephra types. These include cinder and spatter accumulations that are black or reddish brown depending on how oxidized the iron in the material is, tuffs that range from massive to delicately bedded and from buff or tan to dark-colored depending on the proportions of basaltic and sedimentary material they contain, and deposits of generally unsorted material containing large blocks of earlier basaltic material that was quarried and moved about by explosive activity or that caved from crater walls. The distal deposits generally consist of layers a few millimeters to a few centimeters thick of fine-grained basaltic fallout ash interbedded with lake-deposited sedimentary sequences, or of thicker debris-flow deposits produced by the partial collapse of vents and preserved in lacustrine environments at distances as much as several kilometers from their sources. More details regarding the basaltic pyroclastic vents and their deposits are given by Godchaux and others (1992), McCurry and others (1997), and Godchaux and Bonnichsen (this volume).

INTERACTION OF BASALTIC LAVA AND WATER

Basaltic lavas interacted with surface water in many interesting fashions in southwestern Idaho, especially in the western SRP where Lake Idaho existed for part of the time the eruptions were occurring. Below, some of the main ways basaltic lava and water interacted are summarized briefly. Many more details regarding these interactions are presented and discussed in Godchaux and Bonnichsen (this volume). In many instances, after basaltic lavas had been erupted from subaerial volcanos, the lavas ran into standing bodies of water. These situations led to the widespread development of pillow basalts, commonly in the form of pillow deltas. In pillow deltas, the individual pillows generally are elongated, inasmuch as each one represents a blob of lava that flowed directly down the foreslope of the delta as it was being constructed. Pillow deltas are commonly configured in a manner similar to sedimentary deltas, with definite topset, foreset, and bottomset beds.

At many localities in southwestern Idaho, especially in the western SRP region, some basalt flows have an altered or hydrated appearance and show a low resistance to weathering, even though such flows may be quite young, never having been subjected to wet-climate weathering, and may be in contact with perfectly fresh-appearing basalt flows. In fact, some fresh-appearing basalt flows have been traced laterally into other areas where they are extremely altered in appearance. The general association of the various types of altered-appearing basalt flows with such geologic features as lake beds, pillow basalts, and basaltic tuff beds suggests that water affected the basalts in various ways during and just after their solidification, with the internal heat of the basalt being the energy source that drove the reactions. We have collectively referred to this group of variably hydrated and altered basalts as water-affected basalts (WAB), regardless of their specific alteration patterns or exactly how they were brought about. Sublacustrine basaltic eruptions in the western SRP area include the underwater extrusion of pillow piles and associated tuffs, the development of invasive blobs and flows within the lake-bottom sediments (although some invasive flows are subaerial), and the formation of lava flows (mostly WABs) that were erupted under water. Redeposition of much underwater-deposited incompetent materials after collapse of unstable piles of pillows and pillow fragments, tuffs, and other fragmental materials has resulted in many layers of subaqueous debris flows.

BASALT CHEMICAL CATEGORIES IN THE SNAKE RIVER PLAIN

The southwestern Idaho SRP basalts vary considerably in chemical composition, but in a systematic way. Basalt analyses range from relatively primitive basalts with fairly high Mg and Al contents to those that are quite evolved with high Fe, Ti, P, and alkali abundances. Table 1 shows the average, maximum, and minimum concentrations for the major oxides for the four regions of southwestern Idaho. These average values show that the basalts from the Owyhee-Humboldt and Bruneau-Jarbidge regions have nearly identical compositions. The basalts from the Twin Falls and western SRP regions are somewhat more evolved, however, and show more compositional diversity. More details about basalt compositions in the various regions are presented later.

Of the most abundant oxides, Fe_2O_3 and Al_2O_3 vary about the most within the body of compositional data; Figure 4 shows the variation in these two key oxides and what sort of distribution pattern the analyses have. Figure 4 confirms (1) that the basalts in the Owyhee-Humboldt and Bruneau-Jarbidge regions are nearly alike, (2) that the Twin Falls region basalts are generally more Fe-rich and Al-poor than the region to the southwest along the SRP hotspot track, (3) that the western SRP region shows the greatest variation in basalt compositions, and (4) that the western SRP iron compositional distribution pattern is bimodal.

The wide variation in the iron and aluminum abun-

Table 1. Average basalt compositions for different southwestern Idaho regions.

	Owyhee-Humboldt Region (70 analyzed rocks)				Bruneau-Jarbidge Region (140 analyzed rocks)		
	Average	**Minimum**	**Maximum**		**Average**	**Minimum**	**Maximum**
SiO_2	47.86	46.21	49.47	SiO_2	47.59	45.90	49.67
TiO_2	1.66	0.76	2.51	TiO_2	1.87	0.98	3.03
Al_2O_3	15.74	13.85	17.25	Al_2O_3	15.60	13.81	17.20
Fe_2O_3	12.50	10.06	14.36	Fe_2O_3	12.91	10.57	15.23
MnO	0.18	0.17	0.21	MnO	0.19	0.16	0.21
MgO	8.46	6.21	12.61	MgO	8.14	5.98	10.10
CaO	10.58	9.19	12.13	CaO	10.69	9.06	12.18
Na_2O	2.37	1.92	2.76	Na_2O	2.35	2.08	2.85
K_2O	0.35	0.11	0.59	K_2O	0.35	0.17	0.87
P_2O_5	0.30	0.11	0.58	P_2O_5	0.30	0.12	0.62
Mg No.	57.08	47.76	65.37	Mg No.	55.46	46.07	63.25
	Western Snake River Plain (295 analyzed rocks)				**Twin Falls Region (126 analyzed rocks)**		
	Average	**Minimum**	**Maximum**		**Average**	**Minimum**	**Maximum**
SiO_2	46.55	43.20	49.82	SiO_2	46.21	44.64	48.60
TiO_2	2.86	1.50	4.56	TiO_2	3.06	1.33	4.24
Al_2O_3	14.80	11.71	16.91	Al_2O_3	14.30	11.53	16.40
Fe_2O_3	14.69	10.69	18.11	Fe_2O_3	15.54	11.26	19.21
MnO	0.21	0.17	0.32	MnO	0.22	0.17	0.29
MgO	6.95	2.89	9.65	MgO	7.09	4.33	10.16
CaO	9.80	6.91	12.35	CaO	9.86	8.97	11.93
Na_2O	2.70	2.21	3.73	Na_2O	2.48	1.95	2.86
K_2O	0.79	0.19	2.27	K_2O	0.59	0.19	0.97
P_2O_5	0.65	0.21	2.21	P_2O_5	0.65	0.24	1.95
Mg No.	48.25	25.32	59.26	Mg No.	47.37	33.46	63.78

dances suggests that further studies should explore basalt compositions from region to region in southwestern Idaho. The variations in these constituents likely are partly related to magma fractionation processes, such as the segregation of crystals from melts in magma chambers in the Earth's crust or uppermost mantle. Segregation of phenocrysts away from a magma body, by settling or floating of phenocrysts for example, leads to compositional diversity. Aluminum concentrations are lowered in magmas by the crystallization and segregation of plagioclase, and iron concentrations are increased relative to magnesium in magmas during the crystallization and segregation of olivine. The crystallization and separation of plagioclase and olivine together cause the Al content of the remaining magma to decrease and the Fe content to increase. The most primitive lavas would be the most Al-rich and Fe-poor ones, having had the least amount of plagioclase and olivine removed. The most evolved would be the most Al-poor and Fe-rich ones, having had the largest amounts of plagioclase and olivine removed. Moreover, part or all of the compositional diversity of the southwest Idaho basalts may be related to initial compositional differences during the generation of the magmas in the Earth's mantle, or to the depths at which both melting and crystallization processes occurred. Such features as the considerable variation in the potassium content in the basalts may be related to such a cause, and some of the variation in the iron and aluminum contents may also possibly have been generated at deep levels during magma genesis. At present, we do not have much insight into how important these alternate roads to compositional diversity of the SRP basalts are relative to one another.

To discuss the variation in basalt compositions, we have used the following nomenclature, based on the proportions of Fe and Al, expressed as Fe_2O_3 and Al_2O_3.

High-Al basalt: Contains 17.0 percent or more of Al_2O_3.

Al-enhanced basalt: Contains between 16.00 and 16.99 percent of Al_2O_3.

SROT basalt: Contains 15.99 percent or less of Al_2O_3 and 14.99 or less of Fe_2O_3.

Fe-enhanced basalt: Contains between 15.00 and 15.99 percent of Fe_2O_3.

Ferrobasalt: Contains 16.00 percent or more of Fe_2O_3.

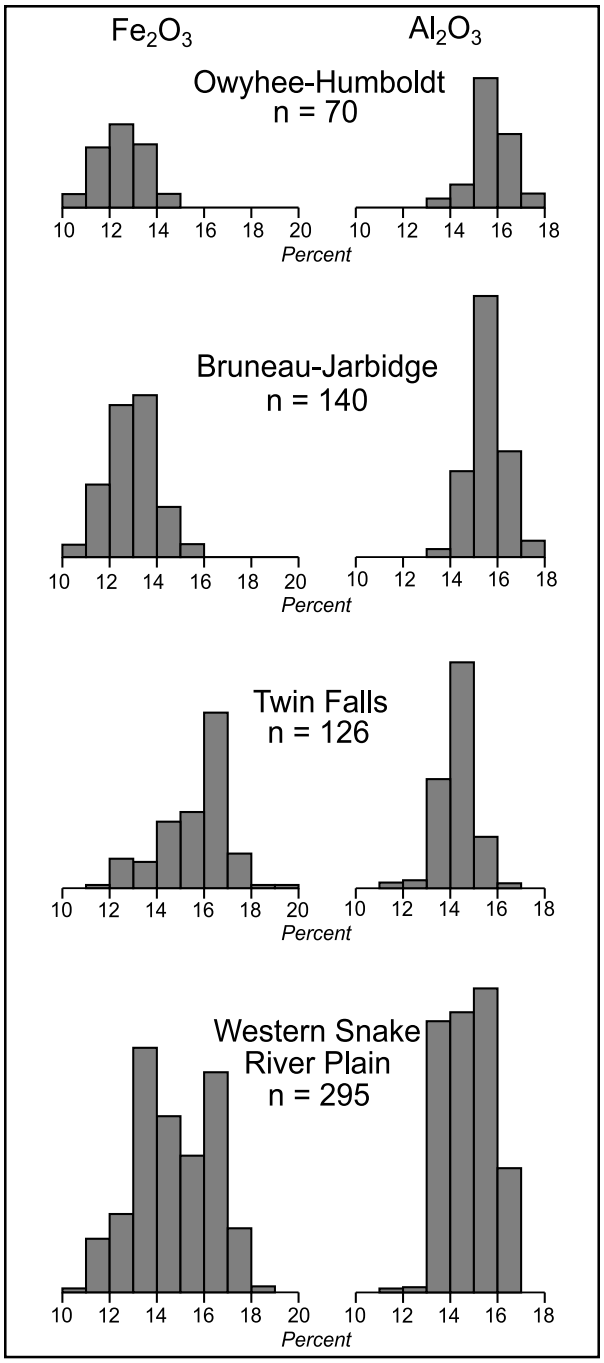

Figure 4. Histograms of the abundances of Fe_2O_3 and Al_2O_3 in basalts from the four principal regions of the SRP volcanic province in southwestern Idaho and vicinity. A total of 631 basalt analyses are represented. For each analysis, the total iron was expressed as Fe_2O_3, and the sum of the major element oxides was normalized to 100 percent. These are the same analyses used to calculate the average values compiled in Table 1. Data sources are (1) B. Bonnichsen, unpublished analyses from University of Massachusetts at Amherst and Washington State University; (2) Bonnichsen and others, 1994a, 1994b; (3) W.P. Leeman, unpublished analyses from Rice University and Edinburgh University; (4) Hart, 1982; (5) Othberg and others, 1995; (6) Stone, 1967; and (7) White and others, this volume.

The acronym SROT refers to Snake River olivine tholeiite, an established term that describes most of the basalts in the SRP volcanic province (Leeman, 1982; White and others, this volume). In our paper, as seen above, we have restricted the usage of SROT to a specific range of Fe and Al contents. Most previous workers, however, have included a wider range of compositions when using the term SROT. The basalt-type categories noted above are based on the premises that all of the iron in an analysis is expressed as Fe_2O_3 and that the percentages of the ten major-element oxides (SiO_2, TiO_2, Al_2O_3, Fe_2O_3, MnO, MgO, CaO, Na_2O, K_2O, and P_2O_5) have been normalized to a sum of 100 percent. So far, all of the southwestern Idaho basalt analyses that we know of fit into only one of these self-explanatory categories. This system of mutually exclusive basalt compositional categories has become a very practical way to briefly describe how the basalt chemistry varies. Admittedly, this classification does not include some other compositional parameters, such as the MgO or SiO_2 concentrations, that commonly are used in basalt classification schemes. However, of the several ways we have tried to categorize SRP basalts compositions, we find by trial and error that using Fe and Al as outlined above works best for our descriptive purposes.

GEOLOGY OF THE BRUNEAU-JARBIDGE REGION

The volcanism in the Bruneau-Jarbidge and Owyhee-Humboldt regions is similar in style and in the chemical composition of the resulting basalt. The histograms for iron and aluminum contents for the basalts from the two regions shown in Figure 4 are practically identical, and the average compositions in Table 1 also show no significant difference between the two areas. In both regions, the volcanism mainly resulted in subaerial lava flows and the concomitant building of small monogenetic shield volcanoes. There are many basalt volcanoes in the interior of the Bruneau-Jarbidge eruptive center (Bonnichsen, 1982a), the elliptical, 90 km by 65 km structural zone from which the Cougar Point Tuff was erupted and which was then flooded with rhyolite lava flows. However, only a few basalt volcanoes fall outside the limits of that buried structure. All of the known basalt volcanoes in the Bruneau-Jarbidge region are shown in relation to the Bruneau-Jarbidge eruptive center outline in Figure 5, and are listed in Table 2. In the north part of the Bruneau-Jarbidge region, the now-drained Lake Idaho existed during most, if not all, of late Miocene and Pliocene time. In the area where this lake existed, beds of sediments were deposited and a few basalt eruptions occurred that led to

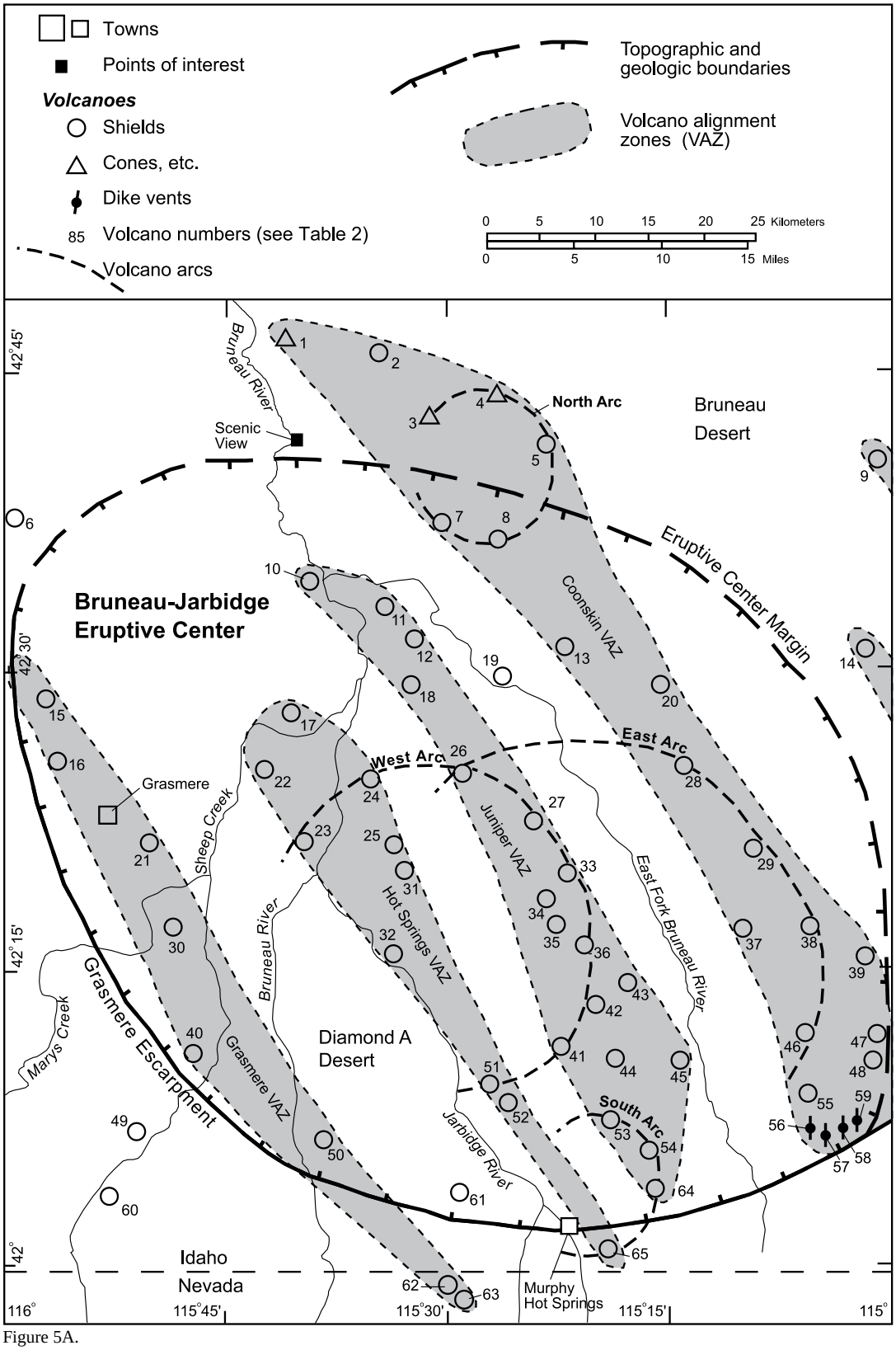

Figure 5A.

Figure 5. Volcano locations for the Bruneau-Jarbidge (left page) and Twin Falls (right page) regions. See Table 2 for the names of the volcanoes.

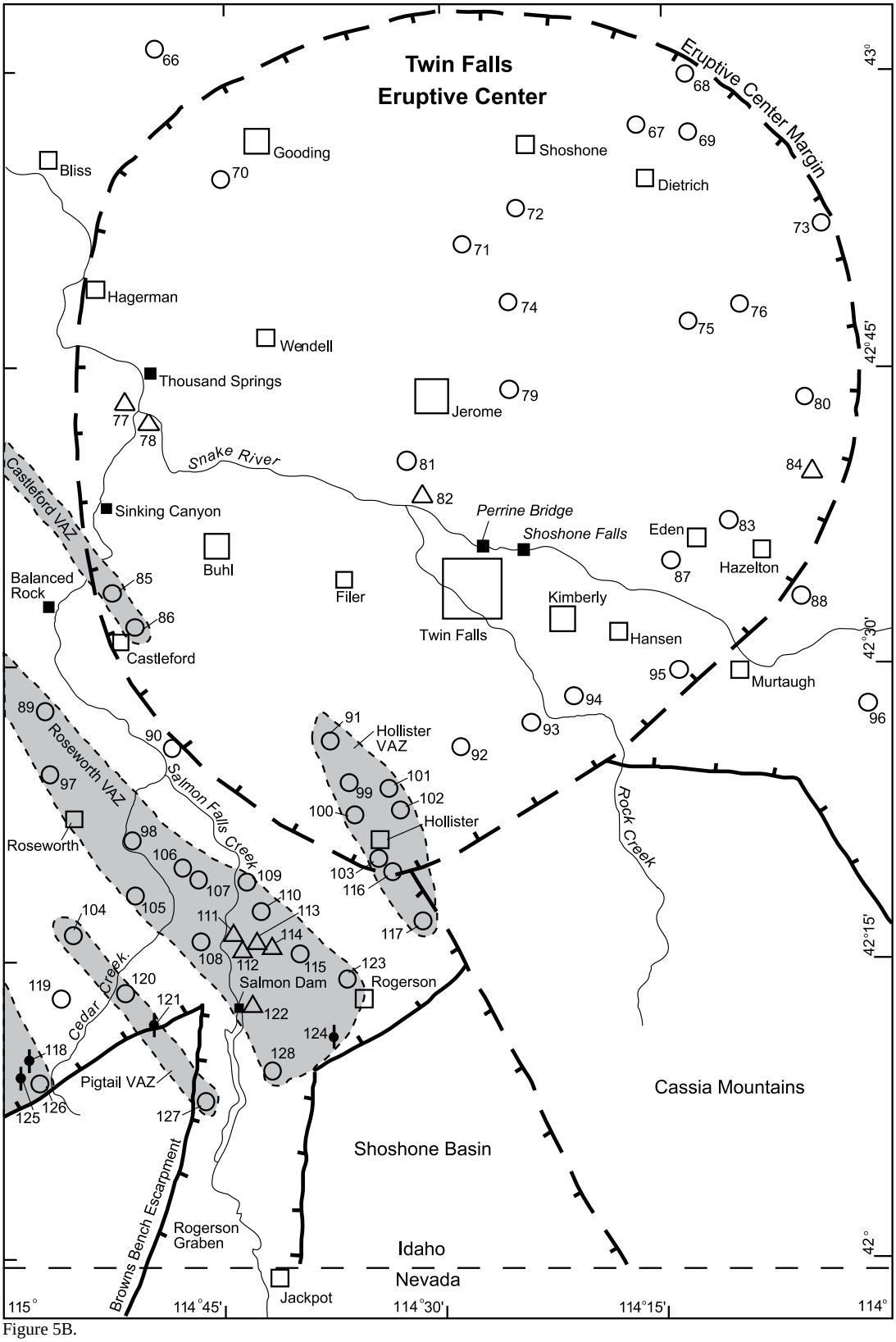
Twin Falls
Eruptive Center
Eruptive Center Margin
Bliss
Gooding
Shoshone
Dietrich
Hagerman
Wendell
Thousand Springs
Jerome
Snake River
Sinking Canyon
Perrine Bridge
Shoshone Falls
Eden
Hazelton
Buhl
Filer
Kimberly
Twin Falls
Hansen
Murtaugh
Balanced Rock
Castleford
Castleford VAZ
Roseworth VAZ
Roseworth
Hollister VAZ
Hollister
Salmon Falls Creek
Rock Creek
Cedar Creek
Salmon Dam
Rogerson
Pigtail VAZ
Cassia Mountains
Shoshone Basin
Browns Bench Escarpment
Rogerson Graben
Jackpot
Idaho
Nevada
43°
42°45'
42°30'
42°15'
42°
115°
114°45'
114°30'
114°15'
114°

Figure 5B.

Table 2. Volcanoes in the Bruneau-Jarbidge and Twin Falls regions. See Figure 5 for locations.

Part A. Bruneau-Jarbidge region volcanoes:

Number	Name	Type	Unit	Chemistry	Location
10	Austin Butte	shield	Tab	SROT	sec. 8, T. 10 S., R. 7 E.
5	Black Butte (north)	shield	—	unknown	sec. 34, T. 8 S., R. 9 E.
38	Black Butte (south)	shield	—	SROT	sec. 19, T. 13 S., R. 12 E.
50	Black Rock Hill	shield	Tbr	Al-enhanced	sec. 21, T. 15 S., R. 7 E.
43	Burnt Butte	shield	—	unknown	sec. 4, T. 14 S., T. 10 E.
21	Buster Butte	shield	Tbub	Al-enhanced	sec. 26, T. 12 S., R. 5 E.
14	Castleford Butte	shield	—	SROT	sec. 34, T. 10 S., R. 12 E.
27	Clover Butte	shield	—	SROT	sec. 16, T. 12 S., R. 9 E.
29	Coonskin Butte	shield	—	Al-enhanced	sec. 26, T. 12 S., R. 11 E.
9	Elmas Hill	shield	—	unknown	sec. 1, T. 9 S., R. 12 E.
45	Forks Hill	shield	—	Al-enhanced	sec. 36, T. 14 S., R. 10 E.
46	Grassy Hills	complex shield	Tgh	SROT	sec. 19, T. 14 S., R. 12 E.
1	Hill 3001	tuff and cinder cone	Tsog	ferrobasalt	sec. 36, T. 7 S., R. 6 E.
8	Hill 4310	shield	—	unknown	sec. 30, T. 9 S., R. 9 E.
13	Hill 4442	shield	—	unknown	sec. 35, T. 10 S., R. 9 E.
19	Hill 4510	shield	—	SROT	sec. 6, T. 11 S., R. 9 E.
18	Hill 4553	shield	Tsd	unknown	sec. 8, T. 11 S., R. 8 E.
6	Hill 4630	shield	Thir	Fe-enhanced	sec. 21, T. 9 S., R. 4 E.
20	Hill 4692	shield	—	unknown	sec. 15, T. 11 S., R. 10 E.
24	Hill 4726	shield	Tbc	SROT	sec. 1, T. 12 S., R. 7 E.
17	Hill 4735	shield	Tbib	SROT	sec. 18-19, T. 11 S., R. 7 E.
25	Hill 4770	shield	—	unknown	sec. 30, T. 12 S., R 8 E.
31	Hill 4830	shield	—	unknown	sec. 5, T. 13 S., R 8 E.
23	Hill 4882	shield	Tbl	unknown	sec. 29, T. 12 S., R. 7 E.
32	Hill 4983	shield	—	unknown	sec. 30, T. 13 S., R. 8 E.
33	Hill 4997	shield	—	SROT	sec. 2, T. 13 S., R. 9 E.
26	Hill 5090	shield	—	SROT	sec. 2, T. 12 S., R. 8 E.
35	Hill 5152	shield	—	Al-enhanced	sec. 23, T. 13 S., R. 9 E.
15	Hill 5158	shield	Twhc	SROT	sec. 14, T. 11 S., R. 4 E.
30	Hill 5191	shield	Tdp	unknown	sec. 24, T. 13 S., R. 5 E.
34	Hill 5199	shield	—	SROT	sec. 10, T. 13 S., R. 9 E.
37	Hill 5278	shield	—	unknown	sec. 21-22, T. 13 S., R. 11 E.
40	Hill 5363	shield	—	SROT	sec. 29, T. 14 S., R. 6 E.
52	Hill 5518	shield	Tpb	unknown	sec. 8, T. 15 S., R. 9 E.
44	Hill 5570	shield	—	Al-enhanced	sec. 32, T. 14 S., R. 10 E.
53	Hill 5583	shield	Tbf	SROT	sec. 17, T. 15 S., R. 10 E.
47	Hill 5728	shield	Twor	unknown	sec. 23, T. 14 S., R. 12 E.
61	Hill 5770	shield	Tdt	SROT	sec. 2, T. 16 S., R. 8 E.
56	Hill 5850	dike vent	Tdw	unknown	sec. 19, T. 15 S., R. 12 E.
59	Hill 5880	dike vent	Tcs	unknown	sec. 15, T. 15 S., R. 12 E.
57	Hill 5890	dike vent	Tcs	unknown	sec. 20, T. 15 S., R. 12 E.
58	Hill 5950	dike vent	Tcs	unknown	sec. 22, T. 15 S., R. 12 E.
65	Hill 5981	shield	Tbf	SROT	sec. 20, T. 16 S., R. 10 E.
60	Hill 6430	shield	—	Al-enhanced	sec. 8-9, T. 16 S., R. 5 E.
63	Hill 6485	shield	Tda	Al-enhanced	sec. 7, T. 47 N., R. 58 E.
49	Hills 6028 & 5890	complex shield	—	SROT	sec. 22-23, T. 15 S., R. 5 E.
28	Horse Butte	shield	—	Al-enhanced	sec. 1, T. 12 S., R. 10 E.
64	Horse Hill	shield	Tbf	SROT	sec. 3, T. 16 S., R. 10 E.
36	Juniper Butte	shield	—	Al-enhanced	sec. 25, T. 13 S., R. 9 E.
62	Knight Hill	shield	Tda	Al-enhanced	sec. 2, T. 47 N., R. 57 E.
55	Little Grassy Hill	shield	Tlgh	unknown	sec. 7, T. 15 S., R. 12 E.
11	Long Butte	shield	Tjt	SROT	sec. 18, T. 10 S., R. 8 E.
12	Lookout Butte (west)	shield	Tlb	SROT	sec. 29, T. 10 S., R. 8 E.
39	Marshall Butte	shield	Tmab	unknown	sec. 26-27, T. 13 S., R. 12 E.
41	Middle Butte	shield	Tmb	SROT	sec. 26, T. 14 S., R. 9 E.
22	Monument Butte	complex shield	Tjp	unknown	sec. 1, T. 12 S., R. 6 E.
42	Mosquito Lake Butte	shield	—	SROT	sec. 7, T. 14 S., R. 10 E.
2	Pence Butte (north)	shield	Tsay	ferrobasalt	sec. 1, T. 8 S., R. 7 E.
54	Pence Butte (south)	shield	Tbf	SROT	sec. 28, T. 15 S., R. 10 E.
51	Poison Butte (east)	shield	Tpb	high-Al	sec. 6, T. 15 S., R. 9 E.
16	Poison Butte (west)	shield	Twhc	SROT	sec. 36, T. 11 S., R. 4 E.
3	Pot Hole Butte	tuff ring	Tsay	ferrobasalt	sec. 21, T. 8 S., R. 8 E.
4	Sailor Cap Butte	tuff cone	Tscv	SROT	sec. 18, T. 8 S., R. 9 E.
48	Signal Butte	shield	Tsig	Al-enhanced	sec. 35, T. 14 S., R. 12 E.

Table 2.Continues.

7	Winter Camp Butte	shield	Twc	Fe-enhanced	sec. 22, T. 9 S., R. 8 E.
Part B. Twin Falls region volcanoes:					
Number	**Name**	**Type**	**Unit**	**Chemistry**	**Location**
74	Bacon Butte	shield	Qbac	SROT	sec. 23, T. 7 S., R. 17 E.
91	Berger Butte	shield	Tsuk	ferrobasalt	sec. 31, T. 11 S., R. 16 E.
68	Brown Butte	shield	—	unknown	sec. 8-17, T. 5 S., R. 19 E.
90	Canyon Hill	shield	Tchb	SROT	sec. 34, T. 11 S., R. 14 E.
119	Cedar Butte	shield	—	SROT	sec. 9-10, T. 14 S., R. 13 E.
103	Checking Station Hill	shield	Tsuk	unknown	sec. 33-34, T. 12 S., R. 16 E.
84	Cinder Butte	cinder-spatter cone	Qcin	unknown	sec. 11, T. 9 S., R. 20 E.
67	Crater Butte	shield	—	unknown	sec. 25-26, T. 5 S., R. 18 E.
89	Devil Creek Butte	shield	Tdev	unknown	sec. 20, T. 11 S., R. 13 E.
69	Dietrich Butte	shield	—	unknown	sec. 32-33, T. 5 S., R. 19 E.
105	Emery Butte	shield	—	unknown	sec. 7, T. 13 S., R. 14 E.
79	Flat Top Butte	shield	Qflt	various	sec. 13, T. 8 S., R. 17 E.
70	Gooding Butte	shield	QTgb	ferrobasalt	sec. 11, T. 6 S., R. 14 E.
95	Hanson Butte	complex shield	QTha	Fe-enhanced	sec. 3-4, T. 11 S., R. 19 E.
88	Hazelton Butte	shield	QThz	unknown	sec. 15, T. 10 S., R. 20 E.
93	Hill 4197	shield	Trck	Fe-enhanced	sec. 19, T. 11 S., R. 18 E.
76	Hill 4272	shield	—	unknown	sec. 19, T. 7 S., R. 20 E.
80	Hill 4526	shield	Qrh	various	sec. 14, T. 8 S., R. 20 E.
101	Hill 4534	shield	Tsuk	unknown	sec. 15, T. 12 S., R. 16 E.
102	Hill 4535	shield	Tsuk	unknown	sec. 15, T. 12 S., R. 16 E.
116	Hill 4613	shield	Tsuk	ferrobasalt	sec. 3, T. 13 S., R. 16 E.
99	Hill 4645	shield	Tsuk	ferrobasalt	sec. 8, T. 12 S., R. 16 E.
106	Hill 4902	shield	—	unknown	sec. 3, T. 13 S., R. 14 E.
123	Hill 4943	shield	—	SROT	sec. 8, T. 14 S., R. 16 E.
107	Hill 4965	shield	—	unknown	sec. 11, T. 13 S., R. 14 E.
109	Hill 4970	shield	—	unknown	sec. 5-8, T. 13 S., R. 15 E.
114	Hill 5012	cinder-spatter cone	—	unknown	sec. 33, T. 13 S., R. 15 E.
112	Hill 5028	cinder-spatter cone	—	unknown	sec. 29, T. 13 S., R. 15 E.
115	Hill 5036	shield	—	unknown	sec. 35, T. 13 S., R. 15 E.
113	Hill 5038	cinder-spatter cone	—	SROT	sec. 28, T. 13 S., R. 15 E.
111	Hill 5070	cinder-spatter cone	—	SROT	sec. 30, T. 13 S., R. 15 E.
110	Hill 5089	shield	—	Fe-enhanced	sec. 16, T. 13 S., R. 15 E.
124	Hill 5130	dike vent	—	SROT	sec. 30, T. 14 S., R. 16 E.
117	Hill 5155	shield	Tsuk	Fe-enhanced	sec. 24, T. 13 S., R. 16 E.
108	Hill 5208	shield	—	SROT	sec. 26, T. 13 S., R. 14 E.
127	Hill 5366	shield	—	unknown	sec. 11, T. 15 S., R. 14 E.
128	Hill 5384	shield	—	Al-enhanced	sec. 4, T. 15 S., R. 15 E.
120	Hill 5436	shield	—	unknown	sec. 7, T. 14 S., R. 14 E.
121	Hill 5475	dike vent	—	SROT	sec. 20, T. 14 S., R. 14 E.
118	Hill 5731	dike vent	—	unknown	sec. 31, T. 14 S., R. 13 E.
125	Hill 5822	dike vent	—	SROT	sec. 6, T. 15 S., R. 13 E.
126	Hill 5991	shield	—	SROT	sec. 5, T. 15 S., R. 13 E.
100	Holly Hill	shield	Tsuk	unknown	sec. 20, T. 12 S., R. 16 E.
92	Hub Butte	shield	Thub	ferrobasalt	sec. 32, T. 11 S., R. 17 E.
82	Jerome Golf Course	maar-tuff ring	Qjer	Fe-enhanced	sec. 13, T. 9 S., R. 16 E.
71	Lincoln Hill	shield	QTlh	ferrobasalt	sec. 31, T. 6 S., R. 17 E.
86	Lookout Butte (east)	shield	Tluc	Fe-enhanced	sec. 30, T. 10 S., R. 14 E.
66	McKinney Butte	shield	Qmck	various	sec. 5, T. 5 S., R. 14 E.
96	Milner Butte	shield	QTmi	unknown	sec. 20, T. 11 S., R. 21 E.
72	Notch Butte	shield	Qnot	various	sec. 22, T. 6 S., R. 17 E.
73	Owinza Butte	shield	—	unknown	sec. 27, T. 6 S., R. 20 E.
104	Pigtail Butte	shield	—	SROT	sec. 22, T. 13 S., R. 13 E.
78	Riverside Ferry	tuff cone	Tbhs	SROT	sec. 29, T. 8 S., R. 14 E.
122	Salmon Butte	cinder-spatter cone	QTsb	ferrobasalt	sec. 17, T. 14 S., R. 14 E.
98	Secret Cabin Butte	shield	—	ferrobasalt	sec. 30, T. 12 S., R. 14 E.
87	Skeleton Butte	shield	QTsk	ferrobasalt	sec. 4, T. 10 S., R. 19 E.
81	Sonnickson Butte	shield	Tson	Al-enhanced	sec. 2, T. 9 S., R. 16 E.
94	Stricker Butte	complex shield	QTst	ferrobasalt	sec. 16, T. 11 S., R. 18 E.
85	Sunset Butte	shield	Tluc	ferrobasalt	sec. 13, T. 10 S., R. 13 E.
77	Thousand Hill	tuff cone	Tbhs	unknown	sec. 19, T. 8 S., R. 14 E.
97	Tuanna Butte	shield	—	unknown	sec. 5, T. 12 S., R. 13 E.
75	Wilson Butte	shield	Qwil	various	sec. 27, T. 7 S., R. 19 E.
83	Wilson Lake Res. Hill	shield	QTwl	unknown	sec. 30, T. 9 S., R. 20 E.

the formation of tuff beds, water-affected basalt flows, and pillow deltas.

Geologic mapping in the Bruneau-Jarbidge region includes the reconnaissance work by Malde and others (1963) at 1:125,000 scale that covers the northern part of the region, the compilation by Rember and Bennett (1979) at 1:250,000 scale, and the more detailed map of the Glenns Ferry-Hagerman area by Malde and Powers (1972) at 1:48,000 scale. More detailed maps that cover wide strips on either side of Sheep Creek, Jarbidge, and Bruneau canyons and much of the Jacks Creek area at 1:50,000 scale were prepared by Bonnichsen and others (1990), Bonnichsen and Jenks (1990), Jenks and Bonnichsen (1990a), and Kauffman and Bonnichsen (1990). In the Grand View-Bruneau area in the northwestern part of the Bruneau-Jarbidge region and the northeastern part of the Owyhee-Humboldt region, nineteen 7.5-minute quadrangles (scale 1:24,000) were mapped by Jenks and others (1993). Later, this same information was summarized at 1:100,000 scale (Jenks and others, 1998). Three additional 7.5-minute quadrangles in the southern part of the Bruneau-Jarbidge region were published at 1:24,000 scale by Bonnichsen and Jenks (1995a, 1995b, 1995c).

For the Owyhee-Humboldt region, the principal summary map of the Idaho portion was published at 1:125,000 scale by Ekren and others (1981). In the Owyhee-Humboldt region, the late Miocene basalt flows have been lumped into very general units, although numerous shield volcanoes are evident on topographic maps and in the landscape. Most of the samples from which the histograms in Figure 4 and the average values in Table 1 were derived were collected from many lava flows and vents of varying ages. This information indicates that the Owyhee-Humboldt region basalt mainly is SROT and Al-enhanced basalt. Ferrobasalts have yet to be found in the region. All of the identified Owyhee-Humboldt region basalt volcanoes are shields; phreatomagmatic vents have not been found there. Some may exist, however, because water-affected basalt is intercalated within some of the sedimentary sequences in the region.

Only a few radiometric dates are available for the basalt units in the Owyhee-Humboldt and Bruneau-Jarbidge regions (Figure 6). These data indicate that the ages of basalt units in the Owyhee-Humboldt region may generally be older than those in the Bruneau-Jarbidge region, but that there is considerable time overlap between the two regions. The dated basalts in the Owyhee-Humboldt region are late Miocene, whereas some of the dated basalts in the Bruneau-Jarbidge region are late Miocene and Pliocene. The age-spread patterns in Figure 6 suggest that most of the basalts in the eastern part of the Owyhee-Humboldt area are between 10.5 Ma and 7.0 Ma, whereas most of the basalts associated with the Bruneau-Jarbidge area are between 9.5 Ma and 3.5 Ma.

The general stratigraphic setting of the Bruneau-Jarbidge region is given in Figure 2. In that illustration it can be seen that several episodes of basalt eruption occurred between the late Miocene and the early part of the Pleistocene. These basalt eruptions were interspersed in time with the eruption of the last of the rhyolite lava flows and the deposition of lacustrine and fluvial sediments. The principal individual basalt units in the Bruneau-Jarbidge region and the eastern part of the Owyhee-Humboldt region are noted in Figure 7. This illustration shows the approximate stratigraphic relationships of the basalt units. Establishing a stratigraphic order for the region is incomplete because of limited overlap among basalt units from area to area and few radiometric dates. A more-detailed example of the type of stratigraphic relationships that exist between the basalt and rhyolite flows and some of the sediments in the region is presented for a 26-km-long part of Bruneau Canyon in the longitudinal section shown in Figure 8.

The basalt units in the Bruneau-Jarbidge region mainly have Al-enhanced and SROT compositions (Figure 4), with a few analyses from units in the southern part of the region falling in the high-Al category and some from the northern part of the region being Fe-enhanced basalt and ferro-basalt. Examples of basalt compositions from the various parts of the region, and which illustrate the compositional range, are given in Table 3.

STRUCTURAL GEOLOGY OF THE BRUNEAU-JARBIDGE REGION

The main structural features exposed in the Bruneau-Jarbidge region are parts of the Bruneau-Jarbidge eruptive center boundary, small-displacement normal faults that typically trend about N. 30º W. in the main part of the region, and similar faults that trend N. 60º W. in the northern part. Undoubtedly, other faults with large vertical displacements are buried beneath the cover of volcanic rocks and sediments. Additional structural features include alignment patterns observed among the basalt volcanoes in the region. These patterns include both northwest-trending volcano alignment zones that enclose most of the volcanoes in the region and broad arcuate zones that are defined by several of the larger shields in the region.

The Bruneau-Jarbidge region was the site of some of the most voluminous explosive and effusive eruptions of rhyolite in the Earth's history (Bonnichsen, 1982a, 1982b; Bonnichsen and Citron, 1982; Bonnichsen and Kauffman, 1987). These eruptions led to the development of a large,

elliptical zone of structural collapse that occupies much of the region (Figures 1 and 5), and which has been called the Bruneau-Jarbidge eruptive center (Bonnichsen, 1982a). This basin of structural collapse is somewhat like a caldera, but it is larger, took longer to develop, and is believed to merge beneath the cover of basalt into the similarly collapsed zone in the central SRP known as the Twin Falls eruptive center. We believe that buried within the interior of the Bruneau-Jarbidge eruptive center is a complex of calderas whose collapse accompanied the eruption of some of the largest of the ignimbrites of the Cougar Point Tuff.

The structural features that define the western and southern margins of the Bruneau-Jarbidge eruptive center include the Grasmere escarpment along the southwestern segment (Figure 9), a down-to-the-north faulted zone accompanied by the Black Rock shield and Murphy Hot Springs along the southern segment, and the general physiographic margin of the SRP along the southeastern segment (Bonnichsen, 1982a). The eastern and northern segments were defined partly by both geophysical (gravity and aeromagnetic patterns) and indirect geological evidence. The position of these defining structures generally is consistent with the locations of subsidence and accompanying faults thought to have accompanied the eruption of an enormous volume of rhyolitic magma, the Cougar Point Tuff, from fissures in the eruptive center. During an interval of about a million years, the interior of the eruptive center foundered as a series of large silicic magma chambers were partially evacuated. In effect, the Bruneau-Jarbidge eruptive center is viewed as a very large caldera complex in which the several major eruptive events were accompanied by subsidence. Although speculative, the locations of hidden bounding faults of calderas thought to be buried within the eruptive center may be discerned where basalt magmas were delivered to the surface along highly fractured zones.

The northwest- to west-northwest-trending faults in the northern part of the Bruneau-Jarbidge region are parallel to the faults in the western SRP in areas farther north and northwest. This structural continuity and the resemblance in composition of the generally younger basalt in the northern part of the Bruneau-Jarbidge area with some in the western SRP suggest that the development of the structures and basaltic volcanism in the northern part of the region is more closely related to the evolution of the western SRP than it is to events in the Bruneau-Jarbidge eruptive center farther south.

Most of the basalt volcanoes in the region are grouped into long narrow zones, referred to as volcano alignment zones (Figure 5), that are elongate approximately parallel to the N. 30° W.-trending faults and to other linear features such as canyon segments and basalt dikes. Each of these zones is tens of kilometers long and several kilometers wide. From southwest to northeast, we have referred to them as the Grasmere, Hot Springs, Juniper, and Coonskin volcano alignment zones. In each zone there are two or more nearly straight-line groupings of basalt shields that are nearly parallel to one another and only a few kilometers apart. Very few basalt shields within and adjacent to the Bruneau-Jarbidge eruptive center fall outside the volcano alignment zones. This arrangement suggests that buried zones of deep fracturing have exerted control on the positions at which the basalt magmas appeared at the surface. The volcano alignment zones are oriented perpendicular to the topographic southeastern margin of the SRP. We have not found any particular age or basalt compositional groupings that relate to particular zones; however, such a relationship might be discovered with a more complete radiometric age set.

The distribution of shield volcanoes in the Bruneau-Jarbidge region shows that four arcs of volcanoes (Figure 5), each convex toward the east, can be discerned from the positions of some of the most voluminous shields. Each arc might indicate the position of a buried ring-fracture zone, inside of which subsidence occurred during the development of a specific caldera as one of the Cougar Point Tuff units erupted. Each arc is a part of a circle, the approximate diameters of which are 12-13 km for the southern and northern arcs, about 30 km for the western arc, and about 45 km for the eastern arc. These dimensions are consistent with the size of calderas that might be expected to have formed during the eruption of the largest Cougar Point Tuff units.

LANDSCAPE EVOLUTION IN THE BRUNEAU-JARBIDGE REGION

The landscape in the Bruneau-Jarbidge region includes a mountainous highland mainly in Nevada adjacent to the southern side, the Grasmere escarpment that extends for about 50 km along the southwestern margin of the eruptive center, a large plateau capped mainly by basalt flows that form much of the interior of the eruptive center, a series of steep-walled canyons incised deeply into the volcanic plateau, and an area of easily eroded, fine-grained to gravelly lacustrine and fluvial sediments in the northern part in which the course of the Snake River was established. The Snake River, which has incised itself into the sediments and underlying volcanic units, forms the southern boundary of another basalt-flow capped plateau, along the northern edge of the Bruneau-Jarbidge region, that extends northward through the Mountain Home part of the western SRP.

In the southern highlands, the principal rock units are the extensive, thoroughly welded ignimbrites of the Cougar Point Tuff and older rocks. The land surface there generally dips northward into the Bruneau-Jarbidge eruptive center. This regional slope is a dip-slope controlled by the resistant upper surfaces of the welded ignimbrite sheets. It probably formed in response to subsidence that occurred in the SRP area at the end of and after the eruption of the rhyolitic units. The Grasmere escarpment is another topographic feature created when the Bruneau-Jarbidge eruptive center formed. It is cut into one or more thick and strongly welded ignimbrites that came from the eruptive center and had their northeastern portions cut off and downdropped at the escarpment. The escarpment appears to be a caldera-margin segment traceable for nearly 50 km along the southwestern side of the eruptive center (Figure 5).

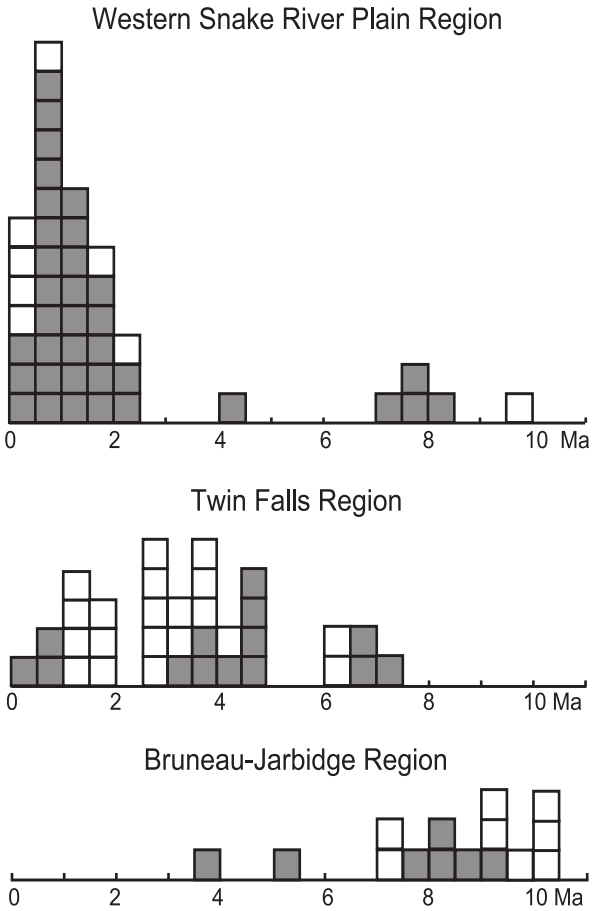

Figure 6. Summary of radiometric dates of basalt samples from the western SRP, Twin Falls, and Bruneau-Jarbidge regions. For the western SRP region, each shaded box represents a date from within the plain, and each open box represents a date from the adjoining Boise Front or Smith Prairie areas. For the Twin Falls region, each shaded box represents a date from within the region shown in Figure 5, and each open box represents a date from the adjacent Glenns Ferry area to the northwest. For the Bruneau-Jarbidge region, each shaded box represents a date from within the region shown in Figure 5, and each open box represents a date from the adjoining part of the Owyhee-Humboldt region immediately to the west. Dates were selected from Amini and others (1984), Armstrong (1975), Armstrong and others (1975, 1980), Clemens and Wood (1993), Ekren and others (1984), Evernden and others (1964), Hart (1982), Hart and Brueseke (2002), Hart and Carlson (1983), Howard and others (1982), Kuntz and others (1986), Othberg and others (1995), Vetter and Shervais (1992), White and others (this volume), and Williams and others (1990).

At various levels in the Bruneau and Jarbidge canyons, the earliest basalt flows are intercalated with sedimentary layers that consist mainly of fine-grained detrital material deposited in lacustrine and fluvial environments. Evidently, when these early basalts were erupted, the landscape was of low relief and contained shallow lakes in some places. Such ephemeral lakes probably were present from the beginning of basaltic volcanism in the region. The Indian Hot Springs basalt, which lies beneath the 8.1 Ma old Dorsey Creek rhyolite unit (Figure 8), contains conspicuous amounts of water-affected basalt especially in its more distal parts. Evidently it flowed into shallow water. Similarly, the other early basalt units—the basalts of Tindall Trail, Homer Bedal Homestead, and Columbet Creek—are associated with thick, mainly fine-grained sediment sequences.

In much of the southern part of region, the basalt flows and associated sediments form only a thin veneer above the great thickness of rhyolite associated with the earlier formation and filling of the eruptive center. The margins of these rhyolite units and of faults that cut them have had considerable influence on the distribution of the later basalt flows and sediments that form the present landscape. An example of this control is where the basalts of Wickahoney Creek and Hole In Rock were confined to the broad channel formed between the eastward-dipping rhyolite units erupted from the Jacks Creek area and the western margin of the large Sheep Creek rhyolite lava flow near the northwestern end of the Bruneau-Jarbidge eruptive center (Figure 10).

Topographic relief began to develop near the end of the plateau-forming basalt volcanism in the Bruneau-Jarbidge region. This probably occurred in the early Pliocene as Lake Idaho, which occupied a large part of the western SRP north of the developing plateau, started to recede. This lowering permitted the Bruneau River, its tributaries, and other through-going streams to develop and then become entrenched into their present courses across the volcanic plateau. Some of the youngest units on the plateau are gravels whose clasts indicate southern sources in the northern Nevada highlands. The streams were transporting gravel and other detritus northward across the volcanic plateau to the margin of Lake Idaho, and their deposits reveal where the courses for the ances-

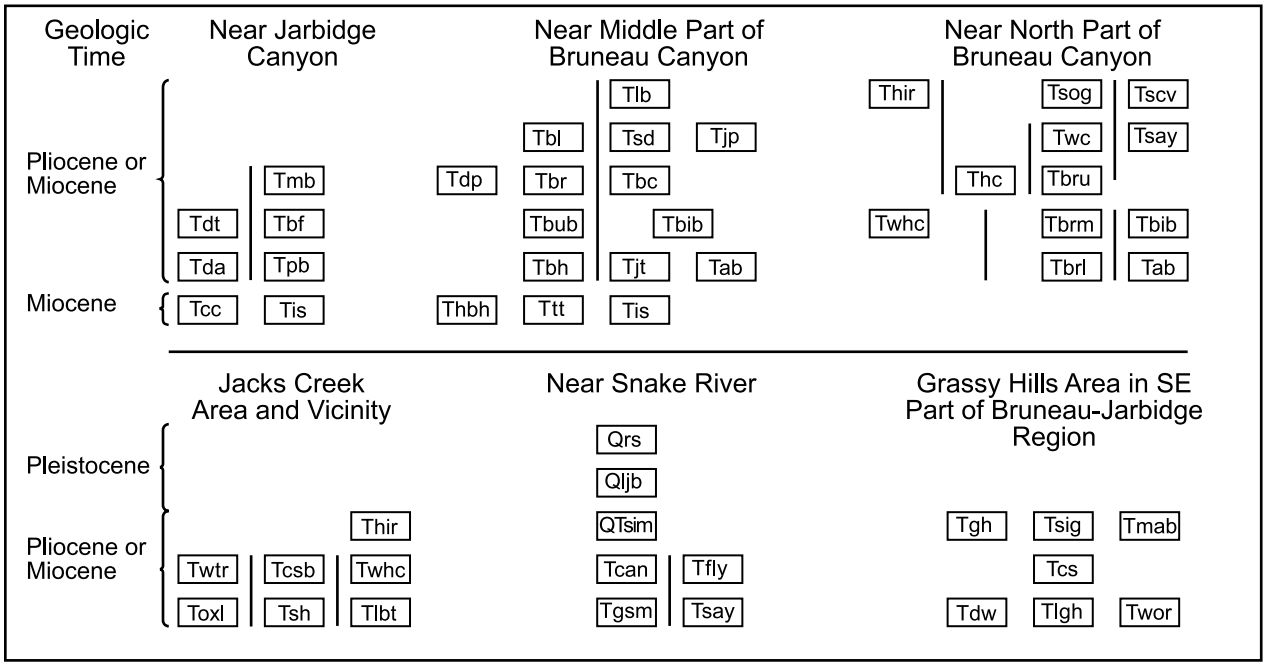

Figure 7. Stratigraphic chart for basalt units in parts of the Bruneau-Jarbidge region. Side-by-side boxes indicate that adjacent units are about the same age. Stratigraphic relations between adjacent boxes are unknown where parts of adjacent columns are separated by heavy vertical lines. See text for unit symbol identifications and information sources.

tral Bruneau River and other streams were first established. As Lake Idaho continuously receded, gravel accumulations prograded farther and farther northward across previously deposited finer grained detritus and basalt flows, forming extensive delta systems. Eventually, the lake level receded enough for rivers to begin cutting canyons and forever after to be confined. Gravels deposited on the plateau surface were left stranded at canyon rims and other localities away from the canyons where they occupy broad areas in the upstream parts of the region. Some of these early gravels lie above the youngest basalt flows, but others are intercalated between some of the earlier flows. Such unit sequences suggest that the Lake Idaho drawdown had commenced before the basaltic volcanism on the high plateau of the Bruneau-Jarbidge region ended. The lake's drawdown history has not been worked out in detail, but it likely was more complex than just a long decline of the lake's surface over time. Wood and Clemens (this volume) indicate that at least two stands of high water occurred during the lake's evolution, the first during Chalk Hills time (late Miocene) and the second during Glenns Ferry time (Pliocene).

That there was significant interaction between Lake Idaho and the basaltic volcanism that formed the plateau is substantiated by the presence of basalt-pillow deltas and large amounts of WAB in several flows in the northern parts of the plateau, and by the development of some phreatomagmatic volcanism. Some of the youngest basalt units in the northern part of the Bruneau-Jarbidge area flowed into the lake and formed extensive pillow deltas with wide lateral extents, thus establishing the approximate elevations of Lake Idaho's surface at the time of these particular basalt eruptions. Moreover, at the time, some of the basalt erupted into water-saturated ground at the lake's margin or into shallow parts of the lake, resulting in explosively generated basaltic phreatomagmatic deposits (Figure 5, Table 2). After Lake Idaho vanished, the Snake River was able to incise itself into the lake sediments and the post-lake fluvial deposits to form the present-day landscape.

VOLCANISM IN THE BRUNEAU-JARBIDGE REGION

The first part of the SRP volcanism in the Bruneau-Jarbidge region was the eruption between about 12.6 Ma and 8.1 Ma of numerous rhyolite units (Bonnichsen, 1982a, 1982b; Bonnichsen and Citron, 1982; Bonnichsen and Kauffman, 1987). The first was a series of voluminous, high-temperature, typically rheomorphic ignimbrites that constitute the Cougar Point Tuff, which is exposed along the southern part of the region and extends many kilometers to the east and west in southernmost Idaho and to the south into Nevada. The Cougar Point

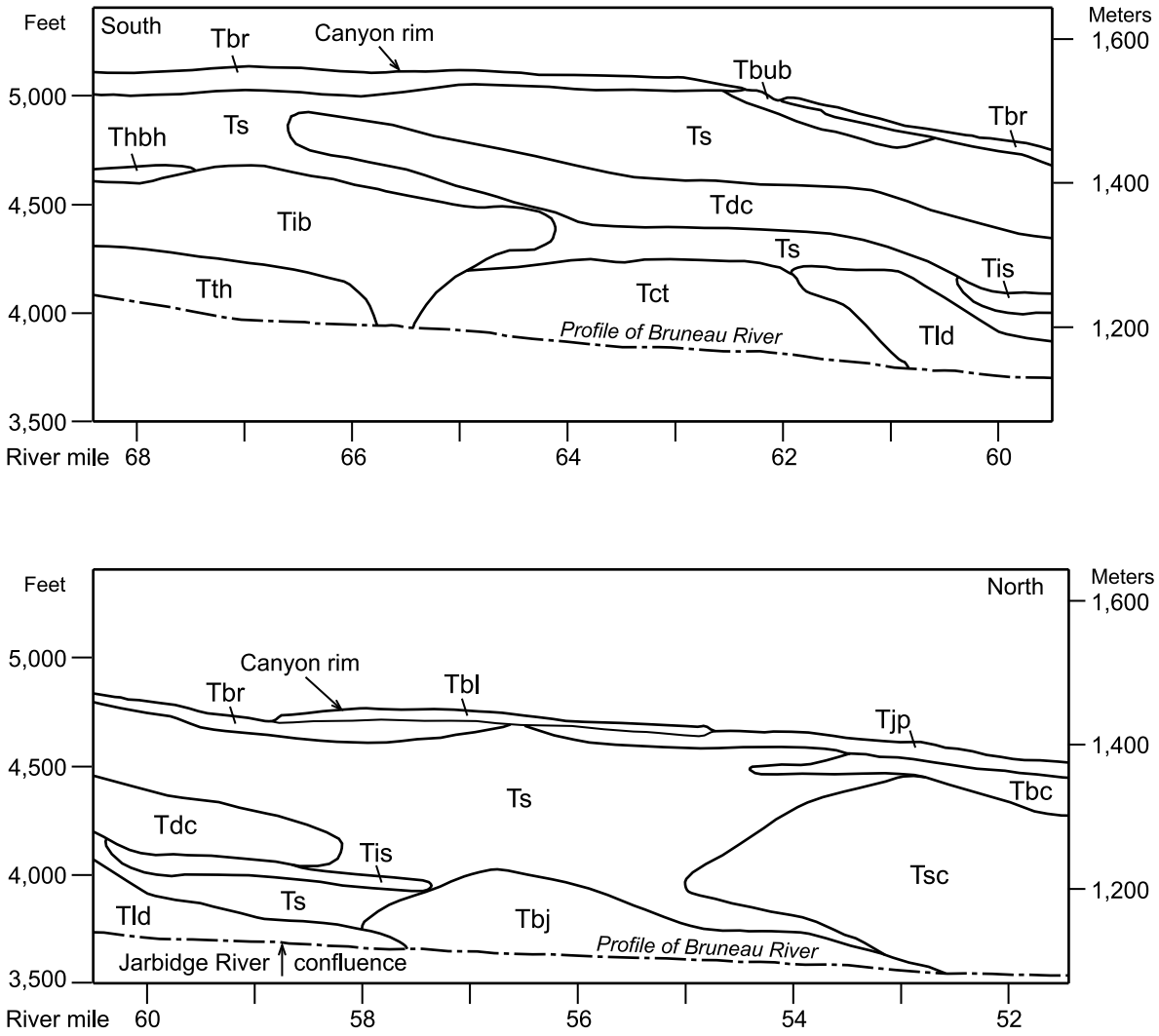

Figure 8. Longitudinal section along Bruneau Canyon in the vicinity of the confluence of the Bruneau and Jarbidge rivers. The section shows the stratigraphic relationships among the late Miocene rhyolite and basalt units in this part of the Bruneau-Jarbidge region. The extent of the rhyolite units is constructed from information on both the east and west sides of Bruneau Canyon, and the extent of the basalt units near the canyon rim is constructed from information only on the west rim. Units are identified as follows: Tbr—basalt of Black Rock, Tbub—basalt of Buster Butte, Tbl—basalt of Big Lakes Draw, Tjp—basalt of the J-P Desert, Tbc—basalt of Bengoechea Cabin, Tis—basalt of Indian Hot Springs, Thbh—basalt of Homer Bedal Homestead, Tdc—Dorsey Creek rhyolite, Tsc—Sheep Creek rhyolite, Tib—Indian Batt rhyolite, Tth—Triguero Homestead rhyolite, Tct—Cedar Tree rhyolite, Tld—Long Draw rhyolite, Tbj—Bruneau Jasper rhyolite, and Ts—undifferentiated sediments. River miles are those designated on U.S. Geological Survey 7.5-minute topographic maps.

Tuff consists of nine recognized ignimbrite sheets, units III, V, VII, IX, X, XI, XII, XIII, and XV. Altogether, the Cougar Point Tuff may include a few thousand cubic kilometers of material, which was erupted during about 2 million years. The loss of the large volume of material expelled from the earth during the eruption of the Cougar Point Tuff ignimbrites is why the large collapsed depression, called the Bruneau-Jarbidge eruptive center, was formed. After being formed, continued eruption of rhyolitic magma, now as large lava flows, partially filled the depression over about 3 million years. The first rhyolite lavas were erupted before the end of ignimbrite formation, but most of the lavas followed the ignimbrites in time. Most of the principal rhyolite lava flows and their relative stratigraphic positions are shown in Figure 8.

Other high-temperature rheomorphic ignimbrites and rhyolite lava flows in the Bruneau-Jarbidge region, which also were formed by the same magmatism that led to the development of the Bruneau-Jarbidge eruptive center, occur to the west along the Grasmere escarpment (the

Table 3. Chemical analyses of basalt samples from the Bruneau-Jarbidge region.

Number	**1**	**2**	**3**	**4**	**5**	**6**	**7**	**8**	**9**	**10**
Sample	**I-3040**	**I-1126**	**I-511**	**I-1867**	**X-11**	**I-1869**	**I-1856**	**B-66**	**I-1927**	**I-728**
Unit	**Twtr**	**Tis**	**Tpb**	**Tbr**	**Tab**	**Tbib**	**Twc**	**Tscv**	**Thir**	**Tgh**
Type	**Al-enh**	**SROT**	**high-Al**	**high-Al**	**SROT**	**SROT**	**Fe-enh**	**SROT**	**Fe-enh**	**SROT**
Major Oxides, weight percent:										
Lab	**UMass**	**UMass**	**UMass**	**UMass**	**UMass**	**UMass**	**UMass**	**Rice**	**UMass**	**Edin**
SiO_2	47.46	47.74	47.14	47.83	47.73	47.88	46.71	53.50	48.81	47.76
TiO_2	1.29	1.68	1.47	1.14	2.20	1.77	3.09	2.50	3.49	1.74
Al_2O_3	16.83	15.40	17.14	17.19	15.73	15.82	14.33	13.70	13.78	15.70
Fe_2O_3	11.28	12.49	12.20	11.44	13.46	13.00	15.81	12.50	15.76	12.10
MnO	0.18	0.18	0.18	0.18	0.19	0.19	0.21	0.16	0.20	0.18
MgO	9.21	9.25	8.63	8.98	7.46	8.20	6.39	4.33	5.65	8.65
CaO	11.02	10.78	10.58	10.90	10.39	10.77	9.77	7.13	9.05	11.24
Na_2O	2.20	2.34	2.45	2.60	2.61	2.88	2.39	2.75	2.44	2.20
K_2O	0.23	0.27	0.24	0.20	0.38	0.35	0.71	2.08	0.46	0.28
P_2O_5	0.23	0.29	0.22	0.14	0.39	0.24	0.81	0.42	0.45	0.27
Total	99.93	100.42	100.25	100.60	100.54	101.10	100.22	99.07	100.09	100.12
Major Oxides, normalized:										
SiO_2	47.49	47.54	47.02	47.54	47.47	47.36	46.61	54.00	48.77	47.70
TiO_2	1.29	1.67	1.47	1.13	2.19	1.75	3.08	2.52	3.49	1.74
Al_2O_3	16.84	15.34	17.10	17.09	15.65	15.65	14.30	13.83	13.77	15.68
Fe_2O_3	11.29	12.44	12.17	11.37	13.39	12.86	15.78	12.62	15.75	12.09
MnO	0.18	0.18	0.18	0.18	0.19	0.19	0.21	0.16	0.20	0.18
MgO	9.22	9.21	8.61	8.93	7.42	8.11	6.38	4.37	5.64	8.64
CaO	11.03	10.73	10.55	10.83	10.33	10.65	9.75	7.20	9.04	11.23
Na_2O	2.20	2.33	2.44	2.58	2.60	2.85	2.38	2.78	2.44	2.20
K_2O	0.23	0.27	0.24	0.20	0.38	0.35	0.71	2.10	0.46	0.28
P_2O_5	0.23	0.29	0.22	0.14	0.39	0.24	0.81	0.42	0.45	0.27
Mg No.	61.80	59.47	58.36	60.87	52.34	55.55	44.47	40.70	41.53	58.62
Minor Elements, parts per million:										
Lab	**ISU**	**UMass**	**Edin**	**UMass**	**UMass**	**UMass**	**UMass**	**Rice**	**UMass**	**Edin**
Sc	33	—	27	—	—	—	—	21	—	33
Cr	316	398	137	188	220	284	113	127	109	315
Co	60	—	—	—	—	—	—	42	—	—
Ni	—	128	118	132	120	129	52	42	71	130
Zn	73	91	87	88	132	107	149	120	146	95
Rb	—	4	3	3	6	6	14	—	9	4
Sr	240	169	199	170	255	192	289	237	362	221
Zr	40	122	94	72	163	114	328	352	191	128
Ba	215	220	197	183	293	215	499	691	365	1341
V	—	227	217	224	227	221	273	217	240	257
Y	—	28	26	22	35	27	47	51	37	36
Nb	—	10	7	6	20	9	32	—	18	11
Ga	—	20	—	18	21	21	24	—	23	—
Cu	—	—	53	—	—	—	—	11	—	50
Pb	—	5	2	2	4	3	8	—	7	3
La	19	10	13	5	18	14	42	—	14	28
Ce	22	29	20	14	43	30	92	—	37	30
Nd	13	—	14	—	—	—	—	—	—	23

Samples were analyzed at the following institutions: UMass—University of Massachusetts at Amherst, ISU—Idaho State University, Edin—Edinburgh University, and Rice—Rice University.

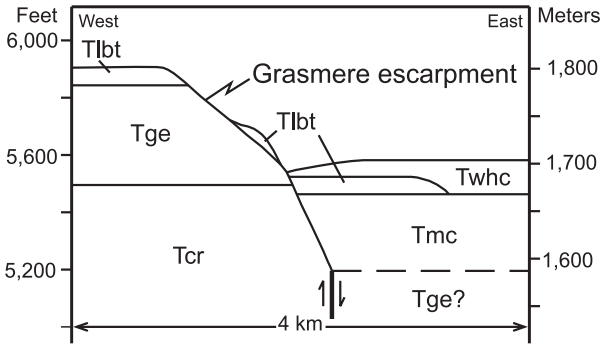

Figure 9. Schematic cross-section of the Grasmere escarpment west of Grasmere near Crab Creek in the western part of the Bruneau-Jarbidge region. The section illustrates the sequence of volcanic events accompanying and following the subsidence of the area east of the escarpment. This subsidence evidently occurred during and immediately after the eruption of the voluminous Grasmere escarpment ignimbrite; the collapse likely was the first major caldera-forming event in the evolution of the Bruneau-Jarbidge eruptive center. Following the collapse, the Marys Creek rhyolite lava flow partly filled the subsided zone. After this, minor amounts of lava of the Little Blue Table basalt, whose sources are farther west on the Owyhee Plateau, flowed down the escarpment to the basin floor. Later, these flows were partially covered by lava flows of the Wickahoney Creek basalt unit erupted from shields within the Bruneau-Jarbidge eruptive center. Units are identified as follows: Twhc—Wickahoney Creek basalt, Tlbt—Little Blue Table basalt, Tmc—Marys Creek rhyolite, Tge—Grasmere escarpment ignimbrite, and Tcr—Crab Creek ignimbrite.

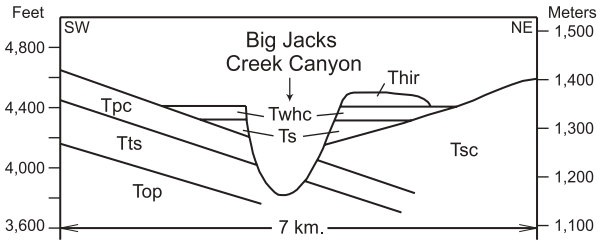

Figure 10. Schematic cross-section of Big Jacks Creek Canyon in the western part of the Bruneau-Jarbidge region near Hill 4630, the vent for the Hole In Rock basalt. The section illustrates how a broad valley formed between the eastward-dipping rhyolite units of the Jacks Creek area and the western margin of the Sheep Creek rhyolite lava flow. Basalt flows of the Wickahoney Creek and Hole In Rock basalt units subsequently flowed northward along this valley and eventually were partly eroded by the incision of Big Jacks Creek to form the canyon. Units are identified as follows: Thir—Hole In Rock basalt, Twhc—Wickahoney Creek basalt, Ts—undifferentiated Miocene sediments, Tsc—Sheep Creek rhyolite, Tpc—Perjue Canyon rhyolite, Tts—Tigert Springs rhyolite, and Top—O X Prong rhyolite.

Marys Creek rhyolite and three thick, densely welded ignimbrites, informally called the rhyolites of Grasmere escarpment, Buckhorn, and Crab Creek; see Figure 9) and to the area east of Jarbidge Canyon in the southeastern part of the Bruneau-Jarbidge eruptive center (the Three Creek rhyolite and the thin, high-temperature, informally named ignimbrites of Deadwood Creek and of House Creek). Additional rhyolite units in the contiguous Jacks Creek area to the west (Figure 1) that were erupted during the same time as the Cougar Point Tuff and rhyolite lava flows in the Bruneau-Jarbidge eruptive center include several large rhyolite lava flows (the Rattlesnake Creek, O X Prong, Tigert Springs, Perjue Canyon, and Horse Basin rhyolites; see figure 10); several of these units extend into the western side of the Bruneau-Jarbidge region (Bonnichsen and Kauffman, 1987; Kauffman and Bonnichsen, 1990). Two more rhyolite units that probably were erupted from the Bruneau-Jarbidge eruptive center occur a few kilometers northeast of the center. These are the upper and lower rhyolites of the Crows Nest area. The upper is a rhyolite lava flow, and the lower likely is a dense, rheomorphic ignimbrite (Bonnichsen, 1982b). Altogether more than a twenty-five major rhyolitic ignimbrites and lava flows are known to have erupted from the Bruneau-Jarbidge eruptive center over 4 to 5 million years, and additional units were erupted during the same time in the contiguous Jacks Creek area.

Nearly all basaltic volcanism in the Bruneau-Jarbidge region occurred after the end of rhyolitic volcanism. In Figure 5, sixty-five basalt volcanoes are plotted in the region. Fifty-eight of these are shields. Four are dike-vents, and the other three are tuff-cone or tuff-ring phreatomagmatic constructs. The shield volcanoes occur throughout the region, and nearly all are of the simple type; only three are complex. The dike vents are localized in the southeastern part of the region, near the margin of the area covered by basalt, and the phreatomagmatic volcanoes are in the northern part (Figure 5, Table 2).

In those areas where sufficiently detailed geologic mapping has been conducted, the basalt flows have been correlated with their source volcanoes. This has been done mainly in the western part of the region in the vicinity of Bruneau and Jarbidge canyons, and in the southeastern part of the region. Elsewhere, although many basalt volcanoes are known to exist (Figure 5, Table 2), our knowledge is not yet sufficient to outline the extent of the flows from specific volcanoes. Accordingly, we have not attempted to discuss the details of the basaltic volcanism in much of the eastern part of the region. There are many more basalt units at lower stratigraphic levels for which the source volcanoes have not been identified. These can be seen primarily in the walls of Bruneau Canyon and its tributaries and in other canyons. Most basalt units that are discussed below and identified in Figure 7 are in the vicinity of Bruneau Canyon and its tributaries in the western part of the region.

BASALT UNITS IN THE BRUNEAU-JARBIDGE REGION

We have studied several groups of basalt units in the Bruneau-Jarbidge region and another in the adjacent Jacks Creek area, so our discussion of the basalt in these regions is organized accordingly. Descriptions of the basalt units in the Jacks Creek area appear first and are then followed by three Bruneau-Jarbidge groups, which are: (1) basalt units that are older than some of the rhyolite units; (2) postrhyolite basalt units of late Miocene and Pliocene age, discussed as units near Jarbidge Canyon, units near the middle part of Bruneau Canyon, and units near the northern part of Bruneau Canyon; and (3) basalt units of Pliocene and Pleistocene age that erupted late in the development of the region and which are in the northern part, mainly north of Bruneau near the Snake River. Finally, several basalt units of probable Miocene age are described for the Grassy Hills area in the southeastern part of the region. Although additional basalt flows and volcanoes occur elsewhere in the region, especially in the eastern part, these have not been studied and cannot be described at this point.

In the Jacks Creek area, geological mapping has separated the various basalt units from one another. The Jacks Creek area is in the northeastern part of the Owyhee-Humboldt region, just northwest of the Bruneau-Jarbidge eruptive center and adjacent to the western SRP graben (Kauffman and Bonnichsen, 1990; Jenks and others, 1993, 1998). The relative ages of these units are given in Figure 7. These basalt flows are probably late Miocene and were deposited on top of the Jacks Creek rhyolite lava-flow succession (Bonnichsen and Kauffman, 1987; Kauffman and Bonnichsen, 1990).

Only in two places are basalt units clearly below some of the rhyolitic units. These are in Jarbidge Canyon and in Bruneau Canyon near its confluence with Jarbidge Canyon where the basalts of Indian Hot Springs and Columbet Creek lie beneath the Dorsey Creek rhyolite lava flow. The age of these two basalt units is late Miocene and probably between 8.1 and 9.5 Ma, the respective ages of the Dorsey Creek and Bruneau Jasper rhyolites (Figure 8). Two other nearby basalt units, the basalts of Tindall Trail and Homer Bedal Homestead, occur beneath substantial thicknesses of sediments and directly on top of rhyolite units older than the Dorsey Creek unit. These basalt units likely are older than some of the latest rhyolite units, so they also are included as part of this early group. Also included is the basalt of Little Blue Table; however, since the vents for this unit lie west of the Bruneau-Jarbidge region, it has been placed in the Jacks Creek part of Figure 7.

Many basalt units are known from our geologic mapping near Bruneau and Jarbidge canyons. The larger, more important units are discussed below, and their relative stratigraphic positions are given in Figure 7. For many of them, the source volcano has been identified, but for some that are lower in their local stratigraphic successions, the source volcanoes have not been identified and in many instances are probably buried by later basalt flows. Throughout the Bruneau-Jarbidge eruptive center, the basalts have Al-enhanced and SROT compositions and came from subaerial eruptions during which small shield volcanoes were formed. In the northern part of the region, however, the basalts are younger and have compositions dominated by Fe-enhanced basalt and ferrobasalt. In a very few places just north of the Bruneau-Jarbidge center, alkali-enriched basalts have been found; their presence suggests an evolutionary progression of basalt compositions similar to those in the western SRP, to be discussed later. Moreover, in the area just north of the Bruneau-Jarbidge eruptive center, phreatomagmatic eruptions formed spatter and tuff constructs and bedded basaltic tuffs, clearly indicating the presence of abundant water when these eruptions occurred.

Along the Snake River and on the bluffs north of the river in the northwestern part of the Bruneau-Jarbidge region are several basalt units (Jenks and others, 1993, 1998). The older ones probably are Pliocene, but may be late Miocene, and appear to have been emplaced subaqueously in Lake Idaho. The sources of many of these units have not been identified, but they are likely buried beneath younger basalt flows to the north. The younger units in this area came from volcanoes to the north and were erupted subaerially (Shervais and others, this volume). Many of them flowed into shallow water and formed pillow deltas as they approached the area along the present course of the Snake River. The youngest of these lavas, the basalt of Little Joe Butte, came from the northwest and flowed into and partly filled the valley that the ancestral Snake River had eroded in the sediments.

Several basalt units have been identified in the Grassy Hills area in the southeast part of the Bruneau-Jarbidge region (Bonnichsen and Jenks, 1995b). All were erupted subaerially. Some formed shield volcanoes during their eruptions, but others were coalesced from lavas that erupted from dikes and ran across the landscape without building noticeable volcanic constructs. These units likely are late Miocene in age and, based on the general compositional pattern of the region, are likely to consist of Al-enhanced and SROT basalt.

Authors' note: The remainder of the "Basalt Units in the Bruneau-Jarbidge Region" section describes individual units. Readers not interested in these details can skip ahead to the next major section, "Geology of the

Twin Falls Region," without losing the continuity of discussion.

BASALT UNITS IN THE JACKS CREEK AREA

The following late Miocene basalt units in the Jacks Creek area are described in this section:

Twtr—basalt of Whickney Tree Reservoir
Toxl—basalt of O X Lake
Tcsb—basalt of Crab Spring Butte
Tsh—basalt of Sugarloaf Hill

One of the main basalt units in the Jacks Creek area is the **basalt of Whickney Tree Reservoir** (Twtr), which erupted from the Hill 6062 shield volcano. It covers about 35 square km, ranges from 4 m to 36 m in thickness, and consists of both Al-enhanced basalt and SROT. A typical analysis is given in Table 3 (number 1). The Whickney Tree Reservoir basalt overlaps the **basalt of O X Lake** (Toxl), which erupted from the Hill 5910 shield, covers about 16 square km, and ranges from 14 m to 35 m in thickness. The **basalt of Crab Spring Butte** (Tcsb) erupted from the shield of that name, covers about 11 square km, and ranges between 10 m and 30 m in thickness. It overlies the **basalt of Sugarloaf Hill** (Tsh), which erupted from the shield of that name, covers about 80 square km, ranges from 5 m to 18 m in thickness, and consists of Al-enhanced basalt. The volcanoes for these four Jacks Creek area units have not been included with the information compiled in Table 2, since they are not located within the area shown on Figure 5. Their locations can be seen on the map by Kauffman and Bonnichsen (1990).

Along the boundary between the Owyhee-Humboldt and Bruneau-Jarbidge regions are two prominent basalt units. The older is the basalt of Wickahoney Creek (Twhc), and the younger is the basalt of Hole In Rock (Thir). These units are discussed below with the other basalt units in the Bruneau-Jarbidge area, but they are also shown in Figure 7 with the units of the Jacks Creek area.

EARLIEST BASALT UNITS IN THE BRUNEAU-JARBIDGE REGION

The following Miocene basalt units that are intercalated with rhyolite in the Bruneau-Jarbidge region are described in this section:

Tlbt—basalt of Little Blue Table
Tis—basalt of Indian Hot Springs
Tcc—basalt of Columbet Creek
Ttt—basalt of Tindall Trail
Thbh—basalt of Homer Bedal Homestead

The **basalt of Little Blue Table** (Tlbt) occurs south of the Jacks Creek area along the boundary between the Owyhee-Humboldt and Bruneau-Jarbidge regions. The Little Blue Table basalt is a composite unit that erupted from Hills 6227 and 5826 and covers at least 80 square km near the western margin of the Bruneau-Jarbidge eruptive center. It probably is older than the units in the Jacks Creek area. At some localities along the base of the Grasmere escarpment, the Little Blue Table basalt occurs within the confines of the Bruneau-Jarbidge eruptive center and may have flowed into place there rather than being downfaulted (Figure 9). Hart (1982) reports K-Ar dates of 8.27 and 9.11 Ma for samples that probably are from this unit, or perhaps from even earlier basalts. This basalt unit is Al-enhanced. The volcanoes for the Little Blue Table basalt are not included in Table 2, since they are outside the area of Figure 5.

The **basalt of Indian Hot Springs** (Tis) is stratigraphically above the Bruneau Jasper and Long Draw rhyolites and below the Poison Creek and Dorsey Creek rhyolites (Bonnichsen and Jenks, 1990), as indicated in Figure 8. It is exposed in the walls of the lower part of Jarbidge Canyon for more than 12 km between the mouth of Poison Creek and the confluence of the Jarbidge and Bruneau rivers, and for more than 4 km upstream from there in Bruneau Canyon. The Indian Hot Springs basalt consists of a series of flows without intervening layers of sedimentary material, although the unit is intercalated within a series of sedimentary layers. The volcano from which the basalt erupted lies beneath the Dorsey Creek rhyolite and probably is in sec. 24, T.13 S., R.7 E., where the unit is thickest in Jarbidge Canyon. The more distal parts of the unit, exposed near where the Jarbidge and Bruneau rivers join, appear to be water-affected and commonly contain calcite-rich amygdules with probable zeolites and other minerals. The unit has a reverse paleomagnetic signature (Bonnichsen, 1982a), contains sparse olivine phenocrysts and abundant plagioclase phenocrysts, and consists of SROT. An analysis of a typical sample is given in Table 3 (number 2).

The **basalt of Columbet Creek** (Tcc) occurs stratigraphically between Unit XV of the Cougar Point Tuff (below) and the Dorsey Creek rhyolite (above) in Jarbidge River canyon immediately downstream from where the East and West Forks join near Murphy Hot Springs (Bonnichsen and Jenks, 1990). The Columbet Creek basalt is exposed for about 5 km along the bottom of Jarbidge Canyon between the confluence of the two forks and the mouth of Columbet Creek. The location of its vent is unknown. The unit has a reverse paleomagnetic signature (Bonnichsen, 1981), contains clumps of olivine phenocrysts, and is chemically like the Indian Hot

Springs basalt, consisting of SROT basalt.

The **basalt of Tindall Trail** (Ttt) is exposed for about 9 km along the walls of Sheep Creek Canyon south of the mouth of Louse Creek and for about 2 km up Marys Creek Canyon. The Tindall Trail basalt lies beneath a thick section of sediments and almost directly on the Indian Batt rhyolite and lower rhyolite at Louse Creek (Jenks and Bonnichsen, 1990). The unit consists of three flow packages separated by thin layers of sediments, but its source volcanoes have not been identified, and no chemical analyses are available.

The **basalt of Homer Bedal Homestead** (Thbh) is exposed discontinuously for about 6 km in the walls of Bruneau Canyon roughly between Long Draw and upstream to the Homer Bedal Homestead (Bonnichsen and Jenks, 1995c). The Homer Bedal Homestead basalt lies on the Indian Batt rhyolite and beneath as much as 100 m of sedimentary material (Figure 8). It contains scattered olivine and plagioclase phenocrysts and probably has a normal paleomagnetic signature (Bonnichsen, 1981). The location of its source is unknown, and no chemical analyses are available.

LATE MIOCENE AND PLIOCENE BASALT UNITS NEAR BRUNEAU AND JARBIDGE CANYONS

In our discussion below, we proceed from south to north, first discussing the units near Jarbidge Canyon, then those near the middle part of Bruneau Canyon, and finally the ones near the northern part of Bruneau Canyon (see Figures 5 and 7).

Basalt Units Near Jarbidge Canyon

The following late Miocene and Pliocene basalt units that are near Jarbidge Canyon are described in this section:

Tda—basalt of the Diamond A Desert
Tdt—basalt of Dorsey Table
Tpb—basalt of Poison Butte
Tbf—basalt of Big Flat
Tmb—basalt of Middle Butte

The **basalt of the Diamond A Desert** (Tda) occurs in the Diamond A Desert between Jarbidge Canyon and Bruneau Canyon in the southern part of the region (Bonnichsen and Jenks, 1990, 1995a). The Diamond A Desert basalt lavas erupted from two shield volcanoes in northernmost Nevada, Hill 6485 and Knight Hill, and apparently flowed more than 32 km northward across sediments and parts of the Dorsey Creek rhyolite lava to beyond where Arch Canyon (Cougar Creek) joins the Jarbidge River, assuming that areas previously mapped as undifferentiated basalt are part of the Diamond A Desert basalt. The flow generally follows the west side of Jarbidge Canyon, is as much as 11 km wide in its southern portion, and ranges between 12 m and 48 m thick on canyon rims. The basalt is nearly aphyric, with only scattered plagioclase microphenocrysts and sparse olivine phenocrysts, and consists of Al-enhanced and high-Al basalt.

The **basalt of Dorsey Table** (Tdt) also occurs in the Diamond A Desert, lying on the Diamond A Desert basalt through most of its extent (Bonnichsen and Jenks, 1990, 1995c). The Dorsey Table basalt erupted from a small irregular-shaped shield volcano, Hill 5770, and flowed generally northward to cover an area about 9 km long (N-S) and 7 km wide (E-W). It is the uppermost basalt unit throughout its extent, occupies the area west of Jarbidge Canyon between Columbet Creek and Dorsey Creek canyons, and is as much as 12 m thick along canyon rims. The basalt typically contains olivine phenocrysts and rounded scoria fragments, and consists of SROT basalt.

The **basalt of Poison Butte** (Tpb) occurs on the east side of Jarbidge Canyon in the southern part of the Bruneau-Jarbidge region (Bonnichsen and Jenks, 1990). It was erupted mainly from Poison Butte (east), a prominent shield volcano, and from Hill 5518, a second, smaller shield that lies about 2 km southeast of the main shield (Figure 5, Table 2). These two shields are thought to be along the same northwest-trending feeder dike. The Poison Butte basalt flowed northwestward from these two sources to form a flow field about 18 km long (including the small area previously called the basalt of Post Office Crossing surrounding the subsidiary southeastern shield). It now occupies an area east of Jarbidge Canyon approximately from the mouth of Dorsey Creek on the south to the north side of Poison Creek Canyon where it joins Jarbidge Canyon. At canyon rims this unit varies from 6 m to 24 m in thickness. The exposed part of the flow field is narrow because it is overlapped by younger flows to the east and south. The basalt is aphyric at most localities but in some places carries large olivine phenocrysts and even cumulophyric clusters of olivine. It consists of Al-enhanced and high-Al basalt; an analysis of a high-Al basalt sample is given in Table 3 (number 3).

The **basalt of Big Flat** (Tbf) is a composite unit east of Jarbidge Canyon in the southern part of the Bruneau-Jarbidge region that occupies an area about 20 km long (N-S) and 10 km wide (Bonnichsen and Jenks, 1990). The Big Flat basalt flows were erupted from a least four small shields, Horse Hill, Pence Butte (south), Hill 5981, and Hill 5583. These four volcanoes form the southern volcanic arc noted in Figure 5. The Big Flat basalt flows

are exposed along the east rim of Jarbidge Canyon for many kilometers with only discontinuous, thin zones of sediments occurring at places between them. The thickness of the unit along this canyon rim ranges from 6 m to 42 m. Radiometric K-Ar dates of 5.08 and 5.10 Ma for this unit (Hart, 1982) suggest it is early Pliocene in age. These dates probably were determined on basalt erupted from Hill 5981. Several analyses of the unit show it to be SROT.

The **basalt of Middle Butte** (Tmb) is east of Jarbidge Canyon and west of the East Fork of the Bruneau River in the southern part of the Bruneau-Jarbidge region. It erupted from the Middle Butte shield volcano (Figure 5, Table 2), which is relatively large and elongate from southeast to northwest but somewhat irregular in shape, and apparently had several eruptive points (Bonnichsen and Jenks, 1990). The extent of the Middle Butte basalt field has not been entirely mapped but extends for more than 15 km northwestward from the source. The unit ranges from 6 to 18 m in thickness. The basalt contains abundant large olivine phenocrysts and sparse plagioclase phenocrysts and is SROT basalt.

Basalt Units Near the Middle Part of Bruneau Canyon

The following late Miocene and Pliocene basalt units near the middle part of Bruneau Canyon are described in this section:

Tbh—basalt of Big Holes
Tbub—basalt of Buster Butte
Tbr—basalt of Black Rock
Tdp—basalt of Dans Place
Tbl—basalt of Big Lakes Draw
Tjt—basalt of Juniper Tree Draw
Tab—basalt of Austin Butte
Tbib—basalt of Big Bend
Tbc—basalt of Bengoechea Cabin
Tsd—basalt of Sheepshead Draw
Tjp—basalt of the J-P Desert
Tlb—basalt of Lookout Butte
Twhc—basalt of Wickahoney Creek

The **basalt of Big Holes** (Tbh) is west of Sheep Creek and south of Louse Creek in a northwest-trending area 2 km wide and 10 km long (Jenks and Bonnichsen, 1990a). Its full extent and source volcano are unknown, but the unit likely extends southward from its exposure for many kilometers beneath the Buster Butte basalt. The Big Holes basalt typically ranges from 6 m to 24 m in thickness and lies on the Sheep Creek rhyolite. It is essentially aphyric, but no samples have been analyzed.

The **basalt of Buster Butte** (Tbub) is exposed on both sides of Sheep Creek between Louse Creek on the north and Marys Creek on the south, and also in an isolated area on the west side of Bruneau Canyon as shown in Figure 8 (Bonnichsen and Jenks, 1990; Jenks and Bonnichsen, 1990a). The unit was erupted from the Buster Butte shield located 4 km southeast of Grasmere. The Buster Butte basalt flow field extends more than 15 km north-south and probably exceeds 10 km east-west. Since Buster Butte is in the southwestern part of the flow field, the lava from this shield apparently flowed mainly north and east. Along canyon rims, the unit typically is between 6 m and 24 m thick. It probably has a reverse paleomagnetic signature (Bonnichsen, 1981). The basalt typically is aphyric, although at some localities it shows widely scattered plagioclase laths and large olivine phenocrysts. A chemical analysis indicates that it is Al-enhanced basalt.

The **basalt of Black Rock** (Tbr) is widely distributed in the southern part of the Bruneau-Jarbidge region between the canyons of the Bruneau River and Sheep Creek, as well as east of Bruneau Canyon south of its confluence with Jarbidge Canyon (Bonnichsen and Jenks, 1990, 1995a, 1995c; Jenks and Bonnichsen, 1990a). The Black Rock shield volcano is near the intersection of the Bruneau-Jarbidge eruptive center buried ring fault and a north-south normal fault with a down-to-the-west displacement of about 150 m. Where the volcano is cut by this fault, the interior layers and a small diabase plug are exposed. The basalt flows traveled mainly north, reaching a distance of about 31 km from the vent (Figure 8). Flows that were directed eastward and southward traveled as much as 5 km from the shield. Near the vent, the sequence of flows, as seen in the canyon walls, is around 30 m thick; in distal areas, the Black Rock basalt is a single flow only a few meters thick. The unit has a relatively modest volume of perhaps between 1 and 3 cubic km. The basalt has a normal paleomagnetic signature. It typically is aphyric, although locally sparse olivine phenocrysts are present. Chemical analyses indicate that most of the unit consists of Al-enhanced basalt, although the diabasic plug is SROT basalt. An analysis of a high-Al basalt sample, the most primitive of the group of analyses from this unit, is shown in Table 3 (number 4).

The **basalt of Dans Place** (Tdp) occurs between Marys Creek on the west and Sheep Creek on the east in the southern part of the Bruneau-Jarbidge region (Jenks and Bonnichsen, 1990a). The source of the Dans Place basalt is a small shield, Hill 5191, probably located toward the south part of the flow field, which is 6-7 km long (N-S) and about 5 km wide. The unit ranges from 6 to 12 m in thickness and contains fairly abundant plagioclase phenocrysts. No chemical analyses are available.

The **basalt of Big Lakes Draw** (Tbl) covers an area

between Bruneau Canyon on the east and Sheep Creek Canyon on the north and west and then north of the Indian Hot Springs area (Figure 8), which makes the unit about 7 km long (SW-NE) and 5 km or more wide (Bonnichsen and Jenks, 1990; Jenks and Bonnichsen, 1990a). The Big Lakes Draw basalt was erupted from the Hill 4882 elongate shield, which stretches for nearly 3 km southwest to northeast. The flow generally traveled northward and ranges from 6 m to 30 m in thickness. It contains sizeable olivine phenocrysts and plagioclase laths that vary in abundance. No chemical analyses are available for this unit.

The **basalt of Juniper Tree Draw** (Tjt) is south of the East Fork of the Bruneau River and north and east of the main fork. It is exposed in the walls of Juniper Tree Draw and the walls of the adjacent part of Bruneau Canyon for a distance of about 4 km; the full extent of the unit is unknown (Jenks and Bonnichsen, 1990a). The Juniper Tree Draw basalt was erupted from the Long Butte shield. Except for the area near Long Butte and the canyon-wall exposures, it is mainly covered by the Lookout Butte basalt. Near the vent, it consists of numerous thin flows, but in the more distal canyon-wall exposures, where the unit is between 30 m and 120 m thick, it consists of only two or three thick flows. The basalt contains abundant plagioclase phenocrysts and sparse olivine phenocrysts and is SROT basalt.

The **basalt of Austin Butte** (Tab) is exposed toward the northern part of the Bruneau-Jarbidge area on the west side of Bruneau Canyon and in the adjacent canyon walls (Jenks and Bonnichsen, 1990a; Jenks and others, 1993, 1998). The Austin Butte basalt was erupted from the Austin Butte shield on the west side of Bruneau Canyon opposite the mouth of the East Fork of Bruneau Canyon. The lavas from this volcano traveled mainly east and north and are exposed as a package of several flows that ranges in thickness from 120 m at the vent to 24 m in distal areas. The unit has been traced for about 7 km along the walls of Bruneau Canyon and for more than 5 km eastward in the walls of the East Fork of Bruneau Canyon. The vent area has been dissected by Bruneau Canyon; there, the lower part of the basalt sequence consists of a few, fairly massive flows, whereas the upper part of the shield has as many as fifteen thin and very scoriaceous flows. The volume of erupted material is estimated to be between 1 and 3 cubic km. The basalt encloses plagioclase laths and clumps of pervasively altered olivine as phenocrysts. Chemical analyses of the unit show it to be predominantly SROT basalt (Table 3, number 5).

The **basalt of Big Bend** (Tbib) is exposed on both sides of Sheep Creek upstream for about 11 km from its confluence with the Bruneau River and forms a flow field with a north-south extent of about 15 km and a width of about 8 km (Jenks and Bonnichsen, 1990a; Jenks and others, 1993, 1998). The Big Bend basalt erupted from Hill 4735 shield located west of Bruneau Canyon and just north of Sheep Creek. This shield is elongate east-west; there is not a clear distinction between the shield and the outflow sheet. Most of the lava flowed northward and extends almost 12 km from the volcano. The unit is about 30 m thick near the volcano on the Sheep Creek Canyon rim but only a few meters thick in distal parts to the north. Near its source, the Big Bend basalt consists of numerous thin scoriaceous flows, but at distal localities it is made of one to three massive flows. The estimated volume of the Big Bend basalt is between 0.5 and 2 cubic km. At many localities, the basalt is nearly aphyric with only sparse small plagioclase phenocrysts. At other localities, it contains large olivine phenocrysts accompanied by small plagioclases, and elsewhere it has sparse large equant plagioclase phenocrysts. This unit is SROT basalt (Table 3, number 6).

The **basalt of Bengoechea Cabin** (Tbc) is in the middle of the Bruneau-Jarbidge region on the east side of Bruneau Canyon between a little south of Stiff Tree Draw on the south (Figure 8) and Sheepshead Draw on the north (Jenks and Bonnichsen, 1990a). It is exposed in the walls of Bruneau Canyon or at the surface for nearly 16 km (N-S) and as much as 5 km (E-W). It was erupted from the Hill 4726 shield and flowed northward, following a paleovalley between the Sheep Creek rhyolite flow to the west and the rhyolite of the Juniper-Clover area to the east. The north end of the unit has not been identified; there, it merges into an undifferentiated basalt unit. Near its source, the Bengoechea Cabin basalt is characterized by numerous thin flows with an aggregate thickness of as much as 42 m, whereas in distal areas the unit is 6 m to 12 m thick. Both plagioclase and olivine phenocrysts range from large and abundant near the source to small and sparse in the distal portions of the flow. The unit is SROT basalt.

The **basalt of Sheepshead Draw** (Tsd) is in the interior of the Bruneau-Jarbidge region on the east side of Bruneau Canyon from near Sheepshead Draw on the south to the East Fork Bruneau Canyon on the north (Jenks and Bonnichsen, 1990a). It is exposed at the surface over an area about 6 km long (SW-NE) and about 3 km wide and also for an undetermined distance in the walls of Bruneau Canyon where it ranges from 3 m to 12 m thick. The Sheepshead Draw basalt was erupted from the Hill 4553 shield and generally flowed northwestward. It contains plagioclase and sparse olivine phenocrysts; no samples have been analyzed.

The **basalt of the J-P Desert** (Tjp) occurs between Sheep Creek Canyon and Bruneau Canyon in the interior of the Bruneau-Jarbidge region (Jenks and Bonnichsen,

1990a). The unit is a composite of flows erupted principally from Monument Butte, with possible contributions from adjacent small vents that are part of this complex shield. The flows traveled mainly northeastward to form a flow field about 13 km long and 7 km wide, assuming that the unit includes the basalt categorized as undivided by Jenks and Bonnichsen (1990) and which extends to the confluence of the Sheep Creek and Bruneau canyons. Exposures of the unit at canyon rims (Figure 8), which are somewhat distal from the source, range from 6 m to 12 m thick. No samples of this unit have been analyzed.

The **basalt of Lookout Butte** (Tlb) forms a flow field at the surface between the main Bruneau Canyon and the East Fork of Bruneau Canyon and probably extends all the way to the confluence of these canyons, having flowed northwestward from its source at the Lookout Butte (west) shield for 11 km. The flow field is as much as 6 km wide (Jenks and Bonnichsen, 1990a). At canyon rims, it is as much as 24 m thick. The basalt shows abundant plagioclase and olivine phenocrysts that at some localities are grouped into clumps. A chemical analysis shows the unit is SROT basalt.

The **basalt of Wickahoney Creek** (Twhc) occurs along the boundary between the Owyhee-Humboldt and Bruneau-Jarbidge regions. It is a composite unit believed to have erupted from Poison Butte (west) and Hill 5158 in the western part of the Bruneau-Jarbidge eruptive center (Kauffman and Bonnichsen, 1990; Jenks and others, 1993, 1998). The lavas from these shields flowed northward, generally following a paleovalley between the Grasmere escarpment and the Tigert Springs rhyolite lava flow on the west and the southwestern margin of the Sheep Creek rhyolite lava flow on the east (Figures 9 and 10). The Wickahoney Creek basalt consists of two flow sequences, presumably representing the two sources, separated by as much as 2 m of sediments. The unit's overall north-south length is about 24 km, but the flow field is only a few kilometers wide because of its confinement to the paleovalley. The flows are well exposed in Wickahoney Creek Canyon where the unit ranges from 5 to 67 m thick. Analyzed samples show the basalt is SROT.

Basalt Units Near the Northern Part of Bruneau Canyon

The following late Miocene and Pliocene basalt units near the northern part of Bruneau Canyon are described in this section:

Tbrl—lower basalt of Bruneau River
Tbrm—middle basalt of Bruneau River
Tbru—upper basalt of Bruneau River
Thc—basalt of Hot Creek
Twc—basalt of Winter Camp Butte
Tsog—Seventy One Gulch volcanic complex
Tsay—Saylor Creek ferrobasalt field
Tscv—Sailor Cap Butte volcanic complex
Thir—basalt of Hole In Rock

Three composite basalt units, the **lower basalt of Bruneau River** (Tbrl), the **middle basalt of Bruneau River** (Tbrm), and the **upper basalt of Bruneau River** (Tbru) occur in the walls of Bruneau Canyon in the northern part of the Bruneau-Jarbidge region (Jenks and Bonnichsen, 1989; Jenks and others, 1993, 1998). These units appear along a stretch of Bruneau Canyon that is about 10 km long, starting at the south about where Miller Water joins Bruneau Canyon and where the older Sheep Creek rhyolite has been downfaulted to the north so that the number of basalt flows and their aggregate thickness increase markedly to the north. The zone where these three Bruneau River basalt units occur extends northward about 10 km to where the edge of the Bruneau Desert plateau is reached, and the elevation of the land decreases as one enters the dried-up basin of former Lake Idaho. Through this zone, the individual basalt flows exposed in the walls of Bruneau Canyon have not been mapped separately; rather, the three composite units, the lower, middle, and upper basalts of Bruneau River have been recognized, each consisting of flows from a variety of sources.

The Bruneau Canyon Scenic View site (Figure 5), west of the Saylor Creek Air Force Range, is an excellent place to view these units in the walls of Bruneau Canyon. The lower basalt of Bruneau River is the lowest sequence in Bruneau Canyon north of Miller Water and forms the sheer cliffs in the bottom of the canyon. The lower basalt consists of four or five individual flows that are separated from one another by very thin red sediment layers. The individual flows appear to be less rubbly than the flows within the two composite units higher on the canyon wall, which may be a result of having been subaerially emplaced. The middle basalt of Bruneau River contains three or four basalt flows, each separated by thin layers of red sediment. The middle basalt unit is above a slope break that probably represents a thicker section of sediments. The upper basalt of Bruneau River is also a sequence of three or four flows that are separated from the middle unit by another prominent slope break that may represent a significant thickness of sediment. In the part of the canyon downstream from the Bruneau Canyon Scenic View site, some of the upper flows in the upper basalt of Bruneau River appear to be extremely water affected.

Analyzed samples from the lower basalt unit are a combination of Al-enhanced and SROT basalt, and the samples from the middle unit are SROT basalt. For the upper basalt of Bruneau River, most of the analyses are

Fe-enhanced basalt, so this composite unit would seem to have more in common with the Pliocene Fe-enhanced and ferrobasalt units discussed in the following section, rather than with the Miocene basalts in the areas farther south.

The **basalt of Hot Creek** (Thc) occupies an area about 13 km long (N-S) and 8 km wide and probably was erupted mostly from a single but unidentified source. The unit is located mainly between Bruneau Canyon on the east and Hot Creek on the west in the northern part of the Bruneau-Jarbidge region (Jenks and Bonnichsen, 1989; Jenks and others, 1993, 1998). The Hot Creek basalt is as much as 30 m thick and likely equivalent to one of the flows that constitute the upper basalt of Bruneau River. Throughout much of its exposure area and particularly in the northern part, the Hot Creek basalt is extremely water affected to the point where, from a distance, it resembles a layer of brown sediment. Where it is strongly water affected, it overlies a thin but prominent layer of sediment that has been baked and stained bright red. At most localities, the basalt is aphyric, although locally it contains plagioclase or olivine phenocrysts, or both. Analyses indicate the unit is partly SROT and partly Fe-enhanced basalt, but both types are compositionally close to one another.

The **basalt of Winter Camp Butte** (Twc) covers a broad area in the northern part of the Bruneau-Jarbidge region mainly east of Bruneau Canyon (Jenks and Bonnichsen, 1989, 1990a; Jenks and others, 1993, 1998). The flow field is more than 22 km from southeast to northwest and more than 25 km from southwest to northeast, if the probable correlative outlier map units, the basalt of Miller Water and the pillow basalt of West Fork Browns Creek, are included in the unit. The shield, Winter Camp Butte in the southern part of the flow field, is somewhat elongate in an east-west direction and is accompanied by a probable satellite vent, Hill 4285, located just over 2 km to the southeast, which suggests the Winter Camp Butte eruption may have started through a fissure and later became restricted to these point sources. The Winter Camp Butte flows extend nearly 20 km northwest from the vent to their distal margin at the rim of Bruneau Canyon. They also traveled many kilometers west, north, east, and even southeast from the volcano. The maximum thickness along the rim of Bruneau Canyon is about 30 m. The Winter Camp Butte basalt likely has a relatively large volume, probably 5 to 20 cubic km of erupted lava. The unit is stratigraphically above the Austin Butte and Big Bend basalt units and lies on several meters of fluvial and lacustrine Glenns Ferry age sediments, especially in its northern part. It seems to be one of the youngest basalt units on the Bruneau Desert plateau and is believed to be Pliocene in age. Along its northern margin, the Winter Camp Butte basalt ran into the margin of Lake Idaho and formed an extensive pillow delta that is well exposed along the Bruneau Canyon rim between 3,400 and 3,500 feet (1,037-1,067 m) in elevation, and at the same elevation at other localities along the northern part of the unit. The basalt typically contains abundant plagioclase phenocrysts accompanied by scattered olivine phenocrysts. Chemical analyses indicate the unit to be Fe-enhanced basalt (Table 3, number 7).

The **Seventy One Gulch volcanic complex** (Tsog) is a small tuff and cinder cone and associated basalt dike near the southeast end of Bruneau Valley in the northern part of the Bruneau-Jarbidge region (Godchaux and others, 1992; Jenks and Bonnichsen, 1989; Jenks and others, 1993, 1998). The tuff and cinder cone (Hill 3001) probably was built in shallow water but in a subaqueous setting. It is capped by scattered basalt pillows and accompanied by a peperitic dike of quenched basalt clots in a matrix of volcanically reworked sedimentary material. Extending for about a kilometer southeastward from the cone is a vertical basalt dike that evidently extruded fragmental hyaloclastitic tuff and coarser material onto the lake floor that now is interstratified with lake sediments. The basalt at the preserved top of the dike is pillowed. The dike also extends several hundred meters northwest of the volcano so that it is exposed alongside the road, but apparently the volume of material extruded was insufficient to form a lava flow. A chemical analysis indicates the basalt is ferrobasalt.

The **Saylor Creek ferrobasalt field** (Tsay) is a composite unit in the northern part of the Bruneau-Jarbidge region that covers a broad area in and adjacent to the Saylor Creek Air Force Range. Most of the basalt field is between West Fork Brown Creek on the west and Pot Hole Creek on the east. Several eruptive sources of ferrobasalt contributed to the development of the field, and the lava flows from them spread as far northward as the valley of the Snake River, so that the field extends about 30 km north-south and has a width greater than 10 km. The eastern part has not been mapped, so the width could be considerably more, particularly if Black Butte (north) just to the east were to have the same composition and be included in the Saylor Creek field. Three previously distinguished units—the basalt of Pence Butte (north), the basalt of Browns Creek, and the Pot Hole Butte volcanic complex that occur in the source area of this unit—and a fourth unit—the basalt of Chalk Gulch that occurs along the Snake River in the Indian Cove area and north of Bruneau Dunes State Park—are compositionally identical and have been grouped together in the Saylor Creek ferrobasalt field (Jenks and Bonnichsen, 1989; Jenks and others, 1993, 1998). The vents for the field include Pot Hole Butte, which is a series of small

phreatomagmatic tuff and spatter constructs, Pence Butte (north) which is a small shield, and some unnamed low topographic rises just northwest of Pothole Butte. Together, these sources constitute a southeast- to northwest-trending zone about 10 km in length along the southwest side of the field. As the field is followed northward from its source area, the basalt flows become progressively buried by greater thicknesses of sedimentary materials that evidently were deposited after the volcanism. Near the Snake River, however, the ferrobasalt included in the field was exhumed by the Bonneville Flood; this represents the farthest travelled part. The flows along the Snake River typically are water affected and contain pillows at many locations. The basalt in this field contains widely varying amounts of plagioclase and olivine phenocrysts, in some instances arranged as large rosette clumps, and has a composition that mainly is ferrobasalt.

The **Sailor Cap Butte volcanic complex** (Tscv) is a subaerially emplaced phreatomagmatic tuff ring with a spatter cap and associated layers of basaltic tuff extending away from the vent; it is in the northern part of the Bruneau-Jarbidge region, just to the east of the Saylor Creek ferrobasalt field (Godchaux and others, 1992; Jenks and Bonnichsen, 1989). Although the Sailor Cap volcanic complex is about the same age as the nearby Saylor Creek ferrobasalt field, the composition of the juvenile volcanic rocks in the two are quite different. With 54 percent silica, the Sailor Cap volcanic rock might better be called a basaltic andesite or ferrolatite instead of a basalt (Table 3, number 8). This is a very unusual rock type for the SRP, although similar analyses have been found for a couple of rocks from the undifferentiated basalts in the area west of Bruneau Canyon in the northern part of the Bruneau-Jarbidge region. This compositional variation pattern is reminiscent of the juxtaposition of vents with widely differing compositions in the Birds of Prey basalt field and at other localities in the western SRP, which are discussed below.

The **basalt of Hole In Rock** (Thir) occurs along the boundary between the Owyhee-Humboldt and Bruneau-Jarbidge regions where it forms a flow field about 8 km long (N-S) and as much as 3 km wide (Jenks and others, 1993, 1998; Kauffman and Bonnichsen, 1990). It is well exposed in the canyons of Wickahoney and Big Jacks creeks. The Hole In Rock basalt ranges from 11 m to 20 m in thickness and lies on a layer of sedimentary material as much as 27 m thick and on the basalt of Wickahoney Creek below that. It erupted from the Hill 4630 shield volcano and flowed northward along the same paleovalley that channelized the Wickahoney Creek basalt between the Sheep Creek rhyolite flow on the east and the rhyolite units of the Jacks Creek area on the west (Figure 10). The basalt contains plagioclase phenocrysts that range from sparse to common and from small to large. Some chemically analyzed samples are Fe-enhanced basalt, and some are ferrobasalt. An example of an analyzed Fe-enhanced sample is given in Table 3 (number 9).

BASALT UNITS NORTH OF BRUNEAU NEAR THE SNAKE RIVER

The following basalt units north of Bruneau near the Snake River are described in this section:

Tgsm—basalt of Goldsmith Road
Tcan—basalt of Canyon Creek
Tfly—basalt of Flying H Ranch Road
QTsim—basalt of Simco Road
Qljb—basalt of Little Joe Butte
Qrs—basalt of Rattlesnake Springs

The **basalt of Goldsmith Road** (Tgsm) occurs along the valley of the Snake River through an east-west distance of about 17 km from north of Bruneau Dunes State Park on the east to the Bruneau River arm of C.J. Strike Reservoir on the west; it forms a discontinuous series of occurrences as much as 2 km wide (Jenks and others, 1993, 1998). It is the oldest basalt unit in the area and has been eroded by the Snake River. The small adjacent unit, referred to as the basalt of Katie Lane, should be included as part of the Goldsmith Road basalt. The source of the basalt is unknown, but it probably lies to the north of the Snake River and has been covered by later sediments and basalt units. It evidently was emplaced into Lake Idaho because it is extensively water affected and shows several areas where pillows are developed. Some pillowed areas have associated tuffaceous zones of hyaloclastic debris that probably formed as the pillows were developing. West of Idaho Highway 51 in the lower canyon of Rattlesnake Creek, each flow within the unit has a pillowed base. The basalt contains phenocrysts of plagioclase, which range from larger in the east to smaller in the west, and small- to medium-sized olivine phenocrysts. Analyzed samples of the unit indicate SROT and Fe-enhanced basalt.

The **basalt of Canyon Creek** (Tcan) occurs as benches and in canyonwall exposures along the Snake River valley for about 20 km from north of Bruneau westward to the Simplot Feedlot area in the southeastern part of the region described in the later western SRP section (Jenks and others, 1993, 1998). The small adjacent unit, the basalt of Crane Falls, should be included as part of the Canyon Creek basalt. Its southern edge is irregular, suggesting it may be close to the original flow margin. The source of the basalt has not been determined but probably is some distance to the north; the small basalt vents, which constitute Hills 3110, 3198, and 3203 west of

Mountain Home and about 20 km north of the Snake River, are the probable candidates. The Canyon Creek basalt lies on the Goldsmith Road basalt in the area north of Bruneau, but farther west in the area east of Simplot Feedlot, it forms part of the plateau surface north of the river. The Canyon Creek basalt is pillowed at some places and water affected to some extent, supporting the idea that it ran into standing water, probably part of Lake Idaho. The basalt commonly is aphyric or contains sparse, small plagioclase phenocrysts. The unit consists of Fe-enhanced basalt.

The **basalt of Flying H Ranch Road** (Tfly) is exposed in the bluffs and benches along the north side of the Snake River for about 5 km north of Bruneau Dunes State Park (Jenks and others, 1993, 1998). Its source is unknown but probably somewhere to the north. The Flying H Ranch Road basalt overlies the Saylor Creek ferrobasalt field in the canyon, and the flows at its western margin constitute a fairly large pillow delta. The unit contains plagioclase phenocrysts that range from small to medium in size and at places are abundant; compositionally the unit is Fe-enhanced basalt.

The **basalt of Simco Road** (QTsim) is exposed for about 15 km (E-W) along benches and in canyon walls in the Snake River Valley between due north of Bruneau on the east and north of the confluence of the Bruneau River arm of C.J. Strike Reservoir with the main part of the reservoir on the west. The unit has been traced northward on the east side of Canyon Creek to about 5 km north of the reservoir (Jenks and others, 1993, 1998; Shervais and others, this volume). The source of the Simco Road basalt has not been identified but most likely is one or more of the vents west of Mountain Home about 15 to 20 km north of C.J. Strike Reservoir. In several places, the basalt formed extensive pillow deltas at its southern margin. The unit is SROT basalt.

The **basalt of Little Joe Butte** (Qljb) occurs in Snake River Canyon and on the plateau to the north, and extends west of C.J. Strike Dam where it was mapped by Jenks and others (1993, 1998) as the basalts of Strike Dam Road and Dixie Road. The unit is described later with the other western SRP basalt flows.

The **basalt of Rattlesnake Springs** (Qrs) forms a broad flow field north of the Snake River and is exposed as the canyon rim basalt for an east-west distance of 25-30 km north of Bruneau and Bruneau Dunes State Park (Jenks and others, 1993, 1998; Shervais and others, this volume). Where it occurs, it is the uppermost basalt unit throughout the region and appears to be entirely subaerial. The Rattlesnake Springs basalt was erupted from a broad, very low-profile shield, Hill 3242, located a few kilometers west of Mountain Home and about 20 km north of the Snake River. Thus, the basalt field is relatively large, covering a few hundred square kilometers; it probably contains between 10-50 cubic km of basalt. The basalt contains plagioclase and olivine phenocrysts and is SROT basalt.

BASALT UNITS IN THE GRASSY HILLS AREA, SOUTHEASTERN PART OF THE BRUNEAU-JARBIDGE REGION

The following late Miocene and Pliocene basalt units in the Grassy Hills area are described in this section:

Tdw—basalt of Deadwood Creek
Tlgh—basalt of Little Grassy Hills
Twor—basalt of Worley Draw
Tcs—basalt of Camas Slough
Tgh—basalt of Grassy Hills
Tsig—basalt of Signal Butte
Tmab—basalt of Marshall Butte

The **basalt of Deadwood Creek** (Tdw) is exposed for nearly 3 km along the northeast side of Deadwood Creek in the southeastern part of the Bruneau-Jarbidge region (Bonnichsen and Jenks, 1995b). It was erupted from a small dike vent, Hill 5850, that is elongate from southeast to northwest. The lava flowed an undetermined distance northward from the vent area and subsequently was covered by the Camas Slough basalt unit. The Deadwood Creek basalt contains plagioclase and olivine phenocrysts that in places are fairly large and may occur in clumps. No chemical analyses are available.

The **basalt of Little Grassy Hills** (Tlgh) covers an area more than 5 km (E-W) and nearly 3 km (N-S) north of Deadwood Creek in the southeastern part of the Bruneau-Jarbidge region (Bonnichsen and Jenks, 1995b). The exposed area of the Little Grassy Hills basalt consists mainly of the shield, which is elongate from southeast to northwest. The lava from this shield flowed northward an undetermined distance. To the north, the Grassy Hills basalt overlies the Little Grassy Hills basalt. Much of this unit is nearly aphyric, although scattered plagioclase phenocrysts occur at some places near the vent.

The **basalt of Worley Draw** (Twor) is exposed as a series of basalt flows along Worley Draw in the southeastern part of the Bruneau-Jarbidge region (Bonnichsen and Jenks, 1995b). The flow field extends more than 11 km north-south and is as much as a few kilometers wide, although the margins of the unit are covered by the Signal Butte basalt on the east and the Grassy Hills basalt on the west. The vent area, Hill 5728 and the adjacent topographic depression, is at the south end of the flow field in sec. 23, T. 14 S., R. 12 E. The presence of dense, vesicle-poor basalt suggests the vent area contains a frozen lava

pond. The Worley Draw basalt ranges from being aphyric to containing scattered plagioclase and olivine phenocrysts.

The **basalt of Camas Slough** (Tcs) is a composite unit made of overlapping basalt flows that erupted from three dike vents northeast of Deadwood Creek (Bonnichsen and Jenks, 1995b). The Camas Slough basalt field occurs along both sides of Devil Creek and is more than 15 km from north to south and a little over 6 km wide in the southern part, but less in the northern part where it is overlain by the Grassy Hills basalt on the west. The three dike vents are Hills 5890, 5950, and 5880 spaced out over a distance of a little more than 3 km along the southern margin of the flow field. At some localities, the basalt is aphyric; at others, it contains plagioclase and olivine phenocrysts.

The **basalt of Grassy Hills** (Tgh) is a large basalt unit east of East Fork Bruneau Canyon in the southeastern part of the Bruneau-Jarbidge region (Bonnichsen and Jenks, 1995b). The source volcano, Grassy Hills, is a complex shield with a southeast- to northwest-trending ridge at its top about 3 km long as the main eruptive zone, and other possible eruptive points at the southeastern end of the shield. The flow field, which extends northwestward from the shield, is at least 23 km long and as much as 13 km wide. The basalt contains sparse to abundant olivine phenocrysts but lacks plagioclase phenocrysts. Chemical analyses of the unit indicate SROT basalt (Table 3, number 10).

The **basalt of Signal Butte** (Tsig) is exposed on the west side of House Creek and continues on to the north in the southeastern part of the Bruneau-Jarbidge region (Bonnichsen and Jenks, 1995b). The basalt was erupted from the Signal Butte shield volcano at the south end of the flow field. The Signal Butte basalt lava ran more than 10 km north and northeast from the volcano and formed a flow that typically is 1 to 4 km wide. The basalt contains phenocrysts of olivine and plagioclase that vary from small and sparse in the distal part of the flow to large and more abundant in the vent area. The unit consists of Al-enhanced basalt.

The **basalt of Marshall Butte** (Tmab) erupted in the southeastern part of the Bruneau-Jarbidge region from the Marshall Butte shield and flowed northward for several kilometers (Bonnichsen and Jenks, 1995b). The Marshall Butte basalt contains olivine and plagioclase phenocrysts that vary in abundance and size and commonly occur in clumps.

GEOLOGY OF THE TWIN FALLS REGION

Many basalt volcanoes of late Miocene and Pliocene age exist in the southwestern part of the Twin Falls region; these include scattered volcanoes of Pliocene and Pleistocene age several kilometers south of the city of Twin Falls, and more widely scattered volcanoes of mainly Pleistocene age northeast, north, and northwest of the city (Figure 5). Considerable geologic mapping has been done in most parts of the Twin Falls region, except for the southern part. Older geologic maps include the north part of the region at 1:500,000-scale and a narrow strip along the Snake River at 1:63,360-scale (1 inch per mile) by Stearns and others (1938), much of the region at 1:125,000-scale by Malde and others (1963), a compilation at 1:250,000-scale by Rember and Bennett (1979), the Glenns Ferry-Hagerman area at 1:48,000-scale by Malde and Powers (1972), and the Snake River Canyon at 1:24,000-scale by Covington (1976). Recent mapping by the U.S. Geological Survey was conducted at 1:48,000-scale in the southeastern part of the region by Williams and others (1990, 1991) and at 1:24,000-scale for the north wall of Snake River Canyon and vicinity by Covington and Weaver (1989, 1990a, 1990b, 1990c, 1991).

Our own geologic mapping at 1:24,000-scale has concentrated on the basalt units in the agricultural region south of the Snake River in the Buhl, Filer, Twin Falls, and Kimberly areas. These maps will eventually be included in a 1:100,000-scale geologic map produced by the Idaho Geological Survey. These maps include the Twin Falls and Filer 7.5-minute quadrangles and the Jerome 7.5-minute quadrangle south of the Snake River (Bonnichsen and Godchaux, unpub. mapping, 1994-1995), the Clover and southern part of the Niagara Springs 7.5-minute quadrangles (Bonnichsen and Godchaux, unpub. mapping, 1995-1996), the Buhl and eastern part of the Balanced Rock 7.5-minute quadrangles (Bonnichsen and Godchaux, unpub. mapping, 1996-1997), and the Kimberly and Eden 7.5-minute quadrangles (Bonnichsen and Godchaux, unpub. mapping, 2002).

The general stratigraphic relations in the Twin Falls region are summarized in Figure 2, and the more detailed stratigraphic relations among many of the basalt units, mainly in the northern part of the region, are presented in Figure 11. An even more detailed view summarizing the stratigraphic relations among the volcanic units in Snake River Canyon near Twin Falls is presented in Figure 12.

Very few radiometric dates are available for basalt units in the Twin Falls region; the few that exist are compiled in the middle part of Figure 6 along with the available dates from the Glenns Ferry area just northwest of the Twin Falls region. These dates show that basaltic volcanism has been fairly constant in the region for nearly

the last 7 million years. The few gaps in this continuity simply may represent the small number of units that have been dated, compared to the number of units known to exist there. The data in Figure 6 show that the period of basaltic volcanism in the Twin Falls region is somewhat younger than in the Bruneau-Jarbidge region, although the two intervals overlap by 3 to 4 million years, and that the basaltic volcanism in both regions went on for about 7 million years.

The average chemical composition and range of compositions for basalt samples from the Twin Falls region are somewhat more Fe-rich and Al-poor than for the basalts of the Bruneau-Jarbidge region, although there is large overlap in the compositional ranges for the two regions (Figure 4; Table 1). Generally, the compositions of the older basalts in the Twin Falls region are like those of the Bruneau-Jarbidge region, whereas the younger basalts in the region, from which the preponderance of analyses were taken, are more evolved in that they are higher in Fe and lower in Al than the Bruneau-Jarbidge basalts. Analyses of ten representative basalt samples selected to show the range of compositions in the Twin Falls region are given in Table 4.

STRUCTURAL GEOLOGY OF THE TWIN FALLS REGION

The main geologic features of the Twin Falls region are the older highlands in the southern part where prebasaltic rocks are exposed outside the SRP, and the basalt plain that covers the central and northern parts (Figure 5). The older southern highlands consist of the Cassia Mountains area in the southeast and additional but unnamed highlands separated by a north-south valley, the Rogerson graben, in the southwest. The highlands are underlain mainly by Miocene silicic volcanic rocks that erupted from the interior of the central SRP and flowed generally southward to cover earlier Tertiary volcanic rocks and Mesozoic and Paleozoic marine sediments. The Cassia Mountains and other parts of the southern highlands represent the transition zone between the Basin and Range Province farther south and the SRP province. The basalt-capped plateau in the middle and northern part of the Twin Falls region constitutes much of the central part of the SRP where the hotspot trace that trends southwest-northeast from the Owyhee Plateau to the Yellowstone region is intersected by the southeast- to northwest-trending western SRP rift zone that is elongate nearly perpendicular to the hotspot trace (Figures 1 and 3). The late Miocene to Pleistocene basalt flows that cap the plateau in the central and northern part of the Twin Falls region were erupted over a period of several million years following the development of the main SRP zone and during the concurrent and subsequent formation of the western SRP rift. These basalts overlie silicic volcanic rocks that were formed earlier in the development of the central part of the SRP, coeval with those exposed in the southern highlands. Immediately north of the Twin Falls region, there are additional highlands, the eastern Bennett Hills, underlain by Miocene silicic volcanic rocks similar to those in the southern highlands and that, in turn, overlie older Tertiary volcanic rocks and granitic rocks of the Idaho batholith. The Bennett Hills are cut off on the north by a Pliocene-Pleistocene east-west oriented graben known as the Camas Prairie in which there are abundant accumulations of late Pliocene and Pleistocene SRP-type basalt and fluvial and lacustrine sediments.

Numerous faults cut the silicic volcanic rocks in the Cassia Mountains south of the SRP (Malde and others, 1963; Mytton and others, 1990; Williams and others, 1990, 1991). The fault pattern is complex, with the older Paleozoic and Mesozoic rocks cut by faults with many orientations, including some thrust faults. The younger Miocene volcanic rocks are cut by numerous normal faults in a pattern that generally includes closely spaced faults oriented north-south or northeast-southwest with lengths

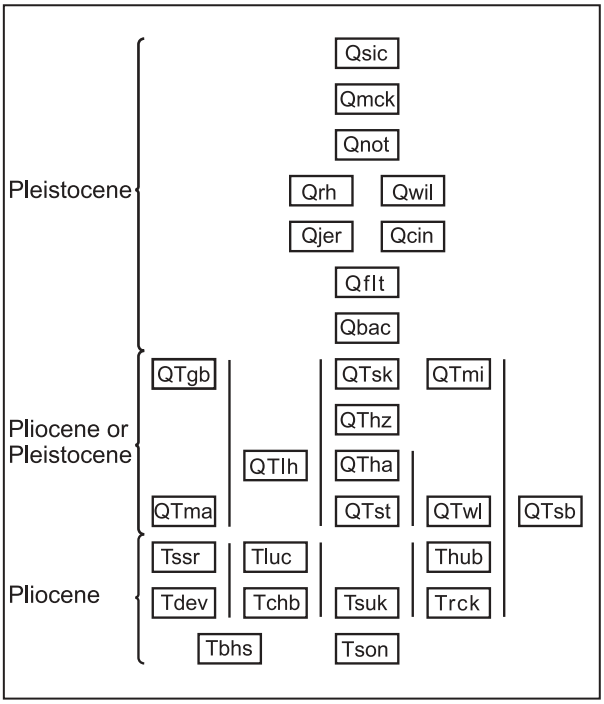

Figure 11. Stratigraphic chart for basalt units in parts of the Twin Falls region. Side-by-side boxes indicate that adjacent units are about the same age. Stratigraphic relations between adjacent boxes are unknown where parts of adjacent columns are separated by heavy vertical lines. See text for unit symbol identifications and information sources.

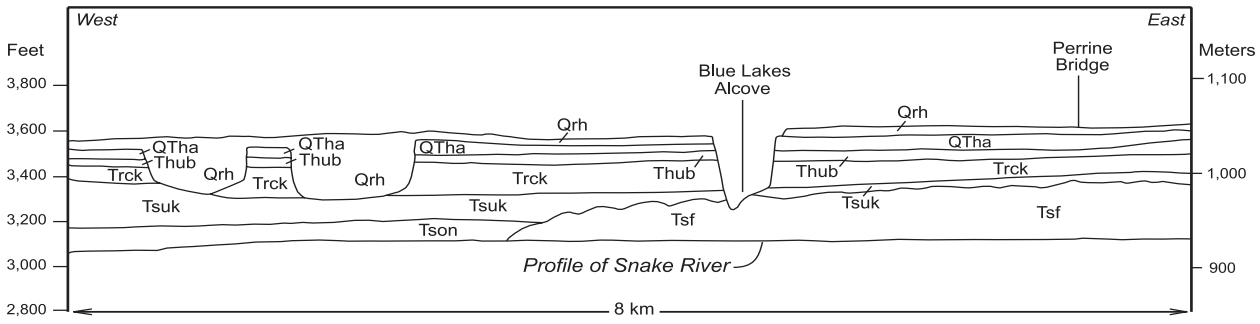

Figure 12. Longitudinal section along the north wall of Snake River Canyon for the zone extending westward from the Perrine Bridge north of Twin Falls. Marginal lobes belonging to the western margin of the Shoshone Falls rhyolite lava flow are exposed in the area west of Blue Lakes Alcove. The lowest basalt unit was likely erupted from Sonnickson Butte north of the canyon, based on chemical similarity. The overlying basalt flows are units of the Magic Valley ferrobasalt that were erupted from volcanoes south of the canyon, and the uppermost unit, the Rocky Hill basalt (Sand Springs basalt of Stearns and others, 1938) erupted from a vent to the northeast. Note how the Rocky Hill basalt has filled channels that were cut into the Magic Valley ferrobasalt units probably by the ancestral Snake River. Units are identified as follows: Qrh—Rocky Hill basalt, QTha—Hansen Butte basalt, Thub—Hub Butte basalt, Trck—Rock Creek basalt, Tsuk—Sucker Flat basalt, Tson—Sonnickson Butte basalt, and Tsf—Shoshone Falls rhyolite. Modified from a canyon wall map in Covington and Weaver (1990b).

of more than 20 km; faults in these orientations tend to cut one another. Cutting these older faults are several normal faults with northwest-southeast strikes that have lengths of more than 20 km. Both groups of faults probably formed in response to extensional stresses. The earlier north-south and northeast-southwest faults likely formed in response to pre-SRP stresses, in a fashion similar to the abundant faults with similar orientations farther west (Ekren and others, 1981). The later northwest-southeast faults, which generally are oriented perpendicular to the elongation of the SRP and parallel to the elongation of the western SRP rift, likely were developed after the major SRP silicic eruptions in the Twin Falls region had occurred, and probably accompanied the widening of the western SRP rift (Figure 3).

The topographically low region in the central SRP from which some or all of the large, high-temperature ignimbrites exposed in the Cassia Mountains and Bennett Hills were erupted is probably a large caldera complex or eruptive center similar to the Bruneau-Jarbidge eruptive center farther west (Bonnichsen, 1982a; McCurry and others, 1997; Pierce and Morgan, 1992). The proposed but mainly buried outline for the Twin Falls eruptive center is indicated in Figures 1 and 5. The evidence for where we have drawn the location of the eruptive center boundary actually is fairly thin. It rests mainly on the position of where the ignimbrites dip northward beneath younger volcanic rocks along the north side of the Cassia Mountains, on a plexus of faults with varying orientations along the east side of Salmon Falls Creek canyon in the Balanced Rock area, and on the presumption that the Shoshone Falls and Balanced Rock rhyolite lava flows are within the eruptive center, which is analogous to the many rhyolite lava flows within the Bruneau-Jarbidge center.

The remainder of the Twin Falls eruptive center margin shown in Figure 5 is speculative. We have drawn it as a semicircular entity mainly to portray the idea that such a structurally downdropped zone from which hundreds if not thousands of cubic kilometers of silicic ignimbrite erupted, is hidden within the central SRP. As noted earlier, the region between the Bruneau-Jarbidge and Twin Falls eruptive centers, as drawn on Figures 1 and 5, eventually may need revision. Since probably many kilometers of southwest-northeast extension related to the same tectonic forces that developed and widened the western SRP rift occurred in the central SRP, the original boundaries of such an entity as the Twin Falls eruptive center likely were considerably modified by the extension (Figure 3). Moreover, we may find through further study that before the extension there really was not much, if any, of a gap between the Bruneau-Jarbidge and Twin Falls centers, and they simply are parts of the same structurally downdropped zone that formed during and after the thousands of cubic kilometers of high-temperature ignimbrites were erupted from the region now occupied by the two centers.

The Rogerson graben separates the Cassia Mountains in the southeastern part of the Twin Falls region from a southwestward continuation of similar highlands (Figure 5). The Rogerson graben is a complex structure bounded by a large escarpment, the Browns Bench es-

Table 4. Chemical analyses of basalt samples from the Twin Falls region.

Number	**1**	**2**	**3**	**4**	**5**	**6**	**7**	**8**	**9**	**10**
Sample	**I-2249**	**I-3234**	**I-3309**	**I-3209**	**I-3207**	**I-3302**	**I-3367**	**I-3377**	**I-3381**	**I-3372**
Unit	**dike**	**Tson**	**Tsuk**	**Trck**	**QTst**	**Tchb**	**QTlh**	**Qflt**	**Qrh**	**Qnot**
Type	**SROT**	**Al-enh**	**ferrobs**	**Fe-enh**	**ferrobs**	**SROT**	**ferrobs**	**ferrobs**	**ferrobs**	**SROT**
Major Oxides, weight percent:										
Lab	**WSU**	**UMass**	**UMass**	**UMass**	**UMass**	**UMass**	**UMass**	**UMass**	**UMass**	**UMass**
SiO_2	48.82	47.90	45.96	46.35	46.02	48.09	44.43	46.03	46.49	47.31
TiO_2	1.40	1.88	3.36	2.98	3.27	2.69	4.17	3.32	3.30	2.27
Al_2O_3	15.20	16.04	13.61	14.55	13.97	14.94	11.47	13.78	13.89	15.45
Fe_2O_3	12.25	12.52	16.59	15.44	16.27	14.33	19.11	16.34	16.00	13.39
MnO	0.18	0.20	0.23	0.21	0.22	0.19	0.29	0.23	0.23	0.20
MgO	8.84	7.70	6.57	7.41	7.15	6.51	5.10	6.02	6.63	7.70
CaO	11.91	10.78	9.70	9.67	9.66	9.63	9.85	9.57	9.22	10.28
Na_2O	2.24	2.40	2.55	2.59	2.67	2.64	2.21	2.74	2.68	2.71
K_2O	0.20	0.38	0.60	0.58	0.57	0.67	0.89	0.74	0.75	0.61
P_2O_5	0.21	0.35	0.79	0.60	0.56	0.49	1.94	0.89	0.79	0.48
Total	101.25	100.15	99.96	100.38	100.36	100.18	99.46	99.66	99.98	100.40
Major Oxides, normalized:										
SiO_2	48.22	47.83	45.98	46.17	45.85	48.00	44.67	46.19	46.50	47.12
TiO_2	1.38	1.88	3.36	2.97	3.26	2.69	4.19	3.33	3.30	2.26
Al_2O_3	15.01	16.02	13.62	14.49	13.92	14.91	11.53	13.83	13.89	15.39
Fe_2O_3	12.10	12.50	16.60	15.38	16.21	14.30	19.21	16.40	16.00	13.34
MnO	0.18	0.20	0.23	0.21	0.22	0.19	0.29	0.23	0.23	0.20
MgO	8.73	7.69	6.57	7.38	7.12	6.50	5.13	6.04	6.63	7.67
CaO	11.76	10.76	9.70	9.63	9.63	9.61	9.90	9.60	9.22	10.24
Na_2O	2.21	2.40	2.55	2.58	2.66	2.64	2.22	2.75	2.68	2.70
K_2O	0.20	0.38	0.60	0.58	0.57	0.67	0.89	0.74	0.75	0.61
P_2O_5	0.21	0.35	0.79	0.60	0.56	0.49	1.95	0.89	0.79	0.48
Mg No.	58.85	54.93	43.97	48.74	46.55	47.38	34.59	42.20	45.09	53.26
Minor Elements, parts per million:										
Lab	**WSU**	**ISU**	**ISU**	**ISU**	**ISU**	**ISU**	**ISU**	**ISU**	**ISU**	**ISU**
Sc	41	35	31	30	30	29	36	31	28	34
Cr	509	259	158	222	231	184	78	105	188	242
Co	—	53	57	63	63	67	50	54	54	55
Ni	143	35	55	—	—	69	55	52	65	155
Zn	85	89	161	133	148	127	265	185	167	109
Rb	2	11	19	—	—	18	13	13	10	18
Sr	137	360	215	315	320	220	310	315	330	335
Zr	79	70	150	90	100	120	270	170	150	120
Ba	137	180	315	365	250	295	655	490	445	255
V	280	—	—	—	—	—	—	—	—	—
Y	31	—	—	—	—	—	—	—	—	—
Nb	8	—	—	—	—	—	—	—	—	—
Ga	20	—	—	—	—	—	—	—	—	—
Cu	83	—	—	—	—	—	—	—	—	—
Pb	4	—	—	—	—	—	—	—	—	—
La	0	16	29	21	19	25	75	42	31	19
Ce	19	35	65	47	42	54	162	88	68	43
Nd	—	24	28	31	26	33	80	43	49	29

Samples were analyzed at the following institutions: UMass—University of Massachusetts at Amherst, WSU—Washington State University, and ISU—Idaho State University.

carpment, on its west side and by a series of much smaller escarpments on its east side. The Browns Bench escarpment apparently has a major fault along its base that has a length of about 20 km in Idaho and that extends farther south in Nevada. This fault trends north to north-northeast and has a down-to-the-east displacement of several hundred meters. The Rogerson graben can be thought of as a complex half graben that developed during the time of silicic volcanism in this part of the SRP. The faulting along the Browns Bench escarpment cut ignimbrites with radiometric ages younger than 10.22 ± 0.09 Ma (New Mexico Geochronological Research Laboratory, written commun., 2003) and had deposited on its floor the Greys Landing ignimbrite with a K-Ar age of 7.62 ± 0.4 Ma (Hart and Aronson, 1982), as well as later basalts. We suggest that the Rogerson graben formed during the same time as did much of the extension in the western SRP graben in response to the same set of regional stresses.

Abundant northwest-southeast and a few north-south oriented faults cut the silicic volcanics in Salmon Falls Creek canyon in the central part of the region (Bonnichsen and Godchaux, unpub. mapping, 1996-1997) similar to the fashion seen in the Cassia Mountains. North of the central SRP in the Bennett Hills area, a complex pattern of abundant normal faults also cut the Miocene silicic volcanic rocks (Malde and others, 1963) in a fashion similar to that in the highlands in the southern part of the Twin Falls region. These similar patterns of faulting both north and south of the Twin Falls region and along Salmon Falls Creek canyon strongly suggest that extensive faulting of the older part of the sequence of volcanic rocks occurs at depth beneath the Twin Falls region, even though the upper part of the basalt plain is almost unfaulted.

Only a few faults cut the basalt plain in the central and northern parts of the Twin Falls region. These faults have southeast-northwest strikes and displacements that typically measure no more than a few tens of meters but reach lengths of a few kilometers. The faults parallel those cutting the older silicic volcanic rocks and probably represent a continuation of the same stresses that produced this older group. The northwest-southeast faults displace only the oldest basalts in the interior of the central SRP. Thus, the stresses responsible for their development may have largely been dissipated by the time the younger (late Pliocene and Pleistocene) basaltic volcanism was underway in the Twin Falls region.

The Castleford, Roseworth, Pigtail, and Hollister volcano alignment zones occur in the southwestern part of the Twin Falls region (Figure 5). They are parallel to the volcano alignment zones in the Bruneau-Jarbidge region to the west. These zones encompass all of the basaltic volcanoes in the southwestern part of the region, except the Cedar Butte and Canyon Hill shields. The presence of such southeast-northwest-trending volcano alignment zones apparently does not extend into the northern and eastern part of the Twin Falls region, however. As can be seen in Figure 5, these zones are not evident within the Twin Falls eruptive center, except along its southwestern side. Also interesting for the volcano alignment zones is that the Castleford and Hollister zones are composed of Fe-enhanced basalt and ferrobasalt, whereas the zones farther west are mainly SROT and Al-enhanced basalt. Moreover, the age of the volcanism in the Hollister and Castleford zones appears to be Pliocene in age, whereas the volcanism in the zones farther to the west is Miocene and early Pliocene. These observations are consistent with the idea, expressed earlier, that the volcano alignment zones represent magma rise along previously fractured structural zones, rather than a phenomena produced during the basaltic volcanism. Arcs of large shields like those in the Bruneau-Jarbidge region have not been noted in the Twin Falls region, however.

LANDSCAPE EVOLUTION IN THE TWIN FALLS REGION

The principal elements of the landscape in the Twin Falls region are the two geologic zones mentioned above—the basalt-covered plain in the central and northern parts and the highlands and accompanying Rogerson graben in the southern part. In both areas, canyons have been incised into the bedrock. In the southern highlands, these canyons tend to be fairly deep, with sloping walls, and appear to have evolved over considerable time. In the central and northern part of the region and in the Rogerson graben, the canyons are not as deep as those in the southern highlands, typically have vertical walls, and appear to have evolved over a shorter time than the canyons farther south. These observations are consistent with the age of the volcanic rocks in the central and northern parts of the region being somewhat older than those in the southern highlands, allowing much more time for the canyons to develop there.

Lake Idaho was present in the northern part of the region and farther west in the SRP during the late Miocene and the Pliocene. It likely had drained from the Twin Falls region by the beginning of the Pleistocene. Only in the northwestern part of the region near Hagerman is there abundant evidence for the existence of Lake Idaho. A succession of lacustrine beds, the Glenns Ferry Formation, are capped by beds of gravel-laden fluvial sediments, the Tuanna Gravel (Malde and Powers, 1962, 1972; Link and others, this volume). Lake Idaho apparently existed for a prolonged period during which basaltic volcanism either was explosive to form phreatomagmatic deposits, where eruptions occurred in shallow

parts of the lake, or facilitated the development of pillow deltas and water-affected flows where subaerially erupted lavas ran into the lake. An example of a pillow delta that probably formed at the lake margin is the lowest basalt flows along the Castleford-Roseworth road in Salmon Falls Creek canyon, at an elevation of about 3,700 feet, near the apparent high-stand of the lake. Excellent examples of subaerially erupted lavas that ran into the lake and became WAB can be seen north and northwest of Buhl in the Sucker Flat, Canyon Hill, and Lucerne School basalts.

Once Lake Idaho had been drained and the base level that it had provided was removed, canyons started to incise into the basalt-covered plain in the central SRP. This led to the Snake River and Salmon Falls Creek canyons and their tributaries. Some preexisting streams with their headwaters in adjacent highlands, such as Rock Creek which heads in the Cassia Mountains, reestablished themselves in new canyons that cut across the basaltic plain. While the canyons were being excavated, the basalt volcanism in the central SRP plain was continuing. This led to many situations where newly formed canyons were partly filled by later basalt flows. A clear example of this is in the Salmon Dam area at the north end of the Rogerson graben where the relatively late, probably Pliocene age, Salmon Butte volcano was formed as it erupted basaltic lava that partially filled the nearby ancestral canyon of Salmon Falls Creek. Later, partial erosion of this flow led to a classic intracanyon lava flow confined within an older canyon (Figure 13). Similar relationships occur at several localities along Snake River Canyon (Figure 12), although they are not graphically illustrated in the landscape there. During the latter part of the Pliocene and most of the Pleistocene, the continued basaltic volcanism led to the filling of canyons and the excavation of new ones as additional basalt flows spread across parts of the developing basalt plain. This topography, rearranged by the lava flows, had an especially marked influence on the course of the Snake River and the cutting of canyons by it.

The earlier phase of basaltic volcanism in the central part of the Twin Falls region was mainly eruptions from vents south of the present course of the river to form the Magic Valley ferrobasalt, followed by eruptions from vents mainly north of the river course to form the Northside basalt. We do not know where the ancestral Snake River drainage was located, if in fact it even existed, during Pliocene time as the Magic Valley ferrobasalt formed, but the paleoslopes at that time would infer that such a drainage would have been pushed toward the north side of the central SRP region. The effect of the latter eruptions during the Pleistocene of Northside basalt flows apparently had the opposite effect on the course of the Snake River by pushing it southward to skirt around the margins of flows. Some of these later flows, the Rocky Hill flow for example, apparently followed earlier canyons excavated by the river, but then were reexcavated as the river reestablished its canyon. Evidence for such events can be seen in the local presence of remnants of Northside flows along the southern rim of Snake River Canyon north of Filer and Buhl, across from filled tributaries on the north wall of the canyon (Figure 12). These competing forces of the erosional excavation of canyons concurrent with their filling and refilling by the sequence of basalt flows, then, has led to the development of complex and not yet entirely resolved stratigraphic relations among the basalt flows in the Twin Falls region.

The final evolutionary stages that formed the present landscape in the Twin Falls region include the development of a blanket of loess across the region, the formation of landslides along canyon walls, and the effects of the Bonneville Flood. The loess varies in thickness from place to place and was deposited over several million years, inasmuch as some layers are preserved beneath the basalt flows. The loess is the material upon which the soils across the region are developed. This loess blanket is relatively thicker on the south side of Snake River Canyon than on the north. Its mantling effect restricts the best places for observing the geology of the region to the canyon walls, especially of the Snake River and Salmon Falls Creek.

Along the walls of the canyons, landslides are common, such as the ones in the Sinking Canyon area along Salmon Falls Creek west of Buhl (Figure 14). In most places, these landslides have occurred where several meters or more of unconsolidated to poorly consolidated lacustrine and fluvial beds, most commonly part of the Glenns Ferry Formation, lie beneath a canyon rim of basalt flows. As illustrated in Figure 14, when the incompetent sedimentary beds are weakened, commonly by the undercutting of streams, or during the Pleistocene by the Bonneville Flood, or by marked variations in the height of the ground-water table as has occurred during the past century, they give way and permit the overlying basalt to subside, fragment, and create lowered and tilted benches of basalt-flow fragments and debris avalanches consisting of large basalt blocks in a disorganized sedimentary matrix. This process of landslides along the canyon wall still continues, as witnessed by the 1993 Bliss landslide (Gillerman, 2001) and the current active subsidence in the Blue Gill Pond area just south of Sinking Canyon.

The Bonneville Flood made its way down the course of the Snake River about 14,500 years ago and affected both the Snake River Canyon and some of the upland area to the north (Malde, 1968), but otherwise did not significantly change the landscape of the Twin Falls re-

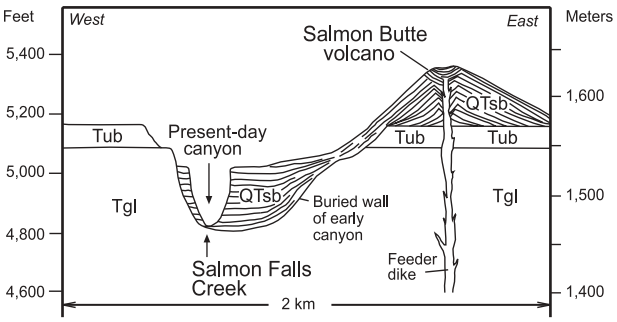

Figure 13. Schematic cross-section of Salmon Falls Creek canyon near Salmon Dam in the southern part of the Twin Falls region. Section shows how an earlier canyon was partly filled with basalt flows erupted from Salmon Butte. The younger flows were then partly eroded to reveal the classic intracanyon basalt signature in which the top of the younger flow appears at a lower elevation in the canyon wall than the older flows. Units are identified as follows: QTsb—basalt of Salmon Butte, Tub—older undifferentiated basalt flows, and Tgl—Greys Landing ignimbrite.

gion. In the canyon, a significant amount of erosion occurred primarily in the form of tearing blocks of basalt as much as 3 m across from the canyon rim and transporting them, with variable amounts of rounding, to downstream localities where they were deposited in large bars. Such erosion undoubtedly widened the canyon and likely caused the deep part of it to migrate headwards an unknown distance. The two waterfalls north of Kimberly, Shoshone Falls and Twin Falls, were likely sculpted during the Bonneville Flood. A large part of the flood veered northward away from the present course of the Snake River and flowed across the basalt plain. In that area, it scoured out a number of channels and left numerous deposits of sand and gravel. Where the flood reentered the canyon of the Snake River north of Kimberly and Twin Falls, it created by headward erosion many short channels and impressive examples of scablands topography as the flood waters fell over the north canyon rim. An example of these Bonneville Flood channels is Blue Lakes Alcove (Figure 12), a short distance downstream from the Perrine Bridge.

VOLCANISM IN THE TWIN FALLS REGION

In the southern part of the Twin Falls region, extensive occurrences of late Miocene silicic volcanic rocks, consisting mainly of densely welded ignimbrites, were apparently erupted from the SRP. These ignimbrites occur as laterally extensive sheets of welded tuff, many of which can be traced tens of kilometers. They typically have volumes ranging from 5 to 50 cubic kilometers, exclusive of volumes that are hidden beneath the younger basalts in the SRP, and were erupted at comparatively high temperatures. Some of the upper Cougar Point Tuff units extend into the southwestern part of the Twin Falls region from the west and are capped by the slightly younger tuffs of Deadwood Creek and House Creek. Large, high-temperature ignimbrites similar to the Cougar Point Tuff units that erupted from the Bruneau-Jarbidge eruptive center are well exposed along the Browns Bench escarpment that forms the western margin of the Rogerson graben. The succession of Cougar Point Tuff-like ignimbrites traces to Browns Bench escarpment, where it is well exposed, contains at least ten separate cooling units, and forms an aggregate section more than 300 m thick. The ignimbrite units at Browns Bench escarpment have not been correlated one by one with the Cougar Point Tuff units exposed 50-75 km to the west in Jarbidge and Bruneau canyons; they fall approximately in the same time span, however, and have similar phenocryst assemblages and chemical compositions as the Cougar Point Tuff units, so very likely they were generated by magmatic processes similar to those that operated in the Bruneau-Jarbidge eruptive center. The Greys Landing ignimbrite was erupted from a hidden source in the SRP after the regional structural collapse that downdropped the central SRP and formed the Bruneau-Jarbidge and Twin Falls eruptive centers, and the subsequent extension that formed the Rogerson graben. The Greys Landing unit flowed up against the tilted ignimbrites along the northern edge of the highlands in the southwestern part of the Twin Falls region and into the Rogerson graben forming much of its floor.

In the Cassia Mountains in the southeastern part of the Twin Falls region is another thick succession of late Miocene, densely welded rhyolitic ignimbrite sheets with petrologic and physical characteristics very similar to those of the Cougar Point Tuff and the unnamed units in the Browns Bench area west of the Rogerson graben. The major units recognized in the Cassia Mountains are, from older to younger, the tuffs of Big Bluff, Steer Basin, Wooden Shoe Butte, and McMullan Creek (McCurry and others, 1996, 1997; Mytton and others, 1990; Parker and others, 1996; Perkins and others, 1995; Watkins, 1998; Williams and others, 1990, 1991; Wright and others, this volume). These ignimbrites are believed to have mainly erupted from the Twin Falls eruptive center north of the Cassia Mountains. None have yet to be definitively correlated with any of the Cougar Point Tuff units or any of the large welded ignimbrite sheets exposed at Browns Bench escarpment, although several suggestions have been proposed. Given the units' proximity and similarity to those regions farther west, it would not be surprising if specific correlations were eventually confirmed.

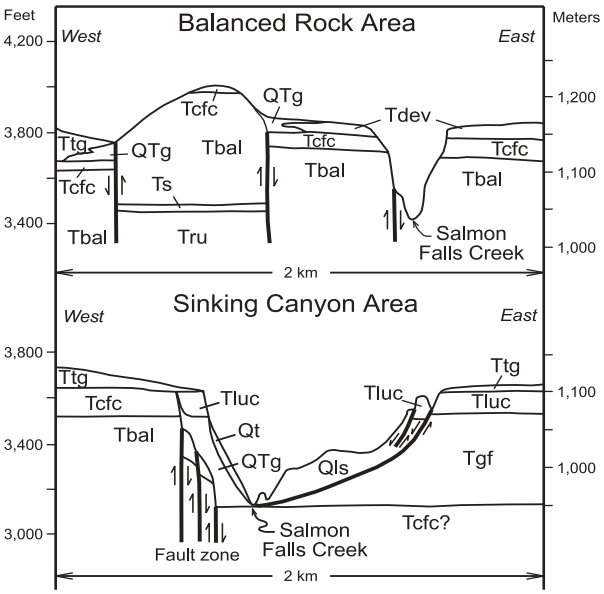

Figure 14. Schematic cross-sections of Salmon Falls Creek canyon in the Balanced Rock and Sinking Canyon areas of the western Twin Falls region. The sections contrast the erosional differences caused by streams cutting narrow canyons into competent volcanic rock layers, as in the Balanced Rock area, with those cutting wide canyons into incompetent lake beds that then allow extensive landslides and slope retreat, as occurred in the Sinking Canyon area. Units are identified as follows: Qls—landslide deposits, Qt—talus, QTg—mixed slope detritus, gravel and lake beds, Ttg—Tuanna Gravel, Tluc—basalt of Lucerne School, Tgf—Glenns Ferry Formation sediments, Tdev—basalt of Devil Creek Butte, Tcfc—Castleford Crossing ignimbrite, Tbal—Balanced Rock rhyolite lava, Ts—older sediments, and Tru—undifferentiated rhyolite.

Additional rhyolitic units occur beneath the basalt flows in the central part of the Twin Falls region and are exposed where the canyons of the Snake River and of Salmon Falls Creek have eroded through the basalt. Along the Snake River in the region from the Twin Falls waterfall to nearly 4 km downstream from the Perrine Bridge (McCurry and others, 1997; Monani, 1997), the upper part of the Shoshone Falls rhyolite lava flow is exposed at the bottom of the canyon beneath various basalt flows (Figure 12). Two rhyolite units are discontinuously exposed along Salmon Falls Creek canyon from the Balanced Rock area west of Castleford northward for about 20 km to near the mouth of the canyon near the Snake River (Figure 14). The lower unit is the rhyolite of Balanced Rock, a lava flow, and the upper is the rhyolite of Castleford Crossing, a very high-temperature, rheomorphic ignimbrite identical in composition to the underlying lava flow (Bonnichsen and Godchaux, unpub. mapping, 1996-1997; Bonnichsen and others, 1988, 1989; McCurry and others, 1997; Monani, 1997). The temporal relationship of these units within the Twin Falls eruptive center to the ignimbrites exposed in the Cassia Mountains is unknown. The units likely are younger than the Cassia Mountains units, if the sequence of events in the Twin Falls eruptive center is analogous to those in the Bruneau-Jarbidge eruptive center.

The sixty-three basalt volcanoes that we know to occur in the Twin Falls region are shown on Figure 5 and are listed in Table 2. As in the Bruneau-Jarbidge region, they mainly are shields. Of the sixty-three, fifty are shields; four are dike vents; six are cinder and spatter constructs that were formed in subaerial environments and that may have produced lava flows later; and three are phreatomagmatic constructs that are dominated by phreatomagmatic tuff and may have started as maars and culminated as tuff rings or cones. Many of these are described in more detail below. Most of the lava formed flows consisting of subaerial pahoehoe basalt; aa basalt flows have not been seen in the region. In some instances, the basalt flows ran into water, either Lake Idaho or streams and rivers, to form WAB and pillow basalt accumulations. The older basalts commonly have formed WAB, whereas a few of the younger flows have associated pillow accumulations, especially in places where the lava flowed down relatively steep slopes or even dropped over cliffs to enter water and become pillowed. The flows vary considerably in size but many exceed a cubic kilometer in volume, and a few contain more than 5 cubic km. The most voluminous unit apparently is the Sucker Flat basalt, which erupted from the group of vents that constitute the Hollister volcano alignment zone (Figure 5) and underlies most of the agricultural region between Twin Falls and Buhl. Most of the lavas from volcanoes south of the Snake River generally flowed north and northwest. Most of the lavas from volcanoes north of the Snake River, however, generally flowed west and southwest. Because many of the flows from these northern sources are younger than the ones from the southern sources, they buried the northern extent of many of the older flows.

BASALT UNITS IN THE TWIN FALLS REGION

Age is the principal basis of subdividing the basalt units in the Twin Falls region into the groups in the following section. Geographic proximity and chemical composition also have been taken into account. The three main basalt groups are those of late Miocene and Pliocene age, those of Pliocene and Pleistocene age, and those of Pleistocene age. The late Miocene and Pliocene group has been subdivided into basalts in the southwest and northern parts

of the region. The Pliocene and Pleistocene basalt units are broken into the informal "Magic Valley ferrobasalt field" and the other basalt units distributed throughout the northern part of the region. The Pleistocene basalts in this northern area have been grouped into the informal "Northside basalt field."

The Magic Valley ferrobasalt field consists of the basalt erupted from the arc of vents around the southern part of the Twin Falls eruptive center, from the nearby vents of the Hollister volcano alignment zone, and from Salmon Butte farther southwest. The field stretches nearly 60 km from southwest to northeast and ranges from about 40 km wide in the west to about 10 km wide in the east. It includes basalt units of strictly Fe-enhanced and ferrobasalt composition. There are other basalt volcanoes farther north that consist entirely of ferrobasalt and Fe-enhanced basalt, but that are not now included in the Magic Valley ferrobasalt field because they either are some distance away or are younger and fit better into the Northside basalt field.

We find it convenient to use these two informally named basalt-unit groupings, the Magic Valley ferrobasalt and the Northside basalt fields, rather than the older Banbury Basalt, Glenns Ferry Formation, and Bruneau Formation of the Idaho Group and the Snake River Group formal stratigraphy (Stearns, 1938; Malde and Powers, 1962; Malde, 1991). Our proposed groupings take geographic and compositional information into account whereas the older system does not. Our groupings should be viewed as complementing rather than replacing the older stratigraphic nomenclature until such time as more information on the age, composition, and geographic extent of specific flows allows a formal revision. For the Banbury Basalt stratigraphic unit, however, we propose that it should be abandoned and present our reasons in the discussion of the basalt of Sucker Flat below.

Authors' note: The remainder of the "Basalt Units in the Twin Falls Region" section describes individual units. Readers not interested in these details can skip ahead to the next major section, "Geology of the Western Snake River Plain Region," without losing the continuity of discussion.

LATE MIOCENE AND PLIOCENE BASALT, SOUTHWEST PART OF THE TWIN FALLS REGION

Although the basalt in the northern part of the Twin Falls region has been studied and mapped in some detail, the basalt in most of the southwest part (basalt that erupted from the volcanoes plotted southwest of the Twin Falls eruptive center boundary on Figure 5) has not. Consequently, even though many basalt volcanoes occur in the southwest, not enough is known to discuss individual units there. The few units with sources in that area, the basalts of Devil Creek Butte, Canyon Hill, and Salmon Butte, are included with similar units from the northern part of the region. Nearly all of the volcanoes in the southwest part of the region are in the Roseworth, Pigtail, and the extreme southeast end of the Coonskin volcano alignment zones (Figure 5). The exceptions are the Canyon Hill and Cedar Creek shields. Many of the southwest area basalt volcanoes are shields, but a few are dike vents and a few others are cinder and spatter cones (Table 2).

The southwestern basalts have high-Al, Al-enhanced, or SROT chemical compositions; a typical example of SROT, from the dike next to the Rogerson-Jarbidge road that fed the Hill 5822 dike vent, is given in Table 4 (number 1). The only radiometric dates are the K-Ar determinations by Hart (1982) for the lower (6.91 ± 0.66 Ma) and upper (6.70 ± 0.63 Ma) basalt flows that make the canyon rim at the west side of Salmon Falls Creek at Salmon Dam. These two dated basalt flows lie on the Greys Landing rhyolite that was K-Ar dated by Hart and Aronson (1982) at 7.62 ± 0.40 Ma.

LATE MIOCENE AND PLIOCENE BASALT UNITS, NORTHERN PART OF THE TWIN FALLS REGION

The following late Miocene and Pliocene basalt units in the northern part of the Twin Falls region are described in this section:

Tson—basalt of Sonnickson Butte
Tbhs—tuff of Blue Heart Springs

The **basalt of Sonnickson Butte** (Tson) occurs on and within 1 to 2 km of the Sonnickson Butte shield volcano, about 7 km south-southwest of Jerome and 14 km northwest of Twin Falls. The flows from this shield are poorly exposed and covered in all directions by younger basalt units, so it is unknown how far they extend. Flows chemically similar to the Sonnickson Butte basalt occur at the bottom of Snake River Canyon downstream from Perrine Bridge and the Blue Lakes Alcove (Figure 12), about 4 km south of the shield. They readily could be from the same source, although they were included within the Banbury Basalt by Covington and Weaver (1990b). The Sonnickson Butte basalt is older than any of the basalt flows contiguous to the vent area and might be Pliocene or late Miocene. An analysis from Sonnickson Butte indicates the unit consists of Al-enhanced basalt (Table 4, number 2).

The **tuff of Blue Heart Springs** (Tbhs) occurs at scattered localities in the bottom of Snake River Canyon on

both sides of the river through an area about 5 km long (north-south) and 3 km wide (east-west) approximately 12 km southeast of Hagerman. Two phreatomagmatic vent areas are known in the Blue Heart Springs tuff field and are indicated on Figure 5. One is the Riverside Ferry tuff cone, and the other is the Thousand Hill tuff cone remnant. Near these vent areas are accumulations of basaltic tuff, which extend outward to become intercalated with Glenns Ferry sediments in some of the outlying areas surrounding the vents, but their full extent has not been traced. One of the vent areas for this unit was mentioned by Stearns and others (1938); they considered the unit to be part of the Banbury Basalt and called it the Riverside Ferry cone and the source for some of the Banbury Basalt flows. Some of these basaltic tuffs are shown on Malde and Powers' (1972) geologic map as the vent facies of the lower member of the Banbury Basalt; however, field inspection makes it clear that the Blue Heart Springs tuff was deposited as a series of thick, explosively erupted layers varying from cinder and spatter laden deposits commonly tilted adjacent to the constructs to subhorizontal, finer-grained material in their more distal parts. The chemical composition of basaltic spatter from the Riverside Ferry vent suggests that the unit consists of SROT basalt.

PLIOCENE AND PLEISTOCENE MAGIC VALLEY FERROBASALT UNITS IN THE TWIN FALLS REGION

The following Magic Valley ferrobasalt units in the Twin Falls region are described in this section:

Tsuk—basalt of Sucker Flat
Trck—basalt of Rock Creek
Thub—basalt of Hub Butte
QTst—basalt of Stricker Butte
QTha—basalt of Hansen Butte
QTsk—basalt of Skeleton Butte
Tluc—basalt of Lucerne School
QTsb—basalt of Salmon Butte

The **basalt of Sucker Flat** (Tsuk) consists of a succession of ferrobasalt lava flows developed extensively south of the Snake River Canyon between Rock Creek near Twin Falls on the east and Deep Creek west of Buhl on the west (Bonnichsen and Godchaux, unpub. mapping, 1994-1995; 1995-1996; 1996-1997). The principal source is the northwest-trending elongate shield, Berger Butte, located about 20 km southwest of Twin Falls in the Hollister area. Additional shields in the Hollister area that were probable and possible sources for the Sucker Flat ferrobasalt are Holly Hill, Checking Station Hill, and Hills 4534, 4535, 4613, 4645, and 5155. Together, these vents form the nearly 20-km-long, northwest-trending Hollister volcano alignment zone. The presence of thin sedimentary interbeds between flows in the Sucker Flat basalt unit in the Snake River Canyon walls supports the probability that it was erupted from more than one source; it is unclear which of the Hollister volcano alignment zone shields was responsible for which flows, although, given its size, Berger Butte probably was the principal source for the uppermost part of the unit.

The Sucker Flat basalt field exceeds 25 km in width (SW-NE) and 30 km in length (SE-NW); the field may be as much as 50 km long (SE-NW), if lavas from the southernmost part of the Hollister vent zone are part of the field. Because this unit covers several hundred square kilometers and typically is as much as a few tens of meters thick where exposed in Snake River Canyon, it probably has a volume of 15 to 20 cubic kilometers. This is exceptionally large for a Snake River Plain basalt and is even more interesting because the unit has a very evolved Fe-rich composition.

In the area northwest of the city of Twin Falls, the unit lies above the Shoshone Falls rhyolite and the Sonnickson Butte basalt and beneath the Rock Creek basalt (Figure 12). The unit is a 45- to 60-m-thick succession of basalt flows where exposed in the south wall of Snake River Canyon. The Sucker Flat ferrobasalt typically is covered by several feet of loess in plateau areas where the flows are subaerial in character. In the vicinity of Snake River Canyon, the unit is gradational over horizontal distances of hundreds of meters into its water-affected equivalent that represents parts of the unit that flowed into Lake Idaho. The WAB parts of the Sucker Flat ferrobasalt succession consist of partially to thoroughly altered basalt that weathers to gruslike material.

Three K-Ar dates in good agreement (Armstrong, 1975; Mitchell and others, 1985) from localities we believe are Sucker Flat basalt exposures give ages of 4.6 ± 0.3 Ma (sample YU-69-42L from the source region near Hollister), 4.5 ± 0.6 Ma (sample YU-70-44L from an upper Banbury Basalt locality), and 4.6 ± 0.4 Ma (weighted mean of two determinations on sample YU-69-51L that Armstrong thought was Lucerne School basalt but that we have mapped as Sucker Flat basalt). The paleomagnetic signature of the Sucker Flat basalt is probably reverse. Flows of the unit generally have abundant plagioclase phenocrysts and scattered olivine phenocrysts. Chemical analyses show the unit to characteristically be ferrobasalt; a representative analysis is shown in Table 4 (number 3).

In the Banbury Hot Springs-Clear Lakes-Thousand Springs area near the course of the Snake River, which constitutes the northwestern part of the Sucker Flat ferrobasalt field, Malde and Powers (1972) mapped a unit they called the Banbury Basalt and in places distinguished

upper and lower parts of it separated by a layer of sediments. The name, Banbury volcanics, was first proposed by Stearns and others (1938) to the Pliocene basalts exposed for 63 miles along the Snake River Canyon from near Twin Falls downstream to near King Hill. Subsequently, the name "Banbury Basalt" has been indiscriminately applied to many basalt flows of varying ages at different localities in southwestern Idaho, so that the meaning of the term has become confusing. We have found that the Banbury Hot Springs-Clear Lakes-Thousand Springs part of the original Banbury Basalt to simply be a continuation of the Sucker Flat ferrobasalt field into the environment where the basalt became water-affected largely because it was subaqueously emplaced. This correlation is confirmed by the composition of samples of the Banbury Basalt from that area; they are ferrobasalts essentially indistinguishable from those in the Sucker Flat unit at locations east and south of the Banbury Basalt area (Figure 15). In addition, the three radiometric ages of 4.6, 4.5, and 4.6 Ma cited above support the idea that the part of the Banbury Basalt along the Snake River is simply a continuation of the Sucker Flat basalt. This equivalence supports the suggestion that the old stratigraphic unit, the Banbury Basalt, should be abandoned since it has no real stratigraphic, geochemical, or volcanological significance and especially since the probable age of the Sucker Flat basalt is somewhat younger than originally proposed by Malde and Powers (i.e., Miocene-age pre-Chalk Hills Formation vs. part of the Pliocene-age Glenns Ferry Formation interval of time).

The **basalt of Rock Creek** (Trck) is exposed south of Twin Falls and erupted as one or more basalt flows from the Hill 4197 shield about 13 km south-southeast of Twin Falls (Bonnichsen and Godchaux, unpub. mapping, 1994-1995; Covington and Weaver, 1990b; Williams and others, 1991). The vent area is nearly covered by the younger basalt flows from Hub Butte and Stricker Butte. The best exposures are along Rock Creek. The Rock Creek basalt unit extends at least 17 km from south to north; at its northern extent, where it is directly on the Shoshone Falls rhyolite lava flow in the bottom of Snake River Canyon near the Shoshone Falls and Twin Falls waterfalls, it lies beneath several younger basalt units and extends northward beneath younger flows. Downstream, it lies above the Sucker Flat basalt unit as well (Figure 12). The Rock Creek basalt is equivalent to unit Qo of Williams and others (1991) and probably is the same basalt as unit Qi10 of Covington and Weaver's Idaho Group. At the Twin Falls waterfall, this is the unit that forms the falls because it is about 50 m thick and quite massive. It typically is covered by several feet of loess in plateau areas. The Rock Creek basalt is nearly aphyric but contains as much as 1 percent of tiny, single-crystal plagioclase and olivine phenocrysts. The composition of most Rock Creek basalt (and Qi10) samples is Fe-enhanced basalt (Table 4, number 4), but it locally varies from SROT to ferrobasalt.

The **basalt of Hub Butte** (Thub) is a sequence of basalt flows that erupted and flowed mainly northward from the Hub Butte shield, located 15 km south of Twin Falls. The Hub Butte shield generally is equant in shape. The unit forms a flow field greater than 20 km long, from south to north, and a few kilometers wide; the unit is as much as 30 m thick 15 km north of the shield near the confluence of the Rock Creek and Snake River canyons. At its northernmost exposures, the unit extends to the north beneath younger lavas in the walls of Snake River Canyon (Figure 12), so the full length of the field is unknown (Bonnichsen and Godchaux, unpub. mapping, 1994-1995; Covington and Weaver, 1990b; Williams and others, 1991). The Hub Butte basalt probably is equivalent to unit Qi9 of Covington and Weaver's Idaho Group. It typically is covered by several feet of loess in plateau areas. The basalt probably has a reverse paleomagnetic signature. It contains plagioclase and olivine phenocrysts as individual crystals that make up 1 to 10 percent of typical samples; the plagioclases range from 1 to 4 mm long, and the olivines range from 0.5 to 1.0 mm in diameter and are strongly altered to iddingsite. Chemical analyses indicate the unit is ferrobasalt.

The **basalt of Stricker Butte** (QTst) consists of the basalt flows that erupted from the Stricker Butte complex shield located about 13 km southeast of Twin Falls. The basaltic lavas flowed generally northwestward from this source to form a flow field at least 25 km southeast-northwest and as much as a few kilometers wide (Bonnichsen and Godchaux, unpub. mapping 1994-1995; Covington and Weaver, 1990b; Williams and others, 1991). The Stricker Butte basalt probably is equivalent to unit Qi8 of Covington and Weaver's Idaho Group. The maximum thickness is 12 m. The unit typically is covered by several feet of loess in plateau areas. At its distal northwest extent the unit lies on a layer of sand and gravel at the Snake River Canyon rim. Our magnetic polarity determinations from drilled, oriented samples indicate a normal polarity, although Williams and others (1991) report reverse polarity as determined by field fluxgate measurements. The basalt is nearly aphyric but contains as much as 1 percent of plagioclase and olivine phenocrysts as single crystals and clusters. Chemical analyses indicate the unit is ferrobasalt; a representative analysis is shown in Table 4 (number 5).

The **basalt of Hansen Butte** (QTha) is a sequence of basalt flows erupted from the Hansen Butte complex shield located about 20 km east-southeast of Twin Falls. The Hansen Butte shield is large and elongate from SSE

to NNW, with a topping ridge 3-4 km long that suggests the eruptions probably were emitted from a fissure. The lavas from the shield traveled northeast, north, and especially northwest to form a flow field that probably exceeds 30 km in length from southeast to northwest and is several kilometers wide (Bonnichsen and Godchaux, unpub. mapping, 1994-1995, 2002; Covington, 1976; Covington and Weaver, 1990b, 1990c; Williams and others, 1990, 1991). The Hansen Butte basalt flows reach an aggregate thickness of 61 m in Snake River Canyon near Hansen Bridge where they may have filled a preexisting canyon. Between the Hansen Bridge area and downstream along the Snake River, the unit consists of several flows without any intervening sedimentary layers; it is sandwiched between the Hub Butte basalt and the Rocky Hill basalt downstream from Perrine Bridge (Figure 12). The Hansen Butte basalt is the same unit as Covington and Weaver's unit Qi7 of the Idaho Group. Its base is pillowed at some localities, and typically it is covered by several feet of loess in plateau areas, except in low places near the Snake River Canyon that were stripped by the Bonneville Flood. The unit has a reverse paleomagnetic signature. Plagioclase and olivine phenocrysts, as single crystals and small clusters, constitute 1 to 10 percent of the rock. The plagioclase crystals are as much as 3 mm long, and the olivines are as much as 1 mm in diameter; the olivines have iddingsite rims. Chemical analyses indicate the unit consists of Fe-enhanced basalt and ferrobasalt.

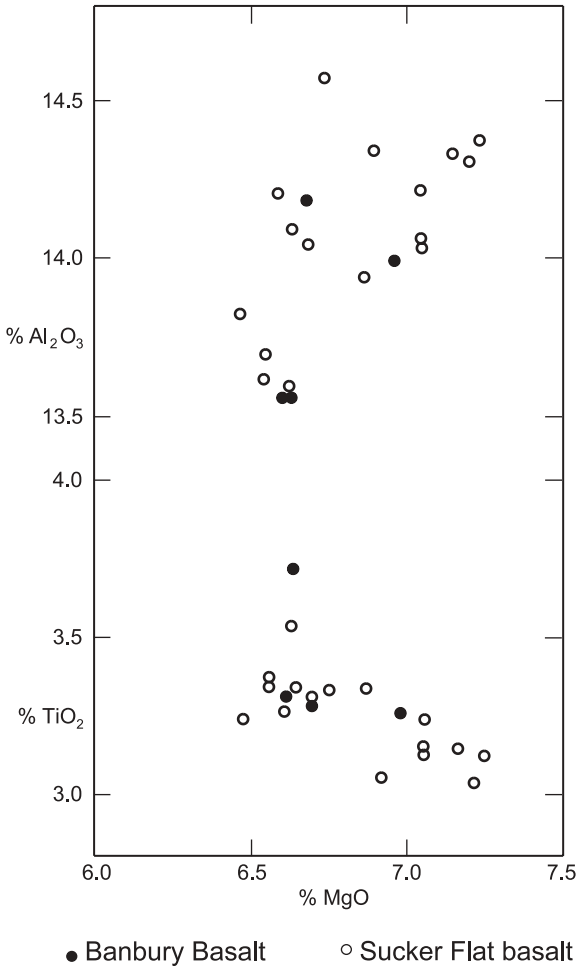

Figure 15. Plots of Al_2O_3 versus MgO and of TiO_2 versus MgO, comparing the compositions of Sucker Flat basalt with the basalt near Banbury Hot Springs northwest of Buhl that Malde and Powers (1972) mapped as Banbury Basalt. These plots show the Banbury Basalt within the compositional range of the Sucker Flat basalt unit.

The **basalt of Skeleton Butte** (QTsk) makes an irregular flow field about 14 km from east to west and about 9 km from north to south surrounding the Skeleton Butte shield; most of the basalt from this source flowed west and south from the source, although a tongue extends to the southeast (Bonnichsen and Godchaux, unpub. mapping, 2002; Covington, 1976; Covington and Weaver, 1990b, 1990C). The Skeleton Butte shield is about 19 km east of Twin Falls and 3 km southwest of Eden. The Skeleton Butte basalt is well exposed as a single flow, generally 7-8 m thick, for about 15 km along the north rim of Snake River Canyon. A subdued topographic high, located about 4 km southeast of the top of Skeleton Butte ($NW^1/_4$, sec. 14, T. 10 S., R. 19 E.) suggests a possible second vent area also fed the Skeleton Butte flow field, although this has yet to be investigated carefully. If there is a second vent, then perhaps both represent a NW-trending fissure system. The Skeleton Butte basalt is the same as Covington and Weaver's Qi3 Idaho Group unit. The unit has a reverse paleomagnetic signature. It is rich in olivine phenocrysts and also contains sparse plagioclase phenocrysts. Chemical analyses indicate it is ferrobasalt.

The **basalt of Lucerne School** (Tluc) is a composite unit erupted from two shields, Lookout Butte (east) and Sunset Butte, both about 11 km southwest of Buhl and 32 and 35 km, respectively, west of Twin Falls (Bonnichsen and Godchaux, unpub. mapping, 1996-1997; Malde and Powers, 1972). These two shields along with the Elmas Butte shield farther northwest form a linear array of vents, the Castleford volcano alignment zone about 20 km long that probably lies above a feeder dike system (Figure 5). The top of the Lookout Butte shield is only 4 km southwest of the top of the Sunset Butte shield. The basalt lavas from both shields flowed generally northward and are similar in composition. The Lucerne School

basalt was included as part of the Glenns Ferry Formation by Malde and Powers (1972). This unit is present along the rim of Salmon Falls Creek canyon for 13-14 km and is as much as 20 m thick in places. In the Sinking Canyon area along Salmon Falls Creek, the unit lies on more than 100 m of unconsolidated Glenns Ferry Formation sediments. Variations in the water table over time have led to several large landslides into the canyon and the breaking up of the rim basalt layer for several miles along the east side of the canyon in that area (Figure 14). The Lucerne School basalt flow field probably extends for about 17 km from south to north and is a few kilometers wide. At its northern end, the basalt has been turned into WAB where the lavas ran into Lake Idaho. It has plagioclase and olivine phenocrysts and mainly is ferrobasalt, although locally on the Lookout Butte shield, it is Fe-enhanced basalt.

The **basalt of Salmon Butte** (QTsb) occupies an area a few kilometers across on the east side of Salmon Falls Creek surrounding the source volcano, the Salmon Butte cinder and spatter cone. The unit's best exposures are a sequence of thin, intracanyon flows in the walls of Salmon Falls Creek canyon (Figure 13). Salmon Butte is about 10.5 km west of Rogerson and 1 km east of Salmon Dam. The volcano is a small accumulation of cinders and spatter with several eruptive points preserved along its top. The volcano is elongate from southeast to northwest, measuring about 2 km long and 1 km wide. It is within the Roseworth volcano alignment zone. The Salmon Butte basalt is demonstrably younger than the other basalt flows in the southern part of the Twin Falls area. The other basalt units were dissected by the erosional events that led to the present course of Salmon Falls Creek canyon, after which the Salmon Butte basalt partially filled the canyon and then was partly removed by erosion. The upper surface of the Salmon Butte basalt forms a prominent bench within the canyon that can be traced for about 5 km north of Salmon Dam. It is a truly classic example of an intracanyon sequence of flows. The geomorphic control that originally led to the initial development of the canyon was the lowering of the base level of ancestral Salmon Falls Creek that accompanied the draining of Lake Idaho during Glenns Ferry time. It is clear that the eruption of the Salmon Butte basalt occurred after the canyon had been excavated in response to the base-level lowering. Thus, the Salmon Butte basalt is either late Pliocene or Pleistocene in age, whereas the nearby basalt units are late Miocene. The Salmon Butte basalt is characterized by abundant and fairly large plagioclase and olivine phenocrysts commonly in the form of cumulophyric aggregates. It is a ferrobasalt that is extremely rich in Fe and Ti.

OTHER PLIOCENE AND PLEISTOCENE BASALT UNITS IN TWIN FALLS REGION

The following additional Pliocene and Pleistocene units in the Twin Falls region are described in this section:

Tdev—basalt of Devil Creek Butte
Tchb—basalt of Canyon Hill
Tssr—basalt of Shoestring Road
QTma—the Madson basalt
QTwl—basalt of Wilson Lake Reservoir
QTlh—basalt of Lincoln Hill
QTgb—basalt of Gooding Butte
QThz—basalt of Hazelton Butte
QTmi—basalt of Milner Butte

The **basalt of Devil Creek Butte** (Tdev) forms a flow field about 14 km long from south to north and a few kilometers wide that erupted from the source vent, the Devil Creek Butte shield, located about 43 km west-southwest of Twin Falls and about 24 km southwest of Buhl. The northernmost extent of the flow is at the rim of Salmon Falls Creek canyon about 4 km northeast of the Balanced Rock area (Bonnichsen and Godchaux, unpub. mapping, 1996-1997). In that area, the Devil Creek basalt lies on the Castleford Crossing rhyolite unit, but it was erupted after an episode of faulting had offset the surface of the earlier rhyolite units, so that this basalt flow was banked up against some of the older rhyolite-cored hills (Figure 14). The Devil Creek Butte shield is west of Salmon Falls Creek canyon in the northern part of the Roseworth volcano alignment zone and is elongate in a southeast-northwest direction; the flows traveled north from the vent. No chemical analyses are available for the unit.

The **basalt of Canyon Hill** (Tchb) was erupted from the Canyon Hill shield volcano on the east side of Salmon Falls Creek canyon about 32 km southwest of Twin Falls and 19 km south of Buhl (Bonnichsen and Godchaux, unpub. mapping, 1996-1997). Flows may have traveled north to at least as far as the south rim of Snake River Canyon northwest of Buhl, a distance of 28 km, where they ran into Lake Idaho and became pervasively water-affected. Throughout most of its extent, however, the Canyon Hill basalt flows are covered by the Lucerne School basalt and probably by some of the upper flows of the basalt of Sucker Flat, so the full extent of its flow field is unknown. Chemical analyses indicate the unit is SROT basalt, as noted in Table 4 (number 6).

The **basalt of Shoestring Road** (Tssr) occurs intercalated within, and is part of, the Glenns Ferry Formation in the northern part of the Hagerman Valley and in nearby bluffs along the Snake River in the northwest part

of the Twin Falls region (Covington and Weaver, 1989; Malde and Powers, 1972). Malde and Powers suggested that the vent might be located about 5 km south of Bliss; we have not verified the location so have not included it on Figure 5. In the Hagerman Fossil Beds National Monument area, the Shoestring Road basalt has a radiometric date of 3.40 ± 0.02 Ma (Hart and Brueseke, 2002). Interestingly, at the same stratigraphic level, a second basalt unit occurs with a radiometric date of 3.68 ± 0.02 Ma; Hart and Brueseke suggest this second flow is the basalt of Deer Gulch, which is a widespread member of the Glenns Ferry Formation west of the National Monument (Malde and Powers, 1972). The Shoestring Road basalt contains phenocrysts of plagioclase and olivine and has a Fe-enhanced basalt composition (Stone, 1967).

The **Madson basalt** (QTma) occurs as discontinuous exposures of canyon-filling basalt between Tuttle on the east and Swiss Valley on the west along the northeastern wall of Snake River Canyon north of Hagerman Valley in the northwestern part of the Twin Falls region (Covington and Weaver, 1989; Malde and Powers, 1972; Stearns and others, 1938). The location of the venting area is unknown, but probably lies east of the exposures of the unit. A radiometric date of 0.54 ± 0.08 Ma and a normal paleomagnetic polarity have been reported by Armstrong (1975). The unit contains phenocrysts of olivine and plagioclase, and the chemical composition is SROT basalt (Stone, 1967).

The **basalt of Wilson Lake Reservoir** (QTwl) occupies an area of a few square kilometers north of Eden and east of Wilson Lake Reservoir (Bonnichsen and Godchaux, unpub. mapping, 2002). The vent is the shield volcano at the west end of Wilson Lake Reservoir about 19 km east-northeast from Twin Falls. The lava apparently flowed westward from the shield. The Wilson Lake Reservoir basalt is mainly covered by younger lava flows and heavily covered by loess except where that cover was stripped by the Bonneville Flood. The unit probably has a normal paleomagnetic signature. It contains fairly abundant small plagioclase phenocrysts but no olivine; no chemical analyses are available.

The **basalt of Lincoln Hill** (QTlh) occupies an area of 4 to 5 km from north to south and as much as 3 km wide mainly extending south of the Lincoln Hill shield volcano (Hill 4071), which is about 32 km north of Twin Falls and 11 km southwest of Shoshone. The shield is small, only about a kilometer long and elongate in a north-south direction. The Lincoln Hill basalt flow is blanketed by thick loess deposits and is overlain by the younger basalts of Notch Butte on the north and Bacon Butte on the south, so its full original extent is unknown. The Lincoln Hill basalt contains abundant small plagioclase phenocrysts, but no olivine phenocrysts were noted. This is the ferrobasalt with the highest known Fe content (19.31 percent Fe_2O_3) of any southwestern Idaho basalt (Table 4, number 7). Whether it should be included as part of the Magic Valley ferrobasalt field is unclear at this point. It might be younger and is some distance away from the units in that grouping, so it has not been included at this time.

The **basalt of Gooding Butte** (QTgb) forms an irregular-shaped flow field that exceeds 20 km from north to south and is nearly as wide from east to west (Covington and Weaver, 1989; Malde and Powers, 1972). The flows were erupted from the Gooding Butte shield volcano located about 4 km southwest of Gooding. The lavas flowed mainly south and west and went as far as the northeastern rim of Snake River Canyon where they are exposed along the rim and canyon wall east of Hagerman for about 15 km. The unit was previously referred to as the Malad basalt (Stearns and others, 1938) and as the Malad basalt member of the Thousand Springs basalt (Malde and Powers, 1972). The basalt of Gooding Butte has large and abundant plagioclase phenocrysts and sparse to abundant olivine phenocrysts as well. Chemical analyses indicate it is ferrobasalt. Like the Lincoln Hill basalt, it has not been included in the Magic Valley ferrobasalt at this time.

The **basalt of Hazelton Butte** (QThz) consists of the basalt flows erupted from the Hazelton Butte shield located about 30 km east of Twin Falls. The shield is generally equant in shape, and it released lavas that mainly flowed westward to form a flow field that exceeds 10 km in length from east to west and is nearly as wide from north to south (Bonnichsen and Godchaux, unpub. mapping, 2002; Covington, 1976; Covington and Weaver, 1990c; Williams and others, 1990). The full extent of the field has yet to be resolved, as parts of it are covered by younger lavas. The Hazelton Butte basalt is the same set of flows as Covington and Weaver's Qi4 Idaho Group unit. In most areas, the unit is covered by a thick blanket of loess. It has a varied to erratic paleomagnetic pattern. The unit contains 10 to 15 percent phenocrysts as single crystals and crystal-clusters of plagioclase and olivine; the plagioclases are as much as 4 mm long and the olivine grains as much as 5 mm in diameter. No chemical analyses are available for this unit, so it is unclear yet if it is part of the Magic Valley ferrobasalt field, even though it is contiguous to other flows of that group and about the same age.

The **basalt of Milner Butte** (QTmi) is in the eastern part of the Twin Falls region where it forms a flow field almost 13 km from south to north and at least 13 km from east to west (Covington and Weaver, 1990c; Williams and others, 1990). This is the same basalt unit as Covington and Weaver's unit Qi2 of the Idaho Group. The source volcano is the Milner Butte shield, located about 10 km

east of Murtaugh Lake and 38 km east-southeast of Twin Falls. The shield is about 3 km in diameter and generally equant in outline; it is cut by a northwest-trending normal fault. The Milner Butte basalt contains 20-25 percent phenocrysts, including plagioclase laths 2-2.5 mm long and olivine grains about 0.5 mm in diameter with iddingsite rims. No chemical analyses are available.

THE PLEISTOCENE NORTHSIDE BASALT FIELD OF THE TWIN FALLS REGION

The following Pleistocene Northside basalt units in the Twin Falls region are described in this section:

Qbac—basalt of Bacon Butte
Qflt—basalt of Flat Top Butte
Qjer—basalt of Jerome Golf Course
Qcin—basalt of Cinder Butte
Qwil—basalt of Wilson Butte
Qrh—basalt of Rocky Hill
Qnot—basalt of Notch Butte
Qmck—the McKinney basalt
Qsic—basalt of Shoshone Ice Cave

The **basalt of Bacon Butte** (Qbac) forms a flow field about 10 km wide and 25 to 35 long, extending west-southwest from its source shield to the Snake River Canyon (Covington and Weaver, 1991; Gillerman and Schiappa, 2001). The source volcano is the Bacon Butte shield, which has a pit(?) crater at its summit that is approximately 0.8 long and 0.5 km wide. Hill 4054 is the high point of the vent area and is located 2 to 2.5 km northwest of the Bacon Reservoir Ranch and about 17 km north of Twin Falls. The distal part of the Bacon Butte basalt was included as part of Malde and Power's (1972) Sand Springs basalt field; however, it clearly is a different basalt than the main part of their Sand Springs basalt, as discussed below in the Rocky Hill basalt description. The Bacon Butte lavas travelled west-southwest from the vent area, but their full extent is unclear owing to the extensive overlying loess and dune sand deposits. Marginal parts of the flow field of the younger Flat Top Butte and Notch Butte basalts, respectively at the south and north sides of the Bacon Butte flow field, also obscure the true extent of the Bacon Butte basalt. The unit has a normal paleomagnetic signature and contains abundant, fairly large olivine phenocrysts accompanied in some places, mainly near the shield, by small plagioclase phenocrysts. Plagioclase microphenocrysts are common in the unit, and chemical analyses of the basalt show it to be SROT basalt. Although our preliminary investigations suggest that the Bacon Butte basalt is older than the Flat Top Butte basalt (Figure 11), recent geologic mapping by the Idaho Geological Survey suggests it actually may be younger (John Kauffman, oral commun., 2004).

The **basalt of Flat Top Butte** (Qflt) forms a flow field that stretches about 38 km from east to west and is as much as 10 km wide along the north side of Snake River Canyon and to the north where it caps the adjacent upland. The lavas were erupted from the Flat Top Butte shield volcano located about 19 km north of Twin Falls and 8 km east of Jerome. The Flat Top Butte basalt was previously called the Thousand Springs basalt (Covington and Weaver, 1990b; Stearns and others, 1938). Earlier, Flat Top Butte was considered by them to be one of several Thousand Springs basalt sources (Covington, 1976; Gillerman and Schiappa, 2001; Malde and Powers, 1972). The Flat Top Butte shield is near the eastern end of the Flat Top Butte basalt field; lavas from the shield flowed west-southwest from the shield in the more proximal area and then more or less westward in the more distal parts of the field. The field slightly overlaps the Bacon Butte flow field on the north and in turn is overlapped by the flow fields of the Rocky Hill and Wilson Butte basalts on the southeast. Basalt of the Flat Top Butte shield surrounds the earlier basalt of Sonnickson Butte. The southern margin of the Flat Top Butte flow field apparently guided the position of the ancestral Snake River before its incision from about the mouth of Cedar Draw to the Banbury Hot Springs area. In that area in the north wall of the canyon, the Flat Top Butte basalt principally is subaerial and lies on the older Sucker Flat basalt, which is thoroughly and spectacularly water affected. Where cut through by the Snake River Canyon, the Flat Top Butte basalt ranges from a single flow to several flows stacked upon each other without any intervening sediments. The basalt has a normal paleomagnetic signature and typically contains phenocrysts of plagioclase and olivine; in places, these phenocrysts are quite abundant, and in other places the olivines are fairly large. Chemical analysis indicates the unit ranges from SROT basalt to ferrobasalt; a representative ferrobasalt analysis is given in Table 4 (number 8). Although our preliminary investigations suggest that the Flat Top Butte basalt is younger than the Bacon Butte basalt and older than the Jerome Golf Course basalt (Figure 11), recent geologic mapping by the Idaho Geological Survey suggests that it actually may be older that the Bacon Butte basalt but younger than the Jerome Golf Course basalt (John Kauffman, oral commun., 2004).

The **basalt of Jerome Golf Course** (Qjer) occurs in a small area in and adjacent to the Jerome Golf Course on the north side of Snake River Canyon downstream from Perrine Bridge. The source vents are two "cinder pits" about 9 km south of Jerome and 10 km northwest of Twin Falls, and 0.5 km north-northwest of the golf course. These vents clearly are phreatomagmatic and aligned from

east-northeast to west-southwest. Their lower deposits consist of fragmental tuff that probably was erupted into a subaerial environment. These tuffs are overlain by spatter deposits. Dikes cut the vent deposits, and a small flow was erupted from the area, evidently to travel mainly to the south and west. These vents are classified as maars or tuff rings in Table 2, although we do not know if maars were formed during the initiation of the eruptions because the lower part of the vents are buried. Where exposed at the Snake River Canyon rim about 0.8 km south of the vent area, the flow has well-developed pillows in its lower part. Apparently, it flowed into a stream or standing water. Covington (1976) included the "cinder pits" as part of his Thousand Springs basalt unit but commented that the thin flow from the pits might be younger than the nearby Sand Springs (i.e., Rocky Hill) basalt. The Jerome Golf Course basalt has a normal paleomagnetic signature and typically contains large and abundant phenocrysts of plagioclase and olivine in places as cumulophyric clumps. A chemical analysis indicates the unit is Fe-enhanced basalt. Although our preliminary investigations suggest that the Jerome Golf Course basalt is younger than the Flat Top Butte basalt (Figure 11), recent geologic mapping by the Idaho Geological Survey suggests that it actually may be older (John Kauffman, oral commun., 2004).

The **basalt of Cinder Butte** (Qcin) and its vent, Cinder Butte, are located just northeast of the Milner-Gooding Canal, approximately 33 km east-northeast of Twin Falls. Cinder Butte is a small cinder and spatter construct about the same age as the basalt of Jerome Golf Course; the butte is surrounded by lavas that flowed from Hill 4526, the source shield of the Rocky Hill basalt. Because of the limited exposure, it is unclear how much lava issued from Cinder Butte. The structure of Cinder Butte is suggestive of a cone within a cone, with the younger inner cone consisting principally of agglutinated spatter, whereas the older outer cone contains both basaltic tuff and spatter accumulations. The nature of the early Cinder Butte erupted materials suggests a substantial phreatomagmatic component in the early stages of the eruption, as is the case for the Jerome Golf Course cinder pits. Certain layers of the basaltic spatter of Cinder Butte contain lithics of intrusive mafic rocks and possibly of granitoid material. Such inclusions are most prevalent in the thinner more densely welded layers of spatter that occur in the phreatomagmatic-to-magmatic transition zone of the outer cone. No analyses are available for this basalt unit.

The **basalt of Wilson Butte** (Qwil) occurs in the northeastern part of the Twin Falls region and was erupted from the Wilson Butte shield, located about 32 km northeast of Twin Falls, 23 km southeast of Shoshone, and 4 km northeast of the Milner-Gooding Canal. The Wilson Butte shield is nearly circular in plan, about 6 km in diameter, and characterized by rough topography and abundant exposures of basalt because very little loess has been deposited on it. Near the top of Wilson Butte, located just west of the top of the shield, is a small lava tube known as Wilson Butte Cave, which is an important archeological site known for early-man materials that exceed 10,000 years in age. The Wilson Butte lavas generally flowed west and southwest from the shield and have been traced for a distance of about 20 km; the width of the flow field seems to be about 20 km but has yet to be fully mapped. The basalt contains varied amounts of plagioclase and olivine phenocrysts that are relatively small. Chemical analyses indicate the unit ranges from SROT basalt to ferrobasalt.

The **basalt of Rocky Hill** (Qrh) refers to the uppermost basalt flows that cover the plateau surface north of Snake River Canyon and that were erupted from the Hill 4526 shield located 36 km east-northeast of Twin Falls in the eastern part of the Twin Falls region (Bonnichsen and Godchaux, unpub. mapping, 2002). The Rocky Hill basalt flowed generally west-southwest and then westward from the shield to form a flow field 40-50 km long and about 10 km wide. For part of the length, the unit determined the location of the pre-incision ancestral Snake River along the south margin of its flow field. Locally, these lavas filled tributary canyons and flowed farther. The pillowed deposits of the Rocky Hill unit in the area west of Blue Lakes Alcove on the north side of Snake River Canyon are excellent examples of the results of this process (Figure 12). The Hill 4526 shield is relatively large; it is approximately circular in plan, about 8 km across, and has a very hummocky surface because there has been little deposition of wind-blown material since it formed. The Rocky Hill basalt has previously been referred to as the Sand Springs basalt (Covington, 1976; Covington and Weaver, 1989, 1990b, 1991; Gillerman and Schiappa, 2001; Malde and Powers, 1972). Stearns and others (1938) originally named the unit for Sand Springs and Sand Springs Creek located near Snake River Canyon just east of Thousand Springs to the north and Blue Heart Springs to the south; they believed it had been erupted from Rocky Ridge (Hill 4526). This location is many kilometers away from the westernmost documented extent of the flows that originated from the source shield; thus, we believe it is inappropriate to continue to use the Sand Springs name, and the name Rocky Hill is suggested for the Rocky benchmark noted on the Hill 4526 shield. The westernmost extent of the Rocky Hill basalt that we are aware of is at the rim of Snake River Canyon between Jerome and Filer. The basalt has a normal paleomagnetic signature. It contains abundant small phenocrysts of plagioclase and olivine. Chemical analyses show

that the unit ranges from SROT basalt to ferrobasalt; a representative ferrobasalt analysis is given in Table 4 (number 9).

The **basalt of Notch Butte** (Qnot) forms a flow field in the northern part of the Twin Falls region about 45 km long from east-northeast to west-southwest and as much as 15 km wide. The Notch Butte basaltic lavas erupted from the Notch Butte shield, located about 36 km north of Twin Falls and 6 km south of Shoshone. They generally flowed westward, reaching the Snake River Canyon in the Hagerman area. The Notch Butte shield is several kilometers across, generally circular in outline, and hummocky on its surface. It is topped by a small irregular-shaped spatter and cinder accumulation. Throughout its extent the flow-field surface is very rough, with many pits and pressure ridges. It is one of the youngest basalt flows in the central part of the SRP and has had very little windborne material deposited on its top. The unit previously was referred to as the Wendell Grade basalt (Covington and Weaver, 1989; Malde and Powers, 1972; Stearns and others, 1938). The Notch Butte basalt contains abundant phenocrysts of plagioclase and olivine. Chemical analyses indicate the unit ranges from SROT basalt to ferrobasalt; a representative analysis of SROT basalt is given in Table 4 (number 10).

The **McKinney basalt** (Qmck), a subaerial pahoehoe lava flow and pillow lava basalt unit, occupies an irregular area north of the Snake River in the northwestern part of the Twin Falls region and extends farther west. The unit measures more than 30 km east-west and nearly 20 km north-south (Covington and Weaver, 1989, 1990a; Malde and Powers, 1972; Stearns and others, 1938). The source vent is the McKinney Butte shield volcano in the northeastern corner of the flow field, 12-13 km northwest of Gooding and 15 km northeast of Bliss. The McKinney basalt flowed generally southwestward from the shield for 16-18 km across a relatively gently sloping plain and then intersected the ancestral canyon of the Snake River, which was nearly as deep at the time of eruption as it is now. The flows partially filled the canyon and spread along the bottom of it, so that extensive lava cascades and pillow-delta deposits occur along the Snake River from its confluence with the Big Wood River on the southeast to about 3 km southeast of King Hill at its northwesternmost extent. The unit is relatively young, probably late Pleistocene, so its vent area and flow surfaces are fairly rugged, with many drainaway pits and pressure ridges throughout the flow field. The McKinney basalt has been studied in considerable petrologic detail (Leeman, 1976; Leeman and Vitaliano, 1976), so much more information is available on this unit than on other basalts in southwestern Idaho. The unit covers an estimated 300 square km and ranges in thickness from 5-10 m in the upland area to 175 m where it ponded in the ancient Snake River channel. This unit's overall volume is estimated to be 1-2 cubic km. The McKinney basalt contains abundant plagioclase and olivine phenocrysts and varies widely in composition (Leeman and Vitaliano, 1976; Stone, 1967) from Al-enhanced basalt to SROT to Fe-enhanced basalt. Most of the analyzed samples have the composition of SROT basalt; however, in some of the late-stage segregations within the unit, the composition is ferrobasalt.

The **basalt of Shoshone Ice Cave** (Qsic) is the youngest basalt unit in the Twin Falls region and flowed into that area from the north. The Shoshone Ice Cave basalt erupted from Black Butte Crater, a small shield with a complex summit crater area about 2 km north-northwest of Shoshone Ice Caves, 7 km south of Magic Reservoir Dam on the west side of the Big Wood River, and 28 km north of the town of Shoshone (Black Butte is north of the area shown in Figure 5). This basalt flow is about 60 km long; the more proximal 25 km is elongate north-south whereas the more distal 35 km is elongate east-west. The lavas evidently followed the course of the ancestral Big Wood River nearly to Gooding and still are relatively fresh in appearance, although some vegetation covers parts of the flow. The flow field typically is 3-5 km wide; in its more distal east-west section, it separated the present-day Big and Little Wood rivers, that prior to the formation of this lava flow had joined near the town of Shoshone. The Shoshone Ice Cave, a well-known local tourist attraction, is in a section of the prominent lava tube system that can be followed for many kilometers from the source area. In the vent area, there evidently was some late-stage phreatomagmatic activity; numerous fragments of the underlying Magic Reservoir rhyolite are incorporated into the basalt and scattered on the surface of the volcano as loose blocks along with blocks of spatter and older basalt flows. Such phreatomagmatic activity is not surprising given that the volcano was built in an existing stream course and would have blocked the stream temporarily. The unit has been radiometrically dated by Kuntz and others (1986, 1992) at 10,130 ± 350 years old. Chemical analyses of several samples (Kuntz and others, 1985, 1992) indicates it is SROT basalt.

GEOLOGY OF THE WESTERN SNAKE RIVER PLAIN REGION

There is great diversity in the basaltic volcanism associated with the development of the western SRP rift. The basalts erupted during two different times: the first about 9-7 Ma ago, and the second about 2.2-0.4 Ma ago (Figure 6). Only a minor amount of basalt volcanism oc-

curred between these two episodes, in contrast to the pattern of fairly continuous volcanism in the central SRP and Owyhee Plateau regions. During these volcanic episodes, the large lake, Lake Idaho, continued to evolve in the western SRP. This development involved variations of the lake's surface elevation through time (Wood and Clemens, this volume) until the lake drained completely during the late Pliocene or early Pleistocene. The lake level fluctuations and the lake's eventual demise led to wide variations in the style of the basalt eruptions and products (Jenks and Bonnichsen, 1989; Godchaux and others, 1992; McCurry and others, 1997; Hearst, 1999; Wood and Clemens, this volume). See Godchaux and Bonnichsen (this volume) for a discussion on how the presence of water influenced the style of basaltic volcanism in the western SRP. Figure 16 is a northwest-southeast strip map along the Snake River in the western SRP region showing the distribution of many of the volcanoes there. The volcanoes in the area of that map are identified in Table 5.

Several geologic maps exist for the western SRP. The earlier ones, such as those by Savage (1958), Mitchell and Bennett (1979), and Ekren and others (1981), cover large areas but lack detail, especially for the basalt units. More recent mapping in the western SRP and adjacent regions includes the Boise quadrangle (1:100,000 scale) by Othberg and Stanford (1992), the Vale and Mahogany Mountain quadrangles (1:100,000 scale) by Ferns and others (1993a, 1993b), and the maps (1:24,000 scale) by Malde (1989a, 1989b, 1989c, 1989d, and 1990) of the Bruneau Formation. We have found that the earlier geologic mapping, although of considerable value in a broad sense, does not offer sufficient detail to clarify the nature of the basaltic volcanism in the western SRP. Consequently, in preparing the following discussion on the western SRP basalt units, we have relied principally on our own geologic mapping, a small amount of it already published (Bonnichsen and Godchaux, 1998; Jenks and Bonnichsen, 1990b; Jenks and others, 1993, 1998), but much only now in preparation for publication at 1:100,000 (Bonnichsen and Godchaux, unpub, mapping, 1987-2002, Murphy quadrangle).

The general stratigraphic relations among the major basalt groups in the western SRP region are summarized in Figure 2, and a summary of existing radiometric dates for the western SRP basalts units is included in Figure 6. For more detail on the stratigraphy among the individual basalt units, Figure 17 gives the approximate relative time-space relations among all of the units discussed below. The cross-section of the Guffey Table-Melba Alcove area near Walters Ferry and Melba (Figure 18) shows in more detail the relationships among the various basalt units, which are somewhat typical for the western SRP region.

Superimposed on the volcanic-style variations is the chemical composition of the basaltic lavas eruptions that also varied widely over time. The earliest basalts were dominantly SROT. Compositions changed progressively with time to an intermixing of SROT and ferrobasalt. Later, nearly all eruptions were ferrobasalt, and then the final basalts were enriched in alkali elements, but lacked significant Fe enrichment. The pattern above seems to have been followed most strictly in the western part of the western SRP. Details about how the basalt composition varied over time in the Melba-Walters Ferry area are described by White and others (this volume). Examples of typical basalt compositions in the western SRP region are presented in Table 6.

STRUCTURAL GEOLOGY OF THE WESTERN SNAKE RIVER PLAIN

The dominant structural aspect of the western SRP is that it appears to be a complex graben or rift that over time has undergone northeast-southwest extension and widening in a direction essentially perpendicular to the northwest-southeast elongation of the rift. As discussed earlier, this widening seems to have started about 11.7-11.0 Ma ago when rhyolite units were erupted on the uplands west of the western SRP region and flowed northeastward into the nascent rift (Godchaux and Bonnichsen, this volume). At present, we do not know how much of the extension occurred during this time or later, probably when the 7-9 Ma basalts were erupted. Nor do we know how much extension occurred in various parts of the western SRP, but this could readily amount to several kilometers, especially in the southeast part where it joins the main SRP (Figure 3). The principal structural features apparent at the surface are a few normal faults, generally with northwest to west-northwest strikes and small vertical displacements, and the generally steep northwest- to southeast-trending physiographic boundaries on both the northeast and southwest sides of the graben that suggest the presence of large-displacement but covered faults. These hypothesized graben-bounding fault zones likely have thousands of meters of vertical throw but are covered by later deposits.

Several pieces of evidence support the idea that the western SRP is a rift or widened complex graben that accumulated a considerable thickness of materials as it evolved. The long-lived, large and deep Miocene to Pleistocene lake, which was impounded in a physiographic low, strongly suggests sufficient tectonic extension occurred to create the depression in which the lake formed. The lake persisted until its basin was filled with kilometers of basalt and sediments and it was ultimately cap-

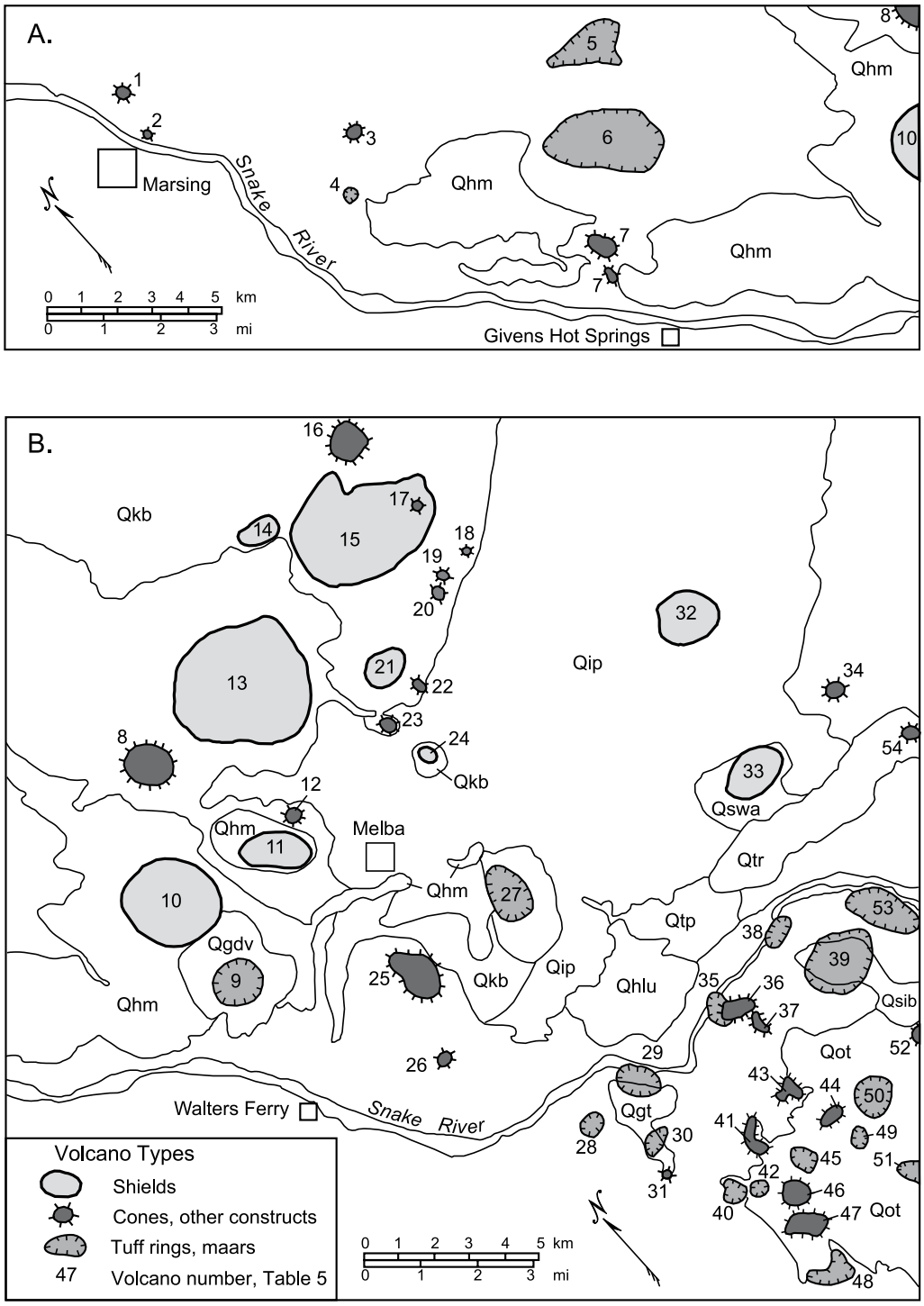

Figure 16. Map along the Snake River in the western SRP showing the locations of volcanoes and selected basalt units. See Table 5 for names of volcanoes. Units are identified as follows: Tbrb—basalt of Brooks Ranch, Ttad—basalt of Tadpole Lake, QTdor—basalt of Dorsey Butte, QTbfb—basalt of Big Foot Butte, Qtr—basalt of Trio Hill, Qswa—basalt of Swan Falls Road, Qtp—basalt of Tombstone Patch Rapids, Qhm—basalt of Hat Butte and McElroy Butte, Qsib—Sinker Butte volcanic complex, Qot—Oregon Trail volcanic field, Qgt—basalt of Guffey Table, Qgdv—Grouch Drain volcanic complex, Qip—basalt of Initial Point, Qkb—Kuna Butte basalt field, Qhlu—upper basalt of Halverson Lake, and Qbppu—upper basalt of Promontory Point.

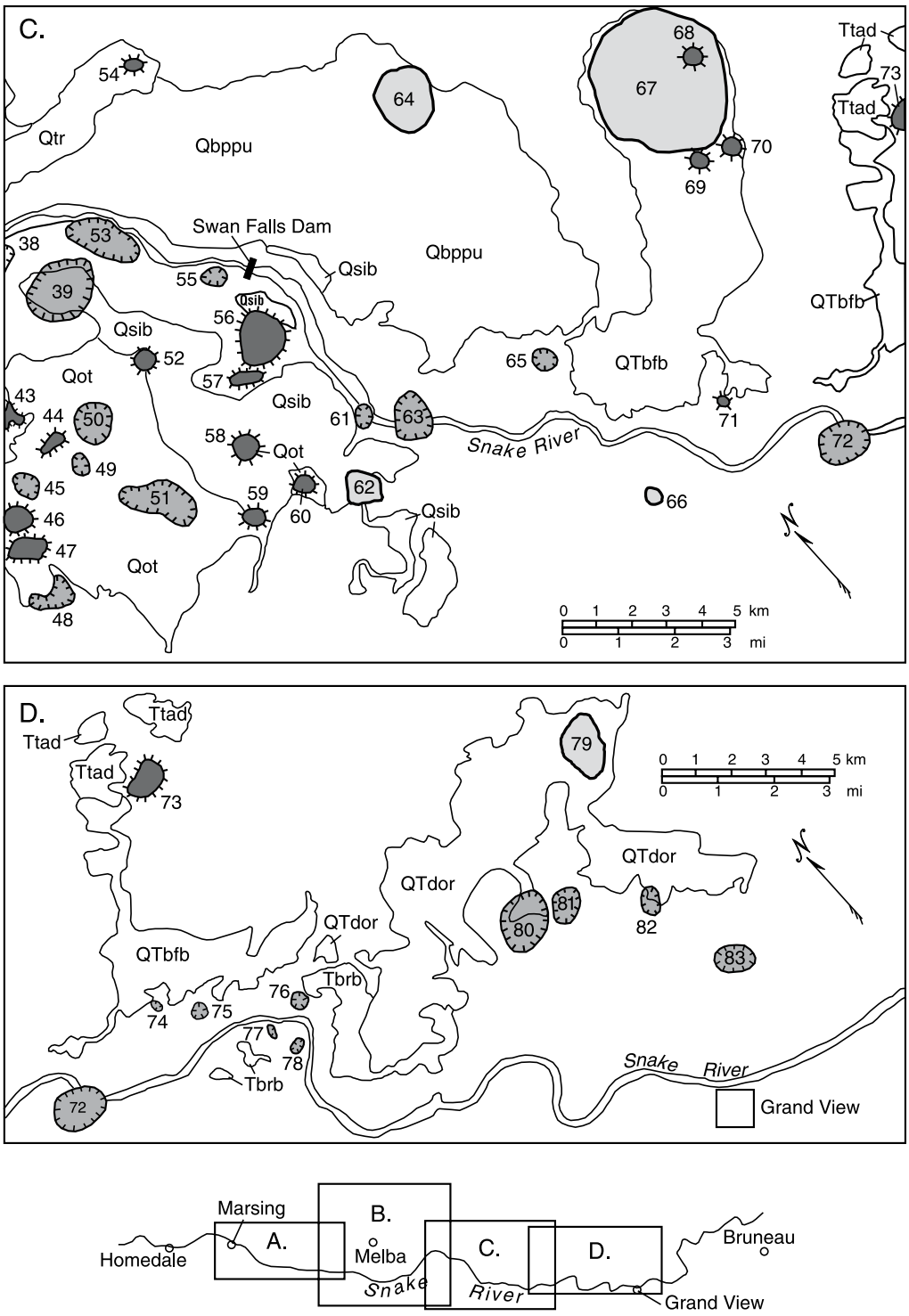

Figure 16. Continues.

Table 5. Volcanoes along the Snake River in the western Snake River Plain region. See Figure 16 for locations.

Number	Name	Type	Unit	Chemistry	Location
74	Big Foot Bar East	maar-tuff ring	Tjvc	SROT	sec. 4, T. 4 S., R. 2 E.
71	Big Foot Bar North	cinder-spatter cone	—	unknown	sec. 25, T. 3 S., R. 1 E.
67	Big Foot Butte	shield	QTbfb	SROT	sec. 33, T. 2 S., R. 2 E.
75	Birthday Gulch	maar-tuff ring	Tjvc	unknown	sec. 33, T. 3 S., R. 2 E.
55	Boise-Meridian	maar-tuff ring	Qbmv	ferrobasalt	sec. 13, T. 2 S., R. 1 W.
72	Castle Butte	maar-tuff ring	Qcas	Fe-enhanced	sec. 6, T. 4 S., R. 2 E.
30	Celebration	maar-tuff ring	Qgbv	unknown	sec. 1, T. 2 S., R. 2 W.
81	Chattin Flat East	maar-tuff ring	Tfl	SROT	sec. 22, T. 4 S., R. 3 E.
80	Chattin Flat West	maar-tuff ring	Tfl	SROT	sec. 21, T. 4 S., R. 3 E.
40	Con Shea Crater	maar-tuff ring	Qot	Fe-enhanced	sec. 13, T. 2 S., R. 2 W.
61	Conservancy Flats	maar-tuff ring	QTcfv	unknown	sec. 6, T. 3 S., R. 1 E.
34	Coyote Butte	cinder-spatter cone	Qcoy	ferrobasalt	sec. 20, T. 1 S., R. 1 E.
79	Dorsey Butte	shield	QTdor	SROT	sec. 12, T. 4 S., R. 3 E.
35	Graveyard Rapids	subaqueous vent	QTgv	unknown	sec. 32, T. 1 S., R. 1 W.
9	Grouch Drain	maar-tuff ring	Qgdv	Al-enhanced	sec. 32, T. 1 N., R. 2 W.
28	Guffey Butte	maar-tuff ring	Qgbv	Fe-enhanced	sec. 35, T. 1 S., R. 2 W.
10	Hat Butte	shield	Qhm	ferrobasalt	sec. 20-21, T. 1 N., R. 2 W.
83	Hayland School	maar-tuff ring	Tfl	unknown	sec. 2, T. 5 S., R. 3 E.
6	Hidden Valley	maar-tuff ring	Qhvc	Fe-enhanced	sec. 34, T. 2 N., R. 3 W.
12	Hill 2725	cinder-spatter cone	Qss	ferrobasalt	sec. 26, T. 1 N., R. 2 W.
66	Hill 2781	shield	Twhbu	SROT	sec. 27, T. 3 S., R. 1 E.
14	Hill 2812	shield	Qkb	Al-enhanced	sec. 32, T. 2 N., T. 1 W.
65	Hill 2829	maar-tuff ring	QTnrl, QTnru	SROT	sec. 10, T. 3 S., R. 1 E.
24	Hill 2830	shield	Qkb	unknown	sec. 29-32, T. 1 N., R. 1 W.
23	Hill 2883	cinder-spatter cone	Qkb	Al-enhanced	sec. 29, T. 1 N., R. 1 W.
36	Hill 2890	cinder-spatter vent	Qtp	ferrobasalt	sec. 4, T. 2 S., R. 1 W.
33	Hill 2930	shield	Qswa	ferrobasalt	sec. 24, T. 1 S., R. 1 W.
18	Hill 2950	cinder-spatter cone	Qkb	unknown	sec. 14, T. 1 N., R. 1 W.
31	Hill 3007	maar-tuff ring	Qgt	SROT	sec. 12, T. 2 S., R. 2 W.
45	Hill 3028	maar-tuff ring	Qot	unknown	sec. 17-18, T. 2 S., R. 1 W.
41	Hill 3045	cinder-spatter cone	Qot	unknown	sec. 7, T. 2 S., R. 1 W.
60	Hill 3048	cinder-spatter cone	Qot	unknown	sec. 2, T. 3 S., R. 1 W.
52	Hill 3054	cinder-spatter cone	Qot	unknown	sec. 14, T. 2 S., R. 1 W.
59	Hill 3086	cinder-spatter cone	Qot	ferrobasalt	sec. 3, T. 3 S., R. 1 W.
58	Hill 3114	tuff cone	Qot	unknown	sec. 35, T. 2 S., R. 1 W.
47	Hill 3125	cinder-spatter cone	Qot	ferrobasalt	sec. 19, T. 2 S., R. 1 W.
42	Hill 3137	maar-tuff ring	Qot	unknown	sec. 18, T. 2 S., R. 1 W.
43	Hill 3147	cinder-spatter cone	Qot	unknown	sec. 8, T. 2 S., R. 1 W.
17	Hill 3148	cinder-spatter cone	Qkb	unknown	sec. 11, T. 1 N., R. 1 W.
57	Hill 3157	tuff cone	QTsfd	unknown	sec. 25, T. 2 S., R. 1 W.
70	Hill 3160	cinder-spatter cone	QTbfb	unknown	sec. 9, T. 3 S., R. 2 E.
73	Hill 3166	cinder-spatter cone	—	unknown	sec. 13, T. 3 S., R. 2 E.
46	Hill 3173	cinder-spatter cone	Qot	Fe-enhanced	sec. 19, T. 2 S., R. 1 W.
69	Hill 3175	cinder-spatter cone	QTbfb	Al-enhanced	sec. 5, T. 3 S., R. 2 E.
44	Hill 3205	cinder-spatter cone	Qot	unknown	sec. 16-17, T. 2 S., R. 1 W.
64	Hill 3207	shield	Qbppu	SROT	sec. 14, T. 2 S., R. 1 E.
50	Hill 3217	maar-tuff ring	Qot	ferrobasalt	sec. 16, T. 2 S., R. 1 W.
49	Hill 3256	maar-tuff ring	Qot	ferrobasalt	sec. 21, T. 2 S., R. 1 W.
68	Hill 3505	cinder-spatter cone	QTbfb	SROT	sec. 33, T. 2 S., R. 2 E.
7	Hills 2798 & 2712	cinder-spatter vent	Qsky	unknown	sec. 9, T. 1 N., R. 3 W.
39	Hulet Ranch	maar-tuff ring	Qhr	unknown	sec. 3, T. 2 S., R. 1 W.
32	Initial Point	shield and spatter cone	Qip	Al-enhanced	sec. 31, T. 1 N., R. 1 E.
77	Jackass Butte NE	maar-tuff ring	Tjvc	unknown	sec. 10, T. 4 S., R. 2 E.
78	Jackass Butte SE	maar-tuff ring	Tjvc	SROT	sec. 15, T. 4 S., R. 2 E.
15	Kuna Butte	complex shield	Qkb	Al-enhanced	sec. 10, T. 1 N., R. 1 W.
20	Kuna Cave Hill	cinder-spatter cone	Qkb	Al-enhanced	sec. 22, T. 1 N., R. 1 W.
19	Kuna Cave Road Ridge	cinder-spatter cone	Qkb	unknown	sec. 15, T. 1 N., R. 1 W.
16	Kuna-Mora Road Hill	cinder-spatter vent	Qkb	Al-enhanced	sec. 35, T. 2 N., R. 1 W.
4	Liberty Butte	maar-tuff ring	Qlbv	Fe-enhanced	sec. 24, T. 2 N., R. 4 W.

Table 5. Continues.

Number	Name	Type	Unit	Chemistry	Location
1	Lizard Butte	cinder-spatter cone	Qliz	Fe-enhanced	sec. 35, T. 3 N., R. 4 W.
11	McElroy Butte	shield	Qhm	ferrobasalt	sec. 27, T. 1 N., R. 2 W.
21	Melba Hill	shield	Qkb	Al-enhanced	sec. 20, T. 1 N., R. 1 W.
22	Melba Hill Southeast	cinder-spatter vent	Qkb	unknown	sec. 29, T. 1 N., R. 1 W.
5	Missouri Avenue	maar-tuff ring	Qmav	ferrobasalt	sec. 26, T. 2 N., R. 3 W.
63	Montini	maar-tuff ring	QTmvc	SROT	sec. 6, T. 3 S., R. 1 E.
2	Pickle Butte	cinder-spatter cone	Qpb	Fe-enhanced	sec. 34, T. 3 N., R. 4 W.
37	Point 2650	cinder-spatter vent	—	unknown	sec. 4, T. 2 S., R. 1 W.
13	Powers Butte	shield	Qpow	Al-enhanced	sec. 13, T. 1 N., R. 2 W.
53	Priest Ranch	maar-tuff ring	Qpr	ferrobasalt	sec. 1, T. 2 S., R. 1 W.
76	Rabbit Creek Canyon	maar-tuff ring	Tjvc	SROT	sec. 11, T. 4 S., R. 2 E.
29	Sign Island	maar-tuff ring	Qgbv	ferrobasalt	sec. 36, T. 1 S., R. 2 W.
82	Simplot Feedlot	maar-tuff ring	Tfl	unknown	sec. 26, T. 4 S., R. 3 E.
56	Sinker Butte	tuff cone	Qsib, QTsfd	ferrobasalt	sec. 24, T. 2 S., R. 1 W.
62	Sinker Creek Butte	shield	QToms	SROT	sec. 12, T. 3 S., R. 1 W.
8	Sleepy Hollow	cinder-filled basin	Qsh	Fe-enhanced	sec. 10, T. 1 N., R. 2 W.
3	Stewart Lateral Hill	cinder-spatter cone	—	unknown	sec. 18, T. 2 N., R. 3 W.
27	Stoddard	maar-tuff ring	QTjl	unknown	sec. 7, T. 1 S., R. 1 W.
48	Striker Basin Gulch	maar-tuff ring	Qot	unknown	sec. 25, T. 2 S., R. 2 W.
54	Trio Hill	cinder-spatter cone	Qtr	ferrobasalt	sec. 29, T. 1 S., R. 1 E.
51	Tumbleweed Ridges	maar-tuff ring	Qot	Fe-enhanced	sec. 28, T. 2 S., R. 1 W.
25	Walters Butte	tuff cone	QTwa	SROT	sec. 11, T. 1 S., R. 2 W.
38	Wees Bar	maar-tuff ring	QTwbv	SROT	sec. 34, T. 1 S., R. 1 W.
26	White Butte	tuff cone	Qwb	ferrobasalt	sec. 22, T. 1 S., R. 2 W.

tured by tributaries of the Columbia River. Shoreline features for this paleolake system are still preserved and show very little deviation from the range of 1,100 to 1,160 m for the high-stand elevations (Jenks and Bonnichsen, 1989; Wood and Clemens, this volume), attesting to the general stability of the area surrounding the lake, even as its interior apparently subsided thousands of meters.

We believe extensive older faulting lies beneath the younger late Pliocene and Pleistocene basalt flows, though we cannot verify it. Evidence to support this includes the observations about the subsurface geology of the western SRP (Wood, 1994; Wood and Clemens, this volume) and the results of deep drilling that reveals the thick succession of materials buried in the interior of the western SRP (Arney and others, 1984; Lewis and Stone, 1988; McIntyre, 1979; Wood and Anderson, 1981). In addition, gravity and seismic data suggest that great thicknesses of reflective and dense material are unequally distributed through various parts of the structure (Mabey, 1982; Wood, 1994). These subsurface perturbations of geophysical data and rock sequences, compared to the geology exposed at the western SRP margins, are wholly consistent with the existence of much faulting at depth.

The occurrences of a few tilted basalt flows as young as about a million years and of tilted lake sediments in places in the western SRP, along with the few faults that can be seen at the surface, support the notion that the tectonic rifting has continued episodically from its inception between 11.7 and 11.0 Ma to the present. The relatively straight-line course of the Snake River parallel to the elongation of the western SRP and the southeastward extension of this trend into Bruneau Valley at the southeast end of the western SRP suggests that a buried set of faults may also have helped guide the course of the river. There are a few faults along this trend, such as in the Jackass Butte area northwest of Grand View. The concentration of hot springs and the availability of hot ground water all along this trend also support the possibility of a long but buried fault system along the trend of the Snake River for the length of the western SRP.

LANDSCAPE EVOLUTION IN THE WESTERN SNAKE RIVER PLAIN

The principal physiographic features of the western SRP are its relatively abrupt and steep margins flanked with extensive gravel-capped fanglomeratic accumulations, the little-dissected low-relief interior plain with numerous small volcanoes aligned in southeast- to northwest-trending alignments, and a northwest-trending zone of escarpments and bluffs near the Snake River where the river has eroded the sediments and capping volcanic materials. The steep margins are thought to reflect the down-faulting of the interior of the rift as it evolved over the past several million years, whereas the low relief of the interior plain resulted from the accumulation of lacustrine sediments and volcanic materials. The erosion of the escarpments and bluffs near the Snake River mainly

has occurred since Lake Idaho drained in the late Pliocene, although some of that topography may have developed earlier when the lake was drawn down to low levels, as suggested by the plots of lake elevation through time in Hearst (1999) and Wood and Clemens (this volume).

The course of the Snake River lies much closer to the southwest margin of the western SRP than to the northeast margin. Its position there likely results from the concentration of the late Pliocene and Pleistocene volcanism in the middle of the plain, which formed a slightly elevated medial zone, with the valleys of the Snake and Boise rivers respectively offset to the southwest and northeast sides of the rift. The volcanism in the central part of the plain, coupled with downcutting during the Pleistocene as the base-level of the river was lowered, kept the course of the Snake River mainly in the zone of sedimentary materials along the southwest margin.

Although the history of the now permanently drained lake system is incompletely understood, enough information has been gathered in the last few years to propose the following ideas about its evolution (Jenks and Bonnichsen, 1989; Godchaux and Bonnichsen, this volume; Godchaux and others, 1992; Hearst, 1999; Wood and Clemens, this volume; Bonnichsen and Godchaux, unpub. mapping, 1987-2002). We are uncertain when the lake started to fill in the western SRP graben, but likely this happened as the rift started to develop. A body of standing water already existed by the time of the early rhyolite eruptions along the southwest side of the western SRP about 11.7-11.0 Ma ago; this is suggested by the interaction of the distal parts of rhyolitic lava flows with large amounts of surface water (Godchaux and Bonnichsen, this volume). Between then and the late Pliocene or early Pleistocene when this large tectonically impounded lake was finally drained, Lake Idaho probably was continuously present but with marked variations in its surface elevation and thus of its depth and areal extent. The broad regional extent of paleo-shoreline features in the 1,100- to 1,160-m elevation range, we suggest, represents the high stand of the lake during late Miocene and early Pliocene time. The high lake levels coincide with when much basaltic volcanism occurred and when substantial amounts of the Chalk Hills and Poison Creek formations accumulated. When the lake level was high, much of the basalt was emplaced subaqueously, and this brought about the wide variety of basalt physical types and structures described in Godchaux and Bonnichsen (this volume).

Later, the lake surface dropped to much lower levels, probably below the present land surface elevation in the

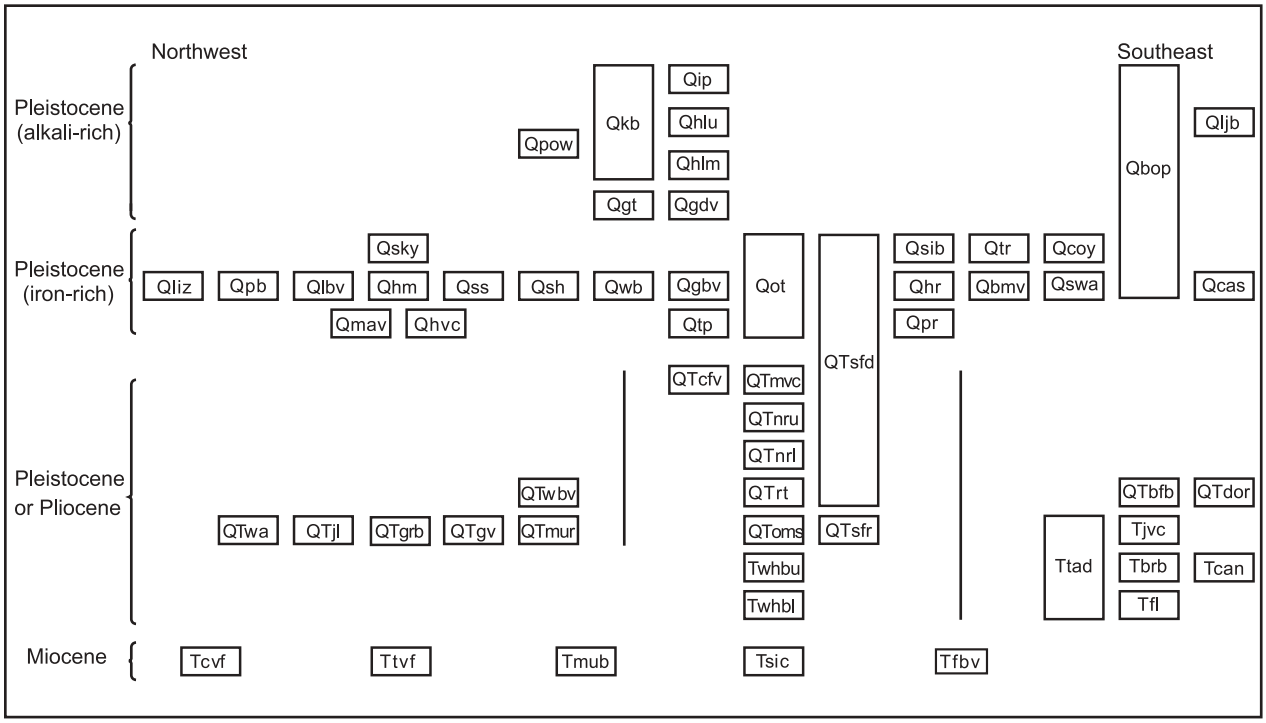

Figure 17. Stratigraphic chart for basalt units in the western SRP. Side-by-side boxes indicate that adjacent units are about the same age. Stratigraphic relations between adjacent boxes are unknown where portions of adjacent columns are separated by heavy vertical lines. See text for unit symbol identifications and information sources.

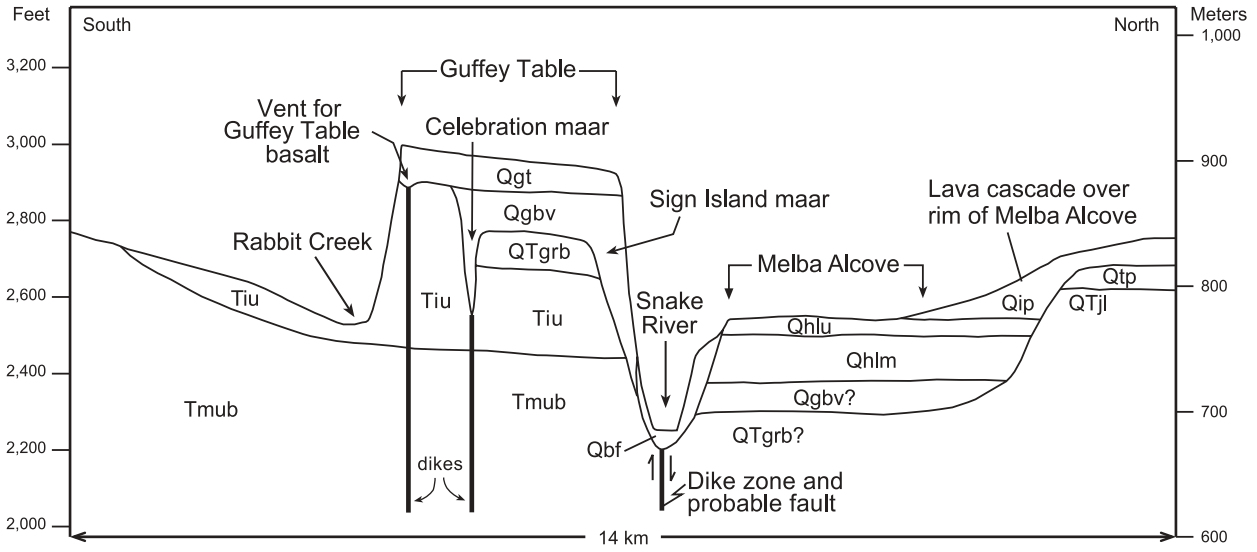

Figure 18. Schematic cross-section along a SSW-NNE line through Guffey Table and the Melba Alcove illustrating some of the volcanic, structural, and landscape evolutionary events in the western SRP. The first events were the eruption of the Miocene Murphy basalt and the deposition of the Idaho Group sediments as Lake Idaho waxed and waned. As the lake finally declined, the late Pliocene Guffey Railroad Bridge basalt, which is water-affected in a fashion suggestive of eruption into a swampy environment, flowed across the sediments. About this time, phreatomagmatic deposits were erupted from the Jinx Lateral volcanic complex and other localities. This was followed by the eruption of the Pleistocene Tombstone Patch Rapids basalt and other ferrobasalt units. During this time, the ancestral Snake River eroded the Melba Alcove into the lake sediments and volcanic units. The eruption of iron-rich basalts continued so that basaltic tuffs, which were erupted in a subaerial environment from the various vents of the Guffey Butte volcanic complex, were deposited in the Melba Alcove. Soon thereafter, the first of the alkali-rich lavas, the Guffey Table basalt, arrived at the surface at about 0.76 Ma. About this same time, the faulting proposed to follow the approximate present course of the Snake River occurred, as indicated by the probable hidden fault beneath the Snake River. While the alkali-rich basaltic volcanism continued, the middle and upper basalts of Halverson Lake, whose sources are unknown, flowed into and partly filled the Melba Alcove. Afterwards, the river began to incise itself along its present course between the Halverson Lake basalt flows and the previously formed Guffey Table. At about 0.41 Ma, Initial Point basalt flows cascaded over parts of the Melba Alcove rim and flowed across the alcove floor. Eventually, the Bonneville Flood scoured out the Snake River channel and left behind extensive boulder and gravel deposits. Units are identified as follows: Qbf—Bonneville Flood deposits and alluvium, Qip—Initial Point basalt, Qhlu—upper basalt of Halverson Lake, Qhlm—middle basalt of Halverson Lake, Qgt—Guffey Table basalt, Qgbv—Guffey Butte volcanic complex, Qtp—Tombstone Patch Rapids basalt, QTjl—Jinx Lateral volcanic complex and affiliated basaltic tuffs, QTgrb—Guffey Railroad Bridge basalt, Tiu—undifferentiated Idaho Group sediments, and Tmub—Murphy basalt.

interior of the western SRP. This lowering led to incisions of nearby streams into canyons, to localized erosion adjacent to the lake basin, and to the development of a minor amount of subaerial-appearing basaltic volcanic deposits in the middle of the Pliocene. The abundance of gypsum and calcite cement in some parts of the Chalk Hills sediments throughout the region may also reflect the lowering of the lake level during this time, as seen by the higher concentrations of the elements in the cementing materials in the lake. Soon, however, the lake returned to higher levels, perhaps as high as 1,100 m or nearly as high as the earlier high stand. During this second high stand, much of the Glenns Ferry Formation was deposited, and the late Pliocene-early Pleistocene basaltic volcanism was starting. Near the end of the Pliocene, the lake almost had drained permanently as its exit through Hell's Canyon of the Snake River eroded deeper and deeper. The demise of the lake permitted the beginning incision of the river into lake and fluvial sediments, and locally into volcanics. As incision continued, there was an accompanying lowering of the ground-water level adjacent to the river course as the channels were deepened.

The draining of the lake and then the lowering of the ground-water level had a marked effect on the style of basaltic volcanism during the late Pliocene and early Pleistocene. At first, there were extensive areas of water-affected basalt and pillow deltas formed where subaerially erupted flows ran into water, and tuff cones and even subaqueous vents developed where eruptions occurred in standing water. Then, after the lake had drained but before significant incision had occurred so that marshy ground and high ground-water tables were present, much of the basalt volcanism became increasingly explosive and formed many maars and tuff rings. Later, after the ground-water level had dropped, the style of volcanism

Table 6. Chemical analyses of basalt samples from the western Snake River Plain region.

Number	**1**	**2**	**3**	**4**	**5**	**6**	**7**	**8**	**9**	**10**
Sample	**I-3061**	**I-3033**	**I-3028**	**I-2996**	**I-3113**	**I-2831**	**I-3674**	**X-220**	**X-362**	**X-215**
Unit	**Tmub**	**QTdor**	**Tfl**	**Tjvc**	**Qss**	**Qcas**	**Qliz**	**Qbop**	**Qbop**	**Qbop**
Type	**SROT**	**SROT**	**Fe-enh**	**SROT**	**ferrobs**	**Fe-enh**	**Fe-enh**	**SROT**	**ferrobs**	**Al-enh**
Major Oxides, weight percent:										
Lab	**WSU**	**UMass**	**UMass**	**WSU**	**WSU**	**UMass**	**WSU**	**UMass**	**UMass**	**UMass**
SiO_2	48.38	46.64	46.10	48.15	49.35	47.94	48.11	47.57	43.62	48.47
TiO_2	2.36	2.90	3.30	2.92	2.45	3.53	3.55	2.55	4.07	1.99
Al_2O_3	15.88	14.87	14.15	13.89	14.11	13.82	13.88	16.01	14.13	16.51
Fe_2O_3	12.56	14.51	15.87	14.72	17.15	15.23	15.97	13.64	17.49	11.10
MnO	0.18	0.21	0.22	0.20	0.34	0.21	0.22	0.20	0.26	0.17
MgO	7.25	6.80	6.66	5.71	2.46	5.05	6.00	6.49	5.38	6.39
CaO	10.59	10.08	10.18	11.17	6.85	10.18	9.66	9.12	8.64	9.03
Na_2O	2.48	2.52	2.45	2.35	3.50	2.49	2.32	3.08	3.15	3.41
K_2O	0.19	0.60	0.46	0.70	2.12	0.71	0.77	1.37	1.35	1.96
P_2O_5	0.32	0.66	0.65	0.75	2.01	0.63	0.76	0.47	1.78	0.61
Total	100.19	99.79	100.04	100.56	100.34	99.79	101.24	100.50	99.87	99.64
Major Oxides, normalized:										
SiO_2	48.29	46.74	46.08	47.88	49.18	48.04	47.52	47.33	43.68	48.65
TiO_2	2.36	2.91	3.30	2.90	2.44	3.54	3.51	2.54	4.08	2.00
Al_2O_3	15.85	14.90	14.14	13.81	14.06	13.85	13.71	15.93	14.15	16.57
Fe_2O_3	12.54	14.54	15.86	14.64	17.09	15.26	15.77	13.57	17.51	11.14
MnO	0.18	0.21	0.22	0.20	0.34	0.21	0.22	0.20	0.26	0.17
MgO	7.24	6.81	6.66	5.68	2.45	5.06	5.93	6.46	5.39	6.41
CaO	10.57	10.10	10.18	11.11	6.83	10.20	9.54	9.07	8.65	9.06
Na_2O	2.48	2.53	2.45	2.34	3.49	2.50	2.29	3.06	3.15	3.42
K_2O	0.19	0.60	0.46	0.70	2.11	0.71	0.76	1.36	1.35	1.97
P_2O_5	0.32	0.66	0.65	0.75	2.00	0.63	0.75	0.47	1.78	0.61
Mg No.	53.36	48.15	45.40	43.46	22.13	39.65	42.68	48.53	37.87	53.29
Minor Elements, parts per million:										
Lab	**WSU**	**ISU**	**ISU**	**WSU**	**WSU**	**ISU**	**WSU**	**ISU**	**ISU**	**ISU**
Sc	34	30	31	35	38	31	28	28	30	25
Cr	186	218	164	160	0	131	122	141	35	141
Co	—	54	57	—	—	45	—	55	49	50
Ni	68	—	—	62	5	—	47	70	60	62
Zn	116	152	145	135	265	173	150	112	208	87
Rb	3	—	—	11	45	—	12	30	11	46
Sr	242	355	280	298	330	375	320	330	365	525
Zr	127	130	120	276	564	120	278	110	200	90
Ba	167	595	320	461	1149	375	449	415	680	555
V	282	—	—	245	70	—	338	—	—	—
Y	32	—	—	43	105	—	42	—	—	—
Nb	12	—	—	25	88	—	29	—	—	—
Ga	21	—	—	21	31	—	23	—	—	—
Cu	42	—	—	47	22	—	38	—	—	—
Pb	5	—	—	7	0	—	7	—	—	—
La	14	30	20	29	75	23	38	20	48	27
Ce	38	65	46	69	180	52	87	45	111	54
Nd	—	31	27	—	—	27	—	30	67	31

Samples were analyzed at the following institutions: UMass—University of Massachusetts at Amherst, WSU—Washington State University, and ISU—Idaho State University.

became much more effusive, leading to the formation of the latest volcanoes in the area, which are a mixture of cinder and spatter constructs and shield volcanoes, and the related eruption of entirely subaerial lava flows.

During the final stages of volcanism, the erosion by the ancestral Snake River and other streams led to the development of small temporary lakes where erupting lavas flowed into and dammed the water courses. These lakes were places where additional basaltic tuffs and lacustrine sediments, sometimes reworked from previous lacustrine accumulations, could collect and where additional explosive interactions between rising basaltic lava and surface waters could occur. Channel-filling basalt units are common but difficult to recognize, and the

lateral extent of many volcanic and sedimentary units is difficult to trace unless the exposures are excellent. The accumulative effect of these events led to complex stratigraphic relationships among the various basalt units and sediments deposited in the western SRP.

VOLCANISM IN THE WESTERN SNAKE RIVER PLAIN

Rhyolitic volcanism along the Owyhee Front on the southwest side of the western SRP and along the Boise Front on the northeast side of the western SRP preceded the eruptions of basalts in the western Snake River Plain. Only small amounts of rhyolite are present along the Boise Front in the area near Boise (Othberg and Stanford, 1992; Wood and Clemens, this volume) and in the Pearl area west of Boise (Clemens, 1993). In the western Bennett Hills area near Mountain Home, adjacent to where the western SRP joins the central SRP (Figure 1), however, a thick succession of rhyolite units, mainly lava flows, range from about 11.0 Ma at the base of the section to 10.0 Ma at the top (Clemens and Wood, 1993). Ten rhyolite units are recognized in the western Bennett Mountains, and they are in two groups. The older, topographically higher group—the rhyolite of Bennett Mountain—consists of the earliest six units. The younger, topographically lower group—the rhyolite of Danskin Mountain—contains four units (Wood and Gardner, 1984). The thickness of the western Bennett Mountain section of rhyolitic rocks has been estimated to be greater than 1 km (Wood, 1989) and may be the thickest exposed accumulation of SRP-affiliated silicic volcanics in southwestern Idaho.

Along the Owyhee Front at the southwest side of the western SRP, rhyolite units occur discontinuously from near the Idaho-Oregon border to where the western and central SRPs join. In the area southwest to southeast of Marsing (Figure 1), several occurrences of rhyolite, collectively referred to as the Owyhee Front rhyolite (Figure 2), have been recognized (Ekren and others, 1981, 1984; Godchaux and Bonnichsen, this volume). Included in this group are the Jump Creek rhyolite field and Reynolds Creek rhyolite lava flow, the Wilson Creek ignimbrite, and the Cerro el Otoño dome field; all fall in the age range of 11.7-11.0 Ma. Farther to the southeast along the Owyhee Front in the area southeast of Murphy and southwest of Grand View (Figure 1), several rhyolite units occur in the Browns Creek area. This Browns Creek group includes rhyolite lava flows and rheomorphic ignimbrites that have ages in the 11.0-11.2 Ma range (Ekren and others, 1981, 1984; Bonnichsen and others, 1988). Even farther southeast along the southwest margin of the western SRP, in the Jacks Creek area near the intersection of the western and central parts of the SRP, are several rhyolite lava flows and perhaps some high-temperature rheomorphic ignimbrites (Bonnichsen and Kauffman, 1987; Ekren and others, 1981, 1984; Kauffman and Bonnichsen, 1990; Jenks and others, 1998) that have radiometric dates ranging from 14.2 Ma to younger than 9.6 Ma. Altogether, at least eight major rhyolite units are in the Jacks Creek area.

About 150 basaltic volcanoes have been identified in the western SRP region between the Idaho-Oregon border on the west and the Mountain Home area on the east (Bonnichsen and Godchaux, unpub. mapping 1987-2002). These are more than have been identified in the Bruneau-Jarbidge and Twin Falls regions combined. However, many of these volcanoes produced only small volumes of ejecta, on average much smaller amounts than ejected by the volcanoes in the Bruneau-Jarbidge and Twin Falls regions. The western SRP volcanoes vary widely in eruptive style, in volume of erupted materials, and in composition. With so many volcanoes, it is impractical to discuss all of them in this paper, so the following overview of the principal units and volcanoes indicates the variety of physical, chemical, and age-group types. Several basaltic volcanoes have previously been described (Jenks and Bonnichsen, 1989; Godchaux and others, 1992; McCurry and others, 1997) or are discussed elsewhere in this volume (Godchaux and Bonnichsen; White and others; Shervais and others).

In the Bruneau-Jarbidge and Twin Falls regions, about 90 percent of the volcanoes are shields and dike vents accompanied by only a few vents of other types. In the western SRP, however, many types of volcanoes occur in abundance and generally are confined to their own regions. Compared with the Bruneau-Jarbidge and Twin Falls regions, a wider variety of eruptive products than just basalt flows occur in the western SRP. Many units contain significant to dominant amounts of pyroclastic materials, ranging from spatter and cinders to extensive beds of basaltic tuff. Of the types of volcanoes mentioned earlier, cinder and spatter cones account for 32 percent of the total, and shields for 30 percent. Nearly all of the shields are simple shields, and most are less than a kilometer in diameter. Both of these general types of volcanoes are subaerial constructs, and they occur primarily as a broad curvilinear band about 15 km wide and nearly 100 km long from the Mountain Home area to the Melba area on the plateau north of the Snake River. More than 80 percent of the shields and cinder and spatter cones lie within this band and are late Pliocene or Pleistocene in age.

Some 28 percent of the volcanoes are best described as maars, tuff rings, or tuff cones. They formed either in emergent situations or in subaerial environments where

the ground was water saturated at the time of volcanism, so that copious quantities of phreatomagmatic deposits were generated (see Godchaux and Bonnichsen, this volume, for discussion). The phreatomagmatic volcanism was mainly restricted to a linear zone trending about N. 40º W. on either side of the Snake River southwest of the band of shields and cinder and spatter cones. This linear zone of dominantly phreatomagmatic volcanism generally is 5 km or less wide, except northeast of Murphy where it swells to about 11 km, and extends for 85 km. The phreatomagmatic volcanoes in this zone also are late Pliocene and Pleistocene in age.

The third group of volcanoes erupted in a subaqueous setting beneath the surface of Lake Idaho. This type accounts for about 10 percent of the western SRP volcanoes. Nearly all of the subaqueous vents are Miocene in age, when the lake may have had a greater extent than later. Most are concentrated in a northwest-trending linear zone southwest of the Snake River that parallels the zone of phreatomagmatic volcanoes along the river. This zone of subaqueous volcanoes trends about N. 35º W. and is nearly 44 km long and as much as 5 km wide in the area northwest of Murphy. Since this style of volcanism is somewhat older than the later emergent and subaerial styles in the zones to the northwest, many subaqueous vents may lie buried under late Pliocene and Pleistocene basalt units northeast of this zone. Thus, the linear zone of subaqueous vents may be more of a landscape evolution artifact than a true linear array of vents. This is somewhat borne out by the occurrence of great thicknesses of basalt, much of which likely was emplaced during the late Miocene in the central part of the western SRP graben at the bottom of Lake Idaho (Lewis and Stone, 1988; McIntyre, 1979; Shervais and others, this volume; Wood, 1994; Wood and Anderson, 1981; Wood and Clemens, this volume).

BASALT UNITS IN THE WESTERN SNAKE RIVER PLAIN REGION

In the western SRP, many volcanoes and basalt units (Figures 16 and 17; Table 5) vary significantly in age, style of eruption, and chemical composition. We have used these three parameters to subdivide the basalt units of the region into the following groups. The main groups are (1) late Miocene basalt units, (2) late Pliocene and early Pleistocene basalt units, (3) Pleistocene iron-rich basalt units, and (4) Pleistocene alkali-rich basalt units. Both the late Pliocene and early Pleistocene, and the Pleistocene iron-rich groups, are further subdivided into units erupted from nonexplosive vents and those from explosive vents. The Pleistocene alkali-rich group has been subdivided into units in the Melba-Walters Ferry area and units in the Birds of Prey and Little Joe Butte area.

The late Miocene group of basalt units occur along the southwestern SRP margin, south of the Snake River, where extensive lacustrine and fluvial sediments of the Idaho Group are exposed. These basalts are exposed because they were never covered by the late Pliocene and Pleistocene basalts that occupy most of the central and northeastern part of the western SRP. The late Miocene basalts probably extend beneath most of the western SRP, with only a small amount exposed at the surface. This suggestion is supported by the presence of Miocene basalts in the Boise foothills region (Clemens and Wood, 1993) and by a thick section of buried basalt at the Mountain Home Air Force Base (Lewis and Stone, 1988; Shervais and others, this volume).

The radiometric ages of the late Miocene western SRP basalts are in the 7-9 Ma range (Figure 6). White and others (this volume) report Ar-Ar ages of 7.85 and 7.92 Ma, for samples respectively from the Teapot and Chalky volcanic fields. Amini and others (1984) report K-Ar dates of 7.07 and 7.24 Ma for the Fossil Butte volcanic complex. The late Miocene basalts consist principally of SROT, which is accompanied by minor amounts of Al-enhanced basalt and even smaller amounts of Fe-enhanced basalt. Chemical analyses of representative samples are presented by White and others (this volume). These late Miocene, western SRP basalts are essentially the same chemically as many of the SROT basalts of similar age in the Bruneau-Jarbidge region, and they correspond to the category M1 basalts of White and others. Plagioclase and olivine commonly are phenocryst minerals in this group of basalts.

During the late Pliocene after the early Pliocene volcanism hiatus and extending well into the early Pleistocene, extensive volcanism occurred in many parts of the western SRP. Some of it was effusive, producing basalt lavas from subaerial shields and cinder and spatter cones, and some of it was explosive, producing bedded tuffs and spatter in and adjacent to vents. In addition, WABs, pillow deltas, and littoral fans formed at many localities during the late Pliocene where subaerial lava flows entered bodies of water. The dominant composition of the ascending magma was SROT basalt, but a few Fe-enhanced basalt flows and even ferrobasalts are intercalated with the SROT basalts. These late Pliocene-early Pleistocene basalts commonly contain plagioclase and olivine phenocrysts and correspond to the M2 category basalts of White and others (this volume). The basaltic volcanism during this time seems to have occurred from the eastern part of the western SRP to as far west as Guffey and Walters Buttes south of Melba. But most vents and units near the Snake River are east and southeast of the

Swan Falls Dam area. The locations of many late Pliocene and Pleistocene volcanoes near the Snake River are shown on Figure 16 along with the outlines of some of the larger basalt flows.

As the Pleistocene epoch progressed, the style of basaltic volcanism remained similar to that during the late Pliocene. It was a mixture of effusive and explosive eruptions, depending on the near-surface environment into which a particular batch of basaltic magma ascended. However, the composition of the ascending magma changed to become more and more iron rich. By the middle of the Pleistocene, essentially all of the ascending magma batches were ferrobasalt in composition, and only locally were they merely Fe-enhanced. From all appearances, the change through time from dominantly SROT basalt to dominantly ferrobasalt is a gradational transition rather than an abrupt break. The Pleistocene ferrobasalts are within the M2 basalt category of White and others (this volume). The ferrobasalts typically contain both olivine and plagioclase phenocrysts. In some units, the plagioclase phenocrysts are large and abundant, and in places are grouped together as cumulophyric aggregates. By mid-Pleistocene, the region undergoing most of the ferrobasalt volcanism was near the Snake River northwest of the Swan Falls Dam area and extending northwestward through the Walters Ferry-Melba area to as far as Lizard Butte near Marsing. The ferrobasalt units in this zone were erupted from both nonexplosive and explosive sources and are described below. In addition to the ferrobasalt volcanism near the Snake River, similar volcanism was occurring during the Pleistocene in the Mountain Home area (Shervais and others, this volume) and near the fault zone bounding the northeast margin of the western SRP between Mountain Home and Boise (Othberg, 1994).

A group of basalt vents and flows that are younger and characterized by greater amounts of alkali elements than the SROT basalts and ferrobasalts of the western SRP occur along a zone in the central part of the western SRP. This zone extends as a somewhat irregular and generally NW-trending broad, but low, ridge that encompasses the Little Joe Butte, Christmas Mountain, Initial Point, and Kuna Butte areas. For our discussion, we refer to these basalts as being alkali-rich because many, although not all, contain more than 4 percent K_2O plus Na_2O. A few contain less, but compared to the SROT basalts and ferrobasalts they still are enriched in alkali elements. The two principal groups of these alkali-rich basalts are in the Melba-Walters Ferry area and farther southeast in the uninhabited part of southern Ada County dedicated to the National Guard Maneuver Area and the Snake River Birds of Prey Area.

The basalt magmas coming to the surface in the Melba-Walters Ferry area changed abruptly from ferrobasalt to distinctly different compositions in mid-Pleistocene at about 0.80 Ma. These later basalts generally are enriched in Al relative to SROT and ferrobasalt and are enriched in alkali elements, in some instances having as much as twice the alkalis as the SROT-ferrobasalt group. These late-stage alkali-rich basalts correspond to the M3 basalt category of White and others (this volume). The M3 basalts do not show high Fe contents like those in the SROT-ferrobasalt group. Rather they have relatively low Fe contents similar to those in the Al-enhanced basalts that form the primitive end of the SROT-ferrobasalt group, but they clearly do not share the relatively low alkali contents of that group. Other differences between these two basalt compositional groups can be seen in the analyses of Table 6 and in White and others (this volume). The alkali-rich M3 basalts typically contain both olivine and plagioclase phenocrysts, and many of the units of this group have a greater abundance of phenocrysts than do most of the basalts in the M2 SROT-ferrobasalt group.

By the middle of the Pleistocene when the alkali-rich basalts started to erupt, nearly all of the standing water and water-saturated ground in the Melba-Walters Ferry area had been drained; thus, most of the vents for this type of basalt are either shields or cinder and spatter cones. Only the earliest two eruptions, which led to formation of the Guffey Table lava flow and the Grouch Drain volcanic complex, had substantial explosive phreatomagmatic activity. The later eruptions, which led to formation of the basalt of Initial Point, the Kuna Butte basalt field, the basalt of Powers Butte, and the middle and upper basalt units of Halverson Lake, seem to have been relatively effusive subaerial outpourings of lava and pyroclastic emissions that developed shields and cinder and spatter cones.

In contrast to the sharp time break between the eruptions of ferrobasalts and alkali-rich basalts in the Melba-Walters Ferry area, there was some temporal overlap between the eruptions of these two types in the southern part of Ada County. We have referred to this group of basalt units and vents in that area as the Birds of Prey basalt field. Moreover, some of the ferrobasalts in the Birds of Prey basalt field are markedly enriched in alkali elements.

The Birds of Prey basalt field lies north of the segment of the Snake River between Grand View and Swan Falls Dam and occupies an area extending more than 30 km (N-S) and almost 40 km (E-W; Figure 19). In effect, the basalt field is a giant shield volcano with an extremely low profile. Only about 200 m of relief occurs from the flows at the margins of the unit to the highest point, Christmas Mountain, in the middle of the field. Unlike nearly

all of the other shields in the SRP and there are hundreds, the Birds of Prey "shield" is polygenetic in that basalt flows erupted from many sources over a long time. By contrast, nearly all the other SRP shields are monogenetic, an eruption of one magma batch during a short time. The Birds of Prey "shield" is made up of vents and flows of quite diverse composition erupted from a series of magma batches that rose to the surface as the construct evolved.

The range of compositions in the Birds of Prey basalt field is essentially the same as among the various units in the Walters Ferry-Melba area. These include iron-rich basalts with only slightly more than ordinary amounts of alkali elements and iron-rich basalts with greatly enriched abundances of alkali elements. In addition, many Birds of Prey basalts are similar in character to White and others' M3 category, with an abundance of alkali elements that vary from ordinary amounts to greatly enriched, but no iron enrichment. Among the cinder and spatter cones in the central ridge vent complex, some of the vents have one composition and adjacent vents another, and these various compositions are interstratified among the flows. In contrast, in the Walters Ferry-Melba area the ferrobasalt eruptions stopped abruptly at about 0.8 Ma and soon were replaced by the eruption of alkali-rich M3 basalts. In the Birds of Prey field, the overlap in time and location of the eruptions of iron-rich and alkali-rich basalts suggests the contemporaneous existence of the two magma types. In the Walters Ferry-Melba area, however, the time difference between eruption of the two magma types does not suggest such a coexistence. Stratigraphically, the Birds of Prey basalt field appears to be mainly or entirely Pleistocene. Two radiometric K-Ar ages are available (Amini and others, 1984). One (sample 80H15) appears to be the lower basalt of Promontory Point and has an age of 0.78 Ma; the other (sample 79H3A) probably is the basalt of Corder Creek and has a date of 0.47 Ma.

Author note: The remainder of the "Basalt Units in the Western Snake River Plain Region" section of this article describes individual units. Readers not interested in these details can skip ahead to the next major section, "Variations in Basalt Chemical Composition," without losing the continuity of discussion.

LATE MIOCENE BASALT UNITS IN THE WESTERN SNAKE RIVER PLAIN

The following late Miocene basalt units in the western SRP are described in this section:

Tsic—basalt of Sinker Creek
Tfbv—Fossil Butte volcanic complex
Tmub—basalt of the Murphy area
Ttvf—Teapot volcanic field
Tcvf—Chalky volcanic field

The **basalt of Sinker Creek** (Tsic) consists of water-affected basalt flows, pillow basalt, and a debris flow of basalt, sediment, and basaltic tuff fragments distributed for several kilometers along Sinker Creek that we believe were mainly erupted from the Hill 3337 volcano (NE¼ sec. 29, T. 3 S., R. 1 W.), located about 11 km southeast of Murphy near where State Highway 78 crosses Sinker Creek. Beneath the Hill 3337 vent are extensive palagonite tuff deposits cut by peperitic dikes. This sequence of materials suggests that the early part of this eruption was explosive, and the latter part, responsible for the WAB flows and pillow basalts, was more effusive. See Godchaux and Bonnichsen (this volume) for a discussion of the Hill 3337 volcano and the Sinker Creek basalt. Recent investigations of the Sinker Creek basalt unit and its volcano, Hill 3337, have established Joyce Ranch volcano as a new and more distinctive name for this volcano (Mary O'Malley, oral commun., 2004).

The **Fossil Butte volcanic complex** (Tfbv) is an eroded palagonite tuff accumulation capped by a small basaltic spatter layer. Fossil Butte (NW¼ sec. 3, T. 4 S., R. 1 W.) is an eroded tuff cone 15 km southeast of Murphy near State Highway 78. Only inner crater-wall deposits are preserved in the cone itself; poor exposures of possible outer crater-wall deposits can be seen in small gullies flanking the butte. Amini and others (1984) report K-Ar dates on Fossil Butte samples of 7.07 Ma and 7.24 Ma. The basalt spatter layer at the top of the butte consists of SROT basalt.

The basalt of the Murphy area, the Teapot volcanic field, and the Chalky volcanic field are three closely related contiguous areas of late Miocene basalt along the Owyhee Front near Murphy. The **basalt of the Murphy area** (Tmub) is a poorly exposed zone of thoroughly water-affected basalt with minor amounts of admixed basaltic tuff and lacustrine sediments. It occurs as a northwest- to southeast-trending zone about 5 km wide extending both northwest and southeast from Murphy and lies beneath younger sedimentary and basalt units to the northeast (Figure 18). No vents have been identified in the unit, but these basalts probably erupted from several sources and were emplaced on the floor of Lake Idaho. The Murphy area basalt consists mainly of SROT; a typical analysis is presented in Table 6 (number 1).

The **Teapot volcanic field** (Ttvf) occupies an irregular-shaped zone 3-4 km across located 5-7 km northwest of Murphy. The basalt in the Teapot field was emplaced subaqueously, at least in part from vents in the area and perhaps also from nearby subaerial vents. Five probable vents within the field have been identified. Strong inter-

action between the Teapot field basalts and the enclosing sediments led to the development of invasive features and thermal metamorphic rinds adjacent to some of the large basalt blobs. Much of the basalt in the Teapot field is WAB, but adjacent to some of the invasive blobs the basalt was quenched and now forms curvilinear, locally dikelike zones of competent basalt typically 0.5 to 2 m thick surrounding the blobs (McCurry and others, 1997; Godchaux and Bonnichsen, this volume). White and others (this volume) report an Ar-Ar age on the Teapot basalt of 7.85 Ma. Analyzed samples from the Teapot volcanic field are a mixture of Al-enhanced and SROT basalt in composition.

The **Chalky volcanic field** (Tcvf) is 2-5 km north and northwest of the Teapot field and occupies an irregular area principally underlain by fragmented pillow basalt. The Chalky field is about 5 km across and 7-12 km northwest of Murphy. Many of the fragmented basalt pillows evidently formed as copious quantities of basalt were extruded onto the floor of Lake Idaho through dikes. The fragmentation may have occurred as the brittle quenched pillows broke apart in response to being shoved aside by the continued eruption of more pillows. Several of the feeder dikes are exposed around the south side of the unit, and pockets of basaltic tuff, measuring a few meters in thickness and a few tens of meters across, have developed at the base of the unit adjacent to some of the feeder dikes. The uppermost parts of some feeder dikes are also pillowed. Further details on the basalts of the Murphy area and the Teapot and Chalky volcanic fields are presented in Godchaux and Bonnichsen (this volume). White and others (this volume) report an Ar-Ar age for the Chalky volcanic field of 7.92 Ma. Analyzed samples from the field have SROT basalt compositions.

LATE PLIOCENE AND EARLY PLEISTOCENE BASALT UNITS IN THE WESTERN SNAKE RIVER PLAIN

Late Pliocene-Early Pleistocene Units Erupted From Nonexplosive Vents

The following late Pliocene and early Pleistocene basalt units, erupted from nonexplosive vents in the western SRP, are described in this section:

Tcan—basalt of Canyon Creek
QTdor—basalt of Dorsey Butte
Tbrb—basalt of Brooks Ranch
Ttad—basalt of Tadpole Lake
QTbfb—basalt of Bigfoot Butte
Twhbl—lower basalt of Wild Horse Butte
Twhbu—upper basalt of Wild Horse Butte
QTnrl—lower basalt of Nahas Ranch
QTnru—upper basalt of Nahas Ranch
QToms—basalt of Otter Massacre Site
QTsfr—basalt of Swan Falls Reservoir
QTmur—basalt of Murphy Rim
QTgrb—basalt of Guffey Railroad Bridge

Several late Pliocene or early Pleistocene basalt flows are exposed near the Snake River in the southeastern part of the western SRP. Some are strictly subaerial, but most show portions, sometimes major, that consist of WAB, and several of these flows developed pillow deltas. For some, the source vents have not been determined, but for others the source volcanoes are exposed shields and cinder and spatter cones. Progressing from southeast to northwest, some of the more extensive basalt units are itemized below (Bonnichsen and Godchaux, 1998 and unpub. mapping, 1987-2002; Jenks and Bonnichsen, 1990b). Along the canyon rim generally north of Grand View is the basalt of Canyon Creek, which is overlain by the basalt of Dorsey Butte. The **basalt of Canyon Creek** (Tcan), which probably was erupted from a source about 20 km west of Mountain Home, was discussed with the basalt units of the Bruneau-Jarbidge region. The **basalt of Dorsey Butte** (QTdor) was erupted from the Dorsey Butte shield, located about 11 km north-northeast of Grand View (Figure 16). This shield is elongate but somewhat irregular in shape and about 2 km long from south to north. Its subaerial lavas flowed about 6 km south from the vent and probably as much as 12 km to the west. The Dorsey Butte basalt has a SROT composition; a typical analysis is given in Table 6 (number 2).

Beneath the western part of the Dorsey Butte basalt are flows of the **basalt of Brooks Ranch** (Tbrb). The Brooks Ranch basalt is exposed for several kilometers along the bluffs northeast of the Snake River opposite Jackass Butte. It overlies the Feedlot tuff and lies beneath the basaltic tuffs of the Jackass Butte volcanic field (Figures 16 and 17). The basalt is water affected throughout most of its area, but in places along the Snake River it shows a well-developed pillow-delta facies. It is cut by northwest-trending faults near the river. The source volcano has not been identified but presumably lies to the north beneath younger basalt flows. The prominent hill within the area of the flow, Black Butte about 12 km northwest of Grand View, is not a shield; rather, it is an anticline that deforms the basalt unit and is cut on the south and east by faults so that the hill superficially resembles a shield. The Brooks Ranch basalt is one of the earliest of the late Pliocene basalt flows in the western SRP, with a probable age of about 2.2 Ma (Amini and others, 1984). Its composition ranges between Fe-enhanced basalt and ferrobasalt.

About 10 km north of Black Butte, which is about 20

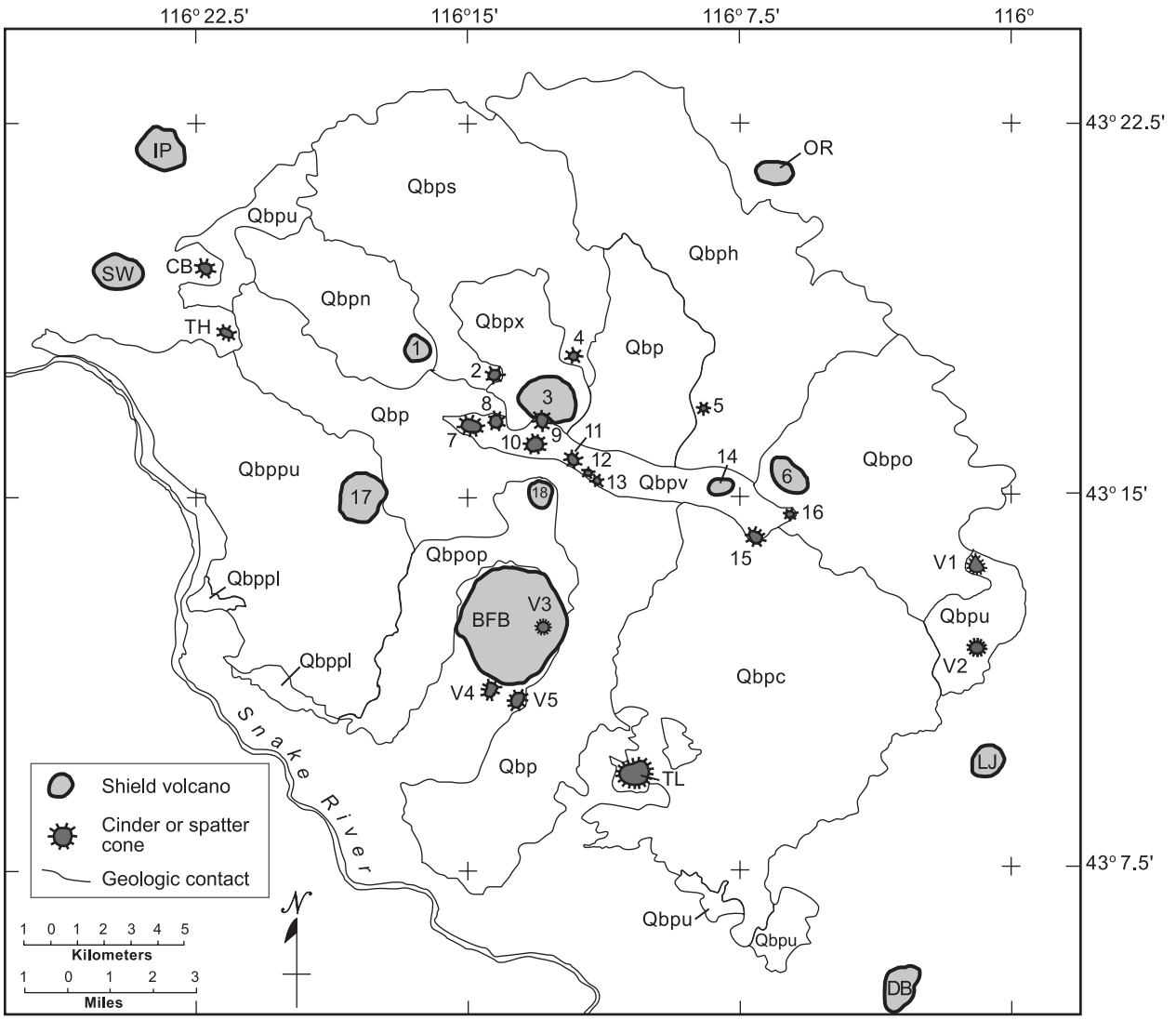

Figure 19. Birds of Prey basalt field in southern Ada County. Units are identified as follows: Qbpv—Central ridge vent complex, Qbpc—Corder Creek basalt flow, Qbph—Higby Cave basalt flow, Qbpop—Old Powerline Road basalt flow, Qbpn—National Guard area basalt flow, Qbpo—Orchard railroad siding basalt flow, Qbps—Sand Creek basalt flow, Qbpx—Christmas Mountain basalt flow, Qbppl—lower basalt of Promontory Point, Qbppu—upper basalt of Promontory Point, Qbp—unnamed basalt flows from south-central part and western end of central ridge vent complex, and Qbpu—Birds of Prey basalt, undifferentiated. Birds of Prey basalt field volcanoes: 1—Hill 3234, 2—Hill 3269, 3—Christmas Mountain, 4—Hill 3353, 5—Flagstaff Butte, 6—Hill 3342, 7—Hill 3346, 8—Hill 3305, 9—Hill 3370, 10—Hill 3349, 11—Hill 3365, 12—Hill 3355, 13—Hill 3391, 14—Hill 3456, 15—Wind Butte, 16—Hill 3330, 17—Hill 3207, and 18—Hill 3315. Other volcanoes: IP—Initial Point, SW—Swan Falls Road Hill, TH—Trio Hill, CB—Coyote Butte, OR—Orchard Ranch hill (Hill 3202), LJ—Little Joe Butte, DB—Dorsey Butte, BFB—Big Foot Butte, TL—Tadpole Lake area hill (Hill 3166), V1—Hill 3171, V2—Hill 3152, V3—Hill 3505, V4—Hill 3175, and V5—Hill 3160.

km north-northwest of Grand View, are some low hills that expose the basalt of Tadpole Lake (Figure 16). The **basalt of Tadpole Lake** (Ttad) is SROT, and its source has not been identified. Many of the exposures of the Tadpole Lake basalt are faulted, and some of the layers dip moderately to steeply in a manner similar to the deformed basalt flows of the Brooks Ranch basalt at Black Butte.

The **basalt of Big Foot Butte** (QTbfb) was erupted from one of the most prominent shield volcanoes in the western SRP, Big Foot Butte, which is 25-28 km north-northwest of Grand View and the same distance east of Murphy (Figure 16). Big Foot Butte is nearly circular in outline and about 4 km in diameter. It is accompanied by three satellite cinder and spatter vents, one high on its east flank (Hill 3505) and two just to the south (Hill 3175)

and southeast (Hill 3160) of the main butte. The Big Foot Butte lava flowed mainly south and southwest to at least as far as the present-day Snake River Canyon rim, 8 to 12 km from the shield. Near the canyon, the subaerial flows entered standing water, probably Lake Idaho, to form extensive pillow deltas. The Big Foot Butte basalt lies stratigraphically above the Brooks Ranch basalt, the tilted flows of the Tadpole Lake basalt, and the Jackass Butte volcanic complex basaltic tuff beds, but it is below several of the lava flows from the Birds of Prey basalt field to the north (Figure 17). Its composition is SROT basalt, and its eruptions may have been sometime between 0.95 and 1.57 Ma (Amini and others, 1984).

Along the Snake River for about 15 km between the mouth of Fossil Creek on the southeast and the Swan Falls Dam area on the northwest are a series of basalt flows exposed in the canyon walls. These flows were erupted from various sources, only some of which are known. This sequence of flows typically is several tens of meters thick, and the flows from individual sources commonly are separated by layers of basalt tuffs from various sources and locally by lacustrine silts of the Idaho Group. Also occurring in this zone are several phreatomagmatic basaltic vents, which are discussed in the next section. Altogether, this is a complex area that is only partly understood. The principal basalt units in this zone, generally from southeast to northwest, are the upper and lower basalts of Wild Horse Butte, the upper and lower basalts of the Nahas Ranch, the basalt of the Otter Massacre Site, and the basalt of Swan Falls Reservoir.

The **lower basalt of Wild Horse Butte** (Twhbl), which lies on sediments deposited in Lake Idaho, is a ferrobasalt from an unknown source. The **upper basalt of Wild Horse Butte** (Twhbu) is SROT basalt and was erupted from the relatively small Wild Horse Butte shield (Hill 2781), located 25 km northwest of Grand View and 20 km southeast of Murphy. Both the **lower and upper basalts of Nahas Ranch** (QTnrl and QTnru) appear to have been erupted from the Hill 2829 ($SW^1/_4$ sec. 10, T. 3 S., R. 1 E.) maar-tuff ring vent complex about 19 km east-southeast of Murphy. The lower basalt is Fe-enhanced, whereas the upper basalt is SROT. Both Nahas Ranch units contain substantial amounts of pillow basalt.

The **basalt of Otter Massacre Site** (QToms) was erupted from the Sinker Creek Butte, an irregular-shaped probable shield 12 km east-southeast of Murphy, and flowed northward down a paleoslope to enter Lake Idaho, where it formed large amounts of pillow basalt and WAB (Jenks and Bonnichsen, 1989). The Otter Massacre Site basalt is SROT. The **basalt of Swan Falls Reservoir** (QTsfr) is a series of flows that probably erupted from several unidentified sources. These flows are variably water-affected, but only nominal quantities of pillow basalt occur in the unit. Some flows of the Swan Falls Reservoir basalt unit are SROT, and some are Fe-enhanced.

For about 21 km farther north and west along the river between the Swan Falls Dam and Walters Ferry areas, many additional flows exposed in the canyon walls were erupted from various sources. Two of the most widespread units are the **basalt of Murphy Rim** (QTmur), which principally occurs a few kilometers northeast of Murphy, and the **basalt of Guffey Railroad Bridge** (QTgrb), which occurs mainly within Guffey Table, a prominent hill across the Snake River from Celebration County Park and located 6 to 9 km north-northeast of Murphy (Figure 18). The sources for these units have not been determined, and both consist mainly of WAB deposited on Lake Idaho sediments. The Murphy Rim basalt is SROT, whereas the Guffey Railroad Bridge basalt is Al-enhanced and uncharacteristically low in MgO.

Late Pliocene-Early Pleistocene Units Erupted From Explosive Vents

The following Late Pliocene and early Pleistocene basalt units, erupted from explosive vents in the western SRP, are described in this section:

Tfl—basaltic tuff of the Feedlot
Tjvc—Jackass Butte volcanic field
QTrt—tuff of Red Trails
QTsfd—tuff of Swan Falls Dam
QTmvc—Montini volcanic complex
QTcfv—Conservancy Flats volcanic complex
QTwbv—Wees Bar volcanic complex
QTgv—Graveyard Rapids volcanic complex
QTjl—Jinx Lateral volcanic complex
QTwa—Walters Butte volcanic complex

Many small-sized phreatomagmatic basaltic eruptions apparently happened during the late Pliocene or early Pleistocene. Vents for these eruptions occur near the present course of the Snake River between the area north of Grand View and Walters Ferry. Most of these eruptions formed maars and tuff rings in subaerial but generally wet environments. A few formed tuff cones in emergent environments (Godchaux and Bonnichsen, this volume), and one apparent subaqueous vent complex has been identified. Accompanying the formation of these small volcanic complexes was the deposition of extensive beds of basaltic tuff and admixed sedimentary material; many of these tuff beds have been traced for several kilometers in the canyon walls where they are interstratified with the basalt flows.

The **basaltic tuff of the Feedlot** (Tfl), a layer several kilometers long that underlies the Brooks Ranch basalt,

was erupted from a series of maar and tuff ring complexes a few kilometers north of Grand View. Progressing from southeast to northwest along the bluffs north of the Snake River, the phreatomagmatic volcano sources for the Feedlot tuff may include the Hayland School, Simplot Feedlot, and the eastern and western Chattin Flat maar and tuff ring complexes (Figure 16, Table 5). Most of the basalt spatter associated with the Feedlot tuff is SROT, although some from the Chattin Flat vent area (Table 6, number 3) is Fe-enhanced basalt.

The **Jackass Butte volcanic field** (Tjvc) occurs farther northwest along the river, between the Jackass Butte and Big Foot Bar areas. This field contains five maar and tuff ring complexes that erupted the basaltic tuffs (Godchaux and Bonnichsen, this volume; McCurry and others, 1997). The unit lies above the Brooks Ranch basalt and contains accidental blocks of both the Brooks Ranch basalt and the Feedlot tuff, as well as abundant sedimentary material. From southeast to northwest, the vents are the Jackass Butte Southeast and Jackass Butte Northeast volcanic complexes on the southwest side of the Snake River, and the Rabbit Creek Canyon, Big Foot Bar East, and Birthday Gulch volcanic complexes on the northwest side of the river (Figure 16, Table 5). Analyzed basaltic spatter samples from the Jackass Butte volcanic field have SROT basalt compositions; a representative analysis from the Rabbit Creek Canyon volcanic complex is given in Table 5 (number 4).

Farther to the northwest along the Snake River are two additional basaltic tuff units, the **tuff of Red Trails** (QTrt) (Jenks and Bonnichsen, 1989) and the **tuff of Swan Falls Dam** (QTsfd), both of which are interstratified with the basalt flows of this late Pliocene-early Pleistocene group and hence about the same age as, or perhaps slightly younger than, the Feedlot and Jackass Butte tuffs. The Red Trails tuff mainly lies between the Big Foot Bar area on the east and the Sinker Creek area on the west, whereas the Swan Falls Dam tuff lies farther northwest, appearing mainly from Sinker Creek to about 3 km northwest of the Swan Falls Dam area. Both tuff units appear to have been accumulated from materials erupted from multiple sources, some of which would include the volcanic complexes identified below and other sources that may be covered by later basalt flows.

Explosively erupted phreatomagmatic maar and tuff ring complexes are by the river near the mouth of Sinker Creek, about 6 km south of Swan Falls Dam and 14-15 km east-southeast of Murphy. These include the **Montini volcanic complex** (QTmvc) and **Conservancy Flats volcanic complex** (QTcfv). Of the two, the Montini volcanic complex is larger and especially well exposed, with its maar form almost perfectly preserved (Godchaux and Bonnichsen, this volume; Jenks and Bonnichsen, 1989). Snake River Canyon was incised through the middle of the Montini volcanic complex to expose the ring dikes that rose along its margins, the cutoff beds discontinuously exposed in its inner walls, and the tuff beds that lie beneath it, as well as the complete sequence of basaltic tuff and spatter layers that form the construct. The Montini complex started as a maar and still retains the form of an open excavation about a kilometer across. At the end of the Montini eruption, basalt flows or a lava pond covered the bottom of the maar. The composition of the basalt in this volcanic complex is SROT basalt, and the age of the eruption may be between 1.67 and 1.81 Ma (Amini and others, 1984).

Additional late Pliocene-early Pleistocene explosive volcanic centers near the Snake River between the Swan Falls Dam and Walters Butte areas include the Wees Bar, Graveyard Rapids, Jinx Lateral, and Walters Butte volcanic complexes. The **Wees Bar volcanic complex** (QTwbv) is a maar and tuff ring that erupted spatter of SROT basalt composition. The **Graveyard Rapids volcanic complex** (QTgv) evidently was a subaqueous vent that generated a great thickness of yellowish brown basaltic tuff exposed on the south side of Snake River Canyon. The **Jinx Lateral volcanic complex** (QTjl) is about 4 km southeast of Melba (Figure 18) and was erupted from the Stoddard tuff ring. This complex includes the fairly extensive surrounding beds of basaltic tuff.

The **Walters Butte volcanic complex** (QTwa) is 3-4 km south-southwest of Melba and north of the Snake River in the middle of the Melba Alcove. The Walters Butte volcanic complex (Godchaux and others, 1992) is a dissected tuff cone sitting on Lake Idaho sediments capped by a thin gravel layer. The phreatomagmatic deposits are accompanied by a small cinder deposit at the summit and at the north end, and by probable dike-generated, subaqueous basaltic hyaloclastic tuffs to the south. Part of the Walters Butte basalts are SROT, and part are Fe-enhanced basalt. White and others (this volume) indicate that this complex is earliest Pleistocene in age at 1.79 Ma.

PLEISTOCENE IRON-RICH BASALT UNITS IN THE WESTERN SNAKE RIVER PLAIN

Pleistocene Iron-Rich Units Erupted From Nonexplosive Vents

The following Pleistocene iron-rich basalt units, erupted from nonexplosive sources in the western SRP, are described in this section:

Qtr—basalt of Trio Hill

Qcoy—basalt of Coyote Butte
Qswa—basalt of Swan Falls Road
Qtp—basalt of Tombstone Patch Rapids
Qhm—basalt of Hat and McElroy Buttes
Qss—basalt of South Side Boulevard

Several nonexplosive shields and only mildly explosive cinder and spatter vents from which ferrobasalt lavas erupted occur near the Snake River between Swan Falls Dam and the Walters Ferry area and also a few kilometers north of the river on the basaltic plateau. Progressing generally from east to west, these vents are Trio Hill 16 km southeast of Melba, Coyote Butte 14 km southeast of Melba, Hill 2930 11 km southeast of Melba, Hill 2890 from which the basalt of Tombstone Patch Rapids was erupted located 11 km south-southeast of Melba, McElroy Butte 3 km northwest of Melba, Hill 2725 3 km north-northwest of Melba, and Hat Butte 6 km northwest of Melba.

The **basalt of Trio Hill** (Qtr) was erupted from Trio Hill, a small cinder and spatter construct that emitted ferrobasalt which flowed westward about 7 km (Figure 16). The **basalt of Coyote Butte** (Qcoy) was erupted from another small cinder and spatter cone, Coyote Butte. It is ferrobasalt, but the flow's extent has not been determined because it is covered by younger basalts. The Coyote Butte ferrobasalt contains anomalously high quantities of alkali elements, similar to some of the ferrobasalts from the Birds of Prey basalt field just to the east (see analysis by White and others, this volume).

The **basalt of Swan Falls Road** (Qswa) was erupted from a small shield, Hill 2930 (Swan Falls Road Hill) that is surrounded and partly covered by younger basalts, so the full extent of the flows has not been determined (Figure 16). The basalt of Swan Falls Road is extremely rich in phosphorus and impoverished in silica relative to other ferrobasalts. Like the Coyote Butte basalt, it is relatively enriched in alkali elements (White and others, this volume). White and others report an age of 0.9 Ma for the Swan Falls Road basalt.

The **basalt of Tombstone Patch Rapids** (Qtp) was erupted from a small vent (Hill 2890) that is best described as a cinder and spatter construct and is on the south side of Snake River Canyon (Figure 16 and Table 5). The lava from this vent flowed northward for 5 km or more to beyond where it is covered by younger basalt flows erupted from Initial Point. The Snake River Canyon cuts this flow, clearly establishing that this segment of the canyon is younger (Figure 18). The composition of several samples of this unit are ferrobasalt.

In the Melba-Walters Ferry area are two shield volcanoes, Hat Butte and McElroy Butte from which were erupted ferrobasalts referred to as the **basalt of Hat and McElroy Buttes** (Qhm). Also in the area is a small cinder and spatter cone that is the source of the basalt of South Side Boulevard, which has an extremely evolved composition. Hat Butte is about 6 km northwest of Melba. McElroy Butte is about 3 km northwest of Melba, and Hill 2725 is about 3 km north-northwest of Melba near the east end of McElroy Butte (Figure 16). The basalt of Hat and McElroy Buttes is exposed for about 25 km from southeast to northwest along the rim of Snake River Canyon. It is present as a band about 3 km wide on the southwest side of the plateau northwest of Hat Butte, and also extends northward 7-8 km from Hat Butte. Most of this unit was erupted from Hat Butte, especially the flows that extend north and northwest. For the eastern part of the flow field, however, it is unclear which flows came from Hat Butte and which came from McElroy Butte. In the area along the north part of the broad Melba Alcove of the Snake River Canyon near Melba, the flows from these two volcanoes evidently filled earlier channels excavated in Glenns Ferry Formation sediments. Where it fills the paleochannel, the basalt unit consists of several flows. Along the Snake River Canyon rim extending northwestward from the Hat Butte area, as well as in the Melba Alcove, the basal part of the unit is commonly pillowed; evidently it ran into water at those locations, perhaps in ancestral Snake River channels. At the northwesternmost extent of the unit, in the Pickles Butte area 10 km southeast of Marsing, the basalt flow has been domed upward and perhaps faulted. The age of the Hat Butte-McElroy ferrobasalt has been reported as 0.92 Ma by White and others (this volume). An analysis of the flow is presented in their paper.

The **basalt of South Side Boulevard** (Qss), which mainly occurs as spatter in the small Hill 2725 cone, is much more evolved in composition than any other ferrobasalts, being characterized by less than 3 percent MgO while maintaining a silica content of less than 50 percent and with very high alkalis (Table 6, number 5).

Pleistocene Iron-Rich Units Erupted From Explosive Vents

The following Pleistocene basalt units, erupted from explosive vents in the western SRP, are described in the following section:

Qcas—Castle Butte volcanic complex
Qsib—Sinker Butte volcanic complex
Qbmv—Boise Meridian volcanic complex
Qpr—Priest Ranch volcanic complex
Qhr—Hulet Ranch volcanic complex
Qot—Oregon Trail volcanic field
Qgbv—Guffey Butte volcanic complex
Qwb—White Butte volcanic complex

Qsh—Sleepy Hollow cinder deposit
Qmav—Missouri Avenue volcanic complex
Qhvc—Hidden Valley volcanic complex
Qsky—Skyline Road volcanic complex
Qlbv—Liberty Butte volcanic complex
Qpb—Pickle Butte volcanic complex
Qliz—Lizard Butte volcanic complex

Many explosive vents erupted ferrobasalt or Fe-enhanced basalt during the Pleistocene near the present course of the Snake River between Castle Butte, 19 km northwest of Grand View on the southeast, and Lizard Butte, 2 km northeast of Marsing on the northwest. Most of these eruptions formed maar and tuff ring constructs, but some formed tuff cones and associated tuff beds and lava flows.

The **Castle Butte volcanic complex** (Qcas) consists of a tuff ring capped by an extensive spatter layer of Fe-enhanced basalt. This feature lies on the south margin of a possible initial maar that was filled by detritus during the Bonneville Flood so that now it is hidden. Also present on the west side of the hypothesized maar are thick fragmental deposits of material believed to have been erupted during maar excavation and deposition of the tuff ring. More details about Castle Butte are given in Godchaux and Bonnichsen (this volume), Jenks and Bonnichsen (1989), and McCurry and others (1997). A radiometric date is not available for the Castle Butte volcanic complex, so it may be either late Pliocene or early Pleistocene. A representative chemical analysis is given in Table 6 (number 6).

The greatest concentration of Pleistocene vents that erupted ferrobasalt, accompanied by subordinate amounts of Fe-enhanced basalt, occurs near the Snake River between Swan Falls Dam and Walters Ferry. The principal units, generally from southeast to northwest, are the following: Sinker Butte volcanic complex; the Boise Meridian volcanic complex; the Priest Ranch volcanic complex; the Hulet Ranch volcanic complex; the Oregon Trail volcanic field; the Sign Island, Celebration, and Guffey Butte maars and tuff rings that make up the Guffey Butte volcanic complex; and the White Butte volcanic complex.

The **Sinker Butte volcanic complex** (Qsib) consists of Sinker Butte located 13 km east of Murphy and about 2 km southwest of Swan Falls Dam, extensive bedded tuff deposits and several dikes exposed in the walls of Snake River Canyon, and basalt flows that extend both south and north of the volcano for about 15 km (Figure 16). The basalt that flowed south has been traced into an extensive and thick pillow delta complex in the walls of Sinker Creek Canyon. Sinker Butte itself is a large tuff cone capped by a lava pond or layer of basaltic spatter about 1 km in diameter. It is a conspicuous landmark in the western SRP region and has been described by Godchaux and Bonnichsen (this volume), Godchaux and others (1992), and McCurry and others (1997). The basalt of the Sinker Butte volcanic complex is Fe-enhanced basalt to ferrobasalt in composition and may be between 1.26 and 0.61 Ma in age from the K-Ar dates of Amini and others (1984).

The **Boise Meridian volcanic complex** (Qbmv) is on the west side of the Snake River about a kilometer northwest of Swan Falls Dam. It consists of a small maar excavated in the basalt of the Swan Falls Reservoir and an accompanying tuff and spatter ring; no lava flows are in evidence, although some could lie to the west under younger deposits. Its tuffs overlie those erupted from Sinker Butte, but the Sinker Butte basalt flow ran into the Boise Meridian crater. Basaltic spatter of this volcanic complex is ferrobasalt.

The **Priest Ranch volcanic complex** (Qpr) also is on the west side of the Snake River and is about 4 km northwest of Swan Falls Dam. In the canyon wall, the complex is seen to consist of massive tuff deposits enclosing a megablock deposit of material filling the maar excavation. Tuff and spatter deposits formed a ring around the maar and now are buried by later units. Lava flows associated with this maar have not been identified. The initial width of the Priest Ranch maar was about 2 km, and the composition of several samples is ferrobasalt and Fe-enhanced basalt similar to the basalts in the Sinker Butte and Boise-Meridian volcanic complexes.

The **Hulet Ranch volcanic complex** (Qhr), located on the tableland south of Snake River Canyon 5 to 7 km northwest of Swan Falls Dam, consists of two elongate to arcuate tuff ring segments on the northeast and southwest sides of a basin that is 2 km across. Presumably, these tuff-ring segments were formed during the excavation of a large maar, which now is filled by basalt that erupted from Sinker Butte and flowed in from the south.

The **Oregon Trail volcanic field** (Qot) occupies much of the tableland south of the Snake River Canyon and west of the Swan Falls Dam-Sinker Butte area (Figure 16, Table 5). It is about 3 to 10 kilometers east and northeast of Murphy. Sixteen separate eruptive points identified in this field supplied the basaltic tuff and spatter accumulations that constitute the unit. The eruptive vents include both maar and tuff ring constructs, which formed where basalt rose into fairly wet surface sediments, and small cinder and spatter constructs, which formed where the feeding dikes erupted into less wet surface environments. Maar and tuff ring vents include Hill 3028, Hill 3137, Hill 3217, Hill 3256, Con Shea volcanic complex, Stricker Basin Gulch volcanic complex, and Tumbleweed Ridges volcanic complex. Tuff, cinder, and spatter cone vents include Hills 3045, 3048, 3054, 3086, 3114, 3125,

3147, 3173, and 3205. Some, such as the Tumbleweed Ridges volcanic complex, are a composite resulting from several adjacent explosive eruptions. The composition of basaltic spatter ranges from ferrobasalt similar to that of the Sinker Butte volcanic complex to slightly less-evolved Fe-enhanced basalts. Nearly all of the basalt associated with this unit is spatter and cinders; lava flows larger than ones on the flanks of the eruptive constructs have not been found. Stratigraphically, the unit is partly to entirely earlier than the Sinker Butte volcanic field to the east, inasmuch as Sinker Butte basalt flows surround some of the eastern vents of the Oregon Trail volcanic field and lie on some of the bedded tuffs from the Oregon Trail field.

In the area a few kilometers southeast of Walters Ferry, the Sign Island maar, the Celebration maar, and the Guffey Butte maar and tuff ring complex contributed to the formation of the **Guffey Butte volcanic complex** (Qgbv), which consists mainly of basaltic tuffs that underlie much of Guffey Butte and Guffey Table (Figure 18). The Sign Island maar, 10 km south of Melba and exposed on the northeast side of Guffey Table, was filled with fragmental material during its eruption and later was cut through by the Snake River. It has a width of about a kilometer. The Celebration maar is beneath the central part of the lava flow that caps Guffey Table; bedded tuffs from it protrude from the east and west sides of the hill. Guffey Butte, which lies a kilometer west of Guffey Table, consists of visually spectacular bedded tuff deposits erupted as the maar formed and of extensive basaltic spatter rim deposited on top of the bedded tuff deposits. Guffey Butte has been described in considerable detail by Godchaux and Bonnichsen (this volume), Godchaux and others (1992), McCurry and others (1997), Morrow (1996), Watson (1999), and White and others (this volume). Basalt lava flows have not been found in association with the Sign Island and Celebration maars or the Guffey Butte maar and tuff ring complex. Basaltic spatter from these sources show mainly a mixture of ferrobasalt and Fe-enhanced basalt with a minor amount of SROT basalt. The basaltic tuff of Guffey Butte lies above the Guffey Railroad Bridge basalt flow and beneath the basalt of Guffey Table.

The **White Butte volcanic complex** (Qwb) is north of the Snake River, nearly 4 km east-southeast of Walters Ferry, and about 6 km south-southwest of Melba. The complex consists almost exclusively of a runty little vent, a remnant of a previously somewhat larger tuff cone. The butte measures only 0.4 km (E-W) by 0.3 km (N-S), but the exposures are quite illuminating as they show what the interior of a tuff cone is like. This volcano has been discussed in more detail by Godchaux and others (1992) and by McCurry and others (1997). White Butte was in the path of the Bonneville Flood and consequently had most of its outer walls stripped away. These materials were deposited in a northwest-trending bar of material about 2 km long on the downstream side of the butte. This stripping of material exposed the core of the vent, which consists of a complex of dikes cutting one another, and the adjacent tuffs. The composition of the basalt is ferrobasalt. No age is available for the volcano, and not enough stratigraphic control exists to establish whether it is late Pliocene or Pleistocene, so a Pleistocene age has been assumed on the basis of the basalt composition.

North and northwest of the Walters Ferry area, extending as far as the Marsing area, are several explosive vent complexes from which ferrobasalt or Fe-enhanced basalt was erupted during the Pleistocene epoch. Some of these are best described as maar and tuff ring constructs, and the others are better described as cinder and spatter cones, although nearly all consist of a mixture of both phreatomagmatic tuffs that usually formed first and cinders and spatter that generally were deposited later. Basaltic lavas that flowed away from these vents have not been found. Most of the vents are on the tableland north of the Snake River, though a few are in the bottomland closer to the river. These vent complexes include the Sleepy Hollow cinder deposit, the Missouri Avenue maar and tuff ring construct, the Hidden Valley maar and tuff ring complex, the Skyline Road cinder and spatter complex, the Liberty Butte maar and tuff ring or perhaps tuff cone complex, and the Pickle Butte and Lizard Butte cinder and spatter constructs.

The **Sleepy Hollow cinder deposit** (Qsh) about 7 km north-northwest of Melba is an enigmatic accumulation of shallowly northward-dipping, generally red cinders exposed in a quarry 400-500 m long and perhaps 30 m deep. No topographic construct extends above the general level of the tableland, so evidently these cinders fill some sort of excavation that formed during the eruption of the cinders. At the base of the deposit are locally exposed bedded phreatomagmatic layers, but the quarry is not deep enough to expose the base of the volcanic sequence. These cinders were deposited in a crater excavated in fine-grained Lake Idaho sediments and coarse-grained Ten Mile Gravel, although none of the margins of the deposit is exposed. Throughout the deposit there are baked white silt clasts from the Glenns Ferry Formation and cobbles derived from the Ten Mile gravel, but no clasts of preexisting basalt flows, or dikes, or layers of spatter. Analysis of a cinder sample indicates an Fe-enhanced basalt composition.

The **Missouri Avenue volcanic complex** (Qmav) consists of a maar and tuff ring and associated tuffs about 17 km northwest of Melba. The volcanic complex consists of scattered occurrences of phreatomagmatic tuff

beds, cinder layers, and spatter accumulations in quarries and roadcuts and at hill tops. The materials were probably erupted from a now-filled maar excavated into Glenns Ferry Formation lake sediments and the Ten Mile gravel. The hypothesized maar is about 2 km long from SE to NW and 1 km or more wide. What probably are outer-flank spatter deposits erupted from the maar cap high points to the south of the covered excavation. The composition of basaltic spatter from this construct is ferrobasalt.

The **Hidden Valley volcanic complex** (Qhvc) consists mainly of a large maar and cinder ring complex just to the southwest of the Missouri Avenue complex and 14-17 km northwest of Melba. It is another hypothesized maar that has been filled by later materials. This probable maar is more than 3 km long from southeast to northwest and nearly 2 km wide. The main mass of erupted material forms an arcuate rampart that probably represents outer-wall deposits of spatter or strongly welded, or sintered, cinders that wraps around the north and west sides of the enclosed maar basin. Locally, fragmental phreatomagmatic deposits are exposed beneath the capping spatter layer, but we do not know how thick or continuous these may be. Like the Missouri Avenue maar, the Hidden Valley maar is thought to have been excavated in Glenns Ferry Formation lake sediments and the overlying Ten Mile Gravel. The composition of the spatter is Fe-enhanced basalt.

The **Skyline Road volcanic complex** (Qsky) consists of a cinder and spatter construct at the edge of the tableland on the north side of the Snake River and 3 km north of Givens Hot Springs. The vent area consists of two small hills, Hill 2712 to the southwest and Hill 2798 on the northeast, capped by spatter and separated by a valley about 250 m wide. Most likely this medial valley holds a hidden dike from which the cinders and spatter were erupted.

The **Liberty Butte volcanic complex** (Qlbv) consists mainly of a small crater filled and overtopped by tuff and cinders about 7 km southeast of Marsing. The construct consists of a block-filled crater, which probably started as a maar, and has outer flanks capped by ferrobasalt spatter accompanied by some SROT basaltic spatter.

The **Pickle Butte volcanic complex** (Qpb) is tiny, only a little more than 100 m across, and located 1 km east of Marsing. Here, bedded phreatomagmatic tuffs and cinders are capped by Fe-enhanced basaltic spatter. The occurrence is basically an excavation at a road junction and should not be confused with Pickles Butte farther southeast, which is not considered a vent complex.

The **Lizard Butte volcanic complex** (Qliz) consists mainly of a cinder and spatter vent. Lizard Butte is about 2 km northeast of Marsing and is a well-known local landmark. This construct, which is about 300 m across, consists of phreatomagmatic tuff overlain by a layer as much as 10 m thick of basaltic cored bombs. The bomb layer, in turn, is capped by a tilted layer of Fe-enhanced basaltic spatter. The layer, which surely is tilted because of initial dip, might be either an inner-wall or outer-wall remnant, but the former is more likely. All three of these volcanic complexes, Liberty Butte, Pickle Butte, and Lizard Butte, were in the path of earlier stages of the Snake River as well as the Bonneville Flood, so some of the eruptive products were likely removed by erosion. A chemical analysis of basaltic spatter from Lizard Butte is given in Table 6 (number 7).

PLEISTOCENE ALKALI-RICH BASALT UNITS IN THE WESTERN SNAKE RIVER PLAIN

Pleistocene Alkali-Rich Units in the Melba-Walters Ferry Area

The following Pleistocene alkali-rich basalt units in the Melba-Walters Ferry area in the western SRP are described in this section:

Qgt—basalt of Guffey Table
Qgdv—Grouch Drain volcanic complex
Qip—basalt of Initial Point
Qkb—Kuna Butte basalt field
Qpow—basalt of Powers Butte
Qhlm—middle basalt of Halverson Lake
Qhlu—upper basalt of Halverson Lake

The two earliest alkali-rich basalt units are the basalt of Guffey Table and the Grouch Drain volcanic complex. They respectively have Ar-Ar dates of 0.76 Ma and 0.73 Ma (White and others, this volume). The **basalt of Guffey Table** (Qgt) is a basalt flow about 3 km long that traveled northward from a small vent at the south end of Guffey Table (Hill 3007) about 6 km north-northeast of Murphy (Figure 16). The interior of the flow is a very dense, nondiktytaxitic basalt, and the flow base is fragmental, suggesting at least part of the unit was an aa flow in contrast to the almost universal occurrence of pahoehoe lavas elsewhere in southwest Idaho. The Guffey Table basalt vent area consists of a small crater filled with bedded phreatomagmatic tuff. The basalt was deposited on the tuff of Guffey Butte, and the northern distal end of the flow at the north end of Guffey Table appears to have been eroded by the Snake River (Figure 18). The original extent of the unit is unknown, but it is not present on the north side of the river. An analysis of Guffey Table basalt indicates it is relatively enriched in Al and Mg and has some, but not marked, enrichment in alkali elements

(White and others, this volume).

The **Grouch Drain volcanic complex** (Qgdv) is 5 km west of Melba on the edge of the tableland north of the Snake River (Figure 16). It consists of an open maar, a bedded phreatomagmatic tuff ring surrounding the maar, localized cinder and spatter deposits on the north and east sides of the tuff-ring, and a small lava pond at the bottom of the maar from which lava flowed through a breach on the south side of the maar to travel downhill to the south for a kilometer or so. The complex covers an area that is about 3 km across, and the maar, which is a little more than a kilometer across, occurs in the middle. The phreatomagmatic deposits lie on top of the Hat Butte basalt, and exposures of the Hat Butte basalt appear in the walls of the maar as a cutoff bed. The Grouch Drain maar and its deposits are discussed further by Godchaux and Bonnichsen (this volume), McCurry and others (1997), and White and others (this volume). The basalt is relatively enriched in Al but only modestly in alkali elements (White and others, this volume). We concur with White and others that the basalts of Guffey Table and the Grouch Drain volcanic complex are part of the M3 group.

The **basalt of Initial Point** (Qip) forms a relatively large basalt field about 22 km from southwest to northeast and about 18 km from southeast to northwest mainly on the tableland north of the Snake River, south of Kuna and east of Melba (Figure 16). The Initial Point basalt flowed away in all directions from the Initial Point shield volcano located 11 km east of Melba in the southeastern part of the basalt field. The shield is about 2 km across, and its north side appears to have been breached or removed, so that in the northern part of the vent complex, this being Initial Point Hill itself, there is a thick, dense basalt layer. The dense basalt may have been a small lava pond that has had its original cinders and other friable materials eroded away. In the southwestern part of the Initial Point basalt field are two places where the Initial Point lava cascaded over the Melba Alcove rim and formed flows on the floor of the alcove (Figure 18). These frozen cascades are each about a kilometer wide and are located about 1.5 and 6 km southeast of Melba. The Initial Point basalt overlies the Kuna Butte basalt field and all other basalt units in the region and has a reported Ar-Ar age of 0.414 Ma (Othberg, 1994; Othberg and others, 1995). Several analyses indicate the basalt composition varies from ordinary abundances of Al to Al-enhanced, but with relatively low Fe contents and with high alkali element abundances. Typical analyses clearly show this unit belongs to the M3 basalt category (White and others, this volume).

The **Kuna Butte basalt field** (Qkb) occupies a large area north of the Initial Point basalt field southwest of Kuna and both south and north of Melba (Figure 16, Table 5). The basalt field is a composite of flows from several different sources and contains at least eleven different eruptive sources. It stretches 23 km from south to north and as much as 11 km east to west. Relatively thick deposits of soil, mainly loess, cover the Kuna Butte basalt field, so not much can be seen of how flows from the various sources within it might relate. The vents in this field form a crude band a few kilometers wide that stretches from 3 to 13 km southwest of Kuna and from 3 to 13 km northeast of Melba. Most of the vents are small cinder and spatter constructs; these are Hill 2883, Hill 2950, Hill 3148, Kuna-Mora Road Hill, Kuna Cave Hill, Kuna Cave Road Ridge, and Melba Hill Southeast. The others are relatively small shields (Hills 2812, Hill 2830, and Melba Hill) except Kuna Butte itself, which measures about 3 km by 4 km and has its peak about 6 km southwest of Kuna. Topographically, Kuna Butte looks superficially like a simple shield volcano; however, the volcanic construct was built on an existing hill of lacustrine and fluvial sediments of the Glenns Ferry Formation and Ten Mile Gravel that are exposed on the northeastern part of the butte, and which evidently were erosional remnants already in existence when the Kuna Butte basalt field formed. Many of the Kuna Butte basalt flows were erupted from near the top of this hill and drape over the preexisting sediment hill, nearly covering it. A series of west-northwest-trending faults and probable accompanying dikes at the top of Kuna Butte mark the location of one of the most active eruptive zones in the basalt field.

Kuna Butte lavas flowed several kilometers both to the south and to the north from the zone of vents. Some of the Kuna Butte basalt field lavas flowed over the rim of the Melba Alcove onto the floor of the alcove where they are partially covered by the Initial Point basalt. One of the flows that extended northward has an Ar-Ar age of 0.387 Ma (Othberg, 1994; Othberg and others, 1995). This date is younger than that of the Initial Point basalt even though the Initial Point lava clearly flowed over the top of lavas from the Kuna Butte basalt field along their mutual contact near Kuna Cave and in the Melba Alcove area. Rather than a dating error, which of course is possible, this discrepancy may reflect an interval of a few tens of thousands of years over which the Kuna Butte basalt field formed. The dated sample from the north may simply be somewhat younger than the southern part of the field that preceded the Initial Point basalt. Many analyses from the Kuna Butte basalt field indicate it characteristically is Al-enhanced and rich in alkali elements, more so than the other units of the alkali-rich M3 group. Three Kuna Butte basalt analyses are given by White and others (this volume).

The **basalt of Powers Butte** (Qpow) was erupted from the Powers Butte shield located 5-7 km north of Melba

and just east of Kuna Butte. Powers Butte is about 4 km across and erupted flows that traveled northward as much as 2 km from the vent. Faults similar in orientation to those at Kuna Butte cut the top of Powers Butte. The Powers Butte basalt has not been dated, but it presumably is very similar in age to the adjacent Kuna Butte basalt field. The composition of the Powers Butte basalt is similar to that of Kuna Butte, being alkali-rich and Al-enhanced.

The **middle and upper basalts of Halverson Lake** (Qhlm and Qhlu) are exposed on the north side of the Snake River across from the Guffey Table area and are separated from one another by a thin layer of basaltic tuff (Figure 16). The upper basalt occupies an area about 3 km across on the floor of the Melba Alcove; it is overlain by the Initial Point basalt on the northern margin and is cut by the Snake River Canyon on the southern margin (Figure 18). The middle basalt of Halverson Lake is known only from exposures along the cliffs on the north side of the Snake River Canyon. Although the source of both of these basalts has not been identified, one or both conceivably are early phases of the Initial Point basalt or correlative with some of the flows of the Kuna Butte field, or they simply may be from buried sources. The upper basalt is not as enriched in Al or alkalis as the Initial Point or Kuna Butte basalts, or as the middle basalt of Halverson Lake, which is fairly similar to the Initial Point and Kuna Butte basalts. The basalts of Powers Butte and of Halverson Lake are all part of White and others (this volume) M3 group.

The Birds of Prey Basalt Field and the Basalt of Little Joe Butte

The following Pleistocene basalt units in the Birds of Prey basalt field and Little Joe Butte area of the western SRP are described in this section:

Qbop—Birds of Prey basalt field

Qljb—basalt of Little Joe Butte

The **Birds of Prey basalt field** (Qbop) underlies much of southern Ada County. The lava flows of the Birds of Prey field were erupted from many vents; eighteen have been identified, and others in the form of hidden dikes are suspected. The vents are in the central part of the field, and the basalt flows radiate away as much as 10 to 15 km. Of the identified vents, twelve are small cinder and spatter cones, and six are best classified as small to medium-sized shields. Christmas Mountain, the largest of these shields, is about 2 km across. Most of the cinder and spatter cones are in a linear central ridge vent complex, which is a little more than a kilometer wide that stretches for 14 km east-southeast to west-northwest (Figure 19). In addition, a probable series of dikes, parallel to and beneath this zone, likely erupted some of the Birds of Prey lava flows. This observation is based on the occurrence of elongate spatter ramparts in the middle part of this central ridge vent complex. Most of the shields in the Birds of Prey field are peripheral to the central ridge vent complex and erupted lavas that flowed even further from the center of the field.

Ten small vents are in the central ridge vent complex (Qbpv) along with several others in flank areas were the sources of the flow units that built the Birds of Prey basalt field. Lava-flow units in the field are the basalts of Corder Creek (Qbpc), Higby Cave (Qbph), Old Powerline Road (Qbpop), the National Guard area (Qbpn), Orchard Railroad Siding (Qbpo), Sand Creek (Qbps), Christmas Mountain (Qbpx), and the lower (Qbppl) and upper (Qbppu) basalts of Promontory Point. The upper Promontory Point basalt is shown on Figure 16. An unnamed Birds of Prey unit (Qbp) identifies basalt that flowed north and south from the south-central part of the central ridge vent complex and northwest from the west end of the vent complex. Additional lava flows with compositions like the Birds of Prey flows occur in the walls of the Snake River Canyon north of Swan Falls Dam. These have not been named and, as yet. have not been correlated with units in the main part of the basalt field. They lie beneath the lower and upper basalts of Promontory Point.

A few older volcanoes have been partly to completely surrounded by Birds of Prey lava flows in the peripheral parts of the field. These include the Hill 3202 shield that is the source of the basalt of Orchard Ranch in the northeast, Hills 3152 and 3171 which are two cinder and spatter vents in the east, Big Foot Butte in the south, and Coyote Butte in the west. Also, the faulted and tilted basalt of Tadpole Lake is partly surrounded by Birds of Prey basalt flows in the southern part of the field. Some of the lavas that traveled west and southwest from the Birds of Prey field flowed into earlier canyons of the Snake River system and filled them, leading to the development of pillow basalts and a complex sequence of flows and tuffs with compositions similar to the flows and vents in the middle of the Birds of Prey field. These very thick pillow accumulations are exposed in the northeast wall of Snake River Canyon a few kilometers downstream from Swan Falls Dam. Very likely as this large basalt field developed, the lavas repeatedly dammed the Snake River system to form temporary lakes immediately upstream.

The region underlain by the Birds of Prey basalt field is covered in most places by a blanket of loess, and basically the area has yet to be dissected to any significant amount by streams. Therefore, reliable stratigraphic information among the individual flows and vents in the

field is sparse; we mapped the individual flows mainly by carefully examining topographic-map contours and using geochemical information to check possible correlations. Furthermore, the area coincides in large part with the Idaho National Guard's training range, where tank maneuvers and artillery target practice with large artillery pieces are common, especially during times when geologists conduct field work. So, between the extensive dust wallows that have been generated over the years by tanks and the wide distribution of live but unexploded ammunition (so-called duds!), it is impractical, let alone potentially very unhealthful, to fully work out the details amongst the units and vents in this interesting basalt field. The field also coincides with much of the Snake River Birds of Prey natural preserve; perhaps the region is best left to the ground squirrels, rabbits, and other critters to survive, for the benefit of the actual birds of prey who visit there.

Many chemical analyses from various vents and units in the Birds of Prey basalt field show a wide range of basalt compositions. Three representative analyses are given in Table 6 (numbers 8-10). Number 8 (sample X-220) is SROT from the Hill 3365 vent in the central ridge vent complex; number 9 (sample X-362) is ferrobasalt from the Christmas Mountain flow at Christmas Mountain, and number 10 (sample X-215) is alkali-rich Al-enhanced basalt from the Hill 3456 vent in the central ridge vent complex. These samples are quite enriched in K_2O, and generally enriched in alkalis, compared to other SRP basalt samples.

The **basalt of Little Joe Butte** (Qljb) was erupted from the Little Joe Butte shield volcano on the tableland north of the Snake River and nearly 21 km north-northeast of Grand View. The basalt lavas from this source constructed a flow field approximately 26 km from north to south and 14 km from east to west located just southeast of the Birds of Prey basalt field. The shield is in the northern part of the flow field, indicating that the lavas generally flowed southward. Some of these lavas traveled far enough to enter the valley of the ancestral Snake River and followed it downstream for 8 km or so, but these basalt flows have since been partially eroded away by the river. The basalt of Little Joe Butte is the same unit as the basalts of Dixie Ranch and Strike Dam Road (Jenks and others, 1993, 1998; Shervais and others, this volume). Analyzed samples of the Little Joe Butte basalt are SROT basalt with relatively high Al and alkali contents. The chemistry is quite similar to the other Pleistocene basalt units that erupted from the central zone of the western SRP, including some of the flows in the Birds of Prey field and sources farther west in the Walters Ferry-Melba area, so this unit is also considered to be part of the alkali-rich M3 group of White and others (this volume).

VARIATIONS IN BASALT CHEMICAL COMPOSITION

In this section we explore the variations in chemical composition of the SRP basalt in southwest Idaho, first to determine how much internal variation occurs within representative basalt units that were erupted from individual volcanoes, then to examine the unit-to-unit compositional variations, and finally to compare the variations among the basalt volcanoes and units in the three major regions we have discussed (Figures 20 and 21). To portray the amount of variation in flows from individual volcanoes, we have constructed Figure 20, which shows the ranges of MgO and Al_2O_3 for a number of volcanoes. The number of analyses available for the chosen volcanoes ranges from five to twenty-one, and the number of analyses for each is noted in the caption to Figure 20.

Four basalt units were selected from the Bruneau-Jarbidge region, the basalts of Black Rock (Tbr), Big Bend (Tbib), Austin Butte (Tab), and Winter Camp Butte (Twc). Their plots indicate only limited compositional overlap from volcano to volcano and a general decline in MgO and Al_2O_3 from the most primitive (Tbr), which mainly consists of Al-enhanced basalt, to the most evolved (Twc), which mainly consists of Fe-enhanced basalt. The collective compositional range shown by these four units fairly well represents the compositional range for the entire Bruneau-Jarbidge region, except for the younger and very iron-rich units in the northern part of that area, north of the Bruneau-Jarbidge eruptive center margin (Figure 5). The Miocene and early Pliocene basalts of the eastern part of the Owyhee-Humboldt region and of the southwestern part of the Twin Falls region have compositions quite similar to the four Bruneau-Jarbidge units shown. Thus, we believe that these four indicate the amount of compositional variation in the late Miocene and early Pliocene group of southwestern Idaho basalt units that erupted along the main Yellowstone hotspot track soon after the rhyolite eruptions.

Five basalt units were chosen from the Twin Falls region: the basalts of Sucker Flat (Tsuk), Rock Creek (Trck), and Stricker Butte (QTst) from the Magic Valley ferrobasalt field; and the Notch Butte basalt (Qnot) and McKinney basalt (Qmck) from the Northside basalt field. The Magic Valley ferrobasalt units are plotted separately from the Northside basalt units so that the extent of the individual fields are easier to see, since there is considerable compositional overlap from unit to unit. For the

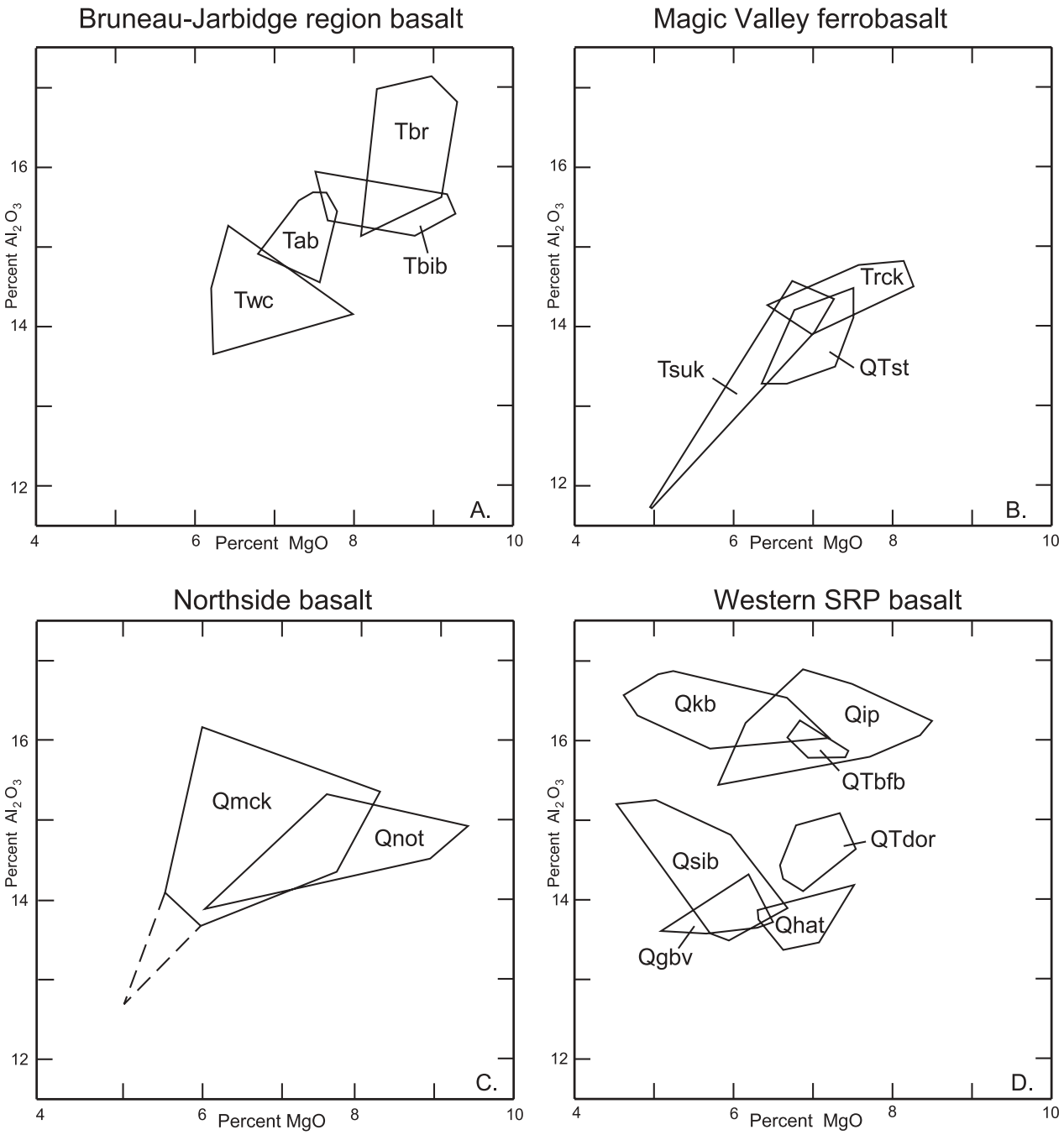

Figure 20. The compositional fields plotted for MgO versus Al_2O_3 of selected volcanoes from the (A) Bruneau-Jarbidge region, (B) Magic Valley ferrobasalt in the Twin Falls region, (C) Northside basalt in the Twin Falls region, and (D) the western SRP region. For the Bruneau-Jarbidge region, the volcanoes and corresponding basalt units are identified as follows: Tbr—Black Rock basalt (9), Tbib—Big Bend basalt (8), Tab—Austin Butte basalt (9), and Twc—Winter Camp Butte basalt (8). For the Magic Valley ferrobasalt in the Twin Falls region, the volcanoes and corresponding units are identified as follows: Tsuk—Sucker Flat basalt (18), Trck—Rock Creek basalt (11), and QTst—Stricker Butte basalt (13). For the Northside basalt in the Twin Falls region, the volcanoes and corresponding units are identified as follows: Qnot—Notch Butte basalt (5) and Qmck—McKinney basalt (21). For the western SRP, volcanoes and corresponding basalt units are identified as follows: QTbfb—Big Foot Butte basalt (9), QTdor—Dorsey Butte basalt (12), Qgbv—Guffey Butte volcanic complex (10), Qsib—Sinker Butte volcanic complex (7), Qhat—Hat Butte flows of the Qhm basalt unit (12), Qkb—Kuna Butte volcanic field (17), and Qip—Initial Point basalt (13). The numbers in parentheses identify how many chemical analyses were used to determine each volcano's compositional field.

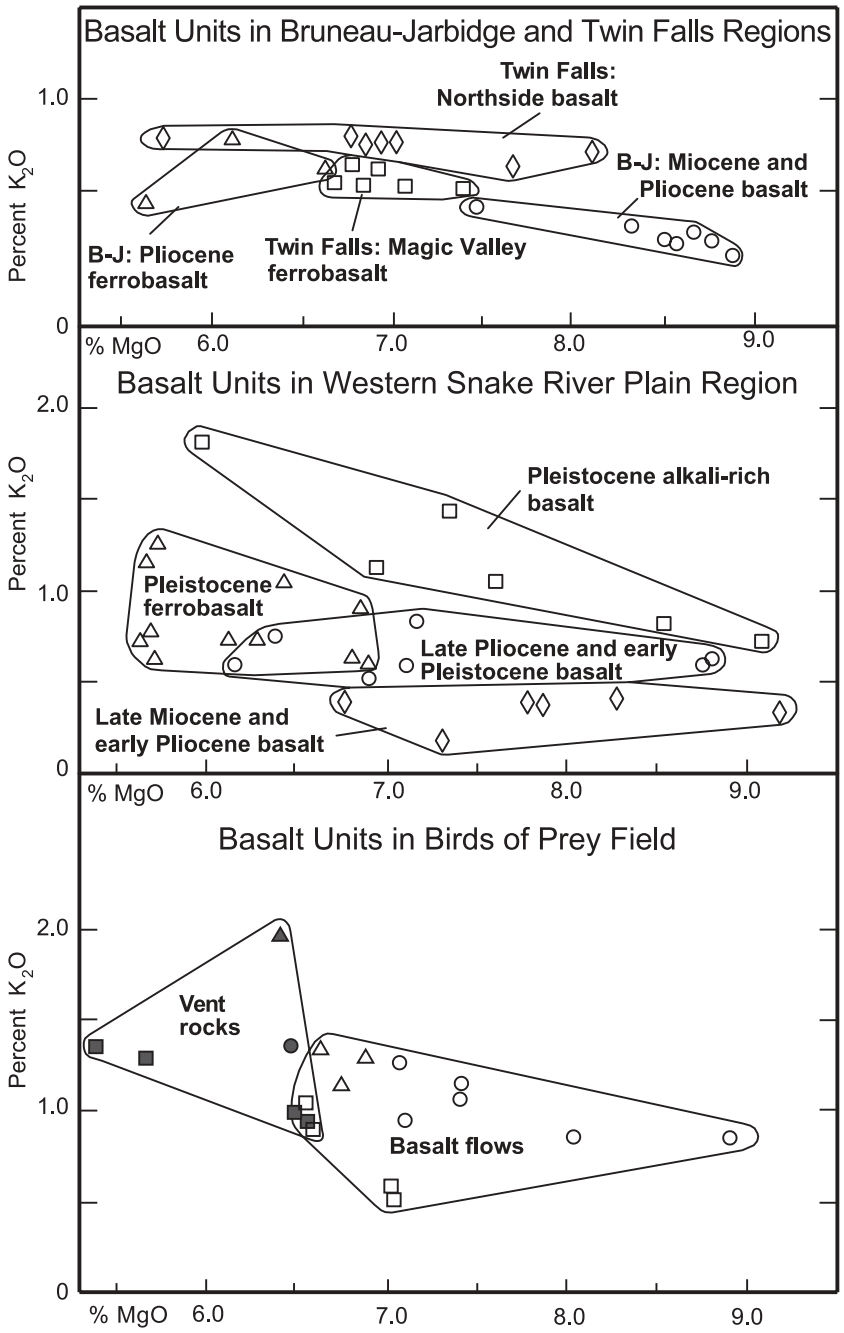

Figure 21. Graphs of MgO versus K_2O for various SRP regions in southwestern Idaho illustrating the compositional differences between the basalt-unit groups. The individual points on the graphs represent the average MgO and K_2O values of several analyses for each of the units.

Upper plot: Basalt units in the Bruneau-Jarbidge and Twin Falls regions. Circles—Miocene and Pliocene basalt units of the Bruneau-Jarbidge region. Triangles—Pliocene ferrobasalt units of the Bruneau-Jarbidge region. Squares—Pliocene and Pleistocene basalt units in the Magic Valley ferrobasalt of the Twin Falls region. Diamonds—Pleistocene basalt units from the Northside part of the Twin Falls region.

Middle plot: Basalt units in the western SRP region. Diamonds—Miocene and early Pliocene basalt units (M1 group). Circles—late Pliocene and early Pleistocene basalt units (M2 group). Triangles—Pleistocene ferrobasalt units (M2 group). Squares—Pleistocene alkali-rich basalt units (M3 group).

Lower plot: Basalt units in the Birds of Prey basalt field, western SRP. Circles—SROT basalt units. Squares—Ferrobasalt units. Triangles—alkali-rich basalt units. Open symbols are samples from lava flows. Filled symbols are samples from the central ridge vent complex.

Magic Valley ferrobasalt units, they collectively form a narrow compositional field extending to lower and lower MgO and Al_2O_3 contents from the relatively more primitive Trck unit to the most evolved part of the Tsuk unit. The two Northside basalt units are similar in composition to the Magic Valley ferrobasalt units, but show much larger compositional fields for the individual units and a much wider spread of compositions overall. Even in the case of the Qnot unit, for which only five analyzes are available, there is a very wide range. For the Qmck unit, the dashed extension to lower MgO and Al_2O_3 contents represent strongly differentiated late-stage interstitial material (Leeman and Vitaliano, 1976). The narrow range of compositions for the Magic Valley ferrobasalt units is consistent with their derivation from one or a succession of magma chambers undergoing very similar fractionation processes from basalt that initially was fairly uniform. The wide range of Northside basalt compositions is consistent with fractionation processes that were quite variable, perhaps representing much more complex magma chambers, and likely formed from magmas with fairly wide ranges of initial compositions.

Seven basalt units were chosen from the western SRP region: the basalts of Big Foot Butte (QTbfb), Dorsey Butte (QTdor), Sinker Butte (Qsib), Guffey Butte (Qgbv), and Hat Butte (Qhat) representing the late Pliocene and Pleistocene, SROT and iron-rich basalt units (the M2 group of White and others, this volume); and the Kuna Butte basalt field (Qkb) and the Initial Point basalt (Qip), representing the Pleistocene alkali-rich basalt units (the M3 group of White and others, this volume). The fields for individual units in the western SRP are relatively small compared to the overall range of compositions there. The late Pliocene and Pleistocene, SROT and iron-rich basalt units are generally lower in Al_2O_3 than are the Pleistocene alkali-rich units, although there clearly is overlap of the two groups inasmuch as the QTbfb unit plots within the same range as the Qip and Qkb units. Still, the overall differences between the SROT-ferrobasalt and alkali-rich groups support the idea that they are from different sources, as also is proposed by White and others (this volume). In addition, the iron-rich units of the western SRP (Qsib, Qhat, and Qgbv), although similar to the iron-rich units in the Twin Falls region, have a tendency toward higher Al_2O_3 contents for a given MgO concentration. Conversely, the Pleistocene alkali-rich units (Qkb and Qip) clearly have lower MgO concentrations than the least-evolved units in the Bruneau-Jarbidge region (Tbr and Tbib) even though the Al_2O_3 contents are comparable. The overall wide range of compositions in the western SRP basalt units infers that diverse fractionation processes occurred and that significant initial compositional differences were present, aside from the results of fractionation processes.

To compare the basalts from region to region and between the major basalt groups within the regions, the Mgo versus K_2O plots of Figure 21 have been prepared. In these plots, the individual points represent the average analyses of separate units rather than individual rock analyses. The upper panel compares the main basalt groups in the Bruneau-Jarbidge and Twin Falls regions with one another. In the middle panel, the main basalt groups in the western SRP are compared with one another, and in the lower panel the units and vents in the Bird of Prey basalt field in the western SRP are compared.

In the upper panel of Figure 21, where the basalt groups in the Bruneau-Jarbidge and Twin Falls regions are compared, the following observations can be made. The lowest K_2O values are in the Miocene and Pliocene units in the Bruneau-Jarbidge region, and these Al-enhanced and SROT basalts generally have higher MgO contents than the other groups. The Magic Valley ferrobasalts and the Pliocene ferrobasalts at the north end of the Bruneau-Jarbidge region are intermediate in K_2O content between the Bruneau-Jarbidge Miocene and Pliocene units and the Pleistocene Northside basalt field in the Twin Falls region. Also, the Pliocene Bruneau-Jarbidge and the Magic Valley ferrobasalts together form a continuous trend, with the Bruneau-Jarbidge ferrobasalts being somewhat lower in MgO than the Magic Valley units. The Northside basalt field shows wide variation in the percentage of MgO but consistently higher K_2O contents than are in the earlier ferrobasalts and even higher than in the earlier Miocene and Pliocene basalt units of the Bruneau-Jarbidge region. Thus, for the basalt units in the Bruneau-Jarbidge and Twin Falls regions, there seems to be an increase of alkalis, as seen by K_2O, from south to north and from older to younger.

In the middle panel of Figure 21, where the basalt units in the western SRP are compared, the following observations can be made. In this plot, the late Miocene and early Pliocene basalt units correspond to White and others' (this volume) M1, low-potassium group; the late Pliocene and early Pleistocene SROT basalts along with the Pleistocene ferrobasalts form a continuous trend across the diagram and correspond to White and others' M2 group, and the Pleistocene alkali-rich units correspond to White and others' M3 group. All of these groups have wide-ranging MgO contents, except the Pleistocene ferrobasalts, but as noted these simply seem to be a continuation of the late Pliocene and early Pleistocene SROT basalt group. The K_2O contents increase from the late Miocene and early Pliocene (M1) group to the late Pliocene and Pleistocene SROT and ferrobasalt (M2) groups, and go on to even higher K_2O concentrations in

the Pleistocene alkali-rich (M3) group. For the Pliocene and Pleistocene SROT and ferrobasalt (M2) group, there is a slight increase in K_2O with a decrease in MgO. For the Pleistocene alkali-rich (M3) group, there is a marked increase in K_2O with a decrease in MgO. Among the groups, there is an increase in K_2O with younger and younger ages but not much variation in the MgO content, except that the ferrobasalt units, all of which are about a million years old, are distinctly lower in MgO than many of the units in the other groups.

When the units in the Bruneau-Jarbidge and Twin Falls regions (upper panel) are compared with the basalt units in the western SRP (middle panel), the following observations can be made from the plots in Figure 21. The Miocene and Pliocene Al-enhanced and SROT basalt groups in the Bruneau-Jarbidge and Twin Falls regions and in the western SRP are very similar in composition, with low K_2O values (below 0.5 percent). All three regions contain ferrobasalts, but some in the western SRP extend to higher K_2O contents than do those in the Bruneau-Jarbidge and Twin Falls regions. However, the lower limit of K_2O concentrations for the ferrobasalts in all regions is similar. Also, the ferrobasalts in the western SRP are somewhat younger than those in the Bruneau-Jarbidge and Twin Falls regions. In all regions, the youngest basalts are the most enriched in K_2O, but those in the western SRP have considerably higher K_2O contents at a given MgO concentration than does the youngest group of basalts in the Twin Falls region, the Northside basalt field.

For the units in the Birds of Prey basalt field, the lower panel of Figure 21 reveals the following observations among the basalt units. There is a wide range of compositions from SROT basalt to ferrobasalt and alkali-rich basalt, although no low-potassium basalts have been found. The Birds of Prey compositions cover about the same range of MgO and K_2O contents as does the combined range, in the middle plot, for the late Pliocene and early Pleistocene basalts and for the Pleistocene ferrobasalts (White and others M2) group along with the Pleistocene alkali-rich group (White and others M3) group. However, in the Birds of Prey basalt field these compositions seem to be intermingled in time and space, whereas in the Walters Ferry-Melba area, farther west in the western SRP, these various compositions are separated in time. The lava flows and the vent rocks from the central ridge vent complex have different compositions, showing very little overlap. The central ridge vent complex basalts are more evolved, with lower MgO contents and ranging to higher K_2O values than the lava flows, many of which were erupted from the central ridge area as well as from shields scattered on the flank of the Birds of Prey basalt field. The central ridge basalts probably are younger than the flows that make up most of the field, as well. Thus, the compositional pattern in the Birds of Prey field suggests that a quite complex pattern of magma composition diversification was occurring during the evolution of the field, but that an overall trend to more evolved compositions took place over time.

CONCLUSIONS

General observations from our preceding descriptions of the SRP basalt units in southwestern Idaho are summarized as follows:

(1) The southwestern Idaho SRP basaltic volcanism follows a long series of volcanic events in the same region. Pre-SRP volcanism occurred during the Eocene, Oligocene, and middle Miocene, and an astounding amount of rhyolitic volcanism accompanied early SRP development just a few million years before the outpourings of basalt.

(2) The southwestern Idaho basaltic volcanism has a complex development pattern in time and space, and the latter part of the volcanism seems to be associated more with the rifting that occurred in the western SRP and across the hotspot track than with the generation of the hotspot track itself.

(3) The physical environment into which basalt erupted and was deposited varied markedly as a function of the amount of water that was available. This formed subaerial flows, WAB, and pillow deltas where flows ran into water, and subaqueous basalt accumulations, which commonly are fragmental. The types of eruptions varied from effusive to very explosive, depending on the availability of water. Much of the volcanism that had a large component of water-induced activity occurred in the western SRP rift, or where the rifting process had propagated itself across the main hotspot track.

(4) The basalt composition varies from high-Al and Al-enhanced (most primitive) to ferrobasalt (most evolved). Although the timing varies from locality to locality, the basalts become more evolved over time. Also, nearly all of the ferrobasalt is associated with the western SRP rift and the extension of the rifted zone across the hotspot track in the Twin Falls region.

(5) In the Bruneau-Jarbidge and Twin Falls regions, the basalts tend to be younger and more K_2O-enriched from south to north.

(6) In the western SRP rift, the latest basalts are mainly alkali-enriched and apparently are from a different source than the earlier SROT-ferrobasalt group. Although there is some late-stage alkali enrichment of the basalts in the other regions, the alkali-rich type of the western SRP has

not been found in those other regions over the hotspot track.

(7) In the Melba-Walters Ferry part of the western SRP, the SROT to ferrobasalt transition was gradational over time. The restriction in time of the ferrobasalts there to being about a million years old is consistent with the possible existence at depth in the crust of one or a group of large differentiated mafic plutons from which ferrobasalt lavas escaped and within which large quantities of olivine and plagioclase were segregated. The late-stage alkali-rich basalts in that area, however, would appear to have come from some other source and perhaps were generated at a deeper level in the mantle, or they were produced by fractionation processes under different temperature and pressure conditions than those that prevailed when the ferrobasalt magmas were formed.

(8) Finally, we have shown that throughout southwestern Idaho, the SRP basalts vary widely but systematically in their compositional and physical volcanological patterns of development. They certainly are not a homogeneous group.

The comprehensive conceptual framework presented in this paper synthesizes current understanding of the stratigraphy and age, chemical differences, and physical volcanology for the SRP basalts of southwestern Idaho. Much remains to be learned, however, about these basalts. We hope that the information provided here will advance future investigations into these fascinating rocks.

ACKNOWLEDGEMENTS

This report represents not only our own efforts but also the wide-ranging assistance from many others over a span of more than twenty years. We take great pleasure in thanking the following individuals affiliated with the Idaho Geological Survey: Roger Stewart, Gayle Wells, Charlotte Fullerton, Jane Freed, Virginia Gillerman, Dan Weisz, John Kauffman, and Kurt Othberg. From Boise State University and Idaho State University, we thank Mike McCurry, Craig White, Scott Hughes, Diana Boyack, Tamra Schiappa, and Spence Wood. Others who have provided valuable assistance over the years include Bill Leeman, John Shervais, Scott Vetter, Margaret Jenks, Mel Kuntz, Bill Hackett, Peter Hooper, John Bernt, Dan Kauffman, Mike Cummings, Mark Ferns, Mike Branney, Graham Andrews, Bill Hirt, Curtis Manley, Bill McIntosh, Bill Hart, James White, Mary O'Malley, and many students from Boise State University, Utah State University, Washington State University, University of Utah, Rice University, University of South Carolina, University of Massachusetts at Amherst, Mount Holyoke College, and the University of Idaho. We could not have developed the data and ideas in this paper without the assistance of Mike Rhodes and Pete Dawson at the University of Massachusetts (Amherst) and Diane Johnson at Washington State University with analyzing more SRP basalt samples than we can count. Also, we appreciate the significant financial help received over the years from several organizations, including the Idaho Geological Survey, the Idaho Department of Water Resources, the U.S. Geological Survey, and Mount Holyoke College. Finally, even with all of the magnificent help we have had from the above individuals and organizations, we take full responsibility for any errors that might eventually be found in our conclusions, and we expect that as research continues on the SRP basalts many of our ideas will be modified for the better.

REFERENCES

Amini, Hassan, H.H. Mehnert, and J.D. Obradovich, 1984, K-Ar ages of late Cenozoic basalts from the western Snake River Plain, Idaho: Isochron/West, no. 41, p. 7-11.

Armstrong, R.L., 1975, The geochronometry of Idaho: Isochron/West, no. 14, p. 1-50.

Armstrong, R.L., J.E. Harakal, and W.M. Neill, 1980, K-Ar dating of Snake River Plain (Idaho) volcanic rocks—new results: Ishochron/West, no. 27, p. 5-10.

Armstrong, R.L., W.P. Leeman, and H.E. Malde, 1975, K-Ar dating, Quaternary and Neogene volcanic rocks of the Snake River Plain, Idaho: American Journal of Science, v. 275, p. 225-251.

Arney, B.H., J.N. Gardner, and S.G. Belluomini, 1984, Petrographic analysis and correlation of volcanic rocks in Bostic 1-A well near Mountain Home, Idaho: Los Alamos National Laboratory Report LA-9966-HDR, 29 p.

Bernt, John, and Bill Bonnichsen, 1982, Pre-Cougar Point Tuff volcanic rocks near the Idaho-Nevada border, Owyhee County, Idaho, *in* Bill Bonnichsen and R.M. Breckenridge, eds., Cenozoic Geology of Idaho: Idaho Bureau of Mines and Geology Bulletin 26, p. 321-330.

Bonnichsen, Bill, 1981, Stratigraphy and measurements of magnetic polarity for volcanic units in the Bruneau-Jarbidge eruptive center, Owyhee County, Idaho: Idaho Geological Survey Technical Report 81-5, 75 p.

————, 1982a, The Bruneau-Jarbidge eruptive center, southwestern Idaho, *in* Bill Bonnichsen and R.M. Breckenridge, eds., Cenozoic Geology of Idaho: Idaho Bureau of Mines and Geology Bulletin 26, p. 237-254.

————, 1982b, Rhyolite lava flows in the Bruneau-Jarbidge eruptive center, southwestern Idaho, *in* Bill Bonnichsen and R.M. Breckenridge, eds., Cenozoic Geology of Idaho: Idaho Bureau of Mines and Geology Bulletin 26, p. 283-320.

Bonnichsen, Bill, John Bernt, and M.D. Jenks, 1990, Geologic map of the Sheep Creek West wilderness study area, Owyhee County, Idaho: U.S. Geological Survey Miscellaneous Field Studies Map MF-2126, 1:50,000.

Bonnichsen, Bill, R.L. Christiansen, L.A. Morgan, F.J. Moye, W.R. Hackett, W.P. Leeman, Norio Honjo, M.D. Jenks, and M.M. Godchaux, 1989, Excursion 4A: Silicic volcanic rocks in the Snake River Plain-Yellowstone Plateau province: New Mexico Bureau of

Mines and Mineral Resources Memoir 47, p. 135-182.

Bonnichsen, Bill, and G.P. Citron, 1982, The Cougar Point Tuff, southwestern Idaho and vicinity, *in* Bill Bonnichsen and R.M. Breckenridge, eds., Cenozoic Geology of Idaho: Idaho Bureau of Mines and Geology Bulletin 26, p. 255-281.

Bonnichsen, Bill, and M.M. Godchaux, 1998, Geologic map of the Walters Butte quadrangle, Ada, Canyon, and Owyhee counties, Idaho: Idaho Geological Survey Geological Map GM-21, scale 1:24,000.

Bonnichsen, Bill, and M.D. Jenks, 1990, Geologic map of the Jarbidge River wilderness study area, Owyhee County, Idaho: U.S. Geological Survey Miscellaneous Field Studies Map MF-2127, scale 1:50,000.

————, 1995a, Geologic map of the Cowan Reservoir quadrangle, Owyhee County, Idaho: Idaho Geological Survey Technical Report 95-1, scale 1:24,000.

————, 1995b, Geologic map of the Grassy Hills quadrangle, Owyhee and Twin Falls counties, Idaho: Idaho Geological Survey Technical Report 95-2, scale 1:24,000.

————, 1995c, Geologic map of the Triguero Lake quadrangle, Owyhee County, Idaho: Idaho Geological Survey Technical Report 95-3, scale 1:24,000.

Bonnichsen, Bill, M.D. Jenks, M.M. Godchaux, W.P. Leeman, and M.D. Norman, 1994a, Analyzed rocks from the Glenns Ferry 30 x 60 minute quadrangle, Owyhee, Twin Falls, Gooding, and Elmore counties, southwestern Idaho: Idaho Geological Survey Technical Report 94-4, diskette and 1:100,000-scale sheet.

Bonnichsen, Bill, and D.F. Kauffman, 1987, Physical features of rhyolite lava flows in the Snake River Plain volcanic province, southwestern Idaho, *in* J.H. Fink, ed., The Emplacement of Silicic Domes and Lava Flows: Geological Society of America Special Paper 212, p. 119-145.

Bonnichsen, Bill, W.P. Leeman, John Bernt, M.M. Godchaux, and M.D. Jenks, 1994b, Analyzed rocks from the Sheep Creek 30 x 60 minute quadrangle, Owyhee and Twin Falls counties, southwestern Idaho: Idaho Geological Survey Technical Report 94-5, diskette and 1:100,000-scale sheet.

Bonnichsen, Bill, W.P. Leeman, M.D. Jenks, and Norio Honjo, 1988, Geologic field trip guide to the central and western Snake River Plain, Idaho, emphasizing the silicic volcanic rocks, *in* P.K. Link and W.R. Hackett, eds., Guidebook to the Geology of Central and Southern Idaho: Idaho Geological Survey Bulletin 27, p. 247-281.

Bushnell, Kent, 1967, Geology of the Rowland quadrangle, Elko County, Nevada: Nevada Bureau of Mines Bulletin 67, 38 p.

Clemens, D.M., 1993, Tectonics and silicic volcanic stratigraphy of the western Snake River Plain, southwestern Idaho: Arizona State University M.S. thesis, 209 p.

Clemens, D.M., and S.H. Wood, 1993, Late Cenozoic volcanic stratigraphy and geochronology of the Mount Bennett Hills, central Snake River Plain, Idaho: Isochron/West, no. 60, p. 3-14.

Coats, R.R., 1964, Geology of the Jarbidge quadrangle, Nevada-Idaho: U.S. Geological Survey Bulletin 1141-M, 24 p.

Covington, H.R., 1976, Geologic map of the Snake River Canyon near Twin Falls, Idaho: U.S. Geological Survey Miscellaneous Field Studies Map MF-809, 14 p., scale 1:24,000.

Covington, H.R., and J.N. Weaver, 1989, Geologic map and profiles of the north wall of the Snake River Canyon, Bliss, Hagerman, and Tuttle quadrangles, Idaho: U.S. Geological Survey Miscellaneous Investigations Series Map I-1947-A, scale 1:24,000.

————, 1990a, Geologic map and profiles of the north wall of the Snake River Canyon, Pasadena Valley and Ticeska quadrangles, Idaho: U.S. Geological Survey Miscellaneous Investigations Series Map I-1947-B, scale 1:24,000.

————, 1990b, Geologic map and profiles of the north wall of the Snake River Canyon, Jerome, Filer, Twin Falls, and Kimberly quadrangles, Idaho: U.S. Geological Survey Miscellaneous Investigations Series Map I-1947-D, scale 1:24,000.

————, 1990c, Geologic map and profile of the north wall of the Snake River Canyon, Eden, Murtaugh, Milner Butte, and Milner quadrangles, Idaho: U.S. Geological Survey Miscellaneous Investigations Series Map I-1947-E, scale 1:24,000.

————, 1991, Geologic map and profiles of the north wall of the Snake River Canyon, Thousand Springs and Niagara Springs quadrangles, Idaho: U.S. Geological Survey Miscellaneous Investigations Series Map I-1947-C, scale 1:24,000.

Cummings, M.L., J.G. Evans, M.L. Ferns, and K.R. Lees, 2000, Stratigraphic and structural evolution of the middle Miocene synvolcanic Oregon-Idaho graben: Geological Society of America Bulletin, v. 112, p. 668-682.

Ekren, E.B., D.H. McIntyre, and E.H. Bennett, 1984, High-temperature, large-volume, lavalike ash-flow tuffs without calderas in southwestern Idaho: U.S. Geological Survey Professional Paper 1272, 76 p.

Ekren, E.B., D.H. McIntyre, E.H. Bennett, and H.E. Malde, 1981, Geologic map of Owyhee County, Idaho, west of longitude 116 degrees W.: U.S. Geological Survey Miscellaneous Investigations Series Map I-1256, scale 1:125,000.

Evernden, J.F., D.E. Savage, G.H. Curtis, and G.T. James, 1964, Potassium-argon dates and the Cenozoic mammalian chronology of North America: American Journal of Science, v. 262, p. 145-198.

Ferns, M.L., H.C. Brooks, J.G. Evans, and M.L. Cummings, 1993a, Geologic map of the Vale 30 x 60 minute quadrangle, Malheur County, Oregon, and Owyhee County, Idaho: Oregon Department of Geology and Mineral Industries, Geological Map Series GMS-77, scale 1:100,000.

Ferns, M.L., J.G. Evans, and M.L. Cummings, 1993b, Geologic map of the Mahogany Mountain 30 x 60 minute quadrangle, Malheur County, Oregon, and Owyhee County, Idaho: Oregon Department of Geology and Mineral Industries, Geological Map Series GMS-78, scale 1:100,000.

Gillerman, V.S., 2001, Geologic report on the 1993 Bliss landslide, Gooding County, Idaho: Idaho Geological Survey Staff Report 01-1, 14 p.

Gillerman, V.S., and Tamra Schiappa, 2001, Geology and hydrology of western Jerome County, Idaho: Idaho Geological Survey Staff Report 01-2, 47 p.

Godchaux, M.M., and Bill Bonnichsen, this volume, Syneruptive magma-water and posteruptive lava-water interactions in the western Snake River Plain, Idaho, during the past 12 million years, *in* Bill Bonnichsen, C.M. White, and Michael McCurry, eds., Tectonic and Magmatic Evolution of the Snake River Plain Volcanic Province: Idaho Geological Survey Bulletin 30.

Godchaux, M.M., Bill Bonnichsen, and M.D. Jenks, 1992, Types of phreatomagmatic volcanoes in the western Snake River Plain, Idaho, USA: Journal of Volcanology and Geothermal Research, v. 52, p. 1-25.

Greeley, Ronald, 1982, The style of basaltic volcanism in the eastern Snake River Plain, Idaho, *in* Bill Bonnichsen and R.M. Breckenridge, eds., Cenozoic Geology of Idaho: Idaho Bureau of Mines and Geology Bulletin 26, p. 407-421.

Hart, W.K., 1982, Chemical, geochronologic and isotopic significance of low-K, high-alumina olivine tholeiite in the northwestern Great Basin, U.S.A.: Case Western Reserve University Ph.D. dissertation, 410 p.

Hart, W.K., and J.J. Aronson, 1982, K-Ar ages of rhyolites from the western Snake River Plain area, Oregon, Idaho, and Nevada: Isochron/West, no. 36, p. 17-19.

Hart, W.K., J.J. Aronson, and S.A. Mertzman, 1984, Areal distribution

and age of low-K high-alumina olivine tholeiite magmatism in the northwestern Great Basin: Geological Society of America Bulletin, v. 95, p. 186-195.

Hart, W.K., and M.E. Brueseke, 2002, Analysis and dating of volcanic horizons from Hagerman Fossil Beds National Monument and a revised interpretation of eastern Glenns Ferry Formation chronostratigraphy: Electronic version from Hagerman Fossil Beds National Monument, 37 p.

Hart, W.K., and R.W. Carlson, 1983, K-Ar ages of late Cenozoic basalts from southeastern Oregon, southwestern Idaho, and northern Nevada: Isochron/West, no. 38, p. 23-26.

Hearst, Jonena, 1999, Depositional environments of the Birch Creek local fauna (Pliocene: Blancan), Owyhee County, Idaho, *in* W.A. Akersten, H.G. McDonald, D.J. Meldrum, and M.E.T. Flint, eds., And Whereas . . . Papers on the Vertebrate Palentology of Idaho Honoring John A. White, V. 1: Idaho Museum of Natural History Occasional Paper 36, p. 56-93.

Howard, K.A., J.W. Shervais, and E.H. McKee, 1982, Canyon-filling lavas and lava dams on the Boise River, Idaho, and their significance for evaluating downcutting during the last two million years, *in* Bill Bonnichsen and R.M. Breckenridge, eds., Cenozoic Geology of Idaho: Idaho Bureau of Mines and Geology Bulletin 26, p. 629-641.

Jenks, M.D., and Bill Bonnichsen, 1989, Subaqueous basalt eruptions into Pliocene Lake Idaho, Snake River Plain, Idaho, *in* V.E. Chamberlain, R.M. Breckenridge, and Bill Bonnichsen, eds., Guidebook to the Geology of Northern and Western Idaho and Surrounding Area: Idaho Geological Survey Bulletin 28, p. 17-34.

————, 1990a, Geologic map of the Bruneau River wilderness study area, Owyhee County, Idaho: U.S. Geological Survey Miscellaneous Field Studies Map MF-2128, scale 1:50,000.

————, 1990b, Geologic map of the Wild Horse Butte quadrangle, Ada and Owyhee counties, Idaho: Idaho Geological Survey Technical Report 90-8, scale 1:24,000.

Jenks, M.D., Bill Bonnichsen, and M.M. Godchaux, 1993, Geologic maps of the Grand View-Bruneau area, Owyhee County, Idaho: Idaho Geological Survey Technical Report 93-2, 21 p., 19 plates, scale 1:24,000.

————, 1998, Geologic map of the Grand View-Bruneau area, Owyhee County, Idaho: Idaho Geological Survey Technical Report 98-1, digitally compiled version, scale 1:100,000.

Kauffman, D.K., and Bill Bonnichsen, 1990, Geologic map of the Little Jacks Creek, Big Jacks Creek, and Duncan Creek wilderness study areas, Owyhee County, Idaho: U.S. Geological Survey Miscellaneous Field Studies Map MF-2142, scale 1:50,000.

Kimmel, P.G., 1982, Strataigraphy, age, and tectonic setting of the Miocene-Pliocene lacustrine sediments of the western Snake River Plain, Oregon and Idaho, *in* Bill Bonnichsen and R.M. Breckenridge, eds., Cenozoic Geology of Idaho: Idaho Bureau of Mines and Geology Bulletin 26, p. 559-578.

Kuntz, M.A., H.R. Covington, and L.J. Schorr, 1992, An overview of basaltic volcanism of the eastern Snake River Plain, Idaho, *in* P.K. Link, M.A. Kuntz, and L.B. Platt, eds., Regional Geology of Eastern Idaho and Western Wyoming: Geological Society of America Memoir 179, p. 227-267.

Kuntz, M.A., N.H. Elsheimer, L.F. Espos, and P.R. Klock, 1985, Major-element analyses of latest Pleistocene-Holocene lava fields of the Snake River Plain, Idaho: U.S. Geological Survey Open-File Report 85-593, 64 p.

Kuntz, M.A., E.C. Spiker, M. Rubin, D.E. Champion, and R.H. Lefebvre, 1986, Radiocarbon studies of latest Pleistocene and Holocene lava flows of the Snake River Plain, Idaho: Dates, lessons, interpretations: Quaternary Research v. 25, p. 163-176.

Leeman, W.P., 1976, Petrogenesis of McKinney (Snake River) olivine tholeiite in light of rare-earth element and Cr/Ni distributions: Geological Society of America Bulletin, v. 85, p. 1582-1586.

————, 1982, Olivine tholeiite basalts of the Snake River Plain, Idaho, *in* Bill Bonnichsen and R.M. Breckenridge, eds., Cenozoic Geology of Idaho: Idaho Bureau of Mines and Geology Bulletin 26, p. 181-191.

Leeman, W.P., and C.J. Vitaliano, 1976, Petrology of McKinney Basalt, Snake River Plain, Idaho: Geological Society of America Bulletin, v. 87, p. 1777-1792.

Lewis, R.E, and M.A.J. Stone, 1988, Geohydrologic data from a 4,403-foot geothermal test hole, Mountain Home Air Force Base, Elmore County, Idaho: U.S. Geological Survey Open-File Report 88-166, 30 p.

Linholm, G.F., 1976, Summary of the Snake River Plain regional aquifer-system analysis in Idaho and eastern Oregon: U.S. Geological Survey Professional Paper 1408-A, 59 p.

Link, P.K., H.G. McDonald, C.M. Fanning, and A.E. Godfrey, this volume, Detrital zircon evidence for Pleistocene drainage reversal at Hagerman Fossil Beds National Monument, central Snake River Plain, Idaho, *in* Bill Bonnichsen, C.M. White, and Michael McCurry, eds., Tectonic and Magmatic Evolution of the Snake River Plain Volcanic Province: Idaho Geological Survey Bulletin 30.

Mabey, D.R., 1982, Geophysics and tectonics of the Snake River Plain, Idaho, *in* Bill Bonnichsen and R.M. Breckenridge, eds., Cenozoic Geology of Idaho: Idaho Bureau of Mines and Geology Bulletin 26, p. 139-153.

Malde, H.E., 1968, The catastrophic late Pleistocene Bonneville Flood in the Snake River Plain, Idaho: U.S. Geological Survey Professional Paper 596, 52 p.

————, 1989a, Geologic map of the Bruneau Formation in the Walters Butte and Initial Point quadrangles, southwestern Idaho: U.S. Geological Survey Miscellaneous Field Studies Map MF-2063-A, scale 1:24,000.

————, 1989b, Geologic map of the Bruneau Formation in the Sinker Butte and Wild Horse Butte quadrangles, southwestern Idaho: U.S. Geological Survey Miscellaneous Field Studies Map MF-2063-B, scale 1:24,000.

————, 1989c, Geologic map of the Bruneau Formation in the Oreana and Castle Butte quadrangles, southwestern Idaho: U.S. Geological Survey Miscellaneous Field Studies Map MF-2063-C, scale 1:24,000.

————, 1989d, Geologic map of the Bruneau Formation in the Jackass Butte and Dorsey Butte quadrangles, southwestern Idaho: U.S. Geological Survey Miscellaneous Field Studies Map MF-2063-D, scale 1:24,000.

————, 1990, Geologic Profiles of the canyon walls of the Snake River, from Sinker Creek to Guffey Butte, Idaho: U.S. Geological Survey Miscellaneous Investigations Series Map I-2096, scale 1:24,000.

————, 1991, Quaternary geology and structural history of the Snake River Plain, Idaho and Oregon, *in* R.B. Morrison, ed., Quaternary Nonglacial Geology, Conterminous U.S.: U.S. Geological Survey, The Geology of North America, v. K-2, p. 251-281.

Malde, H.E., and H.A. Powers, 1962, Upper Cenozoic stratigraphy of the western Snake River Plain, Idaho: Geological Society of America Bulletin, v. 73, p. 1197-1210.

————, 1972, Geologic map of the Glenns Ferry-Hagerman area, west-central Snake River Plain, Idaho: U.S. Geological Survey Miscellaneous Geologic Investigations Map I-696, scale 1:48,000.

Malde, H.E., H.A. Powers, and C.H. Marshall, 1963, Reconnaissance geologic map of west-central Snake River Plain, Idaho: U.S. Geological Survey Miscellaneous Geological Investigations Map I-373, scale 1:125,000.

McCurry, Michael, A.M. Watkins, J.L. Parker, Karen Wright, and S.S. Hughes, 1996, Preliminary volcanological constraints for sources of high-grade, rheomorphic ignimbrites of the Cassia Mountains, Idaho: Implications for the evolution of the Twin Falls volcanic center, *in* S.S. Hughes and R.C. Thomas, eds., Geology of the Crook in the Snake River Plain, Twin Falls and Vicinity, Idaho: Northwest Geology, v. 26, p. 81-91.

McCurry, Mike, Bill Bonnichsen, Craig White, M.M. Godchaux, and S.S. Hughes, 1997, Bimodal basalt-rhyolite magmatism in the central and western Snake River Plain, Idaho and Oregon, *in* P.K. Link and B.J. Kowallis, eds., Proterozoic to Recent Stratigraphy, Tectonics, and Volcanology, Utah, Nevada, Southern Idaho, and Central Mexico: Brigham Young University Geological Studies, v. 42, part 1, p. 381-422.

McIntyre, D.H., 1979, Preliminary description of Anschutz Federal no. 1 drill hole, Owyhee County, Idaho: U.S. Geological Survey Open-File Report 79-651, 15 p.

Mitchell, V.E., and E.H. Bennett, 1979, Geologic map of the Boise quadrangle, Idaho: Idaho Geological Survey Geologic Map 4, scale 1:250,000.

Mitchell, V.E., D.J. Shiveler, G.S. Hustedde, and E.H. Bennett, 1985, Isotopic age dates in Idaho: Idaho Geological Survey Information Circular 38, 29 p.

Monani, Salma, 1997, Rhyolites of the Twin Falls eruptive center, the Snake River Plain volcanic province, southern Idaho: A petrographic and geochemical study: Mount Holyoke College B.A. thesis, 99 p.

Morrow, L.S., 1996, Geology of Guffey Butte, western Snake River Plain, Idaho: University of Idaho M.S. thesis, 106 p.

Mytton, J.W., P.L. Williams, and W.A. Morgan, 1990, Geologic map of the Stricker 4 quadrangle, Cassia County, Idaho: U.S. Geological Survey Miscellaneous Investigations Series Map I-2052, scale 1:48,000.

Othberg, K.L., 1994, Geology and geomorphology of the Boise Valley and adjoining areas, western Snake River Plain, Idaho: Idaho Geological Survey Bulletin 29, 54 p.

Othberg, K.L., Bill Bonnichsen, C.C. Swisher III, and M.M. Godchaux, 1995, Geochronology and geochemistry of Pleistocene basalts of the western Snake River Plain and Smith Prairie, Idaho: Isochron/West, no. 62, p. 1-14.

Othberg, K.L., and L.R. Stanford, 1992, Geologic map of the Boise Valley and adjoining area, western Snake River Plain, Idaho: Idaho Geological Survey Geologic Map 18, scale 1:100,000.

Parker, J.L., S.S. Hughes, and Mike McCurry, 1996, Physical and chemical constraints on the emplacement of the tuff of Wooden Shoe Butte, Cassia Mountains, Idaho, *in* S.S. Hughes and R.C. Thomas, eds., Geology of the Crook in the Snake River Plain, Twin Falls and Vicinity, Idaho: Northwest Geology, v. 26, p. 92-106.

Perkins, M.E., W.P. Nash, F.H. Brown, and R.J. Fleck, 1995, Fallout tuffs of Trapper Creek, Idaho—A record of Miocene explosive volcanism in the Snake River Plain volcanic province: Geological Society of America Bulletin, v. 107, p. 1484-1506.

Pierce, K.L., and L.A. Morgan, 1992, The track of the Yellowstone hot spot: Volcanism, faulting and uplift, *in* P.K. Link, M.A. Kuntz, and L.B. Platt, eds., Regional Geology of Eastern Idaho and Western Wyoming: Geological Society of America Memoir 179, p. 1-53.

Pierce, K.L., L.A. Morgan, and R.W. Saltus, this volume, Yellowstone plume head: Postulated tectonic relations to the Vancouver slab, continental boundaries, and climate, *in* Bill Bonnichsen, C.M. White, and Michael McCurry, eds., Tectonic and Magmatic Evolution of the Snake River Plain Volcanic Province: Idaho Geological Survey Bulletin 30.

Rember, W.C., and E.H. Bennett, 1979, Geologic map of the Twin Falls quadrangle, Idaho: Idaho Geological Survey Geologic Map 17, scale 1:250,000.

Savage, C.N., 1958, Geology and mineral resources of Ada and Canyon counties: Idaho Bureau of Mines and Geology County Report 3, 94 p.

Shervais, J.W., Gaurav Shroff, S.K. Vetter, Scott Matthews, B.B. Hanan, and J.J. McGee, this volume, Origin and evolution of the western Snake River Plain: Implications from stratigraphy, faulting, and the geochemistry of basalts near Mountain Home, Idaho, *in* Bill Bonnichsen, C.M. White, and Michael McCurry, eds., Tectonic and Magmatic Evolution of the Snake River Plain Volcanic Province, Idaho Geological Survey Bulletin 30.

Stearns, H.T., Lynn Crandall, and W.G. Steward, 1938, Geology and ground-water resources of the Snake River Plain in southeastern Idaho: U.S. Geological Survey Water Supply Paper 774, 268 p.

Stone, G.T., 1967, Petrology of upper Cenozoic basalts of the western Snake River Plain, Idaho: University of Colorado Ph.D. dissertation, 392 p.

Swirydczuk, Krystyna, G.P. Larson, and G.R. Smith, 1982, Volcanic ash beds as stratigraphic markers in the Glenns Ferry and Chalk Hills Formations from Adrian, Oregon, to Bruneau, Idaho, *in* Bill Bonnichsen and R.M. Breckenridge, eds., Cenozoic Geology of Idaho: Idaho Bureau of Mines and Geology Bulletin 26, p. 543-558.

Vetter, S.K., and J.W. Shervais, 1992, Continental basalts of the Boise River group near Smith Prairie, Idaho: Journal of Geophysical Research, v. 97, no. B6, p. 9043-9061.

Watkins, A.M., 1998, Geochemistry, petrography, and stratigraphy of the tuff of Steer Basin, Twin Falls and Cassia counties, Idaho: Idaho State University M.S. thesis, 177 p.

Watson, C.A., 1999, The evolution of Guffey Butte tuff cone complex, western Snake River Plain, Idaho: Boise State University M.S. thesis, 73 p.

White, C.M., W.K. Hart, Bill Bonnichsen, and Debra Matthews, this volume, Geochemical and Sr-Isotopic variations in western Snake River Plain basalts, Idaho, *in* Bill Bonnichsen, C.M. White, and Michael McCurry, eds., Tectonic and Magmatic Evolution of the Snake River Plain Volcanic Province: Idaho Geological Survey Bulletin 30.

Williams, P.L., H.R. Covington, and J.W. Mytton, 1991, Geologic map of the Stricker 2 quadrangle, Twin Falls and Cassia counties, Idaho: U.S. Geological Survey Miscellaneous Investigations Series Map I-2146, scale 1:48,000.

Williams, P.L., J.W. Mytton, and H.R. Covington, 1990, Geologic map of the Stricker 1 quadrangle, Cassia, Twin Falls, and Jerome counties, Idaho: U.S. Geological Survey Miscellaneous Investigations Series Map I-2078, scale 1:48,000.

Wood, S.H., 1989, Silicic volcanic rocks and structure of the western Mount Bennett Hills and adjacent Snake River Plain, Idaho, *in* K.L. Ruebelmann, ed., Snake River Plain-Yellowstone Volcanic Province: American Geophysical Union, 28th International Geological Congress Field Trip Guidebook T305, p. 69-77.

————, 1994, Seismic expression and geological significance of a lacustrine delta in Neogene deposits of the western Snake River Plain, Idaho: American Association of Petroleum Geologists Bulletin, v. 78, p. 102.

Wood, S.H., and J.E. Anderson, 1981, Geology, *in* J.C. Mitchell, ed., Geothermal Investigations in Idaho, Part 11, Geological, Hydrological, Geochemical, and Geophysical Investigations of the Nampa-Caldwell and Adjacent Areas, Southwestern Idaho: Idaho Department of Water Resources Information Buletin 30, p. 9-31.

Wood, S.H., and D.M. Clemens, this volume, Geologic and tectonic history of the western Snake River Plain, Idaho and Oregon, *in* Bill Bonnichsen, C.M. White, and Michael McCurry, eds., Tectonic and Magmatic Evolution of the Snake River Plain Volcanic Province: Idaho Geological Survey Bulletin 30.

Wood, S.H. and J.N. Gardner, 1984, silicic volcanic rocks of the Miocene Idavada Group, Bennett Mountain, southwestern Idaho: Final contract report to the Los Alamos National Laboratory from Boise State University, 55 p.

Worl, R.G., T.H. Kilsgaard, E.H. Bennett, P.K. Link, R.S. Lewis, V.E. Mitchell, K.M. Johnson, and L.D. Snyder, 1991, Geologic map of the Hailey 1° x 2° quadrangle, Idaho: U.S. Geological Survey Open-File Report 91-340, scale 1:250,000.

Wright, K.E., Michael McCurry, and S.S. Hughes, this volume, Petrology and geochemistry of the Miocene tuff of McMullen Creek, central Snake River Plain, *in* Bill Bonnichsen, C.M. White, and Michael McCurry, eds., Tectonic and Magmatic Evolution of the Snake River Plain Volcanic Province: Idaho Geological Survey Bulletin 30.

Temporal Controls on Basalt Genesis and Evolution on the Owyhee Plateau, Idaho and Oregon

Kurt A. Shoemaker[1] and William K. Hart[2]

ABSTRACT

The development of the Snake River Plain volcanic province has been attributed to the passage of the North American plate over the Yellowstone mantle plume. As this province was being formed by an eastward progression of younger silicic volcanic centers, basaltic volcanism has continued through the present day in the western regions of the "plume track." Of particular interest is the Owyhee Plateau of southeastern Oregon, located at the westernmost end of the SRP volcanic province. The Owyhee Plateau preserves the best documented continuous record of mid-Miocene to Recent basaltic volcanism in the northwestern United States, allowing an investigation of variations in magmatic sources and processes through time. In addition, this region is underlain by lithosphere transitional between that of the Proterozoic-Archean Wyoming Craton to the east and accreted terranes younger than 200 Ma to the west. Basaltic products that erupted from a variety of vents on the Owyhee Plateau illustrate chemical and Sr isotopic diversity that cannot be solely attributed to lateral lithospheric heterogeneities. Rather, this diversity appears to be a function of eruptive age. For example, Sr isotope data show a systematic increase in $^{87}Sr/^{86}Sr$ from 0.704 to 0.707 with decreasing age from 17.5-11 Ma, but decreasing $^{87}Sr/^{86}Sr$ to 0.704 from 11-0 Ma. The "peak" in Sr values corresponds to a regional change in the dominant basalt type erupted, from large volume, strongly fractionated basalts and basaltic andesites before 11 Ma to smaller volume, more primitive high-alumina olivine tholeiites after 11 Ma. A preliminary model is offered that calls for temporal variations in magma production, lithospheric structure, and the relative contributions from lithospheric and sublithospheric source reservoirs.

Key words: basalt, Owyhee Plateau, lithosphere, Sr isotopes, magmatic evolution, plume track

INTRODUCTION

The initiation of flood basalt volcanism in the northwestern United States at approximately 17.5 Ma marks the onset of a time and longitudinally transgressive sequence of volcanic activity attributed to the passage of the North American plate over the hypothesized Yellowstone mantle plume (Pierce and Morgan, 1992; Geist and Richards, 1993; Camp, 1995). The earliest pulse of flood basalt eruptions (17.5-14 Ma) are represented by the Clarkston Basalt of the Columbia Plateau (Hooper and Hawkesworth, 1993) and Steens Mountain Basalt of the Oregon Plateau (Carlson and Hart, 1987, 1988; Hart and Carlson, 1987). These basalts were erupted from a narrow array of vents extending for nearly 1,000 km from southeastern Washington to central Nevada. This array is believed to represent a rift in the back-arc region of the Cascade arc (Christiansen and McKee, 1978; Carlson and Hart, 1987; Zoback and others, 1994). After 14 Ma, eruptive activity along this rift contracted in a north-south direction, becoming focused in the Owyhee Plateau of the Oregon-Idaho-Nevada border region (Figure 1). Subsequent magmatism to the east formed the Snake River Plain (SRP). It is important to note that, as the SRP was being formed by an eastward progression of silicic eruptive centers, basaltic volcanism has continued essentially

Editors' note: The manuscript was submitted in June 1998 and has been revised at the authors' discretion.

[1]Geology Department, Saint Joseph's College, Rensselaer, IN 47978
[2]Geology Department, Miami University, Oxford OH 45056

Shoemaker, K.A., and W.K. Hart, 2002, Temporal controls on basalt genesis and evolution on the Owyhee Plateau, Idaho and Oregon, *in* Bill Bonnichsen, C.M. White, and Michael McCurry, eds., Tectonic and Magmatic Evolution of the Snake River Plain Volcanic Province: Idaho Geological Survey Bulletin 30, p. 313-328.

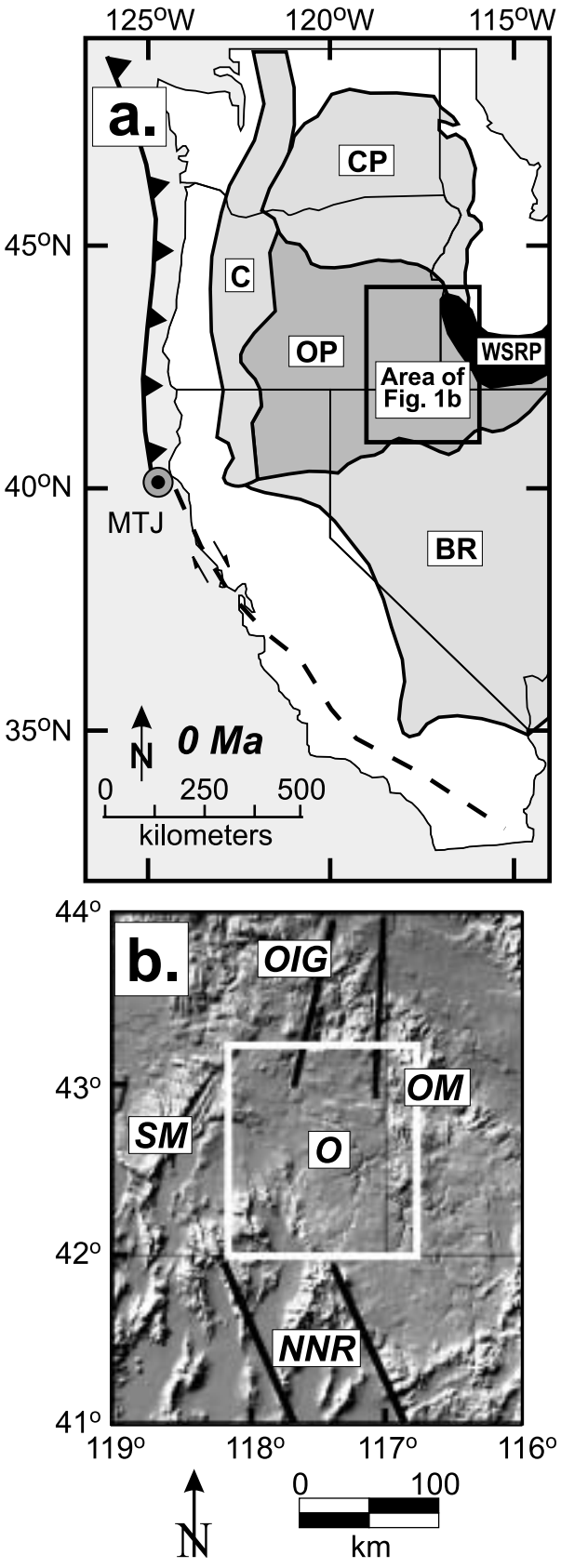

through the present day in the western regions of the "plume track."

Determining the ultimate mantle sources of and the processes responsible for the evolution of these basalts has been hindered by the complication of contamination of the primary magmas by chronologically and chemically heterogeneous lithospheric materials (Leeman and others, 1992). Regional geochemical and isotopic information, combined with regional patterns of crustal deformation, has led some researchers to argue that the initial, large volume flood basalt eruptions were related to the arrival of the Yellowstone plume head at the base of the lithosphere (Geist and Richards, 1993; Hooper and Hawkesworth, 1993; Camp, 1995). Other researchers have used the same evidence to argue that these basalts were erupted as a result of rifting behind the Cascade volcanic arc (Christiansen and McKee, 1978; Carlson and Hart, 1987). Obviously, the current data base is ambiguous with regard to these issues, and questions concerning sources and processes cannot be answered until the influence of the lithosphere on the primary magmas can be adequately determined (Hart, 1997; Hart and others, 1997).

The Owyhee Plateau (Figure 1) provides an excellent opportunity to explore variations in the geochemical and isotopic characteristics of late Cenozoic northwestern United States basalts through time. The basalts in this study constitute a geochemically and isotopically diverse suite erupted over the past 17.5 Ma from vents located within a geographically restricted area between approximately lat 42º00′N. and 43º15′N. and long 116º45′W. and 118º15′W. This area is underlain by lithosphere transitional between that of the Proterozoic-Archean Wyoming craton to the east and accreted terranes younger than 200 Ma to the west (Leeman and others, 1992). Here, the basaltic magmas are assumed to have passed through, and consequently to have had the opportunity to interact with, the same chronologically similar "package" of lithospheric materials. Thus, by eliminating the distinct isotopic signatures attributed to regional, lateral lithospheric variations, a significant variable to investigate is time.

Figure 1. Location of the study area, in relation to major volcanic and tectonic features of the western United States. (a) Generalized map of the major late Cenozoic volcanic provinces of the northwestern United States. C: Cascade arc; CP: Columbia Plateau; OP: Oregon Plateau; WSRP: Western Snake River Plain; BR: Basin and Range; MTJ: Mendocino Triple Junction. (b) Digital elevation model of the Owyhee Plateau study area, modified from Sterner (1997). SM: Steens Mountain; OM: Owyhee Mountains; OIG: Oregon-Idaho Graben; NNR: Northern Nevada Rift; O: Owyhee Plateau and Owyhee River Canyon region. Locations of tectonic and structural features adapted from Bohannon and Parsons (1995), Zoback and others (1994), Carlson and Hart (1987), and Ferns (1997).

Furthermore, to our knowledge, the Owyhee Plateau contains the most complete record of mid-Miocene to Recent basaltic volcanism in the northwestern United States. Thus, it is uniquely suited to an exploration of the temporal variations in lithospheric and sublithospheric contributions to this late Cenozoic basaltic volcanism.

SPATIAL AND TEMPORAL RELATIONSHIPS

Previous investigations of post-17.5 Ma Oregon Plateau basaltic volcanism by Carlson and Hart (1987, 1988), Hart and Carlson (1987, 1992), and Draper (1991) documented a significant change about 11 Ma in the dominant basalt type erupted (Figure 2a). The older eruptions (Steens Mountain Basalt) produced strongly fractionated tholeiitic basalts and basaltic andesites. Post-11 Ma eruptions were dominated by less fractionated low-K, high alumina olivine tholeiites (HAOT). This change coincides not only with the regional shift from large volume, fissure-fed eruptions to small volume eruptions from discrete eruptive centers, but also with the onset of regional lithospheric thinning due to diffuse extension throughout the entire Oregon Plateau area (Hart and Carlson, 1987; Hooper, 1990; Draper, 1991).

Leeman and others (1992) documented that the maximum diversity in $^{87}Sr/^{86}Sr$ for late Cenozoic northwestern United States basalts occurs in a longitudinal "band" corresponding to approximately 117° to 118° west longitude (Figure 2b). This region of maximum diversity coincides with the transition between the Proterozoic-Archean cratonic lithosphere to the east and accreted terranes younger than 200 Ma to the west (Leeman and others, 1992; Elison and others, 1990; Wright and Wooden, 1991). Importantly, the Owyhee Plateau overlies this region of transitional lithosphere (Figure 1).

Hart (1997) further explored the relationships between age and location of eruption and Sr isotope compositions of northwestern United States basalts (Figure 3). Figure 3 substantiates the observations of Leeman and others (1992) that a wide range in basalt $^{87}Sr/^{86}Sr$ values occurs along approximately 117° west longitude, with higher and lower $^{87}Sr/^{86}Sr$ values occurring east and west of this line, respectively. Additionally, Figure 3 shows that those basalts representing the earliest pulse of volcanism (Steens, Clarkston, and Picture Gorge basalts) have lower $^{87}Sr/^{86}Sr$ values than many of the samples representing younger eruptions (e.g., SRP and Saddle Mountains basalts). Furthermore, samples from the Owyhee Plateau define a wide range in $^{87}Sr/^{86}Sr$, from less than 0.704 to greater than 0.707. Another interesting relationship is found when the data are plotted versus the age of eruption. Sr-isotope values increase with decreasing age from the initiation of volcanism to about 11 Ma, at which point the data diverge. Except for the young Yellowstone area basalts that span nearly the entire observed range in $^{87}Sr/^{86}Sr$, SRP basalts retain radiogenic signatures while Owyhee Plateau basalts trend toward lower $^{87}Sr/^{86}Sr$ values from 11 Ma to 0 Ma. The rest of this paper will focus only on the Owyhee Plateau basalts.

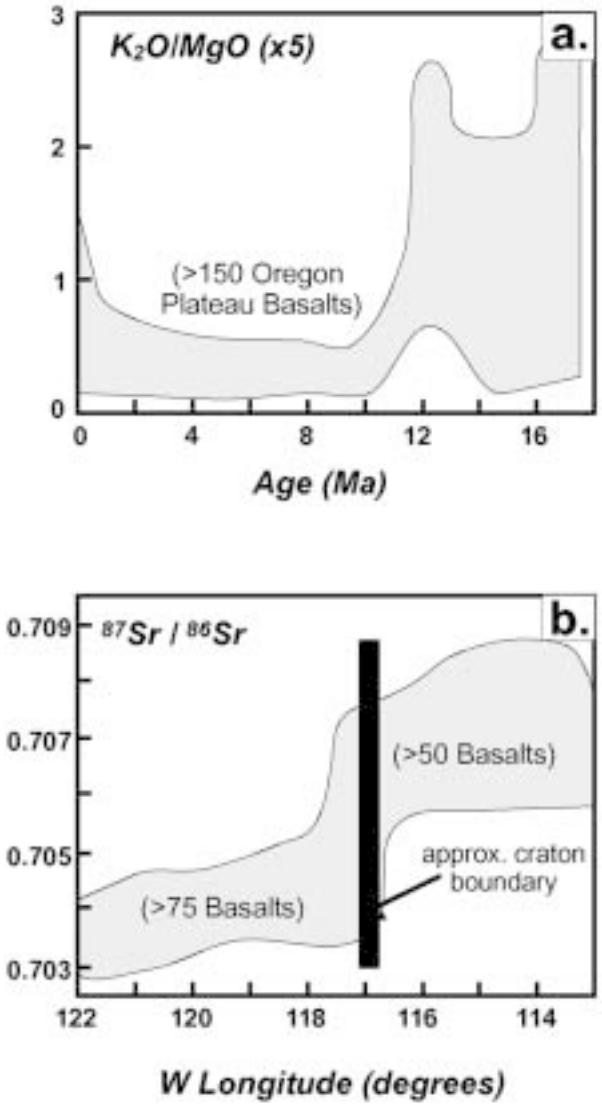

Figure 2. Important regional geochemical and isotopic observations. (a) Illustration of the regional change in basalt geochemistry on the Oregon Plateau, from strongly fractionated basalts and basaltic andesites before approximately 11 Ma to relatively unfractionated basalts after approximately 11 Ma, after Hart and Carlson (1987). (b) Longitudinal variation in Sr isotope compositions of basaltic rocks, after Leeman and others (1992). The area of focus for this study coincides with the cratonic boundary, where the greatest diversity in $^{87}Sr/^{86}Sr$ is observed.

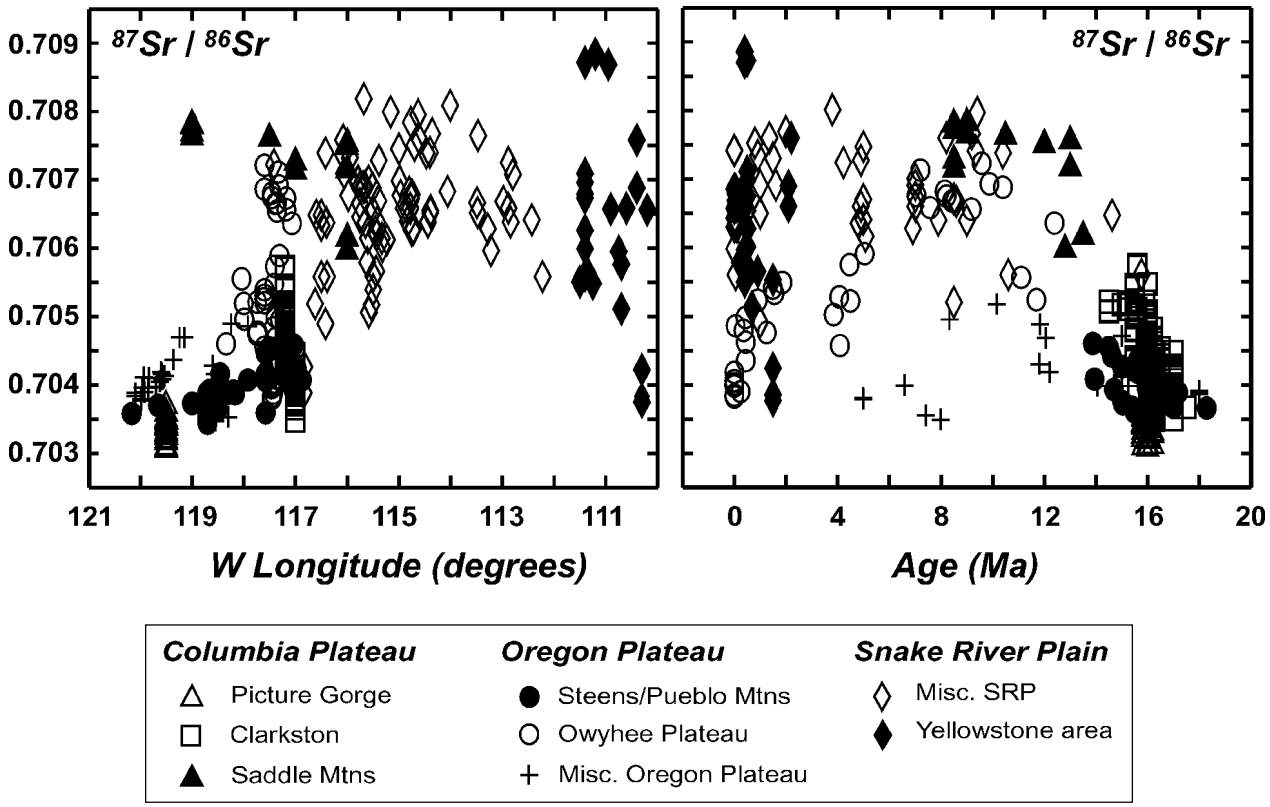

Figure 3. Compilation of Sr isotope data for northwestern United States basalts, after Hart (1997). Where possible, the longitude of the eruption site is used. Data are from Carlson (1984), Carlson and Hart (1987), Carlson and others (1981), Hart (1985), Hart and others (1989), Hooper and Hawkesworth (1993), Lambert and others (1995), Leeman and others (1992), Leeman (1982), Leeman and Manton (1971), Mark and others (1975), Noble and others (1973), and this study.

DATA

CHRONOSTRATIGRAPHY

Careful sampling of basalt flow sequences exposed in fault scarps and in canyons of the Owyhee River and its tributaries (see Figure 1b) combined with new (Table 1) and previously reported (Hart and Mertzman, 1982, 1983; Hart and Carlson, 1983, 1985; and Hart and others, 1984) chronologic data has allowed us to construct a composite chronostratigraphic section representing the history of basaltic volcanism on the Owyhee Plateau over the last 17.5 Ma. Four new $^{40}Ar/^{39}Ar$ method age determinations (Table 1) were obtained in order to better constrain the timing of the older pulse of Owyhee Plateau basaltic volcanism. Age estimates were interpolated for samples with relatively tight (approximately 2 m.y. or less) stratigraphic constraints based on K-Ar or $^{40}Ar/^{39}Ar$ age data. These estimated ages are marked with an asterisk (*) in Table 2.

On the basis of eruptive age, the sample suite has been divided into five groups as indicated in Figure 4. These groups are described briefly below:

17.5-14 Ma. This interval represents the initial, large volume eruptive phase of Oregon Plateau basaltic volcanism, temporally correlative with the eruption of the Clarkston Basalt of the Columbia Plateau (Hart and Carlson, 1985; Hart and others, 1989; Hooper and Hawkesworth, 1993). These flood basalts typically were erupted from isolated fissures and large fissure systems. Magmas erupted at this time were strongly fractionated basalts to basaltic andesites with tholeiitic to calc-alkaline affinities.

14-11 Ma. This interval represents the waning stages of Steens Mountain Basalt eruptions. Basalt compositions are similar to those of the older age group, but the volumes erupted are significantly smaller and individual flows are less areally extensive (Hart and Mertzman, 1982; Hart and Carlson, 1985).

11-6 Ma. This interval marks the regional change in dominant basalt type erupted, from the strongly fraction-

Table 1. New $^{40}Ar/^{39}Ar$ age data.

Sample number	Age Analysis	steps	^{39}ArK (x 10^{-15} mol)	% ^{39}Ar	K/Ca	Age (Ma)	±2 s.d. (Ma)
H85-10A	plateau	6	46.6	82.2	0.33	16.27	0.17
JV96-2	plateau	5	33.4	75.2	0.09	12.37	0.48
JV96-4	plateau	7	27.8	73.1	0.20	14.61	0.35
JV96-7	plateau	7	90.1	66.0	0.28	13.87	0.39

Correction factors:
$(^{39}Ar/^{37}Ar)Ca = 0.00070 \pm 0.00005$
$(^{36}Ar/^{37}Ar)Ca = 0.00026 \pm 0.00002$
$(^{38}Ar/^{39}Ar)K = 0.0119$
$(^{40}Ar/^{39}Ar)K = 0.0002 \pm 0.0003$

ated basalts and basaltic andesites of the early phase of volcanism to relatively unfractionated basalts. This is accompanied by a change from primarily fissural flood basalt activity to a combination of eruptions from local fissures associated with extensional features and from isolated low shield cones similar to those found within the SRP proper. Compositions range from low-K, low-Ti, high alumina olivine tholeiites (HAOT) to high-K, high-Ti Snake River Plain-type olivine tholeiites (SROT). A full spectrum of compositions transitional between these end members (transitional basalts, TB) is present (Hart and others, 1984; Hart, 1985).

6-3 Ma. This interval is defined primarily by increased magmatism between 5-4 Ma following a brief period of low magmatic output (Hart and others, 1984; Figure 3). Magmatism during this interval is dominated by small volume HAOT to SROT eruptions from local fissures and low shield cones (Hart and others, 1984; Hart, 1985).

3-0 Ma. This interval again follows a brief period of low magmatic output and is dominated by small volume HAOT eruptions (Hart and others, 1984). In addition, the only alkaline basalts observed on the Oregon Plateau were produced during this interval (after 1 Ma) and were erupted from low shield and tephra cones (Hart and Mertzman, 1983; Russell and others, 1988; Hart, 1996).

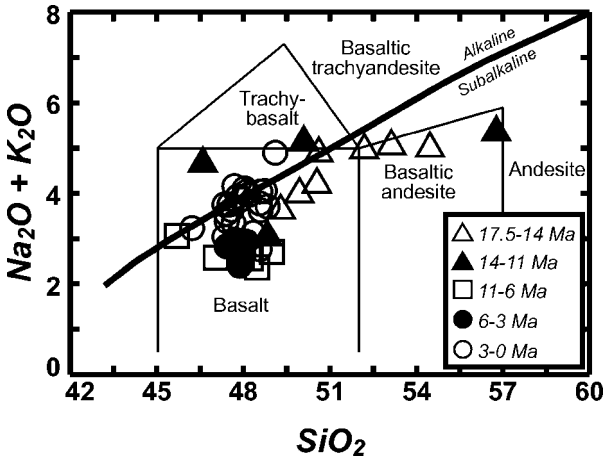

Figure 4. Total alkali-silica diagram of Le Bas and others (1986), showing classification of Owyhee Plateau basalts. Total Fe has been partitioned prior to normalization of analyses to 100 percent anhydrous, according to the method of Le Maitre (1976). Age groups are described in the text.

ELEMENTAL AND SR-ISOTOPE GEOCHEMISTRY

Major and trace element geochemical, Sr-isotope, and chronologic data for the sample suite of this study are given in Table 2. Major element analyses were performed by both X-ray fluorescence and direct current argon plasma spectrometry (DCP) methods. Samples for which both Fe_2O_3 and FeO are reported were analyzed for major elements by XRF at Franklin and Marshall College according to the methods described by Boyd and Mertzman (1987); FeO for these samples was determined by titration. Samples for which only Fe_2O_3 is reported were analyzed for major elements by DCP at Miami University by the method of external standards, using 7-8 international standards to define calibration curves. All trace elements were analyzed by XRF, with the exception of Sc, V, and Cr, which were determined by DCP using external standards. Sr isotope ratios were determined by thermal ionization mass spectrometry at Miami University and at the Department of Terrestrial Magnetism, Carnegie Institution of Washington. Geochronology by the $^{40}Ar/^{39}Ar$ method was performed at the New Mexico Geochronologic Research Laboratory.

Most of the samples are basalts, although some pre-11 Ma samples plot in the basaltic andesite field of Le Bas and others (1986; Figure 4). The samples are dominantly subalkaline, with the exception of some of the samples representing the most recent pulse of eruptive

Table 2. Major and trace element geochemical, Sr-isotope, and chronologic data for Owyhee Plateau basalts. Major element concentrations are reported as weight percent oxides; trace elements are reported in ppm. Samples are arranged according to eruptive age, from oldest to youngest. Estimated ages are marked with an asterisk (see text). With the exception of estimated ages and ages reported in Table 1, all ages are previously published K-Ar ages (Hart and Mertzman, 1982, 1983; Hart and Carlson, 1983, 1985). Sr isotope data are from Hart (1985), Carlson and Hart (1987), and this study. All Sr isotope ratios are age-corrected initial ratios reported relative to $^{87}Sr/^{86}Sr = 0.70800$ for the E&A $SrCO_3$ standard; 2-sigma uncertainties are ± 0.00006 or less.

	Samples:															
	H85-10A	**CH82-32**	**H85-6**	**H85-10B**	**H85-12B**	**H9-47**	**JV96-4**	**JV96-7**	**JV96-2**	**H8-74**	**H9-32**	**H8-29**	**H9-37C**	**SM75-12A**	**H8-69G**	**H8-34**
	Major oxides in wt. %															
SiO_2	53.82	48.46	49.95	48.72	49.26	49.41	51.89	55.38	48.00	46.13	49.80	49.11	45.48	47.65	48.34	48.42
TiO_2	2.00	2.20	1.97	2.07	2.54	2.32	1.21	1.04	2.53	2.86	3.00	1.57	2.80	1.25	1.94	1.82
Al_2O_3	14.72	15.88	14.73	15.76	16.45	15.18	16.71	16.19	14.20	14.80	15.40	15.89	16.25	16.26	15.53	15.78
Fe_2O_3	3.45	12.19	2.93	7.61	9.83	4.85	9.58	8.00	14.05	15.47	7.59	4.77	5.58	2.74	3.36	4.09
FeO	7.09	—	10.41	5.33	3.02	7.56	—	—	—	—	6.40	6.64	8.48	7.33	9.28	7.80
MnO	0.15	0.16	0.25	0.18	0.14	0.19	0.17	0.15	0.20	0.20	0.23	0.19	0.20	0.17	0.20	0.19
MgO	5.01	5.72	2.78	5.67	2.77	4.69	4.88	4.36	6.62	5.01	3.51	7.57	7.50	9.89	8.93	7.35
CaO	7.08	8.17	7.28	9.98	8.66	9.05	8.23	7.09	10.24	8.75	7.24	11.67	9.77	11.49	10.24	11.82
Na_2O	3.52	3.00	3.15	3.09	3.69	3.19	3.57	3.36	2.51	3.25	3.50	2.38	2.53	2.28	2.23	2.06
K_2O	1.41	0.93	1.60	0.48	1.06	0.92	1.36	1.86	0.48	1.02	1.60	0.34	0.53	0.34	0.42	0.31
P_2O_5	0.47	0.41	0.43	0.26	0.42	0.43	0.67	0.62	0.44	0.98	1.37	0.21	0.50	0.15	0.28	0.27
L.O.I.	1.33	3.16	4.75	1.49	2.61	2.37	0.80	1.37	0.11	0.08	0.73	0.93	0.88	0.72	1.03	1.05
TOTAL	100.05	100.28	100.23	100.64	100.45	100.16	99.06	99.42	99.37	98.55	100.37	101.27	100.50	100.27	101.78	100.96
	Trace elements in ppm															
Rb	28	20	44	6.9	17	15	15	40	6.2	16	23	7.4	8.9	6.5	7.5	5.8
Sr	455	440	482	459	561	466	678	595	307	424	468	235	252	201	260	222
Y	36	32	34	29	38	36	31	28	40	48	64	32	36	24	35	35
Zr	263	189	206	146	216	218	206	213	153	270	350	115	159	77	123	156
Nb	11.9	13.8	13.2	9.5	14.9	15.0	14.7	14.5	10.8	23.2	30.5	9.7	14.0	5.6	9.5	10.5
Ni	94	95	63	93	62	49	58	47	86	59	19	118	94	166	145	98
Ga	21.6	22.5	22.0	22.4	24.3	23.1	19.4	18.8	20.7	22.2	22.8	18.5	19.6	16.5	18.3	18.0
Cu	76	74	55	59	72	52	55	45	79	46	31	78	57	89	63	69
Zn	113	124	119	105	116	132	111	103	133	138	167	96	119	77	105	102
U	0.8	1.4	0.3	0.3	0.9	1.7	0.6	1.4	0.1	0.6	1.4	0.7	—	—	—	—
Th	2.6	3.0	5.3	0.6	2.5	4.9	1.8	5.4	—	2.4	1.2	0.6	0.9	1.6	—	0.1
Ba	791	416	662	247	578	538	782	776	548	842	1337	773	574	220	769	352
Ce	45	43	53	40	48	48	74	73	43	65	90	26	43	26	23	27
Co	31	42	35	46	32	39	30	26	45	41	30	46	53	42	52	48
La	23	23	25	16	26	27	34	37	18	38	61	12	24	10	13	15
Cr	177	50	49	33	—	52	114	80	221	70	—	275	53	360	320	288
V	209	280	238	307	—	273	204	158	305	393	—	285	290	240	286	291
Sc	19.5	25.2	21.8	26.9	—	26.0	24.5	19.2	36.6	29.9	—	37.4	32.0	34.7	36.6	37.6
$^{87}Sr/^{86}Sr$	0.70432	0.70409	0.70418	0.70397	0.70436	0.70426	0.70442	—	0.70638	0.70521	0.70557	0.70693	0.70723	0.70667	0.70668	0.70675
Age (Ma)	16.27	16.23	*16	*16	*16	15.01	14.61	13.87	12.37	11.70	11.20	9.87	9.57	8.51	8.42	8.21
Latitude	42.73	43.23	42.84	42.73	42.84	42.92	43.21	43.12	42.99	42.92	42.92	42.85	42.79	42.92	42.68	42.55
Longitude	117.05	116.88	117.22	117.05	117.15	116.98	117.14	117.03	117.07	118.00	118.04	117.32	117.60	117.38	117.36	117.18

Table 2. Continued.

	Samples:															
	H8-36	**H9-39**	**H9-27**	**H8-45**	**H8-47**	**H9-44**	**H9-49**	**H8-50E**	**H9-37D**	**H9-36C**	**H9-36A**	**H8-75A**	**H9-42**	**H9-29**	**H8-70**	**H8-57**
	Major oxides in wt. %															
SiO_2	47.55	46.34	47.71	47.48	47.79	46.96	46.97	47.87	46.07	47.48	47.42	48.68	46.77	47.08	48.79	48.47
TiO_2	1.75	2.15	0.81	1.20	1.30	1.57	1.92	1.58	1.88	1.25	0.94	0.88	1.30	1.80	1.94	2.11
Al_2O_3	15.07	14.84	16.54	16.82	15.75	16.26	15.89	16.13	15.98	16.03	16.52	16.43	16.58	16.16	16.75	16.35
Fe_2O_3	2.25	2.81	1.63	8.34	2.52	3.98	4.81	1.35	1.91	2.76	4.44	1.95	1.68	1.28	6.41	2.74
FeO	8.72	10.00	8.72	2.86	8.00	7.20	7.28	10.00	10.08	8.00	6.24	8.32	8.80	9.36	4.61	9.04
MnO	0.18	0.20	0.17	0.17	0.18	0.17	0.17	0.19	0.18	0.18	0.17	0.18	0.17	0.17	0.17	0.18
MgO	8.53	8.87	9.22	8.90	9.52	8.94	7.88	8.60	8.61	8.73	8.81	9.25	8.68	9.08	6.69	7.18
CaO	11.57	10.20	12.19	11.14	11.03	10.86	10.51	10.91	11.14	10.45	11.59	11.51	11.19	11.00	8.82	10.09
Na_2O	2.26	2.15	2.29	2.65	2.60	2.43	2.63	2.93	2.79	2.69	2.48	2.50	2.55	2.54	3.08	2.93
K_2O	0.28	0.40	0.11	0.33	0.32	0.39	0.72	0.42	0.43	0.38	0.17	0.28	0.26	0.50	1.79	1.23
P_2O_5	0.24	0.42	0.11	0.16	0.26	0.31	0.34	0.22	0.41	0.19	0.10	0.13	0.17	0.23	0.54	0.40
L.O.I.	0.97	1.53	0.89	0.60	0.59	0.44	0.85	0.49	0.86	1.46	0.65	0.93	0.80	0.82	0.61	0.87
TOTAL	99.37	99.91	100.39	100.65	99.86	99.51	99.97	100.69	100.34	99.60	99.53	101.04	98.95	100.02	100.20	101.59
	Trace elements in ppm															
Rb	5.6	6.7	2.1	5.9	5.0	7.9	15	6.3	8.1	5.7	2.7	2.3	4.4	8.7	41	27
Sr	213	292	159	273	229	275	305	261	257	241	191	196	242	282	476	460
Y	33	40	22	23	27	28	27	28	33	22	20	21	23	22	26	30
Zr	144	152	45	96	103	123	131	105	156	86	53	69	88	94	198	174
Nb	9.6	14.9	1.8	8.4	10.4	11.7	16.0	9.8	15.6	10.5	3.3	2.6	7.3	13.7	43.6	32.3
Ni	88	165	152	149	138	141	124	125	130	127	147	183	137	140	86	85
Ga	18.5	18.7	16.3	16.3	17.4	18.4	18.3	19.0	20.2	17.5	18.4	16.3	18.7	18.3	17.9	18.5
Cu	54	74	79	64	61	80	60	73	79	85	84	117	79	74	51	63
Zn	98	119	62	75	76	83	95	89	92	72	71	76	75	77	83	95
U	0.4	—	—	1.3	1.0	0.4	—	—	—	—	0.7	—	0.5	—	2.2	1.0
Th	2.0	—	1.3	0.1	1.3	0.1	1.5	0.4	0.9	—	0.2	—	—	1.4	3.3	2.3
Ba	321	2559	454	141	259	210	404	236	249	130	113	192	116	207	653	499
Ce	23	31	17	25	30	37	34	27	34	23	13	15	21	28	51	43
Co	43	52	49	50	47	45	51	48	47	45	43	50	50	50	43	42
La	12	16	6	10	12	17	13	10	15	12	4	9	8	13	29	22
Cr	306	320	278	—	313	301	253	219	232	270	318	278	240	235	129	132
V	275	277	243	—	249	254	268	265	254	247	253	229	254	248	180	231
Sc	38.1	34.1	37.7	—	36.3	37.0	31.5	34.1	34.0	32.1	35.9	34.6	35.6	31.9	23.0	28.4
$^{87}Sr/^{86}Sr$	0.70658	0.70713	0.70591	0.70457	0.70528	0.70502	0.70549	0.70533	0.70541	0.70476	0.70523	0.70462	0.70435	0.70479	0.70390	0.70486
Age (Ma)	7.58	7.20	5.04	4.09	4.06	3.84	1.86	1.55	1.49	1.25	0.91	0.44	0.44	0.36	0.25	*0
Latitude	42.55	42.62	42.14	43.21	43.21	43.14	42.96	42.89	42.79	42.83	42.83	43.22	43.08	42.63	43.03	43.00
Longitude	117.18	117.33	117.31	117.60	117.60	117.39	117.41	117.60	117.60	117.74	117.74	118.34	117.29	117.73	117.43	117.42

Table 2. Continued.

	Samples:													
	JC-4	**H86-12**	**H86-10**	**H8-62**	**H86-1**	**JC-5**	**JC-3**	**H8-63**	**JC-30B**	**JC-33**	**H8-64**	**85-28B**	**H8-66**	**H86-2**
	Major oxides in wt. %													
SiO_2	47.53	47.73	48.20	47.36	46.99	48.34	48.25	47.66	48.43	48.11	47.18	47.24	48.08	47.35
TiO_2	2.16	2.21	1.86	2.11	2.16	1.78	1.79	2.11	1.72	1.69	2.11	2.21	2.17	2.17
Al_2O_3	15.98	16.31	16.63	16.01	15.97	16.25	15.97	15.98	15.97	16.20	16.02	15.96	16.12	15.90
Fe_2O_3	2.31	1.81	1.52	2.41	2.47	1.75	2.21	2.92	2.04	2.25	4.03	4.16	3.85	6.05
FeO	8.55	8.97	8.44	8.34	8.29	7.84	7.60	7.47	7.46	7.22	6.88	6.81	6.62	5.30
MnO	0.17	0.16	0.17	0.17	0.17	0.16	0.16	0.15	0.15	0.16	0.16	0.17	0.15	0.17
MgO	9.29	9.00	8.24	8.95	9.11	8.62	8.53	8.53	9.13	9.00	8.74	8.51	8.83	9.46
CaO	9.93	9.94	10.45	9.40	9.94	9.98	10.26	9.26	9.85	10.23	9.27	9.60	9.68	9.84
Na_2O	3.08	2.93	3.03	3.21	3.04	2.67	3.01	2.85	3.07	2.80	3.10	3.39	3.26	2.86
K_2O	0.69	0.72	1.02	0.68	0.69	1.00	1.00	0.71	0.96	0.94	0.71	0.74	0.70	0.69
P_2O_5	0.29	0.32	0.39	0.31	0.30	0.41	0.41	0.37	0.43	0.37	0.29	0.32	0.36	0.30
L.O.I.	0.15	0.40	0.57	0.51	0.69	0.80	0.58	1.19	0.31	0.58	1.10	0.51	0.63	0.34
Total	100.13	100.50	100.32	99.46	99.82	99.60	99.77	99.20	99.52	99.55	99.59	99.62	100.45	100.43
	Trace elements in ppm													
Rb	12	20	26	12	12	17	17	12	19	16	15	13	15	20
Sr	655	670	484	668	653	486	498	586	528	502	675	671	585	655
Y	23	28	26	25	26	26	25	24	25	25	35	30	25	34
Zr	117	131	180	121	128	162	157	96	126	136	126	127	91	134
Nb	17.9	—	—	—	—	—	—	—	—	—	—	—	—	—
Ni	156	159	118	180	189	118	120	166	155	120	178	158	153	187
Ga	18.1	—	—	—	—	—	—	—	—	—	—	—	—	—
Cu	65	—	—	—	—	—	—	—	—	—	—	—	—	—
Zn	84	—	—	—	—	—	—	—	—	—	—	—	—	—
U	0.7	—	—	—	—	—	—	—	—	—	—	—	—	—
Th	0.4	—	—	—	—	—	—	—	—	—	—	—	—	—
Ba	262	215	230	240	212	251	240	254	238	244	259	252	277	225
Ce	27	23	39	27	27	40	—	29	34	35	27	29	27	26
Co	49	—	—	—	—	—	—	—	—	—	—	—	—	—
La	12	9	18	11	12	18	—	12	17	16	12	12	12	11
Cr	188	202	251	187	204	264	245	208	289	261	194	178	187	200
V	208	209	239	207	223	226	227	207	191	207	209	210	196	226
Sc	27.9	—	—	—	—	—	—	—	—	—	—	—	—	—
$^{87}Sr/^{86}Sr$	0.70382	0.70385	0.70405	0.70384	0.70383	0.70398	0.70398	0.70385	0.70406	0.70401	0.70385	0.70382	0.70384	0.70383
Age (Ma)	*0	*0	*0	*0	*0	*0	*0	*0	*0	*0	*0	*0	*0	*0
Latitude	43.15	43.15	43.15	43.15	43.15	43.15	43.15	43.15	43.16	43.15	43.15	43.15	43.15	43.15
Longitude	117.46	117.50	117.50	117.50	117.50	117.50	117.50	117.50	117.40	117.50	117.50	117.50	117.50	117.50

activity, and some more evolved members representing the earlier pulse of activity.

Figures 5 and 6 illustrate the relationships between selected major and trace elements and MgO. MgO is used here as an indicator of overall degree of basalt differentiation. Given the wide range in ages, vent locations, and $^{87}Sr/^{86}Sr$ ratios of these basalts (Figures 3 and 4), there is no reason to consider trends between age groups to be indicative of differentiation from a common parental magma. However, major element variations within each age group (Figure 5), such as decreasing SiO_2 and CaO and increasing TiO_2, K_2O, and P_2O_5 with decreasing MgO, do suggest that fractional crystallization has played a significant role in Owyhee Plateau basalt evolution, particularly in the two older (Steens Basalt) age groups. In addition, the wide range of CaO, Al_2O_3, TiO_2, K_2O, and P_2O_5

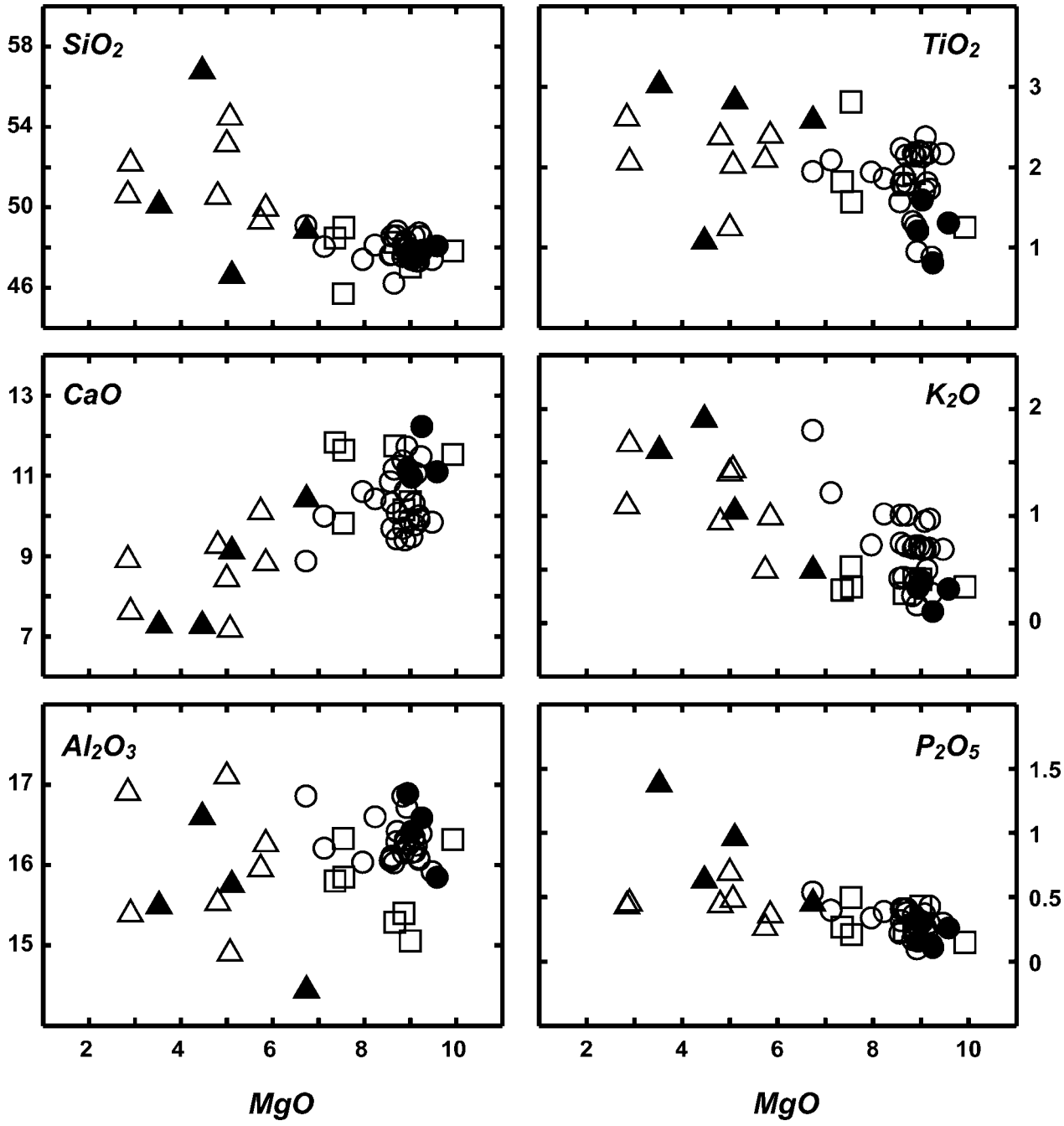

Figure 5. Major element variations with MgO content. Symbols are explained in Figure 4. All oxides reported in weight percent.

contents at the high MgO end of the spectrum suggests that variable depths and degrees of partial melting or the melting of heterogeneous source lithologies, or both, have exerted a primary control on basalt chemical signatures.

The trace element characteristics illustrated in Figure 6 support the above suggestions. For example, the correlated decreases in Ni and MgO within most age groups and decreases in Sc and MgO within the 14-17.5 Ma group suggest olivine fractionation was ubiquitous and hint that clinopyroxene removal was important during the protracted crystallization experienced by pre-11 Ma basalts. The large ion lithophile (Ba), light rare-earth (La), and high field strength (Zr) element variations also are consistent with variable degrees of crystallization, but the scatter in Ba and Zr above approximately 8 weight percent MgO suggests that multiple geochemical reservoirs probably contributed to the overall geochemical patterns. The most intriguing relationships are displayed in the Sr

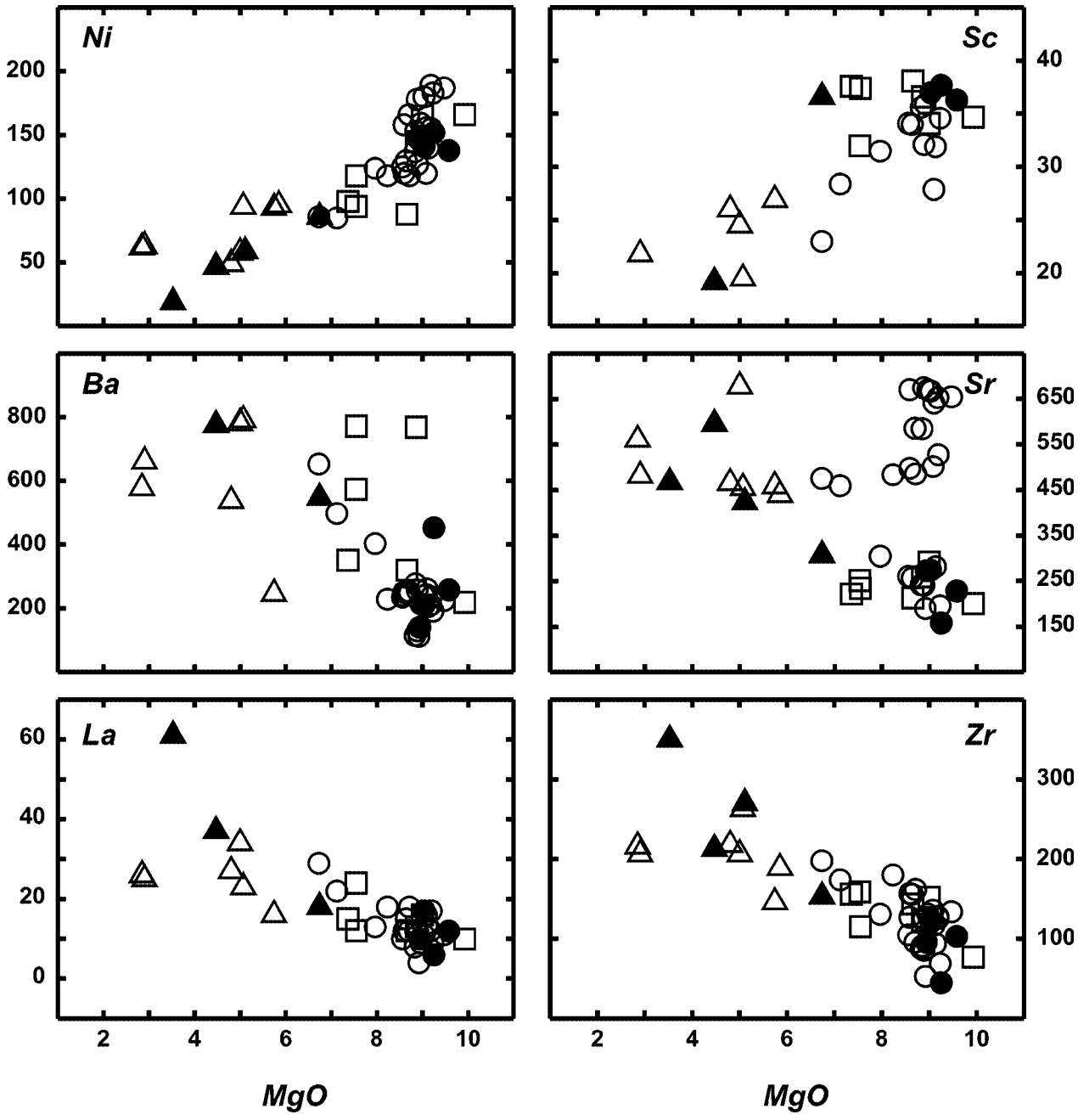

Figure 6. Trace element variations with MgO content. Symbols are explained in Figure 4. All trace elements reported in ppm.

versus MgO plot. The basalt suite is divided into high Sr (greater than 400 ppm) and low Sr (less than 300 ppm) groups. The high Sr samples span the entire observed range of differentiation and include all of the younger than 1 Ma mildly alkaline basalts and most of the older than 11 Ma lavas. These relationships, particularly the occurrence of high (approximately 650 ppm) and low (approximately 200 ppm) Sr content samples at identical high (approximately 9 weight percent) MgO contents, again suggest an important role for partial melting or source composition complexities.

The combined incompatible element characteristics of the least fractionated members of each eruptive age group (i.e., samples with high $Mg^{2+}/(Mg^{2+}+Fe^{2+})$ (Mg number), high Ni, and low SiO_2) are illustrated in the NMORB normalized trace element diagram of Figure 7. These samples have similar overall patterns characterized by strong relative enrichments in Ba and lesser relative enrichments in Nb. The sample with the most MORB-like affinities from La through Y (less than 3 Ma HAOT) has the lowest concentrations of all elements shown, yet still has Sr, K, Rb, and particularly Ba concentrations in excess of NMORB. These characteristics have previously been suggested to indicate a back-arc basin tectonomagmatic setting (Hart and others, 1984; Hart, 1985). Although similar patterns are observed through time, the absolute abundances appear to change as a function of time, as do many incompatible element ratios. These features suggest that similar heterogeneous magma sources and differentiation processes have been involved, but to varying degrees as a function of time, in the evolution of Owyhee Plateau basaltic magmatism.

As shown in Figure 3, basalts from the Owyhee Plateau have a wide range in Sr-isotope values. Close examination of these Sr-isotope characteristics for basalts restricted to the area outlined in Figure 2b reveals an intriguing relationship between the initial $^{87}Sr/^{86}Sr$ composition and the age of eruption (Figure 8). The most radiogenic Sr is associated with the basalts erupted between 11 and 6 Ma, coincident with the regional change in dominant basalt type erupted (Figure 2a). The systematic decrease in $^{87}Sr/^{86}Sr$ from this maximum to values less than or equal to 0.704 in both the oldest and youngest basalts implies a decoupling between isotope and bulk chemical characteristics.

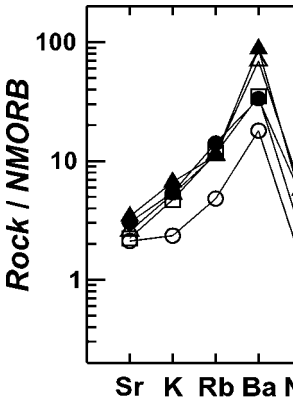

Figure 7. NMORB normalized spider diagram of trace element characteristics of samples representing the least fractionated members of each age group. Symbols are explained in Figure 4.

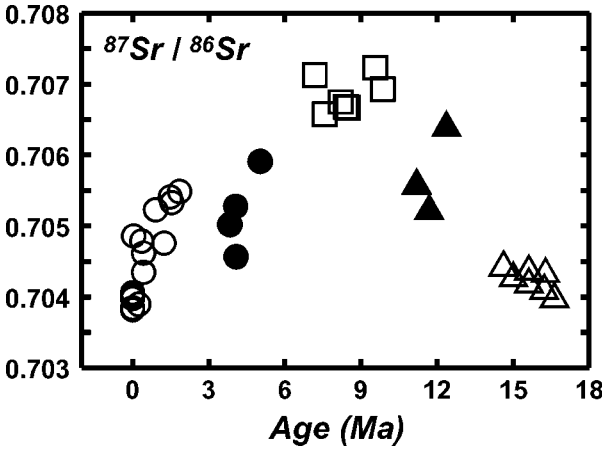

Figure 8. Variations in Sr isotope composition of Owyhee Plateau basalts with age of eruption. Symbols are explained in Figure 4. Samples plotted in this figure include only those thought to be erupted from within the area outlined in Figure 2b, thus not all Oregon Plateau samples plotted in Figure 3 are included. Note that the peak in $^{87}Sr/^{86}Sr$ around 11 Ma coincides with both the change in dominant basalt type erupted and the onset of Oregon Plateau-wide lithospheric extension.

DISCUSSION

The data so far presented clearly illustrate that Owyhee Plateau basalt bulk chemical, trace element, and isotopic parameters vary as a function of age. These variations, while systematic, often are decoupled. For example, basalts with Mg number values around 60 span nearly the entire Sr isotopic range. The discussion below focuses on these issues in an attempt to understand the processes leading to the observed features.

Figure 9 illustrates the relationships between the Sr isotopic composition and the Sr concentration and Rb/Sr ratios of the Owyhee Plateau basalts. Samples with Sr contents less than 300 ppm span a range of $^{87}Sr/^{86}Sr$ from 0.7043 to the highest value measured at 0.7072 (Figure 9a). These samples have Rb/Sr ratios between approximately 0.01 and 0.05 (Figure 9b). In contrast, samples with Sr contents in excess of 400 ppm have Rb/Sr ratios that range from 0.01 to 0.09 and a more limited range in

$^{87}Sr/^{86}Sr$ from 0.7038 to 0.7055. In particular, post-1 Ma and pre-14 Ma high Sr concentration samples (with one exception) all have $^{87}Sr/^{86}Sr$ values less than 0.7045 and define within age group trends of nearly constant $^{87}Sr/^{86}Sr$ with increasing Rb/Sr. Similar trends with flat or slightly positive slopes in $^{87}Sr/^{86}Sr$ versus Rb/Sr are observed for all other age groups with the exception of the 14-11 Ma Steens Basalts. Although defined by only three samples in Figure 9, the 14-11 Ma group occupies an intriguing "intermediate" position in terms of combined Sr concentration, $^{87}Sr/^{86}Sr$, and Rb/Sr characteristics. These characteristics may in part reflect mixing between an end member with high $^{87}Sr/^{86}Sr$ and low Sr and Rb/Sr (11-6 Ma basalts) and an end member with low $^{87}Sr/^{86}Sr$ and high Sr and Rb/Sr (high Sr sample suite).

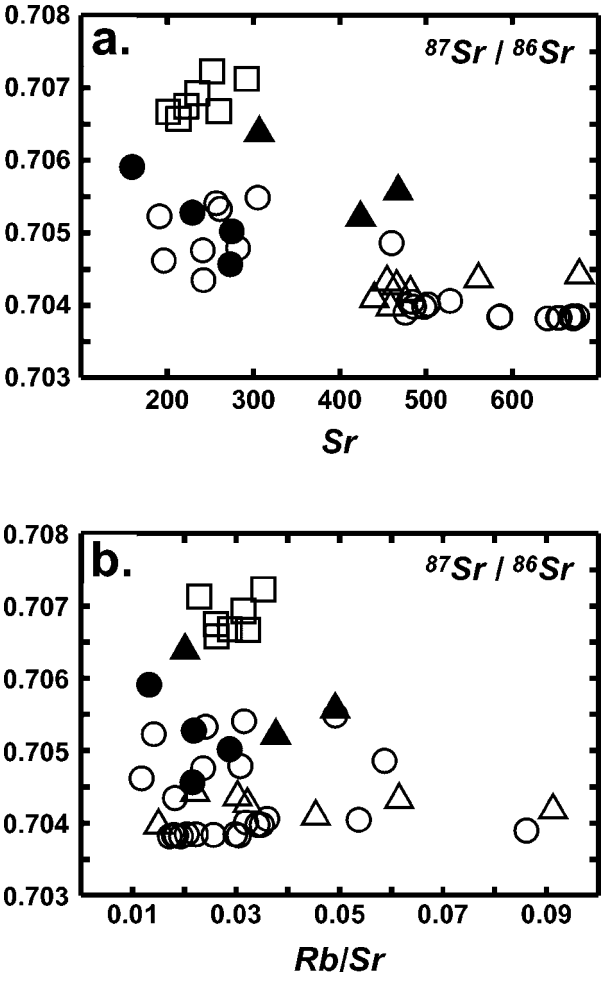

Figure 9. Variations in Sr isotope composition with Sr concentration and Rb/Sr ratio in the context of the eruptive age groups. (a) Relationship between $^{87}Sr/^{86}Sr$ and Sr concentration. (b) Relationship between $^{87}Sr/^{86}Sr$ and Rb/Sr ratio. Symbols are explained in Figure 4.

The above relationships do not rule out a role for felsic upper crustal contamination that in the Owyhee Plateau area could involve heterogeneous lithologies with $^{87}Sr/^{86}Sr$ of 0.705 to greater than 0.710 (Leeman and others, 1992 and references therein). For example, contamination of a low Sr concentration basaltic magma by felsic material at the radiogenic end of this range certainly could contribute to the high $^{87}Sr/^{86}Sr$ of the 11-6 Ma group. Such a contaminant would likely have an elevated Rb/Sr ratio; thus the low Rb/Sr ratios of the 11-6 Ma basalts are at odds with significant felsic crustal addition. This interpretation is extended to the remainder of the Owyhee Plateau basalt suite considering the observed within-group $^{87}Sr/^{86}Sr$, Rb/Sr, and Sr concentration relationships. Therefore, we interpret the relationships displayed in Figure 9 to indicate that felsic crustal contamination was not a dominant contributor to the overall geochemical characteristics observed, that distinct mantle source reservoirs were involved in Owyhee Plateau magma generation, and that magmas erupted just before the regional change in basalt geochemistry at approximately 11 Ma may preserve evidence for a combination of pre- and post-11 Ma source and process inputs.

Additional combined chemical and Sr isotope characteristics of basalts from the Owyhee Plateau are illustrated in Figure 10 in the context of the eruptive age groups. The decoupling of isotope and chemical characteristics is further highlighted by examining variations in differentiation indices such as Mg number (Figure 10a) and trace element ratios such as K/P and Zr/Nb (Figure 10b, 10c) relative to the age of eruption and Sr isotope compositions.

The plot of Mg number versus age (Figure 10a) again illustrates the regional change from strongly fractionated basalts and basaltic andesites before about 11 Ma to relatively unfractionated basalts after about 11 Ma. The same Sr isotope composition, however, can occur over a wide range of Mg number values. This implies that upper crustal assimilation accompanying crystal fractionation exerted little influence on the observed Sr isotope compositions. Thus, the first-order variations in isotopic composition are likely due to variations in relative contributions from different mantle sources through the course of Owyhee Plateau development.

The K/P ratio (Figure 10b) has been used to monitor contamination of low K/P mafic magmas by high K/P upper crustal materials (Carlson and Hart, 1987). In the Owyhee Plateau basalt suite K/P shows the least crustlike signatures at the most radiogenic Sr isotope values, and vice versa. Thus, if crustal contamination is occurring, either it is not the dominant factor controlling the chemical characteristics of these basalts, or it is taking place at

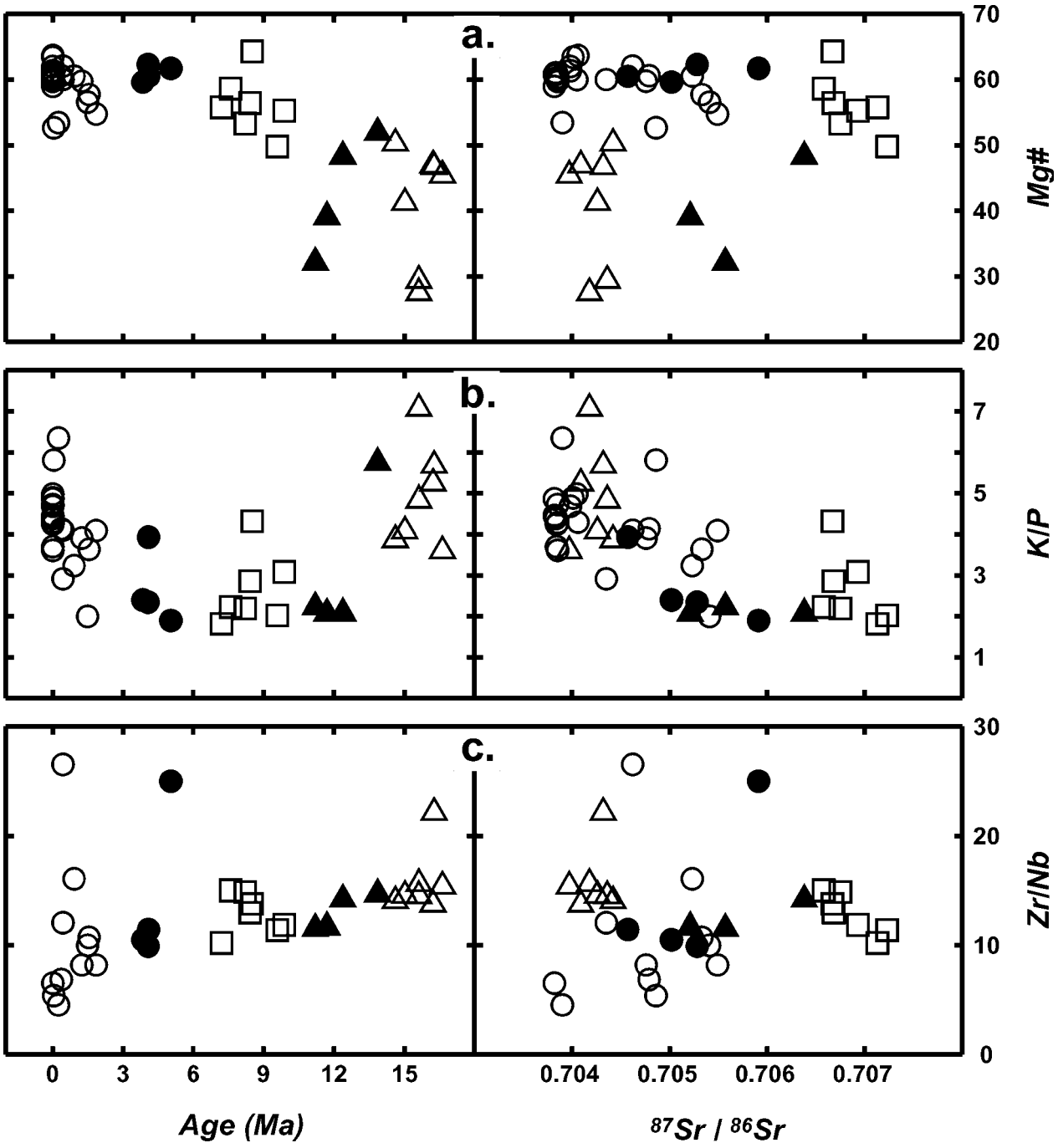

Figure 10. Variations in Mg number, K/P, and Zr/Nb in Owyhee Plateau basalts with age and $^{87}Sr/^{86}Sr$. Symbols are explained in Figure 4.

depth where the crust is likely to be more "basaltic" in composition. The relationships may be best explained by changes in the relative contributions of various source reservoirs. For example, the high $^{87}Sr/^{86}Sr$ values seen in the basalts erupted during the change in basalt geochemistry (approximately 11 Ma) may represent melts derived dominantly from the subcontinental lithospheric mantle (SCLM) that subsequently interacted little with upper crustal rocks or melts. The older and younger basalts may have a more complex history involving a larger contribution from less radiogenic sublithospheric mantle sources plus relatively greater, but still minimal amounts of local crustal contamination. If this is the case, it is significant that the peak in $^{87}Sr/^{86}Sr$ values and the change

in basalt chemistry approximately coincide with the onset of Oregon Plateau-wide lithospheric extension (Hart and Carlson, 1987; Hooper, 1990; Draper, 1991). Such extension would significantly thin the lithosphere, allowing decompression melting of the SCLM (McKenzie and Bickle, 1988; Gallagher and Hawkesworth, 1992). It would also significantly reduce the thickness of crust that the magmas would have to traverse before eruption, resulting in less differentiated basalt chemistries.

In contrast to K/P, Zr/Nb (Figure 10c) appears only to decrease slightly with decreasing age throughout the full age spectrum. Zr and Nb should not be fractionated from each other during typical melting or crystallization processes in relatively anhydrous basaltic systems. While this trend is also apparently decoupled from the trend in $^{87}Sr/^{86}Sr$ values, the implications of this relationship are not as clear. Only a few outliers in the data set, however, approach normal MORB values (Zr/Nb = 30); most samples fall in between values for continental crust and ocean island basalts (Weaver, 1991). These characteristics may lend support to the presence of subduction-modified sublithospheric upper mantle beneath the Owyhee Plateau (Carlson and Hart, 1987; Hart and others, 1997).

The aforementioned relationships suggest that the temporal development of rifting and extension in this narrowly defined region of transitional lithosphere is exerting a strong control on (1) basalt source parameters, in particular the reservoirs involved in the genesis of these magmas, and their relative contributions at various stages during the past 17.5 Ma; and (2) the subsequent magmatic differentiation histories of these basalts.

In light of these observations, the following preliminary model is offered and is keyed to the Sr isotope versus age plot of Figure 11.

Stage 1. The initial, 17.5-14 Ma, large volume flood basalts are generated from hot, upwelling sublithospheric mantle. Although these magmas may be contaminated by small amounts of melt from the SCLM and by crustal lithologies, they retain their less radiogenic Sr isotopic signature because the volume of sublithospheric mantle-derived melt is so great. In addition, these basalts have Sr concentrations in excess of 400 ppm, thus further minimizing the effects of crustal contamination accompanying upper level differentiation on the Sr isotopic composition. Significant residence time in crustal magma chambers is suggested by the evolved bulk compositions characteristic of this time interval and is consistent with the presence of thick crust at the onset of rifting.

Stage 2. The waning stages of the Steens Mountain Basalt eruptions (14-11 Ma) reflect smaller volumes of melt being generated from the sublithospheric mantle. These melts interact with melts of the SCLM as before. However, because the volume of sublithospheric mantle-derived melt is now much less, melts derived from the SCLM exert a stronger control on the Sr isotopic composition and trace element characteristics of the resulting magmas (Figures 9, 10a, and 10c)

Stage 3. The onset of Oregon Plateau-wide lithospheric extension at about 11 Ma allows decompression melting of the SCLM, particularly easily melted mafic constituents (Harry and Leeman, 1995). Basalts erupted during the 11-6 Ma interval reflect the higher $^{87}Sr/^{86}Sr$ values of the SCLM materials as melts derived therefrom dominated over sublithospheric melts. Crustal residence time and input are less significant during this interval due to the active extension of already thinned crust. While some degree of crustal contamination cannot be ruled out, its influence on basalt chemistry is more cryptic. This may reflect the involvement of more mafic crustal lithologies present as a result of the previous pulses of flood basalt activity.

Stage 4. With much of the easily melted portion of the SCLM removed, small volume magmas are produced that represent varying degrees of mixing between sublithospheric and SCLM melts, with the contribution from the SCLM lowest in the young, mildly alkaline basalts. Thus, basalts erupted during short intervals between 6 Ma and the present have more widely varying geochemical signatures.

Further testing and refinement of this model await further detailed modeling of possible basalt source melting scenarios and melt regime physical parameters as well as Nd, Pb, and Os isotopic work on samples spanning the ranges shown in Figures 9-11. In addition, further field and analytical work is in progress south of the area shown in Figure 1b in a region where numerous basalt vent localities have been identified.

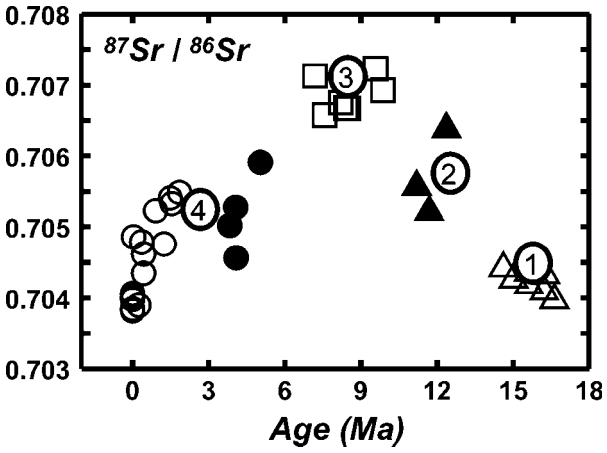

Figure 11. Preliminary model for the development of observed Sr isotope and geochemical characteristics of Owyhee Plateau basalts. Symbols are explained in Figure 4.

CONCLUSIONS

The observed geochemical and isotopic diversity in Owyhee Plateau basalts apparently cannot be attributed solely to lateral lithospheric heterogeneities or to crustal contamination accompanying upper-level differentiation. Rather, this diversity appears to be a function of the age of eruption. Furthermore, the first-order processes responsible for the generation and evolution of these magmas are apparently controlled by temporal variations not only in magmatic volume and lithospheric structure, but also in relative contributions from lithospheric and sublithospheric source reservoirs. The results of this study emphasize the importance of time as a variable in evaluating the evolution of magmas, magmatic processes, and magma source regions in complex continental igneous provinces.

ACKNOWLEDGMENTS

The authors gratefully acknowledge financial support from the Geological Society of America (Lipman Research Award, 5929-96; Shoemaker), the National Science Foundation (EAR-9204780; Hart), the Miami University Graduate School Dissertation Research Support Fund (Shoemaker), the Miami University Committee on Faculty Research (Hart), and the Miami University Geology Department. We would like to thank Stan Mertzman of Franklin and Marshall College for making his XRF facility available, and John Morton of Miami University for his assistance with the Sr isotope and DCP major and trace element analyses. Our gratitude is also extended to Matt Heizler of the New Mexico Geochronological Research Laboratory for performing the $^{40}Ar/^{39}Ar$ analyses. Reviews by Roger Stewart, Craig White, and Scott Hughes helped to clarify the content and improve the readability of this contribution.

REFERENCES

Bohannon, R.G., and T. Parsons, 1995, Tectonic implications of post-30 Ma Pacific and North American relative plate motions: Geological Society of America Bulletin, v. 107, p. 937-959.

Boyd, F.R., and S.A. Mertzman, 1987, Composition and structure of the Kaapvaal lithosphere, southern Africa, *in* B.O. Mysen, ed., Magmatic Processes—Physicochemical Principles: The Geochemical Society Special Publication 1, p. 13-24.

Camp, V.E., 1995, Mid-Miocene propagation of the Yellowstone mantle plume head beneath the Columbia River basalt source region: Geology, v. 23, p. 435-438.

Carlson, R.W., 1984, Isotopic constraints on Columbia River flood basalt genesis and the nature of the subcontinental mantle: Geochimica et Cosmochimica Acta, v. 48, p. 2357-2372.

Carlson, R.W., and W.K. Hart, 1987, Crustal genesis on the Oregon Plateau: Journal of Geophysical Research, v. 92, p. 6191-6206.

———, 1988, Flood basalt volcanism in the northwestern United States, *in* J.D. Macdougall, ed., Continental Flood Basalts: Kluwer Academic Publishers, p. 35-61.

Carlson, R.W., G.W. Lugmair, and J.D. Macdougall, 1981, Columbia River volcanism: The question of mantle heterogeneity or crustal contamination: Geochimica et Cosmochimica Acta, v. 45, p. 2483-2499.

Christiansen, R.L., and E.H. McKee, 1978, Late Cenozoic volcanic and tectonic evolution of the Great Basin and Columbia intermontane regions, *in* R.B. Smith and G.P. Eaton, eds., Cenozoic Tectonics and Regional Geophysics of the Western Cordillera: Geological Society of America Memoir 152, p. 283-311.

Draper, D.S., 1991, Late Cenozoic bimodal magmatism in the northern Basin and Range Province of southeastern Oregon: Journal of Volcanology and Geothermal Research, v. 47, p. 299-328.

Elison, M.W., R.C. Speed, and R.W. Kistler, 1990, Geologic and isotopic constraints on the crustal structure of the northern Great Basin: Geological Society of America Bulletin, v. 102, p. 1077-1092.

Ferns, M.L., 1997, Field trip guide to the eastern margin of the Oregon-Idaho graben and the middle Miocene calderas of the Lake Owyhee volcanic field: Oregon Geology, v. 59, p. 9-20.

Gallagher, Kerry, and Chris Hawkesworth, 1992, Dehydration melting and the generation of continental flood basalts: Nature, v. 358, p. 57-59.

Geist, Dennis, and Mark Richards, 1993, Origin of the Columbia Plateau and Snake River Plain: Deflection of the Yellowstone plume: Geology, v. 21, p. 789-792.

Harry, D.L., and W.P. Leeman, 1995, Partial melting of melt metasomatized subcontinental mantle and the magma source potential of the lower lithosphere: Journal of Geophysical Research, v. 100, p. 10,255-10,269.

Hart, W.K., 1985, Chemical and isotopic evidence for mixing between depleted and enriched mantle, northwestern U.S.A.: Geochimica et Cosmochimica Acta, v. 49, p. 131-144.

———, 1996, Petrogenesis of Quaternary Oregon Plateau alkaline basalts: Geological Society of America Abstracts with Programs, v. 28, p. 73.

———, 1997, Plume-asthenosphere-lithosphere interactions through time: A comparison of Ethiopian and northwestern USA basalts: Geological Society of America Abstracts with Programs, v. 29, p. 298.

Hart, W.K., J.L. Aronson, and S.A. Mertzman, 1984, Areal distribution and age of low-K, high-alumina olivine tholeiite magmatism in the northwestern Great Basin: Geological Society of America Bulletin, v. 95, p. 186-195.

Hart, W.K., and R.W. Carlson, 1983, K-Ar ages of late Cenozoic basalts from southeastern Oregon, southwestern Idaho, and northern Nevada: Isochron/West, v. 38, p. 23-26.

———, 1985, Distribution and geochronology of Steens Mountain-type basalts from the northwestern Great Basin: Isochron/West, v. 43, p. 5-10.

———, 1987, Tectonic controls on magma genesis and evolution in the northwestern United States: Journal of Volcanology and Geothermal Research, v. 32, p. 119-135.

———, 1992, The development of the Oregon Plateau: Perspectives from Neogene mafic to intermediate volcanism: Geological Society of America Abstracts with Programs, v. 24, p. 32.

Hart, W.K., R.W. Carlson, and S.A. Mosher, 1989, Petrogenesis of the Pueblo Mountains basalt, southeastern Oregon and northern Nevada, *in* S.P. Reidel and P.R. Hooper, eds., Volcanism and Tectonism in the Columbia River Flood Basalt Province: Geological Society of America Special Paper 239, p. 367-378.

Hart, W.K., R.W. Carlson, and S.B. Shirey, 1997, Radiogenic Os in primitive basalts from the northwestern U.S.A.: Implications for petrogenesis: Earth and Planetary Science Letters, v. 150, p. 103-116.

Hart, W.K., and S.A. Mertzman, 1982, K-Ar ages of basalts from southcentral and southeastern Oregon: Isochron/West, v. 33, p. 23-26.

———, 1983, Late Cenozoic volcanic stratigraphy of the Jordan Valley area, southeastern Oregon: Oregon Geology, v. 45, p. 15-19.

Hooper, P.R., 1990, The timing of crustal extension and the eruption of continental flood basalts: Nature, v. 345, p. 246-249.

Hooper, P.R., and C.J. Hawkesworth, 1993, Isotopic and geochemical constraints on the origin and evolution of the Columbia River Basalt: Journal of Petrology, v. 34, p. 1203-1246.

Lambert, R. StJ., V.E. Chamberlain, and J.G. Holland, 1995, Ferro-andesites in the Grande Ronde Basalt: Their composition and significance in studies of the origin of the Columbia River Basalt Group: Canadian Journal of Earth Sciences, v. 32, p. 424-436.

Le Bas, M.J., R.W. Le Maitre, A. Streckeisen, and B. Zanettin, 1986, A chemical classification of volcanic rocks based on the total alkali-silica diagram: Journal of Petrology, v. 27, p. 745-750.

Leeman, W.P., 1982, Tectonic and magmatic significance of strontium isotopic variations in Cenozoic volcanic rocks from the western United States: Geological Society of America Bulletin, v. 93, p. 487-503.

Leeman, W.P., and W.I. Manton, 1971, Strontium isotopic composition of basaltic lavas from the Snake River Plain, southern Idaho: Earth and Planetary Science Letters, v. 11, p. 420-434.

Leeman, W.P., J.S. Oldow, and W.K. Hart, 1992, Lithosphere-scale thrusting in the western U.S. Cordillera as constrained by Sr and Nd isotopic transitions in Neogene volcanic rocks: Geology, v. 20, p. 63-66.

Le Maitre, R.W., 1976, Some problems of the projection of chemical data into mineralogical classifications: Contributions to Mineralogy and Petrology, v. 56, p. 181-189.

Mark, R.K., H.R. Bowman, F. Asaro, E.H. McKee, and R.R. Coats, 1975, A high $^{87}Sr/^{86}Sr$ mantle source for low alkali tholeiite, northern Great Basin: Geochimica et Cosmochimica Acta, v. 39, p. 1671-1678.

McKenzie, D., and M.J. Bickle, 1988, The volume and composition of melt generated by extension of the lithosphere: Journal of Petrology, v. 29, p. 625-679.

Noble, D.C., C.E. Hedge, E.H. McKee, and M.K. Korringa, 1973, Reconnaissance study of the strontium isotope composition of Cenozoic volcanic rocks in the northwestern Great Basin: Geological Society of America Bulletin, v. 84, p. 1393-1406.

Pierce, K.L., and L.A. Morgan, 1992, The track of the Yellowstone hot spot: Volcanism, faulting, and uplift, *in* P.K. Link, M.A. Kuntz, and L.B. Platt, eds., Regional Geology of Eastern Idaho and Western Wyoming: Geological Society of America Memoir 179, p. 1-53.

Russell, J.K., G.T. Nixon, and T.H. Pearce, 1988, Petrographic constraints on modeling the crystallization of basalt magma, Cow Lakes, southeast Oregon: Canadian Journal of Earth Sciences, v. 25, p. 486-494.

Sterner, Ray, 1997, Shaded relief map of Oregon: Johns Hopkins University Applied Physics Laboratory, http://fermi.jhuapl.edu/states.

Weaver, B.L., 1991, Trace element evidence for the origin of ocean-island basalts: Geology, v. 19, p. 123-126.

Wright, J.E., and J.L. Wooden, 1991, New Sr, Nd, and Pb isotopic data from plutons in the northern Great Basin, USA: Implications for crustal structure and granite petrogenesis in the hinterland of the Sevier thrust belt: Geology, v. 19, p. 457-460.

Zoback, M.L., E.H. McKee, R.J. Blakely, and G.A. Thompson, 1994, The northern Nevada rift: Regional tectono-magmatic relations and middle Miocene stress direction: Geological Society of America Bulletin, v. 106, p. 371-382.

Geochemical and Sr-Isotopic Variations in Western Snake River Plain Basalts, Idaho

Craig M. White,[1] William K. Hart,[2]
Bill Bonnichsen,[3] and Debra Matthews[1]

ABSTRACT

Secular variations in chemical and Sr-isotopic compositions are examined in a suite of western Snake River Plain basalts exposed in a 1,000 square-km area centered on the town of Melba. Basalts in the area erupted from numerous centers during two major periods of volcanism between about 9 Ma and 0.4 Ma. The first phase (M1) was most active between 9-7 Ma and produced olivine tholeiites characterized by moderate TiO_2 (1.7-2.5 percent), low K_2O (less than 0.5 percent), low excluded trace elements, and $^{87}Sr/^{86}Sr$ ratios of 0.706-0.707. The second phase, at about 2.0-0.4 Ma, produced two chemically distinctive groups of basalts, one strongly tholeiitic (M2) and the other mildly alkaline (M3). The (M2) tholeiites have low Si and Al, high Fe, Ti, and P, low LILE/HFSE ratios, and $^{87}Sr/^{86}Sr$ ratios typically around 0.707 (± 0.0003). The slightly alkaline basalts (M3) are characterized by greater K, Na, Rb, and Sr, higher LILE/HFSE ratios, and $^{87}Sr/^{86}Sr$ ratios between 0.705 and 0.706. Field mapping and $^{40}Ar/^{39}Ar$ dating indicate the M3 lavas are younger than the M2 basalts, with the transition from tholeiitic to more alkaline compositions taking place around 0.8 Ma.

MELTS models indicate that most of the Melba area basalts evolved primarily by fractional crystallization at depths of about 8 km, roughly coincident with the depth at which seismic velocities increase beneath the western SRP. Some of the most evolved lavas within each group have slightly elevated Sr-isotopic ratios relative to other basalts in the same group, and this is attributed to assimilation of shallow crustal rocks. However, the apparent decoupling of the chemical compositions and $^{87}Sr/^{86}Sr$ ratios in the Melba area lavas is inconsistent with a crustal source for the LILE enrichment and greater alkali contents in the M3 basalts. Instead, the data require that the M3 basalts originated in a mantle source that was chemically and isotopically distinctive from the source for M2 and M1 magmas. Chemical similarities between M3 lavas and ocean-island basalts suggest that the M3 magmas had their origin within the asthenosphere. In contrast, the low LILE/HFSE ratios and higher $^{87}Sr/^{86}Sr$ in the M1 and M2 basalts appear to require multiple sources or a single lithospheric source that had a complex history of both enrichment and depletion. The implied shift to deeper mantle source regions is consistent with models in which melting is caused by extension and thinning of the lithosphere and does not necessarily imply a direct role for the Yellowstone mantle plume.

Key words: Snake River Plain, basalt petrology, rift magmas, Sr-isotopes

INTRODUCTION

The western Snake River Plain (SRP) is a northwest-trending topographic lowland that extends from the Twin Falls area, where it intersects the main axis of the northeast-trending Snake River Plain Volcanic Province, past Boise, and into eastern Oregon near the town of Nyssa. Northeast-southwest extension during the last 10-12 Ma produced the complex western SRP graben, which is now filled with as much as 4,000 m of silicic and basaltic volcanic rocks and lacustrine sediments (Mabey, 1982; Wood, 1994; Wood and Clemens, this volume). Volcan-

Editors' note: The manuscript was submitted in July 1998 and has been revised at the authors' discretion.

[1]Department of Geosciences, Boise State University, Boise, ID 83725
[2]Geology Department, Miami University, Oxford, OH 45056
[3]Idaho Geological Survey, University of Idaho, Moscow, ID 83843

White, C.M., W.K. Hart, Bill Bonnichsen, and Debra Matthews, 2002, Geochemical and Sr-isotopic variations in western Snake River Plain basalts, Idaho, *in* Bill Bonnichsen, C.M. White, and Michael McCurry, eds., Tectonic and Magmatic Evolution of the Snake River Plain Volcanic Province: Idaho Geological Survey Bulletin 30, p. 329-342.

ism in the western SRP produced voluminous rhyolitic tuffs and lava flows between about 12-10 Ma, but has been exclusively basaltic since about 9 Ma. Our paper focuses on the basalts in a 1,000-square-km area centered on the town of Melba in the south-central part of the western SRP between about long 116º25′W. and long 116º45'W. (Figure 1). This area is particularly well suited for studying the geochemical variations of western SRP basalts through time because the stratigraphic relations and areal distributions of vents and flows have been well established by geologic mapping (Bonnichsen and Godchaux, 1998; Othberg and Stanford, 1992).

Lake Idaho, which occupied the western SRP for much or all of the time between 11 and 1 Ma (Jenks and Bonnichsen, 1989), was the primary factor that controlled the physical nature of basaltic volcanism in the Melba area. A wide variety of hydrovolcanic deposits and land forms were created depending on water depth and the degree to which magmas interacted with lake water or water-saturated sediments (Godchaux and others, 1992). The oldest basalts in the area occur as pillow lavas, pillow breccias and hyaloclastites, indicating they were erupted beneath a relatively deep Lake Idaho or flowed into the lake from highlands to the south. They range in age between 9-4 Ma, but most were probably erupted between 9-7 Ma (Ekren and others, 1981; Hart and Aronson, 1983; Amini and others 1984). A younger episode of basaltic volcanism, ranging from 2-0.4 Ma, can be divided into two phases. The first, at about 2.0-0.8 Ma, produced hydrovolcanic constructs, including tuff cones and maar-tuff ring complexes. Godchaux and others (1992) attributed these deposits to explosive phreatomagmatic eruptions caused by the interaction of basaltic magma with ground water or shallow surface water during the waning stages of the lake. The second phase, between about 0.8 and 0.4 Ma, mainly produced subaerial lava flows associated with broad, low-profile shield volcanoes.

We refer to the oldest group of dominantly subaqueous basalts as the Group 1 Melba-area basalts (M1). The hydrovolcanic rocks produced during the first phase of the younger volcanic episode we refer to as the M2 basalts, and the youngest, mainly subareal lavas we call the M3 basalts. Mafic lavas erupted during each of these phases have distinctive geochemical characteristics, as illustrated by the triangular diagram of MgO-TiO_2-K_2O used by Hart and others (1984) to distinguish different types of basalt in the northwestern Basin and Range (Figure 2). The M1 lavas plot in or near the field of low K, high Ti transitional basalts (TB). These basalts are intermediate in composition between the mid-oceanic-ridge basalt (MORB)-like high-alumina olivine tholeiites (HAOT) of the Owyhee Plateau and the more evolved tholeiites of the Snake River Plain (SROT). Basalts in the M2 group plot in or near the field of typical SROT, whereas most of the M3 lavas plot within the field of "alkali-olivine basalts"

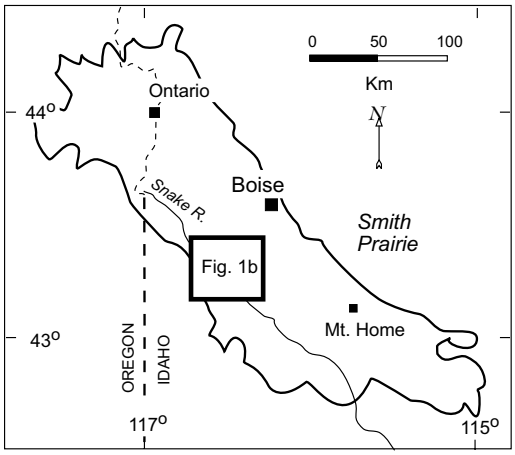

Figure 1A

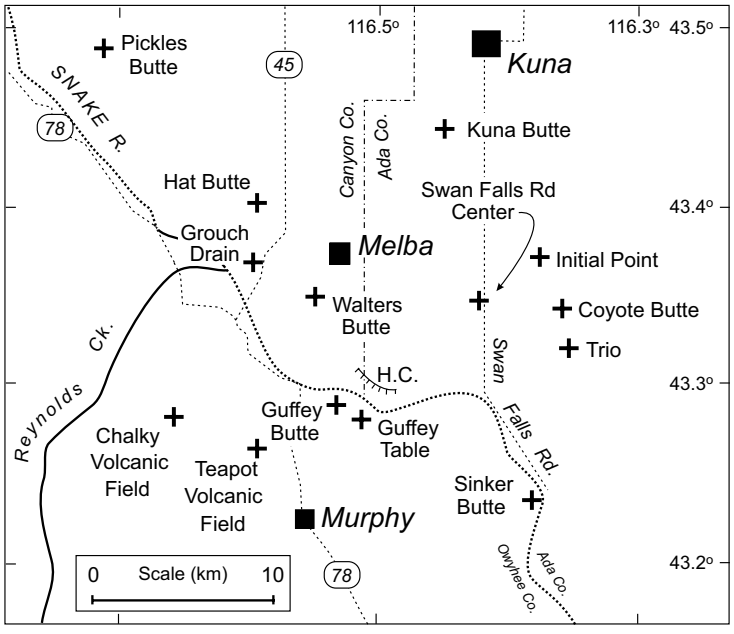

Figure 1B

Figure 1. Index maps: (A) The locations of the Melba area and Smith Prairie relative to the general outline of the western SRP. (B) The Melba area and the locations of basaltic eruptive centers discussed in the text.

(AOB), although most of these rocks would best be described as transitional between olivine tholeiite and AOB. The abrupt change at around 0.8 Ma from strongly tholeiitic basalt volcanism to the eruption of more alkali-rich lavas is the most striking feature of the chemical stratigraphy in the Melba area. It must reflect a shift of regional importance because Vetter and Shervais (1992) reported a similar change from tholeiitic to more alkaline magmatism in the basalts of the Boise River Group in the Smith Prairie region about 25 km north of the SRP (Figure 1). They noted that all of the borderline alkaline lavas in this area are younger than 0.7 Ma, on the basis of the potassium-argon ages of Howard and others (1982).

DESCRIPTION OF BASALTS

ANALYTICAL TECHNIQUES

The major and trace element compositions of fifty Melba area basalts were determined using the Rigaku 3370 XRF spectrometer at Washington State University's Geoanalytical Laboratory. A detailed description of methods and procedures used for XRF analyses in this laboratory is given by Hooper and Johnson (1989). About thirty samples were also analyzed for rare earth elements (REE) and additional trace elements with the Sciex ICP-mass spectrometer at the Washington State University laboratory. These data augmented XRF major-element analyses by Bonnichsen for basalts in the study area (McCurrey and others, 1997). Sr-isotopic ratios were analyzed by thermal ionization mass spectrometry at Miami University; the analytical methods are described by Shoemaker and Hart (this volume). Seven new $^{40}Ar/^{39}Ar$ ages were determined by R. A. Duncan at Oregon State University using total laser fusion of whole rock or plagioclase. A general description of the techniques used in this laboratory can be found in Storey and others (1998).

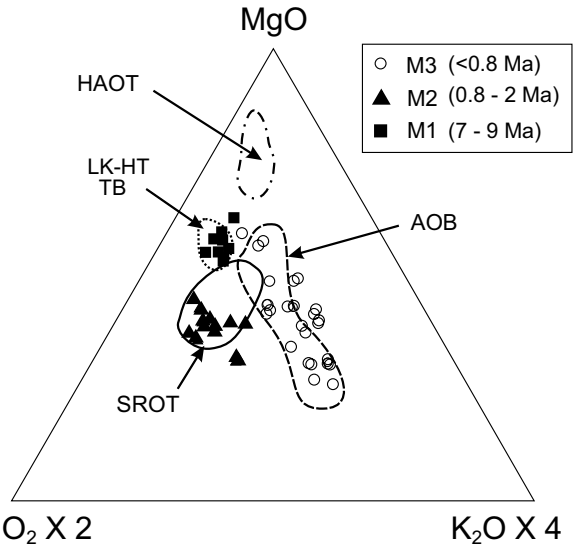

Figure 2. Analyses of Melba area basalts plotted on the diagram of Hart and others (1984) used to distinguish different types of basalt in the northern Basin and Range.

FIELD OCCURRENCES, PETROGRAPHY AND RADIOMETRIC AGES

The best exposures of the pillow lavas, breccias, and tuffs that compose most of the (M1) basalts are located near Murphy and in the Owyhee Mountains foothills near Reynolds Creek (Figure 1). Field descriptions of these rocks are given by Godchaux and others (1992) and McCurry and others (1997). ^{40}Ar-^{39}Ar dating of one sample from the Murphy area and one from near Reynolds Creek yielded ages of 7.85 and 7.92 Ma, respectively (Table 1). The dated samples were fine-grained holocrystalline basalt from the interiors of flows or shallow intrusions, but rocks in this group more typically consist of pillows or hyaloclastites containing small crystals of olivine and plagioclase in a matrix of black glass.

The M2 basalts consist mainly of lavas and pyroclastic rocks associated with hydrovolcanic centers dissected by the Snake River and now well exposed within and adjacent to the Snake River canyon. A subset of this group with distinctive chemical compositions comprises several small eruptive points (Coyote Butte, Trio Butte, Swan Falls Road center) closer to the axis of the western SRP (Figure 1). ^{40}Ar-^{39}Ar ages of M2 basalts range from 1.79 Ma to 0.90 Ma. M2 lavas contain the same phenocryst assemblage as M1 basalts but are generally more coarsely porphyritic and may contain plagioclase phenocrysts as much as 7 mm long.

Most of the analyzed M3 basalts were erupted from vents associated with the broad shield volcanoes at Kuna Butte, Powers Butte, and Initial Point (Figure 1). Othberg and others (1995) reported ^{40}Ar-^{39}Ar incremental-heating ages of approximately 0.40 Ma for basalts at Kuna Butte and Initial Point, and numerous field checks with a fluxgate magnetometer confirmed that all the exposed lavas in this complex have normal remanent magnetic polarities. Basalts from the hydrovolcanic centers at Guffey Table and Grouch Drain are also included in the M3 group because they are closer in chemical composition to the lavas of the Kuna Butte-Initial Point eruptive complex than they are to the strongly tholeiitic M2 basalts. Samples from each of these centers yielded total fusion ^{40}Ar-^{39}Ar ages of about 0.75 Ma (Table 1), indicating they

Table 1. $^{40}Ar/^{39}Ar$ ages of western SRP basalts from the Melba area.

Sample No.	Eruptive Center	Polarity	Age (Ma)	% $^{40}Ar^*$
CM-16B	Chalky	R	7.92 ± 0.19	27.4
MB-5	Teapot	R	7.85 ± 0.19	26.5
CM-17	Walters Butte	R	1.89 ± 0.09	25.0
I-2664	Hat Butte	N	0.96 ± 0.16	5.3
CM-14	Swan Falls Road	R	0.90 ± 0.04	6.3
I-2725	Guffey Table	R	0.76 ± 0.13	9.8
I-2715	Grouch Drain	N	0.73 ± 0.11	24.7

are transitional in age between M2 basalts and the younger Kuna Butte-Initial Point flows. M3 basalts typically contain phenocrysts of olivine from 0.5 to 1.5 mm across and plagioclase from 1 to 2 mm long in a groundmass that ranges in texture from hyaloophitic to intergranular.

CHEMICAL AND SR-ISOTOPIC COMPOSITIONS

Chemical Classification

Most of the chemically analyzed mafic lavas plot as basalts on the alkalis versus silica classification diagram of LeBas and others (1986; Figure 3). Exceptions include two of the M2 lavas, which contain less than 45 percent SiO_2 and plot in the basanite field, and eight of the M3 lavas, which contain enough total alkalis to be classified as trachybasalts. All samples in the M1 group and about half of those in M2 are olivine tholeiites according to the normative classification scheme of Yoder and Tilley (1962). The remaining M2 samples are quartz tholeiites. Most of the analyzed M3 samples are also olivine tholeiites, but three contain normative nepheline and would therefore be classified as alkali-olivine basalt.

Major Elements

Representative analyses of mafic lavas from the Melba area are given in Table 2. Selected oxides are plotted versus MgO in Figure 4, along with the compositional range of basalts from Craters of the Moon (COM; Kuntz and others, 1983) and the averages of multiple analyses of "older" (greater than 5 Ma) and "younger" (less than 5 Ma) SRP basalts based mainly on analyses of lavas from the central SRP (Fitton and others, 1991). The range of differentiation in each of the two older suites is relatively narrow, with the M1 basalts being consistently more MgO rich than the M2 lavas. In contrast, the wide spread of MgO contents in M3 basalts overlaps nearly the entire range of values in both of the older groups. Other notable differences among the three groups are the low SiO_2 and Al_2O_3 and the high total FeO, TiO_2 and P_2O_5 contents of most M2 lavas, and the greater K_2O in M3 basalts (Figure 4).

Major elements in M1 basalts have values similar to those of the average "older" (greater than 5 Ma) central SRP tholeiite of Fitton and others (1991). The average composition of "younger" (less than 5 Ma) central SRP basalts is transitional between M1 and M2 on most of the major-element plots. This suggests that western SRP tholeiites may be, on average, more strongly differentiated than those in the central SRP. On the other hand, the tholeiites in the Melba area are not as strongly evolved as COM lavas, nor do they appear to plot on the differentiation trend connecting COM lavas with the average "young" SRP tholeiite. Despite these differences, however, the major-element trends defined by M1 and M2 lavas are roughly similar to the typically tholeiitic trend for central and eastern SRP basalts, whereas the M3 basalts define very different trends for most oxides.

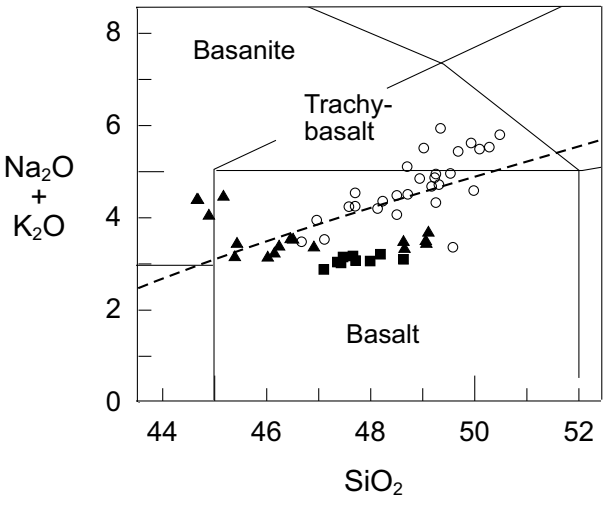

Figure 3. Analyses of Melba area basalts plotted on the alkalis-silica classification diagram of Le Bas and others (1986). The dashed line separates the fields of alkaline and subalkaline rocks (Irvine and Baragar, 1971). Symbols are the same as in Figure 2.

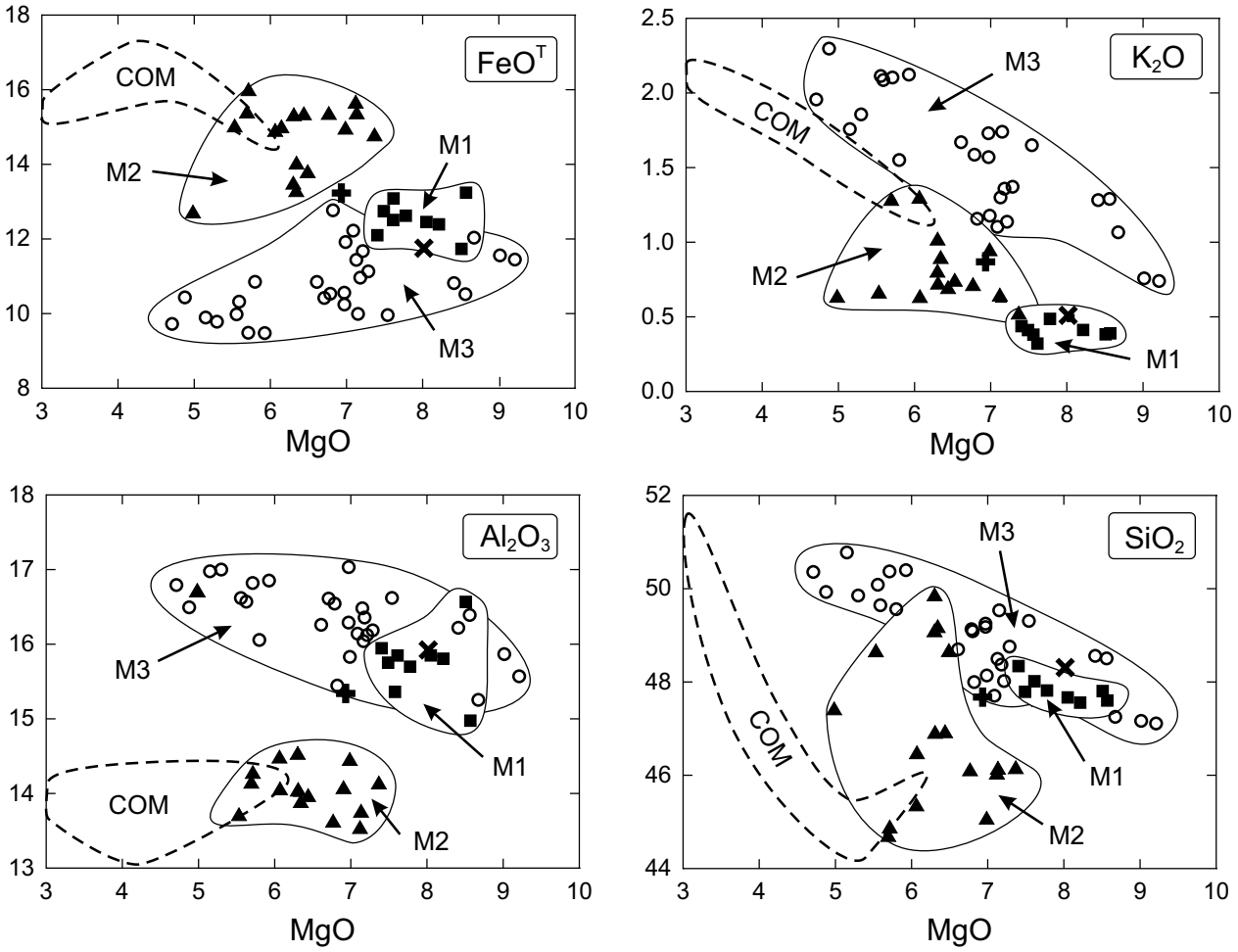

Figure 4. Variations of selected major elements in Melba area basalts plotted versus weight percent MgO. Symbols for Melba area basalts are the same as in Figure 2. The averages of 28 older (greater than 5 Ma) SRP basalts and 112 younger (less than 5 Ma) basalts (Fitton and others, 1992) are indicated by the (X) and (+), respectively. The dashed line indicates the compositional field of evolved lavas from Craters of the Moon (Kunz and others, 1983).

Trace Elements

The division of basalts in the study area into three groups is further supported by systematic differences in the concentrations of incompatible trace elements and in trace-element ratios (Table 2 and Figure 5). M1 lavas have low concentrations of incompatible elements compared to the younger basalts, particularly in Sr, Nb, Ba, Th, and Ta. M2 basalts have high concentrations of Zr, Y, REEs, Hf, and Pb compared to the other groups, and M3 lavas contain the most Rb and Sr. Ratios of large ion lithophile elements to high field strength elements (LILE/HFSE) are generally greatest in the M3 samples, although there is considerable overlap with the M2 basalts for Ba/Nb and Ba/Ta. Ratios of very incompatible elements (VICE) such as Ba, Rb, Nb, Th, and La to moderately incompatible elements (MICE) such as Y, Zr, Hf, and Yb are also greatest in the basalts of the M3 group. Both of these trends appear to reflect a strong tendency for M3 basalts to have higher element ratios when the numerator is a more incompatible element than the denominator according to the criteria of Sun and McDonough (1989) for mantle-derived liquids. This relationship is particularly notable for Th/Hf, K/Ti, Nb/Zr, Sr/Y, Rb/Hf, and La/Yb, but it does not hold for Ba/K, which is consistently greater in the M1 and M2 basalts than it is in the M3 lavas.

All of the analyzed Melba area basalts produce light rare earth element (LREE) enriched patterns on chondrite-normalized diagrams (Figure 6). M1 samples generally have the lowest concentrations of LREEs. M2 lavas have the highest, and the M3 basalts plot between the other two. One notable exception is the sample from Grouch Drain volcano (I-2715), which is included in Group 3 because of its major-element composition but

Table 2. Chemical compositions and $^{87}Sr/^{86}Sr$ ratios of western SRP basalts from the Melba area.

Sample (Group)	**1 (M1)**	**2 (M1)**	**3 (M1)**	**4 (M1)**	**5 (M2)**	**6 (M2)**	**7 (M2)**	**8 (M2)**	**9 (M2)**	**10 (M2)**
Field No.	**MB-5**	**CM-16B**	**CM-11**	**CM-25**	**CM-20**	**I-2664**	**WS1-2**	**CM-7**	**CM-14**	**CM-21**
Eruptive Center	**Teapot**	**Chalky**	**Teapot**	**Sinker Creek**	**Pickles Butte**	**Hat Butte**	**Walters Butte**	**Guffey Butte**	**Swan Falls Road**	**Coyote Butte**
XRF (weight %)										
SiO_2	47.47	48.19	47.71	47.10	46.91	46.15	49.06	48.65	44.66	44.68
TiO_2	1.78	2.31	2.32	2.44	3.61	3.56	3.10	3.40	3.79	3.90
Al_2O_3	16.45	15.82	15.01	15.24	13.96	14.13	13.85	13.97	14.13	14.21
FeO	11.65	12.72	13.27	12.98	15.33	14.77	13.98	13.78	15.37	15.91
MnO	0.19	0.19	0.19	0.21	0.23	0.23	0.21	0.22	0.25	0.23
MgO	8.45	7.84	8.59	7.52	6.44	7.37	6.33	6.49	5.69	5.69
CaO	9.95	10.17	9.71	10.49	9.43	9.90	9.11	9.50	9.49	8.92
Na_2O	2.74	2.69	2.65	2.52	2.63	2.67	2.57	2.57	3.07	3.07
K_2O	0.38	0.49	0.39	0.33	0.69	0.52	0.89	0.72	1.28	1.28
P_2O_5	0.24	0.36	0.39	0.38	0.76	0.71	0.68	0.69	2.20	1.68
Total	99.30	100.78	100.23	99.21	99.99	100.01	99.78	99.99	99.93	99.57
XRF (ppm)										
Ni	83	75	68	94	42	73	68	60	27	41
Cr	94	185	291	232	141	207	150	156	71	77
Sc	30	34	30	27	29	30	27	31	30	30
V	266	284	285	310	371	362	295	343	288	267
Ba	171	280	238	457	630	446	458	464	738	845
Rb	3	5	3	1	7	5	18	15	29	26
Sr	230	241	269	289	320	310	322	333	321	318
Zr	96	125	130	145	262	262	245	253	374	341
Y	29	33	33	34	42	41	46	47	72	61
Nb	10	15	14	19	34	25	27	26	68	59
Cu	44	36	34	58	26	18	27	144	30	43
Zn	100	111	112	115	147	151	145	148	168	174
ICP-MS (ppm)										
La	9.52	15.01	14.53	17.50	35.70	27.68	28.17	27.66	58.51	48.97
Ce	20.91	31.52	30.77	37.50	70.70	57.62	57.55	56.90	122.60	102.20
Pr	2.90	4.17	4.15	4.95	8.62	7.46	7.53	7.46	15.60	13.00
Nd	13.97	19.83	19.15	22.85	37.50	34.32	34.09	34.70	70.15	58.76
Sm	4.30	5.75	5.49	6.32	9.59	9.01	9.08	9.03	16.97	14.88
Eu	1.61	2.03	2.01	2.18	3.22	3.16	3.06	3.11	4.99	4.47
Gd	4.81	5.99	5.81	6.78	9.52	8.83	8.88	8.94	15.58	14.29
Tb	0.90	1.06	1.06	1.17	1.58	1.47	1.50	1.53	2.56	2.34
Dy	5.66	6.63	6.49	6.77	9.03	8.80	9.12	9.13	15.02	13.39
Ho	1.15	1.34	1.31	1.37	1.80	1.74	1.79	1.84	2.91	2.68
Er	3.22	3.76	3.63	3.65	4.57	4.61	4.97	4.97	7.96	6.86
Tm	0.45	0.50	0.49	0.52	0.62	0.62	0.64	0.67	1.04	0.96
Yb	2.63	3.04	2.92	3.10	3.68	3.66	3.89	3.91	6.30	5.78
Lu	0.42	0.48	0.46	0.48	0.56	0.55	0.60	0.60	0.98	0.90
Th	0.39	0.55	0.74	0.62	1.18	0.85	1.91	1.67	2.20	1.90
Hf	2.60	3.47	3.36	3.73	6.48	6.41	6.53	6.69	8.25	8.26
Ta	0.57	0.86	0.80	0.93	1.77	1.62	1.70	1.53	3.49	3.24
U	0.11	0.18	0.68	0.19	0.45	0.29	0.58	0.51	0.78	0.68
Pb	1.98	2.74	3.37	2.71	4.65	3.68	4.38	4.77	5.75	3.28
Cs	0.03	0.06	0.04	0.03	0.17	0.11	0.58	0.61	0.51	0.24
^{87}Sr / ^{86}Sr	0.70648	0.70680	0.70600	0.70638	0.70696	0.70670	0.70730	0.70721	0.70591	—

Table 2. Continued.

11 (M2) CM-23 Trio	12 (M2) CM-27 Sinker Butte	13 (M3) I2725 Guffey Table	14 (M3) I2715 Grouch Drain	15 (M3) ML-5 Halverson Cliffs	16 (M3) ML-3 Halverson Cliffs	17 (M3) DMI-19 Initial Point	18 (M3) DMI-18 Initial Point	19 (M3) I-3105 Kuna Butte	20 (M3) DMK-2 Kuna Butte	21 (M3) DMK-4 Kuna Butte
44.89	46.46	47.11	49.58	46.96	48.13	47.97	49.25	48.70	48.71	49.93
3.97	3.90	1.95	1.54	2.25	2.47	1.84	1.94	2.25	2.08	2.52
14.39	14.05	15.57	16.70	15.16	16.16	16.21	16.29	16.26	16.17	16.65
14.89	15.02	11.45	10.64	11.96	11.70	10.41	10.56	10.85	11.12	9.64
0.24	0.23	0.19	0.18	0.19	0.19	0.17	0.17	0.19	0.18	0.17
6.96	6.07	9.21	6.87	8.62	7.23	8.47	6.97	6.61	7.28	4.67
9.17	9.90	10.58	11.91	9.91	9.63	9.40	9.42	9.34	9.33	9.15
3.07	2.87	2.76	2.91	2.86	3.03	2.72	3.19	3.41	3.11	3.65
0.94	0.63	0.74	0.42	1.06	1.14	1.28	1.73	1.67	1.37	1.94
1.10	0.86	0.44	0.25	0.41	0.55	0.45	0.48	0.72	0.55	0.83
99.62	99.99	100.00	101.00	99.38	100.23	98.91	100.00	100.00	99.90	99.15
67	35	153	60	131	73	135	84	63	80	23
111	136	272	228	249	138	216	166	134	152	76
26	29	34	36	26	28	29	24	30	23	24
316	425	245	285	237	262	224	224	235	229	257
495	529	330	181	363	392	470	636	831	498	810
13	7	17	5	23	19	31	41	34	30	41
322	322	298	220	352	379	411	411	442	426	447
208	306	152	92	151	179	136	156	186	167	225
44	45	27	25	30	33	23	26	31	28	36
37	35	22	14	23	30	26	37	46	40	58
31	37	30	43	48	41	38	28	24	34	43
150	154	95	76	99	109	90	81	92	92	98
27.30	—	18.22	8.82	—	20.53	17.14	21.62	28.78	22.70	34.54
60.50	—	37.54	18.99	—	43.57	35.14	42.77	56.55	45.07	67.75
8.06	—	4.83	2.58	—	5.73	4.37	5.18	6.85	5.50	8.11
37.20	—	21.91	12.08	—	25.34	18.96	21.97	28.72	23.59	33.70
9.80	—	5.69	3.58	—	6.45	4.97	5.25	6.83	5.78	8.07
3.49	—	1.97	1.36	—	2.26	1.76	1.80	2.23	2.00	2.54
10.14	—	5.53	3.88	—	6.81	4.92	5.26	6.64	5.79	8.00
1.66	—	0.97	0.74	—	1.09	0.81	0.84	1.07	0.93	1.31
9.48	—	6.00	4.70	—	6.49	4.95	5.02	6.37	5.57	7.97
1.90	—	1.20	0.98	—	1.28	1.01	0.99	1.26	1.13	1.62
4.97	—	3.35	2.81	—	3.44	2.66	2.57	3.31	2.98	4.37
0.69	—	0.45	0.39	—	0.47	0.38	0.37	0.47	0.42	0.62
4.17	—	2.69	2.37	—	2.89	2.28	2.26	2.81	2.52	3.69
0.65	—	0.42	0.37	—	0.45	0.35	0.34	0.44	0.39	0.58
1.16	—	1.00	0.57	—	1.24	1.34	1.71	2.17	1.79	2.72
5.32	—	3.73	2.33	—	4.22	3.37	3.64	4.29	4.04	5.49
2.20	—	1.81	0.74	—	1.81	1.76	2.31	2.83	2.46	3.66
0.44	—	0.35	0.18	—	0.22	0.49	0.55	0.59	0.61	0.98
2.84	—	2.09	1.29	—	2.18	1.68	2.50	2.94	2.72	3.32
0.08	—	0.13	0.08	—	0.14	0.68	0.47	0.28	0.23	0.30
0.70530	0.70693	0.70500	0.70542	—	0.70510	—	0.70570	—	0.70533	0.70540

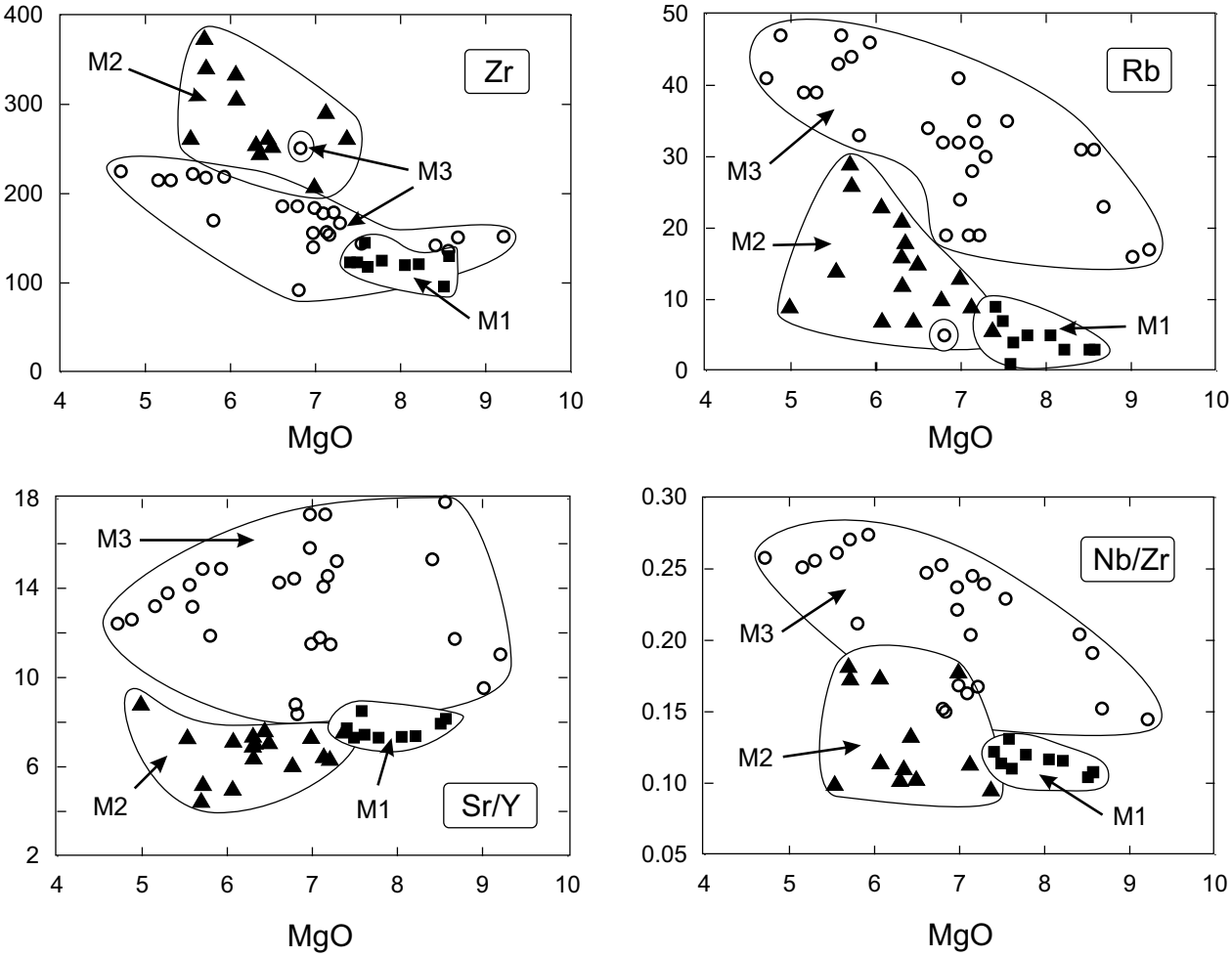

Figure 5. Variations of Rb and Zr (ppm) and Nb/Zr and Sr/Y in Melba area basalts plotted versus weight percent MgO. Symbols are the same as in Figure 2.

has the lowest LREE values of any Melba-area basalt. The chondrite-normalized REE trends for M1 and M2 are roughly parallel; however, most of the M3 basalts are depleted in the heavy REEs relative to those of M1, resulting in the slightly crossed trends on Figure 6. The only specimens that produce Eu anomalies on the chondrite-normalized diagrams are the highly evolved M2 basalts from Coyote Butte and the small shield at Swan Falls Road.

Sr-Isotopes

The Sr-isotopic ratios of twenty-three basalts from the Melba area are given with the chemical analyses in Table 2 and plotted against SiO_2 and Rb/Sr in Figure 7. The most notable feature of these data is their nearly bimodal distribution between M3 basalts, which have $^{87}Sr/^{86}Sr$ ratios less than 0.706, and most of the M1 and M2 samples, which have $^{87}Sr/^{86}Sr$ greater than 0.706. The two M2 samples having Sr-isotopic ratios less than 0.706 are both from the subset of highly evolved basalts with small negative Eu anomalies. Excepting these samples, the $^{87}Sr/^{86}Sr$ ratios appear to increase slightly in the more differentiated basalts of each suite.

PETROGENESIS OF WESTERN SRP BASALTS

In the sections below we discuss the differentiation processes that could have affected the Melba area basalts and speculate about the nature of their mantle source regions. Three observations are presented below about the petrogenetic relationships among and within the three groups.

(1) The M1 basalts and most of the M2 lavas have similar $^{87}Sr/^{86}Sr$ ratios and appear to define two ends of a

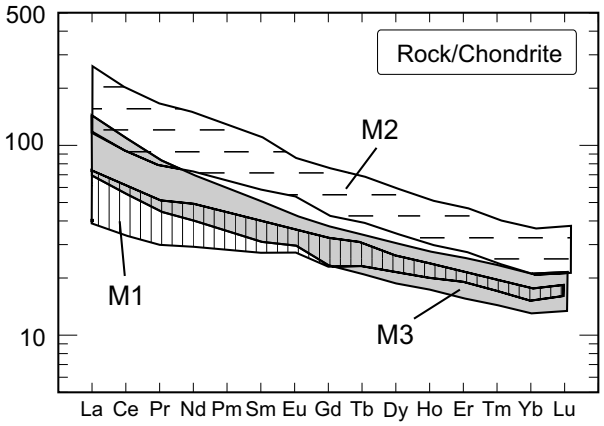

Figure 6. Rare earth element diagram showing the range of compositions in all of the M1 and M2 basalts and in the M3 lavas from Kuna Butte and Initial Point (other M3 lavas not included). Data are normalized to the average chondrite composition of Sun and McDonough (1989).

typical tholeiitic crystal fractionation sequence. Although lavas in these two groups differ widely in age, the parent magmas of most M2 lavas were probably similar in composition to M1 basalts. It follows, therefore, that both groups of basalts may have originated in similar mantle source areas.

(2) In contrast, the M3 basalts are isotopically and chemically distinct from lavas in the two older groups at all values of MgO and Mg-number. The uniformly lower $^{87}Sr/^{86}Sr$ ratios of the M3 basalts cannot be explained by differences in the degree of partial melting or by high versus low pressure fractional crystallization. Nor can the combination of lower $^{87}Sr/^{86}Sr$ and greater K_2O and LILE that characterizes the M3 basalts be easily attributed to greater or lesser degrees of crustal assimilation. The simplest explanation is that the M1 and M2 parent liquids originated in or equilibrated with a mantle source isotopically and chemically different from the source of the M3 basalts. Vetter and Shervais (1992) reached a similar conclusion in their study of basalts near Smith Prairie, where young, slightly alkaline lavas also overlie more typical SROT.

(3) The subset of strongly differentiated M2 basalts having high P_2O_5 and low $^{87}Sr/^{86}Sr$ relative to the other SROT lavas probably included at least a contribution from a third source in the upper mantle or lower crust. Although these lavas are similar in many ways to other M2 tholeiites, they could not have formed from a M1-like parent by simple fractional crystallization or shallow crustal assimilation because neither process would be likely to lower Sr-isotopic ratios or raise P_2O_5 contents relative to other excluded elements. These rocks clearly are not related to the M3 basalts because they plot well off the

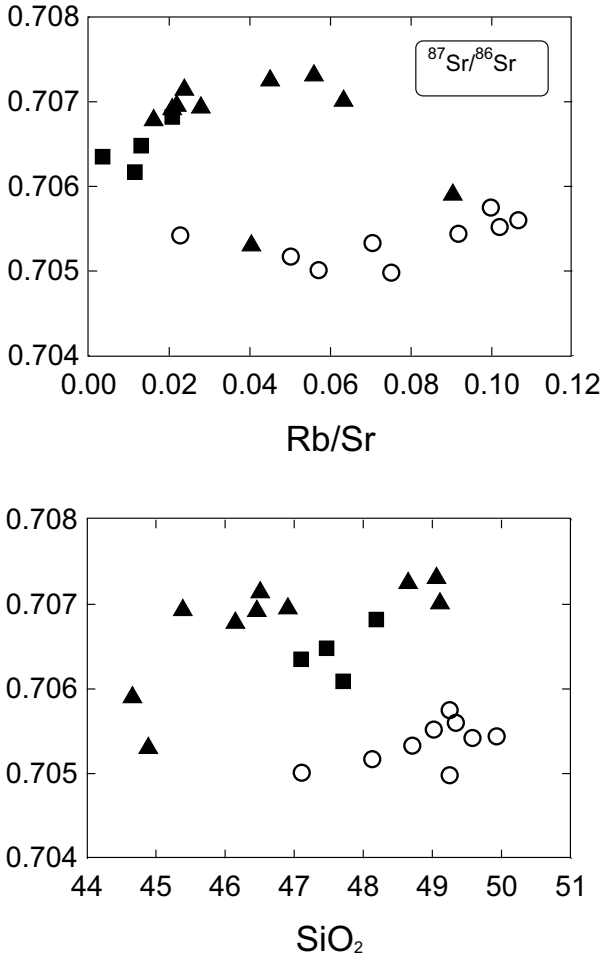

Figure 7. $^{87}Sr/^{86}Sr$ in Melba area basalts plotted versus weight percent Rb/Sr and SiO_2. Symbols are the same as in Figure 2.

geochemical trends for M3 lavas and have very different excluded element ratios (e.g., Th/Hf, Rb/Ba).

DIFFERENTIATION OF THE M1 AND M2 THOLEIITES

Individual M1 and M2 volcanic centers each produced only a narrow range of lava compositions; however, when all of the M1 and M2 basalts are plotted together they define a typical tholeiitic differentiation trend of iron enrichment with decreasing MgO content (Figure 4). To test whether these basalts could simply represent differing degrees of crystal fractionation of similar parent magmas, we performed numerous major element least squares calculations (after Bryan and others, 1969) using analyses of several primitive M1 basalts for the initial liquids. Mineral compositions for these models were taken from analyses of cumulus minerals in the differentiated Graveyard Point intrusion, which is near the western margin of

the western SRP and is similar in age and average composition to M1 basalts (McCurry and others, 1997). The results showed that moderately evolved M2 tholeiites such as the Sinker Butte lava (CM-27, Table 1) could be derived from a primitive M1 magma (MB-5, Table 1) by removing about 13 percent olivine (Fo_{71}), 35 percent plagioclase (An_{61}), and 8 percent augite (En_{35}; $\sum r^2 \approx 0.04$). On the other hand, the major element compositions of samples from the P_2O_5-rich subset of M2 lavas (e.g., CM-14, Table 1) could not be satisfactorily reproduced by the least squares calculations. If these lavas formed by crystal fractionation, their parent liquids must have had more P_2O_5 and a greater P_2O_5/K_2O ratio than any of the analyzed M1 basalts.

An estimate of the pressure at which the M2 magmas fractionated was obtained using the thermodynamically based MELTS program of Ghiorso and Sack (1995). A primitive M1 basalt was again chosen as the parent. Liquid descent lines were calculated for fractional crystallization at a variety of fixed pressures as well as along several specified dP/dT gradients. The model liquid trend that most closely resembles the M1 and M2 rock compositions was obtained when pressure was fixed at 3 kilobars (Figure 8). It is worth noting that this pressure corresponds to a depth just below the boundary at which seismic velocities beneath the western SRP increase to 6.6-6.8 km/s (Prodehl, 1979), and supports the conclusion of Wood and Clemens (this volume) that the seismic boundary marks the top of a zone of abundant mafic intrusions.

Although the least squares calculations and the MELTS models both require the fractional crystallization of pyroxene, none of the M1 or M2 tholeiites contains pyroxene phenocrysts. One explanation for this apparent paradox is suggested by the MELTS model, which indicates that about 80 percent of the total pyroxene in the fractionation mode crystallizes within a temperature range of only two degrees. This event takes place after about 28 percent fractionation of olivine and plagioclase and accounts for the abrupt drop in the Al_2O_3/CaO ratio in the model liquid curve for 3 kilobars in Figure 8. The rapid removal of pyroxene at depths of 7-9 km, followed by the rise and stagnation of magmas in shallow, subvolcanic reservoirs could account for the lack of pyroxene phenocrysts in the M2 lavas.

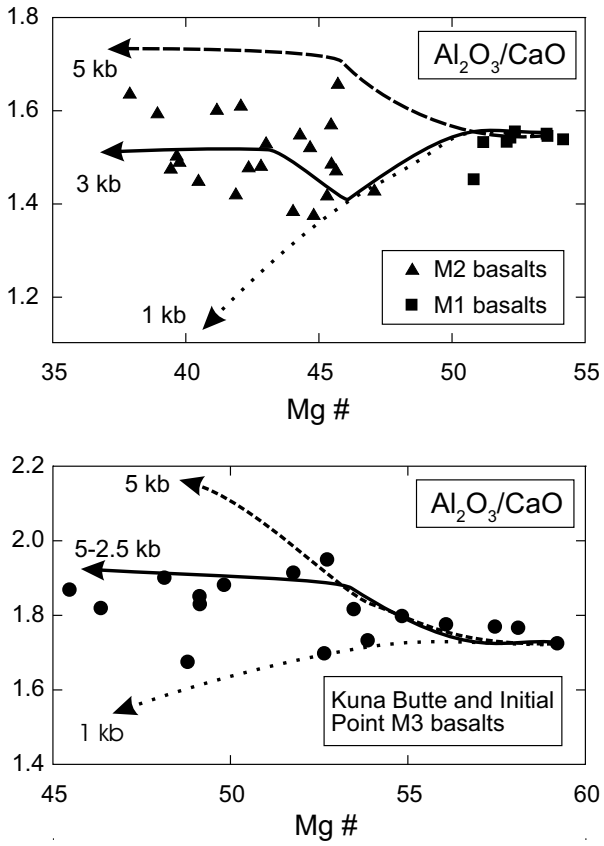

Figure 8. Plots of Al_2O_3/CaO versus Mg-number in Melba area basalts compared with simulated liquid trends resulting from fractional crystallization models using MELTS.

DIFFERENTIATION OF THE M3 BASALTS

Unlike the essentially monogenetic volcanoes of the M1 and M2 groups, several of the M3 centers produced a moderately wide range of mafic rock compositions. Analyzed lavas from Kuna Butte and Initial Point, two temporally and spatially related M3 centers, range in MgO content from 4.7 to 8.6 percent and form well-defined differentiation trends on chemical variation diagrams. In contrast, M3 basalts from Guffey Table, Grouch Drain, and the Halverson Cliffs section (H.C., Figure 1) differ substantially from the Kuna Butte-Initial Point lavas, particularly in their incompatible element abundances.

Least squares computer calculations show that the range of lava compositions at Kuna Butte and Initial Point could have been generated by fractional crystallization of a parent liquid similar to the most MgO-rich basalt (DMI-19, Table 1). For example, the major element composition of the most evolved lava at Kuna Butte (DMK-4, Table 1) can be closely approximated by subtracting about 14 percent olivine (Fo_{71}), 18 percent plagioclase (An_{75}), and 5 percent augite (En_{35}) from the analysis of the most mafic basalt at Initial Point (DMI-19)($\sum r^2 \approx 0.06$). Modeled abundances of incompatible trace elements are generally consistent with the results of the major-element based least squares calculations. Model liquid trends produced by the MELTS program come closest to the Initial Point-Kuna Butte fractionation trend when pressure is

allowed to vary between 5 and 2.5 kilobars, corresponding to a dP/dT path of 20 bars per ºK (Figure 8).

The least squares and MELTS calculations support the conclusion that the Kuna Butte-Initial Point lavas represent one or more crystal fractionation series of the same or similar parent magmas. However, the large differences in trace element abundances and excluded element ratios between this series and M3 basalts at centers such as Guffey Table must be attributed to some process other than fractional crystallization. Because all of the analyzed M3 basalts have similar Sr-isotopic ratios and plot on the same general major-element trends, a possible cause of the trace element variations is that their parent liquids formed by different degrees of partial melting of a chemically and isotopically similar mantle source. Figure 9 shows the variation in Nb/Y versus Nb that would result from the equilibrium partial melting of a source containing twice the primitive mantle abundances of Nd and Y (Sun and McDonough, 1989). The most primitive M3 basalts plot near this melting curve, with the Guffey Table-Halverson Cliffs lavas representing greater percentages of partial melting than the slightly younger Initial Point-Kuna Butte lavas. The more differentiated lavas in each group plot along fractional crystallization curves, as would be expected from the least squares and MELTS calculations.

CRUSTAL ASSIMILATION

Small amounts of crustal assimilation may offer the best explanation for the slight increases in $^{87}Sr/^{86}Sr$ ratios in the more differentiated basalts of the M2 and M3 groups (Figure 7). The clearest indications for shallow level contamination exist for the M2 basalts at Guffey Butte and Walters Butte. Specimens from these centers have slightly greater $^{87}Sr/^{86}Sr$ ratios than the other M2 basalts and have noticeably greater SiO_2 contents and K/P ratios. Direct evidence for the mingling of basalt with partially melted sediments is present at Guffey Butte, where a thin sheet of glassy hybridized rock is exposed near the margin of what was probably once a small lava lake within the crater of the tuff cone (Morrow, 1996; McCurry and others, 1997).

The slightly greater $^{87}Sr/^{86}Sr$ ratios in the more differentiated M3 basalts can also be attributed to crustal assimilation, or more precisely to a combination of assimilation and fractional crystallization (AFC). Models utilizing the AFC equations of DePaolo (1981) indicate that trace element and Sr-isotopic variations in these lavas could result from the assimilation of granitic rocks similar to those in the western border facies of the Idaho batholith (Figure 10). The effect of contamination in M3 lavas is not as pronounced as it appears to be in several of the young Smith Prairie basalts, which erupted North of the western SRP and rest directly on Cretaceous granodiorite. Although assimilation does appear to have played a role in the evolution of some western SRP basalts, it should be emphasized that none of the assimilation or AFC models we tried suggested that M3 lavas could be derived from more primitive M1 or M2 tholeiites.

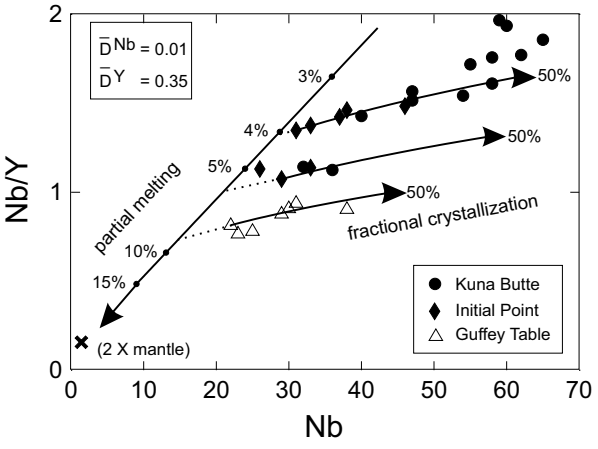

Figure 9. Plot of Nb/Y versus Nb for M3 basalts from Kuna Butte, Initial Point, and the Guffey Table-Halverson Cliffs area. The most primitive samples plot close to the model liquid trend resulting from about 4 to 8 percent partial melting of a spinel peridotite containing twice the Nb and Y concentrations of primitive mantle (Sun and McDonough, 1989). More evolved basalts plot along several model liquid trends for fractional crystallization.

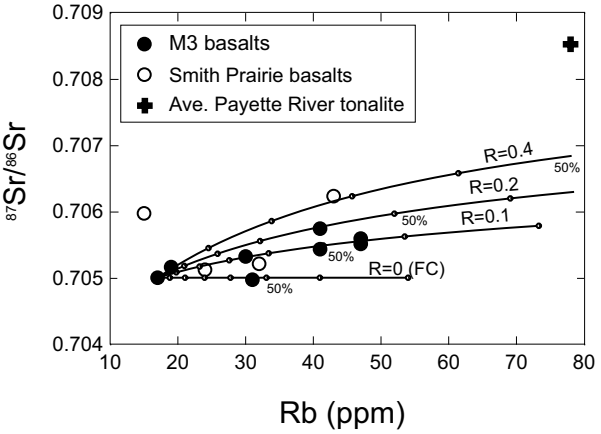

Figure 10. Plot of $^{87}Sr/^{86}Sr$ versus Rb (ppm) for M3 basalts and young basalts (BRG-2) from the Smith Prairie area (Vetter and Shervais, 1992). Liquid trends are shown for AFC models in which the parent liquid is a primitive M3 basalt and the contaminant is average Payette River tonalite from the western margin of the Idaho batholith (Manduca and others, 1992; Manduca, unpubl. data).

SOURCES FOR MELBA AREA BASALTS

Discussions about the sources of continental basalts have typically focused on the relative contributions of partial melts of the asthenosphere versus liquids derived from various types of subcontinental lithospheric mantle (e.g., Hart, 1985; Fitton and others, 1991; Vetter and Shervais, 1992; Shoemaker and Hart, this volume). Although a thorough discussion of the sources of basalts in the Melba area is not yet possible owing to a lack of Pb- and Nd-isotopic data, some preliminary conclusions can be drawn from the trace element and Sr-isotopic analyses. A useful starting point is to compare the incompatible element abundances in Melba area basalts with those of oceanic island basalts (OIB). Figure 11 is a plot of the average compositions of the most primitive basalts in each group normalized to the average OIB analysis of Sun and McDonough (1989). Although all three groups have positive Ba anomalies, which are typical of many late Cenozoic Cordilleran basalts (Fitton and others, 1991), the plots show that average M3 basalt is roughly similar to OIB, whereas the M1 basalts are depleted in the most incompatible elements relative to OIB and more closely resemble enriched MORB. The more evolved M2 group defines a pattern that is generally parallel to the trend for M1 except for a strong negative Sr anomaly that probably indicates fractional crystallization of plagioclase. None of the basalts has the negative Nb anomalies typical of subduction related magmas, but all have small to moderate positive anomalies for Pb and P.

Because the M3 basalts are similar to OIB in their chemical compositions and Sr-isotopic ratios, they were probably derived from an asthenospheric mantle source. Vetter and Shervais (1992) suggested a similar origin for the young, slightly alkaline basalts near Smith Prairie. In contrast, one or more lithospheric sources appear to be necessary to explain the OIB-normalized element trends and higher $^{87}Sr/^{86}Sr$ ratios of the M1 and M2 basalts. Although assimilation of shallow crustal rocks may account for the elevated $^{87}Sr/^{86}Sr$ ratios in a few of the M2 lavas, the more primitive Melba area tholeiites do not show evidence for shallow crustal contamination. These rocks must have inherited their high Sr-isotopic ratios from deep crustal or mantle sources. The nature of this source is problematical because in addition to producing melts with elevated $^{87}Sr/^{86}Sr$ ratios, the source or sources for M1 and M2 basalts also generated liquids with relatively low concentrations of K and Rb, low LILE/HFSE ratios, and low VICE/MICE ratios. Vetter and Shervais (1992) noted a similar combination of isotopic and chemical features in the older, SROT-like basalts near Smith Prairie, which they attributed to the melting of mantle lithosphere that had undergone Fe-Ti metasomatism related to passage of the Yellowstone plume. Lum and others (1989) explained the elevated Sr-isotopic ratios and low VICE/MICE ratios in SRP tholeiites by invoking an ancient lithospheric source that had experienced an early period of high Rb/Sr and rapid growth in $^{87}Sr/^{86}Sr$ followed by an episode of partial melting that substantially reduced the concentrations of the most incompatible elements. Hart and others (1997), using Os-isotopic ratios to support their argument, suggested that HAOT basalts in the Owyhee Plateau originated in a MORB-like source but attributed the basalts' elevated Sr-isotopic ratios to contamination from partial melts of shallow lithospheric mantle.

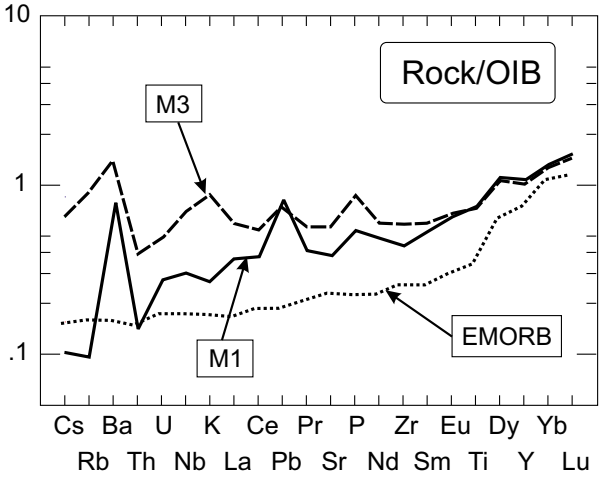

Figure 11. Incompatible element diagram normalized to the average composition of ocean island basalt (OIB). "M1" is an average of all analyzed M1 basalts; "M3" is an average of all Kuna Butte and Initial Point lavas, and "EMORB" is the average enriched MORB composition of Sun and McDonough (1989).

The common idea behind most of these models, that tholeiitic basalts in the western and central SRP were derived from, or contaminated by, a lithospheric mantle source, is consistent with the chemical compositions and $^{87}Sr/^{86}Sr$ ratios in the Melba area basalts. The consistently low VICE/MICE ratios in M1 and M2 basalts indicates they originated in a depleted source, whereas the somewhat elevated $^{87}Sr/^{86}Sr$ ratios require isotopic enrichment. Either the two-stage model of Lum and others (1989) or the two-source model of Hart and others (1997) could plausibly produce this combination of trace-element and isotopic ratios. Although the small subset of M2 samples having low SiO_2 and high P_2O_5 appear at first glance to be extreme fractional crystallization differentiates of less-evolved M2 basalts, their lower $^{87}Sr/^{86}Sr$ ratios and substantially different trace element ratios require that they had a somewhat different combination of source areas, possibly including mafic rocks of the lower crust.

SUMMARY AND CONCLUSIONS

Two major episodes of basaltic volcanism can be identified in the Melba area. The first, at about 9-7 Ma, produced olivine tholeiites (M1 group) with compositions transitional between those of the MORB-like high alumina olivine tholeiite (HAOT) magma type of the northwestern Great Basin and the evolved tholeiites of the Snake River Plain (SROT). The second, at about 2-0.4 Ma, produced two chemically distinctive groups of basalts, an older series of evolved olivine and quartz tholeiites characterized by low LILE/HFSE and having $^{87}Sr/^{86}Sr$ ratios generally greater than 0.706 (M2), and a younger group with compositions transitional between olivine tholeiite and alkali-olivine basalt and having high LILE/HFSE and $^{87}Sr/^{86}Sr$ ratios slightly lower than 0.706 (M3). The compositions of the M1 lavas and the evolved tholeiites of M2 are consistent with their origin in a shallow mantle source that was either MORB-like or was lithospheric mantle that had a complex history of depletion and enrichment. Similarities between the slightly alkaline M3 basalts and OIB suggest a sublithospheric, OIB-like mantle source for these melts. All of the magmas erupted in the Melba area were modified to some degree by fractional crystallization, and some of the M2 and M3 lavas show evidence for small amounts of shallow crustal assimilation.

Although further work is required to understand how the magmatic history of the western SRP relates to its tectonic evolution, we present these preliminary observations on the basalts in the Melba area. It seems reasonable to infer that extension rates within the western SRP may have been greatest between 9-7 Ma, allowing large volumes of the less differentiated M1 basalts to be erupted. Later volcanism produced a greater proportion of differentiated basalts, suggesting that these magmas rose more slowly to the surface, perhaps in response to less rapid extension. The change to more alkaline M3 volcanism at about 0.8 Ma and the implied shift to a deeper mantle source region are consistent with models in which melting is caused by extension and thinning of the lithosphere and does not require the involvement of a mantle plume.

ACKNOWLEDGMENTS

Our paper benefitted greatly from a thorough and insightful review by Dennis Geist. We also thank Martha Godchaux for her invaluable help in the field, Robert Duncan for the $^{40}Ar/^{39}Ar$ dates, and Kathy Manduca for data on the chemical and isotopic compositions of Idaho batholith tonalites. Research was supported in part by an Idaho State Board of Education Faculty Research Grant to Craig White.

REFERENCES

Amini, Hassan, H.H. Mehnert, and J.D. Obradovich, 1984, K-Ar ages of late Cenozoic basalts from the western Snake River Plain, Idaho: Isochron/West, no. 41, p. 7-11.

Bonnichsen, Bill, and M.M. Godchaux, 1998, Geologic map of the Walters Butte quadrangle, Ada, Canyon and Owyhee counties, Idaho: Idaho Geological Survey Geologic Map 21, 1:24,000.

Bryan, W.B., L.W. Finger, and Felix Chayes, 1969, Estimating proportions in petrographic mixing equations by least-squares approximation: Science, v. 163, p. 926-927.

DePaolo, D.J., 1981, Trace element and isotopic effects of combined wallrock assimilation and fractional crystallization: Earth and Planetary Science Letters, v. 53, p. 189-202.

Ekren, E.B., D.H. McIntyre, E.H. Bennett, and H.E. Malde, 1981, Geologic map of Owyhee County, Idaho, west of longitude 116ºW: U.S. Geological Survey, Miscellaneous Investigations Series I-1256.

Fitton, J.G., Dodie James, and W.P. Leeman, 1991, Basic magmatism associated with late Cenozoic extension in the western United States: Compositional variations in space and time: Journal of Geophysical Research, v. 96, p. 13,693-13,711.

Ghiorso, M.S., and R.O. Sack, 1995, Chemical mass transfer in magmatic processes IV: A revised and internally consistent thermodynamic model for the interpolation and extrapolation of liquid-solid equilibria in magmatic systems at elevated temperatures and pressures: Contributions to Mineralogy and Petrology, v. 119, p. 197-212.

Godchaux, M.M., Bill Bonnichsen, and M.D. Jenks, 1992, Types of phreatomagmatic volcanoes in the western Snake River Plain, Idaho, U.S.A.: Journal of Volcanology and Geothermal Research, v. 52, p. 1-25.

Hart, W.K., 1985, Chemical and isotopic evidence for mixing between depleted and enriched mantle, northwestern U.S.A.: Geochemica et Cosmochemica Acta, v. 49, p. 131-144.

Hart, W.K., and J.L. Aronson, 1983, K-Ar ages of rhyolites from the western Snake River Plain area, Oregon, Idaho, and Nevada: Isochron/West, no. 36, p. 17-19.

Hart, W.K., J.L. Aronson, and S.A. Mertzman, 1984, Areal distribution and age of low K, high-alumina olivine tholeiite magmatism in the northwestern Great Basin, U.S.A.: Geological Society of America Bulletin, v. 95, p. 186-195.

Hart, W.K., R.W. Carlson, and S.B. Shirey, 1997, Radiogenic Os in primitive basalts from the northwestern U.S.A.: Implications for petrogenesis: Earth and Planetary Sciences Letters, v. 150, p. 103-116.

Hooper, P.R., and Diane Johnson, 1989, Major and trace element analysis of rocks and minerals by automatic X-ray spectrometry: Available on request from the Geology Department, Washington State University.

Howard, K.A., J.W. Shervais, and E.H. McKee, 1982, Canyon-filling lavas and lava dams on the Boise River, Idaho, and their significance for evaluating downcutting during the last two million years, *in* Bill Bonnichsen and R.M. Breckenridge, eds., Cenozoic Geology of Idaho: Idaho Bureau of Mines and Geology Bulletin 26, p. 629-641.

Irvine, T.N., and W.R.A. Baragar, 1971, A guide to the chemical classification of the common volcanic rocks: Canadian Journal of Earth Science, v. 8, p. 523-548.

Jenks, M.D., and Bill Bonnichsen, 1989, Subaqueous basalt eruptions into Pliocene Lake Idaho, Snake River Plain, Idaho, *in* V.E. Chamberlain, R.M. Breckenridge, and Bill Bonnichsen, eds., Guidebook to the Geology of Northern and Western Idaho and Surrounding Areas: Idaho Geological Survey Bulletin 28, p. 17-34.

Kuntz, M.A., R.H. Lefebvre, D.E. Champion, J.S. King, and H.R. Covington, 1983, Holocene basaltic volcanism along the Great Rift, central and eastern Snake River Plain, Idaho *in* W.P. Nash and K.D. Gurgel, eds., Geologic Excursions in Volcanology: Eastern Snake River Plain (Idaho) and Southwestern Utah: Utah Geological and Mineral Survey Special Studies 61, p. 1-34.

Le Bas, M.J., R.W. Le Maitre, Anton Streckeisen, and Boris Zanettin, 1986, A chemical classification of volcanic rocks based on the total alkali-silica diagram: Journal of Petrology, v. 27, p. 745-750.

Lum, C.C., W.P. Leeman, K.A. Foland, J.A. Kargel, and J.G. Fitton, 1989, Isotopic variations in continental basaltic lavas as indicators of mantle heterogeneity: Examples from the western U.S. cordillera: Journal of Geophysical Research, v. 94, p. 7871-7884.

Mabey, D.R., 1982, Geophysics and tectonics of the Snake River Plain, Idaho, *in* Bill Bonnichsen and R.M. Breckenridge, eds., Cenozoic Geology of Idaho: Idaho Bureau of Mines and Geology Bulletin 26, p. 139-153.

Manduca, C.A., L.T. Silver, and H.P. Taylor, 1992, $^{87}Sr/^{86}Sr$ and $^{18}O/^{16}O$ isotopic systematics and geochemistry of granitoid plutons across a steeply-dipping boundary between contrasting lithospheric blocks in western Idaho: Contributions to Mineralogy and Petrology, v. 109, p. 355-372.

McCurry, Michael, Bill Bonnichsen, C.M. White, M.M. Godchaux, and S.S. Hughes, 1997, Bimodal basalt-rhyolite magmatism in the central and western Snake River Plain, Idaho and Oregon, *in* P.K. Link and B.J. Kowallis, eds., Proterozoioc to Recent Stratigraphy, Tectonics, and Volcanology, Utah, Nevada, Southern Idaho and Central Mexico: Brigham Young University Geology Studies, v. 42, p. 399-404.

Morrow, L.S., 1996, Geology of Guffey Butte, western Snake River Plain, Idaho: University of Idaho masters thesis, 106 p.

Othberg, K.L., Bill Bonnichsen, C.C. Swisher III, and M.M. Godchaux, 1995, Geochronology and geochemistry of Pleistocene basalts of the western Snake River Plain and Smith Prairie, Idaho: Isochron/West, no. 62, p. 1-14.

Othberg, K.L., and L.R. Stanford, 1992, Geologic map of the Boise Valley and adjoining area, western Snake River Plain, Idaho: Idaho Geological Survey Geologic Map 18, scale 1:100,000.

Prodehl, Claus, 1979, Crustal structure of the western United States: U.S. Geological Survey Professional Paper 1034, 74 p.

Shoemaker, K.A., and W.K. Hart, 2002, Temporal controls on basalt genesis and evolution on the Owyhee Plateau, Idaho and Oregon, *in* Bill Bonnichsen, C.M. White, and Michael McCurry, eds., Tectonic and Magmatic Evolution of the Snake River Plain Volcanic Province: Idaho Geological Survey Bulletin 30.

Storey, M.A., R.A. Duncan, A.K. Pederson, L.M. Larsen, and H.C. Larsen, 1998, $^{40}Ar/^{39}Ar$ geochronology of the West Greenland Tertiary volcanic province: Earth and Planetary Science Letters, v. 160, p. 569-586.

Sun, S.S., and W.F. McDonnough, 1989, Chemical and isotopic systematics of oceanic basalts: Implications for mantle composition and processes, *in* A.D. Saunders and M.J. Norry, eds., Magmatism in the Ocean Basins: Geological Society Special Publication 42, p. 313-345.

Vetter, S.K., and J.W. Shervais, 1992, Continental basalts of the Boise River Group near Smith Prairie, Idaho: Journal of Geophysical Research, v. 97, p. 9043-9061.

Wood, S.H., 1994, Seismic expression and geological significance of a lacustrine delta in Neogene deposits of the western Snake River Plain, Idaho: American Association of Petroleum Geologists Bulletin, v. 78, p. 102-121.

Wood, S.H., and D.M. Clemens, 2002, Geologic and tectonic history of the western Snake River Plain, Idaho and Oregon, *in* Bill Bonnichsen, C.M. White, and Michael McCurry, eds., Tectonic and Magmatic Evolution of the Snake River Plain Volcanic Province: Idaho Geological Survey Bulletin 30.

Yoder, H.S., and C.E. Tilley, 1962, Origin of basalt magmas: An experimental study of natural and synthetic rock systems: Journal of Petrology, v. 3, p. 342-532.

Origin and Evolution of the Western Snake River Plain: Implications From Stratigraphy, Faulting, and the Geochemistry of Basalts Near Mountain Home, Idaho

John W. Shervais,[1] Gaurav Shroff,[2] Scott K. Vetter,[3]
Scott Matthews,[3] Barry B. Hanan,[4] and James J. McGee[2]

ABSTRACT

Most models for the origin and evolution of the Snake River Plain (SRP) volcanic province focus on the central role of the Yellowstone hot spot and its effects on the lithosphere of North America in response to plate motions relative to this hot spot. Movement of the North American plate over the Yellowstone hot spot has resulted in a linear track of volcanism that parallels this plate motion, represented today by volcanic rocks of the eastern SRP.

The western SRP is a structural graben oriented at a high angle to the trace of the Yellowstone plume and to the axis of the eastern SRP. It is filled largely with lacustrine sediments related to Pliocene Lake Idaho, a large, long-lived lake system that formed first at the northwestern end of the graben (near Oregon) and extended to the southeast along with the structural graben. High-temperature rhyolite lavas that mark the onset of extension also become younger to the southeast.

Basaltic volcanism in the western SRP occurred in two distinct episodes. The first episode, represented by samples from a deep drill core near Mountain Home and by older surface outcrops that sit directly on rhyolite, is characterized by ferrobasalts that are distinct from other SRP basalts. The second episode is represented by surface flows of Pleistocene age that overlie lacustrine and deltaic sediments of Lake Idaho. These basalts are associated with young faults that reflect Basin and Range extension.

We propose that the western SRP graben represents an aulocogenlike structure formed in response to thermal tumescence above the Yellowstone plume head as it rose under eastern Oregon and Washington. The plume head was deflected northwards either by subduction of the Farallon plate (Geist and Richards, 1993) or by impingement of North American plate lithosphere (Camp, 1995). Basaltic volcanism in the western SRP may be related to the flow of depleted plume source mantle along a sublithospheric conduit beneath the western SRP graben from the Columbia River Plateau. The basalts would form by pressure-release melting of this previously depleted material, along with the overlying mantle lithosphere. The younger volcanic episode apparently formed in response to Basin and Range extension, in a fashion analogous to young basaltic volcanism in the eastern SRP. The source of these basalts is uncertain, but may be plume-modified subcontinental lithosphere.

Key words: continental volcanism, hotspots, basalt, Snake River Plain

INTRODUCTION

The Neogene Snake River Plain (SRP) comprises two distinct tectonic terranes with different crustal structure, stratigraphy, and volcanic history (Figure 1). One is the northeast-trending eastern SRP, a downwarped structural

Editors' note: The manuscript was submitted in June 1998 and has been revised at the authors' discretion.

[1]Department of Geology, Utah State University, Logan, UT 84322
[2]Department of Geological Sciences, University of South Carolina, Columbia, SC 29208
[3]Department of Geology, Centenary College, Shreveport, LA 71134
[4]Department of Geological Sciences, San Diego State University, San Diego, CA 92182

Shervais, J.W., Gaurav Shroff, S.K. Vetter, Scott Matthews, B.B. Hanan, and J.J. McGee, 2002, Origin and evolution of the western Snake River Plain: Implications from stratigraphy, faulting, and the geochemistry of basalts near Mountain Home, Idaho, *in* Bill Bonnichsen, C.M. White, and Michael McCurry, eds., Tectonic and Magmatic Evolution of the Snake River Plain Volcanic Province: Idaho Geological Survey Bulletin 30, p. 343-361.

depression with only minor fault control along its margins (Mabey, 1978, 1982; Malde, 1991; Zentner, 1989; Pierce and Morgan, 1992). This depression becomes progressively elevated towards the east, culminating in the Yellowstone Plateau, the current locus of volcanic activity (Christiansen, 1982; Malde, 1991). The eastern SRP trend is thought to mark the track of the Yellowstone plume from its mid-Miocene location beneath the Owyhee Plateau to its current place under Yellowstone (e.g., Pierce and Morgan, 1992; Malde, 1991; Smith and Braile, 1994), although this hypothesis has been challenged (Humphreys and others, 2000; Christiansen and others, 2002). Recent tomographic data suggest that the plume may actually rise to the west and be tilted eastward by counterflow in the mantle that results from the sinking Farallon slab (Smith and others, 2002; Steinberger and O'Connell, 2002).

The other terrane is the western SRP, a northwest-trending structural graben bounded by en echelon normal faults and filled with sediment up to 1.7 km thick (Malde, 1959, 1991; Malde and others, 1963; Mabey, 1976, 1982; Leeman, 1982). Sedimentary deposits in the western SRP range in age from Miocene through Quaternary and are known collectively as the Idaho Group (Malde and Powers, 1962, 1972; Malde and others, 1963). These deposits are dominantly lacustrine, with subordinate fluviatile and phreatomagmatic deposits (Kimmel, 1982; Smith and others, 1982; Jenks and Bonnichsen, 1989; Malde 1991; Godchaux and others, 1992; Jenks and others, 1993). Sedimentation during this time was controlled by the presence of a large lake, Lake Idaho, which expanded or shrank in response to variations in climate and tectonics (Kimmel, 1982; Jenks and Bonnichsen, 1989).

Volcanic activity in the western SRP began about 11 million years ago with the eruption of rhyolite lavas from fissures that paralleled the range-front faults coeval with extension and graben formation (Ekren and others, 1982, 1984; Bonnichsen, 1982). These rhyolites form the local basement upon which subsequent sediments and basalts were deposited. Basaltic activity in the western SRP began about 9 million years ago, forming lavas that underlie sedimentary deposits of Lake Idaho and, later, local basalt horizons intercalated with these sediments (Malde and Powers, 1962, 1972; Amini and others, 1984; Malde, 1991; Jenks and Bonnichsen, 1989; Jenks and others, 1993).

In this paper we summarize the Neogene volcanic history of the western SRP in the area around Mountain Home, with particular emphasis on the basaltic volcanism and volcanic stratigraphy. Volcanic rocks less than 2.0 Ma are exposed as surface flows near Mountain Home, forming a carapace over sediments of the Idaho Group and documenting an episode of volcanism that occurred some 8 million years after the Yellowstone plume passed this longitude. This area is critical to understanding intracontinental plume tracks because it lies near the intersection of the Yellowstone plume track and the western SRP graben—a tectonic enigma that does not conform to current models of plume-lithosphere interaction (Figure 1). We begin by reviewing first the stratigraphy of volcanic and sedimentary units, their structural deformation, and the geochemistry of the basalts in the Mountain Home area. We then discuss the implications of these data for the Neogene tectonic evolution of the western SRP and the relationship of the western SRP to the Yellowstone plume system.

GEOLOGIC SETTING

Mountain Home is located on the northeast margin of the western SRP, approximately 40 miles southeast of Boise and 70 miles northwest of Twin Falls (Figure 2). The area immediately surrounding Mountain Home is a volcanic plateau, which is underlain by basalt flows and lacustrine sediments of the Idaho Group, at an average

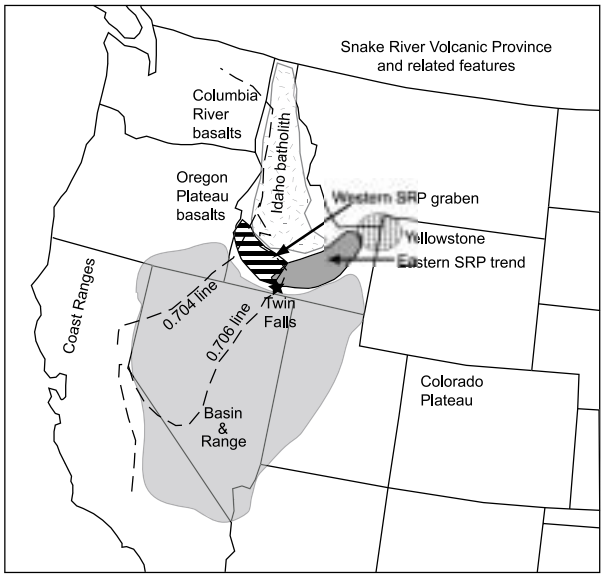

Figure 1. Overview of the northwestern U.S. showing the location of the Snake River Plain and adjacent physiographic regions including the western SRP (horizontal bars), the eastern SRP (dark gray), Columbia River basalt province, the Oregon Plateau basalt province, the Oregon Coast Ranges, the Owyhee Plateau, the Basin and Range Province (pale gray), the Idaho batholith (ticks), the Colorado Plateau, Yellowstone caldera, and the Sr "0.704" and "0.706" lines, which mark the western extent of Proterozoic and Archean crust.

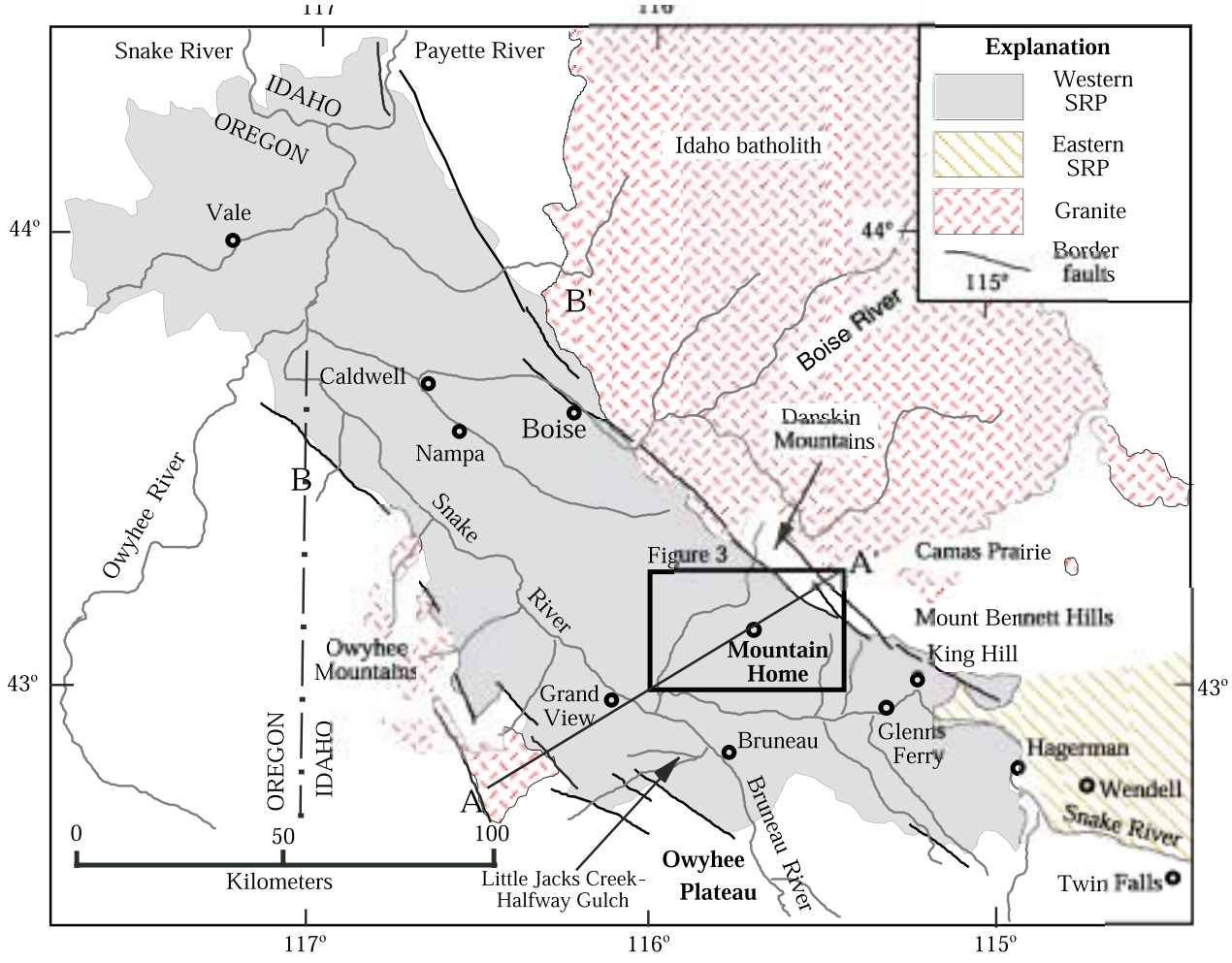

Figure 2. Index map showing southern Idaho and the western Snake River Plain region. Also shown are adjacent parts of the eastern SRP province and the Idaho batholith, and the location of cross sections A-A' (through Mountain Home) and B-B' (through Caldwell; see Figure 6). Unpatterned areas include both rhyolite volcanics and Neogene sediments. Location of the area mapped in Figure 3 is shown by black box.

elevation about 3,200 feet above sea level. The southern limit of this plateau is an escarpment overlooking the current drainage of the Snake River, just upstream from its confluence with the Bruneau River; the elevation at river level is about 2,800 feet. The plateau is truncated along its northern margin by the Danskin Mountains (to the north) and the Mount Bennett Hills (to the northeast). These mountains consist of rhyolite lava flows that have been uplifted along major down-to-the-southwest normal faults, creating a rugged topography with summit elevations from 5,500 to 7,000 feet.

Eight 7.5-minute quadrangles were mapped for this project: Mountain Home North, Mountain Home South, Crater Rings, Crater Rings SW, Crater Rings SE, Cinder Cone Butte, Teapot Dome, and Reverse (Figure 3). The resulting composite map spans 30 minutes of longitude (115°30'W. to 116°0'W.) and 15 minutes of latitude (43°0'N. to 43°15'N.), encompassing about 450 square miles (1,170 square km). Rhyolite lavas of the Idavada Formation crop out in the northeast corner of the map area; lacustrine and fluvial-deltaic sediments of the Idaho Group crop out in embayments along the southern margin. The area between the rhyolitic Mount Bennett Hills and the southern escarpment is underlain largely by basalt flows covered by soil, windblown dust, and alluvial sediments (Figure 3).

There are fifteen identifiable basaltic vents in this area: two maarlike ring structures, three cinder cones, and nine shield volcanoes (Figure 3). One of the shield volcanoes (Crater Rings) has two spectacular pit craters on its summit, which we count as two separate vents. Most of the younger lava flows in this area can be correlated with one of these fifteen vents. There may be another vent near the northern margin of the plateau that has been ob-

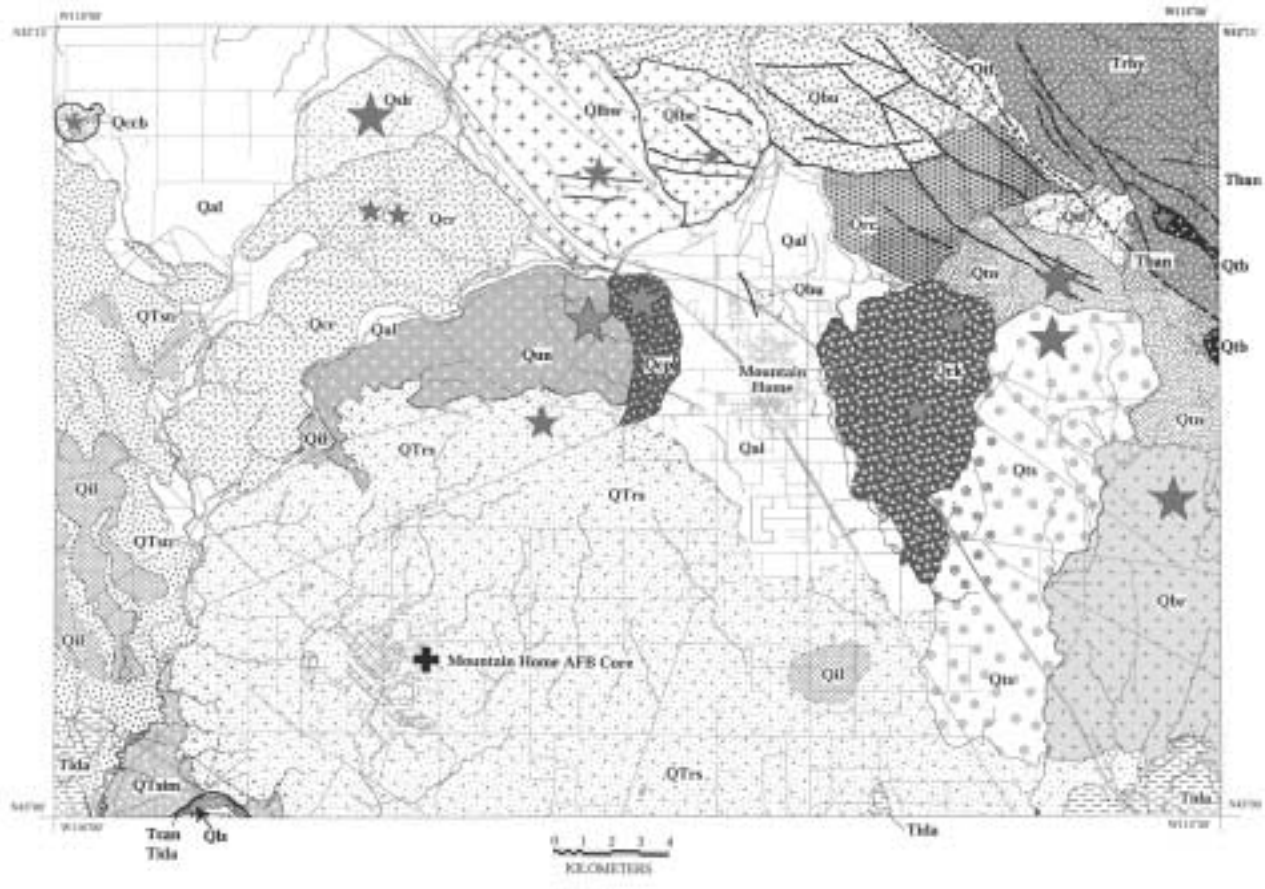

Legend

- Geologic boundary (accurate)
- Geologic boundary (approximate)
- Geologic boundary (inferred)
- Geologic boundary (concealed)
- Fault (accurate)
- Fault (approximate)
- Fault (inferred)
- Fault (concealed)
- Qal Alluvium and gravel
- Qil Intermittent lake
- Qls Landslides
- Qtf Talus and fanglomerate
- Qun Union basalt
- Qcp Basalt of Cinder Pit
- Qcr Crater Rings Basalt
- Qccb Cinder Cone Butte Basalt
- Qlbe Basalt of Lockman Butte East
- Qlbw Basalt of Lockman Butte West
- Qrk Basalt of Rocky
- Qtn Basalt of Teapot North
- Qts Basalt of Teapot South
- Qsh Basalt of Sheep
- Qrc Basaltof Rattlesnake Creek
- Qbu Undifferentiated basalt
- Qtb Basalt of Teapot Basin
- Qbr Basalt of Brush
- QTrs Basalt of Rattlesnake Springs
- QTstr Basaslt of Strike Dam Road
- QTsim Basalt of Simco Road
- Tcan Basalt of Canyon Creek
- Tban Banbury basalt
- Trhy Idavada Volcanic Series (rhyolite)
- Tida Lake Idaho deposits, lacustrine sediments

Figure 3. Geologic map of the Mountain Home area, Elmore County, Idaho. Eight 7.5-minute quadrangles were mapped: Mountain Home North, Mountain Home South, Crater Rings, Crater Rings SW, Crater Rings SE, Cinder Cone Butte, Teapot Dome, and Reverse. Gray stars show the location of vents, where these can be identified. A black cross marks the location of the Mountain Home Air Force Base core.

scured by faulting. Vents for older flows exposed along the southern escarpment have been buried by sediments of the Idaho Group or by younger lava flows.

Mapping of the lava flows and their vents, coupled with flow direction indicators in the pillow lava deltas (dip of foreset beds), shows that lavas generally erupted from vents lying along the northeastern margin of the western SRP graben and flowed to the southwest toward the central axis of the western SRP graben. This pattern is mirrored on the southwest margin of the western SRP by vents which erupted lavas that flowed northeast toward the graben axis (e.g., Bonnichsen and Jenks, 1990; Jenks and Bonnichsen, 1990).

STRATIGRAPHY

The stratigraphic framework of the western SRP was first established by Cope (1883), who recognized evidence for a large, long-lived lake in the western SRP graben and named sediments associated with this lake the "Idaho formation." Malde and coworkers (e.g., Malde and Powers, 1962; Malde and others, 1963; Malde, 1991) discounted the importance of a widespread "Lake Idaho" depositional system, preferring a model in which a meandering river system (ancestral Snake River) coexisted with small, short-lived lakes. Malde and Powers (1962) elevated the Idaho formation to Group status and subdivided it into seven separate formations ranging in age from middle Miocene through Pleistocene (Poison Creek, Banbury Basalt, Chalk Hills, Glenns Ferry, Tuana Gravel, Bruneau, and Black Mesa Gravel).

More recent work has shown that the original concept of a large, long-lived lake is correct and that many of the sediments mapped by Malde and coworkers as fluvial flood-plain deposits are in fact nearshore lacustrine sediments or lacustrine deltaic deposits (Kimmel, 1982; Swirydczuk and others, 1979, 1980; Wood, 1984, 1994; Wood and Anderson, 1981; Jenks and Bonnichsen, 1989). Sediments in the main lacustrine units (Chalk Hills and Glenns Ferry formations) are nearly identical lithologically and can only be distinguished from one another based on paleontological assemblages and age (Chalk Hills = late Miocene, Glenns Ferry = Pliocene). An unconformity lies between the Chalk Hills and Glenns Ferry formations (Kimmel, 1982; Smith and others, 1982); the Glenns Ferry Formation is overlain locally by the Tenmile Gravel (= Tuana Gravel).

Quaternary units formerly in use include the Bruneau Formation (Idaho Group) and the Snake River Group; both units were defined to consist of intercalated sediments and basalt flows (Malde and Powers, 1962; Malde, 1991). Bonnichsen and coworkers have found that this usage is inconsistent with field relations and that basalt flows may be assigned to one formation and their vents assigned to another (Jenks and Bonnichsen, 1989, 1990; Jenks and others, 1993).

In keeping with the practice of Bonnichsen and coworkers (Jenks and Bonnichsen, 1989, 1990; Jenks and others, 1993), we have abandoned the units "Bruneau formation" and "Snake River Group" and prefer instead to map individual basalt flows that in most places can be associated with specific vents and are stratigraphically distinct from other flows. On the southern margins of the map area, these flows are intercalated with lacustrine and fluvial-deltaic sediments deposited during the waning stages of Lake Idaho. Here, individual basalt flows can be mapped on the basis of their stratigraphic position in the sediments, their lateral continuity, and their elevation. We do not assign the sediments above and below these basalts to different formations, because the basalts are laterally finite and at other locations these sediments are contiguous. The basalt flows represent essentially instantaneous events during the slow accumulation of lacustrine sediment.

The mapping conventions followed here are the same as those currently used by the Idaho Geological Survey for mapping in the SRP, and our mapping in the Mountain Home area is tied stratigraphically to published maps of the Idaho Geological Survey along the southern and western margins of our map area (Bonnichsen and Jenks, 1990; Jenks and Bonnichsen, 1990; Jenks and others, 1993).

VOLCANIC UNITS

Volcanic activity in the Mountain Home area can be divided into six distinct phases, one rhyolitic and five basaltic. The phases comprise (from oldest to youngest) rhyolitic volcanism of the Danskin Mountains and Mount Bennett Hills ("Idavada volcanic series"), pre-Lake Idaho basaltic volcanism, late- to post-Lake Idaho plateau-forming basalts that underlie the uplands north of the Snake River drainage, maarlike vents that formed on top of the basaltic plateau, steep-sided shield vents that form the conspicuous hills around Mountain Home, and finally, cinder cone vents that represent the last phase of basaltic volcanism. Eruptive styles seem to be controlled in part by the presence of Lake Idaho and its water-saturated sediments through which many of the later basaltic units erupted.

Volcanic Basement: Idavada Volcanic Series

The oldest volcanic rocks exposed in the Mountain

Home area are rhyolite lava flows that form basement in the Danskin Mountains and the Mount Bennett Hills (northeast corner of map). These rhyolites have been correlated with the Idavada Volcanic Series, which ranges in age from around 9 Ma to 14 Ma (middle Miocene; Armstrong and others, 1975, 1980; Clemens and Wood, 1993).

Clemens and Wood (1993) mapped rhyolite in the area studied here as the Danskin Mountains Rhyolite and mapped rhyolite that crops out farther east as the Mount Bennett Rhyolite. They determined a K-Ar age of 10.0 ± 0.3 Ma for sanidine in a vitrophyre from the summit area on Teapot Dome (Danskin Mountains Rhyolite) and a K-Ar age of 11.0 ± 0.5 Ma for plagioclase in a rhyolite from near Mount Bennett. Possible correlative units on the south side of the western Snake River graben include the Sheep Creek Rhyolite (9.88 ± 0.46 Ma; Hart and Aronson, 1983), the rhyolite of Tigert Springs, the rhyolite of OX Prong, and the rhyolite of Rattlesnake Creek (Kauffman and Bonnichsen, 1990; Jenks and others, 1993). Rhyolite in the eastern Mount Bennett Hills ranges in age from 9.2 ± 0.13 Ma to 10.1 ± 0.3 Ma (Armstrong and others, 1980; Honjo, 1990).

The Danskin Mountains Rhyolite most commonly occurs as a vitrophyre with abundant phenocrysts of sanidine and quartz set in a red, gray-brown, or black volcanic glass. Flow banding appears as laminar variations in the color of the glass or in its crystallinity. The flow banding is commonly folded ptygmatically, indicating rheomorphic mobilization of the rhyolite. Flow banding and axial foliation in the vitrophyre generally trend N. 50º W. to N. 60º W., and dip 15º-45º NE. There are no indications that these rhyolites are rheomorphic ignimbrites; they appear to be rhyolite lavas erupted from fissures that were subparallel to the current range-front faults (B. Bonnichsen, oral commun., 1996, 1997).

Pre-Lake Idaho Basaltic Volcanism

Pre-Lake Idaho basaltic volcanism in the Mountain Home area is represented by core samples from the 4,403-foot Mountain Home Air Force Base (AFB) geothermal test well (Lewis and Stone, 1988) and by basalt horizons that rest directly on rhyolite in the Danskin Mountains and Mount Bennett Hills (Honjo, 1990; Clemens and Wood, 1993). Additional stratigraphic control comes from the 9,676-foot-deep Bostic 1A wildcat petroleum well (Arney and others, 1982, 1984).

The Mountain Home AFB test well was drilled in 1985 on Mountain Home Air Force Base, 10 miles southwest of Mountain Home (Figure 3). The hole was cored continuously from about 1,000 feet to total depth of 4,403 feet, with 60-70 percent recovery above 2,000 feet in the sediments and 90-100 percent recovery below 2,000 feet in the basalts (Lewis and Stone, 1988). Principal rock types are basalt with intercalated sediment (0-532 feet), silty sand and clay (532-1,900 feet), and basalt with minor intercalated hyaloclastites (1,900-4,403 feet). Temperature at the bottom of the hole approached 100ºC (Lewis and Stone, 1988).

Basalts of the Mountain Home AFB drill core have not yet been studied in detail, but our preliminary petrographic and geochemical data indicate that they are dark gray to black, aphanitic aphyric to sparsely phyric (olivine or plagioclase plus olivine) ferrobasalts. These basalts are remarkably fresh and unaltered, except for a few horizons where the basalt appears to have flowed into water.

Basalts in the Danskin Mountains and Mount Bennett Hills that sit directly on rhyolite or are intercalated with lacustrine sediments that sit on rhyolite have been correlated with the Banbury Basalt of Malde and Powers (1962). They are generally altered olivine basalts, but there are little data that can be used to correlate these flows. Armstrong and others (1980) report a mean age of 9.4 Ma for the Banbury Basalt near Twin Falls, but it is unclear if this correlates with the unit referred to as "Banbury Basalt" in the Mount Bennett Hills (e.g., see Clemens and Wood, 1993, for a discussion of this problem).

Plateau-Forming Basalts: Late- to Post-Lake Idaho

Plateau-forming basalts crop out in the bluffs that overlook the current Snake River drainage, especially in the area north of C.J. Strike Reservoir (Figure 4). Younger plateau-forming basalts are also exposed on the tablelands above the bluffs, but the older plateau-forming units are seen only in cross section. Five plateau-forming basalt units are exposed in or near the area mapped (from oldest to youngest, Figure 3): the basalt of Goldsmith Road (Tgsr), the basalt of Canyon Creek (Tcan), the basalt of Simco Road (QTsim), the basalt of Strike Dam Road (QTstr), and the basalt of Rattlesnake Springs (QTrs). Only two units—the basalt of Rattlesnake Springs and the basalt of Strike Dam Road (Jenks and others, 1993)—can be associated with a specific volcanic vent. Vents for the other units have been buried by subsequent eruptive units, and their locations can only be guessed at using lateral variations in flow thickness.

These basalts typically form thin (8 to 35 feet thick), laterally extensive flows that rest directly on the youngest lacustrine or fluvial deltaic sediments of Lake Idaho or on older plateau-forming basalt units. The units tend

Figure 4. Plateau-forming basalts sitting on lacustrine sediments of the Idaho Group (Lake Idaho). Uppermost basalt is basalt of Rattlesnake Springs; lower unit is basalt of Simco Road. Note landslide deposits below main basalt ledge. View to East overlooking C.J. Strike Reservoir. North to left.

to thin near their margins, which allows us to estimate the relative positions of their buried vents or at least the topographic lows that controlled flow distribution.

The basalt of Goldsmith Road is exposed just south of our map area in a lower "plateau" adjacent to C.J. Strike Reservoir (Jenks and others, 1993). Based on its elevation, it appears to correlate with the deepest post-Lake Idaho basalts in the Mountain Home AFB drill core (about 500 feet below surface on the tableland above C.J. Strike Reservoir (Figure 3).

The basalt of Simco Road is commonly pillowed along its southern margin, suggesting a subaerial lava that flowed into standing water of Lake Idaho or its successors. The subaqueous part of the flow consists of hyaloclastite breccia forming foreset delta sequences with individual "rolled" pillows interspersed. The delta foresets dip to the southeast, indicating the direction the lava flowed when it entered the lake (Figure 5).

The basalt of Rattlesnake Springs is the youngest plateau-forming unit in this area. The vent for this unit is a low, topographically subdued shield volcano about 9 miles southwest of the town of Mountain Home (Figure 3). Despite its low topographic profile, this vent is actually a large structure covering all or large parts of five 7.5-minute quadrangles. Lava flows from younger vents to the north, northwest, and northeast of this huge volcano flowed around it. The deflection of younger lava flows around the Rattlesnake Springs vent created a topographic "moat" along its northeast margin that filled with alluvial sediments and loess; this filled "moat" is the location of Mountain Home.

The basalt of Rattlesnake Springs rests directly on fluvial-deltaic sediments (sands, silts, gravels) that form the uppermost part of the Idaho Group. Current structures in these sediments show transport directions from north to south consistent with regional drainage of tributary streams into Lake Idaho from the Danskin Mountains.

Maarlike Vents: Fire Fountain Eruptions

These rather inconspicuous maarlike vents can only be seen clearly on large-scale topographic maps, where the low annular ridges that represent the original tuff rings are generally preserved by subsequent spatter deposition and the onlap of late-stage lavas from the central vents. Some of the older plateau-forming basalts may have erupted from maarlike vents also, but these vents have

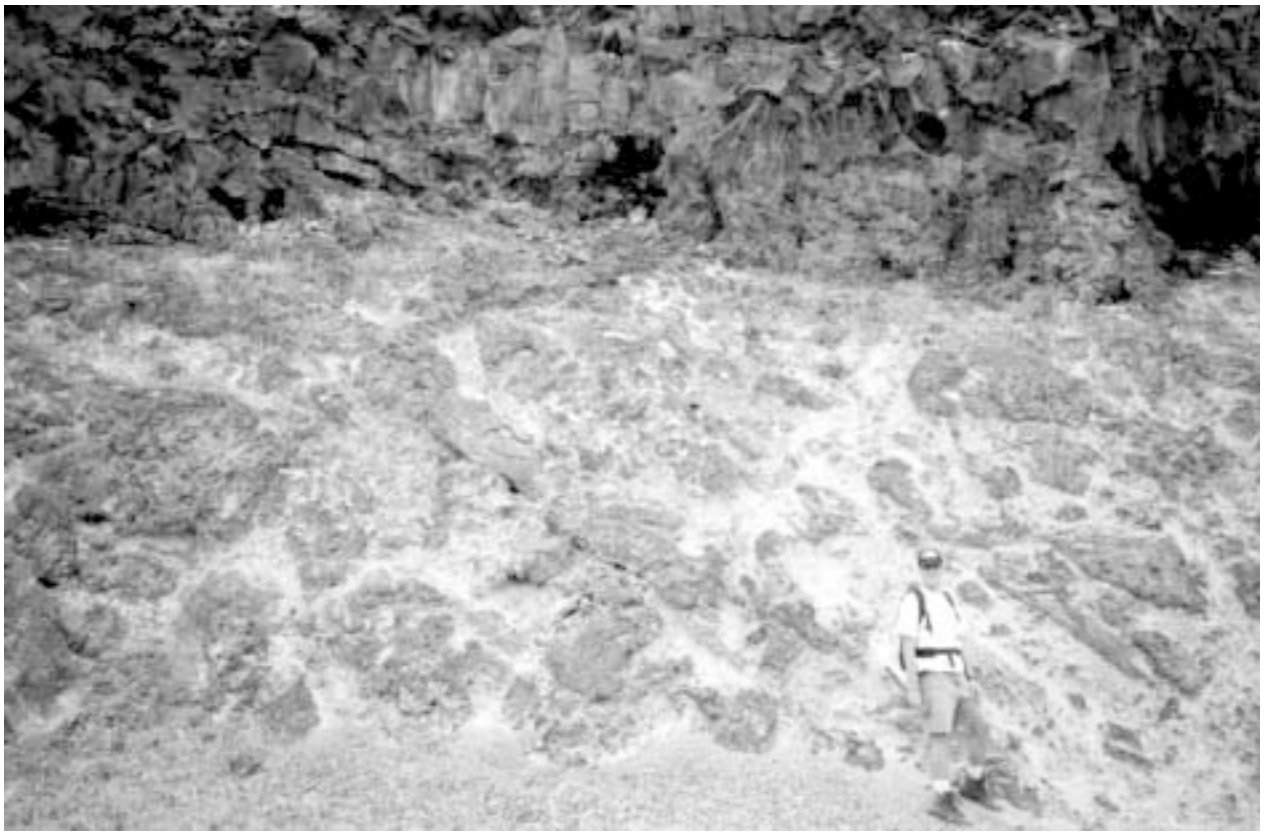

Figure 5. Foreset beds in hyaloclastite breccia + pillow lava delta at the base of the basalt of Strike Dam Road. Delta grades upward from dominantly glassy breccia to breccia + isolated pillows to subaerial basalt. Delta is underlain by lacustrine sediments (silty clay) of Idaho Group. Water depth was about 20 feet here. View to northeast.

been buried by younger flows. Bonnichsen (oral commun., 1996) suggests that these vents began as phreatomagmatic eruptions through water-saturated sediments, then shifted to fire fountain eruption style as the underlying sediments became dewatered. This model is difficult to evaluate, because the surface volcanic deposits cover evidence for the proposed earlier phreatomagmatic event. Nonetheless, an early phreatomagmatic eruptive style is consistent with the overall geometry of these vents.

There are two maarlike vents in the map area: the basalt of Brush (Qbr) and the basalt of Sheep (Qsh). Vents for both units consist of topographically low annular ridges that form ringlike structures about 2 to 3 miles (3 to 5 km) across. The ramparts of these ring structures are constructed largely of welded spatter, but cinder accumulations are found in places. Despite their maarlike structures, the dominant eruptive mode for these vents seems to have been fire fountain eruptions that formed abundant spatter and relatively fine-grained cinders (about 1 to 2 mm).

Shield Volcanoes

Shield volcanoes are the most common volcanic landforms in the Mountain Home area. These steep-sided volcanoes rise conspicuously above the tablelands formed by the plateau-forming basalts with 400 feet to 700 feet of relief (Figure 3). These vents are generally steeper than typical shield volcanoes and may represent magmas that are more viscous than typical Hawaiian tholeiites. These lavas rest on older plateau-forming basalts or on soil horizons developed on top of the older flows. The well-developed soil horizons, with extensive caliche layers, indicate that flows of different ages may be separated by several thousands of years.

Eight basalts are associated with shield volcano vents: the basalt of Teapot Basin (Qtb), the basalt of Rattlesnake Creek (Qrc), the basalt of Teapot South (Qts), the basalt of Teapot North (Qtn), the basalt of Rocky (Qrk), the basalt of Lockman Butte West (Qlbw), the basalt of Lockman Butte East (Qlbe), and the Crater Rings basalt (Qcr; Figure 2). It is not possible to discern the exact

order of eruption since not all of the vents have flows that overlap, but the list above represents their approximate stratigraphic order; the Crater Rings basalt appears to be the youngest unit of this series. In addition, other basalts in the uplands north of Mountain Home cannot be connected with a specific vent because of subsequent faulting. These units are mapped as undifferentiated basalt (Qbu).

The basalt of Lockman Butte West is a plagioclase-phyric ferrobasalt characterized by internal fractionation during flow (McGee and Shervais, 1997). Where well-exposed by a large roadcut along highway I-84, flow units of this basalt show flotation of plagioclase within covered lava tubes, and draining of very Fe-rich (about 16.5 weight percent total iron as FeO) ferrobasalt magma from the plagioclase cumulates into an aphyric bottom layer (McGee and Shervais, 1997). The plagioclase-rich flotation layers are characterized by diktytaxitic textures towards their tops (where exsolved gases have replaced the interstitial magma) and intergranular textures near their bases (where interstitial magma crystallized in place). Partially replaced magnesian olivine phenocrysts (Fo_{90}) suggest that the ferrobasalt was formed by extreme olivine fractionation of a primary picrite. The Fe-rich nature of these lavas is emphasized by the occurrence of Fe-rich K-feldspar, with about 5.5 weight percent Fe_2O_3 (McGee and Shervais, 1997).

The Crater Rings is a spectacular volcanic feature consisting of two large pit craters at the summit of a broad shield volcano about 5 miles west of Mountain Home (Figure 3). The smaller western crater is about 2,500 feet across and 300 feet deep; the larger eastern crater is about 3,000 feet across and 350 feet deep. The eastern crater is surmounted by spatter and agglutinate ramparts on its northern, eastern, and southern sides. Internally, the pit craters consist of welded spatter, agglutinate, and minor intercalated lava flows. The welded spatter and agglutinate are easily identified by their characteristic textures, oxidized coloration, and hollow ring when struck with a hammer.

The internal stratigraphy of the craters shows that they represent former lava lakes, similar to Halemaumau pit crater on the summit of Kilauea volcano and to the paired lava lakes of the 1972 Mauna Ulu eruption (Hawaii: Decker, 1987; Tilling and others, 1987). No fragmental horizons are exposed in the crater walls, which would suggest phreatomagmatic eruption. Fire fountains erupting through the lava lakes fed spatter to the rims, which were occasionally mantled by lava flows when the lava lakes overflowed their ramparts. The final eruptive phase was confined to the eastern vent, where fire fountains built ramparts on three sides of the vent that were not covered by subsequent lava flows, although lava from the eastern vent may have flowed into the western vent during lava highstands at this time. A more recent but equally spectacular example of a double pit crater is Black Butte Crater, the source of the Shoshone flow, located 16 miles north of the town of Shoshone in central Idaho.

Cinder Cone Vents: Last Volcanic Phase

The youngest volcanic features found in the Mountain Home area are cinder cone vents with 150 feet to 300 feet of relief that erupted north of the Rattlesnake Springs shield volcano. The youngest of these is exceptionally well preserved and has no overlying soil in the vent area, consistent with an age of less than 300,000 years. These vents include the Cinder Cone Butte basalt, the Union basalt, and the basalt of Cinder Pit (Figure 2). The Union basalt and the basalt of Cinder Pit erupted from vents immediately north of the Rattlesnake Springs shield volcano, and flows from both of the younger vents were deflected around the older volcano.

SEDIMENTARY ROCKS

Idaho Group (Tida)

Lacustrine sediments and fluvial-deltaic deposits associated with Neogene Lake Idaho are found along the southern rim of the tablelands that underlie the Mountain Home area, much of which lies south of our map (Figure 3). Only 400-450 feet of Idaho Group sediment is exposed in the bluffs that overlook the current Snake River drainage (Figure 4), but drilling on the Mountain Home AFB demonstrates at least 1,400 feet of sediment beneath the deepest postlake basalt (Lewis and Stone, 1988). Farther to the east (about 20 miles east of the Mountain Home AFB core) the 9,676-foot-deep Bostic 1A well penetrated over 4,500 feet of lacustrine sediments with two basalt intercalations, each about 650 feet thick (Arney and others, 1982, 1984).

Generally, the sediments are fine-grained, calcareous, clay-rich muds and silts, with sandy silts higher in the section (Kimmel, 1982; Swirydczuk and others, 1979, 1980; Smith and others, 1982). Ash beds and ash-rich sediments are common (Swirydczuk and others, 1982). The sediments are white to pale green and have fine laminar bedding and rare current structures. The sandy layers may be graded, suggesting deposition from turbidity currents (Jenks and others, 1993). Oolitic limestone horizons are interpreted to represent shoreline facies (Swirydczuk and others, 1979, 1980). Other reefal limestone horizons represent algal or sponge reefs that formed

parallel to the shoreline (Straccia and others, 1990; Jenks and others, 1993).

Sediments intercalated with basalt in the bluffs above C.J. Strike Reservoir are commonly sandy, with both laminar and trough cross-bedding, indicating a fluvial-deltaic environment along the margins of the lake. This is supported by the observation that hyaloclastites and pillow deltas (Figure 5) are found only beneath the southernmost exposures of plateau-forming lavas; exposures farther north show little or no effects of basalt-water interaction. Cross-beds in the fluvial sands beneath the basalt of Rattlesnake Springs show currents moving from north to south, towards the axis of the western SRP graben.

No fossil data are available for this area, but the stratigraphic level of the exposed sediments and their location suggests correlation with sediments of the Pleistocene Bruneau Formation. Older sediments exposed in core or cuttings and lacustrine sediments exposed south of the Mountain Home area probably correlate with the Pliocene Glenns Ferry Formation or Miocene Chalk Hills Formation of Malde and Powers (1962).

Surficial Deposits

Surficial deposits include the Melon Gravel (coarse, unsorted sand, gravel, and boulders deposited by the Bonneville Flood; Malde and Powers, 1962), intermittent lake deposits (clay- to silt-sized sediments transported largely as windblown loess and deposited into intermittent lakes that form in depressions on the surface of basalt flows; Jenks and others, 1993), talus and alluvial fan deposits that form along major range-front fault scarps, landslide deposits (produced by passage of the catastrophic Bonneville Flood, as discussed by Jenks and others, 1993), and alluvium (unconsolidated stream and valley deposits, including clay, silt, sand, and gravel).

STRUCTURE

Structural deformation of the Mountain Home area is restricted to high-angle faulting with two modes: (1) range-front faults that offset rhyolite and resulted in uplift of the Danskin Mountains and Mount Bennett Hills, and (2) younger faults that offset the surface of basalt flows or the alluvium. Tilting is evident in the rhyolite bedrock of the Mount Bennett Hills but is more difficult to establish elsewhere. Nonetheless, faulting clearly spans a range of ages (Neogene to Holocene) and has resulted in significant movement in the recent past.

RANGE-FRONT FAULTS

The range-front faults and related faults that offset rhyolite of the Idavada Formation are responsible for uplift of the Danskin Mountains and Mount Bennett Hills and for faulting within these ranges (Malde, 1959). These faults trend approximately N. 55° W. and have near vertical to steep southwest dips (Figure 3). In general, throw is down to the southwest, so most of these faults are normal (Figure 6). Most actual range-front faults are concealed beneath talus or alluvial fan deposits. Malde (1991) estimates that the accumulated throw across these faults is about 9,000 feet (2,900 m), as shown by the elevation difference between the top of silicic volcanic rocks in the Bostic 1-A well (Arney and others, 1982, 1984) and the rhyolite lavas of the Mount Bennett Hills (Malde, 1959).

Interpretive cross sections of the western SRP show the arrangement of range-front faults, which control subsidence of the graben, and the distribution of volcanic and sedimentary fill within the graben (Figure 6). Cross section A-A' transects the western SRP through Mountain Home, whereas section B-B' (modified from Wood, 1994) depicts a transect through Caldwell (see Figure 3 for locations of cross sections). The Mountain Home section (based on surface maps, deep well logs and regional gravity anomalies) shows rhyolite basement overlain by Banbury Basalt, lacustrine sediments of Lake Idaho, and a thick wedge of early Pliocene basalt (Figure 6). This wedge pinches out to the southeast, as shown by well logs of the Bostic 1A well (Arney and others, 1982). The lacustrine sediments are capped by thin basalt flows intercalated with sediment on the uplands surrounding Mountain Home. The central basement high and the thick sections of basalt on each side of the basement high are required by the regional gravity anomaly (Arney and others, 1982). The Caldwell section (based on surface maps, deep well logs, and seismic reflection data) shows an acoustic basement of basalt overlain by up to 6,000 feet of lacustrine sediment (Wood, 1994). Wells in this region bottomed in basalt, so the depth to rhyolite basement (if present) is not known.

The Mount Bennett Hills block appears to be tilted to the south for most of its length, with north-facing normal faults along its northern margin with the Camas Prairie. The southern margin of the Mount Bennett Hills appears to be a flexural downwarp beneath lavas of the eastern SRP trend, with only minor normal faulting (Cluer and Cluer, 1986). The southwest-facing normal faults that bound the Mount Bennett Hills block in the Mountain Home area lift the western end of this block and accommodate an eastward plunge. These complex relationships reflect the position of the Mount Bennett Hills at the intersection of the western SRP structural graben with the eastern SRP downwarp.

The ages of the range-front faults are unknown but can be estimated as late Miocene to early Pliocene on the

basis of the middle Miocene age of the Mount Bennett rhyolite (about 10 Ma; Clemens and Wood, 1993) and the Pliocene age of Lake Idaho, which filled the western SRP graben that formed during uplift of the rhyolites. The occurrence of Lake Idaho sediments within the Mount Bennett Hills, sitting depositionally on rhyolite vitrophyre or older basalts (Vetter, oral commun., 1998), shows that uplift of the Mount Bennett Hills continued into the Pliocene.

QUATERNARY FAULTING

Recent tectonic activity related to extension of the western SRP graben is demonstrated by fault scarps, with 6 to 30 feet (2 to 9 m) of throw, that crosscut the shield volcanoes and the basaltic flows associated with them. There are two dominant fault sets: one trends N. 85° W.; the other trends N. 60° W. (parallel to the range-front faults) and appears to truncate against the N. 85° W. set (Figure 3). All faults are vertical or high-angle normal faults that dip steeply to the south and are downthrown on the south or southwest side. Similar relationships are observed in the western Mount Bennett Hills where east-west trending faults offset N. 50° W. faults (Clemens and Wood, 1993).

Both sets of faults appear to have been active simultaneously, as shown by asymetric escarpments in the N. 85° W. faults that have larger offsets at the east end than at the west end. This asymetric movement on the N. 85° W. faults was accommodated by movement on the N. 60°

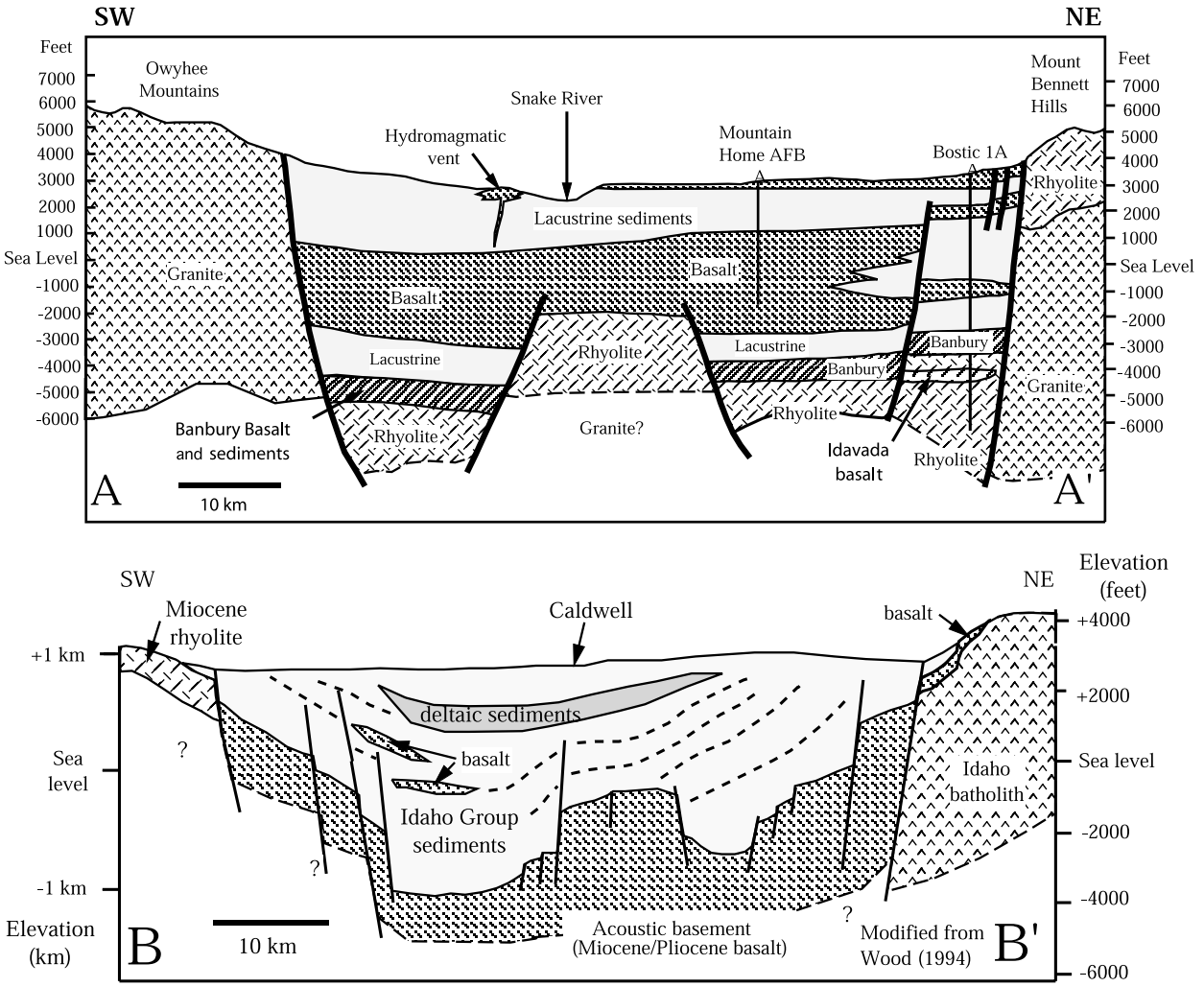

Figure 6. Interpretive cross sections of western SRP: section A-A' from Owyhee Plateau to Mountain Home area; section B-B' through Caldwell (see Figure 2 for location of sections). Section A-A' based on well logs of Mountain Home AFB core (Lewis and Stone, 1988), the Bostic 1A well (Arney and others, 1982, 1984), gravity profiles of the western SRP, and surface mapping (this study; Jenks and others, 1993). Section B-B' near Caldwell, modified from Wood (1994), is based on well logs and seismic reflection data.

W. faults, many of which also preserve asymetric escarpments that have larger offsets on their north ends. The sense of motion here seems to be one in which trapezoid-shaped lozenges of crust accommodated northeast-southwest extension by rotating along pairs of south-dipping and southwest-dipping normal faults.

The age of faulting cannot be determined precisely at this time but must be younger than about 1 Ma, based on the age of the basalt units cut by the faults. In one location, basalt is faulted against alluvial gravel of Canyon Creek (Figure 3), suggesting a late Pleistocene or Holocene age. Beukelman (1997) has shown that similar scarps which offset alluvium in the Halfway Gulch-Little Jacks Creek area south of Mountain Home have ages of about 5,000 to 34,000 years, based on the degradation of scarp profiles. Trenching across one fault indicates five episodes of surface rupture over the last 26,000 years, based on caliche accumulation in the soils (Beukelman, 1997).

GEOCHEMISTRY

Geochemical studies of the volcanic rocks described here are still in progress, so it is not possible to discuss their chemical and petrologic evolution at this time. We can, however, make a general comparison between the older, pre-Lake Idaho lavas sampled by the Mountain Home AFB core and the surface lava flows (Table 1). We can also compare both of these groups to basaltic lavas from the eastern SRP trend (Shervais and others, 1994) and to flood basalts of the Columbia River Plateau province (Tolan and others, 1989; Reidel and others, 1989; Hooper, 1988).

In general, late Pliocene to Quaternary surface flows in the Mountain Home area are similar to basaltic lavas from the eastern SRP in their Fe, Ti, alkali, and silica content (Figure 7). Fe is at the high end of the range for this trend and is higher than typical eastern SRP basalts in many samples. In contrast, early Pliocene, pre-Lake Idaho basalts from the Mountain Home AFB core are much higher in Fe and Ti and lower in alkalis, silica, and phosphorus than typical basalts of the eastern SRP. This suggests a source for the older basalts that is depleted relative to the eastern SRP basalt source in large ion lithophile elements (LILE), but enriched in Fe and Ti, possibly as a result of Fe-Ti metasomatism (Shervais and Vetter, 1992).

When compared with basalts of the SRP province, flood basalts of the Columbia River Plateau (Tolan and others, 1989; Reidel and others, 1989) are much lower in Mg, Fe, Ti, and P and higher in Si and K (Figure 7). This suggests that, relative to basalts of the SRP province, the Columbia River basalts have seen much more exchange with continental materials. This may reflect either assimilation of subcontinental lithosphere or partial melting and assimilation of continental crust (Carlson, 1984; Carlson and Hart, 1988; Carlson and others, 1981).

DISCUSSION

The history of basaltic volcanism in the western SRP is punctuated in the Pliocene by a prolonged hiatus of about 4 million years duration. This is clearly shown by the distribution of basalt and sediment in the Mountain Home AFB core samples, by the stratigraphy of sediments and basalts that crop out in the western SRP, and by seismic profiles of the western SRP (e.g., Wood, 1984, 1994; Wood and Anderson, 1981). The duration of this hiatus corresponds largely with sedimentation in Lake Idaho, but volcanism and sedimentation overlapped in time and space both near the beginning of sedimentation in the early Pliocene and near its end in the late Pleistocene. This overlap is greater farther to the west, near Boise and Caldwell, where phreatomagmatic vents demonstrate the eruption of large volcanos within standing water of the lake (Godchaux and others, 1992). The hiatus in basaltic volcanism shows that development of the western SRP occurred during two separate and possibly unrelated events. We examine each of these events below.

PRE-LAKE IDAHO TECTONICS AND VOLCANISM

Formation of the western SRP graben was preceded by the eruption of high-temperature rhyolites from northwest-trending fissures (Honjo and others, 1992; Bonnichsen, 1997). These rhyolites have anhydrous phenocryst assemblages and calculated eruption temperatures of around 850ºC to 1,000ºC (Honjo and others, 1992). Existing radiometric dates suggest an age progression of high-temperature rhyolites from northwest to southeast. Thus, rhyolites at the northwest end of the western SRP have ages around 11.2 Ma to 11.6 Ma; rhyolites in the Danskin Mountains have ages of 10.0 Ma to 11.0 Ma, and rhyolites in the western and central Mount Bennett Hills have ages of 9.2 Ma to 9.8 Ma (Armstrong and others, 1975, 1980; Honjo, 1990; Clemens and Wood, 1993).

Range-front faults in the western SRP are associated with the formation of the western SRP graben, which became the locus of deposition of Lake Idaho in the late Miocene through Pliocene (Figure 6). The formation of this graben predates Basin and Range extension, and its orientation (about N. 50º W.) is inconsistent with other

Table 1. Representative whole rock geochemistry for selected basaltic lavas from the Mountain Home area. Major elements by fused bead electron-probe analysis. Trace elements by x-ray fluorescence analysis. Latitude and longitude locations are in decimal degrees. Mountain Home AFB core location estimated from map location, with depth below surface in feet for each sample from driller's log.

Sample No.	**96SRP-21-2**	**96SRP-58-2**	**96SRP-V40**	**96SRP-9**	**96SRP-27**	**96SRP-12**	**MH-2538**	**MH-3102**	**MH-4103**
Unit/Vent	**Borrow Pit/ 3245**	**Crater South Flow 3198**	**Lockman/ Lock 3624**	**Radio Tower/ Rocky 3649**	**Teapot North**	**Tuff Ring/ Brush 3291**	**Mtn. Home AFB Core**	**Mtn. Home AFB Core**	**Mtn. Home AFB Core**
Quadrangle USGS 7.5'	**Reverse**	**Cinder Cone Butte**	**Crater Rings**	**Mtn. Home North**	**Teapot Dome**	**Reverse**	**Crater Rings SE**	**Crater Rings SE**	**Crater Rings SE**
Lat. North	**43.078617**	**43.141500**	**43.201817**	**43.132450**	**43.186600**	**43.057400**	**43.057400**	**43.057400**	**43.057400**
Long. West	**115.597217**	**115.909933**	**115.765833**	**115.625117**	**115.605700**	**115.532433**	**115.839333**	**115.839333**	**115.839333**
Depth (in feet)	**NA**	**NA**	**NA**	**NA**	**NA**	**NA**	**2,538**	**3,102**	**4,103**
SiO_2	46.10	46.38	48.49	46.46	47.39	47.17	46.24	47.09	46.19
TiO_2	3.03	3.35	2.17	3.17	3.24	2.58	4.06	3.49	4.48
Al_2O_3	13.69	13.90	17.37	13.91	13.93	13.21	13.87	14.44	13.79
FeO	13.77	15.48	11.99	14.44	14.43	13.11	16.42	15.04	17.75
MnO	0.24	0.24	0.18	0.19	0.19	0.21	0.22	0.25	0.23
MgO	6.93	6.79	5.79	6.72	6.64	6.46	7.18	6.04	5.50
CaO	12.11	9.64	10.46	10.67	9.80	12.76	10.51	9.96	11.07
Na_2O	2.34	2.40	2.68	2.35	2.41	2.23	1.52	2.26	1.09
K_2O	0.60	0.57	0.43	0.58	0.64	0.70	0.26	0.66	0.07
P_2O_5	0.58	0.63	0.74	0.68	0.53	0.51	0.11	0.66	0.14
Total	99.38	99.39	100.29	99.18	99.20	98.94	100.38	99.89	100.32
Nb	19	20	32		19	17	21	31	34
Zr	276	278	355		263	260	297	395	406
Y	43	42	48		42	39	54	61.5	70
Sr	316	315	338		325	320	302	289.5	300
Rb	14	7	2		11	13	4	15.5	3
Zn	136	145	147		144	134	178	161.5	175
Cu	46	31	42		52	48	50	38	49
Ni	62	61	72		80	74	93	76.5	67
Cr	182	181	196		209	199	209	154	134
Sc	36	33	33		30	33			
V	349	333	303		328	298			
Ba	470	441	501		454	514			

Basin and Range grabens (typically N. 20º W. to N. 10º E. in northern Nevada).

This graben appears to be older at its northwest-end and to become progressively younger to the southeast (e.g., Kimmel, 1982; Malde, 1991). This conclusion is based on the age progression of rhyolite lavas discussed above and the age of the oldest sediments filling the graben, which become progressively younger from northwest (late Miocene) to southeast (Pliocene) along the axis of the graben (Kimmel, 1982; Malde, 1991). While the western SRP graben at its northwest end (Oregon-Idaho border) is approximately coeval with the formation of the Bruneau-Jarbidge eruptive center (10-12 Ma), the southeast end of the graben is younger, and structures

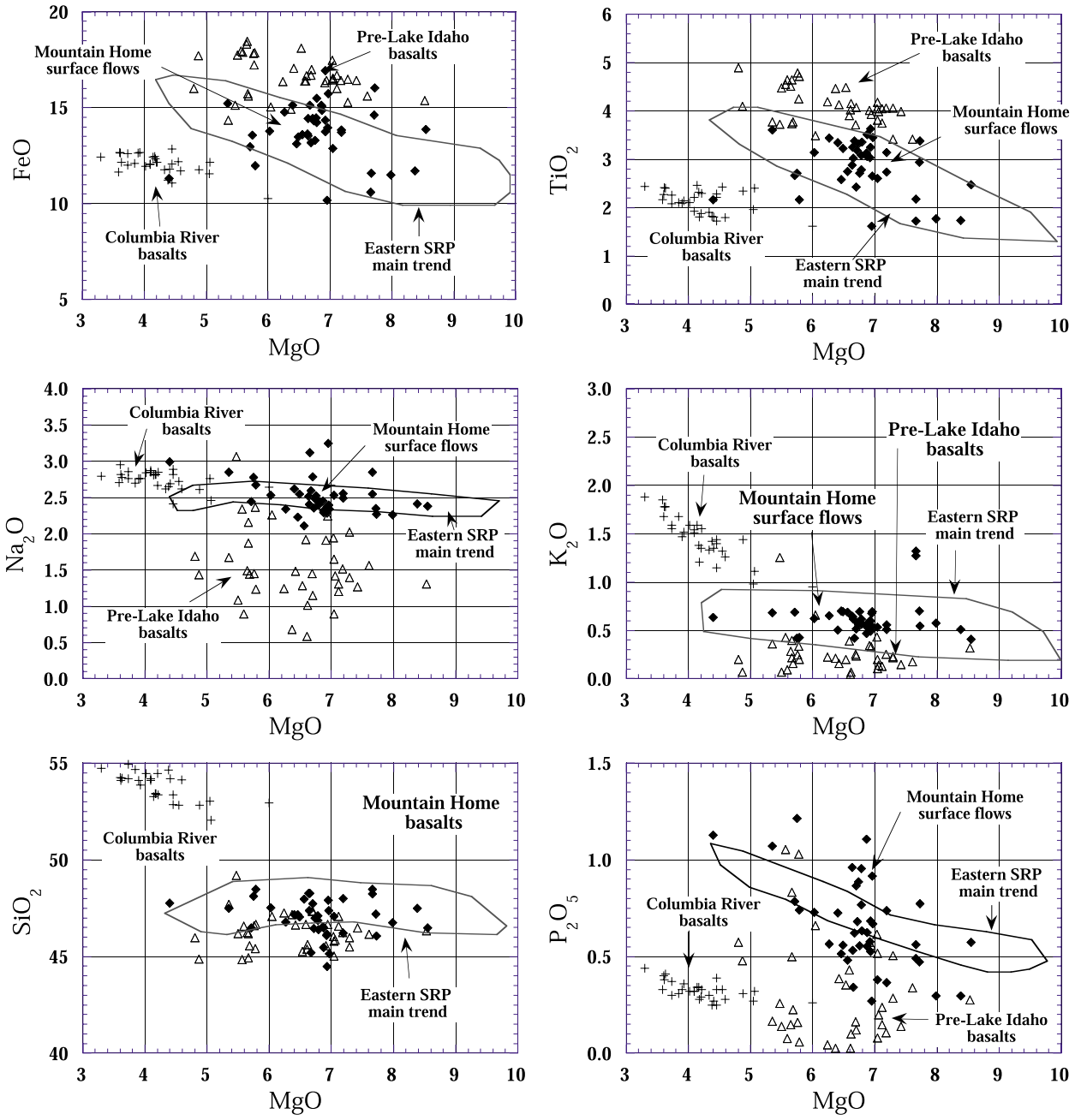

Figure 7. Summary of geochemical data for pre-Lake Idaho and post-Lake Idaho basalts from the Mountain Home region compared to basalts from the eastern Snake River Plain "main trend" and to flood basalts (basaltic andesites) of the Columbia River Plateau.

associated with the graben and its sedimentary fill cross-cut the margins of the Bruneau-Jarbidge eruptive center. The western SRP graben reached its maximum headward extent approximately 3 Ma, as shown by the age of the youngest Glenns Ferry Formation at the southeast end of the Lake Idaho basin (Malde, 1991).

Pre-Lake Idaho basalts are characterized by low alkali contents and by extremely high Fe and Ti (Fe-Ti basalts). These basalts are coeval with plume-tail volcanism of the Bruneau-Jarbidge eruptive center (Bonnichsen, 1982), but they differ compositionally from basalts associated with this eruptive center (e.g., Vetter and others, 1997). They are also coeval with the Saddle Mountains Basalt—the final eruptive phase of the Columbia River flood basalt province (Reidel and others, 1989; Tolan and others, 1989).

The data discussed above suggest that the formation of the western SRP graben and its sedimentary fill is not related to passage of the Yellowstone plume tail from the Owyhee Plateau to the eastern SRP. The data do show a connection between the formation of the western SRP and the flood basalt volcanism of the Columbia River Plateau. To the extent that the Columbia River basalts can be related to the Yellowstone plume head, there is a connection between the western SRP and the Yellowstone plume (e.g., Glen and Ponce, 2002). If so, the plume head was deflected significantly to the north from its proper position in line with the track of the plume tail, as suggested by Geist and Richards (1993) and Camp (1995).

We suggest that the western SRP graben may be thought of as an aulocogenlike rift associated with thermal doming of the lithosphere beneath the Columbia River Plateau; the orientation of this rift was likely controlled by thermal softening of lithosphere by the plume tail, which at this time was located beneath the Bruneau-Jarbidge eruptive center, and by the orientation of large-scale fractures over the plume head beneath the Columbia River plateau (Glen and Ponce, 2002). If this model is correct, then pre-Lake Idaho basalts may be related to the flow of plume-source mantle along a sublithospheric conduit formed by extension of the western SRP. Since the graben is older in the northwest, the flow of this plume-source mantle was most likely from northwest to southeast, that is, from beneath the Columbia River Plateau toward Twin Falls. This implies that the pre-Lake Idaho basalts formed by pressure-release melting of both (1) the previously depleted plume-source mantle and (2) the overlying mantle lithosphere. This is also consistent with the occurrence of high-temperature rhyolites, which are thought to form by crustal anatexis in response to the intrusion of mafic magmas at depth.

This model is illustrated schematically in Figure 8. Between 17 Ma and 14 Ma, the Yellowstone plume head was deflected northward by the Farallon plate (Geist and Richards, 1993) or by North American lithosphere (Camp, 1995), resulting in the eruption of flood basalts on the Columbia River and Oregon plateaus. Thermal tumescence over the plume head elevated eastern Oregon and Washington and initiated the formation of the western SRP graben as an "aulacogen" radial to the center of uplift (Figure 8a). During the period from 12 Ma to 6 Ma, the plume head was compressed and overridden by North America; the compressed plume material "escaped" to southeast along a sublithospheric conduit beneath the developing western SRP graben (Figure 8b). As the plume head cooled and relaxed thermally, the western SRP graben subsided and became the locus of Lake Idaho sedimentation (Figure 8c). At this same time, depleted plume head mantle underplated continental lithosphere beneath the western SRP. The final phase of its development (2 Ma to today) is discussed below.

POST-LAKE IDAHO TECTONICS AND VOLCANISM

Post-Lake Idaho basalts are all less than 2 Ma old and chemically similar to coeval basalts of the eastern SRP (although the common occurrence of ferrobasalt is unique to the western SRP). In the eastern SRP, the youngest basalts are associated with north- to northwest-trending volcanic rift zones oriented perpendicular to the trend of the eastern SRP (Kuntz and others, 1982, 1988, 1992). Rodgers and others (1990) have shown that these volcanic rift zones, which parallel normal faults of the Basin and Range Province, accommodate aseismic extension of the eastern SRP in response to extension within the Basin and Range Province.

Young faults in the western SRP (i.e., those that offset post-Lake Idaho basalt flows or Holocene gravels) appear to reflect Basin and Range extension that has refracted to more westerly orientation to exploit preexisting range-front fault zones of the western SRP (Figure 8d). The occurrence of approximately east-west oriented faults of this age show that a component of north-south extension is also required. The distribution of post-Lake Idaho basalts along the northeast margin of the western SRP graben, and their association with Basin and Range extensional features, suggest that these basalts also formed in response to Basin and Range extension. The mechanism for the formation of the young eastern SRP basalts is still being debated, but there seems to be a consensus that they formed by pressure-release melting of plume-modified lithosphere (e.g., Leeman 1982, Vetter and Shervais, 1992).

The hiatus between the older pre-Lake Idaho basalts and the younger Basin and Range-related basalts prob-

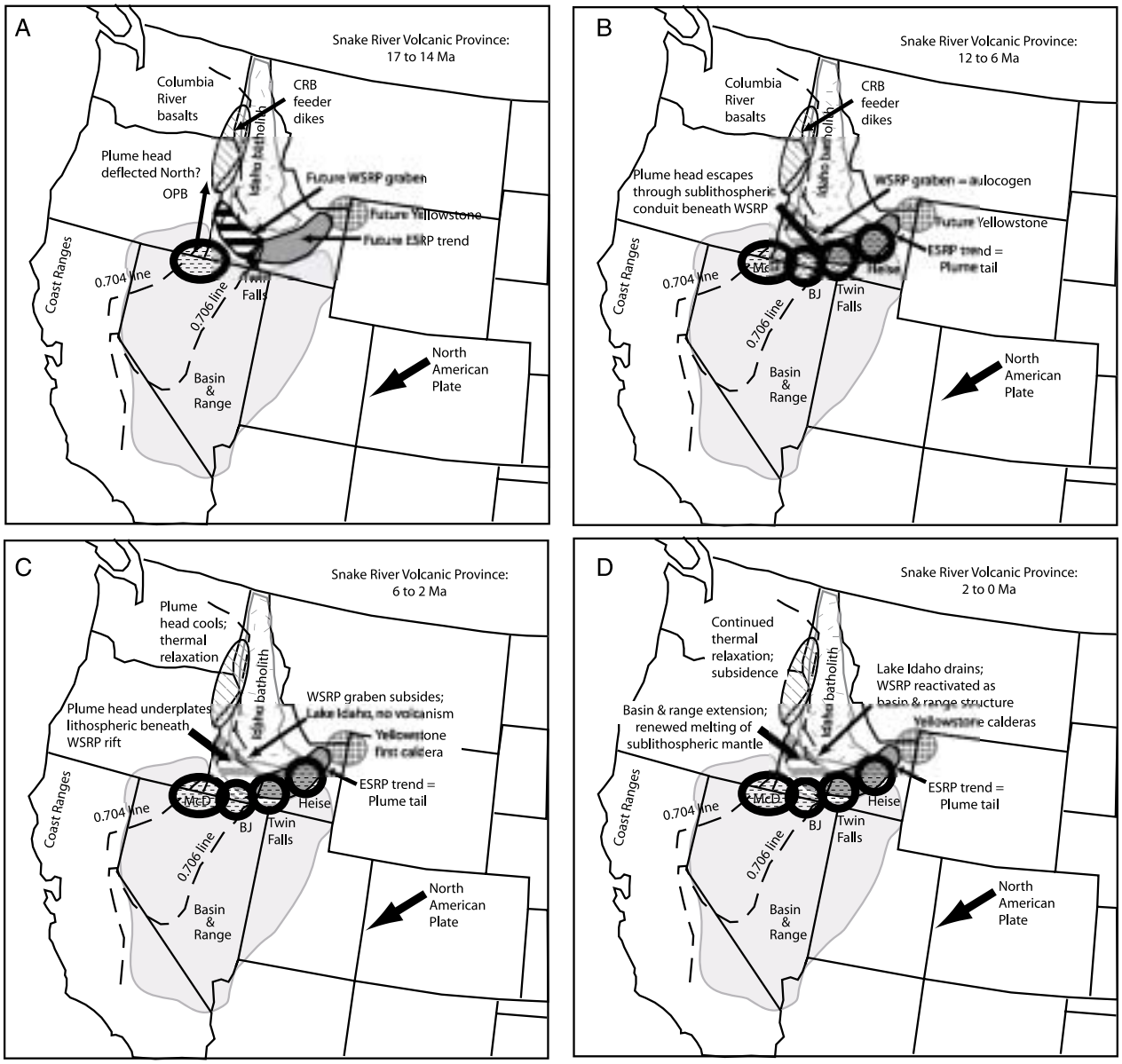

Figure 8. Cartoon depicting the evolution of the western SRP based on model presented here. (a) 17 Ma to 14 Ma: Yellowstone plume head deflected northward by Farallon plate or North American lithosphere; thermal tumescence of eastern Oregon and Washington. (b) 12 Ma to 6 Ma: Plume head compressed and overridden by North America, with continued thermal tumescence of lithosphere; western SRP graben develops as an "aulacogen" (sediment-filled rift) radial to the center of uplift; compressed plume material "escapes" to southeast along sublithospheric conduit beneath western SRP graben. (c) Plume head cools and relaxes, underplates western SRP; western SRP subsides and becomes locus of Lake Idaho sedimentation. (d) 2 Ma to today: Plume tail reaches Yellowstone, Lake Idaho drains, and western SRP reactivated as Basin and Range structure.

ably represents the recovery time of the lithosphere from thermal softening by the plume tail, which seems to have inhibited the propagation of Basin and Range-style extension northwards. The difference in the length of this hiatus in the western SRP (around 4 million years) and the eastern SRP (less than 1 million years?) may reflect differences in the nature, age, and composition of the lithosphere between these two locations (late Proterozoic to Mesozoic in the west, Archean in the east).

CONCLUSIONS

Basaltic volcanism in the western SRP was active in two distinct phases separated by a hiatus of several million years. Lacustrine sediments of the Idaho Group were

deposited largely during this hiatus. Our work in the Mountain Home region of the western SRP, when combined with observations from other parts of the western SRP graben and from the eastern SRP, suggests that these volcanic episodes represent distinct, unrelated events.

The older volcanic episode formed in response to passage of the Yellowstone plume system and thermal tumescence of the Columbia River Plateau. This episode included the formation of the western SRP graben, the eruption of high-temperature rhyolite lavas, and the eruption of pre-Lake Idaho Fe-Ti basalts. The basaltic volcanism may be related to the flow of depleted plume source mantle along a sublithospheric conduit beneath the western SRP graben from the Columbia River Plateau. The basalts would form by pressure-release melting of this previously depleted material along with the overlying mantle lithosphere (Figure 8).

The younger volcanic episode apparently formed in response to Basin and Range extension in a fashion analogous to young basaltic volcanism in the eastern SRP. The source of these basalts is uncertain but may be plume-modified subcontinental lithosphere.

Finally, despite the progress made in the last few years, much remains to be done in understanding the origin and evolution of the SRP volcanic system. It is particularly important that detailed geochemical and isotopic studies, based on careful field studies and modern geologic maps, distinguish between events of different ages and locations. These age-location relationships are especially important in the western SRP, where major changes in tectonic regimes occurred during the Neogene.

ACKNOWLEDGMENTS

Many thanks to Bill Bonnichsen, Kurt Othberg, Martha Godchaux, and Bill Leeman, whose discussions with us on the origin and evolution of the SRP have been valuable. Special thanks to Bill Bonnichsen and Martha Godchaux for guided tours of their field areas and for their special insights into the inner workings of the western SRP. We also wish to thank Craig White for his editorial handling of this manuscript and Dick Smith for a careful and insightful review. Our work was supported by NSF grants EAR-9526594 (Shervais), EAR-9526722 (Vetter), and EAR-9526723 (Hanan).

REFERENCES

Amini, M.H., H.H. Mehnert, and J.D. Obradovich, 1984, K-Ar ages of late Cenozoic basalts from the western Snake River Plain, Idaho: Isochron West, no. 41, p. 7-11.

Arney, B.H., J.N. Gardner, and S.G. Bellnomi, 1984, Petrographic analysis and correlation of volcanic rocks in Bostic 1-A well near Mountain Home, Idaho: Los Alamos National Laboratory Report LA-9966-HDR, 29 p.

Arney, B.H., F. Goff, and Harding Lawson Associates, 1982, Evaluation of the hot dry rock geothermal potential of an area near Mountain Home Idaho: Los Alamos National Laboratory Report LA-9365-HDR, 65 p.

Armstrong, R.L., J.R. Harakal, and W.M. Neill, 1980, K-Ar dating of the Snake River Plain (Idaho) volcanic rocks—new results: Isochron West, no. 27, p. 5-10.

Armstrong, R.L., W.P. Leeman, and H.E. Malde, 1975, K-Ar dating, Quaternary and Neogene volcanic rocks of the Snake River Plain, Idaho: American Journal of Science, v. 275, p. 225-251.

Bonnichsen, Bill, 1982, The Bruneau-Jarbidge eruptive center, southwestern Idaho, *in* Bill Bonnichsen and R.M. Breckenridge, eds., Cenozoic Geology of Idaho: Idaho Bureau of Mines and Geology Bulletin 26, p. 237-254.

———, 1997, Volcanism in the western Snake River Plain, southwestern Idaho: Geological Society of America, Abstracts with Programs, v. 29, no. 6, p. A296.

Bonnichsen, Bill, and D.F. Kauffman, 1987, Physical features of rhyolite lava flows in the Snake River Plain volcanic province, southwestern Idaho, *in* J. Fink, ed., The Emplacement of Silicic Domes and Lava Flows: Geological Society of America Special Paper 212, p. 119-145.

Bonnichsen, Bill, and M.D. Jenks, 1990, Geologic map of the Jarbidge River Wilderness Study Area, Owyhee County, Idaho: U.S. Geological Survey Map MF-2127, scale 1:50,000.

Beukelman, G.S., 1997, Evidence of active faulting in Halfway Gulch-Little Jacks Creek area of the western Snake River Plain, Idaho: Boise State University M.S. thesis, 148 p.

Camp, V.E., 1995, Mid-Miocene propagation of the Yellowstone mantle plume beneath the Columbia River basalt source region: Geology, v. 23, p. 435-438.

Carlson, R.W., 1984, Isotopic constraints on Columbia River flood basalt genesis and the nature of the subcontinental mantle: Geochimica et Cosmochimica Acta, v. 48, p. 2357-2372.

Carlson, R.W., and W.K. Hart, 1988, Flood basalt volcanism in the northwestern United States, *in* J.D. MacDougall, ed., Continental Flood Basalts: Kluwer Academic Publishers, p. 35-61.

Carlson, R.W., G.W. Lugmair, and J.D. McDougall, 1981, Columbia River volcanism: The question of mantle heterogeneity or crustal contamination: Geochimica et Cosmochimica Acta, v. 45, p. 2483-2499.

Christiansen, R.L., 1982, Late Cenozoic volcanism of the Island Park area, eastern Idaho, *in* Bill Bonnichsen and R.M. Breckenridge, eds., Cenozoic Geology of Idaho: Idaho Bureau of Mines Geology Bulletin 26, p. 345-368.

Christiansen, R.L., G.R. Foulger, and J.R. Evans, 2002, Upper-mantle origin of the Yellowstone hotspot: Geological Society of America Bulletin, v. 114, p. 1245-1256.

Clemens, D.M., and S.H. Wood, 1993, Late Cenozoic volcanic stratigraphy and geochronology of the Mount Bennett Hills, central Snake River Plain, Idaho: Isochron West, no. 60, p. 3-14.

Cluer, J.K., and B.L. Cluer, 1986, The late Cenozoic Camas Prairie rift, south-central Idaho: Contributions to Geology, University of Wyoming, v. 24, no. 1, p. 91-101.

Cope, E.D., 1883, A new Pliocene formation in the Snake River valley: American Naturalist, v. 17, p. 867-868.

Decker, R.W., 1987, Dynamics of Hawaiian volcanos: An overview, *in* R.W. Decker, T.L. Wright, P.H. Stauffer, eds., Volcanism in Hawaii: U.S. Geological Survey Professional Paper 1350, ch. 42, p. 997-1018.

Ekren, E.B., D.H. McIntyre, E.H. Bennett, and R.F. Marvin, 1982, Cenozoic stratigraphy of western Owyhee County, Idaho, *in* Bill Bonnichsen and R.M. Breckenridge, eds., Cenozoic Geology of Idaho: Idaho Bureau of Mines and Geology Bulletin 26, p. 215-236.

Geist, D.J., and M. Richards, 1993, Origin of the Columbia River Plateau and Snake River Plain: Deflection of the Yellowstone plume: Geology, v. 21, p. 789-792.

Glen, J.M.G., and D.A. Ponce, 2002, Large-scale fractures related to inception of the Yellowstone hotspot: Geology, v. 30, p. 647-650.

Godchaux, M.M., Bill Bonnichsen, and M.D. Jenks, 1992, Types of phreatomagmatic volcanoes in the western Snake River Plain, Idaho, USA: Journal of Volcanology and Geothermal Resources, v. 52, p. 1-25.

Hackett, W.R., and R.P. Smith, 1992, Quaternary volcanism, tectonics, and sedimentation in the Idaho National Engineering Laboratory area, *in* J.R. Wilson, ed., Field Guide to Geologic Excursions in Utah and Adjacent Areas of Nevada, Idaho, and Wyoming: Utah Geological Society, Miscellaneous Publications, p. 92-93.

Hart, W.K., and J.L. Aronson, 1983, K-Ar ages of rhyolites from the western Snake River Plain area, Oregon, Idaho, and Nevada: Isochron West, v. 36, p. 17-19.

Honjo, Norio, 1990, Geology and stratigraphy of the Mount Bennett Hills, and the origin of west-central Snake River Plain rhyolites: Rice University Ph.D. dissertation, 259 p.

Honjo, Norio, W.P. Leeman, and J.C. Stormer, 1992, Mineralogy and geothermometry of high-temperature rhyolites from the central and western Snake River Plain: Bulletin of Volcanology, v. 54, p. 220.

Hooper, P.R., 1988, The Columbia River basalt, *in* J.D. MacDougall, ed., Continental Flood Basalts: Kluwer Academic Publishers, p. 1-33.

Howard, K.A., and J.W. Shervais, 1973, Geologic map of Smith Prairie, Elmore County, Idaho: U.S. Geological Survey Map I-818.

Howard, K.A., J.W. Shervais, and E.H. McKee, 1982, Canyon-filling lavas and lava dams on the Boise River, Idaho, and their significance for evaluating downcutting during the last two million years, *in* Bill Bonnichsen and R.M. Breckenridge, eds., Cenozoic Geology of Idaho: Idaho Bureau of Mines and Geology Bulletin 26, p. 629-641.

Humphreys, E.D., K.G. Dueker, D.L. Schutt, and R.B. Smith, 2000, Beneath Yellowstone: Evaluating plume and nonplume models using teleseismic images of the upper mantle: GSA Today, v. 10, p. 1-7.

Jenks, M.D., and Bill Bonnichsen, 1989, Subaqueous basalt eruptions into Pliocene Lake Idaho, Snake River Plain, Idaho, *in* V.E. Chamberlain, R.M. Breckenridge, and Bill Bonnichsen, eds., Guidebook of the Geology of Northern and Western Idaho and Surrounding Areas: Idaho Geological Survey Bulletin 28, p. 17-34.

———, 1990, Geologic map of the Wild Horse Butte quadrangle, Ada and Owyhee counties, Idaho: Idaho Geological Survey Technical Report 90-8, scale 1:24,000, 9 p.

Jenks, M.D., Bill Bonnichsen, and M.M. Godchaux, 1993, Geologic maps of the Grand View-Bruneau area, Owyhee County, Idaho: Idaho Geological Survey Technical Report 93-2, scale 1:24,000, 21 p.

Kimmel, P.G., 1982, Stratigraphy, age, and tectonic setting of the Miocene-Pliocene lacustrine sediments of the western Snake River Plain, Oregon and Idaho, *in* Bill Bonnichsen and R.M. Breckenridge, eds., Cenozoic Geology of Idaho: Idaho Bureau of Mines and Geology Bulletin 26, p. 559-558.

Kuntz, M.A., D.E. Champion, R.H. Lefebvre, and H.R. Covington, 1988, Geologic map of the Craters of the Moon, Kings Bowl, and Wapi lava fields and the Great Rift volcanic rift zone, south-central Idaho: U.S. Geological Survey Miscellaneous Investigations Series Map I-1632, scale 1:100,000.

Kuntz, M.A., D.E. Champion, E.C. Spiker, R.H. Lefebvre, and L.A. McBroome, 1982, The Great Rift and the evolution of the Craters of the Moon lava field, Idaho, *in* Bill Bonnichsen and R.M. Breckenridge, eds., Cenozoic Geology of Idaho: Idaho Bureau of Mines and Geology Bulletin 26, p. 423-437.

Kuntz, M.A., H.R. Covington, and L.J. Schorr, 1992, An overview of basaltic volcanism of the eastern Snake River Plain, Idaho, *in* P.K. Link, M.A. Kuntz, and L.B. Platt, eds., Regional Geology of Eastern Idaho and Western Wyoming: Geological Society of America Memoir 179, p. 227-267.

Leeman, W.P., 1982, Development of the Snake River Plain-Yellowstone Plateau province, Idaho and Wyoming: An overview and petrologic model, *in* Bill Bonnichsen and R.M. Breckenridge, eds., Cenozoic Geology of Idaho: Idaho Bureau of Mines and Geology Bulletin 26, p. 155-177.

Lewis, R.E., and M.A.J. Stone, 1988, Geohydrologic data from a 4403-foot geothermal test hole, Mountain Home Air Force Base, Elmore County, Idaho: U.S. Geological Society Open-File Report 88-166, 30 p.

Mabey, D.R., 1976, Interpretation of a gravity profile across the western Snake River Plain, Idaho: Geology, v. 4, p. 53-55.

———, 1978, Regional gravity and magnetic anomalies in the eastern Snake River Plain, Idaho: U.S. Geological Survey Journal of Research 6, p. 553-562.

———, 1982, Geophysics and tectonics of the Snake River Plain, Idaho, *in* Bill Bonnichsen and R.M. Breckenridge, eds., Cenozoic Geology of Idaho: Idaho Bureau of Mines and Geology Bulletin 26, p. 139-153.

Malde, H.E., 1959, Fault zone along northern boundary of western Snake River Plain, Idaho: Science, v. 130, p. 272.

———, 1991, Quaternary geologic and structural history of the Snake River Plain, Idaho and Oregon, *in* R.B. Morrison, ed., Quaternary Non-Glacial Geology: Conterminous United States: Geological Society of America, Boulder, Colorado, The Decade of North American Geology, K2, p. 251-281.

Malde, H.E., and H.A. Powers, 1962, Upper Cenozoic stratigraphy of western Snake River Plain, Idaho: Geological Society of America Bulletin 73, p. 1197-1220.

———, 1972, Geologic map of the Glenns Ferry-Hagerman area, west-central Snake River Plain, Idaho: U.S. Geological Survey Miscellaneous Investigations Map I-696, scale 1:48,000, 2 sheets.

Malde, H.E., H.A. Powers, and C.H. Marshall, 1963, Reconnaissance geologic map of west-central Snake River Plain, Idaho: U.S. Geological Survey Miscellaneous Investigations Map I-373, scale 1:125,000.

McGee, James, and John Shervais, 1997, Flotation cumulate in a Snake River Plain ferrobasalt: Petrologic study of a possible lunar analogue: Geological Society of America, Abstracts with Programs, v. 29, no. 6, P. A136.

McIntyre, D.H., 1979, Preliminary description of Anschutz Federal No 1 drill hole, Owyhee County Idaho: U.S. Geological Survey Open-File Report 79-651, 15 p.

Mitchell, V.E., D.J. Shiveler, G.S. Hustedde, and E.H. Bennett, 1985, Isotopic age dates in Idaho, excluding carbon dates: Idaho Geological Survey Information Circular 38, 29 p.

Othberg, K.L., and L.R. Stanford, 1992, Geologic map of the Boise Valley and adjoining area, western Snake River Plain, Idaho: Idaho Geological Survey Geologic Map 18, scale 1:100,000.

Pierce, K.L., and L.A. Morgan, 1992, The track of the Yellowstone hot spot: Volcanism, faulting, and uplift, *in* P.K. Link, M.A. Kuntz, and L.B. Platt, eds., Regional Geology of Eastern Idaho and Western Wyoming: Geological Society of America Memoir 179, p. 1-53.

Reid, M.R., 1995, Processes of mantle enrichment and magmatic differentiation in the eastern Snake River Plain: Th isotopic evidence: Earth Planetary Science Letters 131, p. 239-254.

Reidel, S.P., T.L. Tolan, P.R. Hooper, M.H. Beeson, K.R. Fecht, R.D. Bentley, and J.L. Anderson, 1989, The Grande Ronde Basalt, Columbia River Basalt Group: Stratigraphic descriptions and correlations in Washington, Oregon, and Idaho, *in* S.P. Reidel and P.R. Hooper, eds., Volcanism and Tectonism in the Columbia River Flood Basalt Province: Geological Society of America Special Paper 239, p. 21-53.

Rodgers, D.W., W.R. Hackett, and H.T. Ore, 1990, Extension of the Yellowstone Plateau, eastern Snake River Plain, and Owyhee Plateau: Geology, v. 18, p. 1138-1141.

Shervais, J.W., and S.K. Vetter, 1992, Young continental basalts of the Snake River Province: Fe-Ti metasomatism of continental lithosphere by an OIB plume component. Eos, Transactions, American Geophysical Union, v. 73, no. 14, p. 334.

Shervais, J.W., S.K. Vetter, and W.R. Hackett, 1994, Chemical stratigraphy of basalts in coreholes NPR-E and WO-2, Idaho National Engineering Laboratory, Idaho: Implications for plume dynamics in the Snake River Plain: Proceedings of the VIIth International Symposium on the Observation of Continental Crust Through Drilling, Santa Fe, New Mexico, p. 93-96.

Smith, G.R., Krystyna Swirydczuk, P.G. Kimmel, and B.H. Wilkinson, 1982, Fish biostratigraphy of late Miocene to Pleistocene sediments of the western Snake River Plain, Idaho, *in* Bill Bonnichsen and R.M. Breckenridge, eds., Cenozoic Geology of Idaho: Idaho Bureau of Mines and Geology Bulletin 26, p. 519-542.

Smith, R.B., and L.W. Braile, 1994, The Yellowstone hot spot: Journal of Volcanology and Geothermal Research, v. 61, p. 121-187.

Smith, R.B., E.D. Humphreys, P.J. Tackley, C.M. Meertens, K.G. Dueker, G. Waite, J. Crosswhite, D. Schutt, C. Puskas, and J.W. Hernlund, 2002, Geodynamics of the Yellowstone hotspot: Plume or not?: Eos Transactions, American Geophysical Union, v. 83, no. 47, Fall Meeting Supplement, Abstract S72C-04.

Steinberger, B.M., and R.J. O'Connell, 2002, Hotspot motion and shape of plume conduits as inferred from global mantle flow models: Eos Transactions, American Geophysical Union, v. 83, no. 47, Fall Meeting Supplement, Abstract S71D-01.

Swirydczuk, Krystyna, G.P. Larson, and G.R. Smith, 1982, Volcanic ash beds as stratigraphic markers in the Glenns Ferry and Chalk Hills formations from Adrian, Oregon, to Bruneau, Idaho, *in* Bill Bonnichsen and R.M. Breckenridge, eds., Cenozoic Geology of Idaho: Idaho Bureau of Mines and Geology Bulletin 26, p. 543-558.

Swirydczuk, Krystyna, B.H. Wilkinson, and G.R. Smith, 1979, The Pliocene Glenns Ferry oolite: Lake margin carbonate deposition in the southwestern Snake River Plain: Journal of Sedimentary Petrology, v. 49, p. 995-1004.

———, 1980, The Pliocene Glenns Ferry oolite: Sedimentology of oolitic lacustrine terrace deposits: Journal of Sedimentary Petrology, v. 50, p. 1237-1248.

Tilling, R.I., R.L. Christiansen, W.A. Duffield, E.T. Endo, R.T. Holcomb, R.Y. Koyanagi, D.W. Peterson, and J.D. Unger, 1987, The 1972-1974 Mauna Ulu eruption, Kilauea volcano: An example of quasi-steady-state magma transfer, *in* R.W. Decker, T.L. Wright, P.H. Stauffer, eds., Volcanism in Hawaii: U.S. Geological Survey Professional Paper 1350, ch. 16, p. 405-469.

Tolan, T.L., S.P. Reidel, M.H. Beeson, J.L. Anderson, K.R. Fecht, and D.A. Swanson, 1989, Revisions to the estimates of the areal extent and volume of the Columbia River Basalt Group, *in* S.P. Reidel and P.R. Hooper, eds., Volcanism and Tectonism in the Columbia River Flood Basalt Province: Geological Society of America Special Paper 239, p. 1-20.

Vetter, S., S.H. Matthews, and J. Shervais, 1997, Basaltic volcanism of the Bruneau-Jarbidge eruptive center, southwest, Idaho: Geological Society of America, Abstracts with Programs, v. 29, no. 6, p. A298.

Vetter, S.K., and J.W. Shervais, 1992, Continental basalts of the Boise River Group near Smith Prairie, Idaho: Journal of Geophysical Research v. 97, no. B6, p. 9043-9061.

Wood, Spencer, 1984, Review of late Cenozoic tectonics, volcanism, and subsurface geology of the western Snake River Plain, *in* P.C. Beaver, ed., Geology, Tectonics, and Mineral Resources of Western and Southern Idaho: Tobacco Root Geological Society, Dillon, Montana, p. 48-60.

———, 1989, Silicic volcanic rocks and structure of the western Mount Bennett Hills and adjacent Snake River Plain, Idaho: Snake River Plain-Yellowstone volcanic province, 28th International Geologic Congress Field Trip Guide T305: American Geophysical Union, Washington, D.C., p. 69-77.

———, 1994, Seismic expression and geologic significance of a lacustrine delta in Neogene deposits of the western Snake River Plain, Idaho: American Association of Petroleum Geologists Bulletin 78, p. 102-121.

Wood, S.H., and J.E. Anderson, 1981, Chapter 2, Geology, *in* J.C. Mitchell, ed., Geothermal Investigations in Idaho, Part 11: Geological, Hydrological, Geochemical, and Geophysical Investigations of the Nampa-Caldwell and Adjacent Areas, Southwestern Idaho: Idaho Department of Water Resources, Water Information Bulletin 30, p. 9-31.

Zentner, N.C., 1989, Neogene normal faults related to the structural evolution of the eastern Snake River Plain, Idaho: Idaho State University M.S. thesis, 48 p.

Evolution of Quaternary Tholeiitic Basalt Eruptive Centers on the Eastern Snake River Plain, Idaho

Scott S. Hughes,[1] Paul H. Wetmore,[2] and Jason L. Casper[1]

ABSTRACT

The tectonic and magmatic evolution of Quaternary olivine tholeiites in the eastern Snake River Plain (SRP) are evaluated by their spatial distribution and geochemical signatures. Individual lava-flow groups and their associated shield-building eruptive centers are either exposed at the surface or inferred to exist beneath overlying volcanic layers. Stratigraphy and dimensions of overlapping subsurface flow groups rely heavily on current well and core-hole correlations interpreted from natural gamma logs of numerous wells in conjunction with petrographic, paleomagnetic, geochemical, and radiometric age investigations. Magmatic sources inferred from vent distribution are dispersed over a wide expanse of the subcontinental mantle beneath the eastern SRP. Major and trace element variations depict at least four general types of sources, although each flow group has a distinct chemical signature representing a separate zone of melting. Basaltic shield dimensions, geochemical signatures, and Sr-Nd isotopic analyses support magma genesis characterized by low-volume batches of melt extracted from local reservoirs within EM2-like upper mantle. The source region was variably enriched in incompatible elements, and perhaps compositionally stratified, by previous subduction and within-plate processes. The wide variation of trace elements observed within some flow groups suggests that, for each monogenetic shield volcano, either (1) a heterogeneous batch of magma is derived by variable low degrees of partial melting and erupted with minimal fractionation, or (2) magma is generated as a homogeneous batch, which undergoes extensive fractionation during successive pulses of eruption. Other scenarios cannot be ruled out entirely.

A comparison of the locations of inferred subsurface (buried) eruptive centers for the basaltic shields with the documented volcanic rift zones suggests that the zones must be either expanded to include the subsurface eruptive centers or broken into numerous smaller, inferred rift zones. This comparison requires that the zone in which strain is accommodated is more diffuse than inferred by previous studies. Extensional stress is not being mitigated within very narrow zones but rather is being distributed throughout a zone that may be as wide as 15 or 20 km. Rift systems probably occur over zones of partial melting that tend to migrate with time depending on ambient conditions and the availability of recently melted lithosphere. Regional tectonic extension allows a diminished component of compressive stress parallel to the eastern SRP axis, thus enabling rift zones to be oriented roughly parallel to Basin and Range faults.

Key words: tholeiitic basalt, eruptive centers, mafic magmatism

INTRODUCTION

The eastern Snake River Plain (SRP), an east-northeast-trending, 400-km-long, 100-km-wide topographic and volcanic depression, extends from Twin Falls to Ashton in southeastern Idaho. The terrain is mostly semiarid steppe developed on eolian and lacustrine soils that variably cover broad expanses of basaltic lava. Mountains and valleys associated with the Basin and Range Province bound the depression on the north and south

Editors' note: The manuscript was submitted in June 1998 and has been revised at the authors' discretion.

[1]Department of Geosciences, Idaho State University, Pocatello, ID 83209
[2]Department of Earth Sciences, University of Southern California, Los Angeles, CA 90089-0740

Hughes, S.S., P.H. Wetmore, and J.L. Casper, 2002, Evolution of Quaternary tholeiitic basalt eruptive centers on the eastern Snake River Plain, Idaho, *in* Bill Bonnichsen, C.M. White, and Michael McCurry, eds., Tectonic and Magmatic Evolution of the Snake River Plain Volcanic Province: Idaho Geological Survey Bulletin 30, p. 363-385.

and trend perpendicular to the eastern SRP axis. Quaternary basaltic volcanic rocks, eolian sand, loess, and alluvial and lacustrine sediments were deposited on Miocene-Pliocene rhyolitic ash-flow tuffs now exposed only in ranges along the margins of the plain. Monogenetic basaltic shield volcanoes dominate the physiography of the eastern SRP (Figure 1) and the upper 1-2 km of the crust (Kuntz and others, 1992). Basaltic lava flows make up most of the stratigraphy, although other important Quaternary volcanic features include rhyolitic domes, phreatomagmatic volcanoes, and polygenetic eruptive centers composed of pyroclastic cones and chemically evolved lavas.

Geologic maps by Kuntz (1979), Scott (1982), and Kuntz and others (1988, 1994) and investigations into mechanisms of eastern SRP basaltic volcanism by Prinz (1970), Greeley and King (1977), Greeley (1982), Kuntz (1992), and Kuntz and others (1982, 1986, 1992) indicate a preponderance of fissure-erupted lavas that produce small coalescent shield volcanoes, each of which has grown over short periods of months or years. Holocene examples include the Wapi and Hells Half Acre

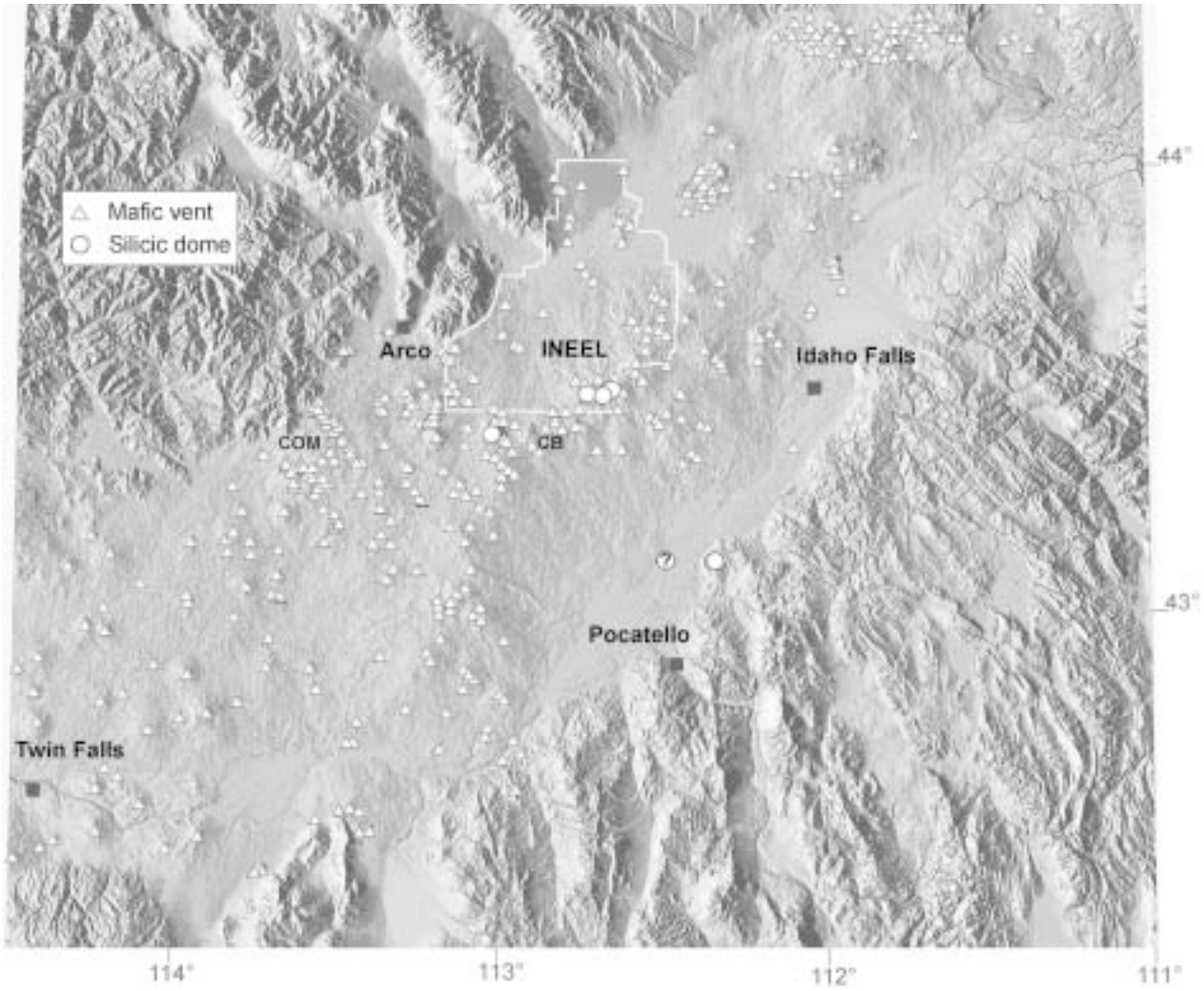

Figure 1. Shaded digital elevation model (DEM) composite map of the eastern SRP showing locations of Quaternary mafic eruptive centers (triangles) and silicic domes (circles). Eruptive centers were obtained from geologic maps of LaPoint (1977), Kuntz and others (1988, 1994) and topographic map interpretations and field investigations by the authors. Several vent clusters, such as those northwest of Idaho Falls, are probably rootless vents over a system of lava tubes from Table Butte, not individual shields. The linear array of vents southwest of Arco represents the latest Pleistocene-Holocene eruptions along the Great Rift. Abbreviations: COM—Craters of the Moon volcanic field, CB—Cedar Butte (both of which are compositionally evolved centers), and INEEL—Idaho National Engineering and Environmental Laboratory boundary.

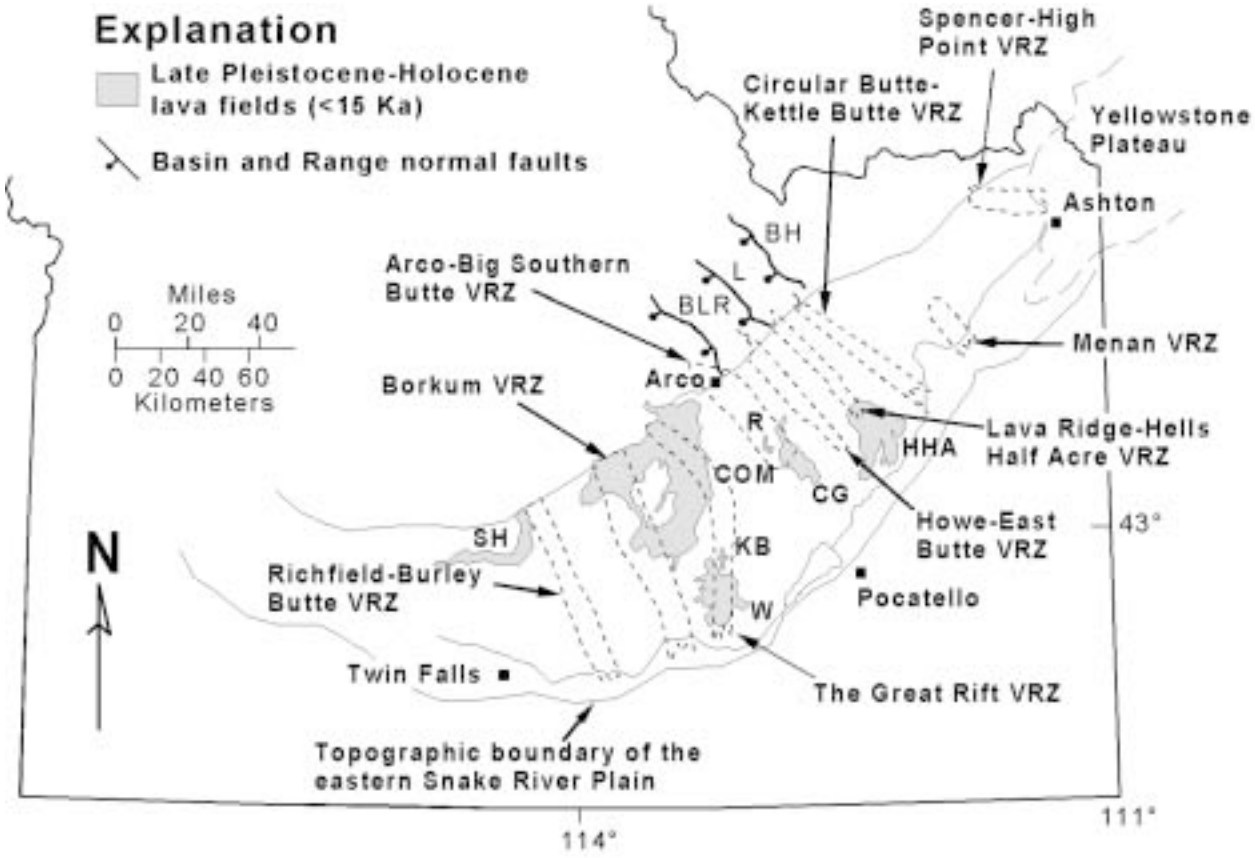

Figure 2. Map of eastern SRP illustrating the relations between volcanic rift zones (VRZs) proposed by Kuntz and others (1992), the location of Basin and Range normal faults northwest of the plain, and the latest Pleistocene-Holocene volcanic fields. Abbreviations for the volcanic fields: SH—Shoshone, COM—Craters of the Moon, KB—Kings Bowl, W—Wapi, R—North and South Robbers, CG—Cerro Grande, HHA—Hells Half Acre. Abbreviations for faults: BLR—Big Lost River, L—Lemhi, BH—Beaverhead.

lava fields (Figure 2), which are fairly uniform chemically and lithologically. Petrologic studies (Leeman, 1982b; Leeman and others, 1976) show that SRP basaltic lavas are dominantly diktytaxitic olivine tholeiites having either mildly enriched and fractionated chemical compositions (Group I) or somewhat primitive compositions with more affinity to magmatic sources (Group II).

Olivine tholeiites are chemically and petrologically distinct from evolved latitic compositions represented by Craters of the Moon (Leeman, 1982c; Kuntz and others, 1982, 1986, 1992), Cedar Butte (Hayden, 1992; Hayden and others, 1992; McCurry and others, 1999), and other locations that have experienced magmatic contamination, hybridization, or extensive fractionation. In contrast to magmatism at evolved centers where eruptions may occur intermittently over several thousand years (Kuntz and others, 1992), monogenetic eruptions represent small batches of magma that ascend from subcrustal sources without appreciable crustal residence time or interaction with crustal components (Leeman, 1982b; Kuntz, 1992).

The spatial distribution and major and trace element geochemical signatures of inferred subsurface eruptive centers (i.e., those that have been buried by younger volcanic or sedimentary deposits) are used in this paper to evaluate the tectonic and magmatic development of the eastern SRP mafic volcanic system. Chemical data were compiled from the literature and an extensive database (Hughes and others, 2000) of major and trace element whole rock analyses by ICP-AES and INAA of core-hole samples obtained in and around the Idaho National Engineering and Environmental Laboratory (INEEL). Stratigraphic and dimensional relations of lava flow groups at the INEEL rely on well and core-hole correlations, summarized by Anderson and others (1996), interpreted from natural gamma logs of numerous wells in conjunction with petrographic, paleomagnetic, geochemical, and radiometric age investigations. Stratigraphic studies at the INEEL have greatly improved the knowledge of eastern

SRP volcanic evolution and are used extensively in the following discussions.

VOLCANIC STRATIGRAPHY

Widespread basaltic volcanism has occurred intermittently on the eastern SRP throughout Pleistocene and Holocene time, an observation that argues for a high probability of mafic volcanism recurring (Hackett and others, this volume). Many of the eastern SRP volcanic landforms and eruptive mechanisms were described as basaltic plains-style volcanism by Greeley (1977; 1982). Interspersed among shields are eruptive and noneruptive fissures, evolved eruptive centers with composite cones, rhyolite domes, and sedimentary interbeds (Figure 3). Basaltic shields are topographically elevated and control the deposition of younger sediments and lavas (e.g., Hughes and others, 1997a). Modern sediments are distributed on the eastern SRP largely in eolian sands, lacustrine (playa-like "sinks"), and fluvial depositional systems (Hackett and Smith, 1992; Kuntz and others, 1992, 1994; Geslin and others, 1997; Gianniny and others, 1997). Eruptive centers exposed on the surface in and around the INEEL and other parts of the eastern SRP range in age from about 1.2 Ma to about 2.1 Ka (Kuntz and others, 1992, 1994), and radiometric ($^{40}Ar/^{39}Ar$) ages for core-hole basalts are as old as 3.2 Ma (D. Champion, written commun., 1998). Hackett and others (this volume) present a more in-depth discussion of the physical volcanology and timing of volcanic events on the eastern SRP. See Welhan and others (this volume) for a detailed assessment of lava-flow morphology and emplacement mechanisms.

The complex volcanic and sedimentary stratigraphy in the eastern SRP (Hughes and others, 1998) is partially solved by the surface and subsurface (test wells and core holes) correlation of flow groups based on uniform physical and chemical properties: natural gamma emissions, paleomagnetic polarity and inclination, radiometric age, petrography, and chemical compositions (e.g., Champion and others, 1988, 1996; Anderson, 1991; Lanphere and others, 1994; Anderson and Bartholomay, 1995; Anderson and Bowers, 1995; Reed and others, 1997). However, the distinction between two or more widely spaced flow groups may not always be evident on the basis of available physical parameters, age relations, and chemical parameters. Thus, flow groups may be combined into a larger "supergroup" of lavas, as used by Welhan and others (1997; this volume) and Wetmore and others (1997), which are coeval in volcanic stratigraphy but represent multiple, essentially unrelated eruptive centers. Subsurface topographic and isopach maps, based on current stratigraphic interpretations of well data by Anderson and others (1996), indicate that many inferred subsurface flow groups are, in fact, supergroups comprising several flow groups erupted from two or more distinct shield volcanoes (Wetmore, 1998; Wetmore and others, 1997).

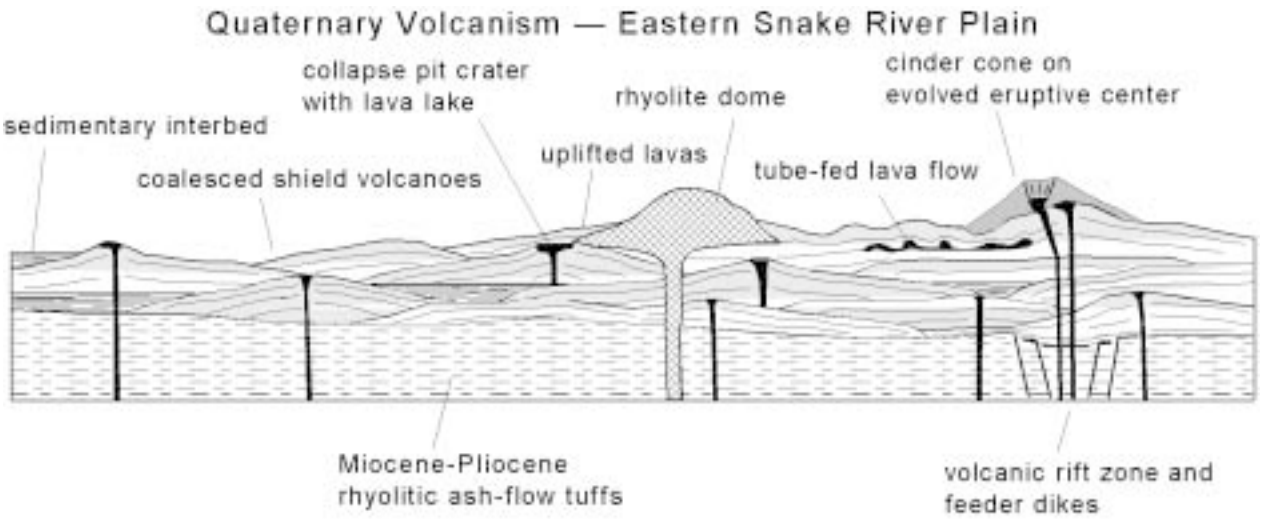

Figure 3. Schematic diagram of basaltic plains-style volcanism on the eastern SRP. Modified from Greeley (1977), the diagram illustrates myriad magmatic and surficial processes that contribute to the evolution of the province.

TECTONIC CONTROLS ON MAGMATISM

Late Tertiary tectonics in the northwestern U.S. produced a complex magmatic system. The currently accepted tectonic explanation for the eastern SRP and its extensions is that the province was formed above the track of the Yellowstone hot spot and possibly created by the passage of the North American plate southwestward over a stationary deep-seated mantle plume (Armstrong and others, 1975; Leeman, 1982a; Pierce and Morgan, 1992; Smith and Braile, 1994). Widespread mid-Miocene volcanism in eastern Oregon, northern Nevada, and southwestern Idaho lends support to the mantle plume hypothesis. Geist and Richards (1993) suggest that the relative volcanic ages and positions of SRP volcanics and the Columbia River basalts can be explained, in part, by the northward deflection of an ascending mantle plume about 20 Ma by the subducting Farallon plate. According to their model, the downgoing slab was subsequently penetrated about 17.5 Ma, and this allowed the plume to pass through to produce the Columbia River basalt and the Yellowstone hot-spot track. Camp (1995) proposes that the north-northwest alignment of mid-Miocene volcanism along the Nevada-Oregon rift zone resulted from compression and distortion of the plume head against the cratonic margin of North America between 17 Ma and 14 Ma. His model allows for a spread in volcanic activity away from the center of the plume and a southward shift in volcanism at about 14 Ma, as the distorted plume crest was overridden by Precambrian crust.

Although the mantle plume hypothesis is consistent with many features of eastern SRP magmatism, it does not account for some regional volcanic features, such as widespread Quaternary SRP volcanism that does not follow a time-transgressive trend and irregular time-space patterns of some major rhyolitic eruptions (e.g., see Hughes and McCurry, this volume). An added complication is the apparent southeast-to-northwest time-transgressive trend in Oregon volcanism that is the mirror image of the SRP trend (Luedke and Smith, 1982). These complications are partly explained by Saltzer and Humphreys (1997) who used seismic tomographic imaging to reveal a narrow, deep low-velocity region beneath, and parallel to, the eastern SRP. The low-velocity mantle corridor, composed of partially melted peridotite, is flanked by zones of high-velocity mantle that is probably depleted, relatively buoyant residual mantle from which SRP mafic magmas were derived. The residuum flattens and widens with distance from the hot spot and acts as a barrier that channels partial melts in the direction of plate motion (southwest) as the hot spot impinges on the craton. Thus, the tomographic model implies local convection controlled by partial melting and melt extraction, and it may help explain the presence of Quaternary volcanism on the eastern SRP subsequent to passage of the hot spot.

Basaltic lavas typically erupted from fissures along, and subparallel to, NW-SE volcanic rift zones that parallel Basin and Range structures. Volcanic rift zones (VRZs) on the eastern SRP (Figure 2) appear as linear sequences of basaltic vents and dikes with associated fissure-fed flows and open fissures generally parallel to, but not collinear with, range-front faults north and south of the plain (Kuntz and others, 1992). Tectonic SW-NE extension on the eastern SRP is possibly accommodated aseismically by dike injection and dilation (Rodgers and others, 1990; Parsons and Thompson, 1991; Hackett and Smith, 1992; Parsons and others, 1998) as opposed to normal faulting associated with Basin and Range extension. Kuntz and others (1992) and Hackett and Smith (1992) suggest that VRZs behave as offset extensions of the range-front faults in that they localize strain. Deformation in areas near eruptive centers includes linear fractures, grabens, and monoclines due to shallow magma injection. The orientation of inferred basaltic feeder dikes, as evidenced by the strong alignments of surface deformation features and vents, suggests that they reflect, at least in part, a regional SW-NE direction of either extensional stress or least-compressive stress.

The eastern SRP and immediately adjacent Basin and Range Province include the seismic collapse shadow of Anders and others (1989), which is an aseismic region surrounded by the seismically active part of the Basin and Range Province. No faults at the surface of the eastern SRP have significant (more than 10 m) offset; consequently, the means by which strain is partitioned between the collapse shadow and the seismically active Basin and Range Province have become debatable. Parsons and Thompson (1991) suggest that seismicity and topography are being suppressed by the dilation of dikes which feed the SRP lava fields. They argue that magmatic overpressure increases the magnitude of the least principle stress (3) and therefore decreases the magnitude of differential stress (1-3), which would otherwise be released in a faulting event. Parsons and others (1998) quantified the strain rate of the eastern SRP since 4.5 Ma and suggest that the eastern SRP has been extending at a rate consistent with that of the seismically active part of the Basin and Range Province. Conversely, Anders and Sleep (1992) conclude that mafic midcrustal intrusions, associated with the passage of the region over a mantle plume, act as a rigid body possessing sufficient strength to resist brittle failure. Their assertion is, therefore, that the eastern SRP is not significantly extending relative to the seismically active Basin and Range Province.

The surficial geometry of eruptive centers, dikes, fis-

sures, and rift zones on the eastern SRP implies that regional stress has some effect on basaltic magma emplacement in reservoirs in the upper mantle or lower crust where primary melts accumulate above the region of partial melting. The magmatic model by Kuntz (1992) indicates basaltic magma stored beneath eastern SRP eruptive centers in narrow elongate sill and dike networks oriented perpendicular to the direction of least-compressive stress. Regional horizontal extension causes magmas to locally penetrate all levels of the lower and middle crust along vertical dikes. This model implies that eastern SRP extension-related magmatism is comparable to that measured or inferred at active basalt rift systems, although the mechanisms of extension may differ somewhat. Noneruptive fissures and grabens (Kuntz and others, 1988, 1994) extending beyond the edges of Holocene volcanic fields and away from their eruptive centers may be related to lateral dike propagation away from the eruptive part of the fissure as well as vertical dike propagation above the reservoir (Pollard and others, 1983; Rubin and Pollard, 1987; Rubin, 1992; Hackett and Smith, 1992). As a dike ascends into overlying basaltic layers, the extension above the advancing dike produces nested grabens (Figure 4), providing topographic lows where lava accumulates.

Dikes propagate when the stress at the dike tip exceeds the fracture toughness of the host rock (Rubin and Pollard, 1987). The stress intensity at the tip is influenced by dike geometry and the difference between magma pressure and the ambient stress, i.e., magmatic overpressure. Ambient stress cannot be isotropic during eastern SRP eruptions as evident in the NW-SE alignment of volcanic fissure systems. Another important factor in the style of eastern SRP magmatism, and its dependency on crustal extension, is a relatively low magmatic supply rate reflected in numerous small batches of magma that produce monogenetic eruptive centers (Figure 1) rather than large complex shields. Compared to regions of high eruption rates, such as Hawaii or Iceland where shield tumescence due to magma injection is followed by deflation during an eruption, eastern SRP magma reservoirs perhaps do not undergo significant readjustment during an eruption. The modeling of eastern SRP basalt magmatism by Kuntz (1992) suggests that a lack of immediate crustal response during an eruption results in low-volume, short-lived eruptions because a progressive pressure drop occurs as the reservoir is depleted. Eastern SRP eruptions terminate at a critical pressure level a relatively short time after the eruption begins. Thus, the extension rate is critically balanced with magma production.

The combination of low magma production rates and regional extension throughout the late Pliocene and Quaternary periods has resulted in the subsidence of the eastern SRP volcanic system. The overall subsidence of the eastern SRP relative to the Basin and Range Province was documented by McQuarrie and Rodgers (1998) in a study of structural attitudes of ranges with respect to distance from the SRP topographic depression. Their analysis indicates that the eastern SRP is a volcanic basin formed as a manifestation of crustal flexuring caused by isostatic readjustment due to an increase in midcrustal density. McQuarrie and Rodgers suggest that the midcrustal load is related to an inferred extensive mafic sill emplaced at approximately 10 Ma, which provided much of the heat for rhyolitic volcanism, and to the continual localized loads added by dikes and sills during Quaternary mafic volcanism. The subsidence rate apparently varies within the volcanic system. Differential subsidence is evident in volcanic-sedimentary stratigraphy and age relations of flow groups. Volcanic stratigraphy beneath the INEEL (Anderson and others, 1996; Reed

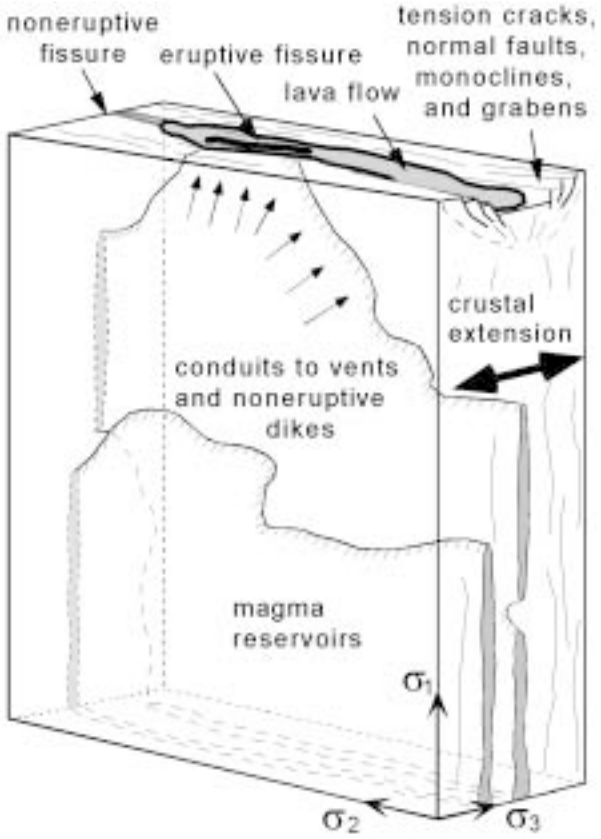

Figure 4. Schematic model of bladelike dike emplacement on the eastern SRP modified from Hughes and others (1997a). Lateral propagation is possible when the fracture toughness of the country rock is exceeded by magma pressure. Orientation of dikes are controlled by the regional stress field and vertical reservoirs probably become more like vertical blobs deeper in the crust (see Figure 16). The diagram is an adaptation of studies by Rubin and Pollard (1987), Kuntz (1992), and Hackett and Smith (1992).

and others, 1997; Hughes and others, 1997a; Wetmore, 1998) suggests that some eruptive centers have subsided significantly with respect to others; however, the relation between possible local subsidence and accommodating structures remains unclear.

DISTRIBUTION OF ERUPTIVE CENTERS

The distribution of eruptive centers reflects the existence and importance of volcanic rift zones (Kuntz and

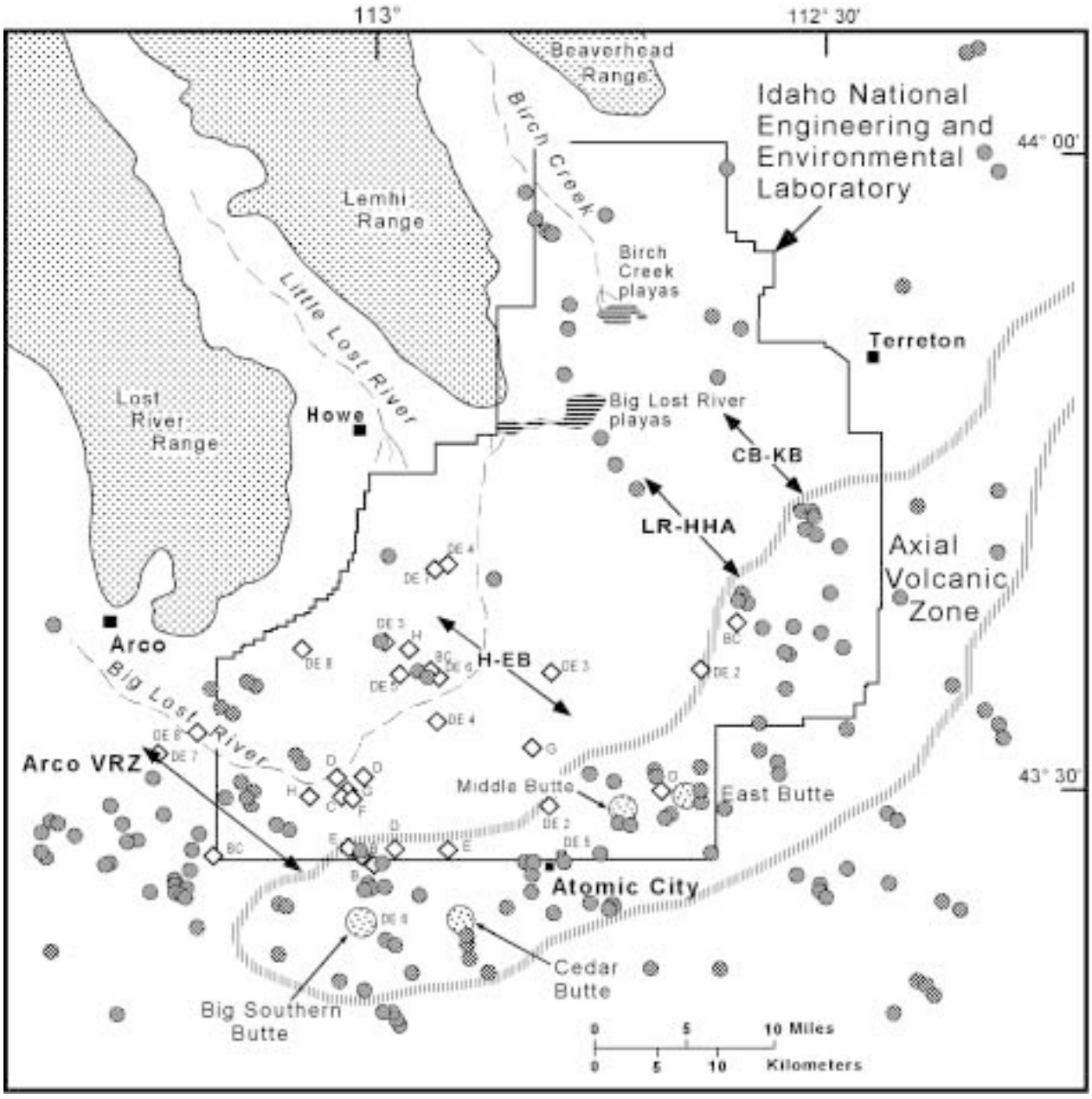

Figure 5. Map of the Idaho National Engineering and Environmental Laboratory region of the eastern SRP with locations of the axial volcanic zone relative to Quaternary volcanic vents exposed at the surface (filled circles) from Kuntz and others (1994) and inferred subsurface vents (diamonds) from Wetmore (1998). Arrows show the axes of volcanic rift zones shown by Kuntz and others (1992): Arco—Arco VRZ; H-EB—Howe-East Butte VRZ; LR-HHA—Lava Ridge-Hells Half Acre VRZ; and CB-KB—Circular Butte-Kettle Butte VRZ.

others, 1992) and can be used to evaluate localization and trends in the development of strain and magmatism (Wetmore, 1998; Anderson and others, 1999). During the past 200 k.y. basaltic volcanism in the central part of the eastern SRP has been concentrated along the northeast-trending axial volcanic zone (Figure 5), which constitutes the topographically high central axis of the eastern SRP (Hackett and Smith, 1992; Kuntz and others, 1992). Repose intervals ranged from 200 k.y. to 1,000 k.y. as evident in surface ages and sedimentary deposits. However, between about 200 Ka and about 600 Ka, the region in what is now the central and southern INEEL was volcanically active, producing as much as 58 cubic km of basalt per 100 k.y. (Wetmore, 1998).

The extensive interpretive stratigraphic database of flow groups and sedimentary interbeds provided by Anderson and others (1996) was used for spatial analysis of sixteen basalt supergroups representing the post-1 Ma time interval. Geochemical analyses and additional core logging since the Anderson and others' paper suggested only minor changes to their interpretations. Thus, the data were used to construct isopach maps of each supergroup (Wetmore and others, 1997) and to infer locations of their respective buried eruptive centers (Wetmore, 1998). These studies identified approximately thirty subsurface eruptive centers at and near the INEEL (Figure 5), most of which are associated with either a previously identified volcanic rift zone (VRZ), Arco-Big Southern Butte or Howe-East Butte, or the axial volcanic zone. Nearly all of the subsurface eruptive centers within the two VRZs lie in clusters so that they are within a few kilometers of each other. The number of middle-to-late Pleistocene eruptive centers in this region is due, in part, to the abundance of data in the southern part of the INEEL; however, surficial basalts and eruptive centers in the northern INEEL region typically are older than 800 k.y. (Kuntz and others, 1994).

Eruptive centers within the Arco-Big Southern Butte and Howe-East Butte VRZs have rough trends of decreasing age from the northwest to the southeast (supergroup and eruptive center ages increase from B to I). Eruptive centers for supergroups DE 8 and DE 7 are in the northwest, whereas supergroups DE 6, BC, and B are in the southeast. Similarly, within the Howe-East Butte VRZ supergroups, DE 7 and DE 4 eruptive centers are in the northwest; one of the supergroup DE 3 eruptive centers is to the southeast, and an eruptive center of supergroup D is still further southeast. Similar trends are apparent just west of the Howe-East Butte VRZ. Thus, volcanism at and near the INEEL appears to make a significant shift through time, producing hiatuses within areas of varied size and duration from 200 k.y. to nearly 1 m.y.

Volcanism between about 625 Ka and 200 Ka occurred in the southwestern and southeastern parts of the INEEL (Figure 6a-d); subsequent volcanism was in the axial volcanic zone (Figure 6e). Locally in the southwestern INEEL, volcanism appears to have shifted with time between the cluster of centers south of Big Lost River and the cluster on the north side of the river. The eruptive centers of supergroups I through F are concentrated within these two areas (Figure 6b). The eruptive centers of the two subsequent supergroups, DE 8 and DE 7, form a linear trend from south of Arco to southeast of Howe (Figure 6c). Eruptive centers of supergroup DE 6 through DE 2 are concentrated in the west-central INEEL north of the river and near Atomic City (Figure 6d). Eruptive centers within supergroup D through B are near the southern INEEL vent cluster, and a single eruptive center (BC) is in the cluster north of the river (Figure 6e). Since the emplacement of supergroup B, the volcanism has been within the axial volcanic zone (Figure 6f), and no eruptions since then have occurred within the INEEL.

GEOCHEMICAL AND LITHOLOGICAL IMPLICATIONS

The SRP volcanic system has been described as "bimodal" (rhyolite and basalt), but there are clearly intermediate compositions such as the evolved latitic rocks at Craters of the Moon and other eastern SRP locations (Leeman, 1982c; Kuntz and others, 1982, 1986, 1992; Honjo and Leeman, 1987; Stout and others, 1994) and latitic to rhyolitic associations at Cedar Butte (Hayden, 1992; Hayden and others, 1992; McCurry and others, 1999). Harker variation diagrams (Figure 7) illustrate well-defined alkalic and tholeiitic compositions based on the classification by Le Bas and others (1986). Chemical trends among the evolved alkalic compositions are clearly separated from the cluster of olivine tholeiites that erupted from monogenetic shields. Tholeiites range in SiO_2 from about 45 to 51 weight percent, whereas lavas in evolved eruptive centers range in SiO_2 from about 43 to 76 weight percent and have alkalic differentiation trends. Eastern SRP tholeiites have lower total alkalis ($Na_2O + K_2O$), higher MgO and CaO, and lower overall TiO_2 relative to Craters of the Moon lavas with equivalent SiO_2 values.

The coherence of major element trends in the evolved compositions implies a uniform process of magmatic evolution in the crust throughout the eastern SRP (Leeman, 1982c). Separation of the alkalic trend from the tholeiitic cluster possibly reflects markedly different magmatic sources; however, some tholeiitic compositions plot close to the alkalic Craters of the Moon trend. An

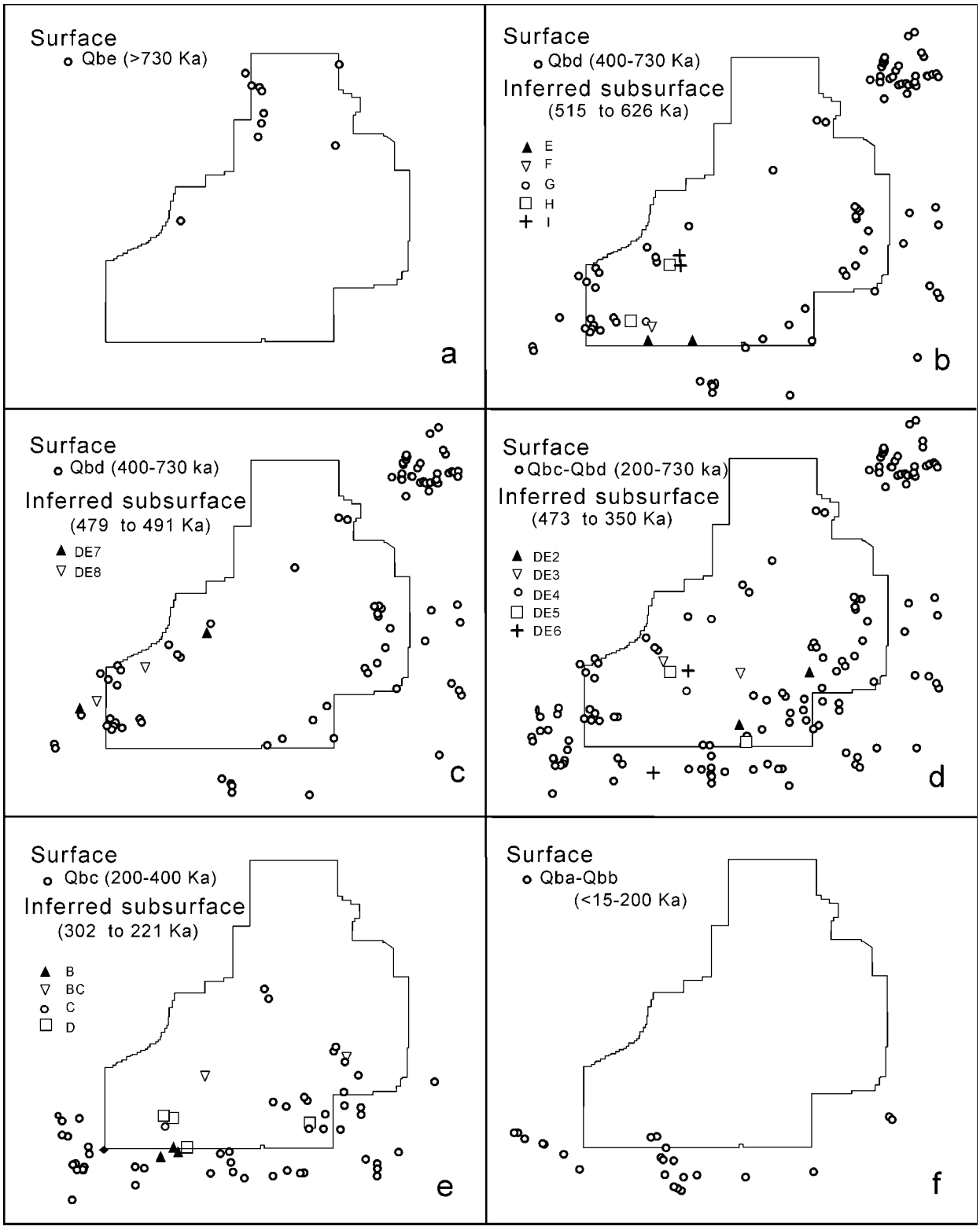

Figure 6. Time-sequential maps of surface and inferred subsurface volcanic centers near the INEEL (compare to Figure 5). Ages for eruptive centers Qba-Qbe are from Kuntz and others (1994); flow group (or supergroup) designations (B-I) are from Anderson and others (1996), and locations of inferred subsurface eruptive centers are from Wetmore (1998). The Qbd vent cluster northeast of the INEEL is probably a system of rootless vents on the flanks of Table Butte shield volcano, not individual shields.

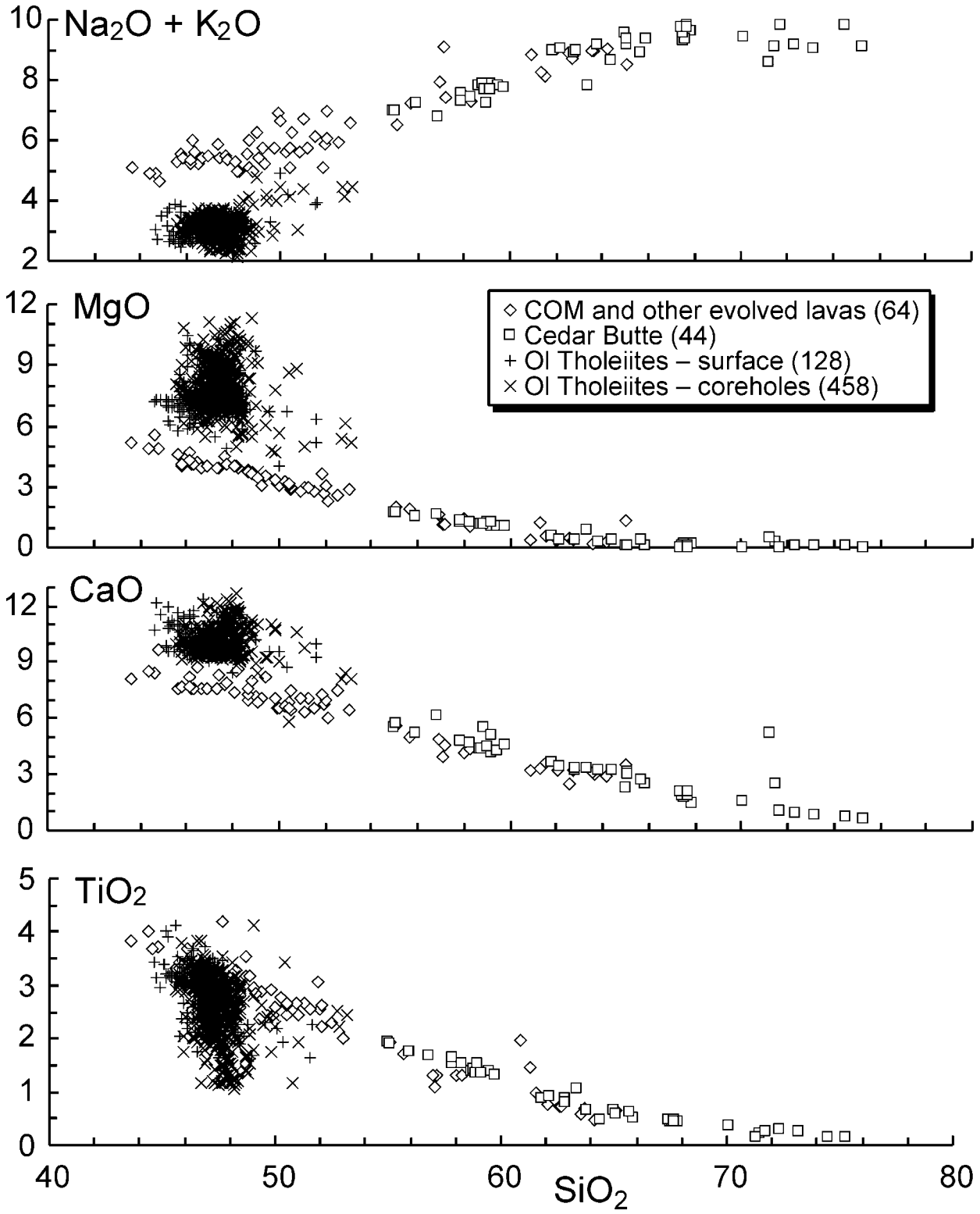

Figure 7. Harker diagrams of $Na_2O + K_2O$, MgO, CaO, and TiO_2 versus SiO_2 for eastern SRP olivine tholeiites, Craters of the Moon (COM), and Cedar Butte. Data sources: Hayden (1992); Knobel and others (1995); Kuntz and others (1985, 1992); Kuntz and Dalrymple (1979); Leeman (1982b, 1982c); Reed and others (1997); Shervais and others (1994); Stout and Nicholls (1977); and new analyses by the Idaho State University geochemical laboratory (Hughes and others, 2002).

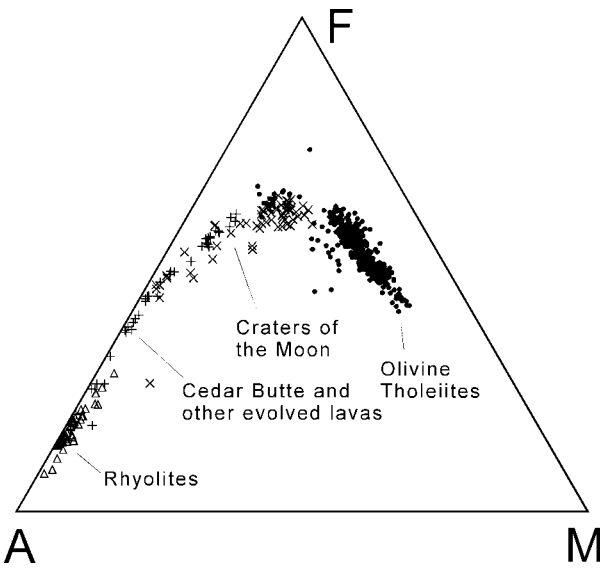

Figure 8. A-F-M diagram (A = $Na_2O + K_2O$, F = FeO, M = MgO — all in weight percent) of eastern SRP Quaternary volcanic rocks. Over 580 analyses are represented, with a few compositionally evolved exceptions, in the olivine tholeiite field. Data sources are the same as those listed in Figure 7.

AFM (Na_2O+K_2O – FeO – MgO) ternary diagram (Figure 8) shows a slight divergence away from the extremely tight cluster of most tholeiite analyses and a possible overlap with the trend observed in Craters of the Moon, Cedar Butte, and SRP rhyolites. This may simply reflect a relatively small amount of crustal evolution (contamination and fractionation) experienced by a few tholeiitic magmas representing the incipient stages of more extensive crustal interaction incurred by the evolved and hybrid compositions.

Chemical variation is significant within the tholeiitic basalts, although SiO_2 remains fairly constant compared to the evolved compositions. For example, TiO_2 ranges from about 1 to 4 weight percent, and MgO ranges from about 3.5 to about 12 weight percent, both of which have an overall 3-4X variation. Dispersion in other major oxides is also evident, although their overall ranges are not as dramatic. Substantial ranges in incompatible trace elements are exemplified in Figure 9 by rare earth element (REE) data normalized to C1 chondritic meteorites (Anders and Ebihara, 1982). Heavy REE (Yb and Lu) have an overall 3X range at 10-30 times chondrites, while light REE (La and Ce) have a nearly 10X overall variation at 22-200 times chondrites.

Compatibility with essential minerals in olivine tholeiites (olivine, plagioclase, pyroxene, and Fe-Ti oxides) increases with atomic number, so the ratio of light REE to heavy REE becomes fractionated during igneous processes. The REE patterns are plotted according to overall

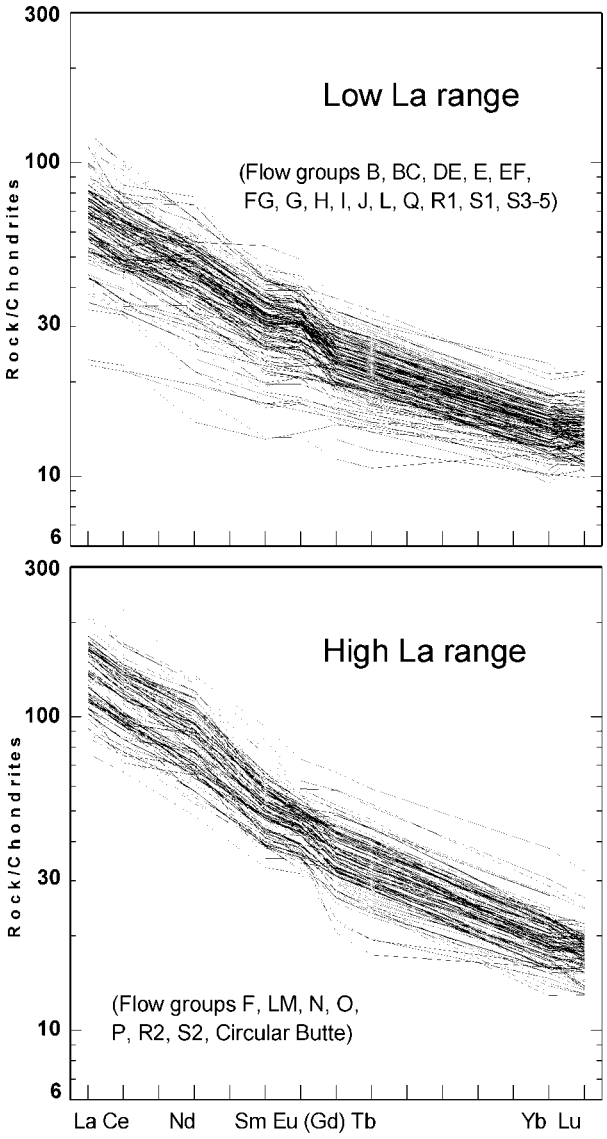

Figure 9. Rare earth element diagrams of tholeiitic basalt flow groups on the eastern SRP arbitrarily separated into compositional ranges with relatively low La (B, BC, DE, E, EF, FD, G, H, I, J, L, Q, R1, S1, S3, S4, and S5) and high La (F, LM, N, O, P, R2, S2, and Circular Butte). Except for Circular Butte lavas, flow group designations follow the terminology of Anderson and others (1996). Data are normalized to C1 chondritic abundances of Anders and Ebihara (1982) recalculated on a volatile-free basis.

flow group chemistries (some are actually supergroups). Those with overall lower La ranges (B, BC, C, D, D3, DE4, DE6 to DE8, E, E1, EF, FG, G, G1, I, Q, R1, S1, S3-5, and Hells Half Acre) are plotted together in the upper part of Figure 9, and those with either relatively high La or a wide range of La (DE1, DE3, DE5, F, F1, LM1 to LM8, N, O , P, R2, S2, Wapi, Shoshone, Kings Bowl, N. Robbers, and S. Robbers) are plotted together

in the lower diagram. Groups N, O, P, and Q, sampled in northern INEEL core holes, are slightly revised from the Anderson and Bowers (1995) and Anderson and others (1996) interpretations on the basis of recent geochemical data. Apparently, there is no relation between the REE signature and vent location in Figure 5. Distinction between the groups based on REE is rather arbitrary and admittedly includes overlapping compositional ranges, but the REE patterns show that some flow groups or supergroups vary widely in REE while others have more uniform REE abundances. Moreover, a gross difference in REE signature is apparent between two major groups of olivine tholeiites. Many additional analyses will be needed to refine this assessment and eliminate possible incorrect groupings.

Geochemical covariant plots of several elements and ratios (Figure 10) suggest that flow groups grossly cluster into separate covariant fields. Considerable overlap with adjacent groups and greater concentration ranges appear more in some components than in others. Individual low La groups have a greater variation in Cr, Sr, and MgO and lower overall Ba and La/Sm relative to the high La groups; high La groups have greater ranges in Sc and K_2O/TiO_2. Covariant trends are not readily defined, but many groups plot in loosely constrained fields that produce somewhat collinear patterns because each covariant plot represents elements that have similar but not equivalent chemical behaviors. Geochemical ranges of high La flow groups P and R2 are slightly more restricted compared with all other flow groups. Several groups, notably R1 and O, have elemental abundances that span the range between other groups. Perhaps all groups would have such high ranges with greater sampling density, but vertical chemical patterns in the INEEL cores (Shervais and others, 1994; Hughes and others, 1997c; Wetmore, 1998) reveal that some flow groups have systematic changes in geochemistry with distance above the base, whereas others are much more uniform throughout the entire thickness of the flow group.

PETROCHEMICAL PROCESSES

Geochemical and isotopic arguments (Leeman and others, 1976; Stout and Nichols, 1977; Leeman, 1982b; Menzies and others, 1984) support the petrogenesis of eastern SRP tholeiitic basalts by partial melting of fairly uniform spinel lherzolite, followed by the fractional crystallization of olivine and plagioclase, along with minor apatite and Fe-Ti spinels. Chemical trends observed in individual flow groups support magmatic fractionation during partial melting and crystallization; however, much of the overall chemical variation may represent local heterogeneity in source regions. This section summarizes the potential effects of these petrologic processes from the recent compilation of an extensive geochemical database and the evaluation of individual flow groups.

Chemical variation in lavas due to mineral-liquid-vapor phase separation is evident in the textures and mineral compositions of eastern SRP basalts. Local differences in phenocryst size and abundance, groundmass texture, and vesiculation may account for some heterogeneity. Eastern SRP basalts erupt as gas-charged magma that produces shelly pahoehoe lava near vents and gradually loses volatiles with distance to produce more massive lava flow interiors (Kuntz and others, 1994). Inspection of numerous flows in INEEL core reveals that many flow tops are highly vesiculated over a 2-4 m thickness, regardless of the total flow thickness, and that highly porous diktytaxitic textures prevail throughout most flow interiors. The petrography of INEEL core-hole and surface basalts by Kuntz (1980), Lanphere and others (1994), and this study reveals that most eastern SRP lavas are mineralogically similar and contain groundmass olivine, plagioclase, clinopyroxene, titanomagnetite, ilmenite, glass, and accessory apatite. Phenocrysts are olivine (0.5-3 mm), plagioclase (0.1-1 cm), and rare clinopyroxene. Textures are generally microporphyritic, glomerophyric, or diktytaxitic; grain size varies, and some coarsely diktytaxitic lavas contain plagioclase laths over 1 cm long. Textural differences in coarsely diktytaxitic lava are evident at outcrop scale and, in some places, at submeter scale where local unmixing of mineral and liquid phases produces bands of subphyric, fine-grained basalt within coarsely crystalline, porphyritic basalt (Hughes and others, 1999).

Microprobe analyses of dominant minerals in Circular Butte lavas (Figure 11) reveal compositional variation in olivine and plagioclases and uniformity in each of two populations of Fe-Ti oxides. Most phenocrysts are relatively unzoned, so olivine and plagioclase compositions tend to cluster near the Mg-rich and Ca-rich ends of their respective trends. The calculated olivine composition ($K_D = 0.3$, Fe-Mg fractionation) shown for Circular Butte lavas represents the initial composition expected during crystallization. The closeness of calculated initial and measured compositions and the lack of zoning suggest that phenocrysts crystallized under stable equilibrium conditions. The Fe-Ti oxide pairs have fixed compositions with the Fe-rich member approximately aligned with the overall trend of whole rock compositions.

The simple mass-balance evaluation of these mineral components (Shervais and others, 1994) shows that small amounts of olivine fractionation will produce significant overall variations in MgO and FeO. Likewise, plagioclase fractionation can account for CaO and Na_2O variations. Crystal fractionation effects would produce signifi-

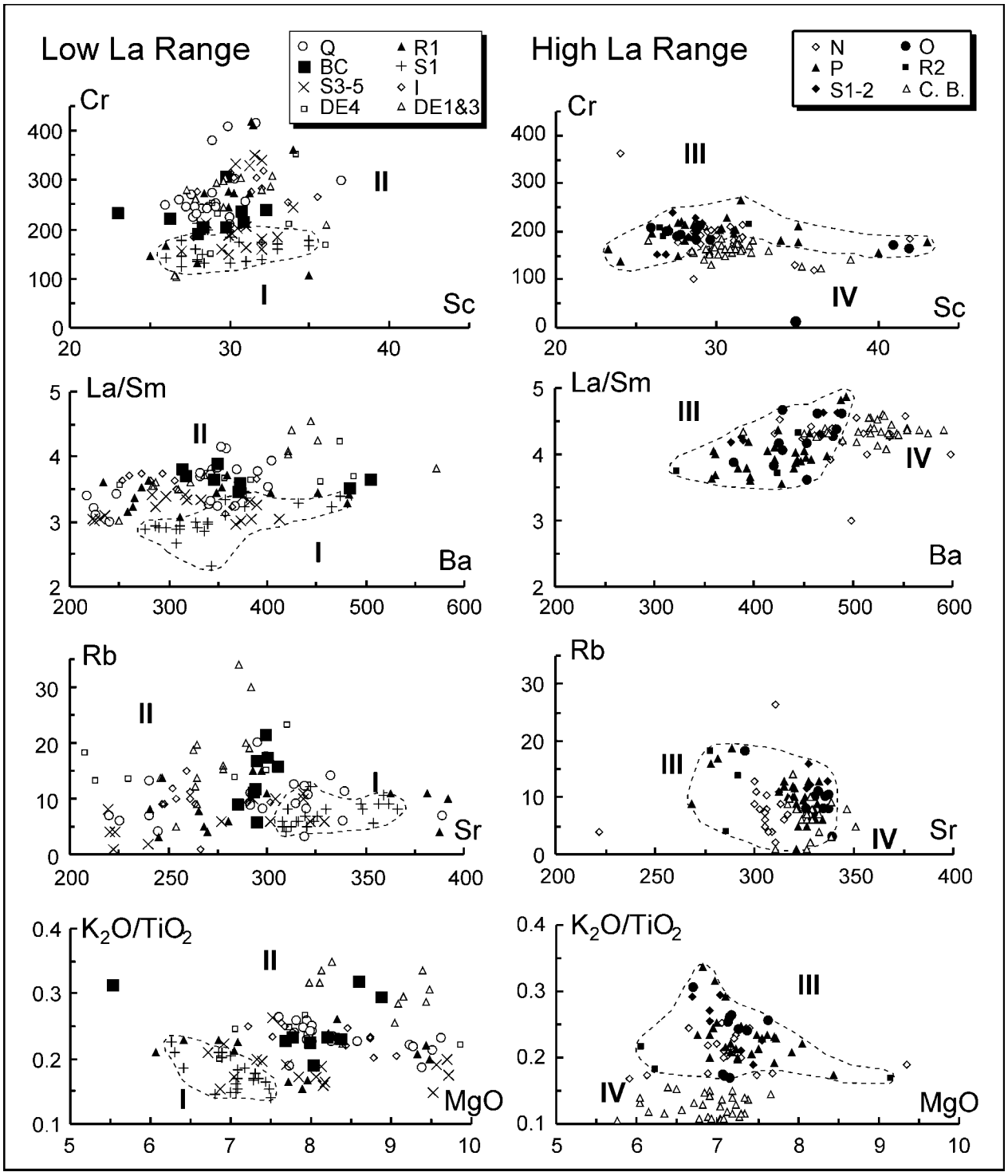

Figure 10. Variation diagrams for elements and element ratios in eastern SRP tholeiitic basalt flow groups. Each major La range is separated into two series based on geochemistry (see Figure 12). Series I and III are outlined to indicate where overlaps occur with series II and IV, respectively. See text for explanation.

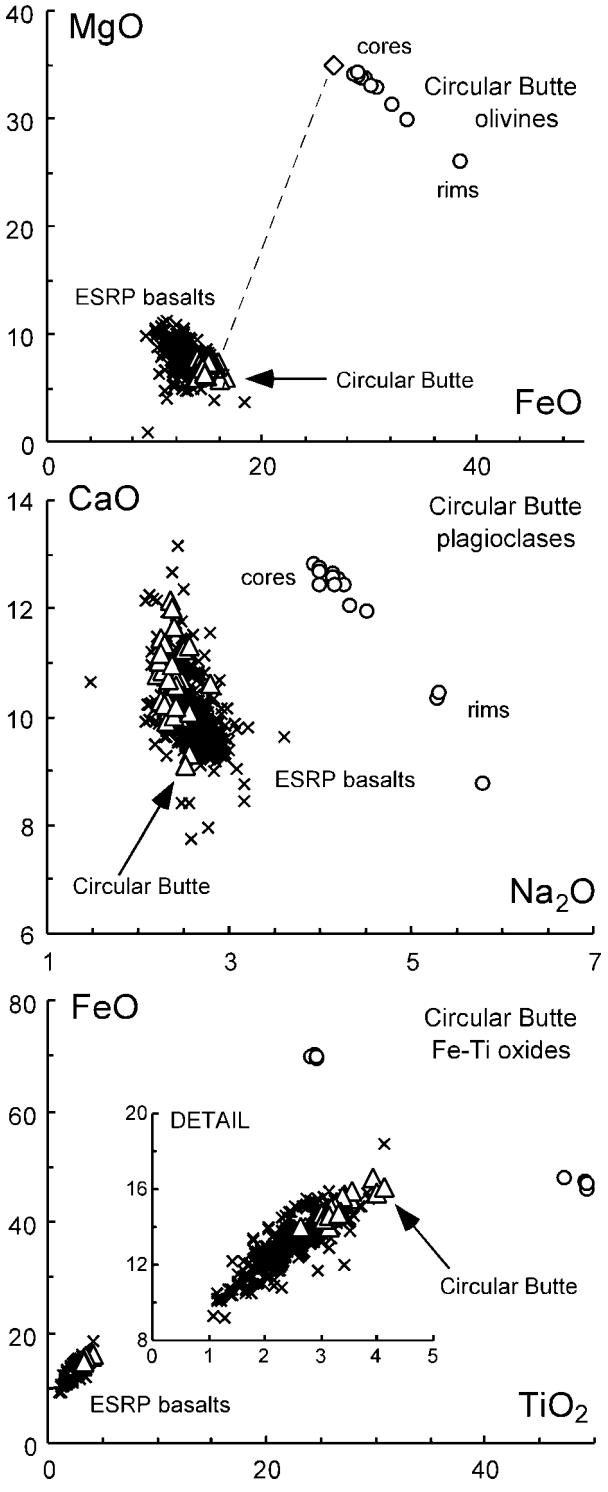

Figure 11. Electron microprobe analyses of essential mineral phases in Circular Butte lavas in the northern INEEL. Open triangles represent whole rock analyses of the Circular Butte basalts and are shown to fall within the clusters for all eastern SRP olivine tholeiites. Dashed line in top diagram connects calculated olivine composition (diamond) in equilibrium with the Circular Butte basalt.

cant trends in bulk MgO/FeO and CaO/Na_2O ratios aligned with phenocryst values. These effects are not evident in Figure 11, although the FeO-TiO_2 trend may be related to a small Fe-Ti oxide effect. Crystallization of olivine and plagioclase would also greatly affect compatible minor and trace elements leading to significant depletion of Sc, Cr, Ni, and Sr in the melt. Chemical variations shown in Figure 10 may be partly related to local mineralogical segregation, yet simple magmatic separation would require density differences and enough time for crystals to form and settle out or produce a mush from which liquid could be separated. Although this mechanism probably occurred on a small scale, it is unlikely responsible for more than minor geochemical changes in light of studies that imply short crustal residence times and the lack of differentiated compositions in the tholeiitic series. Crystal fractionation also does not explain the large ranges in incompatible trace elements (e.g., Shervais and others, 1994) shown by and illustrated in Figures 9 and 10. A three-fold variation in the incompatible elements, assuming a bulk distribution coefficient of zero, requires about 65-70 percent crystallization, which would result in more differentiated lithologic types than what is observed (e.g., see Shervais and others, 1994).

Vapor-differentiation may be responsible for some chemical heterogeneity in eastern SRP lavas. Vesiculation bands, 1- to 10-cm-thick layers of highly vesiculated lava, are common within the upper parts of lava inflationary lobes (Hughes and others, 1997b, 1999) and are often associated with textural variations. Massive diktytaxitic flow interiors commonly have vesicle cylinders and vesicle sheets that locally have chemically evolved compositions relative to other parts of the flow (Bates, 1999). The effect of gas exsolution on geochemical variation is potentially significant, as reported by Goff (1996) in an assessment of vapor-differentiation of diktytaxitic basalts. His results indicate that volatile-rich magmas show positive chemical correlations with lava porosity and increasing groundmass size. Vesicle cylinders and layers are enriched in many incompatible elements, as well as Fe, Mn, Ti, Na, K and P, that are not readily incorporated into minerals during the initial crystallization of the magma. Petrographic and geochemical studies of Circular Butte lavas in the northern INEEL (Casper, 1999) demonstrate that coarse diktytaxitic lavas have higher concentrations of accessory P- and REE-rich apatite and incompatible element-rich glass around irregularly shaped pore spaces.

A plot of La versus MgO for the low-La and high-La ranges (Figure 12) illustrates several important geochemical aspects of eastern SRP tholeiite evolution, most notably a general increase in La content with decreasing MgO

(also noted by Shervais and others, 1994). The relatively low, wide range in MgO contents in SRP basalts (6-10 weight percent) suggest some amount of fractionation is necessary and partly responsible for the range in La. Vectors for model crystal fractionation show paths from any reasonable starting point on the diagram. Ten percent fractionation of olivine alone (X = 10 percent, OL_{100}) yields an increase of only a few ppm (parts per million) La; while 20 percent fractionation of equal amounts of olivine and plagioclase (X = 20 percent, $OL_{50}PL_{50}$) and 30 percent fractionation of pyroxene (X = 30 percent, CPX_{100}) would, respectively, produce somewhat higher variations in La. All three vectors indicate the different models expected for compatible (MgO) and incompatible (La) elements when the ratio of liquid to solid phases is high (Cox and others, 1979). Thus, the variation in La may be unrelated to, and separate from, the MgO trend, so olivine fractionation probably remains the most likely cause of MgO variation among SRP olivine tholeiites. This is best illustrated in the AFM diagram (Figure 5), which shows only limited departure of tholeiite compositions from the main field. The separation of a few samples from the group indicates relative increases in alkalis that may be due to crustal contamination as noted for some Yellowstone and SRP basalts (Hildreth and others, 1991).

The paucity of pyroxene as a phenocryst phase argues against significant fractionation of pyroxene, as a relatively high-pressure phase in deep crustal regimes, unless it can be shown that phenocrysts separated efficiently and the ones that did not became resorbed during magma ascent. Moreover, Cr abundances are not seriously depleted, and there are no significant positive trends in Cr versus Sc (Figure 10). One notable exception is flow group P (Figure 10) that has a range in Sc of approximately 26 to 46 ppm and may have involved a small amount of pyroxene fractionation near the source. Both elements are pyroxene compatible and would be expected to become depleted during pyroxene fractionation. Geologic evidence for this process is not apparent, but the chemical trends do not rule out pyroxene as a variable residual phase during partial melting or depletion in the source region.

Although plagioclase dominates the liquidus mineral assemblage in many SRP tholeiites, the ratio of CaO/Al_2O_3 plotted against Sc/Yb ratio in SRP basalts (Figure 13) suggests minimal involvement of plagioclase as a fractionating phase. Changes in Sc/Yb ratio may be attributed to overall increase in REE while Sc remains fairly constant. There is little change in Ca/Al except for samples collected at Circular Butte, a shield volcano consisting of coarse diktytaxitic flows that show lithologic and chemical evidence of plagioclase fractionation. Phenocryst abundances range from nearly aphyric to 30 percent; phenocryst size ranges from 2 mm to 1.5 cm, and groundmass textures range from fine to coarse. Much of this variation is evident in single flow units and, in many outcrops, little distinction can be made between phenocrystic and groundmass plagioclase (Casper, 1999).

Essentially, the La versus MgO values in Figure 12 and other covariant plots in Figure 10 illustrate the inadequacy of simple crystal fractionation to account for all the variation in trace elements (see also Shervais and others, 1994), although low pressure fractionation (less than 10 kbar) of olivine and plagioclase may be important in petrogenesis of some eastern SRP basalts (Leeman, 1982b). The high-La range diagram further implies that magmas represented by some flow groups, such as N, O, and P, are in the range where liquid to solid ratios are

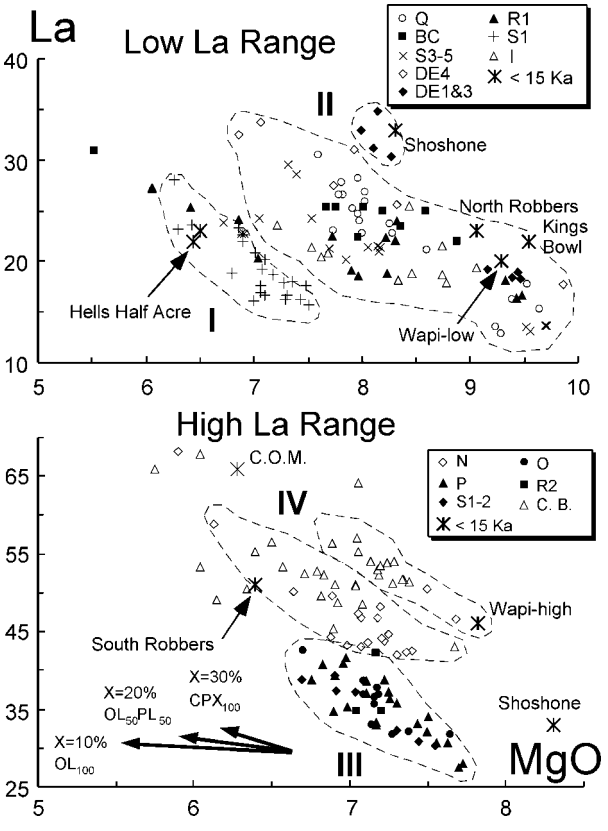

Figure 12. Variation in La (ppm) versus MgO (weight percent) for low-La (I-II) and high-La (III-V) series in eastern SRP tholeiitic basalts. Each series is represented by compositional ranges in one or more flow groups or supergroups. Except for Circular Butte (C.B.) and the <15 Ka representatives, flow group designations follow the terminology of Anderson and others (1996). Dark arrows indicate vectors for fractionation models. See text for explanation.

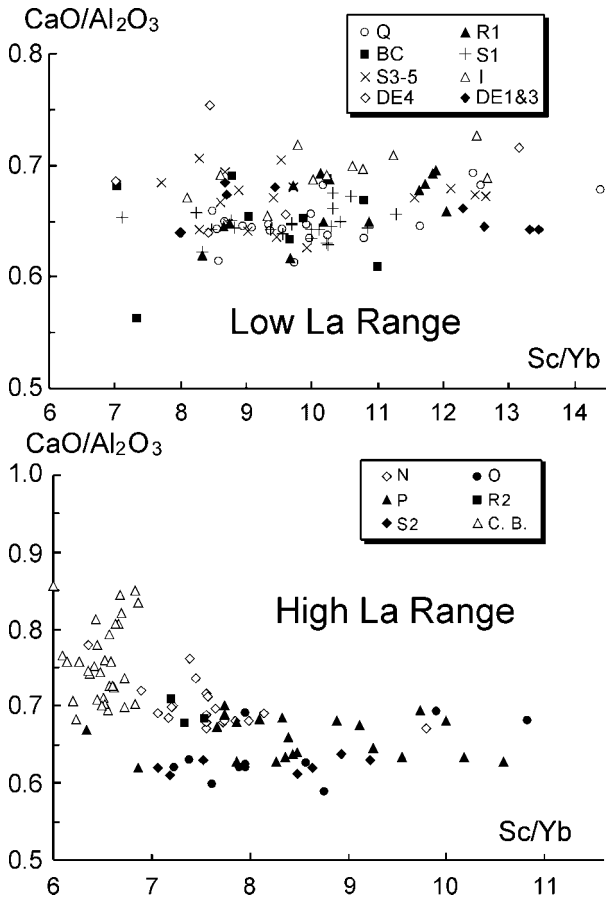

Figure 13. Covariation of CaO/Al_2O_3 ratios with Sc/Yb ratios in low La and High La range eastern SRP tholeiites. The lack of significant variation in Ca/Al ratio, with the exception of Circular Butte lavas argues against significant plagioclase fractionation. Variations in Sc/Yb reflect a large range in REE relative to Sc. See Figure 9 for explanation of flow group designations.

relatively low, such as during partial melting. Thus, the variation shown in these chemical plots supports a scenario that requires a combination of low degrees of partial melting followed by minor fractional crystallization of olivine and plagioclase.

The second major aspect of the chemical variations (Figures 10 and 12) is that several separate chemical series are evident, each of which may be represented by more than one flow group. They each have a similar trend implying similar fractionation and melting processes, albeit with different starting compositions. The late Pleistocene-Holocene examples (data from Kuntz and others, 1992) illustrate significant differences in La and MgO, and they fall along trends shown by other flow groups; however, because few trace element data are available, their individual trends cannot be observed. Separate magmatic sources are the most likely cause of producing at least four petrogenetic series (I-IV) representing two low-La and two high-La magma types. Additional series likely will be defined as more data are accumulated, especially within group II. Except for a few outlying compositions, these series are represented by flow groups using, for the time being, the terminology of Anderson and others (1996): I = S1; II = BC, DE1, DE3, DE4, I, Q, R1, and S3-5; III = O, P, R2, and S1-2; and IV = N and Circular Butte lavas in the northern INEEL.

Series II and IV are each shown as having two fields outlining apparent subseries. Little meaning can be attached to these subseries at present; however, series IV is dominated by Circular Butte lavas that represent two major flow lobes on a single monogenetic shield volcano (Casper, 1999). Also, logs of INEEL drill core show that flow group N (series IV) lies directly beneath and is conformably overlain by Circular Butte lavas, thus providing evidence for a magmatic transition with time. Considerable overlap of flow groups exists within series II and III, yet distinct trends are apparent within most flow groups attesting to their derivation from individual magma batches. Most notable are flow groups R1 and BC which have wide ranges extending to high-La, relatively low-Mg compositions.

MAGMATIC SOURCES

Chemical variations observed between SRP basalt flow group series I-IV and discrete chemical trends within individual flow groups are inconsistent with the production of a single batch of magma that differentiated by crustal assimilation and fractional crystallization. Recurrence of chemical types is apparently unrelated to spatial distribution, so the petrogenetic processes enabling each series, and probably each flow group, are randomly distributed in space and time. A source capable of producing separate batches of magma for each monogenetic shield on the eastern SRP likely would be heterogeneous, but the nature of heterogeneity is unknown. One possibility is a stratified source region (Hughes and others, 1997c) that yields melts over a range of depths and degrees of melting. Chemical variations within and between individual flow groups might be accomplished by invoking variably enriched layered subcontinental lithospheric mantle (SCLM). Each magma batch experienced a range in the amount of partial melting and fractionation.

Heterogeneous enriched subcontinental mantle apparently is important in SRP basalt genesis (e.g., Leeman and Vitaliano, 1976; Menzies and others, 1983; Reid, 1995; Hanan and others, 1997), although isotopic and chemical data suggest crustal contamination in some SRP and Yellowstone basalts (Leeman, 1982c; Hildreth and others, 1991). The covariation of Th/Yb versus Ta/Yb

(Figure 14) allows for an evaluation of source composition by greatly diminishing the effects of fractionation due to crystallization and partial melting (Pearce, 1983). Hildreth and others (1991) argue that Th/Ta enrichment in SRP basalts reflects crustal contamination (vector C); however, the trend in Figure 14 may be too broad to specify a single type of contaminant, and most samples plot within the mantle array defined by the straight boundaries. Crustal contamination of SRP tholeiites has been disregarded as a major contributor on the basis of isotopic constraints (Leeman, 1982b), although magmatic interaction with the lower crust cannot be entirely ruled out. Variations in Nd and Sr isotopic signatures with La and Sr, respectively (Figure 15, bottom), reveal no clear trend in either isotopic Nd with REE or isotopic Sr with Sr abundance. Isotopic Sr and Nd signatures (Figure 15, top) suggest an enriched EM2 type mantle (Zindler and Hart, 1986), which is characteristic of the circumcratonic domain in the western U.S. (Menzies, 1989).

The overall spread in Th/Yb and Ta/Yb (Figure 14) may be related to variable source hybridization due to a combination of subduction zone and within-plate processes (vectors S and W) that introduced components into overlying SCLM. Enrichment possibly occurred during regional Eocene calc-alkaline volcanism or Paleozoic-Mesozoic stages of lithosphere accretion. Additional heterogeneity, including source depletion and enrichment, as well as thermal weakening of lower lithosphere, possibly occurred during Miocene-Pliocene hot spot-related rhyolitic volcanism. As noted by Menzies (1989), vector S is consistent with enrichment of Proterozoic terrane by a subduction component that may have been a significant factor in subcontinental mantle evolution beneath the Snake River Plain.

A viable model of SRP tholeiitic magma generation must account for systematic increase in incompatible elements (e.g., La) during eruption as well as variability of starting compositions. Magma genesis and evolution will be evaluated in a future contribution (Hughes and others, in preparation); however, we present two hypothetical scenarios based on the previous discussion, one in which

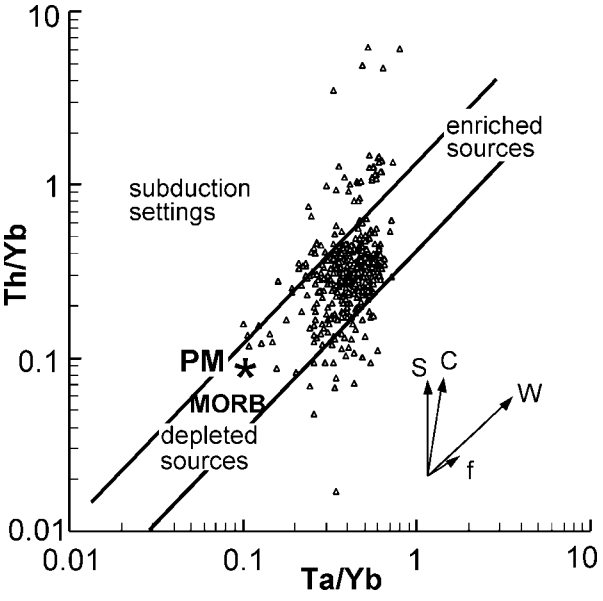

Figure 14. Th/Yb versus Ta/Yb of all eastern SRP olivine tholeiites and a few evolved compositions (see Figure 7 for data sources) showing fields of depleted mantle, enriched mantle, and mantle modified by subduction processes. Vectors represent relative contributions of modification: S—subduction zone mantle enrichment, C—crustal contamination, W—within-plate mantle enrichment, and f—fractional crystallization (after Pearce, 1983). PM—primordial mantle composition.

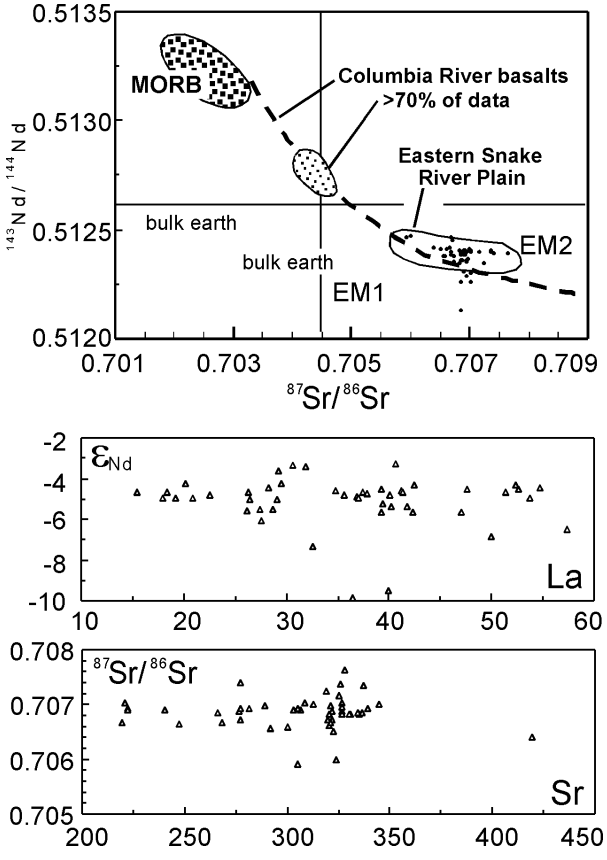

Figure 15. Isotopic Sr and Nd diagram illustrating fields of SRP olivine tholeiites, midocean ridge basalts (MORB), and the trend for Columbia River basalts (Basaltic Volcanism Study Project, 1981). New data for eastern Snake River Plain basalts (Hughes and others, 2000) are represented by small circles (top) and triangles (bottom). The bottom diagrams illustrate the lack of covariance between isotopic Nd with REE represented by La abundance and isotopic Sr with Sr abundance. Top part modified after Wilson (1989, Fig. 10.22). EM1 and EM2 mantle sources from Zindler and Hart (1986).

the chemical variation is due to partial melting and the other in which fractional crystallization is required. Primary magmas are assumed to be generated in a variably enriched, thermally weakened, SCLM source region as shown schematically in Figure 16, and they ascend without significant crustal assimilation. The models allow for variable enrichment and initial fractionation in the source region such that higher incompatible elements and less mafic bulk compositions are expected with increasing height in the SCLM. Both scenarios imply that each monogenetic shield (flow group) is derived from a separate zone of partial melting. Olivine fractionation probably occurs in all cases in order to reduce primary MgO contents below picritic levels.

Scenario 1 supposes that the melt is extracted from the center of a zone of partial melting, and the source then may or may not be tapped farther into the zone of melting where the degree of melting is progressively lower. Some magmas thus ascend with increasingly higher incompatible element abundances with depth. Variably enriched magma ascends through the ductile lower crust, opening and closing pathways plastically, and begins to fractionate olivine ± pyroxene ± plagioclase depending on depth. As the magma batch enters the brittle upper crust, it rises as a thin vertical blade along a typical rift system. Magma representing the highest degree of melting erupts first, followed by lower degree components, if any, to produce the observed time-stratigraphic increase in incompatible elements. Scenario 2 is initially similar to scenario 1, but all of the magma is assumed to be extracted into a homogeneous batch. This magma ascends to some part of the lower-middle crust where neutral bouyancy inhibits further ascent and fractionates extensively prior to continued ascent and eruption. Either successive pulses of the (monogenetic) eruption yield more chemically evolved compositions, or the magma chamber is stratified and the least-evolved tapped first.

Both scenarios present questions that require more detailed assessment. Scenario 1 does not explain the systematic increase in incompatible elements with decrease

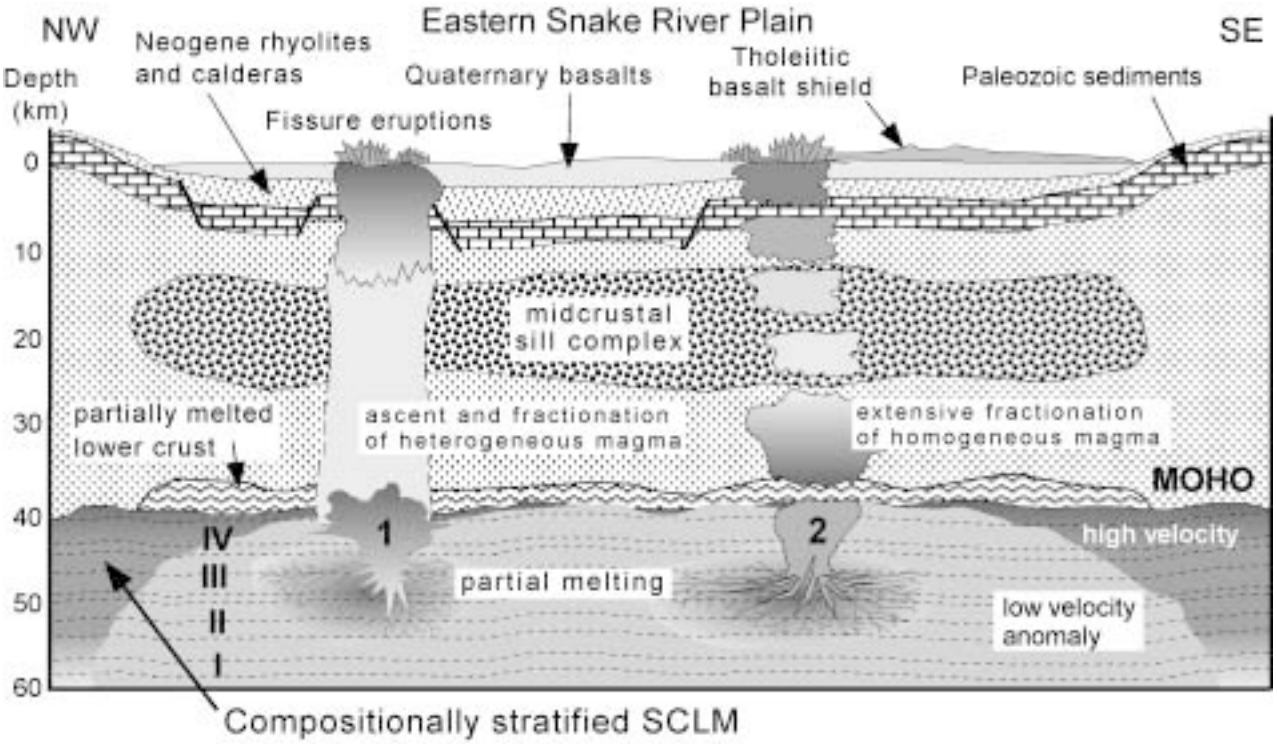

Figure 16. Schematic model of variably enriched subcontinental lithospheric mantle (SCLM) sources I-IV for basalt magma beneath the eastern SRP. View is cross-profile along the axis of the SRP (not edgewise along the rift system) illustrating broad sides of thin bladelike dike reservoirs (see Figure 4). Two hypothetical scenarios are proposed for mafic magma generation, each beginning in a restricted zone of partial melting in a compositionally stratified source region. The location of the melting zone controls the composition of the first melt, and subsequent processes are responsible for compositional diversity in a single monogenetic shield volcano. Scenario 1 requires variable degrees of partial melting followed by ascent of heterogeneous magma with minor crystal fractionation. Scenario 2 requires that a homogeneous batch of magma undergoes extensive crystal fractionation at the level of neutral bouyancy in the lower-middle crust. See text for explanation.

in MgO, unless it can be shown that MgO variability also occurs during the melting event. It also presents difficulties with magma dynamics, such that homogenization might be expected during ascent. Scenario 2 requires that the magma fractionate extensively, perhaps as much as 70 percent or more in some cases. Initial tests of fractionation models predict that any liquidus assemblage would significantly change the bulk composition to something much different than an olivine tholeiite after only 20-30 percent fractional crystallization of the most mafic SRP composition.

Regardless of what is responsible for the chemical variability, tholeiite series I and II require less enrichment than series III and IV, and series II and IV potentially represent large ranges in partial melting relative to the other series. Once a given region has experienced partial melting and magma has been extracted, further melting of the depleted residuum would be unlikely. Support for this scenario is found in chemical stratigraphy (Shervais and others, 1994; Hughes and others, 1997c, 2002) depicting overall increases in incompatible element abundances (e.g., La) with stratigraphic height in core samples, especially for older (>1 Ma) basalts in the northern INEEL region. These studies also demonstrate increases in incompatible elements with stratigraphic level in some individual flow groups as well as gross differences in geochemical signature between and within monogenetic flow groups (Figure 12). The data for Circular Butte suggest that some systems are derived from composite melting zones and yield more than one chemical series in a single volcano.

The petrologic model is consistent with seismic measurements across the eastern SRP, geophysical interpretations of crust and mantle layers, and structural interpretations of bedrock geology. Peng and Humphreys (1998) confirm the presence of an extensive 9-km thick midcrustal gabbroic sill proposed by Sparlin and others (1982). The sill was probably emplaced at approximately 10 Ma and is responsible for much of eastern SRP subsidence (McQuarrie and Rodgers, 1998). Saltzer and Humphreys (1997) indicate a corridor of low-velocity, presumably partially melted mantle extending beneath the plain to depths as great as 200 km. Peng and Humphreys (1998) suggest the low-velocity layer extends into lowermost crust, which is probably a source for more silicic SRP magmas. The model provided by Saltzer and Humphreys (1997) indicates that the low-velocity region is most likely partially melted peridotite and that melt has been extracted from surrounding regions with higher seismic velocities. They further contend that the shape of the low-velocity zone is too narrow and deep to be related to typical mantle plume geometry; thus, small-scale local convection in the upper mantle might be a more appropriate model for the dynamics of the Yellowstone hot spot. Their study demonstrates that the compositional effects of melting and melt extraction (depletion) are dominant processes within the upper mantle. This requires that the low-velocity zone, therefore, must be vertically graded with respect to mineralogy and chemical composition as depicted in Figure 16.

SUMMARY AND CONCLUSIONS

Petrologic and geochemical data suggest separate magma batches for individual shield volcanoes, each of which is represented as a flow group recognized and correlated in drill core and surface exposures. Combined major element, trace element, and isotopic Sr and Nd data support earlier studies (Leeman, 1982b; Kuntz, 1992; Kuntz and others, 1992) that eastern SRP olivine tholeiites are derived by varying degrees of partial melting in enriched subcontinental lithosphere and experience small amounts of olivine fractionation in the crust before eruption. Primary chemical variability between flow groups is caused by their derivation from multiple magmatic sources in a heterogeneous, possibly chemically stratified mantle that has been affected by prior subduction and within-plate processes. At least four broadly defined source types are proposed to account for variability in chemical signatures. Magmas ascend rapidly without significant crustal residence or chemical interaction, so they erupt as gas-charged lavas in which volatile-rich liquid segregation from coarsely crystalline diktytaxitic networks of plagioclase and olivine (and minor Fe-Ti spinel) is possible. This secondary fractionation process occurs during flow emplacement of SRP basalts, especially in zones of high volatile content (Goff, 1996; Bates, 1999).

A comparison between the locations of inferred subsurface eruptive centers and the documented volcanic rift zones (VRZ) of Kuntz and others (1992) suggests that the definition of the rift zones needs to be revised. Many inferred eruptive centers between the Arco-Big Southern Butte and Howe-East Butte VRZ are less than 5 km from the boundary of either one. This suggests that the locations of these VRZ, based upon the location of volcanic features present at the surface, are inconsistent with the location of volcanic features concealed in the subsurface. Therefore, the boundaries of these zones must be either expanded to include these subsurface eruptive centers or broken into numerous smaller, inferred rift zones or "vent corridors" as suggested by Anderson (1999). The latter option is supported by continued evaluations of geologic controls on hydraulic conductivity beneath the INEEL.

The result of either extending these VRZs to include

additional eruptive centers or separating each VRZ into numerous smaller ones is that the zone in which strain is accommodated becomes more diffuse. The existence of discrete VRZs may be questioned, since extensional stress is not being mitigated within very narrow zones but rather is being distributed throughout a zone that may be as wide as 15 or 20 km. This is supported by basaltic shield dimensions and geochemical signatures suggesting magmatism characterized by low-volume batches of melt extracted from local reservoirs that are dispersed over a wide expanse of the subcontinental mantle beneath the eastern SRP. Magmatism controlled by restricted, well-defined rift systems would require structural components extending through the crust, which are not supported by seismicity in the eastern SRP. Instead, rift systems are likely placed over zones of partial melting that tend to migrate with time depending on ambient conditions and how recently melt was extracted from a previous event. Regional tectonic extension allows a diminished component of compressive stress parallel to the eastern SRP axis, thus enabling rift zones to be oriented roughly parallel to Basin and Range faults.

Spatial shifts of the focus of volcanism at and near the INEEL may have implications for the duration of local hiatuses. The INEEL has been the site of volcanic hiatuses that locally lasted anywhere from 200 k.y. to 1 m.y. Much of the southern and central INEEL has been without a volcanic event, with the exception of minor lobes from lava fields within the axial volcanic zone, since at least 200 Ka. Hiatuses such as this are not unusual for relatively small areas; however, a 200 k.y. hiatus for an area the size of the central and southern INEEL has not been demonstrated in the subsurface of that region.

ACKNOWLEDGMENTS

The authors thank all geologists who have worked to define eastern SRP basaltic systems and volcanic stratigraphy over the past two decades. We are indebted to Steve Anderson, U.S. Geological Survey, for collaborating on research to better understand stratigraphic correlations beneath the INEEL. Discussions with Mel Kuntz, U.S. Geological Survey, and David Rodgers and Mike McCurry, Idaho State University, enhanced many of the arguments presented in this paper. Technical reviews by Scott Vetter and Craig White are greatly appreciated and have significantly improved the quality of the manuscript. Much of this research was supported by grant DE-FG07-96ID13420 from the U.S. Department of Energy to the Idaho Water Resources Research Institute, subcontract KEK066-97-B to Idaho State University. Support for neutron irradiation was provided by the Radiation Center at Oregon State University, the U.S. Department of Energy Office of New Production Reactors, and Assistant Secretary for Environmental Management under DOE Idaho Operations Office Contract DE-AC07-94ID13223.

REFERENCES

Anders, E., and M. Ebihara, 1982, Solar-system abundances of the elements: Geochimica et Cosmochimica Acta, v. 46, p. 2360-2380.

Anders, M.H., J.W. Geissman, L.A. Piety, and J.T. Sullivan, 1989, Parabolic distribution of circum-eastern Snake River Plain seismicity and latest Quaternary faulting: Migratory pattern and association with the Yellowstone hot spot: Journal of Geophysical Research, v. 94, no. B2, p. 1589-1621.

Anders, M.H., and N.H. Sleep, 1992, Magmatism and extension: The thermal and mechanical effects of the Yellowstone hot spot: Journal of Geophysical Research, v. 97, p. 15,379-15,393.

Anderson, S.R., 1991, Stratigraphy of the unsaturated zone and uppermost part of the Snake River Plain aquifer at the Idaho Chemical Processing Plant and Test Reactors Area, Idaho National Engineering Laboratory, Idaho: U.S. Geological Survey Water-Resources Investigations Report 91-4058 (DOE/ID-22097), 35 p.

Anderson, S.R., D.J. Ackerman, M.J. Liszewski, and R.M. Feiburger, 1996, Stratigraphic data for wells at and near the Idaho National Engineering Laboratory, Idaho: U.S. Geological Survey Open-File Report 96-248 (DOE/ID-22127), 27 p. and 1 diskette.

Anderson, S.R., and R.C. Bartholomay, 1995, Use of natural gamma logs and cores for determining stratigraphic relations of basalt and sediment at the Radioactive Waste Management Complex, Idaho National Engineering Laboratory, Idaho: Journal of the Idaho Academy of Science, v. 31, no. 1, p. 1-10.

Anderson, S.R., and Beverly Bowers, 1995, Stratigraphy of the unsaturated zone and uppermost part of the Snake River Plain aquifer at Test Area North, Idaho National Engineering Laboratory, Idaho: U.S. Geological Survey Water-Resources Investigations Report 95-4130, (DOE/ID-22122) 47 p.

Anderson, S.R., M.A. Kuntz, and L.C. Davis, 1999, Geologic controls of hydraulic conductivity in the Snake River Plain aquifer at and near the Idaho National Engineering and Environmental Laboratory, Idaho: U.S. Geological Survey Water-Resources Investigations Report 99-4033, 38 p.

Armstrong, R.L., W.P. Leeman, and H.E. Malde, 1975, K-Ar dating, Quaternary and Neogene volcanic rocks of the Snake River Plain, Idaho: American Journal of Science, v. 275, p. 225-251.

Basaltic Volcanism Study Project, 1981, Basaltic volcanism on the terrestrial planets: New York, Pergamon Press, 1286 p.

Bates, David, 1999, The in-situ fractionation of an eastern Snake River Plain basalt flow: Implications for heterogeneous interaction with groundwater contaminants: Geological Society of America Abstracts With Programs, v. 31, no. 4, p. A-3.

Casper, J.L., 1999, The volcanic evolution of Circular Butte: Idaho State University M.S. thesis, 113 p.

Champion, D.E., M.A. Lanphere, and S.R. Anderson, 1996, Further verification and $^{40}Ar/^{39}Ar$ dating of the Big Lost River Reversed Polarity Subchron from drill core subsurface samples of the Idaho National Engineering and Environmental Laboratory, Idaho: Eos, Transactions, American Geophysical Union, 1996 fall meeting v. 77, no. 46, p. 165.

Champion, D.E., M.A. Lanphere, and M.A. Kuntz, 1988, Evidence for a new geomagnetic reversal from lava flow in Idaho: Discussion of

short polarity reversal in the Brunhes and late Matuyama polarity chrons: Journal of Geophysical Research, v. 93, p. 11,667-11,680.

Cox, K.G., J.D. Bell, and R.J. Pankhurst, 1979, The Interpretation of Igneous Rocks: London, George Allen and Unwin Ltd, 450 p.

Fishel, M.L., 1993, The geology of uplifted rocks on Big Southern Butte: Implications for the stratigraphy and geochemistry of the eastern Snake River Plain: Idaho State University M.S. thesis, 178 p.

Geist, Dennis, and Mark Richards, 1993, Origin of the Columbia Plateau and Snake River Plain: Deflection of the Yellowstone plume: Geology, v. 21, p. 789-792.

Geslin, J.K., G.L. Gianniny, P.K. Link, and J.W. Riesterer, 1997, Subsurface sedimentary facies and Pleistocene stratigraphy of the northern Idaho National Engineering and Environmental Laboratory: Controls on hydrology, *in* Sunil Sharma and J.H. Hardcastle, eds., Proceedings of the 32nd Symposium on Engineering Geology and Geotechnical Engineering, p. 15-28.

Gianniny, G.L., J.K. Geslin, Jim Riesterer, P.K. Link, and G.D. Thackray, 1997, Quaternary surficial sediments near Test Area North (TAN), northeastern Snake River Plain: An actualistic guide to aquifer characterization, *in* Sunil Sharma and J.H. Hardcastle, eds., Proceedings of the 32nd Symposium on Engineering Geology and Geotechnical Engineering, p. 29-44.

Goff, Fraser, 1996, Vesicle cylinders in vapor-differentiated basalt flows: Journal of Volcanology and Geothermal Research, v. 71, p. 167-185.

Greeley, Ronald, 1977, Basaltic "plains" volcanism, *in* Ronald Greeley and J.S. King, eds., Volcanism of the Eastern Snake River Plain, Idaho: A Comparative Planetary Guidebook: National Aeronautics and Space Administration, p. 23-44.

———, 1982, The Snake River Plain, Idaho: Representative of a new category of volcanism: Journal of Geophysical Research, v. 87, p. 2705-2712.

Greeley, Ronald, and J.S. King, eds., 1977, Volcanism of the Eastern Snake River Plain, Idaho: A Comparative Planetary Guidebook: National Aeronautics and Space Administration, 308 p.

Hackett, W.R., and R.P. Smith, 1992, Quaternary volcanism, tectonics, and sedimentation in the Idaho National Engineering Laboratory area, *in* J.R. Wilson, ed., Field Guide to Geologic Excursions in Utah and Adjacent areas of Nevada, Idaho, and Wyoming: Utah Geological Survey Miscellaneous Publication 92-3, p. 1-18.

Hackett, W.R., R.P. Smith, and Soli Khericha, 2002, Volcanic hazards of the Idaho National Engineering and Environmental Laboratory, southeast Idaho, *in* Bill Bonnichsen, C.M. White, and Michael McCurry, eds., Tectonic and Magmatic Evolution of the Snake River Plain Volcanic Province: Idaho Geological Survey Bulletin 30.

Hanan, B.B., S.K. Vetter, and J.W. Shervais, 1997, Basaltic volcanism in the eastern Snake River Plain: Lead, neodymium, strontium isotope constraints from the Idaho INEL WO-2 core site basalts: Geological Society of America Abstracts with Programs, v. 29, p. A298.

Hayden, K.P., 1992, The geology and petrology of Cedar Butte, Bingham County, Idaho: Idaho State University M.S. thesis, 104 p.

Hayden, K.P., M. McCurry, W.R. Hackett, and S.A. Mertzman, 1992, Geology and petrology of Cedar Butte volcano, eastern Snake River Plain, Idaho: Geological Society of America Abstracts with Programs, v. 24, p. 6.

Hildreth, Wes, A.N. Halliday, and R.L. Christiansen, 1991, Isotopic and chemical evidence concerning the genesis and contamination of basaltic and rhyolitic magma beneath the Yellowstone Plateau volcanic field: Journal of Petrology, v. 32, p. 63-138.

Hon, K., J. Kauahihaua, R. Denlinger, and K. McKay, 1994, Emplacement and inflation of pahoehoe sheet flows: observations and measurements of active lava flows on Kilauea Volcano, Hawaii: Geological Society of America Bulletin, v. 106, p. 351-370.

Honjo, Norio, and W.P. Leeman, 1987, Origin of hybrid ferrolatite lavas from Magic Reservoir eruptive center, Snake River Plain, Idaho: Contributions to Mineralogy and Petrology, v. 96, p. 163-177.

Hughes, S.S., J.L. Casper, and D.J. Geist, 1997a, Potential influence of volcanic constructs on hydrogeology beneath Test Area North, Idaho National Engineering and Environmental Laboratory, Idaho, *in* Sunil Sharma and J.H. Hardcastle, eds., Proceedings of the 32nd Symposium on Engineering Geology and Geotechnical Engineering, p. 59-74.

Hughes, S.S., J.K. Geslin, and P.K. Link, 1998, Convoluted Quaternary volcanism and sedimentary stratigraphy of the northeastern Snake River Plain (SRP), TAN-INEEL, Idaho: Geological Society of America Abstracts With Programs, v. 30.

Hughes, S.S., and Mike McCurry, 2002, Bulk major and trace element evidence for a time-space evolution of Snake River Plain rhyolites, Idaho, *in* Bill Bonnichsen, C.M. White, and Michael McCurry, eds., Tectonic and Magmatic Evolution of the Snake River Plain Volcanic Province: Idaho Geological Survey Bulletin 30.

Hughes, S.S., M. McCurry, and D. Geist, 2002, Regional geochemical correlations and magmatic evolution of basalt flow groups at INEEL, *in* P.K. Link, L.L. Mink, and Dale Ralston, eds., Geology, Hydrogeology and Environmental Remediation, Idaho National Engineering and Environmental Laboratory, Eastern Snake River Plain: Geological Society of America Special Paper, 353, p. 151-173.

Hughes S.S., R.P. Smith, W.R. Hackett, and S.R. Anderson, 1999, Mafic volcanism and environmental geology of the eastern Snake River Plain, *in* S.S. Hughes and G.D. Thackray, eds., Guidebook to the Geology of Eastern Idaho: Idaho Museum of Natural History, p. 143-168.

Hughes, S.S., R.P. Smith, W.R. Hackett, Mike McCurry, S.R. Anderson, and G.C. Ferdock, 1997b, Bimodal magmatism, basaltic volcanic styles, tectonics, and geomorphic processes of the eastern Snake River Plain, Idaho, *in* P.K. Link and B.J. Kowallis, eds., Proterozoic to Recent Stratigraphy, Tectonics, and Volcanology, Utah, Nevada, Southern Idaho and Central Mexico: Brigham Young University Geology Studies, v. 42, Part I, p. 423-458.

Hughes, S.S., P.H. Wetmore, and J.L. Casper, 1997c, Geochemical interpretation of basalt stratigraphy and Quaternary mafic volcanism, eastern Snake River Plain, Idaho: Geological Society of America Abstracts with Programs, v. 29, p. A-298.

Knobel, L.L., L.D. Cecil, and T.R. Wood, 1995, Chemical composition of selected core samples, Idaho National Engineering Laboratory, Idaho: U. S. Geological Survey Open-File Report 95-748, 59 p.

Kuntz, M.A., 1979, Geologic map of the Juniper Buttes area, eastern Snake River Plain, Idaho: U.S. Geological Survey Miscellaneous Investigations Series, Map I-1115, scale 1:48,000.

———, 1992, A model-based perspective of basaltic volcanism, eastern Snake River Plain, Idaho, *in* P.K. Link, M.A. Kuntz, and L.P. Platt, eds., Regional Geology of Eastern Idaho and Western Wyoming: Geological Society of America Memoir 179, p. 289-304.

Kuntz, M.A., D.E. Champion, R.H. Lefebvre, and H.R. Covington, 1988, Geologic map of the Craters of the Moon, Kings Bowl, Wapi lava fields and the Great Rift volcanic rift zone, south-central Idaho: U.S. Geological Survey Miscellaneous Investigation Series Map I-1632, scale 1:100,000.

Kuntz, M.A., D.E. Champion, E.C. Spiker, and R.H. Lefebvre, 1986, Contrasting magma types and steady-state, volume-predictable volcanism along the Great Rift, Idaho: Geological Society of America Bulletin, v. 97, p. 579-594.

Kuntz, M.A., D.E. Champion, E.C. Spiker, R.H. Lefebvre, and L.A. McBroome, 1982, The Great Rift and the evolution of the Craters of the Moon lava field, Idaho, *in* Bill Bonnichsen and R.M. Breckenridge, eds., Cenozoic Geology of Idaho: Idaho Bureau of

Mines and Geology Bulletin 26, p. 423-438.

Kuntz, M.A., H.R. Covington, and L.J. Schorr, 1992, An overview of basaltic volcanism of the eastern Snake River Plain, Idaho, *in* P.K. Link, M.A. Kuntz, and L.P. Platt, eds., Regional Geology of Eastern Idaho and Western Wyoming: Geological Society of America Memoir 179, p. 227-267.

Kuntz, M.A., and G.B. Dalrymple, 1979, Geology, geochronology, and potential volcanic hazards in the Lava Ridge-Hell's Half Acre area, eastern Snake River Plain, Idaho: U.S. Geological Survey Open-File Report 79-1657, 70 p.

Kuntz, M.A., G.B. Dalrymple, D.E. Champion, and D.J. Doherty, 1980, Petrography, age, and paleomagnetism of volcanic rocks at Radioactive Waste Management Complex, Idaho National Engineering Laboratory, Idaho, with an evaluation of volcanic hazards: U.S. Geological Survey Open-File Report 80-388, 63 p.

Kuntz, M.A., N.H. Elsheimer, L.F. Espos, and P.R. Klock, 1985, Major element analyses of latest Pleistocene-Holocene lava fields of the Snake River Plain, Idaho: U.S. Geological Survey Open-File Report 85-593, 64 p.

Kuntz, M.A., Betty Skipp, M.A. Lanphere, W.E. Scott, K.L. Pierce, G.B. Dalrymple, D.E. Champion, G.F. Embree, W.R. Page, L.A. Morgan, R.P. Smith, W.R. Hackett, and D.W. Rodgers, 1994, Geologic map of the Idaho National Engineering Laboratory and adjoining areas, eastern Idaho: U.S. Geological Survey Miscellaneous Investigations Series Map 1-2330, scale 1:100,000.

Lanphere, M.A., M.A. Kuntz, and D.E. Champion, 1994, Petrography, age, and paleomagnetism of basaltic lava flows in coreholes at Test Area North (TAN), Idaho National Engineering Laboratory: U.S. Geological Survey Open-File Report 94-686, 49 p.

LaPoint, P.J.I., 1977, Preliminary photogeographic map of the eastern Snake River Plain, Idaho: U.S. Geological Survey Miscellaneous Field Studies Map MF-850, scale 1:250,000.

Le Bas, M.J., R.W. Le Maitre, A. Streckeisen, and B. Zanettin, 1986, A chemical classification of volcanic rocks based on the total alkali-silica diagram: Journal of Petrology, v. 27, p. 745-750.

Leeman, W.P., 1982a, Development of the Snake River Plain-Yellowstone Plateau Province, Idaho and Wyoming: An overview and petrologic model, *in* Bill Bonnichsen and R.M. Breckenridge, eds., Cenozoic Geology of Idaho: Idaho Bureau of Mines and Geology Bulletin 26, p. 155-177.

———, 1982b, Olivine tholeiitic basalts of the Snake River Plain, Idaho, *in* Bill Bonnichsen and R.M. Breckenridge, eds., Cenozoic Geology of Idaho: Idaho Bureau of Mines and Geology Bulletin 26, p. 181-191.

———, 1982c, Evolved and hybrid lavas from the Snake River Plain, Idaho, *in* Bill Bonnichsen and R.M. Breckenridge, eds., Cenozoic Geology of Idaho: Idaho Bureau of Mines and Geology Bulletin 26, p. 193-202.

———, 1982d, Rhyolites of the Snake River Plain-Yellowstone Plateau Province, Idaho and Wyoming: A summary of petrogenetic models, *in* Bill Bonnichsen and R.M. Breckenridge, eds., Cenozoic Geology of Idaho: Idaho Bureau of Mines and Geology Bulletin 26, p. 203-212.

Leeman, W.P., and C.J. Vitaliano, 1976, Petrology of the McKinney basalt, Snake River Plain, Idaho: Geological Society of American Bulletin, v. 87, p. 1777-1792.

Leeman, W.P., C.J. Vitaliano, and M. Prinz, 1976, Evolved lavas from the Snake River Plain, Craters of the Moon National Monument, Idaho: Contributions to Mineralogy and Petrology, v. 56, p. 35-60.

Luedke, R.G., and R.L. Smith, 1982, Map showing distribution, composition, and age of late Cenozoic volcanic centers in Oregon and Washington: U.S. Geological Survey Miscellaneous Investigations Series Map I-1091-D.

McGee, J.J., and J.W. Shervais, 1997, Flotation cumulate in a Snake River Plain ferrobasalt: Petrologic study of a possible lunar analogue: Geological Society of America Abstracts with Programs, v. 29, p. A136.

McCurry, Michael, W.R. Hackett, and Karl Hayden, 1999, Cedar Butte and cogenetic Quaternary rhyolite domes of the eastern Snake River Plain, *in* S.S. Hughes and G.D. Thackray, eds., Guidebook to the Geology of Eastern Idaho: Idaho Museum of Natural History, p. 169-179.

McQuarrie, Nadine, and D.W. Rodgers, 1998, Subsidence of a volcanic basin by flexure and lower crustal flow: The eastern Snake River Plain, Idaho: Tectonics, v. 17, no. 2, p. 203-220.

Menzies, M.A., 1989, Cratonic, circumcratonic and oceanic mantle domains beneath the western United States: Journal of Geophysical Research, v. 94, no. B6, p. 7899-7915.

Menzies, M.A., W.P. Leeman, and C.J. Hawkesworth, 1983, Isotope geochemistry of Cenozoic volcanic rocks reveals mantle heterogeneity below western USA: Nature, v. 303, p. 205-209.

———, 1984, Geochemical and isotopic evidence for the origin of continental flood basalts with particular reference to the Snake River Plain Idaho, U.S.A: Philosophical Transactions of the Royal Society of London, v. 310, p. 643-660.

Parsons, Tom, and G.A. Thompson, 1991, the role of magma overpressuring in suppressing earthquakes and topography: Worldwide examples: Science, v. 253, p. 1399-1402.

Parsons, Tom, G.A. Thompson, and R.P. Smith, 1998, More than one way to stretch: a tectonic model for extension along the plume track of the Yellowstone hot-spot and adjacent Basin and Range Province: Tectonics, v. 17, p. 221-234.

Pearce, J.A., 1983, Role of the sub-continental lithosphere in magma genesis at active continental margins, *in* C.J. Hawkesworth and M.J. Norrey, eds., Continental Basalts and Mantle Xenoliths: Cheshire, U.K., Shiva Publishing Ltd., p. 230-249.

Peng, Xiaohua, and E.D. Humphreys, 1998, Crustal velocity structure across the eastern Snake River Plain and the Yellowstone swell: Journal of Geophysical Research, v. 103, no. B4, p. 7171-7186.

Pierce, K.L., and L.A. Morgan, 1992, The track of the Yellowstone hotspot: Volcanism, faulting, and uplift, *in* P.K. Link, M.A. Kuntz, and L.P. Platt, eds., Regional Geology of Eastern Idaho and Western Wyoming: Geological Society of America Memoir 179, p. 1-53.

Pollard, D.D., P.T. Delaney, W.A. Duffield, E.T. Endo, and A.T. Okamura, 1983, Surface deformation in volcanic rift zones: Tectonophysics, v. 94, p. 541-584.

Prinz, Martin, 1970, Idaho rift system, Snake River Plain, Idaho: Geological Society of America Bulletin, v. 81, p. 941-947.

Reed, M.F., R.C. Bartholomay, and S.S. Hughes, 1997, Geochemistry and stratigraphic correlation of basalt lavas beneath the Idaho Chemical Processing Plant, Idaho National Engineering Laboratory: Environmental Geology, v. 30, p. 108-118.

Reid, M.R., 1995, Processes of mantle enrichment and magmatic differentiation in the eastern Snake River Plain: Th isotope evidence: Earth and Planetary Science Letters, v. 131, p. 239-254.

Rodgers, D.W., W.R. Hackett, and H.T. Ore, 1990, Extension of the Yellowstone Plateau, eastern Snake River Plain, and Owyhee Plateau: Geology, v. 18, p. 1138-1141.

Rubin, A.M., 1992, Dike-induced faulting and graben subsidence in volcanic rift zones: Journal of Geophysical Research, v. 97, no. B2, p. 1839-1858.

Rubin, A.M., and D.D. Pollard, 1987, Origins of blade-like dikes in volcanic rift zones: U.S. Geological Survey Professional Paper 1350, Ch. 53, p. 1449-1470.

Saltzer, R.L., and E.D. Humphreys, 1997, Upper mantle P wave velocity structure of the eastern Snake River Plain and its relationship to

geodynamic models of the region: Journal of Geophysical Research, v. 102, no. B6, p. 11,829-11,841.

Scott, W.E., 1982, Surficial geologic map of the eastern Snake River Plain and adjacent areas, Idaho and Wyoming: U.S. Geological Survey Miscellaneous Investigation Map I-1372, scale 1:250,000.

Self, Stephen, Lazlo Keszthelyi, and Th. Thordarson, 1998, The importance of pahoehoe: Annual Reviews of Earth and Planetary Science, v. 26, p. 81-110.

Shervais, J.W., S.K. Vetter, and W.R. Hackett, 1994, Chemical stratigraphy of basalts in coreholes NPR-E and WO-2, Idaho National Engineering Laboratory, Idaho: Implications for plume dynamics in the Snake River Plain: Proceedings of the VIIth International Symposium on the Observation of Continental Crust Through Drilling, Santa Fe, New Mexico, p. 93-96.

Smith, R.B., and L.W. Braile, 1994, The Yellowstone hot spot: Journal of Volcanology and Geothermal Research, v. 61, p. 121-187.

Sparlin, M.A., L.W. Braile, and R.B. Smith, 1982, Crustal structure of the eastern Snake River Plain from ray trace modeling of seismic refraction data: Journal of Geophysical Research, v. 87, p. 2619-2633.

Spear, D.B., 1979, The geology and volcanic history of the Big Southern Butte-East Butte area, eastern Snake River Plain, Idaho: State University of New York at Buffalo Ph.D. dissertation, 136 p.

Stout, M.Z., and J. Nicholls, 1977, Mineralogy and petrology of Quaternary lava from the Snake River Plain, Idaho: Canadian Journal of Earth Sciences, v. 14, p. 2140-2156.

Stout, M.Z., J. Nicholls, and M.A. Kuntz, 1994, Petrological and mineralogical variations in 2500-2000 yr B.P. lava flows, Craters of the Moon lava field, Idaho: Journal of Petrology, v. 35, p. 1682-1715.

Welhan, John, Tim Funderberg, R.P. Smith, and Alan Wylie, 1997, Stochastic modeling of hydraulic conductivity in the Snake River Plain Aquifer: 1. Geologic constraints and conceptual approach, *in* Sunil Sharma and J.H. Hardcastle, eds., Proceedings of the 32nd Symposium on Engineering Geology and Geotechnical Engineering, p. 75-91.

Welhan, J.A., C.M. Johannesen, J.A. Glover, L.L. Davis, and K.S. Reeves, 2002, Overview and synthesis of lithologic controls on aquifer heterogeneity in the eastern Snake River Plain, Idaho, *in* Bill Bonnichsen, C.M. White, and Michael McCurry, eds., Tectonic and Magmatic Evolution of the Snake River Plain Volcanic Province: Idaho Geological Survey Bulletin 30.

Wetmore, P.H., 1998, An assessment of physical volcanology and tectonics of the central eastern Snake River Plain based on the correlation of subsurface basalts at and near the Idaho National Engineering and Environmental Laboratory, Idaho: Idaho State University M.S. thesis, 79 p.

Wetmore, P.H., S.S. Hughes, and S.R. Anderson, 1997, Model morphologies of subsurface Quaternary basalts as evidence for a decrease in the magnitude of basaltic magmatism at the Idaho National Engineering and Environmental Laboratory, Idaho, *in* Sunil Sharma and J.H. Hardcastle, eds., Proceedings of the 32nd Symposium on Engineering Geology and Geotechnical Engineering, p. 45-58.

Wilson, Marjorie, 1989, Igneous Petrogenesis: London, Unwin Hyman, 466 p.

Zindler, A., and S. Hart, 1986, Chemical geodynamics: Annual Reviews of Earth and Planetary Science, v. 14, p. 493-571.

Syneruptive Magma-Water and Posteruptive Lava-Water Interactions in the Western Snake River Plain, Idaho, During the Past 12 Million Years

Martha M. Godchaux[1] and Bill Bonnichsen[2]

ABSTRACT

The western Snake River Plain graben has been the site of interactions of rising magmas and flowing lavas and ignimbrites with surface and near-surface waters during the past 12 million years. These interactions produced volcanic features of many types, making this one of the world's preeminent areas in which to study the role of initial phreatomagmatism in controlling the course of later magmatic rhyolite eruptions, the roles of water depth and near-surface stratigraphy in shaping basaltic phreatomagmatic constructs, and the different modes of entry into water of subaerially erupted lavas. Rhyolite-water interactions produced abundant near-vent breccias and minor subaerial phreatomagmatic tuffs, elongate subaerial flows, and silicified massive breccias at the distal sublacustrine ends of the flows. These eruptions occurred between 12 Ma and 11 Ma, more or less concurrently with large-volume silicic eruptions in the Bruneau-Jarbidge region of the main Snake River Plain. Basalt-water interactions, which occurred during a late Miocene pulse of volcanism between 9 and 7 Ma and again during a Pliocene-Pleistocene pulse between 2.2 and 0.4 Ma, produced pillow deltas, water-affected basalts, littoral cones and fans, hyaloclastites, debris flows, invasive flows, tuff cones of several types, tuff rings, and three types of maars. We describe several types of products to illustrate the variety of processes and edifices that can result from voluminous eruptions within, around, and subsequent to a large deep lake, called Lake Idaho, impounded in an actively extending rift.

Key words: phreatomagmatism, rhyolite, basalt, sublacustrine, emergent, subaerial

INTRODUCTION

During the Miocene, Pliocene, and Pleistocene epochs in the western Snake River Plain (SRP) of southwestern Idaho, there was a complex series of volcanic eruptions of first rhyolitic and then basaltic composition. Many of these eruptions occurred in or near a large lake, Lake Idaho, or in the post-lake basin after the water had drained. This lake, which was large and deep, existed more or less continuously from about 12 million to 2 million years ago in the western SRP graben, waxing and waning in response to a number of controls, such as climatic fluctuations and tectonic extension. It exerted a strong influence on volcanic eruptions, from triggering enormous initial rates of discharge in subaerial phreatomagmatic blasts to disrupting coherent flows that entered the lake after transport down gently sloping upland surfaces or in deeply incised canyons. The numerous ways in which water interacted with magmas and lavas of different compositions led to an amazing diversity of volcanic phenomena. Because of its relative youthfulness and excellent exposures, and the fact that the lake is now drained, the western SRP is one of the very best places in the world in which to study the wide variety of volcanic forms that are produced when magma and lava interact with surface waters.

Editors' note: The manuscript was submitted in October 2003.

[1]Department of Geography and Geology, Mount Holyoke College, South Hadley, MA 01075

[2]Idaho Geological Survey, Morrill Hall, Third Floor, University of Idaho, Moscow, ID 83844-3014

Godchaux, M.M., and Bill Bonnichsen, 2002, Syneruptive magma-water and posteruptive lava-water interactions in the western Snake River Plain, Idaho, during the past 12 million years, *in* Bill Bonnichsen, C.M. White, and Michael McCurry, eds., Tectonic and Magmatic Evolution of the Snake River Plain Volcanic Province: Idaho Geological Survey Bulletin 30, p. 387-434.

For the rhyolite lava flows that ran into the lake, significant amounts of brecciation and pervasive silicification occurred, and where rhyolitic volcanism interacted with lake waters or ground water adjacent to the lake, explosive phreatomagmatic eruptions produced an array of features in lava flows and domes. For the basaltic volcanism, a range of phenomena include basalts extruded in deep water, basalts extruded on land and running into the lake to create pillow deltas and extensive quantities of water-affected basalt (WAB), and explosive eruptions that produced a variety of blast deposits and tuffs blanketing the landscape.

In this paper, we summarize our investigations on the distribution, evolution, and tectonic setting of the interactions between rising magma or erupted lavas and external water in the western SRP. We present ideas of how the various types of volcanic features were produced. Future studies here and elsewhere in the world will continue to provide insights into basic volcanic processes. Observations in the natural southwestern Idaho laboratory where magmas and lavas intersected the now-long-gone lake can be combined with observations of modern basalt-water interactions to further our understanding of the mechanisms of magma-water explosivity.

REGIONAL SETTING

The western Snake River Plain graben has had a long and complex evolution, both tectonically and magmatically, since the middle Miocene. Its tectonic evolution is presented by Wood and Clemens (this volume), and the petrologic and geochemical evolution of the basalt magmatism is discussed by White and others (this volume). The geology, geochemistry, stratigraphy, and other details of basaltic volcanism here and in adjoining regions (Bruneau-Jarbidge and Twin Falls) are provided in Bonnichsen and Godchaux (this volume). Tectonic and magmatic events, mainly episodic extension and the rise and eruption of earlier rhyolitic and later basaltic magmas, occurred in conjunction with changes in the surficial environment, principally with the initiation, waxing and waning, and ultimately final decline of a large freshwater lake, called Lake Idaho. Further study of the patterns of eruption and emplacement of large rhyolite lava flows and domes and ignimbrites (now exposed along the Owyhee Front) during the early part of the graben's history should constrain the timing of the lake's beginning. Similarly, more work on both early (9.0-7.0 Ma) and late (2.2-0.4 Ma) basalts will refine the timing of the lake's growth to its high stand and its eventual slow decline and final demise.

CONTINENTAL TECTONIC AND MAGMATIC EVENTS BEFORE THE OPENING OF THE WESTERN SNAKE RIVER PLAIN GRABEN

Many tectonic events before the development of the present-day NW-SE trending graben structure affected and preconditioned the lithosphere in this region, setting the stage for its response to uplift and heating related to the passage of the neighboring SRP-Yellowstone zone of southwestern Idaho over the Yellowstone hotspot. In late Mesozoic and early Tertiary time, plate evolution along the western borderland of North America was characterized by subduction of Pacific Ocean lithosphere, accretion of diverse terranes of oceanic and exotic continental origin, batholith formation, and the gradual transformation from a mostly convergent margin to a mostly transform margin with remnant convergent domains. These final remnants of the once-extensive Farallon Plate (the present-day Juan de Fuca and Rivera-Cocos plate systems) affect linear volcanic belts at both the northern (Snake River Plain-Yellowstone zone) and the southern (Trans-Mexican Volcanic Belt) margins of large-magnitude Basin and Range extension (Figure 1). Further complicating the already complex subduction pattern of increasingly splintered microplates, the arrival at the base of the lithosphere of the Yellowstone plume head in middle Miocene time (or possibly earlier; see discussion in Pierce and others, this volume) initiated a linear hotspot track across southern Idaho along the approximate northern boundary of major Basin and Range extension.

There is far less evidence for any relationship between a hotspot track and the development of the Trans-Mexican Volcanic Belt (TMVB; although a plume or hotspot-like feature has been proposed to exist beneath present-day Guadalajara). However, these two great Cenozoic volcanic belts, which transect North America at opposite ends of the Basin and Range, have features in common. In both, the dip of the downgoing slab became steadily steeper between early Tertiary time and the present, and an originally large oceanic plate broke up into two or more microplates. Neither belt is parallel to its associated subduction zone, and both the subduction-dominated TMVB and the hotspot-dominated Snake River Plain-Yellowstone zone (SRP-Y) have conspicuous large subsidiary grabens striking at high angles to the main volcanic trend near their western ends, the western SRP graben in the north and the Tepic-Zacoalco graben in the south. These grabens have their own volcanic, hydrologic, and lacustrine systems, so they are loci of phreatomagmatism. Eastward (inland) of these large grabens, both the SRP-Y and the TMVB have numerous

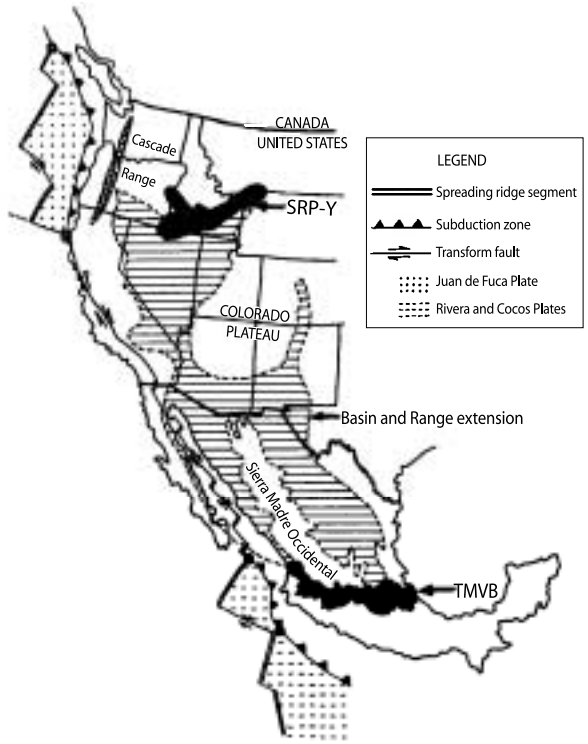

Figure 1. Map of North America, showing Snake River Plain-Yellowstone (SRP-Y) hotspot track and Trans-Mexican Volcanic Belt (TMVB), with present-day configurations of microplates along the Pacific Coast.

smaller grabens oriented nearly perpendicular to the main volcanic trends.

There is also considerable similarity in the pre-Cenozoic crust underlying the two volcanic regions. Precambrian cratonic elements underlie the more easterly parts of each belt; to the west, the Precambrian rocks are overlain or truncated by accreted oceanic arc terranes and oceanic crust of late Paleozoic to late Mesozoic age that are invaded by post-accretion granitoid Mesozoic plutonic rocks. In both belts, several successive volcanic systems developed parallel to the coastline in early Cenozoic time (the Oligocene Sierra Madre Occidental ignimbrites in Mexico and the Eocene Challis and Oligocene Salmon Creek volcanics in Idaho). The present-day volcanic belts were built on the eroded remains of these earlier systems, beginning in middle Miocene time. These similarities between the SRP-Y and the TMVB are worth investigating further, despite their more obvious differences (bimodal volcanism in the SRP-Y versus predominantly intermediate volcanism in the TMVB; clear age progression from older eruptions in the west to younger ones in the east for the SRP-Y versus no clear age trend parallel to the belt in the TMVB). Because these two great Cenozoic belts are symmetrically disposed around the Basin and Range Province and because the similarities between them are so striking, it is important to evaluate critically the contention that the differences result from "pure-end-member" driving forces (mantle plume for the SRP-Y and its flanking graben, subduction for the TMVB and its flanking graben). Both subduction and plume-related processes possibly affected both regions, a suggestion proposed by Humphreys and others (2000) for the SRP-Y and by Marquez and others (1999) for the TMVB.

SUMMARY OF THE HISTORY OF THE WESTERN SNAKE RIVER PLAIN GRABEN

The history of the western SRP graben must be viewed in its relationship to the volcanic-tectonic evolution of the larger setting (geographic region and geologic time frame) in which it is situated. At a minimum, the region includes parts of southwestern and south-central Idaho, southeastern Oregon, and northern Nevada affected by the Yellowstone hotspot from about 17 Ma to the present. Several papers (Manley, this volume; Pierce and others, this volume; McCurry and others, 1997; Wood and Clemens, this volume; Perkins and Nash, 2002; Christiansen and others, 2002; Hooper, this volume, Bonnichsen and Godchaux, this volume) provide brief summaries of events in this setting. On the precise mechanism for generating the silicic melts, there is no general agreement; most workers favor extensive fusion (anatexis or batch melting) of some sort of crustal protolith, whereas some favor the derivation of silicic melts by selective partial fusion of mantle-derived basalts previously injected into the lower crust. As Perkins and Nash (2002) observe from detailed analysis of ash-fall deposits related to ignimbrite-generating eruptions along the hotspot track, there are pronounced temporal and spatial variations in the composition, temperature, discharge, and frequency of erupted silicic materials, and these variations correspond generally to major crustal boundaries.

The history of the western SRP graben (Figure 2) includes a long period of sedimentation in a series of large, deep long-lived lakes that perhaps extended even further back in time than the volcanism, indicating that an initial pulse of graben formation may have occurred as early as 12 Ma. This date is based on the oldest rhyolite flow, dated at 11.69 Ma, that locally invaded and silicified unconsolidated beach sands. Also, gravel deltas with abundant clasts of the Lower Basalt of Ekren and others (1981) appear to underlie the oldest rhyolite. A large lake was certainly present in the area between 11 and 12 Ma, when the first large rhyolite lava flows and ignimbrites advanced downslope along the southwestern margin of the western

SRP into moderately deep water occupying the nascent rift. The oldest rhyolites, in fact, sit on lake sediments possibly as old as 15 Ma, and there is evidence of early phreatomagmatic activity in their vent regions. The distal margins of these flows are broken into large slide blocks and are intensely silicified, and roadcuts along their bases expose tongues of brecciated rhyolite invading downward into the soft lake sediments. Although post-rhyolite movement on faults that generally predate flow emplacement displaces these distal water-affected rhyolites downward with respect to the subaerial parts of the same flows, enough vertical outcrop remains in individual fault blocks to suggest that the water was at least 300 feet deep in places.

Following the rhyolite eruptions was a brief break in volcanic activity while extension apparently continued and the lake deepened. Between 9 Ma and 7 Ma, basalt erupted along the southwestern margin of the graben from subaerial and sublacustrine vents (Bonnichsen and Godchaux, this volume; White and others, this volume). Some of the sublacustrine vents were situated in deep water (from a few hundred feet to perhaps as much as two thousand feet). Following this activity was another pause in the volcanism, while sedimentation and perhaps minor extension continued, until eruptions began again about 2.2 Ma. These eruptions seem to have taken place mainly from a midgraben "hotline," which continues in a SSE direction across the main SRP-Y hotspot track to Salmon Butte, when the lake was undergoing its final demise. Accordingly, these late eruptions were mostly emergent (in water generally less than 300 feet deep). Some were immediately postlake, highly explosive blasts involving interaction between rising magmas and water-saturated sediments; others were cinder-producing Strombolian eruptions of dry subaerial effusions that formed extensive subhorizontal flow fields spreading radially outward from low-profile shields. The most recent of these eruptions for which a radiometric date is available occurred around 400 Ka, but some of the undated flows may be considerably younger.

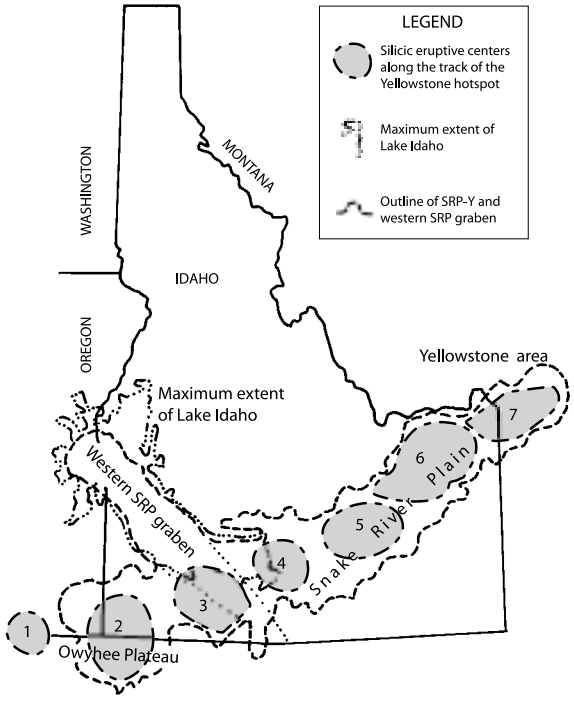

Figure 2. Map of Idaho, with the outlines of SRP-Y and western SRP graben, the maximum extent of Lake Idaho, and silicic eruptive centers along the track of the Yellowstone hotspot. Eruptive centers: 1—McDermitt, 2—Owyhee-Humboldt, 3—Bruneau-Jarbidge, 4—Twin Falls, 5—Picabo, 6—Heise, and 7—Yellowstone.

RHYOLITE ERUPTION AND EMPLACEMENT ALONG THE SOUTHWESTERN MARGIN OF THE WESTERN SNAKE RIVER PLAIN

DISTRIBUTION AND CHARACTERISTICS OF RHYOLITE UNITS

The earliest volcanism associated with the western SRP produced large-volume rhyolite lava flows and a subordinate volume of very high-grade lavalike ignimbrite. These rhyolites were erupted from vents outside the graben and flowed down a regional slope toward the northeast, crossing one or more graben-boundary faults. The oldest and most voluminous flows are at the northwesternmost end of the western SRP, and the units generally become progressively younger and less voluminous toward the southeast. A line separating small-volume units from large-volume ones is coincident with the west edge of the westernmost appearance of Mesozoic granitic rocks at the surface. These outcrops of granite, unlike most granites of the Owyhee Mountains, are strongly lineated gneisses, suggesting that granitic rocks further west were displaced downward along a major tectonic boundary. We speculate that the downfaulted granites were partially melted, generating the magmas which gave rise to the voluminous flows of the Jump Creek Rhyolite. The ages of the western SRP rhyolites are similar to those of Cougar Point Tuff (CPT) units erupted from the Bruneau-Jarbidge eruptive center (Bonnichsen and Godchaux, this volume), but their volumes are smaller than those of most CPT units and their compositions are somewhat different. The western SRP units are described

below in order of decreasing age, starting with the Jump Creek Rhyolite at the northwest end of the western SRP graben. The Jump Creek Rhyolite consists of three large flow-fields, each one produced from a different vent complex. The other units, smaller in map area and in volume, are the Wilson Creek Ignimbrite, the Reynolds Creek Rhyolite, and the Cerro el Otoño Dome Field.

Chemical compositions of all these units are shown in Table 1. The compositions of the Owyhee Front rhyolite units vary widely. The eastern units (Reynolds Creek Rhyolite, Wilson Creek Ignimbrite, and Cerro el Otoño Dome Field) are high-silica rhyolite, whereas the western units (the segments of the Jump Creek Rhyolite) are low-silica rhyolite. Additionally, there are large differences in the minor element contents of these groups of rhyolite. The various parts of the Jump Creek Rhyolite have high Ba, Sr, and Zr contents, and low abundances of Rb in comparison to the other Owyhee Front rhyolite units. These differences are largely correlative with the differences in phenocryst contents of the eastern and western groups of units. The Reynolds Creek Rhyolite, although high in silica and Sr like the Wilson Creek and Cerro el Otoño, has Ba and Zr contents between those of the Jump Creek Rhyolite and those of the other units. The compositions of the Wilson Creek Ignimbrite and Cero el Otoño units seem to be indistinguishable.

JUMP CREEK RHYOLITE

Flow Fields and Principal Features

At the northwesternmost end of the southwestern margin of the western SRP, outcrops of the 11.7-11.5 Ma (New Mexico Geochronological Research Laboratory, written commun., 2000) Jump Creek Rhyolite cover an area of about 100 square miles (Figure 3). The thickness varies and is poorly known, especially in the medial part of the outcrop area, but near the vent areas along the southern margin are thicknesses of 500 to 1,000 feet. The unit was described as an ignimbrite by Ekren and others (1984); they implied that it came from a hypothetical caldera in the western SRP and flowed up a paleovalley, but the known locations of vents and other features described below are inconsistent with that interpretation.

The Jump Creek Rhyolite is a group of petrographically fairly homogeneous low-silica rhyolite lava flows (see Table 1 for analyses) erupted from three principal groups of vents distributed along an east-west line (with an en echelon step to the south just west of U.S. Highway 95) between the southern margin of the Pole Creek Top plateau in Oregon and Shares Snout hill in Idaho. The flow fields that developed from the three groups of vents are referred to (from west to east) as the Pole Creek Top flow field, the Rockville flow field, and the Buck Mountain-Shares Snout flow field.

Each of the vent groups has distinctive breccia rings enclosing its southern, western, and eastern sides, but all are breached on their northern margins. The lava flowed from these vents NNE down a paleoslope and crossed over escarpments formed by down-to-the-northeast normal faults that paralleled the edge of the nascent western SRP graben. They entered standing water at an elevation that today is about 3,000 feet above sea level. We suggest that thermomechanical modeling of the regional uplift, which might have occurred when this area was adjacent to the Yellowstone plume, indicates that the absolute elevation of the lake shore at 11.7-11.5 Ma may have been somewhat higher than it is now. The flows are most voluminous and have the widest breccia ring around the vent group in the Pole Creek Top flow field in the northwestern part of the outcrop area. Around the margins of these flows, their bases are everywhere in depositional contact with either Miocene Succor Creek Formation (fluviatile and lacustrine sediments and unwelded ash flows) or their own associated (precursor) phreatomagmatic tuffs. The aggregate thickness and volume of flows in the Rockville field and the width of the vent-enclosing breccia ring are considerably less than in the Pole Creek Top field (Figure 3). These flows also sit on the Succor Creek Formation but are close to the eastern edge of that unit, where the thickness of the sediments is considerably less than that beneath the Pole Creek Top field, and the upper surface of a thick series of basalts (the Lower Basalt of Ekren and others, 1981) is present at shallow depth. The even less voluminous Buck Mountain-Shares Snout flow field (Figure 3), with relatively little vent-encircling breccia, sits on a heterogeneous group of older volcanic and volcaniclastic rocks, the Oligocene Salmon Creek Formation.

Petrography

The Jump Creek flows are characterized by a relatively high abundance of large equant feldspar phenocrysts set in a variably devitrified brown to dark gray glassy (locally perlitic) matrix material. The most abundant phenocryst mineral is oligoclase, locally with thin discontinuous rims of sanidine. Some grains have conspicuous melt inclusions, especially in the Pole Creek Top flows, and others, without inclusions, have strain features, which may indicate that they are xenocrysts. Rockville and Buck Mountain flows have in addition to the predominant oligoclase some deeply embayed grains of a more calcic plagioclase that also is probably

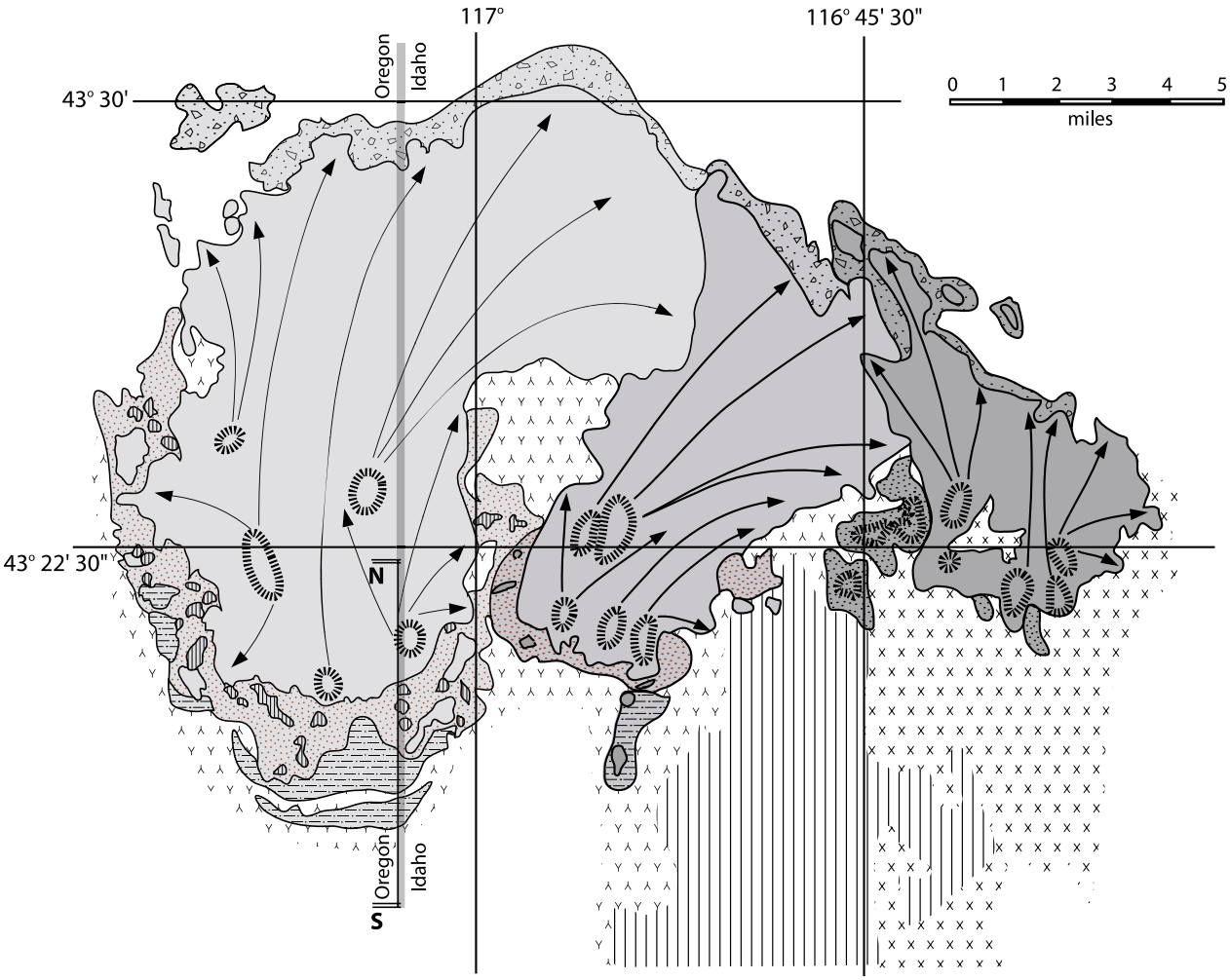

Figure 3. Map of Jump Creek Rhyolite flow-fields (adapted from Bonnichsen and Godchaux, this volume, and sources referenced therein). See Figure 4 for cross section. The cross section line is N-S along the Idaho-Oregon border.

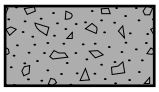	Sublacustrine breccia with large rounded clasts and opal veinlets	Buck Mountain	Jump Creek rhyolite lava flows
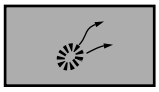	Main body of lava flow, source vents and flow lines	Shares Snout	
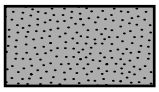	Near-vent breccia with mostly angular clasts and few veins	Flow-field	
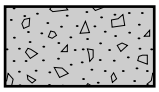	Sublacustrine breccia with large rounded clasts and opal veinlets	Rockville	
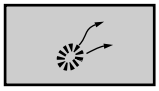	Main body of lava flow, source vents and flow lines		
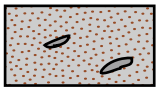	Near-vent breccia with hydrothermal explosion breccia pipes	Flow-field	
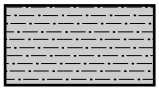	Near-vent phreatomagmatic tuff		
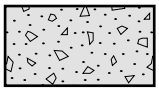	Sublacustrine breccia with large rounded clasts and opal vessels	Pole Creek Top	
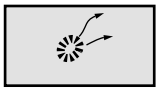	Main body of lava flow, source vents and flow lines		
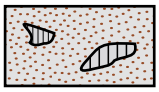	Near-vent breccia with hydrothermal explosion breccia pipes	Flow-field	
	Near-vent phreatomagmatic tuff (cone)		
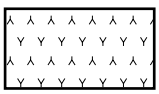	Miocene Sucker Creek Formation: Fossil-bearing fluvio-lacustrine sediments and low-grade ignimbrites, tuffs, pumice falls, and ash falls		
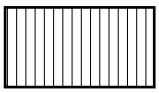	Miocene lower basalt and related volcanic rocks		
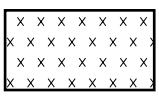	Oligocene Salmon Creek Formation Basalt, basaltic andesite, and andesite welded and unwelded tuffs, lavas, and sediments		

Table 1. Chemical analyses of Owyhee Front rhyolite samples, southwestern Idaho.

Sample	I-3849	I-3747	I-3478	I-3673	I-3846	I-3664	I-3804	I-3672	I-3246	I-3715
Unit	Pole Creek Top segment	Jump Creek Rockville segment	Jump Creek Buck Mountain segment	Jump Creek Shares Snout segment	Reynolds Creek lava flow	Wilson Creek ignimbrite		Cerro el Otoño Hill 3036	Cerro el Otoño Hill 2471	Cerro el Otoño Hill 2781
Weight percent										
SiO_2	69.82	72.98	69.52	71.77	75.11	77.41	75.37	78.89	77.38	80.49
Al_2O_3	14.28	13.11	14.04	14.05	12.49	12.39	12.32	11.63	11.21	10.64
TiO_2	0.50	0.44	0.48	0.50	0.22	0.10	0.12	0.09	0.09	0.07
FeO	3.53	3.15	3.21	3.17	2.03	0.96	1.45	0.94	0.73	0.72
MnO	0.07	0.07	0.08	0.03	0.01	0.01	0.02	0.01	0.01	0.01
CaO	1.67	1.48	1.80	1.29	0.90	0.26	0.61	0.10	1.13	0.22
MgO	0.63	0.40	0.43	0.21	0.28	0.02	0.33	0.08	0.00	0.07
K_2O	4.34	4.08	4.65	4.71	5.08	5.08	5.55	4.79	4.69	4.28
Na_2O	3.96	3.76	3.89	3.92	3.31	3.71	2.53	3.70	3.80	3.19
P_2O_5	0.13	0.12	0.14	0.14	0.07	0.03	0.05	0.02	0.03	0.02
Total	98.93	99.58	98.24	99.78	99.50	99.96	98.36	100.25	99.06	99.71
Parts per million										
Ni	7	4	0	4	5	6	11	10	3	6
Cr	0	0	0	0	0	0	0	1	3	0
Sc	8	7	7	4	4	1	3	7	5	3
V	11	21	20	13	33	11	5	0	4	0
Ba	2063	1874	1945	1930	1477	27	71	14	20	15
Rb	87	82	91	97	150	155	150	176	171	143
Sr	290	246	286	227	73	7	36	7	19	10
Zr	558	483	485	517	362	210	213	282	288	172
Y	51	48	49	56	39	39	65	86	72	39
Nb	44	39	41	42	41	55	53	78	74	53
Ga	21	17	22	21	19	20	20	23	26	21
Cu	3	0	1	2	2	0	3	0	0	0
Zn	117	92	103	99	72	65	91	120	35	41
Pb	22	23	26	24	28	29	30	38	16	22
La	89	71	85	82	100	64	68	52	31	89
Ce	164	139	140	134	180	101	127	119	72	100
Th	11	10	18	13	26	14	12	19	7	13

Analyses by X-ray fluorescence at Washington State University GeoAnalytical Laboratory.

xenocrystic. Sanidine is present in most of the Jump Creek flows in all of these fields, but is invariably much less abundant than plagioclase; it is commonly blue-chatoyant in hand specimen. Mafic minerals are present in minor amounts in all samples; they are pervasively altered to magnetite and other oxides, but a few fresh domains indicate that orthopyroxene is much more abundant than clinopyroxene. The sole exception is in flows from the Buck Mountain vent, in which the principal pyroxene is aegirine-augite. Veinlets of chalcedony and small patches of secondary zeolites occur sporadically, and accessory allanite is present in one breccia sample from the Rockville flow field. Lithic inclusions are present in only one sample from the Pole Creek Top flow field. Matrix glass in most samples is at least incipiently devitrified. Textures are locally spherulitic, suggesting a cooling rate fast enough to preserve glass but not too fast for devitrification to occur at all. Perlitic structure is present in glassy domains, where it is prominent, and as patchy areas in spherulitic domains where it is less prominent. Where a time relationship between spherulite formation and perlitic cracking can be seen, the perlitic cracking seems to postdate the spherulite formation. These features appear most commonly near the toes of flows; they may indicate interaction with external water during cooling.

Breccias

Three types of breccias occur in association with Jump Creek flows. They may be classified as (1) near-vent breccia rings of syneruptive origin, (2) basal breccias developed during transport away from the vent, but not discussed here because they do not involve interaction with surface water, and (3) downflow breccias of syndepositional origin produced when distal parts of the flows broke up as they descended steep topographic breaks or entered the lake.

Near-vent breccia rings. Near-vent breccia rings are crudely bedded and pervasively cemented (Figure 4). The breccias have dense glass fragments, fiamme-like fragments, and isolated mineral grains, all cemented together by silica. The fragments are relatively small, commonly in a jigsaw-puzzle arrangement (Figure 5), and fine matrix is not abundant except in clearly phreatomagmatic layers near the bases of some breccia-ring outcrops. A series of such layers near the Rockville vents is about 60 feet thick and grades upward into fine breccia overlain by massive rhyolite (Figure 5). Rounded pumice lapilli and accretionary lapilli (many with nonjuvenile mineral grains or lithic fragments in their cores) are abundant in the lowest, massive layers, with glass shards and fine ash becoming more abundant in the upper, crudely bedded layers.

Another series of phreatomagmatic deposits, less well preserved, is exposed as small ledges near the Oregon-Idaho state line. These deposits underlie and grade up into the coarse breccias of the ring surrounding the vents of the Pole Creek Top flow field. Although such deposits are preserved only in a few places in the vent areas of the Jump Creek Rhyolite, they suggest that phreatomagmatism was common at the outset of these dominantly flow-producing eruptions. Despite the probable brevity of the phreatomagmatic phase, it had a great influence on the later wholly magmatic phase of the eruption. A moderately deep-focus blast probably triggered an unusually high rate of eruption of poorly vesiculated rhyolite magma at high temperature, producing low fire fountains and forming clastogenic lava flows. The crudely radial pattern of linear arrays of hydrothermal breccia pipes and their re-brecciation textures within the Pole Creek Top breccia ring (Figure 3) suggest that the water powering the initial explosions was drawn from buried wet sediments or gravel layers rather than from standing water at the surface.

These near-vent breccia rings are shown on most published maps as Quaternary landslide deposits. Our interpretation is that disruption by landsliding is a relatively minor, late-stage process and that much of the primary depositional shape of the rings is preserved. An exception to this pattern occurs along the eastern margin of the

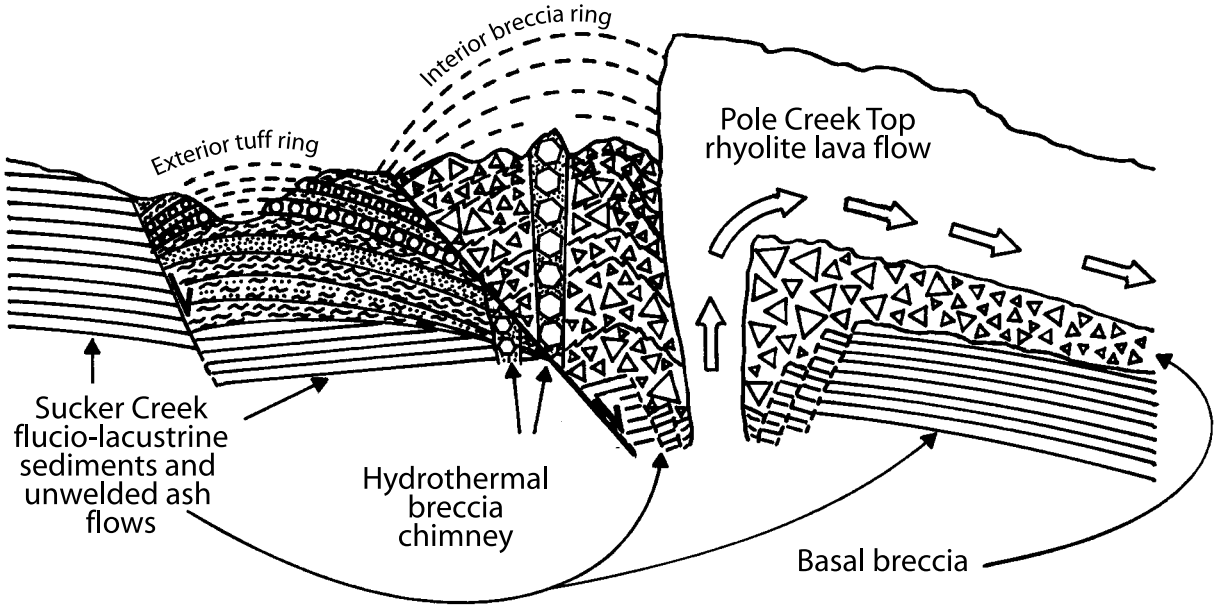

Figure 4. Stateline cross section, vent for Pole Creek Top lava flow (see Figure 3). Exterior tuff ring is dominated by fall deposits and mixed fall-surge deposits. Interior breccia ring is cut by hydrothermal breccia chimneys with fragments of earlier eruptive breccia in jigsaw-puzzle fit and with abundant interstitial secondary silica.

Fig. 5A.

Fig. 5B.

Fig. 5C.

Fig. 5D.

Fig. 5E.

Fig. 5F.

Figure 5. Photographs of Jump Creek Rhyolite near-vent phreatomagmatic tuffs, breccias, and agglutinates. (A) Remnants of main breccia ring around vent areas of Pole Creek Top flow field. (B) Close-up view of second-generation breccia texture in hydrothermal breccia chimney. (C) Tuff of vent area of Rockville flow field. (D) Close-up view of accretionary lapilli in phreatomagmatic tuff. (E) Buck Mountain volcano. (F) Bombs and agglutinate in tephra near vent of Shares Snout flow field.

Rockville field and the western margin of the Buck Mountain-Shares Snout field where lava flows from both vent complexes were descending into the canyon of ancestral Squaw Creek, giving rise to debris flows and penecontemporaneous landslides. When the canyon was reincised by the modern Squaw Creek, downslope movement of large blocks of solid rhyolite was a major factor in shaping the present-day landscape. This region was evidently a paleocanyon into which lavas from both fields descended and produced multiple debris flows and chaotic megabreccias through mixing with unconsolidated water-saturated sediments. Quaternary landsliding acted upon blocks of solid rhyolite during and after the excavation of the present-day canyon.

Downflow breccias. Breccias developed downflow, mostly at and below the present-day 3,400-foot level, have a strikingly different set of textures and outcrop features from those of the near-vent ones (Figure 6). Individual clasts are roughly equant in shape and range in diameter from 6 inches to 3 feet, with larger sizes predominating. They consist mainly of massive and flow-layered, relatively unaltered rhyolite. Matrix is locally abundant, and most clasts are rounded; open space is locally preserved in interstices between large clasts. These breccia accumulations are very thick, in many places equal to the entire flow thickness of several hundred feet. Little cementation is present between the 3,400-foot level and the 3,000-foot level. Below the 3,000-foot level, individual slide blocks appear to have been immersed in water, and tongues of breccia have invaded soft lake-bottom muds, producing spectacular mixtures of rhyolite and sediment. Deposits of opal and other forms of secondary silica fill fractures and voids in these outcrops. From these relationships we can infer the elevation of the lakeshore to have been at the 3,000-foot to 3,100-foot level at the time of lava-flow emplacement.

Semiconsolidated beach sands, which have mineralogy reflecting a granite source and contain no rhyolite fragments, have been invaded by and draped over the margins of the rhyolite lobes. Their dips and degree of silicification and baking decrease away from the rhyolite bodies. In many places, later sandstones that do contain rhyolite pebbles lie with slight to moderate angular unconformity on the steeply tilted sandstones immediately adjacent to the rhyolite. This laterally persistent pattern of coarse thick noncemented breccias passing downflow into silicified breccias, which show a variety of invasion and loading relationships with sediments that were unconsolidated or semiconsolidated at the time of contact, suggests that the Jump Creek flows came down over a series of upland fault scarps into an extensive body of standing water. Some but not all of the faults were reactivated during or soon after emplacement of the rhyolite; in a few places, we have seen evidence of their behaving as growth faults, offsetting lower layers of rhyolite but dying out upwards and causing little or no displacement in the upper part of the rhyolite. Little brecciation is specifically associated with post-rhyolite faulting, although some fault surfaces have fault gouge, slickensides, and local development of secondary minerals such as chlorite and zeolites.

WILSON CREEK IGNIMBRITE

Principal Features

The next major rhyolite unit erupted along the southwestern margin of the western SRP, the Wilson Creek Ignimbrite, covers less than one-tenth as much area as does the Jump Creek unit, but whatever it lacks in volume, it more than makes up in complexity (Figure 7). An earlier or marginal low-grade ignimbrite facies passes laterally into or is overlain by a very high-grade, flow-banded lithophysal facies that has features transitional between those of an ignimbrite and those of a lava flow. We interpret it as a "lava-like" ignimbrite (Branney and Kokelaar, 1992). For most of its runout distance, this ignimbrite is tightly flow-folded with subvertical fold axial surfaces. In the distal third of its length, especially in lower Hardtrigger Creek Canyon, it is characterized by spectacularly developed spherulites and lithophysae as much as 10 inches in diameter, many with "onion-skin" structure (Figure 8).

We concur with Ekren and others (1984) that the Wilson Creek unit is an ignimbrite, but not that it came from a caldera in the western SRP and flowed up a paleovalley. Unlike the Jump Creek Rhyolite, which appears to have been emplaced as lava flows running down a relatively undissected northeast-dipping regional slope, the downslope part of which was cut into stair-steps by northwest-trending, down-to-the-northeast normal faults, the flowing Wilson Creek Ignimbrite was topographically confined by a fairly narrow and deep paleocanyon system. We are unsure if this change in aspect means that not enough time had elapsed between initial basin development in the western SRP and the Jump Creek eruptions for headward erosion to have cut canyons into the fault blocks; by Wilson Creek time 100-200 Ka after Jump Creek emplacement, such canyons were well-developed. Two dates have been obtained on the Wilson Creek unit: one from the vent area at Wilson Bluff is 11.34 Ma, and the other from a distal (probably sublacustrine) outcrop is 11.41 Ma (New Mexico Geochronological Research Laboratory, written commun., 2000).

Fig. 6A.

Fig. 6B.

Fig. 6C.

Fig. 6D.

Fig. 6E.

Figure 6. Photographs of Jump Creek Rhyolite flow-foot breccias. (A) Baked zone in sediments under distal breccia. (B) Breccias downstream from Jump Creek Falls, formed where flows entered Lake Idaho. (C) Large slide block of rhyolite emplaced in shallow part of Lake Idaho. (D) False pyroclastic texture in large slide block. (E) Debris flow packages bounded by shear surfaces, locally invasive into soft sediments, originally emplaced where rhyolite lavas of the Rockville field descended into paleocanyon of ancestral Squaw Creek.

Petrography

The Wilson Creek Ignimbrite differs petrographically and chemically from the Jump Creek Rhyolite as well. Relatively crystal-poor, it is composed mostly of an original groundmass of cloudy brownish glass that has been largely converted to abundant and varied devitrification features. These features include clusters of concentrically banded lithophysal spherulites, delicate flow-banding characterized by alternating glassy and devitrified bands, and radiating fanlike clusters of microlites as matrix around well-formed spherulites. Glass shards and pumice clasts are recognizable in some samples, and irregular patches of tridymite are common. Small and sparse phenocrysts include euhedral to subhedral beta-quartz pseudomorphs and high sanidine of composition Or_{50-60}; the ratio of quartz to feldspar varies considerably, but quartz is generally the more abundant mineral. Sparse clots of brownish mafic material were probably formed by alteration of primary mafic minerals, and magnetite is present in some specimens. A few samples contain embayed grains of symplectite, which may be xenocrysts derived from the source rocks or from older volcanic or plutonic rocks. Chemically the Wilson Creek Ignimbrite is a high-silica rhyolite (average SiO_2 content of 76.5 percent) with less than 100 ppm Ba and more than 5 percent K_2O. FeO and TiO_2 are both low (Table 1).

Breccias

The development of breccia is far less common in the Wilson Creek Ignimbrite than in the Jump Creek Rhyolite, and the style is also very different. Near the Wilson Bluff vent, relatively fine-grained breccias are present as narrow bands intercalated with flow-banded layers and as anastomosing veins. The medial part of the unit has few and restricted breccia zones, in contrast to the laterally persistent thick layers of breccia in the Jump Creek unit. Distal exposures of the Wilson Creek Ignimbrite typically have steeply dipping, tightly folded flow-banding with thin breccia zones both parallel to the bedding and cutting across it, in contrast to the thick piles of very coarse-grained, poorly cemented breccia in distal outcrops of the Jump Creek Rhyolite. Wilson Creek breccia textures are relatively fine-grained and locally show evidence of a hydrothermal origin: a jigsaw puzzle fit of clasts with fine matrix in the interstices (commonly with chalcedony zones), a concentration of (mostly broken) phenocrysts in the matrix, clasts of earlier breccia in later breccia, and scattered clasts of underlying volcanic and plutonic rocks.

Tuffs and tuff-breccias at the base of the unit at Wilson Bluff are probably of phreatomagmatic origin. The lowest exposed layers form a moderately well-bedded but poorly consolidated sequence with matrix material consisting of blocky shards of rhyolitic glass, rhyolitic ash, pumice, and finely comminuted sedimentary rock with abundant lithic clasts, including granite, altered basalt and andesite, and pebbles of Silver City rhyolite (Figure 8). This sequence grades upward through a thickness of several tens of meters into increasingly more densely welded and less lithic-rich tuff and ultimately into lithic-poor vitrophyre at the top. We interpret this sequence as the deposit of an initially phreatomagmatic ignimbrite eruption. The abundance of well-rounded stream pebbles in the basal layers suggests that buried gravel aquifers may have provided the water involved in the earliest phase of the eruption. Breccias at the distal end of the Wilson Creek unit typically occupy the cores of large-amplitude flow folds, fractures in crestal zones of folds, and hydrothermal veins and chimneys. Opal is fairly common as fillings of smaller secondary fractures in distal breccias associated with the Wilson Creek unit, reflecting their deposition in standing water. This opalization is restricted to elevations below 2,900 feet, suggesting a slightly lower lake level than in Jump Creek time. The map pattern of distal outcrops of the Wilson Creek unit suggests that the valley-confined ignimbrites fanned out at the lake shore and traveled northwestward from the present-day mouth of Hardtrigger Creek (Figure 7). They may have been channeled along a small graben parallel to the main western SRP.

REYNOLDS CREEK LAVA FLOW

The Reynolds Creek lava flow, exposed in the Wilson Peak quadrangle, was erupted from a vent near the head of a complex paleovalley cut into granite and partly filled by Salmon Creek Volcanics before this part of the Owyhee Front was reactivated and reincised (Figure 7). It was called the "Tuff of Brown's Creek at Reynolds Creek" by Ekren and others (1984) and was interpreted by them as an ignimbrite whose source was a hypothetical caldera in the western SRP. There is no structural or geophysical evidence for such a caldera. The present-day surface manifestation of the vent consists of well-developed ogives on the upper surface of the flow at elevations between 4,400 and 4,600 feet (Figure 9), but the vent itself is apparently buried by the flow, which ran a short distance back up the paleovalley (Figure 7).

An age of 11.1 Ma has been recalculated to 11.41 Ma (Ekren and others, 1984), contemporaneous with the Wilson Creek unit, but the two units are separated by a high ridge of granite, and no stratigraphic relationship

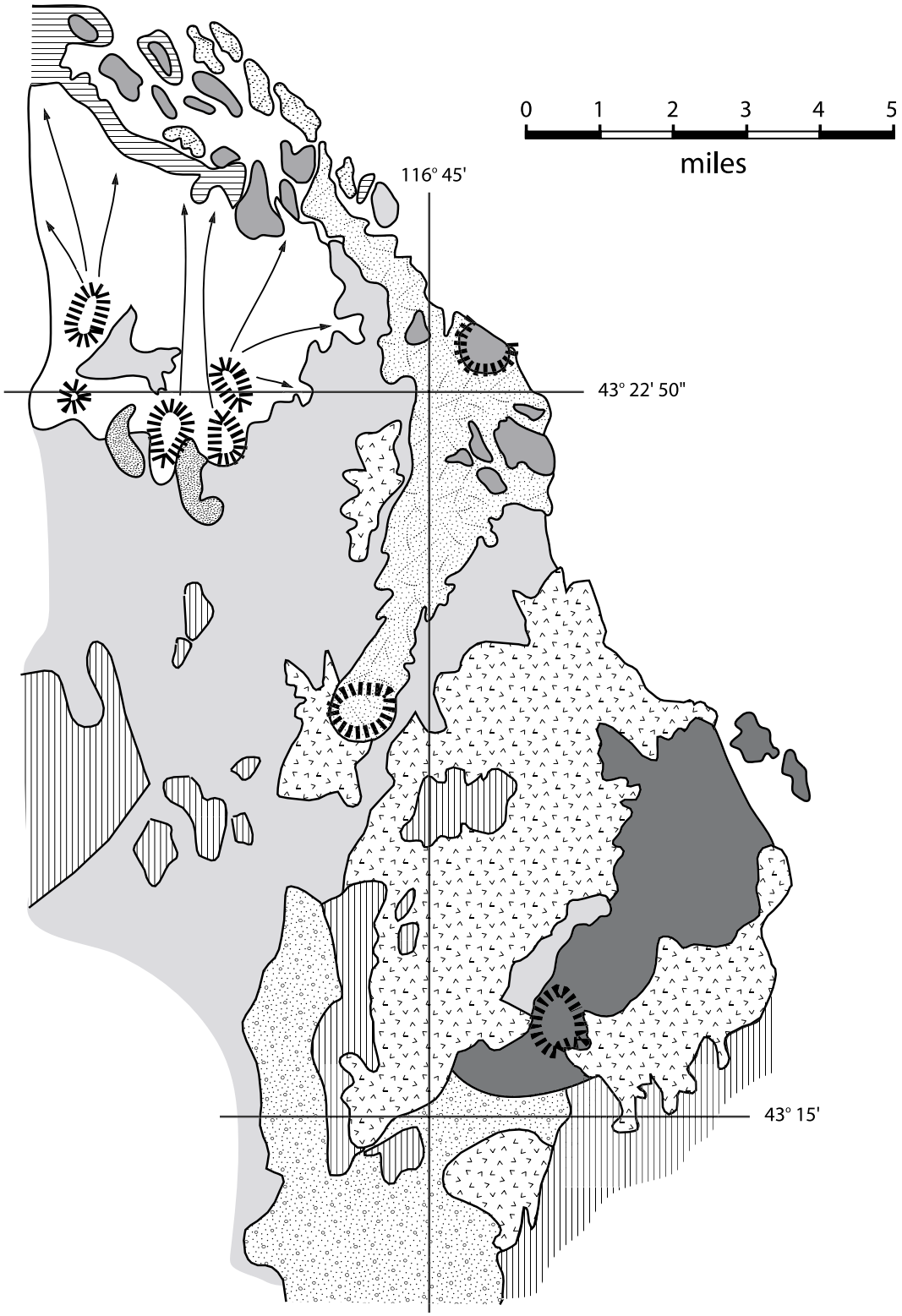

Figure 7. Map of Wilson Creek, Reynolds Creek, and Cerro el Otoño units (adapted from Bonnichsen and Godchaux, this volume, and sources referenced therein.

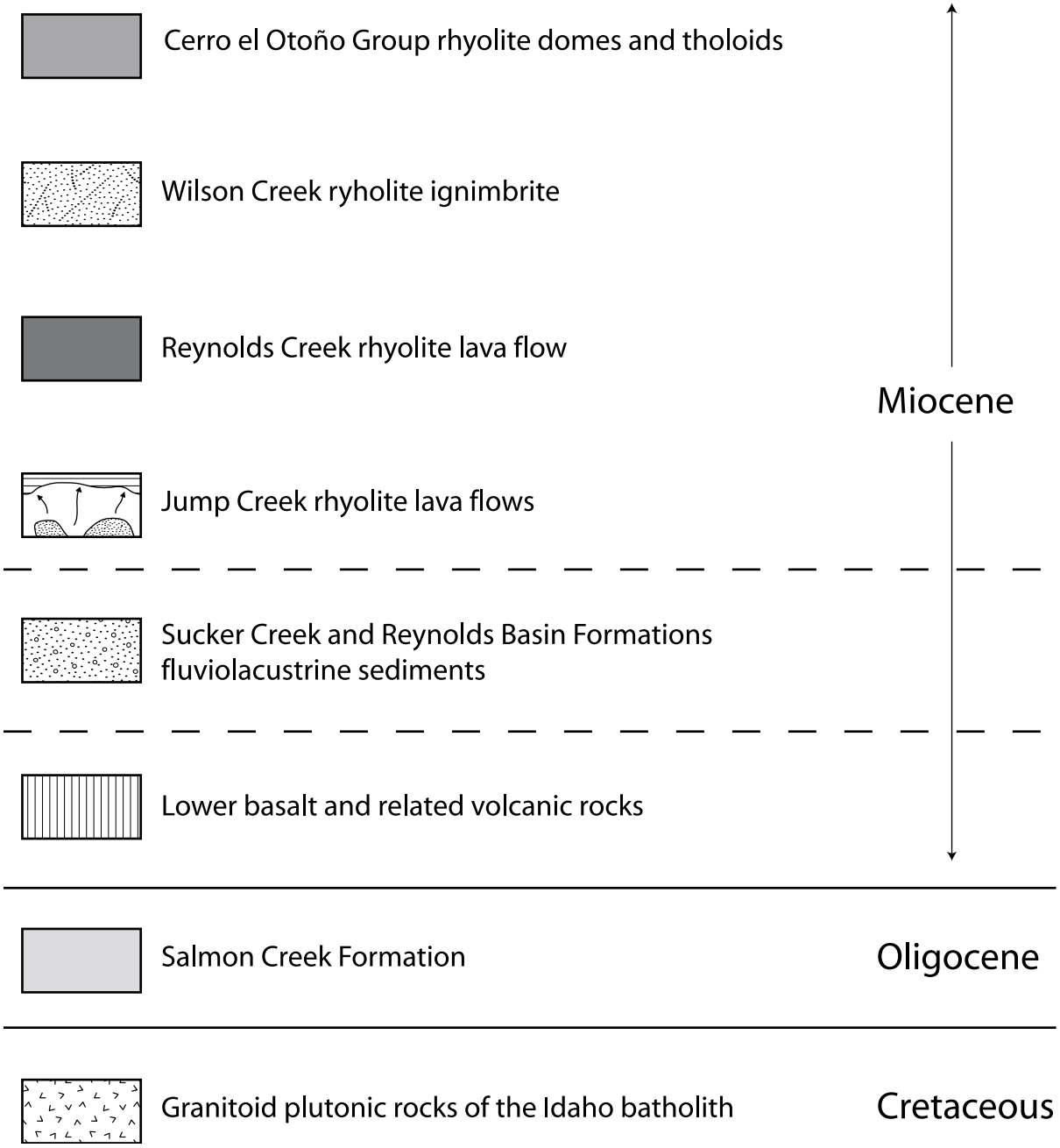
Cerro el Otoño Group rhyolite domes and tholoids
Wilson Creek ryholite ignimbrite
Reynolds Creek rhyolite lava flow
Miocene
Jump Creek rhyolite lava flows
Sucker Creek and Reynolds Basin Formations
fluviolacustrine sediments
Lower basalt and related volcanic rocks
Salmon Creek Formation
Oligocene
Granitoid plutonic rocks of the Idaho batholith
Cretaceous

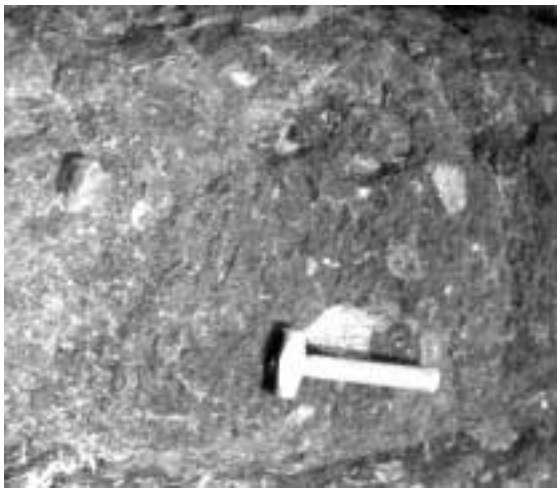

Fig. 8A.

Fig. 8B.

Fig. 8C.

Fig. 8D.

Figure 8. Photographs of Wilson Creek Ignimbrite. (A) Lowermost phreatomagmatic strata at Wilson Bluff vent. (B) Surge, fall, and pyroclastic flow deposits at peripheral outcrop in medial zone of ignimbrite. (C) Onion-skin spherulite with lithophysal cavity at distal end of ignimbrite in lower Hardtrigger Creek. (D) Rats Nest Gulch secondary vent of Wilson Creek Ignimbrite.

Fig. 9A.

Fig. 9B.

Fig. 9C.

Fig. 9D.

Figure 9. Photographs of Reynolds Creek lava flow. (A) Vent region at thickest part of flow. (B) Folded flow-banding near base of flow, south side. (C) Ogives on upper surface of lava flow, near vent area. (D) Red and black breccia rib exposed on upper surface of flow.

exists to tell which is the older, contrary to the assertions of Ekren and others (1984). The Reynolds Creek lava flow is intensely silicified and locally invades lake sediments at and below 3,200 feet, suggesting either that it is in fact a bit older than the Wilson Creek and was emplaced during a short-lived high stand of the lake between Jump Creek time and Wilson Creek time, or that the lake had declined between Jump Creek time and Wilson Creek time and then had risen rapidly, reaching the 3,200-foot level just before the emplacement of the Reynolds Creek lava flow. We prefer the former interpretation, in part because the Cerro el Otoño Group (discussed below) is clearly younger than the Wilson Creek unit, stratigraphically overlying it in places, and at the time of its emplacement the lake level appears to have declined to below 2,600 feet. Obtaining a precise date on the Reynolds Creek lava flow will help to resolve the question of its exact relationship to the Wilson Creek Ignimbrite. If the Reynolds Creek unit turns out to be even older than the Jump Creek unit, then the four Owyhee Front rhyolite units will be seen as recording a steady lowering of the lake level between 12 Ma and 11 Ma.

CERRO EL OTOÑO DOME FIELD

After a hiatus of 300 to 400 Ka, the final series of rhyolite eruptions along the Owyhee Front gave rise to a group of domes and tholoids, the Cerro el Otoño Group (Figure 7). Dates for these rhyolites are 11.03 Ma at the eponymous Cerro el Otoño Dome and 11.14 Ma at a tholoid or possibly a displaced slide block near Givens Hot Springs (New Mexico Geochronological Research Laboratory, written commun., 2000). The aggregate volume of this group is very small, and the vents from which the rhyolite issued were closer to the axis of the western SRP graben than the vents of any of the earlier-erupted units. These vents were a series of short fissures trending NW-SE, following graben-parallel faults that offset the older units or in some places cut obliquely across those older faults. The domes and tholoids of this group are not opalized or strongly silicified except at elevations below 2,600 feet, suggesting a further decline in lake level possibly because the graben widened rapidly between 11.4 Ma (Wilson Creek time) and 11.1 Ma (Cerro el Otoño time). Cerro el Otoño rhyolite is petrographically very

similar to Wilson Creek rhyolite, except that quartz is much more abundant than sanidine in all samples, and oxides and other mafic phases are virtually absent.

The best-developed dome in the group is Cerro el Otoño itself, and it is the only one that has been studied in detail. Although its northeast side is cut off by a fault, it is well exposed elsewhere. Its structure is that of an exogenous dome produced by upwelling of viscous magma inside a low tephra-and-spatter ring (Figure 10). Thin sections of the spatter layers show complex annealing and devitrification textures (Figure 11). One stratigraphic section on the northwest side of the dome exposes progression upward from the unwelded base of the tephra into thin-layered annealed spatter and finally into flow-banded dome rock. Flow banding dips gently inward at the periphery of the dome and becomes steep to vertical in its interior (Figure 12). Narrow dikes and pipelike bodies of hydrothermal breccia cut flow-banded dome rock in many places, but silicification and the development of opal are lacking, suggesting that relatively little magma-water interaction took place during the emplacement of the dome, or that the emplacement was in a wholly subaerial environment.

Other bodies in the Cerro el Otoño field have similar structure and petrography, but all are smaller and less symmetrical than Cerro el Otoño. None appear to have fed flows or to have an invasive relationship with adjacent and underlying sediments, as the Jump Creek Rhyolite and locally the Wilson Creek Ignimbrite do. Although some have been displaced by post-rhyolite faulting, the amount of displacement appears less than that of older units. Breccias appear only as dikes and veins of microbreccia within or marginal to solid rhyolite. The form and distribution of this intriguing group of rhyolites imply that it represents the last bit of silicic magma to seep out of the cracks along the widening western SRP graben.

BASALTIC ERUPTIONS IN AND AROUND LAKE IDAHO

WAYS IN WHICH BASALT AND WATER MAY INTERACT

Basic Considerations

Basaltic magmas differ from rhyolitic magmas in several important ways that impact their interactions with external water. Because basaltic magmas have lower viscosities than rhyolitic magmas and because they are erupted at higher temperatures, their flow thicknesses and velocities and other characteristics also differ. Flow styles vary from blocky to aa to highly fluid pahoehoe. Dissolved gases can exsolve and escape more easily than from rhyolite magmas. The possible interactions with surface and near-surface waters are greater than those for rhyolite magmas. We divide the discussion of interaction styles into three end-member cases: dry subaerial eruption followed by entry of lava into standing water; deep sublacustrine eruption followed by entirely sublacustrine transport and emplacement; and phreatomagmatic eruption characterized by a transition from sublacustrine to subaerial eruption or by substantial interaction with ground water or buried aquifers. Each of these categories is well represented in the western SRP graben.

Important factors. Factors influencing the final product include (1) properties of the lava, such as temperature, viscosity, vesicularity and crystallinity, and the resultant blocky, aa, or pahoehoe flow style, and (2) properties of the flow path, such as the distance traveled over land before entry into water, the velocity, the slope of the lake shore and lake bottom, the type and degree of consolidation of lake-bottom deposits, and the water depth in which each part of a flow comes to rest.

End-member products. End-member products include the following: (1) pillow basalts and pillow deltas, produced when slow-moving pahoehoe lava meets a steeply sloping lake bottom; (2) water-affected basalt (WAB), produced when fast-moving pahoehoe lava meets a gently sloping lake bottom; (3) littoral cones and fans, produced when aa lava enters water; (4) lakemounts and pillow piles, formed during low mass flux sublacustrine eruptions; (5) WAB sheet flows, formed during high mass flux sublacustrine eruptions; (6) hyaloclastite accumulations, formed during sublacustrine eruptions at great depth, generally of higher viscosity basalt magma; (7) debris flows and invasive flows, formed by the collapse of sublacustrine constructs of high relief atop poorly consolidated lake-bottom sediments or by the sinking of flows into areas of especially poorly consolidated substrate; and (8) phreatomagmatic constructs of emergent (tuff cone) type or subaerial (tuff ring or maar) type.

Dry Subaerial Eruption Followed by Entry of Lava into Standing Water

Pillow basalts and pillow deltas. Pillow basalts and pillow deltas occur in several situations. Most commonly, a lava flow enters a large body of water in which the bottom slopes steeply enough (more than 5 degrees) so that the water depth is greater than the thickness of the

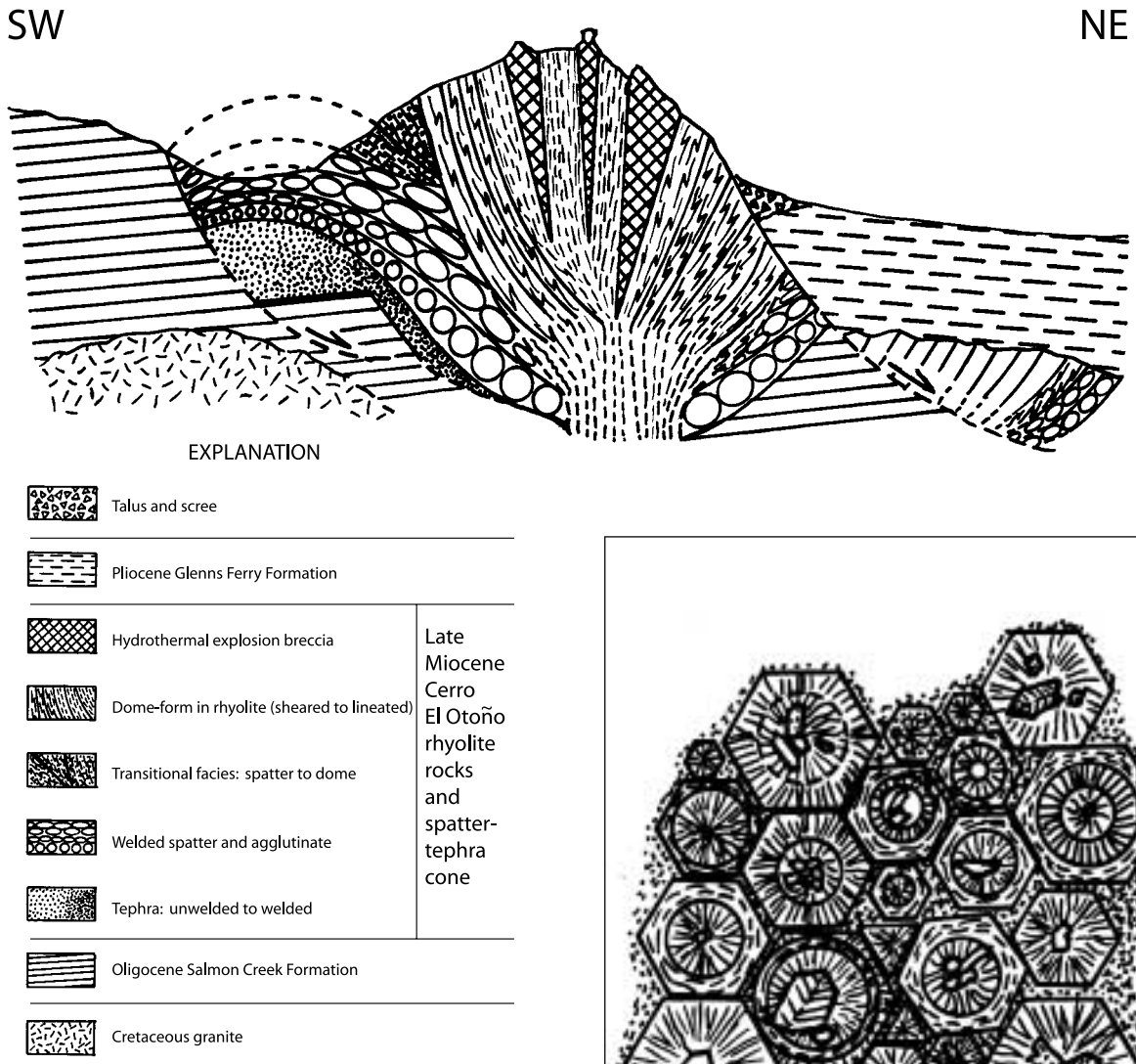

Figure 10. Schematic cross section of Cerro el Otoño Dome and spatter ring.

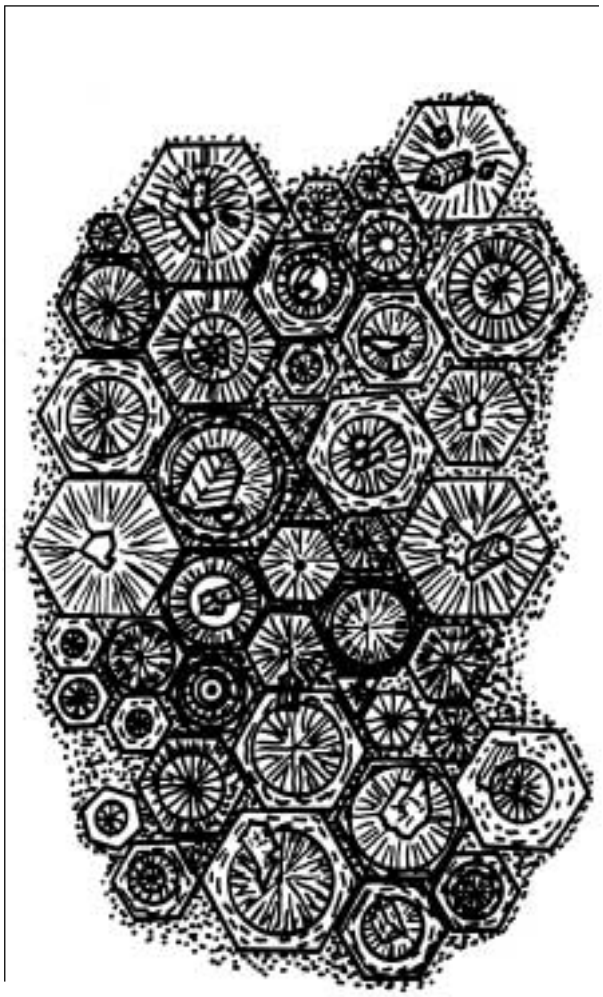

Figure 11. Annealing texture of spatter droplets, Cerro el Otoño. Radiating line pattern indicates devitrified part of droplet. Concentric dashes indicate glassy part. Dot pattern indicates fine ash matrix. Centers of most droplets contain crystals or vesicles.

Fig.12A.

Fig.12B.

Fig.12C.

Fig.12D.

Fig.12E.

Fig.12F.

Figure 12. Photographs of Cerro el Otoño. (A) Faulted margin of Cerro el Otoño Dome, Owyhee Front. (B) Basal spatter deposits on western margin of Cerro el Otoño. (C) Lapilli and bomb in spatter deposit on south side of dome. (D) Inward-dipping spatter layers on north side of dome. (E) Steeply tilted and sheared rhyolite near summit of dome. (F) Breccia tower of hydrothermal origin on upper surface of dome.

lava flow within a few tens of feet from the shoreline. Also common is a second situation in which the water body is extensive but shallow, nowhere as deep as the thickness of the lava flow, so that the flow will be pillowed at its base but will pass upward into subaerial basalt. The third situation in which pillows form is that of a subaqueous eruption, discussed in a later section. The fourth situation, less common than the first three, is where basalt has flowed over a canyon rim or fault scarp and has fallen into water to form a thick deposit that is a mixture of pillows, pillow fragments, and comminuted glassy matrix material.

In pillow deltas, the individual pillows may be considerably elongated, like bolster pillows, as a result of emplacement down the foreslope of the delta. At some localities, such pillows are exposed as lag deposits; they resemble large petrified logs in subparallel or radiating arrangement, with typical plunges ranging from 20 to 40 degrees and from a few feet to tens of feet long. Pillow diameters range from a few tens of inches to several feet; they typically have concentric alternating dark colored and reddish brown layers that formed as pulses of the enclosed lava budded from the downslope end of the pillow, dropped downward, and extended the lower end of the pillow. Large irregular central voids, some as much as 3 feet in length, occur within the upper ends of such pillows as a result of either a drainaway of lava or an inward migration of gases excluded from the melt during solidification. On the outer surfaces of some pillows, a thin skin of glossy black glass is preserved, and there may be additional layers of black glassy or crystalline basalt in the concentric rings, typically alternating with reddish palagonitized rings. A variant of the common bolsterlike pillow shape, a much wider, mattresslike shape, is produced where lava squeezed out of horizontal cracks and flowed down the delta front. Interpillow volcaniclastic material ranges in relative amount from very little to nearly half the volume of the delta. It consists mostly of fragmented glassy basalt (black to reddish brown to yellowish tan), pillow fragments, and sedimentary material that probably originates as muck stirred up from the lake bottom by the advancing delta.

Pillow deltas are commonly configured in a manner similar to sedimentary deltas, with well-defined topset, foreset, and bottomset parts. The foreset part, always the thickest of the three, consists of the plunging pillows described above plus some rounded or bloblike pillows in a fragmental matrix. The foreset part grades into the bottomset part, a subhorizontal relatively thin layer of fragmental glassy basalt, pillow fragments and isolated detached rounded pillows, and admixed sedimentary material. The topset part, also relatively thin, consists of wave-reworked material. Where the water depth was less than the thickness of the flow, the topset part may consist of subaerially emplaced basalt in discrete layers generally less than 10 feet thick. All gradations exist between this case and the type of flow in which only the base is pillowed (generally the typical delta form is not developed, and the pillows tend to be equant rather than elongated) and the "topset" part makes up most of the flow thickness. This form is produced by basalt flows crossing small streams, marshy areas or playa lakes. Commonly found are sedimentary materials intermixed with the glassy matrix, and squeeze-ups and laterally transported rip-ups of hardened and baked mud cut such pillow layers, along with abundant gravel clasts and pillow fragments near the bases of these layers. Locally abundant are downward protrusions of small pahoehoe toes from the bases of the overlying flows into the upper parts of the pillowed layers.

Water-affected basalts. Water-affected basalts (WABs) are even more common in the western SRP than are pillows, but they have received less attention. Earlier workers interpreted their features as the result of deep weathering of ordinary subaerial basalts under humid-climate conditions. Our description of these basalts is organized to proceed from their occurrence and appearance in the field and in thin section to the types of vesicles and amygdules they carry, and to their effects on underlying sediments. We also discuss the major factors and conditions affecting the development of WABs in the western SRP.

Occurrence and Appearance of Water-Affected Basalt

At many localities in southwestern Idaho, especially in the western SRP, certain basalt flows are highly altered and have low resistance to weathering, even though they are very young, have never been subjected to humid-climate weathering, and may be interbedded with basalt flows that are very fresh. In some places, fresh-appearing flows can be traced laterally into thoroughly altered parts. Many of the altered flows are associated with lake beds, pillows, and basaltic tuff beds, suggesting that these flows interacted with water in various ways after eruption, some transport, and partial to complete solidification, but before cooling to ambient temperatures. We have collectively referred to these hydrated and altered basalts as water-affected basalts (WABs), regardless of the specific nature, degree, and pervasiveness of their alteration or exactly how it was produced.

Water-affected basalt has probably developed in a variety of ways, including but not limited to the following: (1) by the slow cooling of subaerially erupted basalt

that was subsequently completely immersed in water, which allowed reactions between water and mafic glass and between water and certain phenocryst minerals to proceed; (2) by even slower cooling of subaqueously erupted basalt at water depths great enough to inhibit explosive magma-water interaction; and (3) by the alteration of basalt by hot water or steam generated from the heating of adjacent wet materials by the lava. The amount of WAB at a given locality in a water-affected flow varies from only scattered small zones or pervasive but relatively minor alteration (incipient WAB) to highly altered but coherent basalt, which forms cliffs or ledges but is nonetheless easily pulverized (moderate WAB), to completely hydrated and disaggregated flows, which form slopes and from which solid samples cannot be extracted (terminal WAB). One WAB characteristic, especially well-developed in terminal WAB, is the formation of a great many closely spaced internal fractures (crackle fractures) throughout the body of the basalt. Upon exposure to the Earth's surface and weathering, these fractures allow the WAB to disaggregate to a gruslike accumulation of small fragments rather than to have the considerable resistance to arid-climate weathering seen in fresh (subaerial) basalts throughout southwestern Idaho. Except for relatively minor chemical changes in the mutual abundances of major oxides at the margins of WAB flows, we have found virtually no change in relative abundances of the major oxides associated with development of WAB from fresh basalt. The development apparently is an isochemical process of hydration of the original basalt through the retention of water in the glassy mesostasis and in microfractures. Mafic phenocrysts, if present, are also commonly converted to their hydrated forms. Certain WABs, probably those with relatively small glass content or abundant crystallites widely dispersed in the glass, develop spectacular spheroidal-weathering features.

Petrography of Water-Affected Basalt

Some of the petrographic features of WAB are indicative of fairly rapid crystal growth, such as swallowtail and hollow plagioclase phenocrysts and even microphenocrysts, skeletal-crystal growth forms of oxides and olivines, and especially ophitic augite crystals that may exceed a half inch across. The ophitic augites are most common in the massive, essentially nonvesicular interior parts of fairly thick WAB flows, and they likely developed in situations where nucleation of new augite crystals was suppressed by moderate degrees of undercooling, thus favoring extensive growth on the margins of the existing crystals. Glass is common in the interstitial parts of WAB flows, and in many instances glasses of two or more colors may be present. Domains may be patchy and irregular, or color variations may be present in well-defined concentric bands. Most such glass is fully converted to palagonite; colors range from pale tan to bright reddish orange, depending on both the degree of hydration and the iron content of the original glass. In some of the massive, nonvesicular forms of WAB, relatively early-formed crystals of zeolites, chlorite, and more rarely biotite have textural configurations suggesting that they grew in the water-saturated hot flow interior directly from part of the glassy mesostasis rather than replaced previously formed olivines, pyroxenes or plagioclases.

Vesicles and Amygdules in Water-Affected Basalt

Vesicles in WAB flows are somewhat different from those typical of fresh subaerial basalt lava flows. Subaerially emplaced lavas contain two quite different populations of vesicles: (1) larger smooth-margined subspherical, tubelike, or discoid vesicles in which gases exsolved from the lava to form bubbles that were trapped within the cooling lava instead of bursting at the fragmentation surface, and (2) a large number of tiny, irregular, rough-walled vesicles bordered by lathlike crystals (diktytaxitic texture) that formed as the last gases were expelled during crystallization of the residual parts of the silicate liquid during its final solidification. In SRP subaerial basalt flows, the earlier-formed smooth-sided vesicles tend to be larger than the later-formed diktytaxitic vesicles, but both types are almost invariably present. In SRP WAB flows, however, diktytaxitic texture normally is absent, and the abundance and size of the larger smooth-sided vesicles typically are lower than in subaerial flows. The lack of diktytaxitic texture in WAB may be due to its crystallization under the somewhat greater confining pressures of a subaqueous environment so that late gases may have been retained in solution in the glass. In WAB, most of the smooth-sided vesicles contain amygdular fillings, which are commonly calcite and various forms of silica. Such amygdules are concentrated near flow surfaces and near fractures. By contrast with subaerial flows, there is rarely any open space left in WAB vesicles, and zeolite minerals are uncommon. Some WAB flows lack vesicles of any sort. These flows commonly have interstitial groundmass zeolites and chlorites, well-developed ophitic textures in their massive interiors, and pervasive crackle-fracturing. Upon exposure to weathering, they yield dark gruslike zones (terminal WAB) rather than coherent outcrops. Our impression is that these ophitic flows formed in relatively deep water that suppressed vesicle forma-

tion and yielded solidification rates rapid enough to favor the growth of large groundmass augite crystals that enclosed previously crystallized plagioclases.

Some WAB flows do contain diktytaxitic vesicles, which have some of the same fibrous and platy minerals that grew in the earlier smooth-sided vesicles. These features probably developed in situations where the lava flow was only partly immersed in water, was traversing wet ground, or entered a zone that was able to liberate a lot of superheated water or steam, which permeated the still hot basalt flow and was able to dissolve, transport, and reprecipitate the chemical constituents that formed the vesicle fillings.

Important Factors in the Development of Water-Affected Basalt

As already noted, the conditions favoring the development of WAB flows, rather than pillow basalts, are gently sloping lake-bottom topography and high rates of flowage of low-viscosity pahoehoe into the body of water. In addition, the lava must solidify rapidly but cool slowly so that the chemical and physical alteration processes can proceed at least partially. Rapid cooling of basaltic lava to ambient temperatures causes quenching and the preservation of abundant anhydrous glass. The early end to hydration reactions prevents glass and minerals in the solidified basalt from being converted to their hydrated equivalents. The requirement for rapid solidification followed by slow cooling implies a certain minimum thickness for individual flows, and most observed WAB flows are more than 10 feet thick. Much evidence can be seen in basalt flows that entered water, which indicates that the time available for WAB formation to proceed is a critical factor. This evidence includes the preservation of selvages of unfractured basalt, which may or may not be glassy, along surfaces and other zones where the abundance of water permitted the rapid chilling of the skin of the flow. Such quenched selvages have been found in many places, including the bases and tops of flows, the margins of columnar joints and other fractures that formed soon after the basalt solidified, and along thin internal subhorizontal surfaces within some flows.

In much WAB, the hydration of the basalt has not gone to its terminal condition; this end to reactions suggests that the amount of time the basalt was within the proper temperature range for the reactions to proceed at a fast enough rate was insufficient. Kernels of fresher basalt completely surrounded by WAB indicate that the cooling curve was too steep for complete conversion. This feature is particularly common in the massive interiors of many flows where residual kernels, which range from a few inches to several feet across, very much resemble the feature referred to as "warm-wet-climate spheroidal weathering" in older rocks. In columnar-jointed parts of some WAB flows, where the WAB-forming process did not go to completion, the outside, joint-bounded parts of individual columns commonly consist of fresh (quenched) basalt, whereas the column interiors are strongly hydrated. Conversely, the opposite zonal pattern has developed in other columns. The core of the column remains fresh and is surrounded by a shell of WAB, which may in turn be enclosed by fresh basalt along the column-bounding joints; it probably was quenched by water flowing along the joints as they developed.

Specific Conditions in the Formation of Water-Affected Basalt

The water depth probably has considerable influence on the formation of WAB and its final appearance and internal features. WABs that formed in water deeper than a few tens of feet generally lack diktytaxitic texture, as noted above; rather, the basalt is dense and massive. If vesicles are present, they tend to be very small, subspherical, and localized in the marginal parts of the flow. They typically are completely filled with calcite, chalcedony, or other secondary minerals. Large augites typically have well-developed ophitic textures, giving many rocks of this class a spotted appearance with the black augite crystals set in a lighter-colored, generally brownish groundmass. Commonly, plagioclase crystals, especially microphenocrysts, are hollow and have swallow-tail terminations. Oxide crystals and some olivines may show skeletal habits indicative of rapid growth. The groundmass commonly contains glass, typically darker, and may contain fibrous minerals, such as zeolites, chlorite, and even biotites and amphiboles that crystallized from the glassy mesostasis. Crackle-fracturing typically is so pervasive that spheroidal-weathering structure is well-developed. Columnar jointing is common in the thick interior parts of many flows.

WABs that formed in water only a few tens of feet deep differ from their deeper-water counterparts by lacking interstitial hydrous minerals and by having fewer and smaller ophitic augites and less developed crackle-fracturing. They have somewhat more extensive palagonitization of basaltic glass and more abundant and larger smooth-sided subspherical vesicles than deeper-water WABs.

For WAB developed where the basalt flow was only partly immersed in water or simply ran across wet ground, the distribution of altered zones tends to be spotty with fresh basalt interspersed irregularly with WAB. Ophitic

textures and rapid-growth habits are not common. Subspherical and smooth-sided vesicles are common, many of them empty or only partly filled by secondary minerals, and diktytaxitic texture commonly occurs (it may be confined to discrete layers within a flow). The glassy part of the flow is incompletely palagonitized. Neither columnar jointing nor crackle fracturing is as well developed as in basalt flows that solidified where they were completely immersed in water. Part or all of the vesicle fillings in these WABs are composed of minerals that have hackly or fibrous growth habits, such as zeolites, rather than more equant crystals such as calcite and various forms of silica. Steam probably coursed up through these basalt flows along multiple fractures after solidification, causing the irregular pattern of the alteration. Small pillows may be present in the basal parts of WAB flows that ran across wet ground or were emplaced in very shallow water.

Effect of Water-Affected Basalts on Underlying Sediments

Beneath some basalt flows that were emplaced on fine-grained water-saturated sediment layers, the sediment has commonly been baked and stained to vivid shades of brown or red. Some of this material is so striking that it can be referred to as "natural brick." The staining dies away, and the sediment is less baked beneath such flows at a depth of a few inches to 10 feet. Most likely, when the hot basalt was emplaced over the wet sediment, a hot water circulation cell was established in which iron was oxidized and leached from the basalt flow and redeposited in a ferric state in the immediately underlying sediment. Once the water was driven off, heat-generated baking of the reddened sediment hardened it to the point where it was rendered a flinty-textured rock.

Littoral cones and fans. Littoral cones and fans were produced when aa flows, which are very rare in the western SRP, entered standing water. Aa flows are characterized by broad flow fronts, high aspect ratios, high crystallinities, and high effective viscosity and shear strain rate at the flow front, all factors that promote explosive interaction with water. Typically, this interaction takes place right at the water's edge, effectively converting the entire flow front to blocky and mosslike glass shards and abundant small angular lithic grains (less than a quarter of an inch in diameter) with scattered larger fragments. A relatively steep-sided cone or half-cone is formed by a single narrow lava stream; more commonly, explosions along a broad flow front produce coalescing cones or fans. Wave reworking of the primary littoral deposits may produce a beveled apron of debris that is characterized by many irregular sets of high-angle cross-beds. Admixture of detrital sediments is less common in these deposits than in most phreatomagmatic tuffs because the lava flow never advances into the water in such a way as to stir up unconsolidated sediment. However, littoral deposits, which accumulate rapidly enough to become unstable, may periodically collapse and produce debris flows that churn up and rip up sediment.

Deep Sublacustrine Eruptions

Sublacustrine basaltic eruptions in the western SRP included the underwater extrusion of pillow piles and associated hyaloclastite tuffs, the development of invasive blobs and flows within the lake-bottom sediments (though some invasive flows are subaerial), and the formation of extensive, sheetlike lava flows (mostly WABs). Redeposition of much underwater-deposited incompetent material, after the collapse of unstable piles of pillows, pillow fragments, hyaloclastite tuffs and entrained sediments, has resulted in sublacustrine debris flows emplaced as sets of radial tongues around vents.

Lakemounts and pillow piles. Lakemounts and pillow piles form where feeders ranging in shape from pipelike conduits to vertical dikes have come up through somewhat consolidated sediments on the lake bottom. The eruption mode appears to have been the slow effusion of lava as equant pillows. In some outcrops, pillows can be seen to have congealed before they were completely extruded and pinched off; they are still trapped within the uppermost few feet of such dikes. Concomitant with the eruption of pillows, considerable quantities of hyaloclastite tuff were formed. These tuffs are preserved as poorly sorted matrix materials around the pillows in some places and as locally developed massive beds of tuff below and adjacent to the pillow accumulations. These tuffs generally are brownish mixtures of glassy fragments (including tachylite, sideromelane, and palagonite) with varying quantities of sediment derived from the beds immediately underlying the basaltic deposits. Some contain larger glassy basalt fragments, scattered pillows, and pillow fragments. The typical breakage of pillows produces three-dimensional pie-shaped, pyramidal, or conical sectors in a matrix composed mainly of fragmental glassy basalt, variably palagonitized. These components may form ragged, irregular piles or well-formed lakemounts with flat tops and steep sides.

Sublacustrine debris flows. Sublacustrine debris flows form when increasingly large and steep-sided accumulations of this type of water-saturated mixed debris become unstable, resulting in a large-scale slumping of material. The resulting debris flows and volcanogenic turbidites

may travel a mile or more across the lake bottom, incorporating disaggregated detrital sediment and rip-ups of better consolidated sediment. These rip-ups range in size from small blocks to tightly folded layers tens of feet in diameter that show a variety of soft-sediment deformation structures. Folds in large rip-ups are commonly isoclinal. At some places near the bases of debris flows, floaters of earlier-deposited layers of the debris flow package have been detached and transported downcurrent in the same way as the sedimentary rip-ups. A common feature of the debris flows is sets of near-vertical cracks that resemble joints but are layer-confined. These planar surfaces apparently served as steam-escape routes or elutriation channels. They are commonly somewhat fines-depleted. Adjacent to some dikes are accumulations of mainly fine-grained bedded hyaloclastite that dip gently away from the dikes. These beds probably formed during long-lasting eruptions at average extrusion rates slightly too fast for pillow formation yet not fast enough to give rise to sheet flows.

Sheet flows of WAB. Sheet flows of WAB are produced where the lava effusion rate is considerably higher than that which would result in pillow formation. If the lake-bottom substrate was well-consolidated to partly lithified sediment or previously erupted basalt, these flows would spread out laterally as sheet flows or shoestring flows, depending on the slope. They tend to be somewhat thicker and shorter than subaerial flows. The bases and tops of these flows consist of fine-grained, rapidly crystallized material with relatively little interstitial glass. In the upper parts of some flows, well-developed columnar joints are present, and in the basal parts there are many closely spaced near-vertical joints with a variety of strike directions. Both the columnar-jointed zones and the fracture-rich zones are conspicuously ophitic in texture. Vent zones from which subaqueous basalt flows were erupted have not been observed; they are probably covered by their own ejecta. At some localities, joints that cut the tops of subaqueous flows permitted residual lava to leak out and be quenched, resulting in small intricately layered and fractured masses of basalt shaped like mushroom caps. The original pahoehoe structure developed on the upper surfaces of some flows is locally preserved. Also preserved on the upper surfaces of parts of some flows are lineations parallel to the flow direction, a feature which may imply flow growth by inflation, temporary ponding, and subsequent drainaway of lava at rates of 10 to 100 cubic yards per second (Chadwick and others, 1999).

Invasive flows. Invasive flows form in places where the sediments were both unconsolidated and relatively thick. The point at which a given flow invades is not commonly preserved; invasion may take place very near the vent or after the flow has advanced a considerable distance across the lake floor. Invasive masses range from dike- and sill-like forms to pods or blobs that may be hundreds of feet across. The interiors of such invasive blobs typically are moderate or terminal WAB and are likely to contain marginal amygdaloidal zones. They also commonly have "coronas" of porcellanized fine-grained sediment. The outer few inches to a few feet of invasive blobs are commonly quenched, producing a selvage of resistant basalt. These selvages, or rinds, commonly appear in the field as curving dikelike bodies. Also associated with some invasive flows are places where sediments and invading basalt became intimately mixed and yielded peperites. Zones atop and adjacent to invasive flows have coverings of chemically precipitated opal or chalcedony, typically a few inches thick, accompanied by calcite in nearby fractures. Blobs that appear very similar to truly invasive flows are produced where lava has flowed down the walls of drowned sublacustrine valleys.

Phreatomagmatic Eruptions: Emergent and Subaerial Types

Factors influencing the final products. Factors influencing the final products of these eruptions are numerous, and their independent variations lead to a plethora of sizes, shapes, and compositions of individual particles and to a multiplicity of shapes, sizes, and preservation potentials of the volcanic constructs formed by the accumulation and postdepositional remobilization of those highly heterogeneous particles. As many researchers have deduced from performing laboratory experiments and from studying phreatomagmatic eruptions, volcanoes, and volcanic fields in other parts of the world (Wohletz and Sheridan, 1979; Sheridan and Wohletz, 1983; Wohletz, 1983; Wohletz, 1986; Valentine, 1987; Sohn, 1996; Valentine and Fisher, 2000; White and Houghton, 2000; Maicher and White, 2001), the operative ratio of water to magma at the site of mixing and the magma volume and supply rate (mass flux) are the most important parameters in determining the nature and progression of the eruption and the shape, size, and other characteristics of the final volcanic construct. Most commonly these parameters change continuously during phreatomagmatic eruptions; the changes may be unidirectional or oscillatory, gradual or abrupt, continuous or discontinuous. A typical scenario is the steady decrease in the water-to-magma ratio, accompanied by a rapid increase in the magmatic mass flux during the early hours of the eruption followed by steady-state conditions throughout most of the eruptive period. The waning phases of such eruptions vary considerably, with some eruptions ending

abruptly and others having a long period of episodic blasts separated by quiet intervals.

Approaches. Popular approaches to the study of phreatomagmatic eruptions and their products include experimental simulations (Wohletz, 1983; Wohletz and McQueen, 1984; Zimanowski and others, 1991), observations of eruptions in progress or of the new volcanic construct immediately after the main phase of activity has ended (Waters and Fisher, 1971; Kienle and others, 1980; Kokelaar, 1986; Moore, 1985; Kokelaar, 1987; Cole, 1991; Mattox and Mangan, 1997; Clague and others, 2000; Cole and others, 2001), and studies of prehistoric, partly eroded deposits and edifices (Fisher and Waters, 1970; Heiken, 1971; Crowe and Fisher, 1973; Lorenz, 1986; Verwoerd and Chevallier, 1987; Sohn and Chough, 1989; Chough and Sohn, 1990; Godchaux and others, 1992; Sohn, 1995; Aranda-Gomez and Luhr, 1996; Houghton and others, 1996; Rinaldi and Camos-Venuti, in press).

Secondary factors. Many secondary factors also influence the courses of phreatomagmatic eruptions. These may be divided somewhat arbitrarily into pre-eruptive and syneruptive. Of course, many posteruptive processes modify the pristine constructional shapes of the volcanoes as well, such as hydrothermal alteration, weathering, erosion, and faulting. Human activities—such as quarrying, cattle and hog feedlots, dams and reservoirs, highways, agriculture, dumps for farm waste and municipal trash, residential subdivisions, military training exercises, civilian target shooting, and motorized off-road recreation—have even more devastating effects on phreatomagmatic volcanoes than do natural processes, especially in desert regions like the western SRP, where protective plant cover is thin and is slow to reestablish itself after it is disrupted.

Pre-eruptive factors include characteristics of the rising magma, such as intrinsic volatile content before contact with external water, viscosity, vesicularity, and crystallinity. The stratigraphy of the uppermost few hundred feet of strata through which the ascending basalt magmas rise constitutes another important factor, its influence increasing with the decreasing depth of surface water. Stratigraphic factors include the ratio of basalt flows and indurated tuffs to sediments, the thicknesses of layers or lenses of highly water-transmissive gravels, the fracture patterns in deeper bedrock units such as rhyolites and granites, and the degree of compaction and lithification of sediments (which influences their porosity and permeability). Near-surface structures, such as faults or monoclines, may control the geometry of the ground-water system and the shape and size of the initial volcanic conduit and therefore will have a profound influence on the shape of the final construct. The topography around the vent may be important in facilitating the destruction of the growing cone by mass-wasting and the mobilization of avalanches and debris flows.

Syneruptive factors include the nature and location of the initial water-magma contact, the balance between magma delivery rate and water delivery rate to the explosion focus as the eruption progresses, the efficiency of downward coring, wind direction, and wind strength, and the collapse or aggressive erosion by waves of sectors of the growing edifice. Clearly these factors are not entirely independent of one another. For example, temperature affects vesicularity and crystallinity, which in turn affect viscosity; near-surface rock types influence the shape and size of the uppermost part of the magmatic conduit; and the lithology of the stratum in which the focus of the explosion is situated determines the fragmentation level of the accidental component. The interplay of relevant major and minor factors will be discussed further in the descriptions of the individual volcanoes.

CLASSIFICATION OF PHREATOMAGMATIC VOLCANOES

The wide variety of surface environments into which the western SRP basaltic magmas rose and the fact that they rose through large, complex, continuously changing systems of fractures and pipes connecting to storage sills at various depths and passing through heterogeneous wall rocks have resulted in a great variety of water-magma interactions. We have mapped more than ninety of the phreatomagmatic volcanoes in the western SRP, although few have been studied in detail. Notwithstanding that no two of these volcanoes are exactly alike, we have classified them, including the sublacustrine ones, on the basis of water depth (a proxy for water-magma ratio) and average rate of magma supply (mass flux) over the courses of the eruptions (Figure 13).

As in our earlier paper (Godchaux and others, 1992), we divide the volcanoes into three groups: sublacustrine, emergent, and subaerial. At that time, we did not identify subtypes within these groups, but as we explored more parts of the large western SRP volcanic field, we accumulated enough evidence to begin to appreciate the importance of eruption rate in producing different types of emergent and subaerial volcanoes. Recent studies of the deep-water volcanoes in the Teapot field and the adjacent Murphy field demonstrated the importance of eruption rate in this setting as well, an understanding that workers studying submarine volcanoes have long had (Batiza and White, 2000). Accordingly we have revised the original classification to include nine basic categories; within each of the nine there are many subtle variations in the deposits (Figure 14).

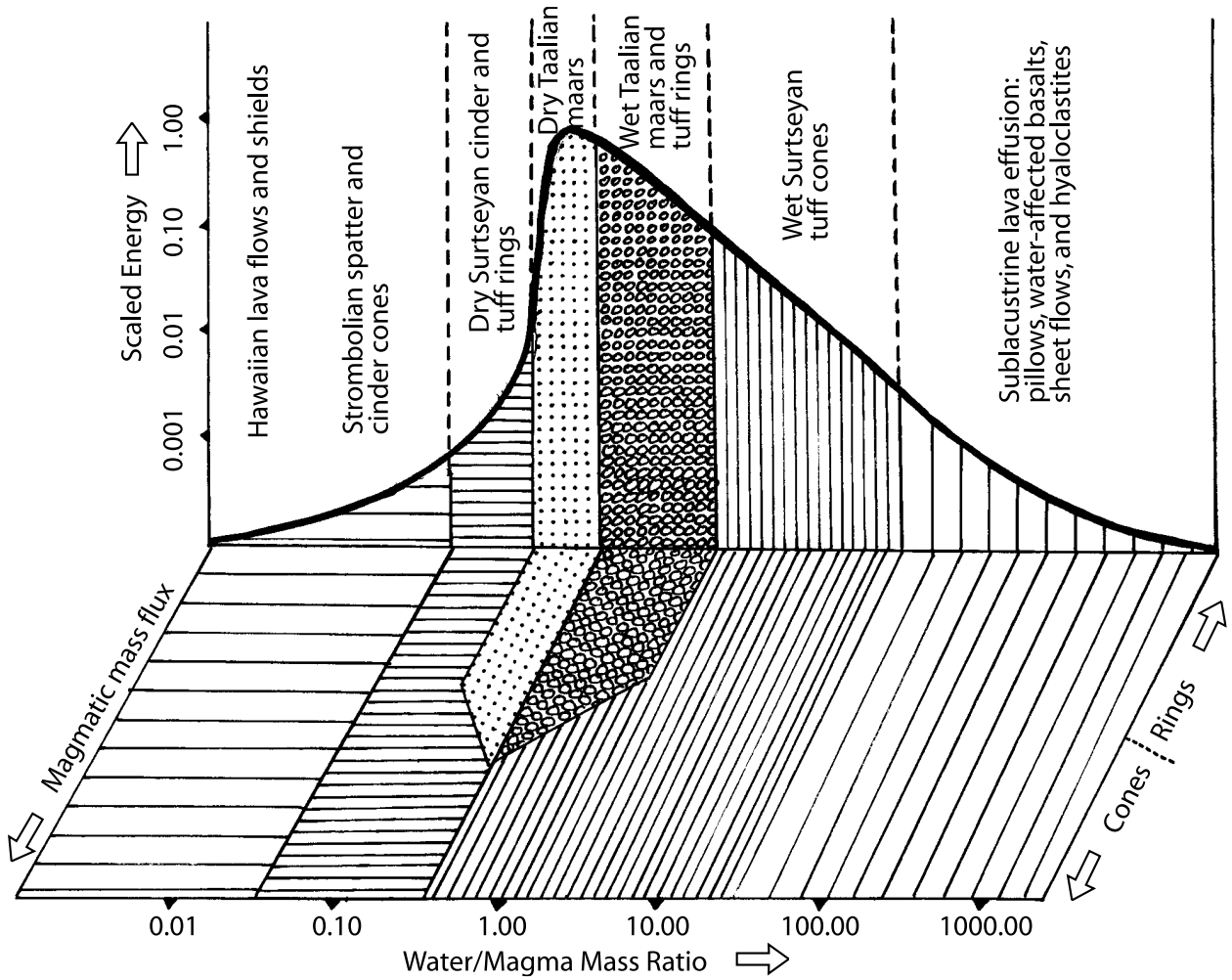

Figure 13. Diagram showing magma:water ratio, explosivity and mass flux in phreatomagmatic eruptions (modified from Wohletz, 1984, Sohn, 1996, and other sources).

Preliminary studies indicate that many of the secondary factors enumerated above interacted continuously or sequentially with the primary ones of water depth and magma supply. With the subaerial volcanoes, the situation is somewhat more complex than in the sublacustrine and emergent ones; in subaerial eruptions, near-surface stratigraphy and total magma supply combine with specific characteristics of the hydrologic system to control the final product.

Sublacustrine Volcanoes

Sublacustrine volcanoes erupted in water too deep for any permanent edifice to appear above lake level, although both gases and pyroclasts may have been ejected briefly above the lake surface. Some of them have horizontal planar upper surfaces, suggesting that they were eroded down to wave base soon after eruptions ceased. We include in this group some occurrences of WAB, invasive flows, and debris flows that appear to have been emplaced in deep water, even though we do not know the locations of their source vents. Some of these incompletely preserved occurrences possibly erupted subaerially very close to the lake shore in recently faulted areas where the drop-off of the lake floor was extremely steep. No subaerial parts of these units are exposed, however. These volcanoes are mostly in the 9-7 Ma group, with a few younger ones constructed in especially deep parts of the generally smaller and shallower later "Glenns Ferry Lake" (Bonnichsen and Godchaux, this volume, Figure 13). Water depths might range from a few hundred to nearly a thousand feet. Although sparse fish fossil evidence suggests that parts of the lake were as deep as 3,000 feet (G. Smith, oral commun., 1990), there is no conclusive evidence that any eruptions occurred at such depths. We

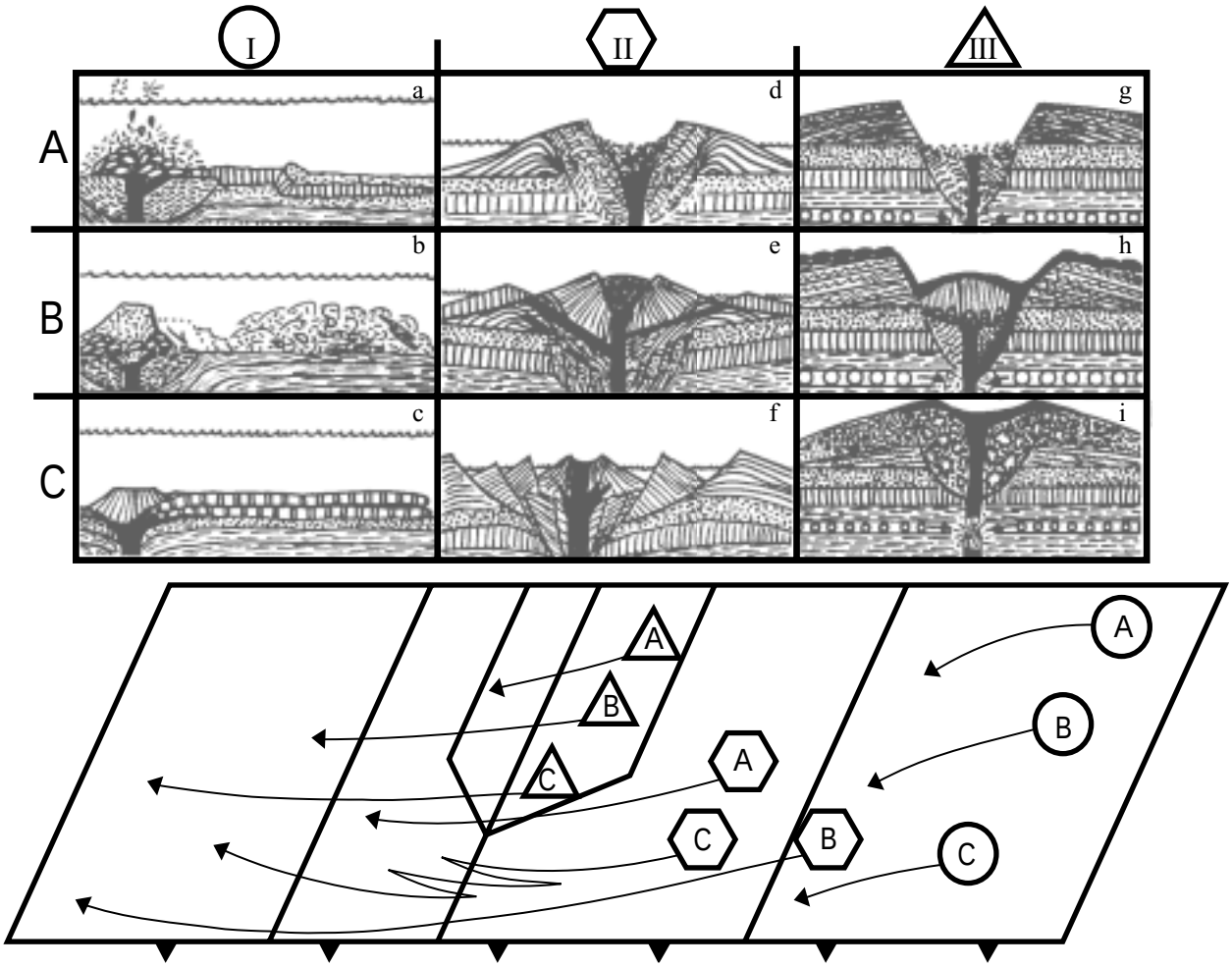

Figure 14. Schematic cross sections of volcanoes produced by eruption paths shown on diagram. (a) Sublacustrine compound lava flows with invasive lobes. (b) Lakemount made of hyaloclastite and pillow fragments collapses to produce sublacustrine debris flow. (c) Sheetlike WABs, emplaced rapidly as thin noninvasive flows. (d) Simple tuff cone or tuff ring with very small late-stage magmatic component. (e) Large tuff cone with lava pond, cinders, and dike-fed lava flows. (f) Compound tuff cone with multiple collapsed segments. (g) Simple open maar or low tuff ring with little or no late-stage magmatic crater fill. (h) Maar partly filled by late-stage lava pond, inner wall spatter, and ejected bombs. (i) Initial maar overtopped by large cinder-and-spatter cone. I—sublucustrine; II—emergent; III—subaerial. A—low effusion rate; B—moderate effusion rate; C—high effusion rate.

recognize three categories of sublacustrine basalt forms.

IA: Sublacustrine compound lava flows. Sublacustrine compound lava flows are dominated by equant pillows or by invasive flow lobes with subordinate marginal hyaloclastite levees and locally developed peperite selvages in adjacent sediments. These levees and selvages are composed of poorly vesiculated blocky shards and angular basalt fragments. These forms are probably produced at a relatively low magma extrusion rate (Figure 14a) in water shallow enough to permit flow-lobe growth by inflation but deep enough to inhibit vesiculation or limit vesicle growth.

IB: Large mounds of hyaloclastite and pillow fragments. Large mounds of hyaloclastite and pillow fragments commonly are emplaced fairly rapidly, forming oversteepened slopes. They collapse periodically, continuing downslope or at least downflow on flat substrates into massive far-traveled sublacustrine debris flows that incorporate large amounts of lake-bottom sediments, both as well-mixed matrix and as folded or flame-shaped giant rip-up clasts. These forms are probably produced at a moderate magma extrusion rate (Figure 14b) and emplaced on lake bottom with a relatively thin layer of unconsolidated mud over indurated sediments or earlier

lava flows. Where several episodes of collapse produced numerous debris flows and turbidites, later flows typically erode U-shaped channels into earlier ones.

IC: Sheetlike, pervasively water-affected lava flows. Sheetlike, pervasively water-affected, commonly columnar-jointed, locally lineated, and variably palagonitized lava flows may cover many square miles and be as much as 40 feet thick. These flows are probably produced at high extrusion rates or are extruded from elongate fissures or multiple vents (Figure 14c).

Emergent Volcanoes

An emergent volcano is erupted in water just deep enough to promote sustained water-magma interaction during most of the eruption, resulting in a permanent cone or ring being built, commonly with a broad apron of lava flows around it, and making a major island in the lake. In the western SRP, these volcanoes were built mostly during the 2.2-1.0 Ma interval by relatively long-lived eruptions (weeks, months, or years); however, a few were built during the 9.0-7.0 Ma interval in shallow parts of the lake. Such eruptions may be represented as unique paths across the water:magma:mass flux diagram (Figure 13), generally crossing several fields. The eruption modes represented by the fields are described in detail by Francis (1993) and by Sigurdsson and others (2000). We recognize three categories of emergent volcanoes.

IIA: Small simple tuff cones or tuff rings. Small simple tuff cones or tuff rings result from an uninterrupted building process (a single wet-to-dry cycle), with little or no late magmatic (Strombolian or Hawaiian) component, produced by a low to moderate mass-flux eruption whose peak energy is generally within the Wet Surtseyan field (Figure 13 and Figure 14d).

IIB: Large simple tuff cones with large late magmatic components. Large simple tuff cones with large late magmatic components include cinders or spatter, variably welded, in the upper parts of the cones, late-stage lava ponds, radial dikes, and extensive aprons of lava flows. These cones are produced by high mass-flux eruptions of long duration (by analogy with the observed eruptions of Capelinhos and Surtsey, these eruptions might continue for 1 to 10 years) whose peak energies of eruption begin in the Wet Surtseyan field and cross the Wet and Dry Taalian fields to end up in the Strombolian or Hawaiian field (Figure 13 and Figure 14e). These long-lasting eruptions typically core downward through the underlying layers, producing a periodic downward movement of earlier-formed rim deposits and a recycling of initial tuffs.

IIC: Small to large compound tuff cones. Small to large compound tuff cones (several wet-to-dry cycles separated by major sector collapse events) with highly variable late magmatic components are produced by medium mass-flux, probably episodic or pulsating, eruptions which follow zig-zag courses across the water:magma ratio spectrum, generally ending in either the Dry Surtseyan or Strombolian fields (Figure 13 and Figure 14f).

Subaerial Volcanoes

Subaerial volcanoes erupted in swampy areas or recently drained or marginal parts of the lake basin either underlain by poorly consolidated water-saturated clays and sands or buried by fan gravels, or they erupted in the courses of the main Snake River and its tributaries. Most subaerial phreatomagmatic volcanoes were constructed in the 1.0-0.5 Ma period after the final drainage of Lake Idaho, but some formed in earlier periods along the shore of the lake. We recognize three categories of subaerial volcanoes.

IIIA: Simple maars or tuff rings. Simple maars or tuff rings are produced in a single brief but very high-energy eruptive episodes at low mass flux, progressing from the Wet Taalian field to the Dry Taalian field (Figure 13 and Figure 14g). The physiographic forms of these maars are perfectly preserved and exposed at the end of the eruption. These volcanoes tend to be small constructs, suggesting that the eruptions are too brief to allow for much downward coring.

IIIB: Simple or multistage partly filled maars. Simple or multistage maars partly filled by late-stage magmatic ejecta or by large lava ponds are produced by eruptive periods that are probably longer than those of IIIA (weeks or months rather than hours or days) and progress from the Taalian fields to the Dry Surtseyan field and then to either the Strombolian or the Hawaiian field, depending on the rate of rise of the remaining basalt magma (Figure 13 and Figure 14h). These eruptions are low-moderate to high mass flux, typically increasing from lower to higher flux as the eruption progresses. The original maar form is largely preserved but is at least partly filled at the end of the eruption. Downward coring and recycling of earlier deposits are effective, and these volcanoes tend to be a bit larger than the previous type. Posteruptive reworking of the crater-fill materials and rapid transport of nonvolcanic sediments into the crater by wind and streams cause these volcanoes to be obliterated as topographic forms in a relatively short time. They may be exhumed following faulting or a change in the base level of nearby streams.

IIIC: Initial maars overtopped by large cinder or spat-

ter cones. Initial maars overtopped by large cinder or spatter cones are produced by relatively high mass-flux eruptions in which the supply of water is exhausted early in the eruption. They progress from Dry Taalian to Strombolian and may produce large constructs (Figure 13 and Figure 14i). These eruptions tend to be somewhat complex in the sense that the position of the eruptive conduit during the robust magmatic phase may change repeatedly, creating a cluster of overlapping cones or cross-cutting spatter ramparts. The stratigraphy within each of those late-stage cones may also be complex with many transitions back and forth between welded and nonwelded spatter or cinders, reflecting variations in eruption rate.

LATE MIOCENE BASALTS

Following the eruption of the rhyolites, a relatively long hiatus occurred before the eruption of basalts began, generally to the southeast of and at somewhat lower elevations than the youngest rhyolite vent areas. These basalts are mapped as three separate larger fields, the Chalky field, the Teapot field, and the Murphy field and also as smaller isolated occurrences grouped for mapping purposes as early western SRP basalts (Bonnichsen and Godchaux, this volume). Basaltic volcanism probably began between 8 and 9 Ma; radiometric dates obtained on these basalts range from 8.10 Ma to 7.07 Ma, and the stratigraphically lowest basalts have not been dated. The Aldape Park Basalt on the northeastern margin of the western SRP graben was dated by Clemens (1993) at 9.0 to 9.5 Ma, and lavas of this age might be present at depth along the southwestern margin as well. Table 2 summarizes the dates from various sources, volcano types, and chemical information (from White and others, this volume, and Othberg and others, 1995) for both the early and the late basalts.

By the time of basalt extrusion in the late Miocene, the shoreline of Lake Idaho had risen to elevations nearly 1,000 feet higher than those of Cerro el Otoño time; the "Chalk Hills Lake" stand was at or near 3,600 feet and apparently had only minor fluctuations until a major drawdown began around 6.5 to 6.0 Ma (Wood and Clemens, this volume). The greatest depths at which eruptions near this western shore of Lake Idaho could have taken place are suggested by the presence of fossils of deepwater fish species in contemporaneous sediments to be at least 3,000 feet (G. Smith, oral commun., 1991). Virtually all the late Miocene basalts interacted with water, but explosive phreatomagmatism was limited, and most outcrops are composed of either WABs or pillow-palagonite complexes dominated by pillow breccias. Although we have located a few of the higher-elevation source vents for these basalts, some lower-elevation vents are likely now concealed beneath younger sediments. Certainly some of the lavas were erupted subaerially and flowed short distances over land before entering the lake, whereas others were erupted within the lake in relatively deep water. Those that flowed over land and then onto the very steeply sloping floor of the lake made pillow deltas with bottomset breccias and subordinate hyaloclastite tuffs. Those that erupted into deep water produced large-diameter contorted and locally invasive lobes (at low eruption rates) or irregular piles of pillow fragments and hyaloclastite, which collapsed to form debris flows (at intermediate eruption rates) or sheetlike water-affected flows (at higher eruption rates).

Data from scattered drill holes in the western SRP and also in the central part of the main SRP (Clemens, 1993), as well as from accidental blocks of early lavas included in the deposits of some of the later, larger, downward-coring phreatomagmatic eruptions, suggest that this early phase of volcanism was widespread and voluminous. Great thicknesses of WAB are present in the subsurface along a broad zone between Mountain Home and Murphy (Wood and others, this volume); the total volume of early basalt may well be in excess of 20 cubic kilometers. Sills emplaced contemporaneously at shallow depths in the region (White and others, this volume) probably account for some of this volume, but the sublacustrine extrusive component is nonetheless very large. White and others (this volume) classify these lavas as M1 types, intermediates between the high-Al olivine tholeiites (HAOT) of the Owyhee Plateau and the more-evolved Snake River Plain olivine tholeiites (SROT). The chemistries are consistent with a petrogenetic model involving partial melting of an upper mantle source, consequent upon rapid extension and thinning of the lithosphere followed by brief storage in large near-surface sills before eruption into and around the lake. In our own geochemical classification, detailed in Bonnichsen and Godchaux (this volume), these Miocene basalts are mostly SROTs.

PLIOCENE AND PLEISTOCENE BASALTS

Following the late Miocene basaltic volcanism, extension slowed to a point where magma production and ascent were suppressed, and a volcanically quiet interval ensued that lasted until a new sequence of eruptions began about 2.2 Ma (see Figure 9 of Bonnichsen and Godchaux, this volume, for locations of volcanoes discussed below). When this second phase of basaltic volcanism began, Lake Idaho was well into its final decline. Although the locus of the late-stage eruptions was a broad linear belt that trended NW-SE approximately along the

Table 2. Basalt volcanoes in the western Snake River Plain: Ages, types, and compositions.

Volcano	Age (Ma)	Type	Composition (White and others' system)
	0.60		
Grouch Drain volcanic complex	0.73*	Simple maar	M3
Guffey Table basalt	0.75*	Subaerial lava flow	M3
	0.90		
Guffey Butte volcanic complex	1.04-1.09**	Filled maar	M2
Sinker Butte volcanic complex	1.37*	Simple tuff cone	M2
Montini volcanic complex	1.64*	Partly filled maar	M2(?)
	1.70		
Walters Butte volcanic complex	1.79*	Multistage tuff cone	M2
Castle Butte volcanic complex	<2.2 <1.8(?)	Complex tuff ring	M2
	1.80		
Jackass Butte volcanic complex	2.2**	Tuff/cinder cone	M1
Feedlot Group volcanic complex	<2.2(?)	Tuff cones	M1(?)
	2.20		
Hill 3337	4.0-5.0(?)	WAB/pillow delta/debris flow	M1
Fossil Butte	7.07-7.24**	Tuff cone	M1
Teapot Field	>7.85*	Invasive WABs	M1
Chalky Field	>7.92*	Pillows and hyaloclastite tuffs	M1
Murphy Field	>8.10***	WAB sheet flows	M1
Aldape Park basalt (oldest basalt on NE margin of WSRP)	9.0-9.5#	WAB(?)	M1
Rhyolites	>10.5		

*White and others (this volume)
**Amini and others (1983)
***Ekren and others (1981)
#Clemens (1993)
– – – 0.60 Ma: changeover from mostly subaerial phreatomagmatic volcanoes to mostly shield volcanoes and cinder cones
------ 0.90 Ma: changeover from chemical type M2 to M3
– – – 1.70 Ma: changeover from mostly emergent to mostly subaerial phreatomagmatic volcanoes
------ 1.80 Ma: changeover from chemical type M1 to M2
– – – 2.20 Ma: changeover from mostly sublacustrine to mostly emergent volcanoes

course of the present-day Snake River in what had once presumably been a fairly deep part of the lake, maximum water depths had declined to less than 300 feet. Eruption rates and total volumes appear to have been smaller than those of the late Miocene volcanism, and magma compositions were heterogeneous and varied through time, as detailed by White and others (this volume; Table 2). In addition to the M1 lava type, which predominated in the earliest part of the late stage, iron-rich M2 basalts became more abundant between 1.8 Ma and 0.9 Ma. Finally, alkaline M3 basalts were erupted from about 0.8 Ma until the youngest eruptions ceased around 0.40 Ma. In general, larger tuff cones, produced by the interaction of magma with shallow standing water, were most abundant between 2.2 and 1.7 Ma. Tuff rings and maars, produced by the interaction of magma with wet sediments, swampy ground, or water trapped in buried gravels, were most common between 1.7 Ma and 0.6 Ma. The youngest eruptions (<< 0.6 Ma) as well as some older ones located above the shore of the declining lake were dominantly subaerial and dry, producing broad flow-fields and very low-aspect shield volcanoes. Cinder cones are rare, but very extensive nearly planar horizontal sheets of red cinders are exposed in deep quarries at several localities in a region parallel to and north of the present-day valley of the Snake River, suggesting that much of this upland area around the young shields is underlain by stratiform cinder deposits beneath the overlying loess and gravel. Although the data are incomplete, a general trend toward decreasing ages of volcanoes from southeast to northwest along the Snake River is indicated for these late basalts. Limited stratigraphic relationships generally are in agreement with radiometric dates.

SELECTED BASALTIC SUBLACUSTRINE AND PHREATOMAGMATIC VOLCANOES

Type IA Volcanic Edifice: The Teapot Field

The small Teapot lava field is in the southwest corner of the Walters Butte quadrangle (Bonnichsen and Godchaux, 1998) and is contiguous with the northern margin of the larger Murphy field of similar age (Bonnichsen and Godchaux, this volume). It is multiply faulted along its northeastern margin, with northeast sides of steeply dipping faults downthrown, and the outcrop pattern and flow directions suggest that some of the faulting was penecontemporaneous. The topographically lowest and most northeasterly exposed lavas flowed into and along a small graben developed in earlier flows, with invasive lobes emplaced from the northwest toward the southeast. Topographic forms that resemble breached craters, locally called "teapots," are well preserved especially on the downthrown block of the largest of the aforementioned faults. These forms result from the erosion of invasive flow lobes whose margins were quenched and fused with adjacent baked sediments, whereas their interiors cooled more slowly and reacted with water, rendering them more susceptible to erosion than the flow margins. An age of 7.85 Ma (White and others, this volume) was obtained on a sample from this field; however, the base of the basalt is nowhere exposed, and somewhat older lavas could be present in the subsurface. Most of the lavas in the higher part of the field southwest of the main fault were emplaced into deep water in a location where the rising lake may have drowned a paleocanyon system. Fine-grained lake-bottom sediments predominate over shoreface sands, suggesting that the lake level was high and thus the shore was fairly far to the west of the Teapot field.

The flow field varies greatly in thickness from a few feet to more than 300 feet over short distances. The pattern is consistent with the piling up of individual flow lobes in the bottoms of sublacustrine valleys, with thinner and somewhat more sheetlike morphology on the drowned interfluves. Some lobes in positions midway between the thinner and thicker parts of the field have steep attitudes and shapes resembling large (20- to 30-foot diameter) pillows; we interpret them as having served as feeder tubes for the thick valley-bottom lava accumulations (Figure 15).

Vesiculation in these lavas was inhibited or retarded, and the tiny calcite amygdules that are found in the dense, black aphyric basalts occur in radial or concentric patterns in each lobe. Intensely baked (porcellanitic) sediments surround many of the invasive lobes (Figure 16), whose eroded quenched margins mimic the outcrop pattern of dikes in some places. The interiors of some of the larger lobes, especially in the thicker piles in presumed valley bottoms, are coarsely crystalline (diabasic to gabbroic) with plagioclase feldspars up to 1.6 inches long. These crystalline domains contrast sharply with the quenched margins and are in sharp contact with them; they may have been produced by the inflation of initial small lobes, although direct evidence for inflation such as rotated crusts, clefts, tumuli, and residual depressions (Chitwood, 1994) is generally lacking.

The unit is exposed over a relatively small area, about 4 square miles, but it may be much more extensive in the subsurface. Outcrops of older basalt sparsely exposed at the base of Guffey Butte on its north side appear very similar to the Teapot field lavas, as do lithic blocks in the tuffs at Sinker Butte.

The small size of the amygdules (generally less than 0.2 cm), their paucity and apparent lack of connected-

ness, and the fact that they contain only calcite leads us to hypothesize, assuming a typical low preemplacement volatile content for these M1 magmas, that the pressure of the overlying water column was sufficiently high that only carbon dioxide had exsolved at the time of the eruption. This carbon dioxide reacted during cooling with the surrounding glass, leaching calcium and producing calcite. If this scenario is correct, water depths of 1,000 to 2,000 feet are implied (Wallace and Anderson, 2000). In any case, the eruption certainly took place entirely within the sublacustrine field of Figures 13 and 14.

Type IB Volcanic Edifices: The Chalky Field and Hill 3337

To the north of the Teapot field is the 7.92 Ma Chalky field (White and others, this volume), composed mainly of pillows, pillow breccias, and partially palagonitized hyaloclastite tuffs intruded by a complex of narrow dikes (Figure 17). The unit is exposed over an area of about 7 square miles; like the Teapot field, it passes beneath younger sediments and is offset by faults, so it too may be more extensive in the subsurface. The water depth in which these lavas were emplaced may have been considerably shallower than that of the Teapot field, less than 500 feet based on the more extensive and interconnected vesicles seen in the pillow fragments. The Chalky lavas appear to have issued from a series of small vents aligned east-west along the southern side of the field; the westernmost of these vents may even have been subaerial. This field has not been studied in detail.

Hill 3337, a small volcano just east of Idaho Highway 78, is the source of the basalt of Sinker Creek (Bonnichsen and Godchaux, this volume). It is an excellent example of a sublacustrine vent whose principal products were water-affected flows passing laterally into a pillow delta that extends westward for several thousand feet along the north side of Sinker Creek Canyon. Collapse of the front of this pillow delta produced a major, highly erosive debris flow that moved along the lake bottom, locally ripping up layers of semiconsolidated sediments and interbedded thin mafic tuffs (O'Malley, oral commun., 2001; Figure 18). Like the Chalky field, this suite of deposits does not suggest especially deep water, even though it is farther to the east of the faulted Owyhee Front than either the Teapot or Chalky fields and thus is presumably closer to the center of the lake basin. Its age is unknown, although nearby Fossil Butte, a tuff cone, was dated by Amini and others (1984) at 7.07-7.24 Ma. Based on its stratigraphic relationship with immediately adjacent sedimentary layers, an age as young as 4-5 Ma is possible for Hill 3337.

Type IC Volcanic Edifice: The Murphy Field

These pervasively water-affected, sheetlike, columnar-jointed lavas (Figure 19) are exposed in an area of about 25 square miles mainly to the west, southwest, and northwest of the town of Murphy, the county seat of Owyhee County and the northern gateway to Cowlands National Park. The principal runway of the local airport was constructed on these lavas. East of the airport, the lava field, like the Teapot and Chalky fields, is overlain by younger sediments, and its extent in the subsurface is unknown. An age of 8.1 Ma reported by Ekren and others (1981) suggests that this flow field predates the Teapot and Chalky fields. The broad extent of these lavas, the thicknesses of individual flows (as much as 40 feet), and their sheetlike morphologies suggest rapid extrusion and emplacement. Two possible source vents are closer to the Owyhee Front than are other vents for the early basalts, and they appear to have been subaerial. They are mapped as shields, one due west of Murphy and one southwest of Murphy (Bonnichsen and Godchaux, this volume). Other vents, which were probably sublacustrine, may be present in the eastern part of the field, but they have not been recognized. If the two mapped vents did indeed produce all the exposed lavas, then this field cannot be classified as truly subaqueous, even though the final emplacement of all its products took place in water more than 200 feet deep, based upon the vertical distance between the topographically highest and lowest elevations of the WABS. Whatever the status of its vents, the Murphy field is a major component of the early basaltic volcanism in this region.

Type IIA Volcano: Castle Butte

Castle Butte was originally a broad low asymmetric tuff ring (possibly evolved from an initial maar) before the Bonneville Flood ripped it in half. It has two preserved remnants: the main spatter-capped butte with a summit elevation of 2,700 feet on the south side, and a lower outlier about a half mile to the northwest across the valley of Castle Creek with a summit elevation of about 2,500 feet (Figure 20). This volcano is described by McCurry and others (1997) and by Bonnichsen and Godchaux (this volume). We interpret these two remnants as two sectors of an originally asymmetrical tuff ring because the deposits as well as their thicknesses differ from north to south. The deposits on the low north side contain evidence of having been wetter. Rounded inclusions of lake sediment show both vesiculation and minicolumnar jointing in radial patterns. The juvenile matrix

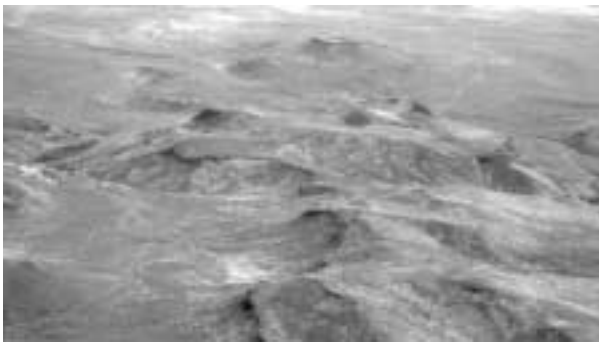

Fig.15A.

Fig.15B.

Fig.15C.

Fig.15D.

Fig.15E.

Figure 15. Photographs of Teapot volcanic field. (A) Aerial view of northeasternmost part of Teapot field, showing eroded invasive lava lobes (view is downflow). (B) Abrupt thickness change in Teapot lavas, suggesting accumulation in a sublacustrine paleocanyon. (C) Invasive lava lobe, emplaced on a paleoslope. (D) Radiating columnar joints in small squeeze-up. (E) Site where lava lobe (top eroded) invades sediments.

hosting them has cavernous weathering, poor sorting, and massive bedding. The deposits on the south side have locally well-developed surge beds, a lack of palagonitization, and fewer and smaller sediment clasts. An unusually vigorous but apparently brief late magmatic stage of the eruption built three small overlapping spatter cones atop the phreatomagmatic deposits of the south wall. Water depth at the time of the eruption is not well constrained, but it was probably shallow; the shoreline elevation of Lake Idaho was probably no higher than 2,450 feet. We do not have a radiometric age on Castle Butte, but its stratigraphy and geochemistry suggest an approximate age between 2.0 Ma and 1.8 Ma. Distal-facies tuffs apparently produced during the eruption of the 2.2 Ma Jackass Butte complex to the south are exposed in an isolated small outcrop immediately to the north of the north side of the Castle Butte rim deposit. This kipuka is surrounded by Castle Butte medial deposits, which flowed around the base of the small hill (Figure 21). The juvenile fraction of the Castle Butte deposits appears transitional between the M1 and M2 lava types, although it is closer to M2 because it is Fe-enhanced (see Table 1); thus, we tentatively place its age between the Jackass Butte eruptions and the changeover from M1 lavas to M2 lavas, but it could be as young as 1.2 Ma.

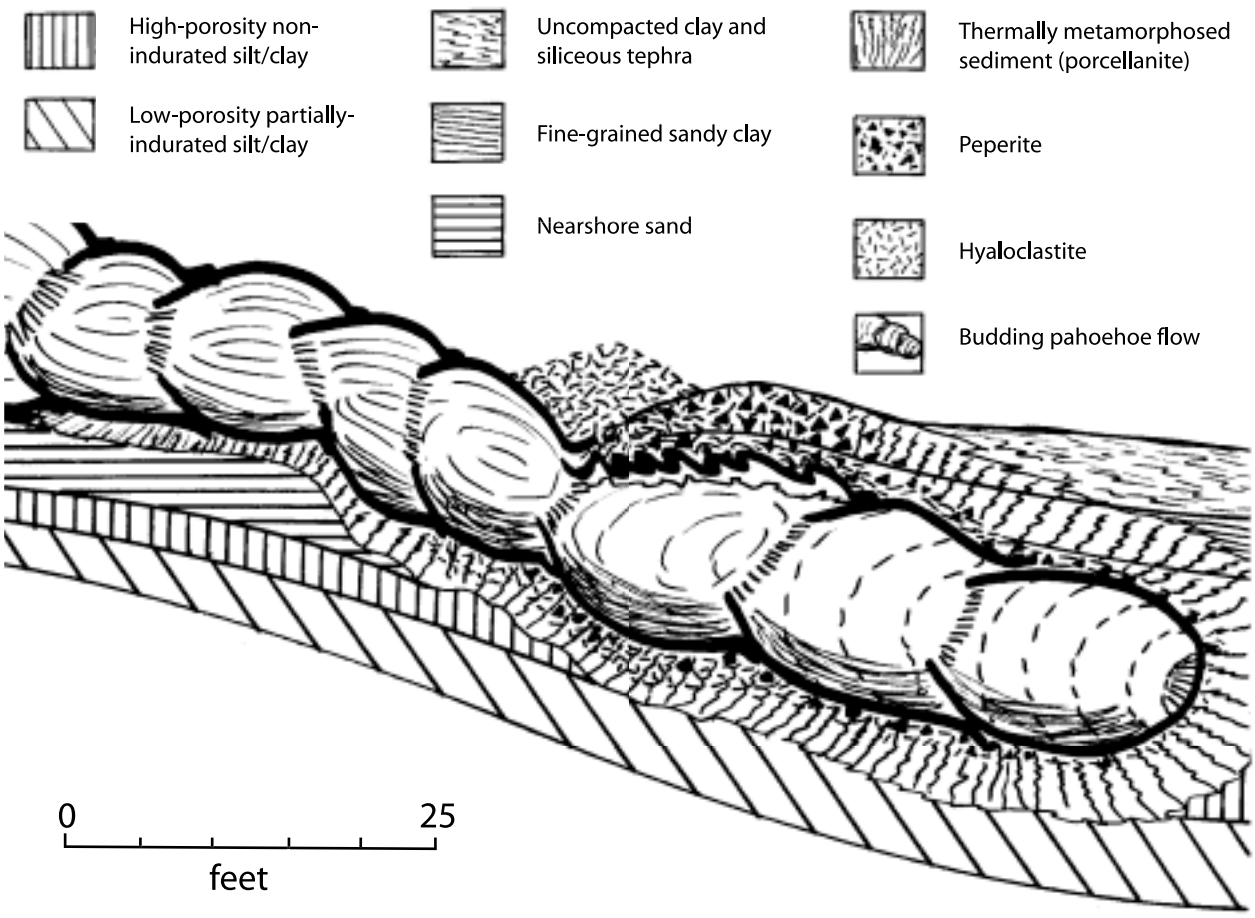

Figure 16. Schematic cross section of invasive lobe of Teapot basalt.

Type IIB Volcano: Sinker Butte

Sinker Butte, the largest tuff cone in the western SRP and maybe in the world, has many components, including early sublacustrine debris flows, reworked basal massive deposits, a thick and locally surge-bedded subaerial tuff accumulation, abundant late-stage Strombolian cinders, a late-stage Hawaiian lava pond, spectacularly developed bladelike radial dikes that propagated outward from a subvolcanic magma reservoir, and far-travelled lava flows (Figure 22). Its location is shown on Figure 9 of Bonnichsen and Godchaux (this volume), and aspects of its formation and features are discussed in McCurry and others (1997). Its age is uncertain; Amini and others (1984) obtained dates of 1.37 Ma and 0.61 Ma (Table 2) on dikes that cut the tuff beds. The stratigraphy suggests that it is closer to the older age. This volcano was described in detail in our earlier paper (Godchaux and others, 1992), and it remains the best example we have found of a long-lived tuff cone that did not have major collapse events during its emergence and that had a robust and long-lasting late magmatic history including both a cinder-producing Strombolian phase and an active Hawaiian fountain-fed lava pond phase, as well as the eruption of dike-fed flows.

Type IIC Volcano: Rabbit Creek Volcanic Complex

The location of the Rabbit Creek volcanic complex is also shown on Figure 9 of Bonnichsen and Godchaux (this volume). It is the part of the Jackass Butte volcanic field located on the northeastern side of the Snake River across from the Jackass Butte volcanic center. Although smaller and less productive in its late magmatic phase than the mighty Sinker Butte, the Rabbit Creek volcanic complex is also an example of an emergent tuff cone with a single wet-dry cycle and progression from phreatomagmatic activity to the building of a late-stage cinder and spatter cone. The principal vent of the complex has an interesting feature common to many emer-

Fig.17A.

Fig.17B.

Fig.17C.

Fig.17D.

Figure 17. Photographs of pillows, dikes, lavas, and tuffs of the Chalky field. (A) Pillows and pillow breccias. (B) Pillows. (C) Invasive flow. (D) Dike cutting bedded hyaloclastite tuffs.

gent tuff cones in the western SRP: the main cone was constructed in a deep hole excavated by initial Wet Surtseyan blasts, although it does not appear to have had a true "open" maar stage. Progressive downward coring was accompanied by cone-building within the deepening depression. Sediment-rich early ejecta deposited atop islands of older tuff have pronounced concentrations of elutriation surfaces, indicating that they were deposited subaerially and rapidly, though they contained abundant water. Similar presumably contemporaneous layers at the base of the main tuff cone lack these surfaces, indicating that they were deposited under water (Figure 23). Late-stage magmatic products include cinders, which grade upward from black to red and are preserved in the uppermost layers of the outer cone wall, and irregular spatter accumulations on the inner wall as well as dikes and plugs preserved as erosional remnants in the inner crater of the cone (Figure 24).

On the opposite side of the river from the Rabbit Creek volcanic complex are at least two more vents, both of which show evidence of having sustained one or more sector collapses during their periods of fastest growth and emergence. Massive beds grade upward into surge-bedded and accretionary lapilli-bearing layers overlain by block-bearing massive layers in which many of the blocks are surge-bedded tuffs apparently recycled after partial collapse of the structure. These vents have not been studied in detail.

Types IIIA and IIIB Volcanoes: Grouch Drain Volcano and Montini Volcano

Grouch Drain and Montini volcanoes are discussed together because they are very similar. They represent the part of the spectrum of maar types from unfilled to partly filled. Both Grouch Drain and Montini show excellent preservation of original maar form, with relatively little dissection, but Montini has more exposure of late-stage magmatic components. Grouch Drain volcano, constructed adjacent to the south flank of a large shield volcano called Hat Butte, is a young open maar whose origi-

Fig.18A.

Fig.18C.

Fig.18E.

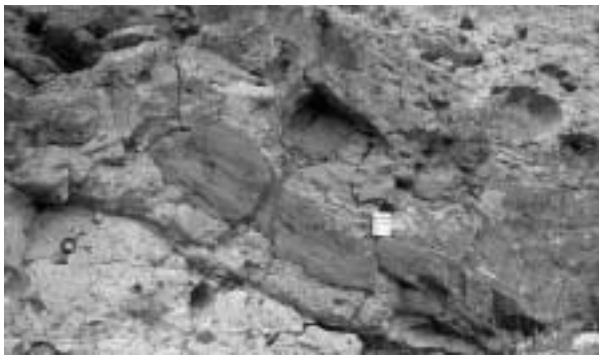

Fig.18F.

Fig.18B.

Fig.18D.

Figure 18. Photographs of Hill 3337 WAB, pillow delta, and debris flow. (A) Tuff, locally peperitic, beneath Hill 3337 vent complex. (B) Shelly pahoehoe WAB near vent. (C) Columnar WAB near vent. (D) Pillow delta, medial to vent. (E) Massive facies of debris flow, distal to vent. (F) Folded rip-up of fine-grained basaltic tuff and interstratified lake sediment in debris flow, distal to vent.

Fig.19A.

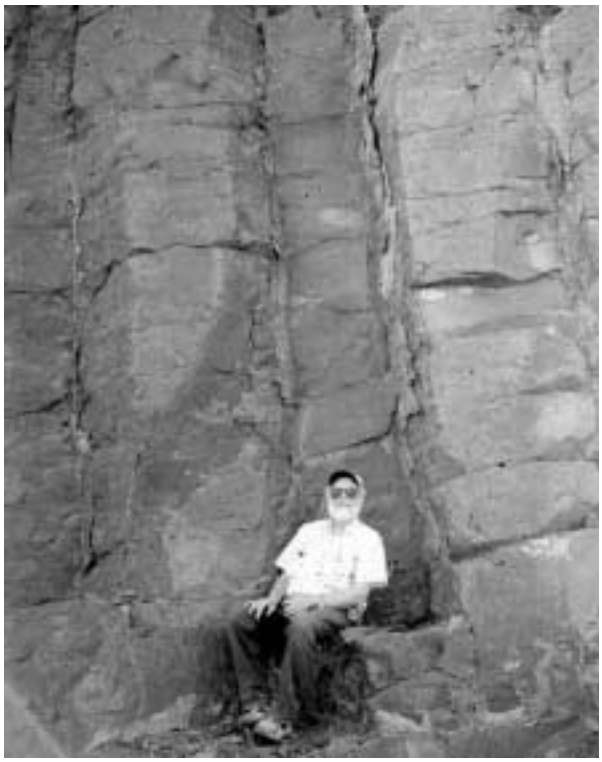

Fig.19B.

Fig.19C.

Figure 19. Photographs of WAB of Murphy field. (A) Panorama of flow layer, showing regular columns with distinctive platy cross joints. (B) Close-up view of altered columns. (C) Columns with quenched margins and altered interiors.

nal form is perfectly preserved on three sides (east, north, and west) and breached by collapse and outflow of lava on the fourth (south) side (Figure 25). Cut-off beds are exposed on its inner wall; rim deposits grade upward from sediment-rich, surge-bedded basal layers to black and red cinders. A small lava pond is exposed in the center of the maar, and the lava flow that issued from that pond breached the south side of the crater and flowed downslope into the paleovalley of the Snake River. It entered standing water about 15 feet deep (the thickness of the pillowed base) and spread out to form a small terrace at an elevation about 100 feet lower than the base of the lava flow where it exited the crater. White and others (this volume) analyzed the Grouch Drain lava and classified it as an M3 (alkaline) type; they also obtained a date of 0.73 Ma. Thus, it is one of the youngest phreatomagmatic centers in the western SRP and the only one identified so far as an M3 type.

Montini volcano, dated by Amini and others (1984) at 1.64 Ma, is similar to Grouch Drain volcano in shape,

Fig.20A.

Fig.20B.

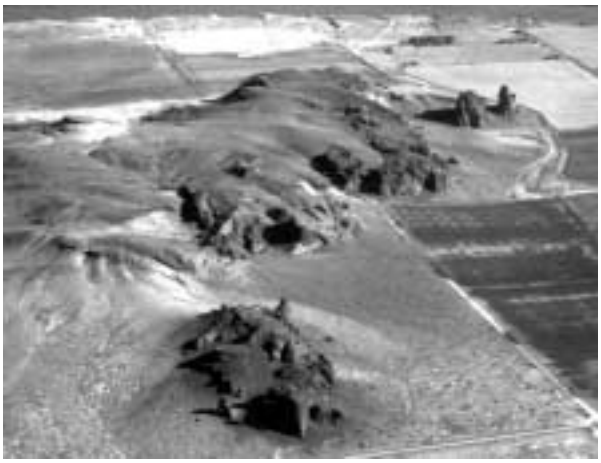

Fig.20C.

Figure 20. Photographs of Castle Butte. (A) Asymmetric tuff ring, viewed from Snake River. (B) Asymmetric tuff ring, viewed from southwest to northeast. (C) Low side of tuff ring, with kipuka of older tuff visible at upper left.

size, and the presence of cut-off beds (Figure 26). Its chemistry places it in the M2 (ferrobasalt) category. It is located at the confluence of Sinker Creek and the Snake River. A special feature of Montini volcano is its tangential dissection by both the Snake River and Sinker Creek, giving excellent exposures of the ring dike segments and other small hypabyssal intrusives that served as eruptive conduits as well as cut through the crater-filling tuff and lava. Inward slumping and downward displacement of early-formed deposits demonstrates that a downward-coring mechanism was active in at least the early part of this eruption, until water no longer reached the rising magma column, which then produced a large lava pond inside the crater.

Figure 21. Castle Butte kipuka. Note elutriated massive tuff overlying finely laminated tuff with flame structures and load-induced deformation.

Type IIIC Volcano: Guffey Butte

Guffey Butte, dated indirectly (from an overlying basalt flow) by Amini and others (1984) as older than 1.04 to 1.09 Ma and by White and others (this volume) as older than 0.76 Ma, is one of the youngest volcanoes with ferrobasalt (M2) chemistry. Its location is shown in Figure 9 of Bonnichsen and Godchaux (this volume). It differs greatly from Grouch Drain and Montini, both in appearance and in the relative amounts of phreatomagmatic and magmatic components. It was described in Godchaux and others (1992) and McCurry and others (1997) and studied further by Morrow (1996) and Watson (1999). It has several interesting features (Figure 27). Exposures along a north-flowing creek that cuts through the north wall of the original maar crater and exposures elsewhere in the Guffey Butte-Guffey Table area demonstrate that the near-surface stratigraphy is quite heterogeneous with a thick section of older WAB overlain by sands, clays, a younger basalt flow (the Guffey Railroad Bridge basalt), and thin gravels. All these lithologies are represented in the population of enormous blocks in the initial blast deposit that unconformably overlies the lake sediments. High-energy (Dry Taalian) deposits overlie the blast deposits and are in turn overlain by a very thick deposit of variably welded cinders and spatter, the remnants of a large complex Strombolian cone. Although the outer walls of this cone have mostly been

Fig.22A.

Fig.22B.

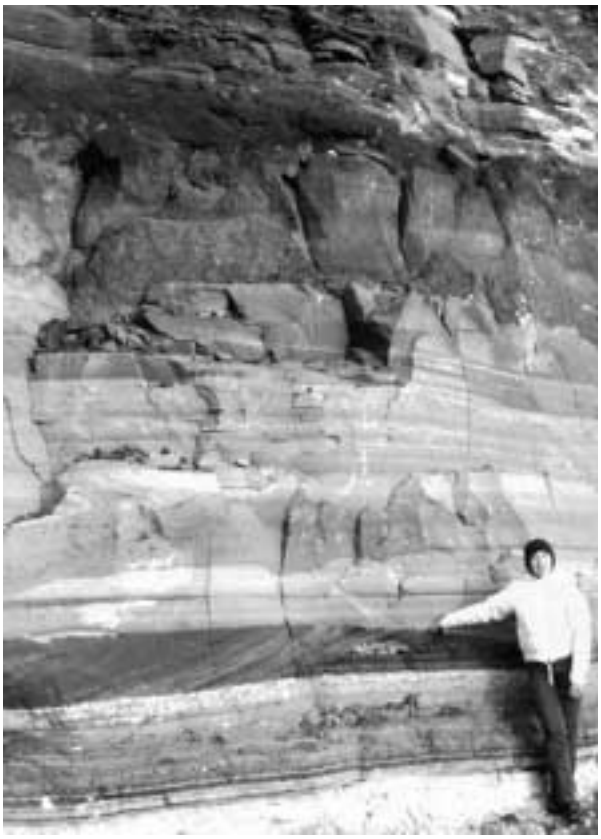

Fig.22C.

Figure 22. Photographs of Sinker Butte. (A) Top of butte. Note lava pond and fire fountain. (B) South alcove, showing tuffs, radial dikes, lava pond, and dike-fed lava flow. (C) Medial facies debris flows and basal turbidites.

removed by erosion, parts of the inner crater walls are well preserved, and a fire-fountain structure high on the western part of the main crater wall can still be recognized. A spectacular partial cone sheet composed of melted sediment and entrained nonmelted sedimentary grains and particles was formed when hot spatter ponded inside the deep initial maar crater and thereby melted and remobilized the sediments with which it was in contact. Magma supply at Guffey Butte long outlasted water supply, resulting in the construction of a complex Strombolian cone that filled and eventually spread beyond the original maar.

CONCLUSIONS

The history of interaction between rising magmas of various compositions and water at or near the surface of the earth extended from nearly 12 Ma to less than 0.5 Ma and has produced an unusual variety of forms within the western SRP and along its margins. The rhyolitic units produced between 12 and 11 Ma have compositions similar to the more voluminous welded tuffs being produced at the same time in the main SRP, but their eruption style is different. Lava flows form most of the erupted volume of the western SRP rhyolites, and most were not preceded by voluminous ash-flow tuffs, as the main SRP rhyolite lava flows were. We suggest that this difference is due to the prevalence of phreatomagmatic opening blasts that favored subsequent development of fountain-fed clastogenic lavas. Thus, the early phreatomagmatic phases, although short-lived, may have guided the courses of entire eruptions. The distal ends of the rhyolite lava flows all entered relatively deep standing water, suggesting an early origin for Lake Idaho. Although these clues do not fully constrain the areal extent or the maximum depth of this early phase of Lake Idaho, further study of these units could be coupled with study of rhyolitic units on the opposite side of the western SRP graben to provide a clearer picture of the paleogeography of this part of Idaho between 12 and 11 Ma. Phreatomagmatic cones and ramparts and breccia rings are associated with vent areas for rhyolite lava flows, ignimbrites, and domes, whereas massive flow-front breccias and slide blocks were produced where those rhyolites flowed into Lake Idaho. Rhyolitic phreatomagmatism is much less well understood than its basaltic counterpart; further study of these features could provide a better understanding of the

Fig.23A.

Fig.23B.

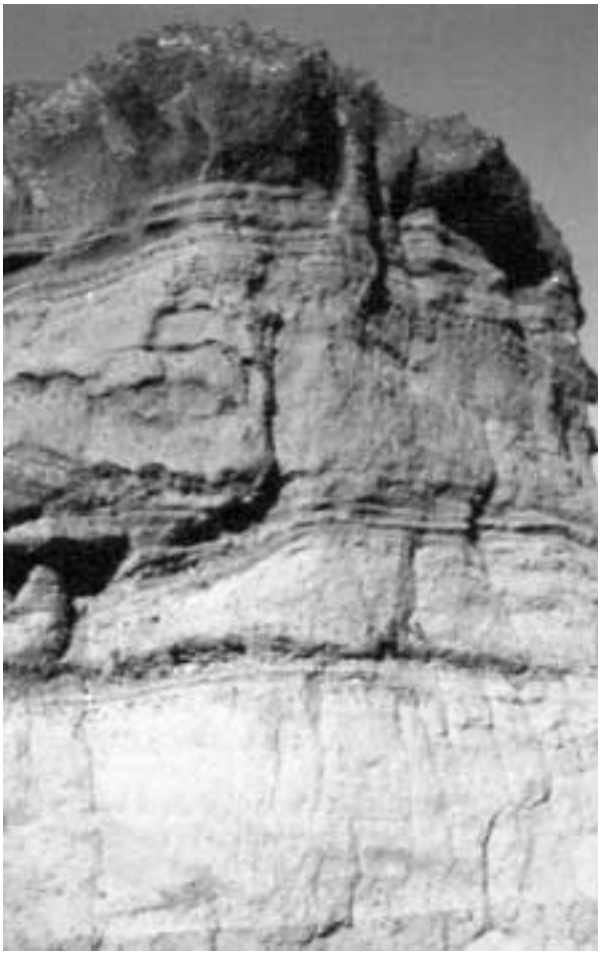

Fig.23C.

Fig.23D.

Figure 23. Photographs of Rabbit Creek volcanic complex, eastern part of Jackass Butte volcanic field. (A) Cone built in center of large self-excavated crater. (B) Massive elutriated tuff overlying laminated distal tuff. (C) Massive tuff grading upward into cinder beds. (D) Block facies in massive tuff.

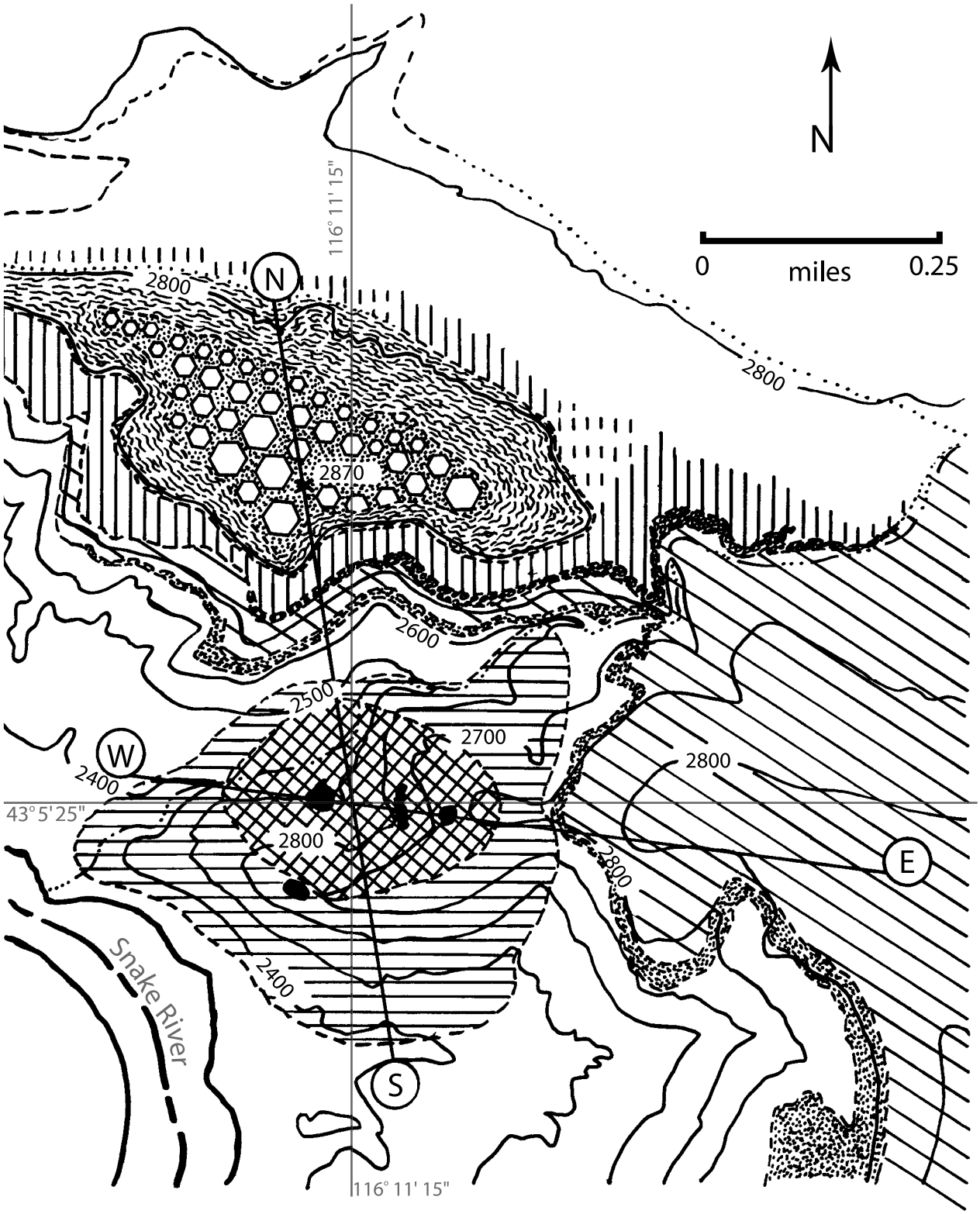

Figure 24. Schematic map and cross section of Rabbit Creek volcanic complex in Jackass Butte volcanic field.

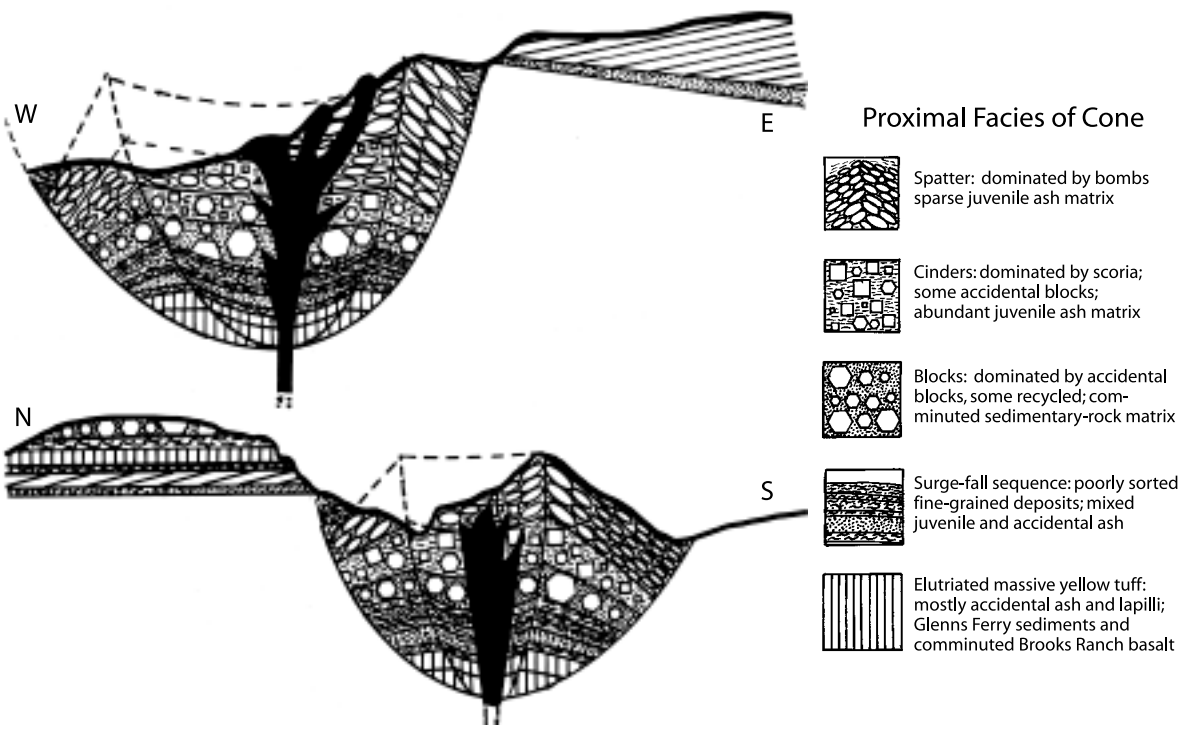
W
E
N
S
Proximal Facies of Cone
Spatter: dominated by bombs sparse juvenile ash matrix
Cinders: dominated by scoria; some accidental blocks; abundant juvenile ash matrix
Blocks: dominated by accidental blocks, some recycled; comminuted sedimentary-rock matrix
Surge-fall sequence: poorly sorted fine-grained deposits; mixed juvenile and accidental ash
Elutriated massive yellow tuff: mostly accidental ash and lapilli; Glenns Ferry sediments and comminuted Brooks Ranch basalt

Map Legend

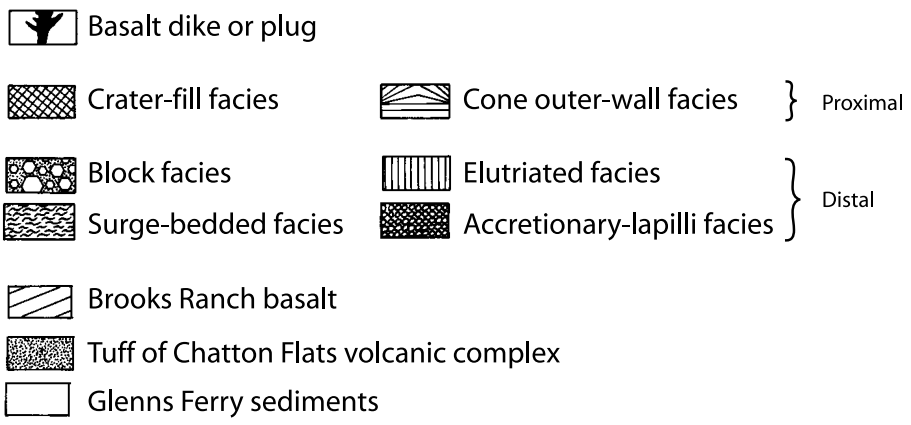
Basalt dike or plug
Crater-fill facies
Cone outer-wall facies
Proximal
Block facies
Surge-bedded facies
Elutriated facies
Accretionary-lapilli facies
Distal
Brooks Ranch basalt
Tuff of Chatton Flats volcanic complex
Glenns Ferry sediments

Fig.25A.

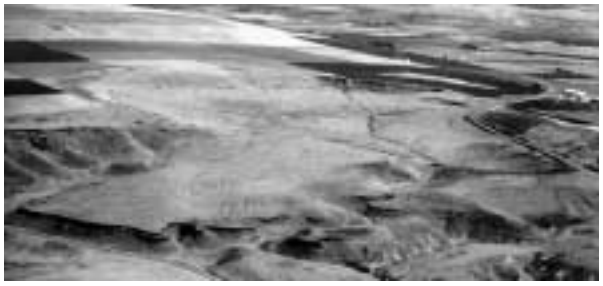

Fig.25B.

Figure 25. Photographs of Grouch Drain maar. (A) Grouch Drain maar and Hat Butte shield volcano, viewed from the southwest. (B) Grouch Drain maar and its lava flow.

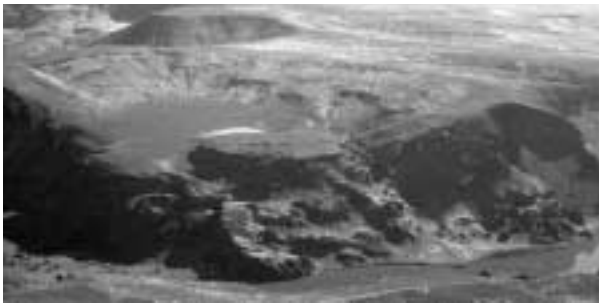

Fig.26A.

Fig.26B.

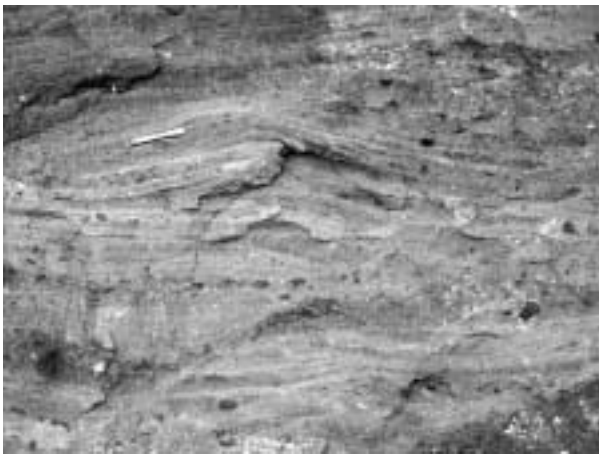

Fig.26C.

Fig.26D.

Figure 26. Photographs of Montini maar. (A) Aerial view of Montini maar, showing side dissected by Snake River. (B) Central part of maar, with small lava pond atop crater-fill material. (C) Surge-bedded layer of rim deposit (transport is from left to right). (D) Rim deposits and ring dike.

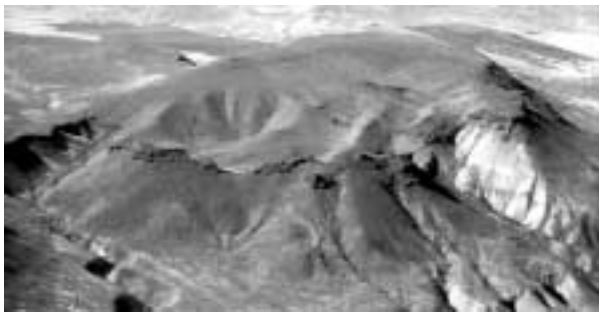

Fig.27A.

Fig.27B.

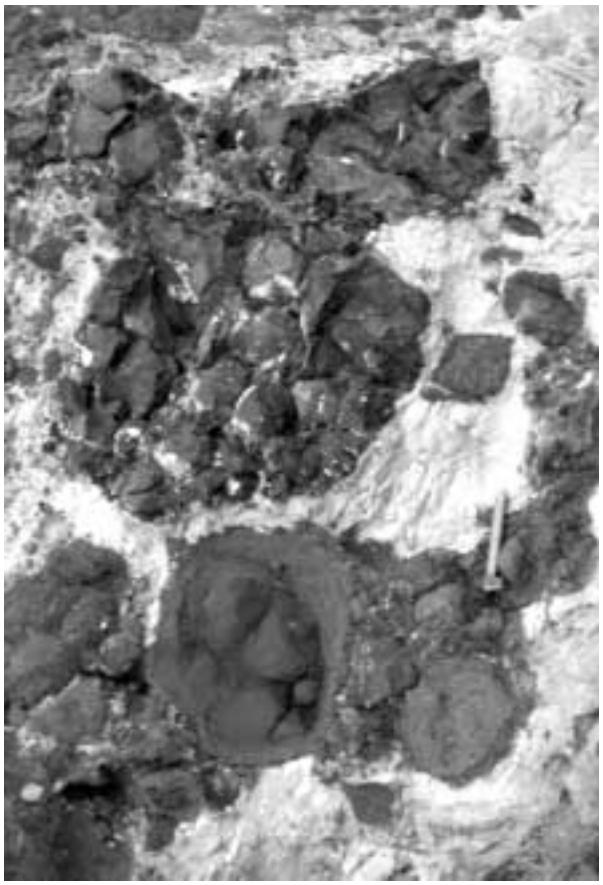

Fig.27C.

Fig.27D.

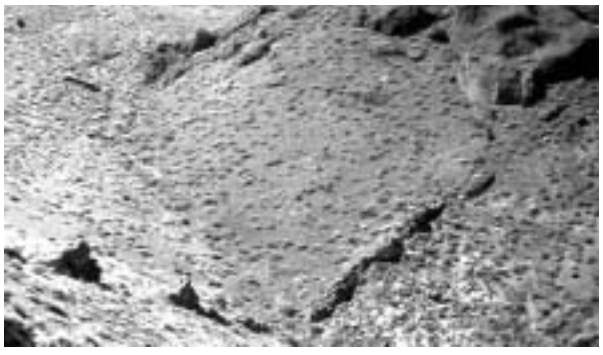

Fig.27E.

Fig.27F.

Figure 27. Photographs of Guffey Butte volcanic complex. (A) Aerial view from east side. (B) Maar wall, maar-rim deposits, and crater fill. (C) Blocks in initial blast deposit. (D) Surge-bedded maar rim deposit. (E) Overview of felsic "dike." (F) Entrained sediment chips in glassy matrix of "dike."

evolution of rhyolitic eruptions in their opening stages.

Early-erupted basalts also interacted with deep water. Some of them were actually erupted at considerable depth, whereas others flowed short distances over land and came to rest in relatively deep water. We have established that there were few truly phreatomagmatic basalt volcanoes during the 9-7 Ma time period; most vents were either subaerial or deep sublacustrine. This suggests that faulting was active at that time and that the lake probably deepened abruptly very close to its southwestern shore. Further work on correlation of 9-7 Ma basalts on the northeastern and southwestern sides of the western SRP graben could provide a clearer picture of the width and depth of Lake Idaho during this period, and it could reveal much about the early stages of graben formation.

Later-erupted basalts, which rose to the surface during and after the final draining of Lake Idaho, built a variety of phreatomagmatic constructs. The different compositions, shapes, sizes, and degrees of induration of these basalt forms reflect the variations in water-to-magma ratios, coupled with changes in rise rate and mass flux of magma as well as being influenced by the local stratigraphy. Study of the largest and most complex volcanoes, particularly those of the emergent type, will yield a better understanding of both the near-surface stratigraphy and the variations in eruptive style that produced them. Because many phreatomagmatic volcanoes are close to large populations throughout the world, and because their eruptions can be among the most violent known, careful study of the well-exposed ones in the western SRP will advance understanding of the hazards faced by at-risk people from Italy to Indonesia. This outdoor laboratory of Idaho, which has been produced by volcanic episodes of long duration, provides examples of every type of water-magma and water-lava interaction known to science.

ACKNOWLEDGMENTS

Field work was supported by COGEOMAP and STATEMAP contracts from the U.S. Geological Survey to the Idaho Geological Survey over the past decade and by faculty grants and a sabbatical grant awarded to Martha Godchaux by Mount Holyoke College between 1988 and 1998.

We thank the following colleagues for spirited and helpful discussions in the field: Curtis Manley, John Wolff, Janet Sumner, Michael Branney, Tiffany Barry, Scott Buroughs, Michael McCurry, Scott Hughes, Craig White, Nancy Riggs, Jocelyn McPhie, Mary O'Malley, James D.L. White, Heather Michaud, Jorge Aranda-Gomez, Gerardo Aguirre-Diaz, Guillermo Labarthe, Spencer Wood, and Kurt Othberg. We are very grateful to B. Benjamin E. Studer for preparing the illustrations and to Gayle Wells for helping scan and digitize photographs. Any errors of fact or interpretation remain the responsibility of the authors.

REFERENCES

Amini, Hassan, H.H. Mehnert, and J.D. Obradovich, 1984, K-Ar ages of late Cenozoic basalts from the western Snake River Plain, Idaho: Isochron/West, v. 41, p. 7-11.

Aranda-Gomez, J.J., and J.F. Luhr, 1996, Origin of the Joya Honda maar, San Luis Potosi, Mexico: Journal of Volcanology and Geothermal Research, v. 74, p. 1-18.

Batiza, R., and J.D.L. White, 2000, Submarine lavas and hyaloclastite, *in* H. Sigurdsson, ed., Encyclopedia of Volcanoes: Academic Press, p. 361-381.

Bonnichsen, Bill, and M.M. Godchaux, this volume, Late Miocene, Pliocene, and Pleistocene geology of southwestern Idaho with emphasis on basalts in the Bruneau-Jarbidge, Twin Falls, and western Snake River Plain regions, *in* Bill Bonnichsen, C.M. White, and Michael McCurry, eds., Tectonic and Magmatic Evolution of the Snake River Plain Volcanic Province: Idaho Geological Survey Bulletin 30.

Branney, M.J., and P. Kokelaar, 1992, A reappraisal of ignimbrite emplacement: Changes from particulate to non-particulate flow during progressive aggradation of high-grade ignimbrite: Bulletin of Volcanology, v. 54, p. 504-520.

Chadwick, W.W., T.K.P. Gregg, and R.W. Embley, 1999, Submarine lineated flows: A unique lava morphology formed on subsiding lava ponds: Bulletin of Volcanology, v. 61, p. 194-206.

Chitwood, L.A., 1994, Inflated basaltic lava—examples of processes and landforms from central and southeast Oregon: Oregon Geology, v. 56, p. 11-21.

Chough, S.K., and Y.K. Sohn, 1990, Depositional mechanisms and sequences of base surges, Songaksan tuff ring, Cheju Island, Korea: Sedimentology, v. 37, p. 1115-1135.

Christiansen, R.L., G.R. Foulger, and J.R. Evans, 2002, Upper-mantle origin of the Yellowstone hotspot: Geological Society of America Bulletin, v. 114, p. 1245-1256.

Clague, D.A., A.S. Davis, J.L. Bischoff, J.E. Dixon, and R. Geyer, 2000, Lava bubble-wall fragments formed by submarine hydrovolcanic explosions on Lo'ihi seamount and Kilauea Volcano: Bulletin of Volcanology, v. 61, p. 437-449.

Clemens, D.M., 1993, Tectonics and silicic volcanic stratigraphy of the western Snake River Plain, northwestern Idaho: Arizona State University M.S. thesis, 209 p.

Cole, P.D., 1991, Migration direction of sand-wave structures in pyroclastic-surge deposits: Implications for depositional processes: Geology, v. 19, p. 1108-1111.

Cole, P.D., J.E. Guest, A.M. Duncan, and J.M. Pacheco, 2001, Capelinhos 1957-1958, Faial, Azores: Deposits formed by an emergent surtseyan eruption: Bulletin of Volcanology, v. 63, p. 204-220.

Crowe, B.M., and R.V. Fisher, 1973, Sedimentary structures in base-surge deposits, with special references to cross-bedding, Ubehebe Craters, Death Valley, California: Geological Society of America Bulletin, v. 84, p. 663-682.

Ekren, E.B., D.H. McIntyre, and E.H. Bennett, 1984, High-temperature, large-volume, lavalike ash-flow tuffs without calderas in southwestern Idaho: U.S. Geological Survey Professional Paper 1272, 76 p.

Ekren, E.B., D.H. McIntyre, E.H. Bennett, and H.E. Malde, 1981, Geologic map of Owyhee County, Idaho, west of longitude 116 degrees W.: U.S. Geological Survey Miscellaneous Investigations Series Map I-1256, scale 1:125,000.

Fisher, R.V., and A.C. Waters, 1970, Base surge bedforms in maar volcanoes: American Journal of Science, v. 268, p. 157-180.

Francis, Peter, 1993, Volcanoes: A Planetary Perspective: Oxford University Press, 443 p.

Heiken, G.H., 1971, Tuff rings: Examples from the Fort Rock-Christmas Lake Valley basin, south-central Oregon: Journal of Geophysical Research, v. 76, p. 5615-5626.

Hooper, P.R., J. Johnson, and C. Hawkesworth, this volume, A model for the origin of the western Snake River Plain as an extensional strike-slip duplex, *in* Bill Bonnichsen, C.M. White, and Michael McCurry, eds., Tectonic and Magmatic Evolution of the Snake River Plain Volcanic Province: Idaho Geological Survey Bulletin 30.

Houghton, B.F., C.J.N. Wilson, M.D. Rosenberg, I.E.M. Smith, and R.J. Parker, 1996, Mixed deposits of Strombolian and phreatomagmatic volcanism: An example from Crater Hill, Auckland, New Zealand: Bulletin of Volcanology, v. 58, p. 59-66.

Humphreys, E.D., K.G. Dueker, D.L. Schutt, and R.B. Smith, 2000, Beneath Yellowstone: Evaluating plume and non-plume models using teleseismic images of the upper mantle: GSA Today, v. 10, no. 12, p. 1-7.

Kienle, J., P.R. Kyle, S. Self, R.J. Motyka, and V. Lorenz, 1980, Ukinrek maars, Alaska I. April 1977 eruption sequence, petrology and tectonic setting: Journal of Volcanology and Geothermal Research, v. 7, p. 11-37.

Kokelaar, B.P., 1986, Magma-water interactions in subaqueous and emergent basaltic volcanism: Bulletin of Volcanology, v. 48, p. 275-289.

————, 1987, Discussion of "Structure and eruptive mechanisms at Surtsey Volcano, Iceland" by J.G. Moore: Geological Magazine, v. 124, p. 79-83.

Lorenz, V., 1986, On the growth of maars and diatremes and its relevance to the formation of tuff rings: Bulletin of Volcanology, v. 48, p. 265-274.

Maicher, D., and J.D.L. White, 2001, The formation of deep-sea *Limu o Pele*: Bulletin of Volcanology, v. 63, p. 482-496.

Manley, C.R., and W.C. McIntosh, this volume, The Juniper Mountain volcanic center, Owyhee County, southwestern Idaho: Age relations and physical volcanology, *in* Bill Bonnichsen, C.M. White, and Michael McCurry, eds., Tectonic and Magmatic Evolution of the Snake River Plain Volcanic Province: Idaho Geological Survey Bulletin 30.

Marquez, A.M., R. Oyarzun, M. Doblas, and S.P. Verma, 1999, Alkalic (ocean-island basalt type) and calc-alkalic volcanism in the Mexican Volcanic Belt: A case for plume-related magmatism and propagating rifting at an active margin?: Geology, v. 27, no. 1, p. 51-54.

Mattox, T.N., and M.T. Mangan, 1997, Littoral hydrovolcanic explosions: A case study of lava-seawater interaction at Kilauea Volcano: Journal of Volcanology and Geothermal Research, v. 75, p. 1-17.

McCurry, M., Bill Bonnichsen, C.M. White, M.M. Godchaux, and S.S. Hughes, 1997, Bimodal basalt-rhyolite magmatism in the central and western Snake River Plain, Idaho and Oregon, *in* P.K. Link and B.J. Kowallis, eds., Proterozoic to Recent Stratigraphy, Tectonics and Volcanology, Utah, Nevada, Southern Idaho, and Central Mexico: Brigham Young University Geological Studies, v. 42, part 1, p. 381-422.

Moore, J.G., 1985, Structure and eruptive mechanisms at Surtsey Volcano, Iceland: Geological Magazine, v. 122, p. 649-661.

Morrow, L.S., 1996, Geology of Guffey Butte, western Snake River Plain, Idaho: University of Idaho M.S. thesis, 106 p.

Othberg, K.L., Bill Bonnichsen, C.C. Swisher III, and M.M. Godchaux, 1995, Geochronology and geochemistry of Pleistocene basalts of the western Snake River Plain and Smith Prairie, Idaho: Isochron/West, no. 62, p. 1-14.

Perkins, M.E., and B.P. Nash, 2002, Explosive silicic volcanism of the Yellowstone hotspot: The ash fall tuff record: Geological Society of America Bulletin, v. 114, p. 367-381.

Pierce, K.L., L.A. Morgan, and R.W. Saltus, this volume, Yellowstone plume head: Postulated tectonic relations to the Vancouver slab, continental boundaries and climate, *in* Bill Bonnichsen, C.M. White and Michael McCurry, eds., Tectonic and Magmatic Evolution of the Snake River Plain Volcanic Province, Idaho Geological Survey Bulletin 30.

Rinaldi, M., and M. Campos-Venuti, in press, The submarine eruption of the Bombarda Volcano, Milos Island, Cyclades, Greece: Bulletin of Volcanology.

Sheridan, M.F., and K.H. Wohletz, 1983, Hydrovolcanism: Basic considerations and review: Journal of Volcanology and Geothermal Research, v. 17, p. 1-29.

Sigurdsson, H., ed., 2000, Encyclopedia of Volcanoes: Academic Press, 1417 p.

Sohn, Y.K., 1995, Geology of Tok Island, Korea: Eruptive and depositional processes of a shoaling to emergent island volcano: Bulletin of Volcanology, v. 56, p. 660-674.

————, 1996, Hydrovolcanic processes forming basaltic tuff rings and cones on Cheju Island, Korea: Geological Society of America Bulletin, v. 108, p. 1199-1211.

Sohn, Y.K., and S.K. Chough, 1989, Depositional processes of the Suwolbong tuff ring, Cheju Island, Korea: Sedimentology, v. 36, p. 837-855.

Valentine, G.A., 1987, Stratified flow in pyroclastic surges: Bulletin of Volcanology, v. 49, p. 616-630.

Valentine, G.A., and R.V. Fisher, 2000, Pyroclastic surges and blasts, *in* H. Sigurdsson, ed., Encyclopedia of Volcanoes: Academic Press, p. 571-580.

Verwoerd, W.J., and L. Chevallier, 1987, Contrasting types of Surtseyan tuff cones on Marion and Prince Edward Islands, southwest Indian Ocean: Bulletin of Volcanology, v. 49, p. 399-417.

Wallace, P., and A.T. Anderson, Jr., 2000, Volatiles in magmas, *in* H. Sigurdsson, ed., Encyclopedia of Volcanoes: Academic Press, p. 149-170.

Waters, A., and R.V. Fisher, 1971, Base surges and their deposits: Capelinhos and Taal Volcanoes: Journal of Geophysical Research, v. 76, p. 5596-5614.

Watson, C.A., 1999, The evolution of Guffey Butte tuff cone complex, western Snake River Plain, Idaho: Boise State University M.S. thesis, 73 p.

White, C.M., W.K. Hart, Bill Bonnichsen, and Debra Matthews, this volume, Geochemical and Sr-isotopic variations in western SRP basalts, Idaho, *in* Bill Bonnichsen, C.M. White, and Michael McCurry, eds., Tectonic and Magmatic Evolution of the Snake River Plain Volcanic Province: Idaho Geological Survey Bulletin 30.

White, J.D.L., and B.F. Houghton, 2000, Surtseyan and related phreatomagmatic eruptions, *in* H. Sigurdsson, ed., Encyclopedia of Volcanoes: Academic Press, p. 495-512.

Wohletz, K.H., 1983, Mechanisms of hydrovolcanic pyroclast formation: Grain size, scanning electron microscopy, and experimental studies: Journal of Volcanology and Geothermal Research, v. 17, p. 31-63.

———, 1986, Explosive magma-water interactions: Thermodynamics, explosion mechanisms, and field studies:Bulletin of Volcanology, v. 48, p. 245-264.

Wohletz, K.H., and R.G. McQueen, 1984, Experimental studies of hydrovolcanic volcanism, *in* Explosive Volcanism: Inception, Evo-

lution and Hazards: National Academy Press, p. 158-169.
Wohletz, K.H., and M.F. Sheridan, 1979, A model of pyroclastic surge: Geological Society of America Special Paper 180, p. 177-194.
Wood, S.H., and D.M. Clemens, this volume, Geologic and tectonic history of the western Snake River Plain, Idaho and Oregon, *in* Bill Bonnichsen, C.M. White, and Michael McCurry, eds., Tectonic and Magmatic Evolution of the Snake River Plain Volcanic Province: Idaho Geological Survey Bulletin 30.
Zimanowski, B., G. Froelich, and V. Lorenz, 1991, Quantitative experiments on phreatomagmatic eruptions: Journal of Volcanology and Geothermal Research, v. 48, p. 341-358.

Overview and Synthesis of Lithologic Controls on Aquifer Heterogeneity in the Eastern Snake River Plain, Idaho

John A. Welhan,[1] Chad M. Johannesen,[2]
Linda L. Davis,[3] Kelly S. Reeves,[4] and John A. Glover[5]

ABSTRACT

The factors controlling basalt permeability and the heterogeneous distribution of permeability in eastern Snake River Plain (SRP) basalt are reviewed and new information summarized. A refined conceptual model of the lithologic architecture has been created on which stochastic models of aquifer heterogeneity and ground-water flow are being based. Basalt lava-flow geometry and internal structures in drill core and in Holocene flow groups are remarkably similar. This suggests that the emplacement style of monogenetic lava flows in the eastern SRP has remained unchanged since the mid-Quaternary, so that Holocene basalts can be used as analogs of the subsurface to identify the features controlling heterogeneity of permeability.

On the basis of core data, inflated pahoehoe lava appears to represent more than 80 percent of eastern SRP basalts. This suggests that the inflated pahoehoe morphology in distal zones of Holocene flow groups is the most volumetrically important basalt morphology of SRP shield volcanoes. Aerial photo and field mapping of large-scale, inflated lava-flow units in the Wapi and Hell's Half Acre flow groups has shown these structures to be characterized by a fractal shape that reflects their growth process. Because of fractal scaling, information on large-scale features may be extrapolated to smaller flow lobes. Length to width aspect ratios of lava-flow lobes can exceed 10 : 1 but median aspect ratios are close to 3 : 1 and remarkably similar in different Holocene flow groups.

Our conceptual hydrogeologic model is based on three principal permeability-controlling lithologies: low-permeability sediments, low-permeability massive basalt, and high-permeability zones within basalt. Two types of high-permeability zones have been identified in inflated pahoehoe lava flows: Type-1 interflow zones of highly porous, rubbly, and broken material at the contacts between lava-flow lobes; and Type-2 networks of fissures which can remain partially open after burial by younger lava. The spatial continuity of interflow zones is expected to be constrained by the dimensions and geometry of flow lobes. If fissures remain sufficiently permeable and interconnected after burial, their spatial continuity could approach kilometer scales and be highly directional. Open-interval permeabilities in individual wells correlate with the number of high-porosity zones (potentially permeable zones) intersected by the well. The large amount of scatter about the correlation suggests that the permeability of individual high-porosity zones is highly variable and that the permeability of any given high-porosity zone will be a stochastic variable.

Key words: basalt morphology, inflated pahoehoe, permeability, heterogeneity

INTRODUCTION

Predictive ground-water flow and transport modeling in heterogeneous aquifers is ultimately limited by the

Editors' note: The manuscript was submitted in June 1998 and has been revised at the authors' discretion.

[1]Idaho Geological Survey, Pocatello Branch Office, Idaho State University, Pocatello, ID 83209-8072
[2]Tetra Tech EMI, 6121 Indian School Rd., NE, Suite 205, Albuquerque, NM 87110
[3]Department of Geology and Environmental Geosciences, Northern Illinois University, DeKalb, IL 60115
[4]Nuclear Placement Services, P.O. Box 52096, Idaho Falls, ID 83405
[5]North Wind Environmental, 1843 W. Del Sol Ln., Yuma, AZ 85364

Welhan, J.A., C.M. Johannesen, L.L. Davis, K.S. Reeves, and John A. Glover, 2002, Overview and synthesis of lithologic controls on aquifer heterogeneity in the eastern Snake River Plain, Idaho, *in* Bill Bonnichsen, C.M. White, and Michael McCurry, eds., Tectonic and Magmatic Evolution of the Snake River Plain Volcanic Province: Idaho Geological Survey Bulletin 30, p. 435-460.

availability of detailed information on the subsurface distribution of rock units and the resulting permeability structure in the aquifer. Traditional, deterministic representations of aquifer heterogeneity are inherently limited, and researchers have developed promising, process- and structure-based stochastic alternatives to modeling aquifer heterogeneity (e.g., Koltermann and Gorelick, 1996). Of these, stochastic simulation is useful in describing the spatial nature of geologic and hydraulic variability, particularly where few data are available, and for quantifying uncertainty in modeled heterogeneity (Srivastava, 1994), thereby allowing for truly probabilistic predictions of contaminant transport.

The eastern Snake River Plain (SRP) aquifer is hydrogeologically complex, with considerable heterogeneity in its permeability field (what we shall subsequently refer to as hydraulic heterogeneity). The aquifer is hosted in a thick sequence of basaltic lava flows and intercalated sedimentary units, whose aggregate permeability as measured in individual wells varies over more than six orders of magnitude (Ackerman, 1991). The aquifer is characterized by highly localized, preferential ground-water flow paths (Lindholm and Vaccaro, 1988) that can cause water and solute mass to travel very rapidly at various spatial scales, thus making predictive modeling of contaminant movement highly uncertain (Sorenson and others, 1997). Previous ground-water models have incorporated heterogeneity on a relatively coarse, regional scale (Garabedian, 1989; Ackerman, 1995) because of insufficient subsurface information. Their predictive utility is consequently low owing to their excessive spatial averaging of heterogeneity.

To accurately predict contaminant movement in this complex aquifer system, the spatial distribution of rock units controlling permeability must be described on a scale that is commensurate with the scale of permeability variations that control contaminant movement. To improve the predictive accuracy of flow and transport models in the eastern SRP aquifer, a refined hydrogeologic conceptual model is needed to impose realistic constraints on stochastically generated models of aquifer heterogeneity.

The conceptual model summarized in this paper forms the basis for recent work on the stochastic simulation of aquifer heterogeneity and ground-water flow and transport in the eastern SRP aquifer. The geostatistical correlation structure of hydraulic conductivity and its relationship to basalt geology, the importance of highly porous and permeable preferential flow zones, and their potential impact on hydraulic behavior are described elsewhere (Welhan and Reed, 1997; Welhan and others, 1997a, 1998, 2002b). Welhan and Wylie (1997) and Welhan and others (2002a) describe the approach taken to build stochastic models of lithologic heterogeneity within this geologic framework, and Gego and others (2002) summarize preliminary flow modeling results.

SCOPE AND OBJECTIVES

By simulating aquifer heterogeneity with stochastic methods, we can predict the likelihood and spatial arrangement of interconnected high- and low-permeability regions that control the movement and dispersal of solutes. The approach strives to reproduce the "flavor" of geologic complexity, while honoring all available information, including that from boreholes, geologic models, and geophysical data (Deutsch and Journel, 1998). To do so, suitable lithologic surrogates for permeability must be chosen, and the spatial continuity of high- and low-permeability lithologic surrogates must be obtained from adequate borehole data or inferred from other geologic information, such as depositional models or geophysical data.

Stochastic simulation of the eastern SRP aquifer is hindered by relatively few monitoring wells with which to constrain model simulations and, more importantly, by an incomplete understanding of the lithologic controls on aquifer heterogeneity. For example, over the 2,315-square-km area of the Idaho National Engineering and Environmental Laboratory (INEEL; Figure 1), less than 300 deep wells sample the aquifer, for an average areal density of about one well per 8 square km. In one of the most densely drilled parts of the INEEL near a large contaminant plume at the Test Area North (TAN) facility, the areal density of monitoring wells is no more than a few wells per square kilometer. Existing conceptual models of the heterogeneous structure of the eastern SRP aquifer are either too generalized (Lindholm and Vaccaro, 1988) or too large in scale (Anderson and others, 1996) to be useful for creating accurate deterministic models of the aquifer or to constrain stochastic models of aquifer heterogeneity.

To overcome these limitations, Knutson and others (1990) suggested that morphologic measurements of exposed Holocene basalts could help define the nature and spatial configuration of hydraulically relevant features

Figure 1. Location of study area and prominent volcanologic features in the north-central part of the eastern Snake River Plain (ESRP). Wells in the Idaho National Engineering and Environmental Laboratory (INEEL) are shown as filled squares. Three major waste-processing facilities are shown inside rectangles. Holocene lava fields and volcanic highland and rift zones are shown in light gray (after Hackett and Smith, 1994; Kuntz and others, 1992). East-northeast oriented ellipse shown in central INEEL represents the scale and anisotropy of spatial autocorrelation of hydraulic conductivity measured in wells at the INEEL (Welhan and Reed, 1997).

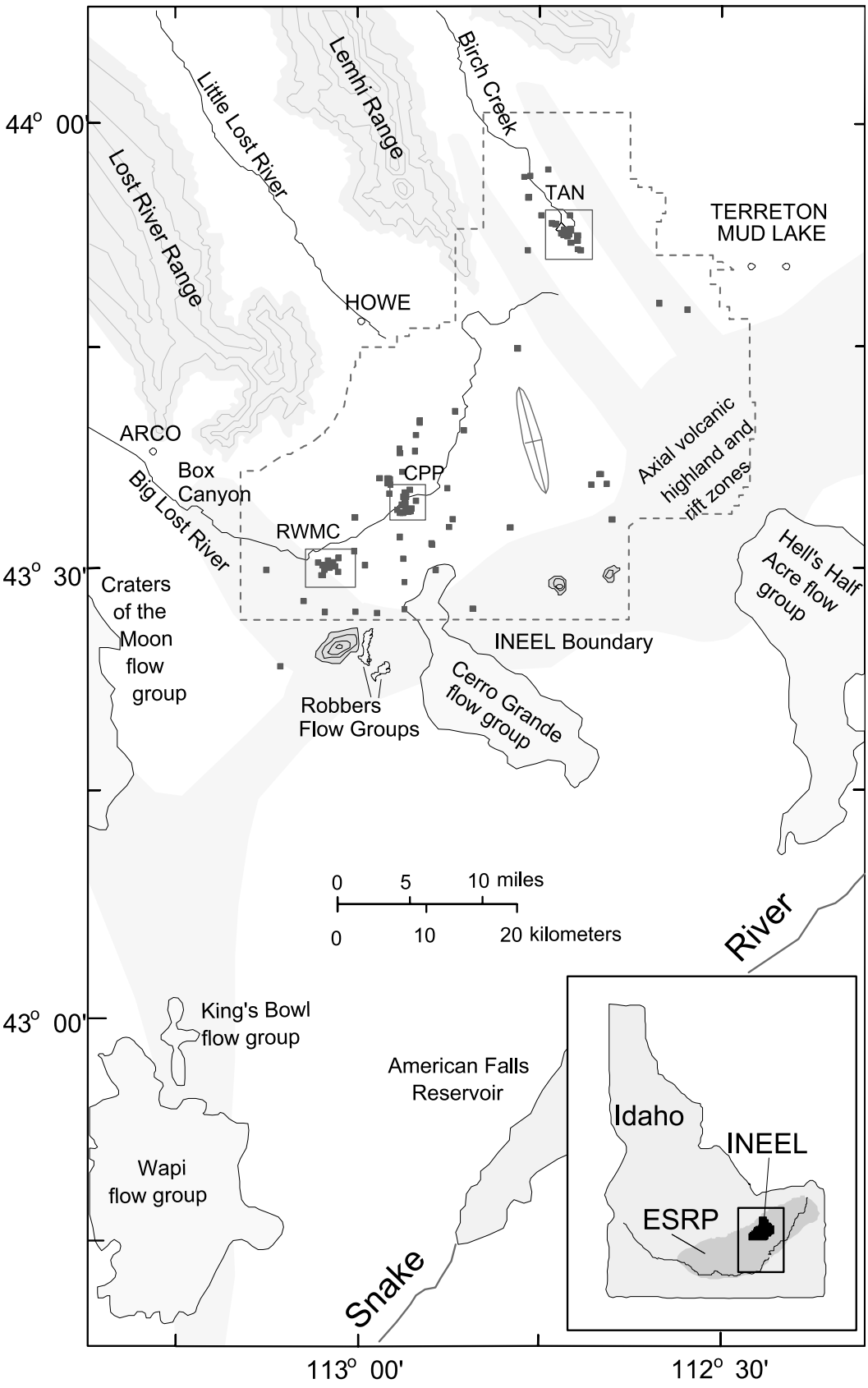
44° 00'
43° 30'
43° 00'
113° 00'
112° 30'
Lemhi Range
Little Lost River
Birch Creek
Lost River Range
TAN
TERRETON
MUD LAKE
HOWE
ARCO
Box
Canyon
Big Lost River
CPP
RWMC
Axial volcanic
highland and
rift zones
Hell's Half
Acre flow
group
Craters
of the
Moon
flow
group
INEEL Boundary
Cerro Grande
flow group
Robbers
Flow Groups
0 5 10 miles
0 10 20 kilometers
River
King's Bowl
flow group
American Falls
Reservoir
Wapi
flow group
Snake
Idaho
INEEL
ESRP

produced during basaltic volcanism. Such information could help to construct refined models of geologic heterogeneity with which to constrain stochastic descriptions of aquifer heterogeneity. Welhan and others (1997a) recommended focusing on the spatial distribution of key lithologies that could be used as proxies to constrain the spatial structure of hydraulic heterogeneity: low-permeability sedimentary interbeds and massive basalt, and high-permeability zones at the contacts between basalt flows. Since then, we have expended significant effort toward understanding the relevant volcanologic processes that created the spatial distributions of permeable zones in basalt lava flows (Welhan and others, 1997b; Glover and others, 1997; Johannesen and others, 1997).

In this paper, we provide an overview and synthesis of significant results obtained from work over the past five years. We develop a refined conceptual model of basalt heterogeneity on the basis of mapping of Holocene basalt morphology, measurements of the internal structure of basalt flows observed in core and in outcrop, and lithologic variations interpreted from geophysical logs. This conceptual model is being used to guide stochastic modeling of aquifer heterogeneity by imposing geologic constraints on hydraulic heterogeneity in the eastern SRP aquifer. Additionally, we hope that this synthesis will stimulate further refinement of pahoehoe emplacement models and future work on the hydraulic heterogeneity of this aquifer.

PREVIOUS WORK AND CONCEPTUAL FRAMEWORK

HYDROGEOLOGIC FRAMEWORK

The eastern SRP is the type locality of plains-style basaltic volcanism, characterized by multiple, low shield volcanoes (Greeley, 1982). Most of these volcanoes are olivine basalts remarkably similar in composition, mineralogy, and texture (Kuntz and others, 1992). Pahoehoe lava and its morphology predominates; aa and block-lava flows are rare. Kuntz and others (1992) estimated that over 95 percent of lavas in the eastern SRP are the products of shield volcanoes and lava cones, and that most of the pahoehoe lavas derived from these are tube fed. The predominance of pahoehoe implies predominantly low-discharge rate eruptions (e.g., Rowland and Walker, 1990). Individual lava fields composing the shield volcanoes are thought to be predominantly monogenetic, having been erupted individually on time scales of a few months, as typified by the Hell's Half Acre, Wapi, and Cerro Grande lava fields (Figure 1). In contrast, the Craters of the Moon lava field is chemically diverse and polygenetic, with some sixty flows erupted over 15,000 years (Kuntz and others, 1992), and is considered atypical of the subsurface.

Figure 2 summarizes the prevailing small-scale conceptual model of the hydraulic characteristics of eastern SRP basalts proposed by Lindholm and Vaccaro (1988) and later refined by Knutson and others (1990, 1992) and Welhan and others (2002b). Because this model is generalized for the entire eastern SRP and enjoys widespread acceptance, it may be termed a paradigm of the aquifer's hydraulic character; it forms the basis of all modern hydrogeologic analyses conducted on the eastern SRP (Knutson and others, 1992; Sorenson and others, 1996; Bennecke, 1996; Welhan and Reed, 1997; Welhan and others, 2002a). Its premise is that the highly fractured, rubbly, vesiculated contacts between basalt lava flows are far more permeable than the flows' massive, intermittently fractured interiors, giving rise to high-permeability, preferential flow zones or "interflow zones" (IFZs) at the contacts between lava flows. These high-permeability zones do not have a simple, three-dimensional geometric shape and are complexly interfingered and interlayered within the basalt section according to the spatial distribution of individual lava flows. Welhan and Reed (1997) postulated that the degree of interconnection of IFZs in lava-flow groups encapsulated within blankets of eolian sediment may be responsible for the kilometer-scale lateral spatial continuity of permeability they documented in INEEL wells.

The Lindholm-Vaccaro paradigm for eastern SRP basalts is entirely consistent with the recent inflationary model of pahoehoe lava flows proposed by Self and others (1998). Self and others combined extensive observations on the internal structure of pahoehoe lavas with data on the growth of pahoehoe lava flows. They proposed that most pahoehoe lava flows form via an inflationary, tube fed mechanism. A cooling crust, encapsulating a molten core supplied from a distant source, inflates in response to topographic obstructions and lava supply. Hon and others (1994) observed that an initially thin sheet flow evolved into an inflated flow where it met slight topographic impediments, which slowed its forward advance, promoted the development of a brittle crust, and initiated inflation by the accumulation of lava beneath the crust. The inflationary growth process explains such characteristic features of pahoehoe as lava morphology, the internal distributions of vesicular zones, and characteristic fracturing patterns (Self and others, 1998). These authors stated that evidence for an inflationary origin is found "throughout the Snake River Plain." As we will show, understanding the morphology of inflated pahoehoe is

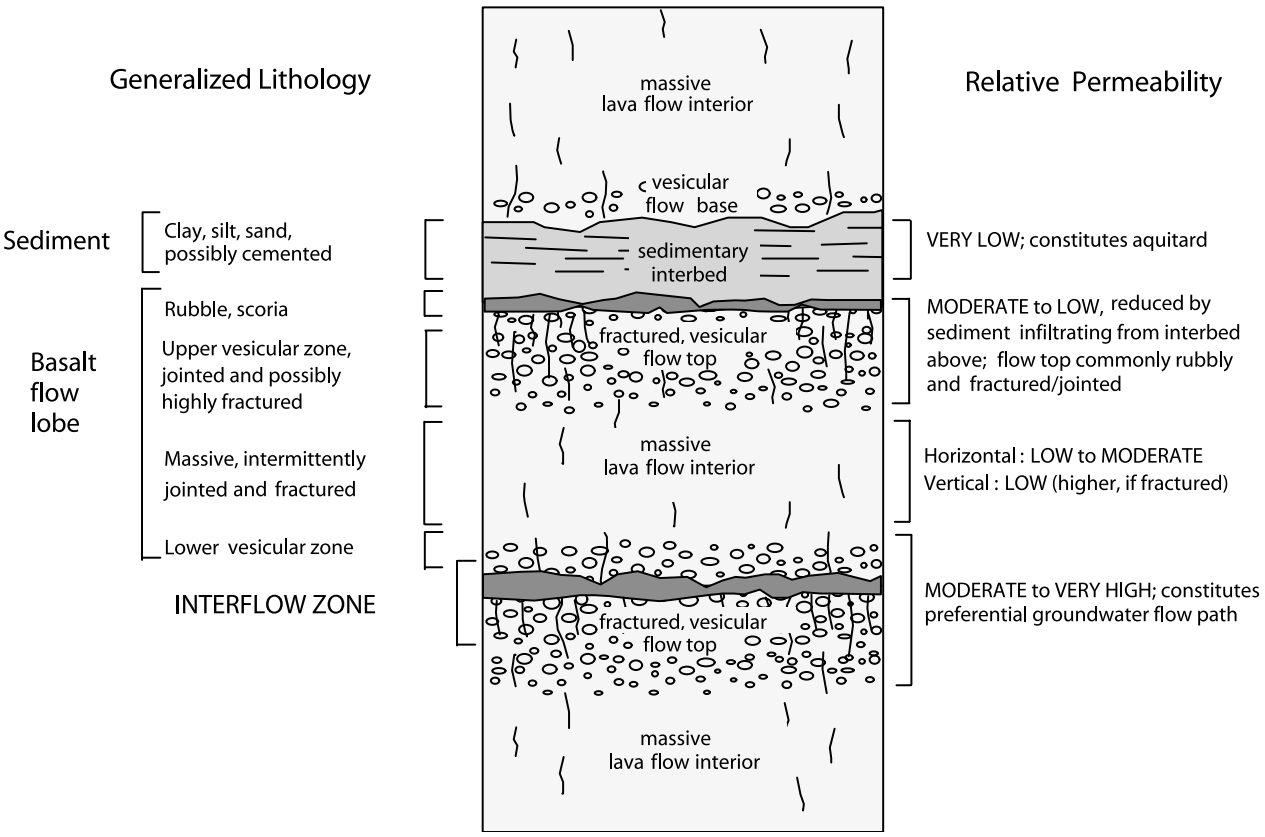

Figure 2. Conceptual model of the principal, hydraulically important lithologic features in Snake River Plain hydrostratigraphy. Modified after Lindholm and Vaccaro (1988), Knutson and others (1990, 1992), and Welhan and others (1997a).

crucial to describing the distribution of high-permeability zones in these subsurface basalts.

Much of our knowledge of the impact that the internal structure of basalt lava flows has on the permeability field of the aquifer is due to the work of Knutson and coworkers (Knutson, 1993; Knutson and others, 1990, 1992) at the outcrop- and core-scales. Knutson's work has provided almost all the data we have on core-scale permeability and porosity variations in these basalts.

Table 1 summarizes existing information on core-scale permeability of basalt and fine-grained sedimentary interbeds at the INEEL. The core-scale permeability of basalt varies by six orders of magnitude in both vesiculated and nonvesiculated rock. Knutson's data indicate that total core porosity consistently doubles or triples within the upper and lower vesicular margins of basalt flows, whereas permeabilities tend to remain very low, only occasionally increasing more than an order of magnitude within vesiculated zones (Welhan and Wylie, 1997). Vesicle-hosted permeability likely arises from the interconnection of vesicle porosity. Its variation within vesiculated basalt may be primarily due to the degree of microfracturing or the presence of diktytaxitic porosity, which can serve to interconnect vesicle porosity. Thus, the importance of vesicular basalt permeability in itself may be overstated in the Lindholm-Vaccaro model of interflow zones.

In contrast, the permeability of basalt rubble and fractured basalt is extremely high and is expected to dominate the hydraulic character of the aquifer (Knutson and others, 1990). Although direct measurements of rubble-hosted permeability are unavailable, Knutson and others (1992) assumed a value of 125 m per day (calculated from field vapor-extraction tests in the unsaturated zone), or about eight orders of magnitude greater than the lowest permeabilities measured in basalt cores. Knutson and others (1993) reported even higher measured permeabilities for outcrop fractures, up to 673 m per day (Table 1). As Lindholm and Vaccaro (1988) pointed out, the degree of fracturing in the interior of lava flows is variable and may be of secondary importance. Thus, the permeability of IFZs appears to be defined primarily by rubble at lava-flow contacts and by the degree of fracturing and jointing in the upper and lower colonnades of basalt flows.

Table 1. Summary of hydraulic conductivity values for sediment and basalt at the Idaho National Engineering and Environmental Laboratory.

		Median (range)	
Aquifer Material	**Reference Source**	**Hydraulic Conductivity meters/day**	**Porosity %**
Sediment			
Sandy silt with clay	Kaminsky and others (1994)	N.A. (0.0003-0.095)	N.A. (6-43)
(TAN/CPP interbeds)	Pudney (1994)	0.00035 (0.00025-0.015)	30 (26-39)
Basalt			
Upper vesicular element	Knutson and others (1992)	0.004 (10^{-6}-4.5)	22 (6-43)
Central massive element	do.	0.008 (10^{-6}-0.4)	11 (1-32)
Lower vesicular element	do.	0.003 (10^{-6}-1.4)	22 (5-35)
Micro fractures	do.	N.A. (0.33-0.67)	N.A.
Interflow rubble zones	do.	ca. 125 (N.A.)*	ca. 50 (N.A.)*
Outcrop fractures (0.03-0.28 mm aperture)	Knutson and others (1993)	N.A. (5-673)	N.A.

* Estimated by Knutson and others (1992).

BASALT LAVA FLOW TERMINOLOGY

Anderson and coworkers (e.g., Anderson and others, 1996) have been instrumental in delineating basalt stratigraphy beneath the INEEL at the regional scale. Their work has spawned detailed stratigraphic correlation studies (Hughes and others, 2002) and focused attention on basalt correlation problems and structural interpretations (Jobe, 1996) and on the volumetric and areal scales of late Quaternary basalt eruptions (Wetmore, 1998). However, these and other authors have used different nomenclature for similar basalt features, or the same nomenclature at different scales of observation. This has led to confusion when synthesizing information from different sources. Because much of what is known of the SRP subsurface is based on exposed basalts, we suggest a common terminology for surface and subsurface basalt features.

Table 2 expands on the terminology originally proposed by Welhan and others (1997a) to make basalt lava-flow terminology consistent with the scale of observational information (i.e., core and borehole data, vertical outcrop, local- and regional-scale mapping), while maintaining consistency with current literature usage. The terminology is arranged into three dimensional scales, in ascending order of size: (1) the local- or outcrop-scale, ranging from 1 m to a few hundred meters; (2) the meso- or plume-scale, at dimensions less than 1 km to 10 km (the scale of interest for most contaminant plume modeling); and (3) the regional- or SRP-scale (the appropriate scale for modeling ground-water flow within the entire eastern SRP).

Lava-flow lobes and lava-flow units are considered the smallest-scale basalt features relevant to modeling aquifer heterogeneity. The diagnostic internal features shown in Figure 2 apply to both lava-flow lobes and flow units. Our usage of "lava-flow lobe" is synonymous with that of Kuntz and others (1992) and Self and others (1998). Lobes range in thickness from less than 1 m to more than 10 m (Knutson and others, 1990). We define a lava-flow unit as a mappable composite of lava-flow lobes derived from a single inflationary advance of a pahoehoe lava flow, typically several hundred to several thousand meters long. The distinction between the two terms is presented in the next section. The dimensions of flow lobes and flow units can extend over a wide range of scales, from tens of meters to several kilometers in length (Self and others, 1998), implying that these features are important at both the local- and meso-scales.

At the meso-scale, the term "flow group" denotes the aggregate of lava-flow units emplaced in a single volcanic eruptive event and from one source area. It is synonymous with the term "lava field" as used by Self and others (1998) and by Kuntz and others (1992) for Holocene lava fields like Hell's Half Acre, Wapi, and Cerro Grande, which have areas up to 400 square km. Anderson and coworkers (e.g., Anderson and others, 1996) applied the term to all correlated subsurface basalt units, regardless of the geographic scale of the correlation. We suggest the term should be applied only to subsurface units correlated on an areal scale of a few hundred square kilometers, such as within the TAN, Radioactive Waste

Table 2. Scale-dependent terminology for basalt lava flows and related features (modified after Welhan and others, 1997a, 2002b).

Local- or Outcrop-Scale	
Lava flow lobe	The smallest coherent lithologic subdivision of inflated pahoehoe identifiable in cores and outcrops, ranging in thickness from <1 m to >10 m; synonymous with the definition of Hon and others (1994) and Self and others (1998) at the local- or outcrop-scale, but herein also used to describe features observed in boreholes or in vertical outcrops where the three-dimensional spatial relationship of individual lobes to one another is not apparent; internally composed of an upper and lower vesicular zone, a central massive zone, and a fractured, possibly rubbly flow top and lateral margins.
Meso- or Plume-Scale	
Lava flow unit	The aggregate of flow lobes created during a single advance of lava from a tube-fed system; mappable in aerial photos, covering a range of length scales from <100 meters to kilometers; for the most part, the spatial relationships between individual lobes and their parent lava flow unit are mappable in the field and in aerial photos, so that the size and geometry of individual lobes can be subjectively estimated.
Lava flow group	Synonymous with the term "lava field" as used by Kuntz and others (1992); a group of many coalesced flow units extruded within a brief time from a common source vent area and typically covering areas up to a few hundred square kilometers (such as Hell's Half Acre, Wapi); use of the term for subsurface correlations should be restricted to areas on the scale of INEEL facilities to avoid confusion with regional-scale stratigraphic correlations between facilities.
Regional- or SRP-Scale	
Flow Member[1]	Laterally and vertically coalesced lava flow groups on a regional scale, originating from different source vent areas, but having similar ages and paleomagnetic signatures; intended to replace Anderson and others' (1996) use of the term "flow group" in regional-scale stratigraphic correlations between INEEL facilities; Kuntz and others' (1994) units Qbb, Qbc, Qbd, and Qbe represent potential surface analogs of this scale of feature.
Composite group	Anderson's regional-scale terminology for multiple flow members combined into larger units for the purpose of regional stratigraphic correlation and structural syntheses.

[1] Replaces the term Supergroup originally proposed by (Welhan and others, 1997a).

Management Complex (RWMC), or Chemical Processing Plant (CPP) facilities, i.e., comparable in scale to the largest Holocene flow groups. Because of the complexity and wide range of dimensional scales of flow lobes and flow units within a flow group, it is probably unrealistic to expect that feasible stratigraphic correlation methods can be developed on any scale smaller than that of the flow group.

The areas and volumes of basalt units that Anderson and coworkers correlated over regional scales (i.e., over thousands of square kilometers) tend to be much larger than those of Holocene lava fields. For example, the mean estimated volume of the four largest[6] Holocene monogenetic lava fields on the eastern SRP is less than 4 cubic km (Kuntz and others, 1992); in comparison, the mean estimated volume of the sixteen youngest of Anderson's subsurface "flow groups" is 16.9 cubic km (Wetmore, 1998).[7] Although this may reflect a change in the style of volcanism toward lower-volume eruptions in the Holocene, Anderson acknowledges that discriminating between vertically stacked or laterally coalesced flow groups of similar age was simply not possible given the correlation methods he employed (S. Anderson, oral commun., 1997). Welhan and others (1997a) and Wetmore (1998) cautioned that a distinction between Anderson's use of the term "flow group" at the facility and regional scales is necessary to avoid misrepresenting the physical volumes and areal extents of stratigraphic packages that may include multiple flow groups.

Anderson (oral commun., 1997) has concurred that the term "flow group" should not be applied to regional-scale basalt correlations. He recognized that his use of the term may lead some to conclude that individual volcanic eruptions in the past were on a different volumetric scale than Holocene eruptions. Welhan and others (1997a) proposed the term "supergroup" to distinguish basalt stratigraphic packages that Anderson and coworkers have correlated over a regional scale from individual flow groups that are equivalent, and comparable in scale, to the largest Holocene lava fields. Welhan and others (2002b) recently used the term "flow member" to avoid confusion with the common stratigraphic connotation of "supergroup." Wetmore and Hughes (1997) concurred with the need for a more precise, scale-dependent terminology, and Wetmore's (1998) work has substantiated this view.

[6] Excluding the very small North and South Robbers and King's Bowl eruptions.

[7] Based on kriging interpolation and volume estimates for flow groups B through I in Anderson's stratigraphy.

The term "supergroup" implies that multiple flow groups of similar age (lacking sedimentary marker horizons to distinguish eruptive hiatuses) are stacked vertically or coalesced laterally, or both, to form larger units of similar age that may extend over hundreds or thousands of square kilometers. From exposed basalt on the eastern SRP, a possible analog may exist in the Quaternary basalt units mapped by Kuntz and others (1994). These workers mapped age relationships within some of the Quaternary basalt units, thereby defining smaller basalt packages whose dimensions Hackett and Smith (1994) subsequently quantified. Their data (R. P. Smith, written commun., 1996) indicate a median area of 24 square km, with a range from less than 1 square km to greater than 200 square km. Welhan and Reed (1997) pointed out that this range is similar to that of Holocene flow groups on the SRP (3 square km to 400 square km; Kuntz and others, 1992). Thus, many of the "lava flows" measured by Hackett and Smith may properly be regarded as flow groups, in which case Kuntz and others' extensive Quaternary basalt units may be informally viewed as a surficial analog of the horizontal spatial distribution of a subsurface supergroup.

FLOW LOBES AND FLOW UNITS

A deliberate distinction between flow lobes and flow units has been retained throughout this work to maintain consistency with the scale-dependent data that have ranged from the decimeter-scale descriptions of lithologic variability in core to the kilometer-scale aerial photo mapping of lava-flow morphology. Because IFZs develop along the contacts between flow lobes, understanding the spatial geometry and configurations of lobes is essential to describing the spatial configuration of IFZs. Borehole data can only provide adequate control on the vertical spacing and locations of lava-flow lobes. To understand and impose realistic constraints on models of the spatial arrangement of lobes in three dimensions, we require subaerial exposures and two-dimensional vertical canyon wall exposures of lobe contacts (Knutson and others, 1992), as well as genetic models of the emplacement of lobes (Welhan and others, 1997a, 2002b).

However, the three-dimensional spatial and genetic relationships between individual lobes identified in core cannot be understood from internal vesicular structures or from the arrangement of cooling surfaces exposed in canyon walls. Mapping subaerial outcrops can identify the spatial relationships between lobes, but their genetic relationships may be obscured by coalescence and fusion of individual lobes during emplacement (Self and others, 1998). Thus, the term "lava-flow unit" is used to describe an aggregate of flow lobes whose overall morphology provides information about the temporal growth and advance of lava.

Growth and Morphology of Flow Lobes

Self and others (1998) proposed that most pahoehoe lava-flow units grow by a tube-fed, inflationary mechanism over a wide range of dimensional scales from less than 100 meters to more than 10 km, resulting in thicknesses ranging from 1 m to 100 m. On the basis of their model and particularly on the work of Hon and others (1994), we define the emplacement and growth of flow lobes as an episodic advance of incandescent lava from a break-out point at the edge of an advancing pahoehoe lava flow. Rapid cooling at the upper surface creates a brittle crust, which continues to extend laterally and to inflate in response to an internal supply of fresh lava. The failure of the brittle crust during this process leads to the creation of a new lobe. This cycle is repeated as long as the lava supply is sustained, and new break-outs occur where the inflation pressure exceeds the tensile strength of the expanding crust. Thus, numerous generations of flow lobes can be created from the parent flow unit, forming a temporal hierarchy of lobes that defines the advance of the lava.

Figure 3 summarizes the growth mechanism of inflated pahoehoe and the limitations of our ability to identify individual flow lobes from outcrop data. Figure 3a, adapted from Hon and others (1994), shows the hierarchical, temporal evolution of a flow unit over a period of 51 hours as observed in an advancing inflationary lava flow on the flank of Kilauea, Hawaii. A large, initial lobe, defined by a distinct cooling surface, was created during the first 6 hours of the event, with smaller lobes appearing along its periphery. A new breakout at the tip of this lobe subsequently fed the growth of a second, larger lobe with smaller lobes subsequently growing along its periphery. Each lobe created during this hierarchical growth, regardless of its dimensional scale, is characterized by a distinct cooling surface and internal structures characteristic of inflated pahoehoe (Figure 2; Self and others, 1998). The final result of this lava advance (Figure 3b) we define as a lava-flow unit.

Without the benefit of the temporal observations in Figure 3a, all flow lobes formed during emplacement of the flow unit cannot be identified from outcrop information alone. For example, the large lobe that had formed by 6 hours and smaller lobes evident in the 6-hour and 27-hour boundaries cannot be distinguished in the final morphology of the flow unit (Figure 3b. From the data of Figure 3, we infer that individual lobes can be identified

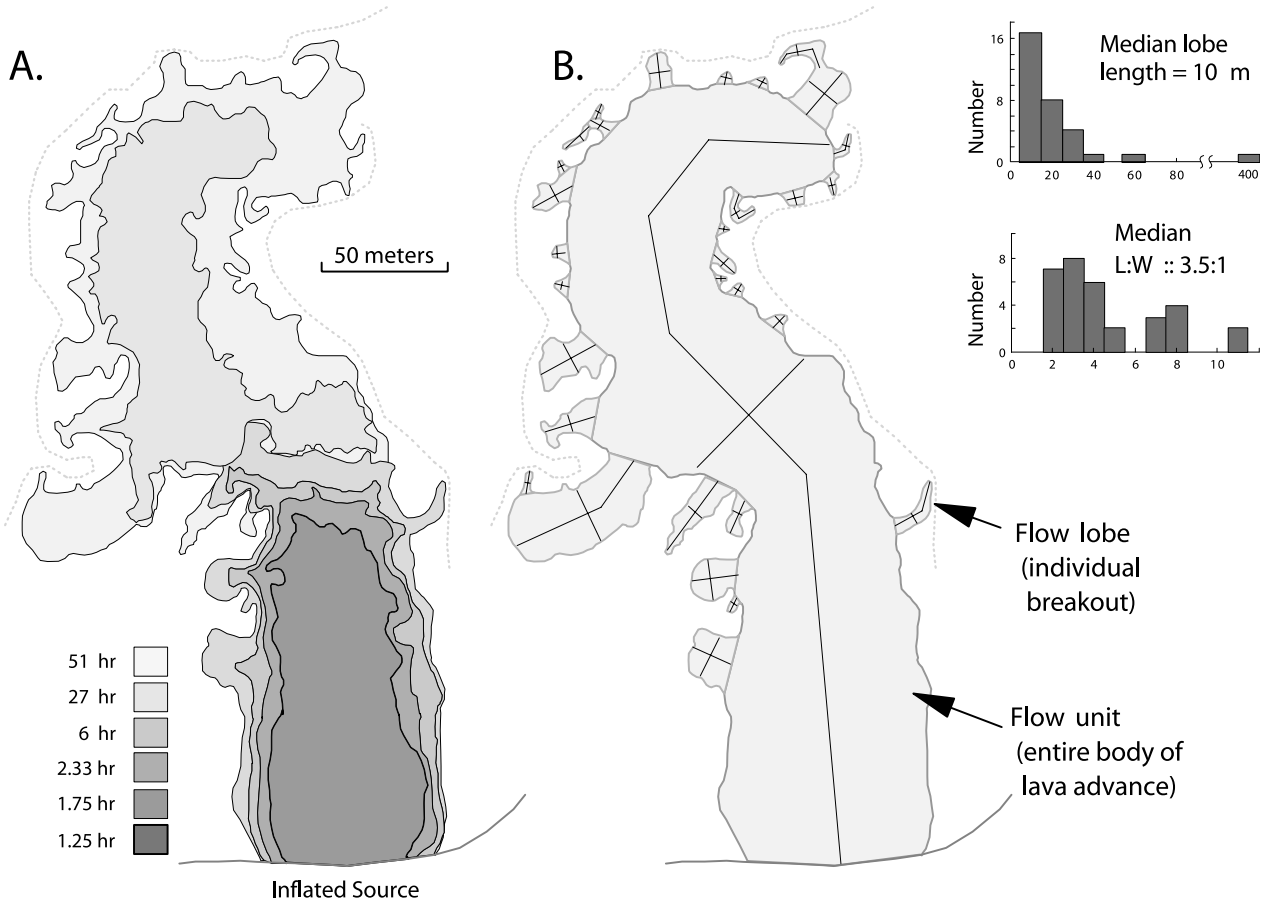

Figure 3. (A) Actual temporal growth of a pahoehoe lava flow, Kilauea Volcano, Hawaii (after Hon and others, 1994); (B) A working definition of flow lobes and flow units. The entire body of inflated lava is termed a "flow unit" in this work. Of the many individual "flow lobes" making up the flow unit, only the latest generation can be identified and mapped; earlier lobe boundaries may have been obliterated during growth of the flow unit. Approximate dimensions of identifiable flow lobes and length to width ratios are shown in the inset.

reliably along the periphery of a flow unit where they are spatially distinct from the parent lobe, and that coalesced flow lobes within the core of a flow unit may be indistinguishable on the basis of subaerial morphology alone. In other words, the distribution of approximate lengths and widths of individual lobes estimated in Figure 3b will be biased because some lobes were obliterated during the emplacement process. For this reason, the distinction between flow lobes in subaerial exposures can be very difficult (Self and others, 1998), and individual lobe geometries mapped from vertical and subaerial outcrops can only provide an approximation of the distribution of their shapes and sizes.

Knutson and others (1990) mapped individual lava-flow lobes in vertical outcrops in Box Canyon (see Figure 1 for location). They measured lobes ranging in thickness from 1 m to 21 m, with a median length to width to height aspect ratio of >8.7 : 4.6 : 1. Because the canyon wall provides a censored sample of lobe dimensions, their lobe lengths were underestimated. Using the same technique shown in Figure 3b as well as other methods, the largest lava-flow lobes and flow units in a portion of Hell's Half Acre were measured by Knutson and others (1990), with a median length to width aspect ratio of 2.9 : 1, almost identical to the 3 : 1 median estimated in the same way for the North and South Robbers flows (Welhan and others, 1997a), Hell's Half Acre, and Wapi flow groups (Welhan and others, 2002b). Combining this with the Box Canyon width to thickness ratio, we arrive at an estimated median length to width to thickness aspect ratio of 15 : 5 : 1. Sorenson and others (1996) suggested that the Box Canyon width to thickness ratio may have been biased low because of outcrop censoring, possibly by as much as a factor of two. If so, the median aspect ratio of flow lobes may be as high as 30 : 10 : 1 (Welhan and others, 1997a).

Fractal Nature of Pahoehoe Lava Forms

The hierarchical growth process of lobes spawning lobes produces a lava-flow unit whose boundary may be fractal. A fractal object is characterized by a shape that has similar features at different scales or, in other words, is self-similar or scale-invariant (Mandelbrot, 1967). A common example is that of a coastline, which when viewed from a great height, looks similar to the shape of a smaller portion when viewed under magnification. Such an object has a fractal dimension, which is a measure of the dependence of perimeter on the scale of measurement. A characteristic of a two-dimensional fractal object is that its perimeter length progressively increases when measured with successively greater attention to small-scale detail (Mandelbrot, 1967).

Bruno (1994) suggested that lavas whose flow margins are controlled predominantly by internal, fluid-dynamic processes rather than by topography have a fractal geometry. If lava is not forced to flow down a steep topographic gradient or along topographically defined pathways, new lobes grow where break-outs occur and tend to produce a flow unit with a boundary whose shape is fractal. Bruno and others (1992) showed that the outer margin of Hell's Half Acre flow group has a fractal geometry similar to pahoehoe flows in Hawaii and elsewhere. The range of lobe dimensions and the hierarchical nature of lobe growth shown in Figure 3b implies that individual lava-flow units may also have fractal shape. Since IFZs are located along lobe surfaces, the implication is that the horizontal dimensions of IFZs may also extend over a range of scales.

SURFACE AND SUBSURFACE OBSERVATIONS

We have used several sources of information to build a conceptual model of the spatial geometry of subsurface basalt heterogeneity. These include descriptions of core from INEEL wells, geophysical logs and borehole permeability profiles from wells at the TAN and CPP facilities, surface mapping of selected parts of Hell's Half Acre and Wapi lava flows, and observations of selected cross-sectional exposures of Quaternary flow lobes. Our work represents one of the first systematic syntheses of subsurface and surface basalt data on lava emplacement in a large basalt volcanic province.

LOCAL-SCALE INFORMATION

Core-Hole Data

Basalt cores from thirteen core holes in the TAN and CPP facilities were examined and logged to identify the thickness, internal vesicular structure, and contacts between flow lobes (Glover and others, 2002). We identified features relevant to the permeability of lava flows, including the thicknesses of upper and lower vesicular zones, the presence and thickness of rubble at lobe contacts, vertical fracturing, broken and fractured material, intervals of missing core (possibly representing broken or rubbly zones, or large voids), and the proportion of lobe contacts that appeared hydraulically "tight." In addition, over a kilometer of borehole video logs were examined to substantiate the inferences from core (J. Glover, written commun., 1998). This work has corroborated much of Bennecke's (1996) and Knutson and others' (1990) findings in the RWMC and CPP areas and has confirmed the generality of the Lindholm-Vaccaro paradigm.

Table 3 summarizes results from our INEEL core-hole data. The distribution of lobe thickness is positively skewed, with median thicknesses ranging from 2.5 to 4.1 m in TAN cores and from 2.8 to 6.1 m at CPP. The thickness range in core is similar to that in flow lobes and flow units in Holocene and late Quaternary flow groups exposed at the surface (less than 1 m to about 20 m; Champion, 1973; Kuntz and others, 1992; Knutson and others, 1990). Even more striking, the distributions of upper and lower vesicular zones within lobes are statistically indistinguishable between TAN and CPP core holes. The distribution and relative proportions of vesicles in upper and lower vesicular zones are entirely characteristic of pahoehoe lavas, having both a relatively thick upper zone that composes about 30-50 percent of the flow thickness and a thin lower zone with an absolute thickness typically less than 1 m (Aubele and others, 1988).

In particular, the distributions of thicknesses and internal vesicular zones of eastern SRP basalts are very similar to those in the Kalapana flow group in Hawaii. Cashman and Kauahikaua (1997) pointed out that Hawaii's inflated pahoehoe is characterized by a relatively constant upper vesicular zone thickness of 40-60 percent of lobe thickness. Self and others (1998) noted that the relative thickness of the upper vesicular zone in examples of ponded lava are much lower, in the range of 6-30 percent and averaging 15 percent. On this basis, they proposed the relative thickness of the upper vesicular zone as a possible discriminant of inflated versus ponded pahoehoe emplacement. If this is correct, then inflated pahoehoe appears to account for more than 80 percent of all flow lobes documented in TAN and CPP cores, in keeping with the large proportion of lavas on the SRP believed to be tube fed (Kuntz and others, 1992).

From the data summarized in Table 3, we have proposed that the occurrence frequencies of rubble in 1 Ma-

Table 3. Summary of statistics on thickness and internal structure of basalt lava-flow lobes of varying ages, as determined from drill core and Box Canyon outcrops in this and other studies.

Geographic Area	**RWMC**	**RWMC**		**Box Canyon**	**CPP**	**TAN**
Wells sampled	15 cores	core C1A		Outcrop	6 cores[1]	6 cores[2]
Data source	(Knutson and others, 1990)	(Knutson, unpubl. data)		(Knutson and others, 1990)	(this work)	
Supergroups[3]	A – C	C – H	LM – T	Qbd	DE5 – J	MN – R+
Age, Ka	100-300	300-800	800-1800	500-700	440 - >640	900- >1400
Number of lobes quantified	114	40	48	372	200	169
Median thickness, m and range, m	4.6 0.3-17	2.4 0.34-16	3.9 0.7-38	3.7 0.3-18	3.0 0.4-46	3.4 0.15-20
Median upper vesicular zone, % of lobe thickness	35	39	42	N.A.	28	30
Median lower vesicular zone Thickness, m	0.45	0.23	0.23	N.A.	0.21	0.27
Occurrence of rubble, % of lobes	11	N.A.	N.A.	N.A.	25 (47)[4]	42 (58)[4]
Rubble thickness median, m / range, m	1.2[5]	N.A.	N.A.	N.A.	0.30 0.03-5.8	0.30 0.03-5.5

[1] NPR-test, W-02(old), W-02(new), USGS-121, USGS-123, CPP-COR-A-023.
[2] GIN-5, GIN-6, TCH-1, TCH-2, 2-2A, USGS-126A.
[3] From Anderson and others (1996).
[4] Includes missing core at lobe contacts as possible rubble.
[5] Reported as "collapse/rubble thickness."

old TAN lavas and in the younger CPP lavas are similar (Welhan and others, 2002b). This suggestion is based on the assumption that apparent rubble occurrence is biased due to incomplete core recovery. As can be seen in the TAN and CPP data, the percentage of rubble at lobe contacts almost doubles if we surmise that the missing core at lobe contacts represents rubbly material lost during drilling. The frequency of rubble at lobe contacts indicates the rubble is discontinuous and patchy over the surface of flow units and lobes, which is consistent with observations on Holocene lavas of the SRP (Knutson and others, 1992; Champion, 1973; Welhan and others, 2002b). The median thickness of rubble zones in all TAN and CPP core is essentially identical.

The striking similarity of lobe characteristics among basalts of different age in the subsurface (Table 3), particularly the relative thicknesses of the upper and lower vesicular zones that Self and others (1998) suggest are diagnostic of inflated pahoehoe lava, indicates a similar character of basalt lava emplacement from 1.4 Ma to at least 100 Ka. Considering the similarities in lobe thickness and rubble occurrence in these and Holocene lava flows, we suggest the eruption style of basaltic lavas has not changed significantly from the mid-Quaternary to the Holocene. On this basis, therefore, we conclude that Holocene lava flows are reasonable analogs from which to deduce the morphology, geometry, and spatial configuration of Quaternary basalts within the eastern SRP aquifer.

Borehole Geophysical Data

Stochastic modeling of aquifer heterogeneity requires that subsurface information be available to condition the probabilistic simulations to the real world. However, because lithologic logs from wells on the SRP do not identify the locations of lobe contacts, information on subsurface lithologic variations, and IFZs in particular, must be obtained indirectly from geophysical logs. Anderson and others (1996) demonstrated the utility of natural gamma logs for identifying and mapping sedimentary interbeds in the subsurface. Knutson (1993) and Hegmann and Wood (1994) showed that induced gamma-density and neutron-porosity logs provide useful information on the locations of basalt flow contacts. However, except for Knutson's (1993) preliminary work, the ability of these methods to resolve lobe contacts at the spatial scale we

required was largely untested.

To document the usefulness of these tools for this purpose and to develop a defensible interpretation protocol, we compared geophysical tool responses with basalt porosity in corresponding core. Unfortunately, the density/porosity logging tools used at the INEEL are not calibrated and porosity could only be visually estimated. In addition, extraneous effects introduced a significant degree of unconstrained variability in geophysical log response, including borehole diameter, the presence or absence of casing, and differences in logging tools used over the years. Therefore, our comparative calibration was of necessity a qualitative effort. In effect, core data were used to document the relative confidence level with which lobe contacts and other porous features could be identified and to provide an estimate of the types of contacts that could and could not be detected.

The interpretation procedure, calibration approach, and results are described by Glover and others (2002). The induced gamma-density and neutron-porosity sondes utilize a gamma-emitting and a fast neutron-emitting source, respectively, to induce secondary gamma radiation or thermal neutron backscatter from the materials they affect. Appropriate detectors record the radiation intensity produced by the interaction of the source radiation with the formation. Induced gamma emissions decrease where bulk density of the formation is high, due to gamma attenuation. Moderation and capture of fast neutrons are most efficient in water-rich (porous) regions of the borehole (Keys, 1997). Therefore, near an IFZ, where bulk formation density decreases and porosity increases, thermal neutron counts decrease and induced gamma counts increase (Knutson, 1993).

Beginning with this premise, we compared the raw count rate produced by these geophysical tools with known occurrences of features such as lobe contacts, rubble, fractures, and massive basalt in core holes at TAN. The overall success rate was highest for the most porous lobe contacts (more than 75 percent). Nonfractured or nonrubbly lobe contacts could not be reliably identified (Welhan and others, 1997b, 2002b). Natural-gamma response was used to identify sedimentary interbeds and sediment accumulations at lobe contacts. Where possible, caliper responses were used to corroborate interpretations derived from the induced-gamma and neutron sondes. An interpretational protocol was developed to qualitatively filter the logging records for casing and drill stem effects, variable quality logs, and the confidence level of the geophysical signal excursions. Because of the attenuating effect of steel well casing and different neutron and gamma attenuation above and below the water table, our interpretations of lobe contacts were confined to those below the steel casing string and within the saturated zone.

Hydraulically relevant features other than lobe contacts are capable of producing responses in the density and neutron tools. Sedimentary interbeds produce density/porosity excursions similar to zones of porous, low-density basalt, but these can be discriminated by their natural gamma signature. The results of our comparison and calibration with core features showed that thick, rubbly, highly fractured lobe contacts can be identified with the highest confidence, whereas welded or nonrubbly lobe contacts and vertically fractured zones within massive basalt could not be detected reliably. In a few places, unequivocal high-porosity/low-density signals within a thick section of massive basalt were identified, for which no corresponding porous features existed in the core. Because the geophysical tools "see" the formation a few decimeters beyond the diameter of the core, these strong signals suggest the presence of large voids in the interior of flow lobes that are near to, but not intersected by, the borehole.

Permeability of Basalt Interflow Zones

Welhan and Wylie (1997) observed that the vertical spatial continuity of well permeability determined from variograms could not be reconciled with the vertical spatial continuity of core-scale permeability measurements, taking into account the difference in measurement scales of the two data sets. They suggested that the lithologic heterogeneity responsible for hydraulic heterogeneity may have a characteristic vertical dimension much greater than the thickness of rubble and broken material at lobe contacts. Their analysis suggested that, rather than being controlled by the thickness of rubbly IFZs (about 0.3 m; Table 3), vertical variations in borehole permeability may be controlled by high-permeability zones 2-3 m thick, possibly representing vertically fractured zones, either at lobe contacts or within massive basalt.

As shown in Figure 4, the highest permeabilities in a vertically profiled section of core-hole TCH-1 correspond with rubbly or multiple flow contacts and with zones of vertically fractured rock. Unfortunately, this core hole is the only one in which such detailed coring and vertical permeability profiling are available. These data do not suggest that vertically fractured zones are important hydraulic features. Vertical fractures and joints commonly occur in the upper colonnades of flow lobes, and core is most commonly missing at flow contacts, suggesting the presence of loose, broken material or large voids (fissures?).[8] If significant vertically oriented fracture poros-

[8]From studying more than 1,200 m of borehole video logs, J. Glover (oral commun., 1998) has observed that large void spaces and subvertical fissures are common at flow contacts.

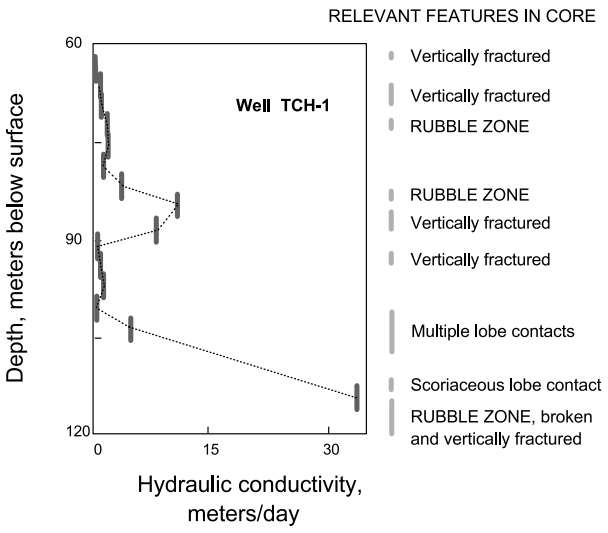

Figure 4. Vertical variation of permeability along a 60-meter section of the aquifer, as measured in a borehole straddle packer profile (A. Wylie, written commun., 1996). Lithologic characteristics in core are noted on the right to point out features relevant to the hydraulic behavior of the aquifer.

ity exists at flow contacts, it would be expected to extend the vertical range of influence of high-permeability IFZ material at lobe contacts, and also to laterally interconnect discontinuous patches of rubble and broken material into more horizontally extensive high-permeability zones.

On the assumption that high-porosity lobe contacts represent potential IFZs, the interpretational protocol developed for INEEL geophysical logs was used to identify high-porosity zones in all TAN wells for which geophysical logs are available. For each borehole, the number of interpreted high-porosity zones within the test interval was plotted against the natural logarithm of permeability estimated from slug tests or pumping tests (A. Wylie, written commun., 1996). Such a cross-plot is expected to be fairly noisy even if the variables are correlated, because conventional hydraulic test interpretation methods can produce inaccurate permeability estimates when applied in a fractured, highly heterogeneous aquifer (Fredericks and Johnson, 1996), and because we inferred potential IFZs from geophysical logs indirectly by their enhanced porosity rather than from their actual permeability.

Figure 5 depicts the relationship between the logarithm of well test permeability and the number of high-porosity zones intersected by the test. The low correlation coefficient reflects the high degree of noise in the relationship. However, it is incorrect to assume that a low regression coefficient signifies lack of a correlation. More importantly, the slope of the regression should be tested for statistical significance relative to the scatter in the data. A Student's-t test was applied to the slope of the regression in Figure 5 and indicated that the correlation is statistically significant at the 99 percent confidence level.

Although some of the scatter about the regression line may be due to error in identifying porous zones from geophysical logs, much of it reflects the variable permeability of IFZs. As discussed in a later section, the permeability of porous zones at lobe contacts is likely variable (Welhan and others, 2002a), depending on the thickness of fractured and rubbly material, the hydraulic interconnection with adjoining permeable zones, the lateral spatial extent, and the degree to which primary IFZ porosity has been plugged by fine-grained sediment. Sediment plugging appears not to be a major factor in the TAN aquifer, since three of the four well test intervals plotted in Figure 5 that contain, or have nearby, sediment occurrences have quite high permeabilities.

Permeability is lognormally distributed in natural materials in general and in the TAN aquifer in particular (Welhan and Wylie, 1997). The semilogarithmic relationship in Figure 5 is consistent with the expectation that the probability of finding highly permeable IFZs increases with the number of high-porosity zones sampled, or in other words, with the scale of the hydraulic test (Neuman, 1990). The relationship in Figure 5 provides important corroboration that IFZs exert a dominant control on the hydraulic character of the aquifer.

MESO-SCALE INFORMATION

The meso-scale is perhaps the most pertinent scale at which aquifer heterogeneity must be described and modeled, because it is the scale at which contaminant plume dynamics must be understood and predicted (Sorenson and others, 1997). Because wells are often spaced too far apart to permit the inference of spatial correlation structure of IFZs from borehole data alone, we require external information to constrain the lateral spatial continuity of basalt flow lobes and their associated IFZs for stochastic simulation purposes (Welhan and others, 1997a). Such information can be obtained from mapping the dimensions, aspect ratios, and orientations of well-exposed Holocene lavas on the SRP. Phillips and Wilson (1989) showed that the spatial correlation parameters of permeability could be estimated from the mapped dimensions of lithologic surrogates for high- and low-permeability zones. Thus, by understanding the spatial configuration (morphology) of basalt flows containing IFZs, we can infer the relevant spatial statistics of high-permeability zones from geologic data and can thereby impose realistic quantitative constraints, as well as honor all available

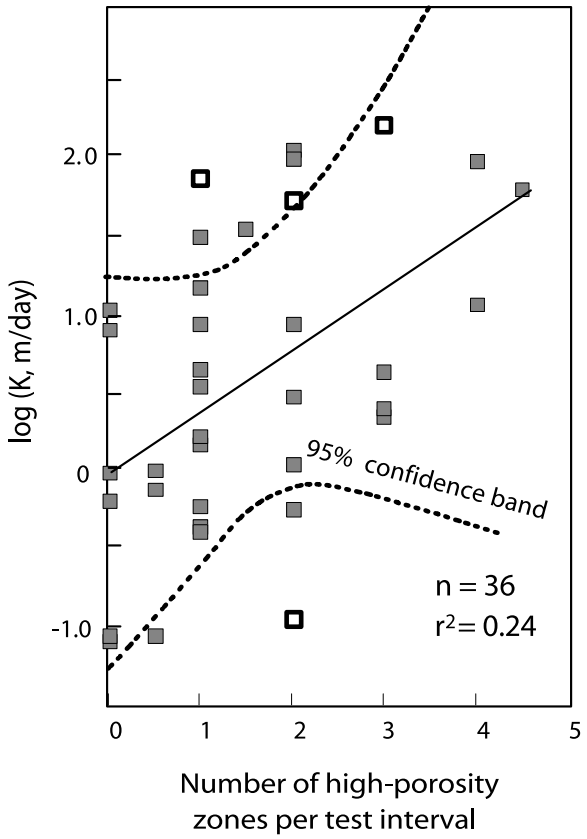

Figure 5. Correlation of the logarithm of permeability measured in TAN well and packer tests (expressed as apparent bulk hydraulic conductivity, or transmissivity/test interval length) and the number of porous zones intersected by the well-test interval. Despite the large scatter, the slope of the regression is significant at the 99 percent confidence level; the 95 percent confidence band of the regression is shown. Porous zones possibly affected by sediment infilling are shown as open squares. Porous zones were picked from interpreted geophysical logs; a porous zone at the edge of a well test interval was assigned half weight. Packer and well test data are from a compilation by A. Wylie (written commun., 1996).

subsurface information, in our stochastic models of permeability distribution.

Data Collection Methods

Field work has focused on parts of the Wapi and Hell's Half Acre flow groups that are relatively accessible and that have been previously mapped (Champion, 1973; Knutson and others, 1990). These areas were chosen as representative of the distal parts of flow groups, in which the morphology of flow units and flow lobes has not been obscured by later flows. The relative importance of topographic slope on flow morphology is different in the two mapped areas. In the eastern salient of the Wapi field (the "eastern lobe" of Champion, 1973), lavas were channeled by a preexisting topographic drainage in an easterly direction until they fanned out on flatter ground (Champion, 1973). In contrast, the northern part of Hell's Half Acre was probably emplaced on a relatively flat, gently undulating surface with no large-scale topographic constraints on flow direction. In both places, the preexisting slopes along which lava flowed were probably low (less than 2 degrees).

The mapping of basalt morphology was initially guided by detailed geologic information in a 4.8-square-km area of the Wapi eastern salient (Champion, 1973). These data were incorporated in a Geographic Information Systems (GIS) format (Figure 6) and referenced to digitized aerial photographs. The Champion geologic map served as a high-resolution training image from which to develop hypotheses about flow morphology and fissure distributions from stereo aerial photographs; using these hypotheses, the mapping of flow units and fissures was extended to areas outside Champion's map area (Figure 7). The same interpretation protocol was also applied to the Hell's Half Acre flow group to map flow units (Figure 8). In all cases, extensive field checks were made on the photogeologic interpretations. Using this approach, fissures greater than about 1.5 m in width and flow lobes greater than about 30 m in areal dimension were mapped. Welhan and others (2002b) also used Global Positioning System (GPS) technology to map a small-scale (<200 m long) lava-flow unit and found that its geometric properties were very similar to those of large-scale lava-flow units mapped from aerial photos.

Characteristics of Large-Scale Inflated Lava-Flow Units

Figure 7 shows flow unit boundaries extended from the Champion (1973) map into the remainder of the Wapi eastern salient from aerial photo and field mapping. The fissures and large-scale flow units shown here represent only the largest features of inflated pahoehoe lavas, since flow lobes and fissures smaller than the resolution of the mapping method were not identified. Figure 7 depicts two of the most important findings in this phase of our work. First, the spatial configuration, hierarchical growth pattern, and fractal-like shape of the large-scale, inflated flow units are the most morphologically distinctive features of these lavas. Second, the spatial arrangement of networks of large fissures near the edges of these flow units is characteristic of all areas in which inflated flow units are exposed.

The unmapped areas between large-scale inflated flow units represent a variety of small-scale inflated lava flows

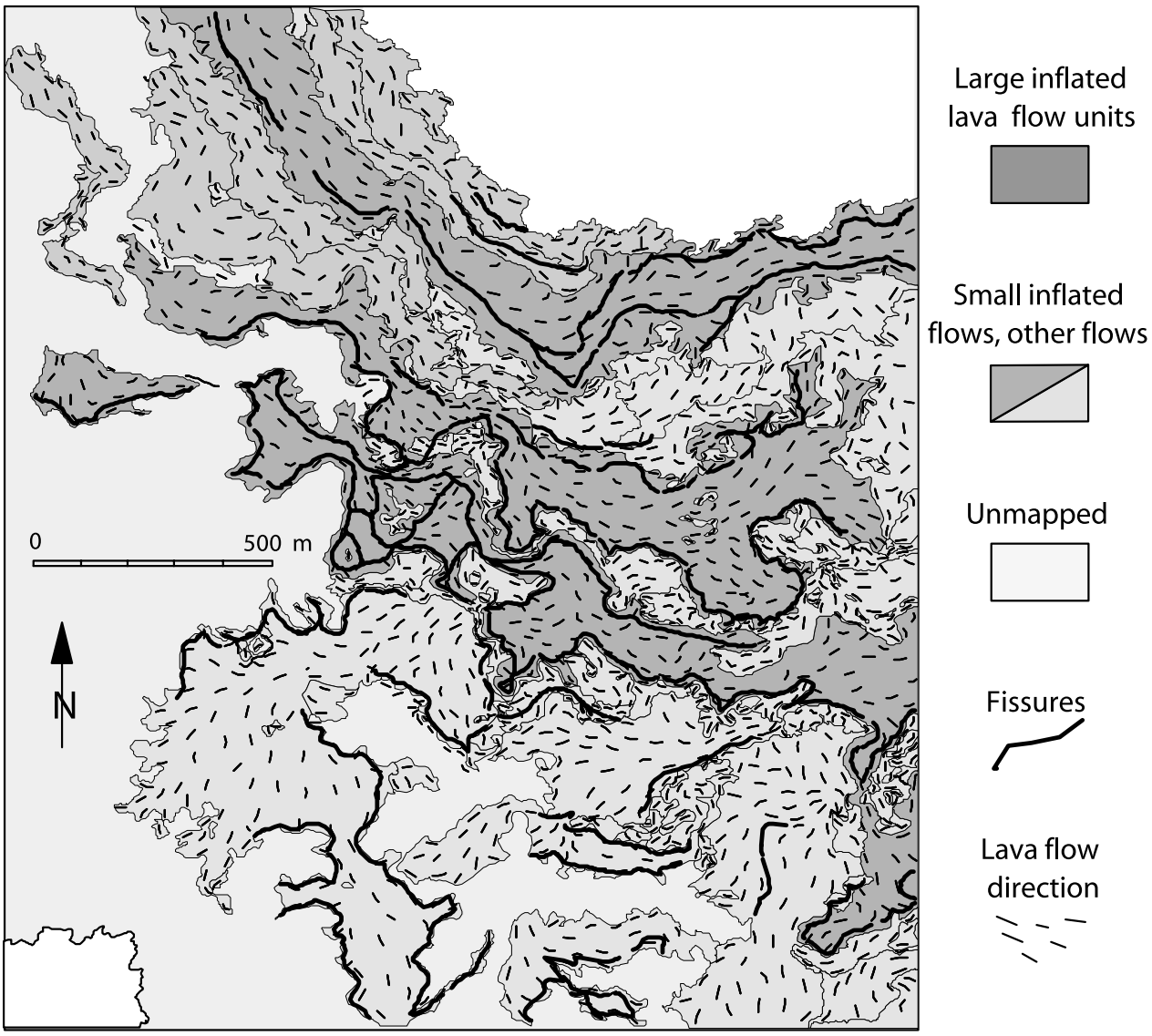

Figure 6. Detailed geologic map of some of the lava-flow features on a part of Wapi flow group, showing large-scale inflated flows, small-scale inflated and other flows, the largest fissures, and lava-flow direction indicators. Predominant lava-flow direction was from the northwest corner of map. Data were digitized from the detailed geologic map of Champion (1973).

(see northernmost section of Figure 6) and chaotic pahoehoe terrain representing lava extruded during deflation of collapsed surfaces or leakage from large-scale inflated flows. These were mapped by Champion (1973) as "secondary flows" (Figure 6). Although not recognized on the Wapi eastern salient, ponded lavas also may occupy part of the areas between the large-scale inflated flows.

Figure 8 shows the same features mapped in a part of the Hell's Half Acre flow group. A third area on the southwestern tip of Wapi (not shown; see Welhan and others, 2002b) that was mapped solely with GPS methods was also found to have the same geometric characteristics at a smaller scale. The similarity of these features (inflated flow units and flow lobes, fissure networks) in the distal parts of different flow groups, in different parts of the same flow group, and at different scales within a flow group suggests that they are characteristic of inflated pahoehoe lava flows on the eastern SRP.

The shapes of these flow units and the arrangement of smaller lobes along their peripheries are similar to inflated pahoehoe flow lobes emplaced during Kilauea eruptions (Figure 3). In accord with the model proposed by Self and others (1998), the thickness of the upper vesicular zones exposed in the walls of large fissures on both the Wapi and Hell's Half Acre flow units appears to be

roughly proportional to the estimated thickness of the flow (from 1-m-thick flow lobes to the largest flow units more than 10 m thick), which is consistent with INEEL corehole observations (Table 3). The flow units and associated lobes are characterized by relatively high topographic relief that is diagnostic of inflated lava flows. Finally, the fissures observed along the margins of flow units are similar to the large, deep tension fissures that are characteristic of inflated pahoehoe lava flows (Self and others, 1998).

The most distinctive morphologic features in the distal parts of Holocene flow groups on the SRP are inflated pahoehoe flow units, composed of smaller flow lobes at various scales. The widely observed characteristics of high relief, fractal-like geometry, and deep fissuring on the surfaces of Holocene flow groups on the SRP indicate that inflated pahoehoe is ubiquitous in the distal and medial parts of Holocene flow groups. From the internal vesicular structure in INEEL basalt core, we inferred that inflated pahoehoe flow lobes are the most volumetrically important component of basalt in the eastern SRP. Therefore, since Holocene basalts are viewed as direct analogs of subsurface basalts, we conclude that inflated flow units are characteristic not only of the distal portions of a flow group but also throughout a flow group's area, obscured beneath ponded lavas and sheet flows.

On this premise, then, we view the inflationary morphology of basalts exposed in the distal parts of Holocene flow groups as an analog of subsurface basalts. In the following sections, we synthesize the relevant spatial characteristics of Holocene basalts. From this information, we will propose a refined conceptual model of the spatial distribution of IFZs in eastern SRP basalts at the local- and meso-scales on which to build quantitative models of lithologic and hydraulic heterogeneity.

Geometry, Fractal Nature, and Surface Characteristics of Flow Lobes

Several factors having relevance for modeling the spatial distribution of IFZs were examined: whether flow units have a fractal shape; the geometry (dimensions and aspect) of flow lobes supporting IFZs; and the proportion of surface area containing high-porosity material (rubble and broken rock). These factors are considered important for inferring the spatial correlation structure of IFZs from mapped geologic information because the spatial extent of IFZs depends on the area and shape of the flow lobes supporting IFZs and because the relative permeability of IFZs depends on the amount and distribution of porous material on lobe surfaces. A fractal geometry would permit extrapolation of inferences derived from the mapping of large-scale features to small-scale features or vice versa.

As discussed previously, a flow unit's geometry is expected to be fractal because of the manner in which lava breakouts and lobe growth occur at the unit's periphery. Figure 9 summarizes the results of fractal dimension analyses on the three flow units and their corresponding fissure networks shown in Figure 8. The fractal dimension was estimated by the box-counting technique (Barnsley, 1988) in which the minimum number, Ni, of boxes of size i, required to cover the boundary or fissure network is determined iteratively. The slope of a log-log plot of Ni versus i defines -D, where D is the fractal dimension. If a flow boundary or fissure network is fractal, its dimension lies between 1.0 (a line) and 2.0 (a plane). As shown in Figure 9, all mapped flow units and fissure networks have similar fractal dimensions, $1.54 \leq D \leq 1.58$; very similar values were obtained for the Wapi flow units at both small and large scales (Welhan and others, 2002b). In contrast, the fractal dimension of the boundary of the flow group shown in Figure 8 is significantly lower, at 1.25. However, this is very similar to the value of 1.21 determined by Bruno and others (1992) using a different measurement method at a much smaller measurement scale.[9] This similarity provides further corroboration that these geologic features are indeed fractal or self-similar over a wide range of scales. The fractal nature of flow unit and flow group boundaries indicates that the process of emplacing pahoehoe lava is a self-similar process producing self-similar geometry in lobes over a range of scales. Because of this fractal nature, the characteristics of large-scale inflated lava flows can be extrapolated and used to infer the geometry and spatial distribution of lobes and fissure networks at smaller scales.

Although the shape of inflated pahoehoe flow lobes is irregular, their approximate lengths, widths, and aspect ratios can be defined by various methods (Welhan and others, 2002b), including the manual approximation approach used in Figure 3b, and the fitting of rectangular or elliptical shapes of equivalent area and perimeter to the measured lobes. The median length to width aspect of lobes mapped in the Wapi eastern salient (Figure 7) is 3.0 : 1. Individual lobe aspect ratios vary from 1 : 1 to more than 10 : 1, but the range of median aspect ratios measured in eastern SRP flow groups is remarkably narrow: 2.9 : 1 and 4 : 1 in Hell's Half Acre (Knutson and others, 1990, and this work, respectively); 3 : 1 in the North and South Robbers flow groups (Welhan and others, 1997a); and greater than 2 : 1 in Box Canyon (Knutson and others, 1990). The median aspect ratio of

[9]Bruno used a rod-counting method to measure the length of the boundary, where the largest measurement scale was a 16-m-long chain; by comparison, our largest box dimension was 2.5 km in the box-counting method.

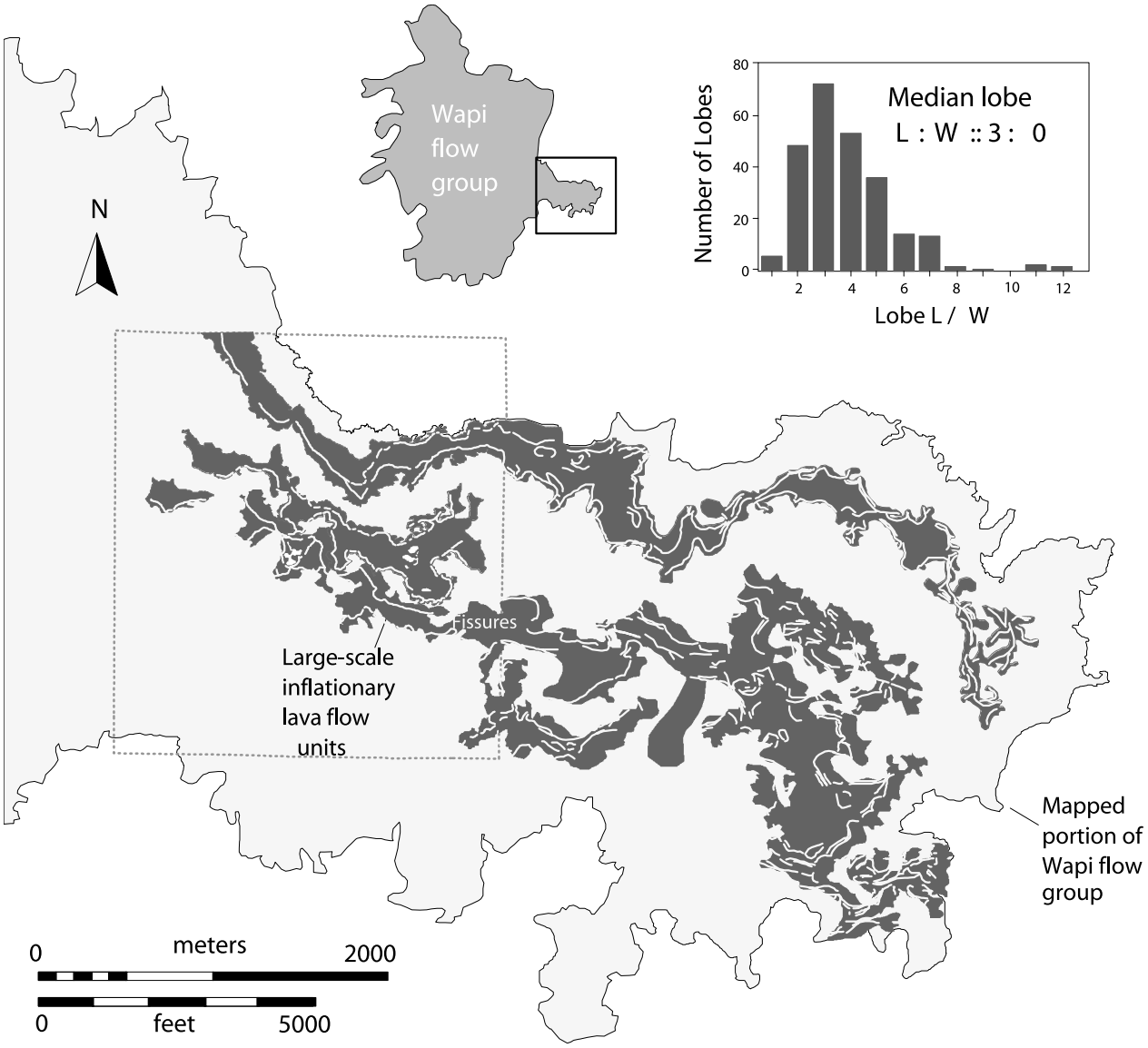

Figure 7. Large-scale, inflated lava-flow units (in black) and fissures (light lines) that have been identified and mapped from aerial imagery on the eastern salient of the Wapi flow group. Dashed rectangle indicates the location of the geologic map of Champion (1973) used to develop the interpretive protocol for air-photo mapping of Holocene lava terrain (see Figure 6).

all lobes mapped in the Wapi and Hell's Half Acre study areas in this work is 3.5 : 1. The uniformity of median aspect ratios among eastern SRP inflated flow lobes and their similarity with the Kilauea flows shown in Figure 3b (L : W :: 3.5 : 1) suggest that this geometry may be characteristic of inflated pahoehoe lava.

The amount of porosity on the lava-flow surface is also an important constraint for modeling the spatial distribution of IFZs on inflated lava flows. High-permeability zones are expected to develop between flow lobes where fractured, broken, or rubbly material occurs. In a limited survey of pahoehoe surfaces in Hell's Half Acre, Knutson and others (1990) found that such high-porosity material covered only about 50 percent of the lava-flow surfaces. An analysis of our field data is consistent with their estimates and indicates that rubble is less frequently found on noninflated (ponded) lava surfaces.

Our field data also corroborate the frequency of rubble observed in core-holes and support the suggestion raised previously in the discussion of Figure 5 that lobe contacts have variable permeability. As shown in Table 3, 25 percent of all lobe contacts in TAN and CPP core have

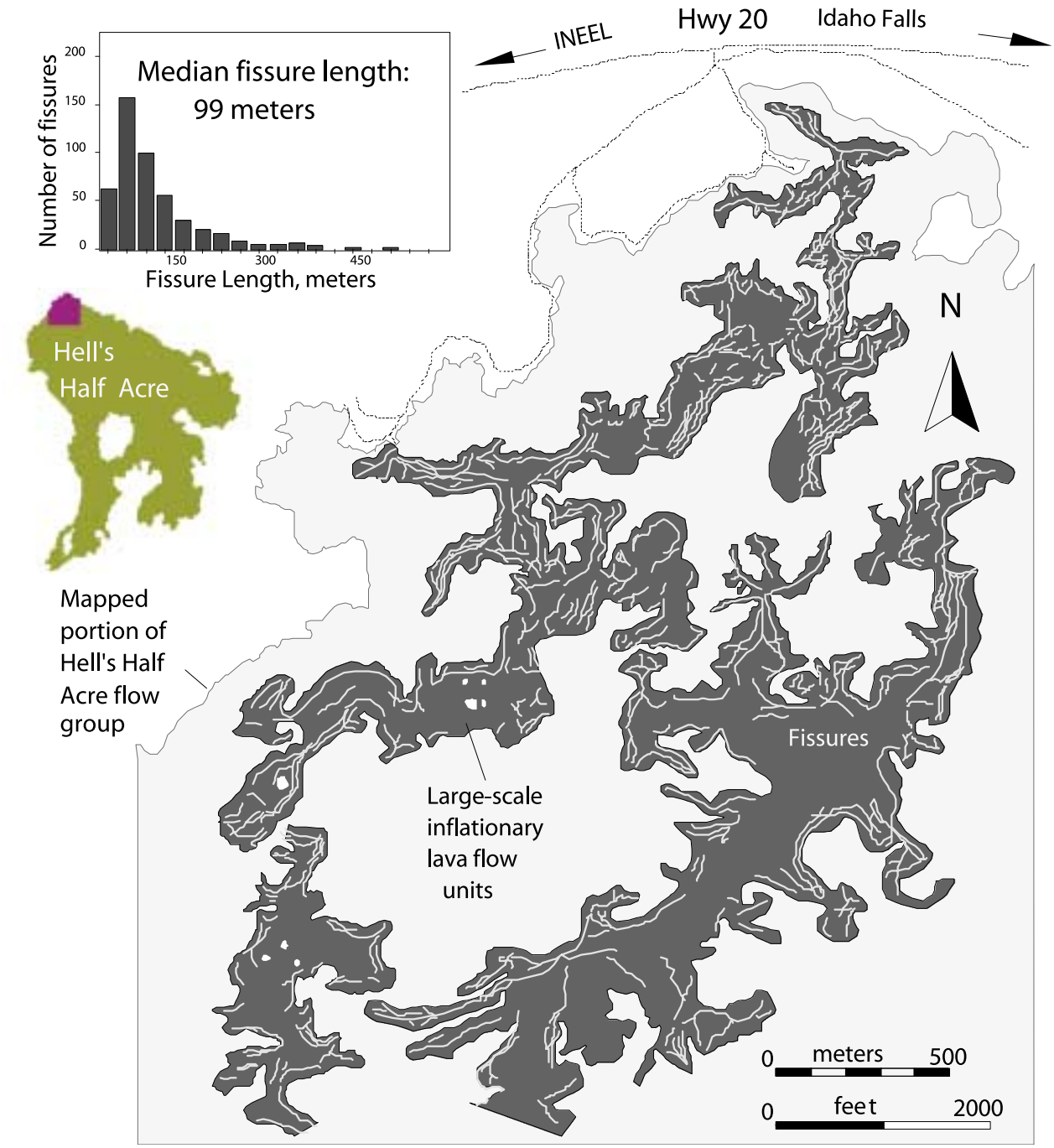

Figure 8. Large-scale, inflated lava-flow units and fissures on Hell's Half Acre flow group. Interflow zones occur at upper and lower surfaces of basalt flows and potentially along fissured zones where fissures remain open and interconnected. Median length of individual fissures is about 100 m.

rubble; if we include those lobe contacts inferred to have rubble the proportion rises to 52 percent. This proportion is very similar to that reported by Knutson and others (1990) for rubbly and broken material on Hell's Half Acre lava surfaces. The implication is that varying amounts of porous material are distributed on lobe surfaces. Once buried beneath younger lava, these lobe contacts will have variable porosity and permeability depending on the amount of porous material present, leading to high-permeability zones that may be discontinuous or patchy. This is in accord with the scatter of permeability values about the correlation shown in Figure 5.

Fissure Networks

Large-scale tension fissures along the tops and near the edges of lava-flow units (Figures 7 and 8) are characteristic of inflated pahoehoe and occur in all sizes of inflated flow lobes. The median length of mapped fissures (those with apertures exceeding about 1.5 m) is as much as 100 m (Figures 7 and 8). Networks of such fissures, however, may extend over kilometer distances depending on the degree of interconnectivity of individual fractures; the aspect ratio of network length to network width is estimated to be at least 10 : 1.

Fissure networks may be much more important to the permeability structure of the aquifer than previously recognized. Clearly, much of their potential hydraulic importance depends on the degree to which they remain open and interconnected after burial. Fissures exposed at the surface during a prolonged volcanic hiatus and then filled with fine-grained sediment will certainly have low permeability. The fate of fissures not filled by sediment but buried by lava, however, is less obvious. In vertical outcrop, numerous examples can be found of fissures completely or partially filled by younger basalt and of others remaining substantially open.

Of twenty-eight buried tension fractures exposed in vertical outcrops in Box Canyon, half remain completely or partially open; a similar proportion can be observed in a roadcut on Interstate-84, west of Massacre Rocks. Of the Box Canyon fractures, the median proportion of original fissure depth that remains open following lava burial is 17 percent. Knutson and others (1992) proposed that large pore voids in rubble that is inundated by younger lava could be bridged owing to the viscosity of the lava; this would serve to preserve the primary rubble porosity, thereby creating a high-porosity IFZ. A viscous bridging mechanism also may be important in fissure filling. Although several Box Canyon fissures wider than 1 m remain wholly or partly open, the mean aperture of fissures wholly or partly open because of lava bridging was found

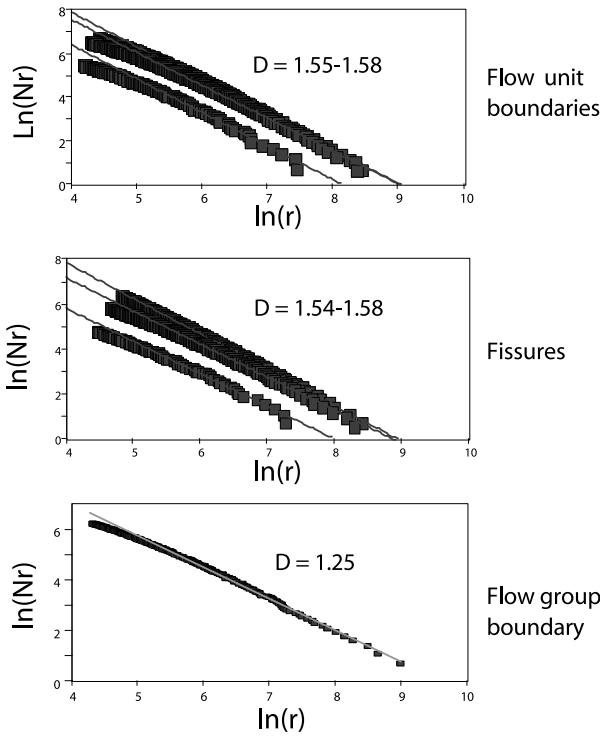

Figure 9. Fractal dimension analyses of the boundaries and fissure networks of the three mapped flow units on Hell's Half Acre and the portion of the flow group boundary adjacent to them. The fractal dimension is determined by the box-counting method, where the logarithm of the minimum number of boxes required to cover the boundary or fissure network, ln(Nr), is plotted against the logarithm of box size, ln(r); the negative slope of the plot gives the fractal dimension.

to be 0.1 m. Of more than 1,000 tension fractures measured on seven lava-flow units in Hell's Half Acre, more than half have a surface aperture less than 0.1 m wide and could remain open following inundation by lavas with viscosities similar to those in Box Canyon. The high spatial density of such small- and medium-aperture fissures near the edges of lobes also makes it likely that they interconnect and could therefore represent an important network of highly connected fracture porosity.

Should such fracture networks prove to be important features of eastern SRP basalts, the high permeability and extreme hydraulic anisotropy they would impart to the aquifer would explain such high-volume, localized spring discharges from the eastern SRP as are found at Thousand Springs. Large-scale, interconnected fracture networks may also explain how chlorine-36 derived from deep injection well disposal at the CPP is able to migrate over 25 km from the point of injection with minimal dispersion (Cecil and others, 2000).

IMPLICATIONS FOR GROUND-WATER FLOW

REFINED CONCEPTUAL MODEL OF INTERFLOW ZONES

The lithologic characteristics of pahoehoe giving rise to high permeability are discontinuous zones of rubble and broken material on the upper surfaces and along the edges of flow lobes, and networks of fissures developed along inflated flow lobes. Since such porous zones are associated with contacts between flow lobes in the subsurface, the original connotation of a permeable "interflow zone" remains appropriate for both. We propose two types of interflow zones: Type-1 is developed in rubbly, broken material at lobe contacts; Type-2 is developed in interconnected networks of fissures along the edges of flow lobes and flow units. The hydraulic characteristics of both types are determined by their porosity, sediment content, the dimensions and aspect ratios of the flow lobes supporting the IFZs, and the manner in which IFZs are spatially arranged and the degree to which they are interconnected.

The lateral spatial continuity and anisotropy of Type-1 IFZs are expected to be a function of the lateral dimensions and aspect ratios of flow lobes and flow units, and of the patchiness and interconnection of rubble and fractured material on flow tops. If fissure networks remain open and interconnected after burial, the lateral spatial continuity of Type-2 IFZs may be orders of magnitude larger than that of Type-1 and with significant directional anisotropy. The permeability measured in a well correlates in a general fashion with the number of IFZs intersected by the well. However, because the permeability of IFZs is highly variable, the well-test permeability should be viewed as a deterministic function of IFZ vertical spatial density plus a substantial stochastic component.

MESO-SCALE CONCEPTUAL MODEL

Figure 10 depicts a conceptual model of the internal structure of an eastern SRP basalt lava-flow group, based on a cross-section by M. Kuntz (written commun., 1997) and our field observations. The zonal designations are based on a combination of topographic relief, the dominant style of lava flows at the surface, and in the case of near-vent facies, internal structures such as cinders, spatter, and shelley pahoehoe (Kuntz and others, 1992; Champion, 1973). Lava advance in the distal zone is primarily via large-scale, tube-fed, inflationary flow units. The resulting morphology of these inflated flows is responsible for the characteristic high relief typical of the distal zone.

During eruption, the position of the distal-medial zonal transition may migrate from the vent area as tube-fed emplacement of inflated lava flows extends the outer perimeter of the flow group, while smaller-scale inflated flows and ponding flows gradually fill the topographic lows between the large-scale inflated features in an expanding medial zone. Alternatively, the inflationary features may first grow laterally outward to substantially their present extent, and the medial zone may not form until late in the eruptive history when the initially high relief of the inflated topography is reduced by later eruptions of lava that fill the topographic lows created by the inflated structures. The most important feature of this conceptual model, however, is that inflated pahoehoe flows are ubiquitous in the basal part of the flow group and are not confined to the distal zone. The volumetric proportion of inflated pahoehoe within the entire flow group is estimated on the basis of INEEL core data to be 80 percent.

The second significant feature of the conceptual model shown in Figure 10 is the relatively small volume of shelly- and slab-pahoehoe in the proximal (near-vent) zone. Although not as important volumetrically as inflated lava flows, these lithotypes are extremely porous and may impart significant permeability localized to areas near source vents. Isolated intervals of extremely frothy, scoriaceous basalt lacking the internal vesicular structure characteristic of inflated lava have been noted in core and identified as near-vent facies (S. Anderson, oral commun., 1997; this work). However, because these occurrences are rare, and because little can be inferred of their spatial distribution, we focus subsequent discussion on porous features in the distal and medial zones.

Figure 11 depicts the meso-scale conceptual model that is the result of stacking numerous flow groups. This concept integrates all the information we have accumulated on hydraulically significant features in Holocene lavas and refines the Lindholm-Vaccaro and Anderson models of the eastern SRP aquifer. A simple "layer-cake" hydrostratigraphy cannot be justified on the meso-scale, because the complex flow-lobe geometry generates a heterogeneous mix of various basalt and sedimentary lithologic elements in a spatially complex arrangement of variably interconnected permeable zones and aquitards. During periods of relatively high volcanic effusion rates, successive generations of lava flows from the same or nearby sources may inundate one another and coalesce laterally and vertically into more extensive supergroups free of sediment influences.

The basalt sections of the stratigraphy are dominated by large-scale, inflated pahoehoe lavas supporting Type-1 and Type-2 permeable IFZs. Their hydraulic nature and

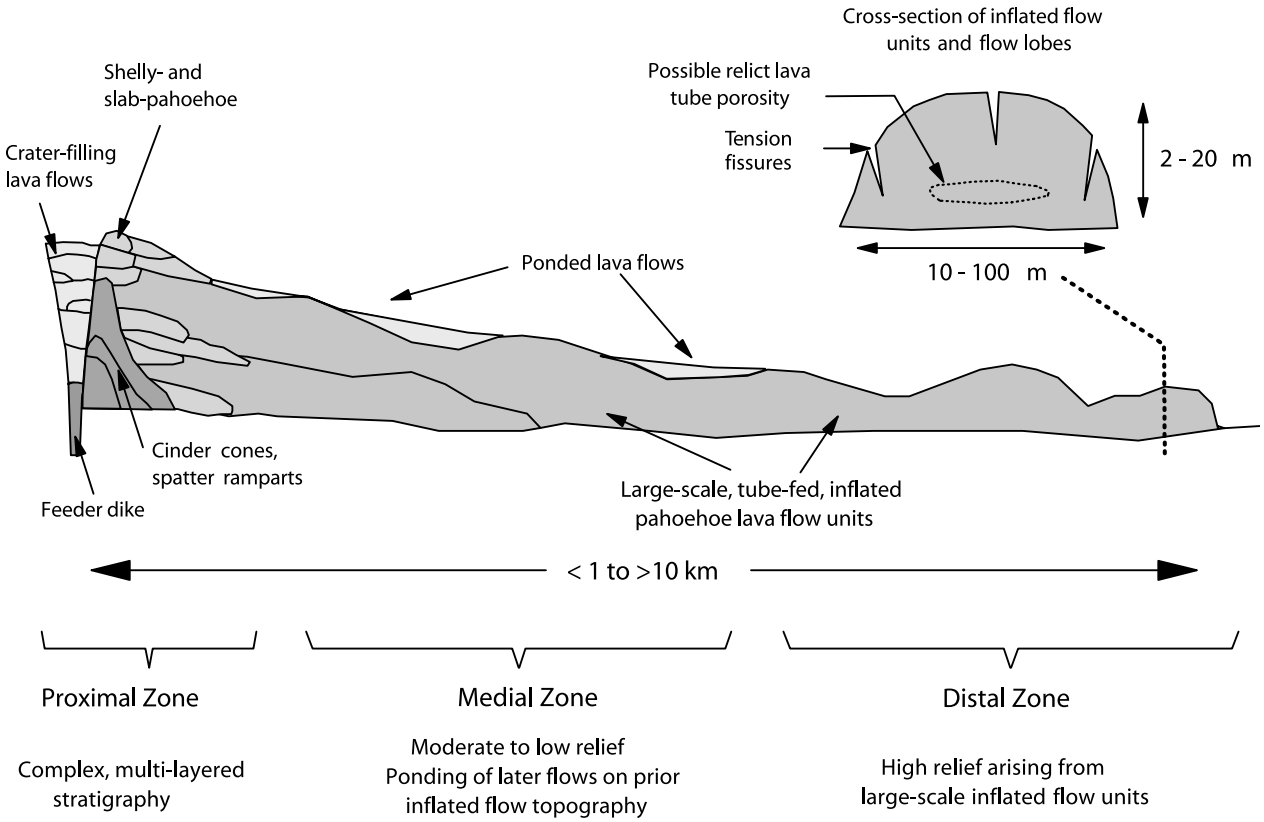

Figure 10. Simplified conceptual model of the internal architecture of a Snake River Plain basalt lava-flow group, based on a cross-section by M. Kuntz (written commun., 1997). Not drawn to scale; vertical dimension is greatly exaggerated. Topographic relief in medial and proximal zones is reduced by later lava that fills depressions between large-scale flow units originally in the distal zone of the evolving flow group. Structures characteristic of the distal zone, therefore, may be common throughout most of the basal layers of the medial zone.

spatial continuity may be quite different, however, leading to different degrees of spatial continuity of permeable regions and preferential flow in the aquifer. The impact of these zones on the measured permeability in well tests will depend on the amount of fine-grained sediment infill and the degree of spatial interconnection within and between IFZs.

Low-permeability elements in the model include massive, regionally extensive sedimentary interbeds and thinner, less spatially continuous accumulations of sediment, which may represent primary deposition or vertical infiltration of fines from higher in the section. During a volcanic hiatus, fine-grained eolian sediment fills the high-porosity zones on exposed surfaces of basalt flow lobes and reduces permeability; in some areas such as TAN, whose topographic elevation has been low for long periods, other fine-grained facies of lacustrine or playa origin also were introduced. In such areas, downward-infiltrating sediment carried by local recharge may reduce the permeability of Type-1 and Type-2 zones at considerable depth below the surface. For the most part, however, permeable zones within the flow group are unaffected and remain laterally interconnected over the scale of the sediment-blanketed flow group or supergroup.

Basalt occurring in the depressions between large, inflated flows can be small-scale inflated flows (supporting small-scale Type-1 and Type-2 permeable zones) and ponded flows. Although we have no data on the relative permeability of ponded lava flows, field observations on Hell's Half Acre indicate that ponded flows lack fissure networks, have substantially fewer fractures than inflated flows, and contain less rubble on their surfaces. This leads us to propose that preferential flow paths are less important in ponded flows relative to inflated flows. On the premise that most of the basalt section is composed of inflated lava flows, we infer that the hydraulic characteristics of large, inflated lavas exert the most important control on hydraulic heterogeneity in the aquifer.

PERMEABILITY CHARACTERISTICS

Figure 12 shows a cumulative frequency distribution of apparent bulk permeabilities derived from well tests in the TAN area (Welhan and others, 2002a) and plotted

as the natural logarithm of hydraulic conductivity (lnK). The distribution is essentially lognormal. Sixty-three percent of these measurements are from open-well tests on intervals spanning multiple lobe contacts. On the basis of the lithology-permeability associations in Table 3 and Figure 5, and the statistical distribution in Figure 12, Welhan and Wylie (1997) and Welhan and others (2002a) proposed that three lithologic categories govern the permeability distribution in the eastern SRP aquifer: (1) high-permeability zones in basalt, represented by hydraulic conductivity values above the 90th percentile lnK threshold of about 100 m per day (rubble and fracture zones, Table 3); (2) massive basalt whose upper permeability range corresponds to the 10th percentile lnK threshold of about 0.3 m per day (Table 3); and (3) low-permeability sediments whose measured hydraulic conductivities also fall below the 10th percentile lnK threshold of about 0.3 m per day.

Welhan and others (2002a) developed a simple model based on linear averaging of IFZ and massive basalt permeabilities within a well test interval to explain the relationship in Figure 5. Their analysis concluded that the statistical distribution in Figure 12 can be modeled as the weighted average of permeabilities representing massive basalt and IFZs in direct proportion to the number of IFZs intersected by the well. In accord with the earlier discussion of factors that affect IFZ permeability, the model also predicts that IFZ permeability must be statistically variable, albeit with a variance far less than that characterizing the distribution in Figure 12.

The relationship of lithology to permeability has been evaluated in thirty-six of these well test zones (see Figure 5) and provides justification for surmising that lnK values intermediate between the 10th and 90th percentiles represent either variable interconnectedness of high-permeability Type-1 and Type-2 IFZs or variable degrees of sediment influence. Sediment interbeds are known aquitards (Kaminsky and others, 1993), so it is reasonable to surmise that they, together with massive basalt, help define the 10th percentile lnK threshold. However, since evidence of their impact on well-test permeability is lacking from the data in Figure 5, we assume that post-

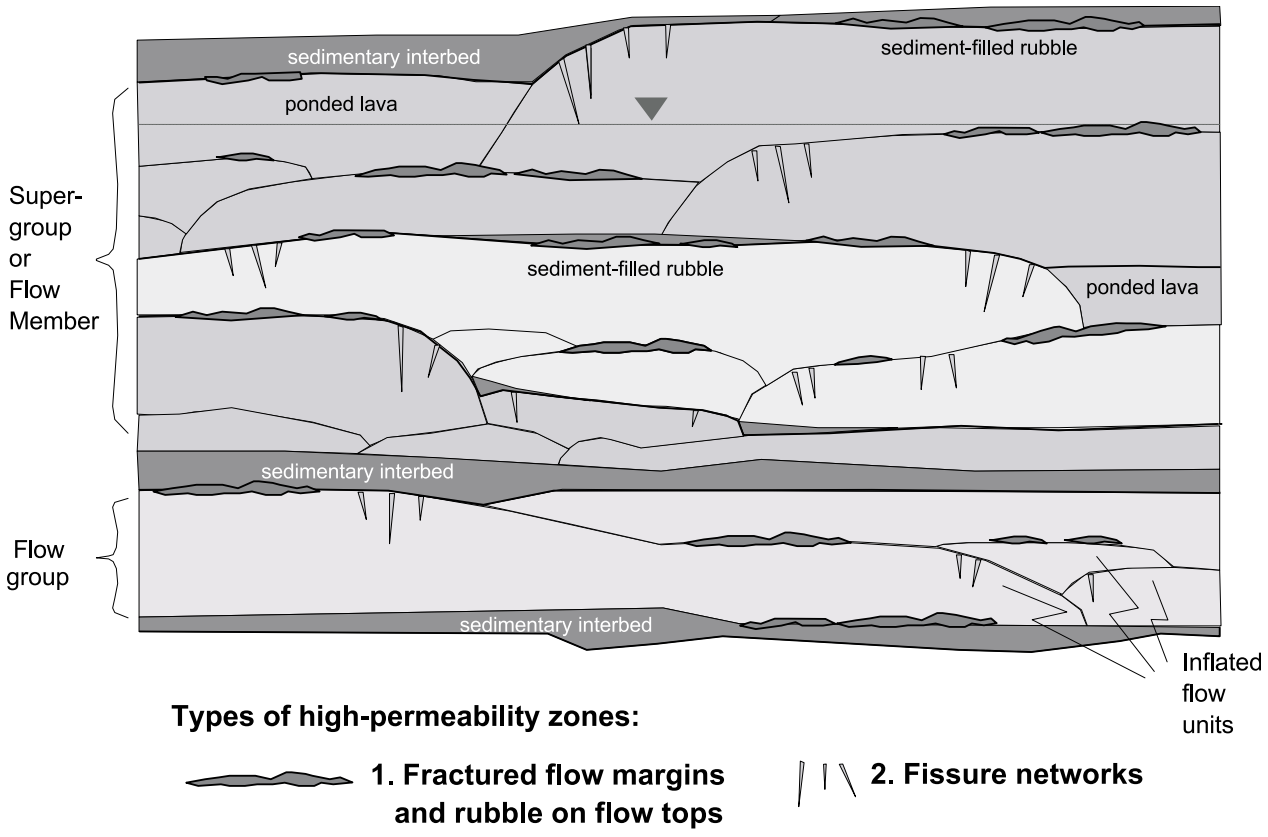

Figure 11. Refined conceptual model of volcanic stratigraphy created by inflated, tube-fed pahoehoe lava flows, showing two types of potential high-permeability zones: (1) rubble and fractured flow tops and margins, and (2) large tension fissures and fissure networks. Also shown are low-permeability sedimentary interbeds and discontinuous sediment accumulations in some interflow zones.

burial sediment infiltration has had a minor effect on IFZ permeability at TAN.

As discussed in reference to Figure 5, the occurrence of high-permeability zones (both Type-1 and Type-2) may be the most important factor in determining the aquifer's hydraulic character. The variability of IFZ permeability inferred from Figure 5 and the permeability model are consistent with the patchy distribution of porous material on Holocene lava flows, but could also reflect the variability of hydraulic interconnection within and between Type-1 and Type-2 zones. A semilogarithmic relationship between permeability and the number of porous zones implies that the probability of finding a highly permeable zone increases with the size of the test interval, in accord with commonly observed behavior in heterogeneous aquifers. This in turn suggests that hydraulic tests conducted in wells with large open-intervals will tend to have a higher apparent bulk permeability than tests conducted in small intervals.

Such an hypothesis may explain the range of well test data from the CPP where median bulk hydraulic conductivity (transmissivity/open-interval length) measured in wells is some forty times higher than at TAN; CPP wells also demonstrate a correlation like that of Figure 5 (Welhan and others, 1997b). Work by Glover and others (1997, 2002) has shown that several factors possibly responsible for higher permeability in CPP wells—such as more or thicker rubbly lobe contacts, the vertical spatial density of lobe contacts, or the occurrence of coarse sediment—can be ruled out. The median well test interval length in CPP wells, however, is seven times greater than that in TAN wells (43 m versus 6 m). Therefore, the higher apparent hydraulic conductivity of CPP wells may simply reflect a greater number of IFZs that are intersected. A comparative analysis of IFZs based on geophysical logs between TAN and CPP wells will afford a test of this hypothesis.

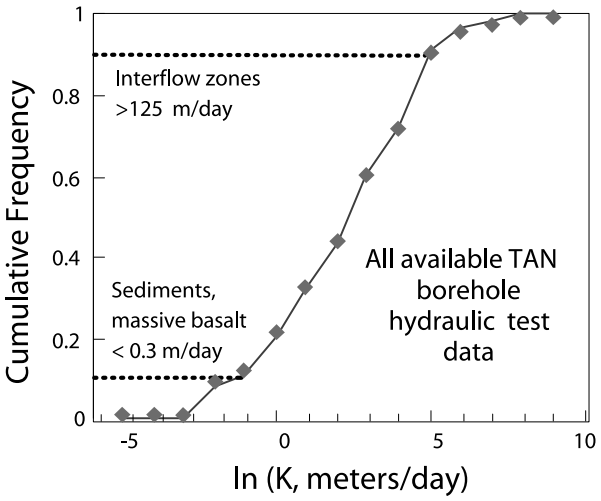

Figure 12. Hydraulic elements in the TAN aquifer defined on the basis of high- and low-permeability thresholds on the cumulative frequency distribution of well permeability data (expressed as apparent bulk hydraulic conductivity, K). Permeability thresholds correspond to massive basalt and sediment with K less than 0.3 m per day; and basalt interflow zones, with K greater than 125 m per day. Well test data was compiled and provided by A. Wylie (written commun., 1996).

SUMMARY AND CONCLUSIONS

We have outlined the basic elements of a refined conceptual model of basalt heterogeneity responsible for the hydraulic heterogeneity in the eastern SRP aquifer. We have developed a descriptive terminology for basalt flow morphology of different scales that has been integrated with data on the hierarchical growth of Hawaiian basalt lava flows to further understand the morphology and spatial geometry of eastern SRP basalts. Comparing internal lava-flow structures in basalt core of widely differing ages with features in Holocene basalts of the SRP supports the contention that the style of emplacement of olivine-tholeiitic lava flows in the eastern SRP has remained unchanged since the mid-Quaternary. Thus, Holocene basalts can be used as analogs of their subsurface counterparts to understand the spatial distribution of preferential ground-water flow zones in this basalt-hosted aquifer.

Core measurements and field mapping indicate that inflated pahoehoe lavas represent more than 80 percent of the lavas in the eastern SRP. This suggests that the inflated pahoehoe morphology exposed in distal zones of Holocene flow groups is the most volumetrically important basalt morphology of SRP shield volcanoes. The geometry of large-scale, inflated pahoehoe lava-flow lobes (as well as the composite flow group) is characterized by a fractal shape, reflecting a hierarchical growth process involving successive lava breakouts, the creation of new lobes through inflation, and subsequent new breakouts where the lobe's inflating surface undergoes brittle failure. The fractal lobe geometry permits generalizing from aerial photo-derived measurements of large lobes having median aspect ratios of the order of 30 : 10 : 1-2 (length to width to height) to smaller scales that are of interest to stochastic ground-water flow modeling.

Two types of potential high-permeability features within inflated lava flows have been identified during mapping of Holocene lava morphology. Type-1 permeable zones occur in highly porous, rubbly, and broken material at the contacts between lava-flow lobes. Their lateral spatial extent is constrained by the areal dimensions of flow lobes, but they may be patchy or discon-

tinuous depending on the distribution of porous material on lobe surfaces. Type-2 permeable zones may exist in fissure networks hosted in inflated lava-flow units. Their relative importance can only be surmised from limited outcrop data where fissures remain partly or wholly open when buried by younger lavas. The horizontal spatial correlation structure of these two types of permeable zones may be quite different.

We have presented evidence that the permeability measured in individual wells is semilogarithmically correlated with the number of porous zones intersected by the well. However, the large scatter about the observed correlation suggests that the permeability of potential interflow zones is highly variable, consistent with the irregular spatial extent of high-permeability zones and the nature of their interconnections. The semilogarithmic relationship is consistent with the expectation that the probability of finding a very permeable zone in a heterogeneous aquifer increases as the spatial scale of the hydraulic test increases.

The variation of permeability in the aquifer, as measured in well tests, is consistent with the premise that three principal lithologies control permeability in this aquifer. The lowest 10 percent of permeabilities (less than 0.3 m per day as hydraulic conductivity) measured at the TAN facility correspond to the permeability of fine-grained sediments and of massive, nonfractured basalts. The highest 10 percent of well permeabilities (greater than 100 m per day) corresponds to the permeabilities of open fractures and rubble. Intermediate permeability values primarily reflect variations in the number of interflow zones intersected by a well.

ACKNOWLEDGMENTS

We wish to thank the many people who have helped to mold the ideas presented in this paper: Duane Champion of the U.S. Geological Survey for providing copies of his Wapi maps; Steve Anderson, USGS-INEEL, for fruitful discussion on his basalt stratigraphic interpretations; Dick Smith at the INEEL for aerial imagery and access to unpublished reports and data and to Cheryl Whittaker for her patience and perseverance in digging up those reports and data files. We also thank Mel Kuntz of the USGS, Denver, Scott Hughes and Mike McCurry of Idaho State University, and Denny Geist of the University of Idaho for their insights into the basalt volcanology of the eastern SRP, and Warren Barrash of Boise State University for his helpful review of the manuscript. This work was funded by the U.S. Department of Energy through grant No. DE-FG07-96ID13420 to the Idaho Water Resources Research Institute and the Idaho Universities Consortium.

REFERENCES

Ackerman, D.J., 1991, Transmissivity of the Snake River Plain aquifer at the Idaho National Engineering Laboratory, Idaho: U.S. Geological Survey Water Resources Investigations Report 91-4058, 35 p.

———, 1995, Analysis of steady-flow and advective transport in the eastern Snake River Palin aquifer system, Idaho: U.S. Geological Survey Water Investigations Report 94-4257, 25 p.

Anderson, S.R. 1991, Stratigraphy of the unsaturated zone and uppermost part of the Snake River Plain aquifer at the ICPP, INEL, Idaho: U.S. Geological Survey Water Resources Investigations Report 91-4010, 71 p.

Anderson, S.R., D.J. Ackerman, M.J. Liszewski, and R.M. Feiburger, 1996b, Stratigraphic data for wells at and near the Idaho National Engineering Laboratory, Idaho: U.S. Geological Survey Open-File Report 96-248, 27 p.

Anderson, S.R., and B. Bowers, 1995, Stratigraphy of the unsaturated zone and uppermost part of the Snake River Plain aquifer at Test Area North, Idaho National Engineering Laboratory, Idaho: U.S. Geological Survey Water Resources Investigations Report 95-4130, 47 p.

Aubele, J.C., L.S. Crumpler, and W.E. Elston, 1988, Vesicle zonation and vertical structure of basalt flows: Journal of Volcanology and Geothermal Research, v. 35, p. 349-374.

Bennecke, W.M., 1996, Basalt features observed in outcrops, cores, borehole video imagery and geophysical logs, and basalt hydrogeologic study at the Idaho National Engineering Laboratory, eastern Idaho: Boise State University M.S. thesis, 178 p.

Bruno, B.C., 1994, Lava flow dynamics: Clues from fractal analysis: University of Hawaii Ph.D. dissertation, 247 p.

Bruno, B.C., G.J. Taylor, S.K. Rowland, P.G. Lucey, and S. Self, 1992, Lava flows are fractals: Geophysical Research Letters, v. 19, p. 305-308.

Cashman, K.V., and J.P. Kauahikaua, 1997, Reevaluation of vesicle distributions in basaltic lava flows: Geology, v. 25, p. 419-422.

Cecil, L.D., J.A. Welhan, J.R. Green, S.K. Frape, and E.R. Sudicky, 2000, Use of chlorine-36 to determine regional-scale aquifer dispersivity, eastern Snake River Plain aquifer, Idaho: Nuclear Instruments and Methods in Physics Research B, v. 172, p. 679-687.

Champion, D.E., 1973, The relationship of large scale surface morphology to lava flow direction, Wapi lava field, southeastern Idaho: State University of New York, Buffalo, M.S. thesis, 44 p.

Deutsch, C.V., and A.G. Journel, 1998, GSLIB Geostatistical Software Library and User's Guide: Oxford University Press, New York, 369 p.

Frederick, D.B., and G.S. Johnson, 1996, Estimation of hydraulic properties and development of a layered conceptual model for the Snake River Plain aquifer at the Idaho National Engineering Laboratory, Idaho: Idaho Water Resources Research Institute, Research Technical Completion Report, 67 p.

Garabedian, S.P., 1989, Hydrology and digital simulation of the regional aquifer system, eastern Snake River Plain, Idaho: U.S. Geological Survey Open-File Report 87-237, 151 p.

Gego, E., and G.S. Johnson, 1998, Stochastic simulations of contaminant transport in the Snake River Plain aquifer: MODFLOW '8 International Conference, Golden, Colorado, October, 1998.

Gego, E.L., G.S. Johnson, M.R. Hankin, A.H. Wylie, and J.A. Welhan, 2002, Modeling groundwater flow and contaminant transport in the

Snake River Plain aquifer: A stochastic approach, *in* P.K. Link and L.L. Mink, eds., Geology, Hydrogeology, and Environmental Remediation: Idaho National Engineering and Environmental Laboratory, Eastern Snake River Plain, Idaho: Geological Society of America Special Paper 353, p. 249-261.

Glover, J., L. Davis, and J. Welhan, 1997, The use of borehole geophysical logs and geologic data for stochastic simulation of hydraulic conductivity in the Snake River Plain aquifer: Connections '97—Ground-Water in the Rocky Mountain Region, Technical Workshop Abstracts, p. 49.

Glover, J.A., J.A., Welhan, and L.L. Davis, 2002, Identification of basalt interflow zones with borehole geophysical and video logs at the Idaho National Engineering and Environmental Laboratory, Idaho: Geologocal Society of America Data Repository Item 2002041, available at <http://www.geosociety.org/pubs/ft2002.htm>.

Greeley, Ronald, 1982, The style of basaltic volcanism in the eastern Snake River Plain, Idaho, *in* Bill Bonnichsen and R.M. Breckenridge, eds., Cenozoic Geology of Idaho: Idaho Bureau of Mines and Geology Bulletin 26, p. 407-422.

Hackett, W.R., and R.P. Smith, 1994, Volcanic hazards of the Idaho National Engineering Laboratory and adjacent areas: Lockheed-Idaho Technologies Company Report INEL-94/0276, 31 p.

Hegmann, M., and S. Wood, 1994, Hydrostratigraphy of the Snake River Plain aquifer beneath the RWMC at the INEL: A preliminary report: Proceedings, 30th Engineering Geology Geotechnical Engineering Symposium, p. 195-206.

Hon, K., J. Kauahikaua, R. Denlinger, and K. Mackay, 1994, Emplacement and inflation of pahoehoe sheet flows: Observations and measurements of active lava flows on Kilauea Volcano, Hawaii: Geological Society of America Bulletin, v. 106, p. 351-370.

Hughes, S.S., M. McCurry, and D.J. Geist, 2002, Geochemical correlations and implications for the magmatic evolution of basalt lava flow groups, *in* P.K. Link and L.L. Mink, eds., Geology, Hydrogeology, and Environmental Remediation: Idaho National Engineering and Environmental Laboratory, Eastern Snake River Plain, Idaho: Geological Society of America Special Paper 353, p. 151-173.

Jobe, S.A., 1996, Petrography and paleomagnetism of core ICPP-COR-A-023 and correlation of a basalt lava flow sequence, Idaho National Engineering Laboratory: San Fransisco State University B.S. thesis, 23 p.

Johannesen, C., L. Davis., T. Funderberg, and J. Welhan, 1997, Basalt surface morphology as a constraint on lateral spatial correlation structure in stochastic simulations of hydraulic conductivity in the Snake River Plain aquifer: Connections '97—Ground-Water in the Rocky Mountain Region, Technical Workshop Abstracts, p. 48.

Kaminsky, J.F., K.N. Keck, A.L. Schafer-Perini, C.F. Hersley, R.P. Smith, G.J. Stormberg, and A.H. Wylie, 1993, Remedial investigation final report with addenda for the Test Area North groundwater operable unit 1-07B at the Idaho National Engineering Laboratory: EG&G Report EGG-ER-10643, 96 p.

Keys, W.S., 1997, A Practical Guide to Borehole Geophysics in Environmental Investigations: Lewis Publishers, New York, 176 p.

Knutson, C., 1993, Geophysical well logging and formation characterization, RWMC area: EG&G Report, unpubl. report, 57 p.

Knutson, C., K.A. McCormick, J.C. Crocker, M.A. Glenn, and M.L. Fishel, 1992, 3D RWMC vadose zone modeling: EG&G Report EGG-ERD-10246.

Knutson, C.F., D.O. Cox, K.J. Dooley, and J.B. Sisson, 1993, Characterization of low-permeability media using outcrop measurements: Proceedings of the 68th Annual Technical Conference and Exhibition of the Society of Petroleum Engineers, Houston, Texas, p. 729-739.

Knutson, C.F., K.A. McCormick, R.P. Smith, W.R. Hackett, J.P. O'Brien, and J.C. Crocker, 1990, RWMC vadose zone basalt characterization: EG&G Report EGG-WM-8949, 126 p.

Koltermann, C.E., and S.M. Gorelick, 1996, Heterogeneity in sedimentary deposits: A review of structure-imitating, process-imitating and descriptive approaches: Water Resources Research, v. 32, p. 2617-2658.

Kuntz, M.A., H.R. Covington, and L.J. Schorr, 1992, An overview of basaltic volcanism of the eastern Snake River Plain, Idaho, *in* P.K. Link, M.A. Kuntz, and L.B. Platt., eds., Regional Geology of Eastern Idaho and Western Montana: Geological Society America Memoir 179, p. 227-267.

Kuntz, M.A., Betty Skipp, M.A. Lanphere, W.E. Scott, K.L. Pierce, G.B. Dalrymple, D.E. Champion, G.F. Embree, W.R. Page, L.A. Morgan, R.P. Smith, W.R. Hackett, and D.W. Rodgers, 1994, Geologic map of the Idaho National Engineering Laboratory and adjoining areas, eastern Idaho: U.S. Geological Survey Miscellaneous Investigations Series, Map I-2330, 1:100,000 scale.

Lindholm, G.F., and J.J. Vaccaro, 1988, Region 2, Columbia Lava Plateau, *in* W. Back, J.S. Rosenshein, and P.R. Seabar, eds., Hydrogeology, Geology of North America: Geological Society of North America, p. 37-50.

Mandelbrot, B.B., 1967, How long is the coast of Britain? Statistical self-similarity and fractional dimension: Science v. 156, p. 636-638.

Neuman, S.P., 1990, Universal scaling of hydraulic conductivity and dispersivities in geologic media: Water Resources Research, v. 26, p. 1749-1758.

Phillips, F.M., and J.L. Wilson, 1989, An approach to estimating hydraulic conductivity spatial correlation scales using geological characteristics: Water Resources Research, v. 25, p. 141-143.

Pudney, W., 1994, Physical properties of sediments affecting saturated vertical water flow at the Idaho National Engineering Laboratory: Idaho State University M.S. thesis, 92 p.

Rowland, S.K., and P.L. Walker, 1990, Pahoehoe and aa in Hawaii: Volumetric flow rate controls the lava structure: Bulletin of Volcanology, v. 52, p. 615-628.

Self, S., L. Keszthelyi, and Th. Thordarson, 1998, The importance of pahoehoe: Annual Reviews of Earth and Planetary Sciences, v. 26, p. 81-110.

Sorenson, K.S., P. Schwind, and T. Aley, 1997, Characterization of flow in a fractured basalt aquifer using fluorescent and ionic tracers at Test Area North, Idaho National Engineering and Environmental Laboratory: Proceedings, Geological Society of America Annual Meeting, Salt Lake City, p. 308.

Sorenson, K.S., A.H. Wylie, and T.R. Wood, 1996, Test Area North site conceptual model and proposed hydrogeological studies, Operable Unit 1-07B: Lockheed-Martin and Idaho Technologies Company Report INEL-96/0105, 139 p.

Srivastava, R.M., 1994, An overview of stochastic methods for reservoir characterization, *in* J.M. Yarus and R.L. Chambers, eds., Stochastic Modeling and Geostatistics: American Association of Petroleum Geologists, Computer Applications in Geology No. 3, p. 3-16.

Welhan, J.A., J.M. Bukowski, A.H. Wylie, and M.R. Hankins, 1998, Directional transmissivity and spatial correlation structure of high-porosity zones in a fractured basalt aquifer: Geological Society of America Annual Meeting, Toronto, Canada, October, 1998.

Welhan, J.A., T.M. Clemo, and E.L. Gego, 2002a, Stochastic simulation of aquifer heterogeneity in a layered basalt aquifer system, eastern Snake River Plain, Idaho, *in* P.K. Link and L.L. Mink, eds., Geology, Hydrogeology, and Environmental Remediation: Idaho National Engineering and Environmental Laboratory, Eastern Snake River Plain, Idaho: Geological Society of America Special Paper 353, p. 225-247.

Welhan, J.A., L. Davis, T. Funderberg, C. Johannesen, and J. Glover, 1997b, Stochastic ground-water modeling in the Snake River Plain aquifer: Hydrogeologic constraints and conceptual approach to the simulation of hydraulic conductivity: EOS, Transactions of the American Geophysical Union, v. 78, p. 147.

Welhan, J.A., T. Funderberg, T., R.P. Smith, and A.H. Wylie, 1997a, Stochastic modeling of hydraulic conductivity in the Snake River Plain aquifer: 1. Hydrogeologic constraints and conceptual approach: Proceedings, 32nd Engineering Geology and Geological Engineering Symposium, Boise, p. 75-92.

Welhan, J.A., C.M. Johannesen, K.S. Reeves, T.M. Clemo, J.A. Glover, and K.W. Bosworth, 2002b, Morphology of inflated pahoehoe lavas and spatial architecture of their porous and permeable zones, eastern Snake River Plain, Idaho, *in* P.K. Link and L.L. Mink, eds., Geology, Hydrogeology, and Environmental Remediation: Idaho National Engineering and Environmental Laboratory, Eastern Snake River Plain, Idaho: Geological Society of America Special Paper 353, p. 135-150.

Welhan, J.A., and M.F. Reed, 1997, Geostatistical analysis of regional hydraulic conductivity variations in the Snake River Plain aquifer, eastern Idaho: Geological Society of America Bulletin 109, p. 855-868.

Welhan, J.A., and A.H. Wylie, 1997, Stochastic modeling of hydraulic conductivity in the Snake River Plain aquifer: 2. Evaluation of lithologic controls at the core and borehole scales: Proceedings, 32nd Engineering Geology and Geotechnical Engineering Symposium, Boise, p. 93-108.

Wetmore, P.H., 1998, An assessment of physical volcanology and tectonics of the central eastern Snake River Plain based on the correlation of subsurface basalts at and near the Idaho National Engineering and Environmental Laboratory, Idaho: Idaho State University M.S. thesis, 115 p.

Volcanic Hazards of the Idaho National Engineering and Environmental Laboratory, Southeast Idaho

William R. Hackett,[1] Richard P. Smith,[2] and Soli Khericha[3]

ABSTRACT

Potential volcanic hazards are assessed, and hazard-zone maps are developed for the Idaho National Engineering and Environmental Laboratory (INEEL) and adjacent areas. The basis of the hazards' assessment and zonation is the past volcanic history of the INEEL region, assuming that late-Quaternary volcanism is representative of future volcanism. The most significant hazards to INEEL facilities are related to basaltic volcanism, chiefly lava flows, which move slowly and threaten property by inundation or burning. Other hazards are volcanic gases and tephra, and the ground disturbance associated with the intrusion of dikes beneath the volcanic zones. Several volcanic zones in the INEEL area contain most of the volcanic vents and fissures of the region and are the most probable sites of future INEEL volcanism.

Volcanic-recurrence estimates are given for each of the volcanic zones based on the geochronology of the lava flows and the lithologic investigations of cogenetic volcanic deposits and magma-induced deformation. Probabilities of basaltic volcanism within the INEEL volcanic zones range from 6 x 10^{-5} per year (16-17 Ka interval between eruptions) for the axial volcanic zone near the southern INEEL boundary and the Arco volcanic-rift zone near its western boundary to 1 x 10^{-5} per year (average 100-Ka interval between eruptions) for the Howe-East Butte volcanic rift zone, a geologically old and poorly defined feature of the central INEEL.

Maps identify hazard zones for basaltic lava flows, tephra and gas, and extensional deformation associated with dike intrusion. The maps are useful in land-use planning, site selection, and safety analysis. The potential effects of ground deformation, tephra, and gases are largely restricted to near-vent areas within the volcanic zones, but lava flows may travel far from their sources. The statistics of INEEL lava flow lengths and areas are used to define two lava-flow hazard zones, which are more extensive than zones for tephra, gases, and ground deformation. The zone of high lava-flow hazard is within 10 km of volcanic vents younger than 400 Ka.

A site-specific volcanic-hazard assessment for the Central Facilities Area, south-central INEEL indicates that the probability of lava inundation is 1 x 10^{-6} per year, if no mitigation is possible, and 4 x 10^{-7} per year if mitigation is attempted.

Key words: basaltic volcanism, volcanic hazards, volcanic-hazard zone maps, eastern Snake River Plain, Idaho National Engineering and Environmental Laboratory

INTRODUCTION

In this paper we discuss the characteristics, frequency, and magnitude of volcanic phenomena in the area of the Idaho National Engineering and Environmental Laboratory (INEEL). We use INEEL geologic data, together with information from analog regions such as Iceland and Hawaii, to construct hazard-zone maps for lava flows, tephra and gas, and ground deformation associated with the intrusion of basaltic dikes. Interpretation of the local

Editors' note: The manuscript was submitted in June 1998 and has been revised at the authors' discretion.

[1]WRH Associates, 100 White Pine Drive, Hershey, PA 17033

[2]Idaho National Engineering and Environmental Laboratory, Lockheed-Martin Idaho Technologies Company, P.O. Box 1625, Mail Stop 2107, Idaho Falls, ID 83415

[3]Idaho National Engineering and Environmental Laboratory Lockheed-Martin Idaho Technologies Company, P.O. Box 1625, Mail Stop 3850, Idaho Falls, ID 83415

Hackett, W.R., R.P. Smith, and Soli Khericha, 2002, Volcanic hazards of the Idaho National Engineering and Environmental Laboratory, southeast Idaho, *in* Bill Bonnichsen, C.M. White, and Michael McCurry, eds., Tectonic and Magmatic Evolution of the Snake River Plain Volcanic Province: Idaho Geological Survey Bulletin 30, p. 461-482.

geology, particularly the record of late-Quaternary volcanism, is the basis for estimating the frequency and magnitude of future INEEL volcanic events, on the premise that "the past is the key to the future." Kuntz and others (1992) and Kuntz (1992) give essential information about eastern Snake River Plain (SRP) regional geology, and recent summaries of INEEL geology include Hackett and Smith (1992) and Kuntz and others (1994). Previous volcanic-hazard assessments of the INEEL area include Kuntz (1978), Kuntz and Dalrymple (1979), and the Volcanism Working Group (1990). These assessments have been outdated by subsequent information, are insufficiently quantitative, or address only specific INEEL localities. In this paper, we give a quantitative assessment of the entire INEEL area.

Volcanic hazards have been evaluated for the INEEL because critical facilities and long-term waste-storage sites have more stringent performance requirements than residential dwellings, and because the regulations governing such facilities demand that all potentially hazardous phenomena be examined in the interests of safety. We have designed the scope and format of this assessment to accommodate future INEEL geologic information. In particular, new geochronologic data might lead to a revision of the recurrence estimates. Recurrence estimates for the INEEL volcanic zones in turn are the basis of probabilistic volcanic-hazard and volcanic-risk assessments for existing or planned INEEL facilities.

Although at times the two terms are used interchangeably, there is a difference between "hazard" and "risk" (Fournier D'Albe, 1986; Reiter, 1990). "Volcanic hazards" describe the potential for dangerous phenomena associated with volcanism. Direct hazards result from eruptions of magma onto the land surface (e.g., lava flows) or into the atmosphere (e.g., volcanic ash or gases). Indirect hazards are attributed to the events that accompany such eruptions, the secondary effects of eruptions, or the underground movement of magma that does not erupt (e.g., dike-induced tensile fissuring and faulting). "Probabilistic volcanic-hazards assessment," the focus of this paper, addresses the probabilities of specific volcanic phenomena occurring within defined source areas. In addition, we develop a site-specific probabilistic volcanic hazards assessment for the Central Facilities Area (CFA) of the south-central INEEL. Here we estimate the annual probability of inundation by lava flows at that site.

"Volcanic risk" describes the extent of losses to people, property, or environment due to occurrences of particular volcanic phenomena. A "probabilistic volcanic-risk assessment" is therefore a quantitative statement concerning the impact or consequences of particular volcanic phenomena. Although we have not addressed the consequences of lava inundation, our assessment is a necessary first step in developing probabilistic volcanic-risk assessments of INEEL facilities.

Our general approach to volcanic-hazards assessment follows Blong (1984) and Latter (1989), with additional information on lava-flow hazards from Fink (1990) and Kilburn and Luongo (1994). Observations of active volcanoes in the analog regions of Hawaii (Decker and others, 1987) and Iceland (Sigurdsson, 1980; Gudmundsson, 1987) also help with understanding the potential effects of future volcanism at the INEEL. We model our quantitative volcanic-hazards assessment after Mullineaux and others (1987) and Wright and others (1992) for the Hawaiian Islands, and our conceptual framework is also influenced by a qualitative study of Iceland (Imsland, 1989).

VOLCANIC GEOLOGY OF THE INEEL AREA

The INEEL is located near the northern margin of the eastern SRP (Figure 1), a region that underwent explosive silicic volcanism during its early development, between about 7 and 4.3 Ma (Pierce and Morgan, 1992). Younger volcanism of the past 4 Ma has largely involved the effusion of basaltic lava flows (Figure 2).

The general characteristics of volcanism in the INEEL area are summarized in Table 1. Early volcanism of the region may be related to the Yellowstone mantle plume, a proposed source of heat and magma that has passed beneath southern Idaho during the past 15 Ma, leaving the 600-km-long SRP in its wake (Pierce and Morgan, 1992; Smith and Braile, 1993). As the North American continent drifted southwestward, the mantle plume left a trail of large silicic eruptive centers that become progressively younger to the northeast and culminate in the Quaternary Yellowstone Plateau volcanic field. The main products of the early explosive eruptions were voluminous and widespread silicic ash-flow tuffs. Beneath the INEEL area, voluminous silicic ash-flow tuffs and lava flows were emplaced about 6.5 to 4.3 Ma (Morgan and others, 1984; Pierce and Morgan, 1992). The present Yellowstone plume is considered to underlie northwestern Wyoming, where it is marked by geophysically anomalous crust and upper mantle (Smith and Christiansen, 1980), by regional uplift of the Yellowstone Plateau, by voluminous silicic volcanism of the Yellowstone Plateau volcanic field during the past 2.1 Ma (Hildreth and others, 1991), and by the present-day high heat flow and geothermal features of the Yellowstone caldera.

The observed, regional space-time pattern of early silicic volcanism on the eastern SRP and the apparent

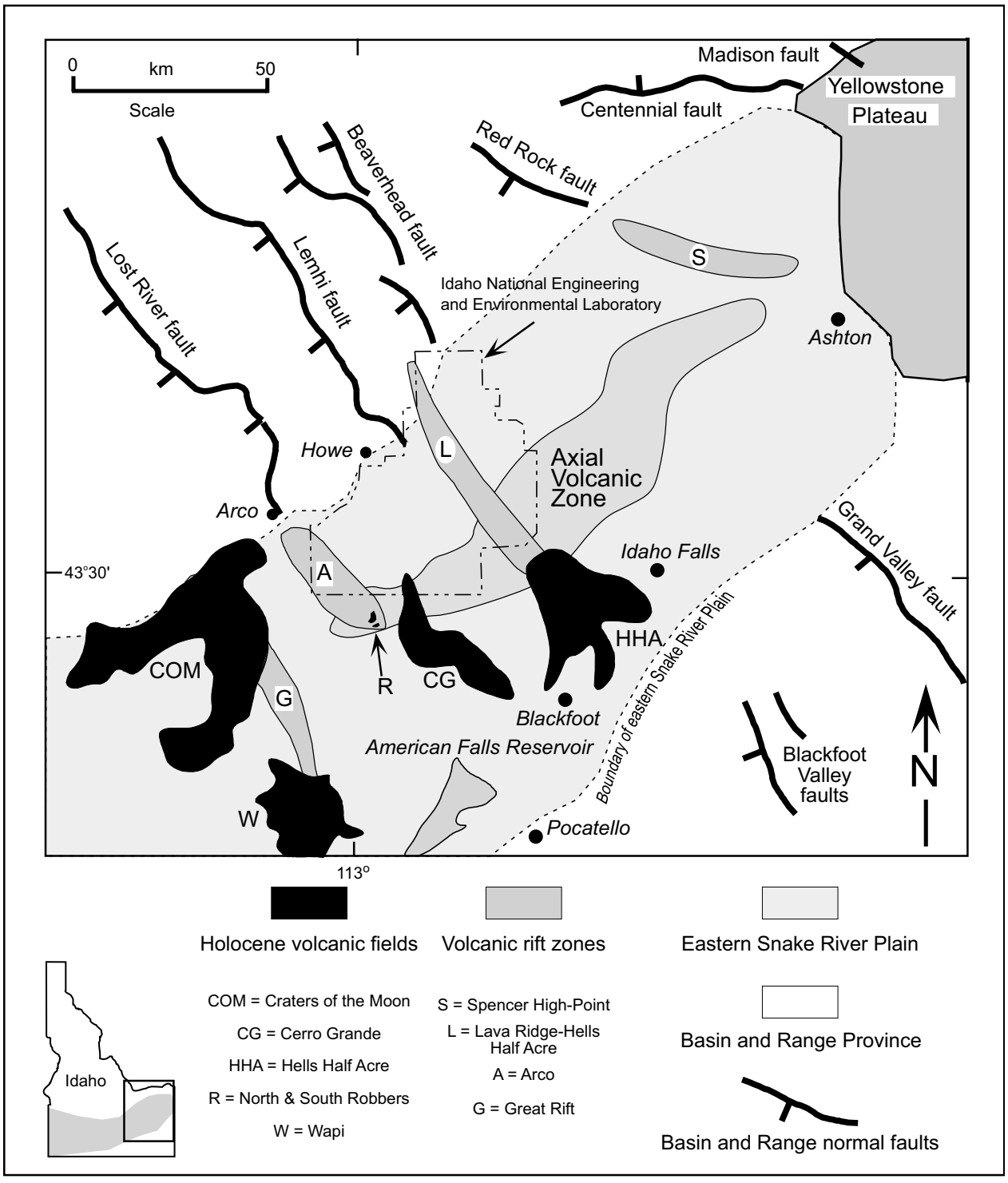

Figure 1. Index map of the eastern SRP, showing INEEL, population centers, and major volcanic and tectonic elements of the region.

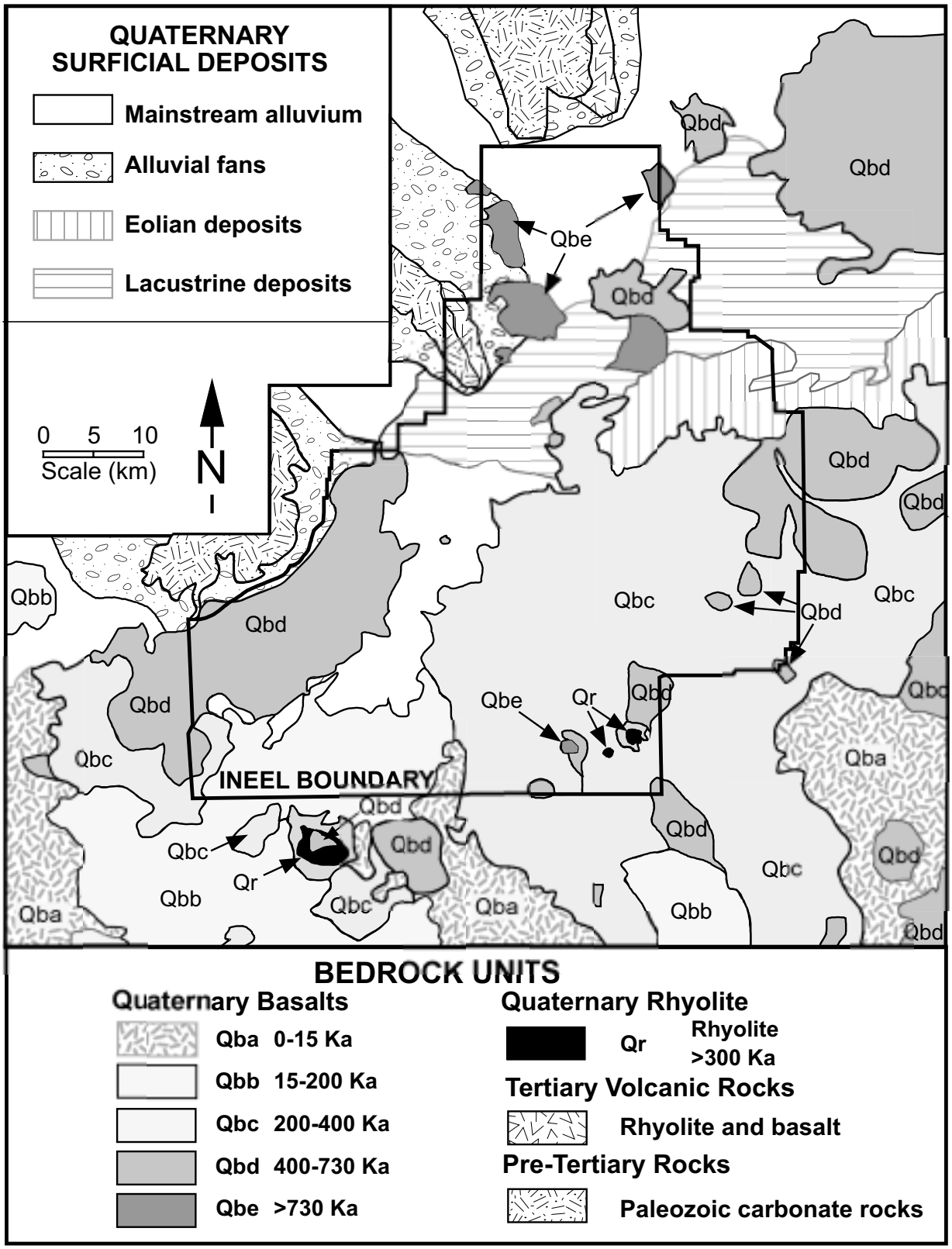

Figure 2. Generalized geologic map of the INEEL area (adapted from Kuntz and others, 1994; Scott, 1982). Quaternary basaltic lava-flow groups Qba through Qbe are based on whole-rock K-Ar (Kuntz and others, 1994) and radiocarbon dates (Kuntz and others, 1986).

Table 1. Characteristics of volcanism in the INEEL area. See Figure 1 for map distribution of volcanic zones and related features.

	Caldera Formation	**Rift-Zone Volcanism**	**Axial-Zone Volcanism**	**Areas Between Volcanic Zones**
Magma Types	Rhyolite (viscous and gas-rich)	Basalt (fluid and gas-poor)	Basalt and subordinate rhyolite	Basalt (and minor rhyolite?)
Volcanic Style and Products	Highly explosive; voluminous pumice and fine ash blankets entire regions	Mild and effusive; erupts mainly lava flows from fissures, low shield volcanoes, and small tephra cones	As per rift zones, but also local rhyolite domes and intrusions (Big Southern, Middle, East buttes) with local explosive phenomena	As per volcanic rift zones and axial volcanic zone
Stratigraphy	Calderas filled with as much as several km of welded, silicic ash-flow tuffs, lava flows, and volcaniclastic sediment [Heise Volcanic Group]	Piles of 1- to 30-m-thick basalt lava flows and minor inter-bedded sediment; total lava thickness as much as 1 km in INEEL area [Snake River Group]	Basaltic lava flows and dispersed small tephra cones; isolated rhyolite domes and intrusions [Snake River Group]	Fine clastic sediment of fluvial, lacustrine, and eolian origin; fewer lava flows than near volcanic rift zones [Snake River Group]
Tectonics and Physical Configuration	Collapse: broad, oval depressions, 10-100 km wide and 1-2 km deep, ringed by inward-dipping fractures	Extensional: NW-trending belts of open fissures, monoclines, small normal faults, and basaltic vents	Extensional, but magma-induced fissures or faults are rare; a diffuse, NE-trending, volcanic highland along the ESRP axis	Subsidence(?): broad, low topographic basins between extensional and constructional volcanic highlands; seldom disturbed by magma intrusion
Geologic Age in INEEL Area	6.5-4.3 Ma, now covered by younger basaltic lava. [2.1-0.6 million years on Yellowstone Plateau]	Surficial INEEL basalts: 1.2-0.05 Ma; most are 0.7-0.1 Ma. Inception of major basaltic volcanism occurred about 4 Ma.	Basalt: >1 Ma (Middle Butte) to 5.4 Ka (Hell's Half Acre). Rhyolite: >1 Ma (near East Butte) to 300 Ka (Big Southern Butte)	As per volcanic rift zones
Quaternary Eruption Frequency	None in INEEL area; Quaternary calderas closest to INEEL occur on Yellowstone Plateau	Low; one eruption per 17 Ka to 100 Ka (see Table 3)	Low: one basaltic eruption per 16 Ka (see Table 3); one rhyolitic intrusion or dome every 200 Ka or longer	Very low; by definition less frequent than within rift zones; one eruption per 100 Ka or longer

northeastward migration of the early silicic volcanic centers have three implications for INEEL volcanic-hazards assessment. First, the available evidence from the Quaternary Yellowstone Plateau volcanic field suggests that major silicic eruptions were separated by about 500 Ka (annual probability less than 2×10^{-6}). Second, explosive silicic volcanism associated with plume passage in the INEEL area took place 6.5 to 4.3 Ma. Recurrence intervals during that period were approximately 700 Ka, and about six recurrence intervals have therefore elapsed since the most recent caldera-forming eruptions of the INEEL area. Third, during the past 4.3 Ma, the major centers of explosive silicic volcanism have migrated to the Yellowstone region, several hundred kilometers northeast of the INEEL. Together, these three factors imply that the INEEL is unlikely to be significantly affected by future, explosive silicic volcanism (Volcanism Working Group, 1990).

During approximately the past 4.3 Ma, the eastern SRP has been repeatedly inundated by basaltic lava flows, which today largely cover the earlier silicic deposits. Much of the 2,315-square-km tract of the INEEL is underlain by basaltic lava flows, either exposed on the present land surface or lying beneath Quaternary sediment of alluvial, eolian, and lacustrine origin (Scott, 1982; Kuntz and others, 1994). Deep boreholes on the INEEL have intersected up to 1 km of late-Tertiary and Quaternary basalt lava flows and interbedded sedimentary deposits overlying Neogene silicic tuffs (Hackett and Smith, 1992). Unlike the early silicic volcanism, no systematic eastward migration of basaltic volcanism is apparent on the SRP, and Holocene lava flows occur across the province. No eruptions have occurred on the eastern SRP during recorded history, but basaltic lava flows of the Hell's Half Acre lava field erupted near the southern INEEL boundary as recently as 5.4 Ka, and eruptions occurred as recently as 2.1 Ka along the Great Rift, 30 km southwest of the INEEL (Kuntz and others, 1986).

Isolated volcanic domes of Quaternary rhyolite also occur on the eastern SRP. The domes were emplaced between about 1.4 and 0.3 Ma along the northeast-trending, central topographic axis of the eastern SRP (Kuntz and others, 1994). They are composed of fractured, lithoidal rhyolite and are surrounded by talus, alluvial-fan deposits, and younger basaltic lava flows.

Five groups of Quaternary basaltic lava flows have been mapped in the INEEL area (Figure 2), based on geologic field relations, geochronology (whole-rock potassium-argon, radiocarbon, and paleomagnetism), degree of weathering, and thickness of sediment cover (Kuntz and others, 1994). Quaternary volcanic rocks, chiefly basaltic lava flows, are exposed over approximately 58 percent of the INEEL and the adjacent land area, and they occur in the subsurface across most of the eastern SRP. Figure 3 shows the relative areas of subaerially exposed Quaternary volcanic rocks in the INEEL region. Several aspects of Figures 2 and 3 are relevant to INEEL volcanic-hazards assessment. More than two-thirds of the subaerially exposed basaltic lava and all of the silicic lava of the INEEL land surface and adjacent areas are older than 200 Ka (Figure 3: map units Qbc, Qbd, Qbe and Qr). No Holocene vents occur on the INEEL, but Holocene basaltic lava flows (Qba) cover 12 percent of the eastern SRP in the INEEL area and have erupted from vents along the axis of the eastern SRP as recently as 5.4 Ka. A minuscule percentage of the INEEL area is occupied by silicic volcanic domes (map unit Qr), and these isolated features occur along the axis of the eastern SRP near the southern INEEL boundary. Relative to basaltic volcanism, future silicic volcanism and its related hazards are, therefore, expected to be infrequent and to affect small areas of the axial volcanic zone.

Volcanic vents are not randomly distributed on the eastern SRP but occur within several volcanic zones (Figure 1). The axial volcanic zone is a northeast-trending, constructional-volcanic highland. Volcanic vents are also abundant in the southern parts of several northwest-trending volcanic rift zones where they merge with the axial volcanic zone. Volcanic rift zones are the surface expressions of underlying dike swarms. During ascent, dikes orient themselves perpendicular to the direction of least horizontal compressive stress, and magma pressure forces overlying rocks apart, forming northwest-trending belts of extensional deformation above the dikes. The resulting structural features include tensile fissures up to a meter wide and several hundred meters long, and normal-fault scarps and monoclines up to 10 m high and several km long (Smith and others, 1989; Hackett and Smith, 1992; Kuntz and others, 1992). The volcanic rift zones are also marked by linear arrays of fissure-fed basaltic lava flows,

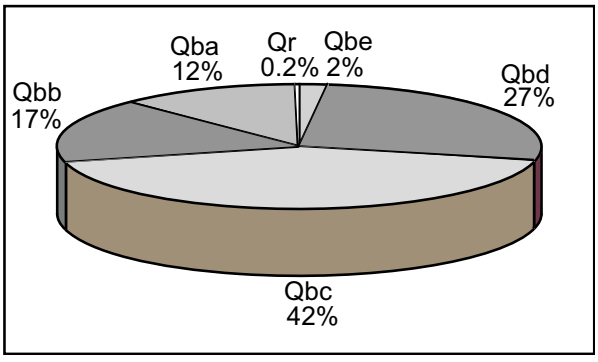

Figure 3. Relative areas of exposed Quaternary volcanic materials in the INEEL region. See Figure 2 for description of map units.

small-shield volcanoes, pyroclastic cones, and collapse craters. The volcanic and structural features of eastern SRP volcanic rift zones are generally similar to those of the Hawaiian and Icelandic rift zones. The eastern SRP volcanic rift zones are more diffuse than those of Hawaii, and their northwest trend conforms with the regional, northeast-southwest extension of the eastern SRP and the adjacent Basin and Range Province, rather than the radial pattern resulting from intrusive and gravitational forces during the growth of huge Hawaiian shield volcanoes. The axial volcanic zone of the eastern SRP has fewer dike-induced fissures and faults than the volcanic rift zones to the north, perhaps because it has a greater number of vents and has been resurfaced more frequently by lava flows. Between the INEEL volcanic rift zones are broad, low-lying basins such as the Big Lost River Sinks of the northern and central INEEL. Borehole data suggest that these basins may have received more late-Quaternary sediment and fewer lava flows than the volcanic zones (Anderson and Lewis, 1989).

The main style of Quaternary eastern SRP basaltic volcanism is Hawaiian, and eruptions typically involved mild effusions of fluid, gas-poor, pahoehoe lava flows from fissures and small shield volcanoes. Many eastern SRP basalt flows are tube fed (Greeley, 1982), as shown by the widespread collapse depressions developed along lava tubes of the region. Strombolian volcanism is marked by small pyroclastic cones on eruptive fissures, many of which occur along the axial volcanic zone. Examples include the summit-forming tephra cone of Cedar Butte and the group of small basaltic tephra cones near Atomic City to the south of the INEEL. Tuff cones and tuff rings, resulting from phreatomagmatic steam explosions during the interaction of basaltic magma with shallow ground water, do not occur in the INEEL area but are found elsewhere on the eastern SRP (Womer and others, 1982; Hackett and Morgan, 1988), probably because the INEEL water table is too deep.

INEEL VOLCANIC HAZARDS

The INEEL area has experienced predominately basaltic volcanism during the past 4.3 Ma, and phenomena associated with basaltic volcanism are, therefore, most important to INEEL hazard assessment. Table 2 outlines the principal hazards associated with eastern SRP basaltic volcanism. Effusion of pahoehoe lava flows (Self and others, 1998) is the most common late-Quaternary phenomenon and, therefore, the most significant hazard on the eastern SRP. Observations of active lava flows in Hawaii (Tilling and Peterson, 1994) indicate that basaltic lava flows on gentle terrain similar to that of the INEEL advance relatively slowly and mainly threaten property by inundation or burning.

Gas release is universally associated with fissuring and eruption, but poisonous or asphyxiating gases are generally serious hazards only within a few hundred meters of active vents. Several kilometers downwind, reactive gases may cause respiratory irritation, affect crops, and cause corrosion. Upon cooling, heavier-than-air gases (carbon dioxide, sulfur, sulfur dioxide, hydrogen fluoride, and hydrogen chloride) may collect in closed topographic depressions. Persistent winds and the broad expanse of most topographic basins on the INEEL mean that volcanic gas is unlikely to be a significant hazard, with the possible exception of the confined basin of the Big Lost River sinks and the Birch Creek sinks in the north-central INEEL (Smith, 1994).

Explosive pyroclastic volcanism and significant tephra fall are rare during mild, Hawaiian-type basaltic eruptions such as those of the eastern SRP. Tephra fallout would involve the deposition of coarse pyroclastic material within a few hundred meters of volcanic vents. Areas of tephra hazard are therefore similar in size and geometry to the areas affected by volcanic gases.

Indirect hazards associated with basaltic volcanism are ground deformation and seismicity associated with dike intrusion beneath volcanic rift zones. Surface fissuring and tumescence occur during dike intrusion with or without the eruption of magma. Tensile fissures on the eastern SRP have widths ranging from 0.1 m to about 1 m, and normal-fault scarps rarely exceed 5 m.

Small- to moderate-magnitude earthquakes also occur during dike intrusion. Most dike-induced seismic events have magnitudes less than 3, and maximum magnitudes are estimated to be less than 5.5 on the eastern SRP (Jackson, 1994; Smith and others, 1996; Hackett and others, 1996).

Future silicic lava domes may erupt along the axial volcanic zone, but the hazardous effects would probably be restricted to a several kilometer radius. Historical observations of active silicic lava domes have shown that such domes commonly produce small-volume pyroclastic flows and tephra-fall deposits as a result of internal explosions and slope failure (Fink, 1990). However, no evidence of such deposits from silicic domes near the INEEL has yet been identified through geologic mapping and borehole investigations. The shallow intrusion of silicic magma during the growth of lava domes may also lead to the uplift of large tracts of land. Middle Butte in the axial volcanic zone is a block of old (Qbe) lava flows that was presumably uplifted by a silicic lava dome that failed to breach the surface (Kuntz and Dalrymple, 1979), and the emplacement of Big Southern Butte raised

Table 2. Hazards associated with basaltic volcanism on the eastern Snake River Plain. Entries are listed from highest to lowest relative hazard.

Phenomenon	**Relative Frequency**	**Size or Area of Influence**	**Comments**
Lava flow	Common	0.1 km^2 to 400 km^2 in area; up to 25 km in length based on sizes of ESRP lava flows of the past 400 Ka	Significant hazard; typical basaltic phenomenon; lava from fissures or shield volcanoes may inundate large areas downslope of vents
Ground deformation: fissuring, faulting, and uplift	Common; associated with virtually all shallow magma intrusion and eruption	Fissuring could affect areas to 2 x 10 km; minor tilting and broad uplift in areas to 5 x 20 km	Significant hazard; due to shallow dike intrusion; "dry" intrusion may occur without lava flows; affects smaller areas than for lava inundation
Volcanic earthquakes	Common; associated with magma intrusion before and during eruption	Maximum M = 5.5 and most events M < 4; ground vibration may affect facilities within 25 km	Low to moderate hazard; swarms of shallow earthquakes (< 4 km focal depth) occur as dikes propagate underground
Gas release (toxic and corrosive vapors)	Common; associated with fissuring and lava eruption	Restricted to near-vent areas; may affect several square-km area downwind	Low hazard; local plume of corrosive vapor, downwind from eruptive vent or fissure; cooled vapor may collect in local topographic depressions
Tephra fall (volcanic ash and bombs)	Common	Restricted to near-vent areas; may affect several square-km area downwind	Low hazard; basaltic eruptions are inherently nonexplosive and may form small tephra cones but little fine ash to be carried downwind
Base surge (ground-hugging blast of steam and tephra)	Rare	Effects limited to radius of several km from vent; < 10 km^2 area	Low hazard; steam explosions due to interaction between ascending magma and shallow ground water; water table too deep under most of INEEL (> 200 m)
Tephra flow (ground-hugging flow of hot, pyroclastic material)	Extremely rare	Near vent; may affect area < 1 km^2	Very low hazard; as per tephra fall but affecting even smaller areas

a 900-m-thick block of basaltic lava flows on its northern flank (Spear and King, 1982; Fishel, 1993).

None of these volcanic phenomena can be effectively controlled, and the most successful mitigation is avoidance through careful land-use planning and site selection. Once a volcanic vent has become established, the paths of lava flows can usually be predicted using terrain analysis. In some places, lava flows can be diverted with rock-rubble barriers (Barberi and others, 1993). Diversions should be constructed well upslope of threatened facilities, in opportune topographic positions, and not at the facilities themselves. Water has been used to chill and halt advancing lava flow fronts, but this requires enormous quantities of water and energy for pumping. It is generally not feasible to engineer structures to withstand ground fracturing or faulting, or the long-term effects of corrosive gases. Tephra fall is not a significant hazard in the INEEL area, and the mitigation of roof collapse by tephra loading is therefore unwarranted.

DEFINITION, FREQUENCY, AND MAGNITUDE OF VOLCANIC EVENTS

The recurrence estimates of Table 3 are based on the number of magmatic events for each INEEL volcanic zone. A magmatic event is defined as a cogenetic assemblage of intrusive and extrusive features that are the products of a single magma batch. An event occurs within the

geologically brief time it takes for a batch of basaltic magma to be injected into the shallow crust and to solidify, generally months to decades. A discrete magmatic event usually produces an assemblage of cogenetic features such as multiple vents along a common eruptive fissure, several lava flows, and a belt of dike-induced extensional structures that may form with or without eruptive products. Interpreting each lava flow, vent, or fissure as the unique product of a discrete volcanic eruption is geologically incorrect and yields inappropriately short recurrence intervals, but this procedure is useful to establish bounding conditions for volcanic recurrence. Equating each lava flow, vent, or deformation feature as the product of a single magmatic event would shorten the preferred recurrence estimates of Table 3 by factors of 1.5 to 3.

To the geologic map data of Kuntz and others (1994), we have added our own field, aerial-photographic, and petrographic investigations of selected vent areas on the axial volcanic zone and the southern Arco volcanic rift zone. We conclude that the geologic field relations as mapped at 1:100,000 scale by Kuntz and others (1994) are adequate for INEEL volcanic-hazards assessment, because the products of individual eruptions are readily distinguished at that scale. We also find that lava flows from individual shield volcanoes commonly differ from lava flows of other vents in phenocryst content, groundmass mineralogy, and texture. These differences support the idea that the clusters of small shield volcanoes, pyroclastic cones, pit craters, and other vents are generally the cogenetic products of single, compositionally uniform magma batches representing a discrete magmatic event. Most eastern SRP volcanoes are small, monogenetic features, as shown by the field relations and by the overall petrographic uniformity among lava flows from the individual shield volcanoes and vent complexes. In the southern Arco volcanic rift zone, the petrographic similarities and field relations among several of the shield volcanoes suggest that in places several shield volcanoes may be the cogenetic products of a single magma batch. In several places, tensile fissures could not be related to cogenetic volcanic materials and were conservatively interpreted as the products of one noneruptive dike-intrusion event.

Cedar Butte, a large central volcano of the axial volcanic zone (Figure 4; Hayden, 1992), is an exception to the typically monogenetic volcanism of the INEEL area. At this polygenetic eruptive center, several eruption cycles have produced diverse lava compositions, ranging from basalt to rhyolite, and pyroclastic as well as effusive volcanic materials, suggesting a complex magma system that evolved either by protracted differentiation of a single batch of parental magma or by magma-reservoir replenishment.

Geologic and geophysical observations during historical rift-zone volcanism in Hawaii and Iceland show that dike intrusion, ground deformation, and lava effusion are cogenetic phenomena that develop during geologically brief eruptive periods of several weeks to a decade or so (Hackett and others, 1996). The inference that multiple lava flows and vents on the eastern SRP formed during geologically brief periods is further supported by paleomagnetic data from drill cores of INEEL lava flows (Champion and others, 1988) and by radiocarbon dates from Holocene lava flows in Craters of the Moon lava field (Kuntz and others, 1986; 1988).

RECURRENCE ESTIMATES

The recurrence estimates for INEEL volcanic zones and boreholes given in Table 3 are based chiefly on the geochronology and geologic map data of Kuntz and others (1994), and are derived by dividing the number of volcanic events into the age range of volcanism. Estimates have been rounded off to avoid implying undue precision and are expressed as frequencies of eruption and as annual probabilities of occurrence. Eruptive periods are separated by an average of about 2 Ka for some parts of the Great Rift, giving a recurrence of 5×10^{-4} per year. Future eruptions of the Great Rift would have little or no impact upon the INEEL, but these data are included because this volcanic rift zone is thoroughly studied and has been frequently active during the past 15 Ka. Its 2-Ka recurrence interval serves as a bounding value of shortest recurrence for the eastern SRP region.

Northwest-trending volcanic rift zones of the INEEL area merge with the axial volcanic zone (Figure 1). The shortest recurrence intervals (greatest annual probabilities of eruption) for INEEL volcanic zones are approximately 16 Ka (6×10^{-5} per year) for the axial volcanic zone and the Arco volcanic rift zone. The axial volcanic zone has the greatest number of volcanic vents of the INEEL volcanic zones and includes four Holocene lava fields. It is a constructional volcanic highland along the axis of the eastern SRP, apparently resulting from a greater magma supply at the center of the volcanic province. The axial volcanic zone includes relatively few dike-induced extensional structures in comparison with the volcanic rift zones. The Arco volcanic rift zone contains more vents than other volcanic rift zones of the INEEL area, and also the greatest number of dike-induced fissures and faults. Together, the Arco and axial volcanic zones account for more than two-thirds of the vents and dike-induced structures of the INEEL area.

Table 3. Estimated volcanic-recurrence intervals and corresponding annual eruption probabilities (in parentheses) for volcanic zones and boreholes of the INEEL area.

Volcanic Zone or Borehole	**Data Sources**	**Time Interval of Volcanism**	**Number of Vents, Fissures, or Flow Groups**	**Comments**	**Estimated Recurrence Interval**
Great Rift (25 km southwest of INEEL)	Kuntz and others, 1986, 1988	2.1-15 Ka (radiocarbon dating)	> 100 vents 8 Holocene eruptive periods (each lasting a few decades or centuries, and each including multiple flows and cones)	No impact on INEEL; most recently and frequently active of all ESRP rift zones; thus provides minimum recurrence for entire ESRP; most probable area of future ESRP volcanism	2 Ka (5×10^{-4}/year)
Axial Volcanic Zone (southern INEEL)	Kuntz and others, 1986, 1994	5-730 Ka (K-Ar dating; radiocarbon; paleomagnetic data)	73 vents and fissure sets; 4 Holocene lava fields, 3 of them shared by volcanic rift zones. 45 cogenetic vent and fissure groups	Could affect much of southern INEEL; most recently and frequently active of all volcanic zones that could impact INEEL	16 Ka (6.2×10^{-5}/year)
Arco Volcanic Rift Zone (southwestern INEEL)	Kuntz, 1978; Smith and others, 1989; Kuntz and others, 1994	10-600 Ka (radiocarbon, K-Ar and thermoluminescence dating; paleomagnetic data)	83 vents and fissure sets; 2 Holocene lava fields. 35 cogenetic vent and fissure groups	Volcanism could affect southwestern INEEL	17 Ka (5.9×10^{-5}/year)
Lava Ridge-Hell's Half Acre Volcanic Rift Zone (includes Circular Butte/Kettle Butte volcanic rift zone) (north and eastern INEEL)	Kuntz and others, 1986, 1994	5 Ka-1.2 Ma (K-Ar dating; radiocarbon; paleomagnetic data)	48 vents and fissure sets; 1 Holocene lava field: Hell's Half Acre. 30 cogenetic vent and fissure groups	Could affect northern and eastern INEEL; extremely long eruptive history; includes oldest and youngest basalts in the INEEL area	40 Ka (2.5×10^{-5}/year)
Howe-East Butte Volcanic Rift Zone (central INEEL)	Kuntz, 1978, 1992; Golder Associates, 1992	230-730 Ka (K-Ar dating; paleomagnetic data)	7 vents and fissure sets; no Holocene features. 5 cogenetic vent and fissure groups	Old, poorly exposed, and sediment-covered; identified in part by subsurface geophysical anomalies	100 Ka (1.0×10^{-5}/year)
Borehole NPR SITE E (south-central INEEL)	Champion and others, 1988	230-640 Ka (K-Ar dating; paleomagnetic data)	9 lava-flow groups (each group contains multiple lava flows, erupted over a short time)	Dates from 600-foot interval of subsurface lavas give recurrence estimate consistent with surficial geology of the area	45 Ka (2.2×10^{-5}/year)
Borehole RWMC 77-1 (southwestern INEEL)	Kuntz, 1978; Anderson and Lewis, 1989	100-565 Ka (K-Ar and TL dating; paleomagnetic data)	11 lava-flow groups (each group contains multiple lava flows, erupted over a short time)	Dates from 600-foot interval of subsurface lavas give longer recurrence interval than nearby Arco and Axial zones, reflecting flow-group (subsurface) vs. vent-counting (surface geology) methods	45 Ka (2.2×10^{-5}/year)

[1] 16 vent/fissure groups in overlap zone of Axial Volcanic Zone and Arco Volcanic Rift Zone are divided between the two zones. 17 vent/fissure groups in overlap zone of Axial Volcanic Zone and Lava Ridge-Hell's Half Acre Volcanic Rift Zone are divided between the two zones.

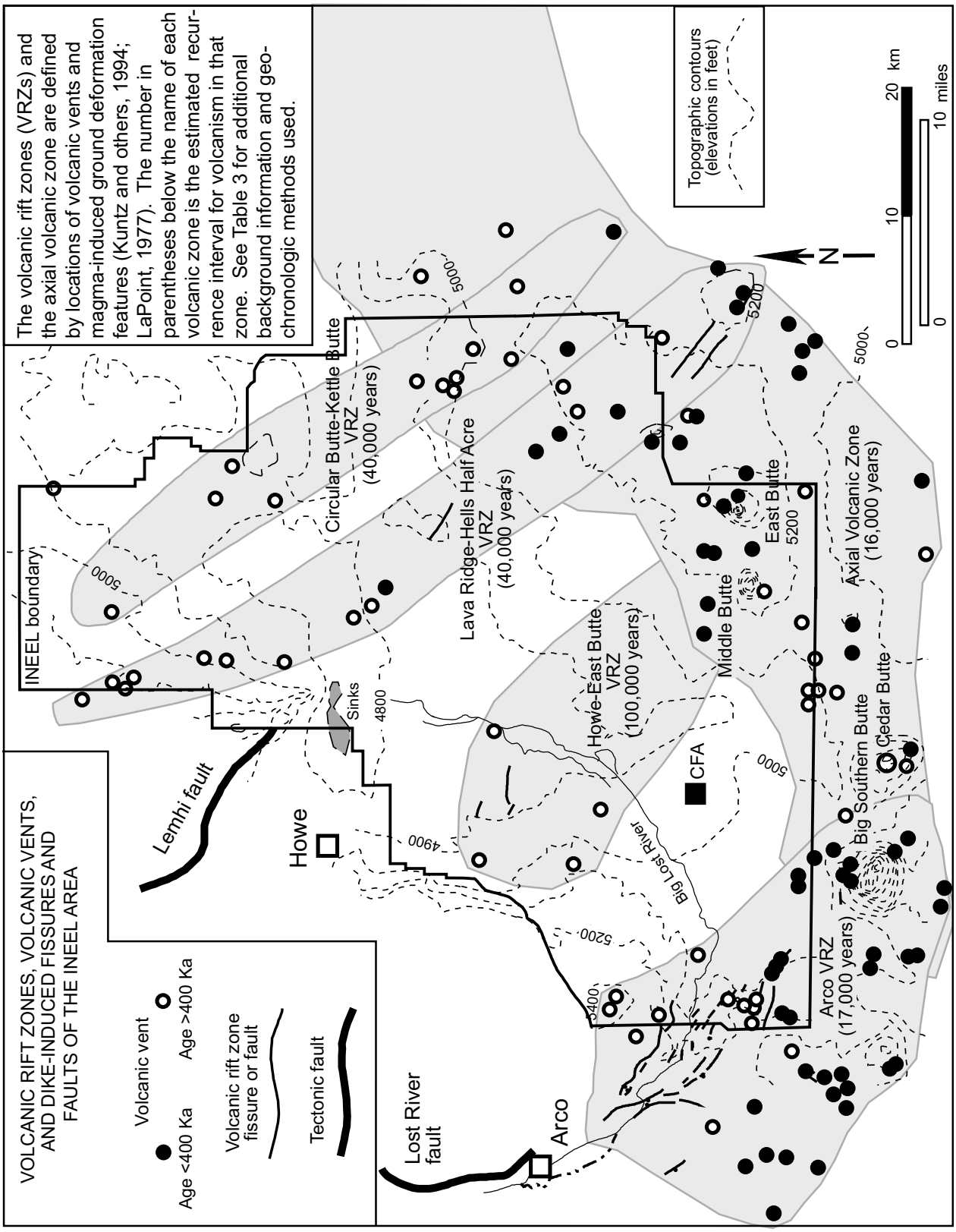

Figure 4. Map of the INEEL area, showing volcanic-vent locations and estimated recurrence intervals for the volcanic zones (gray-filled regions). Filled square shows the location of the Central Facilities Area.

We have combined the Circular Butte-Kettle Butte volcanic rift zone of Kuntz and others (1992) and the Lava Ridge-Hell's Half Acre volcanic rift zone into a single entity. They are diffuse, adjacent features with similar physiographic characteristics, periods of eruptions, and recurrence. Although the number of vents is similar to the Arco volcanic rift zone, the 40-Ka recurrence estimate for the Lava Ridge-Hell's Half Acre volcanic rift zone is longer because the lava flows of its northern part erupted about 1.2 Ma and are among the oldest known from INEEL surface outcrops.

The Howe-East Butte volcanic rift zone, included in Table 3, is identified by Kuntz and others (1992) but is poorly expressed in the INEEL surficial geology. In its northern part, this volcanic rift zone has a few vents and fissures developed in lava flows older than about 400 Ka. In contrast to other eastern SRP volcanic rift zones, its central part is not a topographic highland but a basin containing Big Lost River sediment and younger lava flows from other volcanic zones. The Howe-East Butte volcanic rift zone is marked by a large, northwest-trending, positive aeromagnetic anomaly (Zietz and others, 1978), which may represent a subsurface dike swarm. We therefore interpret the feature as an old volcanic rift zone now largely covered by younger volcanic and sedimentary deposits. Although all Howe-East Butte volcanic vents are older than 400 Ka (Kuntz and others, 1994), the time interval of 230-730 Ka given in Table 3 allows for fissuring and volcanism as young as 230 Ka. This is because the Howe-East Butte volcanic rift zone merges with the axial volcanic zone to the south, and 230 Ka is the age of young vents in this area of the axial volcanic zone. Nonetheless, the 100-Ka estimated recurrence for the Howe-East Butte volcanic rift zone is the longest of any INEEL volcanic zone.

Expansion of the time intervals of volcanism to the present (zero Ma) would be a valid consideration for the INEEL volcanic zones, because hazard assessments are necessarily concerned with the potential effects of future volcanism. This would not substantially change the recurrence estimates for the INEEL volcanic zones because most of them, except the Howe-East Butte volcanic rift zone, include lava flows younger than about 12 Ka.

The northern parts of the Arco- and the Lava Ridge-Hell's Half Acre volcanic rift zones contain fewer and older volcanic vents than their southern parts near the axial volcanic zone, and volcanic recurrence within these rift zones decreases northward. The recurrence estimates reported for the Arco- and for the Lava Ridge-Hell's Half Acre volcanic rift zones represent average values.

Borehole data are shown in Table 3 for comparison with the surface volcanic zones. Borehole recurrence estimates generally conform with those based upon surface geology, although different methods are used. For example, in the NPR Site E borehole, nine basaltic lava-flow groups are separated by sedimentary interbeds. Paleomagnetic data indicate that the lava-flow groups were emplaced within relatively brief periods of centuries to a few millennia, during the 400-Ka-dated interval of the borehole. Each lava-flow group may, therefore, be interpreted as the product of one or a few closely spaced magmatic events, perhaps representing the lava flows from several coalesced shield volcanoes. Nine eruption cycles (lava-flow groups) per 400 Ka gives the 45-Ka recurrence estimate for this borehole. A more detailed dimensional analysis of late Quaternary lava-flow groups in INEEL boreholes is used by Wetmore and others (1997) to derive an INEEL borehole-based recurrence interval of about 19 Ka (5.3×10^{-5} per year).

EVENT MAGNITUDE

To constrain event magnitude and to provide a quantitative basis for establishing INEEL lava-flow hazard zones, we used the map data of Kuntz and others (1994) to measure the lengths and areas of basaltic lava flows from the four youngest Quaternary basaltic lava-flow groups, representing volcanism of the past 750 Ka. Only flows with dimensions not obscured by younger deposits were measured, and a statistical compilation is given in Table 4.

No subaerially exposed lava flow of the INEEL area has traveled farther than about 30 km from its source. The 50th-percentile flow length is 10 km, and the length distribution is strongly skewed toward short flows. The average INEEL lava flow of the past 750 Ka covered about

Table 4. Statistical summary of late Quaternary INEEL basaltic lava-flow lengths and areas. Lava flows were measured from the geologic-map data of Kuntz and others (1994) and LaPoint (1977).

	Length (km)	**Area (km^2)**
Minimum	0.1	0.5
Maximum	31	400
Range	30.9	399.5
Mean	12.4	96.5
Median	10	70
Standard Deviation	7.9	94.2
Number of Flows	46	43

96 square km. Most of the flows are equant, reflecting a tendency to spread laterally on the gently sloping, low-relief terrain.

The magnitude of dike-induced ground deformation is defined as the surface area disturbed by extensional faults and fissures associated with the shallow intrusion of a basaltic dike. Hackett and others (1996) and Smith and others (1996) compile the results of numerical modeling, physical modeling, field observations of deformation during active dike intrusion in Hawaii and Iceland, and field measurements of magma-induced extensional features on the eastern SRP. They show that deformation is largely restricted to narrow belts above intruded basaltic dikes, generally less than 1 km wide and 5 km long (total area of 5 square km), and that the cumulative fault displacement or tensile fracturing associated with intrusion of one several-meter-thick basaltic dike is less than a few meters.

Although coarse pyroclastic material is produced at the onset of nearly all eastern SRP basaltic eruptions, most such material is deposited less than a few hundred meters from vents along a common eruptive fissure up to several kilometers in length. Tephra cones of the Craters of the Moon lava field to the southwest of the INEEL are among the most imposing volcanic features on the eastern SRP. Many are composed of evolved lava having a silica content greater than 50 percent, are about 100 m high, and cover an area of about 1 square km (Kuntz and others, 1988). During an unusual phreatomagmatic event on the eastern SRP, southwest winds deposited several centimeters of basaltic ash up to 1.5 km downwind from the eruptive fissure at the Holocene King's Bowl lava field (Greeley and King, 1977; Kuntz and others, 1988). More representative of the INEEL area are six small basaltic tephra cones, each less than 20 m high and 200 m in diameter, within a 15-square-km area of the axial volcanic zone near Atomic City and the southern INEEL boundary (Kuntz and others, 1992, 1994). Thus, for typical eastern SRP basaltic eruptions, significant effects of tephra fall and toxic or corrosive gases will be limited to areas within 500 m of vents.

Volcanic gas may also be liberated from both eruptive and noneruptive fissures during shallow dike intrusion and would likely be carried northeasterly by prevailing eastern SRP winds. As with ground deformation, the area affected by tephra and gas is anticipated to be a narrow, northwest-trending belt of about 5 square km, developed above and to the northeast of an ascending basaltic dike. Thus, for dike-induced deformation and for tephra and gas, the affected areas are estimated to be about one-twentieth of the area inundated by the average INEEL lava flow.

INEEL HAZARD-ZONE MAPS

Volcanic-hazard zones are founded on the assumption that future eruptions will be similar in style, magnitude and location to those of the recent geologic past, as reconstructed from the INEEL geologic record. The quantitative approach used here incorporates several primary and secondary criteria, including (1) the location and density (number per unit area) of dike-induced fissures and most recent lava flows; (2) volcanic recurrence, estimated from event counts within each of the INEEL volcanic zones and the absolute chronology of the volcanic materials (Figure 4); and (3) distance from volcanic vents or zones, relative to median lava-flow length. Additional criteria include the topographic gradients and barriers that could affect the paths of lava flows or collect volcanic gas, and the prevailing wind directions that would affect the dispersal of gas and fine tephra.

Volcanic-hazard zonation maps are shown for lava flows (Figure 5), tephra fall and volcanic gases (Figure 6), and ground deformation associated with basaltic-dike intrusion (Figure 7). The hazard zone maps show areas in which the level of hazard differs from that of adjacent areas. The level of hazard may vary considerably within a zone, either gradually or abruptly. Direct volcanic hazards (lava flows, tephra, and gases) decrease gradually across zones and away from vents, but abrupt changes may occur along sharp topographic features. The degree of hazard changes gradually rather than abruptly across most zone boundaries, and zones would be most accurately rendered by contours or gradational changes in shading rather than as sharp lines. The zone boundaries are intended to show that differences in hazard exist and to facilitate description of the zones. In spite of these limitations, the hazard zone maps and associated volcanic-recurrence data are useful for land-use planning, site selection, safety analysis, and long-range mitigation planning for volcanic hazards.

LAVA-FLOW HAZARD ZONES

The length statistics of late-Quaternary basaltic lava flows (Table 4) are used to delineate hazard zones for lava inundation from vents within the INEEL volcanic zones (Figure 5). Hazard zone 1 (highest hazard) for lava flows is defined as being within 10 km of a vent or fissure younger than 400 Ka (map units Qba, Qbb, Qbc; Kuntz and others, 1994). Ten km is the median or 50th-percentile length of late Quaternary lava flows (Table 4), meaning that random sites within zone 1 are statistically expected to be inundated by about 50 percent of lava flows that may erupt from nearby sources. The general probability of inundation at the outer limit of zone 1 is, there-

fore, less than or equal to half the annual eruption probability for its adjacent source volcanic zone, ignoring topographic and other site-specific factors. Later, we give a detailed hazard analysis that incorporates these factors for a specific INEEL site. Hazard zone 2 is an area of lower hazard, defined as being within 20 km (the 80th-percentile lava-flow length) of a vent or fissure younger than 400 Ka. Thus, on a statistical basis, less than 20 percent of erupted lava flows are expected to reach the outer limits of hazard zone 2. Areas beyond hazard zone 2 should be inundated by fewer than 20 percent of future lava flows and have probabilities of inundation that are generally about an order of magnitude smaller than the recurrence values for nearby volcanic zones.

The lava-flow hazard zones are truncated in the northern and western INEEL, owing to the topographic effects of mountain ranges near the northwestern INEEL boundary, to the south-sloping alluvial surfaces issuing from intermontane valleys, and to the Big Lost River channel of the central INEEL. Areas outside zone 2 are sufficiently distant or upslope from the volcanic zones to be considered low-hazard areas, beyond the range of most lava flows.

TEPHRA-FALL AND VOLCANIC-GAS HAZARD ZONE

Tephra fall and gas emission are expected to accompany all volcanic eruptions, and gas emission from fissures would accompany dike intrusion even in the absence of lava eruption; our estimated recurrence for tephra and gas emission is therefore the same as for lava flows and dike-induced deformation (Table 3). Tephra deposits, however, constitute a very small part of the total volume of basalt on the eastern SRP (Kuntz and others, 1992) and as discussed earlier, the areas affected by tephra fall are much smaller than the areas inundated by affiliated lava flows. We indicate tephra and gas-hazard zones (Figure 6) within areas 0.5 km southwest and 2 km northeast of vents and fissures younger than 400 Ka within the INEEL volcanic zones. We estimate hazard zones for tephra and gases from future silicic lava-dome eruptions along the center of the axial volcanic zone to be about twice these dimensions (5-km radius). This estimate also includes pyroclastic-flow hazard due to the slope failure and explosions that are typical of silicic lava domes (Blong, 1984; Williams and McBirney, 1979). A separate zone for silicic tephra and gases is not shown within the axial volcanic zone but exists as part of the basaltic-tephra hazard zone for that area. An area of volcanic-gas hazard is indicated in the north-central INEEL, near Test Area North (TAN), within a topographic depression that could trap dense volcanic gas.

GROUND-DEFORMATION HAZARD ZONE

The widespread occurrence of fissure-erupted lava flows and the magma-induced extensional structures of eastern SRP volcanic rift zones indicate that most basaltic eruptions on the eastern SRP were fed by northwest-trending dikes. Ground deformation is expected to accompany all shallow dike-intrusion events, with or without volcanic eruption. The recurrence of ground-deformation phenomena is, therefore, considered equal to or greater than lava-flow recurrence within the INEEL volcanic zones (Table 3). As discussed earlier, the severity of vertical offset and ground fissuring will vary according to the number of dikes and their aggregate thickness, but will generally not exceed 1-2 m of vertical offset or horizontal extension within a few hundred meters of the intruding basaltic dike. The hazardous areas are therefore restricted to the volcanic zones and are substantially smaller than the hazard zones for lava inundation. We define areas within 1 km of Qb a, b, or c (post-400-Ka) vents, and all areas with magma-induced fissures and faults as constituting the zone of ground-deformation hazard (Figure 7). The Arco volcanic rift zone includes many such deformation features associated with fissure-fed lava flows and small pyroclastic cones, indicating repeated dike intrusions in the area. Some of the fissures of the northern Arco volcanic rift zone maybe of tectonic origin and related to the Lost River fault. For purposes of analyzing volcanic hazards, we take a conservative approach by assuming all of these fissures to have been induced by magma. Although generally lacking ground-deformation features, much of the axial volcanic zone is also included as part of the ground-deformation hazard zone, because it can reasonably be inferred that fissures formed but were covered by cogenetic lava flows from the many vents in the area.

Magma-induced fissures and faults of the INEEL area have not been dated, but the ages of host volcanic rocks serve to limit the maximum ages of fissures. We have conservatively assumed that magma-induced fissures without a clear cogenetic relationship to mapped volcanic materials are equivalent in age to a younger lava-flow group than the host rocks. For example, most dike-induced faults and fissures of the northern Arco volcanic rift zone are developed in lava flows older than 400 Ka, but some could have formed during the past 400 Ka and are therefore included as young vents in defining lava-flow hazard zone 1. The isolated fissures mapped near the Naval Reactors Facility (NRF) by Golder Associates (1992) occupy the northern part of the poorly defined Howe-East Butte volcanic rift zone, trend east-west, have no clear relationship to volcanic materials of the area,

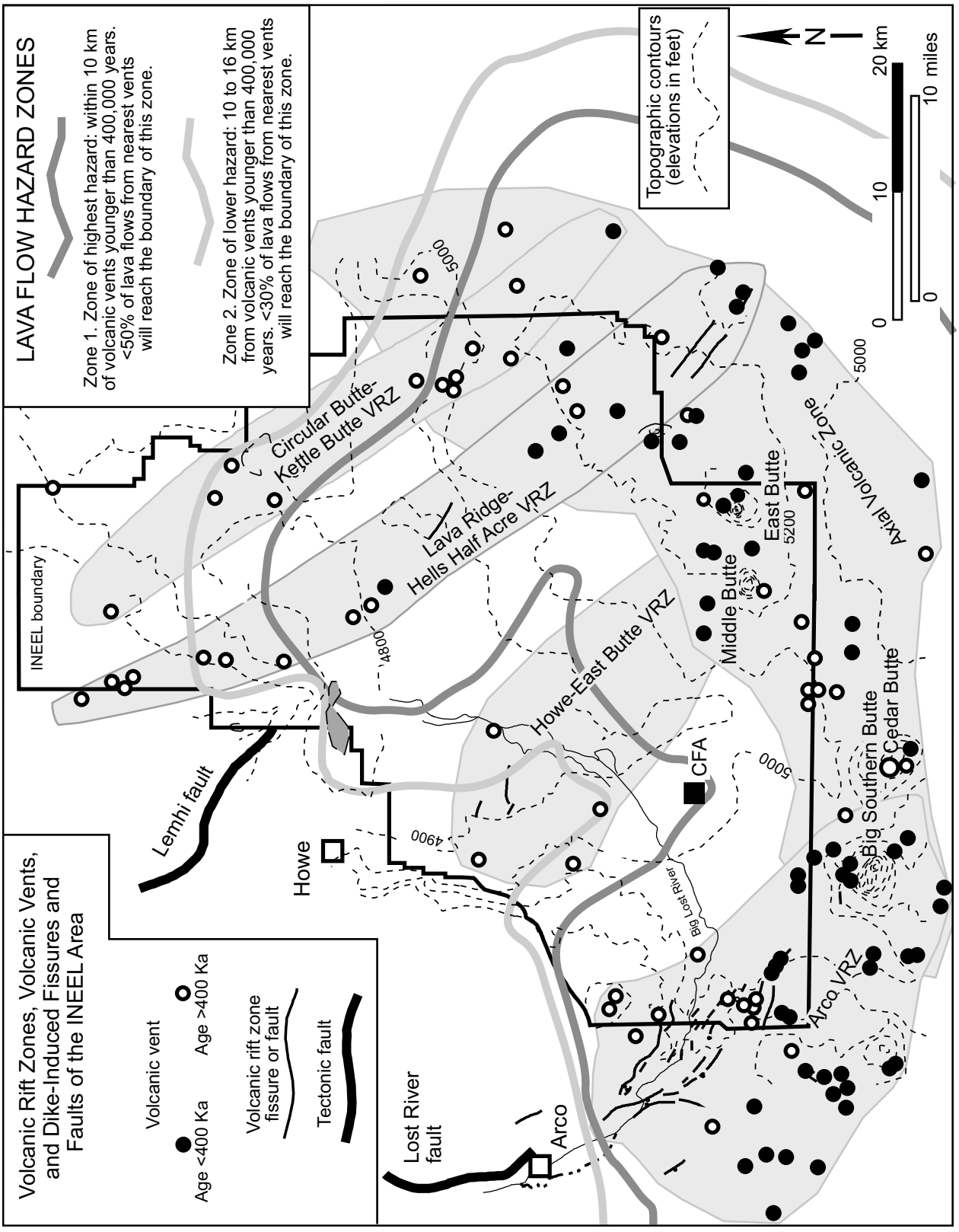

Figure 5. Lava flow hazard-zone map of the INEEL area. Filled square shows the location of the Central Facilities Area.

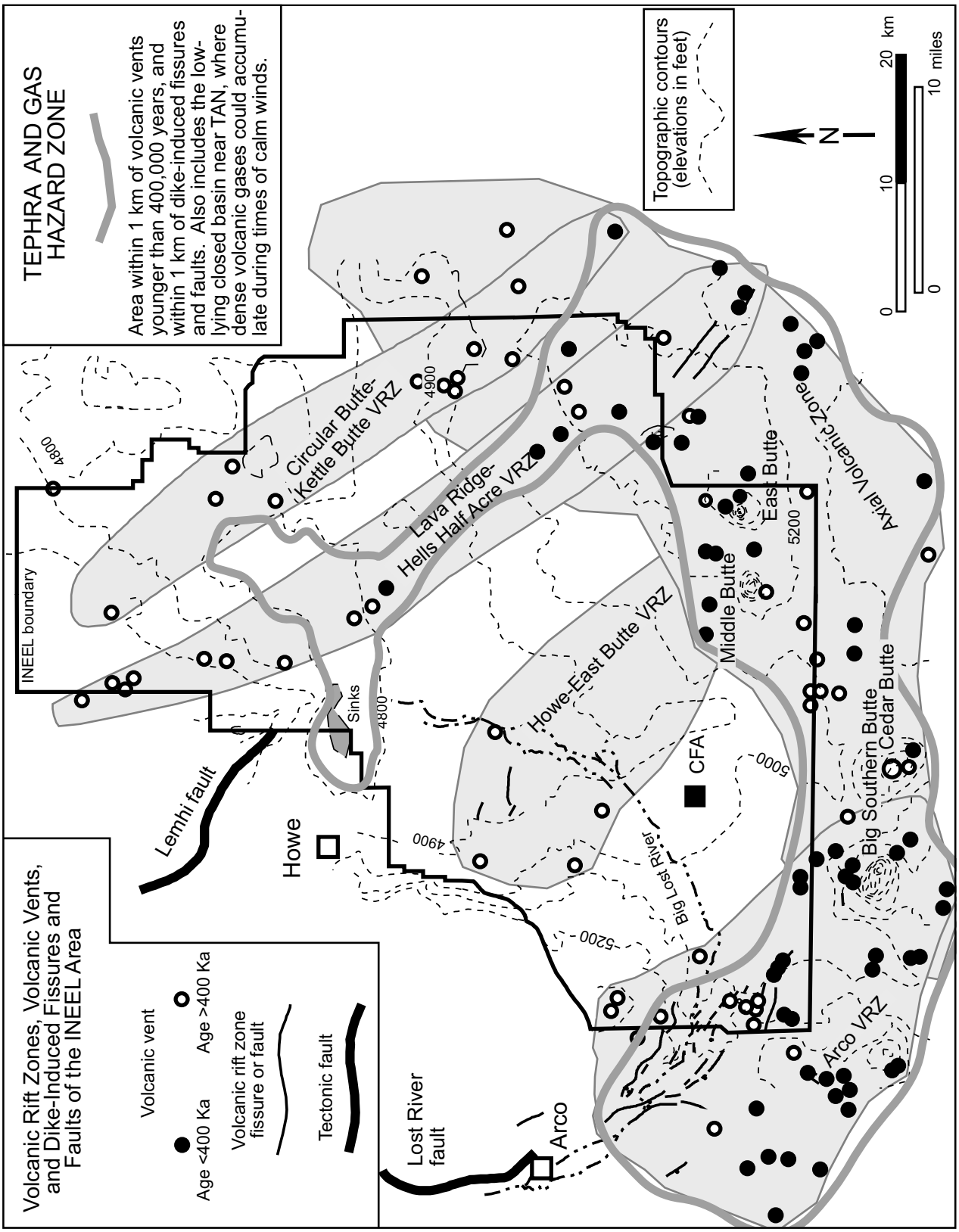

Figure 6. Tephra and gas hazard-zone map of the INEEL area. Filled square shows the location of the Central Facilities Area.

and may be related to basin subsidence rather than dike intrusion. Although these fissures are included in this hazard assessment, we do not consider them to be a likely site of future volcanism.

VOLCANIC-HAZARD ASSESSMENT OF THE CENTRAL FACILITIES AREA

The Central Facilities Area (CFA; Figure 8) is a cluster of buildings and other facilities located on the southwestern INEEL, about 15 km from vents of the volcanic zones to the west and south, and within a topographic basin about 100 m lower in elevation than the surrounding volcanic highlands. Given its distance and physiographic setting, the CFA seems unlikely to be impacted by tephra, gas or dike-induced ground deformation, but the CFA could be inundated by future lava flows from the adjacent volcanic zones. We therefore give a site-specific probabilistic hazard assessment for lava-flow inundation of the CFA.

The parameters needed to estimate the probability of lava inundation are the recurrence intervals of the volcanic source zones, the topographic setting of the CFA and the volcanic zones, the statistics of the lengths and areas of lava flows, the distance from CFA to potential sources of lava flows, the warning time prior to inundation, and the probability of successful mitigation.

We illustrate our approach with an event tree (Figure 9). The event tree is an inductive-logic modeling tool used to identify and depict the chains of events that may result in some outcome of interest, in this case an outcome important as a hazard. The event-tree modeling process begins with an initial condition which may lead to several end-states, depending on the results of subsequent events. The events can be processes, functions, conditions, mitigators, or barriers that are relevant to the outcome of interest. Event-tree branches represent decision points in modeling the combinations of events. Upward branches represent success or the achievement of a desired outcome. Downward branches represent failures of functions or barriers, or the absence of some relevant condition. Application of the event tree uses binary branching (i.e., success vs. failure, condition present vs. condition not present). Each node represents the universe of possible functional or conditional states. Therefore, the probabilities of all the possible states must sum to one. Probabilities are assigned to each event-tree branch, and the probability of each event sequence is the product of the branch probabilities.

"Eruption" is the initial condition, and the 6×10^{-5} per year recurrence value expresses the probability of volcanism at a random location within the Arco volcanic rift zone and the axial volcanic zone (Table 3), which we express as one value because of the nearly identical recurrence estimates.

The second event, "lava flows away from CFA," concerns vent location and topography relative to CFA, which lies outside the volcanic zones. On figure 8, we identify a "critical volcanic source area," which is the region that might send lava flows on a path toward the site. The critical volcanic source area is defined on its southern margin by a topographic divide. Lava flows erupting south of this divide will flow south, away from the CFA. Topographic analysis also shows that lava flows originating from any place on the axial volcanic zone northeast of East Butte will not flow toward CFA. The critical volcanic source area encompasses 660 square km, or 0.29 of the total 2,270 square-km area of the combined Arco and axial volcanic zones.

The third event, "lava stops short of CFA," addresses the probability of lava reaching CFA. If lava reaches CFA, total inundation is assumed; advanced warning and mitigation are addressed later. The CFA is located about 10 km (the 50th-percentile lava-flow length, Table 4) from the critical volcanic source area, and most of the young vents within the source area lie within 20 km (the 80th-percentile lava-flow length). We use the 70th-percentile distance of 16 km as an average distance from inferred lava-flow sources to the CFA. By statistical definition only 30 percent of lava flows from that distance will reach the CFA.

The fourth event addresses warning time for mitigation, and there is considerable uncertainty in deriving this parameter. We assume that 80 percent of lava flows would give at least 1 month advanced warning, and we consider 1 month to be adequate for effective mitigation by the removal of property or the construction of barriers. We justify this by analogy with the active basaltic rift zones of Iceland and Hawaii, where magma usually takes several weeks, commonly several months, to ascend to the surface from upper-mantle source regions. Based on seismic-velocity investigations, the inferred source of magma beneath the eastern SRP is 50-200 km deep, and ascending magma from those depths would be readily tracked by the INEEL seismic network. A second aspect of advanced warning involves lava-flow velocity, or the time to reach CFA after the onset of eruption. Observed basaltic lava flows on low-relief terrain such as the southern INEEL generally move at rates less than several kilometers per day. Tilling and Peterson (1994) summarize field observations of active lava flows from the east rift zone of Kilauea, Hawaii, and find that the average rate of advance of broad lava-flow fronts to be 5 km per day. Fink and Zimbelman (1986) also observed Hawaiian pahoehoe

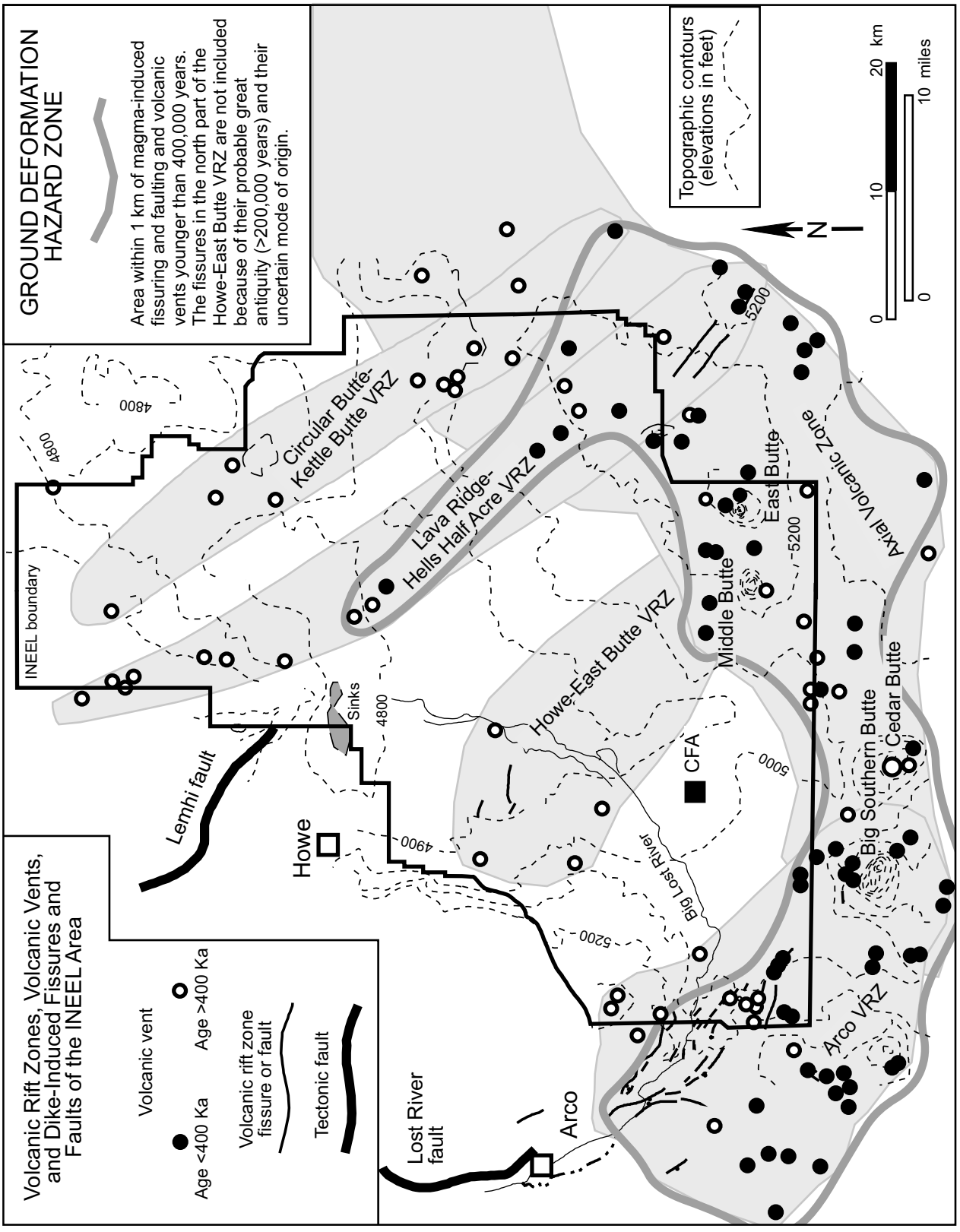

Figure 7. Ground deformation hazard-zone map of the INEEL area. Filled spuare shows the location of the Central Facilities Area.

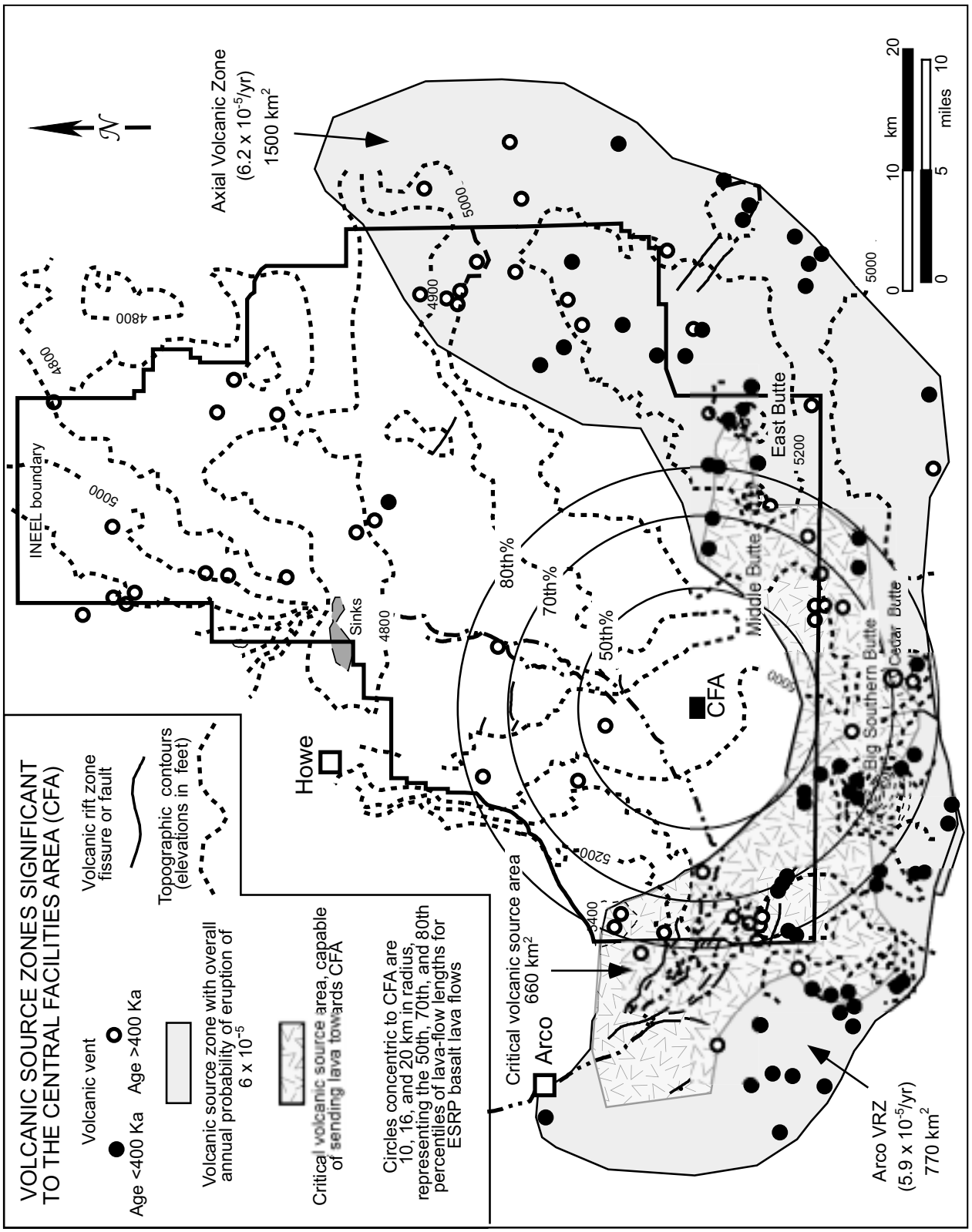

Figure 8. Volcanic source zones significant to the Central Facilities Area (CFA), INEEL.

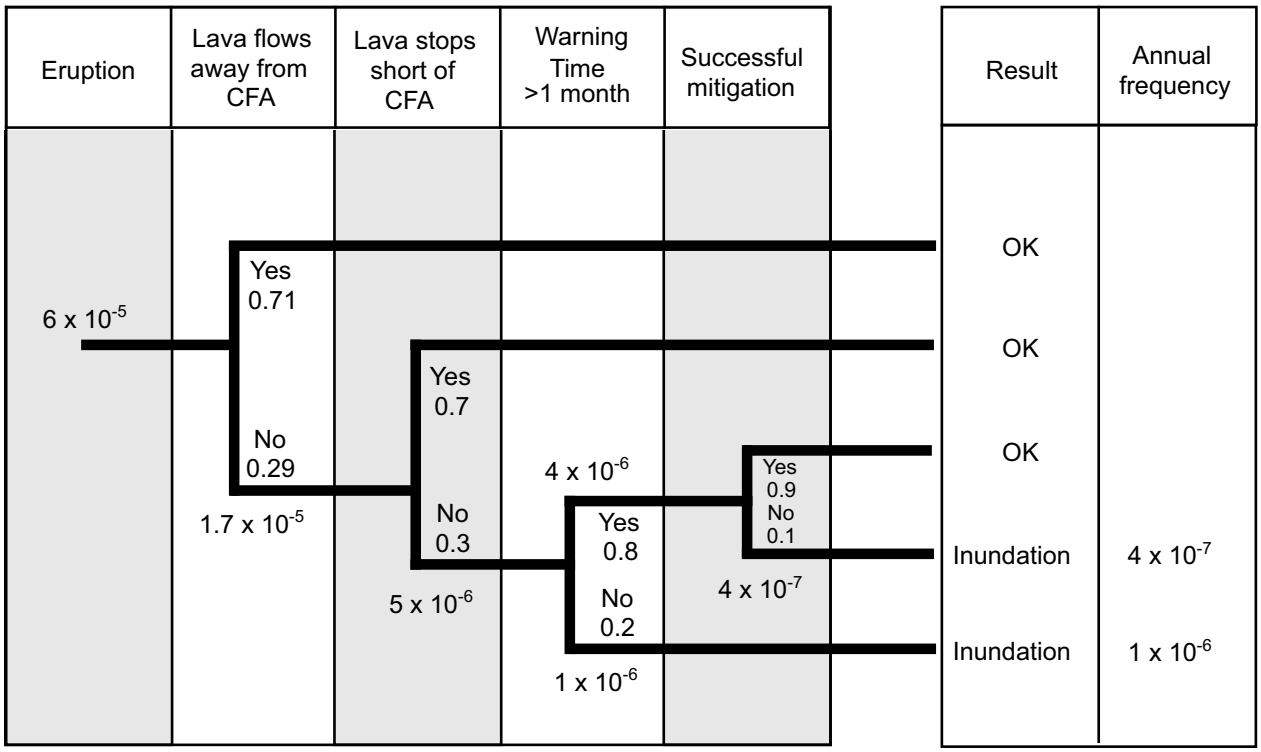

Figure 9. Volcanism event tree for lava-flow inundation of the Central Facilities Area (CFA), INEEL.

flow velocities on terrain similar to that of the INEEL to average 5 km per day. Hon and others (1994) give an average velocity of about 1 km per day for typical pahoehoe sheet flows in Hawaii. Bullard (1962) describes basaltic lava flows from several Hawaiian and Mexican volcanoes and cites near-source velocities of about 1 km per hour during the early stages of eruption, about 400 m per day after the flows had spread on gentle terrain, and as low as 1 m per day in the final stages, weeks or months after onset.

Assuming a rate of 2 km per day, it would take a lava flow about a week to travel the 16-km distance from the center of a nearby volcanic zone to the CFA. Together with several weeks of precursory seismic warning, our analysis suggests that about 1 month of advanced warning of lava inundation is probable. For event 4, our chosen probability of 0.2 assumes that only 20 percent of lava flows will fail to give 1 month of warning.

The fifth event addresses the probability of successful mitigation, given 1 month or more of warning. We assume that mitigation would be unsuccessful only 10 percent of the time. Potential actions (Barberi and others, 1993) include the removal of materials, the construction of earthen berms around CFA facilities, the building of earthen berms in the flow path to slow or divert the lava, the cooling of the lava-flow front with water sprays near critical facilities, and the use of explosives at or near the vent area to route the lava elsewhere.

Results are expressed as annual frequencies on the right of Figure 9. If no mitigation is possible, the estimated frequency of CFA property damage due to lava inundation is 1 x 10^{-6} per year. If mitigation is attempted, the estimated frequency is 4 x 10^{-7} per year.

ACKNOWLEDGMENTS

We thank Suzette Jackson for discussions of magma-induced faulting and seismicity. Scott Hughes, Jennifer Parker, and Rachel Lawrence helped with field work and the measurement of lava flows. Corey Atwood helped with statistical calculations. Our assessment would not have been possible without several decades of field and laboratory work by Mel Kuntz and colleagues at the U.S. Geological Survey. Constructive reviews by Mel Kuntz, Craig White, and Roger Stewart improved the presentation. Our work was performed for the U.S. Department of Energy, under DOE contract no. DE-AC07-94ID13223.

REFERENCES

Anderson, S.R., and B.D. Lewis, 1989, Stratigraphy of the unsaturated zone at the Radioactive Waste Management Complex, Idaho National Engineering Laboratory, Idaho: U.S. Geological Survey Water-Resources Investigations Report 89-4065, 54 p.

Barberi, Franco, M.L. Carapezza, M. Valenza, and L. Villari, 1993, The control of lava flow during the 1991-1992 eruption of Etna: Journal of Volcanology and Geothermal Research, v. 56, p. 1-34.

Blong, R.J., 1984, Volcanic Hazards—A Sourcebook on the Effects of Eruptions: Academic Press, New York, 424 p.

Bullard, F.M., 1962, Volcanoes in History, in Theory, in Eruption: University of Texas Press, Austin, 441 p.

Champion, D.E., M.A. Lanphere, and M.A. Kuntz, 1988, Evidence for a new geomagnetic reversal from lava flows in Idaho: Discussion of short polarity reversals in the Brunhes and late Matuyama polarity chrons: Journal of Geophysical Research, v. 93, p. 11,667-11,680.

Decker, R.W., and Barbara Decker, 1989, Volcanoes: W.H. Freeman and Company, New York, 285 p.

Decker, R.W., T.L. Wright, and P.H. Stauffer, eds., 1987, Volcanism in Hawaii: U.S. Geological Survey Professional Paper 1350, 1667 p.

Fink, J.H., ed., 1990, Lava Flows and Domes—Emplacement Mechanisms and Hazard Implications: IAVCEI Proceedings in Volcanology 2: Springer-Verlag, New York, 249 p.

Fink, J.H., and J.R. Zimbelman, 1986, Rheology of the 1983 Royal Garden basalt flows, Kilauea volcano, Hawaii: Bulletin of Volcanology, v. 48, p. 87-96.

Fishel, Mark, 1993, Geology and petrology of uplifted mafic lavas on the north flank of Big Southern Butte, eastern Snake River Plain, Idaho: Idaho State University M.S. thesis, 178 p.

Fournier D'Albe, E.M., 1986, Reducing vulnerability to nature's violent forces: Cooperation between scientist and citizen, *in* R.H. Maybury, ed., Violent Forces of Nature: Lomond Publications, Mt. Airy, Maryland, p. 1-6.

Golder Associates, 1992, New Production Reactor site characterization, volume 1, volcanic zones geologic mapping report: EG&G Idaho, Inc., Informal Report EGG-NPR-10625.

Greeley, Ronald, 1982, The style of basaltic volcanism in the Eastern Snake River Plain, Idaho, *in* Bill Bonnichsen and R.M. Breckenridge, eds., Cenozoic Geology of Idaho: Idaho Bureau of Mines and Geology Bulletin 26, p. 407-422.

Greeley, Ronald, and J.S. King, 1977, Volcanism of the Eastern Snake River Plain, Idaho: A Comparative Planetary Geology Guidebook: NASA Publication CR-154621, 308 p.

Gudmundsson, Agust, 1987, Tectonics of the Thingvellir fissure swarm, southwest Iceland: Journal of Structural Geology, v. 9, p. 61-69.

Hackett, W.R., S.M. Jackson, and R.P. Smith, 1996, Paleoseismology of volcanic environments, *in* J.P. McCalpin, ed., Paleoseismology: Academic Press, New York, p. 147-179.

Hackett, W.R., and L.A. Morgan, 1988, Explosive basaltic and rhyolitic volcanism of the eastern Snake River Plain, Idaho, *in* P.K. Link and W.R. Hackett, eds., Guidebook to the Geology of Central and Southern Idaho: Idaho Geological Survey Bulletin 27, p. 283-301.

Hackett, W.R., and R.P. Smith, 1992, Quaternary volcanism, tectonics and sedimentation in the Idaho National Engineering Laboratory area, *in* J.R. Wilson, ed., Field Guide to Geologic Excursions in Utah and Adjacent Areas of Nevada, Idaho and Wyoming: Utah Geological Survey Miscellaneous Publication 92-3, p. 1-18.

Hayden, Karl, 1992, Geology and petrology of the Cedar Butte eruptive center, eastern Snake River Plain, Idaho: Idaho State University M.S. thesis, 104 p.

Hildreth, Wes, A.N. Halliday, and R.L. Christiansen, 1991, Isotopic and chemical evidence concerning the genesis and contamination of basaltic and rhyolitic magma beneath the Yellowstone Plateau volcanic field: Journal of Petrology, v. 32, p. 63-138.

Hon, Ken, Jim Kauahikaua, Roger Denlinger, and Kevin MacKay, 1994, Emplacement and inflation of pahoehoe sheet flows: Observations and measurements of active lava flows on Kilauea volcano, Hawaii: Geological Society of America Bulletin, v. 106, p. 351-370.

Humphreys, E.D., and K.G. Dueker, 1994, Western U.S. upper mantle structure: Journal of Geophysical Research, v. 99, no. B5, p. 9615-9634.

Imsland, P., 1989, Study models for volcanic hazards in Iceland, *in* J.H. Latter, ed., Volcanic Hazards—Assessment and Monitoring: IAVCEI Proceedings in Volcanology 1: Springer-Verlag, New York, p. 36-56.

Jackson, S.M., 1994, Maximum magnitudes of earthquakes associated with basalt dike intrusion for use in INEL seismic hazards assessments: INEL-94/0132, 42 p.

Kilburn, C.J., and G. Luongo, eds., 1994, Active Lavas: Monitoring and Modeling: University College London Press, London, 374 p.

Kuntz, M.A., 1978, Geology of the Arco-Big Southern Butte area, eastern Snake River Plain, and potential volcanic hazards to the Radioactive Waste Management Complex and other waste storage and reactor facilities at the Idaho National Engineering Laboratory, Idaho: U.S. Geological Survey Open-File Report 78-691, 70 p.

———, 1992, A model-based perspective of basaltic volcanism, eastern Snake River Plain, Idaho, *in* P.K. Link, M.A. Kuntz, and L.B. Platt, eds., Regional Geology of Eastern Idaho and Western Wyoming: Geological Society of America Memoir 179, p. 289-304.

Kuntz, M.A., D.E. Champion, R.H. Lefebvre, and H.R. Covington, 1988, Geologic map of the Craters of the Moon, Kings Bowl, and Wapi lava fields, and the Great Rift volcanic rift zone, south-central Idaho: U.S. Geological Survey Miscellaneous Investigations Series Map I-1632, scale 1:100,000.

Kuntz, M.A., H.R. Covington, and L.J. Schorr, 1992, An overview of basaltic volcanism of the eastern Snake River Plain, Idaho, *in* P.K. Link, M.A. Kuntz, and L.B. Platt, eds., Regional Geology of Eastern Idaho and Western Wyoming: Geological Society of America Memoir 179, p. 227-268.

Kuntz, M.A. and G.B. Dalrymple, 1979, Geology, geochronology and potential volcanic hazards in the Lava Ridge-Hell's Half Acre area, eastern Snake River Plain, Idaho: U.S. Geological Survey Open-File Report 79-1657, 65 p.

Kuntz, M.A., Betty Skipp, M.A. Lanphere, W.E. Scott, K.L. Pierce, G.B. Dalrymple, D.E. Champion, G.F. Embree, W.R. Page, L.A. Morgan, R.P. Smith, W.R. Hackett, and D.W. Rodgers, 1994, Geologic map of the Idaho National Engineering Laboratory and adjoining areas, eastern Idaho: U.S. Geological Survey Miscellaneous Investigations Map I-2330, scale 1:100,000.

Kuntz, M.A., E.C. Spiker, M. Rubin, D.E. Champion, and R.H. Lefebvre, 1986, Radiocarbon studies of latest Pleistocene and Holocene lava flows of the Snake River Plain, Idaho: Data, lessons, interpretations: Quaternary Research, v. 25, p. 163-176.

LaPoint, P.J., 1977, Preliminary photogeologic map of the eastern Snake River Plain, Idaho: U.S. Geological Survey Miscellaneous Field Studies Map MF-850, scale 1:250,000.

Latter, J.H., 1989, ed., Volcanic Hazards—Assessment and Monitoring: IAVCEI Proceedings in Volcanology 1: Springer-Verlag, New York, 625 p.

Morgan, L.A., D.J. Doherty, and W.P. Leeman, 1984, Ignimbrites of the eastern Snake River Plain: Evidence for major caldera-forming eruptions: Journal of Geophysical Research, v. 89, p. 8665-8678.

Mullineaux, D.R., D.W. Peterson, and D.R. Crandell, 1987, Volcanic hazards in the Hawaiian Islands, *in* R.W. Decker, T.L. Wright, and P.H. Stauffer, eds., Volcanism in Hawaii: U.S. Geological Survey

Professional Paper 1350, p. 599-621.

Pierce, K.L., and L.A. Morgan, 1992, The track of the Yellowstone hotspot—Volcanism, faulting and uplift, *in* P.K. Link, M.A. Kuntz, and L.B. Platt, eds., Regional Geology of Eastern Idaho and Western Wyoming: Geological Society of America Memoir 179, p. 1-54.

Reiter, Leon, 1990, Earthquake Hazard Analysis, Issues and Insights: Columbia University Press, New York, 254 p.

Scott, W.E., 1982, Surficial geologic map of the eastern Snake River Plain and adjacent areas, 111 to 115 degrees W., Idaho and Wyoming: U.S. Geological Survey Miscellaneous Investigations Series Map I-1372, 2 sheets, scale 1:250,000.

Self, Stephen, L. Keszthelyi, and T. Thordarson, 1998, The importance of pahoehoe: Annual Reviews of Earth and Planetary Science, v. 26, p. 81-110.

Sigurdsson, Haruldur, 1980, Surface deformation of the Krafla fissure swarm in two rifting events: Journal of Geophysics, v. 47, p. 154-159.

Smith, R.B., and L.W. Braile, 1993, Topographic signature, space-time evolution, and physical properties of the Yellowstone-Snake River Plain volcanic system: The Yellowstone Hotspot, *in* A.W. Snoke, J.R. Steidtmann, S.M. Roberts, eds., Geology of Wyoming: Geological Survey of Wyoming Memoir 5, p. 694-754.

Smith, R.B., and R.L. Christiansen, 1980, Yellowstone Park as a window on the Earth's interior: Scientific American, February 1980, v. 242, no. 2, p. 104-117.

Smith, R.P., 1994, Potential impacts of selected magmatic processes at Test Area North: EG&G Idaho, Inc., Engineering Design File EDF-TANO-94-23, 7 p.

Smith, R.P., W.R. Hackett, and D.W. Rodgers, 1989, Geologic aspects of seismic-hazards assessment at the Idaho National Engineering Laboratory, southeastern Idaho: Proceedings, Second DOE Natural Phenomena Hazards Mitigation Conference, p. 282-289.

Smith, R.P., S.M. Jackson, and W.R. Hackett, 1996, Paleoseismology and seismic-hazards evaluations in extensional volcanic terrains: Journal of Geophysical Research, v. 101, p. 6277-6292.

Spear, D.B., and J.S. King, 1982, The geology of Big Southern Butte, Idaho, *in* Bill Bonnichsen and R.M. Breckenridge, eds., Cenozoic Geology of Idaho: Idaho Bureau of Mines and Geology Bulletin 26, p. 395-403.

Tilling, R.I., and D.W. Peterson, 1994, Field observation of active lava in Hawaii: Some practical considerations, *in* C.J. Kilburn, and G. Luongo, eds., Active Lavas: Monitoring and Modeling: University College of London Press, London, p. 147-174.

Volcanism Working Group, 1990, Assessment of potential volcanic hazards for New Production Reactor site at the INEL: EG&G Informal Report, EGG-NPR-10624, 98 p.

Wetmore, P.H., S.S. Hughes and S.R. Anderson, 1997, Model morphologies of subsurface Quaternary basalts as evidence for a decrease in the magnitude of basaltic volcanism at and near the Idaho National Engineering and Environmental Laboratory, Idaho: Proceedings 32nd Symposium Engineering Geology and Geotechnical Engineering, Boise, Idaho, p. 45-58.

Williams, Howel, and A.R. McBirney, 1979, Volcanology: Freeman, Cooper and Co., San Francisco, 397 p.

Womer, M.B., Ronald Greeley, and J.S. King, 1982, Phreatic eruptions of the eastern Snake River Plain of Idaho, *in* Bill Bonnichsen and R.M. Breckenridge, eds., Cenozoic Geology of Idaho: Idaho Bureau of Mines and Geology Bulletin 26, p. 453-464.

Wright, T.L., J.Y. Chun, J. Esposo, C. Heliker, J. Hodge, J.P. Lockwood, and S.M. Vogt, 1992, Map showing lava flow hazard zones, island of Hawaii: U.S. Geological Survey Miscellaneous Field Studies Map MF-2193, scale 1:250,000.

Zietz, I., F.P. Gilbert, and J.R. Kirby, 1978, Aeromagnetic map of Idaho: U.S. Geological Survey Geophysical Investigations Map GP-920, scale 1:1,000,000.

IDAHO GEOLOGICAL SURVEY

Main Office at Moscow
Morrill Hall, Third Floor
University of Idaho
PO Box 443014
Moscow, ID 83844-3014
Phone: (208) 885-7991
Fax: (208) 885-5826
E-mail: igs@uidaho.edu

Web site: http://www.idahogeology.org

Branch Office at Boise
Math-Geosciences, Room 223C
Boise State University
MS 1535
Boise, ID 83725-1535
Phone: (208) 426-4002
Fax: (208) 426-4061

Branch Office at Pocatello
Physical Science, Room 235
Idaho State University
MS 8072
Pocatello, ID 83209-8072
Phone: (208) 282-4254
Fax: (208) 282-4414

ADMINISTRATION

Roy M. Breckenridge ..... Director/State Geologist
email: roybreck@uidaho.edu

Kurt L. Othberg ..... Director
email: othberg@uidaho.edu

Roger C. Stewart ..... Manager, Publications & Communications
email: rstewart@uidaho.edu

Charlotte D. Fullerton ..... Management Assistant
email: fullertn@uidaho.edu

PUBLIC INQUIRIES & SALES

Gayle A. Wells ..... Administrative Assistant
email: gaylew@uidaho.edu

Connie Tillotson ..... Secretary, Pocatello Office
email: tillconn@isu.edu

RESEARCH & SERVICE

Roy M. Breckenridge ..... Quaternary geology, urban geology
email: roybreck@uidaho.edu ..... geologic hazards, geomorphology

Jane S. Freed ..... digital map production
email: jfreed@uidaho.edu

Virginia S. Gillerman ..... economic geology,
Boise Office ..... general geology, mineral exploration,
email: vgillerm@boisestate.edu ..... structural geology

John D. Kauffman ..... general geology, geologic mapping,
email: johndk@uidaho.edu ..... Columbia River basalt

Reed S. Lewis ..... general geology, Idaho batholith,
email: reedl@uidaho.edu ..... Belt Supergroup, economic geology

Victoria E. Mitchell ..... mines and prospects,
email: vmitchel@uidaho.edu ..... library information

Kurt L. Othberg ..... environmental geology, geomorphology,
email: othberg@uidaho.edu ..... geologic hazards, earth science education

Loudon R. Stanford ..... Manager, digital mapping
email: stanford@uidaho.edu

Michael J. Weaver ..... Mine Safety Specialist, C.M.S.P.
email: mjweaver@uidaho.edu

John A. Welhan ..... geochemistry, hydrogeology,
Pocatello Office ..... environmental geology,
email: welhjohn@isu.edu ..... hydrothermal investigations

Production

Editor ..... Roger C. Stewart
Digital Illustrator ..... B. Benjamin E. Studer
Designer ..... Barbara A. Ham
Printing and Design Services, University of Idaho
Printer ..... McNaughton Gunn, Inc.
Saline, MI

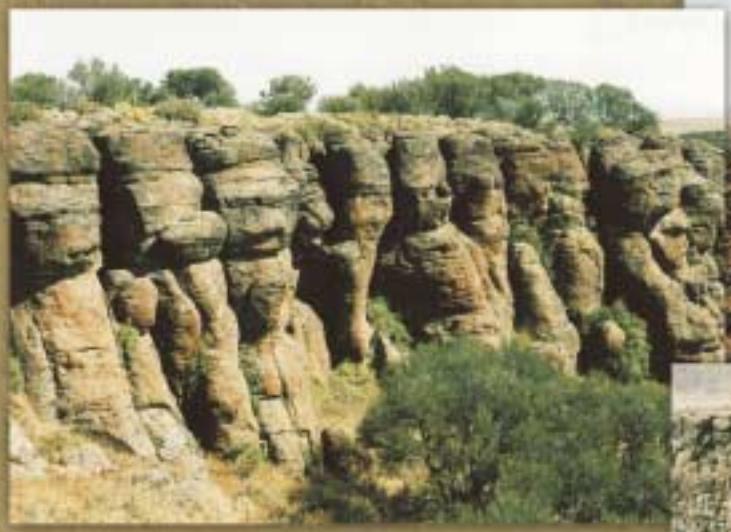

IDAHO
GEOLOGICAL SURVEY
PRESS

ISBN 1-55765-029-2